SPECIALIST PERIODICAL REPORTS

RS•C

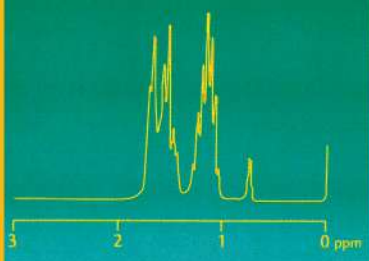

Nuclear magnetic *resonance*

Volume 34

senior reporter G.A. WEBB

Nuclear Magnetic Resonance

Volume 34

A Specialist Periodical Report

Nuclear Magnetic Resonance

Volume 34

A Review of the Literature Published between June 2003 and May 2004

Senior Reporter
G.A. Webb, *formerly Department of Chemistry, University of Surrey, Guildford, UK*

Reporters
A.E. Aliev, *University College, London, UK*
N. Asakawa, *Tokyo Institute of Technology, Tokyo, Japan*
I. Barsukov, *University of Leicester, UK*
A.C. de Dios, *Georgetown University, Washington, DC, USA*
H. Fukui, *Kitami Institute of Technology, Kitami, Japan*
E.F. Hounsell, *Birkbeck College, London, UK*
C.J. Jameson, *University of Illinois at Chicago, USA*
K. Kamieńska-Trela, *Polish Academy of Sciences, Warszawa, Poland*
S. Kuroki, *Tokyo Institute of Technology, Tokyo, Japan*
H. Kurosu, *Nara Women's University, Nara City, Japan*
R.V. Law, *Imperial College of Science, Technology and Medicine, London, UK*
R. Ludwig, *University of Rostock, Germany*
S.J. Matthews, *Imperial College London, UK*
M. Monduzzi, *University of Cagliari, Monserrato, Italy*
M.J.W. Prior, *University of Nottingham, UK*
W. Schilf, *Polish Academy of Sciences, Warszawa, Poland*
R.R. Sharp, *University of Michigan, USA*
T. Watanabe, *Aoyama Women's Junior College, Tokyo, Japan*
J. Wójcik, *Polish Academy of Sciences, Warszawa, Poland*
T. Yamanobe, *University of Gunma, Japan*
H. Yasunaga, *Kyoto Institute of Technology, Kyoto, Japan*

RS•C
advancing the chemical sciences

If you buy this title on standing order, you will be given FREE access to the chapters online. Please contact sales@rsc.org with proof of purchase to arrange access to be set up.

Thank you.

ISBN 0-85404-352-7
ISSN 0305-9804

A catalogue record for this book is available from the British Library

© The Royal Society of Chemistry 2005

All rights reserved

Apart from any fair dealing for the purpose of research or private study, or criticism or review as permitted under the terms of the UK Copyright, Designs and Patents Act, 1988, this publication may not be reproduced, stored or transmitted, in any form or by any means, without the prior permission in writing of The Royal Society of Chemistry, or in the case of reprographic reproduction only in accordance with the terms of the licences issued by the Copyright Licensing Agency in the UK, or in accordance with the terms of the licences issued by the appropriate Reproduction Rights Organization outside the UK. Enquiries concerning reproduction outside the terms stated here should be sent to The Royal Society of Chemistry at the address printed on this page.

Published by The Royal Society of Chemistry,
Thomas Graham House, Science Park, Milton Road,
Cambridge CB4 0WF, UK

Registered Charity Number 207890

For further information see our web site at www.rsc.org

Typeset by Vision Typesetting Ltd, Manchester, UK
Printed by Athenaeum Press Ltd, Gateshead, Tyne and Wear, UK

Preface

Volume 34 of the Specialist Periodical Reports on NMR comprises a comprehensive account of the relevant literature appearing between June 2003 and May 2004. A change in the coverage of Paramagnetic NMR has been put into place. This topic has been covered biennially by Professor R.R. Sharp for the past ten years and I wish to express my gratitude to him for his thorough and interesting reports, the last of which appears in the present volume. In recent years the main developments in paramagnetic NMR have related to contrast agents used in NMR imaging studies. Thus it has been decided that a separate chapter covering this topic is no longer warranted and in future volumes NMR studies on paramagnetic species will be included in other chapters such as those on NMR imaging, applications of nuclear shielding and nuclear relaxation in fluids.

It is a pleasure for me to thank all of the reporters for their timely and interesting accounts and the production team at Thomas Graham House for their support in the realisation of this volume.

G.A. Webb
October 2004

Contents

Chapter 1 NMR Books and Reviews 1
By W. Schilf

1 Books 1
2 Regular Reviews Series 1
3 Edited Books and Symposia 10
4 Reviews in Periodicals 28
5 Reviews and Books in Foreign Languages 48

Chapter 2 Theoretical and Physical Aspects of Nuclear Shielding 57
By C.J. Jameson and A.C. de Dios

1 Theoretical Aspects of Nuclear Shielding 57
1.1 General Theory 57
1.2 *Ab initio* and DFT Calculations 65
2 Physical Aspects of Nuclear Shielding 68
2.1 Anisotropy of the Shielding Tensor 68
2.2 Shielding Surfaces and Rovibrational Averaging 70
2.3 Isotope Shifts 73
2.4 Intermolecular Effects on Nuclear Shielding 74
2.5 Absolute Shielding Scales 80
References 81

Chapter 3 Application of Nuclear Shielding 87
By S. Kuroki, N. Asakawa and H. Yasunaga

1 Introduction 87
2 Shielding of Particular Nuclear Species 87
2.1 Group 1 (^{1}H, ^{2}H, ^{6,7}Li, ^{23}Na, ^{39}K, ^{87}Rb, ^{133}Cs) 87
2.2 Group 2 (^{9}Be, ^{25}Mg, ^{87}Sr) 93
2.3 Group 3 (^{45}Sc, ^{89}Y, ^{139}La, ^{171}Yb) 94
2.4 Group 4 (^{47,49}Ti, ^{91}Zr) 95
2.5 Group 5 (^{51}V and ^{93}Nb) 95
2.6 Group 6 (^{95}Mo, ^{183}W) 96
2.7 Group 7 (^{55}Mn, ^{99}Tc) 97

Nuclear Magnetic Resonance, Volume 34

© The Royal Society of Chemistry, 2005

2.8 Group 8 (^{57}Fe) 98
2.9 Group 9 (^{59}Co, ^{103}Rh) 98
2.10 Group 10 (^{195}Pt) 98
2.11 Group 11 (^{63,65}Cu, ^{107,109}Ag) 99
2.12 Group 12 (^{111,113}Cd, ^{199}Hg) 100
2.13 Group 13 (^{11}B, ^{27}Al, ^{71}Ga, ^{203,205}Tl) 101
2.14 Group 14 (^{13}C, ^{29}Si, ^{73}Ge, ^{117,119}Sn, ^{207}Pb) 105
2.15 Group 15 (^{14,15}N, ^{31}P) 110
2.16 Group 16 (^{17}O, ^{33}S, ^{77}Se, ^{125}Te) 115
2.17 Group 17 (^{19}F, ^{35,37}Cl) 118
2.18 Group 18 (^{3}He, ^{129}Xe) 120
References 121

Chapter 4 Theoretical Aspects of Spin–Spin Couplings 136
By H. Fukui

1 Introduction 136
2 The Sign of Fermi-contact Contribution to Spin–Spin Coupling Constants 136
3 Nuclear Spin–Spin Coupling Density Functions 138
4 Vibrational Corrections to Indirect Nuclear Spin–Spin Coupling Constants 140
5 Residual Dipolar Couplings Between Nuclear Spins 141
6 Fluorine-Fluorine Spin–Spin Coupling Constants 143
7 *Ab initio* Calculation of Spin–Spin Coupling Constants 144
7.1 Full Configuration-Interaction Calculations 144
7.2 Second-order Polarization Propagator Approximation Calculations 144
8 Gas-phase Studies of Spin–Spin Coupling Constants 146
9 Density Functional Theory 146
9.1 Density Functional Theory Calculations of Spin–Spin Coupling Constants using Slater-type Basis Sets 146
9.2 Basis Set Dependence of Spin–Spin Coupling Constants in Density Functional Theory Calculations 147
9.3 Relationship Between the π Character of a C-C Bond and ^{1}J(C,C) 147
9.4 Solvent Effects on the Nuclear Spin–Spin Coupling Constants 148
9.5 ^{1}J(Si,H) and Nonclassical H-Si Interactions 148
9.6 Spin–Spin Coupling Constants in Phosphatrane Molecules 149
9.7 Conformational and Configurational Analysis 149
9.8 Density Functional Theory Calculation of the Nuclear Spin–Spin Coupling Constants in C_{60} 151
9.9 Nuclear Spin–Spin Coupling Constants in Hydrogen Bonded Complexes 152

9.10 Karplus-type Relationships Between Scalar Coupling Constants 153
10 Semiempirical Calculation of ^{13}C-^{13}C Coupling Constants 154
References 154

Chapter 5 Applications of Spin–Spin Couplings 160
By K. Kamieńska-Trela and J. Wójcik

1 Introduction 160
2 New Methods 161
3 One-bond Couplings to Hydrogen 165
4 One-bond Couplings not Involving Hydrogen 168
5 Two-bond Couplings to Hydrogen 177
6 Two-bond Couplings not Involving Hydrogen 178
7 Three-bond Hydrogen–Hydrogen Couplings 181
8 Three-bond Couplings to Hydrogen 187
9 Three-bond Couplings not Involving Hydrogen 191
10 Couplings over More than Three Bonds and Through Space 192
11 Couplings Through Hydrogen Bonds 196
12 Residual Dipolar Couplings 198
References 203

Chapter 6 Nuclear Spin Relaxation in Liquids and Gases 217
By R. Ludwig

1 Introduction 217
2 General, Physical and Experimental Aspects of Nuclear Spin Relaxation 218
2.1 General Aspects 218
2.2 Experimental Aspects 220
2.3 Relaxation in Coupled Spin Systems 222
2.4 Dipolar Couplings and Distance Information 224
2.5 Exchange Spectroscopy 225
2.6 Radiation Damping 227
2.7 Quadrupolar Interactions 228
2.8 Intermolecular Dipolar Interaction in Diamagnetic and Paramagnetic Solution 230
2.9 Slow Motions in Glasses 232
2.10 Models for Molecular Dynamics 234
3 Selected Applications of Nuclear Spin Relaxation 237
3.1 Pure Liquids 237
3.2 Non-electrolyte Solutions 237
3.3 Electrolyte Solutions 237
3.4 Molten Salts 238
4 Nuclear Spin Relaxation in Gases 238

5 Self-diffusion in Liquids 240
5.1 Experimental and Theoretical Aspects 240
5.2 Selected Examples 242
References 243

Chapter 7 Solid State NMR Spectroscopy 253
A. E. Aliev and R. V. Law

1 Introduction 253
2 Reviews and Introductory Articles 254
3 Experimental Developments 257
3.1 Proton NMR. Gradient Experiments 257
3.2 Two-dimensional Experiments 258
3.3 Decoupling 259
3.4 Labelled Materials 260
3.5 NMR Parameter Measurements 262
3.6 Cross-polarisation and Polarisation Transfer 263
3.7 Recoupling Experiments 264
3.8 Selective Pulses and Phase Cycling 265
3.9 Quantitative Measurements 265
3.10 Quadrupolar Nuclei 266
3.11 Instrumental Developments 267
4 Distance and Angle Measurements by Solid State NMR 268
5 NMR Parameters: Experimental and Theoretical Studies 271
5.1 Chemical Shift and its Anisotropy: Spin $\frac{1}{2}$ Nuclei 271
5.2 J-Couplings 272
5.3 Quadrupolar Nuclei 273
6 Applications 274
6.1 Organic Solids 274
6.2 Amino Acids 278
6.3 Peptides 280
6.4 Proteins 284
6.5 Lipids and Membranes 291
6.6 Pharmaceutical Applications 293
6.7 Cellulose and Related Materials 295
6.8 Soils and Related Materials 297
6.9 Coals and Carbonaceous Materials 298
6.10 Polymers 299
6.11 Organometallic and Coordination Compounds 305
6.12 Glasses and Amorphous Solids 305
6.13 Cements 308
6.14 Microporus Solids and Related Materials 308
6.15 Surface Science and Catalysis 309
6.16 Inorganic and Other Related Solids 311
References 315

Chapter 8 Multiple Pulse NMR 328
By I. Barsukov

1 Introduction 328
2 Fast Multidimensional Methods 328
2.1 Hadamard Spectroscopy 329
2.2 Reduced Dimensionality Spectroscopy 331
2.3 Reconstruction of Multidimensional Spectra from Projections 333
2.4 Single Scan Multidimensional Spectroscopy 334
3 NOE, Relaxation and Diffusion 336
3.1 NOE 336
3.2 Relaxation Rate Measurements 336
3.3 Cross-correlated Relaxation Experiments 337
3.4 Diffusion Experiments 340
4 Coupling Constants Measurements 341
4.1 Scalar Couplings 341
4.2 Residual Dipolar Couplings 342
5 Homonuclear Spectroscopy 344
6 Inverse Proton Detected Correlation Spectroscopy 345
6.1 Double-resonance Experiments 345
6.2 Heteronuclear Triple Resonance Experiments 347
References 353

Chapter 9 NMR of Proteins and Nucleic Acids 355
By S. J. Matthews

1 Introduction 355
2 Application and Development of New Methodology 355
2.1 Automated Analysis 355
2.2 Dipolar Couplings 359
2.3 Transverse Relaxation Optimized Spectroscopy (TROSY) 364
2.4 NMR-based Screening 368
3 Macromolecular Structures 369
3.1 Membrane Proteins 369
3.2 Protein Complexes 372
3.3 Nucleic Acid Complexes 377
4 Protein Folding 380
References 384

Chapter 10 NMR of Carbohydrates, Lipids and Membranes 391
By E. F. Hounsell

1 Introduction 391
2 Membranes 391

2.1 Lipid Dynamics 391
2.2 Membrane Proteins 392
2.3 Membrane Interactions with Toxins and Viruses 393
2.4 Antimicrobial Actions 393
2.5 Membrane Transporter Proteins 394
2.6 Protein Folding Disorders 394
3 Hyphenated Techniques, Metabonomics and Data Bases 396
3.1 Reviews on Hyphenated Techniques and Drug Discovery 396
3.2 Metabonomics 397
3.3 Studies of Metabolism 398
3.4 Proteins and Glycosolation 399
4 Mammalian Oligosaccharides as Ligands and Antigens 399
5 Natural Products: Structures, Biological Activities and Antigenicity 402
5.1 Bacteria 402
5.2 Mycobacterium 403
5.3 Fungus 403
5.4 Marine Species 404
5.5 Plants 404
6 Surfactants 406
7 Food 407
References 408

Chapter 11 Synthetic Macromolecules 415
By H. Kurosu and T. Yamanobe

1 Introduction 415
2 Primary Structure 415
3 Liquid Crystalline Polymers 432
4 Imaging 432
5 Characterization of the Synthetic Macromolecules 433
6 Polymer Blend of the Synthetic Macromolecules 440
7 Dynamics of the Synthetic Macromolecules 445
References 449

Chapter 12 NMR in Living Systems 471
By M. J. W. Prior

1 General Applications and Methodologies 471
1.1 Spectral Analysis 471
1.2 New Applications 471
2 Cells 471
2.1 Bacteria 471
2.2 Blood 472
2.3 Mammalian 472

2.4 Tumour 473
3 Plants 473
4 Tissues 474
4.1 Brain 474
4.2 Heart 476
4.3 Eye 479
4.4 Liver 479
4.5 Muscle 480
4.6 Smooth Muscle 481
4.7 Tumour 481
4.8 Whole Organisms 481
5 Clinical Studies 482
5.1 Brain 482
5.2 Heart 486
5.3 Liver 486
5.4 Muscle 487
5.5 Tumour 488
References 489

Chapter 13 Nuclear Magnetic Resonance Imaging 495
By T. Watanabe

1 Introduction 495
2 Overview and Catalysed Reactions 496
2.1 Review 496
2.2 Catalysed Reaction 497
2.3 Xe Ice Melting Process 498
3 Instruments and Materials 498
3.1 Reviews 498
3.2 Magnets 498
3.3 Surface Coil 499
3.4 Optical Pumping System for Polarized Gases 499
3.5 Rapid Sample-mixing Technique 499
4 Pulse Sequences and Data Processing 500
4.1 Force-detected NMR Imaging 500
4.2 Imaging Techniques 500
4.3 Data Processing 501
5 Hyperpolarized Noble Gases, Gas Phase Imaging and Other Nuclei 502
5.1 Review 502
5.2 Hyperpolarized Nobel Gases 502
5.3 Nanopore Structure Analysis 502
5.4 Other Nuclei 503
6 Dynamics: Diffusion, Flow and Velocity Imaging 503
6.1 Diffusion 503
6.2 Flow in Suspensions and Colloids 504

6.3 Flow in Tubes 504
6.4 Gas Flow 505
6.5 Steady State Flow in Porous Media 505
7 Polymer 505
7.1 Reviews 505
7.2 Characterization 505
7.3 Diffusion Process Analysis 506
7.4 Polymer Gel and Sol-Gel Transition 507
7.5 Rubbers, Elastmers and Elastgraphy 508
7.6 Swelling, Drug Release 508
7.7 Silica Network 509
8 Chemical Engineering and Industrial Application 509
8.1 Reviews 509
8.2 Process Analysis 510
8.3 Filtration Process for Air Quality Management 510
8.4 Oil Distribution 511
9 Plants, Trees and Woods 511
9.1 Reviews 511
9.2 Trees 511
10 Food 511
10.1 Review 511
10.2 Freezing Process 511
10.3 Moisture Migration 512
10.4 Fat Contents, Distribution and Migration 512
10.5 Fruits and Vegetables 513
11 *In Vivo* Application 513
11.1 Reviews 513
11.2 Cell and Molecular Imaging 515
11.3 Functional MRI 516
11.4 Contrast Agents 516
11.5 Animal Model 517
References 519

Chapter 14 NMR of Liquid Crystals and Micellar Solutions 523
by M. Monduzzi

1 Introduction 523
2 General Articles: Reviews, Methods, Models 523
3 Liquid Crystals 525
3.1 Thermotropic Liquid Crystals 525
3.2 Lyotropic Liquid Crystals 528
4 Micellar Solutions 537
4.1 Micelles in Amphiphile-Solvent Systems 537
4.2 Solubilization, Microemulsions and Emulsions 541
References 545

Chapter 15 Paramagnetic NMR 553
By R. R. Sharp

1 Introduction 553
2 MRI Contrast Agents 553
2.1 Optimization of Gd Complexes 553
2.2 Macromolecular Agents 557
2.3 Intelligent Contrast Agents 558
2.4 Targeted Contrast Agents 559
2.5 Differentiating Intra- and Extracellular $^{23}Na^{+}$ and $^{35}Cl^{-}$ 560
2.6 Chemical Exchange Saturation Transfer (CEST) 560
2.7 Non Gd-based Contrast Agents 561
2.8 Free Radical Imaging (PEDRI) 562
3 Lanthanide-Induced Shifts (LIS) 562
3.1 Analysis of LIS Data 562
3.2 Solution Structures Deduced from LIS Data 564
4 Characterization of Solution Species 565
5 Analytical Applications 566
5.1 Chemical Shift Reagents 566
5.2 T_1 Relaxation Agents 566
6 Metallo-porphyrins 566
6.1 Low Spin Fe(III) 566
6.2 High Spin Fe (III) 568
6.3 Intermediate $S = 3/2$ Spin State of Fe(III) and Mixed Spin States 568
6.4 Fe(II) Porphyrins 569
6.5 Oxaporphyrins, Corroles and Carbaporphyrins 569
7 Biological Applications 570
7.1 New Spectral Assignment Techniques for Paramagnetic Proteins 570
7.2 Paramagnetic Constraints for Structure Analysis 571
7.3 Spin Labels 574
7.4 Heme Proteins 577
7.5 Copper Proteins 578
7.6 Ferredoxins 579
7.7 Electron Self-Exchange Reactions 580
8 Advances in Theory 580
8.1 NMR Relaxation of $S>1/2$ Paramagnetic Ions 580
8.2 Hyperfine Chemical Shifts 581
9 Chemically Induced Dynamic Nuclear Polarization (CIDNP) 581
9.1 Mechanistic Studies 581
9.2 Switched-Magnetic Field CIDNP 583
9.3 Time-Resolved CIDNP 583
9.4 CIDNP Studies of Proteins 584
References 585

Symbols and Abbreviations

These lists contain the symbols and abbreviations most frequently used in this volume, but they are not expected to be exhaustive. Some specialized notation is only defined in the relevant chapter. An attempt has been made to standardize usage throughout the volume as far as is feasible, but it must be borne in mind that the original research literature certainly is not standardized in this way, and some difficulties may arise from this fact. Trivial use of subscripts *etc.* is not always mentioned in the symbols listed below. Some of the other symbols used in the text, *e.g.* for physical constants such as h or π, or for the thermodynamic quantities such as H or S, are not included in the list since they are considered to follow completely accepted usage.

Symbols

a_N	hyperline (electron–nucleus) interaction constant
A	(i) hyperfine (electron nucleus) interaction constant
	(ii) parameter relating to electric field effects on nuclear shielding
B	(i) magnetic induction field (magnetic flux density)
	(ii) parameter relating to electric field effects on nuclear shielding
B_0	static magnetic field of NMR or ESR spectrometer
B_1, B_2	r.f. magnetic fields associated with ν_1, ν_2
C_X	spin-rotation coupling constant of nucleus X (used sometimes in tensor form): $C^2 = \frac{1}{3}(C_\parallel^2 + 2C_\perp^2)$.
$C_\parallel, C_\perp$	components of C parallel and perpendicular to a molecular symmetry axis
D	(i) self-diffusion coefficient
	(ii) zero-field splitting constant
$\mathbf{D}$	rotational diffusion tensor
$D_\parallel, D_\perp$	components of D parallel and perpendicular to a molecular symmetry axis
D_{int}	internal diffusion coefficient
D_0	overall isotropic diffusion coefficient
E	electric field
E_n	eigenvalue of $\hat{\mathscr{H}}$ (or a contribution to $\hat{\mathscr{H}}$)
g	nuclear or electronic g-factor
G	magnetic field gradient
H_{ij}	element of matrix representation of $\mathscr{H}$
$\mathscr{H}$	Hamiltonian operator–subscripts indicate its nature
$\boldsymbol{I}_i$	nuclear spin operator for nucleus i
$\boldsymbol{I}_{ix}, \boldsymbol{I}_{iy}, \boldsymbol{I}_{iz}$	components of $\boldsymbol{I}_i$
I	(i) ionization potential
	(ii) moment of inertia
^nJ	nuclear spin–spin coupling constant through n bonds (in Hz). Further information may be given by subscripts or in brackets. Brackets are used for indicating the species of nuclei coupled, *e.g.* $J(^{13}C, {}^1H)$ or additionally, the coupling path, *e.g.* J(POCF)
J_r	reduced splitting observed in a double resonance experiment
J	rotational quantum number
^nK	reduced nuclear spin–spin coupling constant (see the notes concerning ^nJ)
m_i	eigenvalue of $\boldsymbol{I}_{iz}$ (magnetic component quantum number)
M_0	equilibrium macroscopic magnetization of a spin system in the presence of B_0
M_x, M_y, M_z	components of macroscopic magnetization
M_n	the number of average mol. wt.

P_A	valence *p* orbital of atom A
P_i	fractional population (or rotamers *etc.*)
P_{uv}	element of bond-order, charge-density matrix
q	electric field gradient
Q	(i) nuclear quadrupole moment (ii) quality factor for an r.f. coil
s_A	valence *s*-orbital of atom A
$S_A^2(0)$	electron density in S_A at nuclear A
S	(i) singlet state (ii) electron (or, occasionally, nuclear spin) *cf. I* (iii) ordering parameter for oriented systems (iv) overlap integral between molecular orbitals
t	elapsed time
T	(i) temperature (ii) triplet state
T_c	coalescence temperature for an NMR spectrum
T_g	the glass transition temperature (of a polymer)
T_1^X	spin–lattice relaxation time of the X nuclei (further subscripts refer to the relaxation mechanism)
T_2^X	spin–spin relaxation time of the X nucleus (further subscripts refer to the relaxation mechanism)
T_2'	inhomogeneity contribution to dephasing time for M_x or M_y
T_2^*	total dephasing time for M_x or M_y; $(T_2^*)^{-1} = (T_2^{-1}) + (T_2')^{-1}$
T_3	decay time following 90_0–τ–90_{90} pulse sequences
$T_{1\rho}^X$, $T_{2\rho}^X$	spin–lattice and spin–spin relaxation time of the X nuclei in the frame of reference rotating with B_1
T_{1D}	dipolar spin–lattice relaxation time
X_i	mole fraction of compound
Z_A	atomic number of atom A
α	(i) nuclear spin wavefunction (eigenfunction of I_z) for a spin $-\frac{1}{2}$ nucleus (ii) polarizability
β	nuclear spin wavefunction (eigenfunction of I_z) for a spin $-\frac{1}{2}$ nucleus
γ_X	magnetogyric ratio of nucleus X
δ_X	chemical shift of a nucleus of element X (positive when the sample resonates to high frequency of the reference). Usually in p.p.m.
δ_{ij}	Kronecker delta (= 1 if $i = j$, and = 0 otherwise)
$\delta(r_{KA})$	Dirac delta operator
Δ	(i) time between field gradient pulses (ii) spectral width
ΔJ	anisotropy in J ($\Delta J = J_{\parallel} - J_{\perp}$, for axial symmetry)
Δn	population difference between nuclear states
$\Delta\delta$	change of difference in δ
$\Delta\nu_{\frac{1}{2}}$	full width (in Hz) of a resonance line at half-height
$\Delta\sigma$	(i) anisotropy in σ($\Delta\sigma = \sigma_{\parallel} - \sigma_{\perp}$, for axial symmetry) (ii) differences in σ for two different situations
$\Delta\chi$	(i) susceptibility anisotropy ($\Delta_{\chi} = \chi_{\parallel} - \chi_{\perp}$, for axial symmetry (ii) differences in electronegativities
ε_r	relative permittivity
ε_0	permittivity of a vacuum
η	(i) nuclear Overhauser effect (ii) asymmetry factor (*e.g.* in e^2qQ/h) (iii) refractive index (iv) viscosity
μ	magnetic dipole moment
μ_0	permeability of a vacuum
μ_B	Bohr magneton
μ_N	nuclear magneton
ν_i	Larmor precession frequency of nucleus *i* (in Hz)
ν_0	(i) spectrometer operating frequency (ii) Larmor precession frequency (general, or of bare nucleus)
ν_2	frequency of 'observing' r.f. magnetic field

ν_2	frequency of 'irradiating' r.f. magnetic field
σ_i	shielding parameter of nucleus i (used sometimes in tensor form). Usually in p.p.m. Subscripts may alternatively indicate contributions to σ.
$\sigma_{\parallel}, \sigma_{\perp}$	components of σ parallel and perpendicular to a molecular symmetry axis
σ^d	diagrammatic contribution to σ
σ^p	paramagnetic contribution to σ
τ	(i) pre-exchange lifetime of molecular species (ii) time between r.f. pulses (general symbol)
τ_c	correlation time
τ_{coll}	mean time between molecular collisions in the liquid state
τ_j	angular momentum correlation time
τ_p	pulse duration
τ_t	translational magnetic relaxation correlation time
χ	(i) magnetic susceptibility (ii) electronegativity (iii) nuclear quadrupole coupling constant ($=e^2qQ/h$)
ω	carrier frequency in rad s^{-1}
$\omega_i, \omega_0, \omega_1, \omega_2$	as for $\nu_i, \nu_0, \nu_1, \nu_2$ but in rad s^{-1}
ω_m	modulation angular frequency (in rad s^{-1})
ω_r	sample rotation (rad s^{-1})

Abbreviations

(a) *Physical properties*

a.f.	audiofrequency
a.u.	atomic unit
a.m.	amplitude modulation
b.c.c.	body-centred cubic
c.m.c.	critical micelle concentration
e.d.	electron diffraction
e.f.g.	electric field gradient
f.c.c.	face-centred cubic
f.m.	frequency modulation
h.c.p.	hexagonal close-packed
h.f.	hyperfine
i.d.	inside diameter
i.f.	intermediate frequency
l.c.	liquid crystalline
mol. wt.	molecular weight
o.d.	outside diameter
p.p.m.	parts per million
r.f.	radiofrequency
r.m.s.	root mean square
s.h.f.	super-high frequency
u.h.f.	ultra-high frequency
ADC	analogue-to-digital converter
AEE	average excitation energy approximation
AQ	acquire
ARP	adiabatic rapid passage
BIRD	bilinear rotation decoupling
CCPPA	coupled cluster polarization propagator approximation
CH-COSY	carbon-hydrogen correlation spectroscopy
CHESS	chemical shift selection
CHF	coupled Hartree–Fock molecular orbital calculations
CIDEP	chemically induced dynamic electron polarization
CIDNP	chemically induced dynamic nuclear polarization
COSY	correlation spectroscopy
CP	cross polarization

CPMG	Carr–Purcell pulse sequence. Meiboom–Gill modification
CSA	chemical shielding anisotropy
CSI	chemical shift imaging
CW	continuous wave
DAC	digital-to-analogue converter
DD	dipole-dipole (interaction or relaxation mechanism)
DEPT	distortionless enhancement by polarization transfer
DLB	differential line broadening
DNP	dynamic nuclear polarization
DQ	double quantum
DQF	double quantum filter
ECOSY	exclusive correlation spectroscopy
EHT	extended Hückel molecular orbital theory
ENDOR	electron- nucleus double resonance
EOM	equations of motion
ESR	electron spin resonance
EXSY	exchange spectroscopy
FC	Fermi contact
FID	free induction decay
FLASH	fast low angle shot
FPT	finite perturbation theory
FT	Fourier transform
GIAO	gauge included atomic orbitals
HMQ	heteronuclear multiquantum
HOHAHA	homonuclear Hartman Hahn
HRPA	higher random phased approximation
IDESS	improved depth selective single surface coil spectroscopy
IGLO	individual gauge for different localized orbitals
INADEQUATE	incredible natural abundance double quantum transfer experiment
INDO	intermediate neglect of differential overlap
INDO/S	intermediate neglect of differential overlap calculations for spectroscopy
INDOR	internuclear double resonance
INEPT	insensitive nuclei enhanced by polarization transfer
IR	infrared
ISIS	image selected *in vivo* spectroscopy
LIS	lanthanide induced shift
LORG	local origin
LSR	lanthanide shift reagent
MASS	magic angle sample spinning
MBPT	many body perturbation theory
MEM	maximum entropy method
MINDO	modified INDO
MQ	multiple quantum
MQC	multiple quantum coherence
MQF	multiple quantum filter
NMR	nuclear magnetic resonance
NOE	nuclear Overhauser enhancement
NOESY	nuclear Overhauser enhancement spectroscopy
NQCC	nuclear quadrupole coupling constant
NQR	nuclear quadrupole resonance
PFG	pulsed field gradient
PRE	proton relaxation enhancement
QF	quadrupole moment/field gradient
QPD	quadrature phase detection
REX	relativistically extended Hückel molecular orbital theory
ROESY	rotating frame Overhauser enhancement spectroscopy
RPA	random phase approximation
SCPT	self consistent perturbation theory
SD	spin dipolar
SECSY	spin echo correlation spectroscopy
SEFT	spin echo Fourier transform

SLITDRESS	slice interleaved depth resolved surface coil spectroscopy
SOPPA	second order polarization propagator approach
SPI	selective population inversion
SPT	selective population transfer
SR	spin rotation (interaction or relaxation mechanism)
TART	tip angle reduced T_1 imaging
TOCSY	total correlation spectroscopy
UV	ultraviolet
WAHUHA	Waugh, Huber and Häberlen (cycle of pulses)
ZQ	zero quantum
ZQC	zero quantum coherence

(b) *Chemical species**

acac	acetylacetonato
ACTH	adrenocorticotropic hormone (corticotropin)
ADP	adenosine diphosphate
AMP	adenosine monophosphate
ATP	adenosine triphosphate
BSA	bovine serum albumin
CMP	cytidine monophosphate
cp	cyclopentadienyl
DAP	dodecylammonium propionate
DME	1,2-dimethoxyethane
DMF	dimethylformamide
DML	dimyristoyl-lecithin
DMS	dimethylsiloxane
DMSO	dimethyl sulfoxide
DNA	deoxyribonucleic acid
DPG	2,3-diphosphoglycerate
DPI	dipalmitoyl-lecithin
dpm	dipivaloylmethanato
DPPH	diphenylpicrylhydrazyl
DSS	2,2-dimethyl-2-silapentane-5-sulfonate (usually as the sodium salt)
DTBN	di-t-butyl nitroxide
EBBA	*N*-(*p*-ethoxybenzylidene)-*p*-butylaniline
EDTA	ethylenediaminetetra-acetic acid
EVA	ethylene-vinyl acetate
fod	1,1,1,2,2,3,3-heptafluoro-7,7-dimethyloctane-4,6-dionato
HAB	4,4′-bis(heptyl)azoxybenzene
HMPA	hexamethylphosphoramide
HOAB	*p*-n-heptyloxyazoxybenzene
IHP	inositolhexaphosphate
KDP	potassium dihydrogen phosphate
MBBA	*N*-(*p*-methoxybenzylidene)-*p*-butylaniline
NADH(P)	nicotinamide adenine dinucleotide (phosphate)
NMF	*N*-methylformamide
PAA	*p*-azoxyanisole
PBA	pyrene butyric acid
PBLG	poly(L-benzyl μ-glutamate)
PC	phosphatidyl choline (lecithin)
PCB	polychlorinated biphenyl
PDMS	polydimethylsiloxane
PMA	poly(methacrylic acid)
PMMA	poly(methyl methacrylate)
POM	poly(oxymethylene)
PS	phosphatidylserine
PTFE	polytetrafluoroethylene
PVC	poly(vinyl chloride)
PVF	poly(vinyl fluoride)

* lower case initials are used when the species is a ligand.

PVP	poly(vinyl pyrrolidone)
RNA	ribonucleic acid (tRNA, transfer RNA)
SDS	sodium dodecyl sulfate
TAB	trimethylammonium bromide
TCNQ	tetracyanoquinodimethane
TFA	trifluoroacetic acid
THF	tetrahydrofuran
TMS	tetramethylsilane
UTP	uridine triphosphate

Amino-acid residues

Ala	alanine	Leu	leucine
Arg	arginine	Lys	lysine
Asn	asparagine	Met	methionine
Asp	aspartic acid	Phe	phenylalanine
Cys	cysteine	Pro	proline
Gln	glutamine	Ser	serine
Glu	glutamic acid	Thr	threonin
Gly	glycine	Trp	tryptophan
His	histidine	Tyr	tyrosine
Hyp	hydroxyproline	Val	valine
Ile	isoleucine		

1
NMR Books and Reviews

BY W. SCHILF

1 Books

No citations available for this section

2 Regular Reviews Series

Accounts of Chemical Research, American Chemical Society, Vol. 36, 2003

R 1 P.B. Crowley and M. Ubbink, 'Close Encounters of the Transient Kind: Protein Interactions in the Photosynthetic Redox Chain Investigated by NMR Spectroscopy', p. 723

R 2 S. Luca, H. Heise and M. Baldus, 'High-Resolution Solid-State NMR Applied to Polypeptides and Membrane Proteins', p. 858

R 3 F.-G. Klaerner and B. Kahlert, 'Molecular Tweezers and Clips as Synthetic Receptors. Molecular Recognition and Dynamics in Receptor-Substrate Complexes', p. 919

Advances in Supramolecular Chemistry, Cerberus Press Inc., Vol. 8, 2002

R 4 W.L. Duax, B.M. Burkhart, W.A. Pangborn, V. Pletnev, Z. Wawrzak and M. Glowka, 'Ion Association, Transport, and Gating in Gramicidin Channels in Lipid Bilayers', p. 245

Annual Reports on NMR Spectroscopy, ed. G.A. Webb, Academic Press Ltd., London, UK.,
Vol. 49, 2003

R 5 E. Kolehmainen, 'Novel Applications of Dynamic NMR in Organic Chemistry', p. 1

R 6 I. Ardelean and R. Kimmich, 'Principles and Unconventional Aspects of NMR Diffusometry', p. 43

R 7 P.J. Wilson, 'Density Functional Theory and Its Application to Nuclear Magnetic Resonance Shielding Constants', p. 117

R 8 G. Lancelot and F. Paquet, 'NMR Studies of Lac Operator and Lac

Nuclear Magnetic Resonance, Volume 34
© The Royal Society of Chemistry, 2005

Repressor', p. 169
R 9 Y. Sasanuma, 'Intramolecular Interactions of Polyethers and Polysulfides, Investigated by NMR, Ab Initio Molecular Orbital Calculations, and Rotational Isomeric State Scheme: An Advanced Analysis of NMR Data', p. 213
Vol. 50, 2003
R 10 B.P. Hills and C.J. Clark, 'Quality Assessment of Horticultural Products by NMR', p. 75
R 11 W.S. Veeman, 'Diffusion in a Closed Sphere', p. 201
R 12 L. Griffiths, 'Automatic Analysis of NMR Spectra', p. 217

Annual Review of Biophysics and Biomolecular Structure, Annual Reviews Inc.,
Vol. 32, 2003
R 13 A.N. Hoofnagle, K.A. Resing and N.G. Ahn, 'Protein Analysis by Hydrogen Exchange Mass Spectrometry', p. 1

Annual Review of Genomics and Human Genetics, Annual Reviews Inc.,
Vol. 3, 2002
R 14 S.K. Burley and J.B. Bonanno, 'Structuring the Universe of Proteins', p. 243

Annual Review of Physical Chemistry, Annual Reviews Inc.,
Vol. 54, 2003
R 15 D.M. Jonas, 'Two-Dimensional Femtosecond Spectroscopy', p. 425
R 16 G.P. Drobny, J.R. Long, T. Karlsson, W. Shaw, J. Popham, N. Oyler, P. Bower, J. Stringer, D. Gregory, M. Mehta and P.S. Stayton, 'Structural Studies of Biomaterials Using Double-Quantum Solid-State NMR Spectroscopy', p. 531

Annual Review of Physiology, Annual Review Inc.,
Vol. 65, 2003
R 17 D.L. Rothman, K.L. Behar, F. Hyder and R.G. Shulman, 'In Vivo NMR Studies of the Glutamate Neurotransmitter Flux and Neuroenergetics: Implantations for Brain Function', p. 401
Vol. 66, 2004
R 18 J.K. Lanyi, 'Bacteriorhodopsin', p. 665

Briefings in Bioinformatics, Henry Stewart Publications,
Vol. 4, 2003
R 19 A. Rodrigues and R.E. Hubbard, 'Making Decisions for Structural Genomics', p. 150

Chemical Reviews, Washington, DC, United States,
Vol. 104, 2004
R 20 J.M. Seco, E. Quinao and R. Riguera, 'The Assignment of Absolute

Configuration by NMR', p. 17

R 21 J.A. Lukin and C. Ho, 'The Structure-Function Relationship of Hemoglobin in Solution at Atomic Resolution', p. 1219

Coordination Chemistry Reviews, Elsevier Science B.V.,
Vol. 238-239, 2003

R 22 J. Autschbach and T. Ziegler, 'Double Perturbation Theory: A Powerful Tool in Computational Coordination Chemistry', p. 83

R 23 I.P. Georgakaki, L.M. Thomson, E.J. Lyon, M.B. Hall and M.Y. Darensbourg, 'Fundamental Properties of Small Molecule Models of Fe-Only Hydrogenase: Computations Relative to the Definition of an Entatic State in the Active Site', p. 238

Vol. 243, 2003

R 24 Y. Li and W.-T. Wong, 'Low Valent Transition Metal Cluster Containing Nitrene/Imido Ligands', p. 191

Vol. 248, 2004

R 25 Y.-G. Chen, J. Gong and L.-Y. Qu, 'Tungsten-183 Nuclear Magnetic Resonance Spectroscopy in the Study of Polyoxometalates', p. 245

Current Medicinal Chemistry, Bentham Science Publishers,
Vol. 10, 2003

R 26 R.C. Glen and S.C. Allen, 'Ligand-Protein Docking: Cancer Research at the Interface between Biology and Chemistry', p. 763

Current Medicinal Chemistry: Anti-Cancer Agents, Bentham Science Publishers,
Vol. 4, 2004

R 27 M.I. Dawson, 'Synthetic Retinoids and Their Nuclear Receptors', p. 199

Current Opinion in Chemical Biology, Elsevier Science Ltd.,
Vol. 7, 2003

R 28 N.J. Ede and Z. Wu, 'Beyond Rf Tagging', p.374

R 29 P.A. Keifer, 'Flow NMR Applications in Combinatorial Chemistry', p. 388

R 30 J.L. Griffin, 'Metabonomics: NMR Spectroscopy and Pattern Recognition Analysis of Body Fluids and Tissues for Characterisation of Xenobiotic Toxicity and Disease Diagnosis', p. 648

Current Opinion in Colloid & Interface Science, Elsevier Science Ltd.,
Vol. 8, 2003

R 31 K. Matsuoka and Y. Moroi, 'Micellization of Fluorinated Amphiphiles', p. 227

Current Opinion in Drug Discovery & Development, Current Drugs,
Vol. 5, 2002

R 32 D.F. Wyss, M.A. McCoy and M.M. Senior, 'NMR-Based Approaches for

Lead Discovery', p. 630
Vol. 6, 2003
R 33 A.P. Watt, R.J. Mortishire-Smith, U. Gerhard and S.R. Thomas, 'Metabolite Identification in Drug Discovery', p. 57
R 34 S.W. Muchmore and P.J. Hajduk, 'Crystallography, NMR and Virtual Screening: Integrated Tools for Drug Discovery', p. 544

Current Opinion in Endocrinology & Diabetes, Lippincott Williams & Wilkins,
Vol. 10, 2003
R 35 A.J. Jenkins, W.T. Garvey and R.L. Klein, 'Lipoprotein Abnormalities in Type 1 Diabetes', p. 245

Current Opinion in Immunology, Elsevier Science Ltd.,
Vol. 15, 2003
R 36 R.G. Pautler and S.E. Fraser, 'The Year(s) of the Contrast Agent – Micro-MRI in the New Millennium', p. 385

Current Opinion in Structural Biology, Elsevier Science Ltd.,
Vol. 13, 2003
R 37 R. Bruschweiler, 'New Approaches to the Dynamic Interpretation and Prediction of NMR Relaxation Data from Proteins', p. 175
R 38 S. Neidle and G.N. Parkinson, 'The Structure of Telomeric DNA', p. 275
R 39 C.B. Post, 'Exchange-Transferred NOE Spectroscopy and Bound Ligand Structure Determination', p. 581
R 40 H. Kogelberg, D. Solis and J. Jimenez-Barbero, 'New Structural Insights into Carbohydrate-Protein Interactions from NMR Spectroscopy', p. 646
Vol. 14, 2004
R 41 J.C. Fromme, A. Banerjee and G.L. Verdine, 'DNA Glycosylase Recognition and Catalysis', p. 43
R 42 P.W. Haebel, S. Gutmann and N. Ban, 'Dial tm for Rescue: tmRNA Engages Ribosomes Stalled on Defective mRNAs', p. 58

Current Organic Chemistry, Bentham Science Publishers Ltd.,
Vol. 7, 2003
R 43 C. Schmuck and L. Geiger, 'Carboxylate Binding by Guanidiniocarbonyl Pyrroles: From Self-Assembly to Peptide Receptors', p. 1485
R 44 X. Cai and C. Dass, 'Conformational Analysis of Proteins and Peptides', p. 1841
Vol. 8, 2004
R 45 K. Yannokopoulou and I.M. Mavridis, 'Threading of Long End-Functionalized Organic Molecules into Cyclodextrins: Structural Analysis in Aqueous Solution by NMR Spectroscopy and in the Solid State by X-Ray Crystallography', p. 25
R 46 Y. Liu, B.-h. Han and H.-y. Zhang, 'Spectroscopic Studies on Molecular

Recognition of Modified Cyclodextrins', p. 35

R 47 D.M. Hatch, J.O. Boles, Z. Li and L.A. Silks, 'Methods for the Synthesis of Heavy-Atom Derivatized Amino Acids: Useful Probes for X-Ray Crystallography, Vibrational, and NMR Spectroscopy of Proteins', p. 47

Current Pharmaceutical Design, Bentham Science Publishers Ltd., Vol. 9, 2003

R 48 A.H. Katz and C.E. Caufield, 'Structure-Based Design Approaches to Cell Wall Biosynthesis Inhibitors', p. 857

Current Protein and Peptide Science, Bentham Science Publishers Ltd., Vol. 4, 2003

R 49 S. Jitrapakdee and J.C. Wallace, 'The Biotin Enzyme Family: Conserved Structural Motifs and Domain Rearrangements', p. 217

R 50 A.L. Wilkins, W. Yang and J.J. Yang, 'Structural Biology of the Cell Adhesion Protein CD2: From Molecular Recognition to Protein Folding and Design', p. 367

Current Topics in Colloid & Interface Science, Research Trends, Vol. 5, 2002

R 51 C. La Mesa, 'Interaction between Surfactants and Polymers', p. 261

Current Topics in Medicinal Chemistry (Hilversum, Netherlands), Bentham Science Publishers, Vol. 3, 2003

R 52 O. Schwardt, H. Kolb and B. Ernst, 'Drug Discovery Today', p. 1

R 53 E. Jacoby, J. Davies and M.J.J. Blommers, 'Design of Small Molecule Libraries for NMR Screening and Other Applications in Drug Discovery', p. 11

R 54 E.R. Zartler, J. Yan, H. Mo, A.D. Kline and M.J. Shapiro, '1D NMR Methods in Ligand-Receptor Interactions', p. 25

R 55 L. Fielding, 'NMR Methods for the Determination of Protein-Ligand Dissociation Constants', p. 39

R 56 A. Ross and H. Senn, 'Automation of Biomolecular NMR Screening', p. 55

R 57 W. Jahnke, A. Florsheimer, M.J.J. Blommers, C.G. Paris, J. Heim, C.M. Nalin and L.B. Perez, 'Second-Site NMR Screening and Linker Design', p. 69

R 58 J. Fejzo, C. Lepre and X. Xie, 'Application of NMR Screening in Drug Discovery', p. 81

R 59 R. Pereda-Miranda and M. Bah, 'Biodynamic Constituents in the Mexican Morning Glories: Purgative Remedies Transcending Boudaries', p. 111

R 60 C.J. Dinsmore and I.M. Bell, 'Inhibitors of Farnesyltransferase and Geranylgeranyltransferase-I for Antitumor Therapy: Substrate-Based Design, Conformational Constraint and Biological Activity', p. 1075

R 61 J. Dornan, P. Taylor and M.D. Walkinshaw, 'Structures of Immunophilins and Their Ligand Complexes', p. 1392

R 62 J.M.J. Tronchet and M. Seman, 'Nonnucleoside Inhibitors of HIV-1 Reverse Transcriptase: From the Biology of Reverse Transcription to Molecular Design', p. 1496

Vol. 4, 2004

R 63 P. Datar, S. Srivastava, E. Coutinho and G. Govil, 'Substance P: Structure, Function, and Therapeutics', p. 75

R 64 J. Malicka, C. Czaplewski, M. Groth, W. Wiczk, S. Oldziej, L. Lankiewicz, J. Ciarkowski and A. Liwo, 'Use of NMR and Fluorescence Spectroscopy as well as Theoretical Conformational Analysis in Conformation-Activity Studies of Cyclic Enkephalin Analogues', p. 123

R 65 A. Naito and K. Nishimura, 'Conformational Analysis of Opioid Peptides in the Solid State and the Membrane Environments by NMR Spectroscopy', p. 135

Current Topics in Peptide & Protein Research, Research Trends,
Vol. 4, 2001

R 66 R. Basosi, N. D'Amelio, E. Gaggelli, N. Gagelli, A. Maccotta, R. Pogni, D. Valensin and G. Valensin, 'NMR and EPR Studies of Copper Complexes with Short-Chain Peptides: The Effect of the cis↔trans Isomerism of Proline', p. 17

Current Topics in Phytochemistry, Research Trends,
Vol. 5, 2002

R 67 R Sanogo, S. Giani, A. Braca, D. Diallo, I. Morelli, C. Pizza and N. De Tommasi, 'Pharmacochemical Investigation on Some Malian Medicinal Plants', p. 225

Methods in Molecular Biology, Humana Press Inc., Totowa, N.J., United States,
Vol. 227, 2003
Membrane Transporters, Methods and Protocols, ed. Q. Yan

R 68 S.J. Opella, 'Membrane Protein NMR Studies', p.307

Mini-Reviews in Medicinal Chemistry, Bentham Science Publishers Ltd.,
Vol. 3, 2003

R 69 A. Maiocchi, 'The Use of Molecular Desciptors in the Design of Gadolinium (III) Chelates as MRI Contrast Agents', p. 845

Vol. 4, 2004

R 70 A. Gill, 'New Generation Strategies for Protein Kinase Inhibitors – Fragment Based Screening Approaches', p. 301

NATO Science Series, 1: *Disarmament Technologies*
Vol. 37, 2002
Environmental Aspects of Converting CW Facilities to Peaceful Purposes.

R 71 W.R. Cullen, P. Andrewes, C. Fyfe, H. Grondey, T. Liao, E. Polishchuk, L. Wang and C. Wang, 'Solidification/Stabilization of Adamsite and Lewisite in Cement and the Stability of Arylarsenicals in Soil', p. 45

NATO Science Series, II: Mathematics, Physics and Chemistry
Vol. 66, 2002
Detection of Explosives and Landmines

R 72 V.S. Grechishkin, 'The Problem of Military TNT in NQR Mine Detector', p. 217

Vol. 76, 2002
Magnetic Resonance in Colloid and Interface Science

R 73 H. Eckert, E. Ratai, T. Torbrugge and M. Witschas, 'Quantifying Structural and Dynamic Disorder in Ionically Conducting Solid Solutions', p. 15

R 74 H.J. Jakobsen, H. Bildsoe, J. Skibsted and T. Giavani, '^{14}N MAS NMR Spectroscopy. An Instrumental Challenge and Informatory Technique', p. 43

R 75 J. Karger and F. Stallmach, 'NMR Diffusion Studies of Molecules in Nanoporous Materials', p. 57

R 76 A. Pines, J.W. Logan and M.M. Spence, "Lighting up' NMR and MRI in Colloidal and Interfacial Systems', p. 97

R 77 M. Pruski, J.P. Amoureux and C. Fernandez, 'Progress in High Resolution Solid State NMR of Quadrupolar Nuclei. Applications to Porous Materials and Catalysts', p. 107

R 78 I.L. Moudrakovski, A.V. Nossov, V.V. Terskikh, S. Lang, E.B. Brouwer, D.V. Soldatov, C.I. Ratcliffe and J.A. Ripmeester, 'Applications of Hyperpolarized ^{129}Xe NMR Spectroscopy to the Study of Materials', p. 115

R 79 R. Simonutti, A. Comotti, S. Bracco and P. Sozzani, 'Solid State NMR Characterization of Polymers and Surfactant Molecules as Confined to Porous Silica Materials', p. 139

R 80 J.H. Strange, L. Betteridge and M.J.D. Mallett, 'Characterisation of Porous Materials by NMR', p. 155

R 81 *E.G.* Bagraynskaya, N.V. Lebedeva, M.V. Fedin and R.Z. Sagdeev, 'Investigation of Radical Pairs in Micelles Using Spin Polarization Techniques', p. 173

R 82 V.D. Skirda, 'The Features of PFG NMR Technique and Some Methodical Aspects of Its Application', p. 245

R 83 M.-A. Springuel-Huet, '^{129}Xe of Adsorbed Xenon Used as a Probe to Study Microporous Solids', p. 255

Vol. 92, 2003
Green Industrial Applications of Ionic Liquids

R 84 O.B. Lapina, V.V. Terskikh, B.S. Bal'Zhinimaev, K.M. Eriksen and R. Fehrmann, 'High-Temperature NMR Studies of Ionic-Liquid Catalysts', p. 85

R 85 V.I. Pekhnyo, S.V. Volkov and N.G. Alexandrova, 'Room-Temperature

Sulfur Chloride Ionic Liquids in Processes for the Isolation of Noble and other Metals', p. 173
Vol. 96, 2003
Molecular Electronics: Bio-Sensors and Bio-Computers

R 86 M. Venanzi, A. Palleschi, L. Stella and B. Pispisa, 'Peptide Foldamers as Building Blocks for Ordered Nanomolecular Architectures: A Structural Investigation', p. 237
Vol. 98, 2003
Polyoxometalate Molecular Science

R 87 T. Yamase, 'Time-Resolved Electron Spin Resonance Spectroscopy of Photoredox Reactions of Polyoxometalates: Formation of Paramagnetic-Species Pair by Triplet Mechanism', p. 211
Vol. 102, 2003
Nanostructured Materials and Coatings in Biomedical and Sensor Applications

R 88 R. Partch, E. Powell, Y.-H. Lee, M. Varshney, S. Kim, N. Barnard, D. Shah, D. Dennis and T. Morey, 'Injectable Nanoparticle Technology for in Vivo Remediation of Overdosed Toxins', p. 27
Vol. 106, 2003
Recent Trends in Theory of Physical Phenomena in High Magnetic Fields

R 89 W.Apel and Yu.A. Bychkov, 'On Deriving Relaxation Equations for Nuclear Spins', p. 223

R 90 P. Averbuch, 'NMR Revisited', p. 235

R 91 Y.V. Pershin, 'Nuclear-Spin-Polarization-Induced Low-Dimensional Electron Structures', p. 263

Phytochemistry Reviews, Proceedings of the Phytochemical Society of Europe, Kluwer Academic Publishers,
Vol. 1, 2002, pub. 2003

R 92 B.M. Abegaz, 'Novel Phenylanthraquinones, Isofuranonaphthoquinones, Homoisoflavonoids, and Biflavonoids from African Plants in the Genera Bulbine, Scilla, Ledebouria, and Rhus' p. 299

Progress in Nuclear Magnetic Resonance Spectroscopy, ed. J.W. Emsley, J. Feeney and L.H. Sutcliffe, Elsevier Science B.V.,
Vol. 41, 2002

R 93 B.J. Stockman and C. Dalvit, 'NMR Screening Techniques in Drug Discovery and Drug Design', p. 187

R 94 D. Frueh, 'Internal Motions in Proteins and Interference Effects in Nuclear Magnetic Resonance', p. 305
Vol. 42, 2003

R 95 A. Cherubini and A. Bifone, 'Hyperpolarized Xenon in Biology', p. 1

R 96 R. Tycko, 'Applications of Solid State NMR to the Structural Characterization of Amyloid Fibrils: Methods and Results', p. 53

R 97 E. Kupce, T. Nishida and R. Freeman, 'Hadamart NMR Spectroscopy', p. 95

Vol. 43, 2003
R 98 A.D. Bain, 'Chemical Exchange in NMR', p. 63
R 99 P. Guntert, 'Automated NMR Protein Structure Calculation', p. 105

Recent Research Developments in Bioconjugate Chemistry, Transworld Research Network,
Vol. 1, 2002
R 100 B. Pragl, H.J. Gruber, G.J. Schutz, M. Trieb, H. Prinz and H.-G. Knaus, 'Fluorescently-Labeled K^+ Channel Toxins – Tools to Study K^+ Channels in Native Tissues', p. 83

Recent Research Developments in Chemical & Pharmaceutical Sciences, Transworld Research Network,
Vol. 2, 2002
R 101 H. Nakayama and M. Tsuhako, 'New Functional Layered Phosphates and Their Characterization by Solid-State NMR', p. 47

Recent Research Developments in Inorganic & Organometallic Chemistry, Research Signpost,
Vol. 1, 2001
R 102 M.R. Bermejo, A.M. Garcia-Deibe, A.M. Gonzalez, O.L. Hoyos, M. Maneiro and M. Rey, 'The Diversity Observed in Manganese(III) – Schiff Base Complexes: Models for a Variety of Biological Systems', p. 61
R 103 L.M. Mink and R.K. Boggess, 'Platinum(II) and Platinum(IV) Tetraphenylporphyrin Complexes: Synthesis, Characterization, and Electrochemistry', p. 125

Recent Research Developments in Non-Crystalline Solids, Transworld Research Network,
Vol. 2, 2002
R 104 T. Akai, 'NMR Investigation of Ion Dynamics in Inorganic Glasses', p. 69

Recent Research Developments in Phytochemistry, Research Signpost,
Vol. 6, 2002
R 105 L.A.D. Williams, H. Roesner, J. Conrad, W. Moeller, U. Beifuss, K. Chiba, J.P. Nkurunziza and W. Kraus, 'Selected Secondary Metabolites from the Phytolaccaceae and Their Biological/Pharmaceutical Significance', p. 13

Reviews in Environmental Science and Bio/Technology, ed. P. Lens, Kluwer Academic Publishers,
Vol. 1, 2002
R 106 N. Nestle, 'NMR Studies on Heavy Metal Immobilization in Biosorbents and Mineral Matrices', p. 215

Trends in Applied Spectroscopy, Research Trends,
Vol. 4, 2002

R 107 P.-A. Eliat, D. Mahmoud-Ghoneim and J.D. de Certaines, 'Texture Analysis and Metabolic Magnetic Resonance Imaging', p. 1

Trends in Biochemical Sciences, Elsevier Science Ltd.,
Vol. 28, 2003

R 108 R. Diaz, 'Spectroscopic Characterisation of Sol-Gel Materials: A Review', p. 253

R 109 H.D. Lutz and B. Engelen, 'Hydrogen Bonds in Inorganic Solids', p. 355

R 110 K.D. Ridge, N.G. Abdulaev, M. Sousa and K. Palczewski, 'Phototransduction: Crystal Clear', p. 479

Trends in Food Science & Technology, Elsevier Science Ltd.,
Vol. 14, 2003

R 111 I. Martinez, M. Aursand, U. Erikson, T.E. Singstad, E. Veliyulin and C. Van der Zwaag, 'Destructive and Non-Destructive Analytical Techniques for Authentication and Composition Analyses of Foodstuffs', p. 489

R 112 F.J. Hidalgo and R. Zamora, 'Edible Oil Analysis by High-Resolution Nuclear Magnetic Resonance Spectroscopy: Recent Advances and Future Perspectives', p. 499

Trends in Pharmacological Sciences, Elsevier Science Ltd.,
Vol. 24, 2003

R 113 J.M. Hakumaki and K.M. Brindle, 'Techniques: Visualizing Apoptosis Using Nuclear Magnetic Resonance, p. 146

R 114 N. Beckmann, B. Tigani, L. Mazzoni and J.R. Fozard, 'Techniques: Magnetic Resonance Imaging of the Lung Provides Potential for Non-Invasive Preclinical Evaluation of Drugs', p. 550

3 Edited Books and Symposia

ACS Symposium Series
Vol. 838, 2002
Synthesis and Properties of Silicones and Silicone-Modified Materials

R 115 J.M. Mabry, M.K. Runyon, J.K. Paulasaari and W.P. Weber, 'Ru-Catalysed Hydrosilylation Polymerization: An Overview of $RuH_2(CO)(PPh_3)_3$ – Catalysed Hydrosilylation Copolymerizations of α,ω-Diketones with α,ω-Dihydrido-oligodimethylsiloxanes and Polymerizations of ω-Dimethylsilyloxy Ketones', p. 50

Vol. 854, 2003
Advances in Controlled/Living Radical Polymerization

R 116 M. Kamigaito, T. Ando and M. Sawamoto, 'Living Radical Polymerization with Designed Metal Complexes', p. 102

Vol. 856, 2003
Ionic Liquids as Green Solvents

R 117 M.M. Abu-Omar, G.S. Owens and A. Durazo, 'Catalytic Olefin Epoxidation and Dihydroxylation with Hydrogen Peroxide in Common Ionic Liquids: Comparative Kinetics and Mechanistic Study', p. 277

Vol. 857, 2003
Beyond Metallocenes

R 118 M. Kang, A. Sen, L. Zakharov and A.L. Rheingold, 'Trends in Alkene Insertion in Late- and Early-Transition Metal Compounds: Relevance to Transition Metal-Catalysed Polymerization of Polar Vinyl Monomers', p. 143

Vol. 858, 2003
Paramagnetic Resonance of Matallobiomolecules

R 119 J. Telser, 'Paramagnetic Resonance of Matallobiomolecules: Introduction and Overview', p. 1

R 120 M. Kostic and T.C. Pochapsky, 'Structure and Dynamics of Paramagnetic Proteins by NMR', p. 214

R 121 J.M. Nocek, K. Huang and B.M. Hoffman, 'An Approach to NMR Treatment of Structural Perturbation in Paramagnetic Proteins too Big for Solution Structure Determination', p. 227

R 122 I. Bertini, F. Capozzi and C. Luchinat, 'Electronic Isomerism in Oxidized High-Potential Iron-Sulfur Proteins Revisited', p. 272

R 123 C.O. Fernandez and A.J. Vila, 'Paramagnetic NMR of Electron Transfer Copper Proteins', p. 287

Vol. 859, 2003
Oriental Foods and Herbs

R 124 S. Sang, A. Lao and Z. Chen, 'Chemistry and Bioactivity of Allium Tuberosum Seeds' p. 317

Vol. 861, 2003
Mesoscale Phenomena in Fluid Systems

R 125 P. Stilbs, 'Characterization Mesoscale Structure and Phenomena in Fluids Using NMR', p. 27

Vol. 864, 2004
Hemicelluloses

R 126 M.A. Kabel, H.A. Schols and A.G.J. Voragen, 'Identification of Structural Features of Various (O-Acetylated) Xylo-Oligosaccharides from Xylan-Rich Agricultural By-Products: A Review', p. 108

R 127 P.T. Larsson, 'Interaction between Cellulose I and Hemicelluloses Studied by Spectral Fitting of CP/MAS ^{13}C-NMR Spectra', p. 254

Vol. 867, 2004
Challenges in Taste Chemistry and Biology

R 128 C.-t. Ho, S. Sang and J.W. Jhoo, 'Chemistry of Theaflavins: The Astringent Taste Compounds of Black Tea', p. 125

Advances in Ceramic Matrix Composites IX, ed. N.P. Bansal, J.P. Singh, W.M. Kriven and H. Schneider in*Ceramic Transactions*, Vol. 153, American Ceramic Society, 2003

R 129 K.J.D. MacKenzie, 'What Are These Thinks Called Geopolymers? A Physico-Chemical Perspective', p. 175

Advances in High Pressure Bioscience and Biotechnology II, Proceedings of the International Conference on High Pressure Bioscience and Technology, 2nd, Dortmund, Germany, Sept. 16-19, 2002, ed. R. Winter, Springer-Verlag, Berlin, Germany, 2003

R 130 K. Akasaka, 'High Pressure NMR Spectroscopy Characterizes Higher Energy Conformers of Proteins', p. 9

Advancing Materials in the Global Economy Applications, Emerging Markets and Evolving Technologies, Book 2 in *International SAMPE Symposium and Exhibition*, Vol. 48, Society for the Advancement of Material and Process Engineering, 2003

R 131 J.W. Gilman, S. Bourbigot, J.R. Shields, M. Nyden, T. Kashiwagi, R.D. Davis, D.L. Vander Hart, W. Demory, C.A. Wilkie, A.B. Morgan, J. Harris and R.E. Lyon, 'High Throughput Methods for Polymer Nanocomposites Research: Extrusion, NMR Characterization and Flammability Property Screening', p. 1459

Analysis and Characterization of Polymers, ed. S. Maiti, Anusandhan Prakashan, Midnapore, India, 2003

R 132 D. Nasipuri, 'Principles of Analysis of Polymer Architecture by NMR Spectroscopy', p. 59

R 133 S.C. Shit and S. Maiti, 'Analysis of Polymer Molecular Weight and Composition by NMR', p. 71

Analytical Advances for Hydrocarbon Research, [Symposium held at the 220th American Chemical Society National Meeting], Washington, DC, United States, Aug. 20-24, 2000, ed. C.S. Hsu, Kluwer Academic/Plenum Publishers, New York, N.Y., 2003

R 134 G.J. Kennedy, 'Advances in NMR Techniques for Hydrocarbon Characterization', p. 369

Analytical Techniques to Evaluate the Structure and Function of Natural Polysaccharides, Glycosaminoglycans, ed. N. Volpi, Research Signpost: Trivandrum, India, 2002

R 135 H.B. Nader and C.P. Dietrich, 'Extraction and Characterization of Heparins', p. 23

Bioactive Natural Products, Part I, ed. Atta-ur-Rahman, in *Studies in Natural Products Chemistry*, Vol. 28, Elsevier Science B.V., 2003

R 136 A. Braca, A.R. Bilia, J. Mendez, C. Pizza, I. Morelli and N. De Tommasi, 'Chemical and Biological Studies on Licania Genus', p. 35

R 137 H.D. Chludil, A.P. Murray, A.M. Seldes and M.S. Maier, 'Biologically Active Triterpene Glycosides from Sea Cucumbers (Holothuroidea, Echinodermata)', p. 587

Bioanalytical Separations, ed. I. Wilson, in *Handbook of Analytical Separations*, Vol. 4, Elsevier Science B.V., 2003

R 138 J.C. Lindon, N.J.C. Bailey, J.K. Nicholson and I.D. Wilson, 'Biomedical Applications of Directly - Coupled Chromatography – Nuclear Magnetic Resonance (NMR) Spectroscopy and Mass Spectrometry (MS)', p. 293

Biofilms in Medicine, Industry and Environmental Biotechnology: Characteristics, Analysis and Control, [Based on the Euro Summer School, 'Biofilms in Industry, Medicine, and Environmental Biotechnology: The Science'], Galway, Ireland, Aug. 24-29, 2002, ed. P. Lens, IWA Publishing, London, UK., 2003

R 139 V. O'Flaherty and P. Lens, 'Biofilms in Wastewater Treatment Systems', p. 132

R 140 P.N.L. Lens and H. Van As, 'Use of ^{1}H NMR to Study Transport Processes in Biofilms', p. 285

Bioinformatics and Genomes, ed. M.A. Andrade, Horizon Scientific Press, Wymondham, UK., 2003

R 141 R.A. George, J. Kleinjung and J. Heringa, 'Predicting Protein Structural Domain Boundaries from Sequence Data', p. 1

BioNMR in Drug Research, ed. O. Zerbe, in *Methods and Principles in Medicinal Chemistry*, Vol. 16, Wiley-VCH Verlag GmbH & Co. KGaA, Weinheim, Germany, 2003

R 142 P. Guntert, 'Structure Calculation Using Automated Techniques', p. 39

R 143 V. Dotsch, 'NMR Strategies for Protein Assignments', p. 79

R 144 R. Fiala and V. Sklenar, 'NMR of Nucleic Acids', p. 121

R 145 C. Griesinger, 'Methods for the Measurement of Angle Restraints from Scalar, Dipolar Couplings and from Cross-Correlated Relaxation: Application to Biomacromolecules', p. 147

R 146 E. de Alba and N. Tjandra, 'Orientational Restraints', p. 179

R 147 A.J. Dingley, F. Cordier, V.A. Jaravine and S. Grzesiek, 'Scalar Couplings Across Hydrogen Bonds', p. 207

R 148 R. Riek, 'TROSY: Transverse Relaxation - Optimized Spectroscopy', p. 227

R 149 P.T.F. Williamson, M. Ernst and B.H. Meier, 'MAS Solid-State NMR of Isotopically Enriched Biological Samples', p. 243

R 150 D. Fushman, 'Determination of Protein Dynamics Using ^{15}N Relaxation Measurements', p. 283

R 151 G.C.K. Roberts, 'The Determination of Equilibrium Dissociation Constants of Protein-Ligand Complexes by NMR', p. 309

R 152 C. Marchioro, S. Davalli, S. Provera, M. Heller, A. Ross and H. Senn, 'Experiments in NMR-Based Screening', p. 321

R 153 W. Jahnke, 'The Use of Spin Labels in NMR-Supported Lead Finding and Optimization', p. 341

R 154 M.J.J. Blommers and S. Ruedisser, 'NMR of Weakly Binding Ligands', p. 355
R 155 G. Gemmecker, 'Isotope Filter and Editing Techniques', p. 373
R 156 C.A. Lepre, 'Strategies for NMR Screening and Library Design', p. 391
R 157 W. Klaus and H. Senn, 'Strategies for Hit Finding Using NMR', p. 417
R 158 M.J.J. Blommers, A. Floersheimer and W. Jahnke, 'Strategies for Drug Discovery Using NMR', p. 439
R 159 M. Pellecchia, X. Huang, D. Meininger and D.S. Sem, 'NMR-Based Drug Design: Approaches for Very Large Proteins', p. 459

Biopolymers, ed. Y. Doi and A. Steinbuchel, Wiley-VCH Verlag GmbH, Weinheim, Germany, 2001
R 160 T.C. de Rijk, P. van de Meer, G. Egging and R.A. Weusthuis, 'Methods for Analysis of Poly(3-hydroxyalkanoate) Composition', p. 1

Biotechnology for the Environment: Soil Remediation, ed. S.N. Agathos and W. Reineke, in *Focus on Biotechnology*, Vol. 3B, Kluwer Academic Publishers, 2002
R 161 J.-M. Bollag, 'Immobilisation of Pesticides in Soil through Enzymatic Reactions', p. 93

Bread Making, ed. S.P. Cauvain, CRC Press LLC, Boca Raton, Fla., 2003
R 162 A.M. Gil, 'Techniques for Analysing Wheat Proteins', p. 97

Carbon Alloys, ed. E.-i. Yasuda, Elsevier Science Ltd., Oxford, UK., 2003
R 163 O.Ito, T. Ikoma and R. Sakurovs, 'Infra-Red Spectra, Electron Paramagnetic Resonance, and Proton Magnetic Thermal Analysis', p. 269
R 164 T. Nishizawa, 'Basics of Nuclear Magnetic Resonance and Its Application to Carbon Alloys', p. 299

Catalysis and Electrocatalysis at Nanoparticle Surfaces, ed. A. Wieckowski, E.R. Savinova and C.G. Vayenas, Marcel Dekker, Inc., New York, N.Y., 2003
R 165 Y.Y. Tong and J.J. Van Der Klink, 'NMR Investigations of Heterogeneous and Electrochemical Catalysts', p. 455

Catalysis: Principles and Applications, [Orientation Programme] Indian Institute of Technology, Department of Chemistry, Madras, India, ed. B. Viswanathan, S. Sivasanker and A.V. Ramaswamy, Narosa Publishing House, New Delhi, India, 2002
R 166 V. Ramaswamy, 'Structural Characterization of Catalysts by X-Ray Analysis', p. 92
R 167 D. Srinivas, 'Application of UV-Visible and Magnetic Resonance Spectroscopic Techniques in Heterogeneous Catalysis', p. 145

Cellular Proteins and Their Fatty Acids in Health and Disease, ed. A.K.

Duttaroy and F. Spener, Wiley-VCH Verlag GmbH & Co. KGaA, Weinheim, Germany, 2003

R 168 C. Lucke, L.H. Gutierrez-Gonzalez and J.A. Hamilton, 'Intracellular Lipid Binding Proteins: Evolution, Structure, and Ligand Binding', p. 95

Chemical and Functional Properties of Food Saccharides, ed. P. Tomasik, CRC Press LLC, Boca Raton, Fla., 2004

R 169 J.J.G. van Soest, 'Spectroscopy of Polysaccharides', p. 371

Comprehensive Coordination Chemistry II, ed. J.A. McCleverty and T.J. Meyer, Elsevier Ltd., Oxford, UK., 2004

R 170 P.S. Pregosin and H. Rueegger, 'Nuclear Magnetic Resonance Spectroscopy', p. 1

R 171 A.M. Bond, 'Electrochemistry. General Introduction', p. 197

R 172 T. Hughbanks, 'Centred Zirconium Clusters', p. 775

Copper-Containing Proteins, ed. J.S. Valentine and E.B. Gralla, in *Advances in Protein Chemistry*, Vol. 60, Academic Press, 2002

R 173 L. Banci, R. Pierattelli and A.J. Vila, 'Nuclear Magnetic Resonance Spectroscopy Studies on Copper Proteins', p. 397

Desiccation and Survival in Plants, ed. M. Black and H.W. Pritchard, CABI Publishing, Wallingford, UK., 2002

R 174 O. Leprince and E.A. Golovina, 'Biochemical and Biophysical Methods for Quantifying Desiccation Phenomena in Seeds and Vegetative Tissues', p. 111

Drug Design: Cutting Edge Approaches, ed. D.R. Flower in *Special Publication – Royal Society of Chemistry*, Vol. 279, Royal Society of Chemistry, 2002

R 175 D.R. Flower, 'Molecular Informatics: Sharpening Drug Design's Cutting Edge', p. 1

Drug-Membrane Interactions, ed. J.K. Seydel and M. Wiese, in *Methods and Principles in Medicinal Chemistry*, Vol. 15, Wiley-VCH Verlag GmbH & Co. KgaA, Weinheim, Germany, 2002

R 176 J.K. Seydel, 'Analytical Tools for the Analysis and Quantification of Drug-Membrane Interactions p. 51

Electrokinetic Phenomena, ed. A.S. Rathore and A. Guttman, Marcel Dekker Inc., New York, N.Y., 2004

R 177 D.A. Jayawickrama, A.M. Wolters and J.V. Sweedler, 'NMR Detection in Capillary Electrophoresis and Capillary Electrochromatography', p. 311

Encephalopathy and Nitrogen Metabolism in Liver Failure, [International Symposium on Hepatic Encephalopathy and Nitrogen Metabolism], 11th, Amsterdam, Netherlands, May 30-June 1, 2002, ed. E.A. Jones, A.J. Meijer and R.A.F.M. Chamuleau, Kluwer Academic Publishers, Dordrecht, Netherlands, 2003

R 178 C. Zwingmann, N. Chatauret, D. Leibfritz and R.F. Butterworth, 'Brain Energy Metabolism in Acute Liver Failure: Studies Using NMR Spectroscopy', p. 225

R 179 C. Zwingmann, T. Shokati, R.F. Butterworth and D. Leibfritz, 'Use of NMR Spectroscopy for the Study of Ammonia Metabolism in Astrocytes and Neurons: Role of Glutamine Synthesis in Astrocytes', p. 299

Encyclopedia of Electrochemistry, Vol. 2, ed. A.J. Bard and M. Stratmann, Wiley-VCH Verlag GmbH & Co. KgaA, Weinheim, Germany, 2003

R 180 Y.Y. Tong and A. Wieckowski, 'NMR Spectroscopy in Electrochemistry', p. 147

Encyclopedia of Nanoscience and Nanotechnology, Vol. 6, ed. H.S. Nalwa, American Scientific Publishers, Stevenson Ranch, Calif., 2004

R 181 T. Ehara, 'Nanocrystalline Silicon. Electron Spin Resonance', p. 495

Encyclopedia of Nuclear Magnetic Resonance, Vol. 9, ed. D.M. Grant and R.K. Harris, John Wiley & Sons Ltd., Chichester, UK., 2002

R 182 M. Ernst and B.H. Meier, 'Adiabatic Polarization-Transfer Methods in MAS Spectroscopy', p. 23

R 183 G.E. Martin, 'Cryogenic NMR Probes: Applications', p. 33

R 184 G.A. Morris, 'Diffusion-Ordered Spectroscopy (DOSY)', p. 35

R 185 H.W. Spiess, 'Double-Quantum NMR Spectroscopy of Dipolar Coupled Spins under Fast Magic-Angle Spinning', p. 44

R 186 A. Samoson, 'Extended Magic-Angle Spinning', p. 59

R 187 A.J. Shaka and V.A. Mandelshtam, 'Filter Diagonalization Methods for Time-Domain Signals', p. 64

R 188 D.M. Grant, 'Five π Pulse Magic-Angle Turning Spectra of Solids', p. 73

R 189 M.H. Levitt, 'Symmetry-Based Pulse Sequences in Magic-Angle Spinning Solid-State NMR', p. 165

R 190 A.E. McDermott and A. Bockmann, 'Assignments and Prospects for Structure Determination of Solid Proteins Using MAS and Isotopic Enrichment', p. 337

R 191 M. Rance, 'Cross-Correlated Relaxation Effects in Biomolecules', p. 354

R 192 G. Navon, H. Shinar and U. Eliav, 'Double Quantum Filtered NMR in Ordered Biological Tissues', p. 374

R 193 T.E. Machonkin and J.L. Markley, 'Electron-Nuclear Interactions', p. 384

R 194 A. Bax, J.J. Chou and B.E. Ramirez, 'Liquid Crystalline Samples: Application to Macromolecular Structure Determination', p. 401

R 195 H. Sun, 'Metallodrugs', p. 413

R 196 S.J. Opella, 'Multiple-Resonance Multi-Dimensional Solid-State NMR of Proteins', p. 427

R 197 J.H. Prestegard, N.U. Jain and S.B. Levery, 'Saccharide-Protein Interactions', p. 441

R 198 H.J. Dyson and P.E. Wright, 'Structure and Dynamics of Disordered Proteins', p. 449

R 199 G.P. Drobny, J.R. Long, W.J. Shaw, M. Cotten and P.S. Stayton, 'Structure and Dynamics of Proteins Adsorbed to Biomaterial Interfaces', p. 458

R 200 K. Wuethrich and G. Wider, 'Transverse Relaxation – Optimized NMR Spectroscopy with Biomacromolecular Structures in Solution', p. 468

R 201 H.-H. Limbach, 'Dynamics of Hydrogen Transfer in Liquids and Solids', p. 520

R 202 J. Jeener, 'Collective Effects in Liquid NMR. Dipolar Field and Radiation Damping', p. 642

R 203 R. Tycko and S.E. Barrett, 'Optically Pumped NMR of Semiconductors and Two-Dimensional Electron Systems', p. 711

R 204 P.T. Callaghan, 'Rheo-NMR: A New Window on the Rheology of Complex Fluids', p. 737

Endofullerenes. A New Family of Carbon Clusters, ed. T. T. Akasaka and S. Nagase, in *Development in Fullerene Science*, Vol. 3, Kluwer Academic Publishers, 2002

R 205 M. Saunders and R.J. Cross, 'Putting Nonmetals into Fullerenes', p. 1

Energetic Materials, Part 2, ed. P.A. Politzer and J.S. Murray, in *Theoretical and Computational Chemistry*, Vol. 13, Elsevier Science B.V., 2003

R 206 S. Zeman, 'A Study of Chemical Micro-Mechanisms of Initiation of Organic Polynitro Compounds', p. 25

EPR of Free Radicals in Solids, Trends in Methods and Applications, ed. A. Lund and M. Shiotani, in *Progress in Theoretical Chemistry and Physics*, Vol. 10, Kluwer Academic Publishers, 2003

R 207 N.P. Benetis, 'Dynamical Effects in CW and Pulsed EPR', p. 95

Ethanol and the Liver, ed. D.I.N. Sherman, V.R. Preedy and R.R. Watson, Taylor & Francis Ltd., London, UK., 2002

R 208 R.F. Butterworth, 'Cerebral Consequences of Alcoholic Liver Disease', p. 512

Field Screening Europe 2001, Proceedings of the International Conference on Strategies and Techniques for the Investigation and Monitoring of Contaminated Sites, 2nd, Karlsruhe, Germany, May 14-16, 2001, ed. W. Breh, Kluwer Academic Publishers, Dordrecht, Netherlands, 2002

R 209 U. Yaramanci, 'Hydrogeophysical Site Characterization – Problems and New Technologies', p. 53

Group 13 Chemistry I, ed. H.W. Roesky and D.A. Atwood, in *Structure and Bonding*, Vol. 103, Springer-Verlag, Berlin, Germany, 2002
R 210 S. Schulz, 'Synthesis, Structure and Reactivity of Group 13/15 Compounds Containing the Heavier Elements of Group 15, Sb and Bi', p. 117

Hallucinogens, ed. R.R. Laing, Elsevier Science Ltd., London, UK., 2003
R 211 J. Hugel and J. Meyers, 'Analysis of the Hallucinogens', p. 191

Handbook of Adhesive Technology (2nd Edition, Revised and Expanded), ed. A.Pizzi and K.L. Mittal, Marcel Dekker Inc., New York, N.Y., 2003
R 212 D.N.-S. Hon, 'Analysis of Adhesives', p. 293

Handbook of Industrial Cell Culture, ed. V.A. Vinci and S.R. Parekh, Humana Press Inc., Totowa, N.J., 2003
R 213 W.M. van Gulik, W.A. van Winden and J.J. Heijnen, 'Metabolic Flux Analysis, Modeling, and Engineering Solutions', p. 349

Handbook on the Physics and Chemistry of Rare Earths, Vol. 33, ed. K.A. Gschneidner Jr., J.-C.G. Bunzli and V.K. Pecharsky, Elsevier, Amsterdam, Netherlands, 2003
R 214 C. Piguet and C.F.G.C. Geraldes, 'Paramagnetic NMR Lanthanide Induced Shifts for Extracting Solution Structures', p. 353

Handbook of Spectroscopy, ed. G. Gauglitz and T. Vo-Dinh, Wiley-VCH Verlag GmbH & Co. KGaA, Weinheim, Germany
Vol. 1, 2003
R 215 L.G. Butler, 'An Introduction to Solution, Solid-State, and Imaging NMR Spectroscopy', p. 177
R 216 G.E. Martin, C.E. Hadden and D.J. Russell, 'Solution NMR Spectroscopy', p. 209
R 217 S.P. Brown and L. Emsley, 'Solid-State NMR', p. 269
Vol. 2, 2003
R 218 L.A. Weisenberger, 'NMR', p. 297
R 219 W. Robien, 'Nuclear Magnetic Resonance Spectroscopy', p. 469

Handbook of Zeolite Science and Technology, ed. S.M. Auerbach, K.A. Carrado and P.K. Dutta, Marcel Dekker Inc., New York, N.Y., 2003
R 220 C.P. Grey, 'Nuclear Magnetic Resonance Studies of Zeolites', p. 205

Heavy Metals Release in Soils, ed. H.M. Selim and D.L. Sparks. Lewis Publishers, Boca Raton, Fla., 2001
R 221 W.L. Kingery, A.J. Simpson and M.H.B. Hayes, 'Chemical Structures of Soil Organic Matter and Their Interactions with Heavy Metals', p. 237

High Magnetic Fields, ed. C. Berthier, L.P. Levy and G. Martinez, in *Lecture Notes in Physics*, Vol. 595, Springer Verlag, 2001

R 222 J.H. Prestegard, 'High Resolution NMR of Biomolecules', p. 426

Interfacial Catalysis, ed. A.G. Volkov, Marcel Dekker Inc., New York, N.Y., 2003

R 223 V.C. Reinsborough, 'Micellar Catalysis', p. 377

Intrinsic Multiscale Structure and Dynamics in Complex Electronic Oxides, Proceedings of the Workshop, Trieste, Italy, June 1-4, 2002, ed. A.R. Bishop, S.R. Shenoy and S. Sridhar, World Scientific Publishing Co. Pte. Ltd., Singapore, Singapore, 2003

R 224 P. Carretta, 'NMR and λSR Investigation of Spin and Hole Texture in $La_{2-x}Sr_xCuO_4$', p. 203

Ionic Liquids in Synthesis, ed. P. Wasserscheid and T. Welton, Wiley-VCH Verlag GmbH & Co. KGaA, Weinheim, Germany, 2003

R 225 J. Richter, A. Leuchter and G. Palmer, 'Translational Diffusion [in Ionic Liquids]', p. 162

R 226 A. Doelle and W.R. Carper, 'Molecular Reorientational Dynamics [in Ionic Liquids]', p. 168

The Lanthanides and Their Interrelations with Biosystems, Vol. 40, ed. A. Sigel and H. Sigel in *Metal Ions in Biological Systems*, Marcel Dekker, Inc., 2003

R 227 C.F.G.C. Geraldes and C. Luchinat, 'Lanthanides as Shift and Relaxation Agents in Elucidating the Structure of Proteins and Nucleic Acids', p. 513

Lead Chalcogenides, in *Optoelectronic Properties of Semiconductors and Superlattices*, Vol. 18, Taylor & Francis Inc., 2003

R 228 T. Story, 'Semimagnetic Semiconductors Based on Lead Chalcogenides', p. 385

Leucocyte Trafficking, Role of Fucosyltransferases and Selectins, ed. A. Hamann, K. Asadullah and A. Schottellius in *Ernst Schering Research Foundation Workshop*, Vol. 44, Springer Verlag, 2004

R 229 B. Meyer, J. Klein, M. Mayer, R. Meinecke, H. Moeller, A. Neffe, O. Schuster, J. Wuelfken, Y. Ding, O. Knaie, J. Labbe, M.M. Palcic, O. Hindsgaul, B. Wagner and B. Ernst, 'Saturation Transfer Difference NMR Spectroscopy for Identifying Ligand Epitopes and Binding Specificities', p. 149

Liquid Chromatography FTIR Microspectroscopy Microwave Assisted Synthesis, in *Advances in Polymer Science*, Vol. 163, Springer-Verlag, Heidelberg, 2003

R 230 T. Chang, 'Recent Advances in Liquid Chromatography Analysis of Synthetic Polymers', p.1

Magnetic Resonance in Food Science, in *Special Publication – Royal Society of Chemistry*, Vol. 286, Royal Society of Chemistry, 2002

R 231 M.J. Gidley, S. Ablett and D.R. Martin, 'The Food Supply Chain: The Present Role and Future Potential of NMR', p. 3

R 232 F. Cornejo and P. Chinachoti, 'NMR in Foods: Opportunity and Challenges', p. 25

R 233 S. Rezzi, C. Guillou and F. Reniero, 'The Application of NMR in the Implementation of European Policies on Consumer Protection', p. 62

R 234 J.P. Renou, G. Bielicki, J.M. Bonny, J.P. Donnat and L. Foucat, 'Assessment of Meat Quality by NMR', p. 161

R 235 B.P. Hills, L. Meriodeu and K.M. Wright, 'NMR Studies of Complex Foods in Off-Line and On-Line Situations', p. 186

R 236 E. Micklander, L.G. Thygesen, H.T. Pedersen, F. van den Berg, R. Bro, D.N. Rutledge and S.B. Engelsen, 'Multivariate Analysis of Time Domain NMR Signals in Relation to Food Quality', p. 239

Magnetism: Molecules to Materials IV, ed. J.S. Miller and M. Drillon, Wiley-VCH Verlag GmbH& Co. KgaA, Weinheim, Germany, 2003

R 237 P. Guetlich, Y. Garcia and H. Spiering, 'Spin Transition Phenomena', p. 271

Melanocortin System, Proceedings of the Fifth International Melanocortin Meeting, August 25-28, 2002, Sunriver, Oregon, ed. R.D. Cone, in *Annals of the New York Academy of Sciences*, Vol. 994, 2003

R 238 G.L. Millhauser, J.C. McNulty, P.J. Jacson, A.D. Thompson, G.S. Barsh and I. Gantz, 'Loops and Links: Structural Insights into the Remarkable Function of the Agouti-Related Protein', p. 27

Membrane Proteins, ed. D. Rees and H. Hughes, *in Advances in Protein Chemistry*, Vol. 63, Elsevier Science, 2003

R 239 W.L. Hubbell, C. Altenbach, C.M. Hubbell and H.G. Khorana, 'Rhodopsin Structure, Dynamics, and Activation: A Perspective from Crystallography, Site-Directed Spin Labeling, Sulfhydryl Reactivity, and Disulfide Cross-Linking', p. 243

Methods in Polyphenol Analysis, ed. C. Santos-Buelga and G. Williamson, Royal Society of Chemistry, Cambridge, UK., 2003

R 240 J.-L. Wolfender, K. Ndjoko and K. Hostettmann, 'Application of LC-NMR in the Structure Elucidation of Polyphenols', p. 128

Modern Aspects of Electrochemistry, Vol. 36, ed. C.G. Vayenas, B.E. Conway, R.E. White and M.E. Gamboa-Adelco, Kluwer Academic/ Plenum Publishers, 2003

R 241 P.K. Babu, E. Oldfield and A. Wieckowski, 'Nanoparticle Surfaces Studied by Electrochemical NMR', p. 1

Modern Methods of Drug Discovery, ed. A. Hillisch and R. Hilgenfeld, Birkhaeusen Verlag, 2003

R 242 M. Vogtherr and K. Fiebig, 'NMR-Based Screening Methods for Lead Discovery', p. 183

Molecular Electronics III, ed. J.R. Reimers, C.A. Picconatto, J.C. Ellenbogen and R. Shashidhar, in *Annals of the New York Academy of Sciences*, Vol. 1006, 2003

R 243 J.P. Parakka, R.R. Schumaker, J.D. Thoburn, B.S. Kesler and S.E. Branz, 'Optical Switching in Chiropticenes', p. 94

Molecular Immunology of Complex Carbohydrates-2, in *Advances in Experimental Medicine and Biology*, Vol. 491, ed. A.M. Wu, Kluwer Academic/Plenum Publishers, 2001

R 244 J.-R. Brisson and H.J. Jennings, 'NMR and Molecular Modeling of Complex Carbohydrates and Carbohydrate-Protein Interactions. Applications to Anti-Bacteria Vaccines', p. 543

Myasthenia Gravis and Related Disorders: Biochemical Basis for Disease of the Neuromuscular Junction, ed.M.A. Agius, D.P. Richman and R.H. Fairclough in *Annals of the New York Academy of Sciences*, Vol. 998, New York Academy of Sciences, 2003

R 245 S. Fuchs, R. Kasher, M. Balass, T. Scherf, M. Harel, M. Fridkin, J.L. Sussman and E. Katchalski-Katzir, 'The Binding Site of Acetylcholine Receptor: From Synthetic Peptides to Solution and Crystal Structure', p. 93

Myocardial Ischemia and Preconditioning, ed. N.S. Dhalla, N. Takeda, M. Singh and A. Lukas, in *Progress in Experimental Cardiology*, Vol. 6, Kluwer Academic Publishers, 2003

R 246 K. Imahashi and H. Kusuoka, 'Mechanisms for Ischemia/Reperfusion Injury: Application of ^{23}Na Magnetic Resonance Spectroscopy', p. 165

Nanostructured Catalysts, ed. S.L. Scott, C.M. Crudden and C.W. Jones, Kluwer Academic/Plenum Publishers, New York, N.Y., 2003

R 247 R. Duchateau, 'Silsesquioxanes: Advanced Model Supports in Developing Silica-Immobilized Polymerization Catalysts', p. 57

Nanotechnology in Catalysis, Vol. 1, ed. B. Zhou, S. Hermans and G.A. Somorjai, Kluwer Academic/Plenum Publishers, New York, N.Y., 2004

R 248 R. Kumar, A. Ghosh, C.R. Patra, P. Mukherjee and M. Sastry, 'Gold Nanoparticles Formed within Ordered Mesoporous Silica and on Amorphous Silica', p. 111

Nanotechnology and Nano-Interface Controlled Electronic Devices, [International Workshop on Nanotechnology and NICE Devices], Nagoya,

Japan, Mar. 19-20, 2002, ed. M. Iwamoto, K. Kaneto and S. Mashiko, Elsevier Science B.V., Amsterdam, Netherlands, 2003

R 249 A. Sugimura and G.R. Luckhurst, 'Explanation of the Static and Dynamic Director Orientation in Thin Nematic Liquid Crystal Films Using Deuterium NMR Spectroscopy', p. 313

Nature-Inspired Methods in Chemometrics: Genetic Algorithms and Artificial Neural Networks, ed. R. Leardi in *Data Handling in Science and Technology*, Vol. 23, Elsevier Science B.V., 2003

R 250 R. Meusinger and U. Himmelreich, 'Neural Networks and Genetic Algorithms Applications in Nuclear Magnetic Resonance Spectroscopy', p. 281

New Horizons and Challenges in Environmental Analysis and Monitoring, [Workshop], Gdansk, Poland, Aug. 18-29, 2003 ed. J. Namiesnik, W. Chrzanowski and P. Zmijewska, Gdansk University of Technology, Centre of Excellence in Environmental Analysis and Monitoring, Gdansk, Poland, 2003

R 251 K. Levsen, A. Preiss and M. Spraul, 'Structure Elucidation of Unknown Pollutants in Environmental Samples by Coupling of HPLC to NMR and MS', p. 150

Nondestructive Characterization of Materials XI, Proceedings of International Symposium, 11th, Berlin, Germany, June 24-28, 2002, ed. R.E. Green Jr., B.B. Djordjevic and M.P. Hentschel, Springer-Verlag, Berlin, Germany, 2003

R 252 G.A. Matzkanin, 'Review of Nuclear Magnetic Resonance for Nondestructively Characterizing Materials', p. 793

R 253 B. Wolter, F. Kohl and N. Surkowa, 'Nondestructive Characterization of Polymers with NMR in One-Sided Access Technique', p. 803

Non-Neuronal Cells of the Nervous System: Function and Dysfunction, Part 2, in *Advances in Molecular and Cell Biology*, Vol. 31, JAI Press Inc., 2004

R 254 R. Gruetter, 'Principles of the Measurement of Neuro-Glial Metabolism Using in Vivo ^{13}C NMR Spectroscopy', p. 409

On-Line LC-NMR and Related Techniques, ed. K. Albert, John Wiley & Sons Ltd., Chichester, UK., 2002

R 255 A. Klaus, 'LC-NMR: Theory and Experiment', p. 1

R 256 U. Braumann and M. Spraul, 'LC-NMR: Automation', p. 23

R 257 J.C. Lindon, J.K. Nicholson and I.D. Wilson, 'Biomedical and Pharmaceutical Applications of HPLC-NMR and HPLC-NMR-MS', p. 45

R 258 J.P. Shockcor, 'Application of On-Line LC-NMR and Related Techniques to Drug Metabolism Studies', p. 89

R 259 M. Sanvoss, 'Application of LC-NMR and LC-NMR-MS Hyphenation

to Natural Products Analysis', p. 111

R 260 T. Glaser and K. Albert, 'Hyphenation of Modern Extraction Techniques to LC-NMR for the Analysis of Geometrical Carotenoid Isomers in Functional Food and Biological Tissues', p. 129

R 261 H. Haendel and K. Albert, 'GPC-NMR Coupling', p. 181

R 262 H. Fischer and K. Albert, 'SFC-NMR and SFE-NMR', p. 195

R 263 M.E. Lacey, A.G. Webb and J.V. Sweedler, 'NMR Spectroscopy in Microdomains', p. 221

R 264 A.B. Schefer and K. Albert, 'Capillary Separation Techniques', p. 237

R 265 K. Albert, 'HPLC-^{13}C NMR', p.249

R 266 A.G. Webb, J.V. Sweedler and D. Raftery, 'Parallel NMR Detection', p. 259

Organometallic Chemistry, Vol. 30 in *Specialist Periodical Reports*, Senior reporter M. Green, Royal Society of Chemistry, 2002

R 267 D.J. Linton and A.E.H. Wheatley, 'Groups 1 and 11: The Alkali and Coinage Metals', p. 51

Organometallic Conjugation, ed. A. Nakamura, N. Ueyama, and K. Yamaguchi, in *Springer Series in Chemical Physics*, Vol. 73, Springer Verlag, 2002

R 268 S. Takeda, 'Dynamic, Electronic and Magnetic Properties of Metal-Ligand and Metal-Metal Interaction Systems Studied by Solid-State High-Resolution Multinuclear NMR', p. 215

Oxazoles: Synthesis, Reactions, and Spectroscopy, Part A, ed. D.C. Palmer in *Chemistry of Heterocyclic Compounds*, Vol. 60, John Wiley & Sons, Inc., 2003

R 269 D. Lowe, 'Spectroscopic Properties of Oxazoles', p. 391

Peptides 2000, Proceedings of the European Peptide Symposium, 26th, Montpellier, France, Sept. 10-15, 2000, ed. J. Martinez and J.-A. Fehrentz, Editions EDK, Paris, France, 2001

R 270 N. Kobayashi, S.M.V. Freund, J. Chatellier and A.R. Fersht, 'NMR Interaction Studies on the Isolated Apical Domain of GroEL with Synthetic Peptides', p. 63

R 271 M. Vilar, V. Esteve, J.F. Marcos and E. Perez-Paya, 'Characterization of an RNA-Binding Peptide from a Plant Virus Movement Protein', p. 119

Perspectives in Molecular Toxinology, ed. A. Menez, John Wiley & Sons Ltd., Chichester, UK., 2002

R 272 M. Delepierre, 'High-Resolution NMR of Venom Toxins in Nanomolar Amounts', p. 125

Perspectives in Organometallic Chemistry, ed. C.G. Screttas and B.R. Steele in *Special Publication – Royal Society of Chemistry*, Vol. 287, Royal

Society of Chemistry, 2003
R 273 A. Macchioni, 'Interionic and Intermolecular Solution Structure of Transition Metal Complexes by NMR', p. 196

Pharmaceutical Analysis, ed. D.C. Lee and M.L. Webb, Blackwell Publishing Ltd., Oxford, UK., 2003
R 274 R.J. Smith and A.J. Edwards, 'Nuclear Magnetic Resonance Spectroscopy in Pharmaceutical Analysis', p. 105

Physics of Superconductors, Vol. 1, ed. K.H. Bennemann and J.B. Ketterson, Springer-Verlag, Berlin, Germany, 2003
R 275 J.P. Carbotte and F. Marsiglio, 'Electron-Phonon Superconductivity', p. 233

PINSA-A, Proceedings of the Indian National Science Academy, Part A: Physical Sciences, Vol. 68, Indian National Science Academy, 2002
R 276 R.E. Williams, 'A Dozen Carborane Structures Refined by Comparison of Quantum Chemical Calculated and Experimental NMR Chemical Shift Values', p. 499

Polymer Characterization Techniques and Their Application to Blends, ed. G.P. Simon, Oxford University Press, Inc., New York, N.Y., 2003
R 277 A.K. Whittaker, 'Nuclear Magnetic Resonance Studies of Polymer Blends', p. 461

Polyoxometalate Chemistry for Nano-Composite Design, [Symposium], Honolulu, HI, United States, Dec. 17-19, 2000, ed. T. Yamase and M.T. Pope, Kluwer Academic/Plenum Publishers, New York, N.Y., 2002
R 278 D.C. Crans, H.S. Bedi, S. Li, B. Zhang, K. Nomiya, N.C. Kasuga, Y. Nemoto, K. Nomura, K. Hashino, Y. Sakai, Y. Tekeste, G. Sebel, L.-A.E. Minasi, J.J. Smee and G.R. Willsky, 'Tetravanadate, Decavanadate, Keggin and Dawson Oxotungstates Inhibit Growth of S. Cerevisiae', p. 181

Prix Nobel 2002, Almqvist & Wiksell International, Stockholm, 2003
R 279 K. Wuethrich, 'NMR Studies of Structure and Function of Biological Macromolecules', p. 235

Proceedings of the International School of Physics 'Enrico Fermi', 148th [*Experimental Quantum Computation and Information*], IOS Press, 2002
R 280 R. Laflamme, E. Knill, C. Negrevergne, R. Martinez, S. Sinha and D.G. Cory, 'Introduction to NMR Quantum Information Processing', p. 411
R 281 Y. Yamamoto, T.D. Ladd, J.R. Goldman and F. Yamaguchi, 'Solid-State Crystal Lattice NMR Quantum Computation', p. 441

Proceedings of SPIE – The International Society for Optical Engineering, [14th Symposium on High-Resolution Molecular Spectroscopy, 2003],

SPIE – The International Society for Optical Engineering, 2004

R 282 N.F. Stepanov, 'State of the Art in Quantum Chemistry Today', p. 5311

Properties of Amorphous Carbon, ed. R. Silva in *EMIS Datareviews Series*, Vol. 29, Institution of Electrical Engineers, 2003

R 283 J.D. Carey, 'Solid-State Nuclear Magnetic Resonance Studies of a-C Thin Films', p. 103

Protein NMR for the Millennium, ed. N.R. Kirshna and L.J. Berliner, in *Biological Magnetic Resonance*, Vol. 20, Kluwer Academic/Plenum Publishers, New York, N.Y., 2003

R 284 K.V. Pervushin, 'Transverse Relaxation Optimized Spectroscopy', p. 3

R 285 J.J. Ottesen, U.K. Blaschke, D. Cowburn and T.W. Muir, 'Segmental Isotope Labeling: Prospects for a New Tool to Study the Structure-Function Relationships in Multi-Domain Proteins', p. 35

R 286 J.L. Battiste, J.D. Gross and G. Wagner, 'Global Fold Determination of Large Proteins Using Site-Directed Spin Labeling', p. 79

R 287 A. McDermott, 'Solid State NMR Studies of Uniformly Isotopically Enriched Proteins', p. 103

R 288 A.J. Wand, C.R. Babu, P.F. Flynn and M.J. Milton, 'NMR Spectroscopy of Encapsulated Proteins Dissolved in Low Viscosity Fluids', p. 121

R 289 C. Griesinger, J. Meiler and W. Peti, 'Angular Restraints from Residual Dipolar Couplings for Structure Refinement', p. 163

R 290 A.M. Gronenborn, 'Protein Structure Refinement Using Residual Dipolar Couplings', p. 231

R 291 S. Grzesiek, F. Cordier and A.J Dingley, 'Hydrogen Bond Scalar Couplings – A New Tool in Biomolecular NMR', p. 255

R 292 T. Peters, T. Biet and L. Herfurth, 'NMR Methods for Screening the Binding of Ligands to Proteins – Identification and Characterization of Bioactive Ligands', p. 287

Protein Structure, ed. D.I. Chasman, Marcel Dekker, Inc., New York, N.Y., 2003

R 293 A.E. Ferentz, 'Prospects of High-Throughput Structure Determination of Proteins by NMR Spectroscopy', p. 95

Quasicrystals, ed. H.-R. Trebin, Wiley-VCH Verlag GmbH & Co, Weinheim, Germany, 2003

R 294 R.A. Brand and J. Voss, 'Local Properties of Quasicrystals: Static and Dynamics', p. 359

Recent Advances in Environmentally Compatible Polymers, International Cellucon Conference, 11th, Tsukuba, Japan, Mar.24-26, 1999, ed. J.F. Kennedy, Woodhead Publishing Ltd., Cambridge, UK., 2001

R 295 M. Kuwahara, 'Characterization and Utilization of Ligninolytic Enzymes Produced by Basidiomycetes', p. 387

Recent Progress in Polycondensation, ed. T. Matsumoto, Research Signpost, Trivandrum, India, 2002

R 296 J. Lin, 'Phase Behavior and Conformation Characteristics of Polypeptide Liquid Crystals', p. 209

Recognition of Carbohydrates in Biological Systems, Part A, General Procedures, ed. Y. Lee and R. Lee, in *Methods in Enzymology*, Vol. 362, Elsevier Science, 2003

R 297 H.-C. Siebert, J. Jimenez-Barbero, S. Andre, H. Kaltner and H.-J. Gabius, 'Describing Topology of Bound Ligand by Transferred Nuclear Overhauser Effect Spectroscopy and Molecular Modeling', p. 417

Research and Development in Neutron Capture Therapy, Proceedings of the International Congress on Neutron Capture Therapy, 10th, Essen, Germany, Sept. 8-13, 2002, ed. W. Sauerwein, R. Moss and A. Wittig, Monduzzi Editore, Bologna, Italy, 2002

R 298 I. Maulana, A. Sterzik, P. Loennecke, S. Blaurock, E. Rys and E. Hey-Hawkins, 'Synthesis and Coordination Properties of Carbaboranylphosphines', p. 25

R 299 A. Sterzik, I. Maulana, S. Blaurock, P. Loennecke, E. Rys, V.N. Kalinin and E. Hey-Hawkins, 'Synthesis of Rac- and Meso-1,2-bis(tert-butylchlorophosphino)-1,2-dicarba-closo-dodecaborane(12) and Transition-Metal Complexes Thereof', p. 85

Science for Materials in the Frontier of Centuries: Advantages and Challenges, International Conference, Kyiv, Ukraine, Nov. 4-8, 2002, Vol. 1, ed. V.V. Skorokhod, Frantsevich Institute for Problems of Materials Science of National Academy of Science of Ukraine, Kiev, Ukraine, 2002

R 300 M.D. Glinchuk, V.V. Laguta and I.P. Bykov, 'New Generation of the Materials for Sensors, Actuators and Ultrasound Technique on the Base of Ferroelectric Relaxors', p. 28

Seminars in Organic Synthesis, Summer School 'A. Corbella', 28th, Gargnano, Italy, June 16-20, 2003, ed. E. Marcantoni and G. Renzi, Societa Chimica Italiana, Rome, Italy, 2003

R 301 L. Lunazzi and A. Mazzanti, 'NMR Analysis of Configurationally Labile Stereoisomers', p. 191

Skin, Hair, and Nails, ed. B. Forslind and M. Lindberg in *Basic and Clinical Dermatology*, Vol. 26, Marcel Dekker, Inc., 2004

R 302 Y.-W. Hsueh, J. Thewalt, N. Kitson and D.J. Moore, 'Stratum Corneum Lipid Structure: Insights from NMR and FTIR Spectroscopic Studies', p. 65

Small Molecule-Protein Interaction, ed. H. Waldmann and M. Koppitz, in *Ernst Schering Research Foundation Workshop*, Vol. 42, Springer-Verlag,

Germany, 2003

R 303 H. Kessler, M. Heller, G. Gemmecker, T. Diercks, E. Planker and M. Coles, 'NMR in Medicinal Chemistry', p. 59

Solid-State Chemistry of Inorganic Materials IV, Materials Research Society Symposium Proceedings, Vol. 755, Materials Research Society, 2002

R 304 T.O. Salami and S.R.J. Oliver, 'Solid State Synthesis and Characterization of Tin-Based Low-Dimensional Materials', p. 235

Solid State Ionics: Trends in the New Millennium, Proceedings of the Asian Conference, 8th, Langkawi, Malaysia, Dec. 15-19, 2002, ed. B.V.R. Chowdari, World Scientific Publishing Co. Pte. Ltd., Singapore, Singapore, 2002

R 305 J. Kawamura, N. Kuwata, T. Hattori and Y. Nakamura, 'Ag-109 NMR of AgJ Based Superionic Conductor Glasses', p. 725

R 306 D. Brinkmann, 'Exploring Fast Ion Conduction by NMR', p. 763

Solid State Physics (India), Proceedings of the DAE Solid State Physics Symposium 43th, 2000, Narosa Publishing House, 2000

R 307 K.V.R. Chary, 'Biomolecular NMR in the Post-Genomic Era', p. 42

Spin Dynamics in Confined Magnetic Structures II, ed. B. Hillebrands and K. Ounadjela, in *Topics in Applied Physics*, Vol. 87, Springer Verlag, 2003

R 308 T. Rasing, H. van den Berg, T. Gerrits and J. Hohlfeld, 'Ultrafast Magnetization and Switching Dynamics', p.213

Structural Bioinformatics, ed. P.E. Bourne and H. Weissig, in *Methods of Biochemical Analysis*, Vol. 44, John Wiley & Sons, Inc., 2003

R 309 S.K. Burley and J.B. Bonanno, 'Structural Genomics', p. 591

Taxus, ed. H Itokawa and K.H Lee in Medicinal and Aromatic Plants – Industrial Profiles, Vol. 32, Taylor & Francis Ltd., 2003

R 310 M. Oyama and H. Itokawa, 'Physical Methods for Identification of the Structures of Taxoids', p. 79

Treatise on Geochemistry, ed. H.D. Holland and K.K. Turekian, Elsevier Ltd., Oxford UK.,
Vol. 1, 2004

R 311 I. Gilmour, 'Structural and Isotopic Analysis of Organic Matter in Carbonaceous Chondrites', p. 269
Vol. 5, 2004

R 312 E.M. Perdue and J.D. Ritchie, 'Dissolved Organic Matter in Freshwaters', p. 273

Unfolded Proteins, ed. G.D. Rose, in *Advances in Protein Chemistry, Vol. 62 Protein Modules and Protein-Protein Interactions*, Academic Press, 2002

R 313 D. Shortle, 'The Expended Denatured State: An Ensemble of Conformations Trapped in a Locally Encoded Topological Space', p. 1

R 314 H.J. Dyson and P.E. Wright, 'Insights into the Structure and Dynamics of Unfolded Proteins from Nuclear Magnetic Resonance', p. 311

Vitamin D Analogs in Cancer Prevention and Therapy, ed. J. Reichrath, M. Friedrich and W. Tilgen, in *Recent Results in Cancer Research*, Vol. 164, Springer Verlag, 2003

R 315 H. Takayama, A. Kittaka, T. Fujishima, Y. Suhara and H. Takayama, 'Design, Synthesis, and Biological Studies of the A-Ring-Modified 1,25-Dihydroxyvitamin D_3 Analogs', p. 289

4 Reviews in Periodicals

R 316 E. Ackerstaff, K. Glunde and Z.M. Bhujwalla, 'Choline Phospholipid Metabolism: A Target in Cancer Cells?', *J. Cell. Biochem.*, 2003, **90**, 525

R 317 S. Aime, W. Dastru, S. G. Crich, E. Gianolio and V. Mainero, 'Innovative Magnetic Resonance Imaging Diagnostic Agents Based on Paramagnetic Gd(III) Complexes', *Biopolymers*, 2002, **66**, 419

R 318 K. Akasaka, 'Highly Fluctuating Protein Structures Revealed by Variable-Pressure Nuclear Magnetic Resonance', *Biochemistry*, 2003, **42**, 10875

R 319 K. Albert, 'NMR Investigations of Stationary Phases', *J. Sep. Sci.*, 2003, **26**, 215

R 320 H. M. Al-Hashimi and A. Gorin, 'Application of NMR Residual Dipolar Couplings in Studies of RNA: Towards High-Throughput Investigations', *Appl. Genom. Proteom.*, 2003, **2**, 3

R 321 J. B. Ames and M. Ikura, 'Structure and Membrane-Targeting Mechanism of Retinal Ca^{2+} – Binding Proteins, Recoverin and GCAP-2', *Adv. Exp. Med. Biol.*, 2002, **514**, 333

R 322 A. Anastasiadis and F. Separovic, 'Solid-State NMR Structural Determination of Components in an Ion Channel Switch Biosensor', *Aust. J. Chem.*, 2003, **56**, 163

R 323 J. P. Andre and H. R. Macke, 'NMR Spectroscopy of Group 13 Metal Ions: Biologically Relevant Aspects', *J. Inorg. Biochem.*,2003, **97**, 315

R 324 O. N. Antzutkin, 'Amyloidosis of Alzheimer's Aβ Peptides: Solid-State Nuclear Magnetic Resonance, Electron Paramagnetic Resonance, Transmission Electron Microscopy, Scanning Transmission Electron Microscopy and Atomic Force Microscopy Studies', *Magn. Reson. Chem.*, 2004, **42**, 231

R 325 F. Arnesano and I. Bertini, 'Structural Genomics on Metalloproteins', *Gene Funct. Disease*, 2002, **3**, 49

R 326 A. Aszalos, 'P-Glycoprotein-Based Drug-Drug Interactions: Preclinical Methods and Relevance to Clinical Observations', *Arch. Pharm. Res.*, 2004, **27**, 127

R 327 M. Auger, 'Biological and Pharmaceutical Applications of Solid-State NMR Spectroscopy', *Can. J. Anal. Sci. Spect.*, 2002, **47**, 184

R 328 K. Awazu and H. Kawazoe, 'Strained Si-O-Si Bonds in Amorphous SiO_2 Materials: A Family Member of Active Centers in Radio, Photo, and Chemical Responses', *J. Appl. Phys.*, 2003, **94**, 6243

R 329 T. Babadagli and S. Al-Salmi, 'A Review of Permeability-Prediction Methods for Carbonate Reservoirs Using Well-Log Data', *SPE Reserv. Eval. Eng.*, 2004, **7**, 75

R 330 V. Bacur, 'Techniques for High Resolution Imaging of Wood Structure: A Review', *Meas. Sci. Technol.*, 2003, **14**, R91

R 331 A. Banerji and P. Sengupta, 'Recent Studies on 1,3-Dipolar Cycloadditions of Nitrones', *J. Ind. Inst. Sci.*, 2001, **81**, 313

R 332 M. H. Baslow, 'N-Acetylaspartate in the Vertebrate Brain: Metabolism and Function', *Neurochem. Res.*, 2003, **28**, 941

R 333 G. Battistuzzi and M. Sola, 'Metal-Ligand Interplay in Blue Copper Proteins Studied by ^{1}H NMR Spectroscopy: Cu(II)-Pseudoazurin and Cu(II)-Rusticyanin', *Chemtracs*, 2003, **16**, 461

R 334 A. Bax, 'Weak Alignment Offers New NMR Opportunities to Study Protein Structure and Dynamics', *Protein Sci.*, 2003, **12**, 1

R 335 A. Bellastella, A. Bizzarro, C. Coronella, G. Bellastella, A. A. Sinisi and A. De Bellis, 'Lymphocytic Hypophysitis: A Rare or Underestimated Disease?', *Eur. J. Endocrinol.*, 2003, **149**, 363

R 336 S. I. Belov and B. I. Kochelaev, 'Magnetic Properties and Spin Kinetics of Two-Dimensional Heisenberg Antiferromagnets', *Mod. Phys. Lett., B*, 2003, **17**, 487

R 337 I. Bertini and R. Pierattelli, 'Copper(II) Proteins Are Amenable for NMR Investigations', *Pure Appl. Chem.*, 2004, **76**, 321

R 338 D. L. Beveridge, S. B. Dixit, G. Barreiro and K. M. Thayer, 'Molecular Dynamics Simulations of DNA Curvature and Flexibility: Helix Phasing and Premelting', *Biopolymers*, 2004, **73**, 380

R 339 S. Bhattacharya and W. J. Chazin, 'Calcium-Driven Changes in S100A11 Structure Revealed', *Structure*, 2003, **11**, 738

R 340 C. Bianchini, A. Meli and W. Oberhauser, 'Catalyst Design and Mechanistic Aspects of the Alternating Copolymerization of Ethane and Carbon Monoxide by Diphosphine-Modified Palladium Catalysis', *Dalton T.*, 2003, **13**, 2627

R 341 M. Billeter, 'Interactive Model Building of Proteins from NMR Data', *Magn. Reson. Chem.*, 2003, **41(Spec. Issue)**, S33

R 342 B. Binotti, A. Macchioni, C. Zuccaccia and D. Zuccaccia, 'Application of NOE and PGSE NMR Methodologies to Investigate Non-Covalent Intimate Inorganic Adducts in Solution', *Comments Inorg. Chem.*, 2002, **23**, 417

R 343 M. Bjerring, T. Vosegaard, A. Malmendal and N. C. Nielsen, 'Method-

ological Development of Solid-State NMR for Characterization of Membrane Proteins', *Concepts Magn. Reson., A*, 2003, **18A**, 111

R 344 W. B. Blanton, 'BlochLib: A Fast NMR C++ Tool Kit', *J. Magn. Reson.*, 2003, **162**, 269

R 345 M. Blaut, L. Schoefer and A. Braune, 'Transformation of Flavonoids by Intestinal Microorganisms', *Int. J. Vitam. Nutr. Res.*, 2003, **73**, 79

R 346 J.-M. Bonmatin, O. Laprevote and F. Peypoux, 'Diversity among Microbial Cyclic Lipopeptides: Iturins and Surfactins. Activity – Structure Relationships to Design New Bioactive Agents', *Comb. Chem. High T. Scr.*, 2003, **6**, 541

R 347 I. Botos and A. Wlodawer, 'Cyanovirin-N: A Sugar-Binding Antiviral Protein with a New Twist', *Cell Mol. Life Sci.*, 2003, **60**, 277

R 348 W. Braun, 'Developing Computational Tools for NMR: The Early Days of Protein NMR', *Magn. Reson. Chem.*, 2003, **41(Spec. Issue)**, S51

R 349 K. L. Bren, 'Recent Advances in NMR Spectroscopy of Cytochromes C', *Chemtracts*, 2002, **15**, 677

R 350 A. M. Brown, 'Brain Glycogen Re-Awakened', *J. Neurochem.*, 2004, **89**, 537

R 351 G. J. B. B. Bruinsma and C. J. A. van Echteld, 'Clinical Motivation for ^{31}P MRS Studies on the Myocardial Energy Metabolism of Brain Dead Cats', *Spectroscopy*, 2003, **17**, 503

R 352 N. A. Brusentsov, F. S. Baiburtskii, V. V. Tarasov, L. Kh. Komissarova and V. I. Filippov, 'Production Technology and Application of Polyfunctional Magnetically Guided Superparamagnetic Preparations (A Review)', *Pharm. Chem. J.*, 2002, **36**, 197

R 353 K. P. Bryliakov and E. P. Talsi, 'Intermediates of Asymmetric Oxidation Processes Catalysed by Vanadium (V) Complexes', *Kinet. Catal.*, 2003, **44**, 334

R 354 L. Bubacco, M. van Gastel, M. Benfatto, A. W. J. W. Tepper and G. W. Canters, 'What Are the Structural Features of the Active Site That Define Binuclear Copper Proteins Function?', *Micron*, 2004, **35**, 143

R 355 W. A. Bubb, 'NMR Spectroscopy in the Carbohydrates: Characterizing the Structural Complexity', *Concepts Magn. Reson.*, 2003, **19A**, 1

R 356 B. Casu and A. Naggi, 'Antiangiogenic Heparin-Derived Heparan Sulfate Mimics', *Pure Appl. Chem.*, 2003, **75**, 157

R 357 F. Cataldo, 'Structural Analogies and Differences between Graphite Oxide and C_{60} and C_{70} Polymeric Oxides (Fullerene Ozopolymers)', *Fuller. Nanotub. Car. N.*, 2003, **11**, 1

R 358 V. Catherinot, T. E. Malliavin, J. -L. Pons and M. -A. Delsuc, 'The Assignment of Protein NMR Spectra: From Manual Analysis to Automatic Processing', *G. I. T. Labor. J. Eur.*, 2003, **7**,200

R 359 B. Chankvetadze, 'Enantiomer Migration Order in Chiral Capillary Electrophoresis', *Electrophoresis*, 2002, **23**, 4022

R 360 I. -Y. Choi, S. -P. Lee, D. N. Guilfoyle and J. A. Helpern, 'In Vivo NMR Studies of Neurodegenerative Diseases in Transgenic and Rodent Models', *Neurochem. Res.*, 2003, **28**, 987

R 361 P. Ciminiello, C. Dell'Aversano, E. Fattorusso, M. Forino and S. Magno, 'Toxins from Adriatic Blue Mussels. A Decade of Studies', *Pure Appl. Chem.*, 2003, **75**, 325

R 362 J. Clarkson and I. D. Campbell, 'Studies of Protein-Ligand Interactions by NMR', *Biochem. Soc. Trans.*, 2003, **31**, 1006

R 363 F. Clemens, M. Wegmann, T. Graule, A. Mathewson, T. Healy, J. Donnelly, A. Ullsperger, W. Hartmann and C. Papadas, 'Computing Fibers: A Novel Fiber for Intelligent Fabrics?', *Adv. Eng. Mater.*, 2003, **5**, 682

R 364 M. Coles, M. Heller and H. Kessler, 'NMR-Based Screening Technologies', *Drug Discov. Today*, 2003, **8**, 803

R 365 L. E. C. Conceicao, H. Grasdalen and I. Ronnestad, 'Amino Acid Requirements of Fish Larvae and Post-Larvae: New Tools and Recent Findings', *Aquaculture*, 2003, **227**, 221

R 366 B. Contreras-Moreira, P. W. Fitzjohn and P. A. Bates, 'Comparative Modeling: An Essential Methodology for Protein Structure Prediction in the Post-Genomic Era', *Appl. Bioinformatics*, 2002, **1**, 177

R 367 B. S. Cooperman, 'Oligopeptide Inhibition of Class I Ribonucleotide Reductases', *Biopolymers*, 2003, **71**, 117

R 368 C. Coperet, 'Molecular Design of Heterogeneous Catalysts: The Case of Olefin Metathesis', *New J. Chem.*, 2004, **28**, 1

R 369 O. Corcoran and M. Spraul, 'LC-NMR-MS in Drug Discovery', *Drug Discov. Today*, 2003, **8**, 624

R 370 I. J. Cox and B. K. Puri, 'In Vivo MR Spectroscopy in Diagnosis and Research of Neuropsychiatric Disorders', *Prostag. Leukotr. Ess.*, 2004, **70**, 357

R 371 G. Cristalli, S. Costanzi, C. Lambertucci, S. Taffi, S. Vittori and R. Volpini, 'Purine and Deazapurine Nucleosides: Synthetic Approaches, Molecular Modeling and Biological Activity', *Farmaco*, 2003, **58**, 193

R 372 P. G. Cummings, P. Offen, M. A. Olsen, S. Kennedy-Gabb and G. Zuber, 'LC/MS, LC/NMR, FTIR: An Integrated Approach to Impurity Identification in Pharmaceutical Development and Formulation', *Am. Pharm. Rev.*, 2003, **6**, 88

R 373 S. Das, 'Nuclear Magnetic Resonance Spectroscopy', *Resonance*, 2004, **9**, 34

R 374 A. K. Dash and W. F. Elmquist, 'Separation Methods That Are Capable of Revealing Blood-Brain Barrier Permeability', *J. Chromatogr., B.* 2003, **797**, 241

R 375 A. M. Davis, S. J. Teague and G. J. Kleywegt, 'Application and Limitation of X-Ray Crystallographic Data in Structure-Based Ligand and Drug Design', *Angew. Chem. Int. Ed.*, 2003, **42**, 2718

R 376 P. V. Desai and E. C. Coutinho, 'NMR: More then a Tool for Structural Elucidation', *Asian Chem. Lett.*, 2001, **5**, 69

R 377 S. -Y. Ding, R. Lamed, E. A. Bayer and M. E. Himmel, 'The Bacterial Scaffoldin: Structure, Function and Potential Applications in the Nanosciences', *Genet. Eng.*, 2003, **25**, 209

R 378 G. F. Dionne, 'Magnetic Relaxation and Anisotropy Effects on High

Frequency Permeability', *IEEE T. Magn.*, 2003, **39**, 3121
R 379 H. Dodziuk, W. Kozminski and A. Ejchart, 'NMR Studies of Chiral Recognition by Cyclodextrins', *Chirality*, 2004, **16**, 90
R 380 P. Di Donato and A. Napolitano, '1,4-Benzotioazines as Key Intermediates in the Biosynthesis of Red Hair Pigment Pheomelanins', *Pigm. Cell Res.*, 2003, **16**, 532
R 381 S. B. Duckett and D. Blazina, 'The Study of Inorganic Systems by NMR Spectroscopy in Conjunction with Parahydrogen-Induced Polarization', *Eur. J. Inorg. Chem.*, 2003, **16**, 2901
R 382 C. J. Durrant, M. P. Hertzberg and P. W. Kuchel, 'Magnetic Susceptibility. Further Insights into Macroscopic and Microscopic Fields and Sphere of Lorentz', *Concepts Magn. Reson.*, A, 2003, **18A**, 72
R 383 J. D. Dyekjaer and K. Rasmussen, 'Recent Trends in Carbohydrate Modeling', *Mini Rev. Med. Chem.*, 2003, **3**, 713
R 384 M. Eden, 'Computer Simulations in Solid-State NMR. I. Spin Dynamics Theory', *Concepts Magn. Reson.*, 2003, **17A**, 117
R 385 L. M. Epstein, N. V. Belkova, E. I. Gutsul and E. S. Shubina, 'Spectral Features of Unconventional Hydrogen Bonds and Proton Transfer to Transition Metal Hydrides', *Polish J. Chem.*, 2003, **77**, 1371
R 386 M. Ernst, 'Heteronuclear Spin Decoupling in Solid-State NMR under Magic-Angle Sample Spinning', *J. Magn. Reson.*, 2003, **162**, 1
R 387 J. W. Faller, J. Parr and A. R. Lavoie, 'Nonrigid Diastereomers: Epimerization at Chiral Metal Centers or Chiral Ligand Conformations', *New J. Chem.*, 2003, **27**, 899
R 388 M. A. Fedotov, 'Nuclear Magnetic Resonance of Donor Atoms as a Tool for Determination of the Structure of Platinum Metal Complexes in Solutions', *Russ. Chem. Bull. (Translation of Izviestiya Akademii Nauk, Seriya Khimicheskaya)*, 2003, **52**, 781
R 389 E. R. Felder, K. Martina, S. Scarpella and M. Tato, 'Versatile Monitoring Tools in Parallel Solid-Phase Synthesis', *Chimia*, 2003, **57**, 229
R 390 M. Ferhat, 'Passage from NMR to MRI and to Medical Biology', *Phys. Chem. News*, 2001, **1**, 1
R 391 C. Fernandez and K. Wuethrich, 'NMR Solution Structure Determination of Membrane Proteins Reconstituted in Detergent Micelles', *FEBS Lett.*, 2003, **555**, 144
R 392 M. Filippi, M. A. Rocca and G. Comi, 'The Use of Quantitative Magnetic-Resonance-Based Techniques to Monitor the Evolution of Multiple Sclerosis', *Lancet Neurol.*, 2003, **2**, 337
R 393 J. R. Forder and G. M. Pohost, 'Cardiovascular Nuclear Magnetic Resonance: Basic and Clinical Applications', *J. Clin. Invest.*, 2003, **111**, 1630
R 394 S. Forsen, 'Calcium', *Chem. Eng. News*, 2003, **81**, 66
R 395 M. Frankenberg-Schwager and D. Frankenberg, 'Tailor-Made Diagnosis and Therapy of Breast Cancer for Familiar Predisposed Women', *Experimentalle Strahlentherapie und Klinische Strahlbiologie*, 2003, **12**, 123
R 396 R. Freeman, 'Beg, Borrow, or Steal. Finding Ideas for New NMR Experiments', *Concepts Magn. Reson.*, 2003, **17A**, 71

R 397 R. Freeman and E. Kupce, 'New Methods for fast Multidimensional NMR', *J. Biomol. NMR.*, 2003, **27**, 101

R 398 L. Frydman, A. Lupulescu and T. Scherf, 'Principles and Features of Single-Scan Two-Dimensional NMR Spectroscopy', *J. Am. Chem. Soc.*, 2003, **125**, 9204

R 399 B. Fuertig, C. Richter, J. Woehnert and H. Schwalbe, 'NMR Spectroscopy of RNA', *ChemBioChem*, 2003, **4**, 936

R 400 B. M. Fung, 'New Angles for NMR Studies of Biological Molecules', *Biophys. J.*, 2003, **85**, 3429

R 401 J. -C. P. Gabriel and P. Davidson, 'Mineral Liquid Crystals from Self-Assembly of Anisotropic Nanosystems', *Top. Curr. Chem.*, 2003, **226**, 119

R 402 T. R. Gadek, 'Strategies and Methods in the Identification of Antagonists of Protein-Protein Interactions', *BioTchniques*, 2003,(Suppl.), 21

R 403 E. Gaggelli, N. D'Amelio, D. Valensin and G. Valensin, '^{1}H NMR Studies of Copper Binding by Histidine-Containing Peptides', *Magn. Reson. Chem.*, 2003, **41**, 877

R 404 M. A. Garcia-Espinosa, T. B. Rodrigues, A. Sierra, M. Benito, C. Fonseca, H. L. Gray, B. L. Bartnik, M. L. Garcia-Martin, P. Ballesteros and S. Cerdan, 'Cerebral Glucose Metabolism and the Glutamine Cycle as Detected by in Vivo and in Vitro ^{13}C NMR Spectroscopy', *Neurochem. Int.*, 2004, **45**, 297

R 405 K. Gawrisch, N. V. Eldho and L. L. Holte, 'The Structure of DHA in Phospholipid Membranes', *Lipids*, 2003, **38**, 445

R 406 P. G. W. Gettins, M. Backovic and F. C. Peterson, 'Use of NMR to Study Serpin Function', *Methods*, 2004, **32**, 120

R 407 P. G. W. Gettins and S. T. Olson, 'Use of Fluorescence Resonance Energy Transfer to Study Serpin-Proteinase Interactions', *Methods*, 2004, **32**, 110

R 408 R. J. Gillies, 'In Vivo Molecular Imaging', *J. Cell. Biochem.*, 2002, **Sup. 39**, 231

R 409 C. Giragossian and D. F. Mierke, 'Determination of Ligand-Receptor Interactions of Cholecystokinin by Nuclear Magnetic Resonance', *Life Sci.*, 2003, **73**, 705

R 410 L. F. Gladden, 'Recent Advances in MRI Studies of Chemical Reactors: Ultrafast Imaging of Multiphase Flows', *Top. Catal.*, 2003, **24**, 19

R 411 W. H. Gmeiner, S. Yu, R. T. Pon, P. Pourquier and Y. Pommier, 'Structural Basis for Topoisomerase I Inhibition by Nucleoside Analogs', *Nucleos. Nucleot. Nucl.*, 2003, **22**, 653

R 412 A. Godelitsas and T. Armbruster, 'HEU-Type Zeolites Modified by Transition Elements and Lead', *Micropor. Mesopor. Mat.*, 2003, **61**, 3

R 413 S. Gorog, 'New Safe Medicines Faster: The Role of Analytical Chemistry', *TrAC, Trend. Anal. Chem.*, 2003, **22**, 407

R 414 K. -E. Gottschalk and H. Kessler, 'The Structures of Integrins and Integrin-Ligand Complexes: Implications for Drug Design and Signal Transduction', *Angew. Chem. Int. Ed.*, 2002, **41**, 3767

R 415 C. P. Grey and Y. J. Lee, 'Lithium MAS NMR Studies of Cathode Materials for Lithium-Ion Batteries', *Solid State Sci.*, 2003, **5**, 883

R 416 J. R. Griffiths and M. Stubbs, 'Opportunities for Studying Cancer by Metabolomics: Preliminary Observations on Tumors Deficient in Hypoxia-Inducible Factor 1', *Adv. Enzyme Regul.*, 2003, **43**, 67

R 417 A. M. Gronenborn, 'The Importance of Being Ordered: Improving NMR Structures Using Residual Dipolar Couplings', *C. R. Biol.*, 2002, **325**, 957

R 418 T. Groth, M. Renil and E. Meinjohanns, 'PEG Based Resins for Protease Drug Discovery Synthesis, Screening and Analysis of Combinatorial On-Bead Libraries', *Comb. Chem. High T. Scr.*, 2003, **6**, 589

R 419 R. Gruetter, G. Adriany, I. -Y. Choi, P. -G. Henry, H. Lei and G. Oz, 'Localized in Vivo ^{13}C NMR Spectroscopy of the Brain', *NMR Biomed.*, 2003, **16**, 313

R 420 J. Guzman and B. C. Gates, 'Supported Molecular Catalysts: Metal Complexes and Clusters on Oxides and Zeolites', *Dalton T.*, 2003, **17**, 3303

R 421 J. Haase, D. Eckert, H. Siegel, H. Eschrig, K. -H. Mueller and F. Steglich, 'Nuclear Magnetic Resonance in Pulsed High-Field Magnets', *Concepts Magn. Reson., B*, 2003, **19B**, 9

R 422 T. Hammen, H. Stefan, K. E. Eberhardt, B. H. W-Huk and B. F. Tomandl, 'Clinical Applications of 1H-MR Spectroscopy in the Evaluation of Epilepsies – What Do Pathological Spectra Stand for with Regard to Current Results and what Answers Do They Give to Common Clinical Questions Concerning the Treatment of Epilepsies?', *Acta Neurol. Scand.*, 2003,**108**, 223

R 423 M. M. Harding, P. I. Anderberg and A. D. J. Haymet, "Antifreeze' Glycoproteins from Polar Fish', *Eur. J. Biochem.*, 2003, **270**, 1381

R 424 V. Haroutunian, S. Dracheva and K. L. Davis, 'Neurobiology of Glutamatergic Abnormalities in Schizophrenia', *Clinic. Neurosci. Res.*, 2003, **3**, 67

R 425 Y. Hatanaka, 'Unusual Behavior of Silicon Oligomers and Polymers Having Functional Groups', *J. Organomet. Chem.*, 2003, **685**, 207

R 426 T. F. Havel, 'Metric Matrix Embedding in Protein Structure Calculations, NMR Spectra Analysis, and Relaxation Theory', *Magn. Reson. Chem.*, 2003, **41(Spec. Issue)**, S37

R 427 T. Hayashi, 'Rhodium-Catalysed Asymmetric Addition of Organo-Boron and – Titanium Reagents to Electron-Deficient Olefins', *Bull. Chem. Soc. Jpn.*, 2004, **77**, 13

R 428 U. Heinemann, 'Establishing a Structural Genomics Platform: The Berlin-Based Protein Structure Factory', *Gene Funct. Disease*, 2002, **3**, 25

R 429 P. Heitjans and S. Indris, 'Diffusion and Ionic Conduction in Nanocrystalline Ceramics', *J. Phys. -Condens. Mat.*, 2003, **15**, R1257

R 430 R. J. Hernandez, 'Influence of a Nontraditional Aluminosilicate Introduction on the Chemical Resistance of a Soda-Lime Glass', *Glass Phys. Chem.*, 2003, **29**, 575

R 431 J. T. Hickey, L. Hickey, W. S. Yancy Jr., J. Hepburn and E. C. Westman, 'Clinical Use of a Carbohydrate-Restricted Diet to Treat the Dyslipidemia of the Metabolic Syndrome', *Metabolic Syndrome and Related*

Disorders, 2003, **1**, 227

R 432 C. W. Hoganson and C. Tommos, 'The Function and Characteristics of Tyrosyl Radical Cofactors', *Biochim. Biophys. Acta*, 2004, **1655**, 116

R 433 E. Holmes and H. Antti, 'Chemometric Contributions to the Evolution of Metabonomics: Mathematical Solutions to Characterizing and Interpreting Complex Biological NMR Spectra', *Analyst*, 2002, **127**, 1549

R 434 G. E. Homanics, Y. Xu and P. Tang, 'Integrated Approaches to the Action of General Anesthetics and Alcohol', *Physiol. Behav.*, 2002, **77**, 495

R 435 S. W. Homans, 'NMR Spectroscopy Tools for Structure – Aided Drug Design', *Angew. Chem. Int. Ed.*, 2004, **43**, 290

R 436 T. Honma, 'Recent Advances in de Novo Design Strategy for Practical Lead Identification', *Med. Res. Rev.*, 2003, **23**, 606

R 437 H. Hori and S. Yamamoto, 'Nuclear Spin-Lattice Relaxation in Ferrimagnetic Clusters and Chains. A Contrast between Zero and One Dimensions', *Los Alamos National Laboratory, Preprint Archive, Condensed Matter*, Avail. URL: http://xxx. lanl. gov/pdf/cond-mat/0306685

R 438 H. Hori and S. Yamamoto, 'Nuclear Spin-Lattice Relaxation in Ferrimagnetic Clusters and Chains: A Contrast between Zero and One Dimensions', *Phys. Rev. B*, 2003, **68**, 054409/1

R 439 F. A. Howe and K. S. Opstad, '^{1}H MR Spectroscopy of Brain Tumours and Masses', *NMR Biomed.*, 2003, **16**, 123

R 440 T. N. Huckerby, R. M. Lauder and I. A. Nieduszynski, 'Recent Studies on the Chondroitin Sulfate/Dermatan Sulfate Polymer Systems Using NMR Spectroscopy', *Polym. Preprints (American Chemical Society, Division of Polymer Chemistry)* [computer optical disk], 2003, **44**, 328

R 441 R. Huo, R. Wehrens, J. Van Duynhoven and L. M. C. Buydens, 'Assessment of Techniques for DOSY NMR Data Processing', *Anal. Chim. Acta*, 2003, **490**, 231

R 442 F. Iborra, P. R. Cook and D. A. Jackson, 'Applying Microscopy to the Analysis of Nuclear Structure and Function', *Methods*, 2003, **29**, 131

R 443 E. Iengo, E. Zangrando and E. Alessio, 'Discrete Supramolecular Assemblies of Porphyrins Mediated by Coordination Compounds', *Eur. J. Inorg. Chem.*, 2003, **13**, 2371

R 444 Y. Iwasa, 'HTS Magnets: Stability; Protection; Cryogenics; Economics; Current Stability/Protection Activities at FBML', *Cryogenics*, 2003, **43**, 303

R 445 K. Jackowski, 'Gas-Phase Studies of Spin-Spin Coupling Constants', *Int. J. Mol. Sci.*, [online computer file], 2003,**4**, 135, Avail. URL: http://www. mdpi. org/ijms/papers/i4030135. pdf

R 446 K. Jackowski, 'Gas-Phase Spin-Spin Coupling Constants in the Zero-Density Limit. A Short Review', *Mol. Phys. Rep.*, 2001, **33**, 22

R 447 E. Jamin and K. Wietzerbin, 'Multielement, Multicomponent, and Multisite Isotropic Profiling for Food and Beverage Authentication', *Am. Lab.*, 2003, **35**, 24

R 448 D. A. Jayawickrama and J. V. Sweedler, 'Hyphenation of Capillary Separations with Nuclear Magnetic Resonance Spectroscopy', *J.*

Chromatogr., A, 2003, **1000**, 819

R 449 D. Jelic, V. Mesar, I. Basic, D. Nadramija and D. Verbanac, 'Novel Approach to Drug Discovery in PLIVA – Establishing of HTS Unit and Unique Compounds Library', *PharmaChem.*, 2003, **2**, 64

R 450 P. Jeschke, H. Uneme, J. Benet-Buchholz, J. Stoelting, W. Sirges, M. E. Beck and W. Etzel, 'Clothianidin (TI-435) – the Third Member of the Chloronicotinyl Insecticide (CNI) Family', *Pflanzenschutz-Nachrichten Bayer (German Edition)*, 2003, **56**, 5

R 451 L. J. C. Jeuken, 'Conformational Reorganisation in Interfacial Protein Electron Transfer', *Biochim. Biophys. Acta*, 2003, **1604**, 67

R 452 M. A. Johnson and B. M. Pinto, 'NMR Spectroscopic and Molecular Modeling Studies of Protein-Carbohydrate and Protein-Peptide Interactions', *Carbohyd. Res.*, 2004, **339**, 907

R 453 D. M. Jonas, 'Chemistry: Optical Analogs of 2D NMR', *Science*, 2003, **300**, 1515

R 454 F. Joubert, P. Mateo, B. G. Gillet, J. -C. Beloeil, J. -L. Mazet and J. A. Hoerter, 'CK Flux or Direct ATP Transfer: Versatility of Energy Transfer Pathways Evidenced by NMR in the Perfused Heart', *Mol. Cell. Biochem.*, 2004, **256/257**, 43

R 455 J. Juneja and J. B. Udgaonkar, 'NMR Studies of Protein Folding', *Curr. Sci.*, 2003, **84**, 157

R 456 N. Kaila and B. E. Thomas IV, 'Design and Synthesis of Sialyl Lewis (x) Mimics as E- and P-Selectin Inhibitors', *Med. Res. Rev.*, 2002, **22**, 566

R 457 S. Kaizaki, 'Spectroscopic Implications for Magnetic Interactions in Metal Complexes with Nitroxide Radicals', *Bull. Chem. Soc. Jpn.*, 2003, **76**, 673

R 458 Y. Kajihara and H. Sato, 'Structural Analysis of Oligosaccharides by Nuclear Magnetic Resonance Method', *Trends Glycosci. Glyc.*, 2003, **15**, 197

R 459 M. Kamao and T. Okano, 'Novel Metabolic Pathways of Vitamin D_3 – Identification of C-3 Epimerization and C-25 Dehydration Pathways and Biological Activity of Novel Metabolites', *J. Health Sci.*, 2003, **49**, 260

R 460 J. Karger, F. Stallmach and S. Vasenkov, 'Structure-Mobility Relation of Molecular Diffusion in Nanoporous Materials', *Magn. Reson. Imaging*, 2003, **21**, 185

R 461 M. R. Kasimova, S. M. Kristensen and J. J. Led, 'Protein Stability Versus Dynamics: A Flexible State of Human Growth Hormone Shows Surprisingly High Stability', *Asian Chem. Lett.*, 2003, **7**, 107

R 462 E. Katchalski-Katzir, R. Kasher, M. Balass, T. Scherf, M. Harel, M. Fridkin, J. L. Sussman and S. Fuchs, 'Design and Synthesis of Peptides that Bind α-Bungarotoxin with High Affinity and Mimic the Three-Dimensional Structure of the Binding-Site of Acetylcholine Receptor', *Biophys. Chem.*, 2003, **100**, 293

R 463 T. Kawashima, 'Syntheses, Structures, and Thermolyses of Three- and Four-Membered Heterocyclic Compounds Containing Highly Coordinate Main Group Elements', *Bull. Chem. Soc. Jpn.*, 2003, **76**, 471

R 464 C. Keeler, M. E. Hodsdon and P. S. Dannies, 'Is There Structural Specificity in the Reversible Protein Aggregates That Are Stored in Secretory Granules?', *J. Mol. Neurosci.*, 2003, **22**, 43

R 465 C. L. Keen, T. Jeu, C. D. Tran, J. Vogel, R. G. Downing, V. Iyengar and R. B. Rucker, 'Analytical Methods: Improvements, Advancements and New Horizons', *J. Nutr.*, 2003, **133**, 1574S

R 466 J. G. Kempf and J. P. Loria, 'Theory and Applications of Protein Dynamics from Solution NMR', *Cell Biochem. Biophys.*, 2002, **37**, 187

R 467 E. Kennett and P. Kuchel, 'Redox Reactions and Electron Transfer Across the Red Cell Membrane', *IUBMB Life*, 2003, **55**, 375

R 468 R. G. Khalifah, 'Reflections on Edsall's Carbonic Anhydrase: Paradoxes of an Ultra Fast Enzyme', *Biophys. Chem.*, 2003, **100**, 159

R 469 A. A. Khrapitchev and P. T. Callaghan, 'Spatial Dependence of Dispersion', *Magn. Reson. Imaging*, 2003, **21**, 373

R 470 I. V. Khudyakov, N. Arsu, S. Jockusch and N. J. Turro, 'Magnetic and Spin Effects in the Photoinitiation of Polymerization', *Des. Monomers Polym.*, 2003, **6**, 91

R 471 G. C. Kite, N. C. Veitch, R. J. Grayer and M. S. J. Simmonds, 'The Use of Hyphenated Techniques in Comparative Phytochemical Studies of Legumes', *Biochem. Sys. Ecol.*, 2003, **31**, 813

R 472 R. L. Kleinberg, C. Flaum, D. D. Griffin, P. G. Brewer, G. E. Malby, E. T. Peltzer and J. P. Yesinowski, 'Deep Sea NMR: Methane Hydrate Growth Habit in Porous Media and Its Relationship to Hydraulic Permeability, Deposit Accumulation, and Submarine Slope Stability', *J. Geophys. Res. - Sol. Ea.*, 2003, **108**, EPM12/1

R 473 G. J. Kleywegt, K. Hendrick, E. J. Dodson and D. M. F. Van Aalten, 'Pound-Wise but Penny-Foolish: How Well Do Micromolecules Fare in Macromolecular Refinement?', *Structure*, 2003, **11**, 1051

R 474 R. Knapp, S. Kelch, O. Schmelz and M. Rehahn, 'Synthesis and Properties in Solution of Ruthenium(II) Coordination Polymers', *Macromol. Symp.*, 2003, **204**, 267

R 475 G. Knothe, 'Quantitative Analysis of Mixtures of Fatty Compounds by ^{1}H · NMR', *Lipid Technol.*, 2003, **15**, 111

R 476 J. Kobayashi, K. Shimbo, T. Kubota and M. Tsuda, 'Bioactive Macrolides and Polyketides from Marine Dinoflagellates', *Pure Appl. Chem.*, 2003, **75**, 337

R 477 Y. Kobuke and K. Ogawa, 'Porphyrin Supramolecules for Artificial Photosynthesis and Molecular Photonic/Electronic Materials', *Bull. Chem. Soc. Jpn.*, 2003, **76**, 689

R 478 H. Koller, 'New Developments of NMR Spectroscopy Applied to Zeolite Catalysts', *Preprints – American Chemical Society, Division of Petroleum Chemistry*, 2003, **48**, 224

R 479 L. Konermann and D. A. Simmons, 'Protein-Folding Kinetics and Mechanisms Studied by Pulse-Labeling and Mass Spectrometry', *Mass Spectrom. Rev.*, 2003, **22**, 1

R 480 I. K. Konstantinou and T. A. Albanis, 'Photocatalytic Transformation of

Pesticides in Aqueous Titanium Dioxide Suspensions Using Artificial and Solar Light: Intermediates and Degradation Pathways', *Appl. Catal. B-Environ.*, 2003, **42**, 319

R 481 I. V. Koptyug and R. Z. Sagdeev, 'Non-Traditional Application of NMR Tomography', *Russ. Chem. Rev.*, 2003, **72**, 165

R 482 W. Kraus, 'Investigation of Biologically Active Natural Products Using Online LC-Bioassay, LC-NMR, and LC-MS Techniques', *J. Toxicol. Toxin. Rev.*, 2003, **22**, 495

R 483 H. -A. Krug von Nidda, R. Bulla, N. Buettgen, M. Heinrich and A. Loidl, 'Heavy Fermions in Transition Metals and Transition-Metal Oxides', *Eur. Phys. J., B*, 2003, **34**, 399

R 484 P. W. Kuchel, B. E. Chapman, W. A. Bubb, P. E. Hansen, C. J. Durrant and M. P. Hertzberg, 'Magnetic Susceptibility: Solutions, Emulsions, and Cells', *Concepts Magn. Reson., A*, 2003, **18A**, 56

R 485 S. Kueppers and M. Haider, 'Process Analytical Chemistry – Future Trends in Industry', *Anal. Bioanal. Chem.*, 2003, **376**, 313

R 486 H. Kumakura, T. Kiyoshi, T. Ohara, H. Kitaguchi, K. Togano and H. Wada, 'Development of Bi-Based Oxide Superconducting Magnets', *Int. J. Condens. Mat. Res.*, 2001, **5**, 241

R 487 S. Kumar, C. Wittmann and E. Heinzle, 'Minibioreactors', *Biotechnol. Lett.*, 2004, **26**, 1

R 488 L. Kwock, J. K. Smith, M. E. Castillo, G. Matthew, S. Cush, T. Hensing, M. Varia, D. Morris and T. W. Bouldin, 'Clinical Applications of Proton MR Spectroscopy in Oncology', *Technol. Cancer Res. Treat.*, 2002, **1**, 17

R 489 T. -L. Lau, K. J. Barnham, C. C. Curtain, C. L. Masters and F. Separovic, 'Magnetic Resonance Studies of β-Amyloid Peptides', *Aust. J. Chem.*, 2003, **56**, 349

R 490 N. Lazar, N. Brakch, M. Panchal, P. Cohen and M. Rholam, 'Secondary Structure as a Conformational Determinant in Processing of Peptide Precursors at Dibasic Amino Acids', *Spectroscopy*, 2003, **17**, 17

R 491 A. LeBail, L. Boillereaux, A. Davenel, M. Hayert, T. Lucas and J. Y. Monteau, 'Phase Transition in Foods: Effect of Pressure and Methods to Assess or Control Phase Transition', *Innovative Food Sci. Emerg. Technol.*, 2003, **4**, 15

R 492 D. L. Lee and R. S. Hodges, 'Structure – Activity Relationships of de Novo Designed Cyclic Antimicrobial Peptides Based on Gramicidin S', *Biopolymers*, 2003, **71**, 28

R 493 W. Leenders, 'Ferumoxtran-10 Advanced Magnetics', *IDrugs*, 2003, **6**, 987

R 494 M. -L. Lehaire and K. Severin, 'Stabilization of Molecular LiF, LiFHF, and Na_2SiF_6 Using Metallamacrocyclic Hosts', *Chimia*, 2003, **57**, 190

R 495 A. Lerf, 'Different Modes and Consequences of Electron Transfer in Intercalation Compounds', *J. Phys. Chem. Solids*, 2004, **65**, 553

R 496 H. Li, M. Carrion-Vazquez, A. F. Oberhauser, P. E. Marszalek and J. M. Fernandez, 'Stretching Single Bio-Macromolecules into Novel Conformations Using the Atomic Force Microscope', *Polym. Mater. Sci. Eng.*,

[computer optical disk], 2003, **88**, 270
R 497 C. D. Lima, 'CUE'd up for Monoubiquitin', *Cell*, 2003, **113**, 554
R 498 C. H. Londergan and C. P. Kubiak, 'Electron Transfer and Dynamic Infrared-Band Coalescence: It Looks like Dynamic NMR Spectroscopy, but a Billion Times Faster', *Chem. Eur. J.*, 2003, **9**, 5962
R 499 F. -D. T. Lung and J. -Y. Tsai, 'Grb2 SH2 Domain-Binding Peptide Analogs as Potential Anticancer Agents', *Biopolymers*, 2003, **71**, 132
R 500 A. Macchioni, 'NMR Investigations in Solution of Non-Covalently Bonded Organometallic Adducts', *Spec. Chem. Mag.*, 2003, **23**, 42
R 501 D. E. MacLaughlin, M. S. Rose, B. -L. Young, O. O. Bernal, R. H. Heffner, D. G. Morris, K. Ishida, G. J. Nieuwenhuys and J. E. Sonier, 'μSR and NMR in f-Electron Non-Fermi Liquid Materials', *Physica B*, 2003, **326**, 381
R 502 A. D. Maher and P. W. Kuchel, 'The Gardos Channel: A Review of the Ca^{2+}-Activated K^+ Channel in Human Erythrocytes', *Int. J. Biochem. Cell Biol.*, 2003, **35**, 1182
R 503 J. P. G. Malthouse, 'Stereospecificity of α-Proton Exchange Reactions Catalysed by Pyridoxal-5'-Phosphate-Dependent Enzymes', *Biochim. Biophys. Acta*, 2003, **1647**, 138
R 504 L. Mannina, C. Calcagni, E. Rossi and A. Segre, 'Review about Olive Oil Characterization Using High-Field Nuclear Magnetic Resonance', *Ann., (Rome, Italy)*, 2003, **93**, 97
R 505 L. Mannina, A. P. Sobolev and A. Segre, 'Olive Oil as Seen by NMR and Chemometrics', *Spectrosc. Eur.*, 2003, **15**, 6
R 506 F. Mari and G. B. Fields, 'Conopeptides: Unique Pharmacological Agents that Challenge Current Peptide Methodologies', *Chim. Oggi*, 2003, **21**, 43
R 507 D. Marsh, 'Lipid Interactions with Transmembrane Proteins', *Cell Mol. Life Sci.*, 2003, **60**, 1575
R 508 G. J. Martin and M. L. Martin, 'Climatic Significance of Isotope Ratios', *Phytochem. Rev.*, 2003, **2**, 179
R 509 T. Matsuo and A. Sekiguchi, 'Cyclobutadiene Dianion', *Bull. Chem. Soc. Jpn.*, 2004, **77**, 211
R 510 T. S. May, 'New High-Throughput NMR', *Targets*, 2003, **2**, 39
R 511 J. E. Mayhew, 'Neuroscience: A Measured Look at Neuronal Oxygen Consumption', *Science*, 2003, **299**, 1023
R 512 R. L. McFeeters and R. E. Oswald, 'Emerging Structural Explanations of Ionotropic Glutamate Receptor Function', *FASEB J.*, 2004, **18**, 428
R 513 B. Meyer and T. Peters, 'NMR Spectroscopy Techniques for Screening and Identifying Ligand Binding to Protein Receptors', *Angew. Chem. Int. Ed.*, 2003, **42**, 864
R 514 R. Micura and C. Hoebartner, 'On Secondary Structure Rearrangements and Equilibria of Small RNAs', *ChemBioChem*, 2003, **4**, 984
R 515 V. N. Mitkin, 'Types of Inorganic Fluorocarbon Polymer Materials and Structure-Property Correlation Problems', *J. Struct. Chem.*, 2003, **44**, 82
R 516 S. Miyahara and K. Ueda, 'Theory of the Orthogonal Dimer Heisenberg

Spin Model for $SrCu_2(BO_3)_2$', *J. Phys. -Condens. Mat.*, 2003, **15**, R327

R 517 K. I. Momot and P. W. Kuchel, 'Pulsed Field Gradient Nuclear Magnetic Resonance as a Tool for Studying Drug Delivery Systems', *Concepts Magn. Reson., A*, 2003, **19A**, 51

R 518 S. H. Moolenaar, U. F. H. Engelke and R. A. Wevers, 'Proton Nuclear Magnetic Resonance Spectroscopy of Body Fluids in the Field of Inborn Errors of Metabolism', *Ann. Clin. Biochem.*, 2003, **40**, 16

R 519 H. Murai, S. Yamauchi, A. Kawai, K. Obi and N. Hirota, 'Developments of Magnetic-Resonance-Related Spin Chemistry in Japan', *Appl. Magn. Reson.*, 2003, **23**, 249

R 520 N. Murali and V. V. Krishnan, 'A Primer for Nuclear Magnetic Relaxation in Liquids', *Concepts Magn. Reson.*, 2003, **17A**, 86

R 521 T. Nakaya and Y. J. Li, 'Recent Progress of Phospholipid Polymers', *Des. Monomers Polym.*, 2003, **6**, 309

R 522 S. Nakayama and J. F. Clark, 'Smooth Muscle and NMR Review: An Overview of Smooth Muscle Metabolism', *Mol. Cell. Biochem.*, 2003, **244**, 17

R 523 S. J. Nelson and S. Cha, 'Imaging Glioblastoma Multiforme', *Cancer J.*, 2003, **9**, 134

R 524 A. A. Nevzorov, M. F. Mesleh and S. J. Opella, 'Structure Determination of Aligned Samples of Membrane Proteins by NMR Spectroscopy', *Magn. Reson. Chem.*, 2004, **42**, 162

R 525 R. A. Newmark, 'Two-Dimensional NMR of Polymers', *Polym. News*, 2003, **28**, 40

R 526 K. L. Ngai and C. M. Roland, 'Unusual Component Dynamics in Poly(ethylene oxide)/Poly(methyl methacrylate) Blends As Probed by Deuterium NMR', *Macromolecules*, 2004, **37**, 2817

R 527 H. G. Niessen, P. Trautner, R. Backhausen and K. Woelk, 'Recent Developments in Toroid Cavity Autoclave Engineering', *Concepts Magn. Reson.*, 2003, **16B**, 15

R 528 J. Nussberger, 'Investigating Mineralocorticoid Hypertension', *J. Hypertension*, 2003, **21**, S25

R 529 N. Ogrinc, I. J. Kosir, J. E. Spangenberg and J. Kidric, 'The Application of NMR and MS Methods for Detection of Adulteration of Wine, Fruit Juices and Olive Oil. A Review', *Anal. Bioanal. Chem.*, 2003, **376**, 424

R 530 O. Ohlenschlaeger, J. Woehnert, R. Ramachandran, C. Sich and M. Goerlach, 'Nuclear Magnetic Resonance Studies of Ribonucleic Acids', *Spectroscopy*, 2003, **17**, 537

R 531 G. Oraedd and G. Lindblom, 'Lateral Diffusion Studied by Pulsed Field Gradient NMR on Oriented Lipid Membranes', *Magn. Reson. Chem.*, 2004, **42**, 123

R 532 J. D. Otvos, 'Why Cholesterol Measurements May Be Misleading about Lipoprotein Levels and Cardiovascular Disease Risk – Clinical Implications of Lipoprotein Quantification Using NMR Spectroscopy', *Laboratoriumsmedizin*, 2002, **26**, 544

R 533 B. Pan and W. J. Fairbrother, 'NMR Structural Analysis of Vascular

Endothelial Growth Factor in Complex with a Phage-Derived Peptide Antagonist', *Spectroscopy*, 2003, **17**, 169

R 534 D. Parra, A. Gonzalez, C. Mugueta, A. Martinez and I. Monreal, 'Laboratory Approach to Mitochondrial Diseases', *J. Physiol. Biochem.*, 2001, **57**, 267

R 535 S. Perez, M. A. Rodriguez-Carvajal and T. Doco, 'A Complex Plant Cell Wall Polysaccharide: Rhamnogalacturonan II. A Structure in Quest of a Function', *Biochimie*, 2003, **85**, 109

R 536 J. Pinkas and H. W. Roesky, 'Organoaluminum Fluorides', *J. Fluorine Chem.*, 2003, **122**, 125

R 537 R. E. Port and W. Wolf, 'Noninvasive Methods to Study Drug Distribution', *Invest. New Drug.*, 2003, **21**, 157

R 538 P. S. Pregosin, E. Martinez-Viviente and P. G. A. Kumar, 'Diffusion and NOE NMR Spectroscopy. Applications to Problems Related to Coordination Chemistry and Homogeneous Catalysis', *Dalton T.*, 2003, **21**, 4007

R 539 K. E. Price, L. H. Lucas and C. K. Larive, 'Analytical Applications of NMR Diffusion Measurements', *Anal. Bioanal. Chem.*, 2004, **378**, 1405

R 540 W. S. Price, 'Recent Advances in NMR Diffusion Techniques for Studying Drug Binding', *Aust. J. Chem.*, 2003, **56**, 855

R 541 T. Radczyk, S. K. Hoffmann and J. Goslar, 'Applications of the Transport Integrals in Solid-State Physics and in Electron Spin Relaxation', *Acta Phys. Pol., A*, 2003, **104**, 469

R 542 V. Ramamurthy, J. Shailaja, L. S. Kaanumalle, R. B. Sunoj and J. Chandrasekhar, 'Controlling Chemistry with Cations: Photochemistry within Zeolites', *Chem. Commun.*, 2003, **16**, 1987

R 543 K. V. Ramanathan and N. Sinha, 'Ordering in Nematic Liquid Crystals from NMR Cross-Polarization Studies', *Pramana*, 2003, **61**, 249

R 544 E. -M. Ratai, M. Janssen, J. D. Epping, J. C. C. Chan and H. Eckert, 'Local and Medium Range Order in Alkali Borate Glasses: An Overview of Recent Solid State NMR Results', *Phys. Chem. Glasses*, 2003, **44**, 45

R 545 R. S. Raymond, D. G. Crabb, V. V. Fimushkin, A. D. Krisch, A. M. T. Lin, V. G. Luppov, C. C. Peters, A. I. Mysnik, A. F. Prukoglyad and K. Yonehara, 'The Status of the University of Michigan Polarized Proton Target', *AIP Conf. Proc.*, 2003, **675**, 916

R 546 R. J. Read, 'Strengthening Molecular Replacement with Maximum Likelihood in Beast', *Crystallogr. Rev.*, 2003, **9**, 33

R 547 H. J. Reich, A. W. Sanders, M. J. Bevan, W. H. Sikorski and R. R. Dykstra, 'Identification and Mechanistic Consequences of Contact and Solvent-Separated Ion Pair Structures in Organolithium Chemistry', *Latvijas Kimijas Zurnals*, 2002, **1**, 93

R 548 D. Reichert, 'Solid-State NMR Spectroscopy and Its Application in Analytical Chemistry', *Anal. Bioanal. Chem.*, 2003, **376**, 308

R 549 M. D. Reily, D. G. Robertson, M. Delnomdedieu and J. D. Baker, 'High Resolution NMR of Biological Fluids: Metabonomics Applications in Pharmaceutical Research and Development', *Am. Pharm. Rev.*, 2003, **6**,

105

R 550 F. Renault and E. Formstecher, 'The Multifunctional Protein PEA-15 is Involved in the Control of Apoptosis and Cell Cycle in Astrocytes', *Biochem. Pharmacol.*, 2003, **66**, 1581

R 551 J. P. Renou, L. Foucat and J. M. Bonny, 'Magnetic Resonance Imaging Studies of Water Interactions in Meat', *Food Chem.*, 2003, **82**, 35

R 552 A. G. Renwick, 'The Safety Testing of Amino Acids', *J. Nutr.*, 2003, **133**, 2031S

R 553 A. C. Ribeiro, P. J. Sebastiao and C. Cruz, 'Contribution of Proton NMR Relaxation to the Investigation of Molecular Dynamics in Columnar Mesophases of Discotic and Polycatenar Molecules', *Pramana*, 2003, **61**, 205

R 554 D. Riesner, 'Biochemistry and Structure of PrP^{C} and PrP^{Sc}', *Brit. Med. Bull.*, 2003, **66**, 21

R 555 M. Rivera and G. A. Caignan, 'Recent Developments in the ^{13}C NMR Spectroscopic Analysis of Paramagnetic Hemes and Heme Proteins', *Anal. Bioanal. Chem.*, 2004, **378**, 1464

R 556 R. J. Robins, I. Billault, J. -R. Duan, S. Guiet, S. Pionnier and B. -L. Zhang, 'Measurement of ^{2}H Distribution in Natural Products by Quantitative ^{2}H NMR: An Approach to Understanding Metabolism and Enzyme Mechanism?', *Phytochem. Rev.*, 2003, **2**, 87

R 557 J. Rocha, C. M. Morais and C. Fernandez, 'Novel Nuclear Magnetic Resonance Techniques for the Study of Quadrupolar Nuclei in Clays and Other Layered Materials', *Clay Minerals*, 2003, **38**, 259

R 558 D. Roy, P. K. Basu, P. Raghunathan and S. V. Eswaran, 'Novolak Resins: Structure Elucidation by Multidimensional NMR Techniques and Correlation with Lithographic Performance', *Polym. Int.*, 2003, **52**, 757

R 559 C. Rumpel and I. Koegler-Knabner, 'Characterisation of Organic Matter and Carbon Cycling in Rehabilitated Lignite-Rich Mine Soils', *Water, Air, & Soil Pollution: Focus*, 2003, **3**, 153

R 560 R. Rusby, D. Head, D. Cousins, H. Godfrin, Yu. M. Bunkov, R. E. Rapp, F. Gay, M. Meschke, C. Lusher, J. Li, A. Casey, Dm. Shvarts, B. Cowan, J. Saunders, V. Mikheev, J. Pekola, K. Gloos, P. Hernandez, S. Triqueneaux, M. de Groot, A. Peruzzi, R. Jochemsen, A. Chinchure, E. van Heumen, G. E. de Groot, W. Bosch, F. Mathu, J. Flokstra, D. Veldhuis, Y. Hermier, L. Pitre, A. Verge, B. Fellmuth and J. Engert, 'European Dissemination of the Ultra-Low Temperature Scale, PLTS-2000', *AIP Conf. Proc.*, 2003, **684**, 89

R 561 M. Russina, O. Russina and F. Mezei, 'Heterogeneous Large Amplitude Atomic Motion in Supercooled Liquids', *Chem. Phys.*, 2003, **292**, 325

R 562 S. Sachdev, 'Colloquium: Order and Quantum Phase Transitions in the Cuprate Superconductors', *Rev. Mod. Phys.*, 2003, **75**, 913

R 563 G. S. Salomons, G. S. Salomons, S. J. M. Van Dooren, N. M. Verhoeven, D. Marsden, C. Schwartz, K. M. Cecil, T. J. DeGrauw and C. Jakobs, 'X-Linked Creatine Transporter Defect: An Overview', *J. Inherit. Metab. Dis.*, 2003, **26**, 309

R 564 X. Salvatella and E. Giralt, 'NMR-Based Methods and Strategies for Drug Discovery', *Chem. Soc. Rev.*, 2003, **32**, 365

R 565 D. J. Sandman, I. -B. Kim, J. M. Njus, D. -C. Lee, A. L. Cholli and S. Sahoo, 'Approaches to Conjugated Polymers *via* Solid State Polymerization', *Macromol. Symp.*, 2003, **192**, 99

R 566 S. P. Sarma, 'Determination of Structure of Proteins in Solution Using Nuclear Magnetic Resonance', *Resonance*, 2003, **8**, 86

R 567 N. K. Sato, 'Magnetism and Superconductivity in UT_2Al_3 (T = Pd, Ni) and UGe_2', *Physica, C*, 2003, **388-389**, 533

R 568 R. Schanen, T. E. Sherline, A. M. Toader, V. Boyko, S. Mat'as, M. Meschke, S. Schottl, E. D. Adams, B. Cowan, H. Godfrin, J. P. Goff, M. Roger, J. Saunders, K. Siemensmeyer and Y. Takano, 'Neutron Scattering from Solid ^{3}He', *Physica B, (Amsterdam, Netherlands)*, 2003, **329-333**, 392

R 569 J. Schiller and K. Arnold, 'Application of High Resolution ^{31}P NMR Spectroscopy to the Characterization of the Phospholipid Composition of Tissues and Body Fluids – A Methodological Review', *Med. Sci. Monit.*, 2002, **8**, MT205

R 570 U. Schmitt, S. K. Branch and U. Holzgrabe, 'Chiral Separations by Cyclodextrin – Modified Capillary Electrophoresis – Determination of the Enantiomeric Excess', *J. Sep. Sci.*,2002, **25**, 959

R 571 D. Schneider and A. Prodoehl, 'Hydrophiles in Hydrophobic Studies: The Role of Polar Amino Acids in Membrane Proteins', *BIOspectrum*, 2003, **9**, 366

R 572 T. Schulte-Herbrueggen, 'Imaging Techniques Boost NMR Spectroscopy; How to Remove Zero-Quantum Artifacts', *Angew. Chem. Int. Ed.*, 2003, **42**, 5270

R 573 A. Schulze, 'Creatine Deficiency Syndromes', *Mol. Cell. Biochem.*, 2003, **244**, 143

R 574 H. Schwalbe, 'Kurt Wuethrich, the ETH Zurich, and the Development of NMR Spectroscopy for the Investigation of Structure, Dynamics, and Folding of Proteins', *ChemBioChem*, 2003, **4**, 135

R 575 J. E. Scott, 'Elasticity in Extracellular Matrix 'Shape Modules' of Tendon, Cartilage, *etc.* A Sliding Proteoglycan-Filament Model', *J. Physiol.*, 2003, **553**, 335

R 576 A. A. Shahkhatuni and A. G. Shahkhatuni, 'Determination of the Three-Dimensional Structure for Weakly Aligned Biomolecules by NMR Spectroscopy', *Russ. Chem. Rev.*, 2002, **71**, 1005

R 577 H. Shimizu, 'Studies on Molecular Interactions of Protein and Their Carbohydrate Ligands by NMR', *Trends Glycosci. Glyc.*, 2003, **15**, 221

R 578 Y. Shrot and L. Frydman, 'Ghost-Peak Suppression in Ultrafast Two-Dimensional NMR Spectroscopy', *J. Magn. Reson.*, 2003, **164**, 351

R 579 E. M. V. Silva, 'Advantages and Disadvantages of Nuclear Magnetic Resonance Spectroscopy as a Hyphenated Technique', *Anal. Chim. Acta*, 2003, **497**, 1

R 580 B. Simon and M. Sattler, 'Speeding up Biomolecular NMR Spectros-

copy', *Angew. Chem. Int. Ed.*, 2004, **43**, 782

R 581 P. M. Singer, A. W. Hunt, A. F. Cederstrom and T. Imai, 'What Has NMR Taught Us about Stripes and Inhomogeneity?', *Physica C, (Amsterdam, Netherlands)*, 2003, **388-389**, 209

R 582 I. Smith and R. Baert, 'Medical Diagnosis by High Resolution NMR of Human Specimens', *IUBMB Life*, 2003, **55**, 273

R 583 H. W. Spiess, 'Supramolecular Aspects of Polymer Science: A Challenge for Solid State NMR', *Macromol. Symp.*, 2003, **201**, 85

R 584 K. Srikanth, R. W. Schurko, I. Hung and A. Ramamoorthy, 'Nuclear Magnetic Resonance Studies of Metals in Solid State Non-Metallic Materials', *Mater. Sci. Technol.*, 2003, **19**, 1191

R 585 R. Stolarski, 'Thermodynamics of Specific Protein-RNA Interactions', *Acta Biochim. Pol.*, 2003, **50**, 297

R 586 S. Stramare, V. Thangadurai and W. Wepper, 'Lithium Lanthanum Titanates: A Review', *Chem. Mat.*, 2003, **15**, 3974

R 587 A. Street, 'Developments in Superconducting Magnets for NMR', *Am. Lab.*, 2003, **35**, 28

R 588 E. M. Strehle, 'Sialic Acid Storage Disease and Related Disorders', *Genet. Test.*, 2003, **7**, 113

R 589 C. Stromberger, O. A. Bodamer and S. Stoeckler-Ipsiroglu, 'Clinical Characteristics and Diagnostic Clues in Inborn Errors of Creatine Metabolism', *J. Inherit. Metab. Dis.*, 2003, **26**, 299

R 590 K. Strzalka, A. Kostecka-Gugala and D. Latowski, 'Carotenoids and Environmental Stress in Plants: Significance of Carotenoid-Mediated Modulation of Membrane Physical Properties', *Russ. J. Plant Physiol.*, 2003, **50**, 168

R 591 T. Su and P. C. Taylor, 'Magnetic Resonance Measurements in Hydrogenated Amorphous Silicon', *Sol. Energ. Mat. Sol. C.*, 2003, **78**, 269

R 592 B. H. Suits, A. N. Garroway, J. B. Miller and K. L. Sauer, '^{14}N Magnetic Resonance for Materials Detection in the Field', *Solid State Nucl. Mag. Reson.*, 2003, **24**, 123

R 593 D. I. Svergun and M. H. J. Koch, 'Small-Angle Scattering Studies of Biological Macromolecules in Solution', *Rep. Prog. Phys.*, 2003, **66**, 1735

R 594 E. Sykova, 'Diffusion Parameters of the Extracellular Space', *Israel J. Chem.*, 2003, **43**, 55

R 595 L. K. Tamm, F. Abildgaard, A. Arora, H. Blad and J. H. Bushweller, 'Structure, Dynamics and Function of the Outer Membrane Protein A (OmpA) and Influenza Hemagglutinin Fusion Domain in Detergent Micelles by Solution NMR', *FABS Lett.*, 2003, **555**, 139

R 596 P. C. Taylor, T. Su, P. Hari, E. Ahn, A. Kleinhammes, P. L. Kuhns, W. G. Moulton and N. S. Sullivan, 'Structural and Photostructural Properties of Chalcogenide Glasses: Recent Results from Magnetic Resonance Measurements', *J. Non-Cryst. Solids*, 2003, **326&327**, 193

R 597 S. S. Taylor, J. Yang, J. Wu, N. M. Haste, E. Radzio-Andzelm and G. Anand, 'PKA: A Portrait of Protein Kinase Dynamics', *Biochim. Biophys. Acta*, 2004, **1697**, 259

R 598 L. K. Thompson, 'Unraveling the Secrets of Alzheimer's β-Amyloid Fibrils', *P. Natl. Acad. Sci. U. S. A.*, 2003, **100**, 383

R 599 T. Timusk, 'The Mysterious Pseudogap in High Temperature Superconductors: An Infrared View', *Solid State Commun.*, 2003, **127**, 337

R 600 P. A. Tishmack, D. E. Bugay and S. R. Byrn, 'Solid-State Nuclear Magnetic Resonance Spectroscopy – Pharmaceutical Applications', *J. Pharm. Sci.*, 2003, **92**, 441

R 601 D. A. Torchia and R. Ishima, 'Molecular Structure and Dynamics of Proteins in Solution: Insights Derived from High-Resolution NMR Approaches', *Pure Appl. Chem.*, 2003, **75**, 1371

R 602 J. Torres, T. J. Stevens and M. Samso, 'Membrane Proteins: The 'Wild West' of Structural Biology', *Trends Biochem. Sci.*, 2003, **28**, 137

R 603 S. Tsimikas, 'Noninvasive Imaging of Oxidized Low-Density Lipoprotein in Atherosclerotic Plaques with Tagged Oxidation-Specific Antibodies', *Am. J. Cardiol.*, 2002, **90**, 22L

R 604 R. Turner and T. Jones, 'Techniques for Imaging Neuroscience', *Brit. Med. Bull.*, 2003, **65**, 3

R 605 T. Uchida, S. Takeya, L. D. Wilson, C. A. Tulk, J. A. Ripmeester, J. Nagao, T. Ebinuma and H. Narita, 'Measurements of Physical Properties of Gas Hydrates and in Situ Observations of Formation and Decomposition Processes *via* Raman Spectroscopy and X-Ray Diffraction', *Can. J. Phys.*, 2003, **81**, 351

R 606 J. R. C. Van Der Maarel, 'Thermal Relaxation and Coherence Dynamics of Spin 3/2. Part 1. Static and Fluctuating Quadrupolar Interactions in the Multipole Basis', *Concepts Magn. Reson., A*, 2003, **19A**, 97

R 607 V. Verougstraete, D. Lison and P. Hotz, 'Cadmium, Lung and Prostate Cancer: A Systematic Review of Recent Epidemiological Data', *J. Toxicol.. Env. Heal. B*, 2003, **6**, 227

R 608 C. Vigano, E. Goormaghtigh and J. M. Ruysschaert, 'Detection of Structural and Functional Asymmetries in P-Glycoprotein by Combining Mutagenesis and H/D Exchange Measurements', *Chem. Phys. Lipids*, 2003, **122**, 121

R 609 M. Vijayan, 'Structural Genomics of Microbial Pathogens – an Indian Programme', *Curr. Sci.*, 2003, **85**, 878

R 610 J. Vreede, M. A. Van Der Horst, R. Kort, W. Crielaard and K. J. Hellingwerf, 'Measuring and Modelling Dynamical Changes in the Structure of Photoactive Yellow Protein', *Phase Transit.*, 2004, **77**, 3

R 611 H. S. Waagepetersen, U. Sonnewald and A. Schousboe, 'Compartmentation of Glutamine, Glutamate, and GABA Metabolism in Neurons and Astrocytes: Functional Implications', *Neuroscientist*, 2003, **9**, 398

R 612 G. Wagner, 'NMR Studies on the Basic Pancreatic Tripsin Inhibitor', *Magn. Reson. Chem.*, 2003, **41(Spec. Issue)**, S3

R 613 F. A. Walker, 'Pulsed EPR and NMR Spectroscopy of Paramagnetic Iron Porphyrinates and Related Iron Macrocycles: How to Understand Patterns of Spin Delocalization and Recognize Macrocycle Radicals', *Inorg. Chem.*, 2003, **42**, 4526

R 614 C. Wang, S. Bi and M. Luo, 'Review on the Progress of Analytical Methodologies for Polynuclear Aluminium in Environmental Water Systems', *Rev. Anal. Chem.*, 2003, **22**, 53

R 615 C. Wang and A. G. Palmer III, 'Solution NMR Methods for Quantitative Identification of Chemical Exchange in ^{15}N- Labeled Proteins', *Magn. Reson. Chem.*, 2003, **41**, 866

R 616 W. -q. Wang, L. Wang, J. -f. Wang and Z. -l. Ma, 'Application of ESR and NMR to Investigation of Metallocene Catalyst and Polyolefin', *Bopuxue Zazhi*, 2003, **20**, 187

R 617 W. W. Warren Jr., 'Nuclear Magnetic Resonance in Expanded Fluid Metals', *Z. Phys. Chem., (Muenchen, Germany)*, 2003, **217**, 775

R 618 E. D. Wemmer, 'The Energetics of Structural Change in Maltose-Binding Protein', *P. Natl. Acad. Sci. U. S. A.*, 2003, **100**, 12529

R 619 H. Wennemers, 'Peptide Receptors – from Selective Molecular Recognition towards Catalytic Activity', *Chimia*, 2003, **57**, 237

R 620 A. E. H. Wheatley, 'The Direct Lithiation of Benzenoid Aromatic Systems', *Eur. J. Inorg. Chem.*, 2003, **18**, 3291

R 621 W. Wiechert, 'An Introduction to ^{13}C Metabolic Flux Analysis', *Genet. Eng.*, 2002, **24**, 215

R 622 M. P. Williamson, 'Solving the First Globular Protein Structure: BUSI IIA', *Magn. Reson. Chem.*, 2003, **41(Spec. Issue)**, S64

R 623 I. D. Wilson and U. A. T. Brinkman, 'Hyphenation and Hypernation. The Practice and Prospects of Multiple Hyphenation', *J. Chromatogr., A*, 2003, **1000**, 325

R 624 M. Wind, R. Graf, A. Heuer and H. W. Spiess, 'Structural Relaxation of Polymers at the Glass Transition: Conformational Memory in Poly(n-Alkyl Methacrylates)', *Phys. Rev. Lett.*, 2003, **91**, 155702

R 625 J. -L. Wolfender, K. Ndjoko and K. Hostettmann, 'Liquid Chromatography with Ultraviolet Absorbance-Mass Spectrometric Detection and with Nuclear Magnetic Resonance Spectrometry: A Powerful Combination for the On-Line Structural Investigation of Plant Metabolites', *J. Chromatogr., A*, 2003, **1000**, 437

R 626 P. Workman, 'The Opportunities and Challenges of Personalized Genome-Based Molecular Therapies for Cancer: Targets, Technologies, and Molecular Chaperones', *Cancer Chemoth. Pharm.*, 2003, **52(Suppl. 1)**, S45

R 627 B. Wrakmeyer, J. Weidinger, A. Pedall and W. Milius, 'N-Silylaminotitanium Chlorides – Synthesis, Structures, Multinuclear Magnetic Resonance, and Some Applications', *Z. Anorg. Allg. Chem.*, 2003, **629**, 862

R 628 H. Wu and S. M. King, 'Backbone Dynamics of Dynein Light Chains', *Cell. Motil. Cytoskel.*, 2003, **54**, 267

R 629 Y. Wu and G. A. Voth, 'Computational Studies of Proton Transport through the M2 Channel', *FEBS Lett.*, 2003, **552**, 23

R 630 K. Wuethrich, 'NMR Studies of Structure and Function of Biological Macromolecules (Nobel Lecture)', *Angew. Chem. Int. Ed.*, 2003, **42**, 3340

R 631 K. Wuethrich, 'NMR Studies of Structure and Function of Biological Macromolecules (Nobel Lecture)', *J. Biomol. NMR.*, 2003, **27**, 13

R 632 K. Wuethrich, 'NMR Structures of Biological Macromolecules', *Magn. Reson. Chem.*, 2003,**41(Spec. Issue)**, S89

R 633 K. Wuethrich, 'NOBEL LECTURE: NMR Studies of Structure and Function of Biological Macromolecules', *Biosci. Rep.*, 2003, **23**, 119

R 634 K. Wuethrich and G. Wider, 'Transverse Relaxation-Optimized NMR Spectroscopy with Biomacromolecular Structures in Solution', *Magn. Reson. Chem.*, 2003, **41(Spec. Issue)**, S80

R 635 G. Wulff and K. Knorr, 'Stoichiometric Noncovalent Interaction in Molecular Imprinting', *Bioseparation*, 2001, **10**, 257

R 636 C. Wunderlich and C. Balzer, 'Quantum Measurements and New Concepts for Experiments with Trapped Ions', *Los Alamos National Laboratory, Preprint Archive, Quantum Physics*, Avail. URL: http://xxx. lanl. gov/pdf/quant-ph/0305129

R 637 C. Wunderlich and C. Balzer, 'Quantum Measurements and New Concepts for Experiments with Trapped Ions', *Adv. Atom. Mol. Opt. Phy.*, 2003, **49**, 293

R 638 C. Yamamoto and Y. Okamoto, 'Optically Active Polymers for Chiral Separation', *Bull. Chem. Soc. Jpn.*, 2004, **77**, 227

R 639 S. Yamamoto, 'Recent Progress of the Low-Dimensional Spin-Wave Theory', *Los Alamos National Laboratory, Preprint Archive, Condensed Matter*, Avail. URL: http://xxx. lanl. gov/pdf/cond-mat/0310004

R 640 N. Yamasaki and J. Masamoto, 'Novel Reaction between Cyclic Formal and Ethylene Oxide', *J. Polym. Sci., A*, 2004, **42**, 520

R 641 C. Yang, G. S. Jas and K. Kuczera, 'Structure, Dynamics and Interactions with Kinase Targets: Computer Simulations of Calmodulin', *Biochim. Biophys. Acta*, 2004, **1697**, 289

R 642 X. Yang, T. Gegan, G. Hodge, G. Munzing and D. Pollick, 'PM Homogeneous Catalyst Characterization Using Advanced Analytical Techniques', *Precious Metals* [computer optical disk], 2002, **26**, 84

R 643 J. Yao, Y. Nakazawa and T. Asukara, 'Structure of Bombyx Mori and Samia Cynthia Ricini Silk Fibroins Studied with Solid-State NMR', *Biomacromolecules*, 2004, **5**, 680

R 644 N. Yao, Z. Hong and J. Y. N. Lau, 'Application of Structural Biology Tools in the Study of Viral Hepatitis and the Design of Antiviral Therapy', *Gastroenterology*, 2002, **123**, 1350

R 645 L. Zeng, C. H. Chen, M. Muller and M. -M. Zhou, 'Structure-Based Rational Design of Chemical Ligands for AMPA-Subtype Glutamate Receptors', *J. Mol. Neurosci.*, 2003, **20**, 345

R 646 S. Zhou, 'Separation and Detection Methods for Covalent Drug-Protein Adducts', *J. Chromatogr., B*, 2003, **797**, 63

R 647 I. Zhukov and A. Ejchart, 'NMR Spectroscopy in Structural Proteomics. NMR-Based Protein Structure Determination', *Polimery (Warsaw, Poland)*, 2003, **48**, 28

R 648 H. Ziegler, J. Benet-Buchholz, W. Etzel and H. Gayer, 'Trifloxystrobin –

A New Strobilurin Fungicide with an Outstanding Biological Activity', *Pflanzenschutz-Nachrichten Bayer (German Edition)*, 2003, **56**, 213

5 Reviews and Books in Foreign Languages

Czech

R 649 P. Cejnar, 'Quantum Calculations with Nuclear Spins', *Ceskoslovensky Casopis pro Fysiku*, 2002, **52**, 263

Chinese

R 650 J. -Y. Chen, H. Zhang, W. -S. Xiao, K. -N. Weng, H. -F. Zheng and Y. -S. Zeng, 'Review of Diamond Anvil Cell for in-Situ High-Temperature and High-Pressure Spectroscopic Study', *Guangpu Shiyanshi*, 2004, **21**, 209

R 651 Y. -h. Fang, 'Principles of High Resolution Solid-State Nuclear Magnetic Resonance and Its Application in Research of Cement Chemistry', *Jianzhu Cailiao Xuebao*, 2003, **6**, 54

R 652 R. Feng, H. Xie and D. -z. Ren, 'Application of Cryogenic NMR Probes', *Bopuxue Zazhi*, 2002, **19**, 447

R 653 I. Green, 'LC-UV-NMR-MS: Information-Rich Separations', *Bopuxue Zazhi*, 2003, **20**, 429

R 654 M. -f. Jeng, 'NMR Spectroscopy and Protein Structure Determination', *Huaxue*, 2003, **61**, 267

R 655 X. Jiang and G. Ji, 'Two Important Frontiers of Physical Organic Chemistry: Aggregation of Organic Molecules and Radical Chemistry', *Huaxue Tongbao*, 2003, **66**, 147

R 656 G. Jin, S. Li, Z. Niu, F. Yang and S. Feng, 'Solid-State Quantum Computing', *Wuli*, 2002, **31**, 773

R 657 W. Ka, 'Medical Physics: The Application of Physics to Medicine', *Wuli*, 2002, **31**, 400

R 658 H. Lei, 'Magnetic Resonance Molecular Imaging Techniques', *Bopuxue Zazhi*, 2003, **20**, 173

R 659 C. -y. Liao, B. -y. Li, M. -j. Zhang and Z. -l. Li, 'Combinatorial Chemistry as an Efficient Technique for Drug Innovation', *Chongqing Daxae Xuebao, Ziran Kexueban*, 2003, **26**, 80

R 660 Q. Liu, L. Tan, Y. Bai, H. Liang and Y. Zhao, 'General Situation of Study on Saponins in Bupleurum Sp. in Recent 10 Years', *Zhongguo Zhongyao Zazhi*, 2002, **27**, 7

R 661 S. -Z. Mao and Y. -R. Du, '^{1}H NMR Studies of Surfactants in Aqueous Solutions', *Wuli Huaxue Xuebao*, 2003, **19**, 675

R 662 X. -a. Mao, 'Outline of NMR Studies of DNA', *Bopuxue Zazhi*, 2003, **20**, 75

R 663 D. Si and D. Zhong, 'Application of Liquid Chromatography-Spectroscopy Coupled Techniques to the Chemical Screening of Natural Products', *Yaoxue Xuebao*, 2002, **37**, 485

R 664 Q. Tian, L. Zhang and M. Cheng, 'Applications and Progress of the NMR

Technique in Solid Phase Synthesis', *Shenyang Yaoke Daxue Xuebao*, 2002, **19**, 221

R 665 D. -x. Wei, X. -d. Yang, J. Luo, X. -p. Sun, X. -z. Zeng, M. -l. Liu and S. -w. Ding, 'Realization of Seven-Qubit Deutsch-Jozsa Algorithm on NMR Quantum Computer', *Yuanzihe Wuli Pinglun*, 2002, **19**, 278

R 666 L. -c. Wu, A. -f. Yu and L. -b. Chen, 'Differentiated Quantitative Analysis of Hydroxyl Groups', *Guangzhou Huaxue*, 2003, **28**, 46

R 667 D. Xiao, 'DEPT and Various 2D NMR Techniques, the Effective Strategies for Identification of Structures of Natural Products', *Tianran Chanwu Yanjiu Yu Kaifa*, 2002, **14**, 75

R 668 J. -h. Yang, Y. -m. Du and C. -q. Qin, 'Application of IR and NMR Spectroscopy in Structural Characterization of Chitin and Chitosan', *Fenxi Kexue Xuebao*, 2003, **19**, 282

R 669 X. Yang, F. Zhang, X. Wang, N. Gan, G. Zou and S. Bi, 'Novel Analytical Techniques for Fractionation and Speciation of Aluminium(III) in Environmental and Biological Systems', *Fenxi Huaxue*, 2003, **31**, 1131

R 670 Z. Yuan and X. Li, 'NMR Methods for Determining the Configuration of 8-O-4' Neolignans', *Bopuxue Zazhi*, 2003, **20**, 307

R 671 H. -c. Zhang, X. -p. Xuan, J. -j. Wang and H. -q. Wang, 'Progress on the Determination of Ionic Transference Numbers in Polymer Electrolytes', *Dianyuan Jishu*, 2003, **27**, 54

R 672 Y. Zheng and F. Wu, 'Advanced Studies on Fingerprint Chromatogram of Traditional Chinese Medicine', *Tianran Chanwu Yanjiu Yu Kaifa*, 2003, **15**, 55

R 673 D. Zhou, L. Li and F. Li, 'Analytical Methodology for Drug-Protein Binding Studies', *Sepu*, 2004, **22**, 116

Danish

R 674 C. Cornett, 'NMR Titration', *Dansk Kemi*, 2003, **84**, 35

French

R 675 S. Akoka and G. Remaud, 'NMR and Isotopic Analyses', *Actualite Chimique*, 2003, **8-9**, 18

R 676 G. Calderone, C. Guillou and N. Naulet, 'Official Methods Based on Stable Isotope Techniques in Food Analysis. Ten Years of European Experience', *Actualite Chimique*, 2003, **8-9**, 22

R 677 S. Godefroy, M. Fleury and J. -P. Korb, 'NMR Study of the Dynamics of Molecules at Liquid-Solid Interfaces', *Petrole et Techniques*, 2003, **443**, 25

R 678 C. Lamoureux, 'Isotopic Analyses at the Customs Laboratory', *Actualite Chimique*, 2003, **8-9**, 31

R 679 B. Leclaire and J. -Y. Lallemand, 'Genetic Diseases: On the Possibilities of Drug Treatments? An Example: Cystic Fibrosis', *Actualite Chimique*, 2003, **4-5**, 97

R 680 M. L. Martin and G. J. Martin, 'Isotope Fingerprinting: Tracing the Origin of Products', *Comptes Rendus de l'Academie d'Agriculture de France*, 2001, **87**, 41

R 681 R. L. McGreevy, 'Modeling by Reverse Monte Carlo (RMC)', *Journal de Physique IV: Proceedings*, 2003, **111**, 347
R 682 F. Moureau, 'The Impact of Molecular Modeling in Rational Drug Design', *Chimie Nouvelle*, 2003, **21**, 86
R 683 D. H. Powell, 'The Structure of Aqueous Solutions', *Journal de Physique IV: Proceedings*, 2003, **111**, 167

German
R 684 D. Bakowies, 'Biomolecular Reality Simulations', *Nachrichten aus der Chemie*, 2003, **51**, 788
R 685 M. Bauser, H. Beck, J. Koebberling, U. Krenz and U. Rosentreter, 'Parallelization in Medicinal Chemistry', *Nachrichten aus der Chemie*, 2003, **51**, 1314
R 686 J. Deberitz and G. Boche, 'Industrial, Medicinal and Scientific Importance. Lithium and Its Compounds', *Chemie in Unserer Zeit*, 2003, **37**, 258
R 687 A. Pieper, R. Vogt, H. Wichmann and M. Bahadir, 'Synthesis and Levels of Polychlorinated Terphenyl (PCT) by Thermal Load', *Mitteilungen der Fachgruppe Umweltchemie und Oekotoxikologie*, 2003, **9**, 6
R 688 M. Regier, K. Knoerzer and G. G. Badolato, 'Applications of Magnetic Resonance for Investigating Water, Temperature, and Pore Distribution in Food Process Engineering', *Chemie Ingenieur Technik*, 2004, **76**, 433
R 689 A. Schaeffer, A. Hoellrigl-Rosta, W. Koerdel and K. Haider, 'The Impact of Pesticides in Soil', *Wasser & Boden*, 2003, **55**, 77
R 690 U. Scheler, 'NMR in Polymer Analysis', *Nachrichten aus der Chemie*,2004, **52**, 386
R 691 R. Suessmuth, 'Biosynthesis', *Nachrichten aus der Chemie*, 2004, **52**, 286
R 692 C. -W. von der Lieth, A. Bohne-Lang and K. K. Lohmann, 'Databases and Bioinformatic Tools for Glycobiology', *BIOspektrum*, 2003, **9**, 635

Greek
R 693 G. Paraskevas, J. Atta-Politou and M. Koupparis, 'Lisinopril – Short Review' *Pharmakeutike*, 2002, **15**, 97

Hungarian
R 694 L. Ettre, 'Where is Chromatography Going?', *Magyar Kemikusok Lapja*, 2003, **58**, 224

Italian
R 695 M. Barbieri, 'Solid-State NMR Spectroscopy', *Laboratorio 2000*, 2002, **16**, 28

Japanese
R 696 K. Akasaka, 'NMR Technologies for Protein Structural Analysis in Aqueous Solution', *Kagaku (Tokyo, Japan)*, 2003, **73**, 74
R 697 H. Akutsu, 'Molecular Miscibility in the Two-Dimensional Solvent of Lipid Bilayer Studied by Solid-State NMR; Molecular Mechanism of the

Microdomain (Raft) Format in the Cell Membranes', *Maku*, 2003, **28**, 102

R 698 H. Akutsu, 'Protein Analytical Method: Development of NMR', *Gendai Kagaku*, 2003, **387**, 12

R 699 F. Amita and O. Kajimoto, 'A Prototype NMR Apparatus for Supercritical Water and Its Technology', *Chorinkai Saishin Gijutsu*, 2003, **7**, 5

R 700 I. Ando, Y. Yamane, S. Koizumi, M. Matsui and S. Kuroki, 'NMR Methods for Characterizing Nano-Scale Structure and Dynamics of Soft and Hard Polymers', *Journal of Ion Exchange*, 2003, **14**, 87

R 701 T. Asakura, 'Structure of Silks Determined with Solid-State NMR and Development of New Silk-Like Materials', *Seibutsu Butsuri*, 2003, **43**, 281

R 702 N. Fujitake, 'Recent Trend and View of Studies on Humic Substances in Japan. 3. Techniques for Humic Substances Analysis and Perspective Techniques in the Future', *Nippon Dojo Hiryogaku Zasshi*, 2003, **74**, 223

R 703 K. Fujiwara, Y. Shimaoka and T. Kobayashi, 'High-Pressure NMR Study of Heavy Fermion Spinel LiV_2O_4', *Koatsuryoku no Kagaku to Gijutsu*, 2003, **13**, 314

R 704 N. Fujiwara, N. Mori, M. Uedoko, T. Matsumoto, N. Motoyama and S. Uchida, 'New Development in NMR Measurement Technology: Research on Pressure Induced Superconductivity under 4Gpa Class Pressure', *JAERI – Conf.*, 2004,2003-21,199

R 705 Y. Fukuzawa, 'Searching for Structure of Supramolecules Using NMR Chemical Shift', *Sentan Kagaku Shirizu*, 2003, **3**, 61

R 706 H. Gouda and S. Hirono, 'Rational Procedure for 3D-QSAR Analysis Using NMR Experiments and Computational Methods', *Bunseki*, 2003, **6**, 294

R 707 M. Hattori, 'Development of Automatic Super Polarized Xenon Gas Preparation Apparatus', *AIST Today (Japanese Edition)*, 2003, **3**, 22

R 708 K. Hayamizu, 'Motions and Diffusion of Ions in Polymer Electrolytes Observed by NMR Spectroscopy', *Nippon Gomu Kyokaishi*, 2003, **76**, 324

R 709 H. Hayashi, 'Fundamentals of Spin Chemistry and Applications of Strong Magnetic Fields', *Teion Kogaku*, 2003, **38**, 530

R 710 K. Hiraoka, 'NMR and NQR Studies of Rare-Earth Compound $YbInCu_4$ under High Pressure', *Koatsuryoku no Kagaku to Gijutsu*, 2003, **13**, 310

R 711 K. Hirayama and H. Miyano, 'Metabolome Analysis by FTICRMS and NMR', *Ensho to Men'eki*, 2003, **11**, 680

R 712 M. Ida, K. Nakamura, T. Arai and T. Tokuyama, 'Clinical Usefulness of Proton MR Spectroscopy (^{1}H-MRS) in Diagnosis Based on NMR Imaging of Diseases of Central Nervous System', *Brain and Nerve*, 2002, **54**, 935

R 713 R. Ikeda and S. Takeda, 'Solid NMR of Polynuclear Metal Complexes', *Shusekigata Kinzoku Sakutai no Kagaku*, ed. H. Okawa and T. Ito, Kagaku Dojin, Kyoto, Japan, 2003, p. 173

R 714 K. Ishida, T. Kato, M. Murakami, M. Watanabe and M. F. Watanabe, 'Microginins, Zinc Matalloproteases Inhibitors from the Cyanobacterium Microcystic Aeruginosa', *Tennen Yuki Kagobutsu Toronkai Koen*

Yoshishu, 2001, **43**, 395

R 715 T. Ito, I. Ibrahim, T. Tanaka, K. -i. Nakaya, M. Iinuma, Y. Takahashi, H. Naganawa, Y. Akao, Y. Nozawa, M. Ohyama, Y. Nakanishi, K. F. Bastow and K. -H. Lee, 'Chemical Constituents of Dipterocarpaceaeous and Gnataceaeous Plants and Their Biological Activities', *Tennen Yuki Kagobutsu Toronkai Koen Yoshishu*, 2001, **43**, 449

R 716 Y. Ito, T. Kigawa, M. Shirouzo and S. Yokoyama, 'Stable Isotope-Labeling of Proteins for NMR Analysis', *Posutoshikuensu Tanpakushitsu Jikkenho*, 2002, **2**, 153, ed. T. Oshima, Tokyo Kagaku Dojin, Tokyo, Japan

R 717 Y. Iwasaki, 'Nuclear Magnetic Resonance', *Bosei Kanri*, 2003, **47**, 388

R 718 S. Kajiyama, M. Yagi, T. Kurihura, A. Okazawa, E. -i. Fukusaki and A. Kobayashi, 'Structure of Hetero Polysaccharide from Desiccation-Tolerant Terrestrial Cyanobacterium Nostoc Commune', *Tennen Yuki Kagobutsu Toronkai Koen Yoshishu*, 2001, **43**, 193

R 719 J. Kawabata and E. Fukushi, 'Aiming at "Practical" Carbon-Carbon Correlation NMR Method', *Kagaku to Seibutsu*, 2003, **41**, 586

R 720 G. Kawai, 'RNA Structure', *RNA ga Wakaru*, ed. Y. Nakamura, Yodosha, Tokyo, Japan, Color Plates, 83-91, 11, 2, 2003

R 721 M. Kitagawa, 'Quantum Computer from Molecule', *Kino Zairyo*, 2003, **23**, 14

R 722 T. Machida, T. Yamazaki, K. Ikushima and S. Komiyama, 'Electrical Manipulation of Nuclear Spins in Semiconductors', *Kotai Butsuri*, 2003, **38**, 791

R 723 S. Maeda, T. Mori, H. Kunimoto and C. Sasaki, 'Molecular Structural Analysis of Poly(ε-Lysine) Derived from Streptomyces', *Kobunshi Kako*, 2003, **52**, 516

R 724 N. Matsubayashi and M. Nakahara, 'NMR Study of the Structure and Dynamics of Supercritical Water', *Koatsuryoku no Kagaku to Gijutsu*, 2003, **13**, 320

R 725 I. Matsuo and Y. Ito, 'Toward Understanding Glycoprotein Quality Control through Chemical Synthesis', *Nippon Nogei Kagaku Kaishi*, 2003, **77**, 983

R 726 S. Matsuoka, N. Matsumori, N. Yamaji, N. Eiraku, T. Oishi and M. Murata, 'Structures and Ion Channel-Formation Activity of Amphotericin-B Conjugates', *Tennen Yuki Kagobutsu Toronkai Koen Yoshishu*, 2001, **43**, 611

R 727 M. Mishima, 'Direct Measurement of Hydrogen Bonds with Multidimensional NMR', *Seibutsu Kagaku Kaishi*, 2003, **81**, 142

R 728 K. Miyamoto, 'Structures of Peptides Related to the Inactivation Gate on Sodium Channels', *Yakugaku Zasshi*, 2002, **122**, 1123

R 729 H. Mokuno, 'Small, Dense LDL and Oxidative Stress', *Kekkan Igaku*, 2003, **4**, 538

R 730 M. Murata, 'Role of NMR in Organic Chemistry', *Nippon Bunko Gakkai Sokuteiho Shirizu*, 2003, **41**, 193

R 731 M. Murata, 'Technology Progress of NMR and Marine Natural Prod-

ucts', *Sentan Kagaku Shirizu*, 2003, **5**, 50
R 732 A. Nagadoi and Y. Nishimura, 'Development of Structural Biology and Protein NMR Analysis', *Nippon Bunko Gakkai Sokuteiho Shirizu*, 2003, **41**, 207
R 733 M. Nakahara, 'The Structure and Properties of Supercritical Water', *Netsu Sokutei*, 2004, **31**, 14
R 734 O. Nakamura, 'Asymmetric Synthesis with Cation-π Interaction', *Kagaku (Kyoto, Japan)*, 2003, **58**, 48
R 735 M. Nakata, 'Magnetic Resonance Spectra', *Gendai Kagaku*, 2004, **394**, 56
R 736 M. Nakata, 'NMR Spectroscopy', *Gendai Kagaku*, 2004, **395**, 56
R 737 N. Niimura, 'Analytical Methods for Coating Films and Their Characteristics. Structural Analysis of Urushi Film as an Example', *Kogyo Toso*, 2003, **185**, 64
R 738 Y. Nishimura, 'Application Development of NMR', *Nippon Bunko Gakkai Sokuteiho Shirizu*, 2003, **41**, 153
R 739 T. Noguchi and H. Iwabuki, 'Recent Studies on Crosslinked Rubbers by Pulsed NMR', *Nippon Gomu Kyokaishi*, 2003, **76**, 178
R 740 Y. Nosaka, 'Behavior of Chemical Species in Photocatalytic Reaction at the Surface of Titanium Oxides', *Kokagaku*, 2003, **34**, 14
R 741 T. Ohara, 'Assessment of Insulin Resistance by NMR', *Bunshi Tonyobyogaku no Shinpo*, 2003, p. 91
R 742 T. Ohkura and A. Kameyama, 'Overview of Current Status and Future Prospects of Structural Analysis of Glycans in Glyco-Biology', *Bio Industry*, 2003, **20**, 18
R 743 M. Ohnishi, 'Analysis of Protein Structure: Its Present Status and Future Prospect', *Bunseki*, 2003, **4**, 189
R 744 E. Okamura, 'Structure and Dynamics of Drugs in Lipid Bilayer Membranes: An NMR Application to Drug Delivery Study', *Maku*, 2003, **28**, 111
R 745 T. Okino, 'Structure Determination of Neuroactive Substances Derived from Cyanobacteria', *Kagaku to Seibutsu*, 2003, **41**, 517
R 746 H. Saito, 'Membrane Structure Modulates the Function of Apolipoproteins', *Maku*, 2002, **27**, 317
R 747 K. Saito, 'Industrial Application of NMR Techniques to Steelmaking Process and Related Materials', *Feramu*, 2003, **8**, 747
R 748 K. Saito, 'NMR Imaging Technology and Its Application', *Interijento Zairyo, Gijutsu no Saishin Kaihatsu Doko*, Shi Emu Shi Shuppan, Tokyo, Japan, 2003, p. 214
R 749 K. Saito, 'Voids Analysis for Porous Materials Using Advanced NMR Technology', *Materia*, 2004, **43**, 206
R 750 Y. Sakaguchi, K. Kawara and S. Imabashi, 'NMR and ATR FT-IR Analysis of Photocuring Process of Flexog. Printing Plates', *Kobunshi Kako*, 2004, **53**, 122
R 751 S. Sasaki and K. M. Itoh, 'Si Nuclear-Spin Quantum Coherence in Silicon Crystal', *Kotai Butsuri*, 2003, **38**, 801
R 752 E. Suzuki, 'Fundamental Role as Analytical Sciences', *Nippon Bunko*

Gakkai Sokuteiho Shirizu, 2003, **41**, 161

R 753 E. Suzuki, 'NMR Analyses of Crystal and Non-Crystal Solid Samples and in Vivo NMR Analysis of the Biological System', *Nippon Bunko Gakkai Sokuteiho Shirizu*, 2003, **41**, 235

R 754 J. Suzuki, K. Furutoh and M. Nishikibe, 'A New System Using NMR Technology for Measurement of Body Composition in Experimental Animals', *Nippon Yakurigaku Zasshi*, 2004, **123**, 281

R 755 Y. Suzuki, O. Aiko, S. Kenji, K. -i. Takao and K. -i. Tadano, 'Total Synthesis of Mniopetals', *Tennen Yuki Kagobutsu Toronkai Koen Yoshishu*, 2001, **43**, 67

R 756 Y. Takao, 'Observation of Dynamic Behaviors of Coordination Compounds by NMR Spectrometry', *Kagaku to Kogyo (Osaka, Japan)*, 2003, **77**, 644

R 757 H. Takeuchi, 'Molecular Structure and Internal Rotation Potential of Liquid Crystal by Liquid Crystal NMR', *Ekisho*, 2002, **6**, 376

R 758 S. Tanaka, Y. Kobashigawa, K. Miura, Y. Nishimiya, A. Miura and S. Tsuda, 'Antifreeze Protein', *Seibutsu Butsuri*, 2003, **43**, 130

R 759 Y. Tanaka, 'Spectroscopic Analyses of the Interaction between Hammerhead Ribozymes and Metal Ions', *Yakugaku Zasshi*, 2003, **123**, 305

R 760 Y. Taniguchi and N. Takeda, 'New Frontier for High-Pressure Biochemistry', *Koatsuryoku no Kagaku to Gijutsu*, 2003, **13**, 127

R 761 S. Tashiro, 'Analysis of Biomacromolecules Using Nuclear Magnetic Resonance Spectroscopy', *Bunseki*, 2003, **9**, 513

R 762 K. Tatsumi, 'Contact Point with Inorganic Chemistry', *Sentan Kagaku Shirizu*, 2003, **1**, 9

R 763 T. Toida, 'Methods of Sugar Chain Analysis Toward Glycome-Function Analysis', *Farumashia*, 2004, **40**, 313

R 764 M. Tsuboi, 'Formation of the Phage fd Capsid Protein Complex', *Gendai Kagaku*, 2004, **395**, 62

R 765 Y. Tsuji, 'Studies on Supramolecular Transition Metal Catalysis', *Asahi Garasu Zaidan Josei Kenkyu Seika Hokoku*, 2003, Avail. URL: http://www. af-info. or. jp/jpn/subsidy/report2/2003/body/03A-B07-P025. TXT

R 766 M. Umeda and T. Tanaka, 'Application of MRS Technology to Diagnoses in Nervous System', *Annual Review Shinkei*, 2003,32

R 767 T. Wada and M. Sekine, 'A Novel Method for Oligonucleotide Synthesis on the Basis of Chemoselective Phospholynation', *Yuki Gosei Kagaku Kyokaishi*, 2003, **61**, 961

R 768 T. Watanabe, 'Freezing and Thawing of Polysaccharide/Water Base Materials', *Kobunshi Kako*, 2003, **52**, 418

R 769 T. Watanabe, M. Tanaka, K. Watanabe, Y. Takamatsu and A. Tobe, 'Research and Development of the Free Radical Scavenger Edaravone as a Neuroprotectant', *Yakugaku Zasshi*, 2004, **124**, 99

R 770 Y. Yamaguchi and K. Kato, 'Stable-Isotope-Assisted NMR Analyses of Glycans', *Tanpakushitsu Kakusan Koso*, 2003, **48**, 1184

R 771 S. Yamamoto, 'Recent Progress of the Low-Dimensional Spin-Wave

Theory', *Kotai Butsuri*, 2003, **38**, 332

R 772 T. Yamamoto and K. Gekko, 'Study on Flexibility of Protein by Mass Spectrometry', *Journal of the Mass Spectrometry Society of Japan*, 2003, **51**, 412

R 773 H. Yamazawa, M. Yamamoto, T. Ando, S. Wakamura and N. Arakaki, 'Novel Epoxy Compounds: Sex Pheromones Secreted by Lymantriid Moths', *Tennen Yuki Kagobutsu Toronkai Koen Yoshishu*, 2001, **43**, 91

R 774 T. Yoshida, 'Structure and Function of Ribosome Recycling Factor (RRF)', *Seibutsu Kogaku Kaishi*, 2003, **81**, 150

R 775 K. Yoshimura, 'Magnetism and Superconductivity of Pyrochlore Type 4d and 5d Transition Metal Oxides', *JAERI – Conf.*, 2004,2003-21,346

Polish

R 776 K. Mojsiewicz-Pienkowska and J. Lukasiak, 'Poly(dimethylsiloxanes) in the Human Environment', *Polimery (Warsaw, Poland)*, 2003, **48**, 403

R 777 J. Przygorzewska, P. Rakoczy and G. Rokicki, 'Calix[4]arene-Based Chromoionophores', *Wiadomosci Chemiczne*, 2003, **57**, 43

Portuguese

R 778 M. *E. G.* Porto and A. A. de Sousa, 'Molecular Motions in Liquids Studied by Nuclear Spin Relaxation and Dielectric Relaxation', *Anais da Associacao Brasileira de Quimica*, 2002, **51**, 113

Rumanian

R 779 C. Andrei and C. Moise, 'Flavonoids. II. Research Methods', *Materiale Plastice (Bucharest, Romania)*, 2003, **40**, 53

Russian

R 780 V. L. Antonovskii and S. L. Khursan, 'Association and Complex Formation of Hydroperoxides in Solution', *Khimicheskaya Fizika*, 2003, **22**, 32

R 781 I. S. Dzhafarov, S. F. Khafizov and P. E. Syngaevsky, 'Permeability Appraisal Models Based on Strong Magnetic Field Nuclear Magnetic Resonance Logs', *Neftyanoe Khozyaistvo*, 2002, **12**, 32

R 782 A. N. Gafarov, G. T. Shakirova and Yu. B. Baranova, 'Effect of Structural Factors on IR, UV, and ^{1}H NMR Spectra of Aliphatic Amines, Hydrazones, Azides, and Nitramines', *Sovremennye Problemy Tekhnicheskoi Khimii, Matarialy Dokladov Vserossiiskoi Nauchno-Tekhnicheskoi Konferentsii, Kazan, Russian Federation, Sept. 26-28, 2002*, 2002,1,223, Izdatel'stvo Kazanskogo Gosudarstviennogo Tekhnologicheskogo Universiteta, Kazan, Russia.

Slovak

R 783 R. Cizmarikova, J. Valentova and J. A. Hutta, 'Beta-Adrenergic Receptor Blockers – a Group of Chiral Drugs: Enantioseparation in the Group of β-Blockers', *Ceska a Slovenska Farmacie*, 2004, **53**, 9

Slovenian

R 784 A. Demsar, J. Kosmrlj and S. Petricek, 'Modification of the Binding of Carboxylate Ligand in Zinc Carboxylate Solutions', *Zbornik Referatov s Posvetovanja Slovenski Kemijski Dnevi, Maribor, Slovenia, Sept. 26-27, 2002*, Part 2, p. 716, ed. P. Glavic and D. Brodnjak-Voncina, Univerza v Mariboru, Fakulteta za Kemijo in Kemijsko Tehnologijo, Maribor, Slovenia, 2002

Spanish

R 785 F. del Rio Portilla, 'Structural Analysis of Proteins by Nuclear Magnetic Resonance and Mass Spectrometry', *Educacion Quimica*, 2003, **14**, 9

R 786 G. G. Gallego, 'Revolutionary Methods for the Analysis of Macromolecules', *Anales de la Real Academia Nacional de Farmacia*, 2003, **69**, 71

R 787 J. M. Natta and M. Gari, 'Contribution of Isotopic Methods (^{2}H-NMR and ^{13}C-MS) to the Alcoholic Beverage Industry for Confirming Brandy Authenticity', *Alimentacion, Equipos y Tecnologia*, 2003, **183**, 47

2
Theoretical and Physical Aspects of Nuclear Shielding

BY CYNTHIA J. JAMESON AND ANGEL C. DE DIOS

1 Theoretical Aspects of Nuclear Shielding

1.1 General Theory. – Although the computational cost in calculating explicitly the small components still limits its application to small molecules, rigorous relativistic treatment of properties depending on the electronic density near the nucleus (such as nuclear magnetic shielding and spin spin coupling) in molecules should be based on the four-component Dirac theory. Recently a number of computational codes for the fully relativistic calculation of both electronic structure and molecular properties have become available. Pioneering work on shielding and spin-spin coupling at the four component level was published in 1983 by Pyper[1] and by Pyykkö[2] using a sum-over states perturbation formulation. In 1993, Aucar and Oddershede developed a full-relativistic scheme to calculate magnetic molecular properties within response theory.[3] Their relativistic polarization propagator approach was shown to be a natural extension of its non-relativistic counterpart. The non-relativistic limit of a given molecular property is reached by considering the corresponding limit of the property matrix elements and the principal propagator separately. They explicitly applied this procedure to the magnetic field interaction operator. However, it was not until late 1997 that the numerical results from first four-component calculations of magnetic properties making use of this formalism started to appear, as the program package DIRAC,[4] a relativistic *ab initio* electronic structure program using analytic response theory for evaluation of molecular properties, started to produce results. DIRAC, now available in a more recent version DIRAC (2000), was used in the calculations of the electric field gradients at the nuclei in hydrogen halides.[5] At about the same time, Nakatsuji and co-workers, who had been doing the more approximate quasi-relativistic calculations earlier, published the first of their calculations of shielding using four-component wavefunctions in molecules,[6,7] using a finite perturbation approach which has the advantage of having no (positron-like) negative energy states appearing explicitly in the evaluation of the shielding. The origin and contribution of the diamagnetic term in shielding in four-component relativistic calculations of magnetic properties have been discovered.[8] When a magnetic field is applied to a molecular system, the electronic spinors are modified in such a way that contributions from

Nuclear Magnetic Resonance, Volume 34
© The Royal Society of Chemistry, 2005

positronic spinors should be considered in calculating the response of the system to the external field. Thereafter, full four-component relativistic calculations of shielding and spin-spin coupling tensors in hydrogen halides could be carried out with the DIRAC suite.[9] These calculations (Dirac-Fock) are the four-component relativistic equivalent of the Hartree-Fock method. Here the one-electron part of the Hamiltonian is given by the relativistic Dirac Hamiltonian while the electron-electron interaction is represented by the full Breit interaction, as in the calculations by Ishikawa *et al.*[6,7] or else by the non-relativistic instantaneous Coulomb interaction, as in the calculations by Visscher *et al.*[5,8,9] The calculations by Ishikawa *et al.*[6] showed that the effect of the Breit interaction (the terms DS-II, ROO, OP-II, and OP-IV defined by Fukui *et al.*) reduces the shielding by less than 0.2% for their heaviest atom (Xe). In the work by the Scandinavian groups, when the Dirac-Fock wavefunction has been obtained, the effect of additional interaction terms in the Hamiltonian are considered by using response theory (a relativistic generalization of the RPA method) where the effect of two perturbing magnetic field operators then permits the calculations of both shielding and spin-spin coupling tensors as zero frequency linear response functions (operators given in their second quantized form), as in Ref. 5, 8, and 9. Sometimes an isotropic Gaussian charge distribution is used to model the finite size of the nuclei in the calculation of the electrostatic electron-nucleus interaction integrals,[10] but for the interaction with the magnetic moment of the nuclei, the nucleus is modeled as a point dipole.[5,8,9] These were followed in the past few years by applications of the finite perturbation method of the Japanese group (Nakatsuji *et al.*) and the relativistic random phase approximation approach of the Scandinavian groups (Jensen *et al.*) to shielding and spin spin couplings, which have been reviewed in this Series.[7,11,12] The most recent applications, in this reporting period, of fully relativistic calculations are in shieldings of rare gas atoms He to Xe in the complete basis set limit,[10] and shieldings and spin-spin couplings of hydrides of group-15 and group-16.[13] Any molecule containing at least one heavy atom may be expected to require a fully relativistic treatment of the NMR parameters: shielding, spin-spin coupling and electric field gradient at the nucleus, for even the light nuclei such as H due to the presence of 'direct' (referred to as 'active', in some papers) and 'indirect' (referred to as 'passive', in some papers) terms.

Some of the important conclusions from four-component calculations are the following:

(1) Both paramagnetic and diamagnetic terms in non-relativistic formalisms are obtained from a single operator in the full relativistic theory. This means that separation into two parts arises from manipulation. The non-relativistic diamagnetic contribution appears naturally for one-electron systems when the magnetic interaction is included from the outset in the Dirac equation.[8] On the other hand, considering electronic and positronic one-electron states obtained for the system in absence of a magnetic field, the non-relativistic diamagnetic contribution appears in perturbation theory if, and only if, the positronic states are taken into account (the (e-p) excitations), as previously shown by the pioneering work of Pyykkö.[2] The fully relativistic second-order energy correction for one-electron

systems shows that it can be divided into three terms. diamagnetic-like, paramagnetic-like, both of which are completely in terms of electronic spinors, and the third term which vanishes when c approaches infinity includes positronic spinors explicitly. The positronic contributions are meant to obtain full relaxation of the reference electronic state to the effect of the perturbation.[8]

(2) The decomposition of the full relativistic value into the electron-like (e-e) excitations and positron-like excitations (e-p) shows clearly that for the rare gas atoms, the (e-e) contributions that are absent in non-relativistic theory are not negligible even from Ne and contribute up to 56% of the total σ in Rn.[10]

(3) In order to save time in molecular applications of the four-component theory, the (e-p) branch of the linear response function has sometimes been approximated by the computationally much more expedient expectation value of the corresponding non-relativistic diamagnetic operator, taken in the relativistic reference state.[8,9,12] This is a good approximation for the spin-spin coupling for which the diamagnetic contribution is quite small, but the diamagnetic contribution is quite important for the shielding. It has been shown by Vaara and Pyykkö[10] that taking this diamagnetic approximation for the (e-p) contributions overestimates the results significantly, as much as by 1000 ppm for Xe.

(4) Additional high-angular momentum, high-exponent functions are found necessary to saturate the basis set,[10] else the calculated shieldings in the four-component calculations lead to underestimates, for example, by 389 ppm for Xe (in the comparison between Ref. 6 and 10). Extension of the basis set with tight functions improves the convergence, as can be expected given the r^{-3} dependence of the operator. Basis set differences may largely be responsible for the differences between two sets of four component relativistic calculations of heavy atom shieldings in H_2O, H_2S, H_2Se, H_2Te, (329.7, 326.7), (750.0, 783.5), (2422.0, 2681.8) and (4769.4, 5638.8) all in ppm, by Ref. 11 and Ref.14, respectively.

(5) Relativistic effects on the heavy atom isotropic shielding increase roughly in proportion to Z^3, with the mass correction (MC) mechanism and the spin-orbit (SO) mechanism both contributing, for the hydrides of the group-15 and -16.[14] SO gives only a part of the relativistic corrections for the heavy atom, the scalar relativistic terms need to be included. The mass correction (MC) contribution proposed for the first time by Fukui *et al.* (their FC-IV and SD-IV terms)[15,16] is a second order expression containing the Fermi contact (FC) and the kinetic energy (p^2) operators.

(6) If the fully relativistic results are manipulated into 'paramagnetic' and 'diamagnetic' contributions according to the definition of Ref. 8, then the two pieces of the total isotropic shielding are very differently affected by relativistic effects. Even though the non-relativistic paramagnetic term is negative, the positive relativistic correction which is roughly proportional to Z^3 overwhelms and changes the sign of the paramagnetic term.[14]

(7) For the proton shieldings, the dominant term is the one-electron spin-orbit interaction coupled to the FC interaction.[5,9] The two-electron SO term and the SD terms are less than 10% of the relativistic correction for HBr and HI. This also indicates that the neglect of the Breit interaction in the four component calculations does not give rise to large errors because it only modifies the

two-electron contribution.

(8) Use of a point-like nuclear model instead of finite Gaussian leads to increase of the σ by 0.04, 2.3, 28, and 1430 ppm for the rare gas atoms Ar to Rn respectively.[10]

(9) It is suggested that the relativistic effects on the core as opposed to the valence electronic structure dominate the difference between the relativistic and the non-relativistic results.[14] A full analysis that examines this suggestion[13,17,18] is discussed below.

Beyond small molecules, one has to consider relativistic approaches less rigorous than the four-component relativistic calculations described above, yet still providing a large part of the relativistic corrections to shielding. Towards this end, several approaches have been tried. We will attempt to summarize the various approaches according to level of completeness. We first consider the elimination of a small component (ESC) scheme. This approach was presented by Melo *et al.*[19] Starting from a full relativistic four-component Rayleigh-Schrödinger perturbation theory (RSPT) formalism, a two-component formalism is constructed by transforming matrix elements using the elimination of small component scheme. A set of operators entering the RSPT expressions in terms of the Schrödinger molecular spectrum are derived by expanding such a four-component expression as a power series in c^{-1}, retaining all formal expressions which are correct up to the order c^{-4}. Consistent to this order, all quantities can be calculated in terms of solutions of the molecular Breit-Pauli Hamiltonian. The explicit expression for the relativistic corrections to the magnetic shielding tensor consist of first, second and third order [RSPT(1), RSPT(2) and RSPT(3)] corrections to the Schrödinger molecular energy.[19] In this way, a strong simplification used in 1996-7 by Fukui *et al.*[15,16] is avoided. The final expressions for the relativistic corrections are found to be equivalent to those of Fukui *et al.* but with additional terms not previously included by the latter. The systematic approach developed by Fukui *et al.* using a formalism in which the external magnetic field is explicitly included in the Breit-Pauli Hamiltonian in order to get a gauge-invariant scheme up to order c^{-4}, although now shown to be somewhat incomplete, introduced the notation for the various contributions that is still in use today. This offers the advantage that the individual contributions (FC-IV, SD-IV, *etc.*) in various numerical calculations at different levels may be identified and compared with each other, and the specific ones that are not included in a particular level of calculation may be identified explicitly. The more complete two-component theory[19] making use of perturbative approach employing the Schrödinger molecular spectrum is an attractive approach in that it can be implemented within any standard quantum chemistry computational program. Some conclusions from this work,[19] in applications to the usual test sets HX and CH_3X molecules, where X = halogen atom, are as follows:

(1) Contributions originating in the Darwin, mass-velocity and spin-orbit corrections to the ground state wave function are obtained in agreement with previous works where the Darwin and mass-velocity scalar effects were included within the unperturbed molecular Hamiltonian.[20,21]

(2) Electronic correlation effects were shown (based on SOPPA vs. RPA

results) to be very small for these relativistic corrections in all the cases considered.[19]

(3) Further contributions beyond these, which were not previously considered in Ref. 20 and 21, expressions appearing here[19] and also in Fukui *et al.*[15,16] are the field-induced spin-orbit contributions (considered by Ref.22) and the term arising from the combination of mass-velocity, external field, Fermi contact operators (analysed by Ref. 9). In addition to these, there are the new terms derived in this work[19] which have not appeared in the literature previously and remain to be treated quantitatively.

(4) Even though the contributions to the absolute value of the nuclear magnetic shielding of the heavy nucleus are very large, they are almost insensitive to the change in chemical environment from HX to CH_3X.

An interesting question arises as to whether such contributions are essentially of atomic character related to the relativistic contraction of the most inner core molecular orbitals, or whether they are sensitive to changes in the chemical environment of the heavy atom. Localized orbital analyses of the numerical results in calculations using the approach of Ref. 19, have been carried out in Ref. 18 and 13 in an attempt to answer this question, and also to find the relative magnitudes of various relativistic correction terms. Using 9 molecular systems as examples, Gomez *et al.*[13] show by analysis of the localized orbitals that the mass correction (MC) contribution (the FC-IV and SD-IV terms of Fukui *et al.*[15,16]) is mainly due to excitation of the inner core orbitals; contributions from bonding and lone pairs are far less significant, thus are relatively independent of the chemical surroundings of the nucleus. The pure zeroth-order approximation of the polarization propagator method provides a good estimate of this mass correction contribution, comparable to the more rigorous four-component calculations. On the other hand, using the X^- ions and HX molecules (X = halogen) as a test set, Ruiz de Azua *et al.*[18] find that some terms are dependent on the chemical environment while others that are dominated by contributions of inner shell electrons are almost insensitive to changes in chemical environment. It had previously been shown by Bouten *et al.* using the ZORA method[17] that for shielding of transition metal nuclei the core contribution to the diamagnetic shielding is large (on the order of 10 000 ppm for the 5d metals) and the additional relativistic corrections to the core diamagnetic part are also large. These large core contributions are important only for the absolute shielding calculations; they are essentially unchanged from one compound to the next and are therefore irrelevant for the chemical shifts.[17]

Three quasi-relativistic approaches that are variationally stable are the Douglass-Kroll-Hess transformation of the no-pair Hamiltonian (for example, see Ref. 11, 20, 23-29), the zeroth order regular approximation, ZORA, (for example, see Ref. 30-34), and the approach of Barysz and Sadlej[35] (for example, see Ref. 36). The results of the first two approaches differ considerably even when used by the same authors,[25,26,32] which led them to try the third approach.[36] A calibration study[32] suggests that relativistic effects on heavy atom shieldings are significantly underestimated by ZORA in comparison to the four-component relativistic treatment, but that the neighboring proton chemical shifts are closer to experi-

ment. Two significant recent reports using ZORA[31,34] deserve a fuller discussion and are described below. The infinite-order Foldy-Wouthuysen transformation, proposed by Barysz and Sadlej,[35] has been used by Fukui *et al.* in a new scheme for calculating shielding.[36] The shielding results, in the most reliable one of the several methods tried in this scheme, were lower than those obtained using four-component relativistic theory, but more work needs to be done to ascertain whether this new scheme is going to be superior to DKH or ZORA approaches.

Finally, obtaining relativistic corrections perturbatively from non-relativistic quantum mechanical calculations is a computationally less demanding alternative, particularly when electron correlation is important. In this approach one starts with a non-relativistic reference wavefunction and includes relativistic terms from the Breit-Pauli Hamiltonian as perturbations on the same footing as the magnetic perturbation operators. Alternatively, response theory can be used. The leading relativistic corrections to the molecular electronic Hamiltonian are the mass-velocity and one- and two-electron Darwin terms, often denoted scalar relativistic corrections, and the one- and two-electron spin-orbit coupling. The spin-orbit terms, in particular the Fermi contact/one-electron spin orbit correction (FC(1) term) received the earliest attention,[37–42] and also the spin dipole/one-electron spin-orbit correction (SD(1) term)[38–45] since the large change in the nuclear shielding of light atoms in the vicinity of heavy elements is caused mainly by spin-orbit coupling. There has been a considerable interest in perturbation calculations of the SO contributions to nuclear shieldings using unrestricted Hartree-Fock (Nakatsuji *et al.*[40–45]) and DFT techniques (Malkin *et al.*[21,46–51]). Later, quadratic response theory using SCF and MCSCF reference wave functions provided the first correlated *ab initio* calculations of the spin-orbit contribution, including both the one- and two-electron parts of the spin-orbit Hamiltonian, as well as the interaction with both the Fermi contact and spin dipolar mechanisms (FC(1), FC(2), SD(1) and SD(2) terms).[22,52] As the mass-velocity and Darwin contributions may induce large perturbations in the electronic structure close to the nuclei, perturbation theory may not be adequate. To circumvent this, techniques like the frozen-core approximation,[53,54] effective core potentials,[55–58] or a relativistic zeroth order Hamiltonian[23] have been used to calculate scalar relativistic corrections to NMR properties. The most recent report of a perturbational approach using a non-relativistic reference wavefunction by Manninen *et el.*[59] extends the response theory approach[22,52] to include the scalar relativistic corrections. Applications to HX (X = halogen), H_2X (X = O to Po), and the rare gases atoms (Ne to Rn) are presented and compared with four-component and quasi-relativistic results for these systems. The present accuracy is comparable to published quasi-relativistic results on the same molecules using the ZORA or Douglas-Kroll-Hess approaches.

Two significant reports of DFT-ZORA applications in this reporting period are the calculations of shieldings and spin–spin couplings which have been observed experimentally in XeF_2, XeF_4, and KrF_2 molecules,[31] and the calculations of the Se and Te shieldings in a series of compounds using an implementation of DFT-ZORA in a gauge-including projected wave approach.[34]

The solid state NMR measurement of the span of the Xe shielding tensor in

XeF_2 provides a strong endorsement of using relativistic approaches in thinking about shielding in molecules containing heavy atoms. The spin-orbit terms and cross terms involving it have been well-known to give rise to relativistic corrections that increase as $\sim Z^3$ for neighboring light atoms. For the heavy atom itself, some of the largest relativistic corrections, as already discussed above, have been established to be largely atomic in nature and nearly independent of the chemical environment. This may lead one to suppose that, at least for the heavy atom shielding, there is some hope that the main relativistic corrections, largely the mass correction terms discussed above, simply go with the atom from one molecule to another and therefore do not radically affect the shielding differences which are the chemical shifts. This may be true in many cases; however, this is not a valid assumption in general. Relativistic calculations of NMR parameters have now reached a level of accuracy that challenges our previous insights based on non-relativistic thinking. Two very important insights, that had been extremely useful in understanding chemical shifts, date back from the time of Ramsey's derivation of the expressions nuclear magnetic shielding in linear and polyatomic molecules using perturbative non-relativistic theory:[60] (1) For a linear molecule, with the gauge origin chosen anywhere along the line of centers, the component of the paramagnetic part of the shielding along the direction of the internuclear axis is identically zero. (2) At a given nuclear configuration, an identity relation exists between the nuclear shielding tensor and the spin-rotation tensor of a nucleus in a molecule. The latter identity, derived also by others in the non-relativistic limit,[61, 62] is the basis for the establishment of the absolute shielding scales for nuclei of light elements. Use of the Flygare approximation for diamagnetic part of the shielding[63] and the two insights listed above leads to:

$$[\sigma_{\parallel}(\text{N in linear molecule}) - \sigma^{\text{diam}}(\text{N in free atom})] \approx 0 \qquad (1)$$

which in turn, leads to

$$(\sigma_{\parallel} - \sigma_{\perp} \approx -(3/2)\,[\sigma_{\text{iso}}(\text{N in linear molecule}) - \sigma^{\text{diam}}(\text{N in free atom})] \qquad (2)$$

and

$$[\sigma_{\perp}(\text{N in linear molecule}) - \sigma^{\text{diam}}(\text{N in free atom})] \approx -(m_p/2m_e g_N)(C_{\perp,N}/B) \qquad (3)$$

where $C_{\perp,N}$ is the spin-rotation constant for nucleus N in the linear molecule and B is the molecular rotational constant. Of course, in deriving accurate absolute shielding scales, the approximations that lead to these are not used; diamagnetic shielding at the nucleus in question in the molecule is calculated accurately and rovibrational corrections are applied. Nevertheless, the more accurate calculations have led to results with only minor deviations from these. There had been no previous observation of a non-zero value for $[\sigma_{\parallel}(\text{N in linear molecule}) - \sigma^{\text{diam}}(\text{N in free atom})]$. On the other hand, the recent experiments on the linear molecule XeF_2[31] leave no doubt as to the necessity of rethinking these two insights derived from the non-relativistic limit. First, $[\sigma_{\parallel}(^{129}\text{Xe in } XeF_2) - \sigma(\text{free Xe atom})]$ was found to be significantly different from zero (by about -1000 ppm!).[31] Second, the span $(\sigma_{\parallel} - \sigma_{\perp}) = +4245$ is found to be substantially different (by about 1430 ppm!) from the $+5678$ ppm $= (3/2)$ times the isotropic

Xe chemical shift in XeF_2 relative to Xe gas (+3785 ppm). Therefore, the experiment itself, separately from any quantum mechanical calculations done concurrently with the experimental work, reveals that the relativistic corrections can not be ignored in XeF_2. The results establish that the internal consistency of the individual tensor components with the free Xe atom is itself at odds with all the previous relationships derived from non-relativistic theory. This is more powerful evidence than any comparison of experiment with relativistic and non-relativistic calculations. Incidentally, DFT-ZORA calculations on XeF_2 isolated molecule leads to values + 4469 ppm for the span and + 3403 ppm for the isotropic values of the Xe chemical shift relative to Xe atom.[31] Both are in very good agreement with the experimental values of +4245 ppm and +3785 ppm, for the solid XeF_2, given the well-known large intermolecular chemical shifts of Xe nucleus. The reference used was external neat liquid $OXeF_4$ at 24°C relative to which a Xe gas sample was at $\delta = -5388$ and XeF_2 solid was at −1603 ppm. Therefore, XeF_2 solid relative to Xe gas was 3785 ppm. [At room temperature the Xe gas chemical shift relative to zero density limit is known to change by a factor of 0.57 ppm times the multiples of the density at STP, which means a gas sample at 1 atm has a chemical shift of +0.57 ppm relative to the free Xe atom.] In the same work, DFT-ZORA calculations were also carried out on Kr and F shieldings in XeF_2 and KrF_2.[31]

Calculations of Se and Te shieldings in small molecules were carried out as first examples of a new method that uses pseudopotentials in a DFT-ZORA calculation based on a gauge-including projector augmented wave approach.[34] The latter method was devised by Pickard and Mauri for large low symmetry structures such as amorphous solids.[64] The recent calculations include only scalar relativistic contributions and at this time the spin-orbit effects have not been included in the theory. Other relativistic calculations have found relatively large spin-orbit contributions to Se and Te shieldings. When this theory is completed, it can be applied to the prediction of chemical shifts in amorphous or crystalline solid materials and for the explanation of trends such as those previously reported in the chalcogenides and semiconductor alloys.[65]

The magnetic field dependence of the nuclear shielding was predicted by Ramsey in 1970.[66] Calculations have recently been reported for the magnitude of the decrease of the shielding with increasing external magnetic field strength for ^{59}Co nucleus in $[Co(NH_3)_6]^{3+}$ and $Co(acac)_3$.[67,68] The method uses analytical response theory, using DFT as well as *ab initio* Hartree-Fock reference states. The calculated results are just large enough to be barely observable in a 900 MHz spectrometer. The predicted sign of the magnetic field coefficient is the same as was found in experimental results reported for these compounds,[69] but the magnitudes are smaller than claimed in the experiments.

Reports of assessment of DFT methods and of various empirical functionals for correlated calculations of nuclear shielding document the need for and attempts for improvement of the DFT method.[70–74] The very useful comparative study carried out by Magyarfalvi and Pulay (reviewed in the previous volume of this series), for the purpose of assessment of density functional methods and the relative performance of various functionals against the CCSD(T) coupled cluster

method as the ultimate benchmark, had included the OLYP density functional from Handy and Cohen.[70] A new hybrid functional, the O3LYP, similar to the popular hybrid B3LYP, but with slightly different mixing coefficients, had not been included in the comparative study. In particular, the proportion of Hartree-Fock exchange in O3LYP is reduced from 20% to just over 11%.[75] Baker and Pulay have carried out the series of calculations to make a comparison of the performance of OLYP and O3LYP for first-row transition metals.[71] The conclusion is that neither of the two new functionals performed well for atomic properties, both giving worse results overall than either BLYP or B3LYP. The results suggest that there is no real incentive to use either OLYP or O3LYP in place of B3LYP for calculations involving first-row transition metals. Keal and Tozer recently developed two new generalized gradient (GGA) functionals named KT1 and KT2, designed specifically to provide high-quality shielding values for light main-group nuclei.[76] The performance of the KT1 and KT2 exchange-correlation functionals for calculations of shielding in fourteen highly correlated molecules has been assessed using GIAOs in the DALTON program.[72] The authors claim the shieldings are a significant improvement over those from conventional functionals (LDA, BLYP, B3LYP), which improvement may be traced directly to the paramagnetic contribution.

Most program suites used for shielding calculations by many laboratories use Gaussian-type orbitals (GTO) whereas others use Slater-type orbitals (STO). There has been some discussion about the relative merits of the two types of functions, in particular whether having the cusp helps make the STO functions perform better. A comparative study has been carried out by Watson *et al.* to compare the two in DFT GGA and hybrid calculations.[74] For the evaluation of energies, they have previously demonstrated that there is little to choose between good GTO calculations and good STO calculations. For the calculation of molecular properties however, the picture for STOs is more encouraging, in particular for electric dipole polarizabilities, for spin-spin coupling and for nuclear magnetic shielding. They showed that the results with STO basis TZ2P-S are comparable with the cc-pVTZ GTO values, with mean absolute errors with respect to the estimated basis set limit being 6.9 and 8.5 ppm, respectively. The accuracy using moderately sized STO basis sets within the DFT framework is highly competitive with the use of GTO basis sets.[74]

Chesnut reports that a constant scaling reducing the paramagnetic component of shielding at the B3LYP/6-311 + G(2d or d,p)//B3LYP/6-311 + G(d,p) level is able to reproduce experimental results in a way that improves upon other density functional methods and rivals more sophisticated *ab initio* approaches.[73] He considered C, N, O, F, P and S shieldings in a range of molecules. A useful review by Facelli describes the power of calculations of nuclear shieldings for a general chemical audience.[77]

1.2 *Ab initio* and DFT Calculations. – For small molecules consisting of light atoms, the *ab initio* correlated methods implemented by Gauss in coupled cluster theory are the most accurate. In this review period the ^{13}C chemical shifts in the (E) and (Z)- isomers of the penta-1,3-dienyl-2-cation were calculated at MP2/tzp

geometries using CCSD(T), CCSD, MP2 and HF-SCF methods and GIAOs based on tzp basis for carbon atoms and dz for hydrogen atoms.[78,79] Unequivocal assignment is made possible by high level correlated (coupled cluster) calculations where the SCF results were not sufficient. The latter led to up to 40 ppm deviations from experimental values for the positively charged carbon atoms. The mean deviation between experimental values in solution and CCSD(T) results for the isolated cation is 1.8 and 2.0 ppm for the two isomers.[78,79]

MP2-GIAO calculations of ^{13}C and ^{1}H chemical shifts in isolated molecules of alkenes having electron-donating and electron accepting functional groups as substituents (so-called push-pull alkenes),[80] ^{13}C chemical shifts in 20 rigid bicyclic compounds,[81] and in substituted acetylenes,[82] have been found to provide the experimental trends in these compounds. In the alkenes, the agreement with experiment was poorest for the carbons of the acceptor functional groups (C=O, C=S, C≡N) even at the largest basis set tried (6-311G**).The agreement with experimental values was good for the sp^3 carbons,[80,81] even at the modest (6-31G*) basis set used for the bicyclic compounds,[81] but not for the sp^2 and sp carbons.[80] The inadequacy of MP2 calculations of shielding for highly correlated systems had been documented against coupled cluster benchmark calculations in previous volumes of this Series. A detailed MO analysis of the tensor components in the substituted acetylenes was carried out using IGAIM,[82] and the MP2-GIAO results using 6-311+G(2d,p) basis sets were compared with DFT results using the MPW1P91 model suggested by Adamo and Barone.[83] The reported work on the acetylenes[82] is a continuation of a series of studies in which an understanding of the ^{13}C shielding tensor is the primary goal.[84] It is found that it is possible to gain additional information about ^{13}C chemical shifts by calculating the tensor components on an MO basis and by examining the matrix elements for the coupling of the occupied orbitals with the virtual orbitals *via* the angular momentum operator.[82,84] While ^{13}C NMR chemical shift tensors for the most part can be routinely calculated for specific molecular systems with satisfactory accuracy using GIAOs, a satisfying accompanying interpretation in terms of simple models is very useful for garnering generalizable insights which are transferable to new systems. This is a worthwhile goal.

Existing basis sets perform poorly for transition metals, the major problem being the D shell. An improved 6-31G* basis set (called m6-31G) for first-row transition metals has been proposed, with new orbital exponents and contraction coefficients for the D shell, which performs uniformly well across the entire first-row transition metal series from Sc to Cu.[85] The quality of the new basis set is demonstrated for accurate prediction of ionization energies and bond dissociation energies, as well as structural parameters and harmonic vibrational frequencies of diatomic and polyatomic molecules. Because of its uniformly good performance for all first row transition metals, this m6-31G basis set, and its derivatives, *e.g.*, m6-31G**, is recommended over the original 6-31G set or its derivatives. We await applications to shielding calculations.

Systematic studies have been carried out on ^{33}S isotropic shielding, in Chesnut's scaled DFT method[73] mentioned in the above Section and in his estimated infinite order Møller-Plesset (EMPI)[86] approaches, for a wide variety of sulfur containing compounds spanning the entire ^{33}S chemical shift range.[87] Agreement

with experiment is estimated to be as good as 3% of the range.

Systematic studies of ^{31}P shielding tensors in transition-metal compounds containing phosphine, phosphido, and phosphinedene ligands provide insights into the chemical bonding.[88] Methods used include uncorrelated *ab initio* (restricted Hartree-Fock) and various DFT methods, with or without relativistic corrections, using hybrid DFT (B3LYP) and the DFT-ZORA method applied to isolated molecules of these compounds. A detailed comparison with individual experimental tensor components permits the identification of the characteristic advantages of each of the methods used. Scalar relativistic corrections are included in the DFT-ZORA calculations. In addition, the spin-orbit corrections were investigated. The powder patterns simulated from the tensor components obtained from the calculations differ dramatically from method to method, although the relative ordering of the three components and their orientations within the molecular frame are preserved. There are systematic deviations of each method from experiment for this class of molecular systems which are instructive in *a priori* gauging one's expectations from any one calculation. The effects of geometry modification show that upon W-P bond extension or M-P-C, M-P-M bond angle modification, one component changes in a direction opposite to the others.[88]

A DFT (B3LYP)-GIAO study of basis set dependence of the isotropic ^{19}F shielding in a series of 53 perfluoro molecules including CF_4, C_2F_6, NF_3, OF_2, SF_4, and SF_6 found that the smaller basis set 6-31++G(d,p) reproduced experimental chemical shifts better than the largest basis set 6-311++G(3df,2p) used.[89] Fortuitous cancellation of errors in shielding calculations can lead to better agreement with shielding differences observed in condensed phases. Other calculations of ^{19}F isotropic shieldings in rigid polycyclic alkyl fluorides using a modest basis set have been reported.[90]

DFT-GIAO calculations of ^{13}C in organic molecules appeared recently. Some examples are in aromatic heterocycles,[91-94] guanyl hydrazone,[95] cyclodextrins,[96] some cyclic and acyclic acetals,[97] and natural products.[98,99] Nitrogen chemical shifts were calculated also in some of these systems,[91,93,95,99] and proton chemical shifts, too, in others.[93,94,96,99-101] The ^{29}Si chemical shift tensors of 21 different simple singlet silylene isolated molecules were predicted to be highly anisotropic, with a very large paramagnetic component in the plane of the central R_2Si unit and perpendicular to its axis.[102] The shielding of interstitial atoms held a fascination for our late colleague Joan Mason. On the one hand, they can be viewed as merely trapped in tightly fitting cages, on the other hand they can be viewed as covalently bonded to the cluster. DFT-GIAO calculations of ^{11}B and ^{13}C chemical shifts of interstitial boron and carbon atoms in centered hexazirconium clusters have found a correlation of the chemical shifts with the energy gap corresponding to the magnetic dipole transition (t_{1u}*-t_{1u}).[103] ^{13}C shieldings in a series of small organic molecules, some containing Cl and Br, (cyclohexane, furan, napththalene, *n*-butyl chloride, *o*-dichlorobenzene, and *o*-bromochlorobenzene) have been investigated using DFT non-relativistic calculations and quasi-relativistic calculations using ZORA, with spin-orbit coupling contributions.[104]

2 Physical Aspects of Nuclear Shielding

2.1 Anisotropy of the Shielding Tensor. – We begin this section by citing the new techniques developed in this reporting period for extracting tensor shielding information. By measuring cross-correlation rates between chemical shift anisotropy and dipolar coupling, and employing pulse sequences based on a symmetrical reconversion of operators, Cisnetti *et al.*[105] have been able to determine the principal values and orientations of the ^{13}C shielding tensor of 63 carbonyl sites in the protein ubiquitin in solution. Based on these results, it is found that the intermediate component of the shielding (σ_{22}) correlates well with the isotropic value, suggesting the dominance of hydrogen bonding in carbonyl carbon chemical shifts in proteins. For tensors characterized by a small span, low spinning rates are normally required to see the spinning sidebands. With properly placed π pulses, Shao *et al.*[106] have demonstrated a two-dimensional experiment capable of extracting sideband patterns that are identical to those obtained at slow spinning rates. On the other hand, Asakawa[107] has utilized a ramped spin-locking radiofrequency field to determine accurately the shielding span of C^{α} and C^{β} in alanine. These sites have relatively low values for their shielding tensor spans (34 and 22 ppm, respectively). The values obtained by Asakawa are in close agreement with single-crystal measurements. Gardiennet and Tekely[108] have revisited the technique of spinning the sample at slightly off the magic angle. Spinning frequencies employed for these experiments are 1/8 to 1/5 of the expected shielding tensor spans and at angles 2–3 degrees from the magic angles. With this method, sharp but scaled principal value peaks are observed.

Chan and Tycko[109] have introduced a novel solid state NMR experiment that combines ROCSA (recoupling of chemical shift anisotropy) and ^{13}C-^{1}H dipolar dephasing. Designed for uniformly labeled samples, this technique is shown to correlate the carbonyl shielding and the $^{13}C^{\alpha}$-$^{1}H^{\alpha}$ dipolar tensors, thereby providing information regarding the peptide torsion angle ψ. Tycko and Ishii[110] have determined that the fibrils formed by residues 11–25 of the amyloid peptide contain an antiparallel β-sheet structure. This observation has been made possible by utilizing a proton-mediated two-dimensional $^{13}C/^{13}C$ exchange experiment. Oyler and Tycko[111] have demonstrated a way of deciphering the relationship of a molecular axis to the principal axis system of a shielding tensor. In this experiment, amyloid fibrils deposited on mica sheets have provided the orientation of the fibril axis with respect to the principal axis of a carbonyl shielding tensor. From the spinning sideband patterns obtained at parallel and perpendicular orientations of the substrate with respect to the rotor axis, an angle of 19° between the Val12 C=O vector and the fibril axis is obtained. Similarly, Kurita and coworkers[112] have used a dilute liquid crystalline medium with the application of magic angle spinning in determining the orientation of the ^{15}N shielding tensor with respect to the molecule's alignment frame. By taking note of the difference between the chemical shifts measured with and without magic angle spinning, an average span of 170 ppm is observed for the amide N sites in ubiquitin. The least shielded component is likewise found to be 20° off the N-H vector. Lastly, using either a train of inversion pulses or rotary resonance,

Nishiyama *et al.*[113] have illustrated a way of measuring the principal components of carbon shielding tensors in uniaxially drawn polypropylene.

Information regarding the dynamics of molecules continues to be inferred from observed shielding tensors at different temperatures. Flip motions of phenylene rings and main-chain fluctuations in amorphous poly(2-hydroxypropyl ester of busphenol A) have been quantitatively examined by measuring the temperature dependence of the line shapes of the ^{13}C sites.[114] Evidence regarding a ring-chain tautomerism of erythromycin A has similarly been obtained from solid state NMR measurements.[115] The principal components of the ^{13}C chemical shift tensor of a cyclic hemiketal have been obtained for the first time. Using a spectral editing technique, it was possible to isolate the resonances of the hemiketal formed in the solid phase ring chain tautomerism of erythromycin A. Externally referenced to TMS, the principal values of the chemical shift tensor found for the hemiketal site are 133,113 and 85 ppm. The δ_{11} and δ_{22} components are unique compared to anomeric carbon values reported in the literature. These principal values are larger (13–16 ppm) than those observed in other anomeric sites. *Ab initio* methods were employed in this study to assign the observed tensors for the ^{13}C sites in erythromycin A.[115] Molecular motions can also manifest in cross-correlated relaxation rates. By comparing results derived from the interference between ^{13}C-^{1}H dipolar interaction and ^{15}N chemical shift anisotropy on sites belonging to the same nucleotide base, and on sites where the dipolar vector is on an adjoining ribose unit while the ^{15}N atom still resides on a base, significant differences can be observed. This comparison essentially distinguishes between global and local motions of a molecule. With these results, internal motions involving the glycosidic linkage between the base and the ribose unit become apparent. The ^{13}C chemical shift tensors have been measured in the solid state for a tripeptide, Tyr-D-Ala-Phe.[116] Its crystal structure has been determined by x-ray diffraction and the peptide chain is seen as adopting a β-conformation.

^{15}N NMR chemical shift tensors have been used to characterize substituted hexaazaisowurtzitanes, which are intermediates in the synthesis of CL-20, a promising new explosive.[117] In the absence of x-ray structures, the tensors combined with *ab initio* calculations provide insights regarding the effects of different functional groups on the principal values of the ^{15}N shift tensors. For silylenes, the least shielded component of the ^{29}Si NMR shielding tensor is found theoretically to correlate strongly with the energy difference between the lowest excited and ground electronic states.[102] Feindel and Wasylishen[88] have evaluated the quality of various shielding computational methodologies in reproducing shielding tensors of ^{31}P in transition metal compounds that contain phosphine, phosphido and phosphinidene ligands. Their results indicate that density functional methods require smaller basis set (double-ζ quality) while restricted Hartree-Fock needs larger basis sets (triple-ζ quality) in order to reproduce experimental results. The first ^{129}Xe shielding tensor to be measured directly from a compound in which Xe is covalently bound has been reported by Forgeron *et al.*[31] In solid XeF_2, the span of the symmetric ^{129}Xe shielding tensor is found to be 4245 ± 20 ppm. Its parallel component, measured at −4433 ppm (referenced to $OXeF_4$

(neat liquid, 24°C)), is about 1000 ppm different from the value of the free atom, illustrating the importance of relativistic effects in the magnetic shielding of Xe.

Deuterium chemical shift tensors have been measured using a 14.1 T magnet.[118] Compounds employed in this study are polycrystalline samples of KD_2PO_4, $ND_4D_2PO_4$, $KDSO_4$, $KDCO_3$, α-$(COOD)_2$, α-$(COOD)_2 \cdot 2D_2O$, and boehmite (AlOOD). Measured anisotropies in this set of compounds range from 10 to 25 ppm. Chemical shift tensors are shown to be more sensitive to polymorphism than quadrupolar coupling constants in a study of monoclinic and orthorhombic polymorphs of triphenylphosphine oxide.[119] Although the ^{17}O quadrupolar coupling constants are essentially identical for the two polymorphs, the spans of the ^{17}O shielding tensors are significantly different, 135 ppm for the orthorhombic form and 155 ppm for the monoclinic form. The isotropic shifts are likewise distinct; the ^{17}O NMR isotropic shifts in the two polymorphs differ by 8 ppm. A combined theoretical and experimental study of the shielding parameters of ^{1}H, ^{13}C, ^{17}O and ^{31}P has been performed for phenylphosphonic acid.[120] ^{31}P shielding tensors have been derived from spectra of nickel(II) and copper(II) phosphorodithioate complexes.[121] The symmetry of a ^{31}P shielding tensor has also been utilized to probe ordered and disordered structural models for oxothiophosphates.[122] A span of 76 ppm is observed for the ^{133}Cs shielding tensor of Cs^+(15-crown-5)I^-.[123] After observing that the anisotropy of the scalar coupling tensor between C and Se in carbon diselenide is significant, corrections have been applied to previously determined ^{13}C and ^{77}Se shielding tensors.[124] ^{119}Sn chemical shift tensors have been reported in some triaryl tin (IV) chlorides, Ar_3SnCl,[125] and the temperature dependence of the tensor components in Ph_3SnCl has been investigated. Solution values of the isotropic chemical shift are different from those in the solid by as much as 17 ppm in one system. The more shielded component is assigned to the unique direction along the three-fold rotation axis containing the Sn-Cl bond in every case. Spans ranged from 24 to 147 ppm, the smallest being that for Ar = mesityl and the largest for Ar = *p*-fluoro.[125] The ^{13}C chemical shift tensor has been determined in bis(cyclopentadienyl) magnesium; the span is 119 ppm and the most shielded component is perpendicular to the plane of the cyclopentadienyl ring.[126] The ^{25}Mg spectrum on the other hand is dominated by the electric field gradient tensor and the chemical shift tensor has not yet been extracted. Calculations predict a span of about 40 ppm.

2.2 Shielding Surfaces and Rovibrational Averaging. – For shielding calculations to mimic exactly what is observed in experiment, not only does one require an accurate equilibrium geometry but also an incorporation of rovibrational averaging is necessary. As an example, Åstrand and Ruud[127] have demonstrated that the rovibrational corrections to shielding in the case of ^{19}F in 2-fluorobutane can be as much as −35 ppm. Dransfeld[128] reports the zero point vibrational corrections to the shielding, in which a complete set of normal vibration modes is taken into account, for a series of small compounds. However, when compared to more accurate calculations by Ruud *et al.* (for example Ref. 127) and by Gauss *et al.* (for example Ref. 129) Dransfeld's results for vibrational corrections are

misleading because the anharmonic terms have not been included. For example, where he gets a correction of 20 ppm without anharmonicity for a ^{13}C site, more accurate calculations including anharmonicity lead to less than 5 ppm. The general overestimation of the vibrational effects by neglect of anharmonicity becomes clear in comparing these corrections for the same molecules with those done by other groups. In the latest benchmark calculations for ^{13}C shielding, Auer *et al.*[129] have tested the coupled-cluster singles and doubles augmented by perturbative corrections for triple excitations (CCSD(T)) with a large basis set (up to 15*s*11*p*4*d*3*f*/10*s*4*p*3*d*). At this level of theory and size of basis set, after including the non-negligible vibrational corrections, the remaining deviation (using absolute shieldings) observed between experiment and theory is in the range of 1–2 ppm. Employing lower levels of theory and smaller basis sets leads to errors. These errors, however, appear to be systematic, thus, when dealing with relative chemical shifts, cheaper calculations may suffice. The DFT(B3LYP)-GIAO calculations of the ^{51}V chemical shifts in peroxovanadate imidazole complexes found the dependence on the angle of rotation of the imidazole group. Averaging of the ^{51}V chemical shifts over this angle made use of Car-Parinello molecular dynamic simulations.[130] Indeed, B3LYP and Hartree-Fock calculations, as illustrated below, are able to provide in several cases, the dependence of the shielding on intra- and intermolecular factors. In the investigation of ^{17}O shielding in polyoxides, the dependence of the ^{17}O chemical shift on the HOOH model system was examined for a flexible rotor as well as a rigid rotor model.[131] The functional dependences on the torsion angle in the two models are substantially different. Although internal rotation of the polyoxides in solution was not investigated, it is assumed that the rotational flexibility of the molecules is considerably limited by hydrogen bonding.

In this reporting period, for example, O'Brien and Moyna[132] have illustrated the usefulness of Hartree-Fock calculations with a 3-21G basis in explaining ^{13}C chemical shifts in cyclodextrins. Calculations for 324 different conformers involving different values of the dihedral angles of the glycosidic bond of a maltose dimer provide the necessary shielding surface on which conformational averaging can be performed. Molecular dynamics simulations for 5 ns are employed for the motional averaging and the results are able to reproduce the observed anomeric shifts in various forms of cyclodextrin. The dependence of ^{13}C chemical shifts on dihedral angles in peptides and proteins continues to be of interest and Sun and Oldfield[133] have recently examined in detail the side chain C atoms of the amino acid tryptophan. In this study, x-ray structures and solid state ^{13}C NMR data are analysed. It should be mentioned that the protein secondary structure effects on ^{13}C chemical shifts were first observed in Trp C^{γ}[134] and finally, with *ab initio* calculations, the observed trends in the chemical shifts of the side chain C atoms of Trp can now be explained.[133] The chemical shift of C^{γ} in Trp depends on the side chain torsion angles, χ_1 and χ_2, and appears to be a consequence of γ-gauche interactions with the backbone carbonyl carbon and amide nitrogen atoms. Perczel *et al.*[135] provide a shielding surface derived from an N-formyl-serine-amide fragment to explain the secondary effects on the backbone chemical shifts of serine residues in peptides and proteins. Manalo and de Dios[136] have

calculated the backbone chemical shifts for a 27-residue peptide, ω-conotoxin GVIA. This work illustrates that errors in NMR structures derived from distance constraints can be revealed upon comparison between experiment and calculated shifts derived from the NMR structures.

The use of the chemical shift tensors of backbone nuclei in determining the conformation of a peptide in the solid state continues to be explored. Strohmeier and Grant recently have performed solid state NMR and x-ray measurements on the tripeptide melanostatin (Pro-Leu-Gly-amide).[137] Using N-formylamino acid-amide fragments, shielding tensor surfaces are obtained and by comparison with experiment, the most probable dihedral angles were extracted for each residue. These values are then compared with those obtained from the x-ray diffraction study. Conclusions drawn from this paper are the following. Multiple solutions for the dihedral angles are obtained if only the principal values are used. If the orientation of the shielding tensor is included, the probable solutions can be reduced. In the case of Leu, incorporating information derived from the C^{δ} shift tensor likewise removes some of the ambiguity regarding the probable values of the dihedral angles. Using the x-ray structure and considering medium effects lead to an rms error of 2.6 ppm in predicting the ^{13}C icosahedral NMR shifts. With an isolated molecule, the rms error is 6.5 ppm. The improvement is seen as well in the ^{15}N icosahedral NMR shifts, which gives an rms error of 5.5 ppm, to be compared with that of an isolated molecule, 13.6 ppm. Interestingly, medium effects of as much as 38 ppm are uncovered in one of the icosahedral shielding components of Gly N. To increase our understanding of shielding tensors in peptides, Chekmenev *et al.*[138] have compiled glycine ^{15}N shielding tensors from crystallographically characterized tripeptides. The range for the tensor spans in these compounds is observed to be 157–176 ppm, while the difference δ_{22}-δ_{33} (the two components of the ^{15}N shielding principal components that are close to each other in value) ranges from 7 to 35 ppm. Glycine residues in sheet and extended conformations exhibit large tensor spans for their amide ^{15}N shielding (169–176 ppm) and large δ_{22}-δ_{33} differences (21–35 ppm). Those in 3_1 helices exhibit the smallest spans (157–167 ppm) and likewise, δ_{22}-δ_{33} differences (7–23 ppm). Helical residues have intermediate values. The ^{15}N isotropic chemical shifts in these systems can apparently be explained with the use of an empirical equation that takes into account the backbone (ϕ,ψ) conformation, sidechain conformation (χ_1), and hydrogen bonding. Czinki and Császár[139] have questioned the adequacy of using a small fragment such as an N-formyl amino acid amide in constructing amino acid shielding surfaces. It is found, as expected, that increasing the fragment up to a pentapeptide does not markedly change the shielding surface for C^{α}, H^{α} and C^{β}. As predicted by other workers in this field, larger fragments are necessary for the amide N and H atoms. Czajlik and Perczel[140] have extended our current understanding of peptide chemical shifts in their work on penetratin fragments and conformational analysis involving chemical shifts have been applied to the study of the structure flexibility of a non-nucleoside HIV-1 Reverse Transcriptase Inhibitor, 9-Cl *TIBO*.[141] Here, the lowest energy conformer provided by geometry optimizations yields calculated shifts closest to experiment. Likewise, ^{13}C chemical shifts have been utilized to characterize

further the structure of a β-amyloid peptide.[142]

For large systems, approaches that make use of clusters or smaller fragments, as illustrated in the work involving peptides and proteins, can be used to probe the dependence of the shielding on the internal coordinates of the molecule. On the other hand, for extended networks such as crystals and glasses, a new method referred to as gauge including projector augmented wave (GIPAW) method, recently introduced by Picard and Mauri[64] has been applied by Charpentier *et al.* to the calculation of the two-dimensional solid state spectra of sodium silicate crystals and glasses.[143] This paper documents a major breakthrough in the theoretical investigations of glasses. The earlier series of computational and experimental studies by Grandinetti *et al.* have uncovered the concomitant changes in bond lengths, bond angles, electric field gradient tensors, by using as test cases silicates of known crystalline structure.[144-147] In other words, chemical electronic structure in these systems requires that more than one structural parameter is changing at the same time. Thus, previous studies which were cluster based, could not arrive at the correct dependence on bond lengths, bond angles found experimentally. The information that solid state two-dimensional NMR would like to discover for a given glass, which is not available by any other means is the distribution of configurations, *i.e.*, bond angles and bond lengths. Charpentier *et al.* have generated their glass model using combined classical and *ab initio* (Car-Parinello) molecular dynamics simulations. At the end of the simulations each model was relaxed to 0 K. Before the NMR calculations all interatomic distances were rescaled so that the volume of the unit cell was reduced by 4.5 % to the experimental values. This is to make sure that the lattice parameters are the appropriate ones. The shielding and electric field gradient calculations were then carried out using the GIPAW method which has been shown to have good accuracy in pure silicate systems. The calculations are in a periodic system but the supercell that is used for the calculations has the built-in distributions of configurations inherent in the glass. Calculations are carried out for ^{29}Si, ^{23}Na and ^{17}O. To investigate the structural significance of the NMR parameters, the coordination numbers of the atoms had to be determined. For example, for oxygen this was taken as the number of sodium atoms located in a sphere of 2.95 Å radius around each of the oxygen atoms. Using this method, the many interesting trends have been uncovered for glassy systems. For example, a linear dependence is seen between the ^{29}Si shielding and the Si-O-tetrahedron angle. The chemical anisotropy at a $Q^{(3)}$ site is predicted to be linear with respect to the bridging and non-bridging Si-O bond lengths, in agreement with experiment. The paper also predicted MQMAS and two-dimensional spectra that would be observed for the particular glass models that their molecular dynamics simulations have generated.[143]

2.3 Isotope Shifts. – Isotope shifts are intimately related to rovibrational corrections. Thus, with the same shielding surfaces used for rovibrational averaging, one can extract expected changes in chemical shift due to isotope substitution. This is once again illustrated in Dransfeld's work,[128] which is cited near the beginning of the preceding section. Here too, some cautionary words are in

order, because Dransfeld's neglect of anharmonicity in general leads to inaccurate average shielding differences resulting from isotopic substitution. Isotope effects are also becoming increasingly important for the study of strong, low barrier hydrogen bonds. One example is Picolinic Acid N-Oxide,[148] which has its hydrogen-bonded proton displaying a chemical shift of 18.5 ppm (from TMS). Shielding surfaces that take into account the effects of the O-H bond length and the O···O hydrogen bond distance, combined with theoretical potential surfaces, are able to reproduce semi-quantitatively the observed primary and secondary isotope effects in this system. In this recent work, the calculated potential surfaces have been constructed with solvent effects using the self-consistent reaction field / polarizable continuum model. Interestingly, isotope effects have also been applied to study of hypoxia and ischemia.[149] In this study, one takes advantage of the ^{18}O-induced isotope effects on the ^{31}P and ^{1}H NMR spectrum of phosphate metabolites. Finally, Golubev *et al.* have reproduced the deuterium-induced isotope effects on the chemical shifts in the hydrogen difluoride ion.[150]

2.4 Intermolecular Effects on Nuclear Shielding. – Probing intermolecular effects on NMR chemical shifts have been very useful in elucidating structure and interactions. With the effects of hydrogen bonding, electric fields and orbital repulsions, the NMR chemical shifts do contain salient information regarding these interactions. This reporting period witnesses further progress in our understanding of intermolecular effects on NMR shielding. And in a paper by Jameson and Murad, it has been demonstrated that in the case of Xe dissolved in water, the average ^{129}Xe NMR chemical shift can be efficiently obtained with the incorporation of molecular dynamics.[151] This is in contrast to other properties of dilute solutions of Xe in water. Mennucci and Cammi[152] continue to explore the usefulness of their integral equation formalism in predicting NMR shielding tensors for solutes in liquid crystals. Their method looks promising as long as the dominant factors influencing the chemical shift are electrostatic in nature.

Hydrogen bonding plays an important role in supramolecular structures that its effects on chemical shifts remain an important area of research. For example, with the aid of *ab initio* calculations that focus on hydrogen bonding effects, a helical structure has been determined for benzoxazine oligomers.[153] This recent study combines data obtained from fast magic-angle spinning spectra, in which assignments can be made in the proton spectra and ^{1}H-^{1}H correlations can be measured. The agreement between calculated and experimental proton shifts has confirmed the supramolecular hydrogen-bonding structure in the oligomer. Wu and Yamada[154] have measured the ^{17}O shielding tensors in potassium hydrogen dibenzoate. In the solid, there are two distinct ^{17}O sites, one is not involved in hydrogen bonding, while another participates in a relatively short hydrogen bond, thus allowing one to measure directly the effects of a strong hydrogen bond on the principal elements of the ^{17}O shielding tensor. The effects are dramatic. A change of almost 200 ppm is seen in the intermediate component of the shielding. This is the component that lies on the plane of the carboxyl group and is nearly parallel to the C-O vector. The span is reduced upon hydrogen bonding by about 170 ppm, indicating the opposing effects of hydrogen bonding

on the other two components, σ_{11} and σ_{33}. It should be noted that the orientation of the shielding tensor is also affected by the hydrogen bond. In the hydrogen-bonded site, the intermediate component is about 20° from the C-O vector, while in the non-hydrogen-bonded site, this angle is 30°. Cybulski *et al.*[155] have used shielding calculations among other things to characterize the interactions present in dihyrogen-bonded complexes. An inverse correlation with the internuclear distance is observed for the complexation shifts of the LiH proton shielding anisotropy in the complex $LiH{\cdots}C_2H_2$. Harris *et al.* have employed *ab initio* calculations in refining the crystal structure of the white form of methylnitroacetanilide.[156] This compound contains an amide group whose N-H bond length is 0.92 Å, as suggested by its x-ray structure. Shielding calculations, however, indicate that the bond length is around 1.03 Å (slightly longer due to hydrogen bonding). This is apparently the bond length that correctly reproduces the observed proton isotropic shielding in the solid state.

Using a chemical shift computation method that employs periodic boundary conditions, one can now explain the proton NMR chemical shifts observed in the proton conducting crystal of imidazole-(ethyleneoxide)$_2$-imidazole.[157] The highly deshielded resonances at 14.5 and 16 ppm arise from the intra-pair and inter-pair NH···N hydrogen bonds, respectively, while the peak at 10 ppm corresponds to a dangling NH in the isolated molecule, demonstrating that there are still noncrystalline domains in the crystal. In addition, even the highly shielded peak observed at 0 ppm can now be attributed to an aliphatic proton that is lying right on top of an aromatic imidazole ring. There are other papers reported in this period that involve hydrogen bonding. The effects of hydrogen bonding on ^{15}N chemical shifts have been used to characterize the active sites in dimetallic hydrolases.[158] Another low barrier hydrogen bond study has been performed on pyridine-dichloroacetic acid complexes by Perrin *et al.*[159] The chemical shift tensors of methoxycarbonyl urea have also been discussed with considerations of hydrogen bonding.[160] Witanowski *et al.*[161] have now included *N*-nitrosamines in their list of compounds whose solvent dependence of ^{15}N shieldings has been measured.

In the presence of a paramagnetic species, pseudocontact shifts can provide additional restraints since these shifts are both distance and orientation dependent. Gaponenko *et al.*[162] have attached a Co^{2+} paramagnetic probe to the N-terminal domain of the protein STAT4. The attachment is achieved by modifying a cysteine residue into a thiol-reactive chelator. With the additional restraints derived from pseudocontact shifts, the NMR structures are improved based on the rmsd value of the family of structures obtained. This approach is likewise illustrated in the work of Barbieri *et al.*[163] on the protein Calbindin D_{9k}. Here, the ions employed are Ce^{3+}, Yb^{3+}, and Dy^{3+}.

^{129}Xe continues to be an excellent probe in characterizing porous materials. Applying the trends predicted by Jameson and de Dios,[164] Koskela *et al.*[165] have interpreted the differences seen in variable temperature ^{129}Xe NMR spectra of Xe adsorbed in aluminophosphate molecular sieves with circular and elliptical cross sections at two different Xe loading values. Autsbach and Zurek[166] have repeated the calculation of the chemical shift of ^{129}Xe in of a Xe atom trapped inside C_{60}.

They have added relativistic corrections based on the zeroth-order regular approximation (ZORA) Hamiltonian. The relativistic contribution is found to be small, about 20 ppm. Several basis sets of various sizes are employed in this work to evaluate the dependence of the calculated ^{129}Xe shielding on the choice of basis sets. A recent calculation of Sears and Jameson,[167] which appeared almost at the same time, has already shown that with the use of a large basis set on Xe (24*s*19*p*15*d*9*f*), a calculated chemical shift of 181.58 ppm is obtained, which compares very well with the experimental value of 182.35 ppm. This compares more favorably with experiment than the calculated shift of 299 ppm from Autsbach and Zurek[166] using their largest basis set (QZ4P). With a TZ2P basis, the calculated shift is 246 ppm, which clearly demonstrates that in the work of Autsbach and Zurek,[166] convergence in basis set size has not yet been achieved. Since the relativistic corrections are likewise basis set dependent, their reported numbers are therefore doubtful. ^{129}Xe NMR has also been applied to the study of phase transitions in liquid crystals. Cifelli *et al.*[168] have studied the ^{129}Xe chemical shift of Xe dissolved in chiral smectogen as a function of temperature. Their study reveals that the ^{129}Xe chemical shift abruptly changes during the isotropic – smectic A and smectic A – smectic C*(ferroelectric) phase transitions. Kobayashi *et al.*[169] have used one-dimensional nanochannels of tris(*o*-phenylenedioxy)cyclotriphosphazene to study Xe-Xe interactions. At high pressures of Xe, it is estimated from the observed chemical shifts that on the average, the distance between Xe atoms inside the nanochannel is about 0.54 nm. As noted previously, with fast magic angle spinning, it is now possible to resolve proton signals in supramolecular nanotubes. Hoffmann *et al.* have taken advantage of this technique to measure the proton shifts in calyx[4]hydroquinone nanotubes.[170] These experimental shifts are nicely reproduced by employing a DFT method based on a pseudopotential plane wave formalism.

To further understand the relationship between chirality and nuclear magnetic shielding, Sears *et al.* have reported four papers on this topic.[171–174] This series of papers are meant to establish the theoretical basis for the diastereomeric splittings observed for Xe in cryptophane cages with attached chiral tethers, reported in a conference [E. J. Ruiz, M. M. Spence, S. M. Rubin, D. E. Wemmer, A. Pines, N. Winssinger, F. Tian, S. Q. Yao, P. G. Schultz, 43rd *Experimental NMR Conference*, 14–19 April 2002, Asilomar, CA]. In the first paper,[171] a Xe atom is placed inside a Ne_8 helix, which provides a chiral environment. An antisymmetric component ($\pm$0.0294 ppm) is calculated inside this environment. In terms of the directly observable symmetric tensor, the left- and right-handed helices are indistinguishable. However, addition of a chiral field arising from other asymmetric groups should lead to diastereomers, which can now have distinct isotropic shifts. In the model, this is achieved by adding a helix of point charges surrounding the Ne_8 helix. A 0.9324 ppm difference is seen between the diastereomers. One can in fact theoretically extract the contribution coming from the induced diastereomerism of the Xe electrons, by repeating the calculation with a naked spin. This is the subject of the second paper,[172] which shows that without the electrons from Xe, a diastereomeric shift of only 0.0191 ppm is observed. The third paper[173] makes use of a single electron confined to travel in a

helical path, a system in which exact analytical solutions are obtainable. A naked spin is used to probe the shielding inside the helix traversed by this electron. The chiral shift obtained in this system is 0.03605 ppm, which turns out to be dominated by the paramagnetic part of shielding. The last paper in the series[174] analyzes the odd and even dependence of the shielding on the chiral potential. It turns out that the difference in chemical shifts between naked spin diastereomers is linear to quite large values of the partial charges employed. On the other hand, with Xe diastereomers, the shielding has a quadratic dependence, yielding the same sign for both positive and negative partial charges. The grand conclusion from this series of papers is that it is now possible to model by *ab initio* calculations the observed diastereomeric splittings in ^{129}Xe NMR spectra that arise from real tethers.

Xe chemical shifts in cryptophane cages can be predicted from *ab initio* calculations as demonstrated by Sears and Jameson.[175] Moreover, the 30 ppm reduction in the ^{129}Xe chemical shift when Xe goes from cryptophane-A cage to cryptophane-E is likewise reproduced. This change in the chemical shift is primarily due to the E cage being larger than the A cage, similar to what is observed in zeolite cavities. To predict these experimental observations, a shielding surface, described as an analytical function of Xe and the cage atom coordinates, is utilized in conjunction with a Monte Carlo canonical averaging of a Xe atom within the cage. The structure of the cryptophane cage used in the shielding calculations has been assembled from geometry-optimized fragments, leading to theoretical conformations of the bridging OCH_2CH_2O groups that are completely in agreement with SPINOE experiments. In clathrate hydrates, the Xe shielding surface can be expressed as a sum over the interactions of Xe with O and H atoms.[176] Combined with Monte Carlo simulations, this shielding surface is able to predict the chemical shifts observed for Xe in a 5^{12} cage (structure I), 214 ppm, in reasonable agreement with the experimental value of 242 ppm.[177] The calculated value for a $5^{12}6^2$ cage is 147 ppm, which likewise compares favorably with experiment, 152 ppm.[177] The same shielding and potential functions applied to structure II hydrates provide a value of 207 ppm for a 5^{12} cage, to be compared with experiment, 225 ppm,[177] and a value of 105 ppm for a $5^{12}6^4$ cage, which reasonably agrees with an experimental value of 80 ppm.[178] Lineshapes can be predicted as well using the shielding tensor surfaces.[179] Since the Xe atom is relatively free to move inside the cage, the shielding anisotropy is averaged down. In a 5^{12} cage (structure I), for example, the predicted anisotropy of 9.0 ppm at the center of the cage, is significantly reduced to 0.7 ppm by Monte Carlo averaging. The sensitivity of the Xe NMR lineshape to the existence of a unique pair of oxygen atoms in the 5^{12} cage of type II is likewise correctly predicted. A larger anisotropy, around 20 ppm, is predicted, in agreement with the experimentally observed line shape by Ripmeester and co-workers.[180]

Since magnetic anisotropy of neighbors or ring currents are very significant in proton chemical shifts, it is important to understand completely their origin. Recently, there has been a question regarding the deshielding of the benzene protons as Wannere and Schleyer have suggested on the basis of their IGLO calculations that the benzene protons lie in the shielding zone of benzene.[181] In

the papers of Viglione *et al.*[182] and Ferraro *et al.*,[183] a more detailed inspection of the shielding tensor component reveals that the out-of-plane components are indeed deshielded, supporting the ring current model. However, in order to reproduce fully the deshielding effect, contributions from σ electrons must be taken into account. This recent work also suggests that the conventional ring current model is still sufficient in describing the shielding of ethyne protons. The shielding experienced by a naked spin (or a neutron) at a specific point in or around a molecule, which has been called the nucleus-independent chemical shift (NICS), continues to be used in evaluating the aromaticity of compounds. Calculations of NICS have primarily used DFT-GIAO schemes. For example, in a paper by Zora and Özkan, NICS values have been used to determine the effects ring fusion has on the aromaticity of benzene rings.[184] It is found that when a benzene ring is fused to heterocycles such as pyrrole, furan and thiophene, the benzene aromaticity is reduced. Other NICS calculations have been carried out in fluorinated homotropilium cations,[185] carbocations from benzo[a]pyrene and azulenophenalenes,[186] carbocations and oxidation dications from azulenes, homoazulene, benzazulenes, benzohomoazulenes and azulenoazulenes.[187] An analysis of individual molecular orbital contributions to NICS reveals that both σ and π electrons in cyclic aromatic molecules can either be shielding or deshielding depending on the number of nodes around the ring.[188] As one goes up to molecular orbitals of higher energy, the number of nodes increases, and this leads to higher deshielding. A careful study using CTOCD, by Lazzeretti and coworkers, of current density maps, magnetizability, and nuclear magnetic shielding tensors of bis-heteropentalenes formed by two furan units used a large basis set to achieve near-Hartree-Fock estimates.[189] *Ab initio* models of the ring currents induced by a magnetic field normal to the molecular plane were obtained for the three isomeric systems of higher symmetry, showing that the pi electrons give rise to intense diamagnetic circulation. Streamlines representing the current density vector field have been calculated. These exhibit sharp localized maxima close to carbon and oxygen nuclei. The pi currents are responsible for enhanced magnetic anisotropy and strong out-of-plane proton deshielding. The work confirms that CTOCD computational schemes for magnetic susceptibilities and nuclear magnetic shieldings are practical and effective tools, alternative to those employing GIAOs.[189] In a closer examination of the proton magnetic shielding of H-4 in phenanthrene and 11-ethynylphenanthrene, it is discovered that the deshielding observed is primarily due to steric compression and not the anisotropy of the triple bond.[190] Steric effects have also been invoked in describing proton shifts in halogen substituted phenanthrenes.[191]

Lastly, Wang and coworkers have calculated ^{3}He shifts for He encapsulated in various fullerenes using GIAO-B3LYP and a small basis, 3-21G, and employing geometries that have been optimized using empirical force fields.[192] Their results are surprisingly able to reproduce the experimental trends.

Other studies during this reporting period that involve intermolecular effects on shielding include a correlation between ^{1}H, ^{15}N, ^{13}C shifts and acid strengths of Bronsted acidic zeolites, as probed by an acetonitrile molecule.[193] From this study, it is unraveled that the isotropic shifts of ^{1}H and ^{15}N in acetonitrile correlate very well with acid strength while ^{13}C shifts are more sensitive to the

orientation of the acetonitrile molecule inside the zeolite. In a hexazirconium halide cluster, the chemical shift of interstitial atoms, such as H, Be, B, C, N, Al, Si, Ge, P, Mn, Fe, Co and Ni, are predicted to be sensitive to the binding of terminal ligands. A study by Shen and Hughbanks[103] finds that the chemical shift, for example, of interstitial ^{11}B and ^{13}C atoms correlate well with the energy gap ΔE (t_{1u}^{*}-t_{1u}), indicating its dominant contribution to the paramagnetic term in the observed interstitial shifts. Lastly, although dehydration has very minimal effects on the structure of tris(ethylenediammine)cobalt(III) chloride, these small differences can be detected by a change of about 6 ppm in the ^{59}Co isotropic NMR shift.[194]

In aqueous solution where ions result from dissociation of molecules, there are usually many structures that need to be considered in calculating the shieldings that may be observed. A consideration of six possible structures of phosphorous acid in aqueous solution and calculations of the isotropic ^{31}P shielding in each one leads to the suggestion that a particular structure agrees with experiment.[195] However, since these calculations are for isolated systems and no water molecules had been included in the calculations, further work has to be done, including hydrogen-bonding partners as part of the structure, and perhaps even molecular dynamic simulations, before a comparison with experiment is warranted. A study of oxocarboxylic acid oximes[100] points the previous study in the correct direction. In this work various intra- and inter-molecular hydrogen-bonded species are considered, dimers and tetramers with internal hydrogen bonds, and also dimers with the solvent DMSO. Clusters have also been used in the description of ^{17}O chemical shifts of polyoxides in the gas phase and in solution, HO_nH, CH_3O_nH, $CH_3O_nCH_3$ (n = 2,3,4).[131] The ^{17}O shifts are found to be strongly dependent on the position of the O atom in the polyoxide chain. O atoms near the terminal are found to be shielded by about 300 ppm compared to the O atoms inside the chain. These calculations were carried out with four different methods: Hartree-Fock, MP2, and CCSD(T), all using GIAOs, and also DFT using IGLO.[131]

Cluster models have been used for solvated or hydrogen-bonded systems, as mentioned above, and are still widely used for extended networks. For example, the ^{19}F shieldings in solids such as MF_2 (M = Zn, Cd), β-PbF_2, MF_3 (M = Al, Ga, In), AMF_3 (A = K, Rb, Cs, Ba; M = Mg, Ca, Li, Zn, Cd), $BaMgF_4$, $BaZnF_4$, and Ba_2ZnF_6 have been investigated using various cluster models such as $[FM_3F_9]^{4-}$, $[FM_3F_{13}M_4]$, $[FM_2A_4]^{7+}$, *etc.* in DFT (B3LYP)-GIAO calculations.[196] Of course, a better approach to shielding in extended networks has to be by calculations in an infinitely extended system, using periodic boundary conditions. A review of calculations of NMR parameters in condensed phases by Sebastiani describes the extension of well-established approaches for the calculation of magnetic linear response to extended systems which are described under periodic boundary conditions.[197] Two major implementations have evolved within density functional theory in a pseudopotential plane wave scheme: The review describes the pioneering work of Mauri *et al.* since 1996, which has been reviewed over the years in this Series, and the more recent work of Sebastiani and Parinello.

A variety of methods have been applied to calculations of shielding for

molecules in solution or in the neat liquid where the intermolecular interactions (such as hydrogen bonding) requires that the effects of the neighboring molecules have to be treated in some fashion, not necessarily at the same level as the subsystem of interest. The earliest examples of these were the shielding calculations for ^{13}C and other nuclei in proteins in which *ab initio* methods with locally dense basis sets were employed for a fragment containing the nucleus in question, with a sufficiently large subsystem to take into account the effects of various torsional angles that influence the shielding and the remainder of the protein is replaced with a charge-field model, using a sufficiently large sphere.[198] Subsequently the ONIOM method was proposed by Morokuma *et al.*,[199] and the idea of using the successively approximate techniques to include large numbers of neighbors around an intensively calculated subsystem has become widely used for shielding calculations. Of course, the use of classical force fields to describe the larger system has been around for a long time, and the general scheme denoted QM/MM has been employed for studying reactions in solution and in enzymes. Application to NMR chemical shifts in solution by Cui and Karplus interfaced, among other possibilities, *ab initio* calculations using the Gaussian suite with molecular mechanics using the CHARMM force field.[200] A recent example by Sebastiani and Rothlisberger uses DFT QM/MM calculations to calculate the ^{1}H and ^{17}O chemical shifts in liquid water,[201] and the results may be compared with those of Cui and Karplus.[200] In the method used in the recent work the quantum part is enclosed into a box of finite volume, in which the Kohn -Sham equations are solved, using a plane-wave basis set under periodic boundary conditions. The interaction of the quantum system with the classical atoms is mediated by the electrostatic potential created by the point charges. The classical system itself is also described using periodic boundary conditions. They introduced a new term, the purpose of which is to mimic the orthogonality constraint that would be imposed on the electrons if also the MM region was treated quantum mechanically. However, there is some question about double counting the interactions, because there already exists a van der Waals term in the classical description to take care of the repulsive atomic forces. It remains to be seen whether it makes sense to add the new terms. They also performed calculations for a snapshot from Car-Parinello molecular dynamics simulation of liquid water using 64 water molecules under periodic boundary conditions.[201] They then analyse the shieldings in each water molecule as the center of the QM system which includes the first solvation shell, with the surrounding water molecules comprising the MM system. Inclusion of waters from the second solvation sphere in the QM part improves the results, which is not a surprise.

2.5 Absolute Shielding Scales. – For lighter elements, the way to the absolute shielding involves a non-relativistically valid relation between the spin-rotation constant, C, and shielding σ, applied to at least one primary reference molecule. A review of how spin-rotation constants relate to shielding constants was provided by Bryce and Wasylishen.[202] The C and σ tensors for the primary reference are corrected for rovibrational effects and then connected to a commonly used secondary reference (usually a neat liquid substance) *via* an NMR measurement in the gas phase at the limit of zero density and in the liquid

reference in the same magnet. At this time we make note of the fact that the spin rotation constant for ^{195}Pt has been recently measured to be 30.98 KHz in the ground vibrational state in the diatomic molecule PtSi.[203] From this and the measured rotational constant of the molecule, it would have been possible to estimate the difference [$\sigma(^{195}$PtSi) – σ (free Pt atom)] = $\pm$3206 ppm, the sign depending on the sign of C (probably negative), if the non-relativistic relations could be expected to hold. However, from relativistic shielding calculations being done currently for linear molecules such as XeF_2, it is quite clear that the zero paramagnetic contribution to the parallel component that holds for nuclei lighter elements in linear molecules is no longer valid in relativistic theory, and also the identity relationship between the spin-rotation tensor and the shielding tensor that had been derived in non-relativistic theory is no longer valid. This means that obtaining the absolute shielding scale for the high atomic number nuclei such as Pt will have to wait until a new relationship, if any, can be found between these two tensor quantities in relativistic theory.

CJJ dedicates this report to the memory of the late Joan Mason whose interest in the NMR chemical shift spanned decades, and who introduced her to this Series of volumes as a junior co-author.

References

1. N. C. Pyper, *Chem. Phys. Lett.*, 1983, **204**, 96.
2. P. Pyykkö, *Chem. Phys.*, 1983, **74**, 1.
3. G. A. Aucar and J. Oddershede, *Int. J. Quantum Chem.*, 1993, **47**, 425.
4. T. Saue, V. Bakken, T. Enevoldsen, T. Helgaker, H. J. Aa. Jensen, J. Laerdahl, K. Ruud, J. Thyssen, and L. Visscher, DIRAC, A Relativistic *Ab initio* Electronic Structure Program, Release 3.2. (2000) (http://dirac.chem.sdu.dk).
5. L. Visscher, T. Enevoldsen, T. Saue and J. Oddershede, *J. Chem. Phys.*, 1998, **109**, 9677.
6. Y. Ishikawa, T. Nakajima, M. Hada and H. Nakatsuji, *Chem. Phys. Lett.*, 1998, **283**, 119.
7. M. Hada, Y. Ishikawa, J. Nakatani and H. Nakatsuji, *Chem. Phys. Lett.*, 1999, **310**, 342.
8. G. A. Aucar, T. Saue, L. Visscher and H. J. Aa. Jensen, *J. Chem. Phys.*, 1999, **110**, 6208.
9. L. Visscher, T. Enevoldsen, T. Saue, H. J. Aa. Jensen and J. Oddershede, *J. Comput. Chem.*, 1999, **20**, 1262.
10. J. Vaara and P. Pyykkö, *J. Chem. Phys.*, 2003, **118**, 2973.
11. M. Hada, R. Fukuda and H. Nakatsuji, *Chem. Phys. Lett.*, 2000, **321**, 452.
12. T. Enevoldsen, LK. Visscher, T. Saue, H. J. Aa. Jensen and J. Oddershede, *J. Chem. Phys.*, 2000, **112**, 3493.
13. S. S. Gomez, R. H. Romero and G. A. Aucar, *Chem. Phys. Lett.*, 2003, **367**, 265.
14. S. S. Gomez, R. H. Romero and G. A. Aucar, *J. Chem. Phys.*, 2002, **117**, 7942.
15. H. Fukui, T. Baba and H. Inomata, *J. Chem. Phys.*, 1996, **105**, 3175.
16. H. Fukui, T. Baba and H. Inomata, *J. Chem. Phys.*, 1997, **106**, 2987.
17. R. Bouten, E. J. Baerends, E. van Lenthe, L. Visscher, G. Schreckenbach and T. Ziegler, *J. Phys. Chem.*, 2000, **104**, 5600.
18. M. C. Ruiz de Azua, J. I. Melo and C. G. Giribet, *Mol. Phys.*, 2003, **101**, 3103.
19. J. I. Melo, M. C. Ruiz de Azua, C. G. Giribet, G. A. Aucar and R. H. Romero, *J.*

Chem. Phys., 2003, **118**, 471.
20. H. Nakatsuji, M. Hada, H. Kaneko and C. C. Ballard, *Chem. Phys. Lett.*, 1996, **255**, 195.
21. S. K. Wolff and T. Ziegler, *J. Chem. Phys.*, 1998, **109**, 895.
22. J. Vaara, K. Ruud and O. Vahtras, *J. Chem. Phys.*, 1999, **111**, 2900.
23. C. C. Ballard, M. Hada, H. Kaneko and H. Nakatsuji, *Chem. Phys. Lett.*, 1996, **254**, 170.
24. M. Hada, R. Fukuda and H. Nakatsuji, *Chem. Phys. Lett.*, 1996, **261**, 7.
25. H. Fukui and T. Baba, *J. Chem. Phys.*, 1998, **108**, 3854.
26. T. Baba and H. Fukui, *J. Chem. Phys.*, 1999, **110**, 131.
27. T. Baba and H. Fukui, *Mol. Phys.*, 2002, **100**, 623.
28. R. Fukuda, M. Hada and H. Nakatsuji, *J. Chem. Phys.*, 2003, **118**, 1015.
29. R. Fukuda, M. Hada and H. Nakatsuji, *J. Chem. Phys.*, 2003, **118**, 1027.
30. S. K. Wolff, T. Ziegler, E. van Lenthe and E. J. Baerends, *J. Chem. Phys.*, 1999, **110**, 7689.
31. M. A. M. Forgeron, R. E. Wasylishen and G. H. Penner, *J. Phys. Chem. A*, 2004, **108**, 4751.
32. H. Fukui and T. Baba, *J. Chem. Phys.*, 2002, **117**, 7836.
33. E. van Lenthe, E. J. Baerends and J. G. Snijders, *J. Chem. Phys.*, 1993, **99**, 4597.
34. J. R. Yates, C. J. Pickard, M. C. Payne and F. Mauri, *J. Chem. Phys.*, 2003, **118**, 5746.
35. M. Barys and A. J. Sadlej, *J. Chem. Phys.*, 2002, **116**, 2696.
36. H. Fukui, T. Baba, Y. Shiraishi, S. Imanishi, K. Kudo, K. Mori and M Shimoji, *Mol. Phys.*, 2004, **102**, 641.
37. I. Morishima, K. Endo and T. Yonezawa, *J. Chem. Phys.* 1973, **59**, 3356.
38. M. I. Volodicheva and T. K. Rebane, *Theor. Exp. Chem. Engl. Ed.* (*USSR*), 1978, **14**, 348.
39. A. A. Cheremisin and P. V. Schastnev, *J. Magn. Reson.*, 1980, **40**, 459.
40. H. Nakatsuji, H. Takashima and M. Hada, *Chem. Phys. Lett.*, 1995, **233**, 95.
41. H. Takashima, M. Hada and H. Nakatsuji *Chem. Phys. Lett.*, 1995, **235**, 13.
42. H. Nakatsuji, H. Takashima and M. Hada, *Chem. Phys. Lett.*, 1995, **247**, 418.
43. H. Nakatsuji, M. Hada, T. Tejima and T. Nakajima, *Chem. Phys. Lett.*, 1996, **249**, 284.
44. H. Kaneko, M. Hada, T. Nakajima and H. Nakatsuji *Chem. Phys. Lett.*, 1996, **261**, 1.
45. H. Nakatsuji, Z. M. Hu and T. Nakajima, *Chem. Phys. Lett.*, 1997, **275**, 429.
46. V. G. Malkin, O. L. Malkina and D. R. Salahub, *Chem. Phys. Lett.*, 1996, **261**, 335.
47. M. Kaupp, O. L. Malkina and V. G. Malkin, *Chem. Phys. Lett.*, 1997, **265**, 55.
48. M. Kaupp, O. L. Malkina, V. G. Malkin and P. Pyykkö, *Chem. Eur. J.*, 1998, **4**, 118.
49. M. Kaupp and O. L. Malkina, *J. Chem. Phys.*, 1998, **108**, 3648.
50. O. L. Malkina, B. Schimmelpfennig, M. Kaupp. B. A. Hess, P. Chandra, U. Wahlgren and V. G. Malkin, *Chem. Phys. Lett.*, 1998, **296**, 93.
51. M. Kaupp, C. Aubauer, G. Engelhardt, T. M. Kalpötke, and O. L. Malkina, *J. Chem. Phys.*, 1999, **110**, 3897.
52. J. Vaara, K. Ruud, O. Vahtras, H. Ågren and J. Jokisaari, *J. Chem. Phys.*, 1998, **109**, 1212.
53. G. Schreckenbach and T. Ziegler, *Int. J. Quantum Chem.* 1996, **60**, 753.
54. G. Schreckenbach and T. Ziegler, *Int. J. Quantum Chem.* 1997, **61**, 899.
55. M. Kaupp, V. G. Malkin, O. L. Malkina and D. R. Salahub, *Chem. Phys. Lett.*, 1995, **235**, 382.
56. M. Kaupp, V. G. Malkin, O. L. Malkina and D. R. Salahub, *J. Am. Chem. Soc.*,

1995, **117**, 1851.
57. M. Kaupp, V. G. Malkin, O. L. Malkina and D. R. Salahub, *J. Am. Chem. Soc.*, 1995, **117**, 8492.
58. J. Vaara, O. L. Malkina, H. Stoll, V. G. Malkin and M. Kaupp, *J. Chem. Phys.*, 2001, **114**, 61.
59. P. Manninen, P. Lantto, J. Vaara and K. Ruud, *J. Chem. Phys.*, 2003, **119**, 2623.
60. N. F. Ramsey, *Phys. Rev.*, 1950, **78**, 699.
61. W. H. Flygare, *J. Chem. Phys.*, 1964, **41**, 793.
62. F. Michelot, *Mol. Phys.*, 1982, **45**, 971.
63. T. D. Gierke and W. H. Flygare, *J. Am. Chem. Soc.*, 1972, **94**, 7277.
64. C. Pickard and F. Mauri, *Phys. Rev. B*, 2001, **63**, 245101.
65. H. Eckert, K. Moran, D. Franke and C. Hudalla, pp.49–73. in J. A. Tossell, ed. *Nuclear Magnetic Shieldings and Molecular Structure*, NATO ASI Series Vol. 386, Kluwer Academic Press, Dordrecht, 1993.
66. N. F. Ramsey, *Phys. Rev. A*, 1970, **1**, 1320.
67. J. Vaara, P. Manninen and J. Lounila, *Chem. Phys. Lett.*, 2003, **372**, 750.
68. P. Manninen and J. Vaara, *Phys. Rev. A*, 2004, **69**(02), 2503.
69. M. R. Bendall and D. M. Doddrell, *J. Magn. Reson.*, 1979, **33**, 659.
70. G. Magyarfalvi and P. Pulay, *J. Chem. Phys.*, 2003, **119**, 1350.
71. J. Baker and P. Pulay, *J. Comput. Chem.*, 2003, **24**, 1184.
72. T. W. Keal, D. J. Tozer and T. Helgaker, *Chem. Phys. Lett.*, 2004, **391**, 374.
73. D. B. Chesnut, *Chem. Phys. Lett.*, 2003, **380**, 251.
74. M. A. Watson, N. C. Handy, A. J. Cohen and T. Helgaker, *J. Chem. Phys.*, 2004, **120**, 7252.
75. W. M. Hoe, A. J. Cohen and N. C. Handy, *Chem. Phys. Lett.*, 2001, **341**, 319.
76. T. W. Keal and D. J. Tozer, *J. Chem. Phys. Lett.*, 2003, **119**, 3015.
77. J. C. Facelli, *Concepts Magn. Reson. A*, 2004, **20**, 42.
78. H. U. Siehl, T. Muller and J. Gauss, *J. Phys. Org. Chem.*, 2003, **16**, 577.
79. H. U. Siehl, T. Muller and J. Gauss, *J. Phys. Org. Chem.*, 2003, **16**, 880.
80. E. Kleinpeter, S. Klod and W. D. Rudorf, *J. Org. Chem.*, 2004, **69**, 4317.
81. A. Koch, B. Mikhova and E. Kleinpeter, *J. Mol. Struc.*, 2004, **694**, 149.
82. K. B. Wiberg, J. D. Hammer, K. W. Zilm, T. A. Keith, J. R. Cheeseman and J. C. Duchamp, *J. Org. Chem.*, 2004, **69**, 1086.
83. C. Adamo and V. Barone, *Chem.Phys. Lett.*, 1997, **274**, 242.
84. K. B. Wiberg, J. D. Hammer, K. W. Zilm, J. R. Cheeseman and T. A. Keith, *J. Phys. Chem. A*, 1998, **102**, 8766.
85. A. V. Mitin, J. Baker and P. Pulay, *J. Chem. Phys.*, 2003, **118**, 7775.
86. D. B. Chesnut *Chem. Phys. Lett.*, 1995, **246**, 235.
87. D. B. Chesnut and L. D. Quin, *Heteroatom Chem.*, 2004, **15**, 216.
88. K. W. Feindel and R. E. Wasylishen, *Can. J. Chem.*, 2004, **82**, 27.
89. H. Fukaya and T. Ono, *J. Comput. Chem.*, 2004, **25**, 51.
90. W. Adcock, J. E. Peralta and R. H. Contreras, *Magn. Reson. Chem.*, 2003, **41**, 503.
91. I. Alkorta and J. Elguero, *Struct. Chem.*, 2003, **14**, 377.
92. A. Balandina, V. Mamedov, F. Xavier, F. Bruno and S. Latypov, *Tetrah. Lett.*, 2004, **45**, 4003.
93. I. Alkorta, J. Elguero, N. Jagerovic, A. Fruchier and G. P. A. Yap, *J. Heterocyclic Chem.*, 2004, **41**, 285.
94. C. Bassarello, P. Cimino, L. Gomez-Paloma, R. Riccio and G. Bifulco, *Tetrah.*, 2003, **59**, 9555.
95. T. L. C. Martins, T. C Ramalho, J. D. Figueroa-Villar, A. F. C. Flores and C. M. P. Pereira, *Magn. Reson. Chem.*, 2003, **41**, 983.

96. J. A. Dobado, N. Benkadour, S. Melchor and D. Portal, *Theochem, J. Mol. Struc.*, 2004, **672**, 127.
97. W. Migda and B. Rys, *Magn. Reson. Chem.*, 2004, **42**, 459.
98. G. Bifulco, L. Gomez-Paloma and R. Riccio, *Tetrah. Lett.*, 2003, **44**, 7137.
99. J. Tousek, J. Dostal and R. Marek, *J. Mol. Struc.*, 2004, **689**, 115.
100. K. Malek, M. Vala, H. Kozlowski and L. M. Proniewicz, *Magn. Reson. Chem.*, 2004, **42**, 23.
101. M. Trabelsi, M. Salem and B. Champagne, *Org. Biomol. Chem.*, 2003, **1**, 3839.
102. T. Muller, *J. Organomet. Chem.*, 2003, **686**, 251.
103. J. Y. Shen and T. Hughbanks, *J. Phys. Chem. A*, 2004, **108**, 350.
104. A. Bagno, F. Rastrelli and G. Saielli, *J. Phys. Chem. A*, 2003, **107**, 9964.
105. F. Cisnetti, K. Loth, P. Pelupessy and G. Bodenhausen, *Chem. Phys. Chem.* 2004, **5**, 807.
106. L. M. Shao, C. Crockford, H. Geen, G. Grasso and J. J. Titman, *J. Magn. Reson.*, 2004, **167**, 75.
107. N. Asakawa, *Theochem, J. Mol. Struc.*, 2004, **675**, 29.
108. C. Gardiennet and P. Tekely, *Concepts Magn. Reson. A* 2004, **22**, 106.
109. J. C. C. Chan and R. Tycko, *J. Am. Chem. Soc.*, 2003, **125**, 11828.
110. R. Tycko and Y. Ishii, *J. Am. Chem. Soc.*, 2003, **125**, 6606.
111. N. A. Oyler and R. Tycko, *J. Am. Chem. Soc.*, 2004, **126**, 4478.
112. J. Kurita, H. Shimahara, N. Utsunomiya-Tate and S. Tate, *J. Magn. Reson.*, 2003, **163**, 163.
113. Y. Nishiyama, A. Kubo and T. Terao, *J. Chem. Phys.*, 2003, **119**, 3297.
114. H. Kaji, K. Fuke and F. Horii, *Macromolecules*, 2003, **36**, 4414.
115. R. J. Iuliucci, J. Clawson, J. Z. Hu, M. S. Solum, D. Barich, D. M. Grant and C. M. V. Taylor, *Solid State Nucl. Magn. Reson.*, 2003, **24**, 23.
116. M. M. Slabicki, M. J. Potrzebowski, G. Bujacz, S. Olejniczak and J. Olczak, *J. Phys. Chem. B*, 2004, **108**, 4535.
117. J. S.. Clawson, K. L. Anderson, R. J. Pugmire and D. M. Grant, *J. Phys. Chem. A*, 2004, **108**, 2638.
118. A. Hauch, H. Bildsoe, H. J. Jakobsen and J. Skibsted, *J. Magn. Reson.*, 2003, **165**, 282.
119. D. L. Bryce, K. Eichele and R. E. Wasylishen, *Inorg. Chem.*, 2003, **42**, 5085.
120. C. Gervais, M. Profeta, V. Lafond, C. Bonhomme, T. Azais, H. Mutin, C. J. Pickard, F. Mauri and F. Babonneau, *Magn. Reson. Chem.* 2004, **42**, 445
121. A. V. Ivanov, A. C. Larsson, N. A. Rodionova, A. V. Gerasimenko, O. N. Antzutkin and W. Forsling, *Russian J. Inorg. Chem.*, 2004, **49**, 373.
122. M. Pompetzki, L. van Wullen and M. Jansen, *Zeit. Anorg. Allgem. Chem.*, 2004, **630**, 384.
123. K. Y. Lee, T. H. Kim, Y. W. Shin and J. Kim, *Bull. Korean Chem. Soc.*, 2004, **25**, 529.
124. J. Jokisaari and J. Autschbach, *Phys. Chem. Chem. Phys.*, 2003, **5**, 4551.
125. J. M. Geller, I. S. Butler, D. F. R. Gilson, F. G. Morin, I. Wharf and F. Belanger-Gariepy, *Can. J. Chem.*, 2003, **81**, 1187.
126. I. Hung and R. W. Schurko, *Solid State Nucl. Magn. Reson.*, 2003, **24**, 78.
127. P. O. Astrand and K. Ruud, *Phys. Chem. Chem. Phys.*, 2003, **5**, 5015.
128. A. Dransfeld, *Chem. Phys.*, 2004, **298**, 47.
129. A. A. Auer, J. Gauss and J. F. Stanton, *J. Chem. Phys.*, 2003, **118**, 10407.
130. M. Buhl, R. Schurhammer and P. Imhof, *J. Am. Chem. Soc.*, 2004, **126**, 3310.
131. A. A. Wu, D. Cremer and J. Gauss, *J. Phys. Chem. A*, 2003, **107**, 8737.
132. E. P O'Brien and G. Moyna, *Carb. Res.*, 2004, **339**, 87.
133. H. H. Sun and E. Oldfield, *J. Am. Chem. Soc.*, 2004, **126**, 4726.

134. A. Allerhand, R. F. Childers and E. Oldfield, *Biochemistry*, 1973, **12**, 1335.
135. A. Perczel, A. K. Fuzery and A. G. Csaszar, *J. Comput. Chem.*, 2003, **24**, 1157.
136. M. N. Manalo and A. C. de Dios, *Theochem, J. Mol. Struc.*, 2004, **675**, 1.
137. M. Strohmeier and D. M. Grant, *J. Am. Chem. Soc.*, 2004, **126**, 966.
138. E. Y. Chekmenev, Q. W. Zhang, K. W. Waddell, M. S. Mashuta and R. J. Wittebort, *J. Am. Chem. Soc.*, 2004, **126**, 379.
139. E. Czinki and A. G. Csaszar, *Theochem, J. Mol. Struc.*, 2004, **675**, 107.
140. A. Czajlik and A. Perczel, *Theochem, J. Mol. Struc.*, 2004, **675**, 129.
141. S. Saen-Oon, S. Hannongbua and P Wolschann, *J. Chem. Informat. Comput. Sci.*, 2003, **43**, 1412.
142. A. T. Petkova, G. Buntkowsky, F. Dyda, R. D. Leapman, W. M. Yau and R. Tycko, *J. Mol. Biol.*, 2004, **335**, 247.
143. T. Charpentier, S. Ispas, M. Profeta, F. Mauri and C. J. Pickard, *J. Phys. Chem. B*, 2004, **108**, 4147.
144. K. Vermillion, P. Florian, and P. Grandinetti, *J. Chem. Phys.*, 1998, **108**, 7274.
145. T. Clark, P. Grandinetti, P. Florian and J. F. Stebbins, *J. Phys. Chem.*, 2001, **105**, 12257.
146. P. Grandinetti, J. Baltisberger, I. Farnan, J. F. Stebbins, U. Werner and A. Pines, *J. Phys. Chem.*, 1995, **99**, 12341.
147. I. Farnan, P. Grandinetti, J. Baltisberger, J. F. Stebbins, U. Werner, M. A. Eastman and A. Pines, *Nature.*, 1992, **358**, 31.
148. J. Stare, A. Jezierska, G. Ambrozic, I. J. Kosir, J. Kidric, A. Koll, J. Mavri and D. Hadzi, *J. Am. Chem. Soc.*, 2004, **126**, 4437.
149. D. Pucar, P. P. Dzeja, P. Bast, R. J. Gumina, C. Drahl, L. Lim, N. Juranic, S. Macura and A. Terzic, *Mol. Cell. Biochem.*, 2004, **256**, 281.
150. N. S. Golubev, S. M. Melikova, D. N. Shchepkin, J. G. Shenderovich, P. A. Tolstoy and G. S. Denisov, *Zeit. Physik. Chem.-Int. J. Res. Phys. Chem. Chem. Phys.*, 2003, **217**, 1549.
151. C. J. Jameson and S. Murad, *Chem. Phys. Lett.*, 2003, **380**, 556.
152. B. Mennucci and R. Cammi, *Intl. J. Quantum Chem.*, 2003, **93**, 121.
153. G. R. Goward, D. Sebastiani, I. Schnell, H. W. Spiess, H. D. Kim and H. Ishida, *J. Am. Chem. Soc.*, 2003, **125**, 5792.
154. G. Wu and K. Yamada, *Solid State Nucl. Magn. Reson.*, 2003, **24**, 196.
155. H. Cybulski, M. Pecul, J. Sadlej and T. Helgaker, *J. Chem. Phys.*, 2003, **119**, 5094.
156. R. K. Harris, P. Y. Ghi, R. B. Hammond, C. Y. Ma and K. J. Roberts, *Chem. Commun.*, **2003**, 2834.
157. D. Sebastiani, G. Goward, I. Schnell and H. W. Spiess, *Theochem, J. Mol. Struct.*, 2003, **625**, 283.
158. B. H. Ye, I. D. Wilhams and X. Y. Li, *J. Inorg. Biochem.*, 2002, **92**, 128.
159. C. L. Perrin, J. S. Lau and B. K. Ohta, *Pol. J. Chem.*, 2003, **77**, 1693.
160. S. Macholl, F. Borner and G. Buntkowsky, *Zeit. Physik. Chem.-Int. J. Res. Phys. Chem. Chem. Phys.*, 2003, **217**, 1473.
161. M. Witanowski, Z. Biedrzycka, W. Sicinska and Z. Grabowski, *J. Magn. Reson.*, 2003, **164**, 212.
162. V. Gaponenko, S. P. Sarma, A. S. Altieri, D. A. Horita, J. Li and R. A. Byrd, *J. Biomol. NMR*, 2004, **28**, 205.
163. R. Barbieri, C. Luchinat and G. Parigi, *Chem. Phys. Chem.* 2004, **5**, 797.
164. C. J. Jameson and A. C. de Dios, *J. Chem. Phys.*, 2002, **116**, 3805.
165. T. Koskela, J. Jokisaari and C. Satyanarayana, *Micropor. Mesopor. Mater.*, 2004, **67**, 113.
166. J. Autschbach and E. Zurek, *J. Phys. Chem. A*, 2003, **107**, 4967.

167. D. N. Sears and C. J. Jameson, *J. Chem. Phys.*, 2003, **118**, 9987.
168. M. Cifelli, J. Saunavaara, J. Jokisaari and C. A. Veracini, *J. Phys. Chem. A*, 2004, **108**, 3973.
169. H. Kobayashi, T. Ueda, K. Miyakubo and T. Eguchi, *Zeit. Naturf. A*, 2003, **58**, 727.
170. A. Hoffmann, D. Sebastiani, E. Sugiono, S. Yun, K. S. Kim, H. W. Spiess and I. Schnell, *Chem. Phys. Lett.*, 2004, **388**, 164.
171. D. N. Sears, C. J. Jameson and R A Harris, *J. Chem. Phys.*, 2003, **119**, 2685.
172. D. N Sears, C. J. Jameson and R. A. Harris, *J. Chem. Phys.*, 2003, **119**, 2691.
173. D. N. Sears, C. J. Jameson and R. A. Harris, *J. Chem. Phys.*, 2003, **119**, 2694.
174. D. N. Sears, C. J. Jameson and R. A. Harris, *J. Chem. Phys.*, 2004, **120**, 3277.
175. D. N. Sears and C. J. Jameson, *J. Chem. Phys.*, 2003, **119**, 12231.
176. D. Stueber and C. J. Jameson, *J. Chem. Phys.*, 2004, **120**, 1560.
177. I. L. Moudrakovski, C. I. Ratcliffe and J. A. Ripmeester, *J. Am. Chem. Soc.* 2001, **123**, 2066.
178. K. A. Udachin, G. D. Enright, C. I. Ratcliffe and J. A. Ripmeester, *J. Am. Chem. Soc.* 1997, **119**, 11481.
179. C. J. Jameson and D. Stueber, *J. Chem. Phys.*, 2004, **120**, 10200.
180. J. A. Ripmeester, C. I. Ratcliffe and J. S. Tse, *J. Chem. Soc. Faraday Trans.* 1988, **84**, 3731.
181. C. S. Wannere and P. v. R. Schleyer, *Org. Lett.* 2003, **5**, 605.
182. R. G. Viglione, R. Zanasi and P. Lazzeretti, *Org. Lett.*, 2004, **6**, 2265.
183. M. B. Ferraro, P. Lazzeretti, R. G. Viglione and R. Zanasi, *Chem. Phys. Lett.*, 2004, **390**, 268.
184. M. Zora and I. Ozkan, *Theochem, J. Mol. Struc.*, 2003, **638**, 157.
185. I. Alkorta, J. Elguero, M. Eckert-Maksic and Z. B. Maksic, *Tetrah.*, 2004, **60**, 2259.
186. T. Okazaki and K. K. Laali, *J. Org. Chem.*, 2004, **69**, 510.
187. T. Okazaki and K. K Laali, *Org. Biomol. Chem.*, 2003, **1**, 3078.
188. T. Heine, P. V. Schleyer, C. Corminboeuf, G. Seifert, R. Reviakine and J. Weber, *J. Phys. Chem. A*, 2003, 107, 6470.
189. I. G. Cuesta, R. S. Jartin, A . S. de Meras and P. Lazzeretti, *J. Chem. Phys.*, 2004, **120**, 6542.
190. E. Kleinpeter and S. Klod, *J. Am. Chem. Soc.*, 2004, **126**, 2231.
191. R. J. Abraham, M. Moblil and R. J. Smith, *Magn. Reson. Chem.*, 2004, **42**, 436.
192. G. W. Wang, X. H. Zhang, H. Zhan, Q. X. Guo and Y. D. Wu, *J. Org. Chem.*, 2003, **68**, 6732.
193. A. Simperler, R. G. Bell and M. W. Anderson, *J. Phys. Chem. B*, 2004, **108**, 7142.
194. T. Ueda, G. M. Bernard, R. McDonald and R. E. Wasylishen, *Solid State Nucl. Magn. Reson.*, 2003, **24**, 163.
195. S. G. Kozlova, S. P. Gabuda and R. Blinc, *Chem. Phys. Lett.*, 2003, **376**, 364.
196. S. H. Cai, X. Y. Yu, Z. Chen and H. L. Wan, *Magn. Reson. Chem.*, 2003, **41**, 902.
197. D. Sebastiani, *Modern Phys. Lett. B*, 2003, **17**, 1301.
198. A. C. de Dios, J. G. Pearson and E. Oldfield, *Science*, 1993, **260**, 1491.
199. P. B. Karadakov and K. Morokuma, *Chem.Phys. Lett.*, 2000, **317**, 589.
200. Q. Cui and M. Karplus, *J. Phys. Chem. B*, 2000, **104**, 3721.
201. D. Sebastiani and U. Rothlisberger, *J. Phys. Chem. B*, 2004, **108**, 2807.
202. D. L. Bryce and R. E. Wasylishen, *Acc. Chem. Research*, 2003, **36**, 327.
203. S. A. Cooke, M. C. L. Gerry, D. J. Brugh and R. D. Suenram, *J. Mol. Spectrosc.*, 2004, **223**, 185.

3
Application of Nuclear Shielding

BY SHIGEKI KUROKI, NAOKI ASAKAWA AND HIDEKAZU YASUNAGA

1 Introduction

The report covers and introduces studies on the application of nuclear shielding and related NMR chemical shifts in the world from 1 June 2003 to 31 May 2004. The shieldings of particular nuclear species are described in the following section according to their position in the periodic table. Although there is a great number of articles on NMR spectroscopy during the period of this review, the coverage of this chapter is restricted to widely available and common journals, which are published in English as a general rule, due to space limitation.

2 Shielding of Particular Nuclear Species

The NMR experiments for most elements contained in molecules were made in the course of physical, chemical or biological studies during the period covered by the report. The simple structure determination and related studies of natural products or macromolecules are excluded in the report, and the review articles are given as necessity requires.

2.1 Group 1 (^{1}H, ^{2}H, ^{6,7}Li, ^{23}Na, ^{39}K, ^{87}Rb, ^{133}Cs). – *2.1.1 Hydrogen* (^{1}H) ($I = 1/2$). The conventional explanations of ^{1}H NMR chemical shifts concerning ring current of conjugated systems were revised.[1] It was revealed by ab initio (IGLO) analyses that the downfield shift of ^{1}H chemical shift for benzene is not due to deshielding ring current effects. Covalently bonded hydrogen nuclei located over the plane of a carbonyl group in a strong magnetic field experience magnetic shielding that results from the combined effect of the magnetic anisotropy of the carbon-oxygen double bond and various other intramolecular shielding effects. Gauge-including AOs - Hartree-Fock (GIAO-HF) in Gaussian 98 was employed to calculate isotropic shielding values and to predict the net proton NMR shielding increment for a simple model system: the proximate proton of methane held in various positions over formaldehyde.[2] An accurate estimation of chemical shift of a proton in the vicinity of a carbon-oxygen double bond could be accomplished and this can assist in spectral assignments and in correct structure determination. The ^{1}H chemical shifts of benzaldehydes were

Nuclear Magnetic Resonance, Volume 34
© The Royal Society of Chemistry, 2005

assigned in $CDCl_3$ and DMSO solution and the carbonyl substituent chemical shifts for the molecules were analysed in terms of the carbonyl electric field, magnetic anisotropy and steric effects for long-range protons together with a model (CHARGE7). The CO anisotropy and O shielding differ appreciably from the corresponding values for the aliphatic aldehydes and ketones.[3] The aromaticity was studied in terms of a delocalized ring current contribution to the ^{1}H NMR shielding of ferrocene, benzene, bis(benzene)chromium, hexamethylbenzene ruthenocene and related compounds.[4] The ^{1}H, ^{13}C and ^{15}N NMR spectra for monomethyl substituted tetramethyl 9a*H*- and 4*H*-quinolizine-1, 2, 3, 4-tetracarboxylate were calculated theoretically at the Hartree-Fock level by using the polarized double zeta (PDZ) basis set of Hansen and Bouman for the geometries optimized at the same level.[5] The structures of cis-[$Os(bpy)_2(CO)(Cl)$] [(PF_6)] and cis-[$Os(bpy)_2(CO)(H)$] [(PF_6)] (bpy = 2, 2′-bipyridine) were clarified by ^{1}H NMR and X-ray measurements.[6] The experimental ^{1}H NMR data were interpreted with the aid of magnetic shielding constant calculations by the GIAO method, and the assignment of the proton spectrum was confirmed by the ^{1}H-^{1}H NOESY results. Twelve secondary phenylselenenylalkanes and cycloalkanes were studied by ^{1}H, ^{13}C and ^{77}Se NMR spectroscopy in the presence of the chiral dirhodium, and two different mechanisms of ligand exchange were characterized and discussed.[7] The degree of aromaticity of neutral and charged cyclic and potentially homoaromatic hydrocarbon species (C_mH_{m+1q}, m = 4-13, q = −1, 0, 1, 2) with (4n + 2; n = 0, 1, 2) p electrons were studied by calculating the magnetic shieldings in selected points. The ring-current susceptibility with respect to an external magnetic field was estimated by employing the aromatic ring-current shielding (ARCS) method.[8] The 1, 3-dipolar cycloaddition reactions of 2-phenylisatogen and its 3-phenylimino derivative with electron-deficient alkenes are reported.[9] Their regioisomers and the chemical shifts were obtained by ab initio calculations of the ^{1}H NMR shielding tensor. The thermolysis products obtained by refluxing a series of vic-dihydroxychlorins in *o*-dichlorobenzene are characterized and studied by extensive NMR (COSY, ROESY) experiments and molecular modelings.[10] Their dimeric structure is tilted toward the opposite ring as evident by the shielding effect in the resonances of some of the protons in the ^{1}H NMR spectroscopy. The synthesis of syn-sesterbicyclo [2.2.2]octene I bilaterally grafted by an exocyclic σ-cis-butadiene moiety is achieved and the ^{1}H NMR demonstrates the anisotropic shielding effect operating within the three parallel laticyclic double bonds.[11] The cyclic triamide of 3′-amino-3-biphenylcarboxlic acid synthesized, which is a novel class of anion receptors with a large central cavity, was studied by ^{1}H NMR.[12] The chemical shift change gives information on the geometry of the bound anion and the hydrogen bond donors for anion binding. Zero-point vibrationally averaged nuclear shielding constants were calculated for 24 fluoro-containing organic compounds ranging in size from fluoromethane to difluorobenzene.[13] The chemical shifts relationships measured relative to TMS (tetramethylsilane) and DSS (sodium salt of 2,2-dimethyl-2-silapentane-5-sulfonic acid) were studied by solution NMR and solid-state magic-angle-spinning (MAS) NMR.[14] The DSS and TMS reference scales for ^{13}C and ^{1}H were related accurately using MAS NMR. A simple

semi-empirical physical local model was presented in order to fit the chemical shift data of mixtures. The 50 sets of data for 14 systems were correlated, indicating that the new model can well correlate the ^{1}H NMR chemical shift literature data of binary mixtures with only one parameter.[15] The ^{1}H NMR chemical shift spectra of proton conducting crystals for systems under periodic boundary conditions were computed and compared with experimental spectra yields an excellent agreement.[16] The information on the intracellular pH (pHI) of oxidative and glycolytic fibers are obtained from ^{1}H NMR signals (7.7-8.6 and 6.8-7.4 ppm regions) of frog muscle.[17] The 4-Aza-5α-androstanone and 4-aza-5β-androstanone I were synthesized in order to obtain the NMR shielding parameters for the secondary amine group. Drastic chemical shift change of protons near-by nitrogen atom of ammonium salt was observed and shielding parameter for the secondary ammonium group was obtained.[18] Magnetic susceptibility and nuclear magnetic shielding at the nuclei of bis-heteropentalenes formed by two pyrrole units were evaluated by a series of different approximations and a large Gaussian basis set. The theoretical findings are used to assess a diatropicity scale for these molecules.[19] The naphthyl protons of the *trans*-10*b*-methyl-10*c*-(2-naphthyl)- and *trans*-10*b*-methyl-10*c*-(1-naphthyl)-10*b*, 10*c*-dihydropyrene **5** and **6**, respectively were measured by ^{1}H NMR and the signals are well resolved in their spectra due to a strong shielding effect of the dihydropyrene ring.[20] It was found that there is free rotation of the 2-naphthyl ring in **5** on the NMR time scale, whereas the 1-naphthyl ring in **6** is conformationally rigid. ^{1}H and ^{13}C NMR spectra of the oxocarboxylic acid oximes 2-(hydroxyimino)propanoic acid (**1**), 2-(4-methylthiazol-2-yl)-2-(hydroxyimino)acetic acid (**2**) and 2-cyano-2-(hydroxyimino)acetic acid (**3**) were measured in DMSO-d_6, D_2O and acetone- d_6 solutions.[21] Total energy calculations of the stability of various hydrogen-bonded species, equilibrium parameters and chemical shifts were calculated using ab initio methods (RHF, MP2) and density functional theory (B3LYP), implemented in the Gaussian 98 software package. The gauge-including AO (GIAO) method was used to predict magnetic shielding constants. The contributions of different vibrational isotope effects to H/D NMR isotope shifts were estimated by using ab initio calculations of ^{1}H, ^{19}F magnetic shielding tensors of hydrogen difluoride ion as the functions of three coordinates of symmetry.[22] An unusually strong paramagnetic deshielding of H for the equilibrium geometry of the [FHF]- ion is noted. The investigation of conformational preference for aldol adducts is conducted employing ^{1}H NMR spectroscopy, X-ray crystallography and computational methods.[23] A lower shielding of poly(ethylene oxide) (PEO) protons was found for PEO/hydroxybenzene and PEO/$LiCF_3SO_3$ complexes in comparison with neat PEO by using solid-state NMR.[24] The proton distances in complexes of PEO and benzene derivatives were estimated from 2D ^{1}H CRAMPS exchange NMR spectra. The two different conformations for different acetylmandelate groups of *D*-1, 4-di-*O*-(*O*-acetylmandeloyl)-2, 3: 5, 6-di-*O*-isopropylidene-myo-inositol shown in X-ray crystal structure was studied complementarily by ^{1}H NMR. The anisotropic shielding effect was observed and rationalized.[25] Norchelerythrine and norsanguinarine, tertiary benzo[*c*]phenanthridine alkaloids, were studied by gradient-selected 2D NMR

spectroscopy and extensive theoretical calculations.[26] ^{1}H, ^{13}C and ^{15}N chemical shifts assignments of the isoquinoline alkaloids based on NOE and multiple-bond chemical shift correlation experiments (GSQMBC) were reported. The experimental ^{1}H NMR spectra for the *E* and *Z* isomers of alkyl Ph ketone phenylhydrazones R1-C(Ph):N-NH-Ph (R1 = Me, Et, *i*-Pr and *t*-Bu) were simulated by ab initio GIAO calculations and the deviations from Karabatsos' rule or from the assignment of Bellamy and Hunter were discussed in the light of the optimized geometrical structures.[27] The concentration dependence of the ^{1}H-NMR chemical shifts of the aromatic protons in sampangine derivatives with a fused imidazole ring was observed and the concentration variation was discussed.[28] There is a computer program named SHIFTX, which rapidly and accurately calculates the diamagnetic ^{1}H, ^{13}C and ^{15}N chemical shifts of backbone and sidechain atoms in proteins. The chemical shift hypersurfaces obtained by SHIFTX capture dihedral angle, sidechain orientation, secondary structure and nearest neighbor effects.[29] Feed-forward neural networks (FFNN) were trained for the general prediction of ^{1}H NMR chemical shifts of CH_n protons in organic compounds in $CDCl_3$.[30] Predictions were obtained for an independent test set of 952 cases with a small mean average error, which significantly better than those obtained with counter propagation neural networks. Moreover, two different ways were explored to incorporate new available experimental data into previously trained ensembles of FFNN, for the structure-based prediction of ^{1}H NMR chemical shifts of organic compounds.[31] One approach uses the new data as the memory of an associative neural network (ASNN) system. Another neural network was trained to predict the ^{1}H, ^{13}C and ^{15}N of proteins using their three-dimensional structure as well as experimental conditions as input parameters.[32] The method has the potential to not only support the assignment process of proteins but also help with the validation and the refinement of three-dimensional structural proposals. Density functional theory (DFT) and HF quantum mechanics calculations were performed on the disaccharides, β-L-Fucp-(1→4)-α-D-Galp-OMe, β-L-Fucp-(1→4)- α-D-Glcp-OMe and β-L-Fucp-(1→3)-α-D-Glcp-OMe.[33] The chemical shifts of hydroxy protons of the disaccharides and a water/methanol/ethers system were obtained and shielding of the hydroxy proton of methanol is observed. The shielding is a consequence of reduced hydration due to intermolecular hydrogen bonding or steric effects. The anisotropic effect of a proximally introduced ethynyl group on the chemical shifts of H-4 and C-4 of the phenanthrene skeleton was calculated by using GIAO-HF/NICS methods and the anisotropic effect was determined to be only negligible in magnitude. Partitioning of the chemical shieldings of H-4 and C-4 by the NCS-NBO method revealed that steric compression is able to account for the large downfield shifts of both H-4 and C-4 in 11-ethynylphenanthrene relative to phenanthrene.[34]

2.1.2 Deuterium (^{2}H) ($I = 1$). The ^{2}H chemical shift anisotropies (CSAs) for polycrystalline samples were determined by ^{2}H MAS NMR spectroscopy at high magnetic field strength (14.1 T). It was shown that the precision of the CSA parameters depends strongly on the asymmetry parameter (η_Q) for the ^{2}H

quadrupole coupling tensor.[35] The inhomogeneous broadening arising from both chemical and/or paramagnetic shift anisotropy and a 1st-order I = 1 quadrupolar interaction was observed by a simple 2-pulse spin-echo ^{2}H NMR experiment.[36] The ^{2}H NMR spectra for a paramagnetic solid ($CuCl_{2.2}$•D_2O) and a non-paramagnetic solid ($D_2C_2O_{4\,2}$·D_2O) obtained by the method are significantly less distorted than those provided by the conventional quadrupolar-echo method.

2.1.3 Lithium (^{6,7}*Li*) (*I* = 1, 3/2). The ^{6,7}Li MAS NMR spectra of lithium ions in paramagnetic host materials such as $LiMO_2$ compounds were studied and density functional theory (DFT) calculations in the generalized gradient approximation were made.[37] ^{7}Li Knight shift and spin-lattice relaxation times for $LiRuSn_4$ prepared indicates that it has a much higher electron density at the Li atom arising from conduction electrons at the Fermi level.[38] ^{6}Li MAS NMR spectroscopy was used to study the structure of $LiMn_2O_4$ spinel samples prepared using different annealing methods. The NMR spectra of the delithiated samples, $Li_xMn_2O_4$, exhibit a gradual shift in the position of main spinel resonances with decreasing lithium content for $0.3 < x < 1.0$.[39] Electrochemical insertion of Li into pyrolysed amorphous carbons prepared from polymeric precursors of methacrylonitrile and divinylbenzene was studied by ^{7}Li variable temperature static and MAS NMR. The large chemical shift effects indicate that the structural and electronic properties of the inserted reversible Li species are sensitively dependent on the extent of loading.[40] The Li_xC_6 contained in a plastic Li/C battery was studied by the continuous in situ static ^{7}Li NMR. By comparing the Knight shift with that of Li_0, the charge transfer from Li to C can be estimated.[41] In situ magnetic resonance was also performed for a Li battery in order to obtain data, which determine of the ^{7}Li Knight shift, the line width and the relaxation time T_1.[42] The data indicates the presence of quasi-metallic Li, which diffuses less in metal and in graphite. The ^{7}Li MAS NMR spectra for the glasses of $(LiCl)_x(LiPO_3)_{1-x}$ ($x \leqslant 0.45$) have a broad signal and a linear dependence of the chemical shift on LiCl composition (x) is observed showing the formation of gamorphous LiCl aggregate regionsh in the glasses.[43] Static ^{7}Li solid-state NMR spectra revealed motional narrowing effects >300 K for Li in $LiAg_2Sn$, which is weakly Pauli paramagnetic and a good metallic conductor. The modestly small ^{7}Li Knight shift is thought to be a nearly complete state of Li ionization.[44]

2.1.4 Sodium (^{23}*Na*) (*I* = 3/2). A variety of Na metallocenes (sodocenes) were studied by ^{23}Na and ^{13}C solid-state NMR and simulations of ^{23}Na MAS NMR spectra yielded ^{23}Na quadrupolar coupling constants and asymmetry parameters.[45] Ab initio calculations were performed on a variety of structural models to gain insight into the nature of the electric field gradient and chemical shielding tensors. $NaCoO_2$ and $HCoO_2$ were studied by ^{59}Co and ^{23}Na NMR at 3 different magnetic field strengths (4.7, 7.1 and 11.7 T) and the ^{59}Co and ^{23}Na quadrupole and anisotropic shift tensors were determined by iterative fitting of the NMR line shapes at the field strengths.[46] The ^{23}Na chemical shift anisotropy

can be reproduced by shift tensor calculations using a point dipole model and considering the magnetic susceptibility. The local environment around Na^+ in charge-balanced aluminosilicate glasses (the $NaAlO_2$-SiO_2) was investigated by ^{23}Na MAS NMR spectroscopy at varying magnetic fields (9.4, 14.1 and 18.8 T), as well as triple-quantum (3Q) MAS NMR spectroscopy at 9.4 T. It was found that ^{23}Na chemical shifts in binary (Al-free) sodium silicate glasses are more deshielded and have ranges distinct from those of aluminosilicate glasses.[47] The effects of NaCl on the aggregation of two typical thiacarbocyanine dyes (3, 3′-di(3-sulfopropyl)-4, 5, 4′, 5′-dibenzo-9-phenyl- thiacarbocyanine tri-Et ammonium salt and 3, 3′-di(3-sulfopropyl)-4, 5, 4′, 5′-dibenzo- 9-methyl-thiacarbocyanine tri-Et ammonium salt) were studied by using ^1H and ^{23}Na NMR measurements.[48] It was found that the J-aggregation of two dyes can be promoted by the addition of NaCl and that the effective coherence length of the J-aggregate is shorter than that obtained without NaCl. The apparent association constants between Na^+ ions and dye molecules in J-aggregates were estimated from the chemical shifts of ^{23}Na. The chelates structure of the Na salt of $[Gd(DOTP)]_5^-$ (H_8DOTP = 1, 4, 7, 10- tetraazacyclododecane 1, 4, 7, 10-tetrakis(methylenephosphonic acid)) in solution was studied by using ^{23}Na NMR shift data.[49]

2.1.5 Potassium (^{39}K) ($I = 3/2$). Three G-quadruplex structures formed by self-assembly of 5′-tert-butyl-dimethylsilyl-2′, 3′-O-isopropylidene guanosine, guanosine and GMP were studied by solid-state ^{39}K NMR, and NMR spectra clearly show different spectral signatures for K^+ ions inside the G-quadruplex channel and for K^+ ions bound to the phosphate groups.[50]

2.1.6 Rubidium (^{87}Rb) ($I = 3/2$). The structure of $Rb_2[Pd(Se_4)_2]\cdot Se_8$ was studied by ^{87}Rb MAS and static NMR and ^{77}Se MAS NMR using their nuclear spin interaction parameters.[51] The dependence of the Rotor Assisted Population Transfer (RAPT) enhancement on offset frequency for nuclei experiencing different quadrupolar couplings was exploited and applied to the ^{87}Rb spectrum of Rb_2SO_4.[52] Rb-loaded LTA-type zeolite was studied in comparison with K-loaded one by ^{87}Rb NMR. It was found that the mass center of the ^{87}Rb spectrum shifts clearly to higher frequency side <10 K and the existence of Fermi contact interaction between σ electron and Rb nuclei was suggested.[53]

2.1.7 Cesium (^{133}Cs) ($I = 7/2$). The $CsAu\cdot NH_3$, which was recently synthesized and belongs to the family of ammoniates, was studied by ^1H and ^{133}Cs NMR. The ^{133}Cs NMR properties of the compound strongly deviate from the corresponding ones in CsAu, and the former can be interpreted consistently within a localized charge distribution due to either an anharmonic charge density wave state induced by a charge transfer process or an Anderson localization mechanism.[54] The ^{133}Cs NMR spectra in a Cs_2CoCl_4 single crystal were measured in the two mutually perpendicular crystal planes. From their angular dependences, the two different ^{133}Cs nuclei have different values for the quadrupole coupling constant and the asymmetry parameter. The electric field gradient tensors of both the two ^{133}Cs nuclei are asymmetric and the orientations of their principal axes do not

coincide.[55] The same research group also studied Cs_2ZnCl_4 single crystal by ^{133}Cs NMR.[56] The Nuclear magnetic octupole moment of ^{133}Cs was observed and the magnetic dipole, electric quadrupole and magnetic octupole hyperfine coupling constants were detected.[57] A series of heptametallic cyanide cages containing $Cs{\bullet}Rh_4Ru_3$ were studied by ^1H and ^{133}Cs NMR measurements using ^{133}Cs NMR shift values.[58] Solid-state ^{133}Cs NMR was used to obtain local structural information about the cation binding sites of Na, K-ATPase and ^{133}Cs NMR spectra and chemical shift values of Cs^+ in equilibrium with Na, K-ATPase membranes were discussed.[59]

2.2 Group 2 (^{9}Be, ^{25}Mg, ^{87}Sr). – *2.2.1 Beryllium (^9Be) (I = -3/2).* A mixture of beryllium fluoride complexes was studied by solution-state cross-polarization (CP) ^9Be NMR, which is a valuable technique for the selective observation of scalar-coupled quadrupolar nuclei in anisotropic phases.[60] The $CpBe(SiMe_3)$ (Cp = h5-C_5H_5), which is chemical vapor deposition precursors of metallic beryllium, was investigated by multinuclear NMR spectroscopy including ^9Be NMR. The ^9Be NMR spectra exhibit a large J(Be-Si) coupling constant and the ^9Be chemical shift is in accordance with the calculated bond-polarity pattern, as well as a bond to silicon.[61] Complexes of beryllium chloride and nitrate with $(Me_2N)_2P(O)F$ were characterized in solution by multinuclear NMR spectroscopy. These compounds show narrow lines in the solution ^9Be NMR spectra indicative of a highly symmetrical environment for beryllium.[62] The quadrupolar interaction parameters (QI) of tugtupite $[Na_8(Al_2Be_2Si_8O_{24})C_{12}]$ were calculated by using full-crystal linearized augmented plane-wave (FC LAPW) or ab initio MO.[63] The calculated values and experimental results obtained by MAS NMR were compared and discussed.

2.2.2 Magnesium (^{25}Mg) (I = -5/2). The bis(pyridine)(5, 10, 15, 20-tetraphenylporphyrinato)magnesium(II), $Mg(TPP){\bullet}Py_2$, was studied by solid-state ^{25}Mg NMR and quantum-mechanics calculation. The ^{25}Mg quadrupole coupling constants for the compound shows the largest value so far observed for ^{25}Mg nuclei. The ^{25}Mg chemical shielding anisotropy is too small to be accurately determined.[64] Application of the quadrupolar Carr-Purcell Meiboom-Gillh (QCPMG) sequence permits the first natural abundance solid-state ^{25}Mg NMR study of bis(cyclopentadienyl)- magnesium. The parameters and orientation of the ^{25}Mg electric field gradient tensor were rationalized from the crystal structure and molecular symmetry.[65]

2.2.3 Strontium (^{87}Sr) (I = -9/2). The magnetic properties of $(Sr_{2-x}Ca_x)RuO_4$ and $Sr_2(Ru_{1-y}Ti_y)O_4$ were studied by ^{87}Sr NMR to shed light on the effect of multibands on the magnetic character in the spin-triplet superconductor Sr_2RuO_4. It was found that the Knight shift of $(Sr_{2-x}Ca_x)RuO_4$ at 1.4 K increases up to x = 1.5 and ferromagnetic fluctuations develop with the increasing Ca content. [66] The same research group also investigated the magnetic properties on $Sr_{2-x}Ca_xRuO_4$ by a microscopic probe of ^{87}Sr and obtained similar results on the relationship between the Knight shift and the nuclear spin-lattice relaxation rate divided by temperature ($1/T_1T$).[67]

2.3 Group 3 (^{45}Sc, ^{89}Y, ^{139}La, ^{171}Yb). – *2.3.1 Scandium* (^{45}*Sc*) ($I = 7/2$). The fast amplitude-modulated (FAM) pulse sequences for the sensitivity enhancement of MAS and multiple-quantum (MQ) MAS spectra for the nuclei of which nuclear spin quantum number (I) is 7/2 were reported and applied to ^{45}Sc NMR of $Sc_2(SO_4)_3{\cdot}5H_2O$ and ^{139}La NMR of $LaAlO_3$.[68] The ^{1}H and ^{45}Sc NMR spectroscopies were used to study the structures formed in [ScCl(15-crown-5)(MeCN)] $[SbCl_6]_2$, $[ScCl_2$(18-crown-6)][$FeCl_4$] and [$ScCl_2$([15]aneS_2O_3)][$FeCl_4$] ([15] aneS_2O_3 = 1, 4-dithia-7, 10, 13-trioxacyclopentadecane) paying attention to their chemical shifts.[69] The solid solutions of $ScBRh_3$-$ScRh_3$ and $CeBRh_3$-$CeRh_3$ synthesized were characterized by using the Knight shift of ^{45}Sc observed by NMR spectroscopy.[70] The Knight shift decreases with increasing boron concentration of the samples showing that the Sc 4s electron density at the Fermi level changes.

2.3.2 Yttrium (^{89}*Y*) ($I = -1/2$). The line shape and Knight shift obtained by ^{89}Y NMR for Ca-doped YBCO compounds were presented and discussed considering the doping effect.[71] The Cu-oxide spin-chain compound, $Ca_{2+x}Y_{2-x}Cu_5O_{10}$, was studied by ^{89}Y NMR and it was found that the spectra exhibit an appreciable average shift and sharpen at lower temperature, possibly due to increasing intrachain ferromagnetic correlations.[72] The local magnetic susceptibility at different distances from the defects for Y_2BaNiO_5 was investigated by ^{89}Y NMR using chemical shift values. Its ^{89}Y NMR spectrum consists of one central peak and several less intense satellite peaks. The information about uniform susceptibility, which displays a Haldane gap and it corresponds to an antiferromagnetic (AF) coupling between the nearest neighbor Ni spins, is obtained from the central peak.[73]

2.3.3 Lanthanum (^{139}*La*) ($I = 7/2$). The temperature dependence of the ^{139}La and ^{19}F NMR spectra was studied for polycrystalline $LaMn(O_{1-x}F_x)_3$ with a partial substitution of fluorine for oxygen.[74] The fast amplitude-modulated (FAM) pulse sequences for the sensitivity enhancement of MAS and MQ/MAS spectra for the nuclei of which nuclear spin quantum number (I) is 7/2 were reported and applied to ^{45}Sc NMR of $Sc_2(SO_4)_3{\cdot}5H_2O$ and ^{139}La NMR of $LaAlO_3$.[68] The effects of substitution of barium by tin on the phase composition, structural imperfection and properties of lanthanum manganite perovskites, $La_{0.7}Ba_{0.3-x}Sn_xMnO_3$ (x = 0, 0.1, 0.15, 0.2, 0.3), were established by comprehensive studies done by x-ray diffraction, resistive methods and ^{55}Mn and ^{139}La NMR. The high-frequency electron exchange between Mn^{3+} and Mn^{4+} and nonequivalence of the environment of those ions and La^{3+} due both to heterovalent ions and to vacancies and clusters were clarified by the ^{55}Mn and ^{139}La NMR spectra.[75] $La_2Fe_{14}BH_x$ was studied by ^{139}La spin-echo NMR and the observed quadrupole splittings are directly proportional to the lattice part of the electric field gradient.[76] The magnetic and transport properties of ferromagnetic $(La_{1-x}Sr_x)_{1-d}MnO_3$ manganites (x = 0, 0.075 and 0.125, d = 0.03-0.05) were investigated by ^{139}La and ^{55}Mn.[77]

2.3.4 Ytterbium (^{171}*Yb*) ($I = 1/2$). The ytterbium (II) β-diketiminates,

$[Yb\{N(SiMe_3)C(R^2)C(H)C(R^4)N(SiMe_3)\}_2]$ ($R^2 = R^4 = Ph$, $R^2 = R^4 = Tol$, $R^2 = R^4 = Dph$ or $R^2 = Tol$ and $R^4 = Ad$) (Tol = C_6H_4Me-4, Dph = C_6H_4Ph-4, Ad = 1-adamantyl), were studied by ^{171}Yb NMR.[78] NOE data obtained lead to the assignments of the two types of $SiMe_3$ groups (adjacent to Tol or Ad) and the conclusion that the two isomers are conformers, one of which probably corresponds to that found in the crystal.

2.4 Group 4 ($^{47,49}Ti$, ^{91}Zr). – *2.4.1 Titanium* ($^{47,49}Ti$) ($I = -5/2, -7/2$). An ultrapure $BaTiO_3$ single crystal was studied by ^{47}Ti and ^{49}Ti NMR.[79] The results demonstrate the coexistence of a displacive and order-disorder component in the phase transition mechanism, and tetragonal breaking of the cubic symmetry due to biased Ti motion between off-center sites in the paraelectric phase above Tc. The ^{29}Si MAS, ^{27}Al MAS/3Q-MAS and $^{47,49}Ti$ wide-line multinuclear solid-state NMR spectroscopies were applied to study the structural characterization of titanium substituted ultra-stable zeolite Y (Ti-USY).[80] The chemical shielding and electric field gradient tensors for the titanium environment in the zeolite were determined by a computer simulation of the quadrupolar broadened static $^{47,49}Ti$ NMR spectra. The $RTiO_3$ (R = Y, Gd and La) was investigated by $^{47,49}Ti$ NMR to get information on the orbital degree of freedom.[81] The nonlinear optical crystal K titanyl phosphate, $KTiOPO_4$ (KTP), was studied by ^{17}O, ^{39}K and $^{47,49}Ti$ solid-state NMR.[82] The results were compared with ab initio calculations using the WIEN2k program and discussed in specific relation to the bond-polarizability approach for the calculation of 2nd-order nonlinear optical properties of KTP.

2.4.2 Zirconium (^{91}Zr) ($I = -5/2$). The vanadium-doped zircon (V-$ZrSiO_4$) samples were studied by ^{29}Si solid state, ^{51}V, ^{17}O and ^{91}Zr NMR to clarify its structure.[83] Static ^{91}Zr NMR data was reported from a pure zircon sample to quantify the amount of vanadium entering the zircon structure, and to elucidate its site preference within the lattice.

2.5 Group 5 (^{51}V, ^{93}Nb). – *2.5.1 Vanadium* (^{51}V) ($I = 7/2$). The orthovanadate $LaVO_4$ was investigated by ^{51}V MQ/MAS NMR determining the chemical shift anisotropy (CSA) parameter along with the asymmetry parameter. Combining MQ/MAS NMR data with least-square analyses of the manifold of spinning sidebands in the single-pulse MAS NMR spectrum resulted in a precise determination of the magnitudes and relative orientation of the ^{51}V quadrupole coupling and CSA tensors for $LaVO_4$.[84] Solid-state ^{51}V NMR spectra were obtained for polycrystalline V_2O_5 and V_2O_5-WO_3 solids by MAS and static NMR spectroscopies.[85] Chemical shift parameters (δ_{iso}, δ_{aniso}, η_{cs}) and quadrupolar parameters (C_Q, η_Q) were obtained by simulation of both MAS and static spectra. Geometric and electronic environments of V in $[VW_5O_{19}]^{3-}$ and $[V_2W_4O_{19}]^{4-}$ were addressed by ^{51}V MAS NMR spectroscopy.[86] The solid-state NMR spectra reflect the details of the local environment of the V site in these hexametalate solids *via* the anisotropic quadrupolar and chemical shielding interactions. The Oxovanadium(V) complexes mimicking the active site of V haloperoxidases were

studied by ^{51}V MAS NMR spectroscopy and density functional theory (DFT).[87] The MAS spectra are dominated by the anisotropic quadrupolar and chemical shielding interactions, and the quadrupolar coupling and chemical shielding tensors as well as their relative orientations were determined by simulations. The $[VO(O_2)_2(Im)]^-$ (Im = imidazole) was investigated by using ^{51}V NMR chemical shifts.[88] Implications for the mechanism of the oxidative chemicals of V-dependent haloperoxidases and requirements for prospective biomimetic analogs were discussed. The complete manifold of spinning sidebands including both the central and satellite transitions in ^{51}V MAS NMR spectra for surface vanadia nanoparticles on titania in $DeNO_x$ catalysts were reported.[89] The ^{51}V quadrupole coupling and chemical shift anisotropy parameters for the dominating vanadia structure were determined from ^{51}V NMR spectra. Carbohydrates containing galactopyranosyl and mannopyranosyl units with vicinal cis-diols were treated with $NaVO_3$ in D_2O, and the complexation occurred was detected by ^{51}V NMR spectroscopy.[90] The NMR signals for complexes are found in the $\delta = 515$ region, consistent with the dimeric trigonal-bipyramidal structure. $V_2O_5 \cdot nH_2O$ used for Li batteries was studied by ^{51}V solid-state NMR and the results showed that its films annealed at low or room temperatures have broad peaks and significant downfield isotropic chemical shifts.[91] It suggests that the interlayered H_2O produces a distorted square-pyramidal ligand field that may favor Li intercalation and electron transfer within the matrix of the films.

2.5.2 Niobium (^{93}Nb) ($I = 9/2$). $PbSc_{1/2}Nb_{1/2}O_3$ (PSN) and $PbMg_{1/3}Nb_{2/3}O_3$ (PMN) were studied by ^{93}Nb and ^{45}Sc NMR. The analysis of the spectra was performed using the NMR line shapes and a numerical Monte Carlo calculations. The ^{93}Nb NMR spectrum for PMN contains practically only the broad component and the NMR data demonstrate that the cubic symmetry at $T \cdot T_m$ in PMN is locally broken due to ion shifts similar to that in disordered PSN.[92] The improved ^{93}Nb NMR spectra for $NaNbO_3$ were obtained by using a multiple rotor-assisted population transfer (RAPT) method and a special data processing procedure.[93] Pure liquid niobium chloride and solid and liquid $NbCl_5$-alkali chloride solutions ($NbCl_5$-(LiCl, NaCl, KCl or CsCl)) were for the first time studied by ^{93}Nb NMR and the chemical shift and line width measurements were made by using a home made probe head at elevated temperatures up to 650 C.[94] The observed temperature dependence of the ^{93}Nb chemical shift in different salt mixtures was found to be in qualitative agreement with a theoretical estimation, which considers the Nb-Cl distance variation with temperature. The framework Ti of silicotitanate (Ti-CST), $HNa_3Ti_4Si_2O_{14} \cdot 4H_2O$, was replaced with Nb (Nb-CST) in order to improve its Cs ion exchange selectivity and was characterized by high-speed ^{93}Nb MAS NMR spectroscopy.[95] It was discussed on the basis of the results that the Nb octahedral present in Nb-CST have near uniform Nb-O bond lengths and are slightly distorted from cubic symmetry.

2.6 Group 6 (^{95}Mo, ^{183}W). – *2.6.1 Molybdenum* (^{95}Mo) ($I = 5/2$). – The ^{95}Mo and ^{183}W NMR chemical shifts of various molybdenum and tungsten compounds were calculated by combining the individual gauge for the localized

orbital approach for density functional theory with the normalized elimination of a small component using an effective potential.[96] The relationship between electronic structure of a molecule and the relativistic paramagnetic corrections was discussed. The 2-(phenylhydrazino)pyridine (2-PHP) complexes, cis-$Mo(CO)_4$(X-2-(phenylhydrazino)pyridine) (X = 4-CH_3O, 4-CH_3, H, 4-Cl, 5-Br, 6-CH_3, 4, 6-Me_2) and cis-$Mo(CO)_4$(2-(2-CH_3-phenylhydrazino)pyridine), were characterized by ^{95}Mo NMR utilizing chemical shifts of the 2-PHP complexes.[97] The $LaMo_6Se_8$ was studied between 15 and 4.2 K by ^{95}Mo NMR spectroscopy and no shift of the spectral line was observed between the normal and the superconducting states, indicating a magnetic susceptibility dominated by a spin-orbit mechanism.[98] The line shape in the superconducting state was simulated by convolution of a spectrum at normal state and the magnetic field distribution. The $(n\text{-}Bu_4N)_3[Mo_6O_{18}(N_2Ar)]$ (Ar = RC_6H_4 ((R = H, *p*-Me, *p*-F, *p*-CN, *p*-CF_3, *p*-OMe, *p*-NO_2, *o*-Cl, *o*-NO_2, *m*-NO_2)), C_6F_5, 2, 4-dinitrophenyl) were studied by ^{95}Mo and ^{17}O NMR spectroscopy and the ^{95}Mo chemical shifts were determined by variation in the paramagnetic shielding term.[99] The strongly deshielded resonance of the Mo^{II} centre spans a large range as 600-1100 ppm.

2.6.2 Tungsten (^{183}W) (I = 1/2). The decatungstates for Eu, Tm, Yb and Lu were synthesized and ^{183}W and ^{17}O NMR spectra were measured for their solutions. The general trend in the change of the ^{183}W NMR chemical shifts for $LaW_{10}O_{36}{}^{9-}$, $Ce^{IV}W_{10}O_{36}{}^{8-}$, $W_{10}O_{32}{}^{4-}$ and $W_6O_{19}{}^{2-}$ depends on the paramagnetic contribution.[100] The solution state of the polyoxotung was studied by multiline ^{183}W NMR and DFT calculations were carried out.[101] The ^{183}W NMR chemical shifts are sensitive to structure, solvent and counterion and a lot of information about them are obtained. The ^{183}W NMR spectra of $[SiW_{11}O_{39}]^8$ isomers in aqueous tungstosilicate equilibrium were measured as a function of pH. The chemical shift assignment was made clarifying the relation of the values to chemical and physical structures of the samples.[102] The ^{95}Mo and ^{183}W NMR chemical shifts of various molybdenum and tungsten compounds were calculated by combining the individual gauge for the localized orbital approach for density functional theory with the normalized elimination of a small component using an effective potential.[96]

2.7 Group 7 (^{55}Mn, ^{99}Tc). – *2.7.1 Manganese* (^{55}Mn) (I = 5/2). The ^{55}Mn NMR measurements were carried out on an oriented powder sample of Mn12 clusters to study microscopically its inner spin structure and spin dynamics. The ^{55}Mn NMR spectrum of the Mn12 cluster depends on an external magnetic field and the relation gives a direct confirmation of the internal magnetic structure.[103] A single crystal of perovskite bilayer manganite $La_{1.2}Sr_{1.8}Mn_2O_7$ was studied by ^{55}Mn NMR and the shape of the spectrum obtained depends strongly on the rf radiation field for exciting and refocusing a spin-echo signal.[104] The $La_{0.84}Sr_{0.16}MnO_3$ single crystal was investigated by ^{55}Mn NMR and the evidence of the charge modulated ferromagnetic state below the metal-insulator transition was found.[105] The NMR spectra at low-temperature phase remain motionally narrowed and this indicates that the hopping time of carriers is shorter than the

period of the Larmor precession of the Mn nuclear spins. The same research group also studied the magnetic structure of fine scale ($\sim$50 and $\sim$100-200 nm) particles of $La_{0.7}Sr_{0.3}MnO_3$.[106] The effects of substitution of barium by tin on the phase composition, structural imperfection and properties of lanthanum manganite perovskites, $La_{0.7}Ba_{0.3-x}Sn_xMnO_3$ (x = 0, 0.1, 0.15, 0.2, 0.3), were established by comprehensive studies done by x-ray diffraction, resistive methods and ^{55}Mn and ^{139}La NMR. The high-frequency electron exchange between Mn^{3+} and Mn^{4+} and nonequivalence of the environment of those ions and La^{3+} due both to heterovalent ions and to vacancies and clusters were clarified by the ^{55}Mn and ^{139}La NMR spectra.[75]

2.7.2 Technetium (^{99}Tc) (I = 9/2). Complexation of the $Tc(CO)_3(H_2O)^{+3}$ ion with halide (F-, Cl-, Br-, I-) and thiocyanate ions in aqueous solutions was studied by ^{99}Tc NMR spectroscopy and the stability constants of the mono-, di- and tri-substituted complexes were calculated.[107, 108]

2.8 Group 8(^{57}Fe). – *2.8.1 Iron*(^{57}Fe)(I = 1/2). To investigate the non-heme peroxo-iron species, a Moessbauer study of the ^{57}Fe-enriched E47A superoxide reductase(SOR) from D. Baarsii reacted quickly with H_2O_2, was performed.[109] The geometries, electronic structures and energies for ligand-exchange reactions of a novel class of metal-centered aromatic compounds $[Fe(Sb_5)]^+$ and $[Fe(Bi_5)]^+$ were studied by DFT methods and the ^{57}Fe NMR chemical shifts were also calculated for these two compounds.[110]

2.9 Group 9(^{59}Co,^{103}Rh). – *2.9.1 Cobalt* (^{59}Co)(I = 7/2). The ^{59}Co NMR experiments were carried out on single-crystal and polycrystalline (powder) samples of (+-)-tris(ethylenediamine)cobalt(III) chloride trihydrate, (+-)-$[Co(en)_3]Cl_3 \cdot 3H_2O$ and its dehydrate.[111] The ^{59}Co and ^{23}Na NMR were applied to the layered Co oxides $NaCoO_2$ and $HCoO_2$ at 3 different magnetic field strengths (4.7, 7.1 and 11.7 T).[46] Investigation were the nature of higher-order effects arising in solid-state NMR when quadrupolar nuclei are subject to significant chemical shift anisotropies.[112]

2.9.2 Rhodium (^{103}Rh)(I = 1/2). The reaction of the La ate-complex $[\{O(SiMe_2\text{-}Ap)_2\}_2LaLi(THF)_4]$ (Ap-H = 2-amino-4-methylpyridine) with $[(cod)RhCl]_2$ (cod = cycloocta-1,5-diene) and $[(C_2H_4)_2RhCl]_2$ gave rise to three La-Rh bimetallic compounds.: $[\{O(SiMe_2\text{-}Ap)_2\}_2LaRh(cod)]$, $[\{O(SiMe_2\text{-}Ap)_2\}_2LaRh(C_2H_4)]$ and $[\{O(SiMe_2\text{-}Ap)_2\}_2(THF)LaRh(C_2H_4)]$, and the structure and ^{103}Rh NMR chemical shifts of the La-Rh-bimetallics were discussed with regard to metal-metal interactions.[113]

2.10 Group 10(^{195}Pt). – *2.10.1 Platinum* (^{195}Pt)(I = 1/2). – Complexes of the types cis- and trans-Pt(amine)$_2$I$_2$ were studied by spectroscopic methods, especially by ^{195}Pt, ^{1}H and ^{13}C NMR spectroscopy.[114] The synthesis, crystal structures, spectroscopic(including ^{195}Pt NMR) and electrochemical properties of new Pt(II) heteroleptic complexes with two diimines (2,2′-bipyridine, 4,4′-dimethyl-

2,2′-bipyridine) and the crown trithioether 9S3 (1,4,7-trithiacyclononane) were reported.[115] The synthesis, spectroscopy(including ^{195}Pt NMR), electrochemical and crystal structures of two new mononuclear homoleptic Pt(II) and Pd(II) complexes with the crown trithioether 1,5,9-trithiacyclododecane (12S3) were reported.[116] The syntheses, crystal structures and spectroscopic properties(including ^{195}Pt NMR) for two new Pt(II) heteroleptic complexes containing the chiral diphosphine ligands, R-BINAP, and R,R-Chiraphos along with crown trithioether [9]aneS3 (1,4,7-trithiacyclononane) were reported.[117] Ion-pair formation between a Na^+ cation and the $[PtCl_{62}]^-$ anion in methanol was observed from ^{195}Pt NMR chemical shift trends as well as from molecular dynamics computer simulations.[118] The preparation of Pt(II) complexes containing L-serine using $K_2[PtCl_4]$ and KI as raw materials was undertaken and investigated by ^{195}Pt NMR.[119] The products of the reactions of $[\{trans\text{-}PtCl(NH_3)_2\}_2\text{-}m\text{-}\{trans\text{-}Pt(NH_3)_2(NH_2(CH_2)_6NH_2)_2\}](NO_3)_4$ (BBR3464;1,0,1/t,t,t,n = 6), $[\{trans\text{-}PtCl(NH_3)_2\}_2\text{-}m\text{-}(H_2N(CH_2)_6NH_2)](NO_3)_2$ (BBR3005;1,1/t,t, n = 6), $[\{trans\text{-}PtCl(NH_3)_2\}_2\text{-m-}(H_2N(CH_2)_3NH_2(CH_2)_4NH_2)]Cl_3$ (BBR3571; 1,1/t,t-spermidine, n = 3,4) and trans-$[PtCl_2(NH_3)_2]$ (*t*-DDP) with reduced GSH in phosphate-buffered saline (pH = 7.35) were characterized by ^{1}H, ^{195}Pt and ^{1}H-^{15}N gradient heteronuclear single-quantum coherence NMR spectroscopy and high-performance liquidchromatography (HPLC) coupled with electrospray ionization time-of-flight massspectrometry to determine likely metabolites of the complexes with GSH.[120] The aqueous reactions of $K[Pt(Ypy)Cl_3]$ (Ypy = pyridine derivative) with acetonitrile were studied under different pH conditions, mainly by ^{195}Pt and ^{1}H NMR.[121] It was known since 1973 that addition of NaOH aqueous solution to an aqueous solution of $[Pt(bipy)_2](NO_3)_2{\cdot}H_2O$ gives rise to changes in both the solution UV/visible and solution ^{1}H and ^{13}C NMR spectra of the complex, and ^{195}Pt NMR spectroscopy was applied to understand the problem.[122] Gel-phase ^{195}Pt NMR spectroscopy of dichloroplatinum peptide complexes attached to a solid support was described.[123] The reactions of $K_2[PtI_4]$ with sulfoxides produce the iodo-bridged dinuclear species $(R2SO)IPt_{(m\text{-}I)}2Pt(R2SO)_I$ and was investigated by^{195}Pt NMR spectroscopy.[124] The ^{195}Pt and ^{205}Tl NMR chemical shifts of the complexes$[(NC)_5Pt\text{-}Tl(CN)_n]^{n\text{-}}$ (n = 0-3) and of the related system $[(NC)_5Pt\text{-}Tl\text{-}Pt(CN)_5]^{3\text{-}}$ were computationally investigated.[125] A variety of para-substituted NCN-pincer palladium(II) and platinum(II) complexes [MX(NCN-Z)] (M = Pd(II), Pt(II); X = Cl, Br, I; NCN-Z = $[2,6\text{-}(CH_{(2)}NMe_{(2)})_{(2)}C_{(6)}H_{(2)}\text{-}4\text{-}Z](\text{-})$; Z = $NO_{(2)}$, COOH, $SO_{(3)}H$, $PO(OEt)_{(2)}$, PO(OH)(OEt), $PO(OH)_{(2)}$, $CH_{(2)}OH$, SMe, $NH_{(2)}$) were synthesized by routes involving substitution reactions, either prior to or, notably, after metalation of the ligand. The solubility of the pincer complexes is dominated by the nature of the para substituent Z, which renders several complexes water-soluble, and the influence of the para substituent on the electronic properties of the metal centre was studied by ^{195}Pt NMR spectroscopy and DFT calculations.[126]

2.11 Group 11($^{63,\ 65}$Cu,^{107,109}Ag). – *2.11.1 Copper($^{63,\ 65}$Cu)(I = 3/2, 3/2).* – The ^{63}Cu and ^{65}Cu NMR and viscosity studies of 0.064 M $CuClO_4$ were made in binary mixtures of acetonitrile (AN) with succinonitrile (SN), adiponitrile

(ADN), n-butyronitrile (*n*-BTN) and iso-butyronitrile (*iso*-BTN) as co-solvents at 298 K using 500 MHz NMR spectrometer and an Ubbelohde viscometer, respectively, and chemical shift (*d*) and linewidth (*D*) for both ^{63}Cu and ^{65}Cu signals were recorded relative to 0.064 M $CuClO_4$ solution in pure anhydrate AN.[127] The local structures of the new phosphorus chalcogenide – copper iodide coordination compounds $(CuI)P_4Se_4$, $(CuI)_2P_8Se_3$, $(CuI)_3P_4Se_4$ and $(CuI)_3P_4S_4$ were studied using comprehensive ^{63}Cu, ^{65}Cu and ^{31}P MAS NMR techniques.[128] The electronic structure of La_2CuO_4 was studied using 1st-principles cluster calculations and the chemical shieldings at the Cu nucleus were determined with several state-of-the-art quantum chemical methods.[129]

2.11.2 Silver($^{107,109}Ag$)($I = 1/2,1/2$). Ag(I) complexes of selenones, $[LAgNO_3]$ and $[AgL_2]NO_3$ (L = imidazolidine-2-selenone or diazinane-2-selenone and their derivatives.) were prepared and characterized by elemental analyses, IR and NMR (^1H, ^{13}C and ^{107}Ag) spectroscopy.[130] The structure of 1,3-bis(2,4,6-trimethylphenyl)-imidazol-2-ylidene-silver(I)chloride, 1, were determined to be a monomer with weak head-to-tail H···Cl interactions in the solid state by $^{107,109}Ag$ NMR study using a ^{13}C(carbene) labeled derivative, 1(^{13}C).[131]

2.12 Group 12($^{111,113}Cd$, ^{199}Hg). – *2.12.1 Cadmium*($^{111,113}Cd$)($I = 1/2,1/2$). A new divalent Cd phosphonate, $Cd_2Cl_2(H_2O)_4(H_2L)$, was synthesized from ethylenediamine-N,N′-bis(methylenephosphonic acid) (H_4L) and the obtained microcrystalline compound was characterized by solid-state IR spectra and ^{13}C, ^{31}P and ^{113}Cd CP/MAS NMR spectra.[132] $[CdX_2(C_5H_4NCOOR)]$ (X = Cl or Br; R = Me, Et, Pr or Pri) and $[CdX_2(C_5H_4NCOOR)_2]$ (X = I; R = Me, Et, Pr or Pri) were obtained by the addition reaction of esters of 2-pyridinecarboxylic acid to Cd(II) halides, and x-ray crystal structures and ^{113}Cd CP/MAS NMR of two complexes $[CdI_2(C_5H_4NCOOR)_2]$, R = Me and R = Pr, are carried out.[133] $[M(Spy)_2(SpyH)_2]$ (Spy- = pyridine-4-thiolate; M = Cd (1) and Hg (2)), of a hitherto unknown type, were prepared by reacting the corresponding metal perchlorates with pyridine-4-thiol in the ratio 1:6 in DMSO-MeOH. $[M(SpyH)_4]_2^+$ (M = Zn, Cd and Hg) were prepared and isolated as their perchlorate salts, and investigated by x-ray crystallography and $^{113}Cd/^{199}Hg$ NMR spectroscopy.[134] Binuclear diisopropyl and dicyclohexyl dithiophosphate Cd complexes, $[Cd_2\{S_2P(OR)_2\}_4]$, were studied by high-resolution heteronuclear (^{13}C, ^{31}P and ^{113}Cd) NMR spectroscopy in the solid state at 295-378 K.[135] Coordination geometry and structure of metal binding sites in biological relevant systems were studied using chemical shift parameters obtained from ^{113}Cd solid-state NMR experiments and quantum chemical calculations.[136] Present were a detailed account of a number of quantum chemical studies aimed at relating isotropic and anisotropic ^{113}Cd chemical shifts to the structure of several biologically relevant complexes with discrete and polymeric structures.[137] Cd hexathiohypodiphosphate ($CdPS_3$) intercalates with K and N,N′-dimethylviologen cations were studied by ^{31}P and ^{113}Cd solid-state NMR experiments.[138] Determination of ^{113}Cd chemical shift was motivated for characterization of metal porphyrins, metal-histidine interactions and other metal-ligand interac-

tions in many bioinorganic complexes and metalloproteins.[139]

2.12.2 Mercury(^{199}Hg)($I = 1/2$). The complexation of mercury(II) cyanide with macrocyclic ligands 15-crown-5, 18-crown-6 and dibenzo-24-crown-8 in dimethylsulfoxide was studied using ^{199}Hg NMR measurements.[140] 3,5-Dichlorophenylmercury cyanide and phenylethynylmercury cyanide dissolved in DMSO-d_6 were studied using ^{13}C, ^{15}N and ^{199}Hg NMR and density functional theory (DFT) calculations.[141] The synthesis, crystal structure and NMR spectroscopy were reported for the Hg(II) complex with the crown thioether 1,4,7-trithiacyclodecane, bis(1,4,7-trithiacyclodecane)mercury(II) hexafluorophosphate.[142] The coordination chemistry of Hg(II) with tris[(1-methylimidazol-2-yl)methyl]amine (TMIMA) was studied, and a ^{199}Hg NMR was performed for the complex.[143] Reaction of *o*-$C_6F_4(HgCl)_2$, *m*-$C_6F_4(HgCl)_2$, C_6F_5HgCl and $C_6F_4H(HgCl)$ with TMSCN in MeCN affords the corresponding organomercury cyanide derivatives *o*-$C_6F_4(HgCN)_2$, *m*-$C_6F_4(HgCN)_2$, C_6F_5HgCN and $C_6F_4H(HgCN)$, respectively, and these compounds were characterized by elemental analyses, ^{1}H, ^{13}C, ^{19}F and ^{199}Hg NMR, and IR spectroscopy.[144] Quasi-relativistic theory of magnetic shielding constants based on the Douglas-Kroll-Hess transformation of the magnetic potential presented in a previous paper was extended to molecular systems that contained heavy elements.[145]

2.13 Group 13(^{11}B, ^{27}Al, ^{71}Ga, ^{203,205}Tl). – *2.13.1 Boron(^{11}B)($I = 3/2$).* The reaction of bis(silyl)ethynes 2-4, bearing one, two and three hydrides at one of the silicon atoms, with triallylborane 1 leads primarily to alkenes 5, 8 and 11 respectively, by 1,1-allylboration, and it was investigated by the observation of isotope-induced chemical shifts $^2D^{10/11}B(^{29}Si)$.[146] 1-Boraadamantane reacted with 1-alkynylsilanes containing one or two Si-H functions adjacent to triple bond, giving 4-methylene-3-borahomoadamantane derivatives with Si-H-B bridging hydrogens and being analysed by IR data, an extensive set of NMR spectroscopic data (^{1}H, ^{11}B, ^{13}C and ^{29}Si NMR) including various unusual isotope effects on chemical shifts and coupling constants, as well as from the crystal structure in the solid state.[147] Dumortierite occurs as small nodules or thin layers along horizontal fractures in the altered volcanic rocks of the Milyang clay deposit, southeastern Korea, and is investigated by ^{29}Si, ^{27}Al and ^{11}B.[148] In a series of mono and mixed-alkali borosilicate glasses($\sim 0.7M_2O{\cdot}B_2O_3{\cdot}2SiO_2$, M = Li, Na, K, ($1/2Li_2O + \sim 1/2Na_2O$), ($1/2Li_2O + 1/2K_2O$) and ($\sim 1/2Na_2O + 1/2K_2O$)), triple-quantum magic-angle-spinning (3QMAS) and ^{11}B and ^{17}O NMR were performed to obtain high-resolution information about short-range structure and the connections among various network structural units, to study the effect of mixed cations on the glass structure and to explore the distribution and mixing of these modifier cations.[149] Zwitterionic boron-carbon mono- and bis-homoaromatics (*e.g.*, 1-azonium-, 1-phosphonium- or 1-arsonium-2,4-diboretane-3-ide derivatives, 1-azonium-2,5-diboracyclopentane- 3-ide derivative) containing positive charged NMe_2, PPh_2 or $AsPh_2$ bridges and anionic three-center two-electron (3c2e) delocalized B heterocyclic units were prepared and characterized by NMR as well as by x-ray structure analyses.[150] The struc-

ture of dimesitylborane dimmer and monomer was explored; the thermodynamic parameters of association were measured and a hydrogen-bridged dimmer $(Mes_2BH)_2$ was found to exist in equilibrium with monomer in solution, which was investigated by variable concentration and variable temperature ^{11}B NMR spectroscopy.[151] The ^{19}F NMR spectra and spin-lattice relaxation rate, R_1, of dichloro(trifluorovinyl)borane were studied as a function of temperature, T, and magnetic field, B, and the linewidths of ^{11}B are measured between 253 and 363 K.[152] The mixed modifier borosilicate glass used in high level radioactive waste immobilization was doped with between 2 and 12 mol% waste stimulants including lanthanum oxide (La_2O_3), aluminum oxide (Al_2O_3) and bismuth oxide (Bi_2O_3) forming three series of glasses, and these were examined by using ^{11}B, ^{29}Si and ^{27}Al MAS-NMR to characterize their structures.[153] Xerogels of compound $La_2B_4Al_2O_{12}$, treated between 200-1100°C, were investigated by ^{11}B MAS NMR and SEM.[154] 1-Sila-2,4-cyclopentadienes (siloles) 1-R1-1-R2-2-R3-3-Et-4-BEt_2-5-R4-C_4Si [3a,b, R1 = R2 = Me, R3 = R4 = Bu (a), Ph (b); 4, R1 = R2 = Me, R3 = Me_3Sn, R4 = Ph; 5, R1 = H, R2 = Me, R3 = R4 = Bu] react by [4+2]cycloaddition with alkyne $MeO_2CC\beta CCO_2Me$ and alkene $(NC)_2C=C(CN)_2$, to give 7-silanorbornadienes and 7-silanorbornenes, respectively, and were characterized in solution by multinuclear magnetic resonance (^1H-, ^{11}B-, ^{13}C-, ^{29}Si- and ^{119}Sn-NMR spectroscopy).[155]

2.13.2 Aluminium(^{27}Al)($I = 5/2$). The crystallization behavior of $8SiO_2.YAl_2O_3.3.75MgO.2.25MgF_2.BaO$ glasses with Y varying between 1.5 and 3.5 were investigated using differential scanning calorimetry (DSC), x-ray diffraction analysis and ^{27}Al, ^{29}Si, ^{31}P and ^{19}F MASNMR spectroscopy.[156] NMR studies using $^{29}Si\{^1H\}$ CP/MAS and ^{27}Al and ^{23}Na MQ/MAS methods provide information about the local structure of amorphous aluminum silicates, isolated from hydrothermal reactions used to form crystalline zeolite A.[157] ^{27}Al MAS and triple quantum (3Q) MAS NMR spectroscopic techniques were used to characterize zeolite Beta samples with framework Si/Al ratios between 9 and 215, obtained by synthesis in fluoride medium.[158] Mixed phosphates $Al_{1-x}Ga_xPO_4$ ($0.0 < x < 1.0$), with orthorhombic structure, were prepared and investigated by using powder X-ray diffraction and ^{27}Al NMR spectroscopy.[159] Multinuclear (^{27}Al and ^{17}O) solid-state NMR and quantum chemical calculations were performed to study the structures of silicate glasses quenched from melts at pressures up to 10 GPa in a multianvil approximation.[160] Two-dimensional ^1H-^{27}Al CP experiments were performed to clay minerals that provides resolution enhancement in ^{27}Al NMR spectra, permitting the differentiation of aluminum ions with one same coordination number, but with different chemical environments.[161] A new sol-gel synthesis route to organic free Na_2O-Al_2O_3-P_2O_5 xerogels was developed and investigated by solid-state ^{27}Al MAS NMR.[162] Electric field gradients (EFG) of ^{23}Na and ^{27}Al in three model fluoride crystalline powders AlF_3, Na_3AlF_6 and $Na_5Al_3F_{14}$ were computed using the density functional based electronic structure code WIEN97 and compared to values derived from NMR (NMR).[163] Five component ionomer glasses (Fuji IX, Ketac Molar, G338, G2 and G2SR) used to produce glass (ionomer) polyalkenoate dental cements were studied by ^{29}Si, ^{27}Al, ^{31}P and ^{19}F

MASNMR spectroscopy to characterize the glasses and the resulting spectra compared with previous studies of model glasses.[164] Trachytic and alkali-trachytic volcanic glasses from the deposits of the Neapolitan Yellow Tuff eruption, in the Campi Flegrei Caldera (Southern Italy), were studied by back-scattered electron microscopy, electron microprobe analyses and ^{27}Al MAS NMR spectroscopy (MAS NMR).[165] Formation of aqueous aluminate-borate complexes was characterized at 25°C using ^{27}Al NMR spectroscopy, and at 50-200°C *via* measurements of gibbsite and boehmite solely in the presence of boric acid.[166] Report were high-resolution solid-state ^{27}Al NMR data for two members of the magnetoplumbite group of structures, strontium hexaluminate ($SrAl_{12}O_{19}$) and calcium hexaluminate ($CaAl_{12}O_{19}$, synthetic hibonite), acquired at 14.1 and 18.8 T fields.[167] The influence of cation exchange on the ^{27}Al-NMR spectra of NaA-zeolites was studied by ^{27}Al-MAS and MQ/MAS solid-state NMR.[168] The feasibility of using ultrasound to enhance the geopolymerisation of metakaolinite/sand and fly ash/metakaolinite mixtures was investigated by ^{27}Al MAS NMR.[169] Buckwheat (Fagopyrum esculentum Moench. cv. Jianxi) is known as an Al-accumulating plant and the process leading to the accumulation of Al in the leaves was investigated, focusing on the chemical form of Al using ^{27}Al-NMR.[170] The structure of calcium aluminosilicate and calcium aluminosilicate fluoride glasses were characterized by ^{29}Si, ^{27}Al and ^{19}F MAS-NMR.[171] A series of monoethyl and diethylaluminum(III) complexes of the types $Et_2Al\{O\text{-}R\text{-}NR_1R_2\}$ and $EtAl\{O\text{-}R\text{-}NR_1R_2\}_2$ [R = $(CH_2)_2$, $R_1 = R_2 = H$; R = $(CH_2)_3$, $R_1 = R_2 = H$; R = $CH_2CH(CH_2CH_3)$, $R_1 = R_2 = H$; R = $(CH_2)_3$, $R_1 = H$, $R_2 = CH_3$; R = $(CH_2)_3$, $R_1 = R_2 = CH_3$; R = o-C_6H_4, $R_1 = R_2 = H$] were prepared by the reactions of triethylaluminum etherate adduct ($Et_3Al{\cdot}Et_2O$) and investigated by ^{27}Al NMR chemical shift.[172] Dumortierite occurs as small nodules or thin layers along horizontal fractures in the altered volcanic rocks of the Milyang clay deposit, southeastern Korea and it was analysed by ^{27}Al, ^{29}Si and ^{11}B MAS NMR.[173] The effects of the addition of clay minerals on the hydration reactions and kinetics of alite and belite were investigated for a white Portland cement (WPC)-kaolinite (20 wt%) blend and a mixture of 90 wt% WPC and 10 wt% bentonite using ^{29}Si and ^{27}Al MAS NMR spectroscopy.[174] Multinuclear solid-state NMR spectroscopy, employing ^{29}Si MAS, ^{27}Al MAS/3Q-MAS and ^{47,49}Ti wide-line experiments, was used for the structural characterization of titanium substituted ultra-stable zeolite Y (Ti-USY).[80] The solid solution behavior of mixed halide (Cl/Br, Cl/I and Br/I) sodalite systems as prepared by hydrothermal synthesis was studied in detail by x-ray diffraction and ^{23}Na and ^{27}Al solid-state NMR.[175] Zeolites NaY and mordenite were dealuminated by $SiCl_4$ and steaming methods and carefully characterized during and after the various synthetic stages by ^{27}Al and ^{29}Si MAS NMR and x-ray diffraction (XRD) to ensure sample quality, and ^{129}Xe NMR spectra for xenon adsorbed in NaX, siliceous Y, mordenite and dealuminated mordenite were also obtained for very low xenon loadings and as a function of temperature.[176] The mixed modifier borosilicate glass used in high level radioactive waste immobilization were doped with between 2 and 12 mol% waste simulants including lanthanum oxide (La_2O_3), aluminum oxide (Al_2O_3) and bismuth oxide (Bi_2O_3) forming three series of glasses, and examined using ^{11}B, ^{29}Si

and ^{27}Al MAS NMR to characterize their structures.[153] The influence of F substitution on the local structure of Al in the tetrahedral and octahedral sheets of synthetic Al-rich phlogopite samples with nominal gel components of $K(Mg_{3-x}Al_x)[Al_{1+x}Si_{3-x}O_{10}](OH)_y(F)_{2-y}$ between $0.0 < x < 0.8$ and $0.5 < y < 1.8$, was studied by ^{27}Al MAS, MQ/MAS, $\{^1H/^{19}F\} \rightarrow {}^{27}Al$ 2D CP/MAS (HETCOR) and $\{^1H/^{19}F\}$ ^{27}Al REDOR solid-state NMR and by IR spectroscopy.[177] Reported were ^{17}O and ^{27}Al NMR results for ^{17}O-enriched synthetic and natural layer silicates with significantly improved resolution of O sites including basal and apical oxygens using ^{17}O 3QMAS NMR spectroscopy.[178] The ^{29}Si and ^{27}Al MAS NMR was used to characterize Laponite RD and synthetic saponites of variable interlayer charge.[179] The dealumination of zeolite H-b by ammonium hexafluorosilicate (*i.e.*, $(NH_4)_2SiF_6$, AHFS) treatment was investigated by ^{27}Al and ^{19}F solid-state NMR, combined with $^{27}Al/^{19}F$ double resonance NMR.[180] The calcium silicate hydrate (C-S-H) phase resulting from hydration of a white Portland cement (wPc) in water and in a 0.3 M $NaAlO_2$ solution was investigated at 14 and 11 hydration times, respectively, ranging from 6 hour to 1 year by ^{27}Al and ^{29}Si MAS NMR spectroscopy.[181] Dicyclopentadienylaluminum alkoxides of general formula $[Cp_2Al\text{-}m\text{-}OR]_2$ (R = Me (1), Et (2), *n*-Bu (3), *i*-Bu (4), CH_2-*t*-Bu (5), *s*-Bu (6), CH_2Ph (7), C_6H_4-4-*t*-Bu (8)) were prepared by reacting CpNa with $ROAlCl_2$ in the molar ratio 2:1, respectively, (2-8) or from reaction of Cp_3Al with alcohol (1) are characterized by multinuclear NMR (^1H, ^{13}C and ^{27}Al) and, in the case of 2, 5 and 6, x-ray crystallography.[182] The dissolution and complex formation of fluoroaluminates in 2 eutectic alkali fluoride mixtures, NaF-KF (FNAK) and LiF-NaF-KF (FLINAK), were studied by Raman, NMR and thermal analyses.[183] The (dimethylamino)methyl compounds $(Me_2AlCH_2NMe_2)_2$, $(Me_2GaCH_2NMe_2)_2$, $(Me_2InCH_2NMe_2)_2$, $[(Me_2AlCH_2NMe_2)(MeClAlCH_2NMe_2)]$, $[ClAl(CH_2NMe_2)_2]_2$ and $[Al(CH_2NMe_2)_3]_2$ were prepared by reacting $LiCH_2NMe_2$ with the corresponding element or organoelement chlorides, and haracterization was undertaken by elemental analyses, NMR spectroscopy (^1H, ^{13}C and ^{27}Al) and mass spectrometry.[184] Electric field gradients (EFG) of ^{23}Na and ^{27}Al in three model fluoride crystalline powders AlF_3, Na_3AlF_6 and $Na_5Al_3F_{14}$ were computed using the density functional based electronic structure code WIEN97 and compared to values derived from NMR.[185] Five commercial ionomer glasses (Fuji IX, Ketac Molar, G338, G2 and G2SR) used to produce glass (ionomer) polyalkenoate dental cements were studied and ^{29}Si, ^{27}Al, ^{31}P and ^{19}F MASNMR spectroscopy was used to characterize the glasses and the resulting spectra compared with previous studies of model glasses.[164] Buckwheat (Fagopyrum esculentum Moench. cv. Jianxi) is known as an Al-accumulating plant. The process leading to the accumulation of Al in the leaves was investigated, focusing on the chemical form of Al using ^{27}Al-nuclear magnetic resonance.[186] Multinuclear solid-state NMR spectroscopy, employing ^{29}Si MAS, ^{27}Al MAS/3Q-MAS and $^{47,49}Ti$ wide-line experiments, was used for the structural characterization of titanium substituted ultra-stable zeolite Y (Ti-USY).[80] The calcium silicate hydrate (C-S-H) phase resulting from hydration of a white Portland cement (wPc) in water and in a 0.3 M $NaAlO_2$ solution was investigated at 14 and 11 hydration times,

respectively, ranging from 6 h to 1 year by ^{27}Al and ^{29}Si MAS NMR spectroscopy.[187]

2.13.3 Gallium($^{69,71}Ga$)($I = 3/2, 3/2$). The ^{19}F isotropic chemical shift, and ^{23}Na, ^{27}Al and $^{69,71}Ga$ quadrupolar parameters were calculated to crystallized and/or disordered inorganic fluorides.[188]

2.13.4 Thallium(^{205}Tl)($I = 1/2$). The ^{195}Pt and ^{205}Tl NMR chemical shifts of the complexes $[(NC)_5Pt\text{-}Tl(CN)_n]_n^-$ (n = 0-3) and of the related system, $[(NC)_5Pt\text{-}Tl\text{-}Pt(CN)_5]_3^-$, were computationally investigated.[189]

2.14 Group 14(^{13}C, ^{29}Si, ^{73}Ge, $^{117,119}Sn$, ^{207}Pb). – *2.14.1 Carbon (^{13}C)($I = 1/2$).* Accurate, practical prediction of ^{13}C NMR chemical shifts was achieved with a new system, CAST/CNMR, taking account of stereochemistry.[190] The CAST/CNMR system has solved the critical problem of the accurate distinction of differences and similarities in stereochemical structures around a specific carbon, which has not yet been achieved by any other database-oriented system for prediction of ^{13}C NMR chemical shifts. The ^{1}H and ^{13}C NMR data for 13 nitrohistidine derivatives are reported, providing a diagnostic method for the elucidation of the N1- and the N3-substituted regioisomers.[191] The ^{13}C NMR chemical shift assignments for 1, 2-$C_{60}H_2$ and a series of ^{13}C-labeled fullerene derivatives with three-, four- and five-membered annulated rings were assigned using 2D INADEQUATE spectroscopy and examined for trends that correspond to the changes in strain in the fullerene cage.[192] Molecular structure and conformational stability of chair and twist conformers of 1, 2-dioxane and halogen substituted compounds of the 1, 2-dioxane were studied using ab initio and density functional theory (DFT) methods.[193] The ^{13}C-NMR chemical shift study for carbon atoms in the compounds are calculated and the results were discussed. A review of available results obtained from studies of the initiation micro-mechanisms of polynitro compounds from the point of view of organic chemistry. Attention is also paid to the basic mechanisms of low-temperature thermal decomposition of these compounds. With consideration of these results, the relations were specified and analysed between the characteristics of impact and electric spark sensitivities, detonation and thermal decomposition, on the one hand, and ^{13}C and ^{15}N NMR chemical shifts of polynitro compounds, on the other.[194] In this review[195], the authors mainly focus on the structural determination of two well-known silk fibroin proteins that are from the domesticated silkworm, Bombyx (B.) mori, and the wild silkworm, Samia cynthia ricini, respectively. The structures of B. Mori silk fibroin before and after spinning were determined by using an appropriate model peptide, $(AG)_{15}$, with several solid-state NMR methods; ^{13}C two-dimensional spin-diffusion solid-state NMR and rotational echo double resonance (REDOR) NMR techniques along with the quantitative use of the conformation-dependent ^{13}C CP/MAS chemical shifts.

2.14.2 Silicon (^{29}Si)($I = 1/2$). Variable temperature high resolution MAS ^{29}Si NMR spectroscopy is used to study the phase transition between the low and

high temperature versions of pure silica ferrierite.[196] ETS-10 zeolite was synthesized under hydrothermal conditions from gels containing $TiCl_4$ and sodium silicate as titanium and silica source in the presence of tetraalkylammonium bromides, TAABr (TAA^+: TMA^+, TEA^+, TPA^+ and TBA^+). The samples were characterized by XRD, thermal anal. (TG, DSC), SEM and multinuclear ^{13}C- and ^{29}Si-NMR.[197] Amorphous aluminum silicates, isolated from hydrothermal reactions used to form crystalline zeolite A, were studied using a number of techniques. NMR studies using $^{29}Si\{^1H\}$ CP/MAS and ^{27}Al and ^{23}Na MQ/MAS methods provide information about the local structure of the solids.[157] Five common ionomer glasses (Fuji IX, Ketac Molar, G338, G2 and G2SR) used to produce glass (ionomer) polyalkenoate dental cements were studied. ^{29}Si, ^{27}Al, ^{31}P and ^{19}F MAS NMR spectroscopy was used to characterize the glasses and the resulting spectra compared with previous studies of model glasses.[164] The existence of ether or ester-like complexes of silicate with organic compounds has long been debated in the literature on biological utilization of silicon. Comparison of theoretically calculated ^{29}Si NMR chemical shifts for such complexes with experimentally measured values in biological systems could provide a diagnostic tool for identifying which, if any of these molecules exist under physiological conditions.[198] The reduction of 1-chloro-1, 2, 3, 4, 5-pentaphenylsilole, ($C_4Ph_4SiPhCl$) with 2 equiv Li gave the pentaphenylsilole anion $[C_4Ph_4SiPh]^-$, silole dianion $[C_4Ph_4Si]^{2-}$ and hexaphenylsilole $C_4Ph_4SiPh_2$ were characterized by ^{29}Si NMR spectroscopy.[199] A nitrate-citrate-silica gel was prepared from metallic nitrates, citric acid and silica powder by sol-gel process, and it was further used to synthesize $Ni_{0.5}Zn_{0.5}Fe_2O_4/SiO_2$ nanocomposites by auto-combustion. The obtained $(Ni_{0.5}Zn_{0.5}Fe_2O_4)_{100-x}(SiO_2)_x$ (x = 5, 10 and 20%) samples were characterized by IR, DTA-TG, ^{29}Si CP/MAS NMR and XRD techniques.[200] He neutral hexacoordinate Si(IV) complex cis-$[(acac)_2Si(NCO)_2]$ (cis-8; acac = acetylacetonato-O,O) was synthesized, starting from $Si(NCO)_4$. Cis-8 was structurally characterized in the solid state (^{13}C, ^{15}N and ^{29}Si MAS NMR; crystal structure analysis) and in solution (^1H, ^{13}C and ^{29}Si NMR).[201] The structure of calcium aluminosilicate and calcium aluminosilicate fluoride glasses were characterized by ^{29}Si, ^{27}Al and ^{19}F MAS-NMR.[202] Periodic density functional theory (DFT) was used to calculate the structure of zircon ($ZrSiO_4$) and reidite (scheelite polymorph of ZrSiO4) at pressures from 0-41 GPa. Subsequently, the ^{29}Si NMR (NMR) chemical shifts at each pressure were determined using the GIPAW method.[203] The $Mg_2Si_xGe_{1-x}$ solid solution was prepared by heating stoichiometric amounts of elemental Mg, Si and Ge in an argon atmosphere. The ^{29}Si solid-state NMR was used to characterize the $Mg_2Si_xGe_{1-x}$ solid solution.[204] The ^{29}Si NMR chemical shift tensors of 16 simple singlet silylenes, R_2Si:, were calculated using GIAO/B3LYP method; correlations with molecular geometry and electronic structure are discussed.[205] ^{29}Si and ^{119}Sn NMR spectroscopy was performed on binary $xSnO_{(100-x)}SiO_2$ and ternary $xR_2O_{(50-x)}SnO_{50}SiO_2$ glasses (R = Li, Na, K, Rb for the ^{29}Si NMR and R = Na for ^{119}Sn NMR).[206] Previously unknown (methyl-β-cyanoethyl)cyclotri-, cyclotetra- and cyclopentasiloxanes were prepared by oxygen-halogen exchange between silicon and tin; the prepared compounds are characterized by ^{29}Si NMR spectra.[207] The effects of the

addition of clay minerals on the hydration reactions and kinetics of alite and belite are investigated for a white Portland cement (WPC)-kaolinite (20 wt%) blend and a mixture of 90 wt% WPC and 10 wt% bentonite using ^{29}Si MAS NMR spectroscopy.[208] Multinuclear solid-state NMR spectroscopy, employing ^{29}Si MAS, ^{27}Al MAS/3Q-MAS and ^{47,49}Ti wide-line experiments, was used for the structural characterization of titanium substituted ultra-stable zeolite Y (Ti-USY).[80] Zeolites NaY and mordenite were dealuminated by $SiCl_4$ and steaming methods and carefully characterized during and after the various synthetic stages by ^{27}Al and ^{29}Si MAS NMR and XRD to ensure sample quality.[176] The mixed modifier borosilicate glass used in high level radioactive waste immobilization was doped with between 2 and 12 mol% waste simulants including lanthanum oxide (La_2O_3), aluminum oxide (Al_2O_3) and bismuth oxide (Bi_2O_3) forming three series of glasses. These series were examined using multinuclear, ^{11}B, ^{29}Si and ^{27}Al MAS NMR to characterize their structures.[153] The compound, $[(Me_3Si)_2N]_2Si$, was prepared by the reduction of $[(Me_3Si)_2N]_2SiBr_2$ with potassium graphite at -78 °C. Unlike the corresponding germanium and tin compounds, 1 is unstable, but it can be studied in solution at low temperatures. The ^{29}Si NMR chemical shift of 1 measured at -20 °C was 223.9 ppm, in good agreement with a value obtained from model calculations of 233 ppm.[209] Li monosilicide (LiSi) was formed at high pressures and high temperatures (1.0-2.5 GPa and 500-700 °C) in a piston-cylinder apparatus. This compound was previously shown to have an unusual structure based on 3-fold coordinated Si atoms arranged into interpenetrating sheets. Lowered synthesis pressures permitted recovery of large (150-200 mg) quantities of sample for structural studies *via* NMR spectroscopy (^{29}Si and ^{7}Li), Raman spectroscopy and electric conduction measurements.[210] Density functional Born-Oppenheimer mol. dynamics (BOMD) is applied to study the evolution of geometry and ^{29}Si NMR chemical shifts of $Si(OH)_4$, which is the smallest zeolite precursor.[211] Nanometer-sized faujasite zeolite (nanoNaX), synthesized with an organic-additive-free approach, was modified with org. functional groups. Raman scattering and ^{29}Si solid-state NMR techniques were employed to study the organic components on the zeolites, the structures of the zeolitic frameworks and the connections between the organosilyl groups and zeolitic silanol groups.[212] The ^{29}Si, ^{27}Al MAS NMR was used to characterize Laponite RD and synthetic saponites of variable interlayer charge.[213] Powder and single-crystal X-ray diffraction, combined with ^{29}Si MAS NMR measurements, was used to study the thermal expansion of siliceous zeolite ferrierite as it approaches a second-order displacive phase transition from a low-symmetry (P_{nnm}) to a high-symmetry (I_{mmm}) structure.[214] In order to unambiguously assign the ^{29}Si-NMR chemical shifts to polycarbosilanes and poly(carbodisilane)s containing structural units $-CH_2Si_1(R_1R_2)Si_2(R_1R_2)CHPh-$, where $R_1 = R_2 =$ Me or Ph, a model polymer, poly(tetramethyl-disilylene-ethylene) was synthesized by dechlorination of 1,2-bis(chlorodimethylsilyl)ethane using potassium in toluene.[215] The calcium silicate hydrate (C-S-H) phase resulting from hydration of a white Portland cement (wPc) in water and in a 0.3 M $NaAlO_2$ solution was investigated at 14 and 11 hydration times, respectively, ranging from 6 h to 1 year by ^{27}Al and ^{29}Si MAS NMR spectroscopy.[216] The ^{29}Si chemical shift anisotropy

(CSA) data were determined from ^{29}Si MAS NMR spectra recorded at 14.1 T for a number of synthetic calcium silicates and calcium silicate hydrates.[217] Norbornyl cations of the group 14 elements Si → Pb (I^+; wherein E = Si, Ge, Sn and Pb; R = Me, Et and *n*-Bu) were synthesized from substituted 3-cyclopentenemethyl precursors by intramolecular addition of transient cations to the C=C double bond of the 3-cyclopentenemethyl substituent (π-route to norbornyl cations). The norbornyl cations 4a (E = Si, R = Me), 4e (E = Si, R = Et), 4f (E = Si, R = Bu), 4g (E = Ge, R = Bu), 4h (E = Sn, R = Bu) and 4i (E = Pb, R = Et) were identified by their characteristic NMR chemical shifts (4a, e, f, δ(^{29}Si) = 80-87, δ(^{13}C)(CH:) = 149.6-150.6; 4g, δ(^{13}C)(CH:) = 144.8; 4h, δ(^{119}Sn) = 334, δ(^{13}C)(CH:) = 141.5; 4i, δ(^{207}Pb) = 1049, δ(^{13}C)(CH:) = 138).[218]

2.14.3 Germanium (^{73}*Ge*)($I = 9/2$). NMR spectra of ^{73}Ge in germanium single crystals with different isotopic components were measured at the frequency of 17.4 MHz at room temperature.[219] Due to the small concentration (apprx.0.1%) of the magnetic (^{73}Ge) isotope, the magnetic dipole-dipole interaction is negligible in the samples studied, and the observed specific features of the resonance line shapes (a narrow central peak and a wide plateau) are determined mainly by the quadrupole interaction of magnetic nuclei with the random electric-field gradient (EFG) induced by the isotopic disorder.

2.14.4 Tin ($^{117,\,119}$ *Sn*)($I = 1/2$, 1/2). New organotin(IV) derivatives with general formulas R_2SnL, where R = n-Bu and L is the dianion of glycyltyrosine (H2L-1), glycyltryptophane (H2L-2), leucyltyrosine (H2L-3), leucylleucine (H2L-4), valylvaline (H2L-5) and alanylvaline (H2L-6) were synthesized in 1:1 molar ratio by the reaction of Bu_2SnO with the respected dipeptide under azeotropic removal of water. Triphenyltin glycylleucinate was obtained by reacting Ph_3SnCl and sodium glycylleucinate with filtration of NaCl formed. The bonding and coordination behavior in these derivatives are discussed on the basis of IR, multinuclear ^{1}H, ^{13}C and ^{117}Sn magnetic resonance and ^{119}Sn Moessbauer spectroscopic studies.[220] Polystannide transition metal complexes form from reactions between the Sn_9^{4-} Zintl ion and various zero-valent Pt precursors. The complexes include $[Sn_9Pt_2(PPh_3)]^{2-}$, $[Sn_{18}Pt_2]^{4-}$ and $[HSn_9Pt]^{3-}$ ions, which were characterized by extensive structural and spectroscopic studies including ESI-MS and MALDI TOF mass spectrometry and variable temperature ^{119}Sn, ^{117}Sn, ^{195}Pt and ^{31}P NMR spectroscopy.[221] The generalized-UHF (GUHF) theory is reviewed in the framework of the two-component quasi-relativistic MO theory. The authors review the theories on the magnetic shielding constants based on the SO-UHF, SO-GUHF and QR-GUHF methods and explain the applications to the ^{1}H shielding constants of hydrogen halides, the ^{13}C chemical shifts of Me halides, ^{119}Sn chemical shifts of tin halides, the shielding constants of noble gas atoms and the ^{199}Hg shielding constants of mercury halides.[222] A new stannide, Li_2AuSn_2, was prepared by reaction of the elements in a sealed Ta tube in a resistance furnace at 970 K, followed by annealing at 720 K for 5 days. The noncubic local symmetry at the Sn site is reflected by nuclear electrical quadrupolar splitting in the ^{119}Sn Moessbauer spectra and by the small chemical shift anisotropy in ^{119}Sn

solid-state NMR spectra.[223] The solid-state ^{119}Sn CP/MAS NMR spectra of triaryltin chlorides Ar_3SnCl were acquired.[224] The reaction of LiPh with Ar*SnPh (Ar* = C_6H_3-2,6-Trip2; Trip = C_6H_2-2,4,6-Pri3) afforded either the monomeric etherate (Et_2O)LiSnPh2Ar* (1) or the dimer $(LiSnPh_2Ar^*)_2$ (2). The reaction of 2 with $SnCl_2$ in a 1:1 ratio in Et_2O yielded the monomeric distannylstannylene $Sn(SnPh_2Ar^*)_2$ (3). The compounds 1-3 were characterized by ^{1}H, ^{7}Li, ^{13}C and ^{119}Sn NMR and UV-vis spectroscopy.[225] The centrosymetric structure of bis(triphenyltin) oxalate contains essentially four-coordinated tin and monodentate carboxylate moieties despite a Moessbauer quadrupole splitting of 2.8 mm s^{-1} and a ^{119}Sn NMR chemical shift of -503 ppm.[226] Application of the chemical vapor transport method to the Sn-S system allowed three different phases (*viz.* SnS, SnS_2 and Sn_2S_3) to be synthesized. By contrast, the chemical shifts, anisotropy and skew parameters for Sn_2S_3 as obtained by ^{119}Sn NMR were markedly different from those for SnS and SnS_2, and reflected the severe distortion of Sn(IV) and, especialy, Sn(II) in the former compound relative to the latter two.[227] ^{29}Si and ^{119}Sn NMR spectroscopy were performed on binary $xSnO(100\text{-}x)SiO_2$ and ternary $xR_2O(50\text{-}x)SnO50SiO_2$ glasses (R = Li, Na, K, Rb for the ^{29}Si NMR and R = Na for ^{119}Sn NMR).[206] The ^{11}B and ^{119}Sn NMR spectroscopies were used to determine the local environments of boron and tin in binary tin borate glasses of general composition $xSnO(1\text{-}x)B_2O_3$ ($0.2 \leqslant x \leqslant 0.7$).[228] Water-solvable (3-methoxypropyl)stannanes $(CH_3OCH_2CH_2CH_2)_xSnCl_{4-x}$ (x = 4, 3, 2, 1) were prepared. For all compounds, structures in $CDCl_3$ and [D6]DMSO solutions were proposed on the basis of their ^{13}C and ^{119}Sn NMR spectra.[229]

2.14.5 Lead (^{207}Pb)($I = 1/2$). Lead (II) and palladium (II) macrocyclic complexes were prepared by the template process using macrocyclic ligands. The mode of bonding was established on the basis of IR, ^{1}HNMR, ^{13}C NMR, ^{207}Pb NMR and mass spectral studies.[230] Lead fluoride, a superionic conductor was prepared in its nanostructured form by Inert Gas Condensation Technique (IGCT) using an Ultra High Vacuum (UHV) chamber. The average grain size was found to be in the range 9 to 43 nm. The existence of mixed phases (α and β-PbF_2) was identified using XRD. Solid state ^{207}Pb MAS NMR was carried to average out the dipolar interaction and the resultant isotropic peaks were assigned to the corresponding phases.[231] The results of the extensive investigations of the variation of the EPR and ^{207}Pb NMR spectra of active centers due to the existence of the native defects generated by disorder in the IV-VI semiconductor matrixes are presented.[232] The ^{207}Pb static, MAS and two-dimensional phase-adjusted spinning sidebands (2D-PASS) NMR experiments were performed on (1-x)PMN/xPSN [where PMN stands for $Pb(Mg_{1/3}Nb_{2/3})O_3$ and PSN stands for $Pb(Sc_{1/2}Nb_{1/2})O_3$] relaxor ferroelecs.[233] Flame at. absorption (FAA) spectroscopy was used to quantitate levels of cadmium (Cd) and lead (Pb) in four mainstream calcium supplements, with ranges of 0.04-0.09 μg/g tablet for Cd and 0.67-0.88 μg/g tablet for Pb being observed. Following this, ^{113}Cd and ^{207}Pb NMR spectroscopy studies were undertaken to observe competitive binding of both metals in three different calcium-binding model systems: calcein (a chelator), casein (Ca^{2+}-rich milk protein) and the calcium-binding protein (CBP) (highly specific for Ca^{2+}).[234]

Novel nonstoichiometric mixed lead and Sn niobates with the pyrochlore structure were synthesized *via* a solid-state route. The materials were characterized by bulk chemical analysis, single-crystal and powder x-ray diffraction, ^{207}Pb, ^{119}Sn and ^{93}Nb (single and triple quantum) solid-state NMR spectroscopy.[235] The ^{207}Pb, ^{45}Sc and ^{93}Nb nuclear-magnetic-resonance spectra of partially ordered relaxor ferroelectric $PbSc_{1/2}Nb_{1/2}O_3$ (PSN) were studied at 77-420 K.[236] The utility of the Carr-Purcell Meiboom-Gill (CPMG) experiment and a modified-CPMG experiment in characterizing NMR chemical shift powder patterns for spin-1/2 nuclei is demonstrated. Heavier NMR-active nuclei such as ^{195}Pt, ^{199}Hg and ^{207}Pb are known to be extremely sensitive to their local environment and as such have very large chemical shift ranges.[237] A Pb(II) complex with three ligands, 4, 4′-bipyridine (4, 4′-bpy), nitrate and thiocyanate, was synthesized and characterized by CHN elemental analysis, IR and ^{1}H, ^{13}C and ^{207}Pb NMR spectroscopy.[238] A 2.8 kV/cm electric field was applied parallel to the external magnetic field along the [111] direction of a PMN single crystal and the ^{207}Pb NMR spectra were measured at 9.1 T.[239] An isotropic ^{207}Pb NMR spectrum corresponding to the glassy matrix with spherical shell type Pb shifts from the cubic sites, as well as an anisotropic spectral component corresponding to polar nanoclusters with a Pb shift parallel to the [111] direction, were observed in a $PbMg_{1/3}Nb_{2/3}O_3$ (PMN) single crystal.[240] The coordination polymer $Pb[B(Im)_4](NO_3)(xH_2O)$, constructed by using Na tetrakis(imidazolyl)borate and $Pb(NO_3)_2$ solutions, is a layered material with the metal centers facing the interlayer spacing. As in naturally occurring layered minerals, this compound can readily undergo anion exchange and reversible intercalation of solvent H_2O in the solid state with retention of crystallinity. The authors observed changes in solvent intercalation by ^{207}Pb solid state NMR and TGA.[241] Reaction of bis(3-cyclopentenylmethyl)diethylplumbane (2) with trityl cation leads to the formation of the cationic complex bis(η1:η2-3-cyclopentenylmethyl)(ethyl)lead$^{(1+)}$, in which the positively charged lead atom interacts with the two C=C double bonds of the cyclopentene groups. The plumbylium cation 1 was characterized by NMR spectroscopy ($\delta(^{207}Pb)$ = 807 ppm, $\delta(^{13}C(C=C))$ = 136.1 ppm, $^1J(Pb,C=C)$ = 14.4 Hz) and x-ray crystallography.[242] ^{207}Pb NMR spectra were used to determine the structure of adducts of triphenyllead chloride and diphenyllead dichloride in CH_2Cl_2 and MeCN.[243]

2.15 Group 15(^{14,15}N, ^{31}P). - *2.15.1 Nitrogen ($^{14,15}N$)(I = 1, 1/2).* The ^{1}H, ^{13}C and ^{14}N NMR chemical shifts for creatinine in water solutions of various acidity were measured.[244] The ^{14}N MAS NMR spectra for a number of tetraalkylammonium halides with short alkyl chains (C_2H_5- to n-C_4H_9-) were recorded following a careful setup of the experimental conditions. Analysis of the spectra demonstrates the presence of ^{14}N chemical shift anisotropies (CSAs) on the order of $|\Delta\sigma|$ = 10-30 ppm along with ^{14}N quadrupole coupling constants in the range of 10-70 kHz.[245] Solvent effect on ^{14}N NMR chemical shifts of oxine (8-hydroxyquinoline) and 2-methyloxine (8-hydroxyquinaldine) was studied.[246] The ^{1}H, ^{13}C, ^{14}N and ^{15}N NMR chemical shifts were used to prove the structures of the products of 2-chloropyrazine oxidation.[247] EIM (embedded ion method), cluster,

combined EIM/cluster and isolated molecule ^{13}C and ^{15}N chemical shielding and quadrupolar coupling constant (QCC) calculations at the B3LYP level with D95**, D95++**, 6-311G** and 6-311+G** basis sets were done on the amino acids L-alanine, L-asparagine monohydrate and L-histidine monohydrate monohydrochloride, and on the α and γ polymorphs of glycine.[248] A new method for determining of nitrogen chemical shift anisotropies (CSAs) employing ^{14}N MAS NMR spectroscopy is presented.[249] Directly detected ammine ^{14}N NMR chemical shifts of 20 amminecobalt(III) compounds are reported.[250] The ^{14}N, ^{15}N and ^{17}O NMR and data are reported for some mesoionic 1, 3-diazoles, 1, 3-oxazoles and 1, 3-thiadiazoles.[251] Solid-state NMR 2-dimensional spectroscopy was used to correlate C atom backbone and side-chain chemical shifts for uniformly ^{13}C, ^{15}N-enriched microcrystalline ubiquitin.[252] Solid-state NMR measurements were performed on the complex of an 18-residue peptide derived from the V3 loop sequence of the gp120 envelope glycoprotein of the HIV-1 MN strain with Fv fragments of the human anti-gp120 monoclonal antibody 447-52D in a frozen glycerol/water solution. The peptide was uniformly ^{15}N- and ^{13}C-labeled in a 7-residue segment containing the conserved GPGR motif in the epitope. The ^{15}N and ^{13}C NMR chemical shift assignments for the labeled segment were obtained from two-dimensional ^{13}C-^{13}C and ^{15}N-^{13}C MAS NMR spectra.[253] Structural and spectroscopic properties of solid tris(3-formyl-5-methyl-2-salicylidenaminoethyl)amine were investigated. The ^{13}C and ^{15}N CP/MAS NMR results (chemical shifts) allow identification of two pairs of Schiff and amino nitrogen nuclei thus supporting formation of the two types of moieties in the crystal lattice.[254] Norchelerythrine and norsanguinarine, tertiary benzo[c]phenanthridine alkaloids, were examined by gradient-selected 2D NMR spectroscopy and the later also by extensive theoretical calculations. ^{1}H, ^{13}C and ^{15}N chemical shifts assignments of the title isoquinoline alkaloids based on NOE and multiple-bond chemical shift correlation experiments (GSQMBC) are reported.[255] In a recent MAS NMR study, two types of histidine residues in the light-harvesting complex II (LH2) of Rhodopseudomonas acidophila were resolved. The isotropic ^{13}C shifts of histidines coordinating to B850 BChl a are similar to fully positive charged histidine, while the ^{15}N shift anisotropy shows a predominantly neutral character.[256] The determination of backbone conformations in powder peptides using ^{13}C and ^{15}N shift tensor information is explored.[57] An approach is presented that allows a detailed, quantitative characterization of conformational exchange processes in proteins on the μs-ms time scale. The approach relies on a combined analysis of ^{15}N NMR relaxation rates and chemical shift changes and requires that the chemical shift of the exchanging species can be determined independently of the relaxation rates.[258] Experimental and theoretical ^{15}N and ^{13}C NMR data for the three nitrobenzaldehyde guanylhydrazones isomers (*o*-, *m*- and *p*-I) are reported.[259] A new indirect detection scheme for obtaining $^{15}N/^{1}H$ shift correlation spectra in crystalline proteins is described.[260] An alternate technique for accurately monitoring the chemical shift in multidimensional NMR experiments using spin-state selective off-resonance decoupling is presented here.[261] The ^{1}H, ^{13}C and ^{15}N chemical shifts of some pyridines and mesoionic oxatriazole aminides were recorded in the absence and

presence of the complex dirhodium tetrakis(trifluoroacetate).[262] The authors describe direct methods for the measurement of the transverse and longitudinal ^{15}N chemical shift anisotropy-dipolar cross-correlation rates based on comparison of the ^{15}N doublet components observed in ^{1}H-coupled ^{1}H-^{15}N HSQC-type spectra.[263] Geometry-dependent chemical shift anisotropy (CSAg) values of ^{1}H and ^{15}N nuclei were determined in solution for ^{15}N-labeled, Nα-t-Boc-L-valine by measurements of CSA/dipole-dipole cross-correlated relaxation rates using longitudinal variants of the recently proposed one-dimensional cross-correlation experiments.[264] The intestinal fatty acid binding protein (IFABP) is a small (15 kDa) protein consisting mostly of 10 antiparallel β-strands (A-J) and a small helical region that serves as a portal for the ligand. Two β-sheet structures (strands A-E and F-J) surround a cavity into which the ligand binds. In this work, the authors investigated how changes in the side chains of specific residues are propagated through the structure. To determine what these changes were and how they relate to changes in stability, ^{15}N chemical shift perturbations were measured and compared to those of the wild-type protein.[265] Two sets of cross-correlated relaxation rates involving chemical shift anisotropy and dipolar interactions were measured in an RNA kissing complex.[266] Solid state NMR sample preparation and resonance assignments of the U-[^{13}C, ^{15}N] $2L10^{4}$ kDa dimeric form of the regulatory protein Crh in microcrystalline, PEG precipitated form are presented.[267] The ^{1}H, ^{15}N and ^{13}C resonance assignments of protein S-824 are reported. The backbone ^{1}H, ^{15}N and ^{13}C resonance assignments of S-824 are virtually complete.[268] The ^{1}H, ^{13}C and ^{15}N NMR spectra in DMSO-d6 were measured for eight nitraminopyridine N-oxides, ten 4-nitropyridine N-oxides, four 2-nitraminopyridines and five 4-nitropyridines. Their chemical shift assignments are based on PFG ^{1}H, X (X = ^{13}C and ^{15}N) HMQC and HMBC experiments.[269] The ^{15}N-labeled Fe dinitrogen complexes trans-$[FeH(N_2)(PP)_2][BPh_4]$ (PP = dppe, depe and dmpe) and cis-$[FeH(N_2)(PP_3)][BPh_4]$ were prepared in situ by exchange of unlabeled coordinated dinitrogen with $^{15}N_2$. The ^{15}N NMR chemical shifts and coupling constants are reported.[270] The ^{15}N NMR chemical shifts of 2-aryl-1, 3, 4-oxadiazoles were assigned on the basis of the ^{1}H-^{15}N HMBC experiment.[271] The ^{15}N NMR spectral data for 3-substituted (chloro, bromo, acetyl, carboxy, carboethoxy, methylsulfanyl, methylsulfinyl, N, N-dimethylsulfamoyl, nitro) 4(1H)-quinolinones and their 1-Me derivatives are presented.[272] Treatment of 2-acetyl-2-methylcyclopentanone with hydrazine hydrate yielded a new condensed hexahydro-1,3,5-triazine (I), which is the first example of the ketimine-type trimers. A complete ^{1}H, ^{13}C and ^{15}N NMR assignment of the compound was achieved.[273] The interaction between the histidine-containing phosphocarrier protein HPr and xenon atoms in solution is studied. Wild-type HPr as well as the exchange mutant I14A were studied. Xenon binding results in pronounced changes of the ^{1}H and ^{15}N chemical shifts of amide groups close to the cavity.[274] Structural and dynamical features of the B18 peptide from the sea urchin sperm bindin protein were determined in the crystalline state and in zwitterionic lipid bilayers at a peptide:lipid molar ratio of 1:12 using solid-state NMR spectroscopy. The study was focused on three ^{13}C and ^{15}N uniformly labeled leucine residues, which were introduced into three

different B18 peptides at positions evenly distributed along the B18 primary structure.[275] The effect of time and spatial averaging on ^{15}N chemical shift/^{1}H-^{15}N dipolar correlation spectra, *i.e.*, PISEMA spectra, of α-helical membrane peptides and proteins is investigated.[276] The theoretical ^{1}H, ^{13}C and ^{15}N NMR spectra were calculated at the Hartree-Fock level by using the polarized double zeta (PDZ) basis set of Hansen and Bouman for the geometries optimized at the same level.[277] A computer program (SHIFTX) is described which rapidly and accurately calculations the diamagnetic ^{1}H, ^{13}C and ^{15}N chemical shifts of both backbone and sidechain atoms in proteins.[278] Three model 2, 4, 6-tris(amino)-1,3,5-triazines, structurally related to a dyestuff molecule, were synthesized in order to enable the effects of rotamer exchange on the ^{1}H, ^{13}C and ^{15}N NMR spectra to be investigated in more detail.[279] LL-37 is an amphipathic, α-helical, antimicrobial peptide. ^{15}N chemical shift and ^{15}N dipolar-shift spectroscopy of site-specifically labeled LL-37 in oriented lipid bilayers indicate that the amphipathic helix is oriented parallel to the surface of the bilayer.[280] Crystals of the Schiff base derivative of 2, 2′-dihydroxybiphenyl-3-carbaldehyde with n-butylamine were examined using x-ray diffraction, FTIR and CP/MAS spectroscopy. The results of the FTIR, ^{1}H, ^{13}C and ^{15}N NMR and CP/MAS study of the crystals are in agreement with the x-ray data. Instead of a continuous absorption, only a broad band is found indicating relatively low proton polarizability in the two types of the cooperative relatively short intramolecular hydrogen bonds. The ^{15}N NMR chemical shift indicates the protonation of the Schiff base.[281] The ^{1}H, ^{13}C and ^{15}N chemical shifts of SAM22 were assigned and its secondary structure was evaluated based on multidimensional heteronuclear NMR data.[282] The 39 kDa receptor associated protein (RAP) is a modular protein consisting of multiple domains. There has been no x-ray crystal structure of RAP available and the full-length protein does not behave well in a NMR tube. To elucidate the 3D structure of the RAP, the authors undertook structure determination of individual domains of the RAP. As the first step, here it was reported the nearly complete assignments of the ^{1}H, ^{13}C and ^{15}N chemical shift signals of domain 1 of the RAP.[283]

A series of well-defined model polypeptides of B. mori silk fibroin, $[Ala\text{-}Gly]_n$ ($n = 12$ and 5-9), $[Alad4Gly]_{12}$ and $[Glyd2Ala]_{12}$, (where Ala, Gly, Alad4 and Glyd2 denote L-alanine, glycine, 2, 3, 3, 3-deuterated L-alanine and 2, 2-deuterated glycine residues, respectively), were successfully synthesized by an automatic solid phase peptide synthesizer. The authors determined the intrinsic ^{1}H, ^{13}C and ^{15}N NMR chemical shifts of Ala and Gly residues, characteristic to the silk I and silk II forms in Bombyx mori, by high-resolution and solid-state ^{13}C CP/MAS, ^{1}H CRAMPS, ^{1}H-^{13}C HETCOR and ^{15}N CP/MAS NMR measurements.[284] RefDB is a secondary database of reference-correlated protein chemical shifts derived from the BioMagResBank (BMRB). The database was assembled by using a recently developed program (SHIFTX) to predict protein ^{1}H, ^{13}C and ^{15}N chemical shifts from x-ray or NMR coordinate data of previously assigned proteins.[285] The role of proline residues in the photocycle of bacteriorhodopsin (bR) is addressed using solid-state NMR. The ^{13}C and ^{15}N chemical shifts from X-Pro peptide bonds in bR are assigned from REDOR difference spectra of

pairwise labeled samples, and correlations of chemical shifts with structure are explored in a series of X-Pro model compounds.[286] The proton transfer equilibrium in a series of double Schiff base derivatives of trans-1, 2-diaminocyclohexane in solution and the solid state was studied by means of ^{15}N NMR spectroscopy and analyse of the deuterium isotope effect on the chemical shifts Δ^{15}N(D).[287] A simple and reliable method for docking protein-protein complexes using ^{1}HN/^{15}N chemical shift mapping and backbone ^{15}N-^{1}H residual dipolar couplings is presented and illustrated with three complexes (EIN-HPr, IIAGlc-HPr and IIAMtl-HPr) of known structure. The ^{1}HN/^{15}N chemical shift mapping data are transformed into a set of highly ambiguous, intermolecular distance restraints (comprising between 400 and 3000 individual distances) with translational and some degree of orientational information content, while the dipolar couplings provide information on relative protein-protein orientation.[288] A new strategy of backbone resonance assignment is proposed based on a combination of the most sensitive TROSY-type triple resonance experiments such as TROSY-HNCA and TROSY-HNCO with a new 3D MQ HACACO experiment. The favorable relaxation properties of the MQ coherences and signal detection using the ^{13}C′ antiphase coherences optimize the performance of the proposed experiment for application to larger proteins. In addition to the ^{1}HN, ^{15}N,^{13}Cα and ^{13}C′ chemical shifts the 3D MQ HACACO experiment provides assignment for the ^{1}Hα resonances in contrast to previously proposed experiments for large proteins.[289] The backbone assignment of the copper-zinc superoxide dismutase amyotrophic lateral sclerosis G93A mutant was performed on an ^{15}N-enriched protein sample.[290] N-terminal myristoylation of the Ig-binding domain of protein G (GB1) from group G Streptococcus provides the means to bind the protein to aligned phospholipid bilayers for solid-state NMR structural studies. The myristoylated protein is immobilized by its interactions with bilayers, and the sample alignment enables orientationally dependent ^{15}N chemical shifts and ^{1}H-^{15}N-dipolar couplings to be measured.[291]

2.15.2 Phosphorus (^{31}P)($I = 1/2$). Variable angle sample spinning (VASS) in NMR studies of membrane-associated biological molecules facilitates the extrication of structural information. VASS NMR was used, for example, to obtain information of ^{31}P chemical shift anisotropy of phosphatidylinositol phosphates embedded in a lyotropic liquid crystal membrane mimic.[292] In contrast to solution NMR spectroscopy, where complete or almost complete averaging leads to isotropic values, the anisotropic character of nuclear interactions is apparent in solid-state NMR spectra. The orientation dependence of chemical shift and dipolar or quadrupolar interactions was used to obtain dynamic as well as angular information from polypeptides that strongly interact with phospholipid bilayers. This article illustrates the advantageous characteristics of the anisotropic ^{15}N or ^{31}P chemical shift interactions that in a direct manner allow one to obtain information on the alignment of helical polypeptides or of phospholipid head groups with respect to the membrane normal.[293] Five commercial ionomer glasses (Fuji IX, Ketac Molar, G338, G2 and G2SR) used to produce glass (ionomer) polyalkenoate dental cements were studied by ^{29}Si, ^{27}Al, ^{31}P and ^{19}F

MAS NMR.[164] The authors studied the interaction between metal ions and the metal ion-binding motif in hammerhead ribozymes, as well as the functions of the metal ion at the motif, with heteronuclear NMR spectroscopy and employed model RNA systems, which mimic the metal ion-binding motif and the altered motif. In $Co(NH_3)_6$(III) titrations, they observed large ^1H and ^{31}P chemical shift perturbations for the motif and found that outer-sphere complexation of $Co(NH_3)_6$(III) is possible for this motif.[294] The phospholipids (PL) occurring in both ewe and cow milk fat globule membrane were identified and quantitatively determined using ^{31}P NMR spectroscopy with inverse gated decoupled sequences, which allowed a rigorous quantitative analysis.[295] The solution structure of d(CGCGAATTCGCG)(2) was determined on the basis of an exceptionally large set of residual dipolar couplings. In addition to the heteronuclear ^{13}C-^1H and ^{15}N-^1H and qualitative homonuclear ^1H-^1H dipolar couplings, previously measured in bicelle medium, more than 300 quantitative ^1H-^1H and 22 ^{31}P-^1H dipolar restraints were obtained in liquid crystalline Pf1 medium, and 22 ^{31}P chemical shift anisotropy restraints.[296]

2.16 Group 16(^{17}O, ^{33}S, ^{77}Se, ^{125}Te). – *2.16.1 Oxygen* (^{17}O)($I=5/2$). – The authors demonstrate that it is possible to calculate with reasonable accuracy the ^{17}O-chemical shift for the gas-to-liquid phase change for water using density functional theory (DFT) and water clusters in which both cluster size and cooperative hydrogen bonding are taken into account.[297] The solvent effect on ^{17}O isotropic shielding was computed by different methods: the polarizable continuum model and a mixed approach, including a few real solvent molecules treated as the solute.[298] The ^1H, ^{13}C, ^{17}O and ^{31}P NMR parameters, including chemical shift tensors and quadrupolar parameters for ^{17}O, were calculated for phenylphosphonic acid, $C_6H_5PO(OH)_2$, under periodic boundary conditions.[299] Structures of the superelectrophilic fluorooxonium dications FOH_3^{2+} and $F_2OH_2^{2+}$ were calculated at the QCISD(T)/6-311G** level. The ^{17}O and ^{19}F NMR chemical shifts of the mono- and dications were also computed by the GIAO-MP2 method.[300] The Gd(III) complexes of the two dimeric ligands [en(DO_3A)$_2$] {N, N′-bis[1, 4, 7-tris(carboxymethyl)-1, 4, 7, 10-tetraazacyclododecan- 10-ylcarbonylmethyl]-N, N′-ethylenediamine} and [pi(DTTA)$_2$]$_8^-$ [bis(diethylenetriaminepentaacetic acid) diamide derivatives with trans-1, 2-cyclohexanediamine] were synthesized and characterized. The ^{17}O NMR chemical shift of H_2O induced by [en{Dy(DO_3A)}$_2$] and [pi{Dy(DTTA)}$_2$]$_2^-$ at pH 6.80 proved the presence of 2.1 and 2.2 inner-sphere H_2O molecules, respectively.[301] PDMS-MxOy (where M = Ge^{IV}, Ti^{IV}, Zr^{IV}, Nb^V and Ta^V) hybrid materials were studied from the solution to the solid state through ^{17}O NMR spectroscopy.[302] A group of para-substituted bis(acetoxy)iodoarenes was studied by ^{17}O and ^{13}C NMR.[303] The ^{17}O NMR chemical shift values of polyoxides HO_nH, MeO_nH and MeO_nMe (n = 2, 3, 4) were calculated using four different methods (GIAO-HF, GIAO-MP2, GIAO-CCSD(T) and IGLO-DFT) and various basis sets ranging from double to quadruple ζ quality.[304] The ^{17}O-enriched phenylphosphonic acid ($PhP_{17}O_3H_2$) was prepared from phosphonic acid dichloride and enriched H_2O. The ^{17}O MAS NMR spectra were recorded at various

magnetic fields (7, 9.4 and 17.6 T) and the isotropic chemical shifts and quadrupolar constants were determined for the different O sites: P:O, P-O-H, P-O-Ti and OTix.[305] The structure and dynamic properties of aqueous mixtures of 1,1,1,3,3,3-hexafluoro-2-propanol (HFIP) were investigated over the whole range of HFIP mole fraction (xHFIP) by large-angle X-ray scattering (LAXS), small-angle neutron scattering (SANS), ^{19}F-, ^{13}C- and ^{17}O-NMR chemical shifts, ^{17}O-NMR relaxation and mass spectrometry.[306] The ^{17}O NMR data for 52 phenoxyethyl derivation were measured and assigned.[307] Solid-state ^{17}O NMR spectra were obtained at 4.70, 11.75 and 19.60 T for potassium hydrogen [$^{17}O_4$] dibenzoate (PHB) under both MAS and stationary conditions.[308] Solid-state ^{17}O NMR spectroscopy is employed to characterize powder samples of known monoclinic and orthorhombic modifications of ^{17}O-enriched triphenylphosphine oxide, Ph_3PO.[309] The authors used single crystal ^{17}O NMR and density functional theory to investigate intermolecular interactions in a strongly H-bonded system. The chemical shielding and quadrupole coupling (QC) tensors are determined in oxalic acid dihydrate by single crystal methods.[310] The ^{17}O NMR chemical shifts were measured for 23 liquid chemical compounds and their vapors at natural abundance of oxygen-17 and the temperature of 333 K.[3011] The authors report ^{17}O and ^{27}Al NMR results for ^{17}O-enriched synthetic and natural layer silicates with significantly improved resolution of O sites including basal and apical oxygens using ^{17}O 3QMAS NMR spectroscopy.[178] A multi-linear-regression analysis using the Kamlet-Abbout-Taft (KAT) solvatochromic parameters in order to elucidate and quantify the solvent effects on the ^{17}O chemical shifts of three 4-dimethylsulfoximide-1,1,1-trifluoro-3-buten-2-ones is reported.[312] Ab initio calculations of the ^{17}O electrical field gradient (EFG) tensor, quadrupolar coupling constant (Cq) and asymmetry parameter (η_q), along with the ^{17}O NMR isotropic chemical shift (δ_{iso}) for the three crystalline polymorphs of P_2O_5 are presented.[313] Special high-temperature and high-pressure multinuclear NMR equipments were constructed, and used for the measurements of ^{17}O-NMR chemical shift and spin-lattice relaxation time (T_1) in water over the range from liquid to supercritical (SC) states.[314] The authors report resolution-enhanced ^{17}O MAS NMR studies of the paraelectric-antiferroelectric phase transition (at TC = 373 K) of the model H-bonded compound squaric acid ($H_2C_4O_4$).[315] The oxidation of the trans, cis-(II) and trans, trans-epoxides (III) (first prefix refers to relative position of C4 carbonyl and C3′ aryl of the epoxide ring, second prefix describes relative position of C2 Ph and epoxide O) of differently substituted (Z)-3-arylidene-1-thioflavan-4-ones with dimethyldioxirane (DMD) yielded the appropriate sulfoxides and sulfones. The structures were elucidated by the extensive application of one- and two-dimensional ^{1}H, ^{13}C and ^{17}O NMR spectroscopy.[316] Hydrosodalites and hydroxosodalites were analysed by ^{17}O, ^{29}Si and ^{1}H MAS NMR in the fields of 17.6 and 11.7 T.[317] With various concentrations of $CaCl_2$ and $MgCl_2$ aqueous solution below 1.0 mol/l, Raman spectra of water in the OH stretch region of 2500-4000 cm^{-1} and ^{17}O NMR chemical shift of water are measured and the Raman spectra are deconvoluted.[318] The two-layer ONIOM2(MP2-GIAO:HF-GIAO) (our own n-layer integrated MO and molecular mechanics approach, in which a small model

system containing the nuclei of interest is described at the MP2-GIAO level of theory, and the rest of the mol.-using the HF-GIAO method) ansatz is applied to the calculation of ^{13}C, ^{1}H and ^{17}O NMR chemical shifts in the 4C1 G+, 4C1 G-, 4C1 T, 1C4 G+ and 1C4 G- conformers of β-D-glucopyranose.[319] The ^{17}O NMR parameters, both the chemical shifts and the quadrupolar parameters, are calculated for SiO_2 polymorphs using density functional theory with the generalized gradient-corrected PBE functional.[320]

2.16.2 Sulfur (^{33}S)($I = 3/3$). Solid state ^{33}S NMR spectra of a variety of inorganic sulfides were obtained at magnetic field strengths of 4.7 and 17.6 T.[321]

2.16.3 Selenium (^{77}Se)($I = 1/2$). The electronic structures and molecular properties of square-planar 6π-electron ring molecules and ions E_2N_2 and E_4^{2+} (E = S, Se and Te) were studied using various ab initio methods and density functions. The ^{77}Se NMR chemical shifts of chalcogen cations $S_xSe_{4-x}^{2+}$ (x = 0-3) were calculated with CAS, BPW91 and B3PW91 methods using the GIAO formalism.[322] Theoretical ^{77}Se chemical shifts of a series of simple organoselenium compounds are compared to known NMR data for various derivatives of selenoenzymes and selenoamino acids.[323] Solid-state CP/MAS ^{13}C, ^{77}Se and ^{15}N NMR spectra were recorded for 1, 3-imidazolidine-2-selenone, its N-substituted derivatives and some related compounds.[324] The Peterson olefination of aromatic aldehydes with an α-silyl selenoacetamide proceeded smoothly with high stereoselectivity to give E-α, β-unsatulated selenoamides in good to high yields. The reaction with aldehydes bearing alkenyl and dienyl groups gave the corresponding selenoamides bearing dienyl and trienyl groups, but the stability of the products depended on the substituents on the aromatic ring. X-ray molecular analysis disclosed that the α, β, γ and δ-unsatulated selenoamides had a nearly planar structure. In the ^{77}Se NMR spectra, signals were observed in the region •130 ppm depending on the substituents on the aromatic ring, whereas the ^{1}J coupling constant between the C atom and the Se atom was almost independent of the substituents.[325] Twelve secondary phenylselenenylalkanes and -cycloalkanes were studied by ^{1}H, ^{13}C and ^{77}Se NMR spectroscopy in the presence of the chiral dirhodium complex $Rh_2[(R)\text{-MTPA}]_4$ [Rh-Rh; MTPA-H = (R)-(+)-methoxytrifluoromethylphenylacetic acid, Mosher's acid].[326] An extensive library of ^{77}Se chemical shifts were generated from the NMR measurements on substituted (phenylseleno)benzenes, including 33 new compounds.[327] The authors present a method for the 1st principles density functional calculation of relativistic all-electron NMR chemical shifts using pseudopotentials and demonstrate its success for a range of Se and Te containing molecules.[328]

2.16.4 Tellurium (^{125}Te)($I = 1/2$). The static and MAS NMR solid-state spectra of Re_6Te_{15} and a series of Re_6-Te cluster compounds demonstrate the positive and negative ^{125}Te NMR chemical shifts indicating that the $[Re_6]$ cluster distorts strongly magnetic field at the neighboring Te sites.[329] Tellurium(IV) complexes $(R_4N)_2[TeCl_6]$ (T6), $(R_4N)[TeCl_5]$ (T5) and $(R_4N)[TeCl_4OH]$ (T4), where $(R_4N)^+$ is tetra-Bu, tetraoctyl and trialkyl benzyl ammonium cations, were synthesized.

Tellurium distribution between aqueous HCl solutions and trialkyl benzyl ammonium chloride solution in caprylic acid was studied. The ^{125}Te NMR spectra of aqueous HCl solutions of tellurium have a single averaged peak, whose chemical shift (CS) depends on the acid concentration. The ^{125}Te NMR spectroscopy has shown that the T4 complex in nonaqeous solution is kinetically inert and the ligand exchange with the T6 and T5 complexes is retarded.[330] Tellurium(II) dimethanethiolate, $Te(SMe)_2$ and tellurium(II) diethanethiolate, $Te(SEt)_2$, were synthesized by reaction of TeO_2 and $Te(OiPr)_4$ with HSMe and HSEt, respectively. The ^{125}Te NMR chemical shift of $Te(SR)_2$ largely depends on R (R = Me, Et, *i*-Pr and *t*-Bu) and shows a nearly linear correlation with the first ionization energy of the corresponding thiol HSR.[331] The authors present a method for the 1st principles density functional calculation of relativistic all-electron NMR chemical shifts using pseudopotentials. Relativistic effects are included at the level of the scalar-relativistic zeroth-order regular approximation. The method allows chemical shifts of large, low symmetry structures containing heavy elements to be calculated efficiently. They demonstrate its success for a range of Se- and Te- containing molecules.[328]

2.17 Group 17(^{19}F, ^{35,37}Cl). – *2.17.1 Fluorine* (^{19}F)($I = 1/2$). The ^{19}F NMR chemical shifts and coupling constants are reported for 215 compounds.[332] Oil-in-water fluorinated microemulsion aggregates were diluted at high water content, thus taking the system outside the regime of thermodynamic stability. The kinetic stability of aggregates was studied by an analysis of ^{19}F NMR chemical shifts.[333] High-speed MAS ^{19}F NMR spectra are recorded and reconstructed for 10 compounds from BaF_2-AlF_3 and CaF_2-AlF_3 binary systems which leads to the determination of 77 isotropic ^{19}F chemical shifts in various environments.[334] Five common ionomer glasses (Fuji IX, Ketac Molar, G338, G2 and G2SR) used to produce glass (ionomer) polyalkenoate dental cements were studied. ^{29}Si, ^{27}Al, ^{31}P and ^{19}F MAS NMR Spectroscopy was used to characterize the glasses and the resulting spectra compared with previous studies of model glasses.[164] Identification of compounds from chemical libraries that bind to macromolecules by use of NMR spectroscopy has gained increasing importance during recent years. A simple methodology based on ^{19}F NMR spectroscopy for the screening of ligands that bind to proteins, which also provides qualitative information about relative binding strengths and the presence of multiple binding sites, is presented here.[335] The reaction of trichloroacetaldehyde with fluorobenzene, followed by a series of transformations, gave 4-fluorobenzil and 4,4′-difluorobenzil which were used in the synthesis of new difluoroaromatic compounds with a heterocyclic central group. The ^{1}H, ^{13}C and ^{19}F NMR spectra of the newly synthesized difluoroaromatic compounds were studied.[336] Murine adenosine deaminase (mADA) is a 40-kDa (b/α)8-barrel protein consisting of 8 central β-strands and 8 peripheral α-helixes containing 4 Trp residues. Here, the authors investigated the urea-dependent behavior of mADA labeled with 6-fluorotryptophan (6-^{19}F-Trp). The ^{19}F NMR spectrum of 6-^{19}F-Trp-labeled mADA revealed 4 distinct resonances in the native state and 3 partly overlapped resonances in the unfolded state. The resonances were assigned unambiguously

by site-directed mutagenesis.[337] The ^{19}F NMR shieldings for 53 perfluoro compounds were calculated by the B3LYP-GIAO method using the 6-31G(d), 6-31+G(d), 6-31G(d, p), 6-31++G(d, p), 6-311G(d, p), 6-311++G(d, p), 6-311G(2d, 2p), 6-311++G(2d, 2p), 6-311++G(2df, 2p), 6-311++G(3d, 2p) and 6-311++G(3df, 2p) basis sets.[338] The authors investigated the crystal structures of poly(vinylidene fluoride) (PVDF) in PVDF/silica (SiO_2) binary and PVDF/poly(Me methacrylate) (PMMA)/SiO_2 ternary hybrid composite films using IR analysis and solid-state, high-speed MAS ^{19}F NMR spectroscopy.[339] A set of 2-fluoro- and 3-fluoro-substituted thiophenes, pyrroles and furans was synthesized by a treatment of the corresponding lithio derivatives with N-fluorodibenzenesulfonamide. For all these compounds, ^{1}JCC and ^{1}JCH coupling constants and ^{19}F NMR chemical shifts were measured.[340] The non-natural amino acid 4-fluorophenylglycine (4F-Phg) was incorporated into several representative membrane-associated peptides for dual purpose. The ^{19}F-substituted ring is directly attached to the peptide backbone, so it not only provides a well-defined label for highly sensitive ^{19}F NMR studies but, in addition, the D and L enantiomers of the stiff side chain may serve as reporter groups on the transient peptide conformation during the biological function.[341] The ^{19}F NMR solution measurements were made for various phenyl-fluorinated Fe porphyrin complexes. Large chemical shifts for Ph fluorine signals of Fe(III) and Fe(II) are observed, and these signals are sensitive to electronic structure.[342] A method that uses both Hartree-Fock and hybrid Hartree-Fock density functional methods at the 6-311+G(2df,p) basis set level was used to calculate the ^{19}F NMR chemical shifts for possible Al-F species in Na aluminosilicate glasses.[343] The association behaviors of three 1-octanols (1-octanol: C_8OH; 1, 1, 2, 2-tetrahydrotridecafluorooctanol: TFC_8OH; and 1, 1-dihydropentadecafluorooctanol: DFC_8OH) in two hydrocarbon solvents (n-hexane and benzene) were examined by vibration spectroscopy from 288.15 to 318.15 K. It was found from ^{19}F NMR chemical shift measurements that the fluorooctanols in the benzene solution aggregated by interaction between the fluorocarbon chains instead of by hydrogen bonding.[344] The structure and dynamic properties of aqueous mixtures. of 1, 1, 1, 3, 3, 3-hexafluoro-2-propanol (HFIP) were investigated over the whole range of HFIP mole fraction (hip) by large-angle x-ray scattering (LAXS), small-angle neutron scattering (SANS), ^{19}F-, ^{13}C- and ^{17}O-NMR chemical shifts, ^{17}O-NMR relaxation and mass spectrometry.[306] Solid state ^{19}F MAS NMR studies of (3, 3, 3-trifluoropropyl)dimethylcholorosilane (TFS) probe molecules covalently bound to low surface area glass fibers are used for the quantive analysis of hydroxyl sites on the surfaces of model E-glass fibers.[345] The ^{19}F NMR shieldings for several remotely substituted rigid polycyclic alkyl fluorides with common sets of substituents covering a wide range of electronic effects were calculated using the DFT-GIAO theoretical model.[346] Based on structural information provided by recently reported crystal structures of rhodopsin, rationales are presented for the regiospecific protein perturbation on the previously reported ^{19}F chemical shifts of the vinyl and trifluoromethylrhodopsins and their photoproducts.[347] A survey of possible structures for the $C_{60}F_8$ molecule was carried out, using both experimental (^{19}F NMR data) and theoretical(structure-energy correlation) con-

siderations to limit the number of isomers to be regarded as candidates for the previously isolated species.[348] Anomalous tendencies in the ^{19}F NMR chemical shifts of certain fluorine-containing, primarily organofluorine, compounds are explained.[349] Solution $^{1}JSi\text{-}F$ and $^{2}JC\text{-}F$ NMR coupling constant and ^{19}F NMR chemical shift data were analysed in pentacoordinate silyl monofluoride complexes used to model nucleophilic substitution at Si.[350] The ^{19}F NMR chemical shifts of CF_4 in CO_2 under extremely dilute concentrations were precisely determined at 299.8, 314.4 and 328.9 K over a wide range of pressure between 0.4 and 33 MPa.[351] The ^{119}Sn and ^{19}F NMR chemical shifts in alkali-metal hexafluorostannates are measured. Data of MAS-spectroscopy and ab initio calculations reveal that $[SnF_6]^{2-}$ has a distorted structure due to intramolecular electron correlation interactions in this anion.[352]

2.17.2 Chlorine ($^{35,37}Cl$)($I = 3/2$, $3/2$). – The ^{133}Cs and ^{35}Cl NMR T_1 relaxation studies of the Cs^+ and Cl^- complexation by Suwannee River natural organic matter (NOM) provide significant, new insight into the interaction of these species with NOM. The ^{35}Cl NMR chemical shift and T_1 relaxation rates show that there is no significant complexation between Cl^- and NOM.[353] The authors studied the efficacy of the tris-glycinatocobaltate(II) complex ($[Co(gly)(3)]^{(-)}$) as a shift reagent (SR) for chloride by ^{35}Cl NMR spectroscopy and compared to that of $Co^{(2+)}$(aq.).[354]

2.18 Group 18 (^{3}He, ^{129}Xe). – *2.18.1 Helium* (^{3}He)($I = 1/2$). Benkeser reduction of $C_{60}H_{36}$ (reduction with lithium metal and ethylenediamine at 90°C) yields mixtures of the hydrogenated fullerenes $C_{60}H_{38}$ to $C_{60}H_{44}$ was prepared by a much milder procedure than previous syntheses of highly hydrogenated fullerenes. The ^{1}H and ^{13}C NMR spectra of fractions isolated by HPLC showed that more highly hydrogenated fullerenes exhibited signals that were shifted upfield. The opposite trend appears to hold in ^{3}He NMR spectra of the corresponding endohedral helium compounds.[355] Eleven mono- and eight di-exocyclically substituted heptafulvene derivatives were optimized at the B3LYP/6-311+G** level of theory. The aromaticity indexes REC (ring energy content), Schleyer's NICS, ^{3}He NMR chemical shift and anisotropy of magnetic susceptibility and the geometry based descriptor HOMA were used to estimate the extent of cyclic π-electron delocalization due to the substituent effect.[356] The purpose of this research was to study the magnetic properties of the anions of higher fullerenes by ^{3}He NMR spectroscopy.[357] The ^{3}He NMR chemical shifts of various ^{3}He-encapsulated fullerenes (^{3}He at Cn) and their derivatives were calculated at the GIAO-B3LYP/3-21G and GIAO-HF/3-21G levels with AM1 and PM3 optimized structures.[358]

2.18.2 Xenon (^{129}Xe)($I = 1/2$). The authors report the variation of ^{129}Xe chemical shift δ vs. the pore size, the temperature and the xenon pressure of xenon adsorbed on mesoporous materials prepared in different synthesis conditions.[359] The xenon and fluorine magnetic shielding tensors, σ, of XeF_2 are characterized using solid-state ^{129}Xe and ^{19}F NMR spectroscopy and nonrelativistic and spin-

orbit relativistic zeroth-order regular approximation density functional theory (ZORA DFT).[360] The pressure dependence of the ^{129}Xe chemical shift tensor confined in the Tris(o-phenylenedioxy) cyclotriphosphazene (TPP) nanochannel was investigated by high-pressure ^{129}Xe NMR spectroscopy.[361] The authors report, for the 1st time, a calculation of the isotropic NMR chemical shift of ^{129}Xe in the cages of clathrate hydrates Structures I and II.[362] The chemical shift sensitivity and significant signal enhancement afforded by laser-polarized ^{129}Xe have motivated the application of ^{129}Xe NMR to imaging and spectroscopy.[363] SBA-15 samples prepared at several different temperature are characterized by hyperpolarized ^{129}Xe NMR spectroscopy.[364] The continuously circulating flow of hyperpolarized (HP) ^{129}Xe NMR technique was used to study the porous structure of ordered purely siliceous and Al-containing MCM-41 and SBA-15 mesoporous materials.[365] The ^{129}Xe-NMR was employed in the characterization of the activation of two Fe silicalites, with different Fe loadings.[366] Zeolites NaY and mordenite were dealuminated by $SiCl_4$ and steaming methods and carefully characterized during and after the various synthetic stages by ^{27}Al and ^{29}Si MAS NMR and XRD to ensure sample quality. The ^{129}Xe NMR spectra for xenon adsorbed in NaX, siliceous Y, mordenite and dealuminated mordenite were obtained for very low xenon loadings and as a function of temperature.[176] The ^{129}Xe NMR method was used for evaluation of the sizes of free volume elements in amorphous glassy materials – random copolymers of tetrafluoroethylene and perfluorodioxoles of different structures.[367] The authors report, for the first time, a reasonably good calculation of Xe shielding in a fullerene.[368] Relativistic contributions to the chemical shift of ^{129}Xe in Xe at C60 were computed by means of a two-component relativistic density functional approach.[369] The measurement of the ^{129}Xe NMR chemical shift as a function of density is reported. The application used in this study enabled the authors to measure the ^{129}Xe NMR chemical shift in the supercritical state up to a pressure of $\sim$70 MPa.[370] The NMR properties (chemical shift and spin-spin coupling constants) of ^{129}Xe in covalent compounds and weakly bound complexes were investigated by DFT methods including relativistic effects.[371] The ^{129}Xe NMR spectroscopy was performed on xenon adsorbents on a iridium single crystal surface.[372]

References

1. C. S. Wannere, P. R. Schleyer, *Organic Letters*, 2003, **5**, 605-608.
2. N. H. Martin, N. W. Allen, J. D. Brown, D. M. Kmiec, L. Vo, *Journal of Molecular Graphics & Modelling*, 2003, **22**, 127-131.
3. R. J. Abraham, M. Mobli, R. J. Smith, *Magnetic Resonance in Chemistry*, 2003, **41**, 26-36.
4. L. Phillips, F. Separovic, M. J. Aroney, *New Journal of Chemistry*, 2003, **27**, 381-386.
5. E. Bednarek, J. Cz. Dobrowolski, K. Kamienska-Trela, *Journal of Molecular Structure*, 2003, **651-653**, 719-727.
6. R. Gobetto, C. Nervi, B. Romanin, L. Salassa, M. Milanesio, G. Croce, *Organometallics*, 2003, **22**, 4012-4019.

7. S. Malik, S. Moeller, G. Toth, T. Gati, M. I. Choudhary, H. Duddeck, *Magnetic Resonance in Chemical istry*, 2003, **41**, 455-465.
8. J. Juselius, M. Patzschke, D. Sundholm, *THEOCHEMICAL*, 2003, **633**, 123-136.
9. P. Astolfi, P. Bruni, L. Greci, P. Stipa, L. Righi, C. Rizzoli, *European Journal of Organic Chemistry*, 2003, (14), 2626-2634.
10. G. Li, M. P. Dobhal, A. Graham, M. Shibata, G. Zheng, A. Kozyrev, R. K. Pandey, *Journal of Organic Chemistry*, 2003, **68**, 3762-3772.
11. C.-T. Lin, K.-Z. Chen, T.-C. Chou, *Tetrahedron*, 2003, **59**, 1493-1500.
12. K. Choi, A. D. Hamilton, *Journal of the American Chemical Society*, 2003, **125**, 10241-10249.
13. P.-O. Astrand, K. Ruud, *Physical Chemistry Chemical Physics*, 2003, **5**, 5015-5020.
14. C. R. Morcombe, K. W. Zilm, *Journal of Magnetic Resonance*, 2003, **162**, 479-486.
15. D. Deng, H. Li, J. Yao, S. Han, *Chemical Physics Letters*, 2003, **376**, 125-129.
16. D. Sebastiani, G. Goward, I. Schnell, H. W. Spiess, *THEOCHEMICAL*, 2003, **625**, 283-288.
17. B. M. Damon, A. C. Hsu, H. J. Stark, M. J. Dawson, *Magnetic Resonance in Medicine*, 2003, **49**, 233-240.
18. H. Iwamoto, Y. Kondo, T. Kawatani, T. Haino, Y. Fukazawa, *Tetrahedron Letters*, 2003, **44**, 5975-5978.
19. I. Garcia Cuesta, R. Soriano Jartin, A. Sanchez de Meras, P. Lazzeretti, *Journal of Chemical Physics*, 2003, **119**, 5518-5526.
20. Y. Ting, Y-H. Lai, *Journal of the American Chemical Society*, 2004, **126**, 909-914.
21. K. Malek, M. Vala, H. Kozlowski, L. M. Proniewicz, *Magnetic Resonance in Chemistry*, 2004, **42**, 23-29.
22. N. S. Golubev, S. M. Melikova, D. N. Shchepkin, I. G. Shenderovich, P. M. Tolstoy, G. S. Denisov, *Zeitschrift für Physikalische Chemie*, 2003, **217**, 1549-1563.
23. J. R. Burgeson, M. K. Renner, I. Hardt, G. M. Ferrence, J. M. Standard, S. R. Hitchcock, *Journal of Organic Chemistry*, 2004, **69**, 727-734.
24. J. Spevacek, J. Brus, *Macromolecular Symposia*, 2003, **203**, 111-121.
25. K. M. Sureshan, T. Miyasou, M. Hayashi, Y. Watanabe, *Tetrahedron:Asymmetry*, 2004, **15**, 3-7.
26. J. Toušek, J. Dostál, R. Marek, *Journal of Molecular Structure*, 2004, **689**, 115-120.
27. M. Trabelsi, M. Salem, B. Champagne, *Organic & Biomolecular Chemistry*, 2003, **1**, 3839-3844.
28. I. Katsuyama, A. A. Khalil, C. Dunbar, J. K. Zjawiony, *Spectroscopy Letters*, 2003, **36**, 477-485.
29. S. Neal, A. M. Nip, H. Zhang, D. S. Wishart, *Journal of Biomolecular NMR*, 2003, **26**, 215-240.
30. Y. Binev, J. Aires-de-Sousa, *Journal of Chemical Information and Computer Sciences*, 2004, **44**, 940-945.
31. Y. Binev, M. Corvo, J. Aires-de-Sousa, *Journal of Chemical Information and Computer Sciences*, 2004, **44**, 946-949.
32. J. Meiler, *Journal of Biomolecular NMR*, 2003, **26**, 25-37.
33. S. Bekiroglu, A. Sandstroem, L. Kenne, C. Sandstrøm, *Organic & Biomolecular Chemistry*, 2004, **2**, 200-205.
34. E. Kleinpeter, S. Klod, *Journal of the American Chemical Society*, 2004, **126**, 2231-2236.
35. A. Hauch, H. Bildsøe, H. J. Jakobsen, J. Skibsted, *Journal of Magnetic Resonance*, 2003, **165**, 282-292.
36. S. Antonijevic, S. Wimperis, *Journal of Magnetic Resonance*, 2003, **164**, 343-350.

37. D. Carlier, M. Menetrier, C. P. Grey, C. Delmas, G. Ceder, *Physical Review B: Condensed Matter and Materials Physics*, 2003, **67**, 174103/1-174103/14.
38. Z. Wu, H. Eckert, J. Senker, D. Johrendt, G. Kotzyba, B. D. Mosel, H. Trill, R.-D. Hoffmann, R. Poettgen, *Journal of Physical Chemistry B*, 2003, **107**, 1943-1948.
39. D. M. Pickup, D. Simon, M. Fooken, H. Krampitz, E. R. H. Van Eck, E. M. Kelder, *Journal of Materials Chemistry*, 2003, **13**, 963-968.
40. S. E. Hayes, R. A. Guidotti, W. R. Jr. Even, P. J. Hughes, H. Eckert, *Journal of Physical Chemistry A*, 2003, **107**, 3866-3876.
41. M. Letellier, F. Chevallier, C. Clinard, E. Frackowiak, J.-N. Rouzaud, F. Beguin, M. Morcrette, J.-M. Tarascon, *Journal of Chemical Physics*, 2003, **118**, 6038-6045.
42. M. Letellier, F. Chevallier, F. Beguin, E. Frackowiak, J.-N. Rouzaud, Journal of Physics and Chemistry of Solids, 2004, **65**, 245-251.
43. M. Hanaya, K. Goto, K. Echigo, K. Watanabe, *Journal of Physics: Condensed Matter*, 2004, **16**, 715-719.
44. Z. Wu, R.-D. Hoffmann, D. Johrendt, B. D. Mosel, H. Eckert, R. Poettgen, *Journal of Materials Chemistry*, 2003, **13**, 2561-2565.
45. M. J. Willans, R. W. Schurko, *Journal of Physical Chemistry B*, 2003, **107**, 5144-5161.
46. R. Siegel, J. Hirschinger, D. Carlier, M. Menetrier, C. Delmas, *Solid State Nuclear Magnetic Resonance*, 2003, **23**, 243-262.
47. S. K. Lee, J. F. Stebbins, *Geochimica et Cosmochimica Acta*, 2003, **67**, 1699-1709.
48. J. Xiang, X. Yang, C. Chen, Y. Tang, W. Yan, G. Xu, *Journal of Colloid and Interface Science*, 2003, **258**, 198-205.
49. F. Avecilla, J. A. Peters, C. F. G. C. Geraldes, *European Journal of Inorganic Chemistry*, 2003, **(23)**, 4179-4186.
50. G. Wu, A. Wong, Z. Gan, J. T. Davis, *Journal of the American Chemical Society*, 2003, **125**, 7182-7183.
51. A. Goldbach, F. Fayon, T. Vosegaard, M. Wachhold, M. G. Kanatzidis, D. Massiot, M.-L. Saboungi, *Inorganic Chemistry*, 2003, **42**, 6996-7000.
52. H.-T. Kwak, S. Prasad, T. Clark, P. J. Grandinetti, *Journal of Magnetic Resonance*, 2003, **160**, 107-113.
53. M. Igarashi, T. Kodaira, T. Ikeda, M. Itoh, T. Shimizu, A. Goto, Y. Nozue, *Physica B: Condensed Matter*, 2003, **327**, 72-78.
54. S. Krämer, M. Mehring, A.-V. Mudring, M. Jansen, *Journal of Physical Chemistry B*, 2003, **107**, 4922-4926.
55. A. R. Lim, H. W. Shin, *Journal of the Physical Society of Japan*, 2003, **72**, 718-722.
56. A. R. Lim, O. H. Han, S.-Y. Jeong, *Journal of Physics and Chemistry of Solids*, 2003, **64**, 933-937.
57. V. Gerginov, A. Derevianko, C. E. Tanner, *Physical Review Letters*, 2003, **91**, 072501/1-072501/4.
58. M. L. Kuhlman, T. B. Rauchfuss, *Journal of the American Chemical Society*, 2003, **125**, 10084-10092.
59. L. O. Jakobsen, N. C. Nielsen, M. Esmann, *Annals of the New York Academy of Sciences*, 2003, **986**, 290-292.
60. T. R. Eykyn, D. J. Philp, P. W. Kuchel, *Chemical Physics Letters*, 2003, **376**, 732-736.
61. D. A. Saulys, D. R. Powell, *Organometallics*, 2003, **22**, 407-413.
62. M. A. M. Khouna, M. T. Ben Dhia, M. R. Khaddar, *Phosphorus, Sulfur and Silicon and the Related Elements*, 2003, **178**, 2309-2317.
63. B. Zhou, B. L. Sherriff, *American Mineralogist*, 2004, **89**, 377-381.

64. G. Wu, A. Wong, S. Wang, *Canadian Journal of Chemistry*, 2003, **81**, 275-283.
65. I. Hung, R. W. Schurko, *Solid State Nuclear Magnetic Resonance*, 2003, **24**, 78-93.
66. K. Ishida, Y. Minami, Y. Kitaoka, S. Nakatsuji, N. Kikugawa, Y. Maeno, *Physical Review B: Condensed Matter and Materials Physics*, 2003, **67**, 214412/1-214412/6.
67. K. Ishida, Y. Minami, Y. Kitaoka, S. Nakatsuji, Y. Maeno, *Journal of Low Temperature Physics*, 2003, **131**, 1227-1236.
68. P. K. Madhu, O. G. Johannessen, K. J. Pike, R. Dupree, M. E. Smith, M. H. Levitt, *Journal of Magnetic Resonance*, 2003, **163**, 310-317.
69. M. D. Brown, W. Levason, D. C. Murray, M. C. Popham, G. Reid, M. Webster, *Dalton Transactions*, 2003, (**5**), 857-865.
70. M. Oku, T. Shishido, T. Shinohara, Q. Sun, Y. Kawazoe, K. Nakajima, K. Wagatsuma, *Journal of Solid State Chemistry*, 2004, **177**, 457-460.
71. P. Carretta, A. Lascialfari, A. Rigamonti, P. Tedesco, F. Tedoldi, *International Journal of Modern Physics B: Condensed Matter Physics, Statistical Physics, Applied Physics*, 2003, **17**, 791-798.
72. G. I. Drandova, T. C. Messina, J.-H. Choi, J. F. Hernandez, J. T. Markert, *Journal of Low Temperature Physics*, 2003, **131**, 305-309.
73. J. Das, A. V. Mahajan, J. Bobroff, H. Alloul, F. Alet, E. S. Sorensen, *Physical Review B: Condensed Matter and Materials Physics*, 2004, **69**, 144404/1-144404/13.
74. K. N. Mikhalev, S. A. Lekomtsev, A. P. Gerashchenko, A. Y. Yakubovskii, A. R. Kaul', JETP Letters (Translation of Pisma v Zhurnal Eksperimental'noi i Teoreticheskoi Fiziki), 2003, **77**, 401-404.
75. V. P. Pashchenko, A. A. Shemyakov, M. M. Savosta, S. I. Khartsev, V. N. Derkachenko, V. K. Prokopenko, V. A. Turchenko, A. V. Pashchenko, V. P. Dyakonov, Y. Buhanzev, H. Szymczak, *Low Temperature Physics* (Translation of Fizika Nizkikh Temperatur), 2003, **29**, 910-916.
76. J. Bartolomé, M. D. Kuz'min, C. Kapusta, P. C. Riedi, M. Ellouze, P. l'Héritier, *Solid State Communications*, 2004, **129**, 331-334.
77. M. M. Savosta, V. D. Doroshev, V. I. Kamenev, V. A. Borodin, T. N. Tarasenko, A. S. Mazur, M. Marysko, *Journal of Experimental and Theoretical Physics*, (Translation of Zhurnal Eksperimental'noi i Teoreticheskoi Fiziki), 2003, **97**, 573-586.
78. A. G. Avent, P. B. Hitchcock, A. V. Khvostov, M. F. Lappert, A. V. Protchenko, *Dalton Transactions*, 2003, (**6**), 1070-1075.
79. B. Zalar, V. V. Laguta, R. Blinc, *Physical Review Letters*, 2003, **90**, 037601/1-037601/4.
80. S. Ganapathy, K. U. Gore, R. Kumar, J.-P. Amoureux, *Solid State Nuclear Magnetic Resonance*, 2003, **24**, 184-195.
81. T. Kiyama, S. Fujisawa, H. Saitoh, M. Itoh, K. Kodama, M. Takigawa, *Physica B: Condensed Matter*, 2003, **329-333**, 733-735.
82. P. A. Thomas, A. Baldwin, R. Dupree, P. Blaha, K. Schwarz, A. Samoson, Z. H. Gan, *Journal of Physical Chemistry B*, 2004, **108**, 4324-4331.
83. N. Dajda, J. M. Dixon, M. E. Smith, N. Carthey, P. T. Bishop, *Physical Review B: Condensed Matter and Materials Physics*, 2003, **67**, 024201/1-024201/9.
84. U. G. Nielsen, H. J. Jakobsen, J. Skibsted, *Solid State Nuclear Magnetic Resonance*, 2003, **23**, 107-115.
85. B. A. Gee, A. Wong, *Journal of Physical Chemistry B*, 2003, **107**, 8382-8387.
86. W. Huang, L. Todaro, L. C. Francesconi, T. Polenova, *Journal of the American Chemical Society*, 2003, **125**, 5928-5938.
87. N. Pooransingh, E. Pomerantseva, M. Ebel, S. Jantzen, D. Rehder, T. Polenova, *Inorganic Chemistry*, 2003, **42**, 1256-1266.

88. M. Buehl, R. Schurhammer, P. Imhof, *Journal of the American Chemical Society*, 2004, **126**, 3310-3320.
89. U. G. Nielsen, N.-Y. Topsoe, M. Brorson, J. Skibsted, H. J. Jakobsen, *Journal of the American Chemical Society*, 2004, **126**, 4926-4933.
90. C. A. Tischer, M. B. M. Oliveira, F. Reicher, M. Iacomini, C. L. O. Petkowicz, M. E. R. Duarte, M. D. Noseda, P. A. J. Gorin, *Carbohydrate Research*, 2004, **339**, 771-775.
91. J. Wang, C. J. Curtis, D. L. Schulz, J.-G. Zhang, *Journal of the Electrochemical Society*, 2004, **151**, A1-A7.
92. V. V. Laguta, M. D. Glinchuk, S. N. Nokhrin, I. P. Bykov, R. Blinc, A. Gregorovic, B. Zalar, *Physical Review B: Condensed Matter and Materials Physics*, 2003, **67**, 104106/1-104106/8.
93. H.-T. Kwak, S. Prasad, T. Clark, P. J. Grandinetti, *Solid State Nuclear Magnetic Resonance*, 2003, **24**, 71-77.
94. E. Schellkes, X. Hong, M. Holz, U. Huniar, R. Ahlrichs, W. Freyland, *Physical Chemistry Chemical Physics*, 2003, **5**, 5536-5543.
95. B. R. Cherry, M. Nyman, T. M. Alam, *Ceramic Transactions*, 2003, **143**(Environmental Issues and Waste Management Technologies in the Ceramic and Nuclear Industries VIII), 377-384.
96. M. Filatov, D. Cremer, *Journal of Chemical Physics*, 2003, **119**, 701-712.
97. M. N. Ackermann, K. B. Moore, A. S. Colligan, J. A. Thomas-Wohlever, K. J. Warren, *Journal of Organometallic Chemistry*, 2003, **667**, 81-89.
98. L. Le Polles, R. Gautier, J. C. Ameline, M. Le Floch, O. Pena, *Solid State Communications*, 2003, **125**, 597-600.
99. C. Bustos, B. Hasenknopf, R. Thouvenot, J. Vaissermann, A. Proust, P. Gouzerh, *European Journal of Inorganic Chemistry*, 2003, (**15**), 2757-2766.
100. M. Inoue, T. Yamase, L. P. Kazansky, *Polyhedron*, 2003, **22**, 1183-1189.
101. A. Bagno, M. Bonchio, A. Sartorel, G. Scorrano, *Chem. Phys. Chem.*, 2003, **4**, 517-519.
102. B. J. Smith, V. A. Patrick, *Australian Journal of Chemistry*, 2003, **56**, 283-286.
103. Y. Furukawa, K. Watanabe, K. Kumagai, F. Borsa, T. Sasaki, N. Kobayashi, D. Gatteschi, *Physical Review B: Condensed Matter and Materials Physics*, 2003, **67**, 064426/1-064426/7.
104. K. Shimizu, M. Velazquez, J.-P. Renard, A. Revcolevschi, *Journal of the Physical Society of Japan*, 2003, **72**, 793-796.
105. M. M. Savosta, P. Novak, Z. Jirak, *Physical Review B: Condensed Matter and Materials Physics*, 2003, **67**, 100411/1-100411/4.
106. M. M. Savosta, V. N. Krivoruchko, I. A. Danilenko, V. Y. Tarenkov, T. E. Konstantinova, A. V. Borodin, V. N. Varyukhin, *Physical Review B: Condensed Matter and Materials Physics*, 2004, **69**, 024413/1-024413/8.
107. N. I. Gorshkov, A. E. Miroslavov, A. A. Lumpov, D. N. Suglobov, V. A. Mikhalev, *Radiochemistry* (Moscow, Russian Federation) (Translation of Radiokhimiya), 2003, **45**, 127-130.
108. N. I. Gorshkov, A. A. Lumpov, A. E. Miroslavov, V. A. Mikhalev, D. N. Suglobov, *Czechoslovak Journal of Physics*, 2003, **53**, A745-A749.
109. O. Horner, J.-M. Mouesca, J.-L. Oddou, C. Jeandey, V. Niviere, T. A. Mattioli, C. Mathe, M. Fontecave, P. Maldivi, P. Bonville, J. A. Halfen, J.-M. Latour, *Biochemistry*, 2004, **43**, 8815-8825.
110. M. Lein, J. Frunzke, G. Frenking, *Angewandte Chemie, International Edition*, 2003, **42**, 1303-1306.

111. T. Ueda, G. M. Bernard, R. McDonald, R. E. Wasylishen, *Solid State Nuclear Magnetic Resonance*, 2003, **24**, 163-183.
112. S. Wi, S. E. Ashbrook, S. Wimperis, L. Frydman, *Journal of Chemical Physics*, 2003, **118**, 3131-3140.
113. H. Noss, W. Baumann, R. Kempe, T. Irrgang, A. Schulz, *Inorganica Chimica Acta*, 2003, **345**, 130-136.
114. F. D. Rochon, V. Buculei, *Inorganica Chimica Acta*, 2004, **357**, 2218-2230.
115. G. J. Grant, K. N. Patel, M. L. Helm, L. F. Mehne, D. W. Klinger, D. G. VanDerveer, *Polyhedron*, 2004, **23**, 1361-1369.
116. G. J. Grant, A. M. Goforth, D. G. VanDerveer, W. T. Pennington, *Inorganica Chimica Acta*, 2004, **357**, 2107-2114.
117. G. J. Grant, J. A. Pool, D. G. VanDerveer, *Dalton Transactions*, 2003, **20**, 3981-3984.
118. K. J. Naidoo, A. S. Lopis, A. N. Westra, D. J. Robinson, K. R. Koch, *Journal of the American Chemical Society*, 2003, **125**, 13330-13331.
119. M. Watabe, M. Kai, K. Goto, H. Ohmuro, S. Furukawa, N. Chikaraishi, T. Takayama, Y. Koike, *Journal of Inorganic Biochemistry*, 2003, **97**, 240-248.
120. M. E. Oehlsen, Y. Qu, N. Farrell, *Inorganic Chemistry*, 2003, **42**, 5498-5506.
121. F. D. Rochon, P.-C. Kong, *Canadian Journal of Analytical Sciences and Spectroscopy*, 2003, **48**, 30-37.
122. C. S. McInnes, B. R. Clare, W. R. Redmond, C. R. Clark, A. G. Blackman, *Dalton Transactions*, 2003, **11**, 2215-2218.
123. M. S. Robillard, J. S. Leith, G. A. van der Marel, J. H. van Boom, J. Reedijk, *European Journal of Inorganic Chemistry*, 2003, **8**, 1529-1532.
124. F. D. Rochon, G. Masserweh, N. Nedelec, *Inorganica Chimica Acta*, 2003, **346**, 197-206.
125. J. Autschbach B. Le Guennic, *Chemistry (Weinheim an der Bergstrasse, Germany)*, 2004, **10**, 2581-2589.
126. M. Q. Slagt, G. Rodriguez, M. M. P. Grutters, G. R. J. M. Klein, W. Klopper, L. W. Jenneskens, M. Lutz, A. L. Spek , G. van Koten , *Chemistry (Weinheim an der Bergstrasse, Germany)*, 2004, **10**, 1331-1344.
127. D. S. Gill, T. I. Quickenden, L. Byrne, V. Pathania, B. K. Vermani, *Journal of Molecular Liquids*, 2004, **111**, 85-93.
128. G. Brunklaus, J. C. C. Chan, H. Eckert, S. Reiser, T. Nilges, A. Pfitzner, *Physical Chemistry Chemical Physics*, 2003, **5**, 3768-3776.
129. S. Renold, T. Heine, J. Weber, P. F. Meier, *Physical Review B: Condensed Matter and Materials Physics*, 2003, **67**, 024501/1-024501/8.
130. S. Ahmad, A. A. Isab, A. P. Arnold, *Journal of Coordination Chemistry*, 2003, **56**, 539-544.
131. T. Ramnial, C. D. Abernethy, M. D. Spicer, I. D. McKenzie, I. D. Gay , J. A. C. Clyburne, *Inorganic chemistry*, 2003, **42**, 1391-1393.
132. E. V. Bakhmutova-Albert, N. Bestaoui, V. I. Bakhmutov, A. Clearfield, A. V. Rodriguez, R. Llavona, *Inorganic Chemistry*, 2004, **43**, 1264-1272.
133. R. March, J. Pons, J. Ros, W. Clegg, A. Alvarez-Larena, J. F. Piniella, J. Sanz, *Inorganic Chemistry*, 2003, **42**, 7403-7409.
134. K. S. Anjali, J. J. Vittal, P. A. W. Dean, *Inorganica Chimica Acta*, 2003, **351**, 79-88.
135. A. V. Ivanov, O. N. Antzutkin, W. Forsling, N. A. Rodionova, *Russian Journal of Coordination Chemistry (Translation of Koordinatsionnaya Khimiya)*, 2003, **29**, 301-306.
136. S. S. Kidambi, D.-K. Lee, A. Ramamoorthy, *Inorganic Chemistry*, 2003, **42**, 3142-

3151.
137. S. S. Kidambi, A. Ramamoorthy, *Inorganic Chemistry*, 2003, **42**, 2200-2202.
138. J. Schmedt auf der Guenne, H. Eckert, A. Leaustic, F. Babonneau, *Physical Chemistry Chemical Physics*, 2003, **5**, 1306-1313.
139. S. S. Kidambi, A. Ramamoorthy, *Inorganic chemistry*, 2003, **42**, 2200-2202.
140. J. S. Jaworski, A. Lewicka, R. Anulewicz, *Journal of Inclusion Phenomena and Macrocyclic Chemistry*, 2003, **46**, 207-211.
141. S. Molchanov, A. Gryff-Keller, *Magnetic Resonance in Chemistry*, 2003, **41**, 788-793.
142. 5 M. L. Helm, D. G. VanDerveer, G. J. Grant, *Journal of Chemical Crystallography*, 2003, **33**, 625-630.
143. D. C. Bebout, M. M. Garland, G. S. Murphy, E. V. Bowers, C. J. Abelt, R. J. Butcher, *Dalton Transactions*, 2003, **12**, 2578-2584.
144. J. B. King, F. P. Gabbaie, *Organometallics*, 2003, **22**, 1275-1280.
145. R. Fukuda, M. Hada, H. Nakatsuji, *Journal of Chemical Physics*, 2003, **118**, 1027-1035.
146. B. Wrackmeyer, O. L. Tok, Y. N. Bubnov, *Applied Organometallic Chemistry*, 2004, **18**, 43-50.
147. B. Wrackmeyer, W. Milius, O. L. Tok, *Chemistry–A European Journal*, 2003, **9**, 4732-4738.
148. C. O. Choo, Y. Kim, *Mineralogical Magazine*, 2003, **67**, 799-806.
149. L.-S. Du, J. F. Stebbins, *Chemistry of Materials*, 2003, **15**, 3913-3921.
150. Y. Sahin, A. Ziegler, T. Happel, H. Meyer, M. J. Bayer, H. Pritzkow, W. Massa, M. Hofmann, P. v. R. chleyer, W. Siebert, A. Berndt, *Journal of Organometallic Chemistry*, 2003, **680**, 244-256.
151. C. D. Entwistle, T. B. Marder, P. S. Smith, J. A. K. Howard, M. A. Fox, S. A. Mason, *Journal of Organometallic Chemistry*, 2003, **680**, 165-172.
152. W. J. Boyko, R. L. Dudley, G. F. Kemmerer, A. J. Leffler, *Journal of Magnetic Resonance*, 2003, **164**, 65-70.
153. A. Duddridge, D. Holland, S, M. Dixon, C. R. Scales, *Glass Technology*, 2003, **44**, 85-89.
154. M. Vasilescu, G. Borodi, S. Simon, *Journal of Optoelectronics and Advanced Materials*, 2003, **5**, 153-156.
155. B. Wrackmeyer, W. Milius, M. H. Bhatti, S. Ali, *Journal of Organometallic Chemistry*, 2003, **665**, 196-204.
156. R. G. Hill, A. Stamboulis, R. V. Law, J. Hawes, J. Henry, *Physics and Chemistry of Glasses*, 2004, **45**, 121-126.
157. H. Yang, R. I. Walton, S. Antonijevic, S. Wimperis, A. C. Hannon, *Journal of Physical Chemistry B*, 2004, **108**, 8208-8217.
158. A. Abraham, S.-H. Lee, C.-H. Shin, S. B. Hong, R. Prins, J. A. van Bokhoven, *Physical Chemistry Chemical Physics*, 2004, **6**, 3031-3036.
159. S. K. Kulshreshtha, O. D. Jayakumar, V. Sudarsan, *Journal of Physics and Chemistry of Solids*, 2004, **65**, 1141-1146.
160. S. K. Lee, *Journal of Physical Chemistry B*, 2004, **108**, 5889-5900.
161. M. D. Alba, M. A. Castro, M. Naranjo, A. C. Perdigon, *Physics and Chemistry of Minerals*, 2004, **31**, 195-202.
162. S. M. Abo-Naf, N. A. Ghoneim, H. A. El-Batal, *Journal of Materials Science: Materials in Electronics*, 2004, **15**, 273-282.
163. G. Silly, C. Legein, J. Y. Buzare, F. Calvayrac, *Solid State Nuclear Magnetic Resonance*, 2004, **25**, 241-251.

164. A. Stamboulis, R. V. Law, R. G. Hill, *Biomaterials*, 2004, **25**, 3907-3913.
165. F. F. Slejko, R. Petrini, C. Forte, *Neues Jahrbuch fuer Mineralogie, Abhandlungen*, 2003, **179**, 311-324.
166. B. Tagirov, J. Schott, J.-C. Harrichoury, J. Escalier, Geochimica et Cosmochimica Acta, 2004, **68**, 1333-1345.
167. L.-S. Du, J. F. Stebbins, *Journal of Physical Chemistry B*, 2004, **108**, 3681-3685.
168. W. Masierak, T. Emmler, G. Buntkowsky, A. Gutsze, *Zeitschrift fuer Physikalische Chemie (Muenchen, Germany)*, 2003, **217**, 1613-1626.
169. D. Feng, H. Tan, J. S. J. van Deventer, *Journal of Materials Science*, 2004, **39**, 571-580.
170. R. Shen, T. Iwashita, J. F. Ma, *Journal of Experimental Botany*, 2004, **55**, 131-136.
171. A. Stamboulis, R. G. Hill, R. V. Law, *Journal of Non-Crystalline Solids*, 2004, **333**, 101-107.
172. A. K. Jain, A. Gupta, R. Bohra, R. C. Mehrotra, *Main Group Metal Chemistry*, 2003, **26**, 111-118.
173. C. O. Choo, Y. Kim, *Mineralogical Magazine*, 2003, **67**, 799-806.
174. H. Kroyer, H. Lindgreen, H. J. Jakobsen, J. Skibsted, *Advances in Cement Research*, 2003, **15**, 103-112.
175. H. Trill, H. Eckert, V. L. Srdanov, *Journal of Physical Chemistry B*, 2003, **107**, 8779-8788.
176. J. M. Kneller, T. Pietrass, K. C. Ott, A. Labouriau, *Microporous and Mesoporous Materials*, 2003, **62**, 121-131.
177. M. Fechtelkord, H. Behrens, F. Holtz, J. L. Bretherton, C. A. Fyfe, L. A. Groat, M. Raudsepp, Nuclear Magnetic Resonance*American Mineralogist*, 2003, **88**, 1046-1054.
178. S. K. Lee, J. F. Stebbins, C. A. Weiss, Jr. , R. J. Kirkpatrick, *Chemistry of Materials*, 2003, **15**, 2605-2613.
179. L. Delevoye, J.-L. Robert, J. Grandjean, *Clay Minerals*, 2003, **38**, 63-69.
180. H.-M. Kao, Y.-C. Chen, *Journal of Physical Chemistry B*, 2003, **107**, 3367-3375.
181. M. D. Andersen, H. J. Jakobsen, J. Skibsted, *Inorganic Chemistry*, 2003, **42**, 2280-2287.
182. S. Szumacher, I. Madura, J. Zachara, A. R. Kunicki, A. Cebulski, L. Jerzykiewicz, *Journal of Organometallic Chemistry*, 2003, **669**, 64-71.
183. J. H. von Barner, C. Bessada, R. W. Berg, *Inorganic Chemistry*, 2003, **42**, 1901-1907.
184. C. Lustig, N. W. Mitzel, *Organometallics*, 2003, **22**, 242-249.
185. G. Silly, C. Legein J. Y. Buzare, F. Calvayrac F, *Solid state nuclear magnetic resonance*, 2004, **25**, 241-251.
186. R. Shen, T. Iwashita, J. F. Ma, *Journal of experimental botany*, 2004, **55**, 131-136.
187. M. D. Andersen, H. J. Jakobsen, J. Skibsted, *Inorganic chemistry*, 2003, **42**, 2280-2287.
188. G. Silly, M. Body, J.-Y. Buzare, C. Legein, B. Bureau, *Comptes Rendus Chimie*, 2004, **7**, 403-416.
189. J. Autschbach, B. Le Guennic, *Chemistry–A European Journal*, 2004, **10**, 2581-2589.
190. H. Satoh, H. Koshino, J. Uzawa, T. Nakata, *Tetrahedron*, 2003, **59**, 4539-4547.
191. C. Escolano, M. J. Kogan, M. Rubiralta, E. Giralt, A. Diez, *Magnetic Resonance in Chemistry*, 2003, **41**, 219-222.
192. M. S. Meier, H. P. Spielmann, R. G. Bergosh, M. C. Tetreau, *Journal of organic chemistry*, 2003, **68**, 7867-7870.
193. K. Senthilkumar, P. Kolandaivel, *Computational biology and chemistry*, 2003, **27**, 173-183.

194. S. Zeman, *Theoretical and Computational Chemistry*, 2003, **13**, 25-52.
195. J. Yao, Y. Nakazawa, T. Asakura, *Biomacromolecules*, 2004, **5**, 680-688.
196. R. J. Darton, P. Wormald, R. E. Morris, *Journal of Materials Chemistry*, 2004, **14**, 2036-2040.
197. C. C. Pavel, J. B. Nagy, N. Bilba, A. Nastro, C. Perri, D. Vuono, P. De Luca, I. V. Asaftei, *Microporous and Mesoporous Materials*, 2004, **71**, 77-85.
198. N. Sahai, *Geochimica et Cosmochimica Acta*, 2004, **68**, 227-237.
199. H. Sohn, *Journal of Organometallic Chemistry*, 2004, **689**, 134-138.
200. K. H. Wu, Y. C. Chang, G. P. Wang, *Journal of Magnetism and Magnetic Materials*, 2004, **269**, 150-155.
201. R. Tacke, R. Bertermann, M. Penka, O. Seiler, *Zeitschrift für Anorganische und Allgemeine Chemie*, 2003, **629**, 2415-2420.
202. A. Stamboulis, H. Artemis, G. Robert; R. V. Law, *Journal of Non-Crystalline Solids*, 2004, **333**, 101-107.
203. I. Farnan, E. Balan, C. J. Pickard, F. Mauri, *American Mineralogist*, 2003, **88**, 1663-1667.
204. E. Ratai, M. P. Augustine, S. M. Kauzlarich, *Journal of Physical Chemistry B*, 2003, **107**, 12573-12577.
205. T. Mueller, *Journal of Organometallic Chemistry*, 2003, **686**, 251-256.
206. D. Holland, A. P. Howes, R. Dupree, J. A. Johnson, C. E. Johnson, *Journal of Physics: Condensed Matter*,2003, **15**, S2457-S2472.
207. V. V. Zuev, A. V. Kalinin, Russian Journal of General Chemistry (Translation of Zhurnal Obshchei Khimii), 2003, **73**, 546-549.
208. H. Kroyer, H. Lindgreen, H. J. Jakobsen, J. Skibsted, *Advances in Cement Research*, 2003, **15**, 103-112.
209. G. H. Lee, R. West, T. Mueller, *Journal of the American Chemical Society*, 2003, **125**, 8114-8115.
210. L. A. Stearns, J. Gryko, J. Diefenbacher, G. K. Ramachandran, P. F. McMillan, *Journal of Solid State Chemistry*, 2003, **173**, 251-258.
211. S. Krishnamurty, T. Heine, A. Goursot, *Journal of Physical Chemistry B*, 2003, **107**, 5728-5732.
212. B. Z. Zhan, M. A. White, M. Lumsden, *Langmuir*, 2003, **19**, 4205-4210.
213. L. Delevoye, J. L. Robert, J. Grandjean, *Clay Minerals*, 2003, **38**, 63-69.
214. I. Bull, P. Lightfoot, L. A. Villaescusa, L. M. Bull, R. K. B. Gover, J. S. O. Evans, R. E. Morris, *Journal of the American Chemical Society*, 2003, **125**, 4342-4349.
215. S. Packirisamy, G. Ambadas, R. M. Rama K. N. Ninan, *European Polymer Journal*, 2003, **39**, 1077-1080.
216. M. D. Andersen, H. J. Jakobsen, J. Skibsted, *Inorganic Chemistry*, 2003, **42**, 2280-2287.
217. M. R. Hansen, J. H. J. Ryan; J. Skibsted, *Inorganic Chemistry*, 2003, **42**, 2368-2377.
218. T. Mueller, C. Bauch, M. Ostermeier, M. Bolte, N. Auner, *Journal of the American Chemical Society*, 2003, **125**, 2158-2168.
219. S. V. Verkhovskii, A. Yu. Yakubovsky, B. Z. Malkin, S. K. Saikin, M. Cardona, A. Trokiner, V. I. Ozhogin, *Physical Review B: Condensed Matter and Materials Physics*, 2003, **68**, 104201/1-104201/10.
220. M. Nath, S. Pokharia, X. Song, G. Eng, M. Gielen, M. Kemmer, M. Biesemans, R. Willem, D. de Vos, *Applied Organometallic Chemistry*, 2003, **17**, 305-314.
221. B. W. Eichhorn, B. Kesanli, J. Fettinger, *Abstracts of Papers, 225th ACS National Meeting, New Orleans*, LA, United States, March 23-27, 2003, INOR-482.
222. R. Fukuda, M. Hada, H. Nakatsuji, *Recent Advances in Computational Chemistry*,

2004, **5**(Recent Advances in Relativistic Molecular Theory), 191-220.
223. Z. Wu, B. D. Mosel, H. Eckert, R-D. Hoffmann, R. Poettgen, *Chemistry–A European Journal*, 2004, **10**, 1558-1564.
224. J. M. Geller, I. S. Butler, D. F. R. Gilson, F. G. Morin, I. Wharf, F. Belanger-Gariepy, *Canadian Journal of Chemistry*, 2003, **81**, 1187-1195.
225. B. E. Eichler, A. D. Phillips, P. P. Power, *Organometallics*, 2003, **22**,5423-5426.
226. L. Diop, B. Mahieu, M. F. Mahon, K. C. Molloy, K. Y. A. Okio, *Applied Organometallic Chemistry*, 2003, **17**, 881-882.
227. M. Cruz, J. Morales, J. P. Espinos, J. Sanz, *Journal of Solid State Chemistry*, 2003, **175**, 359-365.
228. D. Holland, M. E. Smith, A. P. Howes, T. Davies, L. Barrett, *Physics and Chemistry of Glasses*, 2003, **44**, 59-63.
229. T. Lebl, A. Smicka, J. Brus, C. Bruhn, *European Journal of Inorganic Chemistry*, 2003, (**1**), 143-148.
230. A. Bansal, N. Fahmi, R. V. Singh, *Main Group Metal Chemistry*, 2003, **26**, 335-347.
231. P. Thangadurai, S. Ramasamy, P. T. Manoharan, *European Physical Journal B: Condensed Matter Physics*,2004, **37**, 425-432.
232. D. Zayachuk, Ye. Polyhach, E. Slynko, O. Khandozhko, C. Rudowicz, *Spectrochimica Acta, Part A: Molecular and Biomolecular Spectroscopy*, 2004, **60A**, 1247-1256.
233. D. H. Zhou, G. L. Hoatson, R. L. Vold, F. Fayon, *Physical Review B: Condensed Matter and Materials Physics*, 2004, **69**, 134104/1-134104/10.
234. T. L. Whitehead, M. E. Watson, Spectroscopy Letters, 2004, **37**, 105-114.
235. L. P. Cruz, J. M. Savariault, C. M. Morais, C. Fernandez, J. D. Pedrosa de Jesus, J. Rocha, *Journal of Solid State Chemistry*, 2004, **177**, 1549-1558.
236. V. V. Laguta, M. D. Glinchuk, I. P. Bykov, R. Blinc, B. Zalar, *Physical Review B: Condensed Matter and Materials Physics*, 2004, **69**, 054103/1-054103/9.
237. R. Siegel, T. T. Nakashima, R. E. Wasylishen, *Journal of Physical Chemistry B*, 2004, **108**, 2218-2226.
238. A. Morsali, A. R. Mahjoub, *Chemistry Letters*, 2004, **33**, 64-65.
239. R. Blinc, V. V. Laguta, R. Pirc, B. Zalar, *Solid State Nuclear Magnetic Resonance*, 2004, **25**, 185-187.
240. R. Blinc, V. Laguta, B. Zalar, *Physical Review Letters*, 2003, **91**, 247601/1-247601/4.
241. B. H. Hamilton, K. A. Kelly, T. A. Wagler, M. P. Espe, C. J. Ziegler, *Inorganic Chemistry*, 2004, **43**, 50-56.
242. T. Muller, C. Bauch, M. Bolte, N. Auner, *Chemistry–A European Journal*, 2003, **9**, 1746-1749.
243. L. A. Margolis, C. D. Jr. Schaeffer, C. H. Yoder, Applied Organometallic Chemistry, 2003, **17**, 236-238.
244. D. Kotsyubynskyy, S. Molchanov, A. Gryff-Keller, *Polish Journal of Chemistry*, 2004, **78**, 239-248.
245. T. Giavani, K. Johannsen, C. J. H. Jacobsen, N. Blom, H. Bildsoe, J. Skibsted, H. J. Jakobsen, *Solid State Nuclear Magnetic Resonance*, 2003, **24**, 218-235.
246. S. A. Pathan, A. W. K. Khanzada, *Journal of the Chemical Society of Pakistan*, 2003, **25**, 21-25.
247. P. Cmoch, *Magnetic Resonance in Chemistry*, 2003, **41**, 693-698.
248. M. Strohmeier, D. Stueber, D. M. Grant, *Journal of Physical Chemistry A*, 2003, **107**, 7629-7642.
249. T. Giavani, H. Bildsoe, J. Skibsted, H. J. Jakobsen, *Chemical Physics Letters*, 2003, **377**, 426-432.

250. P. Kofod, *Magnetic Resonance in Chemistry*, 2003, **41**, 531-534.
251. J. Jazwinski, B. Kamienski, O. Staszewska-Krajewska, G. A. Webb, *Journal of Molecular Structure*, 2003, **64**, 1-9.
252. T. I. Igumenova, A. E. McDermott, K. W. Zilm, R. W. Martin, E. K. Paulson, A. J. Wand, *Journal of the American Chemical Society*, 2004, **126**, 6720-6727.
253. S. Sharpe, N. Kessler, J. A. Anglister, W. M. Yau, R. Tycko, *Journal of the American Chemical Society*, 2004, **126**, 4979-4990.
254. B. Kolodziej, P. M. Dominiak, A. Koscielecka, W. Schilf, E. Grech, K. Wozniak, *Journal of Molecular Structure*, 2004, **691**, 133-139.
255. J. Tousek, J. Dostal, R. Marek, *Journal of Molecular Structure*, 2004, **689**, 115-120.
256. M. J. Alia; I. de Boer, P. Gast, H. J. van Gorkom, H. J. M. de Groot, *Journal of Biomolecular NMR*, 2004, **28**, 157-164.
257. M. Strohmeier, D. M. Grant, *Journal of the American Chemical Society*, 2004, **126**, 966-977.
258. M. A. S. Hass, M. H. Thuesen, H. E. Christensen, J. J. Led, *Journal of the American Chemical Society*, 2004, **126**, 753-765.
259. T. L. C. Martins, T. C. Ramalho, J. D. Figueroa-villar, A. F. C. Flores, C. M. P. Pereira, *Magnetic Resonance in Chemistry*, 2003, **41**, 983-988.
260. E. K. Paulson, C. R. Morcombe, V. Gaponenko, B. Dancheck, R. A. Byrd, K. W. Zilm, *Journal of the American Chemical Society*, 2003, **125**, 15831-15836.
261. C. R. R. Grace, R. Riek, *Journal of the American Chemical Society*, 2003, **125**, 16104-16113.
262. J. Jazwinski, H. Duddeck, *Magnetic Resonance in Chemistry*, 2003, **41**, 921-926.
263. J. B. Hall, D. Fushman, *Magnetic Resonance in Chemistry*, 2003, **41** 837-842.
264. K. E. Koever, G. Batta, V. J. Hruby, *Magnetic Resonance in Chemistry*, 2003, **41**, 828-836.
265. M. Rajabzadeh, J. Kao, C. Frieden, *Biochemistry*, 2003, **42**, 12192-12199.
266. S. Ravindranathan, C. H. Kim, G. Bodenhausen, *Journal of Biomolecular NMR*, 2003, **27**, 365-375.
267. A. Boeckmann, A. Lange, A. Galinier, S. Luca, N. Giraud, M. Juy, H. Heise, *Journal of Biomolecular NMR*, 2003, **27**, 323-339.
268. Y. Wei, D. Fela, S. Kim, M. Hecht, J. Baum, *Journal of Biomolecular NMR*, 2003, **27**, 395-396.
269. K. Laihia, E. Kolehmainen, E. Virtanen, M. Nissinen, A. Puszko, Z. Talik, *Magnetic Resonance in Chemistry*, 2003, **41**, 721-725.
270. L. D. Field, N. Hazari, H. L. Li, I. J. Luck, *Magnetic Resonance in Chemistry*, 2003, **41**, 709-713.
271. B. Nowak-Wydra, B. Gierczyk, G. Schroeder, *Magnetic Resonance in Chemistry*, 2003, **41**, 689-692.
272. A. Zieba, A. Maslankiewicz, V. Milata, J. Sitkowski, *Magnetic Resonance in Chemistry*, 2003, **41**, 639-640.
273. A. Simon, G. Toth, C. P. Librera, W. Adam, *Magnetic Resonance in Chemistry*, 2003, **41**, 541-544.
274. C. Groeger, A. Moeglich, M. Pons, B. Koch, W. Hengstenberg, H. R. Kalbitzer, E. Brunner, *Journal of the American Chemical Society*, 2003, **125**, 8726-8727.
275. P. Barre, O. Zschoernig, K. Arnold, D. Huster, *Biochemistry*, 2003, **42**, 8377-8386.
276. S. K. Straus, W. R. Scott, A. Watts, *Journal of Biomolecular NMR*, 2003, **26**, 283-295.
277. E. Bednarek, J. C. Dobrowolski, K. Kamienska-Trela, *Journal of Molecular Structure*, 2003, **651-653**, 719-727.

278. S. Neal, A. M. Nip, H. Zhang, D. S. Wishart, *Journal of Biomolecular NMR*, 2003, **26**, 215-240.
279. H. E. Birkett, J. C. Cherryman, A. M. Chippendale, J. S. O. Evans, R. K. Harris, M. James, I. J. King, G. J. McPherson, *Magnetic Resonance in Chemistry*, 2003, **41**, 324-336.
280. K. A. Henzler Wildman, D-K. Lee, A. Ramamoorthy, *Biochemistry*, 2003, **42**, 6545-6558.
281. G. Wojciechowski, M. Ratajczak-Sitarz, A. Katrusiak, W. Schilf, P. Przybylski, B. Brzezinski, *Journal of Molecular Structure*, 2003, **650**, 191-199.
282. P. Neudecker, K. Lehmann, P. Roesch, *Journal of Biomolecular NMR*, 2003, **26**, 191-192.
283. Y. Wu, M. Migliorini, P. Yu, D. K. Strickland, Y. X. Wang, *Journal of Biomolecular NMR*, 2003, **26**, 187-188.
284. S. Kishi, A. Santos, O. Ishii, K. Ishikawa, S. Kunieda, H. Kimura, A. Shoji, *Journal of Molecular Structure*, 2003, **649**, 155-167.
285. H. Zhang, S. Neal, D. S. Wishart, *Journal of Biomolecular NMR*, 2003, **25**, 173-195.
286. J. C. Lansing, J. G. Hu, M. Belenky, R. G. Griffin, J. Herzfeld, *Biochemistry*, 2003, **42**, 3586-3593.
287. T. Dziembowska, K. Ambroziak, Z. Rozwadowski, W. Schilf, B. Kamienski, *Magnetic Resonance in Chemistry*, 2003, **41**, 135-138.
288. G. M. Clore, C. D. Schwieters, *Journal of the American Chemical Society*, 2003, **125**, 2902-2912.
289. K. Pervushin, A. Eletsky, *Journal of Biomolecular NMR*, 2003, **25**, 147-152.
290. E. L. Shipp, F. Cantini, I. Bertini, J. S. Valentine, L. Banci, *Biochemistry*, 2003, **42**, 1890-1899.
291. M. F. Mesleh, K. G. Valentine, S. J. Opella, J. M. Louis, A. M. Gronenborn, *Journal of Biomolecular NMR*, 2003, **25**,55-61.
292. B. M. Fung, *Biophysical Journal*, 2003, **85**, 3429-3430.
293. B. Bechinger, C. Sizun, *Concepts in Magnetic Resonance, Part A*, 2003, **18A**, 130-145.
294. Y. Tanaka, Y. Kasai, S. Mochizuki, A. Wakisaka, E. H. Morita, C. Kojima, A. Toyozawa, Y. Kondo, M. Taki, Y. Takagi, A. Inoue, K. Yamasaki, K. Taira Kazunari, *Journal of the American Chemical Society*, 2004, **126**, 744-752.
295. S. Murgia, S. Mele, M. Maura, Lipids, 2003, **38**, 585-591.
296. D. F. Wu, F. Delaglio, N. Tjandra, V. B. Zhurkin, A. Bax, *Journal of biomolecular NMR*, 2003, **26**, 297-315.
297. R. A. Klein, B. Mennucci, J. Tomasi, *Journal of Physical Chemistry A*, 2004, **108**, 5851-5863.
298. M. Cossi, O. Crescenzi, *Theoretical Chemistry Accounts*, 2004, **111**, 162-167.
299. C. Gervais, M. Profeta, V. Lafond, C. Bonhomme, T. Azais, H. Mutin, C. J. Pickard, F. Mauri, F. Babonneau, *Magnetic Resonance in Chemistry*, 2004, **42**, 445-452.
300. V. P. Reddy, E. Sinn, G. A. Olah, G. K. S. Prakash, G. Rasul, *Journal of Physical Chemistry A*, 2004, **108**, 4036-4039.
301. T-M. Lee, T-H. Cheng, M-H. Ou, C. A. Chang, G-C. Liu, Y-M. Wang, *Magnetic Resonance in Chemistry*, 2004, **42**, 329-336.
302. B. Julian, C. Gervais, M-N. Rager, J. Maquet, E. Cordoncillo, P. Escribano, F. Babonneau, C. Sanchez, *Chemistry of Materials*, 2004, **16**, 521-529.
303. G. Cerioni, G. Uccheddu, *Tetrahedron Letters*, 2004, **45**, 505-507.
304. A. Wu, D. Cremer, J. Gauss, *Journal of Physical Chemistry A*, 2003, **107**, 8737-8745.
305. V. Lafond, C. Gervais, J. Maquet, D. Prochnow, F. Babonneau, P. H. Mutin,

Chemistry of Materials, 2003, **15**,4098-4103.
306. K. Yoshida, T. Yamaguchi, T. Adachi, T. Otomo, D. Matsuo, T. Takamuku, N. Nishi, *Journal of Chemical Physics*, 2003, **119**, 6132-6142.
307. J. L. Jios, H. Duddeck, G. P. Romanelli, J. C. Autino, *Magnetic Resonance in Chemistry*, 2003, **4**, 739-740.
308. G. Wu, K. Yamada, *Solid State Nuclear Magnetic Resonance*, 2003, **24**, 196-208.
309. D. L. Bryce, K. Eichele, R. E. Wasylishen, *Inorganic Chemistry*, 2003, **42**, 5085-5096.
310. Q. Zhang, E. Y. Chekmenev, R. J. Wittebort, *Journal of the American Chemical Society*, 2003, **125**, 9140-9146.
311. W. Makulski, K. Jackowski, *Journal of Molecular Structure*, 2003, **651-653**, 265-269.
312. H. G. Bonacorso, S. R. T. Bittencourt, A. P. Sinhorin, N. Zanatta, M. A. P. Martins, *Journal of Fluorine Chemistry*, 2003, **121**, 135-139.
313. B. R. Cherry, T. M. Alam, C. Click, R. K. Brow, Z. Gan, *Journal of Physical Chemistry B*, 2003, **107**, 4894-4903.
314. T. Tsukahara, M. Harada, H. Tomiyasu, Y. Ikeda, *Journal of Supercritical Fluids*, 2003, **26**, 73-82.
315. N. S. Dalal, K. L. Pierce, J. Palomar, R. Fu, *Journal of Physical Chemistry A*, 2003, **107**, 3471-3475.
316. J. Kovacs, G. Toth, A. Simon, A. Levai, A. Koch, E. Kleinpeter, *Magnetic Resonance in Chemistry*, 2003, **41**, 193-201.
317. T. Loeser, D. Freude, G. T. P. Mabande, W. Schwieger, *Chemical Physics Letters*, 2003, **370**, 32-38.
318. R. Li, Z. Jiang, S. Shi, H. Yang, *Journal of Molecular Structure*, 2003, **645**, 69-75.
319. G. A. Rickard, P. B. Karadakov, G. A. Webb, K. Morokuma, *Journal of Physical Chemistry A*, 2003, **107**, 292-300.
320. M. Profeta, F. Mauri, C. J. Pickard, *Journal of the American Chemical Society*, 2003, **125**, 541-548.
321. T. A. Wagler, W. A. Daunch, P. L. Rinaldi, A. R. Palmer, *Journal of magnetic resonance*, 2003, **161**, 191-197.
322. H. M. Tuononen, R. Suontamo, J. Valkonen, R. S. Laitinen, *Journal of Physical Chemistry A*, 2004, **108**, 5670-5677.
323. C. A. Bayse, *Inorganic Chemistry*, 2004, **43**, 1208-1210.
324. M. I. M. Wazeer, A. A. Isab, H. P. Perzanowski, *Magnetic Resonance in Chemistry*, 2003, **41**, 1026-1029.
325. T. Murai, A. Fujishima, C. Iwamoto, S. Kato, *Journal of Organic Chemistry*, 2003, **68**, 7979-7982.
326. S. Malik, S. Moeller, G. Toth, T. Gati, M. I. Choudhary, H. Duddeck, *Magnetic Resonance in Chemistry*, 2003, **41**, 455-465.
327. J. Oddershede, L. Henriksen, S. Larsen, *Organic & Biomolecular Chemistry*, 2003, **1**, 1053-1060.
328. J. R. Yates, C. J. Pickard, M. C. Payne, F. Mauri, *Journal of Chemical Physics*, 2003, **118**, 5746-5753.
329. S. G. Kozlova, S. P. Gabuda, V. V. Terskikh, *Solid State Nuclear Magnetic Resonance*, 2004, **25**, 72-75.
330. I. M. Ivanov, S. V. Tkachev, S. N. Ivanova, *Journal of Structural Chemistry (Translation of Zhurnal Strukturnoi Khimii)*, 2003, **44**, 146-153.
331. H. Fleischer, N. W. Mitzel, D. Schollmeyer, *European Journal of Inorganic Chemistry*,2003, **5**, 815-821.
332. A. Foris, *Magnetic Resonance in Chemistry*, 2004, **42**, 534-555.

333. S. Mele, A. Chittofrati, B. W. Ninham, M. Monduzzi, *Journal of Physical Chemistry B*, 2004, **108**, 8201-8207.
334. M. Body, G. Silly, C. Legein, J.-Y. Buzare, *Inorganic Chemistry*, 2004, **43**, 2474-2485.
335. T. Tengel, T. Fex, H. Emtenaes, F. Almqvist, I. Sethson, J. Kihlberg, *Organic & Biomolecular Chemistry*, 2004, **2**, 725-731.
336. M. L. Keshtov, C. V. Keshtova, M. M. Begretov, R. B. Tkhakakhov, *Russian Journal of General Chemistry* (*Translation of Zhurnal Obshchei Khimii*), 2003, **73**, 1476-1480.
337. Q. Shu, C. Frieden, *Biochemistry*, 2004, **43**, 1432-1439.
338. H. Fukaya, T. Ono, *Journal of Computational Chemistry*, 2004, **25**, 51-60.
339. J-W. Park, Y-A. Seo, I. Kim, C-S. Ha, K. Aimi, S. Ando, *Macromolecules*, 2004, **37**, 429-436.
340. E. Dvornikova, M. Bechcicka, K. Kamienska-Trela, A. Krowczynski, *Journal of Fluorine Chemistry*, 2003, **124**, 159-168.
341. S. Afonin, R. W. Glaser, M. Berditchevskaia, P. Wadhwani, K. Guehrs, U. Moellmann, A. Perner, A. S. Ulrich, ChemBioChem, 2003, **4**, 1151-1163.
342. B. Song, B. Yu, *Bulletin of the Korean Chemical Society*, 2003, **24**, 981-985.
343. Y. Liu, J. Tossell, *Journal of Physical Chemistry B*, 2003, **107**, 11280-11289.
344. A. Ohta, R. Murakami, A. Urata, T. Asakawa, S. Miyagishi, M. Aratono, *Journal of Physical Chemistry B*, 2003, **107**,11502-11509.
345. C. G. Pantano, R. A. Fry, K. T. Mueller, *Physics and Chemistry of Glasses*, 2003, **44**, 64-68.
346. W. Adcock, J. E. Peralta, R. H. Contreras, *Magnetic Resonance in Chemistry*, 2003, **41**, 503-508.
347. L. U. Colmenares, R. S. H. Liu, . *Journal of Photoscience*, 2003, **10**, 81-87.
348. J. P. B. Sandall, P. W. Fowler, *Organic & Biomolecular Chemistry*, 2003, **1**, 1061-1066.
349. B. A. Suvorov, *Russian Journal of General Chemistry* (*Translation of Zhurnal Obshchei Khimii*), 2003, **73**, 119-122.
350. A. R. Bassindale, Y. I. Baukov, M. Borbaruah, S. J. Glynn, V. V. Negrebetsky, D. J. Parker, P. G. Taylor, R. Turtle, *Journal of Organometallic Chemistry*, 2003, **669**, 154-163.
351. M. Kanakubo, T. Umecky, T. Aizawa, Y. Masuda, Y. Ikushima, *Magnetic Resonance in Chemistry*, 2003, **41**, 75-76.
352. S. P. Gabuda, V. Y. Kavun, S. G. Kozlova, V. V. Tverskikh, *Russian Journal of Coordination Chemistry* (*Translation of Koordinatsionnaya Khimiya*), 2003, **29**, 1-5.
353. X. Xu, R. J. Kirkpatrick, *Abstracts of Papers, 226th ACS National Meeting*, New York, NY, United States, September 7-11, 2003, GEOC-067.
354. C. F. Diven, F. Wang, A. M. Abukhdeir, W. Salah, B. T. Layden, C. Geraldes, *Inorganic chemistry*, 2003, **42**, 2774-2782.
355. A. Peera, R. K. Saini, L. B. Alemany, W. Billups, M. Saunders, A. Khong, M. S. Syamala, R. J. Cross, *European Journal of Organic Chemistry*, 2003, **(21)**, 4140-4145.
356. B. T. Stepien, T. M. Krygowski, M. K. Cyranski, *Journal of Physical Organic Chemistry*, 2003, **16**, 426-430.
357. T. Sternfeld, M. Saunders, R. J. Cross, M. Rabinovitz, *Angewandte Chemie, International Edition*, 2003, **4227**, 3136-3139.
358. G-W. Wang, X-H. Zhang, H. Zhan, O-X. Guo, Y-D. Wu, *Journal of Organic Chemistry*, 2003, **68**, 6732-6738.
359. E. Haddad, A. Nossov, F. Guenneau, A. Gedeon, *Comptes Rendus Chimie*, 2004, **7**,

305-310.

360. M. A. M. Forgeron, R. E. Wasylishen, G. H. Penner, *Journal of Physical Chemistry A*, 2004, **108**, 4751-4758.
361. H. Kobayashi, T. Ueda, K. Miyakubo, T. Eguchi, *Zeitschrift fuer Naturforschung, A: Physical Sciences*, 2003, **58**, 727-734.
362. D. Stueber, C. J. Jameson, Journal of Chemical Physics, 2004, **120**, 1560-1571.
363. T. J. Lowery, S. M. Rubin, E. J. Ruiz, M. M. Spence, N. Winssinger, P. G. Schultz, A. Pines, D. E. Wemmer, *Magnetic Resonance Imaging*,2003, **21**, 1235-1239.
364. A. Nossov, E. Haddad, F. Guenneau, A. Galarneau, F. Di Renzo, F. Fajula, A. Gedeon, *Journal of Physical Chemistry B*, 2003, **107**, 12456-12460.
365. A. Nossov, E. Haddad, F. Guenneau, A. Gedeon, Physical *Chemistry Chemical Physics*, 2003, **5**, 4473-4478.
366. S. Faggian, P. Fisicaro, E. Giamello, R. Gobetto, A. Viale, G. Berlier, C. Lamberti, I. Rossetti, *Journal of Physical Chemistry B*, 2003, **107**, 8922-8928.
367. G. Golemme, J. B. Nagy, A. Fonseca, C. Algieri, Y. Yampolskii, *Polymer*, 2003, **44**, 5039-5045.
368. D. N. Sears, C. J. Jameson, *Journal of Chemical Physics*, 2003, **118**, 9987-9989.
369. J. Autschbach, E. Zurek, *Journal of Physical Chemistry A*, 2003, **107**, 4967-4972.
370. D. Baumer, A. Fink, E. Brunner, *Zeitschrift fuer Physikalische Chemie (Muenchen, Germany)*, 2003, **217**, 289-293.
371. A. Bagno, G. Saielli, *Chemistry-A European Journal*, 2003, **9**, 1486-1495.
372. H. J. Jansch, P. Gerhard, M. Koch, D. Stahl, *Chemical Physics Letters*, 2003, **372**, 325-330.

4
Theoretical Aspects of Spin–Spin Couplings

BY H. FUKUI

1 Introduction

During the past few years, there has been a renewed interest in indirect nuclear magnetic spin-spin coupling constants as probes to study a variety of molecular problems. Physical aspects of spin-spin coupling constants have been extensively studied both experimentally and theoretically, but still present many questions. The aim of this review is to provide readers with information about important development in theoretical aspects of spin-spin couplings which appeared between June 2003 and May 2004.

2 The Sign of Fermi-Contact Contribution to Spin–Spin Coupling Constants

One of the reasons for difficulty in explaining indirect nuclear magnetic spin–spin coupling constants is that this phenomenon has no analogues in classical physics. The main driving force for inducing nuclear spin–spin couplings in molecules is not electromagnetic interactions but the Pauli's exclusion principle, operating on between electrons with the same spin. It is well known that the largest contribution to the coupling constants of J(H,X) type, in which at least one of the coupled nuclei is proton, is the contribution due to the Fermi-contact (FC) interaction. The interaction Hamiltonian for the FC interaction of nucleus N is given by

$$H_{\mathrm{N}}^{\mathrm{FC}} = (16\pi\mu_B/3)(\mu_0/4\pi)\sum_k \delta(\vec{r}_{kN})\vec{s}_k\cdot\gamma_N h\vec{I}_N, \tag{4.1}$$

where μ_B is the Bohr magneton, μ_0 is the magnetic permeability in vacuum, γ_N is the nuclear magnetogyric ratio for the nucleus N, and $\vec{s}_k$ and $\vec{I}_N$ are the spin vectors for the kth electron and Nth nucleus, respectively. The magnetic interaction energy between the two nuclear spins of atoms A and B, E_{AB}, is represented as

$$E_{AB} = K_{AB}\,\gamma_A\,\gamma_B\,\hbar^2\vec{I}_A\cdot\vec{I}_B = hJ_{AB}\vec{I}_A\cdot\vec{I}_B\,, \tag{4.2}$$

where K_{AB} and J_{AB} are the reduced and normal isotropic nuclear spin–spin

Nuclear Magnetic Resonance, Volume 34
© The Royal Society of Chemistry, 2005

coupling constant, respectively. The standard time-independent second-order perturbation theory yields

$$K_{AB}^{FC} = -2\,(16\pi\mu_B/3)^2\,(\mu_0/4\pi)^2 \sum_n (E_n\text{-}E_0)^{-1}$$

$$\times \left\langle {}^1\Psi_0 \,|\, \sum_k \delta(\vec{r}_{kA})\, s_{kz} \,|\, {}^3\Psi_n \right\rangle \left\langle {}^3\Psi_n \,|\, \sum_k \delta(\vec{r}_{kB})\, s_{kz} \,|\, {}^1\Psi_0 \right\rangle \tag{4.3}$$

for the FC contribution to K_{AB}. The fact that the same contribution comes from s_{kx}, s_{ky}, and s_{kz} operators is used above. If the Hartree–Fock (HF) approximation is used in the computation of K_{AB}^{FC}, only the one-electron excitation triplet state wavefunctions contribute to K_{AB}^{FC} as the excited triplet state wavefunctions ${}^3\Psi_n$. At the HF level of approximation, eq. (4.3) can be written as

$$K_{AB}^{FC} = -(16\pi\mu_B/3)^2\,(\mu_0/4\pi)^2 \sum_i^{\text{occ}} \sum_a^{\text{unocc}} (\varepsilon_a - \varepsilon_i - J_{ia})^{-1}$$

$$\times\ \psi_i(\vec{R}_A)\,\psi_a(\vec{R}_A)\,\psi_i(\vec{R}_B)\,\psi_a(\vec{R}_B), \tag{4.4}$$

where ε_i and ε_a are the orbital energies for occupied MO (molecular orbital) ψ_i and unoccupied MO ψ_a, respectively, J_{ia} is the molecular coulomb integral, and $\vec{R}_A$ and $\vec{R}_B$ are the nuclear position vectors for nuclei A and B, respectively. Del Bene and Elguero[1] proposed the NMR triplet wavefunction model (NMRTWM) in which the phase of the excited triplet state wavefunction, made from one-electron excitation from occupied MO ψ_i to virtual MO ψ_a, is defined as that of the product function $\psi_i\,\psi_a$. If we introduce the function P_{ia} defined by

$$P_{ia} = \psi_i\,\psi_a, \tag{4.5}$$

K_{AB}^{FC} can then be written as

$$K_{AB}^{FC} = -(16\pi\mu_B/3)^2\,(\mu_0/4\pi)^2 \sum_i^{\text{occ}} \sum_a^{\text{unocc}} (\varepsilon_a - \varepsilon_i - J_{ia})^{-1}\, P_{ia}(\vec{R}_A)\, P_{ia}(\vec{R}_B). \tag{4.6}$$

The function P_{ia} has a symmetry belonging to one of the irreducible representations of the molecular point group. It is concluded that the sign of each contribution to the coupling constant K_{AB}^{FC} is determined by the sign of $P_{ia}(\vec{R}_A)\,P_{ia}(\vec{R}_B)$. If the phases of $P_{ia}(\vec{R}_A)$ and $P_{ia}(\vec{R}_B)$ have the same sign, the contribution to K_{AB}^{FC} from the triplet state wavefunction ${}^3\Psi_{ia}$ is negative, and *vice versa*. Del Bene *et al.*[2] carried out *ab initio* calculations of $J({}^{19}F, {}^{19}F)$ spin–spin coupling constants for $(HF)_2$ clusters using the equation-of-motion coupled cluster (EOM-CC) method. They showed that the overall features of the J(F, F) coupling surface with respect to the F-F distance and the orientation of the pair of HF molecules reflect those of the FC surface. The J(F,F) coupling constants in the hydrogen-bonded HF dimer exhibited unusual behavior compared to other hydrogen-bonded coupling constants, since ${}^{2h}J$(F,F) exhibited variations in sign and magnitude depending on the F-F distance and the relative orientation between two HF molecules. It was shown that the maximum negative value for the FC term is found for the

linear arrangement F-H···H-F, while the maximum positive value is found for the linear H-F···F-H arrangement. Del Bene *et al.* explained such puzzling data using NMRTWM.

3 Nuclear Spin–Spin Coupling Density Functions

It is well known that nuclear spin–spin couplings are described as the propagation of spin density in the molecule.[3] Using the Hellmann-Feynman theorem,[4] the FC contribution to the reduced coupling constant between two nuclei A and B, K_{AB}^{FC}, can be written as

$$K_{AB}^{FC} = \left[\frac{\partial}{\partial \lambda_B} \left\langle \Psi(\lambda_B) \mid \tilde{H}_A^{FC} \mid \Psi(\lambda_B) \right\rangle \right]_{\lambda_B = 0}, \tag{4.7}$$

where

$$\tilde{H}_A^{FC} = (16\pi\mu_B/3)(\mu_0/4\pi) \sum_k \delta(r_{kA}) \, s_{k\pm} . \tag{4.8}$$

The wavefunction $\Psi(\lambda_B)$ will be given as a single Slater determinant made from spin-unrestricted Hartree–Fock (UHF) molecular orbital functions which are eigenfunctions of the perturbed Fock matrices

$$F_{\mu\nu}^{\alpha} = H_{\mu\nu}^{core} + \lambda_B (8\pi\mu_B/3)(\mu_0/4\pi)\phi_\mu(\vec{R}_B)\, \phi_\nu(\vec{R}_B) + \sum_{\lambda\sigma} [P_{\lambda\sigma}(\mu\nu|\lambda\sigma) - P_{\lambda\sigma}^{\alpha\alpha} (\mu\sigma|\lambda\nu)] \tag{4.9}$$

and

$$F_{\mu\nu}^{\beta} = H_{\mu\nu}^{core} - \lambda_B (8\pi\mu_B/3)(\mu_0/4\pi)\phi_\mu(\vec{R}_B)\, \phi_\nu(\vec{R}_B) + \sum_{\lambda\sigma} [P_{\lambda\sigma}(\mu\nu|\lambda\sigma) - P_{\lambda\sigma}^{\beta\beta} (\mu\sigma|\lambda\nu)] , \tag{4.10}$$

where $H_{\mu\nu}^{core}$, $P_{\lambda\sigma}$, and $(\mu\nu|\lambda\sigma)$ have the usual meanings. ϕ_μ, ϕ_ν are basis functions. Using this type of wavefunction, the expression (4.7) for the FC contribution becomes

$$K_{AB}^{FC} = (8\pi\mu_B/3)(\mu_0/4\pi) \sum_{\mu\nu} \phi_\mu(\vec{R}_A)\phi_\nu(\vec{R}_A) \left[\frac{\partial}{\partial \lambda_B} \rho_{\mu\nu}^{spin}(\lambda_B) \right\rangle \Bigg]_{\lambda_B = 0}, \tag{4.11}$$

where

$$\rho_{\mu\nu}^{spin} = P_{\mu\nu}^{\alpha\alpha} - P_{\mu\nu}^{\beta\beta} . \tag{4.12}$$

The first-order differentiation with respect to λ_B in eq. (4.11) can be evaluated numerically in the finite perturbation theory (**FPT**) or analytically in the coupled Hartree–Fock (CHF) approach.[5] The quantity $\sum_{\mu\nu} \rho_{\mu\nu}^{spin} \phi_\mu(\vec{R}_A)\phi_\nu(\vec{R}_A)$ is the spin density at $\vec{R}_A$ for the state wavefunction $\Psi(\lambda_B)$ which is subjected to the spin

dependent perturbation at $\vec{R}_B$. If the perturbation parameter λ_B is positive, the spin density induced at $\vec{R}_B$ is negative at $\vec{R}_B$. Equation (4.11) indicates that if the spin densities at $\vec{R}_A$ and $\vec{R}_B$ have the same sign, K_{AB}^{FC} is negative, and *vice versa*.

Soncini and Lazzeritti[6] calculated the one- and two-bonds nuclear spin–spin coupling densities and the Fermi hole densities for hydrogen fluoride, water, ammonia, and methane molecules. The pair density function $\rho_2(\mathbf{x}_1, \mathbf{x}_2)$ determines the probability of two electrons being found simultaneously at points $\mathbf{x}_1 = \vec{r}_1\eta_1$ and $\mathbf{x}_2 = \vec{r}_2\eta_2$, where $\vec{r}_1$ and $\vec{r}_2$ are coordinates in three-dimensional space, and η_1 and η_2 are the spin variables of the two electrons. For a system described by a one determinant wavefunction of occupied spin-orbitals $\phi_i(\mathbf{x})$, that is, a wavefunction in the HF approximation, the pair density function becomes

$$\rho_2(\mathbf{x}_1, \mathbf{x}_2) = \sum_{i,j} (\phi_i(\mathbf{x}_1)\phi_j(\mathbf{x}_2) - \phi_j(\mathbf{x}_1)\phi_i(\mathbf{x}_2))\phi_i^*(\mathbf{x}_1)\,\phi_j^*(\mathbf{x}_2). \tag{4.13}$$

On completing the spin coordinate integrations, it is easy to show that, for a closed shell system,

$$\rho_2^{\alpha\beta}(\vec{r}_1,\vec{r}_2) = \rho_\alpha(\vec{r}_1)\rho_\beta(\vec{r}_2) = \rho_\beta(\vec{r}_1)\rho_\alpha(\vec{r}_2) = \rho_2^{\beta\alpha}(\vec{r}_1,\vec{r}_2)\,, \tag{4.14}$$

$$\begin{aligned}\rho_2^{\alpha\alpha}(\vec{r}_1,\vec{r}_2) &= \rho_\alpha(\vec{r}_1)\left\{\rho_\alpha(\vec{r}_2) + h_\alpha(\vec{r}_1,\vec{r}_2)\right\} = \rho_\beta(\vec{r}_1)\left\{\rho_\beta(\vec{r}_2) + h_\beta(\vec{r}_1,\vec{r}_2)\right\} \\ &= \rho_2^{\beta\beta}(\vec{r}_1,\vec{r}_2)\,,\end{aligned} \tag{4.15}$$

where $\rho_\alpha(\vec{r})$, the α-electron density, is determined by a sum over the densities due to the occupied molecular orbitals having α spin,

$$\rho_\alpha(\vec{r}) = \sum_i^{\alpha,\mathrm{occ}} \phi_i^*(\vec{r})\,\phi_i(\vec{r}). \tag{4.16}$$

The pair function $h_\alpha(\vec{r}_1,\vec{r}_2)$, called Fermi hole (FH) density,[7–10] is given by

$$h_\alpha(\vec{r}_1,\vec{r}_2) = -\sum_{i,j}^{\alpha,\mathrm{occ}} \left\{\phi_i^*(\vec{r}_1)\,\phi_j^*(\vec{r}_2)\phi_j(\vec{r}_1)\phi_i(\vec{r}_2)\right\} / \rho_\alpha(\vec{r}_1)\,. \tag{4.17}$$

The FH density distribution (4.17) describes how the density of α-spin electrons at position $\vec{r}_2$ would be changed if one of the α-spin electrons, called the 'reference electron', is fixed at position $\vec{r}_1$. Therefore, the FH density (4.17) is a negative quantity which accounts for the decrease of the α-spin density at $\vec{r}_2$. The FH density $h_\alpha(\vec{r}_1,\vec{r}_2)$ exhibits the limiting value $-\rho_\alpha(\vec{r}_1)$ for $\vec{r}_2 \to \vec{r}_1$, corresponding to the complete removal of same-spin density from the proximity of the reference electron. When $h_\alpha(\vec{r}_1,\vec{r}_2)$ is integrated over the coordinates $\vec{r}_2$, it equals -1, corresponding to the complete removal of one electron from the molecular domain. Nuclear spin–spin coupling density functions yield a three-dimensional picture of the interaction between two nuclear magnetic dipole moments mediated by electron spin density. The Fermi contact coupling density maps present the mechanism whereby the spin polarization induced about one nucleus is transmitted to another nucleus coupled to it. The mechanism for propagation of FH density may be the same as that of spin density transmission. Soncini and Lazzeretti[6] showed that the Fermi hole density functions are characterized by

morhological aspects very similar to those of the Fermi contact coupling density functions. Their results confirmed that the Fermi correlation between same-spin electrons is the fundamental vehicle propagating nuclear spin–spin couplings.

4 Vibrational Corrections to Indirect Nuclear Spin–Spin Coupling Constants

The indirect nuclear spin–spin coupling constants of nuclear magnetic resonance (NMR) spectroscopy may nowadays be calculated by a variety of electronic-structure methods.[11] The current status of the calculation of spin–spin coupling constants is now such that the difference between theoretical and experimental values is often not larger than the vibrational corrections to the couplings, which may constitute as much as 10 % of the coupling.[12-15] Therefore, to make further progress towards the accurate description of indirect nuclear spin–spin coupling constants, it has become important to develop efficient methods for the calculation of vibrational corrections. Ruden *et al.*[16] evaluated vibrational corrections to the indirect nuclear spin–spin coupling constants of HD, HF, CO, N_2, H_2O, HCN, NH_3, CH_4, C_2H_2, and C_6H_6 molecules. The theory for the calculation of vibrational corrections to molecular properties by second-order perturbation theory is well documented.[17-22] Ruden *et al.* calculated the vibrational correction as the zero-point vibrational (ZPV) correction, using the approach of Kern *et al.*[17-19] In this approach, the zeroth-order ground-state vibrational wavefunction $X^{(0)}(Q)$ is written as a product of harmonic-oscillator functions in normal coordinates Q:

$$X^{(0)}(Q) = \Phi_0(Q) = \prod_{K=1}^{3n-6} \phi_0^K(Q_K), \tag{4.18}$$

where $\phi_k^K(Q_K)$ indicates the kth excited harmonic-oscillator state for the Kth vibrational normal mode, Q_K. Next, the first-order groundstate vibrational wave function $X^{(1)}$ is expanded in the full set of virtual excitations from $X^{(0)}(Q)$. Assuming a fourth-order Taylor expansion of the potential energy E surface about equilibrium, only single and triple excitations from $\Phi_0(Q)$ contribute to $X^{(1)}(Q)$. If $\Phi_{klm}^{KLM}(Q)$ indicates the wavefunction obtained from $\Phi_0(Q)$ by exciting the Kth, Lth, and Mth modes to the kth, lth, and mth harmonic-oscillator states, respectively, $k + l + m$ should be 1 or 3. To determine the ZPV correction to the equilibrium value P_{eq} of some molecular property P, we consider the expectation value

$$\langle P \rangle = \langle X^{(0)} + X^{(1)} | P | X^{(0)} + X^{(1)} \rangle. \tag{4.19}$$

The property P in eq. (4.19) can be expanded in a Taylor series about the equilibrium geometry in normal coordinates. To second order in perturbation theory, the ZPV correction to the property P can then be written as

$$\Delta P_{\mathrm{ZPV}} = \langle P \rangle - P_{eq} = \frac{1}{4} \sum_{K=1}^{3n-6} \frac{1}{\omega_K} \frac{d^2P}{dQ_K^2} - \frac{1}{4} \sum_{K=1}^{3n-6} \frac{1}{\omega_K^2} \frac{dP}{dQ_K} \sum_{L=1}^{3n-6} \frac{F_{KLL}}{\omega_L}, \tag{4.20}$$

where ω_K is the harmonic frequency of the mode K, and F_{KLM} is the cubic force

constant defined as

$$F_{KLM} = \frac{d^3E}{dQ_K\ dQ_L\ dQ_M}. \tag{4.21}$$

Ruden *et al.*[16] performed the calculation of ZPV corrections to the indirect nuclear spin–spin coupling constants in which all calculations have been carried out using hybrid density functional theory (DFT) with the Becke 3-parameter Lee-Yang-Parr (B3LYP) functional.[23] Several basis sets, based on the Huzinaga sets[24,25] and contraction patterns of Kutzelnigg *et al.*,[26] were used. In the Huzinaga-type basis sets, the DFT/B3LYP model provided a good representation of the harmonic force field. Once the vibrational corrections to the indirect nuclear spin–spin coupling constants have been calculated theoretically, a set of empirical equilibrium coupling constants J_{eq}^{emp} can be extracted from experimentally observed values J^{exp} by subtracting the calculated ZPV corrections ΔJ_{vib}^{cal} from J^{exp}:

$$J_{eq}^{emp} = J^{exp} - \Delta J_{vib}^{cal}. \tag{4.22}$$

Empirical equilibrium coupling constants J_{eq}^{emp} can be compared as a benchmark with calculated equilibrium coupling constants J_{eq}^{cal} obtained with various methods. A comparison of these empirical equilibrium constants with calculated equilibrium constants suggested that the restricted-active-space self-consistent field (RASSCF) method is the best approach for calculating the indirect nuclear spin–spin coupling constants of small molecules, and that the second-order polarization propagator approximation (SOPPA) and DFT are similar in performance.

Ruden *et al.*[27] calculated the indirect nuclear spin–spin coupling constants of allene, cyclopropane, and cyclopropene at different levels of electronic-structure theory and compared them with experimental equilibrium constants, which were obtained from experiment by subtracting evaluated vibrational contributions. It was found that, even in a relatively small basis set, the coupled-cluster singles-and-doubles (CCSD) method provides very good results. SOPPA consistently performed better than RASSCF. Hybrid DFT performed as well as SOPPA for the one-bond coupling constants, while, for the other coupling constants, it provided results of similar quality as CCSD.

5 Residual Dipolar Couplings Between Nuclear Spins

The influence of anisotropic indirect nuclear spin–spin coupling tensors on residual dipolar coupling constants (RDCs) has been investigated for many small molecules dissolved in liquid crystalline solvents.[28–30] The total nuclear spin–spin coupling Hamiltonian for two nuclear spins $\vec{I}_M$ and $\vec{I}_N$ may be written in Cartesian form as:

$$H_{DD,J} = h\vec{I}_M \cdot \hat{D}_{MN}^{dir} \cdot \vec{I}_N + h\hat{J}_{MN}^{iso}\, \vec{I}_M \cdot \vec{I}_N + h\vec{I}_M \cdot \hat{J}'_{MN} \cdot \vec{I}_N, \tag{4.23}$$

where $\hat{D}_{MN}^{dir}$ is the axially symmetric direct dipolar coupling tensor, J_{MN}^{iso} is the

isotropic indirect nuclear spin–spin scalar coupling constant, and J'_{MN} is the symmetric second-rank anisotropic indirect nuclear spin–spin coupling tensor. Examination of the form of this Hamiltonian indicates that while J^{iso}_{MN} may be measured independently of the other contributions, the effects of the $\hat{D}^{dir}_{MN}$ and J'_{MN} tensors can not be measured separately.[28,31–33] This is due to the fact that the J'_{MN} tensor gives a contribution to the experimentally detectable RDC, D^{exp}_{MN}:

$$D^{exp}_{MN} = D^{dir}_{MN} + \frac{1}{2} J^{aniso}_{MN}, \tag{4.24}$$

where

$$D^{dir}_{MN} = -\frac{\mu_0 \hbar \gamma_M \gamma_N}{8\pi^2} \left\langle \frac{1}{R^3_{MN}} \right\rangle s^B_{MN} \tag{4.25}$$

and

$$J^{aniso}_{MN} = \frac{2}{3} \sum_{\alpha\beta} J'_{MN,\alpha\beta} s^B_{\alpha\beta}. \tag{4.26}$$

In eq. (4.25), s^B_{MN} is the orientational order parameter (relative to the external magnetic field) of the vector $\vec{R}_{MN}$, and $\langle\ \rangle$ indicates averaging over internal vibrations. The coefficients $s^B_{\alpha\beta}$ in eq. (4.26) are Saupe orientational order tensor elements relative to the external magnetic field in a molecular-fixed frame.[34] Consequently, it is necessary to know the $\hat{J}'_{MN}$ tensor in order to be able to determine experimentally the direct dipolar contribution D^{dir}_{MN} from D^{exp}_{MN}.

Jokisaari and Autschbach[35] calculated the isotropic average and anisotropy of the $^1\hat{J}(^{13}C, ^{77}Se)$ and $^2\hat{J}(^{77}Se, ^{77}Se)$ spin–spin coupling tensors in carbon diselenide (CSe_2) by applying relativistic density functional theory. They included scalar relativistic effects as well as spin–orbit coupling in all computations together with flexible basis sets. All contributions to the spin–spin couplings, *i.e.*, Fermi-contact (FC), spin–dipolar (SD), paramagnetic spin–orbit (PSO), diamagnetic spin-orbit (DSO), and cross terms due to spin-orbit coupling,[36] were calculated. The applied methodology is based on the zeroth-order regular approximate (ZORA) two-component relativistic Hamiltonian[37,38] and its implementation in the Amsterdam Density Functional program package.[39–41] They showed that the SD term significantly lowers $\Delta J(Se, Se) = J_{||}(Se, Se) - J_{\perp}(Se, Se)$ and increases $\Delta J(C, Se)$, improving the agreement with experiment in both cases. It was shown that $\frac{1}{2}J^{aniso}_{SeSe} = \frac{1}{3}\Delta J(Se, Se)\, s^B_{zz}$ is a clearly dominating contribution in D^{exp}_{SeSe}. Here, the z-axis is chosen to lie along the C_{∞} symmetry axis of the linear molecule CSe_2.

The measurement and interpretation of RDCs between spatially proximate spin-pairs in biopolymers such as proteins, nucleic acids, and oligosaccharides in partially oriented environments has become a popular method for structure determination.[42] All observed RDCs, D^{exp}'s contain an unknown contribution from the anisotropic part of coupling tensor, $\hat{J}'$ in addition to the direct dipolar contribution, D^{dir}. Bryce and Wasylishen[43] evaluated the influence of $\hat{J}'$ on RDCs through a series of DFT calculation on model peptides. Very small contributions of $\hat{J}'$ were found in one-bond RDCs measured between heavy atoms in peptides

and proteins. The $\hat{J}'$ contributions to RDCs involving at least one proton were negligible. The orientations of $\hat{J}$(N, C′) and $\hat{J}$(C$^{\alpha}$, C′) tensors in the molecular framework were determined for glycylglycine.

Forgeron *et al.*[44] measured the $^{1}J(^{129}\text{Xe}, ^{19}\text{F})$ coupling constant in crystalline XeF_2 to be -5560 ± 50 Hz whose sign was determined using the sign of the $^{129}\text{Xe}-^{19}\text{F}$ direct dipolar interaction. No theoretical calculations have been published for ^{1}J(Xe, F).

6 Fluorine-Fluorine Spin–Spin Coupling Constants

Investigations of $J(^{19}\text{F}, ^{19}\text{F})$ spin–spin coupling constants are attractive experimentally, given that ^{19}F has a natural abundance of 100 %, a nuclear spin of 1/2, and a large magnetogyric ratio of 2.6273 magnetons, which implies that $^{19}\text{F}-^{19}\text{F}$ coupling constants should be large and therefore relatively easy to measure. Del Bene *et al.*[45] computed two- three-, and four-bond $^{19}\text{F}-^{19}\text{F}$ spin–spin coupling constants for a set of small fluoro-substituted organic molecules using *ab initio* equation-of-motion coupled cluster singles and doubles (EOM-CCSD) theory. The computed values reproduced the experimental signs and magnitudes of ^{n}J(F, F). The straight line that relates the experimental and computed coupling constants had a slope of approximately 1 and passed through the point (0,0) within the uncertainties of the fit. It was shown that EOM-CCSD values of ^{n}J(F, F) should be excellent predictors of experimental values when these are not available. Baldeschwieler *et al.*[46] experimentally determined that ^{3}J(F, F) and ^{3}J(H, H) in *cis*-difluoroethene have opposite relative signs, but they were not able to determine the absolute signs of these coupling constants. The calculation by Del Bene *et al.* indicated that the sign of ^{3}J(F, F) is negative, while that of ^{3}J(H, H) is positive. Furthermore, they showed that the present EOM-CCSD results for coupling constants are superior to those obtained by DFT, SOPPA, and SOPPA(CCSD).[47] All of the components of ^{n}J(F, F) except for the DSO term may be large and must be evaluated if agreement between theory and experiment is to be obtained.

Alkorta and Elguero[48] studied the electronic structure of a number of compounds that show experimental F···F coupling constants across the space using the hybrid DFT/B3LYP and Atoms in Molecules (AIM) methodologies.[49] The AIM methodology provides a unique tool for the study of bonding interactions via investigation of a bond critical point (BCP) and the corresponding bond path linking two nuclei in an equilibrium geometry.[50] Alkorta and Elguero presented the formula correlating experimental F···F coupling constants with the electron density at the bond critical point, ρ_{BCP} and the dihedral angle formed by the F−C···C-F groups, α:

$$J(\text{F, F})/\text{Hz} = -(220 \pm 23) + (16826 \pm 1293)\,\rho_{BCP} + (40 \pm 8)\cos\alpha. \quad (4.27)$$

Exponential relationships have been found between the electron density ρ_{BCP} and the interatomic distance d:

$$\rho_{BCP} = (4.1 \pm 0.7)\exp[(-2.17 \pm 0.06)d]\,. \quad (4.28)$$

Barone *et al.*[47] studied substituent effects on ^2J(F, F) couplings in aliphatic and olefinic CF_2 moieties and ^3J(F, F) couplings in fluorinated derivatives of ethylene using SOPPA, SOPPA(CCSD), and DFT/B3LYP calculations. Computed substituent effects on the coupling constants were compared with experimental values where it was possible. It was shown that in general, the SOPPA methodology matches absolute experimental values reasonably well, whereas the DFT/B3LYP approach performs poorly in describing ^2J(F, F) couplings. Fortunately, DFT notably better reproduced substituent effects on J couplings. For a vinyl CF_2 moiety, the accurate prediction of ^2J(F, F) couplings is a challenging task even for high level *ab initio* methods such as SOPPA and SOPPA(CCSD). It was shown that substituent effects on ^2J(F, F) and ^3J(F, F) couplings in fluorinated derivatives of ethylene are dominated by non-Fermi contributions. Because DFT/B3LYP strongly underestimates the FC term, but generally assesses the non-Fermi terms similar to SOPPA, DFT may predict substituent effects reasonably well.

7 *Ab initio* Calculation of Spin–Spin Coupling constants

7.1 Full Configuration-Interaction Calculations. – NMR chemical shift calculations are nowadays carried out routinely, but the computation of spin–spin coupling constants using quantum chemical methods is less common.[11] It is already known in the seventies that the inclusion of electron correlation effects is essential for the accurate prediction of spin–spin coupling constants and that results of Hartree–Fock self-consistent-field (HF – SCF) calculations are often unreliable due to the triplet nature of the perturbing operators. On the other hand, coupled-cluster (CC) approaches have proven most efficient when aiming for quantitative accuracy in quantum chemical calculations.[51,52] A lot of effort has been devoted to the formulation and implementation of CC methods for the calculation of spin–spin coupling constants.[53–56] In order to estimate the error introduced by the approximation of electron correlation effects, full configuration-interaction (FCI) calculations have often been used for calibration.[57–60] Auer *et al.*[61] carried out FCI calculations of the indirect nuclear spin–spin coupling constant of the BH molecule in order to investigate the performance of various CC methods in the treatment of electron-correlation effects. It was shown that the CCSDT results are in excellent agreement with the FCI values in the all-electron calculations. However, frozen-core results obtained with the unrelaxed CC calculations[62] for the FC and DSO contributions were very disappointing, while the core-inactive FCI results showed no significant deviations from the all-electron values. Assuming additivity of correlation and basis set effects, they obtained a theoretical estimate of 50.67 Hz for the ^1J(11B, 1H) spin–spin coupling constant.

7.2 Second-Order Polarization Propagator Approximation Calculations. – Krivdin[63] performed a systematic study of the one-bond and long-range J(C, C), J(C, H), and J(H, H) coupling constants in the series of nine bicycloalkanes at the

second-order polarization propagator approximation (SOPPA) level with special emphasis on the investigation on coupling transmission mechanisms at bridgeheads. The most striking feature of the molecular structure of bicyclo[1.1.1]pentane (**1**), the most unusual member of bicycloalkanes family, is its unprecedentedly short non-bonded distance of *ca.* 1.9 Å between bridgehead carbons, which is one of the shortest non-bonding carbon-carbon distances known so far. Krivdin's calculations demonstrated that *ab initio* SOPPA applied with the Dunning's basis sets[64–66] performs perfectly well in reproducing experimental values of different types of coupling constants (the estimated reliability is *ca.* 1-2 Hz) in relatively large organic molecules of up to 11 carbon atoms. Most of the bridgehead couplings in all but one bicycloalkane appeared to be essentially additive while bicyclo[1.1.1]pentane demonstrated dramatic non-additivity. Non-additivity effects in the latter compound established at the SOPPA level should be attributed to the through-space non-bonded interactions at bridgeheads due to the essential overlapping of the bridgehead rear lobes.

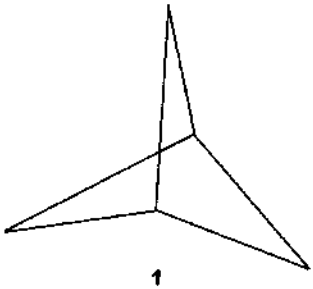

1

Krivdin[67] calculated all possible J(C, C) of the bicarbocyclic frameworks together with J(C, H) and J(H, H) at bridgeheads in the series of six bridged bicycloalkanes at the SOPPA level. It was shown that there are two main factors governing the behavior of carbon-carbon coupling constants in the carbocyclic framework of bridged bicycloalkanes under study, namely (i) the hybridization of the coupled carbons (*s*-characters of bonding hybrids) and (ii) the nature of the coupling route (number of the coupling pathways, number of intervening bonds in each coupling path, *etc.*). Proton-proton coupling constants at bridgeheads markedly decrease with the interproton distance at bridgeheads, which suggests a substantial through-space contribution. Krivdin[68] calculated a full set of carbon-carbon coupling constants in the series of six most representative propellanes at the SOPPA level. Special attention was focused on spin–spin couplings involving both bridgehead carbons, and the data were explained in terms of the hybridization effects and multipath coupling mechanism.

Krivdin and Kuznetsova[69] carried out an *ab initio* calculation for ^{13}C-^{13}C spin–spin coupling constants in a series of saturated three- and four-membered heterocycles within a framework of second-order perturbation theory using SOPPA. It was shown that the main variations in the J(^{13}C, ^{13}C) coupling constants in the heterocycle series under study are governed by the FC contribution and that the FC contribution is highly sensitive to the heteroatom character

and ring size. The calculated values of ^1J(C, C) coincided with available experimental data within 1-2 Hz.

8 Gas-Phase Studies of Spin–Spin Coupling Constants

There is now an urgent question. Can which experimental data straightforwardly be compared with the theoretical results of spin–spin coupling constant? Because all experimental data contain the contributions from molecular interactions and intramolecular nuclear motion, these effects must be accounted if a reliable comparison of theoretical and experimental coupling constants is required. Generally, nuclear spin–spin coupling constant J(X, Y) is modified in a gaseous binary mixture consisting of solute gas A and solvent gas B as follows:

$$J(\mathrm{X, Y}) = J_0(\mathrm{X, Y}) + J_{1\mathrm{AA}}(\mathrm{X, Y})\rho_\mathrm{A} + J_{1\mathrm{AB}}(\mathrm{X, Y})\rho_\mathrm{B} + \cdots, \tag{4.29}$$

where J_0(X, Y) is the spin spin coupling constant between X and Y nuclei at the zero-density limit, and $J_{1\mathrm{AA}}$ (X, Y) and $J_{1\mathrm{AB}}$(X, Y) are parameters representing intermolecular effects in the binary collisions of A-A and A-B molecular pairs, respectively. Usually, the density of A is kept sufficiently low and eq. (4.29) is simplified to

$$J(\mathrm{X, Y}) = J_0(\mathrm{X, Y}) + J_{1\mathrm{AB}}(\mathrm{X, Y})\rho_\mathrm{B}\,. \tag{4.30}$$

Theoretically, J_0(X, Y) is evaluated as the sum of the J_e(X, Y) constant, calculated for an isolated molecule at the equilibrium geometry, and the rovibrational correction ΔJ (X, Y). Jackowski[70] compared the experimentally determined J_0(X, Y) values for 1,2-^{13}C-acetylene at 300 K[71] with the three theoretical values for J_0(X, Y) obtained by Kaski *et al.*[72], Wigglesworth *et al.*[73,74], and Jaszuński and Ruud[75]. It was shown that the theoretical J_0(X, Y) values by Jaszuński and Ruud are closest to the observed J_0(X, Y) values.

9 Density Functional Theory

9.1 Density Functional Theory Calculations of Spin–Spin Coupling Constants Using Slater-type Basis Sets. – Watson *et al.*[76] extended their density functional theory (DFT) calculations,[77,78] with generalized-gradient approximation (GGA) and hybrid functionals, using Slater-type orbitals (STOs), to the determination of second-order molecular properties like nuclear spin–spin coupling constants. The key to their methodology involves the fitting of all STO basis function products to an auxiliary STO basis. For the evaluation of energies, their previous papers[77,78] have demonstrated that there is little to choose between good GTO calculations and good STO calculations. Their results with GGA and hybrid functionals indicated that similar quality values are obtained with both basis sets. However, the cost of the STO hybrid energy calculations exceeded that of the GTO energy calculations. For the calculation of molecular properties, however, the picture for STOs was more encouraging. For the indirect nuclear

spin–spin coupling constants, it was observed that fewer additional tight s functions are required to obtain high-quality results. The addition of many tight GTOs is presumably required to obtain a good description of the electronic cusp at the nucleus, something that is automatically presented with STOs. As a conclusion, it was demonstrated that molecular properties may be determined to a high accuracy using moderately sized STO basis sets within the DFT framework in a manner that is highly competitive with the use of GTOs.

9.2 Basis Set Dependence of Spin–Spin Coupling Constants in Density Functional Theory Calculations. – Peralta *et al.*[79] analyzed the basis set dependence of NMR spin–spin coupling constants calculated using DFT in a set of benchmark molecules (HF, H_2O, NH_3, CH_4, C_2H_4, and FCH_3) containing first row and hydrogen atoms. They presented a systematic study of the basis set dependence of spin–spin coupling constants using the cc-pVXZ (X = D, T, Q, 5, and 6), cc-pCVXZ (X = D, T, Q, and 5), cc-pCVXZ-sd (X = D, T, Q, and 5), and cc-pCVXZ-sd + t (X = D, T, Q, and 5) series of basis sets. The convergence of the cc-pVXZ series was unsatisfactory and a large difference between the cc-pV5Z and the cc-pV6Z results was found. Results of the cc-pCVXZ series of basis set, which consists of the previous cc-pVXZ augmented with extra functions to describe core-core and core-valence correlation,[80] did not show clear convergence and indicated that more basis functions need to be added. The correct evaluation of the FC term requires a good description of the electronic density near the nuclear positions. For this reason, the s-type functions of the cc-pCVXZ basis set was fully decontracted to yeld the cc-pCVXZ-sd series. Results obtained with these cc-pCVXZ-sd basis sets showed a smoother trend of convergence than the former cc-pVXZ and cc-pCVXZ sets. However, most values obtained with the largest cc-pCV5Z-sd set were not far from being converged. Finally, tight s-type functions were added to the cc-pCVXZ-sd basis sets to improve the description of the core region, yelding the cc-pCVXZ-sd + t basis set series. As expected, the addition of tight s-type functions improved the convergence of calculated spin–spin coupling constants, mainly due to its effect on the FC contribution. It was found that the cc-pCV5Z-sd + t basis set is fully converged. Furthermore, they showed that the aug-cc-pVTZ-J basis set, which is much smaller than the cc-pCV5Z-sd + t set, yelds the spin–spin coupling constants closest to converged values.

9.3 Relationship Between the π Character of a C-C Bond and ^1J(C, C). – The ^1J(C, C) coupling constant is a sensitive antenna for investigating the electronic structure in hyper- and π-conjugated hydrocarbons. Gräfenstein *et al.*[81] investigated the dependence of the PSO term in ^1J(C, C) on the C-C multiple bond character. They analyzed the PSO term for the prototypical C-C single, double, and triple bonds in the framework of DFT calculations. It was found that there is a cubic dependence of $^1J^{PSO}$(C, C) on the C-C bond order. They showed that under certain conditions, the degree of hybridization can be determined with the help of the PSO term, and that the PSO term helps to distinguish hyperconjugation and π-conjugation effects. It was shown that the PSO term can be a sensitive

descriptor for the degree of π delocalization.

9.4 Solvent Effects on the Nuclear Spin–Spin Coupling Constants. – Autschbach and Le Guennic[82] studied the nuclear spin–spin coupling constants of the complexes $[(NC)_5Pt\text{-}Tl(CN)_n]^{n-}$, $n = 0-3$, (**I**, **II**, **III**, and **IV**) and the related system $[(NC)_5Pt\text{-}Tl\text{-}Pt(CN)_5]^{3-}$ (**V**). These complexes exhibit outstanding, sometimes unintuitive NMR properties. One typical feature of the NMR spectra of complexes **I** – **V** is the very large Pt-Tl spin–spin coupling constant (the largest coupling constants so far observed between two different nuclei).[83–85] Along the series **I** to **IV**, ^1J(Pt, Tl) decreases from 71 to 39 kHz (25 kHz for complex **V**). Autschbach and Ziegler[86] had previously studied the spin–spin coupling constants for complex **II**. They found that effects from Tl coordination by the solvent (H_2O) could be responsible for almost half of the huge 57 kHz magnitude (experimental value) of the Pt-Tl coupling constant. However, in their computations, a difference of approximately 20 % remained between the calculated and the experimental data. Autschbach and Le Guennic[82] used the statistical average of orbital-dependent model potentials (SAOP).[87–91] It was demonstrated that whole experimental trend among the series is entirely due to solvent effects. An approximate inclusion of the bulk solvent effects by means of a continuum model, in addition to the direct coordination, proved to be crucial. A computational model employng the SAOP in addition to the solvent effects allowed to accurately reproduce the experimental coupling constants within reasonable limits.

Sychrovský *et al.*[92] calculated indirect nuclear spin–spin coupling constants for the discrimination between the inner-shell and the outer-shell binding motif of hydrated divalent cations Mg^{2+} or Zn^{2+} with a guanine base. They used the specific inner-shell binding motif that the hydrated cation binds either with oxygen O6 or with nitrogen N7 of guanine. The calculated coupling constants ^1J(Mg, O6) and ^1J(Zn, O6) were 6.2 and −17.5 Hz, respectively, for the inner-shell complex of cation directly interacting with oxygen O6 of guanine. For the inner-shell coordination of the cation at nitrogen N7, the calculated coupling constants ^1J(Mg, N7) and ^1J(Zn, N7) were 5.6 and −36.5 Hz, respectively. When the binding of the cation was water-mediated, the coupling constant was zero. It was shown that the calculated change of NMR spin–spin coupling constants due to the hydration and coordination of the cation with guanian is caused mainly by the variation of FC coupling contribution. The change of s-character of guanine sigma bonding, sigma antibonding, and lone pair orbitals upon the hydration and cation coordination correlates with the variation of the FC term. It was demonstrated that measurements of NMR intermolecular coupling constants may be used to discriminate between the specific inner- and outer-shell binding of divalent cations to nucleobases in DNA and RNA.

9.5 ^1J(Si, H) and Nonclassical H-Si Interactions. – Recently, a great deal of progress has been made in studyng complexes with nonclassical interligand interactions.[93–98] The most common means for probing the H-Si bonding is measuring of ^1J(Si, H) coupling constant, where magnitudes higher than 20 Hz

are attributed to the presence of a direct H-Si interaction.[95,96] Dubberley *et al.*[99] reported ^{29}Si NMR and DFT studies of a series of silylhydrido complexes of Ta, having nonclassical M-H···Si-X interligand hypervalent interactions (IHIs).[100–102] Complexes of the type Cp(ArN)Ta(PMe$_3$)(H)(SiR$_3$) were investigated. The ^{29}Si NMR spectra showed a remarkable trend in that the magnitude of the ^1J(Si, H) coupling constant sequentially increases as the number of chlorine groups on silicon increases. DFT calculations demonstrated that the larger magnitude of ^1J(Si, H) does not necessarily correspond to the stronger interaction between Si and H atoms.

9.6 Spin–Spin Coupling Constants in Phosphatrane Molecules. – Phosphatranes, also referred to as Verkade's bases, are football-shaped molecule of C_3 symmetry that diplay unusual structures, spectroscopic properties, and reactivities, including catalysis.[103–107] Furthermore, they are very strong bases due to the extraordinary stability of their protonated species.[103–109] From a qualitative standpoint, these features can be attributed to the partial bonding between the bridgehead phoshorus and axial nitrogen (N_{ax}) inside the caged structure. Galasso[110] computed indirect nuclear spin–spin coupling constants of a representative selection of phosphatranes by DFT-based methods. The results were fairly consistent with experimental evidence, in particular for the observables involving the central phosphorus. The full DFT calculations showed that the FC contribution is predominant in ^nJ(X, Y) values in the studied phosphatrane molecules. In the pattern of the ^nJ(X, Y) computed for phosphatranes, the following aspects are remarkable. A small value of $J(^{31}P, ^{15}N_{ax})$ was predicted in all cases, which manifests the long-range rather than one-bond coupling between the bridgehead nuclei, *i.e.*, ^4J instead of ^1J between the bridgehead phospharus and axial nitrogen atoms.

9.7 Conformational and Configurational Analysis. – Ratajczyk *et al.*[111] studied the conformational dependence of the indirect nuclear spin–spin coupling constants of glycolaldehyde by means of DFT using the B3LYP functional. For selected cases, the coupling constants calculated by means of DFT were compared with those obtained with coupled-cluster singles – and – doubles (CCSD) theory. The DFT and CCSD coupling constants of glycolaldehyde were close to each other. The surfaces of the spin–spin coupling constants generated by rotations about the C-C and C-O bonds in glcolaldehyde were calculated, and the resulting surfaces were fit to a truncated Fourier series. The resulting expressions may help to determine the conformation of carbohydrates and their derivatives from measured nuclear spin–spin coupling constants. The relationships between coupling constants and dihedral angles were discussed and compared, whenever possible, with experimental trends.

Tormena *et al.*[112] studied conformational analysis of fluoroacetoxime using the solvent dependence of the 1H, ^{13}C, and 15N NMR spectra of (E)-fluoroacetoxime [(E)-FAO] and of (E)-fluoroacetoxime O-methyl ether [(E)-FAOME]. Recent studies[113–116] using *ab initio* and DFT techniques to calculate all contributions (FC, SD, PSO, and DSO contributions) to J(C, H), J(C, F), and J(H, F) con-

firmed the predominance of the FC contribution to these couplings and agreed with experiment[117-123] that these couplings are dependent on the molecular conformation. On the other hand, it was probable that for the ^3J(N, F) coupling constant, the noncontact contributions (SD, PSO, and DSO contributions) predominate and in this case the coupling was independent of the molecular conformation. The ^4J(H, F) and ^1J(C, F) coupling constants in (E)-FAO were analyzed by solvation theory assuming the *cis* and *gauche* forms to give $E_{cis} - E_{gauche} = 3.3$ kcal mol^{-1} in the vapor phase, decreasing to 1.54 kcal mol^{-1} in CCl_4, and -1.19 kcal mol^{-1} in DMSO. In (E)-FAOME, the observed coupling constants, when analysed similarly by solvation theory, gave $E_{cis} - E_{gauche} = 2.2$ kcal mol^{-1} in vapor phase, 0.91 kcal mol^{-1} in CCl_4, and -1.18 kcal mol^{-1} in DMSO. The ^3J(N, F) coupling constant was independent of the molecular conformation, as it did not change with the solvent polarity.

Lately, the techniques relyng on experimental heteronuclear NMR J values in configurational assignments of organic compounds have shown their great potential, and accordingly, they have been used to tackle a number of stereochemical problems.[124-127] Particularly, an important problem in the configurational assignment of complex natural products is to determine configuration of a molecule with one or more pairs of adjacent stereocenters. There are six main staggered rotamers (g^+, anti, and g^- rotamers for each of *erythro* and *threo*) for each pair of stereocenters. In principle, if one wanted to examine all the possible combinations of staggered rotamers, the number of staggered arrangements to be investigated is 6^n, where n is the number of pairs of stereocenters. However, since magnitudes of coupling constants are affected mainly by the local atomic environment and effects extending further than two atoms away from the nuclei involved in the coupling are usually not relevant. Full independence in the analysis of each pair of adjacent stereocenters requires only $6n$ staggered arrangements to be investigated. Bifulco *et al.*[128] performed the configurational assignment for the side chain of the marine macrolide reidispongiolide A using quantum mechanical calculations of NMR coupling constants at DFT level. They obtained an excellent agreement between calculated and experimental data.

Pihlaja *et al.*[129] studied the solution-state conformational equilibria of *trans*-4′,7-dihydroxysoflavan-4-ol and trans-isoflavan-4-ol based on the temperature dependence of their vicinal coupling constants J(H-2α, H-3) and J(H-3, H-4), which were compared to values calculated with DFT methods with the B3LYP functional. Several rotamers with respect to the C-4 hydroxyl and C-3 phenyl were calculated and the overall diequatorial-to-diaxial ratio at 298 K were assessed.

Bassarello *et al.*[130] performed DFT calculations of the spin–spin coupling constants for the ethyl ester of the *exo*-2-norbornanecarbamic acid. The obtained results were considered to be satisfactory.

There is an extensive literature on interproton coupling over four bonds ^4J(H, H′) in saturated and unsaturated molecules.[131-137] With modern NMR instrumentation, these data are easily obtainable now but are often difficult to interpret because of their sensitivity to conformational, substituent, and ring-size effects.

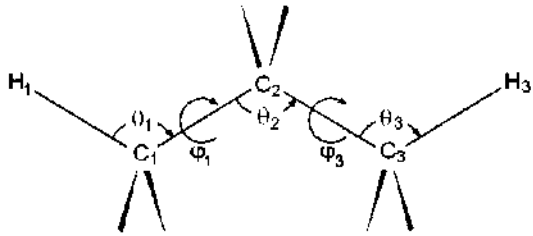

2

Barfield[138] presented a study of the structural dependencies for scalar J-coupling across four bonds in propanic and propenic systems, in which DFT and finite perturbation theory (FPT) were used to obtain the FC contributions to ^{1}H-^{1}H couplings. Interproton couplings ^4J(H, H′) in propane were obtained as a function of the dihedral angles φ_1 and φ_3, and the internal angle θ_2 in Scheme **2**. It was shown that the following trigonometric expression provides a fairly good representation of the DFT/FPT results for ^4J(H, H′) in propane:

$$^4J(\mathrm{H, H'})(\varphi_1, \varphi_3) = 0.82\cos^2\varphi_1\cos^2\varphi_3 - 0.62\cos\varphi_1\cos\varphi_3(\cos\varphi_1 + \cos\varphi_3) + 0.21\cos\varphi_1\cos\varphi_3 - 0.32\ \mathrm{Hz}. \quad (4.31)$$

However, eq. (4.31) was not, in general, applicable to bicyclic systems. The DFT/FPT propane-based results for couplings involving a methyl group (H-C-C-CH_3) were in better conformity with the experimental data. In contrast to the propanic coupling, the trigonometric expressions for propenic coupling constants were generally applicable to conformational analyses in bicycloalkenes.

Bagno *et al.*[139] determined ^{13}C chemical shifts and ^nJ(C, H) coupling constants both experimentally and theoretically (by DFT calculations) for a series of organic molecules. With the exception of halogen-bonded carbon nuclei, a good correlation was observed between experimental and calculated data. The PSO and DSO terms were negligible or canceled out for ^1J(C, H) and ^3J(C, H) couplings, thus leaving the FC term as the only relevant contribution to these couplings, but they became important for ^2J(C, H) in aromatic (but not in aliphatic) compounds. Conformational effects on the long-range ^nJ(C, H) coupling constants were investigated in a model alkane derivative (n-butyl cloride). It was concluded that the implications to structure prediction and determination by NMR spectra perform well and that their results obtained enable the NMR theoretical spectra of larger molecules to be directly synthesized.

9.8 Density Functional Theory Calculation of the Nuclear Spin–Spin Coupling Constants in C_{60}. – Ever since the first experimental evidence for the existence of C_{60}[140] and the subsequent verification that the molecule consists of sixty equivalent carbon atoms by the use of NMR spectroscopy[141,142], C_{60} has attracted a great deal of experimental and theoretical interest.[143] Jaszuński *et al.*[144] performed DFT calculations of the 23 indirect nuclear spin–spin coupling constants of C_{60} using the B3LYP functional. Knowledge of these couplings may help in unravelling the spectrum of ^{13}C-enriched C_{60}. For a highly symmetric molecule such as C_{60}, in which all carbon atoms are equivalent, it suffices to solve the response

equations for only one set of perturbing operators. All coupling constants can then be calculated at little or no extra cost. However, since the symmetry of the D_{2h} subgroup was used in the calculations of couplings for C_{60}, they needed to solve response equations for appropriately selected symmetry-adapted nuclear magnetic moments. They determined all 23 symmetry-distinct indirect nuclear spin–spin coupling constants by solving only 12 singlet and 28 triplet response equations. We note that there are three tensor components for each PSO operator, six for each SD operator, and one for each FC operator. The one-bond couplings within pentagons and between pentagons were 62 Hz and 77 Hz, respectively; the corresponding geminal couplings were 7 Hz and 1 Hz, respectively. Except for the vicinal couplings (about 4 Hz), the long-range couplings were all 1 Hz or smaller. The above calculation for C_{60} is the largest theoretical calculation to date of the complete set of indirect nuclear spin–spin coupling constants of a molecular system.

9.9 Nuclear Spin–Spin Coupling Constants in Hydrogen Bonded Complexes. – Progress in NMR spectroscopy has made it possible to use the nuclear spin–spin coupling constants not only as indirect evidence of hydrogen bonds[145] but also as direct evidence, owing to the recent discovery of intermolecular hydrogen-bond-transmitted spin–spin coupling constants. Such couplings have been observed in biomolecules[146–150] and in fluorine-containing clusters.[151,152] Cybulski *et al.*[153] investigated the nuclear spin–spin coupling constants in the dihydrogen-bonded A-H···H-D complexes, *i.e.*, LiH···H_2, LiH···CH_4, LiH···C_2H_6, and LiH···C_2H_2, in which the proton acceptor A-H is LiH, and the proton donors D-H's are H_2, CH_4, C_2H_6, and C_2H_2. Unlike the other three complexes, which can be classified as week van der Waals complexes, the LiH···C_2H_2 complex resembles a conventional hydrogen-bonded system. ^{1h}J(H, H) in LiH···C_2H_2 decayed exponentially with intermolecular distance as the ^{1h}J(H, H) of conventional hydrogen-bonded complexes does.[154–156] The reduced coupling constants ^{2h}K(H, X) between the proton of LiH and hydrogen or carbon nucleus of the proton donor correlated with the interaction energy, while ^{1h}J(H,H) did not correlate with the interaction energy. The reduced ^{2h}K(H,X) and ^{3h}K(Li, X) couplings correlated with the intermolecular distance.

The experimental observation of spin–spin coupling constants across hydrogen bonds, ^{nh}J, has created many exciting possibilities for the application of these parameters to biologically important compounds such as proteins,[157,158] DNA,[159] *etc.* Tuttle *et al.*[160] calculated the indirect nuclear spin–spin coupling constants across the H-bonds of the protein ubiquitin using coupled perturbed density functional theory (CPDFT) in combination with the B3LYP functional. They used four different models based on either the crystal or the aqueous solution structure of ubiquitin to describe H-bonding for selected residue pairs of ubiquitin. Two different spin–spin coupling mechanisms were identified. While mechanism I transmits spin polarization via an electric field effect, mechanism II involves also electron delocalization from the lone pair of the carbonyl oxigen to the antibonding orbital of the N-H bond. It was shown that mechanism I is more important in the crystal structure of ubiquitin, while in aqueous solution, mech-

anism II plays a larger role. The importance of the ^{3h}J(N, C′) and ^{1}J(N, H) constants was emphasized as descriptors for the H-bond.

Recent developments in computation suggest that genuine information on hydrogen bond strength, geometry, symmetry, and, in particular donor-accepter distance (r_{NN}) in "N-H ···N" systems is available through determination of the NMR coupling constants between the N centers.[149,150,161–164] Lloyd-Jones *et al.*[165] investigated the coupling constant between hydrogen bonded nitrogen centers, ^{2h}J(N, N), in the free-base and protonated forms of the complete series of [$^{15}N_2$]-N-methylated 1,8-diamino naphthalenes in [D_7]DMF solution. It was observed that the ^{2h}J(N, N) increases with increasing methylation. The following two explanations are possible for the increasing ^{2h}J(N, N) due to the methylation: (i) the inductive effect of the methyl groups (relative to hydrogen) results in an increased covalency,[166] and thus increased FC contribution across the cationic N-H···N unit[167] and/or (ii) the stronger hydrogen bonding of the N-H units to solvent in the lower number of methyl groups weakens the intramolecular hydrogen bond. The induction mechanism (i) was unlikely as the computed gas-phase coupling constants remained roughly constant with increasing methylation. In contrast, the solvation mechanism of the free N-H bonds (ii) was supported by the reduction in computed spin–spin coupling constants for lower numbers of the methyl groups. However, Lloyd-Jones *et al.* demonstrated that solvation of N-H groups, within the confines of the structural restrictions imposed by intramolecular N-H···N hydrogen bonding, can result in significant deviation of ^{2h}J(N, N) between experiment and theory. Therefore, until the ^{2h}J(N, N) *vs.* r_{NN} relation is determined in a much broader range of species, caution should be exercised in extracting N···N distances r_{NN} from the experimental ^{15}N, ^{15}N coupling constants ^{2h}J(N, N).

Recently, ^{1}J(C, H) one-bond coupling constants have been used to discuss both electric field effects[168,169] and hydrogen bonds involving CH bonds.[170–173] Hansen[174] investigated ^{1}J(C, H) coupling constants of acetyl groups of a series of substituted 2-hydroxyacetophenones. These ^{1}J(C, H) couplings were compared to that of acetophenone in order to elucidate the cause of the variation. An OR group in the 6-position of 2-hydroxycetophenones led to an increase of ^{1}J(C, H) of ~ 1 Hz. The variations in the ^{1}J(C, H) coupling constants of 6-OR substituted 2-hydroxyacetophenones were discussed as a function of C-H hydrogen bonding and electric field effects. The former was shown not to be at play, whereas the latter was clearly active.

9.10 Karplus-Type Relationships Between Scalar Coupling Constants. – Alkorta and Elguero[175] calculated theoretically the ^{3}J(H, H) coupling constants in the H-X-Y-H systems in six molecules (ethane, methylamine, methanol, hydrazine, hydroxylamine, and hydrogen peroxide) and ^{4h}J(H, H) coupling constants in four H-X···H···Y-H systems in complexes or dimers as a function of the torsion angle φ. The calculated values for coupling constants were fitted to the Karplus equation

$$^{3}J(\mathrm{H, H}) = a\cos 2\varphi + b\cos\varphi + c\,. \tag{4.32}$$

The parameters *a*, *b*, and *c* were analyzed as a function of the electronegativities of X and Y. The hydrogen-bonded ^{4h}J(H, H) values decreased nearly 100-fold from the covalent ^{3}J(H, H) values, but they followed closely a Karplus relationship.

Chou *et al.*[176] compared Karplus curves parametrized by using experimental ^{3}J couplings with those derived by best-fitting the results of DFT calculations carried out on conformers of valine and threonine dipeptide analogues. The experimentally parametrized Karplus curves agreed well with the curves obtained from DFT calculations.

10 Semiempirical Calculation of ^{13}C -^{13}C Coupling Constants

Krivdin and Kuznetsova[177] studied additivity of ^{13}C-^{13}C coupling constants in saturated sterically strained heterocycles using the self-consistent finite perturbation theory (SCFPT) and the contributions of localized molecular orbitals in terms of the polarization propagator theory (CLMOPPT) on a semiempirical level employng the intermediate neglect of differential overlap (INDO) approximation.[3] The fused derivatives of heterocycles, especially those containing 3rd period elements, showed considerable deviations of the calculated coupling constants from the additive values. Danilova and Krivdin[178] calculated ^{13}C-^{13}C coupling constants for all aldopyranoses of the D-series in terms of the SCFPT-INDO approximation. The results obtained made it possible to perform conformational analysis and assign configuration of the anomeric center in molecules of carbohydrates and products of their metabolism, containing a pyranose fragment.

References

1. J. E. Del Bene and J. Elguero, *Chem. Phys. Lett.*, 2003, **382**, 100.
2. J. E. Del Bene, J. Elguero, I. Alkorta, M. Yáñez, and O. Mo, *J. Chem. Phys.*, 2004, **120**, 3237.
3. J. A. Pople and D. L. Beveridge, in 'Approximate Molecular Orbital Theory', McGraw-Hill, New York, 1970.
4. R. P. Feynman, *Phys. Rev.*, 1939, **56**, 340.
5. H. Fukui, H. Inomata, T. Baba, K. Miura, and H. Matsuda, *J. Chem. Phys.*, 1995, **103**, 6597.
6. A. Soncini and P. Lazzeretti, *J. Chem. Phys.*, 2003, **119**, 1343.
7. R. McWeeny, *Rev. Mod. Phys.*, 1960, **32**, 335.
8. R. F. W. Bader and M. E. Stephens, *J. Am. Chem. Soc.*, 1975, **97**, 7391.
9. R. F. W. Bader, A. Streitwieser, A. Neuhaus, K. E. Laidig, and P. Speers, *J. Am. Chem. Soc.*, 1996, **118**, 4959.
10. R. F. W. Bader, S. Johnson, T. -H. Tang, and P. L. A. Popelier, *J. Phys. Chem.*, 1996, **100**, 15398.
11. T. Helgaker, M. Jaszuński, and K. Ruud, *Chem. Rev.*, 1999, **99**, 293.
12. R. D. Wigglesworth, W. T. Raynes, S. Kirpekar, J. Oddershede, and S. P. A. Sauer,

J. Chem. Phys., 2000, **112**, 3735.
13. R. D. Wigglesworth, W. T. Raynes, S. Kirpekar, J. Oddershede, and S. P. A. Sauer, *J. Chem. Phys.*, 2001, **114**, 9192.
14. S. M. Bass, R. L. DeLeon, and J. S. Muenter, *J. Chem. Phys.*, 1987, **86**, 4305.
15. J. S. Muenter and W. Klemperer, *J. Chem. Phys.*, 1970, **52**, 6033.
16. T. A. Ruden, O. B. Lutnæs, T. Helgaker, and K. Ruud, *J. Chem. Phys.*, 2003, **118**, 9572.
17. C. W. Kern and R. L. Matcha, *J. Chem. Phys.*, 1968, **49**, 2081.
18. W. C. Ermler and C. W. Kern, *J. Chem. Phys.*, 1971, **55**, 4851.
19. B. J. Krohn, W. C. Ermler, and C. W. Kern, *J. Chem. Phys.*, 1974, **60**, 22.
20. P. -O. Åstrand, K. Ruud, and P. Taylor, *J. Chem. Phys.*, 2000, **112**, 2655.
21. M. Toyma, T. Oka, and Y. Morino, *J. Mol. Spectrosc.*, 1964, **13**, 193.
22. W. T. Raynes, J. Geertsen, and J. Oddershede, *Int. J. Quantum Chem.*, 1994, **52**, 153.
23. T. Helgaker, M. Watson, and N. C. Handy, *J. Chem. Phys.*, 2000, **113**, 9402.
24. S. Huzinaga, in 'Approximate Atomic Functions', University of Alberta, Edmonton, 1971.
25. S. Huzinaga, *J. Chem. Phys.*, 1965, **42**, 1293.
26. W. Kutzelnigg, U. Fleischer, and M. Schindler, in 'NMR–Basic Principles and Progress', Springer Verlag, Berline, 1990, Vol. 23, p. 165.
27. T. A. Ruden, T. Helgaker, and M. Jaszuński, *Chem. Phys.*, 2004, **296**, 53.
28. J. W. Emsley and J. C. Lindon, in 'NMR Spectroscopy Using Liquid Crystal Solvents', Pergamon, Oxford, 1975.
29. J. Lounila and J. Jokisaari, *Prog. Nucl. Magn. Reson. Spectrosc.*, 1982, **15**, 249.
30. J. Vaara, J. Jokisaari, R. E. Wasylishen, and D. L. Bryce, *Prog. Nucl. Magn. Reson. Spectrosc.*, 2002, **41**, 233.
31. R. E. Wasylishen, in 'Encyclopedia of Nuclear Magnetic Resonance', ed. D. M. Grant and R. K. Harris, Wiley, Chichester, 1996, p. 1685.
32. R. E. Wasylishen, in 'Encyclopedia of Nuclear Magnetic Resonance', ed. D. M. Grant and R. K. Harris, Wiley, Chichester, 2002, p. 274.
33. D. L. Bryce and R. E. Wasylishen, *J. Am. Chem. Soc.*, 2000, **122**, 3197.
34. A. Saupe, Z. Naturforsh., 1964, **19a**, 161.
35. J. Jokisaari and J. Autschbach, *Phys. Chem. Chem. Phys.*, 2003, **5**, 4551.
36. J. Autschbach and T. Ziegler, *J. Chem. Phys.*, 2000, **113**, 9410.
37. E. van Lenthe, E. J. Baerends, and J. G. Snijders, *J. Chem. Phys.*, 1993, **99**, 4597.
38. K. Dyll and E. van Lenthe, *J. Chem. Phys.*, 1999, **111**, 1366.
39. E. J. Baerends *et al.*, Amsterdam Density Functional, Theoretical Chemistry, version 2002. 03, Vrije University, Amsterdam. http://www.scm.com/.
40. G. te Velde, F. M. Bickelhaupt, E. J. Baerends, S. J. A. van Gisbergen, C. Fonseca Guerra, J. G. Snijders, and T. Ziegler, *J. Comput. Chem.*, 2001, **22**, 931.
41. C. Fonseca Guerra, J. G. Snijders, G. te Velde, and E. J. Baerends, *Theor. Chem. Acc.*, 1998, **99**, 391.
42. N. Tjandra and A. Bax, *Science*, 1997, **278**, 1111.
43. D. L. Bryce and R. E. Wasylishen, *J. Biomol. NMR*, 2003, **25**, 73.
44. M. A. M. Forgeron, R. E. Wasylishen, and G. H. Penner, *J. Phys. Chem. A*, 2004, **108**, 4751.
45. J. E. Del Bene, I. Alkorta, and J. Elguero, *Z. Phys. Chem.*, 2003, **217**, 1565.
46. G. W. Flynn, M. Matsushima, J. D. Baldeschwieler, and N. C. Craig, *J. Chem. Phys.*, 1963, **38**, 2995.
47. V. Barone, P. F. Provasi, J. E. Peralta, J. P. Snyder, S. P. A. Sauer, and R. H. Contreras, *J. Phys. Chem. A*, 2003, **107**, 4748.

48. I. Alkorta and J. Elguero, *Struct. Chem.*, 2004, **15**, 117.
49. R. F. W. Bader, in 'Atoms in Molecules: A Quantum Theory (The International Series of Monographs of Chemistry)', ed. J. Halpen, and M. L. H. Green, Clarendon Press, Oxford, 1990.
50. R. F. W. Bader, *J. Phys. Chem. A*, 1998, **102**, 7314.
51. T. J. Lee and G. E. Scuseria, in 'Quantum Mechanical Electronic Structure Calculations with Chemical Accuracy', ed. S. R. Langhoff Kluwer, Dordrecht, 1995, p. 47.
52. J. Gauss, in 'Encyclopedia of Computational Chemistry', ed. P. v. R. Schleyer, N. L. Allinger, T. Clark, J. Gasteiger, P. Kollmann. H. F. Schaefer, and R. R. Schreiner, Wiley, Chichester, 1998, p. 615.
53. S. A. Perera, H. Sekino, and R. J. Bartlett, *J. Chem. Phys.*, 1994, **101**, 2186.
54. S. A. Perera, M. Nooijen, and R. J. Bartlett, *J. Chem. Phys.*, 1996, **104**, 3290.
55. T. Enevoldsen, J. Oddershede, and S. P. A. Sauer, *Theor. Chem. Acc.*, 1998, **100**, 275.
56. A. A. Auer and J. Gauss, *J. Chem. Phys.*, 2001, **115**, 1619.
57. K. Ruud, T. Helgaker, K. L. Bak, P. Jørgensen, and J. Olsen, *Chem. Phys.*, 1995, **195**, 157.
58. J. Gauss and K. Ruud, *Int. J. Quantum. Chem. Symp.*, 1995, **29**, 437.
59. H. Larsen, J. Olsen, C. Hättig, P. Jørgensen, O. Christiansen, and J. Gauss, *J. Chem. Phys.*, 1999, 111, 1917.
60. H. Larsen, J. Olsen, P. Jørgensen, and J. Gauss, *Chem. Phys. Lett.*, 2001, **342**, 200.
61. A. A. Auer, J. Gauss, and M. Pecul, *Chem. Phys. Lett.*, 2003, **368**, 172.
62. E. A. Salter, H. Sekino, and R. J. Bartlett, *J. Chem. Phys.*, 1987, **87**, 502.
63. L. B. Krivdin, *Magn. Reson. Chem.*, 2003, **41**, 417.
64. T. H. Dunning Jr., *J. Chem. Phys.*, 1989, **90**, 1007.
65. R. A. Kendall, T. H. Dunning Jr., and R. J. Harrison, *J. Chem. Phys.*, 1992, **96**, 6796.
66. D. E. Woon and T. H. Dunning Jr., *J. Chem. Phys.*, 1993, **98**, 1358.
67. L. B. Krivdin, *Magn. Reson. Chem.*, 2003, **41**, 885.
68. L. B. Krivdin, *Magn. Reson. Chem.*, 2004, **42**, 1.
69. L. B. Krivdin and T. A. Kuznetsova, *Russ. J. Org. Chem.*, 2003, **39**, 1618.
70. K. Jackowski, *Int. J. Mol. Sci.*, 2003, **4**, 135.
71. K. Jackowski, M. Wilczek, M. Pecul, and J. Sadlej, *J. Phys. Chem. A*, 2000, **104**, 5955.
72. J. Kaski, P. Lantto, J. Vaara, and J. Jokisaari, *J. Am. Chem. Soc.*, 1998, **120**, 3993.
73. R. D. Wigglesworth, W. T. Raynes, S. Kirpekar, *J. Oddershede, and S. P. A. Sauer, J. Chem. Phys.*, 2000, **112**, 736.
74. R. D. Wigglesworth, W. T. Raynes, S. Kirpekar, *J. Oddershede, and S. P. A. Sauer, J. Chem. Phys.*, 2000, **114**, 9192.
75. M. Jaszuński and K. Ruud, *Chem. Phys. Lett.*, 2001, **336**, 473.
76. M. A. Watson, N. C. Handy, A. J. Cohen, and T. Helgaker, *J. Chem. Phys.*, 2004, **120**, 7252.
77. A. J. Cohen and N. C. Handy, *J. Chem. Phys.*, 2002, **117**, 1470.
78. M. A. Watson, N. C. Handy, and A. J. Cohen, *J. Chem. Phys.*, 2003, **119**, 6475.
79. J. E. Peralta, G. E. Scuseria, J. R. Cheeseman, and M. J. Frisch, *Chem. Phys. Lett.*, 2003, **375**, 452.
80. D. E. Woon and T. H. Dunning Jr., *J. Chem. Phys.*, 1995, **103**, 4572.
81. J. Gräfenstein, E. Kraka, and D. Cremer, *J. Phys. Chem. A*, 2004, **108**, 4520.
82. J. Autschbach and B. Le Guennic, *J. Am. Chem. Soc.*, 2003, **125**, 13585.
83. M. Maliarik, K. Berg, J. Glaser, M. Sandström, and I. Tóth, *Inorg. Chem.*, 1998, 37, 2910.
84. G. Ma, M. Kritikos, and J. Glaser, *Eur. J. Inorg. Chem.*, 2001, 1311.

85. G. Ma, A. Fischer, and J. Glaser, *Eur. J. Inorg. Chem.*, 2002, 1307.
86. J. Autschbach and T. Ziegler, *J. Am. Chem. Soc.*, 2001, **123**, 5320.
87. P. R. T. Schipper, O. V. Gritsenko, S. J. A. van Gisbergen, and E. J. Baerends, *J. Chem. Phys.*, 2000, **112**, 1344.
88. O. V. Gritsenko, P. R. T. Schipper, and E. J. Baerends, *Int. J. Quantum Chem.*, 2000, **76**, 407.
89. D. P. Chong, O. V. Gritsenko, and E. J. Baerends, *J. Chem. Phys.*, 2002, **116**, 1760.
90. M. Grüning, O. V. Gritsenko, S. J. A. van Gisbergen, and E. J. Baerends, *J. Chem. Phys.*, 2002, **116**, 9591.
91. S. J. A. van Gisbergen, J. M. Pacheco, and E. J. Baerends, *Phys. Rev. A*, 2001, **63**, 63201.
92. V. Sychrovský, J. Šponer, and P. Hobza, *J. Am. Chem. Soc.*, 2004, **126**, 663.
93. G. J. Kubas, in 'Metal Dihydrogen and σ-Bond Complexes', Kluwer Academic/Plenum, New York, 2001.
94. R. H. Crabtree, *Angew. Chem. Int. Ed. Engl.*, 1993, **32**, 789.
95. U. Schubert, *Adv. Organomet. Chem.*, 1990, **30**, 151.
96. J. Y. Corey and J. Braddock-Wilking, *Chem. Rev.*, 1999, **99**, 175.
97. G. I. Nikonov, *J. Organomet. Chem.*, 2001, **635**, 24.
98. G. I. Nikonov, *Angew. Chem. Int. Ed. Engl.*, 2001, **40**, 3353.
99. S. R. Dubberley, S. K. Ignatov, N. H. Rees, A. G. Razuvaev, P. Mountford, and G. I. Nikonov, *J. Am. Chem. Soc.*, 2003, **125**, 642.
100. G. I. Nikonov, L. G. Kuzmina, S. F. Vyboishchikov, D. A. Lemenovskii, and J. A. K. Howard, *Chem.-Eur. J.*, 1999, **5**, 2497.
101. V. I. Bakhmutov, J. A. K. Howard, D. A. Keen, L. G. Kuzmina, M. A. Leech, G. I. Nikonov, E. V. Vorontsov, and C. C. Wilson, *Dalton Trans.*, 2000, 1631.
102. G. I. Nikonov, P. Mountford, S. K. Ignatov, J. C. Green, P. A. Cooke, M. A. Leech, L. G. Kuzmina, A. G. Razuvaev, N. H. Rees, A. J. Blake, J. A. K. Howard, and D. A. Lemenovskii, *Dalton Trans.*, 2001, 2903.
103. J. G. Verkade, *Acc. Chem. Res.*, 1993, **26**, 483.
104. J. G. Verkade, *Coord. Chem. Rev.*, 1994, **137**, 233.
105. J. -S. Tang and J. G. Verkade, *Synth. Methods Organomet. Inorg. Chem.*, 1996, **3**, 177.
106. J. G. Verkade and P. B. Kisanga, *Tetrahedron*, 2003, **59**, 7819.
107. J. G. Verkade, *Top. Curr. Chem.*, 2003, **223**, 1.
108. P. B. Kisanga and J. G. Verkade, *J. Org. Chem.*, 2000, **65**, 5431.
109. M. A. H. Laramay and J. G. Verkade, *J. Am. Chem. Soc.*, 1990, **112**, 9421.
110. V. Galasso, *J. Phys. Chem. A*, 2004, **108**, 4497.
111. T. Ratajczyk, M. Pecul, J. Sadlej, and T. Helgaker, *J. Phys. Chem. A*, 2004, **108**, 2758.
112. C. F. Tormena, R. Rittner, R. J. Abraham, E. A. Basso, and B. C. Fiorin, *J. Phys. Org. Chem.*, 2004, **17**, 42.
113. J. E. Peralta, V. Barone, R. H. Contreras, D. G. Zaccari, and J. P. Snyder, *J. Am. Chem. Soc.*, 2001, **123**, 9162.
114. J. E. Peralta, V. Barone, M. C. Ruiz de Azúa, and R. H. Contreras, *Mol. Phys.*, 2001, **99**, 655.
115. V. Barone, J. E. Peralta, and R. H. Contreras, *J. Comput. Chem.*, 2001, **22**, 1615.
116. L. B. Krivdin, S. P. A. Sauer, J. E. Peralta, and R. H. Contreras, *Magn. Reson. Chem.*, 2002, **40**, 187.
117. R. J. Abraham, A. D. Jones, M. A. Warne, R. Rittner, and C. F. Tormena, *J. Chem. Soc., Perkin Trans. 2*, 1996, 533.

118. R. J. Abraham, C. F. Tormena, and R. Rittner, *J. Chem. Soc., Perkin Trans. 2*, 1999, 1663.
119. C. F. Tormena, R. Rittner, R. J. Abraham, E. A. Basso, and R. M. Pontes, *J. Chem. Soc., Perkin Trans. 2*, 2000, 2054.
120. R. J. Abraham, C. F. Tormena, and R. Rittner, *J. Chem. Soc., Perkin Trans. 2*, 2001, 815.
121. C. F. Tormena, R. Rittner, and R. J. Abraham, *J. Phys. Org. Chem.*, 2002, **15**, 211.
122. C. F. Tormena, N. S. Amadeu, R. Tittner, and R. J. Abraham, *J. Chem. Soc., Perkin Trans. 2*, 2002, 773.
123. M. P. Freitas, R. Rittner, C. F. Tormena, and R. J. Abraham, *J. Phys. Org. Chem.*, 2001, **14**, 317.
124. N. Matsumori, D. Kaneno, M. Murata, H. Nakamura, and K. Tachibana, *J. Org. Chem.*, 1999, **64**, 866.
125. C. Bassarello, G. Bifulco, A. Zampella, M. V. D'Auria, R. Riccio, and L. Gomez-Paloma, *Eur. J. Org. Chem.*, 2001, **1**, 39.
126. C. Bassarello, G. Bifulco, A. Evidente, R. Riccio, and L. Gomez-Paloma, *Tetrahedron Lett.*, 2001, **42**, 8611.
127. P. Cimino, G. Bifulco, A. Evidente, M. Abouzeid, R. Riccio, and L. Gomez-Paloma, *Org. Lett.*, 2002, **4**, 2779.
128. G. Bifulco, C. Bassarello, R. Riccio, and L. Gomez-Paloma, *Org. Lett.*, 2004, **6**, 1025.
129. K. Pihlaja, P. Tähtinen, K. D. Klika, T. Jokela, A. Salakka, and K. Wähälä, *J. Org. Chem.*, 2003, **68**, 6864.
130. C. Bassarello, P. Cimino, L. Gomez-Paloma, R. Riccio, and G. Bifulco, *Tetrahedron*, 2003, **59**, 9555.
131. S. Sternhell, *Rev. Pure Appl. Chem.*, 1964, **14**, 15.
132. E. W. Garbisch Jr., *Chem. Ind. (London)*, 1964, **41**, 1715.
133. M. Barfield and B. Chakrabarti, *Chem. Rev.*, 1969, **69**, 757.
134. S. Sternhell, *Q. Rev. Chem. Soc.*, 1969, **23**, 236.
135. M. Barfield, R. J. Spear, and S. Sterhell, *Chem. Rev.*, 1976, **76**, 593.
136. W. A. Thomas, *Prog. Nucl. Magn. Reson. Spectrosc.*, 1997, **30**, 183.
137. R. H. Contreras and J. E. Peralta, *Prog. Nucl. Magn. Reson. Spectrosc.*, 2000, **37**, 321.
138. M. Barfield, *Magn. Reson. Chem.*, 2003, **41**, 344.
139. A. Bagno, F. Rastrelli, and G. Saielli, *J. Phys. Chem. A, 2003*, **107**, 9964.
140. H. W. Kroto, J. R. Heath, S. C. O'Brien, R. F. Curl, and R. E. Smalley, *Nature*, 1985, 318, **162**.
141. R. Taylor, J. P. Hare, A. K. Absulsada, and H. W. Kroto, *J. Chem. Soc. Chem. Commun.*, 1990, 1423.
142. H. Ajie, M. M. Alvarez, S. J. Anz, R. D. Beck, F. Diederich, K. Fostiropoulos, D. R. Huffman, W. Krätschmer, Y. Rubin, K. E. Schriver, D. Sensharma, and R. L. Whetten, *J. Phys. Chem.*, 1990, **94**, 8630.
143. J. Cioslowski, in 'Electronic Structure Calculations on Fullerenes and Their Derivatives', Oxford University Press, Oxford, 1995.
144. M. Jaszuński, K. Ruud, and T. Helgaker, *Mol. Phys.*, 2003, **101**, 1997.
145. N. Juranic, P. K. Ilich, and S. Macura, *J. Am. Chem. Soc.*, 1995, **117**, 405.
146. F. Cordier and S. Grzesiek, *J. Am. Chem. Soc.*, 1999, **121**, 1601.
147. G. Cornilescu, J.-S. Hu, and A. Bax, *J. Am. Chem. Soc.*, 1999, **121**, 2949.
148. F. Cordier, M. Rogowski, S. Grzesiek, and A. Bax, *J. Magn. Reson.*, 1999, **140**, 510.
149. A. J. Dingley and S. Grzesiek, *J. Am. Chem. Soc.*, 1998, 120, 8293.

150. A. J. Dingley, J. E. Masse, R. D. Peterson, M. Barfield, J. Feigon, and S. Grzesiek, *J. Am. Chem. Soc.*, 1999, **121**, 6019.
151. I. G. Shenderovich, S. N. Smirnov, G. S. Denisov, V. A. Gindin, N. S. Golubev, A. Dunger, R. Reibke, S. Kirpekar, O. L. Malkina, and H. -H. Limbach, *Ber. Bunsenges. Phys. Chem.*, 1998, **102**, 422.
152. N. S. Golubev, I. G. Shenderovich, S. N. Smirnov, G. S. Denisov, and H. -H. Limbach, *Chem. Eng. J.*, 1999, **5**, 492.
153. H. Cybulski, M. Pecul, J. Sadlej, and T. Helgaker, *J. Am. Chem. Soc.*, 2003, **119**, 5094.
154. M. Pecul, J. Leszczynski, and J. Sadlej, *J. Phys. Chem. A, 2000*, **104**, 8105.
155. M. Pecul and J. Sadlej, *Chem. Phys. Lett.*, 2002, **360**, 272.
156. C. Scheurer and R. Brüschweiler, *J. Am. Chem. Soc.*, 1999, **121**, 8661.
157. Y. -X. Wang, J. Jacob, F. Cordier, P. Wingfield, S. J. Stahl, S. Lee Huang, D. Torchia, S. Grezesiek, and A. Bax, *J. Biomol. NMR*, 1999, **14**, 181.
158. F. Lohr, S. G. Mayhew, and H. Ruterjans, *J. Am. Chem. Soc.*, 2000, **122**, 9289.
159. A. J. Dingley, J. E. Masse, J. Feigon, and S. Grezesiek, *J. Biomol. NMR, 2000*, **16**, 279.
160. T. Tuttle, E. Kraka, A. Wu, and D. Cremer, *J. Am. Chem. Soc.*, 2004, **126**, 5093.
161. H. Benedict, I. G. Shenderovich, O. L. Malkina, V. G. Malkin, G. S. Denisov, N. S. Golubev, and H. -H. Limbach, *J. Am. Chem. Soc.*, 2000, **112**, 1979.
162. J. E. Del Bene and R. J. Bartlett, *J. Am. Chem. Soc.*, 2000, **122**, 10480.
163. J. E. Del Bene, S. A. Perera, and R. J. Bartlett, *Magn. Reson. Chem.*, 2001, **39**, S109.
164. D. L. Bryce and R. E. Wasylishen, *J. Biomol. NMR*, 2001, **19**, 371.
165. G. C. Lloyd-Jones, J. N. Harvey, P. Hodgson, M. Murray, and R. L. Woodward, *Chem. Eur. J.*, 2003, **9**, 4523.
166. W. D. Arnold and E. Oldfield, *J. Am. Chem. Soc.*, 2000, **122**, 12835.
167. S. J. Wilkens, W. M. Westler, J. L. Markley, and F. Weinhold, *J. Am. Chem. Soc.*, 2001, **123**, 12026.
168. D. G. De Kowalewski, V. J. Kowalewski, J. E. Peralta, G. Shuche, R. H. Contreras, A. L. Esteban, M. P. Galache, and E. Diez, *Magn. Reson. Chem.*, 1999, **37**, 227.
169. R. H. Contreras, J. E. Peralta, C. G. Giribet, M. C. Ruiz de Azúa, and J. C. Facelli, *Ann. Rep. NMR Spectrosc.*, 2000, **41**, 55.
170. M. P. M. Marques, A. M. Amorim da Costa, and P. J. A. Ribeiro-Claro, *J. Phys. Chem. A*, 2001, **105**, 5292.
171. H. Satonaka, K. Abe, and M. Hirota, *Bull Chem. Soc. Jpn.*, 1988, **61**, 2031.
172. A. V. Afonin, M. V. Sgalov, S. E. Korostova, I. A. Aliev, A. V. Vaschchenko, and B. A. Trofimov, *Magn. Reson. Chem.*, 1990, **28**, 580.
173. C. Viziolo, M. C. Ruiz. de Azúa, C. G. Giribet, R. H. Contreras, L. Turi, J. J. Dannenberg, I. D. Rae, J. A. Weigod, M. Malagoi, R. Zanasi, and P. Lasseretti, *J. Phys. Chem.*, 1994, **98**, 8858.
174. P. E. Hansen, *Polish J. Chem.*, 2003, **77**, 1683.
175. I. Alkorta and J. Elguero, *Theor. Chem. Acc.*, 2004, **111**, 31.
176. J. J. Chou, D. A. Case, and A. Bax, *J. Am. Chem. Soc.*, 2003, **125**, 8959.
177. L. B. Krivdin and T. A. Kuznetsova, *Russ. J. Org. Chem.*, 2003, **39**, 698.
178. V. A. Danilova and L. B. Krivdin, *Russ. J. Org. Chem.*, 2003, **39**, 663.

5
Applications of spin–spin couplings

KRYSTYNA KAMIEŃSKA-TRELA AND JACEK WÓJCIK

1 Introduction

The material in this chapter covers the period from 1 June 2003 to 31 May 2004. It has been arranged as was done previously,[1] *i.e.* according to (i) the increasing atomic number of the nuclei involved, and (ii) the number of the bonds separating them. We follow the IUPAC[2] recommendations with one notable exception, namely, the nucleus with the smaller mass is given first. For the sake of simplicity the following symbols were used throughout the paper: H for ^{1}H, D – ^{2}H, T – ^{3}H, Li – ^{6}Li, Be – ^{9}Be, B – ^{11}B, C – ^{13}C, N – ^{15}N, O – ^{17}O, F – ^{19}F, Al –^{27}Al, Si – ^{29}Si, P – ^{31}P, S – ^{33}S, V – ^{51}V, Mn – ^{55}Mn, Fe – ^{57}Fe, Co – ^{59}Co, Cu – ^{65}Cu, As- ^{75}As, Se – ^{77}Se, Br – ^{79}Br, Y – ^{89}Y, Nb – ^{93}Nb, Mo – ^{95}Mo, Ru – ^{99}Ru, Tc - ^{99}Tc, Rh – ^{103}Rh, Ag – ^{109}Ag, CD – ^{113}Cd, In – $^{113/115}$In, Sn – ^{119}Sn, Te – ^{125}Te, I – ^{127}I, Cs – ^{133}Cs, W – ^{183}W, Os – ^{187}Os, Pt – ^{195}Pt, Hg – ^{199}Hg, Tl – ^{205}Tl, Pb -- ^{207}Pb. All the other isotopes are described explicitly.

A short review on shielding and spin-spin couplings measured in the gas-phase has been published by Jackowski.[3] These parameters can be at present obtained for gaseous samples containing several micrograms of a solute compound and are therefore free from intermolecular contribution.

An extensive review on intramolecular interactions of polyethers and polysulfides investigated by NMR has been written by Sasanuma.[4] The author also discusses the application of vicinal couplings in conformational analysis of these compounds. Two-dimensional NMR methods of polymers have been reviewed by Newmark.[5]

The methods to determine rotamer populations from NMR homo- and heteronuclear vicinal couplings have been reviewed by Kraszni *et al.*,[6] who also assessed properties and capacities of the Karplus-type equations. NMR studies of chiral recognition by cyclodextrins which manifests itself in all NMR parameters including couplings have been reviewed by Dodziuk *et al.*[7]

Two reviews have been devoted to structure elucidation, mostly by the use of NMR methods, of the compounds isolated from marine organisms. One has been written by Ciminiello and Fattorusso[8] on shellfish toxins from northern Adriatic mussels, the other, by Kobayashi and Tsuda,[9] covers a series of cytotoxic macrolides named amphidinolides, isolated from symbiotic marine dinoflagellates of the genus *Amphidinium* which were separated from inside cells

Nuclear Magnetic Resonance, Volume 34
© The Royal Society of Chemistry, 2005

of marine flatworms.

An extensive review on NMR spectroscopy of RNA in which also homo- and heteronuclear couplings are discussed has been written by Schwalbe and co-workers.[10] A review on the role of NMR spectroscopy in structure-aided drug design, in which a special attention has been paid to dipolar couplings, has been published by Homans.[11]

A short overlook on transverse relaxation-optimized spectroscopy (TROSY) in combination with various isotope-labelling techniques has been published by Fernández and Wider.[12] The method improves, among others, the detection of scalar couplings across hydrogen bonds, providing crucial information on the determination of solution structures of large proteins and oligonucleotides.

Conformational studies in solution, homology models and comparison with other zinc metallopeptidases have been reviewed by Spyroulias *et al.*[13] A review on the application of NMR spectroscopy in the study of carbohydrates has been written by Bubb,[14] and a short review on conformational analysis of arabinofuranosides, galactofuranosides and fructofuranosides has been published by Lowary.[15]

^{19}F NMR chemical shifts and couplings have been collected by Foris for 215 variously substituted halocarbons.[16] The collection includes $^{8}J_{FF}$ and $^{5}J_{HF}$ couplings; the author also briefly discusses the methods used for analysing sometimes very complex spectra.

A review on fluorinated macrocycles, a new donor (C-F) for cations which are characterized *inter alia* by the F-Cs and F-Tl couplings has been written by Takemura.[17] A review on ^{183}W NMR spectroscopy in the study of polyoxometalates has been written by Chen *et al.*[18]

A tool kit, *BlochLib*, designed to be the next generation of NMR simulation packages has been described by Blanton.[19] It enables the user to simulate almost any NMR idea both experimental or theoretical.

2 New Methods

A new HMBC-RELAY pulse sequence that detects simultaneously $^{n}J_{HC}$ and $^{2}J_{HC}$ connectivities has been designed by Sprang and Bigler.[20] The corresponding coherences are created along independent pathways and therefore can be separated into two different subspectra. One spectrum is to show all $^{n}J_{HC}$ connectivities and the other is to show exclusively $^{2}J_{HC}$ connectivities.

Edden and Keeler[21] have described a number of improvements to a method developed by them some time ago[22] which facilitate determination of the values of long-range H-C couplings from heteronuclear multiple bond correlation (HMBC) spectra.

A recently described by Hosur and co-workers[23] triple resonance HN(C)N experiment originally designed for the sequential correlation of H_N and atoms ^{15}N in ^{15}N and ^{13}C enriched proteins has been used by them[24] for the estimation of one-bond C^{α}-N couplings in medium size labelled proteins.

A method which allows accurate and sign-sensitive measuring of J_{HN} and J_{HNH}

couplings has been proposed by Luy.[25] In this approach S^3CT and S^3E-type experiments are created, and CW-cross-polarization as the heteronuclear Hartmann-Hahn sequence has been used.

A new pulse sequence which applies a Carr-Purcell-Meiboom-Gill-type sequence to heteronuclear multiple bond correlation spectroscopy has been designed by Koskela *et al.*[26] It allows one to extract the long-range heteronuclear H-C couplings from a long-range H-C correlation experiment directly from COSY-type antiphase peak patterns. Their approach utilizes CPMG-sequences for polarization transfer, and thus avoids the evolution of homonuclear J_{HH} couplings, which normally may introduce abnormalities into the cross peak pattern.

A selective 2D intermolecular zero-quantum coherences pulse sequence, SEL-HOMOGENIZED, which effectively suppresses strong solvent signals and other trivial signals, has been developed by Chen *et al.*[27] In the homogeneous-like 1D spectrum extracted from the 2D data, chemical shifts, couplings, multiplicity patterns, and relative peak areas are almost independent of the magnetic field inhomogeneity.

A general systematic procedure which allows one to easily analyse first order multiplets has been proposed by del Rio Portilla *et al.*[28] The method has the advantage of measuring couplings while deconvoluting the signals, at the same time using an extension of the modified *J* doubling in the frequency domain.

Direct observation of very small dipolar couplings between distant protons in the overcrowded spectra of biological molecules represents a challenging task. Now Bax and co-workers[29] have presented a method which, by the appropriate manipulation of the nuclear spin Hamiltonian, allows effective decoupling of all protons outside a spectral region of interest and facilitates observation of interactions between remote protons separated by distances of up to 12 Å. The method has been applied to measure remote dipolar couplings in an unlabelled nucleic acid.

A simple and accurate experiment by means of which five RDCs can be extracted from a single E.COSY experiment cross-peak pattern for the ribose sugars in an RNA oligomer has been designed by O'Neil-Cabello *et al.*[30] The $^1D_{HC}$, $^2D_{HC}$ and $^3D_{HH}$ have been determined for the H-C-C-H ribose spin system. Miclet *et al.*[31] have designed a simple 2D NMR experiment that allows accurate measurement of both the sum of the H_A-C and H_B-C and the geminal H_A-H_B coupling in the methylene group, even in the regions of the NMR spectrum that are considered inaccessible due to spectral crowding. The experiment also yields ^1D values, important complementary restraints in structure elucidation.

A 2D-HSQC-carbon selective/proton selective-constant time COSY, 2D-HSQC-(sel C, sel H)-CT COSY experiment, which is applicable to uniformly ^{13}C istopically enriched samples (U-^{13}C) of oligosaccharides or oligonucleotides, has been proposed by Martin-Pastor *et al.*[32] for the measurement of proton-proton RDC in crowded regions of 2D-spectra. In addition, a heteronuclear constant time-COSY experiment, ^{13}C-^{13}C CT COSY, has been proposed for the measurement of one bond carbon-carbon RDC in these molecules.

A new sensitivity improved approach to measure the H_α-C_α scalar and dipolar

couplings in $^{13}C/^{15}N$-labelled proteins using a HA(CA)CONH scheme has been presented by Hu *et al.*[33] A sensitive approach for simultaneous measurement of $^{1}D_{H\alpha C\alpha}$ and $^{2}D_{H\alpha N}$ couplings based on HNCA-type experiments has been proposed by Permi.[34] The magnitude of $^{2}D_{H\alpha N}$ is comparable to that of $^{1}D_{C'N}$, and it can be measured with good accuracy on the slowly relaxing TROSY cross peak from the ^{15}N dimension. Two *J*-modulated HMQC type experiments which allow accurate and individual measurements of the one-bond heteronuclear couplings and their dipolar contributions in methylene and amine moieties have been proposed by Kövér and Fehér.[35] To check the method, 4,6-*O*-ethylidene-α,β-D-glucopyranose has been chosen.

A G-BIRD$^{(r)}$ modified F1 coupled HSQC experiment for the accurate determination of one-bond heteronuclear residual dipolar couplings has been devised by Fehér *et al.*[36] In this approach all the long-range couplings of the heteronucleus are decoupled and only the one-bond coupling to the directly bonded proton is retained. It is worth noting that the G-BIRD module can be easily incorporated in any other variant of HSQC sequence.

Ding and Gronenborn have presented a novel E.COSY N-H^{N} HSQC experiment for accurate simultaneous measurement of one-bond C′-N and two-bond H_N-C′ dipolar couplings[37] as well as a simple, sensitivity-enhanced experiment for measuring the H_N-C_α and N-C_α couplings,[38] based in part on the normal sensitivity-enhanced ^{15}N-$^{1}H_N$ HSQC experiment with backbone H_N-C_α and N-C_α couplings active during the evolution and detection periods, respectively. Furthermore, sensitivity-enhanced 2D IPAP experiments for measuring one-bond C-C_α, H_α-C_α[39] and H_N-N residual dipolar couplings[40] have been proposed by the same authors. In the latter case also sensitivity-enhanced versions of TROSY-anti-TROSY and E.COSY experiments have been described.

Bryce and Bax[41] have proposed a method which exploits the correlated nature of RDCs for structural elements of planar geometry, such as the one-bond C'_i-C^α_i, C'_i-N_{i+1} and N_{i+1}-H^N_{i+1} couplings in peptide bonds of proteins, or suitably chosen combinations of $^{1}D_{H1'C1'}$, $^{1}D_{H2'C2'}$, $^{1}D_{C2'C1'}$, $^{2}D_{H1'C2'}$, $^{2}D_{H2'C1'}$, and $^{3}D_{H1'H2'}$ couplings in nucleic acids, to generate an arbitrarily large number of synthetic RDCs. These synthetic couplings result in substantially improved histograms and values of the magnitude and rhombicity of the molecular alignment tensor compared with histograms generated solely from the original sets of correlated RDCs.

A method which allows testing NMR data such as dipolar couplings, anisotropic chemical shieldings and quadrupolar interactions has been proposed by Žídek *et al.*[42] The authors have used the fact that only a limited number of frequencies corresponding to these parameters can be measured indepedently in a rigid fragment of the macromolecule. Additional values can be predicted as linear combinations of a set of independent frequencies. Comparison of the experimental data with the predicted values of the parameters studied provides a test of the reliability of the former.

Qu *et al.*[43] have designed a computer program, RDC-prospect, for protein structure prediction based on a structural homologue or analogue of the target protein in the Protein Data Bank which best aligns with the N-H RDC data of the protein recorded in a single ordering medium.

Modules that use paramagnetism-based NMR restraints have been designed by Banci *et al.*[44] and included in the well known program for solution structure determination, Xplor-NIH. Among the new restraints involved are residual dipolar couplings due to metal. The program PLATYPUS for fast structure-based assignment of ^{15}N HSQC spectra of selectively ^{15}N-labelled paramagnetic proteins has been developed by Pintacuda *et al.*[45] Among other constraints also RDCs have been included.

An automated procedure for high throughput NMR resonance assignment for a protein of the known structure, or of a homologous structure has been published by Langmead and Donald.[46] The algorithm correlates experimentally measured NH residual dipolar couplings and chemical shifts to a whole-protein 3D structural model given a priori. It requires only uniform ^{15}N-labelling of the protein, and processes unassigned H_N-N RDCs and sparse H_N -H_N NOE's.

An introduction of a coexpressed lanthanide-binding tag (LBT) as a method for protein alignment facilitating the measurement of RDCs has been proposed by Wöhnert *et al.*[47] The LBT chosen by them had the sequence YID-TNNDGWYEGDELLA, and was appended to the terminus of human ubiquitin by standard cloning techniques.

It has been shown by Griesinger and co-workers[48] that it is possible to measure long-range H-C dipolar couplings for the water insoluble compounds in orienting media. The measurements have been performed for menthol dissolved in solution of poly-γ-benzyl-glutamate in chloroform. The results have been used to check the usefulness of the method for elucidation of the stereochemistry of the studied compound.

Two papers by Riek and co-workers[49,50] have been devoted to a technique based on a spin-state selective off-resonance decoupling which allows monitoring the chemical shift in multidimensional NMR. Moreover, the authors indicate that it also facilitates the accurate measurement of the residual scalar coupling.[49]

Two papers have been devoted to improvements of the ADEQUATE method. Kövér and Forgó[51] have described a new method for the accurate determination of carbon-carbon couplings which is based on simultaneous incrementation of C chemical shift and coupling evolution periods. The time increment for the homonuclear carbon-carbon coupling evolution can be suitably scaled with respect to the corresponding increment for the chemical shift evolution. Parella and Sánchez-Ferrando[52] proposed a very simple strategy to extract carbon multiplicity information along with the classic knowledge of carbon-carbon connectivities in ADEQUATE experiments without affecting the sensitivity ratios of the original pulse schemes.

Continued effort is being made to explore the possibilities for measuring NMR spectra in microtesla fields. The main obstacle to low-field studies is the inherently low sensitivity which, however, can be overcome by combining prepolarization in fields on the order of militesla and signal detection with a Superconducting Quantum Interference Device (SQUID). Recently, an enhancement of proton NMR signals by a factor of 10^6 by cross polarization with hyperpolarized liquid ^{129}Xe in an ultralow magnetic field of 1μT has been reported by Heckman *et al.*,[53] who, using a commercial high-Tc SQUID magnetometer, have recorded spectra

of cyclopentane, acetone and methanol. The authors indicate that the technique is especially promising for the detection of intermolecular scalar spin-spin couplings. A variety of heteronuclear systems in both the weak and strong J-coupling regimes has been studied by Trabesinger *et al.*[54] by the use of the low-T_c SQUID spectrometer. They have shown, using examples such as carbonyl labelled glycine, trifluoroethanol and trimethyl phosphate, that J-coupling alone allows one to identify molecules in microtesla fields.

It has been shown by Eykyn *et al.*,[55] who used as an example the ^{9}Be 1D spectrum of an equilibrium mixture of BeF_3^- and BeF_4^{2-} ($^1J_{BeF}$ = 33.9 Hz in BeF_3^- and $^1J_{BeF}$ = 36.8 Hz in BeF_4^{2-}) dissolved in a weakly aligned bicelle solution, that cross-polarization is a valuable tool for the selective observation of scalar-coupled quadrupolar nuclei. They suggested that, by analogy to multiple quantum techniques used in solid-state NMR, the ability to excite higher order coherences can be a useful extension to the single-quantum cross-polarization experiment.

An efficient peak assignment algorithm for two-dimensional NMR correlation spectra of framework structures has been proposed by Brouwer.[56] The algorithm has been primarily developed for assigning the peaks in the high-resolution solid-state ^{29}Si MAS NMR spectra of highly siliceous zeolites based on two-dimensional ^{29}Si INADEQUATE spectra; the zeolites ZSM-12 and ZSM-5 have been used as examples.

It has been shown by Trebosc *et al.*[57] that the FS REDOR (*F*requency *S*elective *R*otational *E*cho *D*ouble *R*esonance) experiment can be used for accurate through-space measurements in spin pairs that involve the quadrupolar nuclei. The experiment reveals both heteronuclear dipolar and scalar couplings, which can be re-introduced selectively site after site. As an example, couplings between the aluminium and phosphorus nuclei in the VPI5 zeolite have been measured. They agree very well with those reported in the literature, which validates the authors' approach.

3 One-bond Couplings to Hydrogen

A crucial piece of information on the electronic structure of the iridium bis(phosphinite) pincer complexes (p-η^2-5-X-C_6H_2[OP-(tBu)$_2$]$_2$-1,3)IrH_2 where X = MeO, Me, H, F, C_6F_5 and 3,5-bis(trifluoromethyl)phenyl, has been derived from isotopic labelling studies.[58] The HD isotopomers of these compounds exhibit *inter alia* $^1J_{HD}$ couplings that are sensitive to the electronic properties of the p-X substituent of the ligand, their values varying from 6.5 Hz for X = MeO to 9 Hz for X = C_6F_5 and 3,5-bis(trifluoromethyl)phenyl. Substantial H-D couplings observed for the H-D isotopomers of *trans*-[(dppe)$_2$-Fe(η^2-H_2)(RCN)] [BF_4]$_2$ complexes provided evidence that the H-H ligand in these compounds remains intact.[59] Temperature dependence of $^1J_{HD}$ couplings has been observed for the *cis* isomer of a new elongated dihydrogen complex of iridium, [Cp*Ir(dmpm)H_2]$^{2+}$, synthesized by Pons and Heinekey.[60] The authors suggest that the complex represents a dihydrogen/*cis*-dihydride equilibrium system, the

structure which is without precedent.

$^1J_{HB}$ couplings have been measured by Yao and Grimes[61] to characterize a series of multinuclear cobaltacarborane complexes, such as, for example, (η^5-$C_5H_4SnMe_3$)Co(2,3-$Et_2C_2B_4H_4$), (η^5-$C_5H_4CMe_3$)Co(2,3-$Et_2C_2B_4H_4$) and similar ones.

Concentration- and temperature-dependent NMR, IR and dipole moment studies on 4-*N*,*N*-dimethylamino-1,1,1-trifluoro-3-buten-2-one and two of its higher homologues performed by Wójcik *et al.*[62] showed that these compounds undergo reversible dimerization in nonpolar solvents. Antiparallel 'closed' dimers are formed with a network of improper intermolecular C-H···O hydrogen bonds which causes an increase of $^1J_{HC}$ by 1.5 Hz.

The potential energy and spin-spin coupling surface of the simplest carbohydrate, glycolaldehyde, have been studied by Ratajczyk *et al.*[63] at the second-order Møller-Plesset (MP2) level of theory. They have also studied the conformational dependence of the indirect C-H and C-C couplings including those across one and more bonds by means of DFT using the B3LYP functional.

H-C couplings of acetyl groups of a series of substituted 2-hydroxyacetophenones have been measured very precisely by Hansen,[64] who analysed them from the point of view of CH hydrogen bonds and electric field effects. The couplings for the aldimine hydrogen have been measured by Montalvo-González and Ariza-Castolo[65] for a series of 25 diaryl-aldimines, their values being characteristic of a given heterocycle.

The application of $^1J_{HC}$ couplings in conformational analysis of six-membered heterocycles has been shortly overviewed by Juaristi *et al.*[66] and by Alabugin *et al.*[67] The couplings have been also shortly addressed by Ribeiro and Rittner[68] in their work on the role of hyperconjugation in the conformational analysis of methylcyclohexane and methylheterocyclohexanes.

The electronic structure of 11 sparteines has been studied by Galasso *et al.*[69] by the use of experimental and DFT calculated NMR parameters, special attention being paid to spin-spin couplings. In particular, the influence of stereoelectronic hyperconjugative effects on $\Delta^1J_{HCeq}/^1J_{HCax}$ has been correctly accounted for by the DFT results.

The distinction between oxazole and isoxazole rings in recently synthesized [1,3]oxazolo[4,5-*e*][2,1]benzisoxazole and naphto[1,2-*d*][1,3]- and phenanthro[9,10-*d*]oxazoles has been made by Katrizky *et al.*[70] by the use of $^1J_{HC}$ couplings, $^1J_{HC}$ of 233 Hz and $^1J_{HC}$ of *ca.* 210 Hz being observed in the oxazole and isooxazole rings, respectively.

An analysis of the ^{13}C NMR spectra of a large series of 1,3-di- and 1,2,3-trisubstituted imidazolidines with aryl, alkyl and aralkyl groups performed by Perillo *et al.*[71] yielded a set of H-C couplings including those across one bond. The differences in the coupling values have been interpreted by the authors in terms of inductive substituent effects and a lone pair orientation.

A conformational analysis of three halothioacetates, *S*-methyl chlorothioacetate, *S*-methyl bromothioacetate and *S*-methyl iodothioacetate has been performed by Basso *et al.*[72] by the use of $^1J_{HC}$ couplings and solvation model yielding the vapour-phase energy difference, the coupling values for each

rotamer, the solution energy difference, and the rotamer population in each solvent.

$^1J_{HC}$ couplings have been published by Martins *et al.*[73] for three cage compounds, 11-amino-8-hydroxypentacyclo[5.4.0.0^{2,6}.0^{3,10}.0^{5,9}]undecane-8,11-lactam, its tautomer, and for *N*-acetyl derivative. $^1J_{HC}$ and $^{2,3}J_{CSi}$ couplings have been used by Wrackmeyer *et al.*[74] to prove the structure of [3-(borabicyclo[3.3.1]non-9-yl)]-2,5-bis(trimethylsilyl)-1,1-dimethyl-1-sila-2,4-cyclopentadiene.

It has been indicated by Stępień *et al.*,[75] who studied weak intramolecular metal-arene interactions in cadmium(II) and nickel(II) complexes of benziporphyrins, that for weak interactions the parameters δ_H, $^1J_{HC}$ and J_{HM} are not necessarily correlated. According to their opinion, the changes of the magnitude of $^1J_{HC}$ seem to be a more reliable probe for the agostic interaction than the variations of the chemical shift.

The partial metalla-alkene character of a novel spiroorganomagnesium compound, $[Cp_2ZrCHSiMe_3(\mu\text{-}Br)]_2Mg$, has been indicated by the short zirconium-carbon bonds, and agostic zirconium-hydrogen interactions by the short zirconium-hydrogen distances (Zr···H-C) and a small $^1J_{HC}$ coupling of 91.4 Hz.[76]

Primary tritium isotope effects have been determined by Schilf *et al.*[77] at various temperatures for proton-nitrogen couplings in two Schiff bases obtained by the condensation of 4-methoxy- and 4,6-dimethoxysalicylaldehyde with methylamine. However, the results are not conclusive and it is not clear if they can be used as an additional probe of the hydrogen bond character.

A typical $^1J_{HN}$ coupling of 93.6 Hz has been measured in the spectrum of 3-phenylhydrazone of 4-dimethylamino-5-(phenyldiazenyl)pent-4-en-2,3-dione.[78]

Three rare, non-classical silane complexes $[Cp^*(PMe_3)Rh(SiMe_3)(\eta^2\text{-}SiMe_3)]BAr_4$, $[Cp^*(PMe_3)Rh(SiEt_3)(\eta^2\text{-}SiEt_3)]BAr_4$ and $[Cp^*(PMe_3)Rh(C_6H_4)(\eta^2\text{-}HSiPh_2)]BAr_4$, have been characterized by Taw *et al.*[79] by the use of NMR. Among others, $^1J_{HSi}$ between 56 and 84 Hz and $^1J_{HRh}$ of *ca.* 28-36 Hz have been measured; the former are diagnostic of the presence of η^2-silane ligands.

One-bond H-Si couplings of *ca.* 200 Hz have been measured by Wrackmeyer *et al.*[80] for a series of bis(silyl)ethynes bearing one, two or three hydrides at one of the silicon atoms and for the products of their 1,1-allylboration where the coupling values vary from *ca.* 130 up to 200 Hz.

A reaction of alkyn-1-yl(diorganyl)silanes with boraadamantane yielded a series of borahomoadamantanes in which the presence of the Si-H-B bridges has been confirmed *inter alia* by the reduced $^1J_{HSi}$ coupling value in comparison with triorganosilanes[81] (Fig. 1).

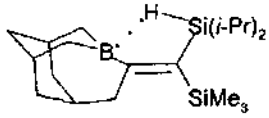

$^1J_{HSi}$ = 116.0 Hz

Figure 1

The unique bonding situation in the Si-H-B bridge is also reflected in the rather large primary isotope effect on the coupling $\Delta_p{}^1J_{HSi}$ of -2.60 ± 0.03 Hz, typical values being -0.05 ± 0.03 Hz. A fairly large positive secondary isotope effect of 1.2 ± 0.03 Hz is observed for the $^2J_{SiSi}$ coupling.

Unusually large $^1J_{HP}$ and $^2J_{PP}$ couplings of 277 and 237 Hz, respectively, have been observed by Weinrich *et al.*[82] for *trans*-bis[dichloro(μ-(tris(*t*-butyl)silyl)phosphino)gallane], $[Cl_2GaP(H)Si^tBu_3]_2$. The corresponding couplings for the *cis* isomer are 277 and 252 Hz. It is noteworthy that the $^2J_{PP}$ values actually lie in the region typical of $^1J_{PP}$ couplings.

Trends in the calculated and measured one-bond H-X reduced spin-spin couplings for twelve XH_4 hydrides (X = C, Si, Ge, N, P, As, O, S, Se, F, Cl, Br) have been interpreted by Cremer and co-workers[83] in terms of orbital contributions by the use of the J-OC-PSP (decomposition of *J* into orbital contributions using the *O*rbital *C*urrents and *P*artial *S*pin *P*olarization) approach. The sign and magnitudes of the orbital contributions have been rationalized with the help of the Fermi contact spin density distribution, the *s*-density of an orbital at the nucleus, the electronegativity, and the polarizability of the central atom X. A new method for calculating the spin-spin couplings for molecules containing heavy elements has been also developed by this group.[84]

The basis set dependence of NMR spin-spin couplings calculated by means of the DFT approach in a set of benchmark molecules containing first row and hydrogen atoms has been studied by Peralta *et al.*[85]

The performance of the KT1 and KT2 exchange-correlation functionals has been assessed by Keal *et al.*[86] for the determination of the GIAO NMR spin-spin couplings in 11 molecules containing light main group nuclei. However, the results are of variable quality; they highlight the sensitivity of the Fermi-contact term to an exchange-correlation functional and are consistent with the previous observations when a self-interaction corrected functional was used.

4 One-bond Couplings not Involving Hydrogen

The dynamics of bimolecular C-Li exchange in several allylic lithium compounds with ligands tethered at C2 has been investigated by Fraenkel *et al.*[87] by the use of the ^{7}Li-C couplings yielding the thermodynamic data of this process.

The products of the reaction of ketones with lithium hexamethyldisilazide have been studied by Collum and co-workers[88] by an extensive use of the ^{6}Li and ^{15}N NMR spectroscopy; $^1J_{LiN}$ couplings have been found to be particularly useful.

Both $^1J_{LiC}$ and $^1J_{LiN}$ couplings have been observed by Sott *et al.*[89] in the spectra of isotopically labelled mixed complexes formed by the lithium salt of acetonitrile ($LiCH_2CN$) and the chiral lithium amides, Li-(*S*)-*N*-(2-methoxybenzyl)-1-amino-1-phenyl-2-ethoxyethane and Li-(*S*)-*N*-isopropyl-2-amino-1-phenyl-3-methoxypropane, providing crucial information on their structures.

A $^1J_{^7LiSn}$ coupling of *ca.* 560 Hz observed by Fukawa *et al.*[90] in the ^{7}Li and $^{117/119}$Sn NMR spectra of the tris(di-*tert*-butymethylsilyl)stannyllithium-benzene

complex measured at room temperature provided evidence that the covalent Li-Sn bond exists in this compound also in solution.

$^1J_{BC}$ and $^1J_{CSi}$ couplings have been derived by Wrackmeyer and Berndt[91] for 1,2-diboretane-3-ylidene, a homoaromatic system with π and σ 3c/2e bonds, from the low temperature NMR spectra. The results shown in Fig. 2 allowed an insight into the electronic structure of this unusual molecule.

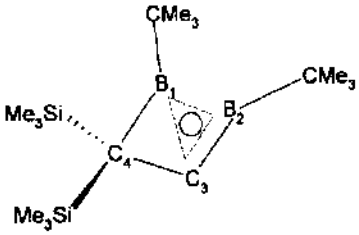

$^1J_{B(1)C}$ = 75 Hz
$^1J_{B(2)C}$ = 84 Hz
$^1J_{B(1)C(4)}$ = < 20 Hz
$^1J_{B(2)C(3)}$ = 110 Hz

Figure 2

A clear correlation between $^1J_{BP}$ and $^1J_{CP}$ couplings has been observed by Schmidbaur and co-workers[92] in a series of trivinylphosphineboranes $(CH_2=CH)_3PBX_3$ (X = H, Cl, Br, I) and interpreted in terms of the influence of the electronegativity of the substituent.

An increasing interest is being paid to spin-spin couplings between directly bonded two carbon nuclei. Four important papers by Cremer and co-workers[93-96] have been devoted to the mechanisms governing NMR spin-spin coupling and to the question if one can derive the information on the π character of a CC bond with the help of this parameter. An analysis of the spin-dipole and paramagnetic spin orbital transmission mechanisms led the authors to the conclusion that these terms are a sensitive indicator of the π character of a CC bond.

$^1J_{CC}$ couplings have been calculated by Biedrzycka and Kamieńska-Trela for a large set of derivatives of acetylene with the help of the DFT method.[97] The DFT calculated coupling data not only follow the trends observed for the experimental results but also the absolute $^1J_{CC}$ values are very well reproduced (in most cases within several Hz). It has been found that the magnitude of the coupling is strongly dependent on the electronegativity of the first atom of the substituent attached to the triple bond, which is described by the equation: $^1J_{C\equiv C}(\text{TOTAL}) = 25.9\ E_XE_Y + 5.4$. The smallest $^1J_{C\equiv C}$ coupling is predicted for Li_2C_2 (42.2 Hz) and the largest for C_2F_2 (416.8 Hz), which reflects the dramatic changes occurring in the electronic structure of the triple bond upon substitution. A rough linear correlation has been found between the $\ln(^1J_{C\equiv C(DFT)})$ and the DFT optimized bond lengths, $r_{C\equiv C}$.

A set of $^1J_{CC}$ couplings has been measured by Kamieńska-Trela *et al.*[98] for a series of 6-substituted quinolines, their *N*-oxides and 2- and 5-methoxyindoles, and compared with the couplings derived for a series of variously substituted 5*H*- and 6*H*-indolo[2,3-*b*]quinolines, which shed new light on the electronic structure of these two groups of compounds.

$^1J_{CC}$ and $^1J_{HC}$ couplings have been determined for a set of 2-fluoro- and 3-fluoro-substituted thiophenes, pyrroles and furans.[99] Invariably, a dramatic increase in the $^1J_{C2C3}$ couplings has been observed in 2-fluoro- and 3-fluoro-substituted compounds in comparison with those measured for the parent compounds. The same is valid for $^1J_{C3C4}$ measured in 3-fluoro derivatives. The experimental *J* values have been well reproduced by the DFT calculated ones.

The effect of the N7 methylation in guanine on the one-bond CC and CN couplings has been studied by Ruszczyńska *et al.*[100] The DFT calculated data for the parent guanine and the experimental *J* values measured for the corresponding nucleoside triphosphate have been compared with those for the N7 methylated compounds, which allowed the authors to estimate the charge distribution in the latter.

The DFT approach has been used by Jaszuński *et al.*[101] to calculate J_{CC} couplings across one and more bonds in fullerene C_{60}. The one-bond CC couplings within pentagons and between pentagons are 62 and 77 Hz, respectively. The DFT calculation of the indirect carbon-carbon couplings across one and two bonds in the C_{70} fullerene has been performed by Peralta *et al.*[102] Very good agreement has been found between the B3LYP/cc-pCVDZ-sd computed $^1J_{CC}$ values and the experimental ones.

The $^1J_{CC}$ and $^2J_{CC}$ couplings of allene and two sterically strained hydrocarbons, cyclopropane and cyclopropene, have been calculated by Ruden *et al.*[103] at different levels of electronic-structure theory and compared with each other and with the experimental equilibrium constants obtained from experiment by subtracting the calculated vibrational contributions.

Chemical shifts and CC couplings have been calculated by Wrackmeyer [104] by the use of the DFT method for cyclic C_4H_2 and C_4H_4 molecules containing carbene centres, and for some of their boron analogues. The author found that scalar CC spin-spin couplings involving carbene centres are frequently dominated by spin-dipole and spin-orbital interactions.

Several papers devoted to non-empirical calculations of carbon-carbon couplings in strained molecules have been published by Krivdin and co-workers. The compounds investigated were bridged bicycloalkanes,[105] propellanes,[106] spiroalkanes[107] and small heterocycles.[108] The additivity of the coupling path in the latter group of compounds has been also studied by the use of the SCPT INDO method.[109] $^1J_{CC}$ couplings within the FPT INDO approach have been calculated by the same group for aldoseptanoses,[110] aldofuranoses[111] and aldopyranoses[112] of the D series.

The feeding experiments with [1-^{13}C], [2-^{13}C] and [1,2-$^{13}C_2$] sodium acetates performed by Tsuda *et al.* for amphidinolide X,[113] a novel 16-membered macrodiolide, and for amphidinolide Y,[114] a novel 17-membered macrolide both isolated from dinoflagellate *Amphidinium sp.*, yielded the ^{13}C enriched compounds

with eight intact acetate units. The presence of these units has been proved by the measurements of the corresponding one-bond carbon-carbon couplings. The results obtained indicate that amphidinolide Y may be a bio-genetic precursor of amphidinolide X.

$^1J_{CC}$ couplings have been measured by Wrackmeyer and co-workers[115] for diethylaminoethynylsilane (152.1 Hz), -germane (152.3 Hz) and -stannane (142.0 Hz). The observed coupling values are, as expected, larger than those found in the corresponding alkynyl-1-yl-silanes or stannanes, which is caused by larger electronegativity of the amino group than the alkyl one. The $^1J_{CC}$ coupling of 141 Hz has been determined by the same group of authors[116] for tetra(propyn-1-yl)silane. The magnitude of this coupling is larger than that in monoalkyl-1-yl(trimethyl)silanes (*ca.* 130 Hz), which indicates that the polar nature of the Si-C≡ bond is reduced.

Carbon-carbon couplings across one bond have been measured by Cmoch[117] for 2-chloropyrazine and its two isomeric *N*-oxides, and by Schilf[118] for five Schiff bases obtained from substituted salicylaldehydes and methylamine. For the parent 2-chloropyrazine also C–C couplings across two and three bonds have been obtained.[117]

Through-bond and through-space solid-state NMR correlation experiments including CP-INADEQUATE at natural isotope abundance have been applied by Brus and Jegorov[119] to establish the structure and dynamic behaviour of simvastatin ($C_{25}H_{38}O_5$), an active metabolite which inhibits 3-hydroxy-3-methyl-glutaryl coenzyme A, (HMG-CoA) reductase, the enzyme that is necessary in an early step of the cholesterol synthesis. 2D INADEQUATE spectroscopy has been applied by Meier *et al.*[120] to establish the structures of a series of fullerene derivatives.

One-bond X-Y couplings have been computed by Del Bene *et al.*[121] for 18 H_mX-YH_n molecules, with X = C, N and P, using the equation-of-motion coupled-cluster singles and doubles method. The calculated values cover the range from *ca.* 200 Hz in acetylene to *ca.* -450 Hz in *E*-diphosphene. However, in the latter case agreement between the experimental and calculated values is rather poor. The same applies to some other molecules, such as, for example, methyl phosphine for which the calculated and experimental *J* values are 0.8 and 9.3 Hz, respectively.

The p*H* dependence of the C-N one-bond couplings on the protonation state and tautomeric form of the imidazole ring has been used by Shimba *et al.*[122] for quantitative idendification of the protonation state of histidines *in vitro* and *in vivo*. The compound studied was the bacterial protein NmerA, and the intracellular p*H* of 7.1 has been determined in the *Escherichia coli* cytoplasm.

One-bond carbon-nitrogen couplings, $^1J_{CN}$ of *ca.* 3 Hz have been measured by Kelemen *et al.*[123] for a series of ^{15}N labelled alkoxyamines, the model compounds for nitroxide-trapping studies in free radical copolymerization. Absolute $^1J_{CN}$ values have been obtained for some mesoionic compounds and related structures by Jaźwinski and Staszewska-Krajewska.[124]

An extensive use of $^1J_{CN}$ couplings has been made by Juranić *et al.*[125] in their studies on polarization of peptide groups in folded proteins. The obtained results

show that H-bonding mediates the peptide-group polarization, which results in the general reduction of the peptide-group polarity of folded proteins in solution. High $^1J_{C'N}$ couplings (>15 *Hz*) characterize the peptide groups structurally shifted toward the 'polar' form, whereas low $^1J_{C'N}$ values often combined with high $^{3h}J_{C'N}$ are typical of the peptide groups that are shifted towards the 'nonpolar' form.

$^1J_{CN}$ couplings are usually large enough to provide information on the position of ^{15}N atoms in the specifically ^{13}C labelled purine nucleosides. A $^1J_{C8N7}$ of <1 Hz only has been found in the spectra of specifically $^{13}C8$ and $^{15}N7$ labelled adenosine, guanosine and their deoxy analogues, and therefore the $^{13}C8$ cannot be used as a direct tag for the adjacent $^{15}N7$ atom. However, it can serve most conveniently as an indirect tag, *via* the larger H8 coupling to both $^{13}C8$ ($^1J_{C8H8}$ > 200 Hz) and $^{15}N7$ ($^2J_{H8N7}$ ~ 12 Hz).[126]

A study of the structure of an active protein splicing precursor, corresponding to an *N*-extein fusion of the Mxe GyrA (*Mycobacterium xenopi* DNA gyrase A) intein, has been carried out by Romanelli *et al.*[127] A $^1J_{CN}$ coupling of ~ 12 Hz measured by them for the (−1) scissile peptide bond at the extein-intein junction provided solid evidence of its presence. Its value indicates that this amide bond is highly polarized.

Due to the small natural abundance of ^{17}O nucleus and its sizeable quadrupole moment little $^1J_{CO}$ coupling data is available in the literature. The DFT $^1J_{CO}$ values derived by Wrackmeyer[128] for carbon dioxide and carbon monoxide are in good agreement with the experimental ones.

The conformational equilibrium of methyl 2-fluoropropionate has been studied by Tormena *et al.*[129] by the use of a combination of NMR, theoretical calculations and solvation theory. The $^1J_{CF}$ couplings have been analysed using theoretical and solvation calculations to give conformer energies in the solvents studied, vapour phase energies, as well as the couplings for the distinct rotamers.

Triflic acid-functionalized Zr-TMS (zirconium oxide with a mesostructured framework; TMS, transition metal oxide mesoporous molecular sieves) have been extensively studied by Chidambaram *et al.*[130] by the use of a variety of spectroscopic methods including ^{13}C DD/MAS NMR. The observed chemical shift of *ca.* 119 ppm and a $^1J_{CF}$ coupling of ca 310 Hz showed that the triflic acid remained intact on the catalyst framework.

An extremely small $^1J_{CSi}$ coupling of 15.7 Hz only has been found between Si and C_b nuclei in the vinyl cation whose structure is shown in Fig. 3, the typical value for trialkylvinylsilanes being of *ca.* 60 Hz. This result, combined with the DFT calculated *J* value of 10.2 Hz indicates, according to the authors, that the s-orbital contribution to the C_b-Si bonds is very small.[131]

Rather small $^1J_{CSi}$ couplings ranging from 1 Hz to 38.6 Hz have been found by Takeda *et al.*[132] for three stable silylene-isocyanide complexes (Fig. 4). The coupling value decreases with the increasing bulkiness of the Ar subsituent. The smallest $^1J_{CSi}$ value of 1 Hz has been found for Ar = 2,4,6-(*t*-Bu)$_3$Ph, the largest, of 38.6 Hz, for Ar = 2,4,6-(*i*-Pr)$_3$Ph.

A new stable pentaorganosilicate whose different configurational isomers coexist in solution has been obtained by Couzijn *et al.*[133] The $^1J_{CSi}$ couplings

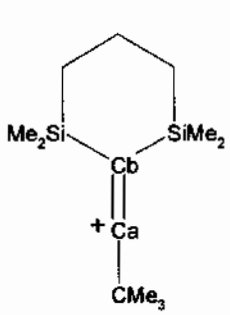

$^1J_{C(b)Si}$ = 15.7 Hz

Figure 3

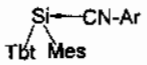

where Tbt denotes 2,4,6-tris[bis(trimethylsilyl)methyl]phenyl

Figure 4

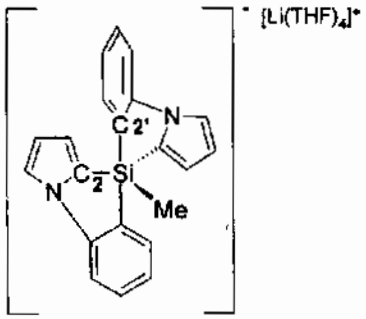

$^1J_{C2Si}$ = 86 Hz; $^1J_{C2'Si}$ = 30 Hz; $^1J_{CMeSi}$ = 64 Hz

Figure 5

measured for the main compound are in agreement with the structure shown in Fig. 5.

A relatively small magnitude of the couplings $^1J_{C(1)Si}$ and $^1J_{C(1)C(2,5)}$ has been observed by Wrackmeyer *et al.*[134] in a series of 1-sila-[1]ferrocenophanes, which reflects the changes in the bonding situation for carbon atom C(1) when compared with the other cyclopentadienyl carbon atoms. Thus, for example, $^1J_{C(1)C(2,5)}$ ($^1J_{C1Si}$) of 31.5 Hz (57.8 Hz) has been found in $[Fe(C_5H_4)_2]SiMe_2$ compared with $^1J_{C(1)C(2,5)}$ ($^1J_{C(1)Si}$) of 36.3 Hz (73.4 Hz) in $Fe(C_5H_4\text{-}SiMe_3)_2$. In the case of $[Fe(C_5H_4)_2]SiMe_2$ where all ring ^{13}C resonances are different, all $^1J_{CC}$ couplings could be determined, and $^1J_{C(1)C(2,5)}$ = 32.1, $^1J_{C(2)C(3)}$ = 45.0, $^1J_{C(3)C(4)}$ = 46.0, $^1J_{C(4)C(5)}$ = 45.2 Hz have been found.

A series of 2-amino-1,3-bis(trimethylsilyl)-1,3,2-diazabora-[3]ferrocenophanes[135] and a novel [6]ferrocenophane containing a N-Si-C-C-Si-N

bridge[136] have been synthesized by Wrackmeyer and co-workers, and characterized by the use of NMR including C-Si couplings.

The absolute DFT $^1J_{CP}$ coupling values calculated by Wrackmeyer[137] for a series of λ^3-1-phosphaalkynes are in reasonably good agreement with the experimental ones. Also the sign (positive) of these couplings has been correctly reproduced. It results mainly from the substantial positive SD contributions, whereas the FC contribution to $^1J_{CP}$ is negative.

$^1J_{CCo}$ and $^1J_{NCo}$ couplings of 102 Hz and 55 Hz, respectively, have been measured by Kofod and Harris[138] for *trans*-$[Co(en)_2(CH_3)(H_2O)]^{2+}$ (en = 1,2-ethanediamine) from the relaxation measurements.

$^1J_{C-Se}$ couplings of *ca.* 200 Hz have been measured by Murai *et al.*[139] for a series of substituted *E*-α,β-unsaturated selenoamides, but no influence of substitution on the coupling value has been observed.

$^1J_{CSn}$ couplings have been applied by Mazhar and co-workers[140] to estimate the dihedral C-Sn-C angle in a series of bimetallic carboxylates of a general type: $[R^4]_2Sn[OOCCH(R^3)CH(R^2)Ge(R^1)_3]_2$ where R's are alkyl and aryl substituents.

A series of novel zwitterionic heterocycles containing hypervalent tin has been obtained by Wrackmeyer *et al.*[141] from (*E*)-2-chloro(dimethyl)stannyl-3-diethylboryl-*N*,*N*-dimethyl-2-pentenylamine and some azoles. The coordinative strong bonding between nitrogen and tin atoms in these compounds is reflected by a large =C-Sn coupling (of *ca.* 800 Hz) and the small value of $^1J_{C(azole)Sn}$ of 131 Hz only (see Fig. 6).

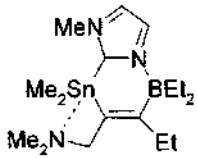

$^1J_{C(olefinic)Sn}$ = 765 Hz

$^1J_{C(azole)Sn}$ = 131.0 Hz

Figure 6

A $^1J_{NN}$ coupling of 10.6 Hz has been measured in the spectrum of 3-phenylhydrazone of 4-dimethylamino-5-(phenyldiazenyl)pent-4-en-2,3-dione.[78]

The ^{15}N NMR spectra of the iron phosphines containing coordinated dinitrogen, *trans*-$[FeH(N_2)(PP)_2]^+[BPh_3]^-$ (PP = 1,2-bis(diphenylphosphino)ethane, 1,2-bis(diethyl diphenylphosphino)ethane and 1,2-bis(dimethyl diphenylphosphino)ethane) exhibit two separate signals for the metal-bound and terminal nitrogen atoms of the coordinated N_2 which are coupled by a $^1J_{NN}$ coupling of *ca.* 4 Hz.[142]

A formation of the hypervalent pentacoordinated and hexacoordinated complex between trifluoro(phenylethynyl)silane and pyridine of the form $PhC{\equiv}CSiF_3{\cdot}C_6H_5N$ and $PhC{\equiv}CSiF_3{\cdot}(C_6H_5N)_2$ (at low temperature), respectively, has been proved by the presence of an intermolecular N-Si coupling across one

bond;[143] $^1J_{NSi}$ = 4 Hz for the pentavalent complex of silicon and $^1J_{NSi}$ = 15.6 Hz for the hexavalent complex have been found.

A strong dependence upon the coordination state and nature of the apical Z substituent has been observed by Galasso[144] for $^1J_{NP}$ and $^1J_{OP}$ couplings calculated in a series of phosphatrane molecules.

A special effort has been made by Wrackmeyer *et al.*[145] to determine $^1J_{NSn}$ couplings in 2,2-di(alkyn-1-yl-1,3-bis(trimethylsilyl)-1,3,2-diazastanna-[3]ferrocenophanes and the products of their 1,1-organoboration with triethylborane, the spirotin compounds which contain both a ferrocenophane and a stannacyclopentadiene ring. The coupling values cover the range of *ca.* 62-124 Hz. They have also measured the $^1J_{NSn}$ coupling (positive) and a set of long-range couplings such as $^2J_{SiSn}$ and $^{2,3}J_{CSn}$ including their signs for cyclic bis(amino)tin chloride with the 1,3,2,4,5-diazastannadisila-cyclopentane ring.[146]

It has been shown by Sychrovsky *et al.*[147] that the calculated intermolecular and intramolecular spin-spin couplings can allow one to distinguish between the specific direct and the water-mediated binding of a divalent metal cation to guanine. The $^1J_{O6,Mg}$ and $^1J_{O6,Zn}$ couplings of 6.2 and −17.5 Hz, respectively, have been calculated for the inner-shell complex of the cation directly interacting with oxygen O6 of guanine. For the inner-shell coordination of the cation at nitrogen N7, the calculated couplings $^1J_{N7,Mg}$ and $^1J_{N7,Zn}$ are 5.6 and −36.5 Hz respectively. When the binding of the cation is water mediated, the coupling is zero.

A $^1J_{OP}$ coupling of 150 Hz has been determined by Bryce *et al.*[148] for the polymorphic ^{17}O-enriched Ph_3PO sample from the MAS NMR spectrum, which is in good agreement with the *J* value reported in the literature for Ph_3PO dissolved in chloroform, 160 Hz.

A $^1J_{FCl}$ coupling calculated by Jaszuński[149] for ClF_3 and $^1J_{FP}$ for PF_3 and PF_5 molecules at the CCSD (coupled clusters singles and doubles) and CCSD(T) (CCSD with noniterative account of triple excitations) level indicate the importance of the electron correlation effects. The results obtained for $^1J_{FCl}$ in ClF_3 confirm the earlier findings of Bryce and Wasylishen[150] that all three contributing terms (FC, SD and PSO) are large and of the same order of magnitude and therefore none of them can be neglected.

$^1J_{FXe}$ of −5560 ± 50 Hz has been measured by Wasylishen and co-workers[151] for XeF_2 from the solid-state spectrum of this compound. The result is in good agreement with the DFT calculated $^1J_{FXe}$ values and those measured in various solutions.

$^1J_{Si=Si}$ of 116.3 Hz across a double SiSi bond and $^1J_{Si\text{-}Si}$ of 75.1 Hz across a single central Si-Si bond have been measured for 1,1,2,3,4,4-hexa-[2,4,6-(*i*-Pr)$_3$C$_6$H$_2$]tetrasiladiene providing solid evidence of its structure.[152] It is worth noting that the $^1J_{Si-Si}$ couplings of 155 to 158 Hz have been reported for tetra(aryl)disilenes. Obviously the value of $^1J_{Si=Si}$ found in tetrasiladiene is considerably lowered by the electropositive silyl substituent.

Three ^{29}Si NMR signals, two couplings across one bond, $^1J_{Si1Si2}$ of 52.7 and $^1J_{Si2Si3}$ of 48.4 Hz, and two couplings across two bonds, $^2J_{Si1Si3}$ of 9.6 Hzand $^2J_{Si3Si2}$ of 8.6 Hz have been measured for heptasilanortricyclene, 3,4,5-tri-*tert*-butyl-1,2,2,6,6,7,7-heptamethyl-heptasilatricyclo[2.2.1.0^{2,6}]-heptane, providing an ex-

perimental proof of its structure.[153]

A large number of the experimental $^1J_{PP}$ couplings for compounds representing a variety of bonding situations have been collected by Wasylishen and co-workers[154] and compared with the DFT calculated J values. The authors used both nonrelativistic and relativistic zeroth-order regular approximation. The obtained data allows one to gain an insight into the mechanism of the coupling. The ^{31}P 2D refocused INADEQUATE experiment has been applied by Fayon *et al.*[155] to study the structure of SnP_2O_7.

The one-bond P-$^{63/65}$Cu couplings have been determined by Brunklaus *et al.*[156] from a lineshape analysis of the ^{31}P MAS NMR spectra of a series of the phosphorus chalcogenide-copper iodide coordination compounds, $(CuI)P_4Se_4$, $(CuI)_2P_8Se_3$, $(CuI)_3P_4Se_4$ and $(CuI)_3P_4S_4$, and discussed together with the couplings reported already in the literature for similar compounds.

Allen and Taylor's suggestion that $^1J_{PSe}$ couplings of phosphorus selenides can be used as a measure of parent phosphine basicity[157] has been applied by Andersen *et al.*[158] to estimate the donor ability of 2,2'-bis(diphenyphosphino)-3,3'-binaphtho[*b*]furan. The $^1J_{PSe}$ coupling of 762 Hz determined for its selenide indicates that this compound is less basic than, for example, triethylphosphine ($^1J_{PSe}$ = 732 Hz in the corresponding selenide). The same parameter has been used by Bolm *et al.*[159] to compare the Lewis basicity of (*S*,*S*p-2-[2-(diphenylphosphino)cyrhetrenyl]-4-*tert*-butyl-4,5-dihydro-1,3-oxazole, with that of (*S*,*S*p)-2[2-(diphenylphosphino)ferrocenyl]-4-*tert*-butyl-4,5-dihydro-1,3-oxazole. The $^1J_{PSe}$ couplings found for the corresponding selenophosphinoyls, 394 Hz for (*S*,*S*p)cyrhetrene and 325 Hz for (*S*,*S*p)ferrocene, indicate that the basicity of the latter is larger than that of the former.

$^1J_{PRh}$ couplings have been used by Cohen *et al.*[160] to characterize the [(PCP)Rh(NCPh)] and [(PCP)Rh(HN=CHPh)] complexes where PCP = *meta*-di-$(CH_2P\text{-}i\text{-}Pr_2)_2Ph$ or *meta*-di-$(CH_2P\text{-}t\text{-}Bu)_2Ph$.

One- and two-bond couplings have been measured by Magiera *et al.*[161] for the adducts of six secondary phosphine oxides existing in two tautomeric forms with the chiral auxiliary dirhodium complex $Rh_2[(R)\text{-MTPA}]_4$, where MTPA-H = methoxytrifluoromethylphenylacetic acid (Mosher's acid). The $^1J_{PRh}$ values in these complexes are between ~106 and 109 Hz and agree well with those of a series of triorganylphosphines (96-106 Hz). The $^2J_{PRh}$ values of *ca.* 20 Hz have been found.

$^1J_{PAg}$ and $^3J_{PAg}$ couplings have been determined by Szłyk *et al.*[162] for a series of silver(I) perfluorinated carboxylate complexes with bis(diphenylphosphino)methane of the general formula $[Ag_2(RCOO)_2(dppm)]$. The couplings were extracted from the higher order spectra measured in solutions at various temperatures and from the solid-state ^{31}P CP MAS NMR spectra. Their analysis indicated that in solution the compounds have a binuclear trigonal Ag(I) geometry with bridging dppm and carboxylates.

$^1J_{P107/109Ag}$ (av.) of 700.1 Hz has been measured for the $AgCl[P(C_7H_7)_3]$ complex, whereas at −45°C the two expected doublets are clearly discernible with the couplings $^1J_{P107Ag}$ = 671.0 Hz and $^1J_{P109Ag}$ = 774.4 Hz, respectively.[163]

A coupling across one bond of 224 Hz between P and $^{113/115}$In nuclei and a P-P

coupling across two bonds of 13 Hz have been found by Iijima *et al.*[164] in undoped and Fe-doped InP semiconductors studied by CP MAS NMR spectroscopy.

The P-Pt coupling data for the platinum- phosphonite complexes published in the literature have been reviewed by Vlugt *et al.*[165] and the $^1J_{PPt}$ couplings for two new complexes containing novel, sterically constrained diphosphonite ligands with 2-*tert*-butyl-phenolate and 2,2'-dioxo-3,3'-di-*tert*-butyl-5,5'-dimethoxy-1,1'-biphenyl groups have been measured by them.

$^1J_{35ClSn}$ couplings ranging from 230 up to *ca.* 330 Hz have been determined by Geller *et al.*[166] for a series of triaryltin(IV) chlorides from the ^{119}Sn CP MAS NMR spectra.

Spin-spin couplings between tungsten and gold of 65 Hz, and gold-gold couplings averaged over all gold positions have been calculated by Autschbach *et al.*[167] for the WAu_{12} molecule which was theoretically predicted by Pyykkö and Runenberg[168] and obtained experimentally by Li *et al.*[169] These coupling values are rather small in comparison with those observed across Hg-Hg bonds[170] reflecting the smallness of the W and Au magnetic moments and the small *s*-character of the W-Au bonds.

Spin-spin couplings between Pt and Tl nuclei in $[(NC)_5Pt\text{-}Tl(CN)_n]^{n-}$ complexes, n = 0-3, belong to the largest reported so far. A theoretical study performed by Autschbach and Le Guennic[171] by the use of a two-component relativistic DFT approach has shown that both the extremely large value of $^1J_{PtTl}$ for the complex $(NC)_5Pt\text{-}Tl$ and the experimental trend among the series are entirely due to solvents effects. Thus, for instance, $^1J_{PtTl}$ of -10 kHz has been calculated for the unsolvated compound while the experimental J value attains 71 kHz.

5 Two-bond Couplings to Hydrogen

Fermi hole density functions have been computed by Soncini and Lazzeretti[172] for the first-row hydrides. The relative maps have been compared with those of one- and two-bonds nuclear spin-spin coupling density. The interesting observation concerns geminal *H*-X-*H* coupling, which is determined mainly by the spin density near the heavy X nucleus. If it were not involved, no geminal coupling could arise.

Geminal and vicinal H-H couplings have been measured by Guthrie *et al.*[173] for new examples of 5-substituted-1-aza-4,6-dioxabicyclo[3.3.0]octanes (bicyclic amide acetals), and for some examples of the new heterocyclic system, 5-substituted-1-aza-4-oxa-6-thiabicyclo[3.3.0]octanes (bicyclic amide monothioacetals). A detailed analysis of this data combined with the X-ray results allowed the authors to elucidate the stereochemistry and conformation of these ring systems.

Geminal and vicinal proton-proton couplings have been measured by Rodríguez and Jimeno[174,175] for a large series of naturally occurring diterpenoids and some synthetic derivatives; the vicinal couplings have been applied to

establish the ring conformations of these compounds. $^2J_{HH}$ and $^3J_{HH}$ couplings have been measured by Reyes-Trejo *et al.*[176] for 14-hydroxymodhephene, a naturally occurring tricyclopentenoid sesquiterpene isolated from *Pluchea sericea*, and used in a conformational analysis of the compound.

Isotope and solvent effects on fluxional hydrogen-bonded complexes of acetic acid and acetate have been studied by Limbach and co-workers.[177] The spectra have been measured in the presence of tetra-*n*-butylammonium acetate around 110 K using liquefied Freon mixture as a solvent. Also spectra of the adduct $CH_3{}^{13}COOH{\cdot}SbCl_3$ have been recorded for comparison. For the first time, a two-bond coupling of the type $^2J(CH_3COOH)$ between a hydrogen-bonded proton and the carboxylic carbon has been observed, $^2J_{HC}$ = 3.0 Hz; for comparison, the corresponding $^2J_{HC}$ value in $CH_3{}^{13}COOH{\cdot}SbCl_3$ equals to 6.7 Hz.

The designed by Murata and co-workers[178] method of $^{2,3}J_{CH}$-based configuration analysis has been applied by Paterson *et al.*[179] to establish the stereochemical structure of dictyostatin, a novel microtubule-stabilising macrolide from the marine sponge *Corallistidae sp.*, and by Tsuda *et al.*[114] to elucidate the configuration of amphidinolide Y, a novel 17-membered macrolide from dinoflagellate *Amphidinium sp.* Two-and three-bond H-C couplings have been used by Toušek *et al.*[180] to assign the ^{13}C chemical shifts in the spectra of norsanguinarine and norchelerythrine, tertiary benzo[*c*]phenanthridine alkaloids.

DFT calculations of H-H and H-C couplings across two and three bonds[181] and a simulation of 2D ^1H homo- and ^1H-^{13}C heteronuclear NMR spectra of organic molecules[182] have been suggested by Biffulco *et al.* as a tool in the determination of the relative configuration of organic compounds.

The $^2J_{HN}$ couplings of the imine nitrogen with the aldimine proton of 3.3 to 6.4 Hz have been measured by Montalvo-González and Ariza-Castolo[65] for a series of 25 diaryl-aldimines indicating that all imines have a *E* configuration.

$^2J_{HO}$ couplings have been calculated by Wrackmeyer *et al.*[128] for methyl formate by the use of the DFT method and good agreement has been found between the calculated and experimental data.

A new elongated dihydrogen complex of iridium, $[Cp^*Ir(dmpm)H_2]^{2+}$, has been synthesized by Pons and Heinekey[60] and characterized by the use of NMR data which also included $^2J_{HP}$ couplings. It has been established that the compound exists in the form of *cis* and *trans* arranged dihydride isomers; $^2J_{HP}$ = 6 Hz for the *trans* and $^2J_{HP}$ = 20 Hz for the *cis* isomer have been found. The obtained data are in agreement with those reported earlier for the related $[CpOs(dppm)H_2]^+$ complex.[183]

6 Two-bond Couplings not Involving Hydrogen

Recently, Hilmersson and co-workers[184] have observed that in heterogeneous aggregates involving lithium amides and alkyllithium compounds, a $^2J_{LiLi}$ coupling can be measured between nonequivalent lithium nuclei belonging to a quadrilateral only if the two complementary atoms are carbons. A similar

observation has been made by Desjardins *et al.*,[185] who studied the aggregates between methyllithium and lithium bromide in toluene. In order to investigate this phenomenon the latter group of authors have calculated the Li-Li couplings in tetramers, $(MeLi)_n(LiBr)_{4-n}$, and found that the coupling values decrease rapidly with the inter-nuclei distances.

An analysis of multipath transmission of spin-spin coupling in cyclic compounds has been made by Wu and Cremer[186] with the help of partially spin-polarized orbital contributions. The calculations have been performed for cyclopropane, cyclopentane, bicyclo[1.1.1]pentane and tetrahydrofuran. The authors have shown that the measured and calculated $^2J_{CC}$ couplings of cyclopentane and tetrahydrofuran are averages over the pseudorotational motion of these ring molecules where each individual coupling of a conformation passed in the pseudorotation is the sum of different path contributions.

Carbon-carbon couplings across one, two and three bonds have been reported and discussed by Frimer *et al.*[187] for a series of cyclobutenones and benzocyclobutenones.

Long-range C-C, C-N and N-N couplings in selectively labelled Ni(II) complexes of the Schiff base derived from (*S*)-*N*-benzylproline(2-benzoylphenyl)amide and glycine have been measured by Popkov *et al.*[188] in $CDCl_3$ solution. Their analysis provided evidence that the donation of electron density from the π-system of the benzyl ring to the nickel orbitals takes place.

$^{1,2}J_{CSi}$ and $^{1,2}J_{CSn}$ couplings supported the proposed by Wrackmeyer *et al.*[189] structures of a series of propargyl derivatives with silicon-carbon and tin-carbon bonds.

$^2J_{CTl}$ couplings between *ca.* 40 and 65 Hz and $^3J_{CTl}$ couplings between *ca.* 35 and 60 Hz have been measured by Claramunt *et al.*[190] in the solid state ^{13}C NMR spectra of some thallium (I) tris-(pyrazol-1-yl)borates (thallium scorpionates).

A $^2J_{NF}$ coupling of *ca.* 95 Hz has been observed in the temperature variable spectra of a novel series of acid-base complexes of HF with 2,4,6-trimethylpiridyne (collidine).[191] The coupling value remains large over the whole range of temperatures applied (94 -170 K).

A $^2J_{NSn}$ coupling of 24 Hz has been observed by Santiago *et al.*[192] in the spectrum of *trans*-4-*tert*-butyl-2-(tributylstannane)piperidine but not in that of its *cis* isomer. In the first case the lone nitrogen pair and the C-Sn bond are eclipsed, in the other antiplanar. The authors also noticed that the tin-lithium transmetallation proceeds very easily for the *trans* compound, whereas isomer *cis* does not undergo this process.

Substituent effects on $^2J_{FF}$ in aliphatic and olephinic CF_2 moieties and on $^3J_{FF}$ couplings in fluorinated derivatives of ethylene have been studied by Barone *et al.*[193] by the use of SOPPA and DFT methods.

A two-bond scalar *J*-coupling between the quadrupolar Al and spin $^1/_2$ P nuclei of *ca.* 30 Hz has been determined successfully by Massiot *et al.*[194] in inorganic solids, such as berlinite ($AlPO_4$), hydrated $AlPO_4$ and VPI-5 molecular sieve using *J*-Resolved experiments, and subsequently used to acquire 2D *J*-HQMC heteronuclear correlation. Similar J_{PAl} coupling values have been measured in VPI-5 by Trebosc *et al.*,[57] who applied the FS REDOR (*F*requency

*S*elective *R*otational *E*cho *D*ouble *R*esonance) for this purpose.

$^2J_{SiSi}$ of 4.6 Hz has been observed in the ^{29}Si NMR spectrum of 2,5-bis(9-borabicyclo[3.3.1]non-9-yl)-2,5-bis(trimethylsilyl)-1,1-dimethyl-1-sila-3-cyclopentene and a $^2J_{SiSi}$ of 5.1 Hz in that of 2,5-bis(9-borabicyclo[3.3.1]non-9-yl)-2,5-bis(trimethylsilyl)-1-methyl-1-sila-3-cyclopentene.[74]

The double zwitterionic form has been suggested by Chęcińska *et al.*[195] for [(diphenoxyphosphinyl)methylidene]triphenylphosphorane, $Ph_3P{=}CH{-}P(=O)(OPh)_2$, on the basis of the NMR data which also included the measurement of the $^2J_{PP}$ coupling (45.5 Hz). The absence of the experimentally observable $^2J_{H\beta P\alpha}$ coupling has been tentatively rationalized in terms of fast pyramidalization of the C_β-anionic site.

A variation of the two-bond P-P coupling has been observed by Morita *et al.*[196-198] for the palladium and platinum complexes according to the type of complex. In the palladium series the coupling value increases from *ca.* 12 Hz in acid-free Pd(0) enone complexes such as $Pd(CH_2{=}CHCOCH_3)(PPh_3)_2$,[197] through Lewis acid adducts (13.5-37.4 Hz)[196], to the largest values for ordinary η^3-allylpalladium(II) complexes, *e.g.* $[Pd(\eta^3\text{-}MeCHCHCH_2)(PPh_3)_2]^+$,[196] where $^2J_{PP}$ of 46.5 Hz has been found. The reverse order has been observed by the authors for the platinum series.[198] Thus, $^2J_{PP}$ of *ca.* 17.1 and 18.9 Hz have been found in $(CH_2CHCCH_3(OBF_3))Pt(PPh_3)_2$ and $(CH_2CHCCH_3(OB(C_6F_5)_3))Pt(PPh_3)_2$, respectively, $^2J_{PP}$ of 37.8 Hz in the $Pt(CH_2{=}CHCOCH_3)(PPh_3)_2$ complex and $^2J_{PP}$ of 9.0 Hz only in the η^3-allylplatinum cation.

$^2J_{PP}$ couplings have allowed Coulliens *et al.*[199] to discriminate easily between the *cis* and *trans* PP isomers of oxo and phenylimido rhenium complexes with 2-[bis(ethoxyethyl)phosphino]phenolato ligand and its derivatives; $^2J_{PP}$ of *ca.* 5 Hz for the *cis* and $^2J_{PP}$ of *ca.* 235 Hz for the *trans* isomers have been observed.

Evidence of the AsAs coupling across two bonds has been obtained by Hari and co-workers[200,201] from the NQR studies on crystalline and glassy As-S/Se compounds. The experimental $^2J_{As\text{-}S\text{-}As}$ coupling values obtained for AsS_3 from the modulation of the decay of the transversal nuclear magnetization are consistent with the values estimated using empirical correlations obtained from the literature.

The anisotropies of the $^1J_{CSe}$ and $^2J_{SeSe}$ spin-spin coupling tensors in carbon diselenide have been obtained by Jokisaari and Autschbach[202] from ZORA DFT calculations and from NMR experiments performed in liquid crystalline solutions. The latter were based on the utilization of experimental D couplings and the computed ratio of the coupling tensor anisotropies.

An extensive NMR data set has been obtained by Wrackmeyer and co-workers[203] for a series of organometallic-substituted allenes. The geminal couplings $^2J_{SnSn}$ whose magnitude changes significantly depending on the other substituents are of particular interest; $^2J_{SnSn}$ of +165 Hz has been found in $(Me_3Sn)_2C{=}C{=}CH_2$ and +443.6 Hz in $(Me_3Sn)_2C{=}C{=}C(Et)C(SnMe_3)_2BEt_2$.

The presence of a $^2J_{PtPt}$ coupling of 130 Hz in *cis,cis*-$[Pt_2(\mu\text{-}SMe_2)(\mu\text{-}PN)]$ and of 275 Hz in $[Pt_2Me_3(O_2CCF_3)(\mu\text{-}SMe_2)(\mu\text{-}PN)]$ where PN = $2\text{-}Ph_2PC_5H_4N$,[204] provided solid evidence of their structure.

7 Three-bond Hydrogen-Hydrogen Couplings

The combined use of the simulated and experimental $^3J_{HH}$ couplings and ^{1}H ROESY spectra has been made by Peter *et al.*,[205] who performed a conformational analysis of the dipeptide Val-Phe isomers. Possible problems and pitfalls, when deriving structural properties of such small and extremely flexible molecules from the NMR data only, have been discussed by them.

^{1}H NMR methodology has been described by Hanna[206] for the determination and characterization of the dietary supplement *S*-adenosyl-L-methionine. The NMR characteristics also included a full set of H-H couplings measured in D_2O for this compound as well as for adenosine and L-methionine.

The thermodynamic data has been determined by Kimura *et al.*[207] for the side-chain conformational equilibrium of aspartic acid residue in both model Asp peptides (di- to tetra-) and neuropeptide achatin-I (Gly-D-Phe-Ala-Asp) in aqueous solution by the use of vicinal HH couplings.

The $^3J_{HH}$ couplings have been measured by Assfalg *et al.*[208] for 83 residues of a monomeric mutant of copper-zinc superoxide dismutase in the unfolded state, at 3.5 GdmCl, and have been found to be in the range of 5.0 to 7.8 Hz (the average value being 6.2 ($\pm$0.5 Hz). At variance with the native protein, none of the measured values falls in the typical range of β-structures (8.5 Hz, on average), while they are close to those reported for unstructured regions of proteins (6.6 Hz on average).

The combined use of 15 $^3J_{HH}$ couplings, 80 NOEs, and the assigned amide and amine protons complemented by the molecular dynamics calculations has allowed Papakyriakou *et al.*[209] to establish a well-defined solution structure of the Ga(III)-bleomycin A2 complex.

The databases which included the $^3J_{HH}$ coupling and the ^{1}H, ^{13}C and ^{1}H(OH) chemical shift databases for contiguous polyols have been reported by Kishi and co-workers.[210] The authors indicate that a stereochemical analysis based on three or two contiguous $^3J_{HH}$ profiles is operationally simpler than one based on ^{13}C and ^{1}H chemical shift profiles.

The calculated and observed vicinal H-H couplings and dihedral angles have been reported for the sugar moiety of 8-*C*-β-D-[2-*O*-(*E*)-*p*-coumaroyl] glucopyranosyl-2-(2-hydroxy)propyl-7-methoxy-5-methylchromone.[211] A conformational analysis based on $^3J_{HH}$ couplings and molecular mechanics calculations has been performed by Mikros *et al.*[212] for the three *C*-linked (1-1) D-glucosyl disaccharides, *C*-trehaloses. The results obtained indicate that α,α-trehalose is quite a rigid molecule adopting only one conformation around the C-glycosidic linkage, whereas the *α,β*- and *β,β*-isomers are rather flexible.

More examples of peptides and proteins for which these couplings have been used in structure determination are listed in Table 1. The corresponding data for nucleotides and carbohydrates are given in Table 2.

Vicinal H-H couplings have been applied in the structural studies of modified cyclodextrins[268] and used as constraints for the elucidation of the conformations around the $Cys_{C\alpha H}$-$Cys_{C\beta H}$ bonds in the selenotrisulfide formed by the reaction of selenite with end-capped phytochelatin-2.[269]

Table 1 *Peptides and proteins for which the solution structure has been calculated with $^3J_{HH}$*

Name	*a*	*b*	*Ref*
antillatoxin, a novel lipopeptide from *Lyngbya majuscula*	3	16	213
a series of the melantropin analogues	6	10-15	214
[MePhe^{2,3}]AVP; [D-MePhe^{2,3}]AVP	9	3;5	215
BVD10 and BVD15, two NPY analogues	9	7	216
BL-1, the linker part of rat brain type IIA Na^+ channel	11	9	217
cLBEL, a peptide derived from the β-subunit of LFA-1	12	25	218
microcin J25	21	14	219
des-(24-28) kalata B1	24	25	220
$IpTx_a$, wild type	33	25	221
SGTx1, a peptide toxin from the venom of the spider *Scodra griseipes*	34	27	222
rSP-C (FFI) a recombinant human PC with FFI substitution	34	23	223
HVcHP (792-826), C-terminal of human villin headpiece	35	10	224
HAcHP (784-819), C-terminal of human advillin headpiece	36	4	224
scarabaecin	36	32	225
palicourein	37	33	226
PhD1 *Petunia hybrida* defensin 1	47	54	227
[C/N] *Tm*Csp, the cold shock protein from the hypertermophilic bacterium *Thermotoga maritima*	63	25	228
[C/N] preCbnB2, the precursor of carnobacteriocin B2 from *Carnobacetrium piscicola*	66	33	229
[N] *apo* CopZ from *Bacillus subtilis*	73	31	230
[C/N] YbcJ from *E. coli*	77	70	231
[C/N] TcPABC (468-550)	83	78	232
[C/N] (M-1,Q1,M23L)rONC, Met^{23} mutated onconase	104	94	233
Gln25-RNase- T_1	104	35	234
[C/N] ALY (77-182)	106	77	235
[C/N] Npl4 NZF/Ub complex	107	>100	236
[C/N] Dy^{3+}-human α-parvalbumin	112	63	237
[C/N] VC0424, *Vibrio cholerae* protein	124	55	238
[C/N] aIF2β, β-subunit of aIF2 from *Methanobacterium thermoautotrophicum*	135	144	239
[C/N] N60D $(CaLn)_N(Ca_2)_C$CaM, Ln = Tb^{3+} or Tm^{3+}	146	93	240

[C/N] Q133M2SOD, *apo* Cu,Zn superoxide dismutase	151	42	[241]
[C/N] *apo* CopAab, N-terminal domain of the ATPase CopA from *Bacillus subtilis*	155	80	[242]
[C/N] Ku80 CTD (566-732)	167	116	[243]
[C/N] *apo* BsSco1 from *Bacillus subtilis*	174	90	[244]
[C/N] ShC PTB domain	191	<102	[245]
[C/N] DEN2C dimer, a flavivirus C protein	2x100	21	[246]
[C/N] IFNAR2-EC/IFNα2 complex	212	88	[247]

[a] the number of amino acid residues
[b] the total number of vicinal backbone and side chain proton-proton couplings measured

Table 2 *Nucleosides, nucleotides, oligonucleotides and carbohydrates for which $^3J_{HH}$ has been used as a structural parameter*

Name	*Ref*
bicyclic nucleosides locked in *S*-type conformations by hydroxyl functionalised 3′,4′-*trans* linkages	248
deoxyribonucleoside methanephosphonamidates	249
3′-amino-3′4′-BNA, a novel bridged nucleoside bearing a fused-azetidine ring	250
a series of 7-halogenated 7-deazapurine nucleosides	251
pyrimidine bi- and tricyclic nucleosides with locked sugars	252
2′- and 3′-modified thymidine analogues	253
[3.2.0]bcANA, a modified dsDNA nonamer	254
an LNA-RNA hybrid	255
DNA-RNA hybrid duplex with 3′-*S*-phosphorothiolate modified DNA	256
carbohydrates	
a series of sulfur-containing 6-deoxy-L-hexose derivatives	257
a series of furanoid ε-sugar amino acid containing cyclic peptides	258
a series of the diisopropylidene derivatives of galactose	259
a cyclic tetrasaccharide with two kinds of glucoses alternatively bonded by α-1,3 and α-1,6 linkages	260
3,4-di-*O*-substituted heptose and several related oligosaccharides	261
a series of per-substituted β-cyclodextrins	262
octakis(3-*O*-butanoyl-2,6-di-*O*-pentyl)-η-cyclodextrin	263
methyl 3-azido-2,3-dideoxy-α-D-*lyxo*-haxapyranoside and its derivatives	264
a series of modified glycopeptides related to cell wall peptidoglycan	265
a series of phenylathanoid glycosides	266
a series of α-D-mannose derivatives	267

Vicinal proton-proton couplings have been applied to establish the stereochemistry of three monoterpene glucosides isolated from the methanol extract of *Portulaca oleracea*,[270] of one new and several known abietane diterpenes isolated from the roots of *Aegiphila lhotzkyana*,[271] and to elucidate the solution-state conformational equlibria of *trans*-4',7-dihydroxyisoflavan-4-ol and *trans*-isoflavan-4-ol.[272] The complete assignment of ^{1}H and ^{13}C NMR including $^3J_{HH}$ couplings has been reported by Vizzotto *et al.*[273] for the sequiterpene (+)-10β,14-dihydroxy-*allo*-aromadendrane. A large $^3J_{H9H11\alpha}$ coupling of 10.3 Hz has been found in the spectrum of 3α-acetyl-20(29)-lupene-24-oic acid, a novel pentacyclic triterpene isolated from the gum resin of *Boswellia serrata*.[274] This value indicates a relaxed chair-chair conformation of both rings, A and B, in this compound. Comparison between the experimental and calculated $^3J_{HH}$ couplings and the analysis of molecular mechanics structures performed for a series of nor-secofriedelanes isolated from the sedative extracts of *Galphimia glauca* has shown that the ring B of these compounds exists in a boatlike conformation.[275]

Wysocka and Brukwicki[276] have continued their studies on quantitative determination of the conformational equilibrium by the use of $^3J_{HH}$ couplings in quinolizidine-piperidine alkaloids. The compound studied, *N*-methylalbine, was synthesized for the first time. The couplings have been also useful in establishing the structure of three new piperidine alkaloids, (−)3-*O*-acetylspectaline, (−)-7-hydroxyspectaline and iso-6-spectaline isolated from *Cassia spectabilis*.[277]

A series of gradient enhanced selective 1D experiments has been applied by Forgo and Kövér[278] yielding unambiguous assignments for signals of the main skeleton and the side-chain of stigmasterol, a phytosterol derivative, and allowing determination of the conformationally important homonuclear proton-proton couplings. A complete ^{1}H and ^{13}C NMR spectral analysis which also included $^{2\text{-}4}J_{HH}$ couplings has been performed by Ciuffreda *et al.*[279] for 17β- and 17α-hydroxy epimers of three biologically active sterols: boldenone, 3-methoxyestradiol and 3-methoxydihydroequilenin, and by Wei *et al.*[280] for two phytosterols isolated from the roots of *Piper nigrum*. $^3J_{HH}$ couplings have been used in structural elucidation of two new withasteroids, withaphysalin M and withaphysalin N, isolated from the leaves of *Acnistus arborescens*.[281]

An extensive use of $^3J_{HH}$ couplings has been made by Tolonen and co-workers[282] in order to elucidate the dihedral bond angles in 5'-*O*-caffeoylquinic acid and three isomeric 1'5'-*O*-, 3',5'-*O*- and 4',5'-*O*-dicaffeoylquinic acids.

Vicinal H-H couplings have been of some help in establishing the structure of the new antraquinone, evariquinone, the new prenylxanthone, isoemericellin, and the known 1,2,3-tetrahydroxy-6-methylanthraquinone, 7-hydroxyemodin, isolated from a sponge derived strain of the fungus *Emericella variecolor*.[283]

Proton-proton couplings have been applied in the elucidation of the structures of three *seco*-iridoids, 7-methoxydiderroside, 6'-*O*-acetyldiderroside and 8-*O*-tigloyldiderroside isolated from the wood bark of *Calycophyllum spruceanum*,[284] to perform a conformational analysis of artemisiifolin isolated from *Stachelina dubia* and three related germacranolides,[285] and to establish the structures of three novel metabolites, tuscolid and tuscoron A and B isolated from the myxobacterium *Sorangium cellulosum*[286] and Palau'amide, a potent cytotoxin

isolated from a species of the marine cyanobacterium *Lyngbya*.[287]

$^3J_{HH}$ and $^4J_{HH}$ couplings have been measured by Katrizky *et al.*[288] for regioisomeric 3-[2- or 5-anilino-2-(alkylamino)phenyl]propanoic acids, 2*H*-1,4-benzothioazin-3(4*H*)-ones and 2,3-dihydro-1,5-benzothiazepin-4(5*H*)-ones, by Suri *et al.*[289] for a series of pyrido[1,2-*a*]pyrimidine derivatives, and by Laatsch and co-workers[290] for helquinoline, a new tetrahydroquinoline antibiotic isolated from *Janibacter limosus*. The configuration around the double bonds and the epoxide stereochemistry of oximidine III, a new antitumor antibiotic against transformed cells from *Pseudomonas sp.*, has been established on the basis of $^3J_{HH}$ by Hayakawa *et al.*[291]

The $^3J_{HH}$ couplings have been used by Abraham and Koniotou[292] to determine the conformer populations of *cis*- and *trans*-cyclopentane-1,3-diol by the use of the Haasnoot, de Leeuw and Altona equation; for the C-CH_2-CH_2-C fragment the following equation has been derived from five- and six-membered cyclic compounds in fixed conformations:

$$^3J_{HH} = 11.16 \cos\varphi^2 - 1.28 \cos\varphi + 0.77$$

Tormena and co-workers[293] have continued their studies on conformational isomerism in 2-substituted cyclohexanones by the use of $^3J_{H2H3}$ couplings and the solvation model. The conformer energies in the solvents studied and the couplings for the distinct conformers have been obtained for 2-*N*,*N*-dimethylamino, 2-methoxy, 2-methylthio and 2-methylseleno derivatives.

A conformational analysis of substituted 1,3-dioxanes[294] and 2,5-disubstituted 1,3,2-dioxaborinanes[295] has been performed by Kuznetsov *et al.* by the use of vicinal proton-proton couplings and quantum-chemical methods.

Conformer populations have been established for two potential antycholinesterasic agents, *cis*-2-*N*,*N*-dimethylaminecyclohexyl 1-*N*',*N*'-dimethylcarbamate and *trans*-2-*N*,*N*-dimethylaminecyclohexyl 1-*N*',*N*'-dimethylcarbamate, by a combination of $^3J_{HH}$ couplings and DFT calculations.[296]

A detailed NMR analysis has been performed by Constantino *et al.*[297] for two polycyclic compounds containing bicyclo[6.2.1]undecane ring systems yielding a full assignment of the ^{1}H and ^{13}C signals and a set of proton-proton couplings.

An interesting conformational analysis by the use of $^3J_{HH}$ couplings has been performed by Murata and co-workers[298] on the acyclic polyamine spermidine and its trihydrochloride or tripolyphosphate salt as model systems for studying the interactions between a bioactive compound and its target molecule. In order to simplify the very complex and extremely difficult to analyse flexible and non-first order ^{1}H NMR spin system the authors undertook an effort to synthesize diastereospecifically deuterated spermidine, (1*S**,2*S**)-1,8-diamino-4-azaoctane-1,2,3,3,5,5,6,6,7,7,8,8-d_{12}. The detailed investigation of the vicinal proton-proton coupling measured for this molecule at different p*H* revealed that spermidine undergoes conformation change upon complexation with polyanion.

$^3J_{HH}$ couplings provided crucial information about the arene-arene influence on the conformation of 2-methyl-1,3-propanediol substituted with different aromatic residues that are linked to the diol spacer by ether or ester functionalities.[299] The vicinal couplings have been used for the calculation of the dipole

moments of some derivatives, and excellent agreement with the experimental values has been found.

In continuation of their studies of conformational equilibria and acid-base behaviour of dicarboxylic acids as a function of solvent, Roberts and co-workers[300] have published the results obtained for 2-carboxy-1,4-butanedioic acid and its mono-, di-, and trianions in dimethyl sulfoxide which were investigated exclusively by the use of $^3J_{HH}$ couplings.

The NMR spectral characteristics has been obtained by Balazs *et al.*[301] for a series of metal-free, metallated and substituted corroles. An excellent correlation has been observed between the C=C bond lengths derived from $^3J_{HH}$ coupling values and the experimental lengths determined by X-ray crystallography of the same molecules.

The first successful application of NMR spectroscopy for the detailed structural assignment of a delocalised carotenoid carbocation has been reported by Lutnaes *et al.*[302] The measurements performed at low temperature allowed the authors to assign completely ^{1}H, and ^{13}C NMR chemical shifts and to measure $^3J_{HH}$ couplings. The latter have been compared with the corresponding couplings of the parent β,β-carotene which allowed an insight into the bonding situation of the cation.

An extensive analysis of $^3J_{HH}$ couplings performed by Ito *et al.*[303] for stable tris-, bis- and mono[9-(azuleno[1,2-*b*]thienyl)]methyl cations provided a valuable insight into the bonding situation of the seven-membered rings in these compounds. Vicinal proton-proton couplings have been used by Borodkin *et al.*[304] to study a series of nitrosonium cations.

Vicinal H-H couplings provided information on the S-C-C-S torsional angles in the Pd(II) complex of 1,4,7,10-tetrathiacyclododec-2-ene-2,3-dicarbonitrile studied by Holzberger and Kleinpeter.[305]

$^3J_{HH}$ couplings have been found to be useful in the investigation of the microstructure of modified polymers. The subsequent papers on this topic have been published by Hooda *et al.*[306,307]

8 Three-bond Couplings to Hydrogen

The combined application of molecular dynamics and NMR data which included $^3J_{HC}$ couplings and NOE-derived distances has allowed Kony *et al.*[308] to establish the conformational preferences around the glycosidic linkages in β-laminaarabinose and β-gentiobiose. They have also suggested that out of two Karplus-type $^3J_{HH}$ equations functioning in the literature that of Stenutz *et al.* is superior to the widely used equation by Haasnoot *et al.*

The combined use of the DFT calculated and experimentally determined $^3J_{HH}$ and $^3J_{HC}$ couplings complemented by the NOE's results has allowed Woods and co-workers[309] to elucidate correctly the conformation of (1*R*,6*R*,7*R*,8*S*)-7,8-dihydroxy-7-thia-1-thioniabicyclo[4.3.0]nonane chloride, a member of the sulfonium salt class inhibitors.

More examples of peptides and proteins for which these couplings have been

Table 3 *Peptides and proteins for which heteronuclear couplings have been used as a structural parameter in 3D structure calculations*

Name	*a*	*b*	*c*	*Ref*
[N] NIP1, the plant disease resistance-triggering protein	60	45	$^3J_{HN}$	310
[C/N] GB1 dimer, immunoglobulin-binding domain B1 of streptococcal protein G	56 × 2	*d*	$^3J_{HN}$, $^3J_{CC}$, $^3J_{CN}$	311
[N] RicC3, a 2S albumin storage protein from *Ricinus communis*	125	100	$^3J_{HN}$	312
[N] $NTR^{PCOLCE1}$	154	370	$^3J_{HN}$	313
[C/N] IIA^{Glc}(11-168)-IIB^{Glc} (12-90/P17A) complex	237	69	$^3J_{CC}$, $^3J_{CN}$	314

[a] number of residues
[b] total number of vicinal couplings measured (homonuclear $^3J_{HH}$ couplings are also included if measured)
[c] types of heteronuclear couplings measured
[d] number not reported

Table 4 *Nucleosides, nucleotides, oligonucleotides and carbohydrates for which heteronuclear vicinal couplings have been used as a structural parameter*

Name	*a*	*b*	*Ref*
2-substituted wyosine derivatives	1	$^{3}J_{HC}$	315
phosphorylated 3′-*O*-β-D-ribofuranosyl-2′-deoxythymidine	1	$^{3}J_{HP}$	316
serine-3′- and 5′-thymidine monophosphate conjugates	1	$^{3}J_{CP}$	317
2′- and 3′methoxy cylic adenosine 5′-diphosphate ribose	1	$^{3,4}J_{HP}$	318
ASL^{Phe}-(Cm_{32},Gm_{34},$m^{1}G_{37}$,$m^{5}C_{40}$) and ASL^{Phe}-(Cm_{32},Gm_{34},$m^{5}C_{40}$)	17	$^{3}J_{HP}$	319
d(CGCGAATTCGCG)$_2$	24	$^{3}J_{HP}$	320
[C/N] d(GCA$_4$T$_4$GC) and d(CGT$_4$A$_4$CG)	24	$^{3}J_{HP}$	321
a DNA with incorporated a disaccharide nucleoside	24	$^{4}J_{HP}$	322
DDI-bulged DNA complex	26+	$^{3}J_{HP}$	323
ent-DDI-bulged DNA complex	26+	$^{3,4}J_{HP}$	324
the stemloop D subdomain of Coxsackievirus B3 cloverleaf RNA	30	$^{3}J_{HP}$	325
carbohydrates			
synthetic pentasaccharides related to the O-specific polysaccharide of *Shigella flexneri* 5a		$^{1}J_{HC}$,$^{3}J_{HC}$	326
polysaccharide O-antigen of *Salmonella* Aberdeen (O:11)		$^{1}J_{HC}$	327
boronate complexes of several monosaccharides		$^{1}J_{HC}$	328
a series of gluco- and galactopyranosides		$^{1}J_{HC}$	329

[a] the number of nucleotides
[b] type of vicinal heteronuclear couplings measured; $^{3}J_{HH}$ homonuclear couplings have also been measured in most cases

used in structure determination are listed in Table 3. The corresponding data for nucleotides and carbohydrates are given in Table 4.

A conformational analysis of a guaiacyl β-O-4 lignin model compound has been performed by Besombes *et al.*[330-332] by the combined use of vicinal proton-carbon and proton-proton couplings. It allowed them to discriminate between *gauche*(−) and *gauche*(+) orientations and revealed that both *trans* and *gauche*(−) orientations of the C1-Cα-Cβ-O4' torsional angle are predominant in solution, precluding an extensive existence of *gauche*(+) orientation.

Vicinal H-C couplings are a valuable tool in the determination of the configuration around the C=C double bond in α,β-unsaturated carbonyl compounds, since those for nuclei with *Z*-orientation are smaller than the couplings for the *E*-oriented nuclei, 2-6 Hz and 8-12 Hz, respectively.[333,334]

The H-C couplings across one, two and three bonds have been measured by Györgydeák *et al.*[335] for a series of 2-amino-4-aryl-1-arylideneaminoimidazoles and their acylation products. The data obtained allowed the authors to assign the configuration (*E*) at the exocyclic C=N bond. The *Z* configuration has been assigned to 2-diisopropylamino-3,5-dihydro-5-[(4-methoxyphenyl)methylene]-3-phenyl-4*H*-imidazol-4-one on the basis of $^3J_{HC}$ = 5.6 Hz.[336]

A recently developed approach based *inter alia* on molecular modelling and on analysis of NMR data including vicinal proton-carbon couplings has been tested by Tanaka *et al.*[337] They used one of the synthetic chiral dihydrofuroangelicines, 4-methyl-8(2-*E*-phenylethenyl)-8,9-dihydro-2*H*-furo[2.3-*h*]-1-benzopyran-2-one, as a model compound and extended the method to establish the absolute stereochemistry of six new dihydrofuroangelicins bearing C-8 substituted double bonds.

The one- and three-bond H-C couplings of the Me_2N group in 8-dimethylamino-napht-1-yl phosphines and their derivatives have been found by Schiemenz *et al.*[338] to be useful indicators of the N-P interactions in these compounds.

The $^3J_{HF}$ and $^3J_{HH}$ couplings have been found to be a reliable criterion in establishing the regiochemistry and stereochemistry of a few [1-fluoroalkyl]-3-ethyl-2-isoxazolines obtained by the cycloaddition of nitrile oxides to some allylic fluorides[339] and of individual regioisomeric and tautomeric pairs of $H(CF_2)_2$-containing isoxazoles and pyrazoles.[340]

The vicinal H-C and H-P couplings measured from the 3D NMR spectra of 1-(*S*)-*N*-[2-(diphenylphosphinyl)naphtyl-2-(hydroxymethyl)pyrrolidine and 1-(*S*)-*N*-[2-(diphenylphosphinyl)naphtyl]-2-(pyrrolidinylmethyl)pyrrolidine have been used to determine the dihedral angles in these compounds.[341]

A set of spin-spin couplings with their signs including those across two and three bonds, $^2J_{HPt}$ and $^3J_{HP}$, have been determined for alkyl and aryl complexes of Pt(II) and Pd(II) containing the tri(1-cyclohepta-2,4,6-trienyl)phosphane ligand.[342]

The *cis*/*trans* stereochemistry of a series of trivalent amino acid derived chiral phosphorus compounds has been established on the basis of $^3J_{HP}$ couplings: all of the *cis* isomers exhibited for the ring hydrogen $^3J_{HP}$ = 3.4-3.7 Hz while all of the *trans* isomers revealed $^3J_{HP}$ = 1.4-1.8 Hz. It should be mentioned that the

geometry of one of the compounds, (2*S*,4*S*)-4-isopropyl-5-oxo-2-phenyl-3-*p*-toluenesulfonyl-1,3,2-oxazaphospholidine, has been established by the use of X-ray and the $^3J_{HP}$ value obtained for it has been used as the reference value for the remaining compounds studied.[343]

A novel silsesquioxanyl phosphine ligand and its Pt and Mo complexes have been fully characterized by the use of NMR spectroscopy.[344] In particular, the $PNCH_3$ groups display a characteristic doublet with $^3J_{HP}$ of *ca.* 10 Hz.

Rochon and co-workers have continued their studies on the platinum complexes by the use of NMR. They have investigated a new type of pyrazine-bridge platinum(II) complexes, *cis* and *trans*-Pt(R_2SO)pyrazine)Cl_2[345] and *trans,trans*-Pt(R_2SO)Cl_2(μ-pyrazine)Pt(R_2SO)Cl_2[346] mainly by the use of IR and NMR spectroscopies; for the *trans* isomers of the compounds studied couplings with the pyrazine protons $^3J_{HPt}$ between 28 and 35 Hz have been observed. Another group of the compounds investigated by them included Pt(amine) complexes, *cis*- and *trans*-Pt(amine)$_2$(NO_3)$_2$[347] and *cis*- and *trans*-Pt(amine)$_2I_2$[348] for which the relationship $^2J_{HPt}$ (*cis*) and $^3J_{HPt}$ (*cis*) larger than the corresponding $^2J_{HPt}$ (*trans*) and $^3J_{HPt}$ (*trans*) couplings has been observed. The same applied to the $^2J_{CPt}$ and $^3J_{CPt}$ couplings.

A full NMR characteristics which also included three-bond N*H*-C*H* and *H*C-N-*Pt* couplings, has been obtained by Al-Najjar *et al.*[349] for a series of complexes of the type *trans*-[$PtCl_2$(η^2-ethene)(*N*-ferrocenylmethyl)amine] where *N*-ferrocenylmethyl)amine = [(η^5-C_5H_5)Fe(η^5-$C_5H_4CH_2NHR$)] and R's are a variety of alkyl and aryl substituents; $^3J_{HH}$ of *ca.* 5 Hz and $^3J_{HPt}$ of *ca.* 30 Hz have been observed.

9 Three-bond Couplings not involving Hydrogen

The new empirical Karplus relationships for $^3J_{C'C\gamma}$ and $^3J_{NC\gamma}$ in proteins have been obtained by Bax and co-workers.[350] The couplings required to parametrize these relationships have been measured for ubiquitin and the third IgG-binding domain of protein G. The experimental Karplus curves have been confirmed by the DFT calculations including an unusual phase shift which causes the maximum $^3J_{CC\gamma}$ and $^3J_{NC\gamma}$ couplings to occur for dihedral angles slightly smaller than 180°. The new Karplus curves permit determination of rotamer populations for the χ_1 torsion angles.

The effects of mutations on the motions of side-chains in the B1 domain of peptostreptococcal protein L and in a pair of point mutants of the domain, F22I and A20V, have been investigated by Millet *et al.*[351] by the aid of methyl ^2H spin relaxation rates and three-bond C_γ-C(O), C_γ-N and C_α-C_δ couplings. It is noteworthy that the measurements of the relaxation rates provide information on a picosecond-nanosecond time scale, whereas *J* couplings span a wide range of time-scales.

$^3J_{CP}$ couplings are a valuable source of information on the geometry of a double CC bond: $^3J_{CP\,(trans)}$ (16 Hz or larger) > $^3J_{CP(cis)}$ (6-10 Hz). This relationship has been applied by Panarina *et al.*[352] to establish the structure of diethyl-2-

diethylaminoalkenephosphonates obtained by the addition of secondary amines to diethyl alkynephosphonates for which $^3J_{CP}$ of 5 Hz have been measured, suggesting *cis* addition.

A spectral characteristics, which also included $^{2,3}J_{CP}$ couplings, has been obtained for three new C-bonded cyclotriphosphazenes, $[N_3P_3(2\text{-thienyl})_6]$, $[N_3P_3(3\text{-thienyl})_6]$ and $[N_3P_3(3,3'\text{-bithienyl-}2,2'\text{-ylene})_3]$, the first examples of non-spiro and trispirocyclotriphosphazene derivatives composed of thiophene and 3,3'-dithiophene substituents, respectively.[353]

$^{1\text{-}3}J_{CP}$ couplings for dichloro(diisopropyloamino)phosphonio[5(4*H*)-oxopyrazol-4-ylide-5-one] and the products of its reaction with various nucleophilic reagents have been measured by Konovets *et al.*[354]

$^{1\text{-}3}J_{CP}$ couplings have been determined by Liu *et al.*[355] for two conformers of fosinopril sodium, the only angiotensin-converting enzyme (ACE) inhibitor that depends on a phosphinyl group to inhibit ACE by a zinc ligand relationship.

The $^{1\text{-}3}J_{CP}$ couplings have been measured by Marinič *et al.*[356] for diethyl 2- and 8-quinolylmethylphosphonates and their palladium(II) dihalide complexes, *trans*-$[PdL_2X_2]$, X = Cl, Br; in the ligands additionally the C-P couplings across four and five bonds have been observed.

A spectral characteristics of 1-(β-apo-8'-carotenoyl)-2-lyso-*glycero*-3-phosphocholine, 1-(β-apo-8'-carotenoyl)-3-lyso-*glycero*-2-phosphocholine, 1-(β-apo-8'-carotenoyl)-3-[(2-bromoethyl)phosphoryl]glycerol and 1-(β-apo-8'-carotenoyl)-2-[(2-bromoethyl)phosphoryl]glycerol has been reported by Foss and Krane,[357] who also measured two- and three-bond C-P couplings of *ca.* 6-7 Hz for these compounds.

The solution conformation of *N*-methyl-2-(tributylstannyl)piperidines has been investigated by Santiago *et al.*[192] by the use of the Kitching-Karplus relationship [358] between the Sn-C-C-C torsion angle and $^3J_{CSn}$ couplings:

$$^3J_{CSn} = 30.4 - 7.6\cos\theta + 25.2\cos 2\theta$$

The authors emphasize that the values of the torsion angles derived in this way are reliable. They have found that the equatorial conformer of the compounds studied is in reality distorted into a half-chair.

A conformational analysis of the cyclohexane, oxane, and thiane derivatives bearing both trimethylsiloxy (or methoxymethyleneoxy) and tributystannyl groups at the geminal position has been performed by Goto *et al.*[359] on the basis of $^3J_{CSn}$ couplings and ^{13}C NMR chemical shifts measured at low temperature.

In an elegant paper recently published by Malkina and Malkin[360] the authors have described a new method which implements real-space functions allowing visualization of nuclear spin-spin coupling pathways. Among others, a picture presenting $^3J_{PP}$ coupling energy density (CED) in the model $H_3P\cdots PH_3$ system has been shown.

10 Couplings over More than Three Bonds and Through Space

The conformations of *cis*- and *trans*-cyclopentane-1,3-diol have been studied by

Abraham and Koniotou[292] by the use of NMR spectroscopy and by *ab initio* and molecular mechanics. The complete analysis of the ^{1}H NMR spectra yielded all the H-H couplings for the *cis* isomer including a long-range $^4J_{HH}$ coupling between H-2*cis* and H-4,5*cis*.

A detailed NMR analysis of a cyclic allylsilane, [(2*R**,3*S**)-1,1-diphenyl-2-vinyl-1,2,3,6-tetrahydrosilin-3-ol], has been performed by Mahieux *et al.*[361] yielding a set of proton-proton couplings including the allylic $^4J_{HH}$ and homoallylic $^5J_{HH}$ ones. These values have been used as NMR constraints to calculate the 3D structure of the compound.

Proton-proton couplings including vicinal and long-range ones have been determined for the sesquiterpene lactone 15-deoxygoyazensolide[362] and a series of six volatile sesquiterpenes.[363] In particular, the $^4J_{HH}$ coupling values determined for (3*S*,4*R*,5*R*,9*S*,10*R*,11*S*)-morelian-7-one are in agreement with the W-type geometries found in the molecular model of this compound.

The steric and electronic structure of 2-(2-acylethenyl)pyrroles has been studied by Ushakov *et al.*[364] by the use of NMR including $^3J_{HH}$ and $^4J_{HH}$ couplings.

The $^5J_{H4H5}$ coupling of 0.55 Hz in phenantrene has been found to be very close to the other ^5J couplings in this compound, *i.e.* $^5J_{H1H4}$ and $^5J_{H4H10}$, which are of *ca.* 0.6 Hz.[365] This result indicates that there is no significant through-space coupling between the 4- and 5-hydrogen.

Long-range $^{5,6}J_{HH}$ couplings have been observed in the spectra of novel β-(styryl)terthiophenes, the key building blocks in the synthesis of functionalized conducting polymers.[366]

An extensive use of proton-proton couplings has been made by Akhmedov *et al.*[367] in their studies on the exchange between rotamers of derivatives of octahydrofuro[3,4-*f*]isoquinoline-7(1*H*)-carboxylate and tetrahydro-2,5,6(1*H*)-isoquinolinetricarboxylate. ^{1}H NMR spectra including a set of long-range couplings have been published by Katrizky *et al.*[368] for a series of thio-substituted N^1-(1,3-dimethylbutyl)-N^4-phenyl-1,4-phenylenediamines.

$^{3\text{-}5}J_{HH}$ couplings have been measured by Brownstein and Zhou[369] for a series of the parent and Ru coordinated 2,2'-bipyridyls, and $^{2\text{-}4}J_{HH}$ couplings have been applied by Engoyan[370] to determine the conformation of 3-oxotiazolidino[3,2-a] piperazine and its derivatives.

The long-range couplings of a series of acetylenic derivatives have been calculated by Alkorta and Elguero[371] by the use of the finite perturbation method. In the case of dimethylated derivatives a Karplus-type relationship has been observed by them for couplings of hydrogen atoms separated up to 15 bonds.

^{13}C chemical shifts and $^nJ_{HC}$ couplings have been determined by Bagno *et al.*[372] both experimentally and theoretically (by DFT calculations) for a series of organic molecules such as furan, *o*-dichlorobenzene, *o*-chloro, bromobenzene and naphthalene. The authors *inter alia* investigated conformational effects on the long-range H-C couplings in a model alkane derivative, *i.e.* *n*-butyl chloride.

The solvent dependent study carried out by Tormena *et al.*[373] on the NMR spectra of (*E*)-fluoroacetoxime and its *O*-methyl ether has shown that $^4J_{HF}$ and

$^1J_{CF}$ couplings, but not $^3J_{NF}$, are sensitive towards conformation of the compounds investigated. An analysis of $^1J_{CF}$ and $^4J_{HF}$ by solvation theory and assuming that both compounds exist in the *cis* and *gauche* forms yielded the ΔE values in the vapour phase, CCl_4 and DMSO.

The β-pyrrole protons of metal-free, metallated and substituted corroles studied by Balazs *et al.*[301] demonstrate long-range heteronuclear couplings including those across six bonds with the *orto*-^{19}F nuclei of the *meso*-carbon aryl rings.

Spectral characteristics including H-H couplings has been reported by Umemiya *et al.*[374] for *meso*-tetrakis(4-*t*-butylphenyl)porphyrinatoplatinum (II) and the parent porphyrin. However, the authors have not been able to observe the long-range H-Pt coupling of *ca.* 8 Hz reported in the literature for the analogous Pt(Pors) complexes.

$^{1\text{-}5}J_{CN}$ couplings have been measured by Schilf for five Schiff bases obtained from substituted salicylaldehydes and methylamine.[118]

$^{1\text{-}4}J_{CF}$ couplings have been measured for three DL-phenylalcoholamide anticonvulsants bearing fluorine at the phenyl ring.[375]

C-P couplings across one up to four bonds have been measured by Gáti *et al.*[376] for four phosphine chalcogenides, $Ph_3P{=}Ch$, Ch = Se, S, O, and $Ph_2(CH_3)P{=}O$ and compared with the couplings obtained for their adducts with the chiral dirhodium complex [Rh-Rh].

Rather large C-Cd(Hg) and H-Cd(Hg) couplings which are transmitted directly between the metal and the arene (a through-space mechanism) have been observed by Stępień *et al.*[75] in the spectra of Cd(II) and Hg(II) complexes of benziporphyrins. DFT calculations performed for two Cd(II) species and the subsequent AIM analysis have shown that the accumulation of electron density between the metal and arene necessary to induce these couplings is fairly small and the interaction is steric in nature.

Very large C(4)-H···Tl couplings between the C(4) atom of a pyrazole fragment and the nearest thallium atom of another molecule have been observed by Claramunt *et al.*[190] in the solid state spectra of thallium (I) tris-pyrazol-1-yl)borates (thallium scorpionates). They varied between 194 and 282 Hz and disappeared in solution, which seems to confirm their rather unusual origin. A related observation has been reported by Janiak and co-workers[377] in the case of a molecular $C_5(CH_2Ph)_5Tl$ complex in solution where the *orto*-phenyl carbon also shows an unusually large C-Tl coupling of 43 Hz.

Good agreement has been observed by Del Bene *et al.*[378] between the experimental two-, three- and four-bond F-F spin-spin couplings and those calculated by the use of the *ab initio* EOM-CCSD (equation-of motion coupled cluster singles and doubles) theory for a set of small fluoro-substituted organic molecules. Interesting calculations of F-F couplings by the use of the second-order polarization propagator approximation approach have been carried out by Provasi *et al.*[379] for four series of compounds: alkanes, conjugated polyenes, conjugated polyynes and cumulenes, where the coupled fluorine nuclei are separated by up to 11 bonds or 1.4 nm. The authors predict that the coupling over 9 bonds or 1.2 nm is of 12 Hz in (1*E*,3*E*,5*E*,7*E*)-1,8-difluoroocta-1,3,5,7-

tetraene, and the coupling over 11 bonds or 1.4 nm is 7 Hz in difluorodecapentayne.

The structure of a number of compounds that show experimental F···F coupling through space has been studied by Alkorta and Elguero,[380] who used the HF-DFT and AIM approaches. For all the cases with strong couplings a bond critical point and the corresponding bond path between the fluorine atoms involved have been found in the electron density map.

F-F through-space couplings have been applied by Schwarz *et al.*,[381] who performed studies on the structural properties of perfluorinated linear alkanes. They proposed a molecular model in which delocalized p-electrons of the fluorines cover the entire surface of the molecule in two pairs of intertwined helices.

Long-range F-F couplings have been applied by Darwish *et al.*[382] in the attempts to assign the structures of numerous products obtained as a result of trifluoromethylation of C_{60}-fullerene.

The first cationic perfluoroaryllanthanoid(II) complexes have been studied by Deacon *et al.*[383] by the use of NMR; for the diamagnetic complex $[Yb(C_6F_5)(THF)_5][BF_4]$ couplings between the F and Yb nuclei across three, four and five, bonds, 48, 33 and 8 Hz, respectively, have been observed in the spectra measured at −30 °C. Similarly, couplings across three and four bonds have been found in the low-temperature spectrum of the $[Yb(C_6F_5)_2(THF)_4]$ compound. These results provide the first examples of the F-Yb couplings reported in the literature.

Unusually large P-P couplings across four bonds of *ca.* 40 Hz have been observed by Omelańczuk *et al.*[384] for two chiral 1,8-bis(*t*-butylphenylphosphino)naphtalene sulfides obtained from the racemic 1,8-bis(*t*-butylphenylphosphino)naphthalene.

Couplings across five bonds between two tin nuclei, $^5J_{117Sn119Sn}$ = 8.6 Hz and $^5J_{119Sn119Sn}$ = 7.0 Hz, have been observed in the spectra of the products of 1,1-organoboration of ethoxyethynyl(trimethyl)stannane, and used by the authors as proof that the tin atoms are in the same molecule[385] (Fig. 7).

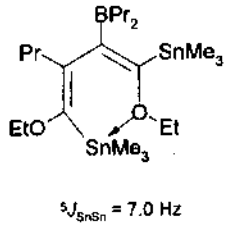

Figure 7

However, the *J* values reported are most obviously inconsistent (also when giromagnetic coefficients are taken into account) and it is not possible to conclude which value is the correct one.

11 Couplings Through Hydrogen Bonds

The $^{3}J_{HH}$ couplings in six H-X-Y-H systems (ethane, methylamine, methanol, hydrazine, hydroxyloamine and hydrogen peroxide) and $^{4h}J_{HH}$ couplings in four systems H-X···H···Y-H, $[H_3N\cdots H\cdots NH_3]^+$ (two arrangements), $HOH\cdots NH_3$ and $HOH\cdots OH_2$ have been calculated theoretically by Alkorta and Elguero[386] in a search of relationship between vicinal H-H and supramolecular couplings.

The structural, energetic, and spectroscopic properties of the dihydrogen-bonded complexes $LiH\cdots H_2$, $LiH\cdots CH_4$, $LiH\cdots C_2H_6$ and $LiH\cdots C_2H_2$ have been investigated by Cybulski *et al.*[387] They have found that the complexation induced changes in the coupling $^{2h}J_{HX}$ between the proton of LiH and the hydrogen or carbon nucleus correlate with the interaction energy, whereas the changes in $^{1h}J_{HH}$ do not.

The positive signs of reduced two-bond spin-spin couplings $^{2h}K_{X,Y}$ across X-H-Y hydrogen bonds have been predicted by Del Bene and Elguero[388] for complexes stabilized by C-H-N, N-H-N, O-H-N, F-H-N, C-H-O, O-H-O, F-H-O and C-H-F hydrogen bonds.

Correlation between hydrogen-bond stability and *J*-coupling through a hydrogen bond has been studied theoretically by Kawahara *et al.*[389] The relationship has been found to be dependent on the type of the nucleus forming the H-bond; the linear correlation has been observed in N-H···O/N type or O-H···N type H-bonded complexes, but not in O···H···O type H-bonded complexes.

A thorough theoretical investigation of the spin-spin coupling mechanism across a H-bond in proteins, N-H···O=C, has been performed by Cremer and co-workers.[390,391] An analysis of the data obtained for the protein ubiquitin[391] has shown that there are simple relationships between the spin-spin couplings associated with the H bond in proteins and the geometrical features of these bonds. In particular, the authors emphasized the importance of the $^{3h}J_{NC'}$ and $^{1}J_{HN}$ couplings as descriptors of the H-bond.

The D_N/H_N isotope effect on $^{3h}J_{NC'}$ and $^{1}J_{NC'}$ couplings as well as on ^{15}N, $^{13}C'$ and $^{1}H_{\alpha}$ chemical shifts in the small globular protein ubiquitin has been studied by Jaravine *et al.*[392] They have found that amide deuteration induces a very slight weakening of 0.03 ± 0.03 Hz for the $^{3h}J_{NC'}$ couplings, whereas the $^{1}J_{NC'}$ couplings are strengthened by 0.25 ± 0.07 Hz. The isotope effect on the $^{3h}J_{NC'}$ couplings is consistent with a recent study by Kojima *et al.*[393] on a limited number of H-bonds in double-stranded DNA.

Additional compounds for which scalar couplings have been measured through the hydrogen bond are listed in Table 5.

Intermolecular $^{2h}J_{NN}$ couplings in multiply hydrogen-bonded ureidopyrimidinone dimers have been determined by Söntjens *et al.*[397] and used to test the relationship between $^{2h}J_{NN}$ values and N-N distances proposed recently by Del Bene and Bartlett.[398,399] The N-N distances calculated by the use of this relationship showed good agreement with the distances observed in the X-ray crystal structures of the studied compound, particularly when the non-linearity of the hydrogen bonds was taken into account.

The scalar coupling between the ^{15}N centres in methylated 1,8-diaminonaph-

Table 5 *Compounds for which scalar couplings have been measured through the hydrogen bond*

Name	*a*	*b*	*c*	*Ref*
[C/N] three variants of the protein Brazzein	N-H···O=**C**	$^{3h}J_{CN}$	14	394
[C/N] CI2, the chymotrypsin inhibitor 2	N-H···O=**C**	$^{3h}J_{CN}$	18	395
[C/N] HIV-1 frameshift inducing stem-loop RNA	N-**H**···**N**	$^{1h}J_{HN}$	26	396

[a] hydrogen bond type, symbols of nuclei involved are given in bold
[b] type of couplings measured
[c] number of couplings measured

talenes and 1,6-diazacyclodecane has been studied by Lloyd-Jones *et al.*[400] They addressed the question to what extent is $^{2h}J_{NN}$ a reliable indicator of the N-N distance.

The factors which determine the sign of the Fermi contact contribution to the NMR spin-spin coupling have been investigated by Del Bene and Elguero.[401] According to the model designed by them, the excited states which contribute to the coupling do so in a regular manner; the sign of an individual contribution is determined by the nodal character of the excited wavefunction and, finally, the response of the nuclei to the phases of this function and the sign of the total coupling is the result of competing positive and negative contributions from various states. The authors conclude that their model can possibly help to explain some unusual results obtained when the orientation dependence of the F-F coupling between two HF molecules has been studied.

A novel series of acid-base complexes of HF with 2,4,6-trimethylpiridyne (collidine) has been studied by Shenderovich *et al.*[191] in the temperature range of 94-170 K. Scalar couplings across the F-H-F and F-H-N hydrogen bridges have been measured for these complexes, which allowed the authors to determine their composition.

The orientation and distance dependence of the sign and magnitude of J_{FF} couplings have been investigated by Del Bene *et al.*[402] for a pair of HF molecules. They have found that the hydrogen-bonded HF dimer exhibits unusual behaviour compared with other hydrogen-bonded complexes, since both the FC term and $^{2h}J_{FF}$ exhibit variations in sign and magnitude as the F-F distance changes and the linearity of the hydrogen bond is destroyed.

12 Residual Dipolar Couplings

NMR residual dipolar couplings (RDCs), in the form of the projection angles between the respective internuclear bond vectors, have been used by Haliloglu *et al.*[403] as structural restraints in the *ab initio* structure prediction of a test set of six proteins. The restraints have been applied using a recently developed SICHO (*SI*de *CH*ain *O*nly) lattice protein model that employs a replica exchange Monte Carlo algorithm to search conformational space. The proteins studied were ACP (77 residues), rubredoxin (53 residues), NS1, a 73 residue RNA binding/dimerization domain, Nodf (35 residues), Crd (137 residues) and Brct domain with 92 residues.

Side-chain C-C residual dipolar couplings have been measured by Vögeli *et al.*[404] in uniformly deuterated and ^{13}C enriched human ubiquitin in the presence of bacteriophages Pf1 by the use of the FLOPSY family experiment, one of the many broadband polarization transfer schemes. An excellent correlation between the measured RDCs and the 3D structure of the protein has been observed, indicating a potential use of the C-C RDCs in the structure determination of perdeuterated proteins.

It has been shown by Clore and Schwieters[405] that the experimental $^{1}D_{HN}$

dipolar coupling data recorded on ubiquitin in 11 alignment media, as well as the $^1D'_{CN}$, $^2D'_{HNC}$ and $^1D'_{C\alpha C}$ recorded in two alignment media can be accounted for, at approximately the level of uncertainty in the experimental measurement, by a single model representation using restrained refinement of the coordinates and optimization of both the magnitudes and orientations of the alignment tensors. Extension to a two-member ensemble representation not only improves the agreement between the observed and calculated dipolar couplings included in the refinement (*i.e.*, the working set), but also results in a significant improvement in the agreement for the cross-validated $^1D_{H\alpha C\alpha}$ dipolar couplings which were not included in the refinement.

The surface dynamics of bacteriorhodopsin has been studied by Barré *et al.*[406] by ^{13}C solid-state NMR. They have measured site-specific H-C dipolar couplings in [3-^{13}C]Ala-labelled bacteriorhodopsin, which allowed an insight into internal fluctuation motions on the millisecond or microsecond timescale relevant to a variety of biological functions.

More examples of proteins whose solution structure has been calculated with RDCs couplings are listed in Table 6. The corresponding data for oligonucleotides and carbohydrates are given in Table 7.

The analysis of the steric and chiral requirements of protein secondary structures has been performed by Mascioni and Veglia,[429] who established a quantitative correlation between structure periodicity and the experimental values of the backbone residual dipolar couplings. Building on the recent interpretation of the periodicity of residual dipolar couplings in α-helices (so-called 'Dipolar Waves'), they have obtained a general parametric equation for fitting the residual dipolar couplings of any regular secondary structure. An extensive paper on Dipolar Waves (DW) as NMR maps of helices in proteins has been published by Mesleh and Opella, who have shown that the DW approach [430] is a useful tool for accurately describing helices and a step towards high throughput structure determination of proteins. They have indicated that ideal candidates for analysis by the use of this method are membrane proteins.[431]

An approach based on exhaustive back-calculation, exSVD, (SVD denotes *S*ingular *V*alue *D*ecomposition) which allows determination of molecular alignment tensors without backbone resonance assignment has been proposed by Zweckstetter.[432] The author has indicated that such calculation can be performed using only $^1D_{HN}$ couplings, which allows one to avoid expensive ^{13}C labelling and, moreover, molecular alignment tensors of proteins as large as 80 kDa can be determined.

Backbone amide RDCs, the tryptophan Nε-H resonance and the amide nitrogen transverse relaxation rates for varying p*H* values and different temperatures have been measured by Ding *et al.*[433] in their studies on equilibrium unfolding of a destabilized mutant of the B1 domain of protein G. The measured RDCs indicate that prior to complete unfolding, two melting hot spots are formed around T11, L12 and K13, and the N terminus of the helix at A24 and T25.

The effects of divalent Mg^{2+} on the conformation and dynamics of the stem-loop transactivation response element (TAR) RNA from HIV-1 have been

Table 6 *Proteins for which the solution structure has been calculated with RDCs*

Name	*a*	*b*	*c*	*Ref*
the ribonuclease S-peptie	20	20	$^1D_{HN}$	407
[N] Vpu (2-30), trans-membrane domain of virus protein 'u' from HIV-1	36	18	$^1D_{HN}$	408
[N] Pf1 coat protein	46	45	$^1D_{HN}$	409
[C/N] GB3, the third IgG-binding domain of Protein G	56	180	$^1D_{HC}$, $^1D_{HN}$, $^1D_{CC}$, $^1D_{CN}$	410
[C/N] the Z domain of Staphylococcal protein A	58	124	$^1D_{HC}$, $^1D_{HN}$, $^1D_{CC}$	411
[N] Zn^{2+}-HIIB NTD, N-terminal domain of TFIIB	60	23	$^1D_{HN}$	412
[C/N] *Tm*Csp, the cold shock protein from *Thermotoga maritima*	63	33	$^1D_{HN}$	228
[C/N] YbcJ from *E. coli*	77	51	$^1D_{HN}$	231
[C/N] TcPABC (468-550)	83	55	$^1D_{HN}$	232
[C/N] eIF4B RRM (88-176)	89	153	$^1D_{HN}$, $^1D_{CC}$, $^1D_{CN}$	413
[C/N] HI1450, the acidic protein from *Haemophilus influenzae*	108	66	$^1D_{HC}$, $^1D_{HN}$, $^1D_{CC}$, $^1D_{CN}$	414
[C/N] the SeV X protein, the nucleocapsid-binding domain of the Sendai virus	109	144	$^1D_{HN}$, $^1D_{CC}$, $^1D_{CN}$	415
[C/N] GB1 dimer, immunoglobulin-binding domain B1 of streptococcal protein G	56 × 2	56	$^1D_{HN}$	311
[C/N] Dy^{3+}-human α-parvalbumin	112	47	$^1D_{HN}$	237
[C/N] Ku86CTR (592-709)	118	96	$^1D_{HN}$	416
[C/N] MuT-Mg^{2+}—8-oxo-dGMP complex	129+	53	$^1D_{HN}$	417
[C/N] aIF2β, β-subunit of aIF2 from *Methanobacterium thermoautotrophicum*	135	44	$^1D_{HN}$	239
[C/N] DcuS (45-180)	136	382	$^1D_{HC}$, $^1D_{HN}$, $^1D_{CC}$, $^1D_{CN}$	418
[C/N] N60D $(CaLn)_N(Ca_3)_C$CaM, Ln = Tb^{3+} or Tm^{3+}	146	67	$^1D_{HN}$	240
[C/N] the FAT domain of FAK (920-1053) plus a 12 aa N-terminal linker	146	[d]	$^1D_{HC}$, $^1D_{HN}$	419
[C/N] Ku80 CTD (566-732)	167	68	$^1D_{HN}$	243
[C/N] the FAT of FAK (920-1053) complexed with LD2 peptide (133-159)	173	50	$^1D_{HN}$	420
[C/N] IFNAR2-EC/IFNα2 complex	212	109	$^1D_{HN}$	247
[C/N] IIA^{Glc}(11-168)-IIB^{Glc} (12-90/P17A) complex	237	138	$^1D_{HN}$, $^1D_{CN}$, $^2D_{HC}$	314
[D/C/N] Oct1·Sox2·*Hoxb*1-DNA ternary transription factor complex	249 + 38 nucleot.	345	$^1D_{HN}$, $^1D_{CC}$, $^1D_{CN}$	421

[a] number of residues
[b] the total number of residual dipolar couplings measured
[c] types of residual dipolar couplings measured
[d] number not reported

Table 7 *Oligonucleotides and carbohydrates for which the solution structure has been calculated with RDCs*

Name	*a*	*b*	*c*	*Ref*
[C/N] HIV-1 frameshift inducing stem-loop RNA	22	20	$^{1}D_{HC}$	396
U6 RNA intramolecular stem-loop harboring an S_P-phosphorothioate	24	31	$^{1}D_{HC}$	422
$d(CGCGAATTCGCG)_2$	24	368	$^{n}D_{HH}$, $^{1}D_{HP}$	320
[C/N] $d(GCA_4T_4GC)$ and $d(CGT_4A_4CG)$	24	72	$^{1}D_{HC}$	321
[C/N] HCV IRES RNA domain IIa (69-98)	30	136	$^{1}D_{HC}$, $^{1}D_{HN}$	423
[C/N D5 RNA, domain 5 of a group II intron ribozyme	34	24	$^{1}D_{HC}$	424
[C/N] WT34 RNA, a construct of *Poliovirus* IRES stem-loop IV, loop B	34	86	$^{1}D_{HC}$	425
[C/N] 10U RNA, a construct of *Poliovirus* IRES stem-loop IV, loop B	34	26	$^{1}D_{HC}$	425
the model Holliday junction J6 with [C] thymidine deoxyriboses	43	28	$^{1}D_{HC}$	426
[C/N] HCV IRES RNA domain IIb (45-69;98-117)	44	105	$^{1}D_{HC}$, $^{1}D_{HN}$	423
[C/N] HCV IRES RNA domain II (45-117)	73	261	$^{1}D_{HC}$, $^{1}D_{HN}$	423
[C/N] mΨ, the core encapsidation signal of the Moloney Murine Leukemia Virus	101	167	$^{1}D_{HC}$	427
carbohydrates				
fucosylated oligosaccharides	3-6	15-28	$^{1}D_{HC}$	428

[a] the number of nucleotides or sugar units
[b] the total number of residual dipolar couplings measured
[c] types of residual dipolar couplings measured
[d] number not reported

studied by Al-Hashimi *et al.*[434] by the use of NMR residual dipolar couplings (RDCs). The order matrix analysis of one bond ^{1}H-^{13}C RDCs measured in TAR at $[Mg^{2+}]$:[TAR] stoichiometric ratios of ~3:1 (TAR(3.0 Mg)) and ~4.5:1 (TAR(4.5 Mg)) revealed that Mg^{2+} reduces the average inter-helical angle from 47(±5)° in TAR (free) to 5(±7)° in TAR(4.5 Mg).

A method for rapid classification to a fold family by the statistical analyses of the unassigned H-N residual dipolar couplings has been presented by Valafar and Prestegard.[435] They have also designed a software package named *RE*sidual *D*ipolar *C*oupling *A*nalysis *T*ool (REDCAT) which allows a convenient and powerful analysis of residual dipolar couplings.[436]

It has been shown by Walsh *et al.*[437] that the periodicity of the duplex, one of the main secondary structural elements of nucleic acid, is reflected in its RDCs. Since there are many more residues per turn in nucleic acids than in proteins, detailed features of the RDC wave emerge containing information on the orientation of both the secondary structure element and individual bond vectors.

The effects of p*H* and molecular charge on dipolar coupling interactions of solutes in skeletal muscle have been studied by Asllani *et al.*[438] by the use of DQF and ^{1}H NMR spectroscopy. Global orientation of bound MMP-3 and N-TIMP-in solution *via* residual dipolar $^{1}D_{HN}$ and $^{1}D_{HC}$ couplings has been studied by Arumugam and Van Doren.[439]

The solution structures of a trisaccharide and a pentasaccharide containing the Lewis^{x} motif have been determined by Berthault *et al.*,[440] who used two independent approaches, either dipolar cross-relaxation (NOE) or residual dipolar coupling (RDC) data. For the trisaccharide, good agreement has been observed between the results of both approaches, whereas for the pentasaccharide strong discrepancies appeared, most probably as a result of interaction between the pentasaccharide and the mesogens. This led the authors to the conclusion that the dilute liquid crystals used to enhance residual dipolar couplings may alter conformational equilibrium in oligosaccharides. As a result, the simultaneous use of NOE and RDC can yield misleading structures.

In combination with the order matrix calculation, RDCs have been used to unambiguously[441] solve the complete relative stereochemistry of substituted bicyclo[3.1.0]hexane with five stereocentres whose structure is shown in Fig. 8. The RDCs measured were C-C, C-F, H-F and H-H, and the complete relative stereochemistry of the compound has been solved by their use only.

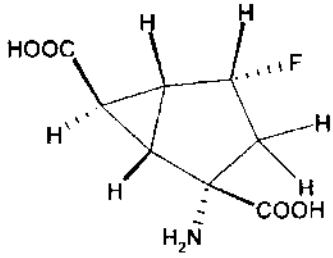

Figure 8

The dipolar H-H couplings have been applied by Chang *et al.*[442] to establish the relative stereochemistry of two new polyclic guanidine alkaloids, crambescidin 826 and dehydrocrambine A isolated from the marine sponge *Monanchora sp.*

References

1. K. Kamieńska-Trela and J. Wójcik, *Nucl. Magn. Reson.*, 2004, **33,** 146.
2. R. K. Harris, J. Kowalewski and S. Cabral de Menezes, *Pure & Appl. Chem.*, 1997, **69,** 2489.
3. K. Jackowski, *Appl. Magn. Reson.*, 2003, **24,** 379.
4. Y. Sasanuma, *Ann. Rep. NMR Spectr.*, 2003, **49,** 213.
5. R. A. Newmark, *Polymer News*, 2003, **28,** 40.
6. M. Kraszni, Z. Szakacs and B. Noszal, *Anal. Bioanal. Chem.*, 2004, **378,** 1449.
7. H. Dodziuk, W. Koźmiński and A. Ejchart, *Chirality*, 2004, **16,** 90.
8. P. Ciminiello and E. Fattorusso, *Eur. J. Org. Chem.*, 2004, 2533.
9. J. Kobayashi and M. Tsuda, *Nat. Prod. Rep.*, 2004, **21,** 77.
10. B. Fürtig, C. Richter, J. Wöhnert and H. Schwalbe, *ChemBioChem*, 2003, **4,** 936.
11. S. W. Homans, *Angew. Chem. Int. Ed.*, 2004, **43,** 290.
12. C. Fernández and G. Wider, *Curr. Opin. Struct. Biol.*, 2003, **13,** 570.
13. G. A. Spyroulias, A. S. Galanis, G. Pairas, E. Manessi-Zoupa and P. Cordopatis, *Curr. Top. Med. Chem.*, 2004, **4,** 403.
14. W. A. Bubb, *Conc. Magn. Reson. Part A.*, 2003, **19A,** 1.
15. T. L. Lowary, *Curr. Opin. Chem. Biol.*, 2003, **7,** 749.
16. A. Foris, *Magn. Reson. Chem.*, 2004, **42,** 534.
17. H. Takemura, *Cyclophane Chem. 21st Cent.*, 2002, 127.
18. Y.-G. Chen, J. Gong and L.-Y. Qu, *Coord. Chem. Rev.*, 2004, **248,** 245.
19. W. B. Blanton, *J. Magn. Reson.*, 2003, **162,** 269.
20. T. Sprang and P. Bigler, *Magn. Reson. Chem.*, 2004, **42,** 55.
21. R. A. E. Edden and J. Keeler, *J. Magn. Reson.*, 2004, **166,** 53.
22. J. J. Titman, D. Neuhaus and J. Keeler, *J. Magn. Reson.*, 1989, **85,** 111.
23. S. C. Panchal, N. S. Bhavesh and R. V. Hosur, *J. Biomol. NMR*, 2001, **20,** 135.
24. N. S. Bhavesh, A. Chatterjee, S. C. Panchal and R. V. Hosur, *Biochem. Biophys. Res. Commun.*, 2003, **311,** 678.
25. B. Luy, *J. Magn. Reson.*, 2004, **168,** 210.
26. H. Koskela, I. Kilpeläinen and S. Heikkinen, *J. Magn. Reson.*, 2003, **164,** 228.
27. Z. Chen, T. Hou, Z.-W. Chen, D. W. Hwang and L.-P. Hwang, *Chem. Phys. Lett.*, 2004, **386,** 200.
28. F. del Rio-Portilla, E. Sanchez-Mendoza, V. U. Constantino-Castillo and J. A. del Rio, *ARKIVOC*, 2003, 213.
29. J. Boisbouvier, F. Delaglio and A. Bax, *Proc. Natl. Acad. Sci. USA*, 2003, **100,** 11333.
30. E. O'Neil-Cabello, D. L. Bryce, E. P. Nikonowicz and A. Bax, *J. Am. Chem. Soc.*, 2004, **126,** 66.
31. E. Miclet, E. O'Neil-Cabello, E. P. Nikonowicz, D. Live and A. Bax, *J. Am. Chem. Soc.*, 2003, **125,** 15740.
32. M. Martin-Pastor, A. Canales-Mayordomo and J. Jimenez-Barbero, *J. Biomol. NMR*, 2003, **26,** 345.
33. W. Hu, Z. Zhang and Y. Chen, *J. Magn. Reson.*, 2003, **165,** 248.

34. P. Permi, *J. Biomol. NMR*, 2003, **27**, 341.
35. K. E. Kövér and K. Fehér, *J. Magn. Reson.*, 2004, **168**, 307.
36. K. Fehér, S. Berger and K. E. Kövér, *J. Magn. Reson.*, 2003, **163**, 340.
37. K. Ding and A. M. Gronenborn, *J. Am. Chem. Soc.*, 2003, **125**, 11504.
38. K. Ding and A. M. Gronenborn, *J. Am. Chem. Soc.*, 2004, **126**, 6232.
39. K. Ding and A. M. Gronenborn, *J. Magn. Reson.*, 2004, **167**, 253.
40. K. Ding and A. M. Gronenborn, *J. Magn. Reson.*, 2003, **163**, 208.
41. D. L. Bryce and A. Bax, *J. Biomol. NMR*, 2004, **28**, 273.
42. L. Židek, P. Padrta, J. Chmelík Jr and V. Sklenář, *J. Magn. Reson.*, 2003, **162**, 358.
43. Y. Qu, J. Guo, V. Olman and Y. Xu, *Nucl. Acids Res.*, 2004, **32**, 551.
44. L. Banci, I. Bertini, G. Cavallaro, A. Giachetti, C. Luchinat and G. Parigi, *J. Biomol. NMR*, 2004, **28**, 249.
45. G. Pintacuda, M. A. Keniry, T. Huber, A. Y. Park, N. E. Dixon and G. Otting, *J. Am. Chem. Soc.*, 2004, **126**, 2963.
46. C. J. Langmead and B. R. Donald, *J. Biomol. NMR*, 2004, **29**, 111.
47. J. Wöhnert, K. J. Franz, M. Nitz, B. Imperiali and H. Schwalbe, *J. Am. Chem. Soc.*, 2003, **125**, 13338.
48. L. Verdier, S. P., M. Zweckstetter and C. Griesinger, *J. Magn. Reson.*, 2003, **163**, 353.
49. C. R. R. Grace and R. Riek, *J. Am. Chem. Soc.*, 2003, **125**, 16104.
50. W. Kwiatkowski and R. Riek, *J. Biomol. NMR*, 2003, **25**, 281.
51. K. E. Kövér and P. Forgó, *J. Magn. Reson.*, 2004, **166**, 47.
52. T. Parella and F. Sánchez-Ferrando, *J. Magn. Reson.*, 2004, **166**, 123.
53. J. J. Heckman, M. P. Ledbetter and M. V. Romalis, *Phys. Rev. Lett.*, 2003, **91**, 067601.
54. A. H. Trabesinger, R. McDermott, S. K. Lee, M. Mück, J. Clarke and A. Pines, *J. Phys. Chem. A*, 2004, **108**, 957.
55. T. R. Eykyn, D. J. Philp and P. W. Kuchel, *Chem. Phys. Lett.*, 2003, **376**, 732.
56. D. H. Brouwer, *J. Magn. Reson.*, 2003, **164**, 10.
57. J. Trebosc, J.-P. Amoureux, J. W. Wiench and M. Pruski, *Chem. Phys. Lett.*, 2003, **374**, 432.
58. I. Göttker-Schnetmann, P. S. White and M. Brookhart, *Organometallics*, 2004, **23**, 1766.
59. H. V. Nanishankar, M. Nethaji and B. R. Jagirdar, *Indian J.Chem., A:Inorg. Bioorg. Phys. Theor. Anal. Chem.*, 2003, **42A**, 2332.
60. V. Pons and D. M. Heinekey, *J. Am. Chem. Soc.*, 2003, **125**, 8428.
61. H. Yao and R. N. Grimes, *Organometallics*, 2003, **22**, 4539.
62. J. Wójcik, K. Kamieńska-Trela, M. Pecul, E. Bartoszak-Adamska, S. I. Vdovienko and I. I. Gerus, *Chem. Phys. Chem.*, 2004, **5**, 209.
63. T. Ratajczyk, M. Pecul, J. Sadlej and T. Helgaker, *J. Phys. Chem. A*, 2004, **108**, 2758.
64. P. E. Hansen, *Polish J. Chem.*, 2003, **77**, 1683.
65. R. Montalvo-González and A. Ariza-Castolo, *J. Mol. Struct.*, 2003, **655**, 375.
66. E. Juaristi, G. A. Rosquete-Pina, M. Vázquez-Hernández and A. J. Mota, *Pure Appl. Chem.*, 2003, **75**, 589.
67. I. V. Alabugin, M. Manoharan and T. A. Zeidan, *J. Am. Chem. Soc.*, 2003, **125**, 14014.
68. D. S. Ribeiro and R. Rittner, *J. Org. Chem.*, 2003, **68**, 6780.
69. V. Galasso, F. Asaro, F. Berti, I. Habuš, B. Kovač and C. De Risi, *Chem. Phys.*, 2004, **301**, 33.
70. A. R. Katritzky, N. G. Akhmedov, Z. Wang, V. A. Roznyatovsky, A. Shestopalov

and C. D. Hall, *Magn. Reson. Chem.*, 2003, **41,** 908.
71. I. A. Perillo, G. Buldain and A. Salerno, *Heterocycles*, 2003, **60,** 2103.
72. E. A. Basso, B. C. Fiorin, C. F. Tormena and R. Rittner, *Can. J. Chem.*, 2004, **82,** 418.
73. F. J. C. Martins, A. M. Viljoen, H. G. Kruger and P. L. Wessels, *Magn. Reson. Chem.*, 2004, **42,** 402.
74. B. Wrackmeyer, H. E. Maisel, W. Milius, M. H. Bhatti and S. Ali, *Z. Naturforsch.*, 2003, **58b,** 543.
75. M. Stępień, L. Latos-Grażyński, L. Szterenberg, J. Panek and Z. Latajka, *J. Am. Chem. Soc.*, 2004, **126,** 4566.
76. M. Hogenbirk, G. Schat, F. J. J. de Kanter, O. S. Akkerman, F. Bickelhaupt, H. Kooijman and A. L. Spek, *Eur. J. Inorg. Chem.*, 2004, 2045.
77. W. Schilf, J. P. Bloxsidge, J. R. Jones and S.-Y. Lu, *Magn. Reson. Chem.*, 2004, **42,** 556.
78. P. Šimunek, V. Bertolasi, A. Lyčka and V. Macháček, *Org. Biomol. Chem.*, 2003, **1,** 3250.
79. F. L. Taw, R. G. Bergman and M. Brookhart, *Organometallics*, 2004, **23,** 886.
80. B. Wrackmeyer, O. L. Tok and Y. N. Bubnov, *Appl. Organomet. Chem.*, 2004, **18,** 43.
81. B. Wrackmeyer, W. Milius and O. L. Tok, *Chem. Eur. J.*, 2003, **9,** 4732.
82. S. Weinrich, H. Piotrowski, M. Vogt, A. Schulz and M. Westerhausen, *Inorg. Chem.*, 2004, **43,** 3756.
83. A. Wu, J. Gräfenstein and D. Cremer, *J. Phys. Chem. A*, 2003, **107,** 7043.
84. M. Filatov and D. Cremer, *J. Chem. Phys.*, 2004, **120,** 11407.
85. J. E. Peralta, G. E. Scuseria, J. R. Cheeseman and M. J. Frisch, *Chem. Phys. Lett.*, 2003, **375,** 452.
86. T. W. Keal, D. J. Tozer and T. Helgaker, *Chem. Phys. Lett.*, 2004, **391,** 374.
87. G. Fraenkel, A. Chow, R. Fleischer and H. Liu, *J. Am. Chem. Soc.*, 2004, **126,** 3983.
88. P. Zhao, A. Condo, I. Keresztes and D. B. Collum, *J. Am. Chem. Soc.*, 2004, **126,** 3113.
89. R. Sott, J. Granander and G. Hilmersson, *J. Am. Chem. Soc.*, 2004, **126,** 6798.
90. T. Fukawa, M. Nakamoto, V. Y. Lee and A. Sekiguchi, *Organometallics*, 2004, **23,** 2376.
91. B. Wrackmeyer and A. Berndt, *Magn. Reson. Chem.*, 2004, **42,** 490.
92. U. Monkowius, S. Nogai and H. Schmidbaur, *Dalton Trans.*, 2003, 987.
93. D. Cremer, E. Kraka, A. Wu and W. Lüttke, *Chem. Phys. Chem.*, 2004, **5,** 349.
94. J. Gräfenstein, T. Tuttle and D. Cremer, *J. Chem. Phys.*, 2004, **120,** 9952.
95. J. Gräfenstein, E. Kraka and D. Cremer, *J. Phys. Chem. A*, 2004, **108,** 4520.
96. J. Gräfenstein and D. Cremer, *Chem. Phys. Lett.*, 2004, **387,** 415.
97. Z. Biedrzycka and K. Kamieńska-Trela, *Polish J. Chem.*, 2003, **77,** 1637.
98. K. Kamieńska-Trela, L. Kania, M. Bechcicka and L. Kaczmarek, *J. Mol. Struct.*, 2003, **661-662,** 209.
99. E. Dvornikova, M. Bechcicka, K. Kamieńska-Trela and A. Krówczyński, *J. Fluor. Chem.*, 2003, **124,** 159.
100. K. Ruszczyńska, K. Kamieńska-Trela, J. Wójcik, J. Stępiński, E. Darzynkiewicz and R. Stolarski, *Biophys.J.*, 2003, **85,** 1450.
101. M. Jaszuński, K. Ruud and T. Helgaker, *Mol. Phys.*, 2003, **101,** 1997.
102. J. E. Peralta, V. Barone, G. E. Scuseria and R. H. Contreras, *J. Am. Chem. Soc.*, 2004, **126,** 7428.
103. T. A. Ruden, T. Helgaker and M. Jaszuński, *Chem. Phys.*, 2004, **296,** 53.
104. B. Wrackmeyer, *Z. Naturforsch.*, 2004, **59b,** 37.

105. L. B. Krivdin, *Magn. Reson. Chem.*, 2003, **41,** 885.
106. L. B. Krivdin, *Magn. Reson. Chem.*, 2004, **42,** 1.
107. L. B. Krivdin, *Magn. Reson. Chem.*, 2004, **42,** 500.
108. L. B. Krivdin and T. A. Kuznetsova, *Russ. J. Org. Chem.*, 2003, **39,** 1618.
109. L. B. Krivdin and T. A. Kuznetsova, *Russ. J. Org. Chem.*, 2003, **39,** 744.
110. V. A. Danilova and L. B. Krivdin, *Russ. J. Org. Chem.*, 2004, **40,** 57.
111. V. A. Danilova and L. B. Krivdin, *Russ. J. Org. Chem.*, 2003, **39,** 1764.
112. V. A. Danilova and L. B. Krivdin, *Russ. J. Org. Chem.*, 2003, **39,** 708.
113. M. Tsuda, N. Izui, K. Shimbo, M. Sato, E. Fukushi, J. Kawabata, K. Katsumata, T. Horiguchi and J. Kobayashi, *J. Org. Chem.*, 2003, **68,** 5339.
114. M. Tsuda, N. Izui, K. Shimbo, M. Sato, E. Fukushi, J. Kawabata and J. Kobayashi, *J. Org. Chem.*, 2003, **68,** 9109.
115. B. Wrackmeyer, O. L. Tok, G. Guldner and S. V. Gruener, *Appl. Organomet. Chem.*, 2003, **17,** 860.
116. B. Wrackmeyer, O. L. Tok and A. Badshah, *Z. Naturforsch.*, 2003, **58b,** 809.
117. P. Cmoch, *Magn. Reson. Chem.*, 2003, **41,** 693.
118. W. Schilf, *J. Mol. Struct.*, 2003, **689,** 245.
119. J. Brus and A. Jegorov, *J. Phys. Chem. A*, 2004, **108,** 3955.
120. M. S. Meier, H. P. Spielmann, R. G. Bergosh and M. C. Tetreau, *J. Org. Chem.*, 2003, **68,** 7867.
121. J. E. Del Bene, J. Elguero and I. Alkorta, *J. Phys. Chem. A*, 2004, **108,** 3662.
122. N. Shimba, Z. Serber, R. Ledwidge, S. M. Miller, C. S. Craik and V. Dötsch, *Biochemistry*, 2003, **42,** 9227.
123. P. Kelemen, J. Lugtenburg and B. Klumperman, *J. Org. Chem.*, 2003, **68,** 7322.
124. J. Jaźwiński and O. Staszewska-Krajewska, *J. Mol. Struct.*, 2004, **687,** 23.
125. N. Juranić, S. Macura and F. G. Prendergast, *Protein Sci.*, 2003, **12,** 2633.
126. A. J. Shallop, B. L. Gaffney and R. A. Jones, *J. Org. Chem.*, 2003, **68,** 8657.
127. A. Romanelli, A. Shekhtman, D. Cowburn and T. W. Muir, *Proc. Natl. Acad. Sci. USA*, 2004, **101,** 6397.
128. B. Wrackmeyer, *Z. Naturforsch.*, 2004, **59b,** 286.
129. C. F. Tormena, M. P. Freitas, R. Rittner and R. J. Abraham, *Phys. Chem. Chem. Phys.*, 2004, **6,** 1152.
130. M. Chidambaram, D. Curulla-Ferre, A. P. Singh and B. G. Anderson, *J. Catal.*, 2003, **220,** 442.
131. T. Müller, M. Juhasz and C. A. Reed, *Angew. Chem. Int. Ed.*, 2004, **43,** 1543.
132. N. Takeda, T. Kajiwara, H. Suzuki, R. Okazaki and N. Tokitoh, *Chem. Eur. J.*, 2003, **9,** 3530.
133. E. P. A. Couzijn, M. Schakel, F. J. J. de Kanter, A. W. Ehlers, M. Lutz, A. L. Spek and K. Lammertsma, *Angew. Chem. Int. Ed.*, 2004, **43,** 3440.
134. B. Wrackmeyer, A. Ayazi, W. Milius and M. Herberhold, *J. Organomet. Chem.*, 2003, **682,** 180.
135. B. Wrackmeyer, E. V. Klimkina, H. E. Maisel, W. Milius and M. Herberhold, *Inorg. Chim. Acta*, 2004, **357,** 1703.
136. B. Wrackmeyer, E. V. Klimkina and W. Milius, *Inorg. Chem. Commun.*, 2004, **7,** 412.
137. B. Wrackmeyer, *Z. Naturforsch.*, 2003, **58b,** 1041.
138. P. Kofod and P. Harris, *Inorg. Chem.*, 2004, **43,** 2680.
139. T. Murai, A. Fujishima, C. Iwamoto and S. Kato, *J. Org. Chem.*, 2003, **68,** 7979.
140. Imtiaz-ud-Din, M. Mazhar, K. M. Khan, M. F. Mahon and K. C. Molloy, *J. Organomet. Chem.*, 2004, **689,** 899.
141. B. Wrackmeyer, W. Milius and S. Ali, *J. Organomet. Chem.*, 2003, **682,** 188.

142. L. D. Field, N. Hazari, H. Lin Li and I. J. Luck, *Magn. Reson. Chem.*, 2003, **41,** 709.
143. M. Nakash and M. Goldvaser, *J. Am. Chem. Soc.*, 2004, **126,** 3436.
144. V. Galasso, *J. Phys. Chem. A*, 2004, **108,** 4497.
145. B. Wrackmeyer, H. E. Maisel, W. Milius and M. Herberhold, *J. Organomet. Chem.*, 2003, **680,** 271.
146. B. Wrackmeyer, W. Milius, H. E. Maisel, H. Vollrath and M. Herberhold, *Z. Anorg. Allg. Chemie*, 2003, **629,** 1169.
147. V. Sychrovsky, J. Šponer and P. Hobza, *J. Am. Chem. Soc.*, 2004, **126,** 663.
148. D. L. Bryce, K. Eichele and R. E. Wasylishen, *Inorg. Chem.*, 2003, **42,** 5085.
149. M. Jaszuński, *Chem. Phys. Lett.*, 2004, **385,** 122.
150. D. L. Bryce and E. Wasylishen, *J. Am. Chem. Soc.*, 2000, **122,** 11236.
151. M. A. M. Forgeron, R. E. Wasylishen and G. H. Penner, *J. Phys. Chem. A*, 2004, **108,** 4751.
152. D. Scheschkewitz, *Angew. Chem. Int. Ed.*, 2004, **43,** 2965.
153. R. Fischer, J. Baumgartner, G. Kickelbick, K. Hassler and C. Marschner, *Chem. Eur. J.*, 2004, **10,** 1021.
154. M. A. M. Forgeron, M. Gee and R. E. Wasylishen, *J. Phys. Chem. A*, 2004, **108,** 4895.
155. F. Fayon, I. J. King, R. K. Harris, R. K. B. Gover, J. S. O. Evans and D. Massiot, *Chem. Materials*, 2003, **15,** 2234.
156. G. Brunklaus, J. C. C. Chan, H. Eckert, S. Reiser, T. Nilges and A. Pfitzner, *Phys. Chem. Chem. Phys.*, 2003, **5,** 3768.
157. D. W. Allen and B. F. Taylor, *J. Chem. Soc. Dalton Trans.*, 1982, 51.
158. N. G. Andersen, M. Parvez, R. McDonald and B. A. Keay, *Can. J. Chem.*, 2004, **82,** 145.
159. C. Bolm, L. Xiao and M. Kesselgruber, *Org. Biomol. Chem.*, 2003, **1,** 145.
160. R. Cohen, B. Rybtchinski, M. Gandelman, L. J. W. Shimon, J. M. L. Martin and D. Milstein, *Angew. Chem. Int. Ed.*, 2003, **42,** 1949.
161. D. Magiera, A. Szmigielska, K. M. Pietrusiewicz and H. Duddeck, *Chirality*, 2004, **16,** 57.
162. E. Szłyk, I. Szymańska, A. Surdykowski, T. (the late) Głowiak, A. Wojtczak and A. Goliński, *Dalton Trans.*, 2003, 3404.
163. M. Herberhold, N. Akkus and W. Milius, *Z. Anorg. Allg. Chemie*, 2003, **629,** 2458.
164. T. Iijima, K. Hashi, A. Goto, T. Shimizu and S. Ohki, *Japn J. Appl. Phys. Part 2:Letters*, 2003, **42,** L1411.
165. J. I. van der Vlugt, R. Sablong, A. M. Mills, H. Kooijman, A. L. Spek, A. Meetsma and D. Vogt, *Dalton Trans.*, 2003, 4690.
166. J. M. Geller, I. S. Butler, D. F. R. Gilson, F. G. Morin, I. Wharf and F. Bélanger-Gariépy, *Can. J. Chem.*, 2003, **81,** 1187.
167. J. Autschbach, B. A. Hess, M. P. Johansson, J. Neugebauer, M. Patzschke, P. Pyykkö, M. Reiher and D. Sundholm, *Phys. Chem. Chem. Phys.*, 2004, **6,** 11.
168. P. Pyykkö and N. Runeberg, *Angew. Chem. Int. Ed.*, 2002, **41,** 4786.
169. X. Li, B. Kiran, J. Li, H.-J. Zhai and L.-S. Wang, *Angew. Chem. Int. Ed.*, 2002, **41,** 4786.
170. J. Autschbach, C. D. Igna and T. Ziegler, *J. Am. Chem. Soc.*, 2003, **125,** 4937.
171. J. Autschbach and B. Le Guennic, *J. Am. Chem. Soc.*, 2003, **125,** 13585.
172. A. Soncini and P. Lazzeretti, *J. Chem. Phys.*, 2003, **119,** 1343.
173. J. P. Guthrie, R. T. Gallant and M. C. Jennings, *Can. J. Chem.*, 2004, **82,** 268.
174. B. Rodríguez and M. L. Jimeno, *Magn. Reson. Chem.*, 2004, **42,** 605.
175. B. Rodríguez, *Magn. Reson. Chem.*, 2003, **41,** 741.

176. B. Reyes-Trejo, M. S. Morales-Rios, E. C. Alvarez-Cisneros and P. Joseph-Nathan, *Magn. Reson. Chem.*, 2003, **41,** 1021.
177. P. M. Tolstoy, P. Schah-Mohammedi, S. N. Smirnov, N. S. Golubev, G. S. Denisov and H.-H. Limbach, *J. Am. Chem. Soc.*, 2004, **126,** 5621.
178. N. Matsumori, D. Kaneno, M. Murata, H. Nakamura and K. Tachibana, *J. Org. Chem.*, 1999, **64,** 866.
179. I. Paterson, R. Britton, O. Delgado and A. E. Wright, *Chem. Commun.*, 2004, 632.
180. J. Toušek, J. Dostál and R. Marek, *J. Mol. Struct.*, 2004, **689,** 115.
181. G. Bifulco, C. Bassarello, R. Riccio and L. Gomez-Paloma, *Org. Lett.*, 2004, **6,** 1025.
182. C. Bassarello, P. Cimino, L. Gomez-Paloma, R. Riccio and G. Bifulco, *Tetrahedron.*, 2003, **59,** 9555.
183. G. Jia, W. S. Ng, J. Yao, C.-P. Lau and Y. Chen, *Organometallics*, 1996, **15,** 5039.
184. P. L. Arvidson, P. Ahlberg and G. Hilmersson, *Chem. Eur. J.*, 1999, **5,** 1348.
185. S. Desjardins, K. Flinois, H. Oulyadi, D. Davoust, C. Giessner-Prettre, O. Parisel and J. Maddaluno, *Organometallics*, 2003, **22,** 4090.
186. A. Wu and D. Cremer, *Phys. Chem. Chem. Phys.*, 2003, **5,** 4541.
187. A. A. Frimer, O. Sharon and H. E. Gottlieb, *Magn. Reson. Chem.*, 2003, **41,** 714.
188. A. Popkov, V. Langer, P. A. Manorik and T. Weidlich, *Trans. Met. Chem.*, 2003, **28,** 475.
189. B. Wrackmeyer, O. L. Tok, M. H. Bhatti, K. Shahid and S. Ali, *Z. Naturforsch.*, 2003, **58b,** 607.
190. R. M. Claramunt, D. Sanz, M. D. Santa María, J. Elguero and S. Trofimenko, *J. Organomet. Chem.*, 2004, **689,** 463.
191. I. G. Shenderovich, P. M. Tolstoy, N. S. Golubev, S. N. Smirnov, G. S. Denisov and H.-H. Limbach, *J. Am. Chem. Soc.*, 2003, **125,** 11710.
192. M. Santiago, E. Low, G. Chambournier and R. E. Gawley, *J. Org. Chem.*, 2003, **68,** 8480.
193. V. Barone, P. F. Provasi, J. E. Peralta, J. P. Snyder, S. P. A. Sauer and R. H. Contreras, *J. Phys. Chem. A*, 2003, **107,** 4748.
194. D. Massiot, F. Fayon, B. Alonso, J. Trebosc and J.-P. Amoureux, *J. Magn. Reson.*, 2003, **164,** 160.
195. L. Chęcińska, Z. H. Kudzin, M. Małecka, R. B. Nazarski and A. Okruszek, *Tetrahedron*, 2003, **59,** 7681.
196. S. Ogoshi, T. Yoshida, T. Nishida, M. Morita and H. Kurosawa, *J. Am. Chem. Soc.*, 2001, **123,** 1944.
197. S. Ogoshi, M. Morita and H. Kurosawa, *J. Am. Chem. Soc.*, 2003, **125,** 9020.
198. M. Morita, K. Inoue, T. Yoshida, S. Ogoshi and H. Kurosawa, *J. Organomet. Chem.*, 2004, **689,** 894.
199. X. Couillens, M. Gressier, Y. Coulais and M. Dartiguenave, *Inorg. Chim. Acta*, 2004, **357,** 195.
200. J. Whitaker, E. Ahn, P. Hari, G. A. Williams, P. C. Taylor and J. C. Facelli, *J. Chem. Phys.*, 2003, **119,** 8519.
201. E. Ahn, P. Hari, J. Whitaker, G. A. Williams, P. C. Taylor and J. Facelli, *J. Non-Crystalline Solids*, 2003, **326-327,** 64.
202. J. Jokisaari and J. Autschbach, *Phys. Chem. Chem. Phys.*, 2003, **5,** 4551.
203. B. Wrackmeyer, O. L. Tok, M. H. Bhatti and S. Ali, *Appl. Organomet. Chem.*, 2003, **17,** 843.
204. M. Rashidi, M. C. Jennings and R. J. Puddephatt, *Organometallics*, 2003, **22,** 2612.
205. C. Peter, M. Rueping, H. J. Wörner, B. Jaun, D. Seebach and W. F. van Gunsteren, *Chem. Eur. J.*, 2003, **9,** 5838.

206. G. M. Hanna, *Pharmazie*, 2004, **59,** 251.
207. T. Kimura, N. Matubayasi and M. Nakahara, *Biophys. J.*, 2004, **86,** 1124.
208. M. Assfalg, L. Banci, I. Bertini, P. Turano and P. R. Vasos, *J. Mol. Biol.*, 2003, **330,** 145.
209. A. Papakyriakou, B. Mouzopoulou and N. Katsaros, *J. Biol. Inorg. Chem.*, 2003, **8,** 549.
210. S. Higashibayashi, W. Czechitzky, Y. Kobayashi and Y. Kishi, *J. Am. Chem. Soc.*, 2003, **125,** 14379.
211. Y. Meng, B. Z. Yan, H. M. Wang, G. F. Hu, F. Y. Liu, Y. G. Song and Y. Liu, *Magn. Reson. Chem.*, 2004, **42,** 564.
212. E. Mikros, G. Labrinidis and S. Pérez, *J. Carbohydr. Chem.*, 2003, **22,** 407.
213. W. I. Li, B. L. Marquez, T. Okino, F. Yokokawa, T. Shioiri, W. H. Gerwick and T. F. Murray, *J. Nat. Prod.*, 2004, **67,** 559.
214. J. F. Ying, K. E. Kövér, X. Y. Gu, G. X. Han, D. B. Trivedi, M. J. Kavarana and V. J. Hruby, *Biopolymers*, 2003, **71,** 696.
215. E. Trzepalka, W. Kowalczyk and B. Lammek, *J. Pept. Res.*, 2004, **63,** 333.
216. S. D. S. Jois and A. Balasubramaniam, *Peptides*, 2003, **24,** 1035.
217. B.-S. Lou, T.-H. Lin and C.-Z. Lo, *J. Pept. Res.*, 2004, **63,** 313.
218. Z. Shuxing, W. S. Ying, T. J. Siahaan and S. D. S. Jois, *Peptides*, 2003, **24,** 827.
219. K. J. Rosengren, R. J. Clark, N. L. Daly, U. Göransson, A. Jones and D. J. Craik, *J. Am. Chem. Soc.*, 2003, **125,** 12464.
220. D. G. Barry, N. L. Daly, R. J. Clark, L. Sando and D. J. Craik, *Biochemistry*, 2003, **42,** 6688.
221. C. W. Lee, E. H. Lee, K. Takeuchi, H. Takahashi, I. Shimada, K. Sato, S. Y. Shin, D. H. Kim and J. I. Kim, *Biochem. J.*, 2004, **377,** 385.
222. C. W. Lee, S. Kim, S. H. Roh, H. Endoh, Y. Kodera, T. Maeda, T. Kohno, J. M. Wang, K. J. Swartz and J. I. Kim, *Biochemistry*, 2004, **43,** 890.
223. B. Luy, A. Diener, R.-P. Hummel, E. Sturm, W.-R. Ulrich and C. Griesinger, *Eur. J. Biochem.*, 2004, **271,** 2076.
224. W. Vermeulen, P. Vanhaesebrouck, M. Van Troys, M. Verschueren, F. Fant, M. Goethals, C. Ampe, J. C. Martins and F. A. M. Borremans, *Protein Sci.*, 2004, **13,** 1276.
225. H. Hemmi, J. Ishibashi, T. Tomie and M. Yamakawa, *J. Biol. Chem.*, 2003, **278,** 22820.
226. D. G. Barry, N. L. Daly, H. R. Bokesch, K. R. Gustafson and D. J. Craik, *Structure*, 2004, **12,** 85.
227. B. J. C. Janssen, H. J. Schirra, F. T. Lay, M. A. Anderson and D. J. Craik, *Biochemistry*, 2003, **42,** 8214.
228. A. Jung, C. Bamann, W. Kremer, H. R. Kalbitzer and E. Brunner, *Protein Sci.*, 2004, **13,** 342.
229. T. Sprules, K. E. Kawulka, A. C. Gibbs, D. S. Wishart and J. C. Vederas, *Eur. J. Biochem.*, 2004, **271,** 1748.
230. L. Banci, I. Bertini and R. Del Conte, *Biochemistry*, 2003, **42,** 13422.
231. L. Volpon, C. Lievre, M. J. Osborne, S. Gandhi, P. Iannuzzi, R. Larocque, M. Cygler, K. Gehring and I. Ekiel, *J. Bacteriol.*, 2003, **185,** 4204.
232. N. Siddiqui, G. Kozlov, I. D'Orso, J.-F. Trempe and K. Gehring, *Protein Sci.*, 2003, **12,** 1925.
233. V. Y. Gorbatyuk, C.-K. Tsai, C.-F. Chang and T.-H. Huang, *J. Biol. Chem.*, 2004, **279,** 5772.
234. K.-I. Hatano, M. Kojima, E.-I. Suzuki, M. Tanokura and K. Takahashi, *Biol.*

Chem., 2003, **384,** 1173.
235. G. C. Pérez-Alvarado, M. Martínez-Yamout, M. M. Allen, R. Grosschedl, H. J. Dyson and W. P. E., *Biochemistry*, 2003, **42,** 7348.
236. S. I. Alam, J. Sun, M. Payne, B. D. Welch, B. K. Blake, D. R. Davis, H. H. Meyer, S. D. Emr and W. I. Sundquist, *EMBO J.*, 2004, **23,** 1411.
237. I. Baig, I. Bertini, C. Del Bianco, Y. K. Gupta, Y.-M. Lee, C. Luchinat and A. Quattrone, *Biochemistry*, 2004, **43,** 5562.
238. T. A. Ramelot, S. S. Ni, S. Goldsmith-Fischman, J. R. Cort, B. Honig and M. A. Kennedy, *Protein Sci.*, 2003, **12,** 1556.
239. P. Gutiérrez, M. J. Osborne, N. Siddiqui, J.-F. Trempe, C. Arrowsmith and K. Gehring, *Protein Sci.*, 2004, **13,** 659.
240. I. Bertini, C. Del Bianco, I. Gelis, N. Katsaros, C. Luchinat, G. Parigi, M. Peana, A. Provenzani and M. A. Zoroddu, *Proc. Nat. Acad. Sci. USA*, 2004, **101,** 6841.
241. L. Banci, I. Bertini, F. Cramaro, R. Del Conte and M. S. Viezzoli, *Biochemistry*, 2003, **42,** 9543.
242. L. Banci, I. Bertini, S. Ciofi-Baffoni, L. Gonnelli and X.-C. Su, *J. Biol. Chem.*, 2003, **278,** 50506.
243. Z. M. Zhang, W. D. Hu, L. Cano, T. D. Lee, D. J. Chen and Y. Chen, *Structure*, 2004, **12,** 495.
244. E. Balatri, L. Banci, I. Bertini, F. Cantini and S. Ciofi-Baffoni, *Structure*, 2003, **11,** 1431.
245. A. Farooq, L. Zeng, K. S. Yan, K. S. Ravichandran and M. M. Zhou, *Structure*, 2003, **11,** 905.
246. L. X. Ma, C. T. Jones, T. D. Groesch, R. J. Kuhn and C. B. Post, *Proc. Nat. Acad. Sci. USA*, 2004, **101,** 3414.
247. J. H. Chill, S. R. Quadt, R. Levy, G. Schreiber and J. Anglister, *Structure*, 2003, **11,** 791.
248. M. Freitag, H. Thomasen, N. K. Christensen, M. Petersen and P. Nielsen, *Tetrahedron*, 2004, **60,** 3775.
249. S. Olejniczak, M. Sobczak, M. J. Potrzebowski, M. Polak, J. Plavec and B. Nawrot, *Tetrahedron*, 2004, **60,** 3979.
250. S. Obika, J.-I. Andoh, M. Onoda, O. Nakagawa, A. Hiroto, T. Sugimoto and T. Imanishi, *Tetrahedron Lett.*, 2003, **44,** 5267.
251. F. Seela and X. H. Peng, *Synthesis*, 2004, 1203.
252. C. Chamorro, S. M. Luengo, M.-C. Bonache, S. Velázquez, M.-J. Pérez-Pérez, M.-J. Camarasa, F. Gago, M.-L. Jimeno and A. San-Félix, *J. Org. Chem.*, 2003, **68,** 6695.
253. P. Van Rompaey, K. Nauwelaerts, V. Vanheusden, J. Rozenski, H. Munier-Lehmann, P. Herdewijn and S. Van Calenbergh, *Eur. J. Org. Chem.*, 2003, 2911.
254. H. V. Tommerholt, N. K. Christensen, P. Nielsen, J. Wengel, P. C. Stein, J. P. Jacobsen and M. Petersen, *Org. Biomol. Chem.*, 2003, **1,** 1790.
255. K. E. Nielsen, J. Rasmussen, R. Kumar, J. Wengel, J. P. Jacobsen and M. Petersen, *Bioconjug. Chem.*, 2004, **15,** 449.
256. A. P. G. Beevers, K. J. Fettes, G. Sabbagh, F. K. Murad, J. R. P. Arnold, R. Cosstick and J. Fisher, *Org. Biomol. Chem.*, 2004, **2,** 114.
257. M. Fragoso-Serrano, G. Guillén-Jaramillo, R. Pereda-Miranda and C. M. Cerda-García-Rojas, *J. Org. Chem.*, 2003, **68,** 7167.
258. R. M. van Well, L. Marinelli, C. Altona, K. Erkelens, G. Siegal, M. van Raaij, A. L. Llamas-Saiz, H. Kessler, E. Novellino, A. Lavecchia, J. H. van Boom and M. Overhand, *J. Am. Chem. Soc.*, 2003, **125,** 10822.
259. M. U. Roslund, K. D. Klika, R. L. Lehtilä, P. Tähtinen, R. Sillanpää and R. Leino,

J. Org. Chem., 2004, **69,** 18.
260. N. Funasaki, S. Ishikawa, S. Hirota, S. Neya and T. Nishimoto, *Chem. Pharm. Bull.*, 2004, **52,** 708.
261. H. Kubo, K. Ishii, H. Koshino, K. Toubetto, K. Naruchi and R. Yamasaki, *Eur. J. Org. Chem.*, 2004, 1202.
262. K. Eliadou and K. Yannakopoulou, *J. Incl. Phenom. Macrocyc. Chem.*, 2002, **44,** 351.
263. A. Mele, G. Raffaini, F. Ganazzoli, M. Juza and V. Schurig, *Carbohyd. Res.*, 2003, **338,** 625.
264. B. Liberek, A. Sikorski, A. Melcer and A. Konitz, *Carbohyd. Res.*, 2003, **338,** 795.
265. K. Fehér, P. Pristovšek, L. Szilágyi, Đ. Ljevaković; and J. Tomašić, *Bioorg. Med. Chem.*, 2003, **11,** 3133.
266. J. Wu, J. Huang, Q. Xiao, S. Zhang, Z. Xiao, Q. Li, L. Long and L. Huang, *Magn. Reson. Chem.*, 2004, **42,** 659.
267. C. Nóbrega and J. T. Vásquez, *Tetrahedron Assym.*, 2003, **14,** 2793.
268. J. A. Dobado, N. Benkadour, S. Melchor and D. Portal, *J. Mol. Struct. Theochem*, 2004, **672,** 127.
269. S. M. Spain and D. L. Rabenstein, *Anal. Bioanal. Chem.*, 2004, **378,** 1561.
270. Y. Seo, J. Shin, H. J. Cha, Y.-A. Kim, J.-W. Ahn, B.-J. Lee and D. S. Lee, *Bull. Korean Chem. Soc.*, 2003, **24,** 1475.
271. M. C. Pinheiro Barros, M. A. Sousa Lima, R. Braz-Filho and E. R. Rocha Silveira, *Magn. Reson. Chem.*, 2003, **41,** 731.
272. K. Pihlaja, P. Tähtinen, K. D. Klika, T. Jokela, A. Salakka and K. Wähälä, *J. Org. Chem.*, 2003, **68,** 6864.
273. L. Vizzotto, R. Marques Muzzi and D. P. de Lima, *Magn. Reson. Chem.*, 2003, **41,** 1034.
274. K. Belsner, B. Büchele, U. Werz and T. Simmet, *Magn. Reson. Chem.*, 2003, **41,** 629.
275. A. T. Cardoso Taketa, J. Lozada-Lechuga, M. Fragoso-Serrano, M. L. Villarreal and R. Pereda-Miranda, *J. Nat. Prod.*, 2004, **67,** 644.
276. W. Wysocka and T. Brukwicki, *Tetrahedron*, 2003, **59,** 8597.
277. C. Viegas Jr., V. da S. Bolzani, M. Furlan, E. J. Barreiro, M. C. M. Young, D. Tomazela and M. N. Eberlin, *J. Nat. Prod.*, 2004, **67,** 908.
278. P. Forgo and K. E. Köver, *Steroids*, 2004, **69,** 43.
279. P. Ciuffreda, S. Casati and A. Manzocchi, *Magn. Reson. Chem.*, 2004, **42,** 360.
280. K. Wei, W. Li, K. Koike, Y. Pei, Y. Chen and T. Nikaido, *Magn. Reson. Chem.*, 2004, **42,** 355.
281. M. L. Veras, M. Z. B. Bezerra, T. L. G. Lemos, D. E. de A.Uchoa, R. Braz-Filho, H.-B. Chai, G. A. Cordell and O. D. L. Pessoa, *J. Nat. Prod.*, 2004, **67,** 710.
282. A. Tolonen, T. Joutsamo, S. Mattlla, T. Kämäräinen and J. Jalonen, *Phytochem. Anal.*, 2002, **13,** 316.
283. G. Bringmann, G. Lang, S. Steffens, E. Günther and K. Schaumann, *Phytochem.*, 2003, **63,** 437.
284. L. M. Cardona-Zuleta, A. J. Cavalheiro, D. H. Siqueira Silva, M. Furlan, M. C. Marx Young, S. Albuquerque, I. Castro-Gamboa and V. da Silva Bolzani, *Phytochem.*, 2003, **64,** 549.
285. M. L. Jimeno, M. C. Apreda-Rojas, F. H. Cano and B. Rodríguez, *Magn. Reson. Chem.*, 2004, **42,** 474.
286. J. Niggemann, M. Herrmann, K. Gerth, H. Irschik, H. Reichenbach and G. Höfle, *Eur. J. Org. Chem.*, 2004, 487.
287. P. G. Williams, W. Y. Yoshida, M. K. Quon, R. E. Moore and V. J. Paul, *J. Nat.*

Prod., 2003, **66,** 1545.
288. A. R. Katritzky, N. G. Akhmedov, M. Wang, C. J. Rostek and P. J. Steel, *Magn. Reson. Chem.*, 2004, **42,** 648.
289. K. A. Suri, O. P. Suri, M. Amina, B. P. Wakhloo and N. K. Satti, *Magn. Reson. Chem.*, 2003, **41,** 747.
290. R. N. Asolkar, D. Schröder, R. Heckmann, S. Lang, I. Wagner-Döbler and H. Laatsch, *J. Ant.*, 2004, **57,** 17.
291. Y. Haykawa, T. Tomikawa, K. Shin-Ya, N. Arao, K. Nagai, K.-I. Suzuki and K. Furihata, *J. Ant.*, 2003, **56,** 905.
292. R. J. Abraham and R. Koniotou, *Magn. Reson. Chem.*, 2003, **41,** 1000.
293. M. P. Freitas, C. F. Tormena, J. C. Garcia, R. Rittner, R. J. Abraham, E. A. Basso, F. P. Santos and J. C. Cedran, *J. Phys. Org. Chem.*, 2003, **16,** 833.
294. V. V. Kuznetsov and E. A. Alekseeva, *Khim. Geterosikl. Soed.*, 2003, 839.
295. V. V. Kuznetsov, A. N. Novikov, I. S. Rublev and P. Y. Markolenko, *Khim. Geterosikl.Soed.*, 2003, 426.
296. P. R. Oliveira, F. Wiectzycosky, E. A. Basso, R. A. C. Gonçalves and R. M. Pontes, *J. Mol. Struct.*, 2003, **657,** 191.
297. M. Gomes Constantino, K. Thiago de Oliveira, A. Beatriz and G. V. J. da Silva, *Magn. Reson. Chem.*, 2003, **41,** 726.
298. K. Maruyoshi, T. Demura, T. Sagane, N. Matsumori, T. Oishi and M. Murata, *Tetrahedron*, 2004, **60,** 5163.
299. P. Bello, N. J. Heaton, A. Chana, J. Jimenez-Barbero, E. Riande and B. Herradon, *J. Phys. Org. Chem.*, 2004, **17,** 71.
300. G. Nair and J. D. Roberts, *Org. Lett.*, 2003, **5,** 3699.
301. Y. S. Balazs, I. Saltsman, A. Mahammed, E. Tkachenko, G. Golubkov, J. Levine and Z. Gross, *Magn. Reson. Chem.*, 2004, **42,** 624.
302. B. F. Lutnaes, L. Bruas, G. Kildahl-Andersen, J. Krane and S. Liaaen-Jensen, *Org. Biomol. Chem.*, 2003, **1,** 4064.
303. S. Ito, T. Kubo, M. Kondo, C. Kabuto, N. Morita, T. Asao, K. Fujimori, M. Watanabe, N. Harada and M. Yasunami, *Org. Biomol. Chem.*, 2003, **1,** 2572.
304. G. I. Borodkin, I. R. Elanov, M. M. Shakirov and V. G. Shubin, *Russ. J. Org. Chem.*, 2003, **39,** 1144.
305. A. Holzberger and E. Kleinpeter, *Magn. Reson. Chem.*, 2004, **42,** 589.
306. S. Hooda and A. S. Brar, *J. Appl. Polymer Sci.*, 2003, **88,** 3232.
307. S. Hooda, R. Kumar and M. Kaur, *Indian J. Chem. A: Inorg. Bioinorg. Physic. Theor. Anal. Chem.*, 2004, **43A,** 527.
308. D. Kony, W. Damm, S. Stoll and P. H. Hünenberger, *J. Phys. Chem. B*, 2004, **108,** 5815.
309. J. Gonzalez-Outerino, J. Glushka, A. Siriwardena and R. J. Woods, *J. Am. Chem. Soc.*, 2004, **126,** 6866.
310. K. A. E. van't Slot, H. A. van den Burg, C. P. A. M. Kloks, C. W. Hilbers, W. Knogge and C. H. M. Papavoine, *J. Biol. Chem.*, 2003, **278,** 45730.
311. I.-J. L. Byeon, J. M. Louis and A. M. Gronenborn, *J. Mol. Biol.*, 2003, **333,** 141.
312. D. Pantoja-Uceda, M. Bruix, G. Giménez-Gallego, M. Rico and J. Santoro, *Biochemistry*, 2003, **42,** 13839.
313. E. Liepinsh, L. Bányai, G. Pintacuda, M. Trexler, L. Patthy and G. Otting, *J. Biol. Chem.*, 2003, **278,** 25982.
314. M. Cai, D. C. Williams Jr., G. S. Wang, B. R. Lee, A. Peterkofsky and G. M. Clore, *J. Biol. Chem.*, 2003, **278,** 25191.
315. D. Baranowski, B. Golankiewicz and J. Plavec, *Nucleos. Nucleot. Nucleic Acids,*

2003, **22,** 1669.
316. E. V. Efimtseva, A. A. Shelkunova, S. N. Mikhailov, K. Nauwelaerts, J. Rozenski, E. Lescrinier and H. P., *Nucleos. Nucleot. Nucleic Acids*, 2003, **22,** 359.
317. Y. Feng, B. Han, B. Tan and Y. Zhao, *Spectroscopy Lett.*, 2003, **36,** 419.
318. S. M. Graham, D. J. Macaya, R. N. Sengupta and K. B. Turner, *Org. Lett.*, 2004, **6,** 233.
319. J. W. Stuart, K. M. Koshlap, R. Guenther and P. F. Agris, *J. Mol. Biol.*, 2003, **334,** 901.
320. Z. G. Wu, F. Delaglio, N. Tjandra, V. B. Zhurkin and A. Bax, *J. Biomol. NMR*, 2003, **26,** 297.
321. R. Stefl, H. H. Wu, S. Ravindranathan, V. Sklená&£345; and J. Feigon, *Proc. Nat. Acad. Sci. USA*, 2004, **101,** 1177.
322. K. Nauwelaerts, K. Vastmans, M. Froeyen, V. Kempeneers, J. Rozenski, H. Rosemeyer, A. Van Aerschot, R. Busson, J. C. Lacey, E. Efimtseva, S. Mikhailov, E. Lescrinier and P. Herdewijn, *Nucl. Acid Res.*, 2003, **31,** 6758.
323. G.-S. Hwang, G. B. Jones and G. I. H., *Biochemistry*, 2003, **42,** 8472.
324. G.-S. Hwang, G. B. Jones and I. H. Goldberg, *Biochemistry*, 2004, **43,** 641.
325. O. Ohlenschläger, J. Wöhnert, E. Bucci, S. Seitz, S. Häfner, R. Ramachandran, R. Zell and M. Görlach, *Structure*, 2004, **12,** 237.
326. M. J. Clément, A. Imberty, A. Phalipon, S. Pérez, C. Simenel, L. A. Mulard and M. Delepierre, *J. Biol. Chem.*, 2003, **278,** 47928.
327. J. Szafranek, M. Kaczyńska, Z. Kaczyński, J. Gajdus, M. Czerwicka, H. Dziadziuszko and R. Głośnicka, *Polish. J. Chem.*, 2003, **77,** 1135.
328. R. Smoum, A. Rubinstein and M. Srebnik, *Magn. Reson. Chem.*, 2003, **41,** 1015.
329. Z. Pakulski, *Synthesis*, 2003, 2074.
330. S. Besombes, J.-P. Utille, K. Mazeau, D. Robert and F. R. Taravel, *Magn. Reson. Chem.*, 2004, **42,** 337.
331. S. Besombes, D. Robert, J.-P. Utille, F. R. Taravel and K. Mazeau, *Holzforschung*, 2003, **57,** 266.
332. S. Besombes and K. Mazeau, *Biopolymers*, 2004, **73,** 301.
333. B. Stanovnik and J. Svete, *Chem. Rev.*, 2004, **104,** 2433.
334. R. Jakše, J. Svete, B. Stanovnik and A. Golobič, *Tetrahedron*, 2004, **60,** 4601.
335. Z. Györgydeák, G. Szabó and W. Holzer, *Monatsh. Chem.*, 2004, **135,** 173.
336. M.-W. Ding, Y. Sun and X.-P. Liu, *Gaodeng Xuexiao Huaxue Xuebao*, 2003, **24,** 1424.
337. K. Tanaka, G. Pescitelli, L. Di Bari, T. L. Xiao, K. Nakanishi, D. W. Armstrong and N. Berova, *Org. Biomol. Chem.*, 2004, **2,** 48.
338. G. P. Schiemenz, S. Petersen and S. Porksen, *Zeit. Naturforsch. B, J.Chem.Sci.*, 2003, **58,** 715.
339. M. Prakesch, D. Grée, R. Grée, J. Carter, I. Washington and K. N. Houk, *Chem. Eur. J.*, 2003, **9,** 5664.
340. V. Y. Sosnovskikh, *Russ. Chem. Bull.*, 2003, **52,** 2087.
341. Y. Sakamoto, K. Kondo, M. Tokunaga, K. Kazuta, H. Fujita, Y. Murakami and T. Aoyama, *Heterocycles*, 2004, **63,** 1345.
342. M. Herberhold, T. Schmalz, W. Milius and B. Wrackmeyer, *Inorg. Chim. Acta*, 2003, **352,** 51.
343. W. H. Hersh, P. Xu, C. K. Simpson, J. Grob, B. Bickford, M. S. Hamdani, T. Wood and A. L. Rheingold, *J. Org. Chem.*, 2004, **69,** 2153.
344. Z. Fei, R. Schmutzler and F. T. Edelmann, *Z. Anorg. Allg. Chem.*, 2003, **629,** 353.
345. F. D. Rochon and J. R. L. Priqueler, *Can. J. Chem.*, 2004, **82,** 649.

346. J. R. L. Priqueler and F. D. Rochon, *Inorg. Chim. Acta*, 2004, **357,** 2167.
347. F. D. Rochon and V. Buculei, *Can. J. Chem.*, 2004, **82,** 524.
348. F. D. Rochon and V. Buculei, *Inorg. Chim. Acta*, 2004, **357,** 2218.
349. I. M. Al-Najjar, A. M. Abdulrahman, J. K. Al-Refai, L. A. Al-Shabanah and L. A. Al-Mutabagani, *Spectrochim. Acta A*, 2003, **59,** 1265.
350. J. J. Chou, D. A. Case and A. Bax, *J. Am. Chem. Soc.*, 2003, **125,** 8959.
351. O. Millet, A. Mittermaier, D. Baker and L. E. Kay, *J. Mol. Biol.*, 2003, **329,** 551.
352. A. E. Panarina, A. V. Dogadina and B. I. Ionin, *Russ. J. Gen. Chem.*, 2003, **73,** 1729.
353. V. Vicente, A. Fruchier, M. Taillefer, C. Combes-Chamalet, I. J. Scowen, F. Plénat and H.-J. Cristau, *New J. Chem.*, 2004, **28,** 418.
354. A. I. Konovets, A. N. Kostyuk, A. M. Pinchuk, A. A. Tolmachev, A. Fischer, P. G. Jones and R. Schmutzler, *Heteroatom Chem.*, 2003, **14,** 452.
355. S. Liu, Y. Shi, Q. Zhang and G. Song, *Magn. Reson. Chem.*, 2003, **41,** 609.
356. Z. Marinić, M. Ćurić, D. Vikić-Topić and L. Tušek-Božić, *Magn. Reson. Chem.*, 2003, **41,** 969.
357. B. J. Foss and J. Krane, *Magn. Reson. Chem.*, 2004, **42,** 373.
358. W. Kitching, H. Olszowy, J. Waugh and D. Doddrell, *J. Org. Chem.*, 1978, **43,** 898.
359. M. Goto, Y. Kotani, K. Kida, S. Tomoda and Y. Nagao, *Heterocyles*, 2004, **62,** 229.
360. O. L. Malkina and V. G. Malkin, *Angew. Chem. Int. Ed.*, 2003, **42,** 4335.
361. C. Mahieux, M. Laguerre, Y. Landais and I. Pianet, *Magn. Reson. Chem.*, 2004, **42,** 467.
362. V. C. Gomes Heleno, A. E. Miller Crotti, M. Gomes Constantino, N. P. Lopes and J. L. Callegari Lopes, *Magn. Reson. Chem.*, 2004, **42,** 364.
363. C. M. Cerda-Garcia-Rojas, M. A. Bucio, L. U. Román, J. D. Hernández and P. Joseph-Nathan, *J. Nat. Prod.*, 2004, **67,** 189.
364. I. A. Ushakov, A. V. Afonin, V. K. Voronov, Z. V. Stepanova, L. N. Sobenina and A. I. Mikhaleva, *Russ. J. Org. Chem.*, 2003, **39,** 1318.
365. Y. Nagano and M. Nakano, *J. Chem. Thermodyn.*, 2003, **35,** 1403.
366. G. E. Collis, A. K. Burrell, S. M. Scott and D. L. Officer, *J. Org. Chem.*, 2003, **68,** 8974.
367. N. G. Akhmedov, E. M. Myshakin and C. D. Hall, *Magn. Reson. Chem.*, 2004, **42,** 39.
368. A. R. Katritzky, N. G. Akhmedov, A. A. A. Abdel-Fattah, M. Wang, C. J. Rostek and O. W. Maender, *Magn. Reson. Chem.*, 2004, **42,** 424.
369. S. Brownstein and M. Zhou, *Magn. Reson. Chem.*, 2003, **41,** 1041.
370. A. P. Engoyan, *Hayastani Kimiakan Handes*, 2002, **55,** 97.
371. I. Alkorta and J. Elguero, *Org. Biomol. Chem.*, 2003, **1,** 585.
372. A. Bagno, F. Rastrelli and G. Saielli, *J. Phys. Chem. A*, 2003, **107,** 9964.
373. C. F. Tormena, R. Rittner, R. J. Abraham, E. A. Basso and B. C. Fiorin, *J. Phys. Org. Chem.*, 2004, **17,** 42.
374. M. Umemiya, K. Sugiura, H. Miyasaka, T. Ishii and M. Yamashita, *Bull. Chem. Soc. Jpn*, 2003, **76,** 2123.
375. J. Peralta-Cruz and S. E. Meza-Toledo, *Magn. Reson. Chem.*, 2004, **42,** 81.
376. T. Gáti, A. Simon, G. Tóth, D. Magiera, S. Moeller and H. Duddeck, *Magn. Reson. Chem.*, 2004, **42,** 600.
377. H. Schumann, C. Janiak, M. A. Khani and J. J. Zuckerman, *J. Organomet. Chem.*, 1987, **330,** 347.
378. J. E. Del Bene, I. Alkorta and J. Elguero, *Z. Phys. Chem.*, 2003, **217,** 1565.
379. P. F. Provasi, G. A. Aucar and S. P. A. Sauer, *J. Phys. Chem. A*, 2004, **108,** 5393.
380. I. Alkorta and J. Elguero, *Struct. Chem.*, 2004, **15,** 117.

381. R. Schwarz, J. Seelig and B. Künnecke, *Magn. Reson. Chem.*, 2004, **42,** 512.
382. A. D. Darwish, A. K. Abdul-Sada, A. G. Avent, Y. Lyakhovetsky, E. A. Shilova and R. Taylor, *Org. Biomol. Chem.*, 2003, **1,** 3102.
383. G. B. Deacon and C. M. Forsyth, *Chem. Eur. J.*, 2004, **10,** 1798.
384. J. Omelańczuk, A. Karaçar, M. Freytag, P. G. Jones, R. Bartsch, M. Mikołajczyk and R. Schmutzler, *Inorg. Chim. Acta*, 2003, **350,** 583.
385. B. Wrackmeyer, S. V. Gruener and A. S. Zolotareva, *Z. Naturforsch.*, 2003, **58b,** 1035.
386. I. Alkorta and J. Elguero, *Theor. Chem. Acc.*, 2004, **111,** 31.
387. H. Cybulski, M. Pecul, J. Sadlej and T. Helgaker, *J. Chem. Phys.*, 2003, **119,** 5094.
388. J. E. Del Bene and J. Elguero, *Magn. Reson. Chem.*, 2004, **42,** 421.
389. S. Kawahara, C. Kojima, K. Taira and T. Uchimaru, *Helv. Chim. Acta*, 2003, **86,** 3265.
390. T. Tuttle, J. Gräfenstein, A. Wu, E. Kraka and D. Cremer, *J. Phys. Chem. B*, 2004, **108,** 1115.
391. T. Tuttle, E. Kraka, A. Wu and D. Cremer, *J. Am. Chem. Soc.*, 2004, **126,** 5093.
392. V. A. Jaravine, F. Cordier and S. Grzesiek, *J. Biomol. NMR*, 2004, **29,** 309.
393. C. Kojima, A. Ono and M. Kainosho, *J. Biomol. NMR*, 2000, **18,** 269.
394. F. M. Assadi-Porter, F. Abildgaard, H. Blad and J. L. Markley, *J. Biol. Chem.*, 2003, **278,** 31331.
395. P. R. Jensen, J. B. Axelsen, M. H. Lerche and F. M. Poulsen, *J. Biomol. NMR*, 2004, **28,** 31.
396. D. W. Staple and S. E. Butcher, *Nucl. Acid Res.*, 2003, **31,** 4326.
397. S. H. M. Söntjens, M. H. P. van Genderen and R. P. Sijbesma, *J. Org. Chem.*, 2003, **68,** 9070.
398. J. E. Del Bene, S. A. Perera and J. E. Bartlett, *Magn. Reson. Chem.*, 2001, **39,** S109.
399. J. E. Del Bene and J. E. Bartlett, *J. Am. Chem. Soc.*, 2000, **122,** 1048.
400. G. C. Lloyd-Jones, J. N. Harvey, P. Hodgson, M. Murray and R. L. Woodward, *Chem. Eur. J.*, 2003, **9,** 4523.
401. J. E. Del Bene and J. Elguero, *Chem. Phys. Lett.*, 2003, **382,** 100.
402. J. E. Del Bene, J. Elguero, I. Alkorta, M. Yánez and O. Mó, *J. Chem. Phys.*, 2004, **120,** 3237.
403. T. Haliloglu, A. Kolinski and J. Skolnick, *Biopolymers*, 2003, **70,** 548.
404. B. Vögeli, H. Kovacs and K. Pervushin, *J. Am. Chem. Soc.*, 2004, **126,** 2414.
405. G. M. Clore and C. D. Schwieters, *J. Am. Chem. Soc.*, 2004, **126,** 2923.
406. P. Barré, S. Yamaguchi, H. Saito and D. Huster, *Eur. Biophys. J.*, 2003, **32,** 578.
407. A. T. Alexandrescu and K. R. A., *Protein Sci.*, 2003, **12,** 2132.
408. S. H. Park, A. A. Mrse, A. A. Nevzorov, M. F. Mesleh, M. Oblatt-Montal, M. Montal and S. J. Opella, *J. Mol. Biol.*, 2003, **333,** 409.
409. S. Lee, M. F. Mesleh and S. J. Opella, *J. Biomol. NMR*, 2003, **26,** 327.
410. T. S. Ulmer, B. E. Ramirez, F. Delaglio and A. Bax, *J. Am. Chem. Soc.*, 2003, **125,** 9179.
411. D. Y. Zheng, J. M. Aramini and G. T. Montelione, *Protein Sci.*, 2004, **13,** 549.
412. M. Ghosh, L. M. Elsby, T. K. Mal, J. M. Gooding, S. G. E. Roberts and M. Ikura, *Biochem. J.*, 2004, **378,** 317.
413. K. Fleming, J. Ghuman, X. M. Yuan, P. Simpson, A. Szendröi, S. Matthews and S. Curry, *Biochemistry*, 2003, **42,** 8966.
414. L. M. Parsons, D. C. Yeh and J. Orban, *Protein Struct. Funct. Genet.*, 2004, **54,** 375.
415. L. Blanchard, N. Tarbouriech, M. Blackledge, P. Timmins, W. P. Burmeister, R. W. H. Ruigrok and D. Marion, *Virology*, 2004, **319,** 201.

416. R. Harris, D. Esposito, A. Sankar, J. D. Maman, J. A. Hinks, L. H. Pearl and P. C. Driscoll, *J. Mol. Biol.*, 2004, **335,** 573.
417. M. A. Massiah, V. Saraswat, H. F. Azurmendi and A. S. Mildvan, *Biochemistry*, 2003, **42,** 10140.
418. L. Pappalardo, I. G. Janausch, V. Vijayan, E. Zientz, J. Junker, W. Peti, M. Zweckstetter, G. Unden and C. Griesinger, *J. Biol. Chem.*, 2003, **278,** 39185.
419. K. C. Prutzman, G. H. Gao, M. L. King, V. V. Iyer, G. A. Mueller, M. D. Schaller and S. L. Campbell, *Structure*, 2004, **12,** 881.
420. G. H. Gao, K. C. Prutzman, M. L. King, D. M. Scheswohl, E. F. DeRose, R. E. London, M. D. Schaller and S. L. Campbell, *J. Biol. Chem.*, 2004, **279,** 8441.
421. D. C. Williams, M. L. Cai and G. M. Clore, *J. Biol. Chem.*, 2004, **279,** 1449.
422. N. J. Reiter, L. J. Nikstad, A. M. Allmann, R. J. Johnson and S. E. Butcher, *Rna*, 2003, **9,** 533.
423. P. J. Lukavsky, I. Kim, G. A. Otto and J. D. Puglisi, *Nature Struct. Biol.*, 2003, **10,** 1033.
424. R. K. O. Sigel, D. G. Sashital, A. D. L., A. G. Palmer III, S. E. Butcher and A. M. Pyle, *Nature Struct. Mol. Biol.*, 2004, **11,** 187.
425. Z. H. Du, N. B. Ulyanov, J. H. Yu, R. Andino and T. L. James, *Biochemistry*, 2004, **43,** 5757.
426. B. N. M. van Buuren, A. Schleucher, V. Wittmann, C. Griesinger, H. Schwalbe and S. S. Wijmenga, *Angew. Chem. Int. Ed.*, 2004, **43,** 187.
427. V. D'Souza, A. Dey, D. Habib and M. F. Summers, *J. Mol. Biol.*, 2004, **337,** 427.
428. A. Almond, B. O. Petersen and J. O. Duus, *Biochemistry*, 2004, **43,** 5853.
429. A. Mascioni and G. Veglia, *J. Am. Chem. Soc.*, 2003, **125,** 12520.
430. M. F. Mesleh and S. J. Opella, *J. Magn. Reson.*, 2003, **163,** 288.
431. M. F. Mesleh, S. Lee, G. Veglia, D. S. Thiriot, F. M. Marassi and S. J. Opella, *J. Am. Chem. Soc.*, 2003, **125,** 8928.
432. M. Zweckstetter, *J. Biomol. NMR*, 2003, **27,** 41.
433. K. Ding, J. M. Louis and A. M. Gronenborn, *J. Mol. Biol.*, 2004, **335,** 1299.
434. H. M. Al-Hashimi, S. W. Pitt, A. Majumdar, W. Xu and D. J. Patel, *J. Mol. Biol.*, 2003, **329,** 867.
435. H. Valafar and J. H. Prestegard, *Bioinformatics*, 2003, **19,** 1549.
436. H. Valafar and J. H. Prestegard, *J. Magn. Reson.*, 2004, **167,** 228.
437. J. D. Walsh, J. Cabello-Villegas and Y.-X. Wang, *J. Am. Chem. Soc.*, 2004, **126,** 1938.
438. I. Asllani, E. Shankland, T. Pratum and M. Kushmerick, *J. Magn. Reson.*, 2003, **163,** 124.
439. S. Arumugam and S. R. Van Doren, *Biochemistry*, 2003, **42,** 7950.
440. P. Berthault, D. Jeannerat, F. Camerel, F. Alvarez Salgado, Y. Boulard, J.-C. P. Gabriel and H. Desvaux, *Carbohydr. Res.*, 2003, **338,** 1771.
441. J. Yan, F. Delaglio, A. Kaerner, A. D. Kline, H. Mo, M. J. Shapiro, T. A. Smitka, G. A. Stephenson and E. R. Zartler, *J. Am. Chem. Soc.*, 2004, **126,** 5008.
442. L. Chang, N. F. Whittaker and C. A. Bewley, *J. Nat. Prod.*, 2003, **66,** 1490.

6
Nuclear Spin Relaxation in Liquids and Gases

BY R. LUDWIG

1 Introduction

The aim of this report is to cover the progress of work in the field of magnetic relaxation and self-diffusion in liquids and gases over a period of twelve months from June 2003 to May 2004, and is a continuation of the report given last year.[1]

As in previous periods, this review is limited to work on comparatively simple liquids and solutions of physico-chemical and chemical interest, as publications in the field of macromolecules and biological chemistry are covered elsewhere in this volume. Of course, such a distinction is sometimes problematic, as innovative work dealing with solutions of complex molecules may be of interest for research in the field covered here. Thus, at the risk of duplication, some interesting studies dealing with more complex systems are mentioned briefly. At the beginning of this chapter it is convenient to quote some authoritative reviews in the subject area. More specialized reviews will be discussed in the corresponding subsections. Details will be discussed later in this chapter.

Reinhardt[2] reviewed the development of NMR for solving structure and dynamics of molecular systems. In particular he focused on the contributions of the first chemist working in the field of NMR, Herbert S. Gutowsky.

During the past two years, significant advances have been made in the development of NMR methods for studying biomolecular dynamics on the microsecond to millisecond timescale. Thuduppathy and Hill[3] reviewed applications of NMR spin relaxation methods for measuring biological motions. Fernandez and Wider[4] discussed transverse relaxation-optimized spectroscopy (TROSY) that promises to further enhance the determination of solution structures of large biomolecules.

The sensitivity of conventional nuclear magnetic resonance (NMR) techniques is fundamentally limited by the ordinarily low spin polarization achievable in even the st rongest NMR magnets. However, by transferring angular momentum from laser light to electronic and nuclear spins, optical pumping methods can increase the nuclear spin polarization of noble gases by several orders of magnitude, thereby greatly enhancing their NMR sensitivity. Cherubini and Bifone[5] surveyed the important role of hyperpolarized xenon in biology.Bain[6] discussed the broad range of NMR experiments for studying chemical exchange. In particular he focused on liquid-state methods. Wang and Palmer[7] reviewed solution

Nuclear Magnetic Resonance, Volume 34
© The Royal Society of Chemistry, 2005

NMR methods for quantitative identification of chemical exchange in ^{15}N-labelled compounds.

Dunand *et al.*[8] reviewed solvent exchange on metal ions. Post[9] summarized recently developed experiments in exchange-transferred NOE spectroscopy for the determination of bound ligand structures. Bain and Khasawneh[10] reviewed the complete range of quadrupole interactions. The spectroscopy is continuously followed from zero through high magnetic field.

Stilbs[11] discussed NMR techniques that provide valuable insight into the structure and dynamics of mesoscale structures. In particular spin relaxation effects were considered. Klein and Ries[12] reviewed the importance of NMR for studying glasses.

Pettersson *et al.*[13] investigated artefacts in electrophoretic NMR experiments in detail. They identified electroosmosis, sample heating, and gas development on the electrodes as main error sources and suggest experimental strategies and setups to suppress their influence on the monitored electrophoretic mobilities. The authors hereby demonstrates essentially artefact-free experiments up to currents and electric fields 3 mA and 70 V/cm, respectively.

2 General, Physical and Experimental Aspects of Nuclear Spin Relaxation

2.1 General Aspects. – Intermolecular zero-quantum and double-quantum-coherences (iZQCs and iDQCs) are frequently discussed in literature since they may provide novel contrast mechanisms in magnetic resonance imaging and possibilities for high-resolution spectra in an inhomogeneous and unstable magnetic field.[14-22]

Branca *et al.*[23] reported a detailed and understandable analysis of the evolution of various coherence orders in a Correlated 2D spectroscopy revamped by asymmetric z-gradient echo detection (CRAZED) like pulse sequence, used to select a signal from intermolecular multi quantum coherences (iMQCs). Because the signal to-noise-ratio of iMQC is much lower than the signal from conventional single quantum coherence (SQC), an optimization of experimental parameters is a necessity when measurements are made with iMQC. For this purpose a phase cycle is shown that not only allows a simpler selection of a particular quantum coherence order, but also removes receiver artifacts.

Intermolecular double-quantum coherence (i-DQC) signals in liquids are usually associated with high magnetic fields. Barros *et al.*[24] demonstrated that, in a magnetic field of only 16 mT, i-DQC imaging of water protons is feasible thanks to the nuclear magnetization enhancement produced by the Overhauser effect. i-DQC images of a phantom containing an aqueous solution of a trityl free radical, with phase encoding in the DQC evolution period or in the acquisition period, are presented. Possible applications of low field i-MQC images are given. Cano *et al.*[25] described a simple and robust method to suppress zero-quantum coherences (ZQC) in a single scan and with very high suppression ratio. It is an appreciable improvement on a previous technique by Thrippleton and Keeler.[26] Bain and Khaswneh[10] mapped out the theoretical transition energies of a spin

3/2 under a combination of quadrupolar and Zeeman interactions as a function of magnetic field. This allows to follow the spectroscopy continuously from zero magnetic field (NQR, nuclear quadrupole resonance) through to high magnetic field (quadrupole-perturbed NMR). This calculation is made possible by a theoretical approach that makes maximum use of the angular momentum properties of the spin system. In this approach, the detailed form of the spin operators are not required, only their angular momentum quantum numbers. No commutators need be evaluated, and the method is easily coded for computer calculation. Application of the Wigner-Eckart theorem and selection rules means that there are only two nonzero reduced matrix elements that are needed for a spin 3/2, and there are explicit formulae for them. In looking at the transition energies, the crucial parameter is the orientation of the quadrupole tensor to the magnetic field. If the angle is nonzero, then the quantization of the spins must shift. At zero field, the quantization is defined by the electric field gradient tensor, which is molecule-fixed at some arbitrary angle to the magnetic field. This direction of quantization must change as the magnetic field increases, to lie close to the z axis at high field. In the region where the two interactions are comparable, all the familiar rules break down and the response is highly non-linear.

In contrast to transverse nuclear magnetizations, longitudinal spin magnetizations are usually considered as insensitive to magnetic field gradients. While this assumption is valid for homogeneously excited samples, the apparent longitudinal spin relaxation behaviour of thin magnetization slices in high magnetic fields is strongly modified by diffusion. Nestle *et al.*[27] presented the results of theoretical and experimental studies on this effect. Furthermore, possible applications and the impact on different types of NMR techniques using strong magnetic field gradients are discussed.

NMR spectroscopy is a unique method for probing microsecond-to-millisecond time scale motions at atomic level resolution. Many dynamic processes that fall in this range are of primary interest for organic, organometallic, and biological chemistry. For example, in the context of protein studies NMR techniques were recently used to probe ligand binding,[28,29] protein folding,[30] and enzymatic catalysis.[31] Information about μs to ms dynamics is obtained from broadening of spectral lines. This effect can be interpreted in a general manner using the master equation for spin density matrix supplemented with an exchange superoperator.[32] In the important case of fast dynamics, exchange broadening can be described by Redfield theory and expressed as a relaxation contribution due to stochastic modulation of isotropic chemical shift, R_{ex}.[33] Redfield-type analyses have been carried out for various motional models including multi-site exchange[34] and in the context of multi-spin systems.[35] Fast-to-intermediate time-scale chemical exchange can be most readily studied using the dependence of R_{ex} on the strength of the applied radiofrequency (RF) field. Two basic experimental schemes have been employed so far toward this goal: (i) continuous-wave spin lock with constant amplitude and phase[33] and (ii) Carr-Purcell-Meiboom-Gill (CPMG) train of hard 180° pulses.[36] The first experiment is usually interpreted in the rotating frame of reference where the energy levels of

the spin-1/2 system are separated by $h\nu_1$ (ν_1 represents the strength of the spin-lock field). The increase in ν_1 widens the gap between the energy levels. As a result, the stochastic motion becomes less efficient in causing relaxation transitions between the said energy levels. This effect manifests itself through the Redfield-theory spectral density, $J(\omega_1) = d\tau G(\tau)\exp(-i\omega_1\tau)$. In the case when correlation function $G(\tau)$ has simple exponential form,[34] $J(\tau_1)$ declines monotonically with τ_1. The resulting dependence of R_{ex} on ω_1 is known as the 'relaxation dispersion curve'. Podkorytov and Skrynnikov[37] proposed a spin lock comprised of radiofrequency pulses with alternating phase as a new technique to probe microsecond time-scale dynamics. A series of $R_{1\rho}$ measurements using different pulse duration t_p allows one to determine exchange rate, k_{ex}, the product $p_a p_b(\Delta\omega_{ab})^2$ involving populations of the exchanging species, p_a and p_b, together with chemical shift difference, $\Delta\omega_{ab}$, and the strength of the spin-lock field, B_1. The interpretation is based on simple analytical expression for $R_{1\rho}$ derived on the basis of Redfield theory. The application of the method is demonstrated for partially deuterated molecule of cyclohexane undergoing chair-to-chair interconversion at −9 °C.

2.2 Experimental Aspects. – Electrophoretic NMR (ENMR,[38,39] also known as DCNMR[40] or magnetic resonance electrophoresis MREP[41,42]) has been available for some time now, adding the electrophoretic mobility dimension to the versatile NMR field.[39-42] Viewed from the electrophoretic side,[43-46] NMR is a useful complement to the existing techniques that are conventionally used to measure electrophoretic mobility; perhaps its greatest advantage is chemical selectivity. Hence, electrophoretic NMR can measure the electrophoretic mobilities of small and large molecular components in complex mixtures. Moreover, NMR diffusion experiments[47-49] are readily available to measure the diffusion coefficient of the electromigrating entities, thereby allowing for separation of charge and size effects. Because the Coulomb interaction is usually dominant at the molecular level, information about charge and surface potential is of great importance when studying various chemical and biochemical systems. Since the first documented attempt,[50] a lot of effort has been invested to improve electrophoretic NMR.[51,52] In general, an ENMR experiment is not as straightforward as an NMR diffusion experiment – it requires control over several nonelectrophoretic motional artefacts, which complicate the measurement of the true electrophoretic mobility of species. The different problems have all been recognized in the general electrophoretic and ENMR literature, but have not been investigated systematically or quantitatively. Petterson *et al.*[13] improved existing explanations and previously suggested remedies.

Loening *et al.*[53] proposed several single-scan experiments for the measurement of the longitudinal relaxation time (T_1). These experiments result in fast and accurate determinations of the relaxation rate, are relatively robust to pulse imperfections, and preserve information about the chemical shift. The method used in these experiments is to first encode the T_1 values as a spatial variation of the magnetization and then to read out this variation either by applying a weak gradient during acquisition or by sequentially observing different slices of the

sample. As a result, it is possible to reduce the time necessary to determine the T_1 values by one or two orders of magnitude. This time saving comes at the expense of the signal-to-noise level of the resulting spectrum and some chemical shift resolution.

NMR imaging by radio-frequency field gradients (B_1 gradients) is especially convenient for heterogeneous samples and/or in the case of relatively short transverse relaxation times. Chaumette *et al.*[54] combined the method with the application of two spin-lock periods of different duration so as to produce rotating-frame spin-lattice relaxation time ($T_{1\rho}$) images. In the case of natural rubber samples with different crosslink densities, such images are not only characteristic of the crosslink density but also reveal the way in which the material has been stressed. The strained parts can be visualized either directly or through histograms showing the $T_{1\rho}$ distribution over the whole sample.

Redfield[55] described an apparatus that can pneumatically move an aqueous liquid NMR sample sealed in a 5 or 8 mm standard tube, from the center of a standard Varian 500 MHz spectrometer and probe out to any position in its fringe field, and back, under computer control. Applications to low-field relaxation and other measurements are discussed briefly, particularly using ^{31}P, and ^{15}N and ^{13}C with proton detection, utilizing the full power of the commercial system for preparation before, and detection after, a relaxation or mixing interval at low field. Transverse relaxation, polarization transfer, and other transverse manipulations are virtually impossible with this apparatus while the sample is at the low (fringe) field, because of the tremendous inhomogeneity of that field.

Ardenkjaer-Larsen *et al.*[56] developed a method for obtaining strongly polarized nuclear spins in solution. The method uses low temperature, high magnetic field, and dynamic nuclear polarization (DNP) to strongly polarize nuclear spins in the solid state. The solid sample is subsequently dissolved rapidly in a suitable solvent to create a solution of molecules with hyperpolarized nuclear spins. The polarization is performed in a DNP polarizer, consisting of a super-conducting magnet (3.35 T) and a liquid-helium cooled sample space. The sample is irradiated with microwaves at approximate to 94 GHz. Subsequent to polarization, the sample is dissolved by an injection system inside the DNP magnet. The dissolution process effectively preserves the nuclear polarization. The resulting hyperpolarized liquid sample can be transferred to a high-resolution NMR spectrometer, where an enhanced NMR signal can be acquired, or it may be used as an agent for in vivo imaging or spectroscopy. The method can be used generally for signal enhancement and reduction of measurement time in liquid-state NMR and opens up for a variety of in vitro and in vivo applications of DNP-enhanced NMR.

Harris *et al.*[57] described a numerical methodology to obtain more efficient relaxation filters to selectively retain or remove components based on relaxation times. The procedure uses linear combinations of spectra with various recycle or filter delays to obtain components that are both quantitative and pure. Modulation profiles are calculated assuming exponential relaxation behavior. The method is general and can be applied to a wide range of solution or solid-state NMR experiments including direct-polarization (DP), or filtered cross-polariz-

ation (CP) spectra. ^{13}C NMR experiments on isotactic poly(I-butene) and dimethyl sulfone showed the utility of the technique for selectively suppressing peaks.

2.3 Relaxation in Coupled Spin Systems. – The ability to transfer coherences between different nuclei in homo- and heteronuclear spin systems is one of the cornerstones of NMR.[58] The transfer of polarization from I = (1/2) to enhance the signal of low-gyromagnetic ratio S = (1/2) nuclei has become routine. In solution state the majority of these methods employ free-precession type techniques such as INEPT[59] where polarization transfer from one spin to another is mediated *via* the scalar coupling. The majority of these techniques are designed for spin-half systems and have shown particular utility in the study of structure and dynamics of biomolecules labeled with ^{13}C and ^{15}N. The use of INEPT for achieving polarization transfer in systems of scalar coupled quadrupolar nuclei has also been investigated.[60,61]

Cross-polarization has been shown to be applicable for coherence transfer in solution state, where the dipolar interaction is motionally averaged to zero. The transfer is therefore usually driven by the scalar coupling interaction,[62-65] and in some circumstances by the interaction with the r.f. fields.[66,67] The scalar coupling is in general at least two orders of magnitude smaller than the dipolar interaction rendering the method susceptible to r.f. mismatch. Cross-polarization in solution state is therefore a less attractive method than its free precession counterparts. Methods developed for mismatch compensation in the solid state[68] have been shown to be applicable to solution state NMR.[69] It has recently been shown that employing r.f. fields whose amplitudes are of the same order as the scalar coupling interaction can largely circumvent this obstacle.[70] The use of weak r.f. fields makes cross-polarization an ideal tool for selective experiments in both solution[71] and solid state.[72]

Recently, there has been significant interest in the use of relaxation interference effects between chemical shift anisotropy (CSA) and dipolar interactions to obtain valuable information about local structure and motions in biological macromolecules.[73-79] Specifically, applications of cross-correlation measurements of ^{15}N CSA and ^{1}H-^{15}N dipolar interaction range from determination of the ^{15}N CSA tensors in molecules in solution[73,74,80,81] to the characterization of the overall and local dynamics in proteins and nucleic acids.[73,74,82,83] In addition, measurements of the ^{15}N CSA-dipolar cross-correlation rates have been used to identify residues involved in conformational exchange and to estimate contributions from these motions.[80,82,84] Hall and Fushmann[85] described direct methods for the measurement of the transverse and longitudinal ^{15}N chemical shift anisotropy-dipolar cross-correlation rates based on comparison of the ^{15}N doublet components observed in ^{1}H-coupled ^{1}H-^{15}N HSQC-type spectra. This allows the determination of the cross-correlation rates with no need for correction factors associated with other methods. The signal overlap problem of coupled HSQC spectra is addressed by using the IPAP scheme.[86] The methods proposed here use a conventional t_1 evolution period, which allows one to minimize the truncation artefacts observed in a constant-time-type experiment.[87]

The NMR signals of insensitive nuclear spins can be enhanced by transferring polarization from a more sensitive species to which they are coupled.[88] The well-known pulse sequences as the polarization transfer techniques are insensitive nuclei enhanced by polarization transfer (INEPT), distortionless enhancement by polarization transfer (DEPT), and reverse insensitive nuclei enhanced by polarization transfer (RINEPT)[89, 90] The INEPT sequence is an alternative to the nuclear Overhauser effect. The INEPT experiment does not require any particular relaxation mechanism and therefore a better enhancement factor can be obtained.[88] Furthermore it is demonstrated that INEPT sequence can be used to determine the multiplicity of each signal in a ^{13}C NMR spectrum.[90] More recently, the INEPT and DEPT experiments were used for the coherence transfer *via* heteronuclear *J*-coupling between spin-1/2 and quadrupolar nuclei in the solids.[91-93] Fyfe *et al.*[91] showed that coherence transfer *via* the scalar coupling between spin-1/2 and quadrupolar nuclei can be obtained in the solid state by using INEPT experiment.

On the other hand to analyse and describe the multi-pulse NMR experiments an effective and useful tool is product operator theory as a simple quantum mechanical method.[94, 95] The product operator formalism has been used for weakly coupled IS ($I=1/2$; $S=1/2$, 1, and 3/2) spin systems.[94, 96-99] The polarization transfer (PT) between spin-1/2 nuclei in an INEPT pulse sequence has been described by using product operator theory.[100] Chandrakumar[101] investigated the polarization transfer between spin-1 and spin-1/2 nuclei by using product operator formalism for INEPT and from spin-1/2 to spin-1 nuclei for refocusing INEPT experiments. Tokatli *et al.*[102] first introduced the results of the applications of the product operators theory to the polarization transfer between spin-3/2 and spin-1/2 nuclei for INEPT and from spin-1/2 to spin-3/2 nuclei for RINEPT experiments. They have taken the molecules that include one of these three organometallic compounds: trimethyltinchloride [$(CH)_3SnCl$] (as IS spin system), dimethyltindichloride [$(CH_3)_2SnCl_2$] (as IS_2 spin system) and methyltintrichloride [CH_3SnCl_3] (as IS_3 spin system) containing the weakly coupled $I=1/2$ (^{119} Sn with $\gamma=-9.53\times10^7$ T^{-1} s^{-1} ; 8.58%) and $S=3/2$ (^{35} Cl with $\gamma=2.62\times10^{-7}$ T^{-1} s^{-1} ; 75.53%) nuclei.[103, 104] It is well know that the scalar or indirect coupling J to the quadrupolar nuclei can be observed provided that some arrangements of ligands can cause to give low or zero electric field gradients at a point of the molecule.[105, 106] In this framework by considering the values mentioned above in the selected real chemical systems the coupling constant $J_{Sn\text{-}Cl}$ was taken as 375 Hz and simulate the intensities and positions of observable signals in INEPT and RINEPT by using Maple programme on computer.[107, 108]

Kupriyanov[109] studied relaxation of spin 1/2 in the scalar coupled spin system AMX with quadrupolar nuclei in the presence of cross correlation effects. Khaneja *et al.*[110] presented optimal control of spin dynamics in the presence of relaxation. Eykyn *et al.*[111] studied selective cross-polarization in solution state NMR of scalar coupled spin 1/2 and quadrupolar nuclei. Tokatli[112] applied the product operator theory to spin 5/2 nuclei. Mahesh *et al.*[113] used strongly coupled spins for quantum information processing. Luy and Glaser[114] inves-

tigated transverse magnetization transfer under planar mixing conditions in spin systems consisting three coupled spins 1/2.

2.4 Dipolar Couplings and Distance Information. – The nuclear Overhauser effect (NOE) arises from dipolar interactions between magnetic moments associated with nuclear spins and it has become a powerful tool to extract relevant pieces of structural information about small molecules, as well as in molecules of biological interest. As a consequence, accurate NOE measurement is a very crucial issue. Walker *et al.*[115] presented a comparison between direct and a new inverse HOESY experiment aimed at the detection of heteronuclear NOE between ^{1}H and ^{13}C, which is particularly well suited for symmetric compounds. It transpires that directly detected data are more suitable for quantitative assessment even if they suffer from lower sensitivity, whereas inverse detection is quite appropriate for a quick and qualitative assessment. In the latter experiment, unwanted cross-correlation effects may hide valuable NOE data (cross-relaxation), this drawback can be circumvented by a slight modification of the pulse sequence.

The direct interaction between magnetic moments associated with nuclear spins (also called dipolar coupling) has proven to be one of the most useful quantities provided by NMR. In an anisotropic medium, through its dependence in r^{-3} (r being the internuclear distance), it yields relevant structural information directly. By contrast, in solution, the dipolar couplings are averaged to zero by molecular motions, and thus do not give rise to any splitting in the NMR spectrum. Nevertheless, dipolar interactions are involved in nuclear spin relaxation and are one of the mechanisms involved in the longitudinal and transverse relaxation times. However, extracting their contributions from the latter parameters is not an easy task. Conversely, cross-relaxation rates are parameters that depend solely on dipolar interactions and these can be accessed relatively directly by appropriate experimental methods, the most popular one being nuclear Overhauser effect (NOE) spectroscopy (NOESY), which turns out to be a powerful tool for structural analysis of small molecules[116] and biological macromolecules.[117,118] Small molecules and proteins were extensively investigated by means of homonuclear cross-relaxation rates[119] so as to gain information on spatial proximity; heteronuclear cross-relaxation rates (*e.g.* ^{13}C-^{1}H or ^{15}N-^{1}H) have been widely used to derive both structural and motional parameters.[120] Several two-dimensional (2D) heteronuclear Overhauser spectroscopy (^{1}H-X) techniques have been applied to different heteronuclei X.[121] Some of them have been designed to detect the signal of the less-sensitive nucleus (*e.g.* X) and used optionally appropriate spin filters to extract the desired piece of information.[122,123] Unfortunately, this methodology suffers from low sensitivity, for the reasons detailed previously.[124] One way to circumvent this disadvantage is to turn to an inverse experiment, *i.e.* performing measurement on the most sensitive nucleus (hence ^{1}H). Bauer[125] proposed a strategy to detect ^{31}P-^{1}H and ^{7}Li-^{1}H interactions by the use of pulsed field gradients but some of these experiments exhibit strong t_1 noise which can blur the spectrum and prevent the accurate measurement of weak heteronuclear Overhauser peaks.[126] Recently,

Alam *et al.*[124] proposed a slight modification of the pulse sequence introduced by Bauer to improve the identification and quantitation of the long-range NOE. Kover and Batta[127] proposed an idea along the same lines using an inverse doubly filtered experiment involving ^{13}C nuclei. HOESY experiments specially designed for symmetric molecules. For both direct and inverse detection, experiments have been designed to observe all possible Overhauser effects, including the following interactions: (i) between the ^{13}C nucleus and its directly bonded ^{1}H; (ii) between the ^{13}C nucleus and a proton not directly bonded to it (remote); (iii) between the ^{13}C nucleus and protons in chemically equivalent sites. For the inverse detected HOESY experiment Walker *et al.*[115] introduced a slight modification of the pulse sequence in order to attenuate possible effects of cross-correlation that may be manifest at the end of the mixing period.

Kramer and Glaser[128] analysed the transfer efficiency of cross-relaxation compensated (Clean) TOCSY sequences for applications to residual dipolar couplings. Surprisingly most conventional Clean TOCSY sequences are very inefficient for dipolar transfer. It is shown theoretically, that this is a general property of all phase-alternating mixing sequences, *i.e.*, for such sequences the suppression of cross-relaxation excludes dipolar transfer in the spin-diffusion limit. A new family of clean dipolar TOCSY sequences is derived which provides excellent transfer efficiencies for a broad range of offset frequencies.

In the weak coupling limit, the spectrum of two scalarly and dipolarly coupled spins does not allow to unequivocally determine the relative sign and size of scalar and residual dipolar coupling constants. One solution to the problem is to use an additional spin to solve the sign ambiguity.[129] Alternatively, the preparation of several samples with different degrees of alignment allows to solve the sign problem. Kramer *et al.*[130] present a different approach, which allows to solve the sign problem for a pair of homonuclear spins in a single aligned sample if the scalar coupling is known. The method relies on the fact that TOCSY transfer functions reflect the full scalar and dipolar coupling tensors. This makes it possible to determine the sign of residual dipolar couplings in the presence of known scalar couplings in a two-spin system. The approach is demonstrated experimentally using a model system and potential problems of the approach are discussed.

Bytchenkoff and Bodenhausen[131] designed a new NMR method for the measurement of the longitudinal relaxation rates of both donor and acceptor ^{15}N nuclei in Watson-Crick base pairs in ^{15}N enriched nucleic acids. The length of four hydrogen bonds could be estimated from the longitudinal relaxation rates.

2.5 Exchange Spectroscopy. – Almost everyone who has done NMR has seen some evidence of chemical exchange. This could be the classic line broadening and coalescence phenomenon, the lack of coupling to hydroxide protons, cross-peaks in a NOESY-type spectrum or several other observations. The ways that chemical exchange affects NMR spectra are very diverse, but the basic mechanism is much the same. In his review, Bain[6] stressed the underlying similarities in the broad range of experimental manifestations. He concentrated on liquid-state NMR, since this is the simplest and most familiar subject. However, exchange

also happens in the gas phase and in the solid state.

Exchange transferred effects in solution-state NMR experiments allow one to determine the conformation of ligands that are weakly bound to macromolecules. Exchange-transferred nuclear Overhauser effect spectroscopy ('TR-NOESY') provides information about internuclear distances in a ligand in the bound state. Recently the possibility of obtaining dihedral angle information from a ligand in the bound state by exchange-transferred cross-correlation spectroscopy ('TR-CCSY') has been reported. In both cases the analysis of the signal amplitudes is usually based on the assumption that rapid exchange occurs between the free and bound forms of the ligand. Ravindranathan *et al.*[132] showed that the fast exchange condition is not easily attained for observing exchange-transferred cross-correlation effects even in systems where exchange-transferred NOE can be observed. Extensive simulations based on analytical expressions for signal intensities corresponding to fast, intermediate, and slow chemical exchange have been carried out on a test system to determine the exchange regimes in which the fast exchange condition can be fulfilled for successfully implementing TR-NOESY and TR-CCSY.

In quantitative NMR studies of chemically exchanging proteins in solution an accurate analysis of the NMR signals is imperative. This holds *inter alia* for paramagnetic metallo-proteins, where valuable information about the dynamics, structure, and function of the proteins can be obtained from an accurate determination of the relaxation rates and Larmor frequencies of the protein nuclei.[133-137]

In chemically exchanging systems, the nuclei reside itinerantly in different conformations that may be characterized by different NMR parameters. Depending on the size of the exchange rate and the difference between corresponding NMR parameters of the exchanging sites, a given nucleus either give rise to a single exchange-averaged signal, or to separate signals corresponding to the individual conformations. In both cases, the NMR signals may depend on more than one of the conformations and can, therefore, provide information about all of the involved conformations as well as the exchange process.

The NMR signals of chemically exchanging systems are described by the Bloch-McConnell equations[138,139] If a sufficiently versatile dataset is available, all the relevant NMR parameters of a chemically exchanging system can be determined simultaneously using the *general* solution of these equations. However, because of limited experimental information approximate solutions of the Bloch-McConnell equations[140] are often used to obtain information about systems of biological interest, the specific form of the equations being dependent on the system under investigation, the applied experimental conditions, and the type of data available. In the case of a limited dataset, approximate solutions of the equations may be used incorrectly and can, therefore, result in erroneous estimates of the parameters. This was clearly emphasized in a recent theoretical study of relaxation in the rotating frame of a system outside the fast exchange limit.[141] Moreover, the available dataset may be analysed using non-optimal computational procedures.

Hansen[142] now present an evaluation of the approximate solutions of the Bloch-McConnell equations of a chemically exchanging system. The evaluation

is based on a comparison with the results of a complete analysis of the NMR signals of chemically exchanging nuclei that allows an independent and accurate determination of all the involved parameters. The complete analysis is based on the general solution of the Bloch-McConnell equations. It includes a simultaneous analysis of the chemical shift, and the transverse and longitudinal relaxation rates of the observed nuclei as well as the variation of these parameters with the molar fractions of the exchanging species and the rate of the chemical exchange process.

Chemical exchange phenomena in NMR spectra reveal protein motions on microsecond to millisecond time scales that are associated with biological functions, including catalysis, ligand binding, allosteric conformational changes and protein folding. Wang and Palmer[7] surveyed solution NMR methods for identifying chemical exchange in proteins by measuring transverse relaxation rate constants for backbone ^{15}N spins. The relaxation-compensated-I_zS_z and in-phase Hahn echo methods are suitable for small- to medium-sized proteins. The transverse relaxation optimized spectroscopy method is suitable for large, deuterated proteins. Differential multiple quantum relaxation is also a signature of chemical exchange and provides unique information about exchange processes. The various methods are illustrated by application to basic pancreatic trypsin inhibitor and triosephosphate isomerase.

Massi *et al.*[143] measured spin relaxation in the rotating frame $R_{1\rho}$ to characterize chemical exchange kinetic processes occurring on μs-ms time scales. The new two-dimensional experiment allow the use of weak r.f. fields between 150 and 1000 Hz. The new experiments also extend the capability of the $R_{1\rho}$ technique to study exchange processes outside the fast exchange limit.

Abergel and Palmer[144] presented expressions for $R_{1\rho}$ for two-site chemical exchange using both the conventional perturbation approach for evolution of the density operator and the stochastic Liouville equation for evolution of the average density operator. This way slow and fast chemical exchange is covered. Shapira and Frydman[145] presented an arrayed acquisition of 2D exchange NMR spectra within a single scan experiment. Hernandez and LeMaster[146] showed relaxation compensation in chemical exchange measurements for the quantitation of amide hydrogen exchange in larger proteins. Post[9] performed exchange-transferred NOE spectroscopy to determine bound ligand structures. Korzhnev *et al.*[147] performed new multi-quantum relaxation dispersion NMR spectroscopy probing millisecond time-scale dynamics in proteins. The approach allows robust measures of exchange parameters. Askin and Yilmaz[148] determined correlation time τ_c for T_1 spin-lattice and T_2 spin-spin relaxation times in agar solutions. They observed fast chemical exchange of water protons between free water and water bound to agar. Callaghan and Furo[149] performed diffusion exchange spectroscopy to study local order and dynamics. Theodorou *et al.*[150] studied the proton exchange rates in aminio acid derivates.

2.6 Radiation Damping. – Diffusion measurements by NMR have a wide range of uses; in particular DOSY (Diffusion Ordered Spectroscopy) is a powerful method for the analysis of mixtures. As with many other NMR techniques,

however, the combination of concentrated samples, high Q probe hardware and high magnetic field can lead to problems with the phenomenon of radiation damping.[151] Diffusion measurements on concentrated samples are important not only in the application of DOSY to the analysis of intact concentrated mixtures and in studies of aggregation, binding and so on, but also in the calibration of pulsed field gradient systems. Although approximate methods using known phantom or r.f. coil dimensions are available, the principal accurate method for calibrating field gradient strength is to perform a pulsed field gradient spin echo experiment on a material for which the diffusion coefficient has been accurately determined by other means. Such materials are generally pure liquids, and are therefore susceptible to radiation damping. The best available diffusion data are those for H_2O, which of course also has one of the highest proton concentrations (110.7 M at 25°C) of any liquid.

Radiation damping arises where the nuclear magnetism is sufficiently strong that the current it induces in the probe coil is large enough to perturb its own motion. Its classic manifestation is in the excess line broadening seen for strong singlet signals such as the proton resonance of water. The broadening arises because in a single pulse Fourier transform NMR experiment the radiofrequency current induced in the probe coil generates a rotating magnetic field which rotates the nuclear magnetization back towards equilibrium at a rate fast compared to spin-spin and spin-lattice relaxation. In more complex experiments a variety of effects may be seen, including severe lineshape anomalies and signal phase errors.

A recent paper by Price and Wälchli[152] has described a direct, hardware-based approach to reducing problems caused by radiation damping, in which the probe tuned circuit is rapidly switched between a high Q and a low Q. This allows experiments to retain high Q for producing powerful radiofrequency pulses and for sensitive signal detection, while effectively eliminating radiation damping at source during the magnetization evolution parts of the pulse sequence. Unfortunately this is not a solution that is available to the great majority of users of NMR diffusion measurements, and also it does not address the problem of radiation damping during signal detection, which can cause both amplitude-dependent broadening of the strong signal and phase anomalies of nearby weaker signals. Connell *et al.*[153] described an alternative approach, using a very slight modification of conventional methods to allow the detected magnetization to be scaled down sufficiently to avoid radiation damping. It follows two principles laid down by Price and coworkers in an earlier paper on background gradient and radiation damping effects[154] : keeping transverse magnetization dephased wherever possible, and reducing the initial magnetization. Louis-Joseph *et al.*[155] found new experimental evidence for nonlinear dynamics of a magnetization subject to r.f. feedback field. The role of B_0 inhomgeneity is discussed.

2.7 Quadrupolar Interactions. – Quadrupolar coupling constants are sensitive probes of hydrogen bonding. Their accurate knowledge is a major prerequisite when trying to extract dynamical information from relaxation data of quadrupo-

lar nuclei. If the relaxing nucleus is covalently bound, the NQCC is determined by the electric field gradient (e.f.g.) arising from the intramolecular charge distribution at the nuclear site. Liquid phase values for NQCC can be obtained only in an indirect way. Details are very difficult to interpret without the help of theoretical calculations. As noted in previous reports[1] there are now theoretical methods to predict the e.f.g in the liquid state. The first method is based on Molecular Dynamics Simulations (MD). From the bulk configurations, molecular clusters are chosen and used in supermolecular ab initio calculations. This technique has been successfully applied by Huber *et al.* [156,157] to determine ^{2}H and ^{17}O NQCC in liquid water. In a second method, molecular clusters were calculated by pure ab initio methods. A Quantum Cluster Equilibrium (QCE) Model,[158,159] which is fully based on quantum thermodynamics treatment, generates temperature- and pressure-dependent molecular cluster populations. Changing cluster distributions lead to temperature-dependent H-bond-sensitive properties such as NQCC, chemical shifts and vibrational frequencies, which are calculated for each of the clusters.

Hardy et al[160] performed model calculations to investigate the DQCC in liquid water. Techniques not amenable to experiment, such as switching on and off the intermolecular or intramolecular electric field gradients and simulating rigid liquid water, give insight into microscopic effects leading to relaxation. In experimental studies it is usually assumed that the deuteron quadrupolar relaxation is governed largely by the reorientational motion of an average electric field gradient, and the error in this assumption is readily extracted from the model calculations. The results show that the evaluation procedure used in most experimental determinations of DQCC lead to values which are 15 kHz to small. The deviation stems from the librations where coupling with the vibrational motion occurs and the e.f.g. across the hydrogen bond has a strong influence.

Müller *et al.*[161] presented an novel approach that allows NMR relaxation rates to be determined for a complex mixture, and it is applied to a dimethyl sulfoxide/water solution. It involves use of a predetermined, quantum mechanical, multidimensional property surface in a simulation. The results are used in conjunction with simulated rotational correlation time to calculated the DQCC, in an analogous approach to the one used by experimentalists, and to examine the surprising experimental findings for the composition dependence of the DQCC in the dimethyl sulfoxide/water mixture. In this respect, Müller and Huber[162] showed that the contributions of solvent molecules to NMR properties of the solute molecule in liquids is approximately pair-additive. Because water is an extreme case, the authors assume that for other systems an even better additivity might be found.

Gill *et al.*[163] measured copper quadrupole coupling constants in binary mixtures of acetonitrile with some other nitriles. Victor *et al.*[164] investigated magnetic relaxation dispersion of lithium ion in solution of DNA. The ^{7}Li ion relaxes through the nuclear electric quadrupole coupling and the dipole-dipole coupling. Bakhmutov[165] determined the orientations of the principle components of the e.f.g. and internal motions in dyhydrogen ligands from ^{2}H T_1 NMR relaxation data in solution. Umecky *et al.*[166] measured precisely ^{17}O longitudinal

relaxation times T_1 of CO_2 under gaseous, liquid and supercritical conditions. The reorientational correlation time of CO_2 was obtained by using a known value of the OQCC. The rotational dynamics of CO_2 was discussed over a wide range of density and temperature. Troganis *et al.*[167] measured ^{14}N NMR relaxation times of several protein amino acids in aqueous solution. The authors concluded that the NQCCs are influenced by the protonated state of the carboxyl group.

2.8 Intermolecular Dipolar Interaction in Diamagnetic and Paramagnetic Solution. – NMR resonance frequencies and relaxation properties of nuclear spins residing in paramagnetic transition metal complexes in solution are strongly influenced by the presence of unpaired electron spin.[168] In particular, the nuclear spin relaxation rates in paramagnetic solutions are very much higher than in the diamagnetic counterparts. In the context of nuclear spin-lattice relaxation, one commonly speaks about the paramagnetic relaxation enhancement (PRE). Strong PRE effects can also be seen for nuclear spins belonging to the solvent or to ligands that spend only a small portion of the time in the coordination sphere of the paramagnetic metal ion. The PRE effect, especially when studied as a function of the magnetic field (the nuclear magnetic relaxation dispersion (NMRD) experiment) can be an important source of information on structural as well as dynamic properties of a system, provided that an adequate theoretical model is available. The NMRD profiles are an important and commonly used tool in the characterisation of paramagnetic complexes, such as Gd(III) chelates, considered for possible applications as contrast agents for magnetic resonance imaging, MRI.[169, 170]

The theory of PRE has developed along two lines. First, the 'classical' theory of the PRE for a nuclear spin in a paramagnetic molecule, T_{1I}^{-1}, is known as the Solomon-Bloembergen-Morgan (SBM) approach.[168, 171-174] The SBM theory was developed in the high-field limit and for highly symmetric complexes. It assumes that the PRE arises through simple stochastic modulation of the hyperfine interaction between the nuclear and electron spins by molecular tumbling, electron spin relaxation and, possibly, chemical exchange. The hyperfine interaction consists of a dipolar part and a scalar term. The dipolar part, usually considered dominant for proton relaxation, is assumed to have a constant strength corresponding to a certain nuclear spin-electron spin distance. The electron spin relaxation is assumed to originate from the collisional modulation of the zero-field splitting (ZFS),[174] with zero average, and is described by a second-order perturbation Redfield-type theory.[175] Luz and Meiboom[176] formulated a simple expression for the measured enhancement of the nuclear spin-lattice relaxation rate, T_{1P}^{-1}, in a situation when the nuclear spin exchanges, with lifetime τ_M, between an in-complex site with the spin-lattice relaxation rate T_{1I}^{-1} and the bulk.

This contribution to the PRE is called inner-sphere relaxation. The ligand or solvent molecules can also experience PRE without ever entering the inner coordination sphere of the paramagnetic species. This second mechanism, referred to as outer-sphere (OS) relaxation, is usually less important and more

difficult to describe, as it allows for stochastic variation of the nuclear spin-electron spin distance. The outer-sphere contribution to the PRE, $T_{1,os}^{-1}$, can be added as a second term. An important theoretical model for the outer-sphere relaxation was given by Hwang and Freed[177] and was modified by Freed.[178] Both the SBM approach and the Hwang-Freed formulation are based on a very simple description of the electron spin relaxation. An improved description of electron relaxation, but still valid only in the high-field limit and in the perturbation regime (the Redfield limit), was proposed by Rubinstein *et al.*[179] Kruk and Kowalewski [180] developed a new theoretical model for nuclear spin relaxation in paramagnetic systems in solution. Fast rotational motion is included in the model, both as a source of modulation of the static zero-field splitting, which provides a mechanism for electron spin relaxation, and as an origin of the stochastic variation of the electron spin-nuclear spin dipole-dipole interaction leading to nuclear spin relaxation. At the limit of low magnetic field, the model is essentially identical to the earlier formulations from our laboratory, but new closed-form expressions are given for the inner- and outer-sphere relaxation at the high-field limit. Numerical comparisons with a general theory are reported for the inner-sphere case. In addition, some nuclear magnetic relaxation dispersion (NMRD) profiles from the literature are considered for systems where experiments have been done with both low-molecular weight paramagnetic complexes and their adducts with proteins. Previously developed theories are used to interpret data for the slowly rotating protein adducts, and good fits of the fast-rotating counterparts are obtained by further adjustment of one or two additional parameters.

Miller *et al.*[181] stimulated NMR-PRE produced by the electron spin $S = 3/2$ complex Cr(III)(acac)3 (acac = acetylacetonato) by spin dynamic (SD) simulation methods in order to test current theory of NMR-PRE. This system provides a particularly demanding test of theory, since the Zeeman and zero field splitting contributions to the electron spin Hamiltonian are of comparable magnitude in the range of magnetic field variation of the data, and Brownian reorientation of both the z.f.s. tensor and the interspin vector play important roles in the relaxation mechanism. For Cr(III)(acac)3, all of the sensitive parameters of theory were known from independent experiments, so that a calculation was possible without variation of parameters. The R_1 field dispersion profile (f.d.p.) exhibits a single pronounced dispersive feature between 0.23 and 2.1 T. SD simulations showed that this feature results physically from the change in spatial quantization of the electron spin motion that occurs in the intermediate regime of field strengths where the Zeeman and zfs energies are comparable. Thus, the observed R_1 dispersion for Cr(III)(acac)3 has a qualitatively different physical origin than the dispersions of Solomon-Bloembergen-Morgan theory, where R_1 dispersions result from Zeeman breaking of level degeneracies. The shape of the experimental fdp suggests that the point-dipole approximation is invalid for Cr(III)(acac)3 due to delocalization of electron spin density onto the p-system of the acac ligand. After accounting for the altered geometry, good agreement with experiment was obtained.

Kateb and Piccioli[182] proposed a new pulse sequence to measure cross correla-

tion rates between ^{1}H Curie spin relaxation and ^{1}H-^{15}N or ^{1}H-^{13}C dipole-dipole coupling in paramagnetic systems. The new sequence has been conceived to obtain quantitative measurements of cross correlation rates in the close proximity to the paramagnetic center, preventing the loss of information due to fast transverse relaxation. The approach was tested on the dicalcium protein calbindin D_{9k} in which Ca^{2+} has been substituted at site II with Ce^{3+}. At variance with previously reported experiments, all peaks observed in HSQC experiments tailored to paramagnetic signals give quantitative estimates the dipole-dipole coupling. This is crucial to refine the immediate proximity of the metal ion.

Iwahara *et al.*[183] presented an ensemble approach for NMR structure refinement against ^{1}H paramagnetic relaxation enhancement data arising from a flexible paramagnetic group attached to a macromolecule. Tamburine *et al.*[184] characterized a macrocyclic Schiff base Gd^{3+} complex as a relaxation agent for a faster acquisition of ^{2}H NMR spectra of ethanol. Fries *et al.*[185] studied the rotational motion and electronic relaxation of the Gd^{3+} aqua complex in water. Bonnet and Fries [186] investigated the competition of Gd^{3+} and Lu^{3+} towards DTPA in water.

2.9 Slow Motions in Glasses. – The concept of heterogeneity in the dynamics around the glass transition was first introduced in 1969 by Addams and Gibbs,[187] who suggested the existence of cooperative, cluster-like motion. The idea has been strongly supported by recent theoretical and molecular dynamics developments. The theoretical approach of Colby[188] uses the idea of free volume in a simple mean-field model to point out the existence of this kind of heterogeneous motion. In the glassy state there is no free volume of a sufficient size and the particles are trapped in the 'cage' of surrounding particles. On microscopic time scales the atoms vibrate in the cages around quasi-equilibrium positions. With increasing temperature the free volume grows and opens up the way for rapid cooperative rearrangement of groups of particles in the form of large amplitude motion. However, only a fraction of atoms in the sample can move at a given time, the rest has to wait for free volume to become available. Hence the heterogeneity in the dynamics: a small fraction of particles is mobile on a short time scale, while the rest follows conventional slow viscous flow. This picture is in agreement with molecular dynamics simulation studies[189] revealing the existence of correlated atomic motion in form of loops or chains ('string'-like motion) observed by identifying those atoms that moved to large distances compared to the average within a given time. In contrast to the Johari-Goldstein hypothesis,[190] this proposed mechanism of heterogeneity in the dynamics is rather a spontaneous one, it does not require the existence of structural heterogeneity or 'islands of mobility'. Heterogeneous as well as homogeneous[191,192] scenarios have been intensively explored in the last decade on a broad time scale for the different relaxation processes observed around the glass transition.

The current picture of relaxation behavior of supercooled liquids is complex. Mode coupling theory[191] introduced slow α- and fast β-processes, whose existence has been confirmed experimentally in almost all known glass forming liquids. The fast β-process takes place on the picosecond time scale at all

temperatures where it is observable, while the α-relaxation moves from macroscopic times to picoseconds with increasing temperature. In addition in some systems one finds the slow Johari-Goldstein β-process on a strongly temperature dependent time scale, which is shorter but close to that of the α-relaxation.

Previous experimental studies related to dynamic heterogeneity focused on the α- or the slow (Johari-Goldsdtein) β-processes. The question whether homogeneous and heterogeneous scenarios can be distinguished by the momentum transfer dependence of the α-relaxation time has been investigated by incoherent neutron scattering. The authors in[192] conclude that the stretching of the α-relaxation is related to homogenous sublinear diffusion. In NMR studies[193,194] the heterogeneity of α-relaxation is probed by selecting a dynamically distinguishable ensemble and monitoring its return to the equilibrium. The conclusion in these works is that above the glass transition temperature one observes heterogeneities with life times of order of α-relaxation time. The slow β-process was also investigated by NMR[194,195] and dielectric spectroscopy experiments. Although both studies found that all molecules contribute to the process in similar fashion, authors in[194] believe that the non-exponential ^{2}H spin-lattice relaxation observed at low temperatures ($T<1.1T_g$) and at times $t<\tau_\alpha$ is due to the heterogeneity of the β-processes. However, no evidence of distinguishable 'islands of mobility' has been obtained. Russian *et al.*[196] tried to answer the questions about the nature and homogeneity/heterogeneity of the fast β-process by probing glassy systems on the picosecond time scale.

Giovambattista *et al.*[197] have studied heterogeneities in supercooled water. The molecular dynamics simulations were compared to multidimensional NMR data. Rault *et al.*[198] investigated the melting of ice in porous glasses. The authors tried to answer the question why water and solvents confined in small pores do not crystallize. Wolak *et al.*[199] reported direct experimental observation of local conformational dynamics in a polymer chain at the calorimetric glass transition temperature T_g. Variable-temperature two-dimensional (2D) solid-state exchange NMR, at natural abundance, reveals segmental dynamics in pure polyisobutylene (PIB) occurring on a time scale of several seconds over the T_g range observed by DSC (203-208 K). This is the first direct observation of molecular-level conformer interchange at the caloric glass transition temperature.

Wind *et al.*[200] introduced conformational memory is as a new aspect of structural relaxationof polymers. In poly(*n*-alkylmethacrylates) extended backbone chain conformations are identified by advanced NMR techniques as the molecular units involved instructural relaxation. They retain conformational memory over many steps of restricted axial chain motion. Randomization of conformation and isotropization of backbone orientation occur on the same time scale, yet much slower than the slowest relaxation process identified so far. Behavior typical of fragile glass formers is found for this new process of chain relaxation. Dyre and Olsen[201] rationalized contrasts between beta relaxation in equilibrium viscous liquids and glasses in terms of a double-well potential model with structure-dependent asymmetry, assuming structure is described by a single order parameter.The model is tested for tripropylene glycol where it accounts for the hysteresis of the dielectric beta loss peak frequency and magnitude

during cooling and reheating through the glass transition.

Li *et al.*[202] used nuclear magnetic resonance to characterize local atomic motions in the glassy and supercooled liquid states of the bulk metallic glass system $Pd_{43}Ni_{10}Cu_{27}P_{20}$. The temperature dependence of the Knight shift reveals that certain local atomic motion decreases rapidly below a crossover temperature T_c down to the glass transition temperature T_g. Above T_c as well as below T_g the mean-squared amplitude of local motions depends linearly on the temperature. The observed gradual transition below T_c is inconsistent with heterogeneity effects. It reveals that qualitative changes of microscopic properties in the supercooled liquid take place at temperatures significantly above T_g.

Rao and Kumar[203] studied the ion transport in multialkali phosphate glasses. A new mechanism has been proposed to understand ion transport in oxide glasses. Tambelli *et al.*[204] investigated the glass structure and fluorine emotion dynamics in lead-cadmium fluorogermanate glasses by ^{19}F NMR techniques. Ardelean *et al.*[205] studied the vapor contribution to diffusion in silica glasses with the aid of field-gradient NMR diffosometry. Chae *et al.*[206] analysed the effect of methyl substitution of the ethylene unit on the physical properties of poly(butylene succinate). Urakawa *et al.*[207] measured self-diffusion of low molecular weight polystyrene over a wide temperature range. The results are interpreted in terms of the length scale of the spatially heterogeneous dynamics which develop near T_g. Cherry *et al.*[208] determined the structure and properties of germanium glasses. Alba-Simionesco *et al.*[209] investigated the consequences on thermodynamic, static and dynamical properties of benzene and toluene if confined in mesoscopic cylindrical pores. Berriot *et al.*[210] used NMR to determine the gradient of glass transition temperature in filled elastomers. Sekhon *et al.*[211] studied the ionic diffuse motion in some fluoride doped polymer electrolytes. Weaver and Quitevis[212] measured the relaxation of the methylen blue monomer-dimer equilibrium in supercooled glycerol near the glass transition. The local conformation of glassy polystyrene is investigated by Nakaoki and Kobayashi.[213] Panatno *et al.*[214] used heteronuclear correlation NMR experiments to study the long range order in barium aluminoborate glasses. Tien *et al.*[215] studied size effects for molten gallium particles.

2.10 Models for Molecular Dynamics. – The liquid state of matter is of great importance in nature and technology. Almost all reactions in biological and chemical systems proceed in solution or liquid like environments. Therefore, it is of interest to develop further the existing models and theories for describing the molecular structure and dynamics of liquids. These models and theories should mediate a better understanding, for example, of the arrangement of the molecules relative to each other or of the dynamic behaviour of the molecules and thus of the route of chemical reactions in liquid systems. The model that is usually applied for the description of molecular reorientational processes in liquids is the rotational diffusion model. A particularly important experimental method to obtain information on the reorientational dynamics of molecules is the measurement of nuclear spin-lattice relaxation rates. Most of the experimental findings on the reorientation of molecules and molecular segments by means of nuclear

relaxation rates were obtained in the extreme narrowing region where the product of the resonance frequency and the reorientational correlation time is much less than unity. Outside the extreme narrowing region the relaxation rates become frequency-dependent. Bloembergen, Purcell and Pound [141] employed in their study of relaxation effects on nuclear magnetic resonance phenomena the model of rotational diffusion by Debye.[216] Another way to describe the deviations from the BPP spectral density is the so-called model-free approach by Lipari and Szabo,[217] which corresponds to a discrete distribution of correlation times and is a generalization of the two-step model by Wennerström *et al.*[218] It was originally developed for taking internal motions in macromolecules into account without giving an explicit model when calculating the relaxation data.[219] The model free approach allows straightforward extraction of generalized order parameters and correlation times for internal and overall bond vector reorientational fluctuations from NMR spin relaxation measurements for macromolecules in solution. The drawback of this approach is the use of a decoupling approximation that neglects correlations between internal and overall molecular motions. These correlations are significant when fluctuation amplitudes are less than the size of the 'cage' that restricts the bond vector. In this regime, motion of the bond vector is only indirectly affected by molecule fluctuations through the orienting potential for the local director axis. By separating the regimes of large and small amplitude molecular fluctuations, Vugmeyster et al[220] derived an expression for the spectral density function that does not invoke the decoupling approximation, but that relies on the same macroscopic level of description as the original MF approach. The parameters of the spectral density function provide insight into the effects on the MF parameters that result from violation of the decoupling approximation.

Lang *et al.*[221] studied molecular reorientation and local mobility of two isomers of 25,26,27,28-tetrapropoxy-2,8,14,20-tetrathiacalix[4]arene, *cone* and 1,3-*alternate*, by means of NMR relaxation. The chemical shift anisotropy of ^{13}C nuclei was determined in the solid state. Nuclear relaxation due to dipole-dipole interaction and chemical shift anisotropy was analysed in the framework of the Lipari-Szabo approach. The aromatic core of both isomers was found rigid on the subnanosecond time scale. The amplitude of the local motion of the lower rim propoxy substituents increases towards the methyl ends. The methylene groups of the propoxy residues of the *cone* isomer possess more motional freedom than in the 1,3-*alternate*, where they are sterically hindered by the adjacent aromatic rings. Global reorientation of the *cone* is slower than the motion of the 1,3-*alternate*, which rotates partly anisotropically. Denkova *et al.*[222] applied the model-free approach to low molecular weigth systems with internal rotation. Carnet *et al.*[223] calculated cross-correlation spectral density functions within the model-free approach. Beside the model-free approach, Friedrich *et al.*[224] fit longitudinal relaxation rates of glycerol to a Cole-Davidson model extended by the Vogel-Fulcher-Tammann temperature dependence.

In the recent years there has been significant interest in the characterization of the overall hydrodynamic properties of biomacromolecules. Because the overall tumbling provides a dominant contribution to spin-relaxation rates, its accurate

characterization is essential for the accuracy of the derived picture of protein dynamics.[225-228] In particular, a failure to take the rotational anisotropy into account could result in spurious conformational exchange motions. Other emerging applications include structure characterization in multidomain systems[229-232] and analysis of protein-ligand interactions[229,233] and protein association.[234]

The information on the overall rotational diffusion of a molecule is encoded in the rates of nuclear spin relaxation that can be measured in various groups in a protein. Several experimental and analytical methods,[233,235] have been developed to determine the overall rotational diffusion tensor of a protein from nuclear spin-relaxation data.[229, 235-244] Models for computer prediction of the diffusion tensor based on atomic structure of a molecule are also available.[245,246] Several computational approaches have been developed, which employed a combination of simplex and grid searches,[229,233,242] simulated annealing,[244] or Bayesian statistics.[247] In the simplex-based methods,[229,243] the optimization was separated into a simplex search in a 3D space of the principal values of the tensor and a grid search in the Euler angle space. This was done to circumvent the problem of implementing periodic boundary conditions for the Euler angles in the simplex algorithm. The angular-grid search turned out to be time consuming, particularly in the case of a fully anisotropic tensor. Walker *et al.*[248] presented a software program ROTDIF that uses a different computational strategy to determine the full set of diffusion tensor parameters and Euler angles. A novel feature of the proposed method is that the optimization search is performed in a full six-dimensional space without separating it into the individual subspaces for the principal values and the angles. This is achieved by using a constrained Levenberg-Marquardt algorithm, which leads to a significant, up to 50-fold gain in the computational efficiency of the analysis without any loss in the accuracy. The authors demonstrated the accuracy and efficiency of the method by applying it to both synthetic data sets and experimental data of a real protein. They also analysed the expected accuracy and precision of the diffusion tensor derivation depending on the experimental noise in relaxation data.

Halle and Davidovic[249] developed a dynamic model that explicitly links protein hydrodynamics to hydration dynamics. With the aid of this model structure-based predictions of global biomolecular dynamics become possible. The validity of the model was demonstrated for a set of proteins for which accurate experimental rotational diffusion coefficients are available. Boisbouvier *et al.*[250] derived the rotational diffusion tensor of nucleic acid from ^{13}C relaxation times. The results were in excellent agreement with values obtained from hydrodynamic modelling.

Derbyshire *et al.*[251] used a series of mathematical functions has been used to fit the proton free-induction decays of concentrated carbohydrate-water samples. For the solid protons, these functions included a sinc function, as well as the Fourier transforms of single and multiple Pake functions multiplied by a Gaussian broadening. The NMR signal from the mobile protons is described by an exponential function. It is found that in most cases the sinc function gives a satisfactory result and provides valuable information about the second moment

M_2 and the ratio of solid to mobile protons (f_s/f_m).

3 Selected Applications of Nuclear Spin Relaxation

3.1 Pure Liquids. – Iwahashi *et al.*[252] studied the dynamical dimer structure and liquid structure of fatty acids in their binary liquid mixture. Celebre *et al.*[253] investigated the planarity of styrene in the liquid phase. The NMR data are consistent with the ring fragment, averaged over the ring-ene rotation, planar, while the ene fragment is not.

Vilfan and Vuk[254] discussed the nuclear spin relaxation resulting from molecular translational diffusion of a liquid crystal in the isotropic phase confined to spherical microcavities. Their analysis can be also applied to other fluids in porous media. Nilsson *et al.*[255] used high-resolution NMR and high-resolution diffusion-ordered spectroscopy (DOSY) for the characterization of selected Port wine samples of different ages with the aim of identifying changes in composition.

3.2 Non-Electrolyte Solutions. – Fojud *et al.*[256] determined the molecular dynamics of n-dodecylammonium chloride in aqueous solutions by ^{2}H and ^{1}H NMR dispersion of spin-lattice relaxation in the 2 kHz to 90 MHz frequency range. Uchino *et al.*[257] studied the segmental motion of poly(L-histidine) in aqueous solution. The ^{13}C relaxation times were measured at six resonance frequencies ranging from 15 to 100 MHz. Müller *et al.*[161] investigated NMR relaxation in complex mixtures such as dimethyl sulfoxide/water solution. The authors presented an approach for calculating DQCC which analogous to the one used by experimentalists. Gao *et al.*[258] measured ^{1}H and ^{13}C spin-spin relaxation times of nylon 11 solution. The relaxation processes shows a bi-exponential behaviour which suggests suggest the existence of two states in the polymer. Crassous and Hediger[259] studied the dynamics of CHFClBr and CDFClBr inside cryptophane.

3.3 Electrolyte Solutions. – Melnichenko *et al.*[260] studied the temperature dependence of NMR relaxation rates in some aqueous electrolytes of semimolar concentration. The activation energies of molecular motions in the near and far hydration regions and in the unperturbed structure region can be determined separately. Abbrent *et al.*[261] measured diffusion coefficients and relaxation times of Lithiumions in an electrolyte solvent. The same NMR techniques were used by Jeffrey *et al.*[262] to investigate the dynamics of the hydrogen and phosphate ions in proton conducting gel/D_3PO_4 electrolytes. The results show that the Grotthus mechanism involving the hopping of the proton from one molecular site to another are most responsible for the motion of the protons in these electrolytes.

Hayamizu and Price[263] presented a new type of sample tube for reducing convection effects in PGSE-NMR measurements of self-diffusion coefficients of liquid samples. The performance of this tube was demonstrated by conducting measurements on an electrochemically important system.

Hayamizu and Akiba[264] measured self-diffusion coefficients of lithium ion, anion and solvent in the electrolytes for lithium batteries. The self-association of some anions is discussed. Sekhon *et al.*[211] investigated the diffusive motion of cations and anions in polyethylene oxide based polymer electrolytes. Translational motion was found above T_g.

3.4 Molten Salts. – Structural and dynamic aspects of molten salts were studied by several authors. Palmer *et al.*[265] measured self-diffusion coefficients of molten salts as a function of pressure. The same authors[266] studied room-temperature molten salts using a recently published high-pressure probe. Dai *et al.*[267] characterized novel room-temperature inorganic ionic liquids by NMR. Schellkes *et al.*[268] applied 93Nb NMR to study the structure and dynamics of liquid $NbCl_5$-alkali chloride solutions. Helmer *et al.*[269] found evidence for spin diffusion in a H,H-NOESY study of imidazolium tetrafluoroborate ionic liquids. Fischer *et al.*[270] used inorganic molten salts as efficient solvents for cellulose. ^{7}Li and ^{13}C NMR were used to describe the solvent-cellulose interactions. Antony *et al.*[271] studied the molecular reorientational dynamics of neat ionic liquids by measurement of ^{13}C relaxation data. The same authors[272] studied Bloembergen-Purcell-Pound ^{13}C NMR relaxation of the ionic liquid 1-butyl-3-methyl-imidazolium hexafluorophosphate. Yonker *et al.*[273] performed high-pressure NMR to investigate the reaction chemistry in a simple salt hydrate. Jodry and Mikami[274] analysed the three-dimensional network of hydrogen bonding in new chiral imidazolium ionic liquids. Ohlin *et al.*[275] determined the carbon monoxide solubility in ionic liquids. Rangits *et al.*[276] investigated platinium-diphosphane complexes in ionic liquids.

4 Nuclear Spin Relaxation in Gases

The sensitivity of conventional nuclear magnetic resonance (NMR) is rather poor compared with other spectroscopic techniques like EPR or optical spectroscopy. This is a result of the small population difference between the nuclear Zeeman energy levels even in the highest magnetic fields currently available in the laboratory. At room temperature, and in a magnetic field of 9.4 T, the polarisation of the protons is less than 4×10^5 . In order to overcome this inherent limitation, methods to improve the signal to noise ratio (SNR) in magnetic resonance experiments have been the subject of active research since the discovery of NMR.

In the past few years, optical methods able to increase the NMR sensitivity of noble gas nuclei by several orders of magnitude have proven particularly successful, and have found applications in biology and medicine. Large nuclear spin polarisations for ^{129}Xe and ^{3}He can be produced through the transfer of angular momentum from circularly polarised laser light to the nuclear spins of these noble gases. Since the nuclear spin polarisation created through this method is far from the equilibrium Boltzmann polarisation, these gases are sometimes referred to as 'hyperpolarized' gases. Although the application of optical

methods for the production of hyperpolarized gases for NMR applications is a relatively recent accomplishment, the basic idea dates back to the 1950s, when Kastler[277] demonstrated that circularly polarised light could be used to produce non-equilibrium populations of electronic spins in gaseous metals, a process called 'optical pumping' that earned him the Nobel Prize. Currently, two optical methods are widely used for production of hyperpolarized noble gases. Spin-exchange with optically pumped alkali metals, a technique pioneered by Happer and co-workers,[278,279] can be applied to produce polarisations up to 70%[280] for both ^{129}Xe and ^{3}He. Hyperpolarized ^{3}He can also be produced through metastability exchange, a method that does not require the presence of alkali metals,[281,282] and that results in higher levels of polarisation. Non-optical methods, like 'brute force' polarisation at temperatures T<10 mK and magnetic fields B>10 T, have been proposed recently as an alternative technique for production of large volumes of hyperpolarized ^{129}Xe, ^{3}He, and D_2,[283] and are currently being developed.

In recent years, the large increase in sensitivity of NMR detection brought about by these methods has led to a number of promising applications of hyperpolarized gases in a wide range of different fields, from physics to biology, chemistry and medicine. Hyperpolarized gases have been used in NMR studies of surfaces, porous materials, water clathrates, gas-flow, quantum computing, and low-field NMR, to name just a few examples. The application of magnetic resonance imaging (MRI) with hyperpolarized noble gases to assess the structure and function of the human lung,[284,285] an organ otherwise difficult to study with MR methods, is particularly promising. The potential diagnostic value of this technique has imparted tremendous momentum to hyperpolarized gas research. While ^{3}He seems particularly favourable for this specific application, due to its larger gyromagnetic ratio and smaller relaxivity, the complex interactions of xenon with biological materials and the sensitivity of the ^{129}Xe NMR parameters to its local environment make hyperpolarized ^{129}Xe a very interesting NMR probe for a range of biological applications.

Recently, several excellent reviews have appeared in the literature, discussing the use of hyperpolarized ^{129}Xe from different perspectives.[285-295] Cherubini and Bifone[5] surveyed experiments involving hyperpolarized ^{129}Xe and its biological applications, both in vitro and in vivo. Particular emphasis was put on the physico-chemical properties of xenon that are responsible for the interesting range of interactions with proteins, lipids and other biological materials.

The extension of NMR PGSE experiments to gas systems allows flow and diffusion information to be obtained over a wider range of length and time scales than with liquids, and also for a new range of physical environments and systems. Interactions between stochastic and deterministic motion are fundamental to the theoretical description of transport in porous media, and the time scale dependences are central to an understanding of the resultant dispersive motion. Codd and Altobelli[296] presented a study of the probability density for molecular displacements of gas flowing through bead packs. Cross *et al.*[297] investigated the signal-to-noise ratio of NMR signals from laser-polarized ^{129}Xe gas at different field strengths.

Han *et al.*[298] visualized the melting and dissolution processes of xenon ice into different solvents using the methods of NMR spectroscopy, imaging, and time resolved spectroscopic imaging by means of hyperpolarized ^{129}Xe. The NMR spectra of homogeneous samples of pure ethanol containing thermally polarized xenon and the spectroscopic images of the melting process show that very high concentrations of hyperpolarized xenon can be stored or delivered in pure ethanol.

Ishikawa *et al.*[299] detected the free-induction signals of xenon atoms polarized by spin-exchange optical pumping. The temperature dependence of dissolution and spin-polarization transfer of xenon atoms in ethanol is measured by simultaneous detection of both xenon and ethanol protons.

Dubois *et al.*[300] measured longitudinal relaxation times of laser-polarized xenon in water solutions containing alpha-cyclodextrin and wheat. The contribution of CSA to relaxation is very limited. The energetic mechanisms inducing xenon binding is discussed. Heckman *et al.*[301] reported an enhancement of proton NMR signals by a factor of 10^6 by cross polarization with hyperpolarized liquid ^{129}Xe in an ultralow magnetic field of 1 μT. Nestle *et al.*[302] used NMR relaxometry as a possible analytical tool for the determination of oxygen contents in water. NMR relaxation in oxygen supersaturated water also might offer some interesting possibilities in medical and environmental science MRI applications. Jackowski and Wilczek[303] performed new measurements for acetonitrile in the gas phase for studying the magnitude of intermolecular effects.

5 Self-Diffusion in Liquids

5.1 Experimental and Theoretical Aspects. – Self-diffusion is one of the most fundamental motions of particles in liquids. NMR provides a convenient and noninvasive means of accurately measuring the self-diffusion coefficient of molecules in solution. Lin *et al.*[304] gave the theoretical expressions of diffusion rates of multi-quantum coherences.

Nuclear magnetic resonance logging technology has been widely used in the petroleum industry to measure porosity and permeability in subsurface formation. It typically uses a permanent magnet with a proton Larmor frequency around several hundred kHz to a few MHz and CPMG pulse sequences to measure T_2 distribution of the formation fluids.[305] Since the formation fluids, such as water, oil, and gas, have widely different diffusion coefficients and moderately different relaxation times, it is possible to differentiate these fluids using the diffusion effect in a magnetic field gradient with different echo spacings and/or different degrees of polarization recoveries with different wait times. There were several NMR logging methods proposed for hydrocarbon typing in the past.[306,307] These methods basically use either different echo spacings or different wait times to create differences in T_2 distribution for hydrocarbon typing. They were primarily methods within the 1D NMR framework. Recent advances have extended to 2D NMR inversions, some of which utilize two-window type modified CPMG sequences,[308-310] and another[310] simply uses regu-

lar CPMG sequences. However, 2D inversion require multiple echo trains (4-6 or more) with different echo spacings and wait times. This kind of data is not always available. Common NMR log data are still handled with 1D inversion scheme. Sun and Dunn[311] introduced two NMR inversion methods within the framework of 1D NMR to extract fluid saturations by varying echo spacing and wait time. The first method connects the T_2 distribution of each fluid with the overall apparent T_2 distribution using a shift matrix. Each fluid's saturation and T_2 distribution are extracted by minimizing the difference between the model T_2 distributions and measured apparent T_2 distributions. The second method relates a model T_2 distribution of each fluid with CPMG echo trains using a global evolution matrix that governs the evolution of magnetization under T_1, T_2 relaxation, and diffusion. These methods will be useful whenever data are not sufficient for 2D NMR inversion. They are also much faster than 2D for fluid typing. Topgaard *et al.*[312] presented a methodology for chemical shift resolved molecular self-diffusion measurements in time-independent static and radio-frequency field gradients. Diffusion encoding is provided by a stimulated echo sequence with additional z-storage that allows for a change of diffusion time without affecting the relaxation weighting. The signal is acquired stroboscopically between the pulses of a train of adiabatic double passages that induces a z-rotation counteracting the phase spread resulting from precession in the inhomogeneous static field, as demonstrated in recent approaches to the goal of high-resolution 'ex situ' NMR. Simulations of the pulse sequence show that the acquired signal results from the desired coherence pathway. Successful demonstrations of the experiment were performed on a mixture of water and isopropanol.

Carr-Purcell-Meiboom-Gill (CPMG) measurements are the primary nuclear magnetic resonance (NMR) technique used for evaluating formation properties and reservoir fluid properties in the well logging industry and laboratory sample analysis. The estimation of bulk volume irreducible (BVI), permeability, and fluid type relies on the accurate interpretation of the spin-spin relaxation time (T_2) distribution. The interpretation is complicated when spin's self-diffusion in an inhomogeneous field and restricted geometry becomes dominant. The combined effects of field gradient, diffusion, and a restricted geometry are not easily evaluated analytically. Zhang and Hirasaki[313] used a numerical method to evaluate the dependence of the free and restricted diffusion on the system parameters in the absence of surface relaxation, which usually can be neglected for the non-wetting fluids (*e.g.*, oil or gas). Ardelean and Kimmich[314] reviewed the conventional pulsed gradient Hahn or stimulated echo methods for diffusion measurements. A series of typical pulse sequences representing the diversity of NMR diffusometry methods is described and discussed with respect to advantages and disadvantages. Casieri *et al.*[315] measured self-diffusion by single-sided NMR. The novel method exploits the fixed gradient of an open magnet, as that used in single-sided NMR, and it does not use prior information on T_2. Momot and Kuchel[316] presented a new diffusion experiment which provides simultaneously suppression of an on-resonance solvent peak and compensation for convection. Possible applications include protein NMR and NMR of cellular

and colloidal systems.

In diffusometry, one often uses the short gradient pulse (SGP) limit approximation in the interpretation of data from systems with restricted diffusion. The SGP limit approximation means that the gradient pulse lengths so short that the spins do not diffuse during pulse duration, but this condition is rarely met. Malmborg *et al.*[317] studied highly concentrated emulsions to show how the length of the gradient pulse influences NMR diffusion experiments.

Manz[318] presented a fast method for quantitative imaging of T_2 and diffusion. The pulse sequence combines multi-PGSE NMR with multi-echo acquisition and compensates for flow effects.

Engelsberg *et al.*[319] studied the role of diffusion for intermolecular double-quantum coherences in two-dimensional spectra of binary liquids. There are some inadequacies in standard approximations if two molecular system having significantly different diffusivities are considered. Pennington[320] discussed the prospects of practical requirements of the 'diffusion enhancement of signal and resolution' (DESIRE) scheme as a method to enhance the sensitivity, spatial resolution, and contrast in magnetic resonance microscopy and localized MR spectroscopy. Klein *et al.*[321] performed self-diffusion measurements by a constant-relaxation method in strongly inhomogeneous magnetic fields. The method was applied to measure the diffusion anisotropy of free water in bovine Achilles tendon.

5.2 Selected Examples. – A study of the nature of the anthelmintic *p*-cresol:piperazine complex in chloroform solution has been conducted using different NMR techniques: self-diffusion coefficients using DOSY, NOE, NULL, and double-selective T_1 measurements to determine inter-molecular distances; and selective and non-selective T_1 measurements to determine correlation times. The experimental results in solution and CP-MAS were compared to literature X-ray diffraction data using molecular modelling. De Carvalho *et al.*[322] showed that the *p*-cresol:piperazine complex exists in solution in a very similar manner as it does in the solid state, with one *p*-cresol molecule hydrogen bonded through the hydroxyl hydrogen to each nitrogen atom of piperazine. The close correspondence between the X-ray diffraction data and the inter-proton distances obtained by NULL and double selective excitation techniques indicate that those methodologies can be used to determine inter-molecular distances in solution. Callaghan and Furo[323] demonstrated the use of new two-dimensional NMR experiments in the examination of local diffusional anisotropy under conditions of global anisotropy. Zuccaccia *et al.*[324] performed NOE and PGSE spectroscopic studies of solution structure and aggregation in metallocenium ion-pairs. Pregosin *et al.*[325] applied diffusion and NOE spectroscopy to problems related to coordination chemistry and homogeneous catalysis.

Gottwald *et al.*[326] applied PFG NMR to investigate flow processes. Valiullin *et al.*[327] measured self-diffusion of liquids in nanopores. Kennedy *et al.*[328] studied the association of dimethylsulfoxide using the same method. Gostan *et al.*[329] measured self-diffusion of solutes in polymer gels. Hollingsworth *et al.*[330] performed PFG NMR experiments to study gast emulsion droplet sizing. Hindmarsh[331]

measured self-diffusion in super-cooled liquid droplets. The resultant self-diffusion data were in good agreement with the Vogel-Fulcher-Tamann equation. Price *et al.*[332] discussed analytical applications of NMR diffusion measurements. Palmer *et al.*[265,266] measured diffusion in molten slats.

References

1. R. Ludwig, in 'Nuclear Magnetic Resonance', ed. G.A. Webb, Specialist Periodical Reports, The Royal Society of Chemistry, Cambridge, 2004, vol. 33, p.192-232.
2. C. Reinhardt, *Ann. Sci.*, 2004, **61**, 1.
3. G.R. Thuduppathy and R.B. Hill, *Method Enzymol.*, 2004, **384**, 243.
4. C. Fernandez and G. Wider, *Curr. Opin. Struc. Biol.*, 2003, **13**, 570.
5. A. Cherubini and A. Bifone, *Prog. Nucl. Mag. Res.*, 2003, **42**, 1.
6. A.D. Bain, *Prog. Nucl. Magn. Res.*, 2003, **43**, 63.
7. C. Wang, A.G. Palmer III, *Magn. Reson. Chem.*, 2003, **41**, 866.
8. F.A. Dunand, L. Helm, and A.E. Merbach, *Ad. Inorg. Chem.*, 2003, **54**, 1.
9. C.B. Post, *Curr. Opin. Struc. Biol.*, 2003, **13**, 581.
10. A.D. Bain and M. Khasawneh, *Concepts Magn. Reson.*, 2004, **22A**, 69.
11. P. Stilbs, *ACS Sym. Ser.*, 2003, **861**, 27.
12. P.G. Klein and M.E. Ries, *Prog. Nucl. Mag. Res.*, 2003, **42**, 31.
13. E. Pettersson, I. Furó, and P. Stilbs, *Concepts Magn. Reson.*, 2004, **22A**, 61.
14. Q. He, W. Richter, S. Vathyam, and W.S. Warren, *J. Chem. Phys.*, 1993, **98**, 6779.
15. W.S. Warren, W. Richter, A.H. Andreotti, and B.T. Farmer II, *Science*, 1993, **262**, 2005.
16. A. Ahn, W.S. Warren, and S. Lee, *J. Magn. Reson.*, 1997, **128**, 114.
17. A. Ahn, S. Lee and W.S. Warren, *Mol. Phys.*, 1998, **95**, 769.
18. P. Brokaert, A. Vlassenbroek, J. Jeener, G. Lippens, and J.-M. Wieruszeski, *J. Magn. Reson. A*, 1996, **120**, 97.
19. A.G. Sobol, G. Wider, H. Iwai, and K. Wüthrich, *J. Magn. Reson.*, 1998, **130**, 262.
20. P. Brokaert, J. Jeener, G. Lippens, and J.-M. Wieruszeski, *J. Magn. Reson.*, 2000, **145**, 259.
21. W.S. Warren, S.Y. Huang, S. Ahn, and Y.Y. Lin, *J. Chem. Phys.*, 2002, **116**, 2075.
22. Z. Chen, Z.W. Chen, and J.H. Zhong, *J. Chem. Phys.*, 2001, **115**, 10769.
23. R.T. Branca, S. Capuani, and B. Maraviglia,*Concepts Magn. Reson. Part A*, 2004, **21A**, 22.
24. W. Barros, Jr., P. Loureiro de Sousa, and M. Engelsberg, *J. Magn. Reson.*, 2003, **165**, 175.
25. K.E. Cano, M.J. Thrippleton, J. Keeler, and A.J. Shaka, *J. Magn. Reson.*, 2004, **167**, 291.
26. M.J. Thrippleton and J. Keeler, *Angew. Chem. Int. Ed.*, 2003, **42**, 3938.
27. N. Nestle , B. Walaszek, and M. Nolte, *J. Magn. Reson.*, 2004, **168**, 46.
28. R. Ishima, D.I. Freedberg, Y.-X. Wang, J.M. Louis, and D.A. Torchia, *Structure*, 1999, **7**, 1047.
29. A. Malmendal, J. Evenäs, S. Forsén, and M. Akke, *J. Mol. Biol.*, 1999, **293**, 883.
30. R.B. Hill, C. Bracken, W.F. DeGrado, and A.G. Palmer, *J. Am. Chem. Soc.*, 2000, **122**, 11610.
31. E.Z. Eisenmesser, D.A. Bosco, M. Akke, and D. Kern, *Science*, 2002, **295**, 1520.
32. G. Binsch, *J. Am. Chem. Soc.*, 1969, **91**, 1304.

33. C. Deverell, R.E. Morgan, and J.H. Strange, *Mol. Phys.*, 1970, **18**, 553.
34. H. Wennerström, *Mol. Phys.*, 1972, **24**, 69.
35. K. Kloiber and R. Konrat, *J. Biomol. NMR*, 2000, **18**, 33.
36. Z. Luz and S. Meiboom, *J. Chem. Phys.*, 1963, **39**, 366.
37. I.S. Podkorytov and N.R. Skrynnikov, *J. Magn. Reson.*, 2004, **169**, 164.
38. C.S. Johnson, Q. He, *Adv. Magn. Reson.*, 1989, **13**, 131.
39. C.S. Johnson. 1996. Electrophoretic NMR. In: D.M. Grant, R.K. Harris, editors. Encyclopedia of nuclear magnetic resonance. Chichester: Wiley p 1886-1895.
40. M. Holz, *Chem. Soc. Rev.*, 1994, **35**, 165.
41. F.M. Coveney, J.H. Strange, A.L. Smith, and *E.G.* Smith, *Colloid Surf.*, 1989, **36**, 193.
42. F.M. Coveney, J.H. Strange, and *E.G.* Smith, *Molec. Phys.*, 1992, **75**, 127.
43. A.T. Andrews, 1992, Electrophoresis. Oxford: Oxford University Press.
44. D.R. Baker, 1995, Capillary electrophoresis. New York: Wiley.
45. P. Jandik, G. Bonn, 1993, Capillary electrophoresis of small molecules and ions. New York: Wiley.
46. P.D. Grossman, J.C. Colburn, 1992, Capillary electrophoresis. San Diego: Academic.
47. P. Stilbs, *Prog. Nucl. Magn. Reson. Spectrosc.*, 1987, **19**, 1.
48. J. Kärger, H. Pfeifer, and W. Henk, *Adv. Magn. Reson.*, 1988, **12**, 1.
49. P.T. Callaghan, 1991, Principles of nuclear magnetic resonance microscopy. Oxford: Clarendon.
50. K.J. Packer, *Molec. Phys.*, 1969, **17**, 355.
51. Q.H. He, Y.M. Liu, H.H. Sun, and E.C. Li, *J. Magn. Reson.*, 1999, **141**, 355.
52. Q.H. He and Z.H. Wie, *J. Magn. Reson.*, 2001, **150**, 126.
53. N.M. Loening, M.J. Thrippleton, J. Keeler, and R.G. Griffin, *J. Magn. Reson.*, 2003, **164**, 321.
54. H. Chaumette, D. Grandclaude, and D. Canet, *J. Magn. Reson.*, 2003, **163**, 369.
55. A.G. Redfield, *Magn. Res. Chem.*, 2003, **41**, 753
56. J.H. Ardenkjaer-Larsen, B. Fridlund, A. Gram, G. Hansson, L. Hansson, M.H. Lerche, R. Servin, M. Thaning, and K. Golman, *Proc. Nat. Acad. Sci. USA*, 2003, **100**, 10158.
57. D.J. Harris, E.R. de Azevedo, and T.J. Bonagamba, *J. Magn. Reson.*, 2003, **62**, 67.
58. R. R. Ernst, G. Bodenhausen, and A. Wokaun, Principles of Nuclear Magnetic Resonance in One and Two Dimensions, Oxford University Press, Oxford, 1987.
59. G. A. Morris and R. Freeman, *J. Am. Chem. Soc.*, 1979, **101**, 760.
60. M. Schumacher and J. Lauterwein, *J. Magn. Reson.*, 1989, **83**, 97.
61. R. Kemp-Harper, D. J. Philp, and P. W. Kuchel, *J. Chem. Phys.*, 2001, **115**, 2908.
62. A. A. Maudsley, L. Muller, and R. R. Ernst, *J. Magn. Reson.*, 1977, **28**, 463.
63. L. Muller and R. R. Ernst, *Mol. Phys.*, 1979, **38**, 963.
64. M. Ernst, C. Griesinger, R. R. Ernst, and W. Bermel, *Mol. Phys.* 1991, **74**, 219.
65. S. J. Glaser and J. J. Quant, *Adv. Magn. Opt. Reson.*, 1996, **19**, 59.
66. F. Ferrage, T. R. Eykyn, and G. Bodenhausen, *J. Chem. Phys.*, 2000, **113**, 1081.
67. T. R. Eykyn, F. Ferrage, and G. Bodenhausen, *J. Chem. Phys.*, 2002, **116**, 10041.
68. M. H. Levitt, D. Suter, and R. R. Ernst, *J. Chem. Phys.*, 1986, **84**, 4243.
69. M. H. Levitt, *J. Chem. Phys.*, 1991, **94**, 30.
70. E. Chiarparin, P. Pelupessy, and G. Bodenhausen, *Mol. Phys.*, 1998, **95**, 759.
71. P. Pelupessy and E. Chiarparin, *Conc. Magn. Reson.*, 2000, **12**, 103.
72. M. Baldus, A.T. Pelkova, J. Zerzfeld, and R.G. Griffin, *Mol. Phys.*, 1998, **95**, 1197.
73. N. Tjandra, A. Szabo, and A. Bax, *J. Am. Chem. Soc.*, 1996, **118**, 6986.

74. D. Fushman, N. Tjandra, and D. Cowburn, *J. Am. Chem. Soc.*, 1998, **120**, 10947.
75. D. Yang, R. Konrat, and L.E. Kay, *J. Am. Chem. Soc.*, 1997, **119**, 11938.
76. B.Brutscher, *Concepts Magn. Reson.*, 2000, **12**, 207.
77. D. Fushmana and D. Cowburn, In *Methods in Enzymology*, vol. 339. James T, Schmitz U, Doetsch V (eds). Academic Press: 2001: 109.
78. H. Schwalbe, T. Carlomagno, M. Hennig, J. Junker, B. Reif, C. Richter, and C. Griesinger, *Methods Enzymol.*, 2001, **338**, 35.
79. D. Fushman and D. Cowburn, *J. Am. Chem. Soc.*, 1998, **120**, 7109.
80. K.E. Kover and G. Batta, *J. Magn. Reson.*, 2001, **150**, 137.
81. C.D. Kroenke, J.P. Loria, L.K. Lee, M. Rance, and A.G. Palmer I. *J. Am. Chem. Soc.*, 1998, **120**, 7905.
82. J. Boisbouvier, B. Brutscher, J.-P. Simorre, and D. Marion, *J. Biomol. NMR*, 1999, **14**, 241.
83. K.T. Dayie, A.S. Brodsky, and J.R. Williamson, *J. Mol. Biol.*, 2002, **317**, 263.
84. J.B. Hall and D. Fushman D, *J. Biolmol. NMR*, 2003, **27**, 261.
85. J.B. Hall and D. Fushman, *Magn. Reson. Chem.*, 2003, **41**, 837.
86. M. Ottiger, F. Delaglio, and A. Bax , *J. Magn. Reson.* 1998, **131**, 373.
87. J.B. Hall, K. Dayie, and D. Fushman, *J. Biomol. NMR* 2003, **26**, 181.
88. R. Freeman, A Handbook of Nuclear Magnetic Resonance. , Longman Scientific and Technical, New York (1988) pp.157-162 .
89. G.A. Morris and R. Freeman, *J. Am. Chem. Soc.*, 1979, **101**, 760.
90. D.M. Doddrell, D.T. Pegg, and M.R. Bendall, *J. Magn. Reson.*, 1982, **48**, 323.
91. C.A. Fyfe, K.C. Wong-Moon, Y. Huang, and H. Grondey, *J. Am. Chem. Soc.*, 1995, **117**, 10397.
92. H.M. Kao and C.P. Grey, *J. Magn. Reson.*, 1998, **133**, 313.
93. T.T. Nakashima, R.E.D. McClung, and B.K. Jhon, *J. Magn. Reson.*, 1984, **58**, 27.
94. O.W. Sorensen, G.W. Eich, M.H. Levitt, G. Bodenhausen, and R.R. Ernst, *Progr. NMR Spectrosc.*, 1983, **16**, 163.
95. R.R. Ernst, G. Bodenhausen and A. Wokaun, Principles of nuclear magnetic resonance in one and two dimensions. , Clarendon Press, Oxford (1987).
96. I.S. Podkorytov, *Concepts Magn. Reson.*, 1997, **9**, 117.
97. N. Chandrakumar. In: E. Fluck, and H. Günter, Editors, *Basic Principles and Progress in NMR* **vol. 34**, Springer-Verlag, Berlin (1996).
98. A. Gençten, Ö. Tezel, and S. Bahçeli, *Chem. Phys. Lett.*, 2002, **351**, 109.
99. (214). Tezel, A. Gençten, A. Tokatli, M. Sahin, and S. Bahçeli, *Acta Phy. Pol. A*, 2003, **104**, 503.
100. O.W. Sorensen and R.R. Ernst, *J. Magn. Reson.*, 1983, **51**, 477.
101. N. Chandrakumar, *J. Magn. Reson.*, 1984, **60**, 28.
102. A. Tokatli, A. Gençten, M. Sahin, (214). Tezel, and S. Bahçeli, *J. Magn. Reson.*, 2004, **169**, 68.
103. S.K. Lee and B.K. Nicholson, *J. Organomet. Chem.*, 1986, **309**, 257.
104. J. Lorberth, S. Wocadlo, W. Massa, E.V. Grigoriev, S. Yashina, V.S. Petrosyan, and P. Finocchiaro, *J. Organomet. Chem.*, 1996, **510**, 287.
105. J.W. Akitt and W.S. Mc Donald, *J. Magn. Reson.*, 1984, **58**, 401.
106. J.C.P. Sanders and G.J. Schrobilgin. In: P. Granger and R.K. Harris, Editors, *Multinuclear Magnetic Resonance in Liquids and Solids-chemical Applications*, Kluwer Academic, Dordrecht (1990), p. 157.
107. C. Brevard and P. Granger, Handbook of High Resolution Multinuclear NMR. , Wiley, New York (1981).
108. A. Heck, Introduction to Maple. (Second ed.), Springer-Verlag, New York (1997).

109. G.S. Kupriyanov, *Z. Naturforsch. A*, 2004, **59**, 217.
110. N. Khaneja, T. Reiss, B. Luy, and S.J. Glaser, *J. Magn. Reson.*, 2003, **162**, 311.
111. T.R. Eykyn, D.J. Philip, and P.W. Kuchel, *J. Chem. Phys.*, 2003, **118**, 6997.
112. A. Tokatli, A. Gencten, and S. Bahceli, *Spectros. Lett.*, 2003, **36**, 449.
113. T.S. Mahesh, N. Sinha, A. Gosh, R. Das, N. Suryprakash, M.H. Levitt, K.V. Ramanathan, and A. Kumar, *Curr. Sci.*, 2003, **85**, 932.
114. B. Luy and S.J. Glaser, *J. Magn. Reson.*, 2003, **164**, 304.
115. O. Walker, P. Mutzenhardt, and D. Canet, *Magn. Reson. Chem.*, 2003, **41**, 776.
116. K.E. Koever and G. Batta, *Prog. Magn. Reson.*, 1987, **19**, 223.
117. B. Celda, C. Biamonti, M.J. Arnau, R. Tejero, and G.T. Montelione, *J. Biomol. NMR*,1995, **5**, 161.
118. C. Mumenthaler, P. Guntert, W. Braun, and K. Wüthrich, *J. Biomol. NMR*, 1997, **10**, 351.
119. D. Neuhaus and M.P. Williamson. *The Nuclear Overhauser Effect in Structural and Conformational Analysis*. VCH: New York,1989.
120. J. Cavanagh, W.J. Fairbrother, A.G. Palmer III, and N.J. Skelton, *Protein NMR Spectroscopy*. Academic Press: San Diego, 1996.
121. F. Guenneau, P. Mutzenhardt, X. Assfeld, and D. Canet, *J. Phys. Chem. A*, 1998, **102**, 7199.
122. I. Furo, P. Mutzenhardt, and D. Canet, *J. Am. Chem. Soc.*, 1995, **117**, 10405.
123. H. Python, P. Mutzenhardt, and D. Canet, *J. Phys. Chem. A*, 1997, **101**, 1793.
124. T.M. Alam, D.M. Pedrotty, and T.J. Boyle, *Magn. Reson. Chem.*, 2002, **40**, 361.
125. W. Bauer, *Magn. Reson. Chem.*, 1996, **34**, 532.
126. B. Lix, F.D. Sonnichsen, and B.D. Sykes, *J. Magn. Reson. A*, 1996, **121**, 83.
127. K.E. Kover and G. Batta, *J. Magn. Reson.*, 1999, **138**, 89.
128. F. Kramer and S.J. Glaser, *J. Magn. Reson.*, 2004, **168**, 238.
129. T. Carlomagno, W. Peti, and C. Griesinger, *J. Biomol. NMR* , 2000, **17**, 99.
130. F. Kramer, A. Jung, E. Brunner, and S.J. Glaser, *J. Magn. Reson.*, 2004, **169**, 49.
131. D. Bytchenkoff and G. Bodenhausen, *J. Magn. Reson.*, 2003, **165**, 1.
132. S. Ravindranathan, J.-M. Mallet, P. Sinay, and G. Bodenhausen, *J. Magn. Reson.*, 2003, **163**, 199.
133. D.G.A. Harshani de Silva, D. Beoku-Betts, P. Kyritsis, K. Govindaraju, R. Powls, N.P. Tomkinson, and A.G. Sykes, *J. Chem. Soc. Dalton Trans.*, 1992, 2145.
134. L. Ma and J.J. Led, *J. Am. Chem. Soc.*, 2000, **122**, 7823.
135. L. Ma, A.-M.M. Jørgensen, G.O. Sørensen, J. Ulstrup, and J.J. Led, *J. Am. Chem. Soc.*, 2000, **122**, 9473.
136. L. Ma, E. Philipp, and J.J. Led, *J. Biomol. NMR*, 2001, **19**, 199.
137. M.R. Jensen, D.F. Hansen, and J.J. Led, *J. Am. Chem. Soc.*, 2002, **124**, 4093.
138. F. Bloch, *Phys. Rev.*, 1946, **70**, 460.
139. H.M. McConnell, *J. Chem. Phys.*, 1958, **28**, 430.
140. A.C. McLaughlin and J.S. Leigh, Jr., *J. Magn. Reson.*, 1973, **9**, 296.
141. O. Trott and A.G. Palmer, *J. Magn. Reson.*, 2002, **154**, 157.
142. D. F. Hansen and J.J. Led, *J. Magn. Reson.*, 2003, **163**, 215.
143. F. Massi, E. Johnson, C.Y. Wang, M. Rance, and A.G. Palmer, *J. Am. Chem. Soc.*, 2004, **126**, 2247.
144. D. Abergel and A.G. Palmer, *Concepts Magn. Reson.*, 2003, **19A**, 134.
145. B. Shaipira and L. Frydman, *J. Magn. Reson.*, 2003, **165**, 320.
146. G. Hernandez and D.M. LeMaster, *Magn. Reson. Chem.*, 2003, **41**, 699.
147. D.M. Korzhnev, K. Bloiber, and L.E. Kay, *J. Am .Chem. Soc.*, 2004, **126**, 7320.
148. M. Askin and A. Yilmaz, *Spectrosc. Lett.*, 2004, **37**, 217.

149. P.T. Callaghan and I. Furo, *J. Chem. Phys.*, 2004, **120**, 4032.
150. V. Theodorou, A.N. Troganis, and I.P. Gerothanassis, *Tetrahedron Lett.*, 2004, **45**, 2243.
151. N. Bloembergen and R.V. Pound, *Phys. Rev.*, 1954, **95**, 8.
152. W.S. Price and M. Walchli, *Magn. Reson. Chem.*, 2002, **40**, S128.
153. M.A. Connell, A.L. Davis, A.M. Kenwright, and G.A. Morris, *Analytical Bioanalytical Chem.*, 2004, **378**, 1568.
154. W.S. Price, P. Stilbs, B Jonsson, and O. Soderman, *J. Magn. Reson.*, 2001, **150**, 49.
155. A. Louis-Joseph, J.Y. Lallemand, and D. Abergel, *Compt. Rend. Chim.*, 2004, **7**, 329.
156. R. Eggenberger, S. Gerber, H. Huber, D. Searles, and M. Welker, *J. Chem. Phys.*, 1992, **97**, 5898.
157. R. Eggenberger, S. Gerber, H. Huber, D. Searles, and M. Welker, *Mol. Phys.*, 1993, **80**, 1177.
158. F. Weinhold, *J. Chem. Phys.*, 1998, **109**, 367.
159. F. Weinhold, *J. Chem. Phys.*, 1998, **109**, 373.
160. E.H. Hardy, M.G. Müller, P.S. Vogt, C. Bratschi, B. Kirchner, H. Huber, and D.J. Searles, *J. Chem. Phys.*, 2003, **119**, 6184.
161. M.G. Müller, E.H. Hardy, P.S. Vogt, C. Bratschi, B. Kirchner, H. Huber, and D.J. Searles, *J. Am. Chem. Soc.*, 2004, **126**, 4707.
162. M.G. Müller and H. Huber, *Collect. Czech. Chem. Commun.*, 2003, **68**, 2292.
163. D.S. Gill, T.I. Quickenden, L. Byme, V. Pathania, and B.K. Vermani, *J. Mol. Liq.*, 2004, **111**, 85.
164. K.G. Victor, C.L. teng, T.R.D. Dinesen, J.P. Korb, and R.G. Bryant, *Magn. Reson. Chem.*, 2004, **42**, 518.
165. V.I. Bakhmutov, *Magn. Reson. Chem.*, 2004, **42**, 66.
166. T. Umecky, M. Kanakubo, and Y. Ikushima, *J. Phys. Chem. B*, 2003, **107**, 12003.
167. A.N. Troganis, C. Tsanaktsidis, and I.P. Gerothanassis, *J. Magn. Reson.*, 2003, **164**, 294.
168. I. Bertini, C. Luchinat, and G. Parigi, Solution NMR of paramagnetic molecules. , Elsevier, Amsterdam (2001).
169. P. Caravan, J.J. Ellison, T.J. McMurry, and R.B. Lauffer, *Chem. Rev.*, 1999, **99**, 2293.
170. S. Aime, M. Botta, M. Fasano, and E. Terreno, *Chem. Soc. Rev.*, 1998, **27**, 19.
171. I. Solomon, *Phys. Rev.*, 1955, **99**, 559.
172. I. Solomon and N. Bloembergen, *J. Chem. Phys.*, 1956, **25**, 261.
173. N. Bloembergen, *J. Chem. Phys.*, 1957, **27**, 572.
174. N. Bloembergen and L.O. Morgan, *J. Chem. Phys.*, 1961, **34**, 842.
175. A.G. Redfield, *Adv. Magn. Reson.*, 1965, **1**, 1.
176. Z. Luz and S. Meiboom, *J. Chem. Phys.*, 1964, **40**, 2686.
177. L.-P. Hwang and J.H. Freed, *J. Chem. Phys.*, 1975, **63**, 4017.
178. J.H. Freed, *J. Chem. Phys.*, 1978, **68**, 4034.
179. M. Rubinstein, A. Baram, and Z. Luz, *Mol. Phys.*, 1971, **20**, 67.
180. D. Kruk and J. Kowalewski, *J. Magn. Reson.*, 2003, **162**, 229.
181. J. Miller,1 N. Schaefle, and R. Sharp,*Magn. Reson. Chem.*, 2003, **41**, 806.
182. F. Kateb and M. Piccioli, *J. Am. Chem. Soc.*, 2003, **125**, 14978.
183. J. Iwahara, C.D. Schwieters, and G.M. Clore, *J. Am. Cehm. Soc.*, 2004, **126**, 5879.
184. S. Tamburini, P. Tomasin, P.A. Vigato, S. Aime, M. Botta, and M.A. Cremonini, *Inorg. Chem. Acta*, 2004, **357**, 1374.
185. P.H. Fries, G. Ferrante, E. Beloritzky, and S. Rast, *J. Chem. Phys.*, 2003, **119**, 8636.
186. C.S. Bonnet and P.H. Fries, *Magn. Reson. Chem.*, 2003, **41**, 782.

187. G. Addams and J.H. Gibbs. *J. Chem. Phys.*, 1969, **43**, 139.
188. R. Colby. *Phys. Rev. E*, 2000, **61**, 1783.
189. C. Donati, J.F. Douglas, W. Kob, S.J. Plimpton, P.H. Poole, and S.C. Glotzer. *Phys. Rev. Lett.*, 1998, **80**, 2338.
190. G.P. Johari and M. Glodstein. *J. Chem. Phys.*, 1970, **53**, 2372.
191. W. Götze. *Z. Phys. B* , 1985, **60**, 195. W. Götze and W. Sjögren. *Rep. Progr. Phys.*, 1992, **55**, 242.
192. A. Arbe, J. Colmenero, M. Monkenbusch, and D. Richter. *Phys. Rev. Lett.*, 1998, **81**, 590.
193. H. Sillescu. *J. Phys. Condens. Matt. J. Non-Crystal. Solids*, 2002, **307**, 16.
194. R. Bohmer, G. Hinze, T. Jorg, F. Oi, and H. Sillescu. *J. Phys. Condens. Matt.*, 2000, **12**, A383.
195. A. Doss, M. Paluch, H. Sillescu, and G. Hinze. *J. Chem. Phys.*, 2002, **117**, 6582.
196. M. Russina, R. Olga, and F. Mezei, *Chem. Phys.*, 2003, **292**, 325.
197. N. Giovambattista, M.G. Mazza, S.V. Buldyrev, F.W. Starr, and H.E. Stanley, *J. Phys. Chem. B*, 2004, **108**, 6655.
198. J. Rault, R. Neffati, and P. Judeinstein, *Eur. Phys. J. B*, 2003, **36**, 627.
199. J.E. Wolak, X. Jia, and J.L. White, *J. Am. Chem. Soc.*, 2003, **125**, 13660.
200. M. Wind, R. Graf, A. Heuer, and H.W. Spiess, *Phys. Rev. Lett.*, 2003, **91**, 155702.
201. J.C. Dyre and N.B. Olsen, *Phys. Rev. Lett.*, 2003, **91**, 155703.
202. L.L. Li, J. Schroers, and Y. Wu, *Phys. Rev. Lett.*, 2003, **91**, 265502.
203. K.J. Rao, and S. Kumar, *Curr. Sci.*, 2003, **85**, 945.
204. C.C. Tambelli, J.P. Donoso, C.J. Magon, L.A. Bueno, Y. Messaddeq, S.J.L. Ribeiro, L.F.C. de Oliveira, and I. Kosacki, *J. Chem. Phys.*, 2004, **120**, 9638.
205. I. Ardelean, G. Farrher, C. Mattea, and R. Kimmich, *J. Chem. Phys.*, 2004, **120**, 9809.
206. H.G. Chae, S.H. Park, B.C. Kim, and D.K. Kim, *J. Poly. Sci. Phys.*, 2004, **42**, 1759.
207. O. Urakawa, S.F. Swallen, M.D. Ediger, and E.D. von Meerwall, *Macromolecules*, 2004, **37**, 1558.
208. B.R. Cherry, J.W. Zwanziger, and B.G. Aitken, *J. Non-Cryst. Solids*, 2004, **333**, 28.
209. C. Alba-Simionesco, G. Dosseh, E. Dumont, B. Frick, B. Geil, D. Morineau, V. Teboul, and Y. Xia, *Eur. Phys. J. E*, 2003, **12**, 19.
210. J. Berriot, H. Montes, F. Lequeux, D. Ling, and P. Sotta, *Europhys. Lett.*, 2003, **64**, 50.
211. S.S. Sekhon, M. Kumar, K. Yamada, and T. Okuda, *Chem. Phys. Lett.*, 2003, **379**, 466.
212. F.W. Weaver and E.L. Quitevis, *Chem. Phys. Lett.*, 2003, **378**, 135.
213. T. Nakaoki and M. Kobayashi, *J. Mol. Struc.*, 2003, **655**, 343.
214. C.G. Pantano, S. Prabakar, and K.T. Mueller, *Phys. Chem. Glasses*, 2003, **44**, 125.
215. C. Tien, E.V. Charnaya, P. Sedykh, and Y.A. Kumzerov, *Phys. Solid State*, 2003, **45**, 2352.
216. P. Debye, Polare Molekeln, Verlag von S. Hirzel: Leipzig, Germany, (1929).
217. G. Lipari, A. Szabo, *J. Am. Chem. Soc.* 1982, **104**, 4546.
218. H. Wennerström, B. Lindman, O. Söderman, T. Drakenberg, and J.B. Rosenholm, *J. Am. Chem. Soc.* 1979, **101**, 6860.
219. G. Lipari and A. Szabo, *J. Am. Chem. Soc.* 1982, **104**, 4559.
220. L. Vugmeyster, D.P. Raleigh, A.G. Palmer, and B.E. Vugmeister, *J. Am. Chem. Soc.*, 2003, **125**, 8400.
221. J. Lang, Z. Tošner, P. Lhoták, and J. Kowalewski, *Magn. Reson. Chem.*, 2003, **41**, 819.

222. P.S. Denkova, V.S. Dimitrov, S.M. Bakalova, J. Kaneti, and K. Danov, *Magn. Reson. Chem.*, 2003, **41**, 989.
223. D. Canet, S. Bouguet-Bonnet, and P. Mutzenhardt, *Concepts Magn. Reson.Part A*, 2003, **19**, 65.
224. A. Friedrich, A. Dölle, and M.D. Zeidler, *Magn. Reson. Chem.*, 2003, **41**, 813.
225. J.M. Schurr, H.P. Babcock, and B.S. Fujimoto, *J. Magn. Reson. B*, 1994, **105**, 211.
226. P. Luginbühl, K.V. Pervushin, H. Iwai, and K. Wuthrich, *Biochemistry*, 1997, **36**, 7305.
227. D. Fushman and D. Cowburn, Studying protein dynamics with NMR relaxation. In: R. Sarma and M. Sarma, Editors, *Structure, Motion, Interaction and Expression of Biological Macromolecules*, Adenine Press, Albany, NY (1998), pp. 63-77.
228. J.B. Hall and D. Fushman. *J. Biomol. NMR*, 2003, **27**, 261.
229. D. Fushman, R. Xu, and D. Cowburn, *Biochemistry*, 1999, **38**, 10225.
230. P.M. Hwang, N.R. Skrynnikov, and L.E. Kay, *J. Biomol. NMR*, 2001, **20**, 83.
231. R. Varadan, O. Walker, C. Pickart, and D. Fushman, *J. Mol. Biol.*, 2002, **324**, 637.
232. R. Varadan, M. Assfalg, A. Haririnia, S. Raasi, C. Pickart, and D. Fushman, *J. Biol. Chem.*, 2004, **279**, 7055.
233. D. Fushman and D. Cowburn, Characterization of inter-domain orientations in solution using the NMR relaxation approach. In: N.R. Krishna, Editor, *Protein NMR for the Millenium Biological Magnetic Resonance* **vol. 20**, Kluwer, Dordrecht (2002), pp. 53-78.
234. P. Bernado, T. Akerud, J. Garcia de la Torre, M. Akke, and M. Pons. *J. Am. Chem. Soc.*, 2003, **125**, 916.
235. D. Fushman, Determination of protein dynamics using ^{15}N relaxation measurements. In: O. Zerbe, Editor, *BioNMR in Drug Research*, Wiley-VCH, New York (2002), pp. 283-308.
236. N. Tjandra, S.E. Feller, R.W. Pastor, and A. Bax, *J. Am. Chem. Soc.*, 1995, **117**, 12562.
237. R. Brüschweiler, X. Liao, and P.E. Wright, *Science*, 1995, **268**, 886.
238. L.K. Lee, M. Rance, W.J. Chazin, and A.G. Palmer III, *J. Biomol. NMR*, 1997, **9**, 287.
239. M. Blackledge, F. Cordier, P. Dosset, and D. Marion, *J. Am. Chem. Soc.*, 1998, **120**, 4538.
240. V. Copie, Y. Tomita, S.K. Akiyama, S. Aota, K.M. Yamada, R.M. Venable, R.W. Pastor, S. Krueger, and D.A. Torchia, *J. Mol. Biol.*, 1998, **277**, 663.
241. G.M. Clore, A.M. Gronenborn, A. Szabo, and N. Tjandra, *J. Am. Chem. Soc.*, 1998, **120**, 4889.
242. P. Tsan, J.C. Hus, M. Caffrey, D. Marion, and M. Blackledge, *J. Am. Chem. Soc.*, 2000, **122**, 5603.
243. R. Ghose, D. Fushman, and D. Cowburn, *J. Magn. Reson.*, 2001, **149**, 214.
244. P. Dosset, J.C. Hus, M. Blackledge, and D. Marion, *J. Biomol. NMR*, 2000, **16**, 23.
245. J.G. de la Torre, S. Navarro, M.C.L. Martinez, F.G. Diaz, and J.J.L. Cascales, *Biophys. J.*, 1994, **67**, 530.
246. J. García de la Torre, M.L. Huertas, and B. Carrasco, *J. Magn. Reson. B*, 2000, **147**, 138.
247. M. Andrec, K.G. Inman, D.J. Weber, R.M. Levy, and G.T. Montelione, *J. Magn. Reson.*, 2000, **146**, 66.
248. O. Walker, R. Varadan, and D. Fushman, *J. Magn. Reson.*, 2004, **168**, 336.
249. J. Boisbouvier, Z.R. Wu, A. Ono, M. Kainosho, and A. Bax, *J. Biomol. NMR*, 2003, **27**, 133.

250. B. Halle and M. Davidovic, *Proc. Natl. Acad. Sci.*, 2003, **100**, 12135.
251. W. Derbyshire, M. van den Bosch, D. van Dusschoten, W. MacNaughtan, I. A. Farhat, M. A. Hemming, and J. R. Mitchell, *J. Magn. Reson.*, 2004, **168**, 278.
252. M. Iwahashi, S. Takebayashi, A. Umehara, Y. Kasahara, H. Minami, H. Matsuzawa, T. Inoue, and H. Takahashi, *Chem. Phys. Lipids*, 2004, **129**, 195.
253. G. Celebre, G. de Luca, M. Longeri, G. Pileio, and J.W. Emsley, *J. Chem. Phys.*, 2004, **120**, 7975.
254. M. Vilfan and M. Vuk, *J. Chem. Phys.*, 2004, **120**, 8638.
255. M. Nilsson, I.F. Duarte, C. Almeida, I. Delgadillo, B.J. Goddfellow, A.M. Gil, and G.A. Morris, *J. Agric. Food Chem.*, 2004, **52**, 3736.
256. Z. Fojud, E. Szczesniak, S. Jurga, S. Stapf, and R. Kimmich, *Solid State Nucl. Magn. Reson.*, 2004, **25**, 200.
257. S. Uchino, T. Hiraoki, and A. Tsutsumi, *Japanese J. Appl. Phys.*, 2004, **43**, 2731.
258. H.C. Gao, G.G. Li, S.Z. Mao, H.Z. Yuan, and Y.R. Du, *Acta polym. Sin.*, 2004, 78.
259. J. Crassous and S. Hediger, *J. Phys. Chem. A*, 2003, **107**, 10233.
260. N.A. Melnichenko, A.V. Bazhanov, and A.S. Kuprinyanov, *J. Struc. Chem.*, 2003, **44**, 397.
261. S. Abbrent, S.H. Chung, S.G. Greenbaum, J. Muthu, and E.P. Giannelis, *Electrochim. Acta*, 2003, **48**, 2113.
262. K.R. Jeffrey, G.Z. Zukowska, J.R. Stevens, and G.Z. Zukowska, *J. Chem. Phys.*, 2003, **119**, 2422.
263. K. Hayamizu and W.S. Price, *J. Magn. Reson.*, 2004, **167**, 328.
264. K. Hayamizu and E. Akiba, Electrochemistry, 2003, **71**, 1052.
265. G. Palmer, J. Richter, and M.D. Zeidler, *Z. Naturforsch. A*, 2004, **59**, 51.
266. G. Palmer, J. Richter, and M.D. Zeidler, *Z. Naturforsch. A*, 2004, **59**, 59.
267. L.Y. Dai, S.Y. Yu, Y.K. Shan, and M.Y. He, *Eur. J. Inorg. Chem.*, 2004, **2**, 237.
268. E. Schellkes, X. Hong, M. Holz, U. Huniar, R. Ahlrichs, and W. Freyland, *Phys. Chem. Chem. Phys.*, 2003, **5**, 5536.
269. N.E. Heimer, R.E. Sesto, and W.R. Carper, *Magn. Reson. Chem.*, 2004, **42**, 71.
270. S. Fischer, H. Leipner, K. Thummler, E. Brendler, and J. Peters, *Cellulose*, 2003, **10**, 227.
271. J.H. Antony, D. Mertens, A. Dölle, P. Wasserscheid, and W.R. Carper, *Chem. Phys. Chem.*, 2003, **4**, 588.
272. W.R. Carper, P.G. Wahlbeck, J.H. Antony, D. Mertens, A. Dölle, und P. Wasserscheid, *Anal. Bionanal. Chem.*, 2004, **378**, 1548.
273. C.R. Yonker and J.C. Linehan, *J. Supercrit. Fluids*, 2004, **29**, 257.
274. J.J. Jodry and K. Mikami, *Tetrahedron Lett.*, 2004, **45**, 4429.
275. C.A. Ohlin, P.J. Dyson, and G. Laurenczy, *Chem. Comm.*, 2004, **9**, 1070.
276. G. Rangits, G. Petocz, Z. Berente and L. Kollar, *Inorg. Chim. Acta*, 2003, **353**, 301.
277. A. Kastler, *J. Phys. Radium* , 1950, **11**, 255.
278. W. Happer, E. Miron, D. Schreiber, W.A. van Wijngarden, and X. Zeng, *Phys. Rev. A* 1984, **29**, 3092.
279. T.G. Walker and W. Happer. *Rev. Mod. Phys.*, 1997, **69**, 629.
280. U. Ruth, T. Hof, J. Schmidt, D. Fick, and H.J. Jansch, *Appl. Phys. B*, 1999, **68**, 93.
281. F.D. Colegrove, L.D. Schearer, and G.K. Walters, *Phys. Rev.*, 1963, **132**, 2561.
282. E. Stoltz, M. Meyerhoff, N. Bigelow, M. Leduc, P.J. Nacher and G. Tastevin, *Appl. Phys. B* 1996, **63**, 629.
283. G. Frossati, *J. Low Temp. Phys.*, 1998, **111**, 521.
284. M.S. Albert, G.D. Cates, B. Driehuys, W. Happer, B. Saam, C.S. Springer, Jr., and A. Wishnia, *Nature*, 1994, **370**, 199.

285. H.E. Moller, X.J. Chen, B. Saam, K.D. Hagspiel, G.A. Johnson, T.A. Altes, E.E. de Lange, and H.U. Kauczor, *Magn. Reson. Med.*, 2002, **47**, 1029.
286. T. Pietrass and H.C. Gaede, *Adv. Mater.*, 1995, **7**, 826.
287. M.S. Albert and D. Balamore, *Nucl. Instrum. Meth. Phys. Res. A*, 1998, **402**, 441.
288. T. Pietrass, *Colloids Surf. A*, 1999, **158**, 51.
289. A. Bifone, J. Wolber, and N.J. Shah, *Magnetic Resonance and Brain Function: Approaches from PhysicsMagnetic Resonance and Brain Function: Approaches from Physics*, IOP Press (1999).
290. B.M. Goodson, *Concepts Magn. Reson.*, 1999, **11**, 203.
291. B.M. Goodson, L. Kaiser, and A. Pines, *Magnetic Resonance and Brain Function: Approaches from Physics Magnetic Resonance and Brain Function: Approaches from Physics*, IOP Press (1999).
292. Y.Q. Song, *Concepts Magn. Reson.*, 2000, **12**, 6.
293. T. Chupp and S. Swanson, *Adv. At. Mol. Opt. Phys.*, 2001, **45**, 41.
294. R.W. Mair and R.L. Walsworth, *Appl. Magn. Reson.*, 2002, **22**, 159.
295. B.M. Goodson, *J. Magn. Reson.*, 2002, **155**, 157.
296. S.L. Codd and S.A. Altobelli, *J. Magn. Reson.*, 2003, **163**, 16.
297. A.R. Cross, M. McDonald, J.P. Robles, and G.E. Santyr, *J. Chem. Phys.*, 2003, **162**, 241.
298. S. Han, H. Kuhn, F.W. Hasing, K. Munnemann, B. Blümich, and S. Appelt, *J. Magn. Reson.*, 2004, **167**, 298.
299. K. Ishikawa, H. Imai, and Y. Takagi, *J. Chem. Phys.*, 2004, **120**, 7602.
300. L. Dubois, S. Parres, J.G. Huber, P. Berthault, and H. Desvaux, *J. Phys. Chem. B*, 2004, **108**, 767.
301. J.J. Heckmann, M.P. Ledbetter, and M.V. Romalis, *Phys. Rev. Lett.*, 2003, **91**, 067601.
302. N. Nestle, T. Baumann, and R. Niessner, *Water Res.*, 2003, **37**, 3361.
303. K. Jackowski and M. Wilczek, *J. Mol. Struc.*, 2003, **651**, 1.
304. Q.L. Lin, S.H. Cai, Z. Chen, and C.B. Cai, *Chinese J. Chem. Phys.*, 2004, **17**, 155.
305. K.J. Dunn, D.J. Bergman, and G.A. LaTorraca, Numclear Magnetic Resonance: Petrophysical and Logging Applications. , Pergamon Press, Oxford (2002).
306. R. Akkurt, H.J. Vinegar, P.N. Tutunjian, and A.J. Guillory, *Log Analyst*, 1996, **37**, 33.
307. S. Chen, D.T. Georgi, O. Olima, H. Gamin and J. Minetto, *SPE Reservoir Evaluat. Eng.*, 2000, **3**, 6.
308. M.D. Hürlimann and L. Venkataramanan, *J. Magn. Reson.*, 2002, **157**, 31.
309. M.D. Hürlimann, L. Venkataramanan, and C. Flaum, *J. Chem. Phys.*, 2002, **117**, 10223.
310. B. Sun and K.-J. Dunn, *Phys. Rev. E* , 2002, **65**, 051309.
311. B. Sun and K.-J. Dunn, *J. Magn. Reson.*, 2004, **169**, 118.
312. D. Topgaard and A. Pines, *J. Magn. Reson.*, 2004, **168**, 31.
313. G.Q. Zhang and G.J. Hirasaki, *J. Magn. Reson.*, 2003, **163**, 81.
314. I. Ardelean and R. Kimmich, *Israel J. Chem.*, 2003, **43**, 9.
315. C. Casieri, S. Bubici, and F. de Luca, *J. Magn. Reson.*, 2003, **162**, 348.
316. K.I. Momot and P.W. Kuchel, *J. Magn. Reson.*, 2004, **169**, 92.
317. C. Malmborg, D. Topgaard, and O. Söderman , *J. Magn. Reson.*, 2004, **169**, 85
318. B. Manz, *J. Magn. Reson.*, 2004, **169**, 60.
319. M. Engelsberg, W. Barros, and F. Hallwass, *J. Chem. Phys.*, 2004, **120**, 10659.
320. C.H. Pennington, *Concepts Magn. Reson.*, 2003, **19A**, 71.
321. M. Klein, R. Fechete, D.E. Demco, and B. Blümich, *J. Magn. Reson.*, 2003, **164**, 310.

322. E.M. de Carvalho, M.H. Rodrigues Velloso, L. Wanderley Tinoco , and J.D. Figueroa-Villar, *J. Magn. Reson.*, 2003, **164**, 197.
323. P.T. Callaghan and I. Furo, *J. Chem. Phys.*, 2004, **120**, 4032.
324. C. Zuccaccia, N.G. Stahl, A. Macchioni, M.C. Chen, J.A. Roberts, and T.J. Marks, *J. Am. Chem. Soc.*, 2004, **126**, 1448.
325. P.S. Pregosin, E. Martinez-Viviente, and P.G.A. Kumar, *Dalton Trans.*, 2003, **21**, 4007.
326. A. Gottwald, P. Kuran, and U. Scheler, *J. Magn. Reson.*, 2003, **162**, 364.
327. R. Valiullin, P. Kortunov, J. Kärger, and V. Timoshenko, *J. Chem. Phys.*, 2004, **120**, 11804.
328. A. Kennedy, C.J. Long, P.J. Hmel, and T.J. Reid, *Spectroscopy*, 2004, **18**, 265.
329. T. Gostan, C. Moreau, A. Juteau, E. Guichard, and M.A. Delsuc, *Magn. Reson. Chem.*, 2004, **42**, 496.
330. K.G. Hollingworth, A.J. Sedermann, C. Buckley, L.F. Gladden, and M.L. Johns, *J. Colloid Interface Sci.*, 2004, **274**, 244.
331. J.P. Hindmarsh, D.I. Wilson, and M.L. Johns, *Colloids Surfaces*, 2004, **234**, 129.
332. K.E. Price, L.H. Lucas, and C.K. Larive, *Analyt. Bioanalyt. Chem.*, 2004, **378**, 1405.

7
Solid state NMR Spectroscopy

BY A.E. ALIEV AND R.V. LAW

1 Introduction

The aim of our contribution is to outline important recent advances and applications achieved in the area of solid state NMR based on the literature published between July 2003 and June 2004. A very large number of papers making use of solid state NMR techniques have been published during this period, however, not all of these papers have been included in this report. Specifically, over 700 references that included solid state NMR and related terms either in the title or in the keywords were initially retrieved for the preparation of this report, and approximately half of these were included in the final report. In choosing sources for this report we have aimed at highlighting publications that uses solid state NMR as the only or the primary technique for structural and/or dynamics studies of solid materials as well as those that have applied the technique in an innovative manner. In selecting references, we have also aimed at illustrating diversity of problems and subject areas covered by modern solid state NMR applications.

The format used in this report is similar to that used in the previous years. The following section of the report includes review articles (Section 2) on both general and specific aspects of solid state NMR spectroscopy and its applications. Publications about recent experimental developments and novel applications that are of general methodological interest are arranged in sections 3-5. A few general trends can be noticed regarding developments of the solid state NMR in the last year. With regard to experimental aspects (Section 3), developments of specific solid-sate NMR techniques suitable for the studies of uniformly isotope labelled solids (mainly ^{13}C and ^{15}N) have attached a considerable amount of research by various groups. In respect to structure determinations (Section 5), some interesting examples include application of REDOR measurements for the 3D structure determination of peptides and proteins. In general, the number of publications making use of solid state NMR for biological applications has considerably increased. In addition to experimental techniques, various quantum-mechanical techniques are now used routinely for the calculation of various NMR parameters (mainly chemical shifts and J-couplings) and their anisotropy in the solid state (Sections 5 and 6). Many publications have demonstrated that combination of DFT or similar type of quantum-mechanical calculations with

Nuclear Magnetic Resonance, Volume 34
© The Royal Society of Chemistry, 2005

both solution and solid state NMR measurements allows a significantly improved structural or conformational analysis. However, the number of publications combining solid state NMR and MD calculations for solids dynamics studies still remains extremely limited. Various examples of solid state NMR applications are collected in the final Section 6. This section is divided into 16 subsections depending on the type of the material studied. Amongst various multinuclear applications, an increased number of useful ^{17}O NMR studies are noteworthy.

2 Reviews and Introductory Articles

Some new developments and applications of the solid state NMR published between October 2001 and October 2003 have been reviewed briefly by Dybowski *et al.*[1] Reviews section of this publication highlights important new articles published in the recent years. A selection of new NMR techniques and chemical shift and *J*-coupling measurements has been reviewed. In addition, applications of solid state NMR techniques to study porous materials, semiconductors and ionic conductors, glasses, polymers and biological materials have been described.

Number of publications making use of quantum-mechanical calculations of the NMR parameters and their anisotropy has increased substantially in the last few years. This is also reflected by the review articles published in 2003-04. Sebastiani has reviewed the development of electronic structure methods for the calculation of NMR properties in condensed matter over the recent years.[2] The theoretical basis of the *ab initio* methods, as well as further recent developments and a variety of selected applications have been presented. The applications are accompanied by solid state NMR experimental data, and the advantage of combining high-level *ab initio* calculations with experimental research is emphasised.

In another review on a related subject, Alkorta and Elguero have summarised the GIAO calculations of chemical shifts and absolute shieldings and their correlation with experimentally measured chemical shifts for aromatic heterocycles.[3] Automatic assignment, conformational analysis, E/Z isomerism, and, in particular, tautomerism, have been discussed in detail. In addition, solid state and solvent effects, as well as the problem of heteroaromaticity have been examined. The review ends with the discussion of some methodological aspects with a special emphasis on the calculation of reference chemical shifts, such as those for TMS and nitromethane.

The recent advances in *ab initio* quantum chemical calculations of calixarenes and calixarene complexes have been highlighted in a short review by Schaltz.[4] The main focus of this article lies on the results obtained mainly during the last 2-3 years.

In terms of experimental aspects, two articles have been published on the subject of ^{13}C CP MAS NMR. The first one by Taylor presents the basics of setting up the CP MAS experiment.[5] The polarisation transfer from the protons

to the carbons is described briefly with the usual thermodynamic and quantum mechanical models. The setup and use of the experiment for routine analyses are discussed. In addition, this article also illustrates such NMR phenomena as rotational echoes, homogeneous and inhomogeneous interactions, continuous wave proton decoupling, and coupling of quadrupolar ^{14}N nuclei to ^{13}C nuclei.

In another article on ^{13}C CP MAS, Conte *et al.* have reviewed its applications to study humified natural organic matter.[6] Despite the problems due to the presence of paramagnetic impurities and the generally low organic matter concentration, ^{13}C CP MAS NMR is one the most informative techniques used in soil chemistry and geochemistry mainly because of its relevance in studying bulk samples such as soils and sediments. Current issues of CP MAS ^{13}C NMR spectroscopy applied to natural organic matter are presented and future possible developments of ^{13}C CP MAS technique related to natural organic matter are discussed. In addition, quantitative aspects of the CP MAS technique are discussed and a brief summary of the most common experimental procedure used to obtain reliable solid state ^{13}C CP MAS NMR spectra is presented.

Another experimental aspect of NMR related to the high precision measurement of target polarisation has been reviewed by Court.[7] Solid state polarised targets have been in use in both particle and nuclear physics experiments for nearly 40 years and the vast majority of these experiments have used the continuous wave NMR technique to measure the target polarisation. The development of this technique over this time period has been presented.

Specific applications of the solid state NMR for various structural and dynamics studies have been reviewed in a number of articles. Aliev and Harris have presented an overview of the hydrogen bonding studies in the solid state using NMR.[8] Of particular interest in this regard are solid state NMR experiments that investigate either the hydrogen atom directly involved in the hydrogen bond (employing ^{1}H or ^{2}H NMR techniques) or the atoms within, or in close proximity of, the hydrogen bond donor and acceptor groups (employing ^{13}C, ^{15}N, ^{17}O, ^{29}Si or ^{31}P NMR techniques). The versatility of solid state NMR arising from its multinuclear capability is highlighted. In addition, the dependence of NMR measured parameters (mainly chemical shifts, their anisotropy and quadrupole coupling constants) on the strength and geometry of hydrogen bonding is discussed in detail.

Structural studies of biomaterials using double quantum solid state NMR have been reviewed by Drobny *et al.*[9] Both the theory and practice of double-quantum solid state NMR techniques for determining the secondary structures of surface-adsorbed peptides and proteins are presented. In particular, the use of solid state NMR dipolar techniques to provide the high-resolution structural and dynamic characterisation of a hydrated biomineralisation protein, salivary statherin, adsorbed to its biologically relevant hydroxyapatite surface is presented. This article also reviews NMR data on peptides designed to adsorb from aqueous solutions onto highly porous hydrophobic surfaces with specific helical secondary structures.

In another article of biological interest, recent developments of novel solid state NMR techniques and their application to the study of fully or significantly

isotopically labelled ^{13}C, ^{15}N or $^{13}C/^{15}N$ biomolecules are presented.[10] The first structure solutions of $^{13}C/^{15}N$-labelled peptides, and a protein, Src-homology 3 domain, by MAS NMR without recourse to any structural information obtained from other methods are highlighted. Future prospects for the application of solid state NMR to interesting biological questions are also discussed.

An overview of high-resolution solid state NMR applications to polypeptides and membrane proteins has been presented by Luca *et al.*[11] The importance of the MAS based techniques at ultrahigh magnetic fields for the studies of insoluble or noncrystalline molecules at the atomic level is highlighted. Recently developed NMR methods suitable for the study of multiply or uniformly [^{13}C,^{15}N]-labelled polypeptides and proteins are discussed. In addition, latest biophysical applications are reviewed.

A related article by Bechinger reviews the membrane interactions of a variety of peptides including alamethicin, melittin, cecropins, magainins, and defensins.[12] The biological activities of the peptides are discussed and are correlated to the results from biophysical and structural studies.

Biological applications of solid state NMR in the area of model membrane systems have been reviewed by Drechsler and Separovic.[13] The advantages of solid state NMR in providing information about how the peptides or proteins interact with the lipids or other peptides/proteins in the membrane, as well as their effect on the membrane and the location of the peptides or proteins relative to the membrane surface are presented. The importance of both recent technique developments and improvements in sample labelling has been emphasised. This review also discusses aligned systems and MAS techniques, bilayers and bicelles, and measurement of chemical shift anisotropy and dipolar coupling. A number of specific experiments such as CP, rotational resonance, REDOR, PISEMA and multidimensional experiments are described. In addition to traditional ^{2}H, ^{13}C and ^{15}N studies, recent solid-sate ^{1}H, ^{17}O and ^{19}F NMR applications are also included in this review. Finally, several examples of the use of solid state NMR to determine the structure of membrane peptides and proteins are given.

Applications of solid state NMR along with FTIR and Raman spectroscopy and X-ray crystallography to study the structural changes in the proton transport cycle of the light-driven pump, bacteriorhodopsin, have been reviewed by Laniy.[14]

Techniques and applications of both liquid- and solid state NMR to membrane proteins have been described by Nielsen *et al.*[15] It has been shown that solid state NMR has undergone a tremendous evolution towards characterisation of membrane proteins in native membrane and oriented phospholipid bilayers. In this mini-review, some of the technological challenges behind these efforts and examples on their use in membrane biology are highlighted.

Solid state NMR techniques, such as CP, RAMP CP, CP TOSS, MQ DEPT, 2D HETCOR, which are relevant to the characterisation of natural organic matter have been reviewed by Cook.[16] The pros and cons of many of the techniques are compared in an effort to provide guidance to the most beneficial utilisation of the NMR techniques for researchers interested in natural organic matter.

Recent developments in structural elucidation of supramolecular systems by advanced solid state NMR techniques have been presented by Spiess.[17] Special emphasis is placed on hydrogen-bonded sytems and columnar stacks of aromatic moieties, as well as imidazole-based proton conductors.

Dzwigaj has reviewed recent major advances in the incorporation and identification of vanadium species in microporous materials.[18] Applications of different spectroscopic techniques, including solid state ^{51}V NMR, are discussed.

NMR studies of metals in solid state non-metallic materials such as zeolites, inorganic complexes, glasses, coals, polymers, metalloproteins, and RNA have been reviewed.[19] The role of solid state NMR spectroscopy in investigating the structural and functional aspects of these materials with no long range order is evaluated. This overview presents several developments of solid state NMR to the study of a variety of metal containing materials. In particular, the use of the quadrupolar Carr-Purcell-Meiboom-Gill pulse sequence for the acquisition of solid state NMR spectra of quadrupolar nuclei with low natural abundances and low NMR frequencies, and applications of solid state ^{113}Cd NMR are covered in detail.

Recent progress in solid state NMR studies of electrode materials for lithium ion batteries has been presented by Zhang *et al.*[20] Applications of NMR here are based on the changes of the ^{6}Li and ^{7}Li NMR spectra, which often reflect changes in the coordination of lithium and the structural changes of the materials during the charge/discharge cycle. New developments in the micro-structural analysis of the electrode materials and mechanistic study of Li^{+} intercalation into a variety of materials by using solid NMR techniques have been presented.

Finally, an overview of the novel NMR techniques for the study of quadrupolar nuclei in clays and other layered materials has been presented by Rocha *et al.*[21] In particular, advances in MQ MAS NMR techniques and their use for recording ^{11}B, ^{17}O, ^{23}Na, ^{27}Al and $^{69/71}Ga$ spectra of synthetic and natural clays are highlighted.

3 Experimental Developments

3.1 Proton NMR. Gradient Experiments. – Chevelkov *et al.* have demonstrated the feasibility of ^{1}H detection in MAS solid state NMR for a microcrystalline, uniformly ^{2}H,^{15}N-labelled sample of a SH3 domain of chicken α-spectrin, using pulsed field gradients for suppression of water magnetisation.[22] In analogy with routine solution NMR measurements, B_0 gradients were employed for coherence order selection and solvent suppression. The achievable gain in sensitivity for ^{1}H detection was in the order of 5 compared to the ^{15}N detected version of the experiment. It is expected that this newly developed approach combined with the possibility to measure long range ^{1}H-^{1}H distances will become a useful tool for the determination of protein structures in the solid state.

In a related paper, WATERGATE and DANTE pulse sequences were used under MAS condition to selectively excite or suppress peaks in ^{1}H solid state spectra.[23] As known from solution NMR studies, signal selection or suppression

can be achieved by pulsed-field gradients which selectively dephase and rephase transverse magnetisation. Under MAS, the required field gradients were provided by a simple pair of coils, which were built into a standard fast-MAS probe. It has been shown that PFG-assisted techniques enable efficient selection or suppression of ^{1}H peaks in a single transient of the pulse sequence without the need for phase cycles. Therefore, these tools can be readily incorporated into solid state MAS NMR experiments, which has been demonstrated for ^{1}H-^{1}H double-quantum NMR spectra of supramolecular systems. In the examples presented, the ^{1}H signals of interest were relatively weak relative to the strong ^{1}H signal of long alkyl sidechains. PFG-assisted suppression of the strong perturbing signal was shown to be particularly useful.

Haeberlen *et al.* have continued their efforts in deepening our understanding of proton NMR lineshape.[24] The possible variation of the lineshape of the high-field ^{1}H spectrum of methyl groups was explored by simulation and experiment. The spectrum of an isolated methyl group was shown to depend on the orientation of the applied field B_0 relative to the C_3-axis of the group, on its rotational tunnel frequency ν_t and on its stochastic reorientation rate κ. For quantitative analyses, the directional mobility of the C_3-axis was also taken into account. It was found that a distinct but frequently occurring case arises when the methyl groups are present as pairs of magnetically equivalent close neighbours. For the experiments, single crystals of four different compounds were used that were isotopically substituted such that they contained protons only in the methyl positions.

3.2 Two-dimensional Experiments. – Various modifications of the two-dimensional solid state NMR experiments have been proposed. Carravetta *et al.* have shown that in many cases, the commutation properties of the mixing Hamiltonian leads to selectivity in the allowed coherence transfer processes leading to enhanced resolution in the cross-peaks of 2D solid state NMR spectra.[25]

Through-bond correlation NMR experiments have been of particular interest in the last year and developments and applications relevant to bio- and microporous materials have been proposed. In particular, through bond correlations were used to characterise the structure of MP_2O_7 crystalline compounds and disordered phosphates.[26] For MP_2O_7 materials, the refocused INADEQUATE experiment allowed discrimination between the possible space group symmetries of the room temperature structure. For lead phosphate glasses, the refocused INADEQUATE experiment was appied to determine the P-O-P through-bond connectivities between the different types of PO_4 tetrahedra. In addition, a correlation between the distributions of J-couplings and ^{31}P isotropic chemical shifts was shown by using the 2D J-resolved experiment.

Total through-bond correlation technique using adiabatic pulses and fast MAS has been suggested by Hardy *et al.*[27] It has been shown that above a certain threshold, the polarisation transfer achieved with these sequences is largely insensitive to the amplitude and homogeneity of the radiofrequency field employed. An experimental transfer efficiency of up to 76% was achieved in a two-spin system. Applications to resonance assignments in the dipeptide L-Val-

L-Phe and in the cyclic decapeptide antamanide have been demonstrated.

A new through-bond correlation method for disordered solids has been proposed.[28] The new approach is based on the uniform-sign cross-peak double quantum filtered correlation spectroscopy experiment, which is a refocused version of the popular double quantum filtered correlation spectroscopy experiment in liquids. Its key feature is that it provides in-phase and doubly absorptive line shapes, which renders it robust for chemical shift correlation in solids. It has been shown that both theory and experiment point to distinct advantages of this protocol, which are illustrated by several experiments under challenging conditions, including fast MAS up to 30kHz, anisotropic molecular motion, and ^{13}C correlation spectroscopy at the natural abundance isotope level.

Ernst *et al.* have demonstrated that 2D solid state NMR chemical-shift correlation spectra can be recorded under low-power conditions.[29] Except for the CP period, no RF field amplitudes above 40 kHz were used. However, such experiments require the use of fast MAS (>50 kHz). Low-power spectra were compared to those obtained under high-power conditions. No line broadenings were found, though some changes in the polarisation-transfer dynamics were observed.

Finally, an algorithm has been described by Brouwer for efficiently assigning the resonances of the inequivalent atoms in the 2D NMR correlation experiments.[30] The algorithm, which is based on basic graph theory concepts, finds all possible assignment sets, which are consistent with the experimentally observed correlations and known connectivities in a very efficient manner. It is designed to deal with less than ideal experimental data in which there may be overlapping peaks and uncertainty about the presence or absence of correlation peaks. The algorithm was primarily developed for assigning the peaks in the high-resolution solid state ^{29}Si MAS NMR spectra of highly siliceous zeolites based on 2D ^{29}Si INADEQUATE spectra and is demonstrated using zeolites ZSM-12 and ZSM-5 as working examples. The algorithm is likely to be a useful tool for efficient peak assignments in various types of correlation spectra.

3.3 Decoupling. – In solid state MAS NMR experiments the potential of heteronuclear ^{1}H decoupling employing a continuous train of adiabatic inversion pulses has been assessed using numerical simulations and experimental measurements.[31] It has been shown that, with a ^{1}H RF field strength of the order of 100 kHz that is typically available with MAS NMR probes, it is possible to achieve efficient adiabatic ^{1}H decoupling at low MAS frequencies. It is pointed out that in the presence of ^{1}H inhomogeneities it will be advantageous to employ adiabatic decoupling in solid state MAS NMR experiments.

Ernst *et al.* have introduced low-power XiX proton decoupling under fast MAS.[32] The method is applicable if the MAS frequency exceeds the ^{1}H-^{1}H interactions. For rigid organic solids this is the case for MAS frequencies above approximately 40 kHz. It has been shown that the quality of the decoupling as well as the sensitivity to frequency offsets can be improved compared to low-power CW decoupling. The decoupling efficiency is somewhat reduced compared to optimised high-power decoupling. For example, in a peptide sample

investigated at an MAS frequency of 50 kHz a loss of about 10% in signal intensity for CH_3 and CH groups, and of about 40% for CH_2 groups was observed. Note that the RF amplitude in the low-power XiX was about 15 times lower than in high-power XiX decoupling.

It has been shown that a direct spectral optimisation scheme can be implemented to obtain improved heteronuclear dipolar decoupling schemes for solid state MAS NMR experiments.[33] The resulting schemes, which turn out to have a particularly simple form, are shown to be applicable over the whole range of commercially available spinning speeds (from 5 to 35 kHz), and are shown to improve on the performance of the best existing sequences.

An increased robustness of hetronuclear decoupling has been demonstrated by Gerbaud *et al.* using a simple approach for expanding the stability of the resonant condition by convolution of the basic modulation used in the decoupling schemes with a Gaussian envelope.[34]

A new approach to markedly reduce RF power for observed nuclei during ^{1}H-homonuclear decoupled CP has been described Nishimura and Naito.[35] The reduction of RF power to satisfy the Hartmann-Hahn matching condition for observed nuclei and homonuclear dipolar decoupling at ^{1}H nuclei were achieved simultaneously based on time averaging of nutation frequency of ^{1}H nuclei by frequency switched Lee-Goldburg decoupling with unequal duration times. The RF nutation frequency and RF field for observed nuclei were shown experimentally to be reduced by factor 3 and 10, respectively, at ^{13}C NMR signals.
An interesting application of the XiX decoupling to mobile solids has been demonstrated by Ashida and Asakura.[36] It has been shown that the XiX decoupling is more effective than the usual CW proton decoupling.

Finally, anomalous line-broadenings of carbon resonances close to ^{19}F commonly observed in the ^{13}C NMR of liquid crystals and solids have been investigated.[37] A number of different line-broadening mechanisms were elucidated: decoupling effects, magic angle misset, and ^{19}F lifetime-broadening. In relatively mobile systems, such as liquid crystals or soft solids, the limiting factor on ^{13}C resolution (and the ability to directly quantify the ^{13}C-^{19}F interactions) was found to be the efficiency and robustness of the proton decoupling. In rigid solids, the lifetime of the ^{19}F spin states was found to be an additional critical factor.

3.4 Labelled Materials. – A new technique for restoring nuclear magnetic dipole-dipole couplings under MAS in solid state NMR spectroscopy has been described by Chan and Tycko.[38] In this technique, called broadband rotational resonance (BroBaRR), the coupling between a pair of nuclear spins with NMR frequency difference close to the MAS frequency is restored by the application of a train of weak RF pulses at a carrier frequency close to the average of the two NMR frequencies. Phase or amplitude modulation of the pulse train at half the MAS frequency splits the carrier into sidebands close to the two NMR frequencies. The pulse train then removes offsets from the exact rotational resonance condition, leading to dipolar recoupling over a bandwidth controlled by the amplitude of the pulse train. ^{13}C NMR experiments on uniformly ^{13}C,^{15}N-

labelled L-valine •HCl •H_2O powder were used to validate the theoretical analysis. BroBaRR is expected to be useful in studies of molecular structures by solid state NMR, for example in the detection of long-range couplings between carbons in uniformly labelled organic and biological materials

A highly sensitive solid state ^{19}F NMR strategy has been described to determine the orientation and dynamics of membrane-associated peptides from specific fluorine labels.[39] Several analogues of the antimicrobial peptide PGLa were synthesised with the non-natural amino acid 4-trifluoromethyl-phenylglycine (CF_3-Phg) at different positions throughout the α-helical peptide chain. A simple ^{19}F experiment allowed the simultaneous measurement of both the anisotropic chemical shift and the homonuclear dipolar coupling within the rotating CF_3-group in a macroscopically oriented membrane sample. The value and sign of the dipolar splitting determines the tilt of the CF_3-rotational axis, which is rigidly attached to the peptide backbone, with respect to the external magnetic field direction. Using four CF_3-labelled peptide analogues it was confirmed that PGLa is aligned at the surface of lipid membranes with its helix axis perpendicular to the bilayer normal at a peptide:lipid ratio of 1:200. The azimuthal rotation angle of the helix was also determined. It has been shown that the new approach allows highly sensitive NMR measurements over a wide range of experimental conditions and dynamic regimes of the peptide.

An improved variant of the popular double cross-polarisation (DCP) experiment for heteronuclear dipolar re-coupling in solid state NMR spectroscopy under MAS was introduced by Bjerring and Nielsen.[40] By simple phase and amplitude modulation of the RF irradiation at the Hartman-Hahn sideband conditions, the new pulse sequence, dubbed *i*DCP, was shown to enable broadband excitation with the high efficiency of γ-encoded coherence transfer. The efficiency and robustness of *i*DCP towards isotropic chemical shift variations and chemical shift anisotropies in the case of uniformly ^{13}C,^{15}N-labelled proteins has been demonstrated numerically and experimentally by ^{15}N to ^{13}C coherence transfer for ^{15}N-labelled *N*-Ac-L-valyl-L-leucine and ^{13}C,^{15}N-labelled-L-threonine.

Petkova and Tycko have described investigations of the effects of rotational resonance (R^2) on solid state ^{13}C NMR spectra of uniformly ^{13}C-labelled samples obtained under MAS.[41] The utility of R^2 measurements as structural probes of peptides and proteins with multiple uniformly labelled residues has been demonstrated. Results for uniformly ^{13}C-labelled L-alanine and L-valine in polycrystalline form and for amyloid fibrils formed by the 15-residue peptide with uniform labeling of a four-residue segment have been reported. The MAS NMR spectra revealed a novel *J*-decoupling effect at R^2 conditions that may be useful in spectral assignments for systems with sharp ^{13}C MAS NMR lines. Pronounced dependences of the apparent isotropic ^{13}C NMR chemical shifts on MAS frequency near R^2 conditions were also observed. The feasibility of quantitative ^{13}C-^{13}C distance determinations in L-valine, and qualitative determinations of inter-residue ^{13}C-^{13}C contacts in fibrils has been demonstrated. In addition, it has been shown that a 'relayed' R^2 technique can be useful in structural measurements on systems with poorly resolved ^{13}C MAS NMR lines.

The experimental lineshapes of the carboxyl and methyl carbon resonances of fully ^{13}C enriched L-Alanine have been studied in detail at different MAS frequencies and decoupling field strengths.[42] Complex lineshapes at intermediate spinning speeds were explained by the joint effect of off rotational resonance and coherent CSA-dipolar cross-correlation. It was found that coherent CSA-dipolar cross-correlation introduces either a differential intensity and/or a differential broadening of the lines of the *J*-multiplet. The conditions that lead to such effects were explained and experimentally verified. Additional simulations showed that these effects can be expected over a wide range of static magnetic fields and are not restricted to L-Alanine.

Spin-state selection in solid state NMR has been demonstrated, using pulse sequences similar to those used in solution NMR.[43] Different transitions of all three carbon resonances in fully ^{13}C-labelled L-alanine were separated in different spectra. By selecting spin-states, the contribution of the *J*-coupling to the linewidth was removed, leading to a considerable enhancement in resolution. The spin-state selective technique was demonstrated for MAS frequencies from 6 to 35 kHz. Other experimental conditions affecting the sensitivity of the experiments were also discussed. Sensitivity losses due to the introduction of the spin-state selective filter were shown to be acceptable. In addition, spin-state selection was used to experimentally confirm the differential broadening expected for the two transitions of the CH_3 resonance.

3.5 NMR Parameter Measurements. – Here we include new NMR techniques used for measuring chemical shift anisotropies and dipolar couplings. In particular, a novel method for accurate determination of small chemical shielding anisotropy was described by Asakawa.[44] This method is based on the adiabatically ramped spin-locking of transverse magnetisation. It relies on the fact that in the presence of chemical shielding and the ramped spin-locking RF field the equation for the time evolution of the spin dynamics for a system is analogous to that for the case of homonuclear magnetic dipolar coupling. It was shown that by carrying out experiments under the on-resonance condition, the span and skew values could be determined. The sample of L-alanine was used. The asymmetry of the chemical shift anisotropy tensor for the C_β was shown to be due to the asymmetrical molecular field, which was further supported by the *ab initio* chemical shielding calculations.

Heavy NMR active nuclei such as ^{195}Pt, ^{199}Hg, and ^{207}Pb are known to be extremely sensitive to their local environment and as such have very large chemical shift ranges. In the solid state, such nuclei commonly exhibit chemical shifts that range well over 1000 ppm, depending upon the orientation of the molecule within the applied magnetic field. Thus, acquiring NMR spectra of polycrystalline samples is often an experimental challenge because of these very broad powder patterns. The utility of the CPMG experiment and a modified CPMG experiment in characterizing NMR chemical-shift powder patterns for spin-1/2 nuclei has been demonstrated.[45] Several examples were provided that demonstrate a considerable time saving on using the CPMG experiment as opposed to the standard single pulse or spin-echo experiments. In general, this

time saving was shown to be even greater if a modified CPMG experiment is used. Homonuclear dipolar interactions were considerably reduced in the CPMG experiment and were almost completely removed in the modified CPMG experiment. For samples containing protons, larger enhancements were realised by combining the CPMG experiment with CP. The principal components of the chemical shift tensors were determined for each of the samples studied using the CPMG and modified-CPMG experiments.

A new solid state NMR pulse sequence has been described that accomplishes efficient broadband dipolar recoupling in systems with small dipolar couplings and large chemical shift anisotropies.[46] The method involves a supercycled symmetry-based recoupling sequence incorporated in a constant-interval data acquisition strategy. The supercycle removes destructive higher-order average Hamiltonian terms, and makes the method more robust at long time intervals. For diammonium [1,4-$^{13}C_2$]-fumarate used the corresponding ^{13}C-^{13}C dipolar coupling was estimated to be 136.5 ± 5.1 Hz.

A novel MAS NMR approach has been presented for the determination of motionally averaged heteronuclear dipolar couplings in unoriented materials.[47] The technique is based on the proton-detected local field protocol and achieves dipolar recoupling by R-type RF irradiation. The experiment, which is called R-PDLF spectroscopy, is demonstrated on solid and liquid-crystalline systems. For mobile systems, it is shown that the R-PDLF scheme provides better dipolar resolution as compared to techniques combining conventional separated local field spectroscopy with R-type recoupling.

3.6 Cross-Polarisation and Polarisation Transfer. – Continuous-wave, ramped amplitude, and frequency modulated CP schemes (abbreviated as CWCP, RACP, and FMCP, respectively) were evaluated for static samples in anisotropic phases, such as peptides oriented in lipid environments.[48] It has been shown experimentally that both RACP and FMCP give rise to 20% higher polarised signal intensity in comparison to CWCP. The CP matching bandwidths for CWCP and RACP were about the same. Because of its adiabaticity, FMCP was shown to have a much broader CP matching bandwidth than CWCP and RACP. A sample of [^{15}N]-Leu labelled gramicidin A oriented in lipid bilayers was used to demonstrate these experiments.

Tycko has shown that the sensitivity of 2D ^{13}C-^{13}C solid state NMR spectroscopy under MAS can be enhanced by the use of transverse polarisation transfer in place of the conventional longitudinal polarisation transfer.[49] Experimental results were reported for 2D spectroscopy of a 20-residue, filament-forming peptide, containing five uniformly ^{13}C-labelled residues, performed at 14.1 T with high-speed MAS and with finite pulse RF-driven recoupling of dipolar interactions in the mixing period. Significant sensitivity enhancements observed at short mixing periods results from a more rapid build-up of cross-peaks under transverse mixing than under longitudinal mixing.

A new NMR method for the characterisation of materials at different length scales has been proposed by Alonso and Massiot.[50] It combines a selection of ^{1}H-^{13}C pairs by a through-bond polarisation transfer and exploration of larger

distances by the introduction of ^{1}H spin diffusion. This characterisation method is adapted to the highest MAS rates. The effect of ^{1}H dephasing on the efficiency of the ^{1}H-^{13}C through-bond polarisation transfer was determined allowing the quantification of signals. Mesostructured spherical silica-based particles were studied by this multi-scale characterisation method. Contrasted spin diffusion curves were found and qualitatively explained by differences in terms of mobility and spatial distributions.

A new adiabatic double quantum polarisation transfer experiment has been proposed, which is an adiabatic variant of the POST-C7 experiment.[51] A continuous variation of the phase increment between pulses in this experiment leads to the introduction of a fictitious Zeeman field that allows for an adiabatic passage through the recoupling condition. This results in a chemical shift offset-compensated adiabatic experiment, which leads to an efficient and broadbanded polarisation transfer or to a double quantum excitation.

3.7 Recoupling Experiments. – The average Hamiltonian theory (AHT) of several classes of symmetry based RF pulse sequences has been developed to second order, allowing quantitative analyses of a wide range of recoupling and decoupling applications in MAS NMR.[52] General closed analytical expressions have been presented for a cross term between any two interactions recoupled to second order AHT. The results are applied to examine a novel homonuclear recoupling strategy. General features and design principles of such triple quantum recoupling sequences are discussed. Numerical simulations and experiments are used to demonstrate that they provide more efficient excitation of ^{13}C triple quantum coherences compared to previous techniques. Uniformly ^{13}C labelled alanine and tyrosine were used. Second order recoupling-based ^{13}C homonuclear triple quantum correlation spectroscopy was introduced and demonstrated on tyrosine.

Rotor modulations and recoupling strategies suitable for molecular orientation and dynamics studies by ^{13}C solid state MAS NMR spectroscopy have been presented by Fishbach *et al.*[53] In general, recoupling strategies for anisotropic interactions enable the investigation of molecular structure, order and dynamics in a sensitive and site-specific fashion by solid state NMR spectroscopy. Whereas MAS efficiently averages anisotropic interactions and enhances spectral resolution, recoupling pulse sequences selectively restore certain parts of rotor-modulated dipole-dipole couplings or chemical shift anisotropies. In principle, it is possible to recouple certain terms of an interaction Hamiltonian, which exhibit different orientation dependencies and, in this way, provide a means of distinguishing whether the observed NMR spectra are affected by molecular motion or by molecular orientation. As demonstrated by Fishbach *et al.*,[53] sideband patterns generated by reconversion rotor encoding allow for a precise and selective determination of coupling constants and anisotropies, which contain site-specific information on structure, orientation and/or dynamics of individual molecular segments. Corresponding recoupling schemes have been presented in a common context, and the possibilities of exploiting these effects for the determination of order parameters of oriented materials, such as oriented polymer

chains or extruded fibres of a discotic mesogen, have been discussed. The obtained orientational order parameters were compared to results from 2D wide-angle X-ray scattering.

A new pulse sequence has been described for the recoupling of heteronuclear dipolar interactions under MAS.[54] The method is similar to the PISEMA experiment, but employs a well-defined amplitude modulation of one of the two RF fields. The technique was used for measurements of ^{1}H-^{13}C dipolar couplings in unoriented solid and liquid-crystalline samples.

Enhanced symmetry-based dipolar recoupling pulse sequences have been described, which provide efficient dipolar recoupling in MAS NMR.[55] For homonuclear and heteronuclear recouplings, it has been shown that the dipolar scaling factors may be increased by replacing previously introduced pulse elements of such sequences by windowed ones. Uniformly ^{13}C-labelled glycine and alanine powders were used to illustrate the advantages of the new pulse sequence. The limitations of the proposed windowed pulse sequences and their use in other recoupling scenarios were also discussed.

3.8 Selective Pulses and Phase Cycling. – Computer-optimised selective pulses are routinely used in solution NMR spectroscopy. At the same time, their utility and importance for solid state applications is rather restricted. A new computational approach has been introduced by Veshtort and Griffin that makes the design of soft selective pulses with desired properties relatively straightforward.[56] By applying this technique to the generic selective excitation problem, the authors have arrived at a family of high performance selective excitation pulses, dubbed E-Family, that allows more flexibility and better performance than analogous pulses previously reported in the literature. The new pulses have been successfully tested in both solution and solid state NMR experiments. A theoretical treatment of the effects of chemical shift anisotropy on the selective excitation in MAS experiments in solids is also presented. The set of heuristics that comprise the new strategy were incorporated into a general NMR simulation program SPINEVOLUTION.

Cogwheel phase-cycling schemes were applied by Ivchenko *et al.* to sideband suppression and sideband separation experiments in solid state NMR.[57] It has been shown that cogwheel phase cycles lead to the elimination of most pulse imperfection effects, while using far fewer experimental signal acquisitions than conventional phase-cycling methods.

3.9 Quantitative Measurements. – A new scheme combining a Lee-Goldburg (LG) sequence with frequency modulation has been proposed for CP (LG-FMCP) in solid state MAS NMR.[58] During the CP contact time, the ^{1}H magnetisation is spin-locked along the magic angle by the LG sequence and the irradiation offset of the S spins (*e.g.*, ^{15}N) is modulated sinusoidally with a constant RF amplitude. It is shown experimentally that the LG sequence significantly lengthens the ^{1}H spin-lattice relaxation time in the tilted rotating frame and that the frequency modulation shortens the CP time for non-protonated *S* spins. As a result of substantially increasing the difference in these relaxation

rates, the non-protonated and protonated S spins can be more efficiently and more uniformly polarised with a relatively long CP contact time, making quantitative CP measurements possible. A sample of lyophilised $^{15}N(\delta_1)$-L-histidine and a $^{15}N(\delta_1)$-L-His labelled transmembrane helical peptide in hydrated lipid bilayers were used to illustrate the advantages of this scheme.

^{13}C CP MAS NMR is widely used as a non-destructive technique to measure the distribution of carbon types in humic substances. Although it is well known that quantification of CP MAS is problematic because different parts of the spectrum have different optimal contact times, a single contact time is used in most studies and in such cases ^{13}C CP MAS NMR is only qualitative. It has been shown that the use of variable contact time experiments and back-extrapolation of the signals for the various chemical shift regions significantly improves quantification of ^{13}C CP MAS NMR.[59] Because signals decrease markedly during the beginning of an experiment, samples need a steady-state condition before acquisition of the FID. The authors have shown that well-defined processing of the raw data significantly improves the quality of measurements. The effect of these various treatments on overall accuracy is also discussed.

3.10 Quadrupolar Nuclei. – A geometrical description of the quadrupolar interaction has been presented.[60] First- and second-order effects on all transitions were represented by quadrics and quartics. This approach allows a simple and exhaustive description of the Solomon multiple echoes; the location of the echoes in the time domain, as well as their nature, is determined without calculation. Experimental evidence of multiple echoes in the case of an Al-O-P cluster is presented. In addition, the selection of double quantum coherences by appropriate phase cycling is presented. DAS and MQ MAS experiments are also described in this particular frame.

A robust, easy to optimize, and efficient homonuclear correlation NMR experiment for half-integer quadrupolar nuclei in solids has been described and has been experimentally tested on anhydrous Na_2HPO_4 by ^{23}Na NMR and as-synthesised $AlPO_4$-14, an aluminophosphate molecular sieve, by ^{27}Al NMR.[61]

A comprehensive experimental and numerical study of the potential of fast amplitude (FAM) irradiation for improving the triple quantum MAS NMR spectra of half-integer $I > 1/2$ nuclei (^{23}Na, ^{27}Al, ^{45}Sc, ^{93}Nb) has been presented.[62] Materials of academic and industrial importance, such as infrared-emitter $Na_3YSi_3O_9$, microporous aluminophosphate VPI-5, mineral andalusite, calcined kaolinite and Sc_2O_3 were investigated. It was found that fast amplitude pulses are indeed of practical relevance and particularly useful for the observation of the NMR resonances given by nuclei in distorted local environments (*i.e.* exhibiting large quadrupole coupling constants). In addition, a novel strategy for the optimisation of the FAM-II MQ MAS NMR experiment, which improves the multiple- to single-quantum coherence transfer efficiency, was also reported.

Two signal enhancement schemes capable of providing large signal-to-noise gains in static and MAS NMR spectra of the central transition of half-integer quadrupolar nuclei have been presented by Schurko *et al.*[63] Amplitude-modulated double-frequency sweeps (AM-DFS) and rotor-assisted population

transfer (RAPT) pulse sequences were used as preparatory sequences in combination with the quadrupolar-CPMG pulse sequence to obtain large signal enhancements ranging from one to two orders of magnitude. Specific applications to two spin-3/2 nuclei (^{87}Rb and ^{39}K) and one spin-5/2 nucleus (^{85}Rb) were presented.

Rotor-assisted population transfer has been developed as a method for enhancing MAS NMR sensitivity of quadrupolar nuclei by transferring polarisation associated with satellite transitions to the central $m = 1/2 \rightarrow -1/2$ transition.[64] After a single RAPT transfer, there still remains polarisation in the satellite transitions that can be transferred to the central transition. This polarisation is available without having to wait for the spill system to return to thermal equilibrium. A new RAPT scheme has been described that uses the remaining polarisation of the satellites to obtain a further enhancement of the central transition by performing RAPT-enhanced experiments multiple times before waiting for re-equilibration of the spin system. For ^{27}Al ($I = 5/2$) in albite a 48% increase over single RAPT was obtained. For ^{93}Nb ($I = 9/2$) in $NaNbO_3$ an 89% increase over single RAPT was obtained. A data processing procedure is also described for obtaining the maximum possible signal-to-noise ratio.

The extension of their previously developed low temperature method to an 18.8 T system has been described by Lipton *et al.*[65] A new probe was used with a cross coil and variable capacitors that are operational at cryogenic temperatures. The limitations to sensitivity are discussed, including a new diode network, the utilisation of a cryogenic band pass filter, and the consequences of the RF profiles of the coil. Further, details of the spectroscopy of quadrupolar nuclei in a protein are discussed, such as the observation of the outer transitions and how to distinguish them from the desired $\pm 1/2$ transition.

3.11 Instrumental developments. – Strategies for successful solid state NMR experiments in high-field Bitter and hybrid magnets have been discussed and implemented on an older generation 24 T system.[66] In general, the stability and homogeneity of this type of magnets did not meet the requirements for most NMR experiments. Nevertheless, the authors have shown that a new type of shimming with ferromagnetic inserts, combined with feedback control of the power supply and NMR reference deconvolution can be used to obtain well-resolved solid state NMR spectra. They also demonstrate that this approach is especially useful for the study of half-integer quadrupolar nuclei. Experimental examples included static and MAS ^{27}Al NMR spectra of minerals, such as sillimanite and andalusite.

A home-built solid state NMR probe for membrane protein studies has been described by Kim *et al.*[67] Proteins in highly oriented lipid bilayer samples are useful to study membrane protein structure determination. Planar lipid bilayers aligned and supported on glass slide were prepared. The stack of glass slide with planar lipid bilayers is not well fit for commercial solid state NMR probe with round coil. Therefore, homebuilt solid state NMR probe was built by Kim *et al.* The overall filling factor of the coil was much better and the large surface area increased the extent to orientation by providing uniform environments for the

phospholipids. ^{1}H and ^{15}N double resonance probe for 400 MHz NMR (9.4T) with a flat coil (coil size: 11 mm × 20 mm × 4 mm) was constructed and tested. In another paper on probe design, solenoid microcoils with an inner diameter of 300-400 μm were developed for the study of mass-limited solid samples.[68] Special attention was paid to the mechanical properties of the probes allowing sample changing. The performance, in terms of sensitivity and RF-characteristics, of these probeheads was studied for ^{1}H, ^{31}P, and ^{27}Al in different model compounds in view of the feasibility of specific applications. A specific advantage of microcoils for solid state NMR applications is that they can generate extremely high RF-fields if implemented in appropriate circuits. Using RF-powers in the hundreds of Watts range, RF-fields well in excess of 1 MHz can be generated. This allows the excitation of spectra of nuclei the resonance lines of which are dispersed over several MHz. The latter is particularly useful for quadrupolar nuclei experiencing large quadrupolar interactions.

4 Distance and Angle Measurements by Solid State NMR

A simple method to compensate for pulse-angle errors in rotational-echo double resonance (REDOR) experiments for determining heteronuclear distances in solids has been presented.[69] By using composite π pulses on the unobserved dephasing spin and EXORCYCLE for the single π pulse on the observed channel, the REDOR curve is shown to become much less sensitive to pulse angle errors. Both improvements are demonstrated by experiments on the model compound, $^{13}C^{\alpha}$,^{15}N-labelled *N-t*-BOC-glycine, and are confirmed by numerical simulations. The advantage of EXORCYCLE is also shown analytically using the product operator formalism. The proposed simple schemes compensate for unavoidable pulse angle errors that arise, for example, from RF field inhomogeneity. They also make REDOR experiments more accurate and robust for low-sensitivity samples where direct pulse length calibration is difficult.

Solid state NMR has been employed to determine a number of distances and torsion angles in an elastin-mimetic peptide, $(VPGVG)_3$, to understand the structural basis of elasticity.[70] Elastin is an extracellular-matrix protein that imparts elasticity to tissues. The C . . . H and C . . . N distances between the V6 carbonyl and the V9 amide segment were measured using ^{13}C-^{15}N and ^{13}C-^{1}H rotational-echo double-resonance experiments. The results indicate the coexistence of two types of intramolecular distances: a third of the molecules have short C-H and C-N distances of 3.3 ± 0.2 and 4.3 ± 0.2 Å, respectively, while the rest have longer distances of about 7 Å. Complementing the distance constraints, the authors measured the (ϕ,ψ) torsion angles of the central pentameric unit using dipolar correlation NMR. The ψ-angles of P7 and G8 were ~ 150°, thus restricting the majority of the peptide to be extended. Combining all torsion angles measured for the five residues, the G8 C^{α} chemical shift, and the V6-V9 distances, a bimodal structure distribution for the PG residues in VPGVG was obtained. The observed conformational distribution around Pro and Gly has been related to the molecular mechanism of elastin elasticity.

Computations of the proton chemical shift by DFT for the intermolecular hydrogen bond in the white form of methylnitroacetanilide, together with the experimental value obtained by high-speed MAS NMR were used by Harris *et al.* to determine the N-H distance as 1.03 ± 0.02 Å.[71]

The relative merits of different isotopic enrichment strategies that might be used in solid state NMR protein structure determinations have been discussed by Gehman *et al.*[72] The basis for comparison of these merits is the determination of the relative uncertainties in rates measured by a generalised dipolar recoupling experiment. The different schemes considered use ^{13}C, ^{15}N and ^{2}H labelling of ubiquitin with homonuclear magnetisation-transfer type experiments under MAS. Specific attention is given to the sensitivity of the predicted relative precisions to variation in natural nuclear density distribution and noise levels. A framework is suggested to gauge the precision of measurement of a given dipolar coupling constant, and the potential for a set of such measurements to constrain structure calculations is explored. The distribution of nuclei in homonuclear ^{15}N and ^{1}H dipolar recoupling spin-exchange experiments appeared to provide the most promising tertiary structure information for uniformly labelled ubiquitin It has been demonstrated that internuclear distances can be evaluated from rotational-resonance experiments in uniformly ^{13}C-labelled compounds.[73] The errors in the obtained distances are less than 10%, without the need to know any parameters of the spin system except the isotropic chemical shifts of all spins. The multi-spin system with a simple fictitious spin-1/2 model has been described. The influence of the couplings to the passive spins (J and dipolar coupling) is described by an empirical constant offset from the rotational resonance condition. Using simulated data for a three-spin system, the authors showed that the two-spin model describes the rotational-resonance transfer curves well as long as none of the passive spins is close to a rotational-resonance condition with one of the active spins. The usability of the two-spin model is demonstrated experimentally using a sample of acetylcholine perchlorate with labelling schemes of various levels of complexity. Doubly-, triply-, and fully labelled compounds led to strongly varying rotational resonance polarisation transfer curves but the evaluated distances using the two-spin model were identical within the expected error limits and coincided with the distance from the X-ray structure. It was shown that rotational resonance distance measurements in fully labelled compounds allow the measurement of weak couplings in the presence of strong couplings.

Solid state NMR methods for the determination of internuclear dipole-dipole couplings between homonuclear spin-1/2 nuclei have been presented by Gunne.[74] The methods considered are suitable for relatively dense dipolar networks which are still dominated by two-spin interactions. Symmetry derived pulse sequences with improved compensation against chemical shift anisotropies were found assuming a small isotropic chemical shift difference and using numerical calculations of the spin dynamics. It has been shown that a constant time procedure can be used to acquire reliable double quantum build up curves even in systems in which damping obscures oscillations in their symmetric build up curve. This technique has been demonstrated on four crystalline model com-

pounds with ^{31}P and ^{13}C spin systems typical for inorganic and biological applications. Comparison to crystal structure data indicates that the distances derived this way from ^{31}P and ^{13}C double quantum NMR carry only small systematic errors caused for example by anisotropic *J*-coupling, dipolar contributions from adjacent spins and relaxation.

Identification of NH . . . N hydrogen bonds by solid state MAS NMR in a double-stranded RNA associated with myotonic dystrophy has been reported by Leppert *et al.*[75] RNA plays a central role in biological processes and exhibits a variety of secondary and tertiary structural features that are often stabilised *via* hydrogen bonds. The distance between the donor and acceptor nitrogen nuclei involved in NH . . . N hydrogen bonds in nucleic acid base pairs is typically in the range of 2.6-2.9 Å. Leppert *et al.* showed that such spatial proximity between ^{15}N nitrogen nuclei can be conveniently monitored *via* MAS NMR on a uniformly ^{15}N-labelled RNA. The presence of NH . . . N hydrogen bonds is reflected as cross-peaks between the donor and acceptor nitrogen nuclei in 2D ^{15}N dipolar chemical shift correlation spectra.

A combination of $^{15}N\{^{19}F\}$, $^{31}P\{^{15}N\}$, and $^{31}P\{^{19}F\}$ REDOR NMR has been used to characterise the conformation of a bound trifluoromethylketal, shikimate-based bisubstrate inhibitor of 5-enolpyruvylshikimate-3-phosphate synthase.[76] The solid state NMR experiments were performed on the complex formed in solution and then lyophilised at low temperatures in the presence of stabilizing lyoprotectants. The results of these experiments indicate that none of the side chains of the six arginines that surround the active site forms a compact salt bridge with the phosphate groups of the bound inhibitor.

$^{19}F/^{29}Si$ REDOR, θ-REDOR and Hartmann-Hahn CP NMR techniques have been applied under fast MAS to a powder sample of fluoride-containing octadecasil.[77] The internuclear distance of the ^{19}F-^{29}Si spin pairs deduced directly from the CP and REDOR measurements was in good agreement with the X-ray crystal structure.

MAS NMR has been used to probe the local structure of as-made zeolite SFF containing occluded fluoride and *N,N*-diethyl-2,6-dimethylpiperidinium.[78] The Si-F bond distance has been measured using two methods: variable contact time CP studies (1.74 Å) and spinning sideband intensity fitting at relatively slow spinning speeds (1.79 Å). Both measurements yield results that were significantly shorter than the internuclear Si-F distance as measured by single-crystal X-ray diffraction ($\sim$1.9 Å), which is based on the average positions of the atoms due to disorder and hence does not reflect the true bond distance.

Olsen *et al.* have performed solid state $^{31}P/^{19}F$ REDOR NMR experiments for the determination of DNA minor groove width in distamycin-DNA complexes.[79] Binding of a single drug molecule was found to cause a 2.4 Å decrease in the groove width. The $^{31}P/^{19}F$ REDOR results demonstrate the ability of solid state NMR to measure distances in the range of 7-14 Å in DNA-drug complexes and provide the first example of a direct spectroscopic measurement of minor groove width in nucleic acids.

A new procedure for the site-selective measurement of heteronuclear magnetic dipole-dipole interactions involving quadrupolar nuclei has been developed.[80]

Particular attention is given to the case of $S\{I\}$ REDOR with $S = 1/2$ and $I = 3/2$, where the nuclear electric quadrupole splitting affects the efficiency of the π_I pulses in recoupling the S-I dipolar interactions. Detailed two- and three-spin simulations using the SIMPSON code indicated that the REDOR response is sensitively affected by the quotient of the nutation frequency and the nuclear electric quadrupole frequency. It was shown that multispin systems could be conveniently analysed using a curvature determination of REDOR data in the limit of short dipolar evolution times to yield dipolar second moment values. Based on this finding, a robust method has been developed to analyse experimental REDOR data in multispin systems, in terms of average dipolar M_2 values, which are affected by distributions of magnetic dipolar and nuclear electric quadrupolar coupling constants only to a minor extent. Validation experiments on suitable model compounds indicated that dipolar M_2 values can be measured within 10% accuracy in this fashion for crystalline compounds. For glasses, the accuracy is expected to be lower, because of possible cumulative errors that may occur from unknown geometries and distribution effects. Experiments conducted on glassy sodium phosphates indicated that the ^{31}P-^{23}Na dipolar interaction strengths in these systems are differentiable for the various Q sites and increase as the charge of the phosphate moiety increases.

5 NMR Parameters: Experimental and Theoretical Studies

5.1 Chemical Shift and its Anisotropy: Spin 1/2 Nuclei. – Calculations of NMR chemical shifts in crystalline phases of some representative amino acids such as glycine, alanine, and alanyl-alanine have been reported.[81] The effect of environment on the chemical shifts was explored in selected glycine geometries ranging from the crystalline phase to completely isolated molecules. In the crystalline and dilute molecular limits, the calculated distinct NMR chemical shifts have been attributed to intermolecular hydrogen bonds and dipole electric field effects, respectively.

Density functional theory combined with the continuous set of gauge transformations (CSGT) method was employed to calculate chemical shielding of the carbonyl carbon (^{13}CO) and nitrogen (^{15}N) atoms of the backbone amide groups in ω-conotoxin GVIA, as well as α- and β-carbon shielding.[82] Experimental ^{13}C and ^{15}N chemical shifts were determined using multidimensional NMR spectroscopy. The 3D solution structure of ω-conotoxin was solved using a hybrid distance geometry-simulated annealing protocol. Peptide fragments with experimentally measured bond lengths, bond angles, and torsion angles were used as model structures in the CSGT-DFT calculations. Linear correlation plots were constructed to compare theoretical data with experiment.

The xenon and fluorine magnetic shielding tensors, σ, of XeF2 were measured using solid state ^{129}Xe and ^{19}F NMR spectroscopy and nonrelativistic and spin-orbit relativistic zeroth-order regular approximation density functional theory (ZORA DFT).[83] Analysis of ^{129}Xe and ^{19}F NMR spectra acquired with MAS at several spinning rates indicated that the Xe and F magnetic shielding

tensors are axially symmetric, as determined by the crystal symmetry. The isotropic ^{129}Xe chemical shift was found to be -1603 $\pm$ 5 ppm with respect to $OXeF_4$ (neat liquid, 297K) and the Xe magnetic shielding anisotropy was 4245 $\pm$ 20 ppm, the first anisotropy measured directly for a xenon compound. The value of the parallel component of the experimentally determined xenon chemical shift tensor, $\delta_{//}$ = -4433 ppm, reveals that relativistic effects play an important role in the nuclear magnetic shielding for xenon. Both the sign and magnitude of the isotropic indirect $^{129}Xe,^{19}F$ nuclear spin-spin coupling constant were determined, -5560 $\pm$ 50 Hz. The ZORA DFT method has been employed to calculate σ(Xe) and σ(F) for isolated XeF_2 and XeF_4 molecules, as well as σ(Kr) and σ(F) for an isolated KrF_2 molecule, at the relativistic and nonrelativistic levels of theory. Spin-orbit relativistic DFT results for Xe chemical shift snisotropy were in very good agreement with those determined experimentally and highlight the importance of relativistic effects.

5.2 *J*-Couplings. – In MAS NMR, the homonuclear *J*-couplings between pairs of spin-1/2 nuclei may be determined by studying the modulation of the spin echo induced by a π-pulse, as a function of the echo duration. The theory of *J*-induced spin-echo modulation in MAS NMR has been reported, and a set of modulation regimes has been derived which apply under different experimental conditions.[84] It was found that in most cases the dominant spin-echo modulation frequency is exactly equal to the *J*-coupling and that the chemical shift anisotropies and dipole-dipole couplings tend to stabilise, rather than obscure, the *J*-modulation. The theoretical conclusions were supported by numerical simulations and experimental results obtained for three representative samples containing ^{13}C spin pairs

Small scalar *J*-couplings between quadrupolar nuclei and spin-1/2 have been measured in inorganic solids using *J*-Resolved experiments.[85] These were further used to acquire 2D *J*-HMQC heteronuclear correlation spectra, giving detailed insight into the chemical bonding scheme in the solid state.[85]

In the study by Forgeron *et al*, one-bond $^{31}P,^{31}P$ indirect nuclear spin-spin coupling tensors, $^1J(^{31}P,^{31}P)$, were calculated using nonrelativistic and relativistic ZORA DFT methods for various model molecules and ions.[86] In the models chosen the values of $^1J_{iso}(^{31}P,^{31}P)$ varied from approximately -480 to +770 Hz, thereby spanning the known range of experimentally measured one-bond $^{31}P,^{31}P$ indirect nuclear spin-spin coupling constants. However, in many cases, the sign of $^1J_{iso}(^{31}P,^{31}P)$ has not been determined by experiment. From the DFT results for $^1J_{iso}(^{31}P,^{31}P)$ and the anisotropy of *J* were found to be in qualitative agreement with experimental values. Furthermore, the DFT calculations provided the absolute sign of $^1J_{iso}(^{31}P,^{31}P)$ in cases where it was unknown experimentally. A number of empirical trends between $^1J_{iso}(^{31}P,^{31}P)$ and various structural parameters were reproduced by theoretical calculations. Inspection of the mechanisms which contribute to $^1J_{iso}(^{31}P,^{31}P)$ indicated that the Fermi contact mechanism dominates in all cases where formal single P,P bonds exist and that the paramagnetic spin-orbit mechanism is of equal or greater importance in comparison with the Fermi contact mechanism in cases where formal multiple P,P

bonds exist. Results from relativistic ZORA DFT calculations differ from the nonrelativistic calculations by less than 10%, indicating that inclusion of relativistic effects is not crucial, as anticipated, given that the systems investigated herein contain relatively light atoms.

The ^{31}P CP MAS NMR spectra have been reported for undoped and Fe-doped InP semiconductors.[87] The isotropic contribution of the electron-coupled nuclear spin-spin coupling of neighbouring $^{113/115}$In-^{31}P in the InP semiconductors were measured as $|J| = 225 \pm 10$ Hz.

5.3 Quadrupolar Nuclei. – ^{2}H chemical shift anisotropies have been determined for the first time for polycrystalline samples employing ^{2}H MAS NMR spectroscopy at high magnetic field strength (14.1 T).[88] The ^{2}H CSA is reflected as distinct asymmetries in the manifold of spinning sidebands observed for the two overlapping single-quantum transitions. Least squares fitting to the manifold of spinning sidebands allowed determination of the ^{2}H CSA parameters along with the quadrupole coupling parameters. This was demonstrated for KD_2PO_4, $ND_4D_2PO_4$, $KDSO_4$, $KDCO_3$, α-$(COOD)_2$, α-$(COOD)_2 \cdot 2D_2O$, and boehmite, which exhibit ^{2}H shift anisotropies in the range $13 \leqslant \Delta\sigma \leqslant 27$ ppm. For fixed values of the shift anisotropy and the ^{2}H quadrupole coupling it was shown that the precision of the CSA parameters depends strongly on the asymmetry parameter η_Q for the quadrupole coupling tensor, giving the highest precision for $\eta_Q \sim 0$. The ^{2}H CSA parameters ($\Delta\sigma$ and η) were in good agreement with ^{1}H CSA data reported in the literature for the corresponding protonated samples from ^{1}H NMR spectra employing various homonuclear decoupling techniques. It has been shown that the determination of ^{2}H quadrupole coupling parameters and ^{2}H (^{1}H) CSAs from the same ^{2}H MAS NMR experiment may be particularly useful in studies of hydrogen bonding since the ^{2}H quadrupole coupling constant and the CSA appear to characterise bond lengths in a hydrogen bond in a different manner.

^{14}N MAS NMR spectra for a number of polycrystalline, symmetrical tetraalkylammonium halides with short alkyl chains (C_2H_5- to n-C_4H_9-) have been recorded following a careful setup of the experimental conditions.[89] Analysis of the spectra demonstrated the presence of ^{14}N CSAs on the order of $\Delta\sigma = 10$-30 ppm along with ^{14}N quadrupole coupling constants in the range of 10-70 kHz. The magnitude and sign of the CSAs determined from ^{14}N MAS NMR were confirmed by the analysis of the corresponding slow-speed spinning (500-650 Hz) ^{15}N CP MAS NMR spectra. It was found that these CSAs are reflected in the spinning sideband intensities of the ^{14}N MAS spectra at much higher spinning speeds than can be applied to retrieve the corresponding ^{15}N CSAs from the spinning sideband pattern in the ^{15}N CP MAS spectra.

Solid state ^{17}O NMR spectroscopy has been employed to characterise powdered samples of known monoclinic and orthorhombic modifications of ^{17}O-enriched triphenylphosphine oxide, Ph_3PO.[90] Precise data on the orientation-dependent ^{17}O electric field gradient (EFG) and chemical shift tensors were obtained for both polymorphs. While the ^{17}O nuclear quadrupolar coupling constants were essentially identical for the two polymorphs [-4.59 $\pm$ 0.01 MHz

(orthorhombic) and -4.57 ± 0.01 MHz (monoclinic)], the spans (Ω) of the chemical shift tensors were distinctly different [135 ± 3 ppm (orthorhombic) and 155 ± 5 ppm (monoclinic)]. The oxygen chemical shift tensor was discussed in terms of Ramsey's theory and the electronic structure of the phosphorus-oxygen bond. The NMR results were in favour of the hemipolar σ-bonded R_3P^+-O^- end of the resonance structure continuum over the multiple bond representation. Indirect nuclear spin-spin (J) coupling between ^{31}P and ^{17}O was observed directly in ^{17}O MAS NMR spectra as well as in ^{31}P MAS NMR spectra. *Ab initio* and DFT calculations of the ^{17}O EFG, chemical shift and $^1J(^{31}P,^{17}O)$ tensors were performed with a variety of basis sets to complement the experimental data. An example chosen by the authors represents an interesting spin system for which the chemical shift, quadrupolar, indirect and direct dipolar interactions contribute significantly to the observed ^{17}O NMR spectra and demonstrates the wealth of information available from NMR studies of solid materials.

Electric field gradients of ^{23}Na and ^{27}Al in three model fluoride crystalline powders AlF_3, Na_3AlF_6 and $Na_5Al_3F_{14}$ were computed using the density functional based electronic structure code WIEN97 and compared to values derived from experimental NMR.[91] The results of measurements of ^{23}Na and ^{27}Al quadrupolar parameters in AlF_3, Na_3AlF_6 and $Na_5Al_3F_{14}$ were revisited by using high-resolution solid state NMR measurements. To determine chemical shifts and quadrupolar parameters with a high precision, the experimental procedure involved MAS, satellite transition spectroscopy and MQ techniques applied to the quadrupolar nuclei together with a simulation of the NMR spectra. In some cases the large discrepancies were observed compared to the previously published results, justifying the use of *ab initio* calculations of the corresponding EFG tensor based on the known structural data of the crystalline phases. The agreement obtained between these calculations and the experimental results, which were better than 10% in almost all cases, supported the reliability of the latest NMR and crystallographic data.

Application of the quadrupolar-CPMG sequence permitted the first natural abundance solid state ^{25}Mg NMR study of an organometallic magnesium compound, bis(cyclopentadienyl)magnesium.[92] Analytical and numerical simulations of both static and MAS quadrupolar-CPMG NMR spectra revealed an axially symmetric ^{25}Mg EFG tensor with a nuclear quadrupole coupling constant of 5.8 MHz. Restricted Hartree-Fock and hybrid density functional theory (B3LYP) calculations were in good agreement with experimental EFG values and predict a chemical shielding anisotropy of about 40-50 ppm. The parameters and orientation of the ^{25}Mg EFG tensor were rationalised from examination of the crystal structure and molecular symmetry. The NMR properties of the cyclopentadienyl rings were examined by ^{13}C CP MAS NMR, RHF and hybrid-DFT (B3LYP) calculations, and simulations of the effects of chemical exchange on the ^{13}C powder pattern.

6 Applications

6.1 Organic Solids. Separated local-field NMR spectroscopy under MAS

conditions has been employed as a means of studying molecular reorientation in solid inclusion compounds.[93] Site-resolved ^{1}H-^{13}C dipolar couplings were estimated in complexes between cryptophane-E and chloromethanes. It was found that the mobilities of encaged guests in the solid state and of guests inside the host cavity in the isotropic liquid solution are very similar.

Solvent molecules of water and acetone trapped in calix[4]hydroquinone supramolecular nanotubes have been studied by solid state ^{1}H and ^{2}H fast MAS NMR and DFT calculations.[94] It has been shown that both water and acetone molecules occupy well-defined average positions, but undergo fast reorientation motions during which their protons interchange their positions.

The nature of the phase transitions and proton-deuteron dynamics in the crystals of 9-hydroxyphenalenone derivatives have been investigated by means of solid state ^{2}H NMR spectroscopy.[95] It was found that the antiferroelectric ordering of deuterons along the hydrogen bonds in 5-methyl-9-deuterioxyphenalenone and 5-bromo-9-deuterioxyphenalenone occurs below the phase transition temperatures at 44 K and 34 K, respectively. The microscopic origin of the incommensurate modulation in 5-bromo-9-deuterioxyphenalenone below 34 K was attributed to slight rotational displacements, which are fixed at commensurate angles below the lock-in transition at 22 K.

^{1}H, ^{13}C, ^{17}O and ^{31}P NMR parameters, including chemical shift tensors and quadrupolar parameters for ^{17}O, have been calculated for phenylphosphonic acid, $C_6H_5PO(OH)_2$, under periodic boundary conditions.[96] The results were in good agreement with experimental data and allowed the unambiguous assignment of all the sites present in the structure. In particular, the ^{17}O NMR parameters of the P=O and P-OH environments were precisely determined, which is important for the characterisation of the bonding mode of phosphonate molecules in hybrid solids. In addition, the effects of intermolecular interactions on the NMR parameters were investigated by comparing the results of the calculations in the crystal and in an isolated molecule of phenylphosphonic acid.

The ^{1}H solid state NMR spectra of four sulfonamide derivatives of 1,2,4-benzothiadiazine-1,1-dioxides (thiazides) were recorded at different temperatures in the range 100-400 K and the temperature dependencies of the second moment (M_2) of the resonant line and spin-lattice relaxation time (T_1) were measured.[97] The minimum in the temperature dependence of the T_1 revealed an activation process related to the hindered rotation (jumps) of the $-NH_2$ group. The activation energy of this motion was estimated on the basis of the fit of the theoretical model to the experimental points and was close to that calculated by the DFT B3LYP/6-311 + G(2d,p) method for the model assuming the $-NH_2$ jumps between two equilibrium positions. Thiazides were also found to perform a quasi-isotropic tumbling whose activation energy was higher than that of the hindered jumps of the NH_2 group.

The dehydration of a thiamine hydrochloride (vitamin B_1) hydrate, commonly referred to as the monohydrate, was investigated by solid state NMR and X-ray diffraction.[98] The hydrate was classified as a nonstoichiometric solvate since the water content depends on the water vapor pressure of the surrounding atmos-

phere and essentially maintains the 3D molecular arrangement upon dehydration. The loss of water led to a shrinkage of the unit cell volume of about 5% and to a slight increase in the free volume. This was also accompanied by an increase in molecular motion, as demonstrated by solid state NMR ^{1}H and ^{13}C T_1 measurements. The largest change in T_1 was observed for the carbons of the hydroxyethyl functional group that is hydrogen bonded to the water molecules in the hydrate. It was confirmed that an increase in free volume results in an increase in molecular mobility.

Evidence for reorientation of imidazolium rings in imidazolium methylsulfonate has been demonstrated using solid state NMR.[99] This material is a model system for new proton-conducting materials based on imidazole. Two advanced NMR methods, including ^{1}H-^{13}C and ^{1}H-^{15}N recoupled polarisation transfer with dipolar sideband pattern analysis and analysis of the coalescence of ^{13}C lineshapes, were used to characterise the ring reorientation. The process was found to occur at temperatures well below the melting point of the salt, between 240 and 380 K, with single activation energy of 38 ± 5 kJ mol^{-1}.

The ^{13}C NMR CP MAS spectra of 2-naphthylphenylsulfoxide in the solid state were used to study the restricted rotation about the Ph-S bond.[100] Line shape simulations of the temperature-dependent spectra allowed the corresponding barrier to be determined in the solid state (14.7 kcal mol^{-1}). It was shown that by using the single-crystal X-ray structure, this barrier could be satisfactorily reproduced by theoretical calculations (14.5 kcal mol^{-1}) that take into account the correlated phenyl motion involving a large set of molecules in the crystalline state.

Various physicochemical characterisation techniques were used to study *tris*(5-acetyl-3-thienyl)methane (TATM) inclusion compounds with 1,*n*-dichloroalkane guests (n = 1-10).[101] Thermogravimetric analysis allowed to determine host-guest stoichiometric ratios. From the multiplicity of the host signals in the ^{13}C CP MAS NMR spectrum, the number of host molecules in the asymmetric unit of each inclusion compound was determined. It was found that only 1,9-dichlorononane and 1,10-dichlorodecane form isostructural TATM inclusion compounds. The obtained results were compared with those for urea-carboxylic acid complexes.

The crystal structure and solid state ^{13}C NMR of methyl α-D-mannofuranoside have been reported.[102] The hydrogen bonding patterns were found, consisting of O-H . . . O interactions which include the anomeric oxygen but exclude the ring oxygen atom. The analysis of ^{13}C CP MAS NMR chemical shifts for solid methyl α-D-mannofuranoside confirmed hydrogen-bonding pattern established by X-ray.

Hydrogen-bonded adducts of solid dicarboxylic acids of variable chain length $HOOC(CH_2)_nCOOH$ (n = 1-7) with solid 1,4-diazabicyclo[2.2.2]octane were studied by X-ray diffraction and solid state NMR.[103] The acid-base adducts, whether involving proton transfer from the COOH group to the *N*-acceptor, or the formation of neutral hydrogen bonds, showed a melting point alternation phenomenon analogous to that shown by the neutral carboxylic acids. It was shown that the ^{13}C chemical shift tensors of the COOH group obtained from the

spinning sideband analysis provide a reliable criterion for assigning the protonation state of the adducts.

Solid state NMR and powder X-ray diffraction of the two-component molecular complex composed of tryptamine and benzoic acid were used to investigate the nature of the intermolecular interaction in the molecular complex.[104] Both ^{13}C CP MAS NMR spectrum and powder X-ray diffraction pattern of the complex were different from the convolution of each spectrum of the single component. 2D ^{1}H-^{13}C HETCOR NMR indicated that the intermolecular interaction between the primary amine of tryptamine and the carboxyl group of benzoic acid must be related to the complex formation.

Solid state ^{13}C NMR measurements were made for the B2 and B4 phases of the achiral banana-shaped molecules.[105] In both phases, an NMR signal assigned to carbonyl carbons of the ester linkages appeared as doublets, showing that the two carbonyl carbons are in different electronic environments. The chemical shifts of the two peaks are 165.6 and 163.9 ppm in the B2 phase, and these values did not change on transformation into the low-temperature B4 phase. To explain this distinct splitting of the carbonyl carbon signal, various possibilities were considered. Based on the ^{13}C NMR results, it was concluded that the banana-shaped molecules exhibit a chiral twisted conformation.

The crystal structure of 1-(3′-methylphenylazo)-2-naphthylamine was determined by the X-ray diffraction method.[106] No dynamic disorder was observed in the crystalline state, and the azo group was found to adopt *trans*-conformation with six-membered ring formed by the intramolecular hydrogen bond. In the solid state, ^{13}C CP MAS NMR spectrum of its acetamide derivative the doublet signals were found. The DFT computations were employed for the conformational analysis of 2-naphthylamines.

The reversible solid state phase transition between the γ and α phases of oleic acid was followed by ^{13}C solid state NMR spectroscopy.[107] All the peaks in the γ and α phases were assigned based on the corresponding crystal structures determined by X-ray diffraction method. On the $\gamma \rightarrow \alpha$ phase transition at 271 K, the methyl-sided methylene carbons exhibited upfield shifts due to the gauche effect. Characteristic peaks shifts due to the conformational change of the *cis*-olefin group were observed for *cis*-olefin carbons. The peaks due to carboxyl-sided chains showed no large shifts on this transition. Each oleic acid carbon showed a discontinuous decrease in T_1, except for the methyl carbon, which was in the extreme narrowing limit in both phases.

Solid state NMR studies of 1,3-imidazolidine-2-thione, 1,3-imidazolidine-2-selenone and some of their *N*-substituted derivatives have been reported.[108] Spinning sidebands of thione and selenone carbons were analysed to yield chemical shift anisotropies for these carbons. The NMR spectrum of imidazolidine-2-thione showed some evidence for the presence of thiol tautomer. Molecular computations were carried out for imidazolidine-2-thione and its *N*-methyl derivative to yield relative energies of various possible tautomers.

VT studies of a polymorphic system comprising two pairs of enantiotropically related forms have been reported.[109] All four forms of [*S*,*S*]-ethambutol dihydrochloride have been characterised, and their relative thermodynamic relation-

ships have been investigated by VT solid state ^{13}C NMR, VT powder X-ray diffraction studies, differential scanning calorimetry and optical microscopy. Solid state NMR has been employed to study the structure of *p-tert*-butylcalix[4]arene inclusion compounds of fluorinated benzenes.[110]

^{13}C and ^{15}N NMR studies of the three solid forms of sulfanilamide have been reported.[111] These studies led to an interpretation of the solid state effects seen in CP MAS spectra. Relaxation times for the different forms were measured. These showed different behaviour for the three forms, arising from mobility variations. To obtain information on local environments, static spectra and spinning sideband manifolds were recorded and analysed for the ^{15}N resonances, using isotopically enriched samples. Shielding asymmetries and anisotropies for the two nitrogen nuclei were obtained, showing very different behaviour for the two sites. Shielding calculations were carried out for both ^{13}C and ^{15}N nuclei, and the results are discussed in relation to the experimental values.

The structure of 3(5)-[(4-diphenylphosphinoyl)phenyl]pyrazole has been investigated using X-ray crystallography and ^{13}C, ^{15}N and ^{31}P CP MAS NMR.[112] The NMR results together with DFT calculations (B3LYP/6-31G** + ZPE) were used for the identification of the predominant tautomeric form.

Solid state ^{13}C, ^{15}N and ^{77}Se CP MAS NMR spectra were reported for 1,3-imidazolidine-2-selenone, its *N*-substituted derivatives and some related compounds.[113] The spinning sideband analysis was used to obtain principal values of ^{13}C and ^{77}Se chemical shift tensors. Large selenium chemical shift anisotropies were observed for these selenones.

Conformational studies of highly hindered naphthylphenyl atropisomers by solution and solid state NMR have been reported.[114]

Neutron and X-ray diffraction, inelastic neutron scattering and solid state ^{13}C NMR investigations of polymorphic *p*-chlorophenylformamide (ClC_6H_4NHCHO) have been described.[115] The structural analysis revealed that the formamide group is essentially coplanar with the chlorophenyl ring. The possibility of hydrogen atom transfer between amide and iminol tautomers was ruled out based on the crystallographic results and additional ^{13}C CP MAS NMR and inelastic neutron scattering investigations. Only infinite chains of hydrogen-bonded formamide units were found in the crystal.

Several cage-substituted hexaazaisowurtzitanes have been characterised using the ^{15}N NMR isotropic and chemical shift tensor principal values, obtained by CP MAS and FIREMAT methods.[116] The effects of the different functional groups on the chemical shift tensor principal values of these caged amines were evaluated and were shown to be reflected in the total anisotropy. It was found that the position of the amine within the cage is reflected by the δ_{22} values. ^{15}N NMR shielding calculations using the embedded ion method to account for long-range intermolecular interactions showed a good correlation with the observed chemical shift tensor values (rmsd = 4 ppm).

6.2 Amino Acids. – In MAS NMR spectra of highly and uniformly ^{13}C,^{15}N-enriched amino acids and proteins, homonuclear coupling interactions contribute significantly to the ^{13}C linewidths, particularly for moderate applied magnetic

field strengths and sample spinning frequencies. Igumenova and McDermott have attempted to dissect, analyse and control the contributions of J-coupling and residual homonuclear dipolar couplings into the linewidths of uniformly $^{13}C,^{15}N$-enriched crystalline alanine.[117] Their studies were carried out at 9.4 T using a range of spinning frequencies from 5 to 15 kHz. The anisotropic second-order dipolar shifts and the J-splittings observed were comparable in their contribution to the linewidths, but behaved differently in terms of experimental protocols for line narrowing. Experiments were carried out to remove or refocus the ^{13}C J-coupling interactions using a selective DANTE pulse in the centre of the indirect evolution period. Inversion profiles and bandwidths of selective DANTE pulses acting on transverse magnetisation, in the regime of moderate spinning frequencies, were characterised computationally and experimentally. A dramatic improvement in the resolution of the 2D spectrum was achieved when this decoupling protocol was employed.

Experimental strategies for the acquisition of high-quality ^{14}N MAS NMR spectra of the simple amino acids, which exhibit ^{14}N quadrupole coupling constants (χ) on the order of 1.2 MHz, have been described.[118] These are the first useful ^{14}N MAS spectra reported for nitrogen compounds having a χ value in excess of 1 MHz. The complete manifolds of 300 spinning sidebands for a spinning frequency of 6.0 kHz, were observed in the ^{14}N MAS NMR spectra of a series of amino acids. In their crystal structure these amino acids all exhibit the zwitterionic form and thus the ^{14}N MAS NMR spectra represent those of a rotating $-NH_3^+$ group and not of an amino group. Computer simulations combined with fitting to the experimental spinning sideband intensities resulted in the determination of precise values for the ^{14}N quadrupole coupling and its associated asymmetry parameter for the nitrogen sites in the amino acids studied.

Solid state ^{17}O NMR results for 14 amino acids have been reported.[119] In most cases well-separated resonances from carbonyl and hydroxyl oxygens with distinct second-order quadrupolar line shapes are observed using a 600 MHz spectrometer with fast MAS. This is in contrast to the motionally averaged resonances usually seen from amino acids in solution. It was shown that for amino acids double angle rotation (DOR) produces a decrease in the linewidth by more than a factor of 40, providing very high-resolution (~ 1 ppm) spectra. The oxygen lines in alanine and the carbonyl oxygens in L-glutamic acid hydrochloride were assigned using ^1H-decoupled DOR. The NMR interaction parameters for amino acids showed a wide variation of quadrupole coupling χ (from 6.4 to 8.6 MHz), its asymmetry parameter η (from 0.0 to 0.9), and chemical shift δ_{iso} (from 83 to 353 ppm). The D- and L-forms of glutamic acid hydrochloride were shown to have the same NMR parameters to within error, which were very different from those reported in the literature for the D,L-form. A strong correlation ($\sim$ -1200 ppm/Å) was found between δ_{iso} and the C-O bond length of the carbonyl oxygens. Based on these data, it is suggested that enriching specific amino acids in more complex polypeptides and proteins could provide site-selective information about the bonding and functionality of different sites in biomolecules. An es-

timate of the possible detection limit for such species is provided.

6.3 Peptides. – ^{15}N chemical shielding parameters have been reported for central glycyl residues in crystallographically characterised tripeptides with α-helix, β-strand, polyglycine II with 3_1-helix conformation and extended structures.[120] Accurate values of the shielding components were determined from MAS and stationary spectra of peptides containing [2-^{13}C,^{15}N]-Gly. Two dipolar couplings, ^{1}H-^{15}N and $^{13}C^{\alpha}$-^{15}N, were used to examine ^{15}N shielding tensor orientations in the molecular frame and the results indicate that the δ_{11}, δ_{33}-plane of the shielding tensor is not coincident with the peptide plane. It was found that the observed isotropic shifts, which vary over a range of 13 ppm, depend on hydrogen bonding (direct and indirect) and local conformation. Furthermore, tensor spans, $\Omega = \delta_{11}$-δ_{33}, and their deviations from axial symmetry, δ_{22}-δ_{33}, vary over a larger range. A prediction scheme for the 2° structure of glycyl residues in proteins based on shielding parameters was proposed.

Sun and Oldfield have reported the ^{13}C NMR spectra of a series of tryptophan containing peptides and model systems, together with their X-ray crystallographic structures, and used quantum chemical methods to predict the ^{13}C NMR shifts (or shieldings) of all nonprotonated aromatic carbons (C^{γ}, C^{δ}, and $C^{\epsilon 2}$).[121] Overall, a generally good agreement between theory and experiment was found. The chemical shifts of Trp C^{γ} in several proteins, hen egg white lysozyme, horse myoglobin, horse heart cytochrome c, and four carbonmonoxyhemoglobins, were also well predicted. The overall Trp C^{γ} shift range seen in the peptides and proteins was 11.4 ppm, and individual shifts (or shieldings) were predicted with an rms error of ~1.4 ppm. Unlike C^{α} and N-H chemical shifts, which are primarily a function of the backbone ϕ,ψ torsion angles, the Trp C^{γ} shifts were shown to be correlated with the side-chain torsion angles χ_1 and χ_2 and appear to arise, at least in part, from γ-gauche interactions with the backbone atoms.

Solid state ^{31}P NMR spectroscopy was applied to measure the isotropic chemical shifts, chemical shift anisotropies and asymmetry parameters of three phosphorylated amino acids, O-phospho-L-serine, O-phospho-L-threonine and O-phospho-L-tyrosine.[122] The CP buildup rates and longitudinal relaxation times of ^{31}P and ^{1}H were determined and compared with the values measured for a triphosphate bound to a crystalline protein. It was shown that the phosphorylated amino acids are well-suited model compounds, *e.g.* for the optimisation of experiments on crystalline proteins. In addition, from 2D exchange experiments on O-phospho-L-tyrosine the existence of an exchange between the two different conformations of the molecule was deduced.

Chan and Tycko have reported a new technique suitable for the determination of the backbone torsion angle ψ in peptides with isolated uniformly labelled residues.[123]

NMR, IR, CD and X-ray crystallography have been applied to study the conformational properties of peptides of β^3-aminoxy acids ($NH_2OCHRCH_2COOH$) having different side chains on the β carbon atom.[124] Theoretical studies on a series of model diamides were also used to rationalise the experimentally observed conformational features of the β^3-aminoxy peptides.

^{1}H, ^{13}C and ^{15}N NMR spectra of several polypeptide samples were compared in order to determine the useful features of each technique.[125] ^{13}C CP MAS was shown to be useful for quick determination of secondary structure. ^{15}N CP MAS was shown to be better suited for resolving end effects and structural types in short oligomers. ^{1}H CRAMPS spectra were found to be similar to ^{13}C CP MAS in terms of the information obtained, but the resolution was not as good. Using ^{13}C CP MAS, the conformation of polyglycine was investigated in detail. Precipitation from solvents such as DCA or TFA resulted in the rippled β-sheet structure (PG I), while 3_1-helix (PG II) was formed by precipitation from aqueous solutions. Interestingly, grinding the sample resulted in an increase of PG I, indicating that this form is more stable in the solid state. These results were in agreement with those for poly(L-alanine), showing that the β-sheet form is more stable in the solid state. It was also found that homopolypeptides with larger side chains did not change their conformation upon grinding.

The natural abundance ^{13}C CP MAS spectrum of polylysine provides spectral resolution of all types of backbone and side chain carbons and thus, dynamic parameters could be determined separately for each of them. This possibility was exploited by Krusheinitsky *et al.* by using the following natural abundance ^{13}C-NMR relaxation methods: measurements of the relaxation times T_1 at two resonance frequencies, off-resonance T_{1r} at two spin-lock frequencies, and proton-decoupled T_{1r}.[126] Experiments were performed at different temperatures and hydration levels (up to 17% H_2O by weight). Additionally, the conformational properties of polylysine were also investigated by FTIR spectroscopy. The data obtained from the different NMR experiments were simultaneously analysed using the correlation function formalism and model-free approach. The results indicated that in dry polylysine both backbone and side chains take part in two low amplitude motions with correlation times of the order of 10^{-4} s and 10^{-9} s. Upon hydration, the dynamic parameters of the backbone remained almost constant except for the amplitude of the slower process that increased moderately. The side chain dynamics revealed a much stronger hydration response: the amplitudes of both slow and fast motions were found to increase significantly and the correlation time of the slow motion was reduced by about five orders of magnitude. At hydration levels of more than 10% H_2O fast and slow side chain motions were experimentally indistinguishable. It was shown that these changes in the molecular dynamics cannot be ascribed to any hydration-dependent conformational transitions of polylysine because IR spectra revealed almost no hydration dependence in either backbone or side chain absorption domains. The physical nature of the fast and slow motions, their correlation time distributions, and hydration dependence of microdynamic parameters are discussed.

The fully extended peptide conformation has been investigated for the first time in the solid state by ^{13}C CP MAS NMR.[127] The compounds examined were members of a terminally protected, homo-oligopeptide series (from monomer through hexamer) based on C^{α},C^{β}-didehydroalanine.

^{13}C and ^{15}N signals of fully isotope-labelled 15-residue peptide, glycinated mastoparan-X, in a solid state were assigned by 2D and 3D NMR experiments under MAS conditions.[128] Intraresidue spin connectivities were obtained with

multidimensional correlation experiments for C-C^{α}-C^{β} and N-C^{α}-C^{β}. Sequence specific assignments were performed with interresidue correlation experiments. Pulse sequences for these experiments use mixing periods under recoupled zero- and double-quantum ^{13}C-^{13}C and ^{15}N-^{13}C dipolar interactions. These correlation spectra allowed the complete assignment of the ^{13}C and ^{15}N backbone and $^{13}C^{\beta}$ signals. Chemical shift analysis of the ^{13}C and ^{15}N signals based on empirical and quantum chemical databases for proteins indicated that the backbone between residues 3 and 14 forms α-helix and residue 2 has extended conformation in the solid state. This structure was compared with the membrane-bound structures of mastoparan-X.

The conformation of an elastin-mimetic recombinant protein, $[(VPGVG)_4(VPGKG)]_{39}$, has been investigated using solid state NMR spectroscopy.[129] The sample was labelled with ^{13}C and ^{15}N. 2D ^{13}C-^{13}C and ^{13}C-^{15}N correlation experiments were carried out to resolve and assign the isotropic chemical shifts of the various sites. The Pro ^{15}N, $^{13}C^{\alpha}$ and $^{13}C^{\beta}$ isotropic shifts, and the Gly-3 $^{13}C^{\alpha}$ isotropic and anisotropic chemical shifts supported the predominance of type-II β-turn structure. The Val-1 preceding Pro was shown to adopt mostly β-sheet torsion angles, while the Val-4 chemical shifts were intermediate between those of helix and sheet. A significant conformational distribution was found, manifested by the broad linewidths of the ^{15}N and ^{13}C spectra.

In another related report, the elucidation of structure-function relationships in insoluble elastin has been approached using elastin-like polypeptide.[130] Solid state NMR experiments indicated that $(LGGVG)_n$ has structural similarities to elastin and some elastin peptides, providing support for the utility of the mimetic peptides. The structure of this elastin-like polypeptide in solution was described as a 'conformational ensemble' with a mixture of type I and II β-turns, in addition to unfolded regions. New data obtained indicated that the peptide does not adopt a single conformation in the solid state, lending further support to models for elastin that involve significant conformational heterogeneity.

The dynamics and aggregation of a β-sheet antimicrobial peptide, protegrin-1 (PG-1), have been investigated using solid state NMR.[131] Measurements of ^{13}C chemical shift anisotropies of carbonyl carbons, as well as ^{1}H-^{13}C dipolar couplings were used to elucidate motional effects involved. Exchange NMR experiments showed that the peptide undergoes slow reorientation with a correlation time of 0.7 ± 0.2 s in lipid bilayers. Based on this long correlation time, it was concluded that geometric constraints in the membrane might contribute to immobilisation of PG-1. From ^{1}H spin-diffusion measurements it was found that the PG-1 aggregates contact both the surface and the hydrophobic center of the lipid bilayer.

Solid state NMR methods employing ^{2}H NMR and geometric analysis of labelled alanines (GALA) were used to study the structure and orientation of the transmembrane α-helical model peptides in oriented and non-oriented lipid bilayers.[132]

Solid state NMR REDOR was applied for detection of oligomeric β strand structure of the membrane-bound HIV-1 fusion peptide.[133] Comparison of REDOR spectra on samples that were labelled at different residue positions sugges-

ted that there are both parallel and antiparallel arrangements of peptide strands.

A recently developed solid state NMR method for measurement of depths in membrane systems was applied to gramicidin A, a membrane-bound peptide of known structure, to investigate the potential of this method.[134] ^{15}N-detected ^{1}H spin-diffusion experiments allowed measurements of the 4-5 Å depth differences between three ^{15}N-labelled backbone sites (Trp13, Val7, Gly2) in gramicidin A. It was also shown that ^{13}C-detected ^{1}H spin diffusion experiments on unlabelled gramicidin A are sufficient to discriminate between the end-to-end dimer and double-helix structures of gramicidin A.

Structural and dynamical features of the B18 peptide from the sea urchin sperm bindin protein were determined in the crystalline state and in zwitterionic lipid bilayers at a peptide:lipid molar ratio of 1:12 using solid state NMR spectroscopy.[135] The study was focused on three ^{13}C and ^{15}N uniformly labelled leucine residues, which were introduced into three different B18 peptides at positions evenly distributed along the B18 primary structure. Isotropic ^{13}C and ^{15}N chemical shift measurements showed that while B18 possesses a nonhelical and non-sheet-like structure in the crystalline state, the peptide adopts an oligomeric β-sheet structure in the membrane in the presence of Zn^{2+} ions at high peptide:lipid ratio. Torsion angle measurements for the three leucine sites supported these results, with ϕ torsion angles between $-80°$ and $-90°$ in the crystalline state and between $-110°$ and $-120°$ in the membrane-bound form. These ϕ torsion angles determined for membrane-bound B18 were consistent with a parallel β-sheet secondary structure. Analysis of motionally averaged dipolar coupling measurements established an increase of the mobility in the leucine side chains upon binding to the membrane, whereas the backbone mobility remained essentially unchanged, except in the binding site of Zn^{2+} ions. It was hypothesised that the oligomeric β-sheet secondary structure represents an active state of the peptide in a membrane environment during fusion.

Solid state NMR measurements for the complex of an 18-residue peptide have been reported.[136] The peptide molecule was uniformly ^{15}N- and ^{13}C-labelled in a 7-residue segment containing the conserved GPGR motif in the epitope. ^{15}N and ^{13}C NMR chemical shift assignments for the labelled segment were obtained from 2D ^{13}C-^{13}C and ^{15}N-^{13}C MAS NMR spectra. Reductions in ^{13}C NMR linewidths and changes in chemical shifts upon complex formation indicated the adoption of a well-defined, antibody-dependent structure. Intramolecular ^{13}C-^{13}C distances in the complex, which constrain the peptide backbone and side chain conformations in the GPGR motif, were determined from an analysis of rotational resonance data. Structural constraints from chemical shifts and rotational resonance measurements were in good agreement with recent solution NMR and crystallographic studies, although differences regarding structural ordering of certain peptide side chains were noted.

Antimicrobial peptides, isolated from the dorsal glands of Australian tree frogs, have been studied using multinuclear solid state NMR.[137] Specifically ^{15}N-labelled peptides were studied using solid state NMR to determine their structure and orientation in model lipid bilayers. The effect of these peptides on phospholipid membranes was determined by ^{2}H and ^{31}P solid state NMR

techniques in order to understand the mechanisms by which they exert their biological effects that lead to the disruption of the bacterial cell membrane.

Finally, the interaction of the neuropeptide methionine-enkephalin with bicelles has been investigated by solid state ^{2}H and ^{31}P NMR.[138]

6.4 Proteins. – *Sample Preparation.* Preparation of proteins in their crystalline state has been known to be important for structural studies. Of these studies only X-ray crystallography requires large crystals. Smaller crystals are just as useful in structure determination by solid state NMR as are large crystals. In the paper by Martin and Zilm a simple set of procedures have been outlined for preparing nanocrystalline protein samples for solid state NMR and other applications, and the characterisation of their crystallinity by NMR and X-ray powder diffraction has been described.[139] The approach has been demonstrated in application to five different proteins: ubiquitin, lysozyme, ribonuclease A, streptavidin and cytochrome c. In all instances the nanocrystals produced were found to be highly crystalline as judged by natural abundance ^{13}C NMR and optical and electron microscopy. It was shown that for ubiquitin nanocrystals prepared by rapid batch crystallisation yield equivalent ^{13}C NMR spectra to those of larger X-ray diffraction quality crystals. Single crystal and powder X-ray diffraction measurements were made to compare the degree of order present in polycrystalline, nanocrystalline, and lyophilised ubiquitin. Solid state ^{13}C NMR was also used to show that ubiquitin nanocrystals are thermally robust, giving no indication of loss of local order after repeated temperature cycling between liquid nitrogen and room temperature. The methods developed are expected to find wide utility in the preparation of protein nanocrystals for applications in catalysis, separations, and especially in sample preparation for structural studies using solid state NMR.

Technique Developments. In the recent years significant progress has been achieved in the field of solid state NMR of isotope-enriched biomolecules, leading to the protein structure solution by solid state NMR. Nevertheless, spectral resolution is still the main limiting factor for the solid state NMR studies of larger systems. In uniformly ^{13}C-labelled proteins, the ^{13}C-^{13}C J-couplings constitute a significant contribution to the linewidth in MAS spectra. J-decoupling techniques using semiselective pulses can be used to enhance the spectral resolution in indirectly detected spectral dimensions. The application of spin-state selective and transition-selective polarisation transfer to multidimensional solid state NMR correlation experiments of ^{13}C-labelled proteins has been reported by Duma *et al.*[140] It has been shown that single-transition selection removes the line broadening due to the ^{13}C-^{13}C J_{COC_α}-coupling in both direct and indirect dimensions of a 2D CO-C^α correlation experiment. As a result, a nearly two-fold improvement in linewidth was obtained on a sample of microcrystalline Crh, an 85-residue protein. In addition, the new technique also allows an easy distinction between 'direct' and 'relayed' transfer cross-peaks.

In another paper, a 3D NMR based approach for the determination of the fold of moderately sized proteins by solid state MAS NMR is presented and applied to the α-spectrin SH3 domain.[141] This new methodology includes the measure-

ment of multiple ^{13}C-^{13}C distance restraints on biosynthetically site-directed ^{13}C-enriched samples, obtained by growing bacteria on [2-^{13}C]glycerol and [1,3-^{13}C]glycerol. 3D ^{15}N-^{13}C-^{13}C dipolar correlation experiments were applied to resolve overlap of signals, in particular in the region where backbone carbon-carbon correlations of the C^{α} - C^{α}, CO – CO, C^{α} - CO, and CO – C^{α} type appear. Additional restraints for confining the structure were obtained from ϕ and ψ backbone torsion angles of 29 residues derived from C^{α}, C^{β}, CO, NH and H^{α} chemical shifts. Using distance and angular restraints, a refined structure was calculated with a backbone rms deviation of 0.7 Å with respect to the average structure.

Techniques Based on Nuclear Overhauser Effect. A recently introduced ^{13}C polarisation technique based on the nuclear Overhauser polarisation (NOP MAS) has been applied to uniformly ^{13}C,^{15}N-labelled proteins.[142] NOP enhancement factors per scan of 1.5-2.0 were obtained, while that by CP was less than 1.0. It was shown that uniform enhancement of all ^{13}C signals by CP is difficult to attain, while it is easily achieved by NOP, thus enabling quantitative comparison of signal intensities. In addition, NOP is easy to carry out under fast MAS and works well even for somewhat mobile molecules, for which CP does not work. Moreover, in labelled protein samples containing nonlabelled additives, NOP can be used to eliminate the signals of nonlabelled species. It was concluded that in the case of uniformly ^{13}C labelled proteins NOP is superior to CP.

Some pioneering advances have been achieved in observing NOEs between exchangeable protons in proteins. A highly sensitive new ^{1}H-detected 3D solid state NMR method has been described by Paulson *et al.* for characterizing ^{1}H-^{1}H spin exchange in nanocrystalline samples of ^{15}N- and ^{2}H-enriched protein.[143] In particular, long-range contacts were observed in human ubiquitin. The method was successfully applied to measure numerous NOEs between backbone amides and crystal water protons.

Pure Exchange Solid state NMR Spectroscopy. Spin-exchange experiments are useful for improving the resolution and establishment of sequential assignments in solid state NMR spectra of uniformly ^{15}N-labelled proteins oriented macroscopically in phospholipid bilayers. To exploit this advantage fully, the diagonal peaks in the 2D exchange spectra need to be suppressed. This may be accomplished using the recently developed pure-exchange experiments (PUREX), which, however, suffer from up to a threefold reduction of the cross-peak intensity relative to experiments without diagonal-peak suppression. A 2D exchange experiment (*i*PUREX), which improves the PUREX sensitivity by 50%, has been reported by Vosegaard and Nielsen.[144] The performance of *i*PUREX is demonstrated experimentally by proton-mediated ^{15}N-^{15}N spin-exchange experiments for a ^{15}N-labelled N-acetyl-L-valyl-L-leucine dipeptide. The relevance of exchange experiments with diagonal-peak suppression for large, uniformly ^{15}N-labelled membrane proteins in oriented phospholipid bilayers has also been demonstrated.

Motional Effects. The effect of time and spatial averaging on ^{15}N chemical shift/^{1}H-^{15}N dipolar correlation spectra (PISEMA) of α-helical membrane peptides and proteins has been investigated.[145] Three types of simple motion were

considered: (a) librational motion of the peptide planes in the α-helix; (b) rotation of the helix about its long axis; and (c) wobble of the helix about a nominal tilt angle. A 2 ns molecular dynamics simulation of helix D of bacteriorhodopsin was used to determine the effect of librational motion on the spectral parameters. For the time averaging, the rotation and wobble of this same helix were modelled by assuming either Gaussian motion about the respective angles or a uniform distribution of a given width. For the spatial averaging, regions of possible ^{15}N chemical shift/^{1}H-^{15}N dipolar splittings were computed for a distribution of rotations and/or tilt angles of the helix. The computed spectra showed that under certain motional modes the ^{15}N chemical shift/^{1}H-^{15}N dipolar pairs for each of the residues do not form patterns, which mimic helical wheel patterns.

Secondary structure and backbone dynamics of Escherichia coli diacylglycerol kinase (DGK) have been studied.[146] To gain insight into secondary structure and backbone dynamics, ^{13}C NMR spectra of [3-^{13}C]Ala-, [1-^{13}C]Val-labelled sample was recorded using CP MAS and single-pulse excitation. Broad lines were observed in the ^{13}C NMR spectra at physiological temperatures due to interference of motional frequencies of DGK with frequencies of MAS or proton decoupling (10^4 or 10^5 Hz, respectively). In gel phase lipids, however, up to six distinct ^{13}C peaks were well-resolved due to lowered fluctuation frequencies ($< 10^5$ Hz). The fact that the enzymatic activity is low under conditions where motion is restricted and high when conformational fluctuations can occur suggested that acquisition of low frequency backbone motions (on the microsecond to millisecond time scale) might facilitate the efficient enzymatic activity of DGK.

The backbone dynamics of free *vs.* binase-bound barstar has been investigated.[147] Two types of dynamic solid state NMR experiments (relaxation and 1D MAS exchange) were combined for the investigation of the backbone dynamics of a 15% randomly ^{15}N-enriched protein barstar in both free and binase-bound states. The main novelty of this work was a simultaneous quantitative processing of the results of these two types of experiments (named SREDA) approach. The latter extends the well-known model-free approach, allowing discrimination between various motional models (jumps between different sites, wobbling in a cone, *etc.*). The SREDA approach was applied to probe a modification of the average backbone dynamics of barstar upon forming a complex with another protein binase. T_1 and off-resonance $T_{1\rho}$ relaxation times of ^{15}N backbone nuclei were measured at three different temperatures between 0 and 45°C; 1D MAS exchange (CODEX) data were obtained at room temperature within the mixing time range from 0.3 to 200 ms. It was found that the barstar backbone participates in two molecular processes with correlation times in the 10^{-9}-10^{-7} and 10^{-3}-10^{-2} s ranges. Forming the complex with binase results in a significant decrease of the amplitudes of both motions, suggesting that the complex is a more rigid and stable structure than free barstar.

Hydration Effects on Protein Dynamics. Solid state NMR investigations of the effect of temperature and hydration on the molecular mobility of collagen isolated from bovine achilles tendon have been reported.[148] ^{13}C CP MAS experiments were performed on samples at natural abundance using NMR methods

that detect motionally averaged dipolar interactions and chemical shift anisotropies and also slow reorientational processes. The data revealed that increasing hydration has a much stronger effect on the amplitude of the molecular processes than increasing temperature. In particular, the C^{γ} carbons of the hydroxyproline residues showed a strong dependence of the amplitude of motion on the hydration level. The applicability of 1D MAS exchange experiments to investigate motions on the millisecond timescale is discussed and first results were presented. Slow motions with correlation times of the order of milliseconds were detected for hydrated collagen.

Water-protein interactions in microcrystalline Crh were measured by ^{1}H-^{13}C solid state NMR.[149] Using ^{1}H-^{13}C dipolar correlation spectroscopy, proton exchange on the millisecond time scale was observed between water molecules and protein protons in a solid sample. These interactions were related to important structural features of the protein such as hydrogen-bonding or salt-bridge networks.

The effect of hydration on the molecular dynamics of soft wheat gluten was investigated by solid state NMR.[150] For this purpose, static and MAS ^{1}H spectra and single pulse, CP and other selective ^{13}C MAS spectra were recorded on samples of dry and H_2O and D_2O hydrated gluten. Measurements of ^{1}H-^{13}C CP times and several relaxation times (carbon T_1 and proton T_1, $T_{1\rho}$ and T_2) were also performed. The combination of these techniques allowed both site-specific and domain-averaged motional information to be obtained in different characteristic frequency ranges. Domains with different structural and dynamic behaviour were identified and the changes induced by hydration on the dynamics of different domains were monitored. The proton spin diffusion process was exploited to get information on the degree of mixing among different gluten domains. The results were consistent with the 'loop and train' model proposed for hydrated gluten.

Ubiquitin. A new indirect detection scheme for obtaining $^{15}N/^{1}H$ shift correlation spectra in crystalline proteins has been described.[151] Excellent water suppression was achieved without the need for pulsed field gradients, and using only a 2-step phase cycle. Careful attention to overall NMR instrument stability was found critical for obtaining the best resolution and sensitivity. Magnetic dilution by deuteration of the protein in combination with high-speed MAS produced ^{1}H resonances averaging only 0.22 ppm in width, and in some cases lines as narrow as 0.17 ppm were obtained. In application to two different polymorphs of ubiquitin, structure dependent differences in both ^{15}N and ^{1}H amide chemical shifts were observed. In one case, distinct shifts for different molecules in the asymmetric unit were seen, which differ substantially from solution NMR shifts. A gain of 7 in sensitivity makes this new approach competitive with solution NMR, provided that nanocrystalline samples are available.

Solid state NMR 2D spectroscopy was used to correlate carbon backbone and side-chain chemical shifts for uniformly ^{13}C,^{15}N-enriched microcrystalline ubiquitin.[152] High applied field strengths, 800 MHz for protons, moderate proton decoupling fields, 80-100 kHz, and high MAS frequencies, 20 kHz, were used to narrow the most of the carbon linewidths to 0.5-0.8 ppm. Homonuclear magnet-

isation transfer was achieved by matching the proton RF field to the spinning frequency, the so-called dipolar-assisted rotational resonance (DARR) and a mixing time of 20 ms was used to maximise the intensity of one-bond transfers between carbon atoms. This polarisation transfer sequence resulted in roughly 14% transfer efficiencies for directly bonded carbon pairs and 4% transfer efficiencies for carbons separated by a third carbon. With this simple procedure, the majority of the one-bond correlations was identified with moderate transfer efficiencies and many two-bond correlations were also observed with weaker intensities. Spin systems were identified for more than half of the amino acid side chains and site-specific assignments were readily possible *via* comparison with 400 MHz ^{15}N-^{13}C correlation spectroscopy.

In a related work by the same group, site-specific assignments in the solid state NMR spectra of uniformly ^{13}C,^{15}N-enriched ubiquitin were described.[153] The assignments were derived from three 3D ^{15}N-^{13}C correlation spectra collected at 400 MHz on microcrystalline material. The results showed close agreement between the chemical shifts observed in solution and those in microcrystalline or precipitated solids. The methods utilised are applicable for other noncrystalline insoluble proteins.

Membrane Proteins: Bacteriorhodopsin. The orientation data provided by solid state NMR provides a great deal of structural information about membrane proteins. However, the quality of the information provided is somewhat degraded by sign degeneracies in measurements of the dipolar coupling tensor. This is reflected in the dipolar coupling penalty function used in atomic refinement, which is less capable of properly restraining atoms when dipolar sign degeneracies are present. Bertman *et al.* have generated simulated solid state NMR data using a variety of procedures, including back-calculation from crystal structures of α-helical and β-sheet membrane proteins.[154] It has been demonstrated that a large fraction of the dipolar sign degeneracies are resolved if anisotropic dipolar coupling measurements are correlated with anisotropic chemical shift measurements, and that all sign degeneracies can be resolved if three data types are correlated. The advantages of correlating data were demonstrated with atomic refinement of two test membrane proteins. When refinement was performed using correlated dipolar couplings and chemical shifts, perturbed structures converge to conformations with a larger fraction of correct dipolar signs than when data are uncorrelated. In addition, the final structures were closer to the original unperturbed structures when correlated data were used in the refinement.

Site-directed solid state ^{13}C NMR spectra of [3-^{13}C]Ala- and [1-^{13}C]Val-labelled bacteriorhodopsin as a typical membrane protein in lipid bilayers, have been reported.[155] Well-resolved ^{13}C NMR signals were observed for monomeric [3-^{13}C]Ala- bacteriorhodopsin in egg phosphatidylcholine bilayer at ambient temperature, although several ^{13}C NMR signals from the loops and transmembrane α-helices were still suppressed. The ^{13}C NMR results were used to elucidate the effect of 2D array formation on the backbone dynamics of membrane proteins in lipid bilayers.

The surface dynamics of bacteriorhodopsin was examined by measurements of

site-specific ^{13}C-^{1}H dipolar couplings in [3-^{13}C]Ala-labelled bacteriorhodopsin.[156] The 2D dipolar and chemical shift (DIPSHIFT) correlation technique was utilised to obtain the dipolar coupling strength for each resolved peak in the ^{13}C MAS solid state NMR spectrum, providing the molecular order parameter of the respective site. In addition to the rotation of the Ala methyl group, which scales the dipolar coupling to 1/3 of the rigid limit value, fluctuations of the C^{α}-C^{β} vector result in additional motional averaging. Typical order parameters measured for mobile sites in bacteriorhodopsin were between 0.25 and 0.29. These were assigned to Ala residues of the mobile regions. Such order parameters departing significantly from the value of 0.33 for rotating methyl groups were explained by the fluctuations of the Ala C^{α}-C^{β} vectors in fully hydrated wild-type bacteriorhodopsin at ambient temperature.

A general feature of dynamic aspect of membrane proteins has been revealed by site-directed ^{13}C NMR studies on bacteriorhodopsin as a typical membrane protein and a variety of mutants at ambient temperature.[157] NMR signals in the ^{13}C spectrum of [3-^{13}C]Ala- or [1-^{13}C]Val-labelled proteins were assigned regiospecifically with reference to the data of the conformation-dependent ^{13}C chemical shifts from model polypeptides, followed by site-specific assignment based on site-directed mutants. Revealed picture of membrane protein at ambient temperature is not static in contrast to anticipation from crystalline structures but flexible enough to undergo a variety of local fluctuations with frequencies from 10^2 to 10^8 Hz. This dynamic picture was further refined by taking into account residue-specific motional freedom of interfacial domains between the surface and inner part of the transmembrane helices and conformational fluctuation induced by the presence of a kinked structure. The presence of molecular fluctuations in the interfacial domains was further confirmed by insensitivity of the peak intensities from the interfacial domains in spite of the presence of accelerated relaxation rate of nearby residues due to surface bound Mn^{2+} ion. It was shown that the observed displacement of [3-^{13}C]-labelled Ala184 peak at 17.4 ppm in the presence of kinked structure in this model peptide is consistent with that of intact protein at 17.3 ppm.

In a related work, ^{13}C NMR spectra of [3-^{13}C]Ala- and [1-^{13}C]Val-labelled bacteriorhodopsin and a variety of its mutants have also been reported.[158] These studies were undertaken in order to clarify contributions of the extracellular Glu residues to the conformation and dynamics of bacteriorhodopsin. Significant dynamic changes were induced for the triple or quadruple mutants, as shown by broadened ^{13}C NMR peaks of [1-^{13}C]Val-labelled proteins. These changes were due to acquired global fluctuation motions of the order of 10^{-4}-10^{-5} s as a result of disorganised trimeric form. It was concluded that the Glu residues at the extracellular surface play an important role in maintaining the native secondary structure of bacteriorhodopsin in the purple membrane.

Finally, Saito *et al.* have demonstrated that well-resolved and site-specifically assigned ^{13}C peaks as recorded by site-directed NMR study of ^{13}C-labelled membrane proteins can serve as a convenient probe to reveal their local conformation and dynamics.[159]

Amyloid Peptide Fibrils. Solid state NMR measurements have been reported

that probe the supramolecular organisation of β-sheets in β-amyloid peptide associated with Alzheimer's disease.[160] The solid state NMR data indicated that the central hydrophobic segment (sequence LVFFA) adopts a β-strand conformation and participates in antiparallel β-sheets and that the registry of intermolecular hydrogen bonds is pH-dependent. The results suggested that the supramolecular organisation of β-sheets in amyloid fibrils is determined by a sensitive balance of multiple 'side-chain-side-chain' interactions. Recent structural models based on X-ray fiber diffraction data were found to be inconsistent with the solid state NMR data.

Fibril formation in human calcitonin (hCT) from aqueous solution at pH 4.1 was examined and compared with those at pH 3.3 and 7.5 by means of site-directed ^{13}C solid state NMR.[161] The observed ^{13}C chemical shifts and lineshapes of the ^{13}C CP MAS spectra differed substantially among fibrils prepared at different pHs. It was found that antiparallel β-sheet structures were formed at pH 7.5 and 4.1 in the central core regions. Further, an attempt was made to assess interatomic distances by ^{13}C REDOR measurements between amide nitrogen and carbonyl carbon of neighboring chains of ^{13}C,^{15}N-labelled hCT. A unique chain packing of the antiparallel β-sheets was proposed as a dominant fibril structure.

Oyler and Tycko have demonstrated that absolute, molecular-level structural information can be obtained from solid state NMR measurements on partially oriented amyloid fibrils.[162] In particular, it has been shown that the direction of the fibril axis relative to a carbonyl ^{13}C CSA tensor can be determined from MAS sideband patterns in ^{13}C NMR spectra of fibrils deposited on planar substrates. Deposition of fibrils on a planar substrate creates a highly anisotropic distribution of fibril orientations (hence, CSA tensor orientations) with most fibrils lying in the substrate plane. The anisotropic orientational distribution gives rise to distorted spinning sideband patterns in MAS spectra from which the fibril axis direction can be inferred.

Silk. Structural studies of the model peptides of Bombyx mori silk-elastin like protein were undertaken using solid state NMR.[163] Detailed structural analyses were performed using deconvolution subroutines assuming Gaussian line shapes for the Ala C^{β} peaks.

Structural role of tyrosine in Bombyx mori silk fibroin was studied using a model peptide prepared as silk I and II.[164] The influence of the bulky and H-bonding Tyr side-chain on its Ala- and Gly-rich environment in Bombyx mori silk fibroin was examined by ^{13}C CP MAS, static ^{2}H and ^{19}F NMR and molecular mechanics calculations. Model peptides of the type $(AG)_{15}$ were synthesised with Tyr in a number of different positions, precipitated under conditions favoring either of the two characteristic protein conformations, and the resulting structures were assigned from their ^{13}C chemical shifts. It was found that the introduction one or more Tyr into $(AG)_{15}$ can have a dramatic effect not only on the local backbone conformation but also on the long-range intermolecular chain packing in the samples. The role of H-bonding was tested by replacing Tyr with Phe or fluorinated Phe. Static ^{2}H NMR of ring-deuterated [3′,5′-$^{2}H_2$]Tyr located in the central region of $(AG)_7YG(AG)_7$ showed that the side-chain is immobilised in

both silk I and II, which was also observed by static ^{19}F NMR of the fluorinated analogue.

Dependence of mechanical properties on the amino acid content in the silk of Nephila clavipes has been investigated using solid state NMR and amino acid analysis.[165]

A decrease in strength and increase in elasticity have been reported when the silk is in contact with water. For example, the addition of water to spider dragline silk results in fiber contraction to 50% its initial length and significant changes to the mechanical properties of the silk. 2D wide-line separation (WISE) NMR was employed to correlate ^{13}C chemical shifts with mobility by observing the corresponding ^{1}H linewidths and line shapes in water-saturated spider dragline silk.[166] The WISE NMR spectrum of the native silk exhibits ^{1}H linewidths that are ~ 40 kHz for all ^{13}C environments characteristic of a rigid organic system. In contrast, the water-saturated case displays a component of the ^{1}H line that is narrowed to ~ 5 kHz for the Gly C^{α} and a newly resolved Ala helical environment, while the Ala C^{β} corresponding to the β-sheet conformation remains broad. It was concluded that water permeates the amorphous, glycine-rich matrix, but not the crystalline, polyalanine β-sheets. A delay time is added to the WISE NMR pulse sequence to monitor spin diffusion between the amorphous, mobile region and the crystalline domains. The time required for spin diffusion to reach spatial equilibrium was related to the length scale of the polyalanine crystallites. This technique was employed to measure crystalline domain sizes on the nanometer length scale in water-solvated spider dragline silk.

The structure of silk fibroin from a wild silkworm was examined by using solution and solid state NMR methods.[167] The structural transition of the silk fibroin in aqueous solution was monitored by using solution ^{13}C NMR spectroscopy as a function of temperature. The torsion angles of several Ala and Gly residues in the model peptide, GGAGGGYGGDGG$(A)_{12}$GGA-GDGY-GAG, were determined by the conformation-dependent ^{13}C chemical shifts, REDOR and 2D spin-diffusion techniques in the solid state.

Finally, structural studies of two well-known silk fibroin proteins, Bombyx mori and Samia cynthia ricini, have been reported.[168] Solid state NMR methods, such as ^{13}C 2D spin-diffusion NMR and REDOR were used in addition to the quantitative use of the conformation-dependent chemical shifts, measured by ^{13}C CP MAS.

6.5 Lipids and Membranes. – The first application of ^{2}H solid state NMR spectroscopy and spin-labelled EPR spectroscopy has been utilised to probe the structural orientation and dynamics of a stearic acid incorporated into magnetically aligned phospholipid bilayers or bicelles.[169] Both methods provided similar qualitative information on the phospholipid bilayer, high order and low motion for the hydrocarbon segment close to the carboxyl groups of the stearic acid and less order and more rapid motion at the end towards the terminal methyl groups. However, the segmental order parameters differed markedly due to the different orientations of the nitroxide and C-D bond axes and because of the difference in dynamic sensitivity between NMR and EPR over the timescales examined. The

influence of the addition of cholesterol and the variation of temperature on the fatty acid hydrocarbon chain ordering in phospholipid bilayers was also studied. It was found that cholesterol increases the degree of ordering of the hydrocarbon chains. Conversely, as the temperature of the magnetically aligned phospholipid bilayers increased, the order parameters decreased due to the higher random motion of the acyl chain of the stearic acid. The results indicate that magnetically aligned phospholipid bilayers are a suitable model membrane system and can be used for both NMR and EPR studies.

Solid state ^{2}H NMR studies of the effects of cholesterol on the acyl chain dynamics of magnetically aligned phospholipid bilayers have been reported.[170] The results suggest that cholesterol is incorporated into the bicelle discs. The order parameters were extracted directly from the ^{2}H quadrupolar splittings, and indicated an overall degree of ordering of the acyl chains of the phospholipids in the presence of cholesterol.

The effects of cholesterol on magnetically aligned phospholipid bilayers (bicelles) have also been studied using both solid state NMR spectroscopy and EPR spectroscopy.[171] It was shown that EPR spectroscopy and ^{2}H NMR spectroscopy exhibit different degrees of sensitivity in detecting the phospholipid molecular motions in the membrane.

Structural changes in the lipid bilayer upon insertion of the transmembrane domain of the membrane-bound protein phospholamban (PLB) were studied using ^{31}P and ^{2}H solid state NMR.[172] Phospholamban is a 52-amino acid integral membrane protein that regulates the flow of Ca^{2+} ions in cardiac muscle cells. Solid state NMR experiments were carried out to study the behavior of lipid bilayers in the presence of the hydrophobic PLB at different temperatures. ^{31}P NMR was used to study the different phases formed by phospholipid membranes. Simulations of the ^{31}P NMR spectra were carried out to reveal the formation of different vesicle sizes upon PLB insertion. Molecular order parameters were calculated by performing ^{2}H solid state NMR studies on deuterated phospholipid bilayers.

Peptide-related alterations of membrane-associated water has been investigated using solid state ^{2}H and ^{31}P NMR of phosphatidylcholine membranes at different hydration levels.[173] The NMR spectra were recorded as a function of hydration in the range between 15 and 93% relative humidity and of sample composition. In the presence of peptides an increased association of water was observed. A quantitative analysis suggested that the peptide-induced changes in the lipid bilayer packing have a significant effect on membrane-water association. The quadrupolar splittings of water ^{2}H at a given degree of hydration indicated that the changes of the water deuterium order parameter are specific for the peptide sequence and the lipid composition.

Solid state ^{2}H NMR investigations of exchange labelled oriented purple membranes at different hydration levels have been reported.[174] Four ^{2}H populations were resolved. Deuterons that have exchanged with amide protons of the protein exhibited a broad spectral line shape (<150 kHz). A broadened signal of deuterons tightly associated with protein and lipid was also detected at low hydration, as well as two additional water populations that were present when

the samples were equilibrated at higher relative humidity.

The theory of the susceptibility corrections in solid state NMR experiments with oriented membrane samples has been described.[175] To determine the necessary corrections, a general analysis is presented for the demagnetizing field of a layered sample of rectangular block geometry, with the normal of the layers parallel to the main field or tilted about an axis of the block. The correction to the line position of the block sample was found to be approximately equal to that of the spheroid which can be inscribed into the block, and for which the correction is well known. It was shown that sample and support materials contribute to that average according to their volume filling factors.

Applications of the susceptibility corrections in solid state NMR experiments with oriented membrane samples have also been reported.[176] Referencing schemes were proposed to compensate for bulk magnetic susceptibility effects that are associated with the non-spherical sample shape. Further aspects related to magnetic susceptibility are discussed, such as air gaps in susceptibility-matched probeheads, the benefits of shimming, and limitations in the accuracy of orientational constraints. A biological application is illustrated by a series of experiments on the antimicrobial peptide PGLa. It was found that accurate referencing was critical to reveal a small but significant change over 5 ppm in the anisotropic chemical shift of the ^{19}F label on the peptide, indicative of a change in the orientation and/or dynamics of PGLa in the membrane.

6.6 Pharmaceutical Applications. – Through-bond and through-space solid state NMR correlation experiments at natural isotopic abundance (CP INADEQUATE, ^{1}H-^{13}C HETCOR, ^{1}H-^{13}C MAS *J*-HMQC) have been applied to study a moderately sized molecule of simavastatin ($C_{25}H_{38}O_5$).[177] Refocused ^{13}C CP INADEQUATE with an optimised performance of high-power decoupling provided full correlation spectrum within a day of acquisition. Complete unambiguous ^{1}H and ^{13}C signal assignment was achieved by ^{1}H-^{13}C MAS *J*-HMQC and dipolar heteronuclear correlation spectroscopy. Dipolar ^{1}H-^{13}C correlation with Lee-Goldburg CP was used to promote long-range polarisation transfer. More than 80 heteronuclear contacts were detected in 2D spectra with LG CP. The majority of these interactions reflected polarisation transfer between neighboring structural units. The obtained ^{1}H-^{13}C and ^{1}H-^{1}H contacts used in conjunction with ^{13}C and ^{1}H NMR aggregation shifts appeared to be a practical and efficient tool to determine conformation and mutual orientation of well-organised molecules within crystal at natural isotopic abundance.

Microscopic molecular mobility of amorphous AG-041R was chracterised by solid state ^{13}C NMR.[178] In order to investigate the molecular mobility microscopically, the spin-lattice relaxation time $T_1(^{13}C)$ was measured at temperatures below and above glass transition temperature (T_g).

Through-bond ^{13}C-^{13}C correlation at the natural abundance level in the solid state has been applied for refining dynamic regions in the crystal structure of vitamin-D_3.[179]

Solid state NMR studies of pharmaceutical solids in polymer matrices have been presented by Lubach *et al.*[180] Two systems were chosen. The first system

studied involved bupivacaine, a local anesthetic compound, which was incorporated into microspheres composed of tristearin and encapsulated using a solid protein matrix. Solid state ^{13}C NMR spectroscopy was used to investigate the solid forms of bupivacaine in their bulk form or as incorporated into the tristearin/protein matrix. In the second case, the possibility of using solid state ^{13}C NMR spectroscopy to characterise biomolecules lyophilised within polymer matrices was evaluated by studying uniformly ^{13}C-labelled asparagine in 1:250 (w/w) formulations with poly(vinyl pyrrolidone) and poly(vinyl alcohol).

A ^{13}C and ^{31}P solid state NMR study was undertaken to study chlorpromazine interaction with phosphatidylserines.[181] Chlorpromazine is widely used as an antipsychotic drug. ^{13}C and ^{31}P solid state NMR techniques were employed to study phospholipid bilayers with and without chlorpromazine.

The effect of tricyclic antidepressants (TCA) on phospholipid bilayer structure and dynamics was studied to provide insight into the mechanism of TCA-induced intracellular accumulation of lipids (known as lipidosis).[182] Solid state ^{31}P and ^{14}N NMR techniques were used. Changes in bilayer architecture in the presence of TCAs were observed to be dependent on the TCA's effective charge and steric constraints.

Solid state ^{15}N NMR studies of tobacco leaves have been reported.[183] Nitrogen-containing compounds are one of important class of constituents in tobacco because of various pharmacological and biological properties. Three types of tobacco leaves (burley, bright, and oriental) were studied using ^{15}N CP MAS and FIREMAT experiments. The results show that burley tobacco leaves contain significantly more pyridinic nitrogen than bright or oriental tobacco leaves. The principal values of ^{15}N chemical shift tensors of nitrogen functional groups were obtained from the FIREMAT data. Possible assignments of solid state ^{15}N NMR resonances were made using nitrogen chemical shift tensors in some model compounds or isotropic chemical shift values from solution NMR results.

Investigations of the physical stability of amorphous drug and drug/polymer melts using VT solid state NMR have been presented by Forster *et al.*[184]

Ring-chain tautomerism in solid-phase of erythromycin A has been characterised by solid state NMR.[185] Chemical shift modeling, utilizing the DFT B3LYP/D95** method, was employed to provide the spectral assignment of the 35 visible ^{13}C resonances from the solid-phase erythromycin A dihydrate. A new resonance at 110.8 ppm was observed in the high-resolution ^{13}C CP MAS spectrum upon the application of heat or sample desiccation. With the use of the dipolar-dephasing spectral editing technique, this resonance was identified as a hemiketal carbon and the alternative hypothesis, a conformational change to the anomeric carbon of the desosamine sugar, was ruled out. The principal components of the ^{13}C chemical-shift tensor corresponding to this hemiketal were also reported. The δ_{11} and δ_{22} components were unique compared to anomeric carbon values reported in the literature.

The structure of gramicidin A in a lipid bilayer environment has been determined using molecular dynamics simulations and solid state NMR.[186] The obtained results underscore the utility of molecular dynamics simulations in the analysis and interpretation of structural information from solid state NMR.

Two different crystalline polymorphs of valinomycin, the triclinic and monoclinic forms, have been studied using ^{13}C CP MAS NMR.[187] Although the two polymorphs of the crystal are remarkably similar, there were distinct differences in the isotropic chemical shifts between the two spectra. For the triclinic form, the carbon chemical shift tensor components for the a carbons adjacent to oxygen in the lactic acid and hydroxyisovaleric acid residues and the ester carbonyls of the valine residue were obtained using the FIREMAT experiment. From the measured components, it was found that the behavior of the isotropic chemical shift, δ_{iso}, for valine residue ester carbonyl carbons is predominately influenced by the intermediate component, δ_{22}. Additionally, it was found that the smallest shift component, δ_{33}, for the L-lactic acid and D-α-hydroxyisovaleric acid C^{α}-O carbon was significantly displaced depending upon the nature of individual amino acid residues, and it is the δ_{33} component that governs the behavior of δ_{iso} for these a carbons.

6.7 Cellulose and Related Materials. – High and low resolution solid state NMR methods have been applied to characterise a few samples of ancient wood. In an ancient larch wood sample, by applying ^{1}H low resolution NMR methods as a function of the temperature, the average pore size and its distribution have been determined. In addition, high resolution NMR techniques have allowed addressing of the question of the proximity of water pools to cellulose and lignin.[188] ^{13}C CP MAS was used to examine changes in carbon composition of harvest residues and examine its effect of soil organic matter (SOM). The ^{13}C NMR spectra of the harvest residues indicated the presence of lignin in the pine wood, foliage and newly incorporated organic matter (NIOM). Condensed tannin structures were found in the decay-resistant bark, small wood and foliage, but were absent in other residue components and SOM. NIOM showed a shift from celluloses to lignin-type structures, indicating an incorporation of woody residues from the decomposing harvest residues.[189] Solid state ^{13}C NMR spectroscopy was used to determine the degree of cellulose crystallinity (CrI) in kraft, flow-through kraft and polysulfide-anthraquinone (PS-AQ) pulps of pine and birch containing various amounts of hemicelluloses. ^{1}H spin-relaxation based spectral edition (PSRE) method to remove the interfering hemicellulose signals prior to the determination of CrI were also compared.[190] A new cellulose based fluorescent polymer has been successfully synthesized by esterificaction of 1-pyrenebutyric acid and cellulose. This polymer was characterized by solid state ^{13}C CP MAS and other techniques.[191] To investigate the domain structure and dynamics of polysaccharides in the native starch granules, a variety of high resolution, solid state ^{13}C NMR techniques have been applied to all three types of starch with different water content. Both SPE MAS and CP MAS methods have been employed together with the PRISE (proton relaxation induced spectral-editing) techniques to distinguish polysaccharide fractions in different domains and having distinct dynamics. It has been found that, for all three types of dry starch granules, there are two sets of NMR signals corresponding to two distinct ordered polysaccharides.[192] Highly crystalline samples of cellulose triacetate (CTA) were prepared from cellulose I by heterogeneous acetylation in an equal

amount mixture of acetic anhydride and toluene. Highly crystalline and oriented films of cellulose I from green alga *Cladophora sp.* was used as a starting material. Prepared samples were studied by FTIR, solid state ^{13}C NMR, and X-ray diffraction. Spectroscopic data indicate a complete degree of acetylation. In the solid state ^{13}C NMR spectrum, each carbon atom appears only as a single resonance, indicating that the asymmetric unit in the CTA I crystal includes only a single chemical repeat unit.[193] The characterization of several size classes of logyard fines sampled from coastal and interior operations were carried out by ^{13}C CP MAS and other techniques. ^{13}C CP MAS spectra were consistent with the chemical data, with high O-alkyl intensity and similarity to naturally occurring woody forest floor; no samples were high in aromatic or phenolic carbon.[194] A review on work with spectral fitting of ^{13}C CP MAS NMR spectra recorded on isolated cellulose, on a mixtures of cellulose I and xylan and, on kraft pulps was presented. The conceptual model for cellulose I used was presented. References demonstrating the validity of the spectral fitting model were given.[195] Xyloglucans (XG) with different mobilities were identified in the primary cell walls of mung beans (*Vigna radiata L.*) by solid state ^{13}C NMR spectroscopy. To improve the signal:noise ratios compared with unlabelled controls, glucose labelled at either C-1 or C-4 with ^{13}C isotope was incorporated into the cell-wall polysaccharides of mung bean hypocotyls. Using cell walls from seedlings labelled with d-[1-^{13}C]glucose and, by exploiting the differences in rotating-frame and spin-spin proton relaxation, a small signal was detected which was assigned to Xyl of XGs with rigid glucan backbones. After labelling seedlings with D-[4-^{13}C] glucose and using a novel combination of spin-echo spectroscopy with proton spin relaxation-editing, signals were detected that had ^{13}C-spin relaxations and chemical shifts which were assigned to partly rigid XGs surrounded by mobile non-cellulosic polysaccharides.[196] In an interesting study a 2D ^{13}C spin-exchange NMR experiment was applied to the uniformly ^{13}C enriched cellulose II in order to obtain interatomic distance information in the cellulose II crystal. A radio frequency-driven recoupling (RFDR) rotor-synchronized π pulse sequence was incorporated during the mixing time of the 2D experiment. The 2D spin-exchange NMR recorded with a short mixing time provided the correlations between a pair of strongly coupled ^{13}C spins such as neighbor carbon nuclei. Interatomic distances and all ^{13}C resonances were obtained.[197] The elucidation of the crystal structures of the two crystalline allomorphs of cellulose triacetate (CTA), namely CTA I and CTA II, 2D solid state through-bond ^{13}C and ^{1}H-^{13}C correlations NMR techniques applied to the two crystalline allomorphs of CTA. As a result, the ^{13}C and ^{1}H chemical shifts of the glucopyranose ring of CTA I and CTA II were completely assigned by the 2D NMR spectra of these allomorphs.[198] Local motions in the cyanogenic glycoside amygdalin have been characterized by VT ^{13}C solid state NMR spectroscopy. ^{13}C chemical shift tensors and ^{1}H-^{13}C dipolar couplings were measured by MAS NMR techniques over the temperature range 0-90°C.[199] The chemical structure and interactions of the cell wall polysaccharides from the red edible seaweed Palmaria palmata were studied by liquid-like MAS and CP MAS solid state ^{13}C NMR spectroscopy. The liquid-like MAS and CP MAS ^{13}C NMR spectra of the rehydrated algal powder revealed

the presence of β-(1-4)/β -(1-3)-linked D-xylan with chemical shifts close to those observed in the solution ^{13}C NMR spectrum of the polysaccharide.[200]

6.8 Soils and Related Materials. – The particle-size separation of subalpine soils was used for delineating the different functional C pools of soil organic matter (SOM) by ^{13}C CP MAS NMR spectroscopy. The obtained data show that organic matter fractions differ according to particle-size distribution and vegetations. Being more aliphatic, clay-size fractions were significantly different from bulk soils.[201] The investigation of the chemical composition of soil organic matter (SOM) in The investigation of the chemical composition of soil organic matter (SOM) in Brazilian Ferralsols by means of CP MAS ^{13}C NMR spectroscopy is limited by their high iron oxide concentration and their low organic carbon content. In order to circumvent those limitations, such samples are often treated with hydrofluoric acid (HF) to remove paramagnetic material and to concentrate the amount of SOM.[202] Dissolved organic matter (DOM) was isolated from water sampled from an oligotrophic river, the River Tagliamento (Italy). Both solution-state and 1-D solid state ^{13}C NMR spectroscopy were used for the DOM characterization.[203] To understand better the chemical characteristics and source of DOM leached from the plow layer of rice paddies. This was characterized by a series of techniques including ^{13}C CP MAS NMR.[204] Three mineral soils were treated by different chemical methods to evaluate their effect on the quality of ^{13}C CP MAS spectra. This was further checked by ^{1}H relaxation data.[205] Solid state ^{13}C NMR spectroscopy was used to characterise sedimentary organic matter sampled from three estuaries on the central New South Wales coast (Australia). CP and Bloch decay (BD) experiments were used to determine the chemical composition of the samples. Proton-spin relaxation editing (PSRE) was used to probe the physical structure of the sedimentary organic matter at the sub-micron scale.[206] Spin counting on solid state ^{13}C CP MAS spectra of two humic fractions isolated from tropical lowland soils showed that only 32-81% of potential ^{13}C NMR signal was detected. The observability of ^{13}C NMR signal (C-obs) was higher in the mobile humic acid (MHA) than in the calcium humate (CaHA) fraction, and increased with increasing intensity of irrigated rice cropping. NMR observability appeared to be related to the nature of the organic carbon, with phenol- and methoxyl-rich samples having the higher values of C-obs. The Bloch decay (BD) technique provided more quantitatively reliable ^{13}C NMR spectra, as evidenced by values of C-obs in the range 91-100% for seven of the eight humic fractions studied.[207] The composition of functional light soil organic matter pools of arable Cambisols with a gradient in clay content was investigated. Using density fractionation in combination with ultrasonic dispersion, two types of particulate organic matter (POM) were obtained: (1) free POM and (2) POM occluded in soil aggregates. Both POM fractions were analysed by elemental analysis (C, N) and ^{13}C CP MAS NMR spectroscopy.[208] Peat samples subjected to thermal oxidation were studied by solid state ^{13}C- and ^{15}N NMR spectroscopy, so as to gain information on the thermal alteration of organic matter during processes such as natural fires or prescribed fires affecting soils.[209] Humic acid was fractionated into eight different molecular size components

using ultrafiltration. ^{13}C CP MAS NMR demonstrated that fractions larger than 100 000 Daltons were primarily aliphatic in character, while fractions smaller than 30 000 Daltons were predominantly aromatic in character. Solid state ^{19}F NMR was used to examine the sorptive uptake of hexafluorobenzene (HFB) by the HA.[210] An improved approach for accurately determining the aromatic carbon fraction (f(a)) and nonprotonated aromatic carbon fraction (f(a)N) in natural organic matter by solid state ^{13}C NMR is described. Quantitative peak areas are obtained from direct polarization ^{13}C NMR under high-speed MAS. The problem of overlap between aromatic and alkyl carbon resonances around 90-120 ppm in ^{13}C NMR spectra is solved by a ^{13}C chemical shift anisotropy (CSA) filter technique. After correction for residual spinning sidebands, an accurate value of the aromaticity f(a) is obtained.[211] Since the toxicity of Al depends on their chemical forms, the importance of Al speciation has been recognized worldwide The NMR spectral characteristics of environmentally important Al-containing components, such as hydoxyaluminum ions, Al-inorganic complexes, Al-organic complexes, and primary and secondary minerals, are summarized for the nuclei of ^{27}Al and ^{29}Si determined by solution NMR and solid state MAS NMR.[212]

6.9 Coals and Carbonaceous Materials. – It is established experimentally using ^{1}H NMR wide line spectroscopy that methane can exist in coals not only in open or closed porosity and fracture systems but also in solid solutions in coal substance, in particular, under methane pressure 2 MPa or higher.[213] CP MAS was used in this work to assess the carbon distribution in coals of different rank (peat, lignite. xyllite. sub-bituminous coal) from important deposits in Greece and Bulgaria.[214] Among the many complicated chemical and physical changes occurring in coal in the plastic temperature range, this study examined the changes in the size of polycondensed aromatic rings. The average size of the aromatic rings for the studied coals and heat-treated coals (chars) was evaluated by solid state NMR.[215] A combination use of the catalysed oxidation reaction and measurement of solid state ^{13}C NMR spectra was applied to the evaluation of the amount of bridge bonds and side chains in two brown coals. NMR data give the information on the amount of methyl group bonded directly to the aromatic ring.[216] Simplified equations are used in common approaches to describe CP dynamics of solids. The CP behavior may be modulated by several nuclei interactions and physicochemical sample properties. At high magnetic fields and spinning speeds, these modulations can obscure the results. To elucidate their impact on the CP behavior of natural organic materials variable contact time (VCT) experiments were acquired with a high temporal resolution for two coal samples.[217] High-resolution 2D ^{27}Al MQMAS NMR, was applied in order to characterize the mineral matter in coals that have been spotlighted recently in new approach to the coal utilization. Octahedral aluminum compounds which consist of kaolin and other mineral phases could be clearly distinguished by ^{27}Al MQMAS method.[218] NMR measurements have revealed that methane can exist in coal samples in the state of solid solution rather than only adsorbed gas. NMR lines in various coals at room or low temperatures and

have found that there exist three species of methane molecules differing in molecular mobility.[219] Solid state ^{13}C MAS NMR spectroscopy has been used to quantify the different carbon species observed in synthetically produced nanodiamonds. Two different diamond-like carbon species were observed using ^{13}C MAS NMR, which have been attributed to a highly ordered crystalline diamond phase and a disordered crystalline diamond phase.[220] Solid state NMR spectroscopy was used to study molecular hydrogen trapped inside an open-cage fullerene.[221] Two separate samples of Na_3C_{60} were prepared by direct reaction of C_{60} with sodium metal vapor, and subjected to different annealing times of 10 days and 16 days. Solid state ^{13}C and ^{23}Na NMR, along with elemental analysis, powder X-ray diffraction (XRD) and Raman spectroscopy, were used to characterize both samples.[222]

6.10 Polymers. – Advanced 2D solid state NMR techniques revealed weak intermolecular interactions that cooperatively sustain nanostructures of high molecular mass aliphatic polymers entrapped as guests in channels formed by an aromatic host.[223] ^{2}H NMR spectroscopy on blends of poly(ethylene oxide) (PEO) with poly(methyl methacrylate) (PMMA) was analysed using a model for the blend dynamics based on the coupling model. This model has previously been shown to describe the relaxation properties of blends whose component dynamics are strongly composition dependent. It was shown that the unusual feature of PEO/PMMA blends, an invariance of the PEO dynamics to composition, is a natural consequence of the high frequency and temperature of the NMR experiments.[224] The phase structures of thermally processed wheat proteins (WP) and polyvinyl alcohol (PVOH) blends were studied by solid state high-resolution NMR spectroscopy. The intermolecular interactions among the multi-component systems and the behavior of each component in the blends on scales of nanometers were examined.[225] 2D DQ ^{1}H MAS NMR has been used to investigate the local structure of a surfactant-templated silicate thin film prepared from adding 4% polyoxyethylene acetyl ether to an acidic TEOS silica sol. A close spatial contact between the surfactant and the silicate present in these materials could be demonstrated, while the high sensitivity of the NMR experiments allowed systems with limited amounts of material to be investigated.[226] Bicomponent nanophase-separated poly(2-hydroxyethyl methacrylate)-linked-polyisobutylene (PHEMA-l-PIB) amphiphilic conetworks were synthesized. The PIB content of the resulting conetworks, determined by elemental analysis and solid state ^{1}H NMR under fast MAS, varied between 17 and 63% w/w. Phase separation and morphology of these conetworks were investigated by DSC, small-angle X-ray scattering (SAXS), and for the first time by ^{1}H spin diffusion solid state NMR.[227] ^{1}H-^{1}H MQ MAS investigations were carried out on a series of monomodal and strongly bimodal end-linked poly(dimethylsiloxane) model networks. A robust pulse sequence characterized by a well-defined DQ Hamiltonian along with a specific normalization approach is used to obtain DQ build-up curves. These curves are analysed in terms of the spin dynamics of a local subsystem of monomer-fixed spins, where analytical fitting functions yielding residual dipole-dipole coupling constants are derived on the basis of exact

solutions provided by simulations.[228] The complex morphology of high-speed melt spun nylon-6 fibres hydrated with D_2O was investigated using ^1H double-quantum-filtered spin-diffusion NMR experiments. The magnetisation exchange from selected crystalline domains along the fibrils and interfibrils was simulated with the help of a 3D solution of a spin-diffusion equation approximated by a product of 1D analytical NMR signals, which correspond to a lamellar morphology.[229] A spinodal demixing technique was employed for the preparation of linear poly(ethylene oxide) (PEO) confined in nanoscopic strands, which in turn are embedded in a quasi-solid methacrylate matrix impenetrable to PEO. Chain dynamics of the PEO in the molten state were examined with the aid of field-gradient NMR diffusometry and field-cycling NMR relaxometry.[230] Advanced ^1H solid state NMR methods were applied for studying the hydrogen bond formation occurring in polymer hydrogels based on N-isopropylacrylamide (NIPAAm) and methacrylic acid (MAA). For P(NIPAAm-co-MAA) copolymers collapsed at low pH, two populations of water can be distinguished in ^1H MAS NMR spectra, one of which is probably situated near stable hydrogen-bonded regions, while the other behaves similarly to free water. The pH-induced polymer collapse can be followed in detail using 2D ^1H-^1H DQ MAS NMR experiments on dried samples.[231] The nature of the pH dependent collapse of poly(methacrylic acid) (PMAA) hydrogels is investigated using recent ^1H solid state NMR methods. In aqueous solution, PMAA changes from an expanded conformation at high pHs to a compact contracted form at low pHs, where hydrogen bonds play a central role. In solid state ^1H NMR spectra, recorded under fast MAS, dried PMAA samples previously collapsed at low pHs show characteristic signals in the spectral region of the carboxylic acid protons.[232] From solid state NMR spectra, a lower shielding of poly(ethylene oxide) (PEO) protons, in contrast to higher shielding of PEO carbons, has been found for PEO/hydroxybenzene and PEO/$LiCF_3SO_3$ complexes in comparison with neat PEO. The same PEO chemical shifts were found both for crystalline and amorphous phase of PEO/ $LiCF_3SO_3$ polymer electrolyte, confirming the same interaction in both phases.[233] A series of ethylene-acrylic acid copolymers either isothermally crystallized or melt-quenched were studied by ^{13}C CP MAS and variable-temperature ^1H wide-line NMR spectroscopy, with the emphasis on the mobility of the noncrystalline region. It is found that with the increase of the comonomer (acrylic acid) content, the chain mobility of the noncrystalline region decreases, while the content of the noncrystalline ethylene segments increases, which was due to hydrogen bonding.[234] Advanced solid state NMR methods under fast MAS are used to study the structure and dynamics of large supramolecular systems, which consist of a polymer backbone with dendritic side groups and self-assemble into a columnar structure. The NMR experiments are performed on as- synthesized samples, *i.e.*, no isotopic enrichment is required. The analysis of ^1H NMR chemical-shift effects as well as dipolar ^1H-^1H or ^1H-^{13}C couplings provide site-specific insight into the local structure and the segmental dynamics, in particular, of phenyl rings and -CH_2O- linking units within the dendrons.[235] The microdomain structure of poly (L-alanine)-β-poly (ethylene glycol) monomethyl ether, MPEG-PLA, used as a new amphiphilic diblock copolymer was

characterized by proton spin diffusion experiments with ^{13}C detection and ^{1}H wideline separation 2D ^{1}H, ^{13}C NMR experiment (WISE-NMR spectroscopy).[236] Solid state NMR spectroscopy is used to monitor the layer-by-layer growth of polyelectrolyte multilayers on colloidal silica. The dynamics and conformation of polyelectrolyte multilayers comprised of the weak polycation, poly(allylamine) hydrochloride, and the strong polyanion, poly(sodium-4-styrene sulfonate), assembled at pH 7 and pH 10 were studied by a combination of ^{1}H and ^{13}C NMR measurements.[237] The high degree of self-assembling of epoxide-based products made from functionalized organosilica building blocks, functionalized oligo(oxypropylene)-diamine and/or -triamine, and colloidal silica nanoparticles was evidenced by solid state NMR spectroscopy, small-angle X-ray scattering (SAXS), and atomic force microscopy (AFM). 2D solid state NMR experiments (2D CRAMPS, 2D ^{1}H-^{13}C and ^{1}H-^{29}Si HETCOR, WISE) revealed differences in structure and segmental dynamics of final films as well as in self-organization and homogeneity degree depending on reaction conditions.[238] ^{1}H wideline and ^{13}C CP MAS spin-lattice T_1 relaxation solid state NMR experiments have been performed in order to investigate the cure state of phenolic novolac resins. Due to the process of spin diffusion, a single averaged T_1 decay time was found which was sensitive to the cure state of the network structure.[239] Chain-level mixing in polyolefins is investigated for blends of polyisobutylene (PIB) and polyethylene-co-1-butene (PEB). Previous reports suggest that PIB exhibits unusual mixing behavior in certain saturated blends relative to other polyolefins, even though it is immiscible with most. VT ^{1}H, ^{2}H, ^{13}C, and ^{129}Xe NMR experiments are used to characterize local PIB chain dynamics in blends with PEB in which the concentration of 1-butene comonomer units is 23 or 66 wt %. Results from 1D and 2D solid state ^{13}C exchange experiments, ^{1}H relaxation measurements, and ^{2}H line shape analysis indicate that local conformational dynamics of the PIB CH_2 group in the polymer backbone increase significantly in blends with PEB copolymers containing 66 wt % butene comonomer (PEB-66).[240] The extent of mixing in blends of poly(hydroxybutyrate-co-hydroxyvalerate) (PHBV) and poly(vinyl acetate) (PVAc) has been measured using a number of different techniques, principally solid state NMR. DSC measurements indicated effective mixing of the polymer chains on a scale of several nanometres. The results of ^{1}H T_1 and ^{1}H $T_{1\rho}$, measurements confirm intimate mixing of the chains.[241] ^{13}C and ^{2}H NMR relaxation time measurements were performed on four linear styrene-isoprene tetrablock copolymers (SISI) of overall molecular weight about 12 000 g/mol in order to characterize the segmental dynamics of both components. The two isoprene blocks are equal in length as are the two styrene blocks. A wide range of temperatures (from 285 to 530 K) and several compositions (volume fraction of styrene: 23%, 42%, 60%, and 80%) were investigated. The NMR measurements show that the segmental relaxation times of styrene and isoprene segments differ by orders of magnitude.[242] Nanocomposites result from combinations of materials with vastly different properties in the nanometer scale. These materials exhibit many unique properties such as improved thermal stability, reduced flammability, and improved mechanical properties. Many of the properties associated with polymer-clay nanocomposites are a function of the extent of

exfoliation of the individual clay sheets or the quality of the nanodispersion. This work demonstrates that solid state NMR can be used to characterize, quantitatively, the nanodispersion of variously modified montmorillonite (MMT) clays in polystyrene (PS) matrices.[243] The chiral conducting polyaniline (PANI) nanocomposites [polyacrylic acid/polyaniline/(-)camphorsulfonic acid (CSA)] were synthesized using enzyme, horseradish peroxidase (HRP). It appears that the enzyme HRP apart being a biocatalyst, plays an important role during the polymerization, which allows PANI to prefer a specific helical conformation whether the induced chirality in the monomer-CSA complex is either by (+)CSA or (-)CSA. The structural characterization of these nanocomposites was examined by solid state ^{13}C CP MAS NMR.[244] A series of poly(ethylene oxide) (PEO)/fullerene (C_{60}) complexes are prepared by lyophilization. The intermolecular interaction and molecular motion in the complex are investigated by solid state ^{13}C NMR spectroscopy. An intense C_{60} signal due to the intermolecular CP was observed in the ^{13}C CP MAS spectra of the complex samples, indicating a high degree of dispersion of C_{60} in the complexes. By measuring the ^{13}C spin-lattice relaxation times and ^{1}H transverse relaxation times of the complex sample and by comparing the static ^{13}C spectrum of the pure C_{60} sample with that of the complex sample, it is demonstrated that there exist n-π interactions between the n-orbitals of the PEO ether oxygen and the π-system of C_{60}.[245] Dry and hydrated poly(vinyl alcohol) (PVA) gels with 55% (aPVA) and 61% (s-PVA) syndiotacticity and related PVA/lactyl chitosan (LC) blends have been investigated with ^{129}Xe and CP MAS ^{13}C NMR techniques.[246] A simple 2D solid state exchange NMR method to suppress significant undesirable diagonal signals was shown using dimethyl sulfone. This technique was extended and combined with MAS and was applied to polyethylene.[247] Isotactic polypropylene (iPP) modified by heterogeneous nucleation and molten state drawing was investigated using the DMTA and NMR methods. Changes in the macromolecular mobility, depending on the iPP structure and molten state drawing, was found by NMR lineshape and second moment measurements.[248] Branch contents in sparsely short-chain branched polyethylenes ($<C_{28}$) and end-group concentrations in linear polyethylenes were investigated by solid- and melt-state ^{13}C NMR using model copolymers of 1-octene, 1-octadecene, 1-hexacosene, and linear PE standards. Benchmark measurements were established for single-pulse acquisition under MAS on these melts at 423 K, using 7 mm ceramic rotors and commercially available solid state probes.[249] Four different bisureas such as hexamethylene bis(ω, N-hydroxyethylurea), tolylene 2,4,bis(ω, N-hydroxyethylurea), hexamethylene bis(ω, N-hydroxypropylurea), and tolylene 2,4-bis(ω, N-hydroxy-propylurea) were prepared by reacting ethanolamine or propanolamine with hexamethylene diisocyanate, (HMDI) or tolylene 2,4-diisocyanate (TDI) were studied by ^{13}C CP MAS NMR spectroscopy.[250] A series of high-resolution solid state ^{13}C NMR experiments were performed on both unstretched and in situ stretched natural rubber samples. From the ^{13}C CP MAS spectra, it was found that natural rubber does form small crystals at room temperature though the degree of crystallinity is very small. Furthermore, from the ^{13}C DD MAS spectra, the crystalline signals were found to increase with the

increase of draw ratio.[251] The structure and chain conformation of the form beta sample newly crystallized from the liquid crystalline (LC) glassy phase have been investigated for a main-chain thermotropic LC polyether, which was polymerized from 3,3′-dimethyl-4,4′- hydroxyl-biphenyl and 1,10-dibromodecane, by solid state ^{13}C NMR spectroscopy.[252] Gel permeation chromatography (GPC) and solid state ^{13}C NMR techniques were used to analyse the structural changes of poly(vinyl chloride) (PVC) in blends of a low-density polyethylene (LDPE) and PVC during melt blending.[253]

Novel polymer nanocomposites having potential anisotropic properties have been synthesized by in-situ intercalative polymerization of 2-ethynylpyridine in the lamellar galleries of Ca^{2+}-montmorillonite and were studied by solid state ^{13}C CP MAS NMR spectroscopy and X-ray diffraction.[254] ^{13}C CP MAS NMR experiments on polypeptides, poly(beta-benzyl L-aspartate) (PBLA), poly(γ-benzyl L-glutamate) (PBLG) and PBLA/PBLG blend have been carried out, in order to elucidate the conformational stability of the polypeptides in the solid state over a wide range of temperatures and its blending effect.[255] Solid state NMR studies of poly(ε-caprolactone)/clay nanocomposites were also carried out.[256] In this study, binary blends formed by poly(methyl methacrylate) (PMMA) and poly(vinyl pyrrolidone) were prepared by solution casting and evaluated by solution and solid state NMR.[257] The fraction of the surviving double bonds was estimated by solid state NMR in the polyisoprene block of a polyisoprene-polydimethylsiloxane (PI-PDMS) diblock.[258] The relationship between the number-average sequence length and the melting temperature of the block copolyesters prepared by quench after the transesterification reaction between poly(ethylene terephthalate) and poly(butylene terephthalate) was reported. In the solid state, ^{13}C NMR spectra was observed as the progress of the transesterification occurred in this system.[259] To study the influence of the stereochemistry on the possibility of cocrystallization of linear and cyclic aliphatic residues in copolyamides, a series of copolyamides 12.6/12.1,4- cyclohexanedicarboxylic acid (CHDA) with variable compositions were synthesized. From solid state NMR studies it could be deduced that cis-1,4-CHDA is present in the amorphous regions whereas the trans residues are located in both the crystalline and the amorphous phase.[260] The variation in molecular and electronic structure of doped (as synthesized) conducting, dedoped base, and redoped conducting forms of polyaniline (PANI) prepared by oxidative enzymatic polymerization of aniline with and without the presence of polyelectrolyte template was analysed by solid state ^{13}C and ^{15}N CP MAS NMR spectroscopy.[261] Poly(vinylimidazole-co-methyl methacrylate)-silica hybrids, bonded through hydrogen bond (PVM-SiO_2) or chemical bond (PVM(5)-SiO_2) between organic and inorganic units, were prepared and characterized. The characterization of PVM-SiO_2 and PVM(5)-SiO_2 hybrids were confirmed by IR, solid state ^{13}C and ^{29}Si NMR spectra.[262] The dynamics of atactic poly(acrylonitrile) (aPAN) have been investigated by variable-temperature ^{15}N CSA, 2D ^{15}N CSA exchange, and 2D ^{15}N pure-exchange NMR experiments on an aPAN sample with 100% ^{15}N-labeled nitrile side groups and by dielectric measurements.[263] Syndiotactic polystyrene (sPS) is known to form a clathrate compound with p-xylene and

m-xylene, called delta-form complex. In this study, the structures of the sPS/p-xylene and sPS/m- xylene systems were investigated by solid state ^{13}C NMR and X-ray diffraction.[264] Natural abundance solid state NMR of ^{15}N was applied to investigate the films of nylon-6 and their blends with poly(propylene oxide) (PPO). The NMR ^{15}N results allowed the identifation of the crystalline forms present in these blends and also confirmed the previous NMR results obtained by ^{13}C NMR study.[265] The effect of electron beam radiation on a perfluoroalkoxy (PFA) resin was examined using solid state high-speed MAS ^{19}F NMR spectroscopy and FTIR spectroscopy.[266] The radiation chemistry of poly(tetrafluoroethylene-co-hexafluoropropylene) (FEP) with a TFE mole fraction of 0.90 has been studied under vacuum using ^{60}Co γ-radiation over a range of temperatures and absorbed doses. The radiolysis temperatures were 300, 363, 423, 523 and 543 K. New structure formation in the copolymers was analysed by solid state ^{19}F NMR spectroscopy.[267] The changes in the conformation and molecular mobility accompanied by a phase transition in the crystalline domain were analysed for ethylene (E) and tetrafluoroethylene (TFE) copolymer, ETFE, using VT solid state ^{19}F MAS and ^{1}H-^{19}F CP MAS NMR spectroscopy.[268] The crystalline structures of poly(vinylidene fluoride) (PVDF) in PVDF/silica (SiO_2) binary and PVDF/poly(methyl methacrylate) (PMMA)/SiO_2 ternary hybrid composite films were investigated using IR analysis and solid state, high-speed MAS ^{19}F NMR spectroscopy.[269] The microphase composition of poly(butylene terephthalate)-block-poly(tetramethylene oxide) multiblock (PBT-block-PTMO) copolymers with varying content of PTMO soft block and varying block length was studied by ^{1}H NMR transverse magnetization relaxation (T_2 relaxation) and ^{1}H 2D DQ NMR experiments under fast MAS. The 2D NMR method showed the existence of the molecular scale mixing of PBT and PTMO blocks.[270] Direct measurement of chemical exchange events in the crystalline polycarbonate monomer 4,4′-isopropylidenediphenol (bisphenol A, BPA) was carried out *via* 2D ^{13}C solid state NMR reveals slow, large-amplitude aromatic ring reorientations. This is in contrast to X-ray diffraction, however, which indicated static crystalline structure.[271] Poly(p-phenylene vinylene) (PPV) has shown a great potential for electro-optical applications due to its electroluminescent and semiconducting properties. In this work, three ^{13}C solid state MAS exchange NMR techniques, in particular CODEX, were used to study conformational dynamics of phenylene rings in PPV.[272] The changes in the phase structures and molecular mobility caused by the ferroelectric-paraelectric phase transition of vinylidene fluoride (VDF) and trifluoroethylene (TrFE) copolymer, P(VDF75/TrFE25), were analysed using VT solid state ^{19}F MAS and ^{1}H -^{19}F CP MAS NMR spectroscopy.[273] Direct spectroscopic probes of individual chain conformation and free volume were used to measure the increasing perturbation in the local glass-transition temperature of one polymer chain with decreasing length scale of mixing in binary polyolefin blends. Solid state ^{2}H and ^{129}Xe NMR experiments reveal a compositional miscibility window in side-chain concentration for polyisobutylene (PIB)/poly(ethylene-co-butene) (PEB) blends.[274] The use of polystyrene beads from different origins in solid-phase organic synthesis was investigated after a simple cleaning procedure of the starting material. The resin

loadings of polystyrene bound phosphines were quantitatively determined by ^{31}P MAS NMR.[275]

The behavior of lithium ions in a comb-like polymer electrolyte with a chelating functional group has been characterized by differential scanning calorimetry (DSC), a.c. impedance, ^{13}C and ^{7}Li solid state NMR measurements.[276] An extensive NMR investigation of filler-free and SiO_2 nanoparticle-containing PEO-LiBETI polymer electrolytes prepared through a solvent-free procedure was reported. ^{7}Li and ^{19}F NMR spectra, spin-lattice relaxation times and self-diffusion coefficients were measured.[277] ^{1}H T_2 NMR relaxation times were used to follow the changes in the macromolecular chain mobility of a chemically (by dicumyl peroxide) cross-linked polybutadiene matrix. The same phenomenon was also studied by an investigation of the ability of the polymer to crystallize using DSC measurements.[278] Films of conjugated polymer blends were studied by NMR relaxometry to improve the understanding of the nanomorphology and segmental chain mobility. Whereas optical microscopy was applied to obtain a rough impression about the surface morphology, the T_1 and T_2 NMR relaxation decay times were determined in the solid state (^{13}C CP MAS and ^{1}H wideline NMR) to judge the homogeneity of the phase morphology, to estimate the size of phase separated molecular domains and to compare the local segmental chain mobility.[279] The information on molecular dynamics in solid state polymers is of importance for controlling mechanical strength, processibility, and biodegradability. The molecular motion at room temperature in the crystalline region of poly(butylene adipate) (PBA) and poly(ethylene succinate) (PES) have been investigated by the a T_{1C} method.[280] Sulfur-vulcanization and heat aging of natural rubber was investigated by solid state ^{13}C NMR along with the measurements of physical properties. ^{13}C NMR detects all of the sulfurization occurring in natural rubber network including inter- and intra-molecular cross-link and pendant linkages, while physical measurements such as modulus at small strain and equilibrium swelling postulate detect only an amount of physically effective crosslinks.[281] Solid state ^{13}C NMR experiments were performed under uniaxial deformation of natural rubber to investigate the changes in the structural and dynamical behavior of the amorphous region induced by elongation. The structural change was detected as the change in the ^{13}C CP chemical shifts and line shapes.[282]

6.11 Organometallic and Coordination Compounds. – Crystallization of ferrocene and ruthenocene substituted in the 1- and 1′-positions by two nitronyl nitroxide radicals gave the new crystal phases β-1 (besides the known phase α-1, α-2, and α-2 whose structures were determined by X-ray analysis and were investigated by ^{13}C and ^{1}H NMR spectroscopy with MAS NMR.[283] The solid state ^{119}Sn CP MAS NMR spectra of a series of triaryltin chlorides of the form Ar_3SnCl have been acquired. The indirect spin-spin coupling constants ($J(^{119}Sn$-$^{35}Cl)$), quadrupolar-dipolar shifts ($\delta(^{119}Sn$-$^{35}Cl)$), and the ^{119}Sn chemical shift tensors were extracted.[284] Powders of the zinc and copper(II) dimethyl-(MDtc), diethyl-(EDtc), and morpholinedithiocarbamate (MfDtc) complexes quantitatively absorb hexamethyleneimine (Hmi) to produce the adducts

$[M\{NH(CH_2)_6\}(S_2CNR_2)_2]$ (M = Zn, Cu; R = CH_3, C_2H_5; R_2 = $(CH_2)_4O$). The ^{15}N isotropic chemical shifts of the dithiocarbamate groups depend on alkyl substituents at the nitrogen atom.[285] Polynuclear silver(I) dialkyldithiocarbamate complexes (R = CH_3, C_2H_5, C_3H_7, iso-C_3H_7) were synthesized and studied by ^{13}C CP MAS and ^{15}N NMR.[286] The nickel(II) and copper(II) complexes $[M\{S_2P(OR)_2\}_2]$ (M = Ni, Cu-63, Cu-65; R = C_2H_5, C_3H_7, i-C_3H_7, C_4H_9, i-C_4H_9, s-C C_4H_9, i-C_5H_{11}, c-C_6H_{11}) with eight symmetric O,O′-dialkyl phosphorodithioates were synthesized, and their structures and spectral properties were studied by EPR and CP MAS ^{13}C and ^{31}P NMR.[287] ^{29}Si and ^{19}F MAS NMR spectra of isolated ^{29}Si-$^{19}F_2$ and ^{29}Si-$^{19}F_3$ spin systems in two organosilicon compounds of the type $RR'SiF_2$ and $RSiF_3$ (R, R′ = organic ligands) were examined by static and MAS NMR.[288] The crystal structure of tetra(propyn-1-yl)silane, $Si(C{=}CMe)_4$ (1), has revealed a completely asymmetric molecule (point group C-1). Since this finding concerns a single crystal, the bulk material of (1) was studied by solid state ^{29}Si and ^{13}C MAS NMR.[289] The first solid state ^{91}Zr NMR spectra of an organometallic zirconium complex, bis(cyclopentadienyl)dichlorozirconium(IV) (Cp_2ZrCl_2), are presented. Overlapping static and MAS ^{91}Zr NMR spectra of Cp_2ZrCl_2 and a zirconium oxide NMR rotor are presented to explore the possibility of conducting ^{91}Zr NMR experiments using standard ZrO_2 rotors.[290] The series of complexes $[CdX_2(C_5H_4NCOOR)]$ (X = Cl or Br; R = Me, Et, Pr-n or Pr-i) and $[CdX_2(C_5H_4NCOOR)_{(2)}]$ (X = 1; R = Me, Et, Pr-n, or Pr-i) have been obtained by the addition reaction of esters of 2-pyriclinecarboxylic acid to cadmium(II) halides. Structural information was compared with that deduced from ^{113}Cd CP MAS NMR experiments.[291] Single-crystal X-ray diffraction and CP MAS ^{13}C and ^{15}N NMR study of zinc N,N-Di-iso-butyldithiocarbamate complex.[292] A solid state multinuclear (^{23}Na, ^{15}N, ^{13}C, and ^{31}P) NMR study was reported on the relative affinity of monovalent cations for a stacking G-quartet structure formed by guanosine 5′-monophosphate (5′-GMP) self-association at pH 8. Two major types of cations are bound to the 5′-GMP structure: one at the surface and the other within the channel cavity between two G-quartets.[293]

6.12 Glasses and Amorphous Solids. – Multinuclear (^{13}C, ^{29}Si, ^{27}Al, ^{1}H) solid state NMR spectroscopy and EPR and FTIR experiments are employed to investigate the thermolysis of aluminum-modified poly(hydridovinylsilazane), $[Al(C_2H_4\text{-}SiH(NH)_3]_{(n)}$, from which Si-Al-C-N ceramics can be formed. In addition, a comparative study is provided for different aluminum-modified polysilazanes and polysilylcarbodiimides in the amorphous state at 1400°C.[294]
Silicon based polymers obtained by ammonolysis of organochlorosilylboranes and their pyrolytic transformation into Si-B-C-N ceramics were studied by a detailed solid state NMR investigation. The polymer to ceramic conversion was analysed by ^{11}B, ^{13}C, ^{15}N, and ^{29}Si MAS NMR spectroscopy as well as by thermal analysis measurements coupled with mass spectroscopy (TGA-MS).[295] Despite their strong implications for magmatic processes in the earth's interior and pressure-induced structural changes in other amorphous, covalent oxide materials, little is known, beyond the coordination numbers of the framework

cations, about the structures of silicate melts and glasses at high pressure. Here, multinuclear (^{27}Al and ^{17}O) solid state NMR and quantum chemical calculations were used to study the structures of silicate glasses quenched from melts at pressures up to 10 GPa in a multianvil apparatus. The pressure-induced changes in atomic configurations in the silicate melts included the formation of highly coordinated framework units.[296]

Colorless and transparent aluminium phosphate gels and glasses with P/Al ratios ranging from 0.5 to 3.0 were prepared *via* the sol-gel process using aluminium lactate and phosphoric acid as precursors.

Optimum pH ranges and thermal treatment conditions have been established on the basis of extensive solution- and solid state NMR spectroscopies. The NMR spectra helped identify the various types of local environments present in the sols, gels and glasses, thereby providing a mechanistic understanding of the molecular transformation processes involved.[297] Chemical structure of human bone mineral was studied by solid state MAS NMR. Trabecular and cortical bone samples from adult subjects were compared with mineral standards. Proton spectra were acquired with excellent spectral resolution provided by ultra-high speed MAS at 40 kHz. 2D ^{1}H-^{31}P NMR heteronuclear correlation was achieved by CP under fast MAS at 12 kHz. ^{31}P NMR was applied with CP from protons under slow MAS at 1 kHz.[298] Calcium aluminosilicate and calcium fluoro-aluminosilicate glasses have been characterized by ^{29}Si, ^{27}Al and ^{19}F MAS NMR. The two calcium aluminosilicate glasses examined were based on the composition $2SiO_2$ - Al_2O_3 - 2CaO and the mineral anorthite $2SiO_2$ - Al_2O_3 - CaO.[299] The crystallisation behaviour of $4.5SiO_2$-$3Al_2O_3$-$1.5P_2O_5$-(5-z)CaO-$zCaF_2$ glasses with z between 0 and 3 was investigated using ^{27}Al, ^{29}Si, ^{31}P and ^{19}F MAS NMR spectroscopy.[300] Five commercial ionomer glasses (Fuji IX, Ketac Molar, G338, G2, and G2SR) used to produce glass (ionomer) polyalkenoate dental cements were studied. ^{29}Si, ^{27}Al, ^{31}P and ^{19}F MAS NMR spectroscopy was used to characterise the glasses and the resulting spectra compared with previous studies of model glasses.[301]

Strontium is often substituted for calcium in order to confer radio-opacity in glasses used for dental cements, biocomposites and bioglass-ceramics. The present paper investigated the influence of substituting strontium for calcium in a glass of the following composition: $4.5SiO_23Al_2O_31.5P_2O5_3CaO_2CaF_2$, having a Ca:P ratio of 1.67 corresponding to calcium fluorapatite ($Ca_5(PO_4)_3F$). The glasses were characterized by MAS NMR, by differential scanning calorimetry (DSC) and X-ray powder diffraction (XRD).[302]

The crystallisation behaviour of $4.5SiO_2.3Al_2O_3.1.5P_2O_5.(5-z)CaO.zCaF_2$ glasses with z between 0 and 3 were investigated using differential scanning calorimetry (DSC), x-ray diffraction analysis and ^{27}Al, ^{29}Si, ^{31}P and ^{19}F MAS NMR spectroscopy.[303] Potassium fluorphlogopite glass ceramics are the basis of machinable ceramics. These materials can he machined to shape using tungsten carbide tooling. The crystallisation behaviour of $8SiO_2.YAl_2O_3.3.75MgO.2.25MgF_2.BaO$ glasses with Y varying between 1.5 and 3.5 were investigated using differential scanning calorimetry (DSC), x-ray diffraction analysis and ^{27}Al, ^{29}Si, ^{31}P and ^{19}F MAS NMR spectroscopy.[304]

6.13 Cements. – It is important to understand physical and chemical processes causing cement degradation in an oilwell downhole environment. In this regard, two cement formulations have been characterised at different ageing conditions using NMR and XRD techniques.[305] Ground granulated blast-furnace slag is a secondary product of cast-iron industry that can be used like a standard hydraulic binder. Solid state NMR and mechanical compression tests were used to determine the hydration products microstructure and performances.[306]

6.14 Microporous Solids and Related Materials. – Calculations have been carried out of ^{1}H, ^{15}N, and ^{13}C NMR chemical shift parameters, which are used to characterize the acid strength and accessibility of Bronsted acid sites in seven high-silica zeolites of structure types CHA, FAU, FER, MFI, MOR, MTW, and TON.[307] ^{109}Ag solid state NMR and optical methods was applied to probe dynamics and local environment of silver cations in a series of silver-exchanged zeolites as a function of hydration.[308] A MAS NMR probe has been developed to allow in situ measurements of NMR spectra. Two applications are targeted with this device: i) in situ and operando MAS NMR spectroscopy of working catalysts and ii) the hyperpolarized (HP) ^{129}Xe spectroscopy of porous materials under MAS and continuous flow conditions.[309] The ^{13}C CP MAS NMR was used to quantify a mixture of cubic MCM-48 and hexagonal MCM-41 mesophases by means of interpretation of their surfactant organization, which cannot be determined by X-ray diffraction (XRD) techniques.[310] Promoter (phosphate)-enhanced crystallization of MCM-41 has been studied by multinuclear solid state NMR spectroscopy with use of ^{13}C, ^{29}Si, and ^{31}P as probe nuclei.[311]

The silicon sites tetrahedrally connected to aluminum in framework positions of a molecular sieve may be identified by a selective reintroduction of the heteronuclear ^{27}Al-^{29}Si dipolar interaction through Rotational Echo Adiabatic Passage DOuble Resonance (REAPDOR) NMR, In this rotor synchronized ^{29}Si MAS experiment, an effective dipolar dephasing of the Si-O-Al, over Si-O-Si, environments is shown to aid in the identification of silicon sites in the immediate vicinity of aluminum.[312] Dynamics of p-nitroaniline (pNA) in FSM-type mesoporous silicas was investigated by means of ^{2}H and ^{13}C solid state NMR. Deuterated pNA (pNA-d) was loaded to FSM-16 (FSM) and modified FSM samples which were prepared by reactions of FSM with trimethylethoxysilane (C_1FSM), n-octyltriethoxysilane (C_8FSM) and 3-aminopropyltriethoxysilane (NH_2FSM).[313] Amorphous aluminum silicates, isolated from hydrothermal reactions used to form crystalline zeolite A, have been studied using a number of techniques. NMR studies using $^{29}Si\{^{1}H\}$ CP MAS and ^{27}Al and ^{23}Na MQ MAS methods provide information about the local atomic structure of the solids.[314] Multinuclear solid state NMR spectroscopy, employing ^{29}Si MAS, ^{27}Al MAS/3Q MAS and ^{47}Ti,^{49}Ti wide-line experiments, has been used for the structural characterization of titanium substituted ultra-stable zeolite Y (Ti-USY). ^{27}Al MAS experiments show the presence of aluminum in four (Al-IV), five (Al-V), and six (Al-V) coordination, whereas the multiplicity within Al-IV and Al-VI is revealed by ^{27}Al 3Q MAS experiments.[315] Mixed phosphates $Al_{1-x}Ga_xPO_4$ ($0.0 \leqslant x \leqslant 1.0$), with orthorhombic structure, have been prepared by co-precipitation method

followed by annealing at high temperature (T approximate to 1350°C) and investigated by using powder X-ray diffraction and solid state NMR spectroscopy.[316] VT high resolution MAS ^{29}Si NMR spectroscopy was used to study the phase transition between the low and high temperature versions of pure silica ferrierite.[317] In this paper, the oxidation of trimethylphosphine as an in situ probe reaction was performed to monitor the oxidation ability of different Ti species in TS-1 zeolite by ^{31}P MAS NMR spectra.[318] Sites and dynamics of p-nitroaniline (pNA) molecules in the micropores of siliceous ZSM-5 zeolite have been investigated by means of ^{2}H solid state NMR. The adsorbed amounts of pNA studied were about 1.5, 4 and 6 molecules per unit cell of ZSM-5. ^{2}H NMR and ^{13}C NMR revealed that the motion of pNA was a 180° flip-flop around the C-2 axis of the molecule when the adsorbed amount was less than four molecules per unit cell.[319] The dynamics of deuterated p-nitroaniline (pNA-d) molecules in zeolite ZSM-5 including Na^+ (NaZSM-5) were investigated by means of ^{2}H and ^{13}C solid state NMR to clarity the effects of Na^+ and hydrated Na^+.[320]

6.15 Surface Science and Catalysis. – The hydrogen bond interaction of pyridine with the silanol groups of the inner surfaces of MCM-41 and SBA-15 ordered mesoporous silica has been studied by a combination of solid state NMR techniques including ^{2}H static, ^{1}H and ^{29}Si MAS and ^{15}N CP MAS.[321] This paper is focused on the characterization and study of the catalytic properties of a natural soil from Etla, Oaxaca, Mexico. Thus, X-ray diffraction, energy dispersive spectroscopy, scanning electron microscopy, thermal methods, infrared spectroscopy, ^{27}Al and ^{29}Si solid state NMR spectroscopy and surface adsorption properties analyses for the target material were carried out.[322] Solid state NMR methods have been used to determine the mechanism for the fluorination reaction of $CHClF_2$ on alumina. The initial stages of fluorination lead to the formation of terminal F-Al groups (*i.e.*, fluorine bound through a single bond to an aluminum atom), which is consistent with a recent XPS report.[323] The well-known reaction between the ethoxy groups of the silane end of the γ-aminopropyltriethoxysilane (APTS) molecule and the silanols of silica, the amino ends of APTS molecules were observed to react in the gas phase with ethoxy groups of other APTS molecules. This was characterized by ^{29}Si CP MAS NMR.[324] The photocatalyic oxidation of dichloromethane over TiO_2 was studied using in situ FTIR and solid state NMR methods.[325] The first observations of the complete manifold of spinning sidebands (ssb) including both the central and satellite transitions in ^{51}V MAS NMR spectra of surface vanadia nanoparticles on titania in $DeNO_x$ catalysts are presented. ^{51}V quadrupole coupling and chemical shift anisotropy parameters for the dominating vanadia structure are determined from ^{51}V MAS NMR spectra recorded at 9.4 and 14.1 T.[326] In situ solid state NMR methodologies have been used to investigate the photocatalytic oxidation of ethanol (CH_3CH_2OH) over a series of SnO_2-based photocatalysts. The adsorption of ethanol on commercially available SnO_2 powder was studied using both CP ^{13}C NMR and REDOR experiments, and showed the formation of two surface ethanol species, hydrogen-bonded ethanol at surface hydroxyl groups and ethanol chemisorbed to the SnO_2 surface ($Sn\text{-}OCH_2CH_3$). ^{119}Sn NMR ex-

periments characterized the tin species on the porous Vycor glass support.[327] The time profiles of the intensities, line widths, and chemical shifts of ^{1}H NMR signals of adsorbed water at 358 K were investigated for six different TiO_2 photocatalysts with different properties by solid state ^{1}H NMR spectroscopy. The apparent single water peak was found to comprise the signals with different line widths and chemical shifts, which correspond to those of the water molecules with different structures and mobility.[328] Distinct hydrogen species are present in important inorganic solids such as zeolites, silicoaluminophosphates (SAPOs), mesoporous materials, amorphous silicas, and aluminas. These H species include hydrogens associated with acidic sites such as Al(OH)Si, non-framework aluminum sites, silanols, and surface functionalities. ^{1}H MAS NMR was used to directly analyse these.[329] In situ solid state NMR spectroscopy was employed to study the kinetics of hydrogen/deuterium exchange and scrambling as well as ^{13}C scrambling reactions of labeled propane over Al_2O_3-promoted sulfated zirconia (SZA) catalyst under mild conditions (30-102°C). This was monitored by ^{1}H, ^{2}H and ^{13}C MAS NMR.[330] Using ^{13}C MAS NMR, conversion of selectively ^{13}C-labelled n-butane on sulfated zirconia catalyst has been demonstrated to proceed initially *via* two parallel routes: scrambling of the selective ^{13}C label in the n-butane molecule and selective formation of isobutane. The combination of the results obtained by both in situ ^{13}C MAS NMR and ex situ GC-MS analysis provides evidence for the monomolecular mechanism of the ^{13}C-label scrambling, whereas isomerization into isobutane proceeds through a pure bimolecular mechanism.[331] New organic-inorganic hybrid catalysts were synthesized by covalent grafting of proline and benzylpenicillin derivatives into mesoporous MCM-41. These catalysts were extensively characterized using FTIR, ^{13}C CP MAS solid state NMR, XRD and TEM techniques.[332] The alkylation reaction of aniline with methanol on zeolites HY and CsOH/CsNaY was studied by in situ ^{13}C NMR spectroscopy under flow and batch conditions. Attention was focused on the identification of intermediates and on the determination of the formation mechanisms of the products.[333] Ethanol associates easily with $MgCl_2$ to form adducts of complex architecture, but until now available characterization methods have failed to identify the pure stoichiometric compounds and their structures. To remedy this, homonuclear and heteronuclear 2D correlated solid state NMR spectroscopy were applied to identify the pure compounds and the ethanol-to-magnesium coordination pattern. High spinning speed and Lee-Goldburg sequences were able to reduce the hydrogen spin-diffusion and homonuclear coupling in the crystalline solid, thus achieving high resolution also in the hydrogen domain.[334] Solid state ^{29}Si CP MAS NMR was used to investigate the microstructurre of SiO_2/polyethyleneglycol(PEG)-based proton conducting hybrid membranes, which were synthesized through acid catalysed sol-gel reactions.[335] Solid state NMR spectroscopy, specifically ^{29}Si and ^{27}Al MAS NMR, together with microactivity testing have been used to characterize the changes that occur in a fluid cracking catalyst (FCC) during gas oil cracking in a refinery fluid catalytic cracking unit (FCCU).[336]

Solid state NMR spectra showing single-quantum excitation of the ^{51}V ($I = 7/2$) central and six satellite transitions were obtained for polycrystalline V_2O_5

and x% V_2O_5-(100 – x%)WO_3 (10 mol % less than or equal to x less than or equal to 40 mol %) solids by MAS and static NMR spectroscopies. All MAS spectra show full spinning sideband manifolds resulting from incomplete averaging of the chemical shift and quadrupolar interaction anisotropies.[337]

6.16 Inorganic and Other Related Solids. – The first metal phosphate incorporating isonicotinate ligand, Zn(HINT)(HPO_4), was hydrothermally synthesized and characterized by single-crystal X-ray diffraction and ^{1}H MAS solid state NMR spectroscopy.[338] Proton dynamics in phase II of $CsHSO_4$ have been studied by ^{1}H NMR. ^{1}H spectral line shapes were traced between 210 and 470 K, and ^{1}H spin-lattice relaxation curves were measured between 310 and 470 K, taking into account the thermal history of the sample. The NMR results demonstrate that proton transfer between two neighboring SO_4 tetrahedra takes place much more easily than the reorientation of the SO_4 tetrahedra in phase II.[339] Solid state ^{1}H, ^{17}O MAS, ^{1}H-^{93}Nb TRAPDOR, and ^{1}H double quantum 2D MAS NMR experiments were used to characterize the oxygen, water, and hydroxyl environments in the monoprotonated hexaniobate material, $Na_7[HnB_6O_{19}]$.$15H_2O$. These solid state NMR experiments demonstrate that the proton is located on the bridging oxygen of the $[Nb_6O_{19}]^{8-}$ Cluster. The solid state NMR results also show that the Nb-OH protons are spatially isolated from similar protons, but undergo proton exchange with the water species located in the crystal lattice.[340]

A series of nano-SiO_2/PEO composites with different compositions were prepared and studied by solid state high-resolution NMR spectroscopy. The ^{1}H T_2 of PEO in the composites was measured *via* ^{1}H-^{13}C CP. It was found that with the increase of nano-SiO_2 content, the crystallinity of PEO decreased greatly while the mobility of PEO chains in the noncrystalline region of PEO decreases dramatically.[343] Nano-building blocks, as metal-oxo-alkoxo clusters, are good models for spectroscopic studies and good candidates for elaboration, by soft chemistry processes, of hybrid organic-inorganic materials. The focus of this work was on the cluster $Ti_{16}O_{16}(OEt)_{32}$ and its reactivity against propyl alcohol. High-resolution liquid and solid state (CP MAS) NMR spectroscopies was used to characterize properly the surface organic groups.[344] ^{29}Si and ^{13}C CP MAS NMR spectroscopy was used to follow the conversion of native silica to a p-chlorobenzamide bonded silica material. The benzamide bonded phase was prepared *via* a hydrosilation reaction of a hydride silica intermediate with p-chloro-N-allylbenzamide.[345] Colloidal poly(4-vinylpyridine)/silica and polystyrene/silica nanocomposite particles comprising 38% and 48% silica by mass, respectively, have been characterized by solid state NMR spectroscopy in order to probe the nature of the molecular interactions between the polymer and silica phases. The high-resolution ^{1}H-^{13}C and ^{1}H-^{29}Si correlation experiments used to extract this information are a novel combination of multipulse proton decoupling and Lee-Goldberg CP.[346] A VT high-resolution ^{13}C and ^{87}Rb solid state NMR study of powder rubidium hydrogen carbonate, $RbHCO_3$, was presented for the first time. At ambient temperature, $RbHCO_3$ is formed by centrosymmetric dimers linked by hydrogen bonds, but almost no information is available on

this compound concerning proton disorder and the low-temperature phase.[347] Reference compounds based on borazine units and polyborylborazines have been characterized by ^{15}N solid state NMR. The various nitrogen sites (B_3N, B_2NH, B_2NX (X = H, Me, Pr-i), BN(H)X and BNX_2 (X = Me, Pr-i) have been discriminated according to their CP behaviour and chemical shift values, which range from -265 to -350 ppm.[348] ^{17}O-enriched phenylphosphonic acid ($PhPO_3H_2$) was prepared from phosphonic acid dichloride and enriched water. This enriched phosphonic acid was used to prepare the titanium oxo-alkoxo-phosphonate as a model compound, and titanium oxide/phenylphosphonate hybrids either by sol-gel processing with $Ti(OPri)_4$ or by surface modification of a titania support. For comparison a gel sample was prepared using nonenriched $PhPO_3H_2$ and enriched water. The ^{17}O MAS NMR spectra of these 5 solids have been recorded at various magnetic fields (7.0, 9.4, and 17.6 T) and the isotropic chemical shifts and quadrupolar constants have been determined for the different oxygen sites: P = O, P-O-H, P-O-Ti, and OTix.[349] Solid state NMR characterization of hybrid aluminosilicate xerogels, by ^{17}O MAS and 3Q MAS techniques, evidences Si-O-Si and Si-O-Al oxygen sites, spectrally separated in MQ MAS experiments.[350] The local environments for oxygen in yttrium-containing pyrochlores and fluorites, $Y_2(B_{1-x}B'_x)_2O_7$ (B = Ti, B-' = Sn, Zr) are investigated by using solid state ^{17}O MAS NMR spectroscopy. The quadrupolar coupling constants of the I = 5/2 nucleus, ^{17}O are sufficiently small for these ionic oxides, that high-resolution spectra are obtained from the MAS spectra.[351] ^{17}O MAS NMR has been used to determine the nature of oxygen exchange in ZrW_2O_8. A highly effective isotopic labelling technique has been developed and 1D NMR and 2D exchange spectroscopy (EXSY) experiments have revealed that mutual exchange occurs between all oxygen sites, even at temperatures considerably below the alpha to beta order-disorder phase transition.[352] PDMS-M_xO_y (where M = Ge(IV), W(IV), Zr(IV), Nb(V), And Ta(V)) hybrid materials have been studied from the solution to the solid state through ^{17}O NMR spectroscopy.[353] ^{17}O, ^{39}K, and ^{47}Ti, ^{49}Ti solid state NMR studies of the nonlinear optical crystal potassium titanyl phosphate, $KTiOPO_4$ (KTP), are reported. The results are compared with ab initio calculations using the WIEN2k program and discussed in specific relation to the bond-polarizability approach for the calculation of second-order nonlinear optical properties.[354] $Al_{13}O_{16}(OH)_{24}$ Keggin structure and a Si_5O_{16} pentamer unit. We used ^{19}F, ^{27}Al, ^{29}Si MAS and ^{27}Al MQ MAS NMR spectroscopy of a series of samples with varying Al:Si and F:OH ratios to investigate the degree of atomic order in zunyite.[355] Potassium hydrogen carbonate $KHCO_3$ is formed of centrosymmetric dimers $(HCO_3^-)_2$ linked by hydrogen bonds, the protons being disordered in an asymmetric double-well potential at ambient temperature. This compound is a model for 0-dimensional hydrogen bonds. It undergoes a nonferroic nonferroelectric phase transition at T_c = 318 K, and the double-well potential becomes symmetric in the high-temperature phase. This phase transition is studied for the first time by variable-temperature ^{13}C and ^{39}K high-resolution solid state NMR experiments.[356] The mobility of water molecules and deuterons of the deuterated analogue of solid 12-tungstophosphoric acid, $H_3PW_{12}O_{40}.nH_2O$ (HPA) (n = 5.5 and 0.1), has been characterized by deuterium

solid state NMR. Analysis of the ^{2}H NMR line shape and spin-lattice relaxation times allowed the characterization of the deuteron and water dynamics in HPA, at different water contents, in the temperature range 103-383 K.[357] Magnetic local structure of a ferromagnetic layer-structured basic copper compound with dicaboxylate anion was examined by solid state high-resolution deuterium NMR above 200 K. The magnetic interaction in a copper layer was probed by the isotropic D NMR shift of OD^{-} ions.[358] MAS NMR was used to study deuterium site occupancy and dynamics in ZrNiD1.0 and ZrNiD3.0.[359] Lead fluoride, a superionic conductor was prepared in its nano-structured form by Inert Gas Condensation Technique (IGCT) using an Ultra High Vacuum (UHV) chamber. The average grain size was found to be in the range 9 to 43 nm. The existence of mixed phases (α- and PbF_2) was identified using XRD. Solid state ^{207}Pb MAS NMR was carried to average out the dipolar interaction and the resultant isotropic peaks were assigned to the corresponding phases.[360] The solid solution behavior of mixed halide (Cl/Br, Cl/I, and Br/I) sodalite systems as prepared by hydrothermal synthesis has been studied in detail by X-ray diffraction and solid state NMR. At a synthesis temperature of 450 K the rate of halide incorporation into the cages of mixed Cl/Br, Br/I, and Cl/I sodalites depends on the halide stoichiometry in the precursor gel and on the particular halogen anion. ^{23}Na and ^{27}Al NMR spectra acquired with MAS are sensitive to both halide composition and distribution and can be used to monitor the onset of phase separation.[361] Crystalline silicotitanate (CST), and the Nb-substituted CST (Nb-CST), are highly selective Cs^{+} sorbents, which makes them attractive materials for the selective removal of radioactive species from nuclear waste solutions. The structural basis for the improved Cs^{+} selectivity in the niobium analogs was investigated through a series of solid state MAS NMR experiments.[362] Solid state NMR is used to study the thermal decomposition of lithium tetrahydroaluminate into metallic aluminum, hydrogen and trilithium hexahydroaluminate. Aluminum sites in $LiAlH_4$ and Li_3AlH_6 were characterized using static, MAS and MQ MAS NMR.[363] The crystal structure of the sialon Ba S-phase $Ba_2Al_xSi_{12-x}N_{16-x}O_{2+x}$ was refined, for x^2, using Mo Ka single-crystal data.The S-phases were studied by ^{29}Si and ^{27}Al MAS NMR and the results are discussed in relation to proposed distributions of Si/Al and O/N atoms in the structure[364] High-resolution solid state ^{27}Al NMR data for two members of the magnetoplumbite group of structures, strontium hexaluminate ($SrAl_{12}O_{19}$, 'SA6') and calcium hexaluminate ($CaAl_{12}O_{19}$, 'CA6,' synthetic hibonite), acquired at 14.1 and 18.8 T fields. The high-field data allow, for the first time, the accurate observation of the NMR signal from the Al_2 sites, which have been previously described as 'pentacoordinate' but which appear instead to be very distorted tetrahedra, which give rise to ^{27}Al isotropic chemical shifts of about 57 ppm and nuclear quadrupolar coupling constants of about 21 MHz.[365] Sodium monothiophosphate(V) Na_3PO_3S is dimorphic. The metastable high temperature modification β-Na_3PO_3S crystallizes hexagonal with a = 8.996(4) and c = 5.216(2) Å. According to ^{31}P solid state NMR experiments, α-Na_3PO_3S exhibits at 20°C a non-axial-symmetric environment for the phosphorus nuclei in contrast to the results of the refined crystal structure. The number of crystallographically distinguishable positions for phos-

phorus and for sodium in Na_3PO_3S and Na_3PO_3S can be confirmed in good agreement with their crystal structures using solid state NMR spectroscopy.[366] A novel poly(vinyl phosphate) ligand was synthesized as a model of biopolymer ligands containing the OH ··· O hydrogen bonds and $CaHPO_4.2H_2O$ (brushite) composites with the polymer ligands were also prepared. Successful detection of the polymer ligand binding to the $CaHPO_4.2H_2O$ crystals is achieved by ^{31}P MAS NMR.[367] Amending poultry litter (PL) with aluminum sulfate (alum) has proven to be effective in reducing water-soluble phosphorus (P) in the litter and in runoff from fields that have received PL applications; it has therefore been suggested as a best management practice. This knowledge is important for the evaluation of the long-term stability and bioavailability of P, which is a necessary prerequisite for the assessment of the sustainability of intensive poultry operations. Both solid state MAS and CP MAS ^{31}P NMR as well as $^{31}P\{^{27}Al\}$-TRAPDOR were used to investigate P speciation in alum-amended and unamended PL.[368] ^{59}Co NMR experiments have been carried out on single-crystal and polycrystalline (powder) samples of (+/-)- tris(ethylenediamine)cobalt(III) chloride trihydrate, (+/-)$[Co(en)_3]Cl_3.3H_2O$, and of its dehydrate. Data collected on single crystals and polycrystalline samples indicated both the C_Q and CSA tensors.[369] The lithium vanadate $Li_xV_2O_5$ (x = 1.0, 1.2 and 1.4) has been prepared by solid state reaction method. The ^7Li MAS NMR, Laser Raman and FTIR spectroscopic analysis reveals the δ-LiV_2O_5 and γ-$LiVO_5$ phase formation. The ^7Li MAS NMR spectrum shows the chemical shift around -1 and -10 ppm, which confirms the presence of gamma and delta phases of lithium vanadate.[370] The structure of $Rb_2[Pd(Se_4)_2].Se_8$ has been investigated using ^{87}Rb MAS and static NMR and ^{77}Se MAS NMR. The number and the integrated intensities of the ^{87}Rb and ^{77}Se resonances are in full agreement with the crystallographic structure of the compound.[371] Solid solutions of $(1 - x)Pb(Mg_{1/3}Nb_{2/3})O_{3x}Pb(Sc_{1/2}Nb_{1/2})O_{-3}$ (PMN/PSN) have been investigated using high-resolution ^{93}Nb 3Q MAS NMR. In previous MAS NMR investigations, the local B-cation ordering in these relaxor ferroelectric solid solutions was quantitatively determined. However, in conventional 1D MAS spectra the effects of chemical shifts and quadrupole interaction are convoluted; this, in addition to the insufficient resolution, precludes reliable extraction of the values of isotropic chemical shift and quadrupole coupling product. In the current, 3Q MAS investigation, ^{93}Nb spectra are presented for concentrations x = 0, 0.1, 0.2, 0.6, 0.7, and 0.9 at high magnetic field (19.6 T) and fast sample spinning speed (35.7 kHz). Isotropic chemical shifts, together with C_Q and CSA tensors were obtained.[372] Analyses of the layer structure of Na-montmorillonite was performed using ^{27}Al MAS and ^{27}Al MQ MAS NMR techniques. Results of ^{27}Al MAS NMR measurements at higher magnetic field strength (16.4 T) suggest that the 4-coordinated Al site in Na-montmorillonite has two different structures. This was confirmed by the fact that two peaks corresponding to 4-coordinated Al are observed in the ^{27}Al MQ MAS NMR at high magnetic field strength.[373]

References

1. C. Dybowski, S. Bai, and S. van Bramer, *Anal. Chem.*, 2004, **76**, 3263-3267.
2. D. Sebastiani, *Mod. Phys. Lett. B*, 2003, **17**, 1301-1319.
3. I. Alkorta and J. Elguero, *Struct. Chem.*, 2003, **14**, 377-389.
4. J. Schatz, *Collect. Czech. Chem. Commun.*, 2004, **69**, 1169-1194.
5. R. E. Taylor, *Concepts in Magn. Reson. Part A*, 2004, **22A**, 37-49.
6. P. Conte, R. Spaccini, and A. Piccolo, *Prog. Nucl. Magn. Reson. Spectrosc.*, 2004, **44**, 215-223.
7. G. R. Court, *Nucl. Instrum. Methods Phys. Res. , Sect. A*, 2004, **526**, 65-69.
8. A. E. Aliev and K. D. M. Harris, *Struct. Bond.*, 2003, **108**, 1-53.
9. G. P. Drobny, J. R. Long, T. Karlsson, W. Shaw, J. Popham, N. Oyler, P. Bower, J. Stringer, D. Gregory, M. Mehta, and P. S. Stayton, *Annu. Rev. Phys. Chem.*, 2003, **54**, 531-571.
10. S. K. Straus, *Philos. Trans. R. Soc. London, B*, 2004, **359**, 997-1008.
11. S. Luca, H. Heise, and M. Baldus, *Acc. Chem. Res.*, 2003, **36**, 858-865.
12. B. Bechinger, *Crit. Rev. Plant Scien.*, 2004, **23**, 271-292.
13. A. Drechsler and F. Separovic, *Iubmb Life*, 2003, **55**, 515-523.
14. J. K. Lanyi, *Annu. Rev. Physiol.*, 2004, **66**, 665-688.
15. N. C. Nielsen, A. Malmendal, and T. Vosegaard, *Mol. Membr. Biol.*, 2004, **21**, 129-141.
16. R. L. Cook, *Anal. Bioanal. Chem.*, 2004, **378**, 1484-1503.
17. H. W. Spiess, *Macromol. Symp.*, 2003, **201**, 85-88.
18. S. Dzwigaj, *Curr. Opin. Solid State Mater. Sci.*, 2003, **7**, 461-470.
19. K. Srikanth, R. W. Schurko, I. Hung, and A. Ramamoorthy, *Mater. Sci. Technol.*, 2003, **19**, 1191-1196.
20. Z. R. Zhang, Y. Yang, and H. S. Liu, *Prog. Chem.*, 2003, **15**, 18-24.
21. J. Rocha, C. M. Morais, and C. Fernandez, *Clay Miner.*, 2003, **38**, 259-278.
22. V. Chevelkov, B. J. van Rossum, F. Castellani, K. Rehbein, A. Diehl, M. Hohwy, S. Steuernagel, F. Engelke, H. Oschkinat, and B. Reif, *J. Am. Chem. Soc.*, 2003, **125**, 7788-7789.
23. I. Fischbach, K. Thieme, A. Hoffmann, M. Hehn, and I. Schnell, *J. Magn. Reson.*, 2003, **165**, 102-115.
24. P. Gutsche, M. Rinsdorf, H. Zimmermann, H. Schmitt, and U. Haeberlen, *Solid State Nucl. Magn. Reson.*, 2004, **25**, 227-240.
25. M. Carravetta, X. Zhao, A. Bockmann, and M. H. Levitt, *Chem. Phys. Lett.*, 2003, **376**, 515-523.
26. F. Fayon, I. J. King, R. K. Harris, J. S. O. Evans, and D. Massiot, *Comptes Rendus Chimie*, 2004, **7**, 351-361.
27. E. H. Hardy, A. Detken, and B. H. Meier, *J. Magn. Reson.*, 2003, **165**, 208-218.
28. L. J. Mueller, D. W. Elliott, G. M. Leskowitz, J. Struppe, R. A. Olsen, K. C. Kim, and C. A. Reed, *J. Magn. Reson.*, 2004, **168**, 327-335.
29. M. Ernst, M. A. Meier, T. Tuherm, A. Samoson, and B. H. Meier, *J. Am. Chem. Soc.*, 2004, **126**, 4764-4765.
30. D. H. Brouwer, *J. Magn. Reson.* , 2003, **164**, 10-18.
31. J. Leppert, O. Ohlenschlager, M. Gorlach, and R. Ramachandran, *J. Biomol. NMR*, 2004, **29**, 319-324.
32. M. Ernst, A. Samoson, and B. H. Meier, *J. Magn. Reson.*, 2003, **163**, 332-339.
33. G. De Paepe, P. Hodgkinson, and L. Emsley, *Chem. Phys. Lett.*, 2003, **376**, 259-267.
34. G. Gerbaud, F. Ziarelli, and S. Caldarelli, *Chem. Phys. Lett.*, 2003, **377**, 1-5.

35. K. Nishimura and A. Naito, *Chem. Phys. Lett.*, 2003, **380**, 569-576.
36. J. Ashida and T. Asakura, *J. Magn. Reson.*, 2003, **165**, 180-183.
37. G. Antonioli and P. Hodgkinson, *J. Magn. Reson.*, 2004, **168**, 124-131.
38. J. C. C. Chan and R. Tycko, *J. Chem. Phys.*, 2004, **120**, 8349-8352.
39. R. W. Glaser, C. Sachse, U. H. N. Durr, P. Wadhwani, and A. S. Ulrich, *J. Magn. Reson.*, 2004, **168**, 153-163.
40. M. Bjerring and N. C. Nielsen, *Chem. Phys. Lett.*, 2003, **382**, 671-678.
41. A. T. Petkova and R. Tycko, *J. Magn. Reson.*, 2004, **168**, 137-146.
42. L. Duma, S. Hediger, A. Lesage, D. Sakellariou, and L. Emsley, *J. Magn. Reson.*, 2003, **162**, 90-101.
43. L. Duma, S. Hediger, A. Lesage, and L. Emsley, *J. Magn. Reson.*, 2003, **164**, 187-195.
44. N. Asakawa, *J. Mol. Struct. – Theochem.*, 2004, **675**, 29-35.
45. R. Siegel, T. T. Nakashima, and R. E. Wasylishen, *J. Phys. Chem. B*, 2004, **108**, 2218-2226.
46. P. E. Kristiansen, M. Carravetta, W. C. Lai, and M. H. Levitt, *Chem. Phys. Lett.*, 2004, **390**, 1-7.
47. S. V. Dvinskikh, H. Zimmermann, A. Maliniak, and D. Sandstrom, *J. Magn. Reson.*, 2004, **168**, 194-201.
48. H. Kim, T. A. Cross, and R. Q. Fu, *J. Magn. Reson.*, 2004, **168**, 147-152.
49. R. Tycko, *ChemPhysChem*, 2004, **5**, 863-868.
50. B. Alonso and D. Massiot, *J. Magn. Reson.*, 2003, **163**, 347-352.
51. R. Verel and B. H. Meier, *ChemPhysChem*, 2004, **5**, 851-862.
52. A. Brinkmann and M. Eden, *J. Chem. Phys.*, 2004, **120**, 11726-11745.
53. I. Fischbach, F. Ebert, H. W. Spiess, and I. Schnell, *ChemPhysChem*, 2004, **5**, 895-908.
54. S. V. Dvinskikh, H. Zimmermann, A. Maliniak, and D. Sandstrom, *J. Magn. Reson.*, 2003, **164**, 165-170.
55. M. Eden, *Chem. Phys. Lett.*, 2003, **378**, 55-64.
56. M. Veshtort and R. G. Griffin, *ChemPhysChem*, 2004, **5**, 834-850.
57. N. Ivchenko, C. E. Hughes, and M. H. Levitt, *J. Magn. Reson.*, 2003, **164**, 286-293.
58. R. Q. Fu, J. Hu, and T. A. Cross, *J. Magn. Reson.*, 2004, **168**, 8-17.
59. B. van Lagen and P. A. de Jager, *Fresenius Environ. Bull.*, 2003, **12**, 1211-1217.
60. C. Bonhomme and T. Azais, *Comptes Rendus Chimie*, 2004, **7**, 417-424.
61. G. Mali and F. Taulelle, *Chem. Comm.*, 2004, 868-869.
62. C. M. Morais, M. Lopes, C. Fernandez, and J. Rocha, *Magn. Reson. Chem.*, 2003, **41**, 679-688.
63. R. W. Schurko, I. Hung, and C. M. Widdifield, *Chem. Phys. Lett.*, 2003, **379**, 1-10.
64. H. T. Kwak, S. Prasad, T. Clark, and P. J. Grandinetti, *Solid State Nucl. Magn. Reson.*, 2003, **24**, 71-77.
65. A. S. Lipton, R. W. Heck, J. A. Sears, and P. D. Ellis, *J. Magn. Reson.*, 2004, **168**, 66-74.
66. P. J. M. van Bentum, J. C. Maan, J. W. M. van Os, and A. P. M. Kentgens, *Chem. Phys. Lett.*, 2003, **376**, 338-345.
67. Y. Kim, J. H. Hwang, and J. J. Park, *Bull. Korean Chem. Soc.*, 2003, **24**, 1281-1283.
68. K. Yamauchi, J. W. G. Janssen, and A. P. M. Kentgens, *J. Magn. Reson.*, 2004, **167**, 87-96.
69. N. Sinha, K. Schmidt-Rohr, and M. Hong, *J. Magn. Reson.*, 2004, **168**, 358-365.
70. X. L. Yao and M. Hong, *J. Am. Chem. Soc.*, 2004, **126**, 4199-4210.
71. R. K. Harris, P. Y. Ghi, R. B. Hammond, C. Y. Ma, and K. J. Roberts, *Chem. Comm.*, 2003, 2834-2835.

72. J. D. Gehman, E. K. Paulson, and K. W. Zilm, *J. Biomol. NMR*, 2003, **27**, 235-259.
73. A. Verhoeven, P. T. F. Williamson, H. Zimmermann, M. Ernst, and B. H. Meier, *J. Magn. Reson.*, 2004, **168**, 314-326.
74. J. S. A. D. Gunne, *J. Magn. Reson.*, 2003, **165**, 18-32.
75. J. Leppert, C. R. Urbinati, S. Hafner, O. Ohlenschlager, M. S. Swanson, M. Gorlach, and R. Ramachandran, *Nucleic Acids Res.*, 2004, **32**, 1177-1183.
76. L. M. McDowell, D. R. Studelska, B. Poliks, R. D. O'Connor, and J. Schaefer, *Biochemistry*, 2004, **43**, 6606-6611.
77. P. Bertani, K. Raya, and K. Hirschinger, *Comptes Rendus Chimie*, 2004, **7**, 363-369.
78. R. J. Darton, D. H. Brouwer, C. A. Fyfe, L. A. Villaescusa, and R. E. Morris, *Chem. Mater.*, 2004, **16**, 600-603.
79. G. L. Olsen, E. A. Louie, G. P. Drobny, and S. T. Sigurdsson, *Nucleic Acids Res.*, 2003, **31**, 5084-5089.
80. W. Strojek, M. Kalwei, and H. Eckert, *J. Phys. Chem. B*, 2004, **108**, 7061-7073.
81. Y. G. Yoon, B. G. Pfrommer, S. G. Louie, and A. Canning, *Solid State Commun.*, 2004, **131**, 15-19.
82. M. N. Manalo and A. C. de Dios, *J. Mol. Struct. Theochem.*, 2004, **675**, 1-8.
83. M. A. M. Forgeron, R. E. Wasylishen, and G. H. Penner, *J. Phys. Chem. A*, 2004, **108**, 4751-4758.
84. L. Duma, W. C. Lai, M. Carravetta, L. Emsley, S. P. Brown, and M. H. Levitt, *ChemPhysChem*, 2004, **5**, 815-833.
85. D. Massiot, F. Fayon, B. Alonso, J. Trebosc, and J. P. Amoureux, *J. Magn. Reson.*, 2003, **164**, 160-164.
86. M. A. M. Forgeron, M. Gee, and R. E. Wasylishen, *J. Phys. Chem. A*, 2004, **108**, 4895-4908.
87. T. Iijima, K. Hashi, A. Goto, T. Shimizu, and S. Ohki, *Physica B-Condensed Matter*, 2004, **346**, 476-478.
88. A. Hauch, H. Bildsoe, H. J. Jakobsen, and J. Skibsted, *J. Magn. Reson.*, 2003, **165**, 282-292.
89. T. Giavani, K. Johannsen, C. J. H. Jacobsen, N. Blom, H. Bildsoe, J. Skibsted, and H. J. Jakobsen, *Solid State Nucl. Magn. Reson.*, 2003, **24**, 218-235.
90. D. L. Bryce, K. Eichele, and R. E. Wasylishen, *Inorg. Chem.*, 2003, **42**, 5085-5096.
91. G. Silly, C. Legein, J. Y. Buzare, and F. Calvayrac, *Solid State Nucl. Magn. Reson.*, 2004, **25**, 241-251.
92. I. Hung and R. W. Schurko, *Solid State Nucl. Magn. Reson.*, 2003, **24**, 78-93.
93. Z. Tosner, O. Petrov, S. V. Dvinskikh, J. Kowalewski, and D. Sandstrom, *Chem. Phys. Lett.*, 2004, **388**, 208-211.
94. A. Hoffmann, D. Sebastiani, E. Sugiono, S. Yun, K. S. Kim, H. W. Spiess, and I. Schnell, *Chem. Phys. Lett.*, 2004, **388**, 164-169.
95. T. Mochida, D. Kuwahara, S. Miyajima, and T. Sugawara, *J. Phys. Chem. B*, 2003, **107**, 12315-12319.
96. C. Gervais, M. Profeta, V. Lafond, C. Bonhomme, T. Azais, H. Mutin, C. J. Pickard, F. Mauri, and F. Babonneau, *Magn. Reson. Chem.*, 2004, **42**, 445-452.
97. J. N. Latosinska, M. Latosinska, R. Utrecht, S. Mielcarek, and J. Pietrzak, *J. Mol. Struct.*, 2004, **694**, 211-217.
98. R. L. Te, U. J. Griesser, K. R. Morris, S. R. Byrn, and J. G. Stowell, *Cryst. Growth & Design*, 2003, **3**, 997-1004.
99. G. R. Goward, K. Saalwachter, I. Fischbach, and H. W. Spiess, *Solid State Nucl. Magn. Reson.*, 2003, **24**, 150-162.
100. D. Casarini, L. Lunazzi, A. Mazzanti, P. Mercandelli, and A. Sironi, *J. Org. Chem.*,

2004, **69**, 3574-3577.
101. P. S. Sidhu and J. A. Ripmeester, *Supramolecular Chem.*, 2003, **15**, 433-446.
102. A. Temeriusz, R. Anulewicz-Ostrowska, K. Paradowska, and I. Wawer, *J. Carbohydr. Chem.*, 2003, **22**, 593-601.
103. D. Braga, L. Maini, G. de Sanctis, K. Rubini, F. Grepioni, M. R. Chierotti, and R. Gobetto, *Chem. Eur. J.*, 2003, **9**, 5538-5548.
104. A. Terakita, H. Matsunaga, T. Ueda, T. Eguchi, M. Echigoya, K. Umemoto, and M. Godo, *Chem. Pharm. Bull.*, 2004, **52**, 546-551.
105. H. Kurosu, M. Kawasaki, M. Hirose, M. Yamada, S. M. Kang, M. Sone, H. Takezoe, and J. Watanabe, *J. Phys. Chem. A*, 2004, **108**, 4674-4678.
106. D. Maciejewska, I. Wolska, and V. Kowalska, *J. Mol. Struct.*, 2004, **693**, 27-34.
107. C. Akita, T. Kawaguchi, F. Kaneko, H. Yamamoto, and M. Suzuki, *J. Phys. Chem. B*, 2004, **108**, 4862-4868.
108. M. I. M. Wazeer, A. A. Isab, and A. El Rayyes, *Spectrsc. Int. J.*, 2004, **18**, 113-119.
109. J. M. Rubin-Preminger, J. Bernstein, R. K. Harris, I. R. Evans, and P. Y. Ghi, *Crystal Growth & Design*, 2004, **4**, 431-439.
110. G. D. Enright, K. A. Udachin, and J. A. Ripmeester, *Chem. Comm.*, 2004, 1360-1361.
111. A. Portieri, R. K. Harris, R. A. Fletton, R. W. Lancaster, and T. L. Threlfall, *Magn. Reson. Chem.*, 2004, **42**, 313-320.
112. R. M. Claramunt, C. Lopez, J. Elguero, A. L. Rheingold, L. N. Zakharov, and S. Trofimenko, *Arkivoc*, 2003, 209-219.
113. M. I. M. Wazeer, A. A. Isab, and H. P. Perzanowski, *Magn. Reson. Chem.*, 2003, **41**, 1026-1029.
114. S. Grilli, L. Lunazzi, A. Mazzanti, and M. Pinamonti, *Tetrahedron*, 2004, **60**, 4451-4458.
115. C. N. Tam, J. A. Cowan, A. J. Schultz, V. G. Young, F. R. Trouw, and A. G. Sykes, *J. Phys. Chem. B*, 2003, **107**, 7601-7606.
116. J. S. Clawson, K. L. Anderson, R. J. Pugmire, and D. A. Grant, *J. Phys. Chem. A*, 2004, **108**, 2638-2644.
117. T. I. Igumenova and A. E. McDermott, *J. Magn. Reson.*, 2003, **164**, 270-285.
118. T. Giavani, H. Bildsoe, J. Skibsted, and H. J. Jakobsen, *J. Magn. Reson.*, 2004, **166**, 262-272.
119. K. J. Pike, V. Lemaitre, A. Kukol, T. Anupold, A. Samoson, A. P. Howes, A. Watts, M. E. Smith, and R. Dupree, *J. Phys. Chem. B*, 2004, **108**, 9256-9263.
120. E. Y. Chekmenev, Q. W. Zhang, K. W. Waddell, M. S. Mashuta, and R. J. Wittebort, *J. Am. Chem. Soc.*, 2004, **126**, 379-384.
121. H. H. Sun and E. Oldfield, *J. Am. Chem. Soc.*, 2004, **126**, 4726-4734.
122. A. Iuga and E. Brunner, *Magn. Reson. Chem.*, 2004, **42**, 369-372.
123. J. C. C. Chan and R. Tycko, *J. Am. Chem. Soc.*, 2003, **125**, 11828-11829.
124. D. Yang, Y. H. Zhang, B. Li, D. W. Zhang, J. C. Y. Chan, N. Y. Zhu, S. W. Luo, and Y. D. Wu, *J. Am. Chem. Soc.*, 2004, **126**, 6956-6966.
125. K. A. H. Wildman, E. E. Wilson, D. K. Lee, and A. Ramamoorthy, *Solid State Nucl. Magn. Reson.*, 2003, **24**, 94-109.
126. A. Krusheinitsky, D. Faizullin, and D. Reichert, *Biopolymers*, 2004, **73**, 1-15.
127. K. A. H. Wildman, A. Ramamoorthy, T. Wakamiya, T. Yoshikawa, M. Crisma, C. Toniolo, and F. Formaggio, *J. Pep. Sci.*, 2004, **10**, 336-341.
128. T. Fujiwara, Y. Todokoro, H. Yanagishita, M. Tawarayama, T. Kohno, K. Wakamatsu, and H. Akutsu, *J. Biomol. NMR*, 2004, **28**, 311-325.
129. M. Hong, D. Isailovic, R. A. McMillan, and V. P. Conticello, *Biopolymers*, 2003, **70**, 158-168.

130. K. K. Kumashiro, T. L. Kurano, W. P. Niemczura, M. Martino, and A. M. Tamburro, *Biopolymers*, 2003, **70**, 221-226.
131. J. J. Buffy, A. J. Waring, R. I. Lehrer, and M. Hong, *Biochemistry*, 2003, **42**, 13725-13734.
132. E. Strandberg, S. Ozdirekcan, D. T. S. Rijkers, P. C. A. van der Wel, R. E. Koeppe, R. M. J. Liskamp, and J. A. Killian, *Biophys. J.*, 2004, **86**, 3709-3721.
133. J. Yang and D. P. Weliky, *Biochemistry*, 2003, **42**, 11879-11890.
134. G. J. Gallagher, M. Hong, and L. K. Thompson, *Biochemistry*, 2004, **43**, 7899-7906.
135. P. Barre, O. Zschornig, K. Arnold, and D. Huster, *Biochemistry*, 2003, **42**, 8377-8386.
136. S. Sharpe, N. Kessler, J. A. Anglister, W. M. Yau, and R. Tycko, *J. Am. Chem. Soc.*, 2004, **126**, 4979-4990.
137. M. S. Balla, J. H. Bowie, and F. Separovic, *Eur. Biophys. J.*, 2004, **33**, 109-116.
138. I. Marcotte, E. J. Dufourc, M. Ouellet, and M. Auger, *Biophys. J.*, 2003, **85**, 328-339.
139. R. W. Martin and K. W. Zilm, *J. Magn. Reson.*, 2003, **165**, 162-174.
140. L. Duma, S. Hediger, B. Brutscher, A. Bockmann, and L. Emsley, *J. Am. Chem. Soc.*, 2003, **125**, 11816-11817.
141. F. Castellani, B. J. van Rossum, A. Diehl, K. Rehbein, and H. Oschkinat, *Biochemistry*, 2003, **42**, 11476-11483.
142. E. Katoh, K. Takegoshi, and T. Terao, *J. Am. Chem. Soc.*, 2004, **126**, 3653-3657.
143. E. K. Paulson, C. R. Morcombe, V. Gaponenko, B. Dancheck, R. A. Byrd, and K. W. Zilm, *J. Am. Chem. Soc.*, 2003, **125**, 14222-14223.
144. T. Vosegaard and N. C. Nielsen, *Magn. Reson. Chem.*, 2004, **42**, 285-290.
145. S. K. Straus, W. R. P. Scott, and A. Watts, *J. Biomol. NMR*, 2003, **26**, 283-295.
146. S. Yamaguchi, S. Tuzi, J. U. Bowie, and H. Saito, *Biochim. Biophys. Acta*, 2004, **1698**, 97-105.
147. A. G. Krushelnitsky, G. Hempel, and D. Reichert, *Biochim. Biophys. Acta*, 2003, **1650**, 117-127.
148. D. Reichert, O. Pascui, E. R. deAzevedo, T. J. Bonagamba, K. Arnold, and D. Huster, *Magn. Reson. Chem.*, 2004, **42**, 276-284.
149. A. Lesage and A. Bockmann, *J. Am. Chem. Soc.*, 2003, **125**, 13336-13337.
150. L. Calucci, C. Forte, L. Galleschi, M. Geppi, and S. Ghiringhelli, *Int. J. Biol. Macromol.*, 2003, **32**, 179-189.
151. E. K. Paulson, C. R. Morcombe, V. Gaponenko, B. Dancheck, R. A. Byrd, and K. W. Zilm, *J. Am. Chem. Soc.*, 2003, **125**, 15831-15836.
152. T. I. Igumenova, A. J. Wand, and A. E. McDermott, *J. Am. Chem. Soc.*, 2004, **126**, 5323-5331.
153. T. I. Igumenova, A. E. McDermott, K. W. Zilm, R. W. Martin, E. K. Paulson, and A. J. Wand, *J. Am. Chem. Soc.*, 2004, **126**, 6720-6727.
154. R. Bertram, T. Asbury, F. Fabiola, J. R. Quine, T. A. Cross, and M. S. Chapman, *J. Magn. Reson.*, 2003, **163**, 300-309.
155. H. Saito, K. Yamamoto, S. Tuzi, and S. Yamaguchi, *Biochim. Biophys. Acta*, 2003, **1616**, 127-136.
156. P. Barre, S. Yamaguchi, H. Saito, and D. Huster, *Eur. Biophys. J.*, 2003, **32**, 578-584.
157. H. Saito, S. Yamaguchi, H. Okuda, A. Shiraishi, and S. Tuzi, *Solid State Nucl. Magn. Reson.*, 2004, **25**, 5-14.
158. H. Saito, S. Yamaguchi, K. Ogawa, S. Tuzi, M. Marquez, C. Sanz, and E. Padros, *Biophys. J.*, 2004, **86**, 1673-1681.
159. H. Saito, J. Mikami, S. Yamaguchi, M. Tanio, A. Kira, T. Arakawa, K. Yamamoto, and S. Tuzi, *Magn. Reson. Chem.*, 2004, **42**, 218-230.

160. A. T. Petkova, G. Buntkowsky, F. Dyda, R. D. Leapman, W. M. Yau, and R. Tycko, *J. Mol. Biol.*, 2004, **335**, 247-260.
161. A. Naito, M. Kamihira, R. Inoue, and H. Saito, *Magn. Reson. Chem.*, 2004, **42**, 247-257.
162. N. A. Oyler and R. Tycko, *J. Am. Chem. Soc.*, 2004, **126**, 4478-4479.
163. K. Ohgo, T. L. Kurano, K. K. Kumashiro, and T. Asakura, *Biomacromolecules*, 2004, **5**, 744-750.
164. T. Asakura, K. Suita, T. Kameda, S. Afonin, and A. S. Ulrich, *Magn. Reson. Chem.*, 2004, **42**, 258-266.
165. D. B. Zax, D. E. Armanios, S. Horak, C. Malowniak, and Z. T. Yang, *Biomacromolecules*, 2004, **5**, 732-738.
166. G. P. Holland, R. V. Lewis, and J. L. Yarger, *J. Am. Chem. Soc.*, 2004, **126**, 5867-5872.
167. T. Asakura and Y. Nakazawa, *Macromol. Biosci.*, 2004, **4**, 175-185.
168. J. M. Yao, Y. Nakazawa, and T. Asakura, *Biomacromolecules*, 2004, **5**, 680-688.
169. N. A. Nusair, E. K. Tiburu, P. C. Dave, and G. A. Lorigan, *J. Magn. Reson.*, 2004, **168**, 228-237.
170. E. K. Tiburu, P. C. Dave, and G. A. Lorigan, *Magn. Reson. Chem.*, 2004, **42**, 132-138.
171. J. X. Lu, M. A. Caporini, and G. A. Lorigan, *J. Magn. Reson.*, 2004, **168**, 18-30.
172. P. C. Dave, E. K. Tiburu, K. Damodaran, and G. A. Lorigan, *Biophys. J.*, 2004, **86**, 1564-1573.
173. C. M. Moraes and B. Bechinger, *Magn. Reson. Chem.*, 2004, **42**, 155-161.
174. B. Bechinger and M. Weik, *Biophys. J.*, 2003, **85**, 361-369.
175. R. Ulrich, R. W. Glaser, and A. S. Ulrich, *J. Magn. Reson.*, 2003, **164**, 115-127.
176. R. W. Glaser and A. S. Ulrich, *J. Magn. Reson.*, 2003, **164**, 104-114.
177. J. Brus and A. Jegorov, *J. Phys. Chem. A*, 2004, **108**, 3955-3964.
178. A. Koga, E. Yonemochi, M. Machida, Y. Aso, H. Ushio, and K. Terada, *Int. J. Pharm.*, 2004, **275**, 73-83.
179. R. A. Olsen, J. Struppe, D. W. Elliott, R. J. Thomas, and L. J. Mueller, *J. Am. Chem. Soc.*, 2003, **125**, 11784-11785.
180. J. W. Lubach, B. E. Padden, S. L. Winslow, J. S. Salsbury, D. B. Masters, E. M. Topp, and E. J. Munson, *Anal. Bioanal. Chem.*, 2004, **378**, 1504-1510.
181. A. U. Gjerde, H. Holmsen, and W. Nerdal, *Biochim. Biophys. Acta*, 2004, **1682**, 28-37.
182. J. S. Santos, D. K. Lee, and A. Ramamoorthy, *Magn. Reson. Chem.*, 2004, **42**, 105-114.
183. Z. R. Ma, D. H. Barich, M. S. Solum, and R. J. Pugmire, *J. Agric. Food Chem.*, 2004, **52**, 215-221.
184. A. Forster, D. Apperley, J. Hempenstall, R. Lancaster, and T. Rades, *Pharmazie*, 2003, **58**, 761-762.
185. R. J. Iuliucci, J. Clawson, J. Z. Hu, M. S. Solum, D. Barich, D. M. Grant, and C. M. V. Taylor, *Solid State Nucl. Magn. Reson.*, 2003, **24**, 23-38.
186. T. W. Allen, O. S. Andersen, and B. Roux, *J. Am. Chem. Soc.*, 2003, **125**, 9868-9877.
187. T. Kameda, G. McGeorge, A. M. Orendt, and D. M. Grant, *J. Biomol. NMR*, 2004, **29**, 281-288.
188. S. Viel, D. Capitani, N. Proietti, F. Ziarelli, and A. L. Segre, *Appl. Phys. A*, 2004, **79**, 357-361.
189. N. J. Mathers, Z. H. Xu, T. J. Blumfield, S. J. Berners-Price, and P. G. Saffigna, *Forest Eco. Manag.*, 2003, **175**, 467-488.

190. T. Liitia, S. L. Maunu, B. Hortling, T. Tamminen, O. Pekkala, and A. Varhimo, *Cellulose*, 2003, **10**, 307-316.
191. S. H. Yang, X. D. Wu, X. Y. Wang, L. A. Samuelson, A. L. Cholli, and J. Kumar, *J. Macromol. Sci. -Pure Appl. Chem.*, 2003, **A40**, 1275-1282.
192. H. R. Tang and B. P. Hills, *Biomacromolecules*, 2003, **4**, 1269-1276.
193. P. Sikorski, M. Wada, L. Heux, H. Shintani, and B. T. Stokke, *Macromolecules*, 2004, **37**, 4547-4553.
194. C. M. Preston and P. D. Forrester, *J. Environ. Qual.*, 2004, **33**, 767-777.
195. P. T. Larsson, *Hemicelluloses: Sci. Tech.*, 2004, **864**, 254-268.
196. T. J. Bootten, P. J. Harris, L. D. Melton, and R. H. Newman, *J. Exp. Bot.*, 2004, **55**, 571-583.
197. H. Kono and Y. Numata, *Polymer*, 2004, **45**, 4541-4547.
198. H. Kono, Y. Numata, T. Erata, and M. Takai, *Polymer*, 2004, **45**, 2843-2852.
199. G. Widmalm, K. Jansson, G. Pellijeff, and D. Sandstrom, *J. Phys. Chem. B*, 2003, **107**, 11794-11798.
200. M. Lahaye, C. Rondeau-Mouro, E. Deniaud, and A. Buleon, *Carbohydr. Res.*, 2003, **338**, 1559-1569.
201. J. S. Chen and C. Y. Chiu, *Geoderma*, 2003, **117**, 129-141.
202. C. N. Goncalves, R. S. D. Dalmolin, D. P. Dick, H. Knicker, E. Klamt, and I. Kogel-Knabner, *Geoderma*, 2003, **116**, 373-392.
203. E. Kaiser, A. J. Simpson, K. J. Dria, B. Sulzberger, and P. G. Hatcher, *Environ. Sci. Tech.*, 2003, **37**, 2929-2935.
204. N. Maie, A. Watanabe, and M. Kimura, *Geoderma*, 2004, **120**, 309-323.
205. M. Schilling and W. T. Cooper, *Anal. Chim. Acta*, 2004, **508**, 207-216.
206. C. J. Golding, R. J. Smernik, and G. F. Birch, *Mar. Fresh. Res.*, 2004, **55**, 285-293.
207. R. J. Smernik, D. C. Olk, and N. Mahieu, *Eur. J. Soil Sci.*, 2004, **55**, 367-379.
208. A. Kolbl and I. Kogel-Knabner, *J. Plant Nut. Soil Sci.-Zeitschrift fur Pflanzenernahrung und Bodenkunde*, 2004, **167**, 45-53.
209. G. Almendros, H. Knicker, and F. J. Gonzalez-Vila, *Org. Geochem.*, 2003, **34**, 1559-1568.
210. M. Khalaf, S. D. Kohl, E. Klumpp, J. A. Rice, and E. Tombacz, *Environ. Sci. Tech*, 2003, **37**, 2855-2860.
211. J. D. Mao and K. Schmidt-Rohr, *Environ. Sci. Tech*, 2004, **38**, 2680-2684.
212. S. Hiradate, *Soil Sci. Plant Nut.*, 2004, **50**, 303-314.
213. A. D. Alexeev, E. V. Ulyanova, G. P. Starikov, and N. N. Kovriga, *Fuel*, 2004, **83**, 1407-1411.
214. A. Georgakopoulos, *J. Serb. Chem. Soc.*, 2003, **68**, 599-605.
215. K. Kidena, K. Matsumoto, M. Katsuyama, S. Murata, and M. Nomura, *Fuel Proces. Tech.*, 2004, **85**, 827-835.
216. K. Kidena, Y. Tani, S. Murata, and M. Nomura, *Fuel*, 2004, **83**, 1697-1702.
217. K. Abelmann, K. U. Totsche, H. Knicker, and I. Kogel-Knabner, *Solid State Nucl. Magn. Reson.*, 2004, **25**, 252-266.
218. K. Kanehashi and K. Saito, *Fuel Proces. Tech.*, 2004, **85**, 873-885.
219. A. D. Alexeev, T. A. Vasylenko, and E. V. Ul'yanova, *Solid State Commun.*, 2004, **130**, 669-673.
220. T. M. Alam, *Mater. Chem. Phys.*, 2004, **85**, 310-315.
221. M. Carravetta, Y. Murata, M. Murata, I. Heinmaa, R. Stern, A. Tontcheva, A. Samoson, Y. Rubin, K. Komatsu, and M. H. Levitt, *J. Am. Chem. Soc.*, 2004, **126**, 4092-4093.

222. R. W. Schurko, M. J. Willans, B. Skadtchenko, and D. M. Antonelli, *J. Solid State Chem.*, 2004, **177**, 2255-2264.
223. P. Sozzani, A. Comotti, S. Bracco, and R. Simonutti, *Chem. Comm.*, 2004, 768-769.
224. K. L. Ngai and C. M. Roland, *Macromolecules*, 2004, **37**, 2817-2822.
225. X. Q. Zhang, I. Burgar, E. Lourbakos, and H. Beh, *Polymer*, 2004, **45**, 3305-3312.
226. T. M. Alam and H. Y. Fan, *Macromol. Chem. Phys.*, 2003, **204**, 2023-2030.
227. A. Domjan, G. Erdodi, M. Wilhelm, M. Neidhofer, K. Landfester, B. Ivan, and H. W. Spiess, *Macromolecules*, 2003, **36**, 9107-9114.
228. K. Saalwachter, P. Ziegler, O. Spyckerelle, B. Haidar, A. Vidal, and J. U. Sommer, *J. Chem. Phys.*, 2003, **119**, 3468-3482.
229. A. Buda, D. E. Demco, B. Blumich, V. M. Litvinov, and J. P. Penning, *Chem. Phys. Chem.*, 2004, **5**, 876-883.
230. N. Fatkullin, E. Fischer, C. Mattea, U. Beginn, and R. Kimmich, *Chem.Phys. Chem*, 2004, **5**, 884-894.
231. E. Diez-Pena, I. Quijada-Garrido, J. M. Barrales-Rienda, I. Schnell, and H. W. Spiess, *Macromol. Chem. Phys.* 2004, **205**, 438-447.
232. E. Diez-Pena, I. Quijada-Garrido, J. M. Barrales-Rienda, I. Schnell, and H. W. Spiess, *Macromol. Chem. Phys.*, 2004, **205**, 430-437.
233. J. Spevacek and J. Brus, *Macromol. Symp.*, 2003, **203**, 111-121.
234. H. P. Zhao, W. X. Lin, G. A. Yang, and Q. Chen, *Acta Polymerica Sinica*, 2003, 631-636.
235. A. Rapp, I. Schnell, D. Sebastiani, S. P. Brown, V. Percec, and H. W. Spiess, *J. Am. Chem. Soc.*, 2003, **125**, 13284-13297.
236. G. L. Wu, P. C. Sun, and J. B. Ma, *Chem. J. Chin. Univ. -Chinese*, 2003, **24**, 1515-1518.
237. R. N. Smith, M. McCormick, C. J. Barrett, L. Reven, and H. W. Spiess, *Macromolecules*, 2004, **37**, 4830-4838.
238. J. Brus, M. Spirkova, D. Hlavata, and A. Strachota, *Macromolecules*, 2004, **37**, 1346-1357.
239. P. Adriaensens, R. Rego, R. Carleer, B. Ottenbourgs, and J. Gelan, *Polym. Int.*, 2003, **52**, 1647-1652.
240. J. Wolak, X. Jia, H. Gracz, E. O. Stejskal, J. L. White, M. Wachowicz, and S. Jurga, *Macromolecules*, 2003, **36**, 4844-4850.
241. D. J. Hill, M. Markotsis, A. K. Whittaker, and K. W. Wong, *Polym. Int.*, 2003, **52**, 1780-1789.
242. Y. Y. He, T. R. Lutz, and M. D. Ediger, *Macromolecules*, 2003, **36**, 8040-8048.
243. S. Bourbigot, D. L. Vanderhart, J. W. Gilman, W. H. Awad, R. D. Davis, A. B. Morgan, and C. A. Wilkie, *J. Polym. Sci. Part B-Polym. Phys.*, 2003, **41**, 3188-3213.
244. M. Thiyagarajan, J. Kumar, L. A. Samuelson, and A. L. Cholli, *J. Macromol. Sci. -Pure Appl. Chem.*, 2003, **A40**, 1347-1355.
245. M. J. Li and Q. Chen, *Polymer* , 2003, **44**, 2793-2798.
246. S. N. Lai, E. Locci, G. Saba, I. Husu, G. Masci, V. Crescenzi, and A. Lai, *J. Polym. Sci. Part B-Polym. Phys.*, 2003, **41**, 3123-3131.
247. H. Kaji and F. Horii, *Chem. Phys. Lett.*, 2003, **377**, 322-328.
248. A. Romankiewicz, J. Jurga, and T. Sterzynski, *Macromol. Symp.*, 2003, **202**, 281-290.
249. M. Pollard, K. Klimke, R. Graf, H. W. Spiess, M. Wilhelm, O. Sperber, C. Piel, and W. Kaminsky, *Macromolecules*, 2004, **37**, 813-825.
250. R. Jayakumar and S. Nanjundan, *J. Polym. Sci. Part B-Polym. Chem.*, 2004, **42**, 1809-1819.
251. W. X. Lin, M. H. Bian, G. Yang, and Q. Chen, *Polymer*, 2004, **45**, 4939-4943.

252. M. Murakami, H. Ishida, H. Kaji, and F. Horii, *Polym. J.* 2004, **36**, 403-412.
253. N. Sombatsompop, K. Sungsanit, and C. Thongpin, *J. Appl. Polym. Sci.*, 2004, **92**, 3167-3172.
254. A. L. Cholli, S. K. Sahoo, D. W. Kim, J. Kumar, and A. Blumstein, *Polym. Micro. Nanoelectron*, 2004, **874**, 294-305.
255. K. Murata, E. Katoh, S. Kuroki, and I. Ando, *J. Mol. Struct.*, 2004, **689**, 223-235.
256. C. Calberg, R. Jerome, and J. Grandjean, *Langmuir*, 2004, **20**, 2039-2041.
257. T. M. F. F. Diniz and M. I. B. Tavares, *J. Appl. Polym. Sci.*, 2004, **93**, 372-377.
258. S. Hansen, M. E. Vigild, R. H. Berg, and S. Ndoni, *Polym. Bull.*, 2004, **51**, 403-409.
259. H. Matsuda, T. Asakura, B. Nagasaka, and K. Sato, *Macromolecules*, 2004, **37**, 4651-4657.
260. B. Vanhaecht, R. Willem, M. Biesemans, B. Goderis, M. Basiura, P. C. M. M. Magusin, I. Dolbnya, and C. E. Koning, *Macromolecules*, 2004, **37**, 421-428.
261. S. K. Sahoo, R. Nagarajan, S. Roy, L. A. Samuelson, J. Kumar, and A. L. Cholli, *Macromolecules*, 2004, **37**, 4130-4138.
262. Y. S. Chiu, K. H. Wu, and T. C. Chang, *Eur. Polym. J.*, 2003, **39**, 2253-2259.
263. H. Kaji, N. Miura, and K. Schmidt-Rohr, *Macromolecules*, 2003, **36**, 6100-6113.
264. Y. Yamamoto, M. Kishi, D. Amutharani, M. Sivakumar, Y. Tsujita, and H. Yoshimizu, *Polym. J.*, 2003, **35**, 465-469.
265. M. I. B. Tavares and C. M. G. de Souza, *J. Appl. Polym. Sci.*, 2003, **90**, 3872-3875.
266. T. R. Dargaville, G. A. George, D. J. T. Hill, U. Scheler, and A. K. Whittaker, *Macromolecules*, 2003, **36**, 7138-7142.
267. D. J. T. Hill, S. Mohajerani, A. K. Whittaker, and U. Scheler, *Polym. Int.*, 2003, **52**, 1725-1733.
268. K. Aimi and S. Ando, *Magn. Reson. Chem.*, 2004, **42**, 577-588.
269. J. W. Park, Y. A. Seo, I. Kim, C. S. Ha, K. Aimi, and S. Ando, *Macromolecules*, 2004, **37**, 429-436.
270. V. M. Litvinov, M. Bertmer, L. Gasper, D. E. Demco, and B. Blumich, *Macromolecules*, 2003, **36**, 7598-7606.
271. J. E. Wolak, J. Knutson, J. D. Martin, P. Boyle, A. L. Sargent, and J. L. White, *J. Phys. Chem. B*, 2003, **107**, 13293-13299.
272. E. R. deAzevedo, R. W. A. Franco, A. Marletta, R. M. Faria, and T. J. Bonagamba, *J. Chem. Phys.*, 2003, **119**, 2923-2934.
273. K. Aimi, S. Ando, P. Avalle, and R. K. Harris, *Polymer*, 2004, **45**, 2281-2290.
274. M. Wachowicz, J. Wolak, H. Gracz, E. O. Stejskal, S. Jurga, E. F. McCord, and J. L. White, *Macromolecules*, 2004, **37**, 4573-4579.
275. D. Rentsch, R. Hany, S. Barthelemy, and R. Steinauer, *Tet. Lett.*, 2003, **44**, 6987-6990.
276. W. H. Hou, C. Y. Chen, and C. C. Wang, *Solid State Ionics*, 2004, **166**, 397-405.
277. S. Suarez, S. Abbrent, S. G. Greenbaum, J. H. Shin, and S. Passerini, *Solid State Ionics*, 2004, **166**, 407-415.
278. J. F. Pilichowski, T. Liptaj, M. Morel, E. Terriac, and M. Baba, *Polym. Int.*, 2003, **52**, 1913-1918.
279. P. Adriaensens, R. Dams, L. Lutsen, D. Vanderzande, and J. Gelan, *Polymer*, 2004, **45** , 4499-4505.
280. K. Kuwabara, Z. H. Gan, T. Nakamura, H. Abe, and Y. Doi, *Polym. Degrad. Stab.*, 2004, **84**, 105-114.
281. M. Mori, *Rubber Chem. Technol.*, 2003, **76**, 1259-1275.
282. T. Kameda and T. Asakura, *Polymer*, 2003, **44**, 7539-7544.

283. C. Sporer, H. Heise, K. Wurst, D. Ruiz-Molina, H. Kopacka, P. Jaitner, F. Kohler, J. J. Novoa, and J. Veciana, *Chem. Eur. J.*, 2004, **10**, 1355-1365.
284. J. M. Geller, I. S. Butler, D. F. R. Gilson, F. G. Morin, I. Wharf, and F. Belanger-Gariepy, *Can. J. Chem. -Rev. Can. Chim.*, 2003, **81**, 1187-1195.
285. A. V. Ivanov, E. V. Novikova, S. A. Leskova, and W. Forsling, *Russ. J. Inorg. Chem.*, 2004, **49**, 95-101.
286. A. V. Ivanov, S. A. Zinkin, A. A. Konzelko, and W. Forsling, *Russ. J. Inorg. Chem.*, 2004, **49**, 593-598.
287. A. V. Ivanov, A. C. Larsson, N. A. Rodionova, A. V. Gerasimenko, O. N. Antzutkin, and W. Forsling, *Russ. J. Inorg. Chem.*, 2004, **49**, 373-385.
288. X. Helluy, R. Pietschnig, and A. Sebald, *Solid State Nucl. Magn. Reson.*, 2003, **24**, 286-300.
289. B. Wrackmeyer, O. L. Tok, and A. Badshah, *Zeit. Naturfors. Section B-A J. Chem. Sci.*, 2003, **58**, 809-812.
290. I. Hung and R. W. Schurko, *J. Phys. Chem. B*, 2004, **108**, 9060-9069.
291. R. March, J. Pons, J. Ros, W. Clegg, A. Alvarez-Larena, J. F. Piniella, and J. Sanz, *Inorg. Chem.*, 2003, **42**, 7403-7409.
292. A. V. Ivanov, E. V. Ivakhnenko, W. Forsling, and A. V. Gerasimenko, *Dok. Chem.*, 2003, **390**, 162-167.
293. A. Wong and G. Wu, *J. Am. Chem. Soc.*, 2003, **125**, 13895-13905.
294. F. Berger, M. Weinmann, F. Aldinger, and K. Muller, *Chem. Mater.*, 2004, **16**, 919-929.
295. C. Gervais, F. Babonneau, L. Ruwisch, R. Hauser, and R. Riedel, *Can. J. Chem. -Rev. Can. Chim.*, 2003, **81**, 1359-1369.
296. S. K. Lee, *J. Phys. Chem. B*, 2004, **108**, 5889-5900.
297. L. Zhang and H. Eckert, *J. Mater. Chem.*, 2004, **14**, 1605-1615.
298. Kaflak-Hachulska, A. Samoson, and W. Kolodziejski, *Calcif. Tissue Int.*, 2003, **73**, 476-486.
299. A. Stamboulis, R.G. Hill and R.V. Law *J. Non-Cryst. Solids*, 2004, **333**, 101-107
300. A. Stamboulis, R.G. Hill, R.V. Law and S. Matsuya *Key Eng. Mat.* 2004, **16**, 99-102
301. A. Stamboulis, R.G. Hill and R.V. Law *Biomaterials* 2004, **25**, 3907-3913
302. R.G. Hill, A. Stamboulis, R.V. Law, A. Clifford, M.R. Towler and C. Crowley *J. Non-Cryst. Solids*,
303. A. Stamboulis, R.G. Hill, R.V. Law and S. Matsuya *Phys. Chem. Glasses* 2004, **45**, 127-133
304. R.G. Hill, A. Stamboulis, R.V. Law, J. Hawes, *Phys. Chem. Glasses* 2004, **45** 121-126
305. G. Le Saout, E. Lecolier, A. Rivereau, and H. Zanni, *Comptes Rendus Chimie*, 2004, **7**, 383-388.
306. S. Murgier, H. Zanni, and D. Gouvenot, *Comptes Rendus Chimie*, 2004, **7**, 389-394.
307. A. Simperler, R. G. Bell, and M. W. Anderson, *J. Phys. Chem. B*, 2004, **108**, 7142-7151.
308. G. E. Pavlovskaya, C. F. Horton-Garcia, C. Dybowski, D. R. Corbin, and T. Meersmann, *J. Phys. Chem. B*, 2004, **108**, 1584-1589.
309. A. Nossov, F. Guenneau, M. A. Springuel-Huet, E. Haddad, V. Montouillout, B. Knott, F. Engelke, C. Fernandez, and A. Gedeon, *Phys. Chem. Chem. Phys.* 2003, **5**, 4479-4483.
310. H. Nur, L. C. Guan, S. Endud, and H. Hamdan, *Mater. Lett.*, 2004, **58**, 1971-1974.
311. S. C. Laha, M. D. Kadgaonkar, A. Anuji, S. Ganapathy, J. P. Amoureux, and R. Kumar, *J. Phys. Chem. B*, 2003, **107**, 14171-14175.
312. S. Ganapathy, R. Kumar, V. Montouillout, C. Fernandez, and J. P. Amoureux,

Chem. Phys. Lett., 2004, **390**, 79-83.
313. Y. Komori and S. Hayashi, *Micro. Mes. Mater.* 2004, **68**, 111-118.
314. H. X. Yang, R. I. Walton, S. Antonijevic, S. Wimperis, and A. C. Hannon, *J. Phys. Chem. B*, 2004, **108**, 8208-8217.
315. S. Ganapathy, K. U. Gore, R. Kumar, and J. P. Amoureux, *Solid State Nucl. Magn. Reson.*, 2003, **24**, 184-195.
316. S. K. Kulshreshtha, O. D. Jayakumar, and V. Sudarsan, *J. Phys. Chem. Solids*, 2004, **65**, 1141-1146.
317. R. J. Darton, P. Wormald, and R. E. Morris, *J. Mater. Chem.*, 2004, **14**, 2036-2040.
318. J. Q. Zhuang, D. Ma, Z. M. Yan, F. Deng, X. M. Liu, X. W. Han, X. H. Bao, X. W. Liu, X. W. Guo, and X. S. Wang, *J. Catal.*, 2004, **221**, 670-673.
319. Y. Komori and S. Hayashi, *Phys. Chem. Chem. Phys.*, 2003, **5**, 3777-3783.
320. Y. Komori and S. Hayashi, *Bull. Chem. Soc. Jpn.*, 2004, **77**, 673-679.
321. I. G. Shenderovich, G. Buntkowsky, A. Schreiber, E. Gedat, S. Sharif, J. Albrecht, N. S. Golubev, G. H. Findenegg, and H. H. Limbach, *J. Phys. Chem. B*, 2003, **107**, 11924-11939.
322. F. Delgado, H. Rios, J. M. Aceves, G. Penieres, G. Arroyo, B. Velasco, and R. Miranda, *Arkivoc*, 2003, 118-131.
323. P. J. Chupas and C. P. Grey, *J. Catal.*, 2004, **224**, 69-79.
324. S. Ek, E. I. Iiskola, L. Niinisto, T. T. Pakkanen, and A. Root, *Chem. Comm.*, 2003, 2032-2033.
325. J. Borisch, S. Pilkenton, M. L. Miller, D. Raftery, and J. S. Francisco, *J. Phys. Chem. B*, 2004, **108**, 5640-5646.
326. U. G. Nielsen, N. Y. Topsoe, M. Brorson, J. Skibsted, and H. J. Jakobsen, *J. Am. Chem. Soc.*, 2004, **126**, 4926-4933.
327. S. Pilkenton and D. Raftery, *Solid State Nucl. Magn. Reson.*, 2003, **24**, 236-253.
328. A. Y. Nosaka, T. Fujiwara, H. Yagi, H. Akutsu, and Y. Nosaka, *J. Phys. Chem. B*, 2004, **108**, 9121-9125.
329. G. J. Kennedy, M. Afeworki, D. C. Calabro, C. E. Chase, and R. J. Smiley, *Appl. Spectrosc.*, 2004, **58**, 698-704.
330. M. Haouas, S. Walspurger, F. Taulelle, and J. Sommer, *J. Am. Chem. Soc.*, 2004, **126**, 599-606.
331. M. V. Luzgin, S. S. Arzumanov, V. P. Shmachkova, N. S. Kotsarenko, V. A. Rogov, and A. G. Stepanov, *J. Catal.*, 2003, **220**, 233-239.
332. D. Dhar, I. Beadham, and S. Chandrasekaran, *Proc. Ind. Acad. Sci. Chem. Sci.*, 2003, **115**, 365-372.
333. I. I. Ivanova, E. B. Pomakhina, A. I. Rebrov, W. Wang, M. Hunger, and J. Weitkamp, *Kin. Cat.*, 2003, **44**, 701-709.
334. P. Sozzani, S. Bracco, A. Comotti, R. Simonutti, and I. Camurati, *J. Am. Chem. Soc.*, 2003, **125**, 12881-12893.
335. H. Y. Chang, R. Thangamuthu, and C. W. Lin, *J. Membr. Sci.*, 2004, **228**, 217-226.
336. M. L. Occelli, U. Voigt, and H. Eckert, *Appl. Cat. A-General*, 2004, **259**, 245-251.
337. B. A. Gee and A. Wong, *J. Phys. Chem. B*, 2003, **107**, 8382-8387.
338. C. M. Wang, S. T. Chuang, Y. L. Chuang, H. M. Kao, and K. H. Lii, *J. Solid State Chem.*, 2004, **177**, 1252-1257.
339. M. Mizuno and S. Hayashi, *Solid State Ionics*, 2004, **167**, 317-323.
340. T. M. Alam, M. Nyman, B. R. Cherry, J. M. Segall, and L. E. Lybarger, *J. Am. Chem. Soc.*, 2004, **126**, 5610-5620.
341. M. Menetrier, C. Vaysse, L. Croguennec, C. Delmas, C. Jordy, F. Bonhomme, and P. Biensan, *Electrochem. Solid State Lett.*, 2004, **7**, A140-A143.

342. H. P. He, R. L. Frost, F. Deng, J. X. Zhu, X. Y. Wen, and P. Yuan, *Clays Clay Min.*, 2004, **52**, 350-356.
343. Y. F. Yao, G. Yang, and Q. Chen, *Chem. J. Chin. Univ.-Chinese*, 2004, **25**, 531-534.
344. S. Le Calve, B. Alonso, L. Rozes, C. Sanchez, M. N. Rager, and D. Massiot, *Comptes Rendus Chimie*, 2004, **7**, 241-248.
345. B. Lynch, G. H. Muller, L. O. Healy, J. D. Glennon, M. Pursch, and K. Albert, *Anal. Bio. Chem.* 2003, **377**, 1014-1019.
346. G. K. Agarwal, J. J. Titman, M. J. Percy, and S. P. Armes, *J. Phys. Chem. B*, 2003, **107**, 12497-12502.
347. C. Odin, *Magn. Reson. Chem.*, 2004, **42**, 381-388.
348. B. Toury, C. Gervais, P. Dibandjo, D. Cornu, P. Miele, and F. Babonneau, *Appl. Organomet. Chem.*, 2004, **18**, 227-232.
349. V. Lafond, C. Gervais, J. Maquet, D. Prochnow, F. Babonneau, and P. H. Mutin, *Chem. Mater.*, 2003, **15**, 4098-4103.
350. A. Lafuma, F. Fayon, D. Massiot, S. Chodorowski-Kimmes, and C. Sanchez, *Magn. Reson. Chem.*, 2003, **41**, 944-948.
351. N. Kim and C. P. Grey, *J. Solid State Chem.*, 2003, **175**, 110-115.
352. M. R. Hampson, P. Hodgkinson, J. S. O. Evans, R. K. Harris, I. J. King, S. Allen, and F. Fayon, *Chem. Comm.*, 2004, 392-393.
353. B. Julian, C. Gervais, M. N. Rager, J. Maquet, E. Cordoncillo, P. Escribano, F. Babonneau, and C. Sanchez, *Chem. Mater.*, 2004, **16**, 521-529.
354. P. A. Thomas, A. Baldwin, R. Dupree, P. Blaha, K. Schwarz, A. Samoson, and Z. H. Gan, *J. Phys. Chem. B*, 2004, **108**, 4324-4331.
355. B. Zhou, B. L. Sherriff, and F. Taulelle, *Canad. Min.*, 2003, **41**, 891-903.
356. C. Odin, *J. Phys. Chem. B*, 2004, **108**, 7402-7411.
357. A. G. Stepanov, T. O. Shegai, M. V. Luzgin, N. Essayem, and H. Jobic, *J. Phys. Chem. B*, 2003, **107**, 12438-12443.
358. K. Morii, G. Maruta, and S. Takeda, *Polyhedron*, 2003, **22**, 1995-2001.
359. N. L. Adolphi, S. Badola, L. A. Browder, and R. C. Bowman, *Physical Review B*, 2004, **69**, art-149901.
360. P. Thangadurai, S. Ramasamy, and P. T. Manoharan, *European Physical Journal B*, 2004, **37**, 425-432.
361. H. Trill, H. Eckert, and V. I. Srdanov, *J. Phys. Chem. B*, 2003, **107**, 8779-8788.
362. B. R. Cherry, M. Nyman, and T. M. Alam, *J. Solid State Chem.*, 2004, **177**, 2079-2093.
363. J. W. Wiench, V. P. Balema, V. K. Pecharsky, and M. Pruski, *J. Solid State Chem.*, 2004, **177**, 648-653.
364. S. Esmacilzadeh, J. Grins, Z. Shen, M. Eden, and M. Thiaux, *Chem. Mater.*, 2004, **16**, 2113-2120.
365. L. S. Du and J. F. Stebbins, *J. Phys. Chem. B*, 2004, **108**, 3681-3685.
366. M. Pompetzki, L. van Wullen, and M. Jansen, *Zeit. Anorgan. Allgem. Chem.*, 2004, **630**, 384-388.
367. A. Onoda, M. Doi, K. Takahashi, T. Okamura, H. Yamamoto, and N. Ueyama, *Chem. Lett.*, 2004, **33**, 466-467.
368. S. Hunger, H. Cho, J. T. Sims, and D. L. Sparks, *Environ. Sci. Tech.*, 2004, **38**, 674-681.
369. T. Ueda, G. M. Bernard, R. McDonald, and R. E. Wasylishen, *Solid State Nucl. Magn. Reson.*, 2003, **24**, 163-183.
370. M. Vijayakumar, S. Selvasekarapandian, K. Nakamura, T. Kanashiro, and R. Kesavamoorthy, *Solid State Ionics*, 2004, **167**, 41-47.

371. A. Goldbach, F. Fayon, T. Vosegaard, M. Wachhold, M. G. Kanatzidis, D. Massiot, and M. L. Saboungi, *Inorg. Chem.*, 2003, **42**, 6996-7000.
372. D. H. Zhou, G. L. Hoatson, and R. L. Vold, *J. Magn. Reson.*, 2004, **167**, 242-252.
373. T. Ohkubo, K. Kanehashi, K. Saito, and Y. Ikeda, *Clays Clay Min.*, 2003, **51**, 513-518.

8
Multiple Pulse NMR

BY I. BARSUKOV

1 Introduction

The report covers the progress in the field of multiple pulse NMR over a period of twelve months from June 2003 to May 2004 and is a continuation of the report from last year. Substantial effort in the reviewed period was directed to further development of methods reducing the spectrometer time required for the acquisition of multi-dimensional spectra. The interest in such methods is caused by the increase in the spectrometer sensitivity, particularly with the use of cryogenic probes, that makes the resolution in the indirect dimensions, rather than the sensitivity, a time-limiting factor of the experiments. In additions, structural genomics projects require the NMR analysis of a large number of proteins that puts premium on the spectrometer time. Currently the most prominent method is GFT spectroscopy that allows to acquire a set of triple-resonance experiments for the backbone protein assignments in a single day. Another interesting approach, related to the reduced dimensionality spectroscopy, is the reconstruction of multidimensional spectra from a series of projections. This possibility was demonstrated for spectra of up to five dimensions. The time reduction methods, however, can only be applied to systems with abundant sensitivity. Cross-correlated relaxation and residual dipolar coupling experiments received considerable attention, with researches still finding the ways to improve the measurements. Several groups described the NMR approaches to large proteins, including optimisation of the existing experiments, selective protonation on methyl groups and the use of ^{13}C detection in deuterated proteins. As before the new and improved experiments are summarised in Table 6.1 at the end of the chapter.

2 Fast Multidimensional Methods

The development of the NMR hardware and the improvements in protein expression and labelling led to the situations when the duration of a multidimensional experiment is governed not by the sensitivity, but by the resolution in each dimension. The intrinsic properties of digital FT require uniform independent sampling of each indirect dimension, leading to the dramatic increase of the total

Nuclear Magnetic Resonance, Volume 34
© The Royal Society of Chemistry, 2005

number of increments with the increase of the number of spectral dimensions, often making 4D methods unacceptably long, and even 2D and 3D methods unnecessary long. Several different schemes for the reduction of the experimental time were introduced in the period, covered by the previous report and further developed in the current period. All the methods are based on the realisation that the uniform sampling wastes a great deal of time on sampling the empty regions of the spectra, where there is no signals. Such regions constitute a major proportion of the spectral space, so a large time gain can arise if the empty regions are avoided or used to store the signals. The main methods for the time reduction in the multidimensional spectra are described and compared by Freeman and Kupce[1] in an excellent review. The advances in the reduction methods are summarised below.

2.1 Hadamard Spectroscopy. – Hadamard spectroscopy is based on the selective spectra manipulation directly in the frequency domain. This is achieved by the application of selective excitation and/or inversion pulses and requires a knowledge on the position of the resonances, usually obtained from 1D or 2D non-selective spectra. Selective pulses are applied simultaneously by combining them into a single polychromatic pulse. To excite individual resonances phase-ramped Gaussian pulses are normally used with duration of ~45ms. The individual pulses are encoded according to Hadamard matrices, resulting in the modulation of the polarity of the individual signals. In case of the excitation pulses the change of the phase by 90° is used for the encoding, while the inversion pulses are either 'on' or 'off' depending on the values in the Hadamard matrices. Each encoding step is recorded separately, analogous to individual increments of the nD FT spectroscopy. The properties of the Hadamard matrices are such that following the complete encoding cycle the individual signals can be extracted through a linear combinations of the recorded 1D spectra. The number of the individual 1D scans is equal to the order of the Hadamard matrix, which is close to the number of selectively irradiated signals, and is much smaller than the number of increments in the corresponding nD FT spectrum. Additional time and sensitivity gain of the Hadamard spectroscopy originates from the full amplitude of the signals alternating between the positive and negative values, while the FT spectroscopy detects a rotating vector, which requires separate measurements of the real and imaginary components. The main drawback of the Hadamard spectroscopy is the need for the predetermined set of the resonance frequencies which may be difficult to obtain for a crowded spectrum. The selectivity of the pulses in such cases may also be insufficient for resolving the overlapped resonances. Additional general drawback of the method is the coherence transfer between the coupled spins during the frequency selective excitation. This phenomenon is often referred to as double-resonance two-spin effect (TSETSE)[2] and leads to the observation of the cross-peak between the coupled sites. The effect depends on the duration of the selective pulses and is sufficiently small for the usually applied pulses of 45 ms. To use the established methods of spectral analysis the decoded 1D spectra are recombined into the appropriate nD ones by positioning them into the spectral regions determined by the excita-

tion frequencies, and adding blank rows to the non-quantified regions. Apart from the detection of complete spectra, the Hadamard method can be used for a selective resonance detection, offering even larger time gain. Such application was demonstrated by Bougault *et al.*[3] who used Hadamard 2D ^{15}N-^{1}H HSQC spectra for the measurement of rapid proton-deuteron exchange for selected amide groups. Each 2D Hadamard spectrum was acquired in 42 s using selective irradiation at seven ^{15}N frequencies. The set-up of the experiment required a prior knowledge on the sites undergoing rapid exchange.

The homonuclear 2D Hadamard spectroscopy is discussed in detailed by Kupce and Freeman[2]. The schemes for COSY, TOCSY and NOESY spectra are described, each applying a single polychromatic selective pulse at the start of the pulse sequence. In case of COSY, 90° selective excitation pulses are used with $\pm 90°$ phase shift according to Hadamard encoding, followed by the non-selective excitation pulse. J-evolution of the experiment takes place during the application of the selective pulse, resulting in anti-phase coherence for the coupled spins. For NOESY and TOCSY spectra 180° selective pulses are applied, set 'on' or 'off' according to Hadamard encoding, followed by the appropriate mixing period and a 90° read pulse. The magnetisation transfer in these experiments occurs only between the pairs of the interacting sites that experience differential perturbation. A pair of gradient pulses flanking the mixing period is applied in both NOESY and TOCSY spectra to reduce the level of artefacts. The mixing sequence of the TOCSY experiment employs WURST-2 adiabatic pulses. The use of the 2D homonuclear Hadamard spectroscopy was illustrated on strychnine. 15 irradiation position were selected from a low-resolution 1D spectrum and encoded using Hadamard matrix of the order 16. The Hadamard spectra took 42-49s to acquire, compared to $\sim$3h for the conventional 2D FT spectra, resulting in time saving factor of more than 220. Due to the nature of the method the Hadamard spectra have a multiplet structure only in the acquisition dimension, while in the indirect dimension the signals consist only of a single point. To generate a multiplet structure in both dimensions the authors proposed to convolute the indirect dimension with a rectangular function of width equal to the excitation bandwidth (45 Hz) and apply a symmetrization routine. This procedure does not add additional information to the spectrum, but may facilitate the visualisation and the analysis.

The following publication by the same authors[4] elaborated on the use of Hadamard spectroscopy for measurement of heteronuclear 3D TOCSY-HSQC spectra. In the proposed sequence both indirect evolution periods and the flanking 90° excitation pulses were replaced with 180° polychromatic pulses, coded 'on' or 'off' according to Hadamard matrices. To remove heteronuclear couplings, the proton polychromatic pulse was combined with a normal carbon CPD decoupling. In case of the carbon polychromatic pulse the decoupling scheme needs to ensure that the protons complete an integral number of 360° rotations. This can be achieved with a pulse train of WURST-40 pulses, combined in a 20-step phase cycle adjusted to match the duration of the polychromatic pulse. The Hadamard TOCSY-HSQC spectrum of strychnine was measured in $\sim$11 min using Hadamard matrix of the order 16 for the proton

dimension. To acquire a 3D FT spectrum of a similar resolution would require nearly three order of magnitude longer experiment. The Hadamard spectrum was reconstructed into a normal 3D spectrum to facilitate the analysis.

2.2 Reduced Dimensionality Spectroscopy. – The method achieves time saving by the joint incrementation of several evolution periods, corresponding to different nuclei, either in step with one another or with a suitable scaling factor between them. The evolution of one of the nuclei is detected in quadrature, while the evolution of other nuclei lead to an additional sine or cosine modulation of the signal, controlled by the phases of the corresponding excitation pulses. As the result cross-peaks are split into a chemical-shift multiplet pattern in the 'combined' dimension with the centre corresponding to the chemical shift of the nucleus detected in quadrature and the components displaced with the linear combination of the chemical shifts of the other 'locked' nuclei. The signs of the multiplet components depends on the type of the modulation for each nucleus (sine of cosine). The modulation is systematically varied for each of the nuclei according to the coefficients in a G-matrix of the appropriate order to acquire several sub-spectra with different combinations of signs of the multiplet components. The sub-spectra are recombined at the initial G-matrix processing stage to extract individual multiplet components. Once the chemical shifts of the individual multiplet components are measured the shift of the contributing nuclei can be deduced by solving a set of linear equations using a least-square fitting procedure as the number of the equations exceeds the number of variables. In practice, due to the ambiguity caused by resonance overlap, additional data sets need to be recorded with the reduced number of the linked evolution periods, including the spectrum recording the chemical shift of the central multiplet peak, the shift of the nuclei detected in quadrature. In total, 5 sub-spectra need to be recorded for two and 15 for three locked dimensions. The main disadvantage of the reduced dimensionality experiments is the complexity of the procedure for the extraction of the individual chemical shifts which may require manual interaction at low signal-to-noise ratios and high cross-peak overlap.

The reduced dimensionally method is generalised by Kim and Szyperski[5] in form of GFT spectroscopy. The authors suggested (N,M)D GFT notation for the reduced dimensionality experiments with N signifying the total number of different evolution periods and M corresponding to the number of dimensions of the sub-spectra. A similar to GFT, but less generalised approach was described by Kozminski and Zhukov[6]. The authors describe the extraction of the individual components of the chemical-shift multiplets of the reduced dimensionality spectra in terms of achieving quadrature detection for each of the linked dimension independently with the procedure very similar to that of the GFT NMR. The complications arising from the resonance overlap and the precision of the extracted chemical shifts are not considered. The method is illustrated on the example of (4,2)D H<u>NCA</u>, H<u>N</u>(CO)<u>CA</u> and (5,2)D <u>HACANH</u> experiments. The first two experiments were based on standard pulse sequences, while a modified sequence for (5,2)D <u>HACANH</u> experiment was presented. The combined CA and HA evolution is measured through the indirect detection of the zero- and

double-quantum coherence in a single evolution period. The quadrature detection of the ^{15}N is achieved through gradient selection in the sensitivity-enhanced scheme.

The application of the GFT NMR spectroscopy for the sequential assignment was extended by Kim and Szyperski[7] by introduction of (5,2)D HACA,CONHN experiment, complementing the previously published (5,2)D HACACONHN, and two pairs of (5,3)D HACA,CONHN/ HACACONHN and (4,3)D CBCACONHN/CBCA,CONHN experiments. The (5,2)D HACA,CONHN sequence register HA, CA, CO and N evolution in a single dimension with the chemical shift multiplet centre corresponding to the ^{15}N chemical shift. The CA and CO evolutions are detected in a single evolution period as zero- and double-quantum coherence. In order to apply phase-shifted selective pulses for the CO excitation, the spectral width for the ^{13}C indirect detection was adjusted to one half of the difference of the CA and CO carrier frequencies to fold CO chemical shifts into the CA region. The CA->N transfer is achieved simultaneously with the excitation and evolution of the multiple-quantum CA/CO coherence in a constant time period. The first order central peaks that provide the splitting with the CA and CO chemical shifts can be obtained simultaneously with the recording of the basic spectra by the use of the ^{13}C steady-state magnetisation, additionally reducing spectrometer time. Alternatively, they are recorded by omitting the HA chemical shift evolution. The second order central peak with splitting on CO chemical shift is recorded with the basic sequence omitting the CA and HA evolutions, and the third-order central peak that provides ^{15}N chemical shift is obtained from 2D [^{15}N,^{1}H]-HSQC spectrum. An improved cross-peak separation can be achieved in the 3D reduced dimensionality spectra. The (5,3)D HACA,CONHN/ HACACONHN pair of the experiments are based on the same sequences as the corresponding (5,2)D experiments, with an independent evolution of the ^{15}N chemical shifts and quadrature detection of the CO evolution. The (4,3)D CBCACONHN/CBCA,CONHN experiments correlate the backbone amide chemical shifts with the CO, CA and CB intraresidue or sequential chemicals shifts detected in the combined dimension with quadrature detection of the CO evolution. The CA and CB evolutions are detected in a constant-time period of the CB->CA coherence transfer, and the CO evolution is detected in a constant-time period of CA/CO two-spin coherence evolution combined with the CA->CO coherence transfer. Experimental data were presented for ubiquitin and a 14 kDa protein, with most of the cross-peaks detected for both proteins. Time saving factor of 225 was reported for the (5,2)D , 25 for the (5,3)D and 6.4 for the (4,3)D experiments. The authors discussed the improved precision of the GFP spectroscopy due to the overdetermined system of linear equations used for the chemical shift extraction.

A different set of reduced dimensionality spectra for the backbone resonance assignment was proposed by Bersch *et al.*[8] All experiments are of (3,2)D-type, where evolution of C^{α}, H^{α} or C^{β} nucleus is registered in the same dimension as N. The spectral analysis is described in terms of double quadrature detection in the combined dimension, where four FIDs are recorded for each time increment and the sub-spectra containing the sum and the difference of the combined chemical

shifts are extracted from the linear combinations of the FIDs. To reduced the number of cross-peaks in the experiments registering intra-residue correlations selective N_i->CA_i coherence transfer based on CA/CO coupling was used in the HNCA, HN(CA)CB and HN(CA)HA experiments. These experiments are complemented by the standard sequential HN(CO)CA, HN(COCA)CB and HN(COCA)HA spectra. In additions, (3,2)D J-HNCO(H) experiment is described that allows to detect CO chemical shifts and measure $^1J(H,N)$ and $^2J(H,C')$ couplings in a single spectrum. The coupling constants are measured through the composite splitting of the cross-peaks in the combined dimension. Individual doublet components are separated into different sub-spectra with the use of α/β-state selection filter. The experiments are most suited for small proteins with good peak separation in [^{1}H,^{15}N]-HSQC spectra.

The problem of resonance overlap in the reduced dimensionality spectra was addressed by Brutscher, proposing to use the method in combination with band-selective Hadamard-type frequency encoding[9] or DEPT-based multiplet selection[10]. The first method was applied in the (3,2)D sequential HN(CO-H_N)CO, sequential HN(CO-H_N)CA and intra-residue (CO-H_N)HNCA experiments correlating CO and CA chemical shifts with the HN group. The frequency encoding is achieved through band-selective inversion pulses applied in the CO region, allowing to extract sub-spectra on the basis of CO chemical shifts. The band-selective pulse is introduced into HNCO and HNCOCA experiments after generating spin polarisation on CO spins. Four unequal frequency bands were used for a 167-residue protein. Some signal loss was observed for the CO resonances close to the edges of the excitation regions. The DEPT-based multiplet selection was introduced into (5,3)D DEPT-HAHBCACB(CO)NH and DEPT-HC(CO)NH-TOCSY experiments[10] correlating side-chain and backbone resonances. The DEPT sequence is used in the initial stage of H->C coherence transfer, allowing to separate the cross-peaks into CH/CH_3 and CH_2 sub-spectra by adding or subtracting the spectra acquired with different flip-angle of the ^{1}H pulse. The side-chain ^{1}H, ^{13}C and backbone ^{15}N resonances are observed in a single dimension with the ^{15}N coherence recorded in quadrature with the gradient-based sensitivity enhancement sequence. Additional cross-peak separation can be achieved through CO band-selective Hadamard frequency encoding.

2.3 Reconstruction of Multidimensional Spectra from Projections. – In a series of publication Kupce and Freeman[11-13] proposed to treat NMR spectra as multidimensional objects and reconstruct the complete spectrum from a series of two-dimensional projections, in a similar way as an anatomical image can be derived from a set of X-ray projections recorded at different angles of incidence. The projections required for the reconstruction can be obtain by incrementing evolution times corresponding to the individual indirect dimensions simultaneously, similar to the reduced dimensionality methods. The tilt angle of a projection is determined by the step-size ratios for the locked evolution delays. In case of 3D spectra, a hypercomplex transformation of the spectrum acquired with the ratio $\Delta t_1/\Delta t_2 = \tan\alpha$ generates two projections tilted through angles $\pm\alpha$

with respect to the F_1F_3 plane. The number of projections required for the reconstruction depends on the complexity of the spectrum. Normally, two projections along the indirect axis are acquired, which generates a lattice of possible cross-peak positions. For a 3D spectrum one or two additional projections are required to identify the real positions of the cross-peaks[11,12]. For a 4D reconstruction four doubly-tilted projections were used, corresponding to the simultaneous incrementation of all three indirect dimensions[14]. These projections are extracted from a single data set in which all locked dimensions are detected in quadrature. Reconstruction of a 5D spectrum requires 8 triply-tilted projection extracted from a hypercomplex data set where three linked dimensions are sampled in quadrature. The formalism for the projection reconstruction spectroscopy was summarised by Coggins *et al.*[15] and illustrated on example of 5D HACACONH experiment. The projection reconstruction method can be used with any triple-resonance sequence without further modification. The resolution of the reconstructed spectrum is similar to that of the full nD spectrum acquired with the same maximum durations of the evolution periods. The reconstructed spectra have the same appearance as the corresponding nD spectra, allowing to use the same methods for the analysis. A time saving factor of 200 was reported for the reconstruction of a 4D spectrum.

2.4 Single Scan Multidimensional Spectroscopy. – Very elegant, albeit of limited practical value, scheme of acquiring a complete 2D spectrum with a single scan was introduced by Shrot and Frydman in the period covered by the previous review. Subsequently they elaborated on the method, extending it to higher dimensions[16] and demonstrating the possibilities to monitor exchange processes[17] and spatial distribution[18] with a single scan experiment. The method is based on the encoding of the indirect chemical shift evolution into a spatial phase distribution that can be refocused by the application of an appropriate gradient pulse. To achieve this an indirect evolution period is replaced by a train of selective excitation pulses applied simultaneously with strong gradient pulses. The selectivity of the r.f. pulses is sufficient to excite the whole spectral range in a thin slice of the sample. The offset of the selective pulses is changed linearly to produce excitation in successive slices throughout the sample. As different slices are excited at different time, the chemical shift evolution leads to the accumulation of the evolution phase shift that has the same distribution throughout the sample as the phase shift caused by the gradient used in the slice selection. This chemical shift de-phasing can then be refocused by applying a gradient with the same spatial distribution. The refocusing conditions depend on the evolution frequency, resulting in the observation of time-separated echo signals from the nuclei with different chemical shifts. Such set of echoes, recorded during the acquisition time in the presence of the refocusing gradient, generate the spectrum in the indirect dimension without a need for Fourier transformation. The modulation in the acquisition dimension is introduced by the recording a successive set of gradient echoes at different time intervals. Fourier transformation of this modulation produces a 2D spectrum. The position-independent mixing is introduced after the spatially selective excitation to generate an appropriate 2D

spectrum. The whole experiment takes a fraction of a second and have the sensitivity that is comparable to that achieved in a single scan in the conventional method. There are some sensitivity loses due to the large bandwidth of the receiver, artefacts generated by rapidly switching gradient pulses and non-idealities of the shaped pulses. The experiment requires the application of strong short gradients, has limited spectral resolution defined by the gradient pulses and distorted line-shapes determined by the gradient function. The spectral limitations and low sensitivity makes the method applicable only to small molecules at high concentrations. The fast 2D acquisition in a single-scan experiment was used in LC-NMR for the characterisation of the continuously eluted compounds.[19]

The use of the orthogonal gradients allows to achieve multiple spatial encoding.[18] To this aim several trains of slice-selective pulses are applied, each associated with a gradient of a different shape. Such encoded signals can only be refocused in the presence of all gradients used for the excitations. The refocusing conditions are different for the nuclei with different evolution frequencies, resulting in the separation of the signals along several independent time axes, as in traditional multidimensional spectroscopy. The theoretical details of the multidimensional extension are described by Shrot and Frydman[18], followed by examples of 3D and 4D homo- and heteronuclear spectra. The orthogonal spatial encoding was also used to record a series of exchange spectra at different mixing time with a single-scan[17]. In this case the additional spatial encoding was used to associate different slices with separate mixing time of the 2D exchange spectra. The gradient refocusing and Fourier transformation in the acquisition dimension produces a series of 2D spectra with different exchange times, allowing to obtain the time dependence of the exchange process in a sing scan. The sensitivity is reduced as only a fraction of the sample is used to record the spectrum at each mixing time. The method can also be applied to the relaxation time measurement in a single scan.

A different type of a single-scan experiment was used by Loening *et al.*[20] for the measurement of T_1 relaxation. In the proposed version the relaxation is encoded in individual slices of the sample which are then sequentially selected for observation with a slice-selective spin-echo sequence in the presence of the gradient. No gradient is used during the acquisition and the chemical shift information is retrieved by the Fourier transformation from an ordinary FID. Each acquisition has to fit between the T_1 increment points. Alternatively, a weak gradient is used in the acquisition time to decode the T_1 information.

Srot and Frydman[18] noted that the line-shape in the indirect dimension of a single-scan experiment depends on the solute distribution throughout the sample. The uniform distribution leads to a Sinc function and the deviation from that can be used to evaluate the deviations of the distribution from uniform. The signals in the proposed 2D single-scan experiments are resolved in two spectral dimensions and include a TOCSY mixing sequence.

The discrete nature of t_1 incrementation during the spatial encoding of the single-scan experiments leads to the appearance of 'ghost' peaks in the indirect dimension, a periodic refocusing artefacts around the central peak. These arte-

facts can be shifted to the outside of the spectral region with the use of sufficiently strong gradients, but with weaker gradients may interfere with the real cross-peaks in the spectra. Srot and Frydman[21] analysed the artefacts and suggested a simple scheme for their elimination. The method is based on the reduction of the effective frequency separation between the successive slices of the selective excitation through the introduction of the additional free evolution delay. This increases the displacement of the ghost peaks and places the outside the spectral region without the need to increase the gradient strength.

3 NOE, Relaxation and Diffusion

3.1 NOE. – A set of 2D ^{13}C filtered/edited experiments was described by Peterson *et al.*[22] The filtering/editing schemes are based on the adiabatic inversion pulses that optimise the experiments for the range of ^{1}H-^{13}C couplings. The same element was used for filtering and editing, differing only in the phases of 90° ^{1}H pulses to select the appropriate in-phase of antiphase ^{1}H coherence at the end of the filer element. Two flittering elements are flanking NOESY sequence to achieve four filtering/editing in 2D spectra. The method was used for base-type-specific isotopically labelled RNA.

The presence of zero-quantum coherence during the mixing time can substantially distort NOE intensities. This coherence can not be removed with phase-cycling or gradient pulses while preserving z-magnetisation. A z-filter scheme was proposed earlier for the elimination of the coherence. It utilises an adiabatic inversion pulse with linear frequency sweep applied simultaneously with a gradient. Cano *et al.*[23] demonstrated that a better suppression is achieved with a z-filter cascade that combines several filter elements. The attainable suppression ration is then equal to the multiplication of the ratios for each element.

3.2 Relaxation Rate Measurements. – The ^{13}C T_1 relaxation in CH_2 groups is complicated by the DD/DD cross-correlation, leading to a multi-exponential decay. A modified T_1 experiment was proposed by Jin *et al.*[24] that suppress the cross-correlated relaxation contribution with the combination of r.f. pulses and gradients. When present, the cross-correlated relaxation leads to the conversion of C_z into the three-spin order $C_zH_{1z}H_{2z}$. In the proposed scheme this term is converted into multiple-quantum proton coherence by the application of ^{1}H 90° pulse. The double-quantum part of the coherence is refocused with the gradient and the zero-quantum term is partially converted into the double-quantum one with a set of additional ^{1}H 90° pulses of different phases and subsequently defocused with the gradients. The N-fold repetition of this process during the relaxation time results in the complete suppression of the three-spin order term, thus suppressing the cross-correlated contribution. Such relaxation time modification was introduced into the INEPT-based experiment for the inversion-recovery T_1measurement. The use of the suppression scheme significantly improved the decay curves measured for ubiquitin. The effect of cross-correlation on the $\{^{1}H\}$-^{13}C NOE values, on the other hand, was found to be insignificant, as

demonstrated by the use of ^{1}H saturation schemes suppressing the cross-relaxation.

The rate of exchange processes can be evaluated from the $R_{1\rho}$ value, often measured using CPMG pulse trains. Kempf *et al.*[25] proposed an experiment that utilise the off-resonance ^{15}N relaxation to access μs to ms dynamics, making available the exchange rates that are faster than the currently available. The adiabatic alignment with the tilted spin-lock field is incorporated into a TROSY sequence to make experiment applicable to large proteins. The spin-lock period is combined with the T_1 relaxation period in the constant-time fashion to produce the signal decay depending on the difference ($R_{1\rho}$-R_1) between the spin-locked and longitudinal rates, reducing the number of parameters for the exchange quantification. During the spin-lock and the longitudinal relaxation periods broad-band spin-lock decoupling with the random-phase alternation scheme are applied to suppress CSA/dipolar cross-relaxation. A different method for evaluation of the chemical exchange contribution was proposed by Wang *et al.*[26] The authors demonstrated that ^{15}N R_{ex} can be calculated from a combination of relaxation rates of TROSY- and anti-TROSY doublet components R_2^{α} and R_2^{β}, and the relaxation rate of two-spin order R_1^{2HzNz}. The experiment for the measurement of the rates is based on the TROSY sequence and include an additional relaxation period prior to the ^{15}N evolution. The appropriate magnetisation relaxing in the relaxation period is then transferred to the TROSY component for detection. The use or TROSY makes the method applicable to large proteins.

The longitudinal relaxation rates of both donor and acceptor ^{15}N in Watson-Crick base pairs can be measured simultaneously in the experiment presented by Bytchenkoff and Bodenhausen.[27] The proton magnetisation is initially converted into the antiphase coherence of the donor ^{15}N, which then evolves with the $^{2h}J(N^D,N^A)$ coupling between the donor and acceptor nitrogens and refocused to generate longitudinal magnetisation on the acceptor ^{15}N. At the same time the longitudinal magnetisation is generated on the donor ^{15}N. Both magnetisations relax simultaneously in the relaxation delay, chemical-shift labelled and transferred back to the ^{1}H for observation. The CSA/DD cross-relaxation is cancelled by the application of the inversion ^{1}H pulses. The longitudinal rates can be used to estimate the length of the hydrogen bonds.

3.3 Cross-Correlated Relaxation Experiments. – ^{1}H-^{13}C dipole-dipole (DD) cross-correlated relaxation rates in CH_2 and CH_3 groups can be used to characterise the degree of freedom of these groups in proteins. The rates are easily acceptable from the ratio of ^{13}C multiplet components in the absence of ^{1}H decoupling. Two CC(CO)NH TOCSY-based sequences for measurement of the relaxation in the CH_2[28] and CH_3[29] groups were proposed. In both sequences proton magnetisation is transferred to the in-phase carbon magnetisation which subsequently evolves during a constant time period without ^{1}H decoupling. This in-phase coherence is then transferred to HN proton *via* CO for observation. In the absence of the cross-correlated DD relaxation a triplet with the ration1:2:1 is observed for CH_2, and a quartet with the ratio 1:1:-1:-1 is observed for CH_3

groups. The deviation of the multiplet intensity ratios from these values is directly related to the cross-correlated relaxation rates. The contributions from the coherences other than ^{13}C in-phase are removed with gradient pulses and transfer process. Using HN protons for observation improves the signal separation in the experiment, but the long transfer process restricts the experiments to low molecular weight proteins. A simple sequence for measurement of ^{1}H-^{13}C dipole-dipole DD cross-correlated relaxation rates in CDH_2 groups of partially deuterated proteins was proposed by Marion.[30] The experiment starts from ^{13}C equilibrium magnetisation that is converted into the transverse coherence which is then evolves in a constant-time period without ^{1}H decoupling. Subsequently it is transferred to the attached protons with the INEPT sequence for acquisition. The cross-relaxation rate is measured from the relative intensity of the multiplet components of the ^{13}C triplet. The pulse sequence is optimised to remove contributions from unwanted ^{13}C coherences.

The ^{15}N CSA/DD cross-correlated relaxation leads to the differential attenuation of the ^{15}N doublet components of HN groups, thus allowing the evaluation of the cross-correlated relaxation rate from their intensity ratio. Hall *et al.*[31] proposed a simple modification of the [^{1}H,^{15}N]-HSQC experiment to extract the components in separate sub-spectra, reducing the cross-peak overlap. The ^{15}N evolution proceeds in a constant-time period without proton decoupling, during which the relaxation takes place. To separate the doublet components an additional spectrum is recorded, where the evolution delay is preceded by an additional INEPT period creating antiphase ^{15}N transverse coherence prior to the indirect detection. As the result the spectrum contains ^{15}N doublets with opposite phase of the multiplet components, attenuated due to the loses during the additional delays. The addition and subtraction of the two spectra scaled accordingly select separate multiplet components. The dependence of the intensity ratio of the multiplet components on the constant-time period is used for the cross-relaxation rate evaluation.

The distortions in the measured cross-correlated relaxation rates due to violations of secular approximation and differential effects of the non-symmetrical coherence transfer periods flanking the relaxation measurement delay can be minimised with the symmetrical reconversion approach introduced in the previous review period. In this approach four experiments are recorded with all combinations of the coherence transfer periods, producing automatic correction of the measured relaxation rate. The method was applied to the measurement of cross-correlated relaxation between CO CSA and long-range CO-HA DD interactions[32] that depends on the backbone angle ψ. The cross-correlated rate is evaluated from the relaxation of $2C'_yN_z$ and $4H^{\alpha}_zC'_yN_z$ coherences, recorded separately. The sequence is based on HNCO and HN(CO)CA experiments. The rates measured for ubiquitin show good correlation with the theoretical values.

The CH-CH DD/DD cross-correlated relaxation in protein side-chains can be easily measured in HCCH experiment. For larger proteins the resolution of the experiment may not be sufficient to extract the relaxation parameters. Carlomagno *et al.*[33] proposed a modification of HBHA(CBCACO)NH sequence for the measurement of $C^{\alpha}H$-$C^{\beta}H$ DD/DD cross-correlated relaxation in the spectra

with higher cross-peak separation. The modified sequence has an additional building block for the magnetisation transfer *via* cross-correlated relaxation that follows C^{β}-C^{α} transfer period. The rate is measured from the intensity ratios of peaks in cross-and reference spectra acquired separately. The rate depends on the $\chi 1$ and can be used for its evaluation. Good correlation was observed between the measured and predicted values for most of the residues in ubiquitin. The few discrepancies can be explained by taking internal motions into account.

Several new experiments were proposed for measurement cross-correlated relaxation in nucletide bases. Dittmer *et al.*[34] described four experiments for measurement of the relaxation rates of various double and triple-quantum coherences that involve imino proton and two neighbouring ^{15}N nuclei, hydrogen bond donor (D) and acceptor (A) of the bases involved in a hydrogen bond. The following cross-correlated relaxation rates can be then deduced from the experiments: $R_{DH,HA}+R_{D,A}$, $R_{D,A}$, $R_{H,A}$ and $R_{D,H}$. All sequence have the same INEPT-based preparation period that utilises $^{2h}J(D,A)=6$-7 Hz across the hydrogen bond to create three-spin order $4D_zH_zA_z$, which is subsequently converted into the desired multiple-spin coherence. The coherence evolves in the relaxation period that contain a series of inversion pulses to restrict the relaxation pathways and to refocus chemical shifts and J-couplings. The rates are evaluated from the intensity ratio of the 'diagonal' peaks in the reference experiment and 'cross-peaks' in the experiments where the desired relaxation mechanism is active. At the end of the relaxation period coherences are transferred back to the three-spin order, and then to the amino proton for the detection. Ravindranathan *et al.*[35] described an HCN-based sequence for the measurement ^{13}C-^{1}H DD/^{15}N CSA cross-correlated relaxations. The ^{13}C nucleus is directly bound to the ^{15}N and is located either in the same base or belongs to the adjoining ribose ring. In general, the experiments measure $R_{N,CH}+R_{C,NH}$ relaxation rates, but the the first term is dominant in the nucleotide systems, so the second term can be neglected. Constant time evolution period is used for the relaxation measurement, in which the undesired relaxation terms are suppressed through the application of inversion pulses. The coherence present at the beginning of the relaxation period evolves with the ^{15}N chemical shift and $^{1}J(C,H)$ coupling. The cross-relaxation rated are evaluated from the ratio of the doublet component. The measured relaxation rated were used to assess the dynamics within an RNA complex.

Motions slower than the overall rotational correlation time, including conformational exchange on the μs-ms time scale, can lead to effects similar to cross-correlated relaxation in multiple-quantum coherences. These slow motions can only modulate isotropic spin interactions, such as J-couplings and isotropic chemical shifts, as the anisotropic interactions are already averaged out by the fast dynamics. The cross-correlated modulation of the isotropic chemical shifts (CSM) of two nuclei has the same effect as their CSA/CSA cross-correlation and can be measured from the difference in relaxation rates of ZQ and DQ coherences of the two nuclei. Two publications presented different schemes for the measurement of the CSM/CSM cross-correlated relaxation. Majumdar and Ghose[36] proposed to evaluate the cross-relaxation rates from the conversion

$2I_aI_b \rightarrow 2I_{a+\pi/2}I_{b+p/2}$ due to the differences in the relaxation rates of ZQ and DQ coherences. The coherence phase change was used to select either the auto- or cross-correlation terms by application of 90° pulses with appropriate phases. Four experiments were described for the measurement of different cross-correlated relaxations involving pairs of backbone nuclei. The sequence for the measurement of NC′ relaxation is based on HNCO-TROSY experiment, creating multiple-quantum coherence $4H_zN_yC'_x$ at the beginning of the relaxation delay. This coherence is converted into $4H_zN_xC'_y$ through the effect of the cross-correlated relaxation, which is then refocussed into the observable magnetisation. The relaxation rate is evaluated from the ration of the intensities of the auto-peaks originated from $4H_zN_yC'_x$ coherence, and cross-peaks from $4H_zN_xC'_y$ coherence that are detected in separate experiments. A set of inversion pulses is applied in the relaxation delay to cancel the undesired relaxation pathways. Similar design was used for three other relaxation experiments: HN(CO)CA-TROSY - based for measurement of $NC^{\alpha(i-1)}$ and $C^{\alpha(i-1)}C'$ relaxation, and HNCA-TROSY based for measurement of $C^{\alpha}C^{\alpha(i-1)}$ relaxation. In the later experiment the four-spin multiple-quantum coherence $8H_zN_zC^{\alpha}{}_xC^{\alpha(i-1)}{}_x$ is used in the relaxation delay. The measured relaxation rates correspond to the sum of CSA/CSA and CSM/CSM cross-correlated rates with the later considered to be dominant when slow-motion modulations are present. The analysis of the relaxtion data for ubiquitin revealed extensive dynamics on the slow time-scale. Wist *et al.*[37] utilised triple-spin coherences $4C'_yN_xH^N{}_y$ and $4C'_xN_yH^N{}_y$ to measure the difference in the pseudo-ZQ and pseudo-DQ NC′ relaxation. The coherences were generated in an HNCO-based experiment and selected with different phase-cycles. The contribution from the CSA/CSA cross-correlated relaxation is evaluated with the CPMG multiple refocusing scheme. The effect of CSM/CSM cross-correlation is reduced with the increase of the repetition rate while the CSA/CSA contribution is repetition rate independent. The offset dependence of the CPMG refocusing was analysed.

3.4 Diffusion Experiments. – Diffusion coefficients of similar size proteins are difficult to separate in ^{1}H spectrum in case of resonance overlap. Nesmelova *et al.*[38] proposed to use isotope filtering in combination with the pulsed gradient spin-echo (PGSTE) experiment to measure the diffusion coefficients selectively for an isotope labelled protein in the presence of unlabelled material. The filter element is combined with WATERGATE sequence for water suppression to improve the quality of the spectra. Additional selective pulses are applied in combination with each excitation pulse of the stimulated-echo sequence to align water magnetisation along z-axis throughout the experiment, reducing the effects of radiation damping. A mathematical method of separating diffusion coefficients in case of the resonance overlap in DOSY spectra was described by Armstrong *et al.*[39] The method applies regularised resolvent transformation iRRT to separate multi-exponential decays observed for the overlapped signals.

4 Coupling Constants Measurements

4.1 Scalar Couplings. – The φ angle in proteins can be determined from $^3J(C',H^\alpha)$ coupling. The measurement of the coupling in triple-resonance experiments is complicated by the comparable values of $^1J(N,C^\alpha_i)$ and $^2J(N,C^\alpha_{i-1})$ couplings, leading to the simultaneous transfer of ^{15}N coherence to both C^α spins. Permi[40] proposed iHN(CA),CO(α/β-J-COHA experiment based on the corresponding sequence for the selective observation of the intraresidue C^α. The selection proceeds through the triple-spin coherence $8N_z(i)C'_z(i-1)C^\alpha_z(i-1)C^\alpha_z(i)$ which is subsequently refocused into $4N_z(i)C'_z(i-1)C^\alpha_y(i)$ coherence. An S^3P spin-state filter is applied to the coherence to select H^α spin-state prior to the C′ evolution which additionally evolves with $^3J(C',H^\alpha)$ coupling. The constant is measured from the cross-peak displacement between the two sub-spectra corresponding to the different polarisations of H^α. A TROSY variant of the experiment is also described. The method, applied to ubiquitin showed good correlation with the values determined previously.

Modification of the ADEQUATE experiment was used by Kover and Forgo[41] to measure single-bond and long-range ^{13}C-^{13}C couplings. The coupling-constant information was introduced into the experiment as J-modulation prior to the ^{13}C-^{13}C coherence transfer. The J-evolution was synchronised with the chemical shift evolution using a variable scaling factor. As the result the cross-peaks have doublet structure in the ^{13}C dimension with the effective splitting equals to the scaled coupling constant. The single-bond and long-range couplings are measured with the same sequence by adjusting the experimental parameters. For the sing-bond coupling the scaling is set to increase the effective value of the the constant by the factor 2-3 and the ^{13}C-^{13}C INEPT transfer delay is tuned to the single bond transfer. For the long-range couplings the small coupling constant is multiplied by the factor 10-15 and the ^{13}C-^{13}C INEPT transfer delay is set for the long-range transfer. The experiment is applicable to small molecules at natural ^{13}C abundance.

Edden and Keeler[42] continued the work on the use of HMBC experiment for the long-range ^1H-^{13}C coupling measurement. In the original application a fitting procedure for the evaluation of the coupling was introduced that used the proton multiplet to generate the shape of the HMBC multiplet. The procedure required the modified HMBC experiment which produced ^1H phase modulation similar to that of a simple delay. The experiment was further improved to include gradient pulses without the perturbation of the form of the cross-peak multiplet. Additional modification allowed to separate single-bond and long-range cross-peaks, so the single-bond peaks can be used in the fitting procedure, removing the requirement of independent detection of proton multiplets. This improves the performance when signals overlap. A ^{13}C frequency selective version of the experiment is also described that can be used for the fast measurement of the small number of couplings in 1D spectra. The experiment is used for small molecules at natural ^{13}C abundance.

4.2 Residual Dipolar Couplings. – One-bond ^{1}H-^{15}N couplings are usually measured in HSQC experiment with the IPAP method, separating individual doublet components into two sub-spectra. A different approach was described by Ding and Gronenborn[43] that separate multiplet components into distinct regions of the same spectrum. The spectra are acquired with sensitivity-enhanced-like sequences without quadrature detection in the indirect dimension and in the absence of ^{1}H decoupling, that introduces phase modulation with the coupling constant evolution and amplitude modulation with the ^{15}N chemical shift. The echo-anti-echo-type phase change and processing result in the doublet components appearing in the mirror-image regions of the spectrum in relation to the ^{15}N chemical shift. This completely separates the components when the sweep width two times larger than for a normal HSQC is used. Additionally, the scheme automatically provides sensitivity enhancement by the factor of 1.4 due to the constructive use of the in-phase and anti-phase ^{15}N coherences. The IPAP, TROSY-anti-TROSY and E.COSY version of the method were described, demonstrating different arrangement of the multiplet components that allow the coupling constant measurement along different spectral dimensions. Systematic difference was observed in the coupling constants measured in ^{1}H and ^{15}N, ascribed to the influence of un-resolved three-bond $^{1}H^{N}$-$^{1}H^{\alpha}$ couplings and cross-correlated relaxation between ^{15}N-$^{1}H^{N}$ and ^{15}N-$^{1}H^{\alpha}$ dipolar interaction. Similar principle was applied for the simultaneous measurement of one-bond ^{15}N-$^{13}C'$ and two-bond $^{1}H^{N}$-$^{13}C'$ couplings.[44] The E.COSY sequence was extended to generate ^{15}N coherence that is anti-phase relative to $^{13}C'$. This coherence is then converted into ^{1}H coherence anti-phase relative to $^{13}C'$ prior to detection. The ^{15}N-$^{13}C'$ coupling is active during ^{15}N evolution and is detected in quadrature. As the result, the E.COSY multiplet components with one-bond ^{15}N-$^{13}C'$ and two-bond $^{1}H^{N}$-$^{13}C'$ coupling splitting in ^{15}N and ^{1}H dimensions, respectively, are separated into mirror-image regions of the spectrum in relation to the ^{15}N chemical shift. The precession of the coupling constant measurement is controlled by the number of increments in the ^{15}N dimension.

A somewhat similar to the above, but this time with the quadrature ^{15}N detection with sensitivity enhancement, was used by Ding and Gronenborn[45,46] to measure different coupling involving back-bone nuclei. In one version[46] of the method the J-evolution was introduced into 2D [^{1}H,^{15}N]-HSQC-like spectrum by synchronising it with the ^{15}N chemical shift using the accordion principle. The sine or cosine J-modulation was selected in the separate FIDs by varying the position of refocussing pulses in an INEPT delay. This selection allows to separate multiplet components into different sub-spectra with IPAP processing. An HNCO-based sequence was used for the measurement of $^{1}J(C',C^{\alpha})$ and an HN(COCA)HA-based sequences were developed for $^{1}J(C',H^{\alpha})$ couplings. The scaling factor of 2 was used for the measurement of $^{1}J(C',C^{\alpha})$ to keep the separation similar to those in ^{15}N-^{1}H IPAP. The detection of signal in the well-resolved [^{1}H,^{15}N]-HSQC-type spectra allows adequate cross-peak separation in a 2D spectrum. In the other variant [45] a similar change in the position of the refocussing pulses in an INEPT delay was used to create E-COSY multiplet

structure. The HNCO experiment was modified to produce E.COSY splitting of ^{15}N-^{1}H peaks with the corresponding couplings to the intraresidue $^{13}C^{\alpha}$, which were further displaced by the passive couplings to the sequential $^{13}C^{\alpha}$ spin. This allows the measurement of $^{2}J(H,C^{\alpha})$, $^{1}J(N,C^{\alpha})$, $^{3}J(H,C^{\alpha})$ and $^{2}J(N,C^{\alpha})$ in a single experiment. The $^{1}J(N,C^{\alpha})$ couplings has a good correlation with y dihedral angle, and $^{2}J(N,C^{\alpha})$ reflects the secondary structure.

Two publications addressed the improvements in measurement of $^{1}H^{\alpha}$ coupling constants. Permi[47] described a modified HNCA-E.COSY experiment that allows simultaneous evaluation of $^{1}J(H^{\alpha},C^{\alpha})$ and $^{2}J(H^{\alpha},N)$ couplings from E.COSY multiplet in a 3D spectrum. The performance of the experiment was improved with the use of TROSY, increasing the precession of $^{2}J(H^{\alpha},N)$ coupling measured in the ^{15}N dimension. The coupling constant evolution is combined with the ^{15}N chemical shift evolution in the semi-constant period. The $^{1}J(H^{\alpha},C^{\alpha})$ coupling is measured in the ^{13}C dimension, where no ^{1}H decoupling is used. A variant of the experiment, HNCA(α/β-J-CAHAN)-TROSY, was presented, that selects individual $^{13}C^{\alpha}$ multiplet components by a filter element that contains a pair of ^{1}H refocussing pulses in the INEPT delay that preserve TROSY component. The positions of the pulses differ in two separate experiment, resulting in either in-phase or anti-phase doublet. Addition and subtraction of the two spectra results in the selection of one of the two multiplet components. The CSA/DD cross-correlated relaxation is suppressed by averaging relaxation rates of doublet components through the inversion of $^{1}H^{\alpha}$ spin-state during the filter element. The use of the multiplet component selection reduced the ^{13}C evolution time without affecting the precision of the coupling constant measurement and halves the number of cross-peaks in the spectrum. Hu *et al.*[48] Proposed to use $^{1}H^{\alpha}$ instead of $^{13}C^{\alpha}$ J-evolution to measure $^{1}J(H^{\alpha},C^{\alpha})$ coupling. This allows to avoid a long constant-time delay that is normally used to remove the contributions from $^{13}C^{\alpha}$-$^{13}C^{\beta}$ couplings, thus increasing the sensitivity of the experiment. The proton inverse pulse in the middle of the J-evolution period removes contribution from cross-correlated relaxation. The J-evolution is synchronised in the $^{13}C'$ evolution of the HA(CA)CONH experiment, so the splitting is observed in the well-resolved C′ dimension.

The measurement of one-bond coupling constants from the distance between the multiplet components in HSQC spectrum becomes unreliable for large proteins due to the differential relaxation that can severely broaden one of the components, and even make it undetectable. Luy and Marino[49] proposed to overcome this problem by introduction of J-modulation to the sharp TROSY component. The JE-TROSY experiment starts with a spin-echo J-evolution period, which is followed by a traditional TROSY detection sequence. As the result the resonances are independently modulated by the single-bond coupling, which leads to the displacement of the cross-peak in the independent spectral dimension after the 3D Fourier transformation. This displacement is measured either relative to zero frequency if real FT is used in the J-dimension, or as the splitting between the pseudo multiplet components if the complex FT is applied. The spectral width in the J-dimension is normally set to twice the value of the

maximum coupling constant expected. The signal intensities are strongly attenuated by the presence of J-modulation delay, limiting the number of increments. The application of the method was demonstrated for a 27 kDa protein-RNA complex.

The residual dipolar couplings in oligosaccharides are usually small due to high flexibility of the system, requiring the measurement with high precision. At the same time the spectra suffer from strong resonance overlap and signals have complex multiplet structures, that complicates the measurements. Feher *et al.*[50] applied G-BIRD(r) module to remove long-range ^{1}H-^{13}C coupling, so the single-bond coupling can be measured from the difference between peak maxima of two singlets. The simplification of the multiplet structure additionally increase the cross-peak intensities, thus improving the sensitivity of the experiment. The module was introduced into the ^{13}C evolution time of the an sensitivity-enhanced HSQC sequence, selectively refocusing the J-evolution over the long-range couplings, while the evolution with the single-bond coupling is unaffected. Martin-Pastor *et al.*[51] introduced chemical shift range selection element into CT-COSY experiments, improving the cross-peak separation. The 2D HSQC-(sel C, sel H)-CT-COSY experiment combines HSQC element for ^{13}C detection with the CT-COSY ^{1}H-^{1}H transfer before the observation. The out- and back-transfer ^{1}H-^{13}C INEPT periods of the HSQC are followed by range-selective selective spin-echo periods on ^{13}C and ^{1}H, based on selective inversion pulses flanked by gradients. The method was applied for measurement of ^{1}H-^{1}H and ^{13}C-^{13}C couplings.

5 Homonuclear Spectroscopy

The assignments of side-chain carbons in uniformly deuterated proteins can be achieved using a novel strategy proposed by Eletsky *et al.*[52] The method is based on 2D homonuclear correlation spectra with ^{13}C-start and ^{13}C-observe. A simple [^{13}C,^{13}C]-TOCSY experiment was described that detects carbon evolution in a constant-time period, followed by FLOPSY-16 magnetisation transfer. The CO decoupling is achieved with SEDUCE sequence. The constant-time experiment was found to be two times less sensitive than the non-constant time version for a 44 kDa protein, but its use was justified by the greatly improved resolution in the indirect dimension and the ability to distinguish resonances from the sites with different number of adjacent ^{13}C spins. The sensitivity of the experiments was improved by introduction of paramagnetic relaxation enhancement agent reducing ^{13}C T_1 relaxation with small effect on the T_2 relaxation. High resolution in the acquisition dimension allowed to separate most of the side-chain spin systems in a 44 kDa protein. Bertini *et al.*[53] proposed to use ^{13}C-^{13}C NOE for the side-chain assignments in large deuterated proteins. The authors demonstrated sufficient sensitivity in the ^{13}C detected 2D NOESY experiments to observe single-bond and some long-range intraresidue NOEs. The NOE intensities increased substantially with the increase of the molecular weight.

6 Inverse Proton Detected Correlation Spectroscopy

6.1 Double-resonance Experiments. – TROSY-type experiments have been traditionally based on the cross-correlation between dipolar and chemical shift anisotropy relaxation mechanisms. Tugarinov *et al.*[54] extended the application of the relaxation compensation principles to cancellation of the intra-methyl ^{1}H-^{1}H and ^{1}H-^{13}C dipole-dipole interactions. The analysis of the relaxation of the individual multiplet components within a methyl group revealed significant differences in the relaxation rates due to the differential contributions of the dipole-dipole interactions into different components. In the commonly used HSQC experiment the slow- and fast-relaxing components are inter-mixed during the INEPT transfer steps, resulting in the averaged relaxation rates. In contrast, the HMQC experiment preserves the individual relaxation components and allows selective transfer between slow-relaxing ^{1}H and ^{13}C coherences. This leads to a sensitivity gain of up to 2.5-fold in the HMQC experiment relative to the HSQC one in case of large proteins with selective protonation on methyl groups. This sensitivity gain is independent on the field strength due to the independence of dipole-dipole interaction on the magnetic field. The interaction with the external protons degrades the performance of the multiple-quantum spectra. This interaction is substantially smaller for the zero-quantum than for the double-quantum coherence, which was used by Tugarinov *et al.*[55] to further enhance the quality of methyl group detection. The authors proposed HZQC scheme that selectively records zero-quantum evolution and avoids the interchange between the zero- and double-quantum coherences. The sequence applies a composite pulse ^{1}H inversion outside the multiple-quantum evolution period. The inversion pulse is positioned either directly before or after the evolution period and the two FIDs are recombined to achieve sensitivity enhancement. The combination of the sensitivity enhancement and reduced relaxation loses results in the sensitivity of the HZQC experiment comparable to that of the HMQC one for a highly deuterated, methyl protonated protein of 810 kDa, making HZQC experiment preferable due to the reduced line widths in the ^{13}C dimension.

DIPSI or FLOPSY schemes with short rectangular pulses are most commonly used for ^{13}C-^{13}C magnetisation transfer in TOCSY-type experiments. Alternative mixing sequences based on adiabatic pulses are currently less popular due to the non-optimum distribution of the transfer efficiency over the chemical shift range despite the large band-width of the pulses. The shortcomings of the adiabatic sequences was addressed by Bennett *et al.*[56] The authors presented an analytical approach to calculating the scaling factor of the J-coupling when a train of inversion pulses is applied. This scaling reflects the efficiency of the mixing, varying between 1 and 0 for the full efficiency and no transfer, respectively. The application of the method to the analysis of adiabatic inversion schemes revealed poor performance of long adiabatic pulses despite their inversion efficiency. Improved adiabatic pulses were derived using numerical simulations to maximise the bandwidth and tolerance for RF inhomogeniety and the J-scaling factor. The mixing sequences with optimised pulses had im-

proved transfer performance over FLOPSY in the case of widely separated ^{13}C resonances even at low r.f. powers of 7-8 kHz.

Currently the majority of heteronuclear pulse sequences are based on the INEPT-type coherence transfer between proton and directly bound nucleus. An alternative method, based on heteronuclei J-cross-polarisation was systematically analysed by Parella.[57] The transfer is achieved by the synchronous application of two r.f. fields at proton and heteronuclear frequencies under matching Hartman-Hahn condition. Depending on the relative amplitude of the magnetic fields and coherences the transfer can be achieved between different types of in-phase and antiphase coherences, with the maximum amplitude at the transfer time equal to 1/J. The publication summarises all main heteronuclear experiments including HSQC, TROSY and spin-state selection. For each of the standard heteronuclear experiment a version based on the cross-polarisation is proposed. All of the proposed experiments follow the same scheme consisting of four basic steps: preparation period generating the desired type of transverse heteronuclear coherence, evolution period that also includes dephasing gradient, back-transfer step and gradient refocusing. The use of gradients allows to combine coherence selection with sensitivity enhancement. The proposed experiments are particularly suitable for the observation of HN spin-systems, which resonate in narrow and very specific region for both ^{1}H and ^{15}N. The proposed experiments were shown to be robust and have good tolerance to r.f. inhomogeneites, and offer advantages over INEPT-based sequences in case of chemical exchange. It was noted that the transfer between in-phase and antiphase coherences require twice as much time when cross-polarisation is used, relative to the INEPT sequence, which may reduce the sensitivity of the corresponding cross-polarisation based experiments. Further experimental evidence is required to assess the merit of the cross-polarisation approach.

Adiabatic inversion pulses are often used in [^{1}H,^{13}C]-HSQC-type spectra to improve the sensitivity of the experiments over the wide range of ^{13}C chemical shifts. The long duration of the adiabatic pulses leads to incomplete refocussing for some of the spins, resulting in the modulation of cross-peak intensity in multiplicity edited HSQC experiments. These modulations can be greatly reduced with the compensation of refocusing inefficiency with synchronised inversion sweep (CRISIS) scheme proposed by Boyer *et al.*[58] The modified sequence CRISIS-HSQC includes additional adiabatic pulses with duration and sweep directions that ensure offset-independent coherence refocusing, that provide substantial increase in sensitivity. The method was demonstrated for small molecules. An improvement of another multiplicity-edited experiment, ADEQUATE was proposed by Parella and Sanchez-Ferrado.[59] The original experiment correlate signals of ^{1}H-^{13}C-^{13}C systems through the use of ^{13}C-^{13}C double-quantum coherence. Gradient selection sensitivity enhancement scheme is used for the coherence detection. The standard sequence was modified to include multiplicity editing that allows to detect signals from CH/CH_3 groups in opposite phase to those of CH_2 groups. The consists of the introduction of ^{1}H pulse of flip angle Θ° during the forward INEPT transfer of coherence between carbon spins that does not change the total length of the pulse-sequence, thus leading to

small sensitivity loss. The experiment is expected to be useful for ^{13}C resonance assignments in small molecules.

6.2 Heteronuclear Triple Resonance Experiments. – The choice of coherence transfer scheme in triple-resonance experiments is critical for very large systems ($\sim$100 kDa). In such cases an optimal strategy is commonly derived on the basis of spin relaxation rates, which are time consuming to measure and difficult to implement with high accuracy. Braun *et al.*[60] suggested to dissect a triple-resonance experiment into individual magnetisation transfer steps and perform optimisation of each step using high-sensitivity 1D and 2D experiments. The method was demonstrated on the optimisation of TROSY-HNCO experiment for a 110 kDa protein. The H->N transfer efficiency was evaluated in a 2D [^{1}H,^{15}N]-TROSY, where the full and truncated TROSY versions were considered. It was found that the truncated version is superior in sensitivity at this molecular weight, producing acceptable level of cross-peak shape distortion. Further increase in the sensitivity was achieved by reducing the duration on the INEPT steps. The experimental results were similar to the estimates based on the relaxation times. Large variation of the transfer efficiency was found for different residues. The efficiency N->CO magnetisation transfer was evaluated from the full TROSY-HNCO experiment. Smaller variation of the transfer efficiency was found for this transfer step throughout the protein and it was concluded that the sensitivity gain is achieved by the optimisation of the TROSY part of the experiment. Similar conclusion was reached by Chung and Kroon[61] after quantitative comparison of TROSY-HNCO sequences at 900 MHz for perdeuterated protein systems with correlation times of 52 and 80 ns (corresponding to molecular weights of 130 and 250 kDa). The authors tested clean-TROSY, Yang/Kay-TROSY (sensitivity-enhanced sequence with an additional 90° ^{15}N pulse at the end and no ^{15}N decoupling in acquisition) and CRINEPT -TROSY, as well as single- and multiple-quantum ^{15}N,$^{13}C'$ correlations. The largest signal loss was observed in the clean-TROSY experiment due to the presence of ^{1}H,^{15}N multiple-quantum coherence. The Yang/Kay-TROSY sequence avoids the multiple-quantum evolution at the expense of transferring both narrow and broad components into the observable magnetisations. Due to the fast relaxation of the broad component only cross-peas corresponding to the narrow component were observed for majority of the HN groups. The sensitivity of CRINEPT-TROSY was $\sim$25% lower that that of the clean-TROSY, making Yang/Kay-TROSY sequence the best out of all considered. The authors additionally compared TROSY experiments at 800 and 900 MHz and found a sensitivity gain higher than expected from the theoretical considerations in case of large systems.

Increased sensitivity in NMR spectra due to the use of cryogenic probes makes it possible to record triple-resonance experiments at natural ^{13}C abundance in the uniformly ^{15}N-labelled samples. Such systems have an advantage of negligible effect of ^{13}C-^{13}C couplings, which was used by Kupce *et al.*[62] to design a combined 3D HNCO/HNCA experiment, where both correlations are recorded simultaneously in a single spectrum. The experiment includes simultaneous N->CO and N->C^{α} transfers, followed by the combined evolution period. To

allow independent setting of the CO and C^{α} sweep widths the CO evolution is split into two parts, one of which is independent from the C^{α} evolution and the other one coincides with it. The CO and C^{α} cross-peaks are observed in the separate regions of the spectra by adjusting the corresponding offsets. The CO excitation is achieved with frequency shifted pulses. The absence of ^{13}C-^{13}C couplings allows to use long values to the ^{13}C evolution time, increasing the spectral resolution.

Additional information can be introduced into the triple-resonance experiments at little sensitivity cost through the use of chemical shift coding of effective coupling constant. This is achieved by a selective pulse with the inversion profile that varies across the range of chemical shifts. The pulse is applied during the indirect evolution to the spins with active single-bond coupling, normally replacing none-selective inversion pulse. As the result the multiplet splitting of the evolving spin varies with the degree of the inversion of the coupled spins, leading to the dependence of the effective splitting on the chemical shift of coupled nuclei. Such chemical shift encoding was introduced into TROSY-HNCACB^{coded}HAHB[63] and TROSY-HNCA^{coded}CB/TROSY-HNCA^{coded}CO[64] experiments, based on the corresponding triple-resonance sequences. In the TROSY-HNCACB^{coded}HAHB experiment the selective Gaussian pulse that decreases to 5% at 2 and 5ppm is applied to H^{α} and H^{β} during C^{α}/C^{β} evolution, leading to the splitting in the ^{13}C dimension with the ^{1}H chemical shift scaled $^{1}J(H,C)$ couplings. Similar pulse is applied to C^{β} in the TROSY-HNCA^{coded}CB or CO in the TROSY-HNCA^{coded}CO experiments, resulting in the chemical shift modulated splitting with the $^{1}J(C^{\alpha},C^{\beta})$ or $^{1}J(C^{\alpha},CO)$ couplings, respectively. The splitting is used to resolve the ambiguity in the matching of the sequential and intraresidue connectivities.

The simultaneous presence of intraresidue and sequential correlations in HN(CA)CO spectra can lead to assignment ambiguities in large proteins due to cross-peak overlap. The intraresidue correlations can be selectively observed in the 3D TROSY intra-HN(CA)CO experiments described by Nietlispach.[65] The pulse sequence uses simultaneous evolution with $^{1,2}J(N,C^{\alpha})$ and $^{1}J(N,C')$ couplings to create triple-antiphase coherence $8N_xC^{\alpha}(i)_zC^{\alpha}(i-1)_zC'_z(i-1)$. The coherence is subsequently converted in multiple-quantum C^{α} coherence that evolves with two $^{1}J(C^{\alpha},C')$ couplings to create $8N_xC^{\alpha}(i)_xC^{\alpha}(i-1)_xC'_z(i)$ coherence that selects intraresidue C' spin. The evolution of the intraresidue C' is then recorded either through the multiple-quantum or single-quantum coherence in respect to C^{α}. The multiple-quantum evolution is achieved in a constant-time manner with simultaneous refocusing of the $^{1}J(C^{\alpha},C^{\beta})$ coupling, that in some cases improves the sensitivity of the experiment. The single-quantum version, on the other hand, reduces the evolution time of the multiple-quantum C^{α} coherence , which is beneficial for large proteins. The experiments were tested on a perdeuterated protein with the correlation time of 28ns (corresponds to ~60kDa). It was found that the sensitivity was reduced by 20-30% relative to the conventional TROSY HN(CA)CO experiment, but the experiment showed clear advantage for the resonance assignment in case of near-degenerate C' chemical shifts.

Selective protonation of side-chain methyl groups in otherwise perdeuterated

and ^{13}C,^{15}N labelled large proteins has been successfully used to obtain valuable structural and dynamical information. Tugarinov and Kay[66] described further development of the strategy, introducing the biothynthetic scheme for protonation and ^{13}C labelling of a single methyl group in otherwise uniformly ^{13}C-labelled side-chains of Leu and Val residues. This creates a linear chain of coupled ^{13}C spins without branching, that can be used to improve the efficiency of the coherence transfer. New experiments Ile,Leu-(HM)CM(CGCBCA)NH, Ile,Leu-HM(CMCGCBCA)NH, Val-(HM)CM(CBCA)NH and Val-HM(CMCBCA)NH were described that correlate the resonances of the methyl group with the backbone HN group. The experiments are a modification of the previously published Ile-(HM)CM(CGCBCA)NH and transfer coherence with a series of INEPT steps. The sensitivity enhancement sequence was used for the N->H transfer. Indirect proton detection is achieved in semi-constant fashion to improve the sensitivity. Additionally, a set of 'out-and-back' experiments HMCM[CG]CBCA and HMCM([CG]CBCA)CO were presented to correlate the resonances of the methyl groups with the other ^{13}C resonances of the side-chains. The sequences are based on a set of sequential INEPT transfer steps. The proposed experiments were used to assign the majority of Val, Ile and Leu residues in a 723 residue protein. A TOCSY-based versions for the correlation of side-chain methyl groups with the rest of the ^{13}C resonances in the uniformly ^{13}C-labelled proteins was described by Yang *et al.*[67] The proposed 3D MQ-(H)CC_mH_m-TOCSY sequence utilises multiple-quantum H-C transfer to record the evolution of ^{13}C spins and create in-phase ^{13}C-coherence at the initial stage of the experiment. This follows by the FLOPSY-8 magnetisation transfer to methyl carbons. The ^{13}C evolution of methyl groups is recorded in constant-time fashion combined with ^{1}H CPD decoupling that reduces the decay of ^{13}C transverse magnetisation. The experiment has higher sensitivity than the HCCH-TOCSY due to the use of the MQ coherence and CPD decoupling. In case of the deuteration of the side-chain with selective protonation on methyl groups the experiment has to be modified to start with the ^{13}C magnetisation.

New experiments for the assignment of quarternary carbons in the aromatic rings of nucleotides were described by Furtig *et al.*[68] The 2D HNC6C5 experiment is derived from the HNCOCA sequence and utilises H1->N1->C6->C5 out-and-back transfer in guanine to correlate H1 and C5 resonances. The 2D H8(H6)-C8(C6)-N9(N1)-C4(C2) and H1′-C1′-N9(N1)-C4(C2) experiments are of HCNC type and correlate H1′ protons or the aromatic H8/H6 protons with C4 and C2 purines and pyrimidines, respectively.

Table 1 *Summary of new or improved experiments and methods*

Experiment/method	*Aims*	*Ref.*
Fast multidimensional methods		
2D Hadamar COSY, TOCSY and NOESY	Time reduction in homonuclear spectra using Hadamard spectroscopy	2
3D Hadamard TOCSY-HSQC	Time reduction in heteronuclear spectra using Hadamard spectroscopy	4
(5,2)D HACA,CONHN	GFT NMR experiments for resonance assignments	7
(5,3)D HACA,CONHN		
(5,3)D HACACONHN		
(4,3)D CBCACONHN		
(4,3)D CBCA,CONHN		
(3,2)D sequential HN(CO-H_N)CO	Combination of GFP NMR and CO band-selective Hadamard frequency encoding to improve cross-peak separation.	9
(3,2)D sequential HN(CO-H_N)CA		
(3,2)D intra-residue (CO-H_N)HNCA		
(5,3)D DEPT-HAHBCACB(CO)NH	Combination of GFP NMR and DEPT-based multiplet selection to improve cross-peak separation.	10
(5,3)D DEPT-HC(CO)NH-TOCSY		
(3,2)D HNCA	Reduced dimensionality experiments for resonance assignments	8
(3,2)D HN(CA)CB		
(3,2)D HN(CA)HA		
(3,2)D HN(CO)CA,		
(3,2)D HN(COCA)CB		
(3,2)D HN(COCA)HA		
(3,2)D J-HNCO(H)		
NOE and diffusion		
2D ^{13}C-filtered/edited NOESY	Isotope-selective NOE observation	22
2D WIF-PGSTE	Selective measurement of diffusion coefficients of ^{15}N-labelled proteins.	38
Relaxation experiments		
2D INEPT-based	Suppression of cross-correlated relaxation in T_1 measurements for CH_2 groups	24
2D TROSY-based	Measurement of off-resonance ^{15}N relaxation to evaluate R_{ex}	25
2D TROSY-based	Measurement of 15N R2a , R_2^b and $R_1^{2H_zN_z}$ to calculate R_{ex}	26

2D INEPT-based	Simultaneous measurement of longitudinal relaxation rates of donor and acceptor ^{15}N in Watson-Crick base pairs	27
2D CC(CO)NH TOCSY-based	1H-^{13}C DD cross-correlated relaxation rates in CH_2 and CH_3 groups	28,29
2D INEPT-based	1H-^{13}C DD cross-correlated relaxation rates in CDH_2 groups	30
2D HSQC-based	15N CSA/DD cross-correlated relaxation rate from the intensities of ^{15}N doublet components	31
2D HNCO and HN(CO)CA-based	Cross-correlated CO CSA/ long-range CO-HA DD relaxation	32
2D HBHA(CBCACO)NH-based	$C^{\alpha}H$-$C^{\beta}H$ DD/DD cross-correlated relaxation	33
2D INEPT-based	$R_{DH,HA} + R_{D,A}$, $R_{D,A}$, $R_{H,A}$ and $R_{D,H}$ cross-correlated relaxation rates involving imino proton and two neighbouring ^{15}N nuclei in hydrogen-bonded nucleotide bases	34
2D HCN-based	1H DD/^{15}N CSA cross-correlated relaxation in nucleotide bases	35
2D HNCO-TROSY-based 2D HN(CO)CA-TROSY-based 2D HNCA-TROSY-based	Cross-correlated relaxation due to slow μs-ms modulation of isotropic chemical shifts of backbone nuclei	36
2D HNCO-based	Cross-correlated relaxation due to slow ms-ms modulation of isotropic chemical shifts of NC′	37
Scalar couplings		
3D iHN(CA),CO(α/β-J-COHA	Measurement of $^3J(C',H^{\alpha})$ couplings	40
2D JM-ADEQUATE	Measurement of single-bond and long-range ^{13}C-^{13}C couplings in small molecules at natural ^{13}C abundance.	41
2D HMBC-based	Measurement long-range ^1H-^{13}C couplings in small molecules at natural ^{13}C abundance.	42
Residual dipolar couplings		
2D IPAP 2D TROSY-anti-TROSY 2D E.COSY	Sensitivity-enhanced experiments for measurement of $^1J(H,N)$ in proteins	43
2D E.COSY	Sensitivity-enhanced experiment for simultaneous measurement of $^1J(N,C')$ and $^2J(H^N,C')$ in proteins	44
2D HNCO-based 2D HN(COCA)HA-based	Measurement of $^1J(C',C^{\alpha})$ and $^1J(C',H^{\alpha})$ in [^1H,^{15}N]-like spectra.	46
2D E.COSY-HNCO	Measurement of $^2J(H,C^{\alpha})$, $^1J(N,C^{\alpha})$, $^3J(H,C^{\alpha})$ and $^2J(N,C^{\alpha})$ in [^1H,^{15}N]-like spectra.	45
3D HNCA-E.COSY-TROSY 3D HNCA(α/β-J-CAHAN)-TROSY	Measurement of $^1J(H^{\alpha},C^{\alpha})$ and $^2J(H^{\alpha},N)$ couplings	47

Table 1 *(cont.)*

Experiment/method	*Aims*	*Ref.*
3D HA(CA)CONH-based	Measurement of $^{1}J(H^{\alpha},C^{\alpha})$ coupling	48
3D JE-TROSY	Single-bond couplings for large macromolecules.	49
2D HSQC-(sel C, sel H)-CT-COSY	Measurement of ^{1}H-^{1}H and ^{13}C-^{13}C couplings.	51
Heteronuclear double resonance		
2D HZQC	TROSY relaxation compensation in methyl groups.	55
2D [^{13}C,^{13}C]-TOCSY	^{13}C assignment in perdeuterated proteins.	52
2D HCP	A set of 2D heteronuclear experiments based on J-cross-polarisation	57
2D CRISIS-HSQC	Offset compensation in multiplicity-edited HSQC experiments with adiabatic pulse inversion.	58
2D multiplicity-edited ADEQUATE	^{13}C assignments in small molecules.	59
Heteronuclear triple resonance		
3D TROSY-HNCACB^{coded}HAHB	Chemical shift modulated splitting of CA and CB with scaled $^{1}J(H,C)$ couplings.	63
3D TROSY-HNCA^{coded}CB 3D TROSY-HNCA^{coded}CO	Chemical shift modulated splitting of CA and CB with scaled $^{1}J(C^{\alpha},C^{\beta})$ or $^{1}J(C^{\alpha},CO)$ couplings.	64
3D TROSY intra-HN(CA)CO	Selective detection of intraresidue CO.	65
3D Ile,Leu-(HM)CM(CGCBCA)NH 3D Ile,Leu-HM(CMCGCBCA)NH 3D Val-(HM)CM(CBCA)NH 3D Val-HM(CMCBCA)NH 3D HMCM[CG]CBCA 3D HMCM([CG]CBCA)CO	Intraresidue correlations in Val and Leu residues, protonated and ^{13}C-labelled on a single methyl group in otherwise uniformly deuterated and ^{13}C-labelled side-chain.	66
3D MQ-(H)CC$_m$H$_m$-TOCSY	Correlation of side-chain methyl groups with the rest of the ^{13}C resonances	67
2D HNC6C5 2D H8(H6)-C8(C6)-N9(N1)-C4(C2) 2D H1′-C1′-N9(N1)-C4(C2)	Assignment of quarternary carbons in the aromatic rings of nucleotides	68

References

1. R. Freeman and E. Kupce, *J. Biomol. NMR*, 2003, **27**, 101.
2. E. Kupce and R. Freeman, *J. Magn. Reson.*, 2003, **162**, 300.
3. C. Bougault, L. M. Feng, J. Glushka, E. Kupce and J. H. Prestegard, *J. Biomol. NMR*, 2004, **28**, 385.
4. E. Kupce and R. Freeman, *J. Magn. Reson.*, 2003, **163**, 56.
5. S. Kim and T. Szyperski, *J. Am. Chem. Soc.*, 2003, **125**, 1385.
6. W. Kozminski and I. Zhukov, *J. Biomol. NMR*, 2003, **26**, 157.
7. S. Kim and T. Szyperski, *J. Biomol. NMR*, 2004, **28**, 117.
8. B. Bersch, E. Rossy, J. Coves and B. Brutscher, *J. Biomol. NMR*, 2003, **27**, 57.
9. B. Brutscher, *J. Biomol. NMR*, 2004, **29**, 57.
10. B. Brutscher, *J. Magn. Reson.*, 2004, **167**, 178.
11. E. Kupce and R. Freeman, *J. Am. Chem. Soc.*, 2003, **125**, 13958.
12. E. Kupce and R. Freeman, *J. Biomol. NMR*, 2003, **27**, 383.
13. E. Kupce and R. Freeman, *J. Am. Chem. Soc.*, 2004, **126**, 6429.
14. E. Kupce and R. Freeman, *J. Biomol. NMR*, 2004, **28**, 391.
15. B. E. Coggins, R. A. Venters and P. Zhou, *J. Am. Chem. Soc.*, 2004, **126**, 1000.
16. Y. Shrot and L. Frydman, *J. Am. Chem. Soc.*, 2003, **125**, 11385.
17. B. Shapira and L. Frydman, *J. Magn. Reson.*, 2003, **165**, 320.
18. Y. Shrot and L. Frydman, *J. Magn. Reson.*, 2004, **167**, 42.
19. B. Shapira, A. Karton, D. Aronzon and L. Frydman, *J. Am. Chem. Soc.*, 2004, **126**, 1262.
20. N. M. Loening, M. J. Thrippleton, J. Keeler and R. G. Griffin, *J. Magn. Reson.*, 2003, **164**, 321.
21. Y. Shrot and L. Frydman, *J. Magn. Reson.*, 2003, **164**, 351.
22. R. D. Peterson, C. A. Theimer, H. H. Wu and J. Feigon, *J. Biomol. NMR*, 2004, **28**, 59.
23. K. E. Cano, M. J. Thrippleton, J. Keeler and A. J. Shaka, *J. Magn. Reson.*, 2004, **167**, 291.
24. C. W. Jin, J. J. Prompers and R. Bruschweiler, *J. Biomol. NMR*, 2003, **26**, 241.
25. J. G. Kempf, J. Y. Jung, N. S. Sampson and J. P. Loria, *J. Am. Chem. Soc.*, 2003, **125**, 12064.
26. C. Y. Wang, M. Rance and A. G. Palmer, *J. Am. Chem. Soc.*, 2003, **125**, 8968.
27. D. Bytchenkoff and G. Bodenhausen, *J. Magn. Reson.*, 2003, **165**, 1.
28. Y. Zheng and D. W. Yang, *J. Biomol. NMR*, 2004, **28**, 103.
29. W. D. Liu, Y. Zheng, D. P. Cistola and D. W. Yang, *J. Biomol. NMR*, 2003, **27**, 351.
30. D. Marion, *J. Magn. Reson.*, 2004, **166**, 202.
31. J. B. Hall, K. T. Dayie and D. Fushman, *J. Biomol. NMR*, 2003, **26**, 181.
32. K. Loth, P. Pelupessy and G. Bodenhausen, *J. Biomol. NMR*, 2003, **27**, 159.
33. T. Carlomagno, W. Bermel and C. Griesinger, *J. Biomol. NMR*, 2003, **27**, 151.
34. J. Dittmer, C. H. Kim and G. Bodenhausen, *J. Biomol. NMR*, 2003, **26**, 259.
35. S. Ravindranathan, C. H. Kim and G. Bodenhausen, *J. Biomol. NMR*, 2003, **27**, 365.
36. A. Majumdar and R. Ghose, *J. Biomol. NMR*, 2004, **28**, 213.
37. J. Wist, D. Frueh, J. R. Tolman and G. Bodenhausen, *J. Biomol. NMR*, 2004, **28**, 263.
38. I. V. Nesmelova, D. Idiyatullin and K. H. Mayo, *J. Magn. Reson.*, 2004, **166**, 129.
39. G. S. Armstrong, N. M. Loening, J. E. Curtis, A. J. Shaka and V. A. Mandelshtam, *J. Magn. Reson.*, 2003, **163**, 139.

40. P. Permi, *J. Magn. Reson.*, 2003, **163**, 114.
41. K. E. Kover and P. Forgo, *J. Magn. Reson.*, 2004, **166**, 47.
42. R. A. E. Edden and J. Keeler, *J. Magn. Reson.*, 2004, **166**, 53.
43. K. Y. Ding and A. M. Gronenborn, *J. Magn. Reson.*, 2003, **163**, 208.
44. K. Y. Ding and A. M. Gronenborn, *J. Am. Chem. Soc.*, 2003, **125**, 11504.
45. K. Y. Ding and A. M. Gronenborn, *J. Am. Chem. Soc.*, 2004, **126**, 6232.
46. K. Ding and A. M. Gronenborn, *J. Magn. Reson.*, 2004, **167**, 253.
47. P. Permi, *J. Biomol. NMR*, 2003, **27**, 341.
48. W. D. Hu, Z. M. Zhang and Y. Chen, *J. Magn. Reson.*, 2003, **165**, 248.
49. B. Luy and J. P. Marino, *J. Magn. Reson.*, 2003, **163**, 92.
50. K. Feher, S. Berger and K. E. Kover, *J. Magn. Reson.*, 2003, **163**, 340.
51. M. Martin-Pastor, A. Canales-Mayordomo and J. Jimenez-Barbero, *J. Biomol. NMR*, 2003, **26**, 345.
52. A. Eletsky, O. Moreira, H. Kovacs and K. Pervushin, *J. Biomol. NMR*, 2003, **26**, 167.
53. I. Bertini, I. C. Felli, R. Kummerle, D. Moskau and R. Pierattelli, *J. Am. Chem. Soc.*, 2004, **126**, 464.
54. V. Tugarinov, P. M. Hwang, J. E. Ollerenshaw and L. E. Kay, *J. Am. Chem. Soc.*, 2003, **125**, 10420.
55. V. Tugarinov, R. Sprangers and L. E. Kay, *J. Am. Chem. Soc.*, 2004, **126**, 4921.
56. A. E. Bennett, J. D. Gross and G. Wagner, *J. Magn. Reson.*, 2003, **165**, 59.
57. T. Parella, *J. Biomol. NMR*, 2004, **29**, 37.
58. R. D. Boyer, R. Johnson and K. Krishnamurthy, *J. Magn. Reson.*, 2003, **165**, 253.
59. T. Parella and F. Sanchez-Ferrando, *J. Magn. Reson.*, 2004, **166**, 123.
60. D. Braun, K. Wuthrich and G. Wider, *J. Magn. Reson.*, 2003, **165**, 89.
61. J. Chung and G. Kroon, *J. Magn. Reson.*, 2003, **163**, 360.
62. E. Kupce, D. R. Muhandiram and L. E. Kay, *J. Biomol. NMR*, 2003, **27**, 175.
63. S. Pegan, W. Kwiatkowski, S. Choe and R. Riek, *J. Magn. Reson.*, 2003, **165**, 315.
64. C. Ritter, T. Luhrs, W. Kwiatkowski and R. Riek, *J. Biomol. NMR*, 2004, **28**, 289.
65. D. Nietlispach, *J. Biomol. NMR*, 2004, **28**, 131.
66. V. Tugarinov and L. E. Kay, *J. Am. Chem. Soc.*, 2003, **125**, 13868.
67. D. W. Yang, Y. Zheng, D. J. Liu and D. F. Wyss, *J. Am. Chem. Soc.*, 2004, **126**, 3710.
68. B. Furtig, C. Richter, W. Bermel and H. Schwalbe, *J. Biomol. NMR*, 2004, **28**, 69.

9
NMR of Proteins and Nucleic Acids

BY S. J. MATTHEWS

1 Introduction

The application of nuclear magnetic resonance (NMR) to proteins and nucleic acids has continued to grow this year, with transverse relaxation optimised spectroscopy (TROSY), liquid crystal NMR and studies on membrane bound systems. Enhanced automated NMR analysis and structure determination procedures have also been described this year, together with the introduction of novel methods. While covering many of the key developments designed to improve throughput, this chapter also emphasises the progress in using NMR to understand important biological problems

2 Application and Development of New Methodology

2.1 Automated Analysis. – NMR protein studies rely on the accurate assignment of resonances. The general procedure is to (1) pick peaks, (2) cluster data from various experiments or spectra, (3) assign peaks to the sequence and (4) verify the assignments with the spectra. Many algorithms and protocols now exist for automating the assignment process.

Complete and accurate NMR spectral assignment is a prerequisite for high-throughput automated structure determination of biological macromolecules. However, completely automated assignment procedures generally encounter difficulties for all but the most ideal data sets. Sources of these problems include difficulty in resolving correlations in crowded spectral regions, as well as complications arising from dynamics, such as weak or missing peaks, or atoms exhibiting more than one peak due to exchange phenomena. SMARTNOTEBOOK is a semi-automated assignment software package designed to combine the best features of the automated and manual approaches[1]. The software finds and displays potential connections between residues, while the spectroscopist makes decisions on which connection is correct, allowing rapid and robust assignment. In addition, SMARTNOTEBOOK helps the user fit chains of connected residues to the primary sequence of the protein by comparing the experimentally determined chemical shifts with expected shifts derived from a chemical shift database, while providing bookkeeping throughout the assignment procedure.

Nuclear Magnetic Resonance, Volume 34
© The Royal Society of Chemistry, 2005

Similarly, Malmodin *et al.* have designed a procedure that yields nearly complete backbone and side chain resonance assignments starting from a set of heteronuclear three-dimensional spectra[2]. By combining two earlier published procedures, AUTOPSY and GARANT, with a new program, PICS, all necessary steps from spectra analyses to sequence-specific assignments were performed fully automatically. Characteristic features of the present approach are a flexible design allowing as input almost any combination of NMR spectra, applicability to side chains, robustness with respect to parameter choices and reproducibility. Also, Coggins and Zhou have developed a novel computer-assisted method for sequential assignment, using an algorithm that conducts an exhaustive search of all spin systems both for establishing sequential connectivities and then for assignment[3]. By running the program iteratively with user intervention after each cycle, ambiguities in the assignments can be eliminated efficiently and backbone resonances can be assigned rapidly.

A flexible interface to help a spectroscopist easily move between assignment steps is also available in the software module, NvAssign, which has been written for use with NMRView. The module provides a flexible interface to cluster data and interact with the existing assignment algorithms. Furthermore, the software module reads the results from other algorithms so that the data can be easily verified by spectral analysis[4]. Hyberts and Wagner have developed a tool for computer-assisted assignments of protein NMR spectra from triple resonance data. The program is designed to resemble established manual assignment procedures as closely as possible. IBIS exports its results in XEASY format, thus, the operator has continuous visual and accounting control over the progress of the assignment procedure. IBIS achieves complete assignments for those residues that exhibit sequential triple resonance connectivities within a few hours or days[5].

Assignment evaluation is a key step in the automated analysis of complex NMR data. Moseleya *et al.* have described a set of utilities and graphical user interface (GUI) tools for evaluating the quality of protein resonance assignments. The Assignment Validation Software (AVS) suite, together with new GUI features in the AutoAssign software package, provides a set of reports and graphs for validating protein resonance assignment data before its use in structure analysis and/or submission to the BioMagResBank (BMRB). Input includes a listing of resonance assignments and a summary of sequential connectivity data used in deriving the assignments. These tools are useful for evaluating the accuracy of protein resonance assignments determined by either automated or manual methods[6].

Residue type and sequential assignments obtained from specifically labeled samples, when combined with 3D heteronuclear data, can significantly increase the efficiency and accuracy of the assignment process, the first step in structure determination by NMR. A protocol for the design of specifically labeled samples with high information content has been developed by Shi *et al.*[7]. In vitro protein synthesis methods were used to produce four specifically labeled samples of the 23.5 kDa protein phosphoserine phosphatase (PSP) from *Methanoccous jannaschii*. Each sample contained two $^{13}C/^{15}N$-labeled amino acids and one ^{15}N-

labeled amino acid. The 135 type and 14 sequential assignments obtained from these samples were used in conjunction with 3D data obtained from uniformly $^{13}C/^{15}N$ -labeled and $^{2}H/^{13}C/^{15}N$-labeled protein to manually assign the backbone $^{1}H(N)$, ^{15}N, $^{13}C'$, ^{13}C(alpha), and ^{13}C(beta) signals. Using an automated assignment algorithm, 30% more assignments were obtained when the type and sequential assignments were used in the calculations.

Langmead and Donald have reported an automated procedure for high-throughput NMR resonance assignment for a protein of known structure, or homologous structure. Their algorithm performs Nuclear Vector Replacement (NVR) by Expectation/Maximization (EM) to compute assignments. NVR correlates experimentally-measured NH residual dipolar couplings (RDCs) and chemical shifts to a given a priori whole-protein 3D structural model. The algorithm requires only uniform ^{15}N-labelling of the protein, and processes unassigned ^{1}H-^{15}N HSQC spectra, ^{1}H-^{15}N RDCs, and sparse HN-HN NOE's. The algorithm was demonstrated on NMR data from a 76- residue protein, human ubiquitin, matched to four structures, including one mutant (homolog), determined either by X-ray crystallography or NMR experiments (without RDCs). NVR achieves an average assignment accuracy of over 99%[8].

High throughput NMR data collection will contribute to the success of proteomics investigations. The G-Matrix Fourier Transformation NMR (GFT-NMR) method significantly shortens experimental time by reducing the number of data dimensions for isotopically labelled proteins. Xia *et al.* have demonstrated a suite of 3D→2D or (3,2)D GFT-NMR experiments using $^{13}C/^{15}N$-labeled ubiquitin. These experiments were completed within 18 hours, representing a 4- to 18-fold reduction in data acquisition time compared to the corresponding conventional 3D experiments. A subset of the GFT-NMR experiments, (3,2)D HNCO, HNCACB, HN(CO)CACB, and 2D ^{1}H-^{15}N HSQC, which are necessary for backbone assignments, were carried out within 6 hours. To facilitate the analysis of the GFT-NMR spectra, automated procedures for viewing and analysing the GFT-NMR spectra were developed. Our overall strategy allows (3,2) D GFT-NMR experiments to be readily performed and analysed[9]. Furthermore, Kim and Szyperski have developed (4,3)D, (5,3)D and (5,2)D GFT triple resonance NMR for polypeptide backbone and ^{13}C(beta) resonance assignment of double labelled proteins[10]. The joint sampling of $m = 2$, 3 or 4 indirect chemical shift evolution periods of 4D and 5D NMR experiments yields the measurement of $2(m) - 1$ linear combinations of shifts. To obtain sequential assignments, these are matched in corresponding experiments delineating either intra or inter-residue correlations. Hence, an increased set of matches is registered when compared to conventional approaches, and the 4D or 5D information allows one to efficiently break chemical shift degeneracy. The new features of GFT NMR based resonance assignment strategies promise to be of particular value for establishing automated protocols. Atreya and Szyperski have also described a GFT NMR spectroscopy-based strategy for resonance assignment of proteins and demonstrate this on three proteins with molecular masses ranging from 8.6 to 17 kDa[11]. Each of the GFT NMR experiments rapidly affords four-, five-, or six-dimensional spectral information in combination with

precise measurements of chemical shifts. The resulting high information content enables one to obtain nearly complete assignments by using only four NMR experiments. For the backbone amide proton detected 'out-and-back' experiments, data collection was further accelerated up to approximate to 2.5-fold by use of longitudinal ^{1}H relaxation optimization.

NMR frequency assignments are usually considered a prerequisite for the analysis of NOESY spectra, which in turn is required for the calculation of biomolecular structures. In contrast, a new method was proposed in which a relatively high numbers of unambiguous NOE assignments can be achieved in an automated manner by relying on the grouping of resonances into connected spin systems. Grishaev and Llinas have developed two protocols, SPI and BACUS, based on Bayesian inference. SPI produces a list of the ^{1}H resonance frequencies from homo- and hetero-nuclear multidimensional spectra, grouped into effective spin systems. BACUS automatically establishes probabilistic identities of NOESY cross-peaks in terms of the chemical shifts provided by SPI. The method exploits the self-consistency of the NOESY graph by taking advantage of a network of J- as well as NOE-connected 'reporter' protons sorted *via* SPI[12]. The development of new high throughput structure determination methods is an essential aspect of modern NMR research. Excellent reviews have been published this year describing automated structure determination of proteins by NMR spectroscopy[13-15]. The quality of NMR-derived biomolecular structure models can be assessed by validation on the level of structural characteristics as well as the NMR data used to derive the structure models. An overview has been presented of the common methods to validate experimental NMR data[16].

Experimental structure determination by X-ray crystallography and NMR spectroscopy is slow and time-consuming compared with the rate at which new protein sequences are being identified. NMR spectroscopy has the advantage of rapidly providing the structurally relevant information in the form of unassigned chemical shifts (CSs), intensities of NOESY crosspeaks (NOEs), and residual dipolar couplings (RDCs), but use of these data are limited by the time and effort needed to assign individual resonances to specific atoms. The rapid calculation of accurate folds is key to subsequent refinement steps and providing immediate information regarding biological function. Kuszewski *et al.* have developed a robust approach to automatically calculate structures with a backbone coordinate accuracy of 1.0-1.5 Angstrom from datasets in which as much as 80% of the long-range NOEs are incorrect. The current algorithm differs from previously published methods in that it has been expressly designed to ensure that the results from successive cycles are not biased by the global fold of structures generated in preceding cycles. The algorithm incorporates three main features: a linear energy function representation of the NOE restraints to allow maximization of simultaneously satisfied restraints during the course of simulated annealing; a method for handling the presence of multiple possible assignments for each NOE cross- peak which avoids local minima by treating each possible assignment as if it were an independent restraint; and a probabilistic method to permit both inactivation and reactivation of all NOE restraints on the fly during the course of simulated annealing[17]. Meiler and Baker have also proposed a method

for generating low-resolution protein structures by using unassigned NMR data that relies on the *de novo* protein structure prediction algorithm, and a Monte Carlo procedure that searches for the assignment of resonances, producing the best fit of the experimental NMR data to a candidate 3D structure[18]. A large ensemble of models is generated from sequence information alone by using ROSETTA, an optimal assignment is identified for each model, and the models are then ranked based on their fit with the NMR data assuming the identified assignments. The method was tested on nine protein sequences between 56 and 140 amino acids and published CS, NOE, and RDC data. The procedure yielded models with rms deviations between 3 and 6 Å, and, in four of the nine cases, the partial assignments obtained by the method could be used to refine the structures to high resolution (0.6-1.8 Å).

Cole *et al.* have developed the program FAST-Modelfree for the fully automated, high throughput analysis of NMR spin-relaxation data[19]. This program interfaces with the program Modelfree 4.1 and provides an intuitive GUI for configuration as well as complete standalone operation during the model selection and rotational diffusion parameter optimization processes. FAST-Modelfree is also capable of iteratively assigning models to each spin and optimizing the parameters that describe the diffusion tensor.

2.2 Dipolar Couplings. – Residual dipolar interactions are very precise reporters on the average orientation of bonds relative to the molecular alignment frame, and they can be used in a variety of ways to further understanding of protein and oligonucleotide structure[20]. Kramer *et al.* have presented an intuitive introduction to the alignment tenser and an elementary derivation of the key equations[21]. An important application of RDCs is in the structure characterisation of macromolecular complexes and multi-domain systems. Based on high-resolution structures of the free molecules accurate structure determination of protein complexes by NMR spectroscopy is possible using RDC data. However, protein backbone resonances have to be assigned first, which is often problematic for large complexes. Zweckstetter has shown that, when NMR resonances belonging to a specific amino acid type are selected either by amino acid specific labelling, characteristic chemical shifts or by dedicated NMR experiments, molecular alignment tensors of proteins up to 80 kDa can be determined without prior backbone resonance assignment[22]. This offers the opportunity to greatly accelerate determination of 3D structures of protein complexes, and validation of multimeric states of proteins. Chen and Reif have demonstrated that transferred residual dipolar couplings (trRDCs) can be useful to restrain the structure of peptide ligand transiently bound to an aligned species. The effect is demonstrated on the spontaneous alignment of amyloid fibrils with the fibril axis parallel to the magnetic field in complex with a peptide inhibitor. This alignment is transferred to the transiently binding peptide inhibitor and is reflected in the size of the trRDCs [23]. Fushman *et al.* have reviewed the use of spin-relaxation and residual dipolar coupling measurements in the determination domain orientation in macromolecules [24].

The increased use of RDCs in high-resolution NMR studies of macro-

molecules, has justified a continued effort towards the development of accurate, sensitive methods for their measurement. Ding and Gronenborn have presented sensitivity-enhanced versions of the IPAP, TROSY-anti-TROSY, and E.COSY experiments for measuring one-bond ^{15}N-^{1}H couplings. Together with the previously developed sensitivity-enhanced E.COSY-type HSQC experiment they comprise a suite of sensitivity-enhanced experiments that allows one to chose the optimal spectrum for accurate measurement of one-bond residual dipolar couplings in proteins[25]. Sensitivity-enhanced 2D IPAP experiments using the accordion principle for measuring one-bond $^{13}C'$-^{13}C(alpha) and ^{1}H(alpha)-^{13}C(alpha) dipolar couplings in proteins have also been presented by this group[26]. Luy and Marino have devised a J-evolved transverse relaxation optimized (JE-TROSY) method for the determination of one-bond couplings that involves J-evolution of the sharpest cross-peak multiplet component selected in a TROSY experiment [27]. Feher and co-workers have reported a G-BIRD(r) modified coupled HSQC experiment for the accurate determination of one-bond heteronuclear RDCs[28]. The G-BIRD(r) module has been employed to refocus the long-range coupling evolution of the heteronucleus. The crosspeaks obtained are split by only the direct one-bond coupling that can be extracted by measuring simple frequency differences between singlet maxima. Additionally, the decoupling of long-range multiple bond splittings leads to considerable sensitivity enhancement. The modification also has been applied in a TROSY sequence resulting in a significant sensitivity and resolution improvement. Permi has designed novel NMR pulse schemes for simultaneous measurement of $^{1}D_{C(alpha)H(alpha)}$ and $^{2}DNH_{(alpha)}$ RDCs in proteins. $^{2}DNH_{(alpha)}$ can be very useful for protein structure determination and can be measured from the ^{15}N dimension utilizing HNCA-TROSY-based experiments, which concomitantly supply the large $^{1}D_{C(alpha)H(alpha)}$ coupling. The HNCA-TROSY-based experiments are optimal for measuring RDCs at high magnetic fields owing to absence of rapid transverse relaxation of carbonyl carbon[29]. These experiments are valuable additions to the suites available for determination of RDCs in biological systems.

Vogeli *et al.* have demonstrated that ^{13}C-start and ^{13}C-observe spectra can be routinely used to measure an extensive set of the side-chain residual ^{13}C-^{13}C dipolar couplings[30]. They established that, among different broadband polarization transfer schemes, the FLOPSY family can be used to exchange magnetization between a J coupled networks of spins while largely decoupling dipolar interactions between these spins. An excellent correlation between measured RDCs and the 3D structure of the protein was observed, indicating a potential use of the ^{13}C-^{13}C RDCs in the structure determination of perdeuterated proteins. Eletsky *et al.* have also discussed the perspectives for structure determination of larger proteins by using novel strategies based on the ^{1}H NOEs in combination with multiple residual dipolar couplings between adjacent ^{13}C spins determined from 2D ^{13}C-only experiments[31].

Recent advancements in RDCs as a means of structure validation and elucidation have demonstrated the need for, not only a more user friendly, but more powerful RDC analysis tools. Valafar and Prestegard have introduced a software package, named REsidual Dipolar Coupling Analysis Tool (REDCAT) that

addresses these issues[32]. REDCAT is a user-friendly program with a GUI developed in Tcl/Tk that is highly portable. In addition to basic utilities to solve for order tensors and back calculate couplings from a given order tensor and proposed structure, a number of improved algorithms have been incorporated. These include the proper sampling of the Null-space (when the system of linear equations is under-determined), more sophisticated filters for invalid order-tensor identification, error analysis for the identification of the problematic measurements and simulation of the effects of dynamic averaging processes. Zidek *et al.* have presented a method of testing structure-related NMR data prior to structure calculations[33]. The test is applicable to second rank tensor interactions (dipolar coupling, anisotropic chemical shielding, and quadrupolar interaction) observed in partially aligned samples of biomacromolecules. The method utilizes the fact that only limited number of frequencies corresponding to these interactions can be measured independently in a rigid fragment of the macromolecule. Internal consistency of sufficiently large sets of frequencies measured in individual molecular fragments is tested by comparing the experimental data with their predicted values.

NMR RDCs, in the form of the projection angles between the respective internuclear bond vectors, have been used as structural restraints in the *ab initio* structure prediction of a test set of six proteins[34]. The restraints were applied using the recently developed SICHO (SIde-CHain-Only) lattice protein model that employs a replica exchange Monte Carlo algorithm to search conformational space. Using a small number of RDC restraints, the quality of the predicted structures is improved as reflected by lower RMSD (root mean square deviation) values from the corresponding native structures and by the higher correlation of the most cooperative mode of motion of each predicted structure with that of the native structure. The latter, in particular, has possible implications for the structure-based functional analysis of predicted structures. Valafar and Prestegard have also presented a simple method for rapid classification of fold families by the statistical analyses of unassigned the ^{15}N-^{1}H RDCs. NMR data can be quickly analysed and structure determination efforts can be focused on unique structures, thereby improving overall efficiency of constructing fold libraries[35].

A new approach to the interpretation of RDCs for the regular secondary structures of proteins has been presented[36]. A quantitative correlation between structure periodicity and the experimental values of the backbone RDCs was established. Building on the recent interpretation of the periodicity of residual dipolar couplings in alpha-helices (*i.e.*, 'dipolar waves'), a general parametric equation for fitting the RDC data of any regular secondary structure was derived. This equation interprets the modulation of the RDC periodicity in terms of the secondary structure orientation with respect to an arbitrary reference frame, laying the groundwork for using backbone RDCs as a fast tool for determining protein folds by NMR. Similar observations have been made in residual dipolar coupling measurements from nucleic acid structures[37].

Alignment of macromolecules in nearly neutral aqueous lyotropic liquid-crystalline media such as bicelles, commonly used in macromolecular NMR

studies, can be predicted accurately by a steric obstruction model. A simple extension of this model is described that results in improved predictions for both the alignment orientation and magnitude of solutes in charged nematic media, such as the widely used medium of filamentous phage Pf1[38]. The extended model approximates the electrostatic interaction between a solute and an ordered phage particle as that between the solute's surface charges and the electric field of the phage. Results indicate that alignment in charged nematic media is a function not only of the solute's shape, but also of its electric multipole moments of net charge, dipole, and quadrupole. For several of the proteins, the calculated alignment is sensitive to the precise position of the charged groups on the protein surface. This suggests that NMR alignment measurements can potentially be used to probe protein electrostatics. Ferrarini has analysed calculated residual dipolar couplings between ^{15}N and ^{1}H nuclear spins in the Ig-binding domain of streptococcal protein G, over a range of ionic strengths, virus dimensions and concentrations[39]. The theoretical predictions enable the NMR observations reported for this protein to be explained. The effects of steric obstruction on random flight chains have been examined by Louhivuori *et al.*[40]. Spatial probability distributions were elaborated to calculate RDCs and residual chemical shift anisotropy parameters. Calculations yielded chain length and residue position-dependent values in good agreement with simulations and provided an understanding of recently acquired data from denatured proteins.

RDCs between nuclear spins in partially aligned samples offer unique insights into biomacromolecular structure and dynamics. To fully benefit from the RDC data, accurate knowledge of the magnitude (Da) and rhombicity (R) of the molecular alignment tensor, A, is important. An extended histogram method (EHM) is presented which extracts these parameters more effectively from dipolar coupling data. The method exploits the correlated nature of RDCs for structural elements of planar geometry, such as the one-bond ^{13}C′(i)-^{13}C(i)alpha, ^{13}C′(i)-^{15}N(i + 1), and ^{15}N(i + 1)-^{1}H(i + 1)N couplings in peptide bonds of proteins, or combinations of $^{1}D_{(C1'H1')}$, $^{1}D_{(C2'H2')}$, $^{1}D_{(C1'C2')}$, $^{2}D_{(C2'H1')}$, $^{2}D_{(C1'H2')}$, and $^{3}D_{(H1'H2')}$ couplings in nucleic acids, to generate an arbitrarily large number of synthetic RDCs. These synthetic couplings result in substantially improved histograms and resulting values of Da and R, compared with histograms generated solely from the original sets of correlated RDCs, particularly when the number of planar fragments for which couplings are available is small. An alternative method, complementary to the EHM, is also described, which uses a systematic grid search procedure, based on least-squares fitting of sets of correlated RDCs to structural elements of known geometry, and provides an unambiguous lower limit for the degree of molecular alignment[41,42].

Wang *et al.* have derived a quadratic equation for computing the direction of an internuclear vector from RDCs measured in two aligning media, and two simple trigonometric equations for computing the backbone (phi, psi) angles from two backbone vectors in consecutive peptide planes[43]. These equations make it possible to compute the backbone (phi, psi) angles for a residue from RDCs in two media on any single backbone vector type. Building upon these exact solutions they have designed a novel algorithm for determining a protein

backbone substructure consisting of alpha-helices and beta-sheets. The algorithm employs a systematic search technique to refine the conformation of both alpha-helices and beta-sheets and to determine their orientations using exclusively the angular restraints from RDCs. Its also computes the backbone fold employing a very sparse distance restraints between pairs of alpha-helices and beta-sheets[43]. Briggman *et al.* describe *de novo* determination of bond orientations and order parameters from residual dipolar couplings with high accuracy[44].

The effect of small amplitude anisotropic peptide plane motion on RDCs measured in proteins has been investigated. RDC averaging effects in the presence of GAF (Gaussian axial fluctuation) motions are found to vary strongly depending on the peptide plane orientation. Even low amplitude dynamics can significantly affect derived alignment tensor parameters if this motion is not taken into account. An analytical description of averaged amide RDCs is introduced that includes basic GAF-like motion. The averaging depends on the orientation of the peptide plane (alpha, beta, gamma) in the alignment frame and on the motional amplitude (sigma). Using the GAF model to describe conformationally averaged RDC is important for two reasons: a more accurate definition of the alignment tensor magnitude can be derived, and the method can be used to detect average small amplitude motions in protein backbones from readily accessible data, on time scales not easily sampled by other NMR techniques[45]. Zhang *et al.* have used magnetic field induced RDCs to probe motions between equivalent RNA domains[46].

Comprehensive evaluation of the peptide bond N-H orientations shows a weak anti-correlation between the deviation of the peptide bond torsion angle omega from 180 degrees and the angle between the N-H vector and the C′NC(alpha) plane. The slope of this correlation is -1, indicating that, on average, pyramidalisation of the peptide N contributes to small deviations from peptide bond planarity to the same degree as true twisting around the C′N bond. Although hydrogen atoms are commonly built onto crystal structures assuming the N-H vector orientation falls on the line bisecting the C′NC(alpha) angle, a better approximation adjusts the C(alpha)C′NH torsion angle to -2 degrees. The ^{1}H-^{15}N dipolar data do not contradict the commonly accepted motional model where angular fluctuations of the NH bond orthogonal to the peptide plane are larger than in-plane motions, but the amplitude of angular fluctuations orthogonal to the Ci-1(alpha)-Ni-Ci(alpha) plane exceeds that of in-plane motions by $\sim$10-15 degrees[47]. Jensen *et al.* have examined how the hydrogen bond geometry is affected when structural restraints based on measurements of residual dipolar couplings are included in the structure calculations. This study revealed the importance of using several types of RDCs to get good hydrogen bond geometry and showed that using a small set of NOEs derived from the amide protons, together with a full set of RDCs resulted in structures of very high quality[48].

NMR spectra of ubiquitin in the presence of bicelles at a concentration of 25% w/v have been recorded under sample spinning for different angles of rotation[49]. For an axis of rotation equal to the magic angle, the coupled ^{1}H-^{15}N HSQC corresponds to the classical spectrum obtained in an isotropic solution and allows the measurement of scalar couplings. For an angle of rotation smaller

than the magic angle, the bicelles orient with their normal perpendicular to the spinning axis, whereas for an angle of rotation greater than the magic angle the bicelles orient with their normal along the spinning axis. This bicelle alignment creates anisotropic conditions that give rise to observable RDCs. The magnitude of these dipolar couplings depends directly on the angle that the rotor makes with the main magnetic field. By changing this angle in a controlled manner, residual dipolar couplings can be either scaled up or down thus offering the possibility to study simultaneously a wide range of dipolar couplings in the same sample. With the aim of determining accurate ^{15}N chemical shielding tensor values for solution proteins, Kurita *et al.* have used magic angle sample spinning (MAS) to observe discriminately the orientation-dependent changes in the ^{15}N chemical shift[50]. The application of MAS to an aligned bicelle solution removes the torque that aligns the bicelles against the magnetic field. Thus, the application of MAS to a protein in a bicelle solution eliminates only the molecular alignment effect, while keeping all other sample conditions the same. The observed chemical shift differences between experiments with and without MAS provides accurate values of the orientation-dependent ^{15}N chemical shifts and remove the accumulated effects of environmental changes, such as protein-bicelle interactions. This provides valuable information on the magnitudes and orientation of the chemical shielding tensors relative to the molecule's alignment frame.

Although an abundance of existing alignment methods is available for the measurement of RDCs in biological macromolecular, new systems are regularly being reported. A molecule with an anisotropic magnetic susceptibility is spontaneously aligned in a static magnetic field. Alignment of such a molecule yields residual dipolar couplings and pseudocontact shifts. Lanthanide ions have recently been successfully used to provide an anisotropic magnetic susceptibility in target molecules either by replacing a calcium ion with a lanthanide ion in calcium-binding proteins or by attaching an EDTA derivative to a cysteine residue *via* a disulfide bond. Ikegami *et al.* have described a novel enantiomerically pure EDTA derived tag that provide a stronger alignment due to a shorter linker and does not suffer from stereochemical diversity upon lanthanide complexation[51]. Residual ^{15}N-^{1}H dipolar couplings of up to 8 Hz at 800 MHz are induced by a single alignment tensor from this tag.

2.3 Transverse Relaxation Optimized Spectroscopy (TROSY). – TROSY, in combination with various isotope-labelling techniques, has opened avenues to study biomolecules with molecular masses of up to 1 MDa by solution NMR. Important recent applications of TROSY include the structure determination of membrane proteins in detergent micelles, structural and functional studies of large proteins in both monomeric form and macromolecular complexes, and investigations of intermolecular interactions in large complexes. TROSY improves the measurement of residual dipolar couplings (RDCs) and the detection of scalar couplings across hydrogen bonds, which promise to enhance the determination of solution structures of large proteins and oligonucleotides[52-55]. Chung*et al.* have provided quantitative signal to noise data and feasibility study

at 900 MHz for ^{1}H-^{15}N-^{13}C triple resonance backbone experiment obtained on a large protein system with correlation time of 80 ns[56]. Results confirmed the prediction that avoiding the unfavourable relaxation properties of multiple quantum coherence in the TROSY phase cycle of the final transfer is crucial for maximal sensitivity from very large molecular weight systems.

A general method for stable-isotope labeling of large proteins has been introduced and applied to the *E. coli* GroEL chaperone proteins by solution NMR[57]. In addition to enabling the residue-specific ^{15}N-labeling of proteins in a highly deuterated background, it is also an efficient approach for uniform labelling. The method meets the requirements of high-level deuteration, minimal cross-labeling and high protein yield, which are crucial for NMR studies of structures with sizes above 150 kDa. Applications to the GroEL system show that these strategies are efficient tools for studies of structure, dynamics and intermolecular interactions in large supramolecular complexes, when combined with TROSY- and CRINEPT-based experimental NMR schemes.

Libraries of new pulse sequences incorporating TROSY-type magnetization transfer have continued to grow this year. A new method for backbone resonance assignment suitable for large proteins with the natural ^{1}H isotope content has been proposed based on a combination of the most sensitive TROSY-type triple-resonance experiments. These techniques include TROSY-HNCO, $^{13}C'$-detected 3D multiple-quantum HACACO and the newly developed 3D TROSY multiple-quantum-HN(CA)HA and 4D TROSY multiple- quantum-HACANH experiments. The method is demonstrated on the 44 kDa uniformly ^{15}N,^{13}C-labeled and fractionally deuterated trimeric *B. Subtilis* Chorismate Mutase [58]. A modified version of the backbone TROSY based 3D HN(CA)CO experiment has been presented that provides uniquely intraresidue correlation shift information, by efficiently suppressing the sequential connectivity data[59]. The resulting reduction in the number of peaks decreases overlap and removes ambiguities in situations where in the conventional HN(CA)CO i and i − 1 correlations are overlapped or are comparable in intensity. The sequential residue connection is obtained in combination with a 3D HNCO. A new strategy of backbone resonance assignment has been devised by Pervushin and Elstsky, based on a combination of the most sensitive TROSY-type triple resonance experiments such as TROSY-HNCA and TROSY-HNCO with a new 3D multiple-quantum HACACO experiment[60]. The favourable relaxation properties of the multiple-quantum coherences and signal detection using $^{13}C'$ antiphase coherences optimize the performance for application to larger proteins. In addition to the $^{1}H(N)$, ^{15}N, ^{13}C(alpha) and $^{13}C'$ chemical shifts the 3D multiple-quantum HACACO experiment provides assignment for the ^{1}H(alpha) resonances. The strategy is demonstrated on larger proteins with molecular weights up to 80 kDa.

The concept of chemical shift-coding monitors chemical shifts in multi-dimensional NMR experiments without additional polarization transfer elements and evolution periods. The chemical shifts are coded in the line-shape of the cross-peak through an apparent scalar coupling dependent upon the chemical shift. This concept has been applied to the 3D triple-resonance experiment HNCA adding the information of ^{13}C(beta) or $^{13}C'$ chemical shifts[61]. On average, the

proposed TROSY-HNCA(coded)CB experiment is a factor of 2 less sensitive than the HNCA experiment. However, it contains correlations *via* the chemical shifts of both ^{13}C(alpha) and $_{13}$C(beta), and provides up to three times higher resolution along the ^{13}C chemical shift axis. Thus, it dramatically reduces ambiguities in linking the spin systems of adjacent residues in the protein sequence during the sequential assignment. The TROSY-HNCA(coded)CO experiment which is conceptually similar contains correlations *via* the chemical shifts of ^{13}C(alpha) and ^{13}C′ without major sensitivity losses. This concept has also been incorporated into the 3D triple-resonance experiment HNCA, by adding the information of ^{1}H(alpha) chemical shifts, HNCA(coded)HA experiment[62]. Furthermore, Pegan *et al.* have introduced the concept of chemical shift- coding to the TROSY-HNCACB experiment[63]. The monitored ^{1}H(alpha) and ^{1}H(beta) chemical shifts are coded in the line shape of the cross-peaks of ^{13}C(alpha), ^{13}C(beta). The information of four sequential correlation pathways enables a rapid backbone assignment. The TROSY HNCACB(coded)HAHB experiment was applied to ^{13}C,^{15}N-labelled amino-terminal fragment of Vaccinia virus DNA topoisomerase I.

Most methods for determining residual dipolar couplings are based on the measurement of the displacement between cross-peak components in J-coupled spectra. However, for large macromolecules and macromolecular complexes, these methods are often unreliable since differential relaxation can significantly broaden one of the multiplet components and thereby make accurate determination of its position difficult. To overcome this problem, a J-evolved transverse relaxation optimized (JE-TROSY) method has been demonstrated for the determination of one-bond couplings that involves J-evolution of the sharpest cross-peak multiplet component selected in a TROSY experiment[27]. Couplings are measured from the displacement of the TROSY component in the additional J-evolution dimension relative to a zero frequency origin.

A comparison of HSQC and HMQC pulse schemes for recording ^{1}H-^{13}C correlation maps of protonated methyl groups in highly deuterated proteins has been made by Tugarinov *et al.*[64,65]. It was shown that HMQC correlation maps can be as much as a factor of 3 more sensitive than their HSQC counterparts and that the sensitivity gains result from a TROSY effect that involves cancellation of intra-methyl dipolar relaxation interactions. The high quality of HMQC spectra obtained in short measuring times strongly suggests that methyl groups will be useful probes of structure and dynamics in supramolecular complexes. The same group proposed an enhanced sensitivity zero-quantum correlation experiment for recording ^{1}H-^{13}C correlations of methyl groups in highly deuterated, methyl protonated large proteins. The zero-quantum spectra benefit from TROSY-effects in which both intra- and inter-methyl dipolar relaxation interactions are minimized. Significant improvements in resolution relative to corresponding HMQC data sets are observed, with only modest decreases ($\sim 10\%$) in sensitivity[66].

Relaxation in methyl groups is strongly influenced by cross-correlated interactions involving the methyl dipoles. One of the major interference effects results from intra-methyl ^{1}H-^{13}C, ^{1}H-^{1}H dipolar interactions and leads to significant

differences in the relaxation of components that contribute to double- and zero-quantum (DQ and ZQ) spectra. Tugarinov and Kay have developed new NMR experiments for the measurement of this differential relaxation effect. It was shown that this difference in relaxation between DQ and ZQ multiplet components can be used as a sensitive reporter of side chain dynamics and that accurate methyl axis order parameters can be measured in proteins that tumble with long correlation times[67]. Korzhnev *et al.* have presented a new CPMG-based multiple quantum relaxation dispersion experiment for measuring millisecond dynamic processes at side-chain methyl positions in high molecular weight proteins[68]. The experiment benefits from the methyl-TROSY effect and the utility of the methodology was illustrated with application to an 82 kDa enzyme consisting of a single polypeptide chain. In TROSY experiments, relaxation interference effects are exploited to produce spectra with improved resolution and signal-to-noise. Such experiments cannot be explained using the standard product operator formalism, but must instead be analysed at the level of individual density matrix elements. Ollerenshaw *et al.* have illustrated this key point with their recent work on TROSY ^{1}H-^{13}C correlation experiments for methyl groups in large proteins[69].

The difference in the relaxation rates of ZQ and DQ coherences is the result of three principal mechanisms. These include the cross-correlation between the chemical shift anisotropies of the two participating nuclei, dipolar interactions with remote protons as well as interference effects due to the time-modulation of their isotropic chemical shifts as a consequence of slow mus-ms dynamics. The last effect when present, dominates the others resulting in large differences between the relaxation rates of ZQ and DQ coherences. Majumdar and Ghose have presented four TROSY-based experiments that measure this effect for several pairs of backbone nuclei. These experiments allow the detection of slow dynamic processes in the protein backbone including correlated motion over two and three bonds[70]. A suite of TROSY-based NMR relaxation dispersion experiments that measure the decay of DG and ZQ ^{1}H-^{15}N coherences as a function of ^{1}H and ^{15}N radiofrequency have been presented for studying millisecond dynamic processes in proteins[71]. When combined, data from all four coherences provide a more quantitative picture of dynamics, making it possible to distinguish between two-site and more complex exchange processes. Furthermore, a TROSY-based pulse scheme is described for measuring the relaxation of amide ^{1}H single-quantum magnetization, obtained by a simple modification of the multiple-quantum experiments.

Chemical exchange phenomena in NMR spectroscopy of proteins in solution arise from motions on μs to ms time scales that can be critical for ligand binding, catalysis, and allosteric regulation. The use of chemical exchange to study these biological processes usually has been restricted to small proteins with molecular weight < 25 kD. Wang *et al.* have presented novel experiments to measure the relevant relaxation rate constants in large proteins[72]. Kempf *et al.* have presented a solution NMR experiment that quantifies conformational exchange rates to time scales at least an order of magnitude faster than previously possible for large proteins and demonstrate the method on a 53-kDa protein[73].

2.4 NMR-based Screening. – One of the prime merits of NMR as a tool for finding leads in drug discovery research is its sensitivity and robustness for detecting weak protein-ligand interactions. This sensitivity allows one to build up ligands for a given target in a modular way, by a fragment-based approach. A number of review papers published this year have discussed current methodology and technology, as well as illustrated the usefulness of NMR screening with key examples[74-81]. Crystallography, NMR and virtual ligand screening are now common tools in structural approaches to drug discovery. These techniques are highly complementary and synergistic, and their integrated impact on the drug discovery cycle has been be highlighted by Muchmore and Hajduk[82]. There are conceptual differences between high-throughput screening (HTS) and fragment-based screening by NMR. The number of compounds in libraries for NMR screening may be significantly smaller than those used for HTS. As one relies on a small library its design is significantly important and Jacoby have provided an introduction to fragment-based NMR screening[83].

NMR-based ligand screening is now an established field and the recent year has seen a number of new developments in the methodology. Several methods have been described that exploit the benefits of ^{19}F NMR spectroscopy. Dalvit *et al.* have devised a novel and sensitive NMR method for rapid, efficient, and reliable biochemical screening. The method named 3-FABS (three fluorine atoms for biochemical screening) requires the labeling of the substrate with a CF_3 moiety and utilizes ^{19}F NMR for the detection of the starting and enzymatically modified substrates[84,85]. The same group has demonstrated the benefits of using ^{19}F NMR in competition-based approaches[86]. The large chemical shift anisotropy of fluorine and the significant exchange contribution allow for the selection of a weak-affinity spy molecule, thus resulting in a lower binding affinity threshold for identified hits. Tengel *et al.* have presented a simple methodology based on ^{19}F NMR and a library of fluorinated compounds for the screening of ligands that bind to proteins, which also provides qualitative information about relative binding strengths and the presence of multiple binding sites[87]. Using variable contact time ^{19}F cross-polarization magic angle spinning (VCT-CP/MAS) NMR, Boland and Middleton have probed competitive inhibition of a membrane-embedded therapeutic target for peptic ulcer disease[88]. This novel approach to probing ligand binding can be applied to a wide range of membrane-embedded pharmaceutical targets, such as G-protein coupled receptors and ion channels, regardless of the size of the protein or strength of binding.

The reported competition STD NMR method combines saturation transfer difference (STD) NMR with competition binding experiments to allow the detection of high-affinity ligands that undergo slow chemical exchange on the NMR time-scale. With this technique, the presence of a competing, high-affinity ligand in the compound mixture can be detected by the disappearance or reduction of the STD signals of a low-affinity indicator ligand. Wang *et al.* have demonstrated this on a BACE1 (beta-site amyloid precursor protein cleaving enzyme 1) protein-inhibitor system and show that it can also used to derive an approximate value for the dissociation constant of the potential ligand[89].

High-throughput ligand-based proton NMR screening performed in the pres-

ence of spy and control molecules is a valuable tool for identifying drug leads. A limitation of the technique is represented by the severe overlap encountered in the screening of large chemical mixtures. An approach for overcoming this overlap problem is the use of multi-selective, R_1-filtered COSY or TOCSY experiments. The precise measurement of the relative intensity of the two resonances permits determination of the binding constant of the NMR-hit. For a simple competition binding mechanism, the rapidly-derived NMR binding constants are in good agreement with the values derived from full-titration ITC and fluorescence spectroscopy measurements[90]. Bertini *et al.* have described a new method involving the influence of paramagnetic metal ions on NMR spectra for ligand screening[91].

Several reports also describe the application of NMR-based ligand screen to specific targets. These include the application of NMR SHAPES screening to an RNA target[92], STD-NMR monitoring of small molecular binding to human factor Xa[93] and human IgG kappa-Fab[94].

3 Macromolecular Structures

In this section I have chosen not to describe solution structures of free proteins, as such publications have increasingly modest impact. Structures of macromolecular complexes are considerably more informative from a biological perspective and this year has seen further impressive studies.

3.1 Membrane Proteins. – The fact that membrane proteins are notoriously difficult to analyse using standard methods for atomic-resolution structure determination has motivated the development of new methodologies. Liquid-state NMR has recently been used with success for studies of peptides and membrane proteins in detergent micelles, and solid-state NMR has undergone a tremendous evolution towards characterization of membrane proteins in native membrane and oriented phospholipid bilayers. This year, several reviews have described some of the technological challenges behind these efforts and provided examples on their use in membrane biology[95-97].

As an alternative to X-ray crystallography, NMR spectroscopy in solution can be readily used for 3D structure determination of small membrane proteins with beta-barrel folds. Fernandez *et al.* have discussed the recent achievements as well as limitations encountered in such studies[98,99]. The structure of the integral membrane protein OmpX from Escherichia coli reconstituted in 60 kDa DHPC micelles (OmpX/DHPC) was calculated from 526 NOE upper limit distance constraints. The structure determination was based on complete sequence-specific assignments for the amide protons and the Val, Leu, and Ile(delta(1)) methyl groups. The solution structure of OmpX in the DHPC micelles consists of a well-defined, eight-stranded antiparallel beta-barrel, with successive pairs of beta-strands connected by mobile loops. These studies also showed that the central part of the protein is covered with a fluid monolayer of lipid molecules, which seems to mimic faithfully the embedding of the protein in the lipid phase of

the biological membrane. The same group have also showed that 50% of all obtainable NOEs involving the diastereotopic methyl groups of Val and Leu can be obtainable from 3D NOESY spectra of the OmpX, using biosynthetically-directed fractional ^{13}C labelling to obtain stereospecific methyl assignments[100]. Detailed characterization of the mixed detergent/protein micelles is of key importance to validate such studies, and to evaluate how faithfully the natural environment of the protein in the biological membrane is mimicked by the micelle. Hilty *et al.* used a series of paramagnetic probes to characterize these 60 kDa mixed micelles. Highly selective relaxation effects on OmpX and DHPC were observed from nitroxide spin labels attached to lipophilic molecules, which yielded novel insights into the protein-detergent interactions in the mixed micelles[101]. Tafer *et al.* have presented an NMR analysis of the urea-denatured OmpX as a platform for investigations of the folding mechanism of this integral membrane protein[102].

Helical membrane proteins are not readily accessible to TROSY NMR techniques because of the narrow chemical shift dispersion and long inter-helical distances. Lee *et al.* have described three solution NMR experiments on a uniformly ^{15}N- labelled membrane protein in micelles that provide sufficient information to describe the structure, topology, and dynamics of its helices[103]. The backbone amide resonances are assigned with an HMQC-NOESY experiment and the backbone dynamics clearly distinguish between the structured helical residues and mobile residues in the terminal and inter-helical loop regions. The structure and topology of the helices are described by dipolar waves and Polar Index Slant Angle (PISA) wheels derived from experimental measurements of residual dipolar couplings (RDCs) and residual chemical shift anisotropies (RCSAs). The results show that the membrane-bound form of Pf1 coat protein has a 20-residue trans-membrane hydrophobic helix with an orientation that differs by about 90degrees from that of an 8- residue amphipathic helix. This combination of three experiments that yields Dipolar waves and PISA wheels has the potential to contribute to high-throughput structural characterizations of membrane proteins. Oxenoid *et al.* have also reported the NMR assignment for the hometrimeric, helical 40 kDa membrane protein, *E. coli* diacylglycerol kinase (DAGK)[104]. Zamoon *et al.* have described the first structure of recombinant, monomeric, helical phospholamban in lipid-mimicking dodecylphosphocholine micelles by solution NMR experiments. The overall structure is 'L-shaped' with the hydrophobic domain approximately perpendicular to the cytoplasmic portion, which is in agreement with our previously published solid-state NMR data[105]. Dmitriev *et al.* have investigated the structure of the 30 KDa helical subunit of the membrane component of *E. coli* ATP synthase in a mixture of chloroform, methanol and water[106]. Near complete backbone chemical shift assignments were made from a set of TROSY experiments and secondary structure was found to consist of multiple elongated alpha-helical segments. Based on data from similar studies, Faulon *et al.* have devised a computational technique for generating helix-membrane protein folds[107].

Dipolar waves describe the structure and topology of helices in membrane proteins. The fit of sinusoids with the 3.6 residues per turn period of ideal

α-helices to experimental measurements of dipolar couplings as a function of residue number makes it possible to simultaneously identify the residues in the helices, detect kinks or curvature in the helices, and determine the absolute rotations and orientations of helices. Since as much as 80% of the structured residues in a membrane protein can be helical, the analysis of dipolar waves provides a significant step toward structure determination of helical membrane proteins by NMR spectroscopy[108]. Solid-state NMR may have a crucial role in structural investigations of membrane proteins and is well suited for the study of helical systems. Li *et al.* have reported methods for sensitivity improvements in membrane protein solid state NMR experiments[58]. Transmembrane helices are more uniform in structure than similar helices in water soluble proteins. Solid state NMR of aligned bilayer samples is being increasingly used to characterize helical membrane protein structures. Traditional spectroscopic methods have difficulty distinguishing between helices with i to i + 3 (3(10)), i to i + 4 (alpha), and i to i + 5 (pi) hydrogen bonding topology. Kim *et al.* have shown that resonance patterns in PISEMA spectra simulated for these different helices show unique and striking features[109]. The size and shape of these PISA wheels, as well as the resonances per turn and clockwise versus counter-clockwise sequential connectivity demonstrate how these different helical structures can be readily distinguished. Park *et al.* used a combined solution and solid state approach to characterise the 3D structure of the channel-forming trans-membrane domain of virus protein 'u' (Vpu) from HIV-1[110,111]. The analysis of the PISA wheels and dipolar waves obtained from both weakly and completely aligned samples show that Vpu has a trans-membrane alpha-helix spanning residues 8-25 with an average tilt of 13 degrees.

Straus has highlighted the problems encountered with such analyses by investigating the effects of time and spatial averaging on PISEMA spectra of alpha-helical membrane peptides[112]. Three types of motion were considered: (a) Librational motion of the peptide planes in the alpha-helix; (b) rotation of the helix about its long axis; and (c) wobble of the helix about a nominal tilt angle. Computed spectra show that under certain motional modes ^{15}N chemical shift/^{1}H-^{15}N dipolar pairs for each of the residues do not form patterns which mimic helical wheel patterns. As a result, the unambiguous identification of helix tilt and helix rotation without any resonance assignments or on the basis of a single assignment may prove problematic.

Castellani have presented a more general 3D NMR-based approach for the fold determination moderately sized proteins by solid-state magic-angle spinning (MAS)[113]. The methodology includes the measurement of multiple ^{13}C-^{13}C distance restraints on biosynthetically site-directed ^{13}C-enriched samples. 3D ^{15}N-^{13}C-^{13}C dipolar correlation experiments were applied to resolve overlap, in particular in the region where backbone carbon-carbon correlations of the Calpha-Calpha, CO-CO, Calpha-CO, and CO-Calpha type appear. Additional restraints for confining the structure were obtained from phi and psi backbone torsion angles of 29 residues derived from C-alpha, C-beta, CO, NH, and H_α chemical shifts. Using distance and angular restraints, a refined structure was calculated with a backbone RMSD of 0.7 Å with respect to the average structure.

Recent applications of solid state NMR to membrane protein characterisation also include the light-harvesting complex II of Rhodopseudomonas acidophila[114], glycinated mastoparan-X[115], diacylglyerol kinase from E. coli[116], phospholamban[117], Rv2433c from Mycobacterium tuberculosis[118] and the ABC transporter LmrA from Lactococcus lactis[119].

Recent progress to determine structures of small membrane proteins in detergent micelles and lipid bilayers has opened a new window to study, for the first time, the dynamics of membrane proteins. Tamm *et al.* have reported attempts to correlate dynamic measurements on OmpA with the ion channel function of this protein[120]. They have summarised how NMR, spin-label electron paramagnetic resonance spectroscopy and selective mutagenesis can be combined to provide a structural basis towards understanding the mechanism of influenza hemagglutinin-mediated membrane fusion. Saito *et al.* have demonstrated general features of the dynamic aspect of membrane proteins by site-directed ^{13}C NMR studies on model protein bacteriorhodopsin (bR). A dynamics picture of membrane proteins, undergoing local fluctuations from 100 to 100000000 H was revealed and contrasted recent anticipation from crystal structures[121,122]. Soubias *et al.* have analysed the ^{15}N T_2 relaxation times of bacteriorhodopsin (BR) amides in oriented membrane samples and provide an account in terms of helix dynamics, mosaic spread and spectral resolution[123]. Barre and co-workers have probed the surface dynamics of bacteriorhodopsin with the measurement of ^{13}C-^{1}H dipolar couplings in [3-^{13}C]Ala-labelled protein. Motions of slow or intermediate frequency (correlation time <50 mus) scaled the ^{13}C-^{1}H dipolar couplings according to the motional amplitude and typical order parameters for mobile sites[124]. These recent examples have demonstrated that a site-directed NMR study on ^{13}C-labeled membrane proteins can serve as a convenient method to reveal local conformation and dynamics. Saito *et al.* have gone on to clarify the extent to which ^{13}C NMR spectra of ^{13}C-labeled fully hydrated bacteriorhodopsin (bR) are visible and well resolved in the presence of inherent fluctuation motions, especially at the membrane surfaces [125]. Backbone dynamics that escape motional frequencies of the order of 10(4)-10(5) Hz are essential for recording ^{13}C NMR spectra, either in the direction of accelerated fluctuation or slowed motions in the direction of forming a 2D array.

3.2 Protein Complexes. It is generally accepted that protein structures are more conserved than protein sequences, and 3D structure determination by computer simulations have become an important necessity in the postgenomic area. Despite major successes no robust, fast, and automated *ab initio* prediction algorithms for deriving accurate folds of single polypeptide chains or structures of intermolecular complexes exist at present. Dobrodumov and Gronenborn have devised new methodology that uses filtering of structural models generated by the docking of known substructures through easily obtainable experimental NMR constraints[126]. In particular, residual dipolar couplings and chemical shift mapping are most efficient. Heuristic inclusion of chemical or biochemical knowledge about point-to-point interactions is combined with NMR data and commonly used contact potentials. The approach is demonstrated for the deter-

mination of protein-protein complexes using the EIN/HPr complex.

The notion that certain proteins lack intrinsic globular structure under physiological conditions and that the attainment of fully folded structure only occurs upon the binding of target molecules has been recently gaining popularity. Farooq *et al.* have reported the solution structure of the PTB domain of the signaling protein Shc in the free form[127]. Comparison of this structure with that of the complex form, obtained previously with a phosphopeptide ligand, reveals that the Shc PTB domain is structurally disordered in the free form, particularly around the regions constituting the peptide binding pocket. The binding of the ligand appears to reorganize this pocket through local folding events triggering a conformational switch between the free and the complex forms.

LMO2 and LMO4 are members of a small family of nuclear transcriptional regulators that are important for both normal development and disease processes. LMO2 is essential for hemopoiesis and angiogenesis, and inappropriate overexpression of this protein leads to T-cell leukemias. LMO4 is developmentally regulated in the mammary gland and has been implicated in breast oncogenesis. B oth proteins comprise two tandemly repeated LIM domains. LMO2 and LMO4 interact with the ubiquitous nuclear adaptor protein ldb1/NLI/CLIM2, which associates with the LIM domains of LMO and LIM homeodomain proteins *via* its LIM interaction domain (ldb1-LID). Deane *et al.* have described the solution structures of two LMO:ldb1 complexes and showed that ldb1-LID binds to the N-terminal LIM domain (LIM1) of LMO2 and LMO4 in an extended conformation, contributing a third strand to a beta-hairpin in LIM1 domains[128]. A mechanism is proposed in which ldb1 can bind a variety of LIM domains that share low sequence homology.

L27 domain, initially identified in the *Caenorhabditis elegans* Lin-2 and Lin-7 proteins, is a protein interaction module that exists in a large family of scaffold proteins. The domain can function as an organization center of large protein assemblies required for establishment and maintenance of cell polarity. Feng *et al.* have solved the high-resolution NMR structure of a tetrameric complex of L27 domains containing two SAP97-mLin-2 L27 domain heterodimers[129]. Each L27 domain contains three alpha-helices. The first two helices of each domain are packed together to form a four-helical bundle in the heterodimer. The third helix of each L27 domain forms another four-helical bundle that assembles the two heterodimers into a tetramer. The structure of the complex provides a mechanistic explanation for L27 domain mediated polymerization of scaffold proteins, a process that is crucial for the assembly of supramolecular complexes in asymmetric cells.

The C-terminal domain of poly(A)-binding protein (PABC) is a peptide-binding domain found in poly(A)-binding proteins (PABPs) and a HECT (homologous to E6-AP C-terminus) family E3 ubiquitin ligase. In protein synthesis, the PABC domain of PABP functions to recruit several translation factors possessing the PABP-interacting motif 2 (PAM2) to the mRNA poly(A) tail. Kozlov *et al.* have determined the solution structure of the human PABC domain in complex with two peptides from PABP-interacting protein-1 (Paip1) and Paip2[130]. The structures show a novel mode of peptide recognition, in which

the peptide binds as a pair of beta-turns with extensive hydrophobic, electrostatic and aromatic stacking interactions. The results provide insight into the specificity of PABC in mediating PABP – protein interactions.

HP1 family proteins are adaptor molecules, containing two related chromo domains that are required for chromatin packaging and gene silencing. Thiru *et al* have presented the structure of the chromo shadow domain from mouse HP1beta bound to a peptide containing a consensus PXVXL motif found in many HP1 binding partners[131]. The shadow domain exhibits a novel mode of peptide recognition, where the peptide binds across the dimer interface. The structure allows the prediction of which other shadow domains bind similar PXVXL motif-containing peptides and provides a framework for understanding their sequence specificity. The authors have also shown that targeting of HP1b to heterochromatin requires shadow domain interactions with PXVXL-containing proteins in addition to chromo domain recognition of Lys-9- methylated histone H3. This finding implies a further complexity to the histone code for regulation of chromatin structure and suggests how binding of HP1 family proteins may lead to its condensation.

The spindle checkpoint delays chromosome segregation in response to misaligned sister chromatids during mitosis, thus ensuring the fidelity of chromosome inheritance. Through binding to Cdc20, the Mad2 spindle checkpoint protein inhibits the target of this checkpoint, the ubiquitin protein ligase APC/C-Cdc20. Luo *et al.* have now shown that without cofactor binding or covalent modification Mad2 adopts two distinct folded conformations at equilibrium (termed N1-Mad2 and N2-Mad2). The structure of N2-Mad2 has been determined by NMR spectroscopy and was shown to be much more potent in APC/C inhibition[132]. Overexpression of a Mad2 mutant that specifically sequesters N2-Mad2 partially blocks checkpoint signaling in living cells. The two Mad2 conformers interconvert slowly *in vitro*, but interconversion is accelerated by a fragment of Mad1, an upstream regulator of Mad2. These results suggested that the unusual two-state behavior of Mad2 is critical for spindle checkpoint signaling.

Ubiquitin (Ub) functions in many different biological pathways, where it typically interacts with proteins that contain modular Ub recognition domains. Monoubiquitylation is a well-characterized signal for the internalization and sorting of integral membrane proteins to distinct cellular organelles. Recognition and transmission of monoubiquitin signals is mediated by a variety of Ub-binding motifs such as NZF, UIM, UBA, UEV, VHS and CUE. The Npl4 zinc finger (NZF) is a compact zinc-binding module found in many proteins that function in Ub-dependent processes. Alam *et al.* recently reported the solution structure of the NZF domain from Npl4 in complex with Ub[133]. The structure revealed that three key NZF residues (13TF14/M-25) surrounding the zinc coordination site bind the hydrophobic 'Ile44' surface of Ub. NZF mutations that inhibit Ub binding by the NZF domain of Vps36/ESCRT-II also inhibit sorting of ubiquitylated proteins into the yeast vacuole. Thus, the NZF is a versatile protein recognition domain that is used to bind ubiquitylated proteins during vacuolar protein sorting, and probably many other biological processes.

Yeast Vps27 protein requires two UIMs for efficient interactions with Ub and for sorting cargo into multivesicular bodies. Swanson *et al.* have shown that the individual UIMs of Vps27 exist as autonomously folded alpha-helices that bind Ub independently, non-cooperatively and with modest affinity[134]. The Vps27 N-terminal UIM engages the Leu8-Ile44-Val70 hydrophobic patch of Ub through a helical surface conserved in UIMs of diverse proteins. The Leu8-Ile44-Val70 Ub surface is also the site of interaction for CUE and UBA domains in endocytic proteins, consistent with the view that Ub-binding endocytic proteins act serially on the same monoubiquitylated cargo during transport from cell surface to the lysosome. Walters *et al.* have used NMR spectroscopy to show that hHR23a, from the Rad23 family of proteins that stimulates nucleotide excision repair, contains an N-terminal Ub-like domain (UBL) that interacts with two internal Ub-associated domains (UBA)[135]. Interestingly, binding of the proteasomal subunit S5a disrupts the hHR23a interdomain interactions and thereby causes it to adopt an opened conformation. Mueller and Feigon have also presented the solution structures of the hHR23A UBL domain, the second UIM of S5a (UIM-2), and the Ubl:S5a-UIM-2 complex[136].

Covalent posttranslational modification of target proteins with Ub and Ub-like proteins regulates many important cellular processes. However, the molecular mechanisms by which these proteins are activated and conjugated to substrates have yet to be fully understood. NMR studies have shown that the Ub-like proteins SUMO-1, -2, and -3 interact with the same N-terminal region of the E2 conjugating enzyme Ubc9 with similar affinities[137]. The conservation of E2 enzymes across the Ub and Ub-like protein pathways indicates that analogous N-terminal sites of E2 enzymes are likely to have similar roles in general. Using NMR, Yoshinaga *et al.* have classified the PC motif-containing region (PCCR) and PB1 (Phox and Bem 1) domain as Ub folds and based on the structural information, the PB1 domains and PCCRs are grouped into a novel family, named the PB1 family[138]. Atypical protein kinase C (aPKC) has been implicated in several signaling pathways and possesses the PB1 domain in its N terminus. The aPKC PB1 domain binds ZIP/p62, Par6, or MEK5 through a PB1-PB1 domain interaction that controls the localization of aPKC. Hirano *et al.* have determined the structure of the PB1 domain by NMR and confirmed that the PB1 domain adopts a Ub fold[139]. Their structural data suggests that the acidic surface of the PKCiota PB1 domain interacts with the basic surface of the target PB1 domains.

The protein CNOT4 possesses an N-terminal RING finger domain that acts as an E3 Ub ligase and specifically interacts with UbcH5B, a Ub-conjugating enzyme. The structure of the CNOT4 RING domain has been solved and the amino acids important for the binding to UbcH5B have been mapped. Residues of UbcH5B important for the binding to CNOT4 RING domain were identified by NMR chemical shift perturbation experiments, and were used to generate structural models of the complex with the program HADDOCK that give structural insights into the E2/E3 specificity[140].

PDZ domains are modular protein interaction domains that bind in a sequence-specific fashion to short peptides and are associated with other protein-

binding motifs in multidomain scaffold proteins. PDZ-containing proteins are typically involved in the assembly of supramolecular complexes that perform localized signaling functions at particular subcellular locations. The cytoplasmic protein Dishevelled (Dvl) and the associated membrane-bound receptor Frizzled (Fz) are essential in canonical and noncanonical Wnt signaling pathways. However, the molecular mechanisms underlying this signaling are not well understood. Wong *et al.* have determined that an internal sequence of Fz binds to the conventional peptide binding site in the PDZ domain of Dvl; this type of site typically binds to C-terminal binding motifs[141]. The C-terminal region of the Dvl inhibitor Dapper (Dpr) and Frodo bound to the same site. In *Xenopus*, Dvl binding peptides of Fz and Dpr/Frodo inhibited canonical Wnt signaling and blocked Wnt-induced secondary axis formation in a dose-dependent manner, but did not block noncanonical Wnt signaling mediated by the DEP domain. These results identified a missing molecular connection within the Wnt pathway. Differences in the binding affinity of the Dvl PDZ domain and its binding partners may be important in regulating signal transduction by Dvl. Feng *et al.* have solved the solution structures of the PDZ45 tandem and the isolated PDZ4 of glutamate receptor interacting protein (GRIP). The two PDZ domains form a compact structure with a fixed interdomain orientation [142]. The interaction of the glutamate receptor subunits 2 and 3 (GluR2/3) with GRIP is important for the synaptic trafficking and clustering of the receptors. Binding of GluR2/3 to GRIP requires both the fourth and fifth PDZ domains (PDZ4 and PDZ5) to be covalently linked, although only one PDZ domain is directly involved in binding to the receptor tail. Interestingly, PDZ4 contains a deformed alphaB-betaB groove that is unlikely to bind to carboxyl peptides. Instead, the domain stabilizes the structure of PDZ5. Au and co-workers have determined the structure of Z band alternately spliced PDZ-containing protein (ZASP) PDZ by NMR and showed that it is a classical class 1 PDZ domain that recognizes the carboxy-terminal sequence of α-actinin-2 calmodulin-like domain[143]. ZASP is a sarcomere Z disk protein expressed in human cardiac and skeletal muscle that is thought to be involved in a dominant familial dilated cardiomyopathy. The alpha-actinin-2/ZASP PDZ interaction involves a binding surface distinct from that recognized by the titin Z repeats.

Classical cadherins mediate cell-cell adhesion through calcium-dependent homophilic interactions and are activated through cleavage of a prosequence in the late Golgi. The first 3D structure of a classical cadherin prosequence was solved by NMR. The prototypic prosequence of N-cadherin consists of an Ig-like domain and an unstructured C-terminal region[144]. The folded part of the prosequence-termed prodomain-has a striking structural resemblance to cadherin 'adhesive' domains that could not have been predicted from the amino acid sequence. The detailed structural and evolutionary analysis revealed that prodomains are distant relatives of cadherin 'adhesive' domains and lack all the features known to be important for cadherin- cadherin interactions. The presence of an additional 'nonadhesive' domain seems to make it impossible to engage homophilic interactions between cadherins that are necessary to activate adhesion, thus explaining the inactive state of prodomain-bearing cadherins.

Cellular adhesion by classical cadherins depends critically on the exact proteolytic removal of their N-terminal prosequences. In a combined solution NMR and X-ray study, the consequences of propeptide cleavage of an epithelial cadherin construct (domains 1 and 2) were followed at atomic level[145]. At low protein concentration, the N-terminal processing induced docking of the tryptophan-2 side-chain into a binding pocket on the same molecule. At high concentration, cleavage induces dimerisation and concomitant intermolecular exchange of the beta A-strands and the tryptophan-2 side-chains. Thus, the cleavage represents the switch from a nonadhesive to the functional form of cadherin.

Adhesive interactions involving CD44, the cell surface receptor for hyaluronan, underlie fundamental processes such as inflammatory leukocyte homing and tumor metastasis. Regulation of such events is critical and appears to be effected by changes in CD44 N-glycosylation that switch the receptor on or off under appropriate circumstances. How altered glycosylation influences binding of hyaluronan to the lectin- like Link module in CD44 is unclear, although evidence suggests additional flanking sequences peculiar to CD44 may be involved. Teriete *et al.* have shown using X-ray crystallography and NMR spectroscopy that these sequences form a lobular extension to the Link module, creating an enlarged HA binding domain and a formerly unidentified protein fold[146]. Moreover, the disposition of key N- glycosylation sites reveals how specific sugar chains could alter both the affinity and avidity of CD44 HA binding.

3.3 Nucleic Acid Complexes. – The low density of tradition NMR restraints make oligonucleotide structures particularly problemsome. Chao and Williamson have highlighted an erroneous NMR structure in which a single imino proton resonance in an internal loop was incorrectly assigned[147]. L30e, a Saccharomyces cervisiae ribosomal protein, regulates its own expression by binding to a purine-rich asymmetric internal loop located in both its prem-RNA and mature mRNA. A crystal structure of an MBP-L30e fusion protein in complex with an RNA containing the pre-mRNA regulatory site was solved at 3.24 Angstrom. A further structural refinement was performed using both the X-ray diffraction data and corrected NMR-derived distance and angle restraints. The joint NMR and X-ray refinement resulted in improved stereochemistry and lower crystallographic R factors. The RNA internal loop of the MBP-L30e-mRNA complex adopts the canonical K-turn fold. Williams *et al.* have proposed novel procedures based on orientational restraints from dipolar couplings and conjoined rigid body/torsion angle dynamics for the determination of protein-oligonucleotide complexes[148]. Using this methodology, the authors present the solution NMR structure of the ternary 42 kDa Oct1.Sox2.Hoxb1.DNA complex which comprises the Oct and Sox transcription factors that control aspects of neural development and embryogenesis.

Recent reports of protein-olidonuecleotide complexes structures are dominated by protein-RNA interactions and the following section reflects this. Specific recognition of double-stranded RNA (dsRNA) by dsRNA-binding do-

mains (dsRBDs) is involved in a large number of biological and regulatory processes. Although structures of dsRBDs in complex with dsRNA have revealed how they can bind to dsRNA in general, these do not explain how a dsRBD can recognize specific RNAs. Rnt1p, a member of the RNase III family of dsRNA endonucleases, is a key component of the *Saccharomyces cerevisiae* RNA-processing machinery. The Rnt1p dsRBD has been implicated in targeting this endonuclease to its RNA substrates, by recognizing hairpins closed by AGNN tetraloops. Wu *et al.* have elucidated the solution structure of Rnt1p dsRBD complexed to the 5′ terminal hairpin of one of its small nucleolar RNA substrates, the snR47 precursor[149]. The conserved AGNN tetraloop fold is retained in the protein-RNA complex. The dsRBD contacts the RNA at successive minor, major, and tetraloop minor grooves on one face of the helix. Surprisingly, neither the universally conserved G nor the highly conserved A are recognized by specific hydrogen bonds to the bases. Rather, the N-terminal helix fits snugly into the minor groove of the RNA tetraloop and top of the stem, interacting in a non- sequence-specific manner with the sugar-phosphate backbone and the two nonconserved tetraloop bases. These results showed how a single dsRBD can convey specificity for particular RNA targets, by structure specific recognition of a conserved tetraloop fold.

RNA interference is a conserved mechanism that regulates gene expression in response to the presence of dsRNAs. The RNase III-like enzyme Dicer first cleaves dsRNA into 21-23-nucleotide small interfering RNAs (siR-NAs). In the effector step, the multimeric RNA-induced silencing complex (RISC) identifies messenger RNAs homologous to the siRNAs and promotes their degradation. The Argonaute 2 protein (Ago2) is a critical component of RISC. Both Argonaute and Dicer family proteins contain a common PAZ domain whose function is unknown. Lingel *et al.* have presented the 3D NMR structure of the Drosophila melanogaster Ago2 PAZ domain[150]. This domain adopts a nucleic-acid-binding fold that is stabilized by conserved hydrophobic residues. The nucleic-acid-binding patch is located in a cleft between the surface of a central beta-barrel and a conserved module comprising strands beta3, beta4 and helix alpha3. Because critical structural residues and the binding surface are conserved, it was suggested that PAZ domains in all members of the Argonaute and Dicer families adopt a similar nucleicacid binding fold that plays an important part in gene silencing.

In HIV type 1 (HIV-1), the dimerization initiation site (DIS) is primarily responsible for initiating the noncovalent linkage of two homologous strands of genomic RNA during viral assembly. The DIS loop contains an autocomplementary hexanucleotide sequence and forms a symmetric homodimer through a loop-loop kissing interaction. In a structural rearrangement catalysed by the HIV-1 nucleocapsid protein (NCp7) and suggested to be associated with maturation of the budded viral particle, the DIS converts from a metastable kissing dinner to an extended duplex. Mihailescu and Marino have demonstrated using NMR that the DIS kissing dimer displays localized conformational dynamics that result from the specific protonation of the N1 base nitrogen of the DIS loop residue A272 at near-physiological pH[151]. These results revealed a previously

unidentified role for base protonation in modulating local RNA structure.

The La protein is a conserved component of eukaryotic ribonucleoprotein complexes that binds the 3 poly(U)-rich elements of nascent RNA polymerase III (pol III) transcripts to assist folding and maturation. Alfano *et al.* have determined the solution structure of N-terminal domain from La show that the La motif adopts an alpha/beta fold that comprises a winged-helix motif elaborated by the insertion of three helices. Chemical shift mapping experiments show that these insertions are involved in RNA interactions[152].

Ramos *et al.* have investigated the role in the fold and RNA-binding properties of the KH modules of a hydrophobic to asparagine mutation of clinical importance in the fragile X syndrome. A detailed comparison of Nova KH3 structure with its RNA/KH complex and with other KH structures suggests a dual role for the alpha2(3) residue, which is involved both in stabilizing the hydrophobic core and in RNA contacts. NMR studies also showed that L447 of Nova-1 in position alpha2(3) is in exchange in the absence of RNA, and becomes locked in a more rigid conformation only upon formation of an RNA complex. This implies that position alpha2(3) functions as a 'gate' in the mechanism of RNA recognition of KH motifs based on the rigidification of the fold upon RNA binding[153].

Cilley and Williamson have determined the solution structure of a 22-amino-acid peptide from the amino-terminal domain of the bacteriophage phi21 N protein in complex with its cognate 24-mer boxB RNA hairpin using NMR[154]. The N peptide binds as an alpha-helix and interacts predominately with the major groove side of the 5′ half of the boxB RNA stem- loop. The exposed face of the phi21 boxB loop, in complex with the N peptide, is strikingly similar to the GNRA tetraloop-like folds of the related lambda and P22 bacteriophage N peptide-boxB RNA complexes. The N peptide-boxB complexes of the various phages, while individually distinct, provide similar structural features for interactions with the *E. coli* host factors to enable antitermination.

A notable publication describing an NMR structure of a protein-DNA complex includes the solution structure of the Cdc13 DNA-binding domain (DBD) complexed with a cognate telomeric ssDNA [155]. Essential budding yeast telomere-binding protein Cdc13 is required for telomere replication and end protection and binds telomeric, single-stranded DNA (ssDNA) 3′ overhangs with high affinity. Analysis of the Cdc13-DBD/ssDNA complex indicated that molecular recognition of extended single-stranded nucleic acids may proceed *via* a folding-type mechanism rather than resulting from specific patterns of hydrogen bonds. The structure provided a foundation for understanding the mechanism by which Cdc13 recognizes GT-rich heterogeneous sequences with both unusually strong affinity and high specificity. NMR chemical shift titration is commonly exploited in characterizing protein-oligonucleotide complexes and two recent studies demonstrate the usefulness of this approach in the absence of a complete structure. Laguri *et al.* have described the structure and NMR titrations of PrrAC with specific and non-specific DNA to show which surfaces are involved in DNA binding[156]. A plausible model of the PrrAC/DNA complex was constructed in which two PrrAC molecules are bound to DNA in a symmetrical manner. Van Melckebeke *et al.* have presented the first solution structure of the

82 amino acid residue DNA-binding domain of *Bacillus licheniformis*, BlaI, a repressors that regulates beta-Lactamase expression[157]. Chemical shift mapping identified residues involved in DNA interaction and a WHP canonical model of interaction with the operators was proposed.

4 Protein Folding

NMR plays a central role in the structural study of unfolded and partially folded states of proteins, as well providing kinetic information. Although our knowledge of basic folded structures of proteins has dramatically improved, the extent of our corresponding knowledge of higher-energy conformers remains extremely slim. The latter information is crucial for advancing the understanding of protein folding and conformational diseases. Akasaka has presented a new experimental strategy using pressure perturbation in conjunction with multidimensional NMR spectroscopy for the study of high energy conformation[158]. They were able to characterise a number of rare conformers at high pressure for the Ras-binding domain of RalGDS, beta-lactoglobulin, dihydrofolate reductase, Ub, apomyoglobin, p13(MTCP1) and prion. Korzhnev *et al.* have describe the use of relaxation dispersion NMR spectroscopy to identify a low-population folding for two mutational variants of the SH3 domain from Fyn tyrosine kinase[159]. By performing the NMR experiments at different temperatures, this approach has enabled characterization of the kinetics and energetics of the folding process as well as providing structures of the intermediates. Di Nardo *et al.* have also used an NMR spin relaxation dispersion technique to study the folding rates of several destabilising mutants of the Src homology 3 domain[160]. They demonstrated that residues that are most stabilizing in the transition-state structure are most destabilizing in the native state, and also cause the greatest reductions *in vitro* functional activity

The rate of stabilisation of side chains during protein folding has not been carefully studied. Recent developments in labelling proteins with ^{19}F-labeled amino acids coupled with real-time NMR measurements have allowed such measurements to be made. Frieden has devised a method to the study of protein folding using 6-^{19}F-tryptophan as the reporting group[161]. It was found that these side chains adopt their final stable state at the last stages of the folding process and that the stabilization of side chains into their final conformation is a highly cooperative process. Also, Mok *et al.* have developed a novel rapid sample-mixing technique for real-time NMR spectroscopy. The apparatus consists of an insert inside a conventional NMR tube coupled to a rapid injection syringe outside the NMR magnet. Efficient and homogeneous mixing of solutions in the NMR tube is achieved with a dead time of tens of milliseconds, without modification of the NMR probe or additional hardware inside the magnet[162].

To search for folding intermediates, Khan *et al.* have examined the folding and unfolding kinetics of wild-type barnase and four mutants[163]. These data combined with direct structural observations and simulation support a minimal reaction pathway for the folding of barnase that involves two detectable folding

intermediates. The first intermediate, I-1, is the denatured state under physiological conditions, D-Phys, which has native-like topology, is lower in energy than the random-flight denatured state U and is suggested by molecular dynamics simulation of unfolding to be on-pathway. The second intermediate, I-2, is high energy, and is proven by the change in rate determining step in the unfolding kinetics to be on-pathway. Vu *et al.* have suggested that barnase folds through partially unfolded intermediates that exist after the rate-limiting step[164].

The ability of proteins to fold to well defined compact structures is one of the most remarkable examples of natural selection on biological molecules. To understand their properties, including the stability, the mechanism of folding, and the possibilities of misfolding and association, it is necessary to know the protein free energy landscape. *Vendruscolo et al.* have used NMR data as restraints in a Monte Carlo sampling procedure to determine the ensemble of structures populated by human alpha-lactalbumin in the presence of increasing concentrations of urea[165]. The ensembles of structures that represent the partially folded states of the protein show that two structural cores, corresponding to alpha and beta domains of the native protein, are preserved even when the native-like interactions that define their existence are substantially weakened. The form of the energy landscape, together with the existence of distinct cores, supports the concept that robustness and modularity are the properties that make the folding of complex proteins possible. The denatured state of a protein contains important information about the determinants of the folding process. By combining site-directed spin-labeling NMR experiments and restrained computer simulations, Lindorff-Larsen *et al.* have determined ensembles of conformations that represent the denatured state of the bovine acyl-coenzyme A binding protein (ACBP)[166]. As the experimentally-determined distance information corresponds to weighted averages over a broad ensemble of structures, the experimental restraints were applied to a system of noninteracting protein replicas using a Monte Carlo sampling scheme. This procedure permits the sampling of ensembles that are compatible with the experimental data and thus to obtain information regarding the distribution of structures in the denatured state. The preferential formation of contacts suggests that the sequence-dependent patterns of helical propensity and hydrophobicity are important determinants of the structure in the denatured state of ACBP[166]. Ripoll *et al.* have investigated structure of the 36 residue villin headpiece subdomain with the electrostatically driven Monte Carlo method[167]. The results of this study provide a basis to understand the effect of the interactions, such as hydrophobicity, charge-charge interaction and solvent polarization, on protein stability.

The characterisation of early folding intermediates is key to understanding the protein folding process. Structures of intermediates and transition states in protein folding are usually characterized by amide hydrogen exchange and protein engineering methods and interpreted on the basis of the assumption that they have native-like conformations. Amide exchange data on the N-domain of phosphoglycerate kinase (PGK) from *Bacillus stearothermophilus* combined with a kinetic model implied the rapid formation of an intermediate with extensive

native-like hydrogen bonding. Reed *et al.* have supplemented this with data for the intact PGK molecule and revealed that the entire N-domain acts concertedly in the formation of the kinetic refolding intermediate rather than there existing a distinct local folding nucleus[168]. Brorsson *et al.* have analysed the folding energy landscape of the 72 amino acid protein MerP by monitoring native state hydrogen exchange as a function of temperature[169]. Analysis at the individual amino acid level showed that exchange is allowed from an ensemble of partially unfolded structures (*i.e.* intermediates) in which the stabilities at the amino acid level form a broad distribution throughout the protein. Feng were able to stabilize and determine the NMR structure of a partially unfolded intermediate that exists after the rate-limiting step of a four-helix bundle protein, Rd-apocyt b(562). The intermediate has partial native-like secondary structure and backbone topology, consistent with amide exchange data. However, non-native hydrophobic interactions exist throughout the structure[170].

Molten globules are partially folded forms of proteins thought to be general intermediates in protein folding. Human alpha-lactalbumin readily forms a molten globule and is thus widely used to study their structural aspects. Quezada *et al.* have used NMR spectroscopy to follow the urea-induced unfolding of the low pH molten globule states of human alpha-lactalbumin variants. The results reveal that different permutations of three of the four major alpha-helices can form a stable, locally cooperative, compact structural core. Their findings demonstrate that the molten globule state of human alpha-lactalbumin is an ensemble of conformations, with different subsets of structures linked by a range of long-range interactions[171]. Ramboarina and Redfield have found that an increase in temperature leads to a dramatic sharpening of peaks in the NMR spectrum of human alpha-lactalbumin. Analysis of NMR chemical shifts of the human alpha-lactalbumin molten globule under these conditions leads to the identification of regions of native-like helix in the alpha-domain and of non-native helical propensity in the beta-domain[172].

The unfolding and refolding of a monomeric mutant of copper-zinc superoxide dismutase has been investigated by NMR spectroscopy in the copper-reduced form by Assfalg *et al.*[173]. It is found that the protein gives rise to a series of intermediates at low guanidinium concentration and to a globular unfolded state at a guanidinium concentration higher than 3.5 M. The transition into the unfolded structure implies the detachment of the metal ions from the native coordination sites, even if non-specific interactions with the metal ions remain. Relaxation experiments provided information on the mobility at the various stages showing how protein rigidity is lost during unfolding. This work demonstrates the importance of metal ions with respect to the unfolding process and protein structure stability. Jimenez *et al.* have evaluated the early steps of unfolding of P43M Calbindin D-9k using the native dicalcium and the paramagnetic monocerium-substituted derivative[174]. The substitution of the calcium ion with the paramagnetic Ce^{3+} ion enabled a number of long-range nonconventional constraints to be obtained, namely, pseudocontact shifts and used to monitor subtle structural variations occurring in the non-native state of the protein. Although the average RMSD between the structures of native and

non-native states is small (0.48 Å), structural rearrangements could be reliably identified.

Many proteins are capable of populating partially folded states under specific solution conditions and, occasionally, coexistence of the folded and an unfolded state can be observed by NMR. Ding *et al.* have reported amide residual dipolar couplings (RDCs), nitrogen transverse relaxation rates for varying pH values and different temperatures on the destabilized mutant of the B1 domain of protein G (GB1). The RDCs for the low pH, thermally unfolded state of GB1 are very small and do not indicate the presence of any native-like structure. Their data provided clear evidence for intermediate conformations and multi-state equilibrium unfolding for this GB1 variant[175].

Protein folding starts from the elusive form of the denatured state that is present under conditions that favour the native state. Mayor *et al.* have studied the denatured state of Engrailed Homeodomain (En-HD) under mildly and strongly denaturing conditions by NMR[176]. The denatured state had extensive native secondary structure and was significantly compact and globular, but the side-chains and backbone were highly mobile. Non-cooperative melting of the residual structure on the denatured state of En-HD was observed, both at the residue and the molecular level, with increasingly denaturing conditions. The starting point for folding under native conditions is highly structured and already poised to adopt the native structure.

In conjunction with other NMR experiments, RDCs can provide valuable insights into the dynamic conformational propensities of unfolded and partly folded states of proteins and thereby help to chart the upper reaches of the folding landscape. Mohana-Borges *et al.* have investigated the conformational propensities of unfolded states for apomyoglobin by measuring RDCs[177]. Results were interpreted on the basis of the statistical properties of the unfolded polypeptide chain, viewed as a polymer of statistical segments. For a folded protein, the magnitude and sign of the RDCs depend on the orientation of each bond vector relative to the alignment tensor of the entire molecule, which reorients as a single entity. For unfolded proteins, there is no global alignment tensor; instead, RDCs are attributed to alignment of the statistical segments or of transient elements of secondary structure. For apomyoglobin in 8 M urea, the backbone is highly extended and local regions of enhanced flexibility are characterized by a decrease in the magnitude of the RDCs. The formation of a small population of helical structure in the acid-denatured state of apomyoglobin leads to a change in sign of the RDCs in local regions of the polypeptide. Moreover, Fieber *et al.* have shown that RDCs in the denatured state of bovine acylcoenzyme A binding protein (ACBP) oriented in strained polyacrylamide gels are a sensitive, sequence-specific probe for residual secondary structure[178]. The data demonstrated alpha-helix propensity in four isolated stretches along the protein backbone provided direct evidence for the existence of native-like hydrophobic interactions in the acid-denatured state

Oxidative folding is the fusion of native disulfide bond formation with conformational folding. This complex process is guided by two types of interactions: first, covalent interactions between cysteine residues, which transform into na-

tive disulfide bridges, and second, non-covalent interactions giving rise to secondary and tertiary protein structure. Cemazar *et al.* have used time-resolved NMR and photochemically induced dynamic nuclear polarization spectroscopies to follow the oxidative folding at the level of amino acid residue conformation[179]. Confinement of a protein in a small inert space and microviscosity are known to increase its thermodynamic stability in a way similar to the mechanisms that stabilize protein fold in the cell. Bolis *et al.* have examined the influence of confinement on protein stability and confirm that proteins are stabilized when confined in the gel[180]. This method could therefore be used as a novel and powerful approach for protein folding studies.

References

1. Slupsky, C. M., Boyko, R. F., Booth, V. K. & Sykes, B. D. *Journal of Biomolecular NMR* 2003 **27**, 313-321.
2. Malmodin, D., Papavoine, C. H. M. & Billeter, M. *Journal of Biomolecular NMR* 2003 **27**, 69-79.
3. Coggins, B. E. & Zhou, P. *Journal of Biomolecular NMR* 2003 **26**, 93-111.
4. Kirby, N. I., DeRose, E. F., London, R. E. & Mueller, G. A. *Bioinformatics* 2004 **20**, 1201-1203.
5. Hyberts, S. G. & Wagner, G. *Journal of Biomolecular NMR* 2003 **26**, 335-344.
6. Moseleya, H. N. B., Sahota, G. & Montelione, G. T. *Journal of Biomolecular NMR* 2004 **28**, 341-355.
7. Shi, J. X., Pelton, J. G., Cho, H. S. & Wemmer, D. E. *Journal of Biomolecular NMR* 2004 **28**, 235-247.
8. Langmead, C. J. & Donald, B. R. *Journal of Biomolecular NMR* 2004 **29**, 111-138.
9. Xia, Y. L., Zhu, G., Veeraraghavan, S. & Gao, X. L. *Journal of Biomolecular NMR* 2004 **29**, 467-476.
10. Kim, S. & Szyperski, T. *Journal of Biomolecular NMR* 2004 **28**, 117-130.
11. Atreya, H. S. & Szyperski, T. Proceedings of the National Academy of Sciences of the United States of America 2004 **101**, 9642-9647.
12. Grishaev, A. & Llinas, M. *Journal of Biomolecular NMR* 2004 **28**, 1-10.
13. Gronwald, W. & Kalbitzer, H. R. *Progress in Nuclear Magnetic Resonance Spectroscopy* 2004 **44**, 33-96.
14. Guntert, P. Progress in Nuclear Magnetic Resonance Spectroscopy 2003 **43**, 105-125.
15. Jung, Y. S., Sharma, M. & Zweckstetter, M. *Angewandte Chemie-International Edition* 2004 **43**, 3479-3481.
16. Nabuurs, S. B., Spronk, C., Vriend, G. & Vuister, G. W. *Concepts in Magnetic Resonance Part A* 2004 **22A**, 90-105.
17. Kuszewski, J., Schwieters, C. D., Garrett, D. S., Byrd, R. A., Tjandra, N. & Clore, G. M. *Journal of the American Chemical Society* 2004 **126**, 6258-6273.
18. Meiler, J. & Baker, D. Proceedings of the National Academy of Sciences of the United States of America 2003 **100**, 15404-15409.
19. Cole, R. & Loria, J. P. *Journal of Biomolecular NMR* 2003 **26**, 203-213.
20. Lipsitz, R. S. & Tjandra, N. Annual Review of Biophysics and Biomolecular Structure 2004 **33**, 387-413.
21. Kramer, F., Deshmukh, M. V., Kessler, H. & Glaser, S. J. *Concepts in Magnetic*

Resonance Part A 2004 **21A**, 10-21.
22. Zweckstetter, M. *Journal of Biomolecular NMR* 2003 **27**, 41-56.
23. Chen, Z. J. & Reif, B. *Journal of Biomolecular NMR* 2004 **29**, 525-530.
24. Fushman, D., Varadan, R., Assfalg, M. & Walker, O. *Progress in Nuclear Magnetic Resonance Spectroscopy* 2004 **44**, 189-214.
25. Ding, K. Y. & Gronenborn, A. M. *Journal of Magnetic Resonance* 2003 **163**, 208-214.
26. Ding, K. & Gronenborn, A. M. *Journal of Magnetic Resonance* 2004 **167**, 253-258.
27. Luy, B. & Marino, J. P. *Journal of Magnetic Resonance* 2003 **163**, 92-98.
28. Feher, K., Berger, S. & Kover, K. E. *Journal of Magnetic Resonance* 2003 **163**, 340-346.
29. Permi, P. *Journal of Biomolecular NMR* 2003 **27**, 341-349.
30. Vogeli, B., Kovacs, H. & Pervushin, K. *Journal of the American Chemical Society* 2004 **126**, 2414-2420.
31. Eletsky, A., Moreira, O., Kovacs, H. & Pervushin, K. *Journal of Biomolecular NMR* 2003 **26**, 167-179.
32. Valafar, H. & Prestegard, J. H. *Journal of Magnetic Resonance* 2004 **167**, 228-241.
33. Zidek, L., Padrta, P., Chmelik, J. & Sklenar, V. *Journal of Magnetic Resonance* 2003 **162**, 385-395.
34. Haliloglu, T., Kolinski, A. & Skolnick, J. *Biopolymers* 2003 **70**, 548-562.
35. Valafar, H. & Prestegard, J. H. *Bioinformatics* 2003 **19**, 1549-1555.
36. Mascioni, A. & Veglia, G. *Journal of the American Chemical Society* 2003 **125**, 12520-12526.
37. Walsh, J. D., Cabello-Villegas, J. & Wang, Y. X. *Journal of the American Chemical Society* 2004 **126**, 1938-1939.
38. Zweckstetter, M., Hummer, G. & Bax, A. *Biophysical Journal* 2004 **86**, 3444-3460.
39. Ferrarini, A. *Journal of Physical Chemistry B* 2003 **107**, 7923-7931.
40. Louhivuori, M., Paakkonen, K., Fredriksson, K., Permi, P., Lounila, J. & Annila, A. *Journal of the American Chemical Society* 2003 **125**, 15647-15650.
41. Bryce, D. L. & Bax, A. *Journal of Biomolecular NMR* 2004 **28**, 273-287.
42. Bryce, D. L. & Bax, A. *Journal of Biomolecular NMR* 2004 **29**, 219-219.
43. Wang, L. C. & Donald, B. R. *Journal of Biomolecular NMR* 2004 **29**, 223-242.
44. Briggman, K. B. & Tolman, J. R. *Journal of the American Chemical Society* 2003 **125**, 10164-10165.
45. Bernado, P. & Blackledge, M. *Journal of the American Chemical Society* 2004 **126**, 4907-4920.
46. Zhang, Q., Throolin, R., Pitt, S. W., Serganov, A. & Al-Hashimi, H. M. *Journal of the American Chemical Society* 2003 **125**, 10530-10531.
47. Ulmer, T. S., Ramirez, B. E., Delaglio, F. & Bax, A. *Journal of the American Chemical Society* 2003 **125**, 9179-9191.
48. Jensen, P. R., Axelsen, J. B., Lerche, M. H. & Poulsen, F. M. *Journal of Biomolecular NMR* 2004 **28**, 31-41.
49. Lancelot, N., Elbayed, K., Bianco, A. & Piotto, M. *Journal of Biomolecular NMR* 2004 **29**, 259-269.
50. Kurita, J., Shimahara, H., Utsunomiya-Tate, N. & Tate, S. *Journal of Magnetic Resonance* 2003 **163**, 163-173.
51. Ikegami, T., Verdier, L., Sakhaii, P., Grimme, S., Pescatore, B., Saxena, K., Fiebig, K. M. & Griesinger, C. *Journal of Biomolecular NMR* 2004 **29**, 339-349.
52. Fernandez, C. & Wider, G. *Current Opinion in Structural Biology* 2003 **13**, 570-580.
53. Permi, P. & Annila, A. Progress in Nuclear Magnetic Resonance Spectroscopy

2004 **44**, 97-137.
54. Sarma, S. P. *Current Science* 2002 **83**, 1304-1306.
55. Wuthrich, K. & Wider, G. *Magnetic Resonance in Chemistry* 2003 **41**, S80-S88.
56. Chung, J. & Kroon, G. *Journal of Magnetic Resonance* 2003 **163**, 360-368.
57. Fiaux, J., Bertelsen, E. B., Horwich, A. L. & Wuthrich, K. *Journal of Biomolecular NMR* 2004 **29**, 289-297.
58. Li, C. G., Hu, J., Tian, C. L., Fu, R. Q., Gao, F., Mo, Y. M., Gorkov, P., Brey, W. & Cross, T. A. *Biophysical Journal* 2003 **84**, 278A-278A.
59. Nietlispach, D. *Journal of Biomolecular NMR* 2004 **28**, 131-136.
60. Pervushin, K. & Eletsky, A. *Journal of Biomolecular NMR* 2003 **25**, 147-152.
61. Ritter, C., Luhrs, T., Kwiatkowski, W. & Riek, R. *Journal of Biomolecular NMR* 2004 **28**, 289-294.
62. Kwiatkowski, W. & Riek, R. *Journal of Biomolecular NMR* 2003 **25**, 281-290.
63. Pegan, S., Kwiatkowski, W., Choe, S. & Riek, R. *Journal of Magnetic Resonance* 2003 **165**, 315-319.
64. Tugarinov, V., Hwang, P. M., Ollerenshaw, J. E. & Kay, L. E. *Journal of the American Chemical Society* 2003 **125**, 10420-10428.
65. Tugarinov, V. & Kay, L. E. *Journal of Biomolecular NMR* 2004 **28**, 165-172.
66. Tugarinov, V., Sprangers, R. & Kay, L. E. *Journal of the American Chemical Society* 2004 **126**, 4921-4925.
67. Tugarinov, V. & Kay, L. E. *Journal of Biomolecular NMR* 2004 **29**, 369-376.
68. Korzhnev, D. M., Kloiber, K., Kanelis, V., Tugarinov, V. & Kay, L. E. *Journal of the American Chemical Society* 2004 **126**, 3964-3973.
69. Ollerenshaw, J. E., Tugarinov, V. & Kay, L. E. *Magnetic Resonance in Chemistry* 2003 **41**, 843-852.
70. Majumdar, A. & Ghose, R. *Journal of Biomolecular NMR* 2004 **28**, 213-227.
71. Orekhov, V. Y., Korzhnev, D. M. & Kay, L. E. *Journal of the American Chemical Society* 2004 **126**, 1886-1891.
72. Wang, C. Y., Rance, M. & Palmer, A. G. *Journal of the American Chemical Society* 2003 **125**, 8968-8969.
73. Kempf, J. G., Jung, J. Y., Sampson, N. S. & Loria, J. P. *Journal of the American Chemical Society* 2003 **125**, 12064-12065.
74. Jahnke, W., Florsheimer, A., Blommers, M. J. J., Paris, C. G., Heim, J., Nalin, C. M. & Perez, L. B. *Current Topics in Medicinal Chemistry* 2003 **3**, 69-80.
75. Pelczer, I. Journal of Molecular Structure-Theochem 2003 **666**, 499-505.
76. Coles, M., Heller, M. & Kessler, H. *Drug Discovery Today* 2003 **8**, 803-810.
77. Clarkson, J. & Campbell, I. D. *Biochemical Society Transactions* 2003 **31**, 1006-1009.
78. Peng, J. W., Moore, J. & Abdul-Manan, N. *Progress in Nuclear Magnetic Resonance Spectroscopy* 2004 **44**, 225-256.
79. Homans, S. W. Angewandte Chemie-International Edition 2004 **43**, 290-300.
80. Ross, A. & Senn, H. *Current Topics in Medicinal Chemistry* 2003 **3**, 55-67.
81. Zartler, E. R., Yan, J. L., Mo, H. P., Kline, A. D. & Shapiro, M. J. *Current Topics in Medicinal Chemistry* 2003 **3**, 25-37.
82. Muchmore, S. W. & Hajduk, P. J. *Current Opinion in Drug Discovery & Development* 2003 **6**, 544-549.
83. Jacoby, E., Davies, J. & Blommers, M. J. J. *Current Topics in Medicinal Chemistry* 2003 **3**, 11-23.
84. Dalvit, C., Ardini, E., Flocco, M., Fogliatto, G. P., Mongelli, N. & Veronesi, M. *Journal of the American Chemical Society* 2003 **125**, 14620-14625.

85. Dalvit, C., Ardini, E., Fogliatto, G. P., Mongelli, N. & Veronesi, M. *Drug Discovery Today* 2004 **9**, 595-602.
86. Dalvit, C., Fagerness, P. E., Hadden, D. T. A., Sarver, R. W. & Stockman, B. J. *Journal of the American Chemical Society* 2003 **125**, 7696-7703.
87. Tengel, T., Fex, T., Emtenas, H., Almqvist, F., Sethson, I. & Kihlberg, J. *Organic & Biomolecular Chemistry* 2004 **2**, 725-731.
88. Boland, M. P. & Middleton, D. A. *Magnetic Resonance in Chemistry* 2004 **42**, 204-211.
89. Wang, Y. S., Liu, D. J. & Wyss, D. F. *Magnetic Resonance in Chemistry* 2004 **42**, 485-489.
90. Dalvit, C., Hadden, D. T. A., Sarver, R. W., Ho, A. M. & Stockman, B. J. *Combinatorial Chemistry & High Throughput Screening* 2003 **6**, 445-453.
91. Bertini, I., Fragai, M., Lee, Y. M., Luchinat, C. & Terni, B. *Angewandte Chemie-International Edition* 2004 **43**, 2254-2256.
92. Johnson, E. C., Feher, V. A., Peng, J. W., Moore, J. M. & Williamson, J. R. *Journal of the American Chemical Society* 2003 **125**, 15724-15725.
93. Fielding, L., Fletcher, D., Rutherford, S., Kaur, J. & Mestres, J. *Organic & Biomolecular Chemistry* 2003 **1**, 4235-4241.
94. Carredano, E., Baumann, H., Gronberg, A., Norrman, N., Glad, G., Zou, J. Y., Ersoy, O., Steensma, E. & Axen, A. *Protein Science* 2004 **13**, 1476-1488.
95. Nielsen, N. C., Malmendal, A. & Vosegaard, T. *Molecular Membrane Biology* 2004 **21**, 129-141.
96. Straus, S. K. Philosophical Transactions of the Royal Society of London Series B-Biological Sciences 2004 **359**, 997-1008.
97. Nevzorov, A. A., Mesleh, M. F. & Opella, S. J. *Magnetic Resonance in Chemistry* 2004 **42**, 162-171.
98. Fernandez, C. & Wuthrich, K. *Febs Letters* 2003 **555**, 144-150.
99. Fernandez, C., Hilty, C., Wider, G., Guntert, P. & Wuthrich, K. *Journal of Molecular Biology* 2004 **336**, 1211-1221.
100. Hilty, C., Wider, G., Fernandez, C. & Wuthrich, K. *Journal of Biomolecular NMR* 2003 **27**, 377-382.
101. Hilty, C., Wider, G., Fernandez, C. & Wuthrich, K. *Chembiochem* 2004 **5**, 467-473.
102. Tafer, H., Hiller, S., Hilty, C., Fernandez, C. & Wuthrich, K. *Biochemistry* 2004 **43**, 860-869.
103. Lee, S., Meslch, M. F. & Opella, S. J. *Journal of Biomolecular NMR* 2003 **26**, 327-334.
104. Oxenoid, K., Kirn, H. J., Jacob, J., Sonnichsen, F. D. & Sanders, C. R. *Journal of the American Chemical Society* 2004 **126**, 5048-5049.
105. Zamoon, J., Mascioni, A., Thomas, D. D. & Veglia, G. *Biophysical Journal* 2003 **85**, 2589-2598.
106. Dmitriev, O. Y., Abildgaard, F., Markley, J. L. & Fillingame, R. H. *Journal of Biomolecular NMR* 2004 **29**, 439-440.
107. Faulon, J. L., Sale, K. & Young, M. *Protein Science* 2003 **12**, 1750-1761.
108. Mesleh, M. F., Lee, S., Veglia, G., Thiriot, D. S., Marassi, F. M. & Opella, S. J. *Journal of the American Chemical Society* 2003 **125**, 8928-8935.
109. Kim, S. & Cross, T. A. *Journal of Magnetic Resonance* 2004 **168**, 187-193.
110. Park, S. H., Mrse, A. A., Nevzorov, A. A., Mesleh, M. F., Oblatt-Montal, M., Montal, M. & Opella, S. J. *Journal of Molecular Biology* 2003 **333**, 409-424.
111. Kochendoerfer, G. G., Jones, D. H., Lee, S., Oblatt-Montal, M., Opella, S. J. & Montal, M. *Journal of the American Chemical Society* 2004 **126**, 2439-2446.

112. Straus, S. K., Scott, W. R. P. & Watts, A. *Journal of Biomolecular NMR* 2003 **26**, 283-295.
113. Castellani, F., van Rossum, B. J., Diehl, A., Rehbein, K. & Oschkinat, H. *Biochemistry* 2003 **42**, 11476-11483.
114. Alia, Matysik, J., de Boer, I., Gast, P., van Gorkom, H. J. & de Groot, H. J. M. *Journal of Biomolecular NMR* 2004 **28**, 157-164.
115. Fujiwara, T., Todokoro, Y., Yanagishita, H., Tawarayama, M., Kohno, T., Wakamatsu, K. & Akutsu, H. *Journal of Biomolecular NMR* 2004 **28**, 311-325.
116. Lorch, M., Mason, A. J. & Glaubitz, C. *Biophysical Journal* 2004 **86**, 99A-99A.
117. Lorigan, G. A., Tiburu, E. K., Dave, P. C., Karp, E. & Abu-Baker, S. *Biophysical Journal* 2004 **86**, 371A-371A.
118. Page, R. C., Korepanova, A. & Cross, T. A. *Biophysical Journal* 2004 **86**, 98A-98A.
119. Mason, A. J., Siarheyeva, A., Haase, W., Lorch, M., van Veen, H. & Glaubitz, C. *Febs Letters* 2004 **568**, 117-121.
120. Tamm, L. K., Abildgaard, F., Arora, A., Blad, H. & Bushweller, J. H. *Febs Letters* 2003 **555**, 139-143.
121. Saito, H., Yamaguchi, S., Okuda, H., Shiraishi, A. & Tuzi, S. *Solid State Nuclear Magnetic Resonance* 2004 **25**, 5-14.
122. Saito, H., Yamamoto, K., Tuzi, S. & Yamaguchi, S. *Biochimica Et Biophysica Acta-Biomembranes* 2003 **1616**, 127-136.
123. Soubias, O., Reat, V., Saurel, O. & Milon, A. *Magnetic Resonance in Chemistry* 2004 **42**, 212-217.
124. Barre, P., Yamaguchi, S., Saito, H. & Huster, D. *European Biophysics Journal with Biophysics Letters* 2003 **32**, 578-584.
125. Saito, H., Mikami, J., Yamaguchi, S., Tanio, M., Kira, A., Arakawa, T., Yamamoto, K. & Tuzi, S. *Magnetic Resonance in Chemistry* 2004 **42**, 218-230.
126. Dobrodumov, A. & Gronenborn, A. M. *Proteins-Structure Function and Genetics* 2003 **53**, 18-32.
127. Farooq, A., Zeng, L., Yan, K. S., Ravichandran, K. S. & Zhou, M. M. *Structure* 2003 **11**, 905-913.
128. Deane, J. E., Mackay, J. P., Kwan, A. H. Y., Sum, E. Y. M., Visvader, J. E. & Matthews, J. M. *Embo Journal* 2003 **22**, 2224-2233.
129. Feng, W., Long, J. F., Fan, J. S., Suetake, T. & Zhang, M. J. *Nature Structural & Molecular Biology* 2004 **11**, 475-480.
130. Kozlov, G., De Crescenzo, G., Lim, N. S., Siddiqui, N., Fantus, D., Kahvejian, A., Trempe, J. F., Elias, D., Ekiel, I., Sonenberg, N., O'Connor-McCourt, M. & Gehring, K. *Embo Journal* 2004 **23**, 272-281.
131. Thiru, A., Nietlispach, D., Mott, H. R., Okuwaki, M., Lyon, D., Nielsen, P. R., Hirshberg, M., Verreault, A., Murzina, N. V. & Laue, E. D. *Embo Journal* 2004 **23**, 489-499.
132. Luo, X. L., Tang, Z. Y., Xia, G. H., Wassmann, K., Matsumoto, T., Rizo, J. & Yu, H. T. *Nature Structural & Molecular Biology* 2004 **11**, 338-345.
133. Alam, S. L., Sun, J., Payne, M., Welch, B. D., Blake, B. K., Davis, D. R., Meyer, H. H., Emr, S. D. & Sundquist, W. I. *Embo Journal* 2004 **23**, 1411-1421.
134. Swanson, K. A., Kang, R. S., Stamenova, S. D., Hicke, L. & Radhakrishnan, I. *Embo Journal* 2003 **22**, 4597-4606.
135. Walters, K. J., Lech, P. J., Goh, A. M., Wang, Q. H. & Howley, P. M. *Proceedings of the National Academy of Sciences of the United States of America* 2003 **100**, 12694-12699.
136. Mueller, T. D. & Feigon, J. *Embo Journal* 2003 **22**, 4634-4645.

137. Tatham, M. H., Kim, S., Yu, B., Jaffray, E., Song, J., Zheng, J., Rodriguez, M. S., Hay, R. T. & Chen, Y. *Biochemistry* 2003 **42**, 9959-9969.
138. Yoshinaga, S., Kohjima, M., Ogura, K., Yokochi, M., Takeya, R., Ito, T., Sumimoto, H. & Inagaki, F. *Embo Journal* 2003 **22**, 4888-4897.
139. Hirano, Y., Yoshinaga, S., Ogura, K., Yokochi, M., Noda, Y., Sumimoto, H. & Inagaki, F. *Journal of Biological Chemistry* 2004 **279**, 31883-31890.
140. Dominguez, C., Bonvin, A., Winkler, G. S., van Schaik, F. M. A., Timmers, H. T. M. & Boelens, R. *Structure* 2004 **12**, 633-644.
141. Wong, H. C., Bourdelas, A., Krauss, A., Lee, H. J., Shao, Y. M., Wu, D. Q., Mlodzik, M., Shi, D. L. & Zheng, J. *Molecular Cell* 2003 **12**, 1251-1260.
142. Feng, W., Shi, Y. W., Li, M. & Zhang, M. J. *Nature Structural Biology* 2003 **10**, 972-978.
143. Au, Y. H., Atkinson, R. A., Guerrini, R., Kelly, G., Joseph, C., Martin, S. R., Muskett, F. W., Pallavicini, A., Faulkner, G. & Pastore, A. *Structure* 2004 **12**, 611-622.
144. Koch, A. W., Farooq, A., Shan, W. S., Zeng, L., Colman, D. R. & Zhou, M. M. *Structure* 2004 **12**, 793-805.
145. Haussinger, D., Ahrens, T., Aberle, T., Engel, J., Stetefeld, J. & Grzesiek, S. *Embo Journal* 2004 **23**, 1699-1708.
146. Teriete, P., Banerji, S., Noble, M., Blundell, C. D., Wright, A. J., Pickford, A. R., Lowe, E., Mahoney, D. J., Tammi, M. I., Kahmann, J. D., Campbell, I. D., Day, A. J. & Jackson, D. G. *Molecular Cell* 2004 **13**, 483-496.
147. Chao, J. A. & Williamson, J. R. *Structure* 2004 **12**, 1165-1176.
148. Williams, D. C., Cai, M. L. & Clore, G. M. *Journal of Biological Chemistry* 2004 **279**, 1449-1457.
149. Wu, H. H., Henras, A., Chanfreau, G. & Feigon, J. Proceedings of the National Academy of Sciences of the United States of America 2004 **101**, 8307-8312.
150. Lingel, A., Simon, B., Izaurralde, E. & Sattler, M. *Nature* 2003 **426**, 465-469.
151. Mihailescu, M. R. & Marino, J. P. Proceedings of the National Academy of Sciences of the United States of America 2004 **101**, 1189-1194.
152. Alfano, C., Sanfelice, D., Babon, J., Kelly, G., Jacks, A., Curry, S. & Conte, M. R. *Nature Structural & Molecular Biology* 2004 **11**, 323-329.
153. Ramos, A., Hollingworth, D. & Pastore, A. *Rna-a Publication of the Rna Society* 2003 **9**, 293-298.
154. Cilley, C. D. & Williamson, J. R. *Rna-a Publication of the Rna Society* 2003 **9**, 663-676.
155. Mitton-Fry, R. M., Anderson, E. M., Theobald, D. L., Glustrom, L. W. & Wuttke, D. S. *Journal of Molecular Biology* 2004 **338**, 241-255.
156. Laguri, C., Phillips-Jones, M. K. & Williamson, M. P. *Nucleic Acids Research* 2003 **31**, 6778-6787.
157. Van Melckebeke, H., Vreuls, C., Gans, P., Filee, P., Llabres, G., Joris, B. & Simorre, J. P. *Journal of Molecular Biology* 2003 **333**, 711-720.
158. Akasaka, K. *Biochemistry* 2003 **42**, 10875-10885.
159. Korzhnev, D. M., Salvatella, X., Vendruscolo, M., Di Nardo, A. A., Davidson, A. R., Dobson, C. M. & Kay, L. E. *Nature* 2004 **430**, 586-590.
160. Di Nardo, A. A., Korzhnev, D. M., Stogios, P. J., Zarrine-Afsar, A., Kay, L. E. & Davidson, A. R. *Proceedings of the National Academy of Sciences of the United States of America* 2004 **101**, 7954-7959.
161. Frieden, C. *Biochemistry* 2003 **42**, 12439-12446.
162. Mok, K. H., Nagashima, T., Day, I. J., Jones, J. A., Jones, C. J. V., Dobson, C. M. &

Hore, P. J. *Journal of the American Chemical Society* 2003 **125**, 12484-12492.
163. Khan, F., Chuang, J. I., Gianni, S. & Fersht, A. R. *Journal of Molecular Biology* 2003 **333**, 169-186.
164. Vu, N. D., Feng, H. Q. & Bai, Y. W. *Biochemistry* 2004 **43**, 3346-3356.
165. Vendruscolo, M., Paci, E., Karplus, M. & Dobson, C. M. *Proceedings of the National Academy of Sciences of the United States of America* 2003 **100**, 14817-14821.
166. Lindorff-Larsen, K., Kristjansdottir, S., Teilum, K., Fieber, W., Dobson, C. M., Poulsen, F. M. & Vendruscolo, M. *Journal of the American Chemical Society* 2004 **126**, 3291-3299.
167. Ripoll, D. R., Vila, J. A. & Scheraga, H. A. *Journal of Molecular Biology* 2004 **339**, 915-925.
168. Reed, M. A. C., Hounslow, A. M., Sze, K. H., Barsukov, I. G., Hosszu, L. L. P., Clarke, A. R., Craven, C. J. & Waltho, J. P. *Journal of Molecular Biology* 2003 **330**, 1189-1201.
169. Brorsson, A. C., Kjellson, A., Aronsson, G., Sethson, I., Hambraeus, C. & Jonsson, B. H. *Journal of Molecular Biology* 2004 **340**, 333-344.
170. Feng, H. Q., Takei, J., Lipsitz, R., Tjandra, N. & Bai, Y. W. *Biochemistry* 2003 **42**, 12461-12465.
171. Quezada, C. M., Schulman, B. A., Froggatt, J. J., Dobson, C. M. & Redfield, C. *Journal of Molecular Biology* 2004 **338**, 149-158.
172. Ramboarina, S. & Redfield, C. *Journal of Molecular Biology* 2003 **330**, 1177-1188.
173. Assfalg, M., Banci, L., Bertini, I., Turano, P. & Vasos, P. R. *Journal of Molecular Biology* 2003 **330**, 145-158.
174. Jimenez, B., Poggi, L. & Picciolo, M. *Biochemistry* 2003 **42**, 13066-13073.
175. Ding, K. Y., Louis, J. M. & Gronenborn, A. M. *Journal of Molecular Biology* 2004 **335**, 1299-1307.
176. Mayor, U., Grossmann, J. G., Foster, N. W., Freund, S. M. V. & Fersht, A. R. *Journal of Molecular Biology* 2003 **333**, 977-991.
177. Mohana-Borges, R., Goto, N. K., Kroon, G. J. A., Dyson, H. J. & Wright, P. E. *Journal of Molecular Biology* 2004 **340**, 1131-1142.
178. Fieber, W., Kristjansdottir, S. & Poulsen, F. M. *Journal of Molecular Biology* 2004 **339**, 1191-1199.
179. Cemazar, M., Zahariev, S., Pongor, S. & Hore, P. J. *Journal of Biological Chemistry* 2004 **279**, 16697-16705.
180. Bolis, D., Politou, A. S., Kelly, G., Pastore, A. & Temussi, P. A. *Journal of Molecular Biology* 2004 **336**, 203-212.

10
NMR of Carbohydrates, Lipids and Membranes

BY E. F. HOUNSELL

1 Introduction

This review begins with NMR studies of membranes which integrates studies on lipids and proteins. The complex interactions at the cell surface are more and more being successfully mimicked by NMR in artificial lipid bilayers. Improvements in methodology are discussed, in particular recent reviews in the area. A large number of studies, the most recent of which are described here, concentrate on the interactions of peptidic components of proteins with membranes in pathology. For example in pore formation for the infiltration of toxins into cells, virus fusion with the cell membrane and the actions of antibiotics. Also included in this Section are NMR studies of the molecules responsible for the pathologies caused by mis-folding and aggregation of proteins leading to inappropriate fibril formation (*e.g.* in Alzheimer's and Creutzfeldt Jakob disease). This leads on to studies of protein glycosylation, which affects all near membrane events at the cell surface and in the extracellular matrix. As with previous years in this review on NMR of carbohydrates, lipids and membranes (the latest being[1]), the increasing importance of metabonomic approaches for *in vivo* and *in vitro* work is highlighted, in particular hyphenated techniques and data base searching. Lipid and carbohydrate-containing natural products and their biological/immunological activities are discussed next with a specific section on those that are surfactants. For the first time a separate section on studies on food is included which brings together relevant studies on oils and polysaccharides.

2 Membranes

2.1 Lipid Dynamics. – A review of principally ^{2}H-NMR of lipid interactions with transmembrane proteins by Marsh[2] indicated that the mean lipid chain ordering at the surface of transmembrane proteins is comparable to that in fluid lipid bilayers. Significantly evidence was produced for what has widely been thought important in membrane organisation that it is the requirement for matching the hydrophobic lengths of lipid and protein that modulate the degree of chain ordering at the lipid-protein interface. The orientation of lipids was studied by solid state ^{2}H and ^{31}P NMR in dimyristoylphosphatidylcholine

Nuclear Magnetic Resonance, Volume 34
© The Royal Society of Chemistry, 2005

(DMPC) entirely or selectively deuterated on the head group, glycerol backbone and acyl chains[3]. Molecular mechanics calculations were also accomplished on fully hydrated DMPC bilayers. From these studies the authors concluded that the glycerol backbone shows a very restricted motional freedom between two fluid zones of the phosphocholine head group and the acyl chains and that the location of the principal axis of motion of the glycerol backbone has the glycerol g2-g3 carbon-carbon bond at about 28 degrees with respect to the bilayer. From Monte Carlo simulations of an hydrophobic peptide with lipid bilayers and NMR obtained in detergent micelles and supported lipid bilayers[4], a value of 14 degrees was given for the tilt between the axis of the helix formed by the peptide and the membrane normal. The simulations showed that starting from an extended conformation in the aqueous phase, the peptide first absorbed onto the membrane surface while acquiring an ordered helical structure. This was followed by formation of a helical hairpin and insertion into the membrane. Cardon et al[5] reported the development of a spin-labelled EPR spectroscopic technique complementary to solid-state NMR to study the structure, orientation and dynamics of uniaxially aligned integral membrane proteins inserted into magnetically aligned discotic phospholipid bicelles and phospholipid bicelles were employed[6] as a membrane bilayer model in the conformational studies of two lipophilic canabinoids using conventional high resolution NMR without isotopic labelling. A preparation of 8% w/v phospholipid concentration and a high DMPC/DHPC ratio (q 2,0 dimyristal/dihexanoyl phosphatidylcholine) was optimal not only for effectively incorporating the ligands but also providing a more bilayer-like environment.

2.2 Membrane Proteins. – A general overview on NMR of membrane associated peptides and proteins is given by Bader et al[7]. Fernandez and Wuthrich review NMR solution structure determination of membrane proteins reconstituted in detergent micelles[8]. For example, for the *Escherichia coli* outer membrane protein X (OmpX) in DHPC it was shown that the central part of the protein is covered with a fluid monolayer of lipid molecules which seems to mimic quite faithfully the embedding of the protein in the lipid phase of the biological membrane. The implication drawn by the authors is that micellar systems used for NMR studies of membrane proteins should be suitable for further investigations of functional interactions with other proteins or low molecular weight ligands.

2D NMR methods for studies of micelle bound proteins are now beginning to answer biologically relevant problems, for example the interactions in membrane mimetics of glucagon[9] and neurokinin[10]. Williamson et al[11] review MAS solid state NMR of isotopically enriched biological samples and studies of them in membrane mimetics including details on sample preparation and different polarisation-transfer techniques. Stable isotope labelling of histamine (H) and its 1D ^{13}C CP MAS and 2D radiofrequency dipolar recoupling (RFDR) spectra were reported[12] and the production of H1 receptor for MAS NMR studies of the ligand receptor interaction are underway to confirm initial findings that histamine interacts with the transmembrane region of the H1 receptor helices III and

V. One of the transmembrane segments of the nicotinic acetylcholine receptor is a 23 amino acid peptide frequently used as a model for peptide-membrane interactions[13]. Continuum-solvent model calculations including data from ten structures from NMR in DPC micelles showed a tendency for the membrane to deform in response to peptide insertion and for kinked forms of the peptide to be the most stable. Yushmanov et al[14] also report on the NMR structure and dynamics of the second transmembrane domain of the neuronal acetyl choline receptor β2 subunit. The topology of factor VIII, a plasma glycoprotein essential in the blood coagulation cascade, binding to phosphatidylserine membranes was studied mainly by X-ray crystallography and electron microscopy[15]. Solid state NMR investigations[16] reported on the depth of insertion of protegrin-1 in lipid bilayers using paramagnetic Mn^{2+}. The preferred conformation of orexin-B, an orphan G-protein coupled receptor antagonist, which is involved in the sleep/wake cycle and feeding regulation, has been determined by ^{1}H and ^{13}C 2D NMR[17] in the membrane mimetic sodium dodecylsulfate-d_{25}. The secondary structure consists of two helical sections Leu7 to Ser18 and Ala 22 to Leu26 of the sequence RSGPPGLQGRLQRLLQASGNHAAGILTM which are thought to be involved in membrane binding as confirmed by spin labelling studies with 5-doxylstearic acid, The lack of apparent structure for Thr27-Met28 was suggested to allow conformational freedom to interact with receptor.

2.3 Membrane Interactions With Toxins and Viruses. – Pore formation in target cell membranes is a common mechanism used by many toxins in order to kill cells[18]. Among various described mechanisms, a toroidal pore concept has emerged where membrane destabilising effects are indicated by an isotropic component *e.g.* as detected by ^{31}P-NMR[18]. In this study the cation selectivity of the toxin-induced pores increased on addition of negatively charged fatty acids to multilamellar vesicles, indicating the presence of lipids in the conductive channel. Saiz et al[19] performed multi-nanosecond molecular dynamics simulations of the pore-forming aggregate of α-helical transmembrane proteins which constitutes a model for the nicotinic acetylcholine receptor inserted in a simple lipid bilayer (a fully hydrated dimyristoyl-*sn*-glycerophosphocholine lipid bilayer) and compared their results to NMR data.

^{1}H MAS nuclear Overhauser effect (NOE) spectroscopy of lipid bilayers with the human immunodeficiency virus (HIV) peptide N-acetyl-LWYIK-amide and cholesterol showed that addition of the former caused reorganisation of phosphatidylcholine and cholesterol to produce membrane domains enriched in cholesterol[20]. These properties helped the authors to explain the observation that the peptide sequence is found to be important in causing the fusion protein of HIV to sequester into rafts in biological membranes. Temperature dependence and resonance assignment of selectively and uniformly labelled fusion peptides of both HIV and influenza virus associated with POPC-POPG (1-palmitoyl-2-oleoyl-*sn*-glycero-3 phosphatidylcholine/glycine 4/1) or lipid/cholesterol membranes were also studied by 1D MAS, 2D ^{13}C-^{13}C correlation[21].

2.4 Antimicrobial Actions. – The dynamics and aggregation of a β-sheet anti-

microbial peptide protegrin-1 (PG-1) were investigated[22] using solid state NMR spectroscopy in 1,2-dilauryl-*sn*-glycero-3-phosphatidylcholine (DPLC) and 1-palmitoyl-2-oleoyl-sn-glycero-3-phosphatidylcholine bilayers. Exchange NMR experiments on ^{13}C -labelled PG-1 showed that it underwent slow reorientation in POPC with a long correlation time (0.7 s) suggesting that, in addition to aggregation (in POPC but not DPLC), geometric constraints in the membrane may also contribute to PG-1 immobilisation in POPC. NMR studies[23] of the 13-residue fragment from the tryptophan rich domain of puroindoline, a wheat endosperm-specific protein with antimicrobial activity indicated that all the possible charged residues of phospholipid vesicles are orientated close to the face of the Trp indole rings (of FPVTWRWWKWWKG) forming energetically favourable cation-π interactions. This characteristic, along with the well-defined amphipathic structure of puroindoline upon binding to membrane mimetic systems, allows the Trp-rich segment to insert more deeply into bacterial membranes and disrupt the regular membrane bilayer structure of Gram-positive and Gram-negative bacteria. Using NMR data as starting parameters, Bingham et al[23] present molecular dynamics simulations of Trp side chain conformational flexibility in the gramicidin A channel (prototypical peptide antibiotic and model ion channel former). Although not specifically related to membranes, but exhibiting useful technology, are studies[24] on plasminogen activator inhibitor-1 (PAI-1) labelled with ^{19}F 5-fluorotryptophan and a Trp-Phe mutation strategy. Detailed interpretation of the ^{19}F -NMR spectra of the PAI-1 mutants provided insights into the local segmental structure of the active form of the proteins and the structural changes that occur on complexation with the proteinase, tissue plasminogen activator t-PA.

2.5 Membrane Transporter Proteins. – A review on the use of NMR to study the structure of membrane transporter proteins appears as a Chapter in the Methods in Molecular Biology Series[25]. Improvements in the preparation of orientated lipid bilayers illustrated for the membrane protein CHIF (channel inhibiting factor), a member of the FXYD family of ion transport regulators, was reported by Marassi[26] using optimisation of hydration to better mimic membrane bound proteins with improved stability. Rosey et al[27] report the use of dynamic nuclear polarisation (DNP) to enhance sensitivity of solid state NMR. MAS DNP was used successfully on cryoprotected solution and membrane proteins *e.g.* signal enhancement of x50 in ^{15}N MAS spectra of bacteriorhodopsin. Several helix-membrane folds were studied by a computational technique matching a predefined set of distance constraints such as those obtained from NMR NOE data chemical cross linking, dipolar EPR and FRET experiments[28]. ^{13}C -labelled substrate affinities for membrane transport proteins (a nucleoside transporter and a glucuronide transporter of *E. coli*) were determined by ^{13}C CP-MAS NMR[29].

2.6 Protein Folding Disorders. – There are twenty five or so known proteins that can misfold and aggregate into fibrils. Of these, three are glycosylated: the amyloid associated membrane protein (AAP) in Alzheimer's; the prion in scrapie,

bovine spongiform encephalopathy (BSE) and Creutzfeldt Jacob Disease (CJD); and some of the immunoglobulin light chains of primary systemic amyloidosis. NMR studies of prions in non-glycosylated form have been reviewed previously[1] and an overview of the work of Wuthrich includes major studies on prion conformation[30]. Updates on studies of prion peptides are included here together with studies on amyloid-β peptides of AAP and the non-glycosylated β2microglobulin.

At pH values between 6.5 and 7.8, *i.e.* the pH at the cell membrane, the octapeptide repeats in recombinant human prion protein (23-230) encompassing the highly conserved peptide sequence PHGGGWGQ were shown by NMR to be structured[31]. By comparison with the crystal structure of HGGGW-Cu^{2+}, indicating that the binding of copper ions induces a conformational transition, the authors proposed that this would modulate PrP aggregation. Reisner[32] reviews the biochemical and structural (including NMR and electron microscopy data) studies of the normal cellular form (PrP^{c}) and pathological forms (PrP^{Sc}) of prions, their conformational transitions and the association of specific lipids and a polyglucose scaffold. Fibril formation of the mouse peptide PrP 106-126 was investigated by electron microscopy, CD spectroscopy, NMR-detected hydrogen-deuterium exchange measurements and molecular dynamics simulations[33] . This peptide induces neuronal cell death by apoptosis and causes proliferation and hypertrophy of glia, reproducing the main neuropathological features of BSE and CJD. The physicochemical studies showed that the fibrils contain approximately 50% β-sheet structure and strong amide exchange protection is limited to the central portion of the peptide spanning the palindromic sequence VAGAAGAV with two four-stranded parallel β-sheets tightly packed against each other by methyl-methyl interactions. The carboxy terminus half of the prion (126-232) contains the two glycosylation sites and two helices. The conversion of helix 1 from α-helical to extended conformation is generally assumed to be an essential step in the conversion of the cellular isoform PrP^{C} to the pathogenic isoform PrP^{Sc}. However NMR and CD analysis of the peptide encompassing helix 1 suggest that the interconversion is representing a barrier rather then a nucleus[34].

A combination of ^{31}P MAS NMR and CD spectroscopy suggested fundamental differences in the functional organisation of the 39-42 amino acid long amphipathic amyloid-β peptide (Aβ1-40 in this study) which was found to be either firmly anchored in the membrane upon proteolytic cleavage thereby being prevented against release and aggregation, or it can have significant adverse effects when bound to membrane surfaces by undergoing accelerated aggregation causing apoptotic cell death[35]. Acidic lipids can prevent release of membrane inserted Aβ1-40 by stabilising its hydrophobic transmembrane C-terminal part (residue 29-40) in an α-helical conformation *via* an electrostatic anchor between its basic Lys28 residue and the negatively-charged membrane surface. However, if Aβ1-40 is released as a soluble monomer, charged membranes act as 2D aggregation templates where an increasing concentration of charged lipids causes an accumulation of surface associated Aβ1-40 followed by accelerated aggregation into toxic structures. Solution NMR studies (^{1}H, ^{13}C and ^{15}N) of the

Aβ1-40 and Aβ1-42 peptides established that the Met35 oxidation state affects the mechanism of amyloid formation[36]. Recent progress in obtaining structural constraints on Ab fibrils from solid state NMR and scanning transmission electron microscopy (STEM) data is presented by Antzutkin[37]. Polymorphism of amyloid fibrils and oligomers of Aβ1-40 was studied by ^{1}H, ^{13}C solid state NMR, TEM and atomic force microscopy (AFM). A real time aggregation of different polymorphs of the peptide was observed (by AFM) and binding of Cu(II) ions and Al-citrate and Al-ATP complexes to amyloid fibrils was observed (by ESR, electron paramagnetic resonance and solid state ^{27}Al NMR). In order to sort out the driving forces for parallel and anti-parallel alignment in the Ab peptide fibril structure, two studies[38,39] report on solid-state NMR of Ab 1-22 made amphiphilic by attaching a long hydrophobic chain to the peptide labelled with ^{13}C and ^{15}N. A third study[40] reports on MAS in ^{13}C NMR spectra of fibrils formed by Aβ1-40 in partially orientated samples.

A review by Tycko[41] describes the solid-state NMR techniques that have been recently applied to amyloid fibrils in general and the information obtained by using these techniques. β2-microgolobulin, lysozyme and calcitonin are others of the 25 or so proteins that causes amyloid. Although their inclusion in this review is tenuous as they are neither glycosylated nor membrane-associated, non-enzymic glycation has been implicated in their fibril formation. The natural turnover of MHC class I to which β2M is bound in the cell gives rise to release of β2M into plasmatic fluids and to its catabolism in the kidney. For those on dialysis, β2M accumulates and forms into fibrils: single amino acid mutants of β2M were studied by NMR and X-ray crystallography to shed light on this process[42]. An increase in the conformational flexibility of β2M upon copper binding monitored by heteronuclear NMR and hydrogen-deuterium exchange was speculated[43] to contribute to the overall destabilisation of the molecule increasing the equilibrium population of the amyloidogenic intermediate which would otherwise not normally happen at physiological pH. Fibril formation in human calcitonin was studied by ^{13}C CP/MAS and a unique packing of anti-parallel sheets proposed as a dominant fibril structure[44]. Glycation-induced changes in the conformation of lysozyme was shown[45] to result in the exposure of its active site region to increased proteolytic activity of trypsin, the opposite effect to what would be expected as previously it has been considered that subsequent formation of advanced glycation end products (AGEs) caused cross-linking and helped fibril formation by increasing stability. Two studies related to glycation are: glucosylation of Ras by *Clostridium sordelli* lethal toxin consequences of effector loop conformation observed by NMR spectroscopy[46]; and modification of peptide Lys residues during Maillard reaction of D-Glc and D-Lac[47].

3 Hyphenated Techniques, Metabonomics and Data Bases

3.1 Reviews on Hyphenated Techniques and Drug Discovery. – Silva Elipe[48] provides a general overview of the advantages and disadvantages of the hy-

phenation of NMR with LC and LC-MS. Kessler et al[49] review NMR spectroscopic methods for the identification of weak binding ligands in medicinal chemistry. They conclude that target-based NMR methods are especially suited to detect initial hits that can be used as chemical scaffolds for further optimisation. Smith[50] reviews NMR structural determination of pharmaceuticals and analysis of drugs by LC-NMR methods, Weisenberger[51] provides a review on the application of NMR to process control and Prior[52] discusses a number of studies using NMR to examine various biologically important phenomena and molecules in human and animal models as well as plants with emphasis on *in vivo* methods. A review entitled 'Purine and sugar chemistry on solid phase – 100 years after Emil Fischer's chemistry Nobel Prize 1902' sums up most of the material published in the field since 1960 and ends by giving a picture of future directions for the field in drug discovery based on sugar and purine chemistry[53]. Automatic spectral processing, spectral analysis, spectral prediction and structural conformation/elucidation are reveiwed[54], particularly for ^{1}H spectra of small to medium sized molecules capable of coping with the explosion in flow-NMR taking place which supports multiple parallel syntheses and combinatorial chemistry. A novel method for analysing 3D protein-ligand binding interactions, called structural interaction fingerprinting (SIFt) has been advocated[55] to deal with the massive amount of information being generated in rational drug design by X-ray crystallography, NMR and *in silico* approaches. Its applications are described in areas as diverse as organising data from 90 known structures of protein-kinase inhibitor complexes, during virtual chemistry library screening process and for the results generated by structure-based docking experiments. A review by Homans[56] focuses on recent developments in NMR spectroscopy and how they might be of value in removing some of the 'bottle-necks' in structure-based drug design.

3.2 Metabonomics. – LC-NMR-MS in natural product, combinatorial chemistry, drug discovery and drug metabolism studies was published in Drug Discovery Today: microcoil probes and capillary separations methods were reported to have a great potential along with recent innovations to improve NMR detection limits such as CryoFlowprobes and on-line solid phase extraction (LC-SPE-NMR)[57]. The SPE unit allows the use of normal protonated solvents for the LC separation and fully deuterated solvents for flushing the trapped compounds to the NMR probe. Thus solvent suppression is no longer necessary. Exarchou et al[58] report the use of LC-UV, SPE-NMR-MS combined with a cryogenic flow probe for the identification of compounds present in Greek oregano. Multiple trapping of the same analyte from repeated LC injections was utilised to solve the problem of low concentration and to obtain 2D heteronuclear NMR spectra. Dalvit et al[59] report a novel and sensitive NMR method for rapid, efficient and reliable biochemical screening of large compounds or natural products and for measuring their IC_{50} values on ligand binding using $^{19}CF_3$ labelled substrate and ^{19}F -NMR spectroscopy. A combined *in vivo* and *in vitro* study using MRS has been reported for the analysis of a drug (a ^{19}F labelled anti-inflammatory) and its metabolites in the liver, in blood plasma and in urine

samples[60]. High resolution NMR of biological fluids is reviewed[61] with a comprehensive profile of abundant endogenous metabolites in peripheral body fluids such as urine or blood focusing mainly on small endogenous molecules and therefore being complementary to studies of protein and nucleic acid: applications of metabonomic technology from drug discovery through early development and clinical applications of metabonomics are discussed.

Nicholoson's group describe in two comprehensive papers toxicity classification from metabonomic data using a density superposition approach 'CLOUDS'[62,63]. Broad identification of bacterial type for pus by ^{1}H NMR spectroscopy showed that the characteristic metabolic pattern of obligate anaerobes may be used as a prototype for their identification[64]. A rapid identification of *Candida* species has been reported by using NMR combined with a statistical classification strategy[65]. Ippel et al[66] describe 'using the greenhouse for structural proteomics' of *in vivo* uniformly labelled ^{15}N plants. In a study on potatoes the glycoprotein patatin and several protease inhibitors were isolated in gram quantities. The use of hyphenated techniques in comparative phytochemical studies of legumes[67] highlighted the advances of the parallel developments in analytical chemistry and systematics.

3.3 Studies of Metabolism. – A comparison of MALDI-TOF MS and ^{31}P NMR was made for the analysis of the neutral phospholipids in lens tissue[68]. Quantification of lipoprotein subfractions using ^{1}H NMR and chemometrics[69] using partial least squares regression gave promising results suggesting that the assessment of coronary heart disease risk is feasible by this method. Supporting this, NMR spectroscopy of plasma lipoprotein concentrations has been used to show the difference in response to women and men to dietary saturated fat and cholesterol[70]. The effect of a high saturated fat and no starch diet on serum lipid subfractions was studied by NMR in patients with documented cardiovascular disease[71]. ^{1}H NMR spectroscopic evidence was given for the interactions of ibuprofen and lipoproteins in human blood plasma with detected alteration in chemical shifts in phosphatidyl choline, sphingomyelin and unsaturated lipids in lipoprotein particles[72]. Oz et al[73] reported the first direct detection of, and measurement of, glycogen metabolism in the brain, achieved using localised ^{13}C NMR with isotopic enrichment of the glucosyl moieties and following incorporation of the label. Measurement of fractional whole body gluconeogenesis in humans from blood samples was possible using ^{2}H NMR spectroscopy[74]. The effects of metformin (an anti-diabetic drug) on both glycogen synthesis and gluconeogenesis were studied in cultured rat hepatocytes[75]. Lipoprotein abnormalities in diabetes have also been revealed by their subclass analysis by NMR[76] and correlated with diabetic neuropathy[77].

A controversial family of drugs at present, the selective serotonin reuptake inhibitors (SSRI, implicated in childhood suicide) have been followed using MRI to study choline metabolic rates[78]. A common characteristic consistently revealed by MRS studies in cancer cells and solid tumours is the elevation of phosphatidyl choline and total choline-containing compounds[79] - a possible target for early detection and therapy?

3.4 Proteins and Glycosylation. – A review recently published on NMR spectroscopy in the study of the structural diversity of carbohydrates provides guidelines for interpretation of 1D and 2D spectra against a background of their tautomeric, configurational and conformational equilibrium in solution and consideration of their biosynthesis and metabolism[80]. Databases and bioinformatics tools for glycobiology were reviewed by von der Leith[81] to further explore the role of glycosylation patterns as sensitive markers of disorders and diseases. Recent trends in carbohydrate modelling are reviewed by Dyekjaer and Rasmussen[82] with emphasis on improving force fields, coupling of NMR measurements with molecular dynamics simulations, calculation of thermodynamic properties and web access to modelling. Vliegenthart[83] has used his considerable experience in glycosylation analysis to review studies of the 3D structure of glycoproteins in solution, in particular the intramolecular interactions between the carbohydrate moieties and the protein backbone are documented. More NMR parameters continue to be published for N-linked glycosylation *e.g.* the Gal(β1-3)GlcNAc(β1-4)Man terminating oligosaccharides of insect royal jelly glycoproteins discussed in terms of the expression of the appropriate transferases[84] and a similar transferase-structure correlation was carried out for both N- and O-linked glycosylation in the milk of transgenic rabbits[85].

Inhibition of N-glycosylation by monosaccharide derivatives (often having N or S in the 'glycosidic' ring rather than O) remains a powerful tool in understanding biosynthesis and as potential drugs. Mellor et al[86] have described an efficient means of generating a series of *N*-alkylated deoxynojirimycin imino sugars to influence tissue selectivity and efficiency for cellular enzyme inhibition. The roles of glycosylation of proteins is being more and more understood in changing cellular behaviour. For example, for the year under review: P-glycoprotein-mediated multi-drug resistance in murine leukaemic cells was shown to be associated with decreases of oligo- (ConA sensitive) and/or polysaccharide content[87]; human insulin like growth factor receptor glycosylation and affinity was shown to be influenced by the co-infection of prions[88]; glycosylation was shown to broaden the substrate profile of type1 matrix metalloproteinases[89]. To understand these various effects in glycoproteins, structural and conformational studies and glyco-specific bioinformatic tools need to be used in consort with protein prediction and modelling algorithms. PROSHIFT is one of the latest tools for protein chemical shift prediction using artificial neural networks, trained to predict the ^{1}H, ^{13}C and ^{15}N of proteins using their 3D structure as well as experimental conditions as input parameters (www.jens-meiler.de/proshift.html)[90]. Spronk et al[91] report a method that yields a more realistic estimation of uncertainty in NMR-derived atomic co-ordinates by maximising the RMSD of an ensemble of structures.

4 Mammalian Oligosaccharides as Ligands and Antigens

A review on saccharide-protein interactions by Prestegard et al[92] discusses the use of NMR to structurally characterise biologically important systems. It

focuses on the methods that give information on internal oligosaccharide geometry and geometry relative to the protein surface. Martin-Pastor et al[93] describe NMR experiments for the measurement of ^{1}H -^{1}H and ^{13}C -^{13}C residual dipolar couplings in uniformly labelled oligosaccharides for studies of their conformation in the free and receptor-bound state. Maltose binding protein (MBP) has been studied by combined protein engineering and NMR spectroscopy which has resulted in a near quantitative structure-energy-binding relationship for a series of MBP mutants to show that this two domain protein undergoes a ligand-mediated conformational rearrangement from an 'open' to a 'closed' structure on binding to malto-oligosaccharides[94]. Two pentasaccharides that are found on the highly sulfated glycoprotein HNK-1 have been synthesised for use as substrates for sulfotransferase and their structure and conformation characterised by ^{1}H NMR[95]. Two new heparin-like hexasaccharides have been synthesised using a convergent block strategy and their solution conformation determined by NMR spectroscopy and molecular modelling to gain insight into the mechanism of fibroblast growth factor activation[96]. The coordination of Cu(II) to a hyaluronate (HA) tetrasaccharide, [GlcA(β1-3)GlcNAc(β1-4)]$_2$ was investigated in aqueous solution by ^{13}C and ^{1}H relaxation measurements at two magnetic fields[97]. Monte Carlo simulations of hyaluronidase were used to follow reactions involving hydrolysis, transglycosylation and condensation[98]. CD44 is the main cell surface receptor for HA and contains a functional HA binding domain, the contact residues of which have been elucidated by NMR[99]. Interestingly, the authors show that the contact residues exhibited only small changes in chemical shift on HA binding whereas residues with large chemical shift changes were located further upstream in the C-terminal extension and first α-helix, suggesting a large conformational change.

The binding of the MUCI transmembrane breast cancer antigen extracellular domain to anti-tumour monoclonal antibodies has been investigated both in the glycosylated and unglycosylated state. Grinstead et al[100] now report on the ^{15}N and ^{13}C NMR relaxation parameters for one and two repeat GVTSAP-DTRPAPGSTA and found that the $^{13}C_{\alpha}T_1$ values best represented changes in the local correlation time on binding of antibody. The implications are discussed within the context of MUC1 breast cancer vaccine design. Starting from a peptide containing the first nine amino acids of the MUCI repeat, Gutierrez et al[101] have added, using a completely enzymatic approach with monitoring by ^{1}H NMR, the core-2 sialyl Lewis X structure, NeuAc(α2-3)Gal(β1-4)GlcNAc(β1-6)[Gal(β1-3)]GalNAc, on the first Thr of the sequence. Brokx et al[102] used heteronuclear NMR of ^{15}N and ^{13}C -labelled forms of recombinant MUC1 construct containing five tandem repeats to characterise the substrate Ser and Thr residues to define the order and kinetics of addition of the core GalNAc. Antifreeze glycoprotein has similarities to mammalian mucins being high in Thr residues. The dynamics of Thr side chains have been investigated using natural abundance ^{13}C NMR spectroscopy: heteronuclear longitudinal and transverse relaxation rates and the ^{1}H -^{13}C NOE were determined and compared to the previously measured ^{15}N parameters[103]. Back to the human, evidence for the regiospecific glycosylation in gastrointestinal mucins was gathered by extensive

NMR analysis of oligosaccharide alditols released by β-elimination[104]. The studies showed the presence of an acidic gradient along the gastrointestinal tract with an increasing gradient of sialic acid from the ileum to the colon, reciprocal to a decreasing gradient of fucose suggested to arise from sialylated Sda/Cad antigens versus (fucosylated, non-sialylated) blood group ABH.

Sialic acids are the ubiquitous interface between eukaryotic cells and their environment and often significant components of prokaryote surfaces and secreted polysaccharides. As discussed by Ringenberg et a[105], a variety of pathogens and commensals use at least 1 of 4 distinct mechanisms for decorating their surfaces with sialic acids as a strategy to avoid, subvert or inhibit host innate immunity. ^{31}P -NMR spectroscopy of *Escherichia coli* K1 derivatives engineered with different combinations of mutations in various enzymes involved in sialylation (aldolase, lyase, kinase, epimerase synthetase and transferase) showed that an UDP-N-acetylglucosamine 2-epimerase generated ManNAc directly from the dinucleotide precursor despite detection of only this enzyme's UDP-hydrolase activity. The authors claim that this is the first use of NMR for analysing intermediate flux within sialate biosynthesis. It certainly is an interesting way to go to help annotate the many genes in eukaryotes and prokaryotes that are involved in monosaccharide transformations and oligosaccharide synthesis.

The sialic acid Kdo is part of the tetrasaccharide repeat [-5)Kdo(β2-3)Gal2Ac (β1-4)Gal(β1-3)Gal(β1-] of the exopolysaccharide produced by a clinical strain of *Burkholderia cepacia* isolated from a patient with cystic fibrosis[106]. In addition when grown in a mannitol-rich medium *B. cepacia* strains produced another polysaccharide established as levan, -2)Fru*f* (β1-2)Fru*f*(β1-. Such polysaccharides may be important in the pathology in the lung in cystic fibrosis. A novel sialylated and galactofuranose-containing O-linked glucan expressed on the sialoglycoprotein of *Trypanosoma cruzi* was characterised by NMR[107].

NMR studies of mimics of the sialyated glycolipid, ganglioside GM1, including (R)-2-hydroxy-3-cyclohexylpropionic acid or (R)-2-hydroxy-3-phenylpropionic acid as replacements for NeuAc, showed that the mimics are stronger cholera toxin binders that the parent ligand which includes (R)-2-hydroxypropionic acid, *i.e.* lipophilic substituents improve affinity for cholera toxin[108]. Using the growth-regulatory interaction of the pentasaccharide of ganglioside GM1 with homodimeric galectin-1 on neuroblastoma cell surfaces, Siebert et al[109] have studied the conformer selection in protein-carbohydrate interactions, principally by transfer NOE and computational methods and not requiring isotope-labelled glycans. The results were relevant to toxin-directed drug design and studies aimed at blocking galactin functionality in malignancy. In another bacterial toxin study[110] a relaxometric investigation of a non-toxic mutant of diphtheria toxin and of its conjugates with capsular polysaccharide of different types of *Neisseria meningitides* was performed in studies to investigate the dynamic properties of glycoconjugate proteins. ^{1}H NMR dispersion profiles of their water solutions showed a reduced protein hydration compared to carrier protein alone, a much larger flexibility of the conjugate compared to macromolecules of the same molecular weight and a strong tendency to aggregate.

5 Natural Products: Structures, Biological Activities and Antigenicity

5.1 Bacteria. – Brisson et al[111] review NMR and molecular modelling of complex carbohydrates and carbohydrate-protein interactions with respect to their applications as anti-bacterial vaccines. They describe how conformational models have proven useful in explaining the serology of the polysaccharides of group B *Neisseria meningitides*, group B *Streptococcus* type III and *S. pneumoniae* type 14. As part of a program for the development of synthetic vaccines against the pathogen *Shigella flexneri*, Clement et al[112] used a combination of NMR and molecular modelling to study the conformations of the O-specific polysaccharide and four related synthetic pentasaccharides. The models were in agreement with NMR data indicating a right handed 3-fold helix of the backbone repeat with a branching Glc pointing outwards. A chemo-enzymatic synthesis approach was used to synthesise tetra-, penta- and hexa-saccharide fragments of the capsular polysaccharide of *Streptococcus pnuemoniae* type 14 to form suitable compounds for conjugation with carrier proteins to be tested as potential vaccines in animal models[113]. Lycknert et al[114] reported the dynamics of the enterohaemorrhagic *E. coli* O19 antigen polysaccharide in solution by ^{13}C -NMR relaxation at low different field strengths. They found that the OPS underwent highly intricate motions both in amplitude and time scales of significance in the presentation of bacterial surfaces to the host immune system.

NMR analysis of the O-polysaccharide of *E. coli* O128, a repeating Gal-GalNAc backbone with Fuc(1-2) side branches on the Gal, was used in the complete sequencing of the biosynthesis gene cluster and flanking regions and a new α-1,2-fucosyl transferase activity detected[115]. Structural and serological characterisation of the O-antigenic polysaccharide of the LPS from *Acinetobacter baumannii* strain 24 showed that a monoclonal antibody raised in mouse is likely to recognise the novel monosaccharide constituents, QuiN4N (2,4-diamino-2,4,6-trideoxyglucose sometimes acetylated at C-4) and GalNAcA (2-acetamido-2-deoxygalacturonic acid)[116].

The O-antigen of *Proteus mirabilis* 038 was shown to be unique among bacterial polysaccharides in having 2-acetamidoethyl phosphate and N-linked D-aspartic acid moieties not previously found. Structural studies were performed using 1D and 2D NMR spectroscopy including experiments run in H_2O/D_2O mixtures to reveal correlations for the NH protons. Solvolysis with triflic acid gave D-GlcNAc6(AcEtnP) showing the suitability of this reagent for the preparation of phosphorylated sugars[117]. The structures and antigenic cross-reactivity of the oligosaccharides of *P. mirabilis* were further discussed in two papers[118, 119] and the structure and immunoreactivity of *P. mirabilis and P. vulgaris* compared[120] together with characterisation of the structure of the novel N-acetyl-L-rhamnosamine containing OPS of *P. vulgaris*[121].

In addition, the following are examples of other natural products identified: conformational studies of modified glycopeptide related to the cell wall peptidoglycan of bacterial cell walls were correlated with immunomodulating activities[122]. The structure of the OPS of the LPS of *Hafnia alvei* strain PCM1546 was characterised fully[123] as Gal(β1-3)GalNAc(β1-6) [3-*O*-Ac]Glc(α1-3)GlcA(α1-

3)[3-*O*-Ac]GalNAc. The structure of the biological repeating groups of the O-antigen of *Pseudomonas aeringinosa* immunotype 4 was shown to contain both 2-acetamido-2,6-dideoxy-D-glucose and 2-acetamido-2,6-dideoxy-D-galactose[124]. The structure of the rough type LPS from *Shewanella onedensis* MR-1 was shown to contain 8-amino-8-deoxy-Kdo and an open chain form of 2-acetamido-2-deoxy-D-galactose[125].

In plant and soil biology: the structure and activity was characterised of the LPS of the phytopathogenic bacterium *Agrobacter larrymoorei* which plays an important role in its pathogenesis in forming plant tumours[126]. A mercury resistant soil bacterium identified as a close relative of *Pseudomonas veronii* was shown to accumulate a compound in the stationary phase of growth that converted to a long-lived radical under oxidising conditions[127]. The compound was characterised by 2D NMR methods and MS etc and shown to be a 6-O-(2-deoxy-2-*N*-methylhydroxyamino-β-D-Glc-*p*)-α-α-trehalose previously discovered in *Micococcus luteus* and named lysodektose. The tetrasaccharide repeat unit of the OPS of a phytopathogenic bacterium *Erminia carotovera* was characterised as exposing branched 4-*O*-methyl rhamnose residues[128]. The major cell wall galactomannan of a *Streptomyces*-causing potato scab was characterised as Gal(β1-6)Gal(β1-6) with Man(α1-3) branches[129]. This was reported to be found for the first time in cell walls together with small amounts of a teichoic acid of the poly(glycerol phosphate) type and 3-deoxy-D-*glycero*-D-*galacto*-non-2-ulopyranosonic acid. A new mannitol teichoic acid containing rhamnose and pyruvic acid acetal was purified from the cell wall of *Brevibacterium permens* and the NMR data suggested to be helpful in determination of the species-specific status of newly isolated strains[130].

5.2 Mycobacterium. – A novel family of surface-exposed glycopeptidolipids were isolated from *Mycobacterium smegmatis* and shown to specifically inhibit the phagocytosis of mycobacterium by human macrophages (the first stage of infection in TB for example)[131]. These potential therapeutic agents (activities in the nano-micromolar level) were composed of a long chain tripeptidyl amino alcohol with a di-*O*-acetyl-6-deoxytalosyl unit substituting the allo-threoninyl residue and a 2-succinyl-3,4-di-*O*-methyl rhamnosyl unit linked to the alaninol ends of the molecules with various glycosylation of the alaninols.

5.3 Fungus. – Minor, but immunodominant components of the peptidogalactomannan fraction of *Aspergillus fumigatus* mycelial cell wall were fractionated to homogeneity by successive gel filtration and HPLC and their primary structures determined based on ESI-QTOF-MS, ^{1}H COSY and TOCSY and ^{1}H -^{13}C HMQC NMR spectroscopy with methylation analysis[132]. The isolated oligosaccharides containing galactofuranose were able to block, on a dose-response basis, recognition between human sera of patients with aspergillosis and the intact peptidogalactomannan. A new metabolite with nematocidal activity was isolated from the culture broth of *Coronphora gregaria* and characterised by 2D NMR as consisting of a highly methylated polyketide skeleton with two β-mannoses[133]. New polyketides of the murine-derived fungus of the genus *Phoma*

were characterised[134] and glycolipids of the filamentous fungus *Absidia corymbifera* F-295[135].

5.4 Marine Species. – The alginates from five species of brown algae from the Egyptian Red Sea were isolated and characterised for their relative contents of guluronic acid and mannuronic acid[136]. Their structure was related to intrinsic velocity and gel strength. The antimicrobial compounds from the brown algae *Sargassum solonifolium* were characterised by ^{1}H, ^{13}C and 2D NMR and identified as free fatty acids and [β-galactopyranosyl(1′-3)]-1,2-*sn*-diacyl glycerols[137]. Characterisation of a β-D-(1-3)-glucan from the marine diatom *Chaetoceros mulleri* was reported by high resolution MAS NMR spectroscopy on whole algal cells[138]. A review of sea cucumbers (holothuroida, *Echinoderma*) characterised by their content of triterpenoid glycosides showed that of nearly 100 holothurins isolated in the last twenty years, all of them can grouped into three main aglycon types[139]. The recently discovered marine sponge fatty acid (±)-2-methoxy-13-methyltetradecanoic acid was synthesised and characterised fully by NMR to substantiate the proposed structure and characterise its cytotoxicty to leukaemia cells[140].

5.5 Plants. – Water soluble polyphenol polymers isolated from cinnamon have been characterised that increase insulin-dependent *in vitro* glucose metabolism roughly X20 fold and display anti-oxidant activity[141]. They were characterised as A-type doubly-linked procyanidin oligomers of the catechins and/or epicatechins. The organic solvent extraction of the leaves of the native North American prairie plant, *Ipomea leptophylla* (big root morning glory) showed *in vitro* activity against *Mycobacterium tuberculosis*[142]. Bio-assay guided fractionation of this extract resulted in the identification of new resin glycosides: operculinic acid was identified as the glycosidic acid, as well as trans-cinnamic acid, propanoic acid and lauric acid[142]. Two new pregnane glycosides from the rhizomes of *Disocorea futschauensis* R. Kunth having two Rha and one Glc residue each were characterised by 2D NMR and for bioactivity against plant pathogenic fungi[143]. *Rhodiola rosea* L. (golden root) has been reported to have many pharmacological properties: four new compounds have now been isolated from a methanol extract of the whole plant and identified as cinnamyl- and benzyl-derivatives of mono- (Glc) and di- (Xyl-Glc and Ara-Glc) saccharides[144]. Cinnamoyl derivatives have also been isolated of triterpene saponins from the roots of *Polygala arenaria* [145]. Their structures were mainly established by 600MHz 2D NMR techniques (COSY, TOCSY, NOESY, HSQC, HMBC) with Glc, Rha, Xyl, Fuc and Gal containing oligosaccharides. The acyl oligosaccharidic moiety was shown to be important for immunomodulating effects in a lymphocyte proliferation assay. On a more mundane level, glucosylation at the 3′ and 5′ positions of anthocyanin was shown to be a critical step in producing blue petals in the plant *Clitoria ternata* [146]. The pigment triacylated and tetraglucosylated anthocyanins from *Ipomea asariflora* flowers were elucidated by GC, MS and NMR methods (^{1}H and ^{13}C TOCSY, DQF-COSY, DIFFNOE and HMBC)[147]. Anthocyanins from the red onion *Allium cepa* containing mainly Glc

residues were characterised[148].

A model oxidation system was developed and optimised in order to provide a relevant tool to study the oxidation products generated during the manufacture of black tea[149], monitored by ^{1}H NMR spectroscopy. The structure of the antioxidative carbazole alkaloids of the leaves of *Murraya koenigii* were characterised by ^{1}H and ^{13}C NMR[150]. The authors suggested that an aryl hydroxyl substituent on the carbazole rings plays a role in stabilising the thermal oxidation and rate of reaction against the 1,1-diphenyl-2-picrylhydrazyl (DPPH) radical. A digalactosyl ononitol with the structure Gal(α1-6)Gal(α1-3)[4-O-Me] -D-myoinositol isolated after hydrolysis from the seeds of the adzuk bean (*Vigna angularis*) was characterised by NMR[151]. The seed oil of *Paullinia cupana* was shown to contain cyanolipids[152].

Crude extracts of the plants of the *Licania* genus (*Chrysobalanaceae*) were found to be cytotoxic to hepatoma, carcinoma and melanoma cell lines and in addition to having a potent molluscicidal activity[153]. Structural characterisation by MS and NMR gave mainly flavanoids (especially flavanoid glycoside), clerodane diterpenes and triterpenes having lupan, ursane and oleanane skeletons. In addition, the diterpenes showed anti-fungal properties whilst the triterpenes were mainly active against Gram-positives. Acylated flavanoid and phenylethanoid glycosides (mono to tetrasaccharide) were isolated from the aerial parts of *Marrubium celutinum* and characterised by NMR[154]. NMR has been used to characterise the flavanol glycosides from cranberry (*Vaccinium macrocarpon*) [155] and the authors speculated that the variations in the sugar moiety may play a role in the bioavailability of the flavanol glycosides *in vivo*. Five new diterpenoids were isolated from the roots of *Caesalpinia pulcherrima* and their structures completely assigned using a combination of 2D NMR experiments including ^{1}H -^{1}H COSY, HSQC, HMBC and T-ROESY sequences[156]. Novel antibacterial iridoid and triterpene were isolated from the aerial parts of *Caiophora coronata*[157] with activity that included that against MRSA at 4μg/ml. Nine new triterpenoid saponins were isolated from aerial parts of *Conysa blinii* and characterised[158] as sharing an unusual pentasaccharide unit attached at C-28 of the aglycon, *i.e.* Api*f* (β1-3)Xyl*p* (β1-4)[Api*f* (β1-3)Rha*p*(α1-2)Ara*p* (β1-). New triterpene saponins with strong anti-leishmanial activity were isolated from the methanol extract of the leaves of *Maesa balansae*. They were shown by COSY, NOESY, HMQC, HMBC, TOCSYand DEPT to contain a pentaglycosidic side chain and varied in the esterification of the triterpenoid part[159]. Their activity against amastigotes was reported to be better than the reference compound, pentostam, which is currently used as the first line treatment for leishmaniasis. The structure and bioactivity of secoirdoid glycosides from *Centaurium erythreae* growing in Scotland were characterised and shown to be potent anti-bacterials at LD_{50} 8-34 μg/ml[160].

A large number of steroidal saponins were characterised from the methanol extract of a Taiwanese yam (cultivar *Dioscorea pseudojaponica* Yamamoto) and characterised by NMR as having various Glc and Rha containing oligosaccharides[161] and the conversions from seroid saponins to diosgenin after acid hydrolysis were found to be around 68 and 90% for furostanol and spirostanol glyco-

sides, respectively. Lanosterol and tetranorlanosterol glycosides were isolated from the methanol extract of *Muscari paradoxum* (*Liliaceae*) bulbs, characterised by NMR and evaluated for their cytotoxic activity against HSC-2 human oral squamous cell carcinoma cells[162]. An antimicrobial cerebroside, pinelloside, was isolated from the air-dried tubers of *Pinella ternata*[163] and its structure determined as 1-)-β-D-glucopyranosyl-(2s,3R,4E,11E)-2-(2′R-hydroxyhexadecenoylamino)4,11-octadecadiene-1,3-diol by chemical transformation and extensive spectroscopic analysis (IR, MS, ^{1}H and ^{13}C NMR, DEPT as well as 2D NMR techniques HMBC, HMQC, ^{1}H -^{1}H COSY and NOESY). This had activity against a broad range of bacteria and fungi at 50-10 mg/ml (only 10-50 times less active than penicillin G or ketoconazole, for example). NMR analysis of oleanolic glycosides from the stem bark of *Pometia ridleyi* gave six triterpenoid saponins containing Api*f*, Glc*p*, Gal*p* and Ara*p* which were shown to have haemolytic activity[164].

A biologically active antitussive fructofuranan of the inulin type was isolated[165] from the roots of *Arctcum lappa*. Several studies have characterised various parts of the prickly pear *Opuntia ficusindica*: most recently, the spines have been shown by optical microscopy, scanning and transmission electron microscopy, wide angle X-ray and solid state ^{13}C NMR analysis to contain arabinan in 1:1 interaction with cellulosic crystals[166]. Structural features of various (*O*-acetylated) xylo-oligosaccharides from xylan-rich agricultural biproducts (*e.g.* wheat bran, brewery's spent grain, corn cobs, Eucalyptus wood) were characterised[167]. Using the α and β anomeric C-1 protons as probes of their concentrations, Kiemle et al[168] have developed an algorithm to quantify the relative molar concentrations of sugars released from lignocellulosic biomass (wood pulp, agricultural residues etc) upon acid hydrolysis. Solution-state NMR studies of the milled wood lignan and cellulytic enzyme lignan showed subtle differences which could explain the degree of condensation[169]. Additional studies are: the isolation and characterisation of pectin from the pericarp of *Citrus depressa*[170]; and NMR structural determination of dissolved *O*-acetylated galactoglucomannan isolated from spruce thermomechanical pulp[171].

6 Surfactants

During cultivation on medium containing medium-chain-length n-alkanes, *Rhodococcus* bacteria strains produced surfactants which halved the surface tension of the cultures[172]. Glycolipids were extracted from the supernatant and characterised by ^{1}H and ^{13}C NMR and MS. The two major constituents consisted of α,α-trehalose esterified at C-2 and C-4 with a succinic acid at C-2′ with a deconoic with additional octanoic or deconoic substitution. The biochemical, genetic and zoosporicidal properties of surfactants produced by *Psuedomonas fluorescens*, which rendered zoospores of several fungi immobile (and hence uninfectious) within 30 s of exposure, were characterised by NMR and MS[173].The main component was a cyclic lipopeptide containing nine amino acids and a 10-carbon hydroxy fatty acid (*m/z* 1139). Other related lipopeptides had molecu-

lar masses ranging from 1111-1169. A prominent group of bioactive lipopeptides produced by *Bacillus* species including iturins, surfactants and lichenysins have been reported[174] as having exceptional surfactant power and anti-fungal, anti-bacterial, anti-tumoral and anti-mycoplasmal properties. Activity-structure relationships were extensively explored by these authors including MS data for characterisation and 2D NMR methods to give 3D structure and dynamics.

Novel amphiphilic cyclodextrins have been prepared by grafting a phospholipid on a modified cyclodextrin[175]. The detergent properties have been evaluated and the aggregation process in water characterised by light scattering, DSC and ^{31}P NMR. A proton NMR study of an α-cyclodextrin inclusion of short chain surfactants[176] and the study of ^{13}C chemical shift surfaces in the study of carbohydrate conformation and application to cyclodextrins in the solid state and in solution[177] were reported.

Physicochemical characterisation was characterised of self-assembled nanoparticles based on glycol chitosan-bearing 5β-cholanic acid and their surfactant activity[178]. Fluorescence spectroscopy and pulsed field gradient NMR (PFG-NMR) revealed information concerning the polydispersity of micelle polymers – chiral polymeric surfactants developed over the past decade for use as chiral selectors in the analytical separation of enantiomers[179]. The authors suggest that polydispersity is a crucial factor in understanding the chiral interactions of these species.

7 Food

A special publication of the Royal Society of Chemistry on Magnetic Resonance in Food Science discusses many aspects of the use of conventional and less conventional NMR methods in food analysis (such as oil, meat, beer, wine, moisture in biopolymers) including multivariate analysis of time domain NMR (TD-NMR) [180], the use of an NMR-MOUSE (mobile universal surface explorer)[181] for portable NMR and a review of the challenges in transferring NMR technology to the on-line industrial situation[182]. Quantitative analysis methods of mixtures of fatty compounds by ^{1}H -NMR are reviewed[183]. Rapid simultaneous determination by ^{1}H NMR of unsaturation and composition of acyl groups have also been reported in vegetable oils[184]. The use of IR, Raman, NMR, and MS was reviewed for the analysis of polysaccharides related to food[185].

The effects of microwave heating on potato texture has been investigated by magnetic resonance imaging: MRI quantitation of the spin-spin relaxation times provided a measure of texture[186]. A comparison of the structural features of arabinoxylans from whole wheat flour and wheat bran was made[187] using methylation analysis, ^{13}C NMR, FT-IR and periodate oxidation: Xyl residues with β-(1-4) linkage varied in the amount of branching through C-3 and C-2. Cutin is a polyester biopolymer component of plant leaf and fruit cuticles most often associated with waxes and cuticular polysaccharides and sometimes with another aliphatic polymer called cutan[188]. The insolubility of these cuticular biopolymers has made it difficult to apply traditional analytical techniques for

structure determination. By using the relatively new techniques 1D and 2D high resolution MAS NMR spectroscopy with added information from solid state ^{13}C NMR spectroscopy, detailed through-bond connectivities were made on cutin for the tomato fruit. Based on the data obtained, tomato cutin was found to be predominantly an aliphatic polyester with some olefinic and aromatic moieties. Aside from esters, the authors found free primary and secondary alcoholic groups as well as free fatty acids. A significant finding was the presence of α-branched fatty acids/esters which could point towards cross-linking. Turning briefly to the soil, humic acids have been studied by CPMAS ^{13}C NMR[189] and ^{27}Al-NMR[190].

References

1. E. F. Hounsell, *Nuclr. Magn. Reson.* RSC Specialist Periodical Reports, Ed G. A. Webb, 2003, **32**, 335.
2. D. Marsh, *Cellular Molec. Life Sci.*, 2003, **60**, 1575.
3. F. Aussenac, M. Laguerre, J-M. Schmitter, E. J. Dufourc, *Langmuir*, 2003, **19**, 10468.
4. A. Kessell, D. Shental-Bechor, T. Haliloglu, N. Ben-Tal, *Biophys. J.*, 2003, **85**, 3431.
5. T. B. Cardon, E. K. Tiburu, G. A. Lorigan, *J. Magn. Reson.*, 2003, **161**, 77.
6. J. Guo, S. Pavlopoulos, X. Tian, D. Lu, S. P. Nikas, D-P. Yang, A. Makriyannis, *J. Medicinal Chem.*, 2003, **46**, 4838.
7. R. Bader, M. Lerch, O. Zerbe, , *Meth. Princip. Medicinl. Chem.*, 2003, **16**, 95.
8. C. Fernandez, K. Wuthrich, *FEBS Letts.*, 2003, **555**, 144.
9. G. Wider, *Magn. Reson. Chem.*, 2003, **41**, S56.
10. I. R. Chandrashekar, S. M. Cowsik, *Biophys. J.*, 2003, **85**, 4002.
11. P. T. F. Williamson, M. Ernst, B. H. Meier, *Meth. Princip. Medicinl. Chem.*, 2003, **16**, 243.
12. V. R. P. Ratnala, F. B. Hulsbergen, H. J. M. de Groot, W. J. de Grip, *Inflammatn. Res.*, 2003, **52**, 417.
13. A. Kessel, T. Haliloglu, N. Ben-Tal, *Biophys. J.*, 2003, **85**, 3687.
14. V. E. Yushmanov, Y. Xu, P. Tang, *Biochem.*, 2003, **42**, 13058.
15. V. S. Purohit, K. Ramani, R. S. Kashi, M. J. Durrani, T. J. Kreiger, S. V. Balasubramanian, *Biochim. Biophys. Acta*, 2003, **1617**, 31.
16. J. J. Buffy, T. Hong, S. Yamaguchi, A. J. Waring, R. I. Lehrer, M. Hong, *Biophys. J.*, 2003, **85**, 2363.
17. M. Miskolzie, S. Lucyk, G. Kotovych, *J. Biomolec. Struct. Dynam.*, 2003, **21**, 341.
18. G. Anderluh, M. D. Serra, G. Viero, G. Guella, P. Macek, G. Menestrina, *J. Biol. Chem.*, 2003, **278**, 45216.
19. L. Saiz, S. Bandyopadhyay, M. L. Klein, *J. Phys. Chem. B*, 2004, **108**, 2608.
20. R. M. Epand, B. G. Sayer, R. F. Epand, *Biochem.*, 2003, **42**, 14677.
21. M. L. Bodner, C. M. Gabrys, P. D. Parkanzky, J. Yang, C. A. Duskin, D. P. Weliky, *Magn. Reson. Chem.*, 2004, **42**, 187.
22. J. J. Buffy, A. J. Waring, R. I. Lehrer, M. Hong, *Biochem.*, 2003, **42**, 13725.
23. W. Jing, A. R. Demcoe, H. J. Vogel, *J. Bacteriol.*, 2003, **185**, 4938.
24. G. L. Abbott, G. E. Blouse, M. J. Perron, J. D. Shore, L. A. Luck, A. G. Szabo, *Biochem.*, 2004, **43**, 1507.
25. S. J. Opella, *Meth. Molec. Biol.*, (*Membrane Transporters*) *Humana Press Inc*, 2003,

227, 307.
26. F. M. Marassi, K. J. Crowell, *J. Magn. Reson.*, 2003, **161**, 64.
27. M. Rosay, J. C. Lansing, K. C. Haddad, W. W. Bachovchin, J. Herzfeld, R. J. Temkin, R. G. Griffin, *J. Amer. Chem. Soc.*, 2003, **125**, 13626.
28. J-L. Faulon, K. Sale, M. Young, *Prot. Sci.*, 2003, **12**, 1750.
29. S. G. Patching, A. R. Brough, R. B. Herbert, J. A. Rajakarier, P. J. F. Henderson, D. A. Middleton, *J. Amer. Chem. Soc.*, 2004, ACS ASAP (English).
30. K. Wuethrich, *Magn. Reson. Chem.*, 2003, **41**, S89.
31. R. Zahn, *J. Molec. Biol.*, 2003, **334**, 477.
32. D. Riesner, *Brit. Med. Bulltn.*, 2003, **66**, 21.
33. K. Kuwata, T. Matumoto, H. Cheng, K. Nagayama, T. L. James, H. Roder, *Proc. Natl. Acad. Sci. U. S. A.*, 2003, **100**, 14790.
34. J. Ziegler, H. Sticht, U. C. Marx, W. Mueller, P. Roesch, S. Schwarzinger, *J. Biol. Chem.*, 2003, **278**, 50175.
35. M. Bokvist, F. Lindstrom, A. Watts, G. Grobner, *J. Molec. Biol.*, 2004, **335**, 1039.
36. L. Hou, H. Shao, Z. Y. Haiyan, H. Li, N. K. Menon, E. B. Neuhaus, J. M. Brewer, I-J. L. Byeon, D. G. Ray, M. P. Vitek, T. Iwashita, R. A. Makula, A. B. Przbyla, M. G. Zagorski, *J. Amer. Chem. Soc.*, 2004, **126**, 1992.
37. O. N. Antzutkin, *Magn. Reson. Chem.*, 2004, **42**, 231.
38. L. Hou, M. G. Zagorski, *Biophys. J.*, 2004, **86**, 1.
39. D. J. Gordon, J. J. Balbach, R. Tycko, S. C. Meredith, *Biophys. J.*, 2004, **86**, 428.
40. N. A. Oyler, R. Tycko, *J. Amer. Chem Soc.*, 2004, **126**, 4478.
41. R. Tycko, *Prog. Nuclr. Magn. Reson. Spectroscopy*, 2003, **42**, 53.
42. C. Rosano, S. Zuccotti, P. Mangione, S. Giorgetti, V. Bellotti, F. Pettirossi, A. Corazza, P. Viglino, G. Esposito, M. Bolognesi, *J. Molec. Biol.*, 2004, **335**, 1051.
43. J. Villanueva, M. Hoshino, H. Katou, J. Kardos, K. Hasegawa, H. Naiki, Y. Goto, *Prot. Sci.*, 2004, **13**, 797.
44. A. Naito, M. Kamihira, R. Inoue, H. Saito, *Magn. Reson. Chem.*, 2004, **42**, 247.
45. F. K. Yeboah, I. Alli, V. A. Yaylayan, K. Yasuo, S. F. Chowdhury, E. O. Purisima, *Bioconjug. J.*, 2004, **15**, 27.
46. M. Geyer, C. Wilde, J. Selzer, K. Aktories, H. R. Kalbitzer, *Biochem.*, 2003, **42**, 11951.
47. R. Tressi, C. T. Piechotta, D. Rewicki, E. Krause, *Int. Congr. Series*, 2002, **1245**, 203.
48. M. V. Silva Elipe, *Analyt. Chim. Acta*, 2003, **497**, 1.
49. H. Kessler, M. Heller, G. Gemmecker, T. Diercks, E. Planker, M. Coles, *Ernst Schering Research Foundation Workshop*, 2003, **42**, 59.
50. R. J. Smith, *Pharmaceut. Anal.*, 2003, 203.
51. L. A. Weisenberger, *Handbook of Spectroscop.*, 2003, **2**, 297.
52. M. J. W. Prior, *Nuclr. Magn. Reson.*, 2003, **32**, 401.
53. R. Franzen, J. Tois, *Combinatorial Chem. High Throughput Screening*, 2003, **6**, 433.
54. L. Griffiths, *Ann. Reports NMR Spectrosc.*, 2003, **50**, 217.
55. Z. Deng, C. Chuaqui, J. Singh, *J. Medicin. Chem.*, 2004, **47**, 337.
56. S. W. Homans, *Angewandte Chemie, Int. Edit.*, 2004, **43**, 290.
57. O. Corcoran, M. Spraul, *Drug Disc. Today*, 2003, **8**, 624.
58. V. Exarchou, M. Godejohann, T. A. Van Beek, I. P. Gerothanassis, J. Vervoort, *Analyt. Chem.*, 2003, **75**, 6288.
59. C. Dalvit, E. Ardini, M. Flocco, G. P. Fogliatto, N. Mongelli, M. Veronesi, *J. Amer. Chem. Soc.*, 2003, **125**, 14620.
60. D. Bilecen, A-C. Schulte, A. Kaspar, E. Kuestermann, J. Seelig, D. Elverfeldt, K. Scheffler, *NMR Biomed.*, 2003, **16**, 144.

61. M. D. Reily, D. G. Robertson, M. Delnomdedieu, J. D. Baker, *Am. Pharm. Rev.*, 2003, **6**, 105.
62. T. Ebbels, H. Keun, O. Beckonert, H. Antti, M. Bollard, E. Holmes, J. Lindon, J. Nicholson, *Analyt. Chim. Acta*, 2003, **490**, 109.
63. O. Beckonert, M. E. Bollard, T. M. D. Ebbels, H. C. Keun, H. Antti, E. Holmes, J. C. Lindon, J. K. Nicholson, *Analyt. Chim. Acta*, 2003, **490**, 3.
64. M. Garg, M. K. Misra, S. Chawla, K. N. Prasad, R. Roy, R. K. Gupta, *Eur. J. Clin. Invest.*, 2003, **33**, 518.
65. U. Himmelreich, R. L. Somorjai, B. Dolenko, O. C. Lee, H-M. Daniel, R. Murray, C. E. Mountford, T. C. Sorrell, *Appl. Environ. Microbiol.*, 2003, **69**, 4566.
66. J. H. Ippel, L. Pouvreau, T. Kroef, H. Gruppen, G. Versteeg, P. van den Putten, P. C. Struik, C. P. M. van Mierlo, *Proteomics*, 2004, **4**, 226.
67. G. C. Kite, N. C. Veitch, R. J. Graver, M. S. J. Simmonds, *Biochem. Systematics Ecol.*, 2003, **31**, 813.
68. M. Rujoi, R. Estrada, M. C. Yappert, *Analyt. Chem.*, 2004, **76**, 1657.
69. M. Dyrby, M. Petersen, S. B. Engelsen, L. Norgaard, U. G. Sidelmann, , *Special Publication – Roy. Soc. Chem. Magnetic resonance in Food Science. Royal Society of Chemistry Press*, 2002, **286**, 101.
70. Z. Li, J. D. Otvos, S. Lamon-fava, W. V. Carrasco, A. H. Lichtenstein, J. R. McNamara, J. M. Ordovas, E. J. Schaefer, *J. Nutrit.*, 2003, **133**, 3428.
71. J. H. Hays, A. DiSabatino, R. T. Gorman, S. Vincent, M. E. Stillabower, *Mayo Clin. Proc.*, 2003, **78**, 1331.
72. Y. Yang, G. Bai, X. Zhang, C. Ye, M. Liu, *Analyt. Biochem.*, 2004, **324**, 292.
73. G. Oz, P-G. Henry, E. R. Seaquist, R. Gruetter, *Neurochem. Int.*, 2003, **43**, 323.
74. O. Kunert, H. Stingl, E. Rosian, M. Krssak, E. Bernroider, W. Seebacher, K. Zangger, P. Staehr, V. Chandramouli, B. R. Landau, P. Nowotny, W. Waldhaeusl, E. Haslinger, M. Roden, *Diabetes*, 2003, **52**, 2475.
75. M. Otto, J. Breinholt, N. Westergaard, *Diab. Obes. Metab.*, 2003, **5**, 189.
76. A. J. Jenkins, W. T. Garvey, R. L. Klein, *Curr. Opins. Endocrinol. Diabetes*, 2003, **10**, 245.
77. A. J. Jenkins, T. J. Lyons, D. Zheng, J. D. Otvos, D. T. Lackland, D. McGee, W. T. Garvey, R. L. Klein, *Kidney Int.*, 2003, **64**, 817.
78. M. J. Kaufman, M. E. Henry, B. Frederick, J. Hennen, R. A. Villafuerte, E. P. Stoddard, M. E. Schmidt, B. M. Cohen, P. F. Renshaw, *Biol. Psychiatry*, 2003, **54**, 534.
79. E. Ackerstaff, K. Glunde, Z. M. Bhujwalla, *J. Cell. Biochem.*, 2003, **90**, 525.
80. W. A. Bubb, *Concepts Magn. Reson. Prt. A.*, 2003, **19A**, 1.
81. C. W. von der Leith, A. Bohne-Lang, K. K. Lohmann, *BIO spektrum*, 2003, **9**, 635.
82. J. D. Dyckjaer, K. Rasmussen, *Mini-Revs. Medicin. Chem.*, 2003, **3**, 713.
83. J. F. G. Vliegenthart, *Adv. Exp. Med. Biol.*, 2001, **491**, 133.
84. Y. Kimura, K. Tsumura, M. Kimura, K. Okihara, H. Sugimoto, H. Yamada, *Biosci. Biotechnol. Biochem.*, 2003, **67**, 1852.
85. K. Koles, P. H. C. van Berkel, F. R. Pieper, J. H. Nuijens, M. L. M. Mannesse, J. F. G. Vliegenthart, J. P. Kamerling, *Glycobiol.*, 2004, **14**, 51.
86. H. R. Mellor, J. Nolan, L. Pickering, M. R. Wormald, F. M. Platt, R. A. Dwek, G. W. J. Fleet, T. D. Butters, *Biochem. J.*, 2002, **366**, 225.
87. R. Fiala, Z. Sulova, A. H. El-Saggan, B. Uhrik, T. Liptaj, I. Dovinova, E. Hanusovska, Z. Drobna, M. Barancik, A. Breier, *Biochim. Biophys. Acta*, 2003, **1639**, 213.
88. C. Fernandez, K. Wurthrich, *FEBS Letts.*, 2003, **555**, 144.

89. Y. I. Wu, H. G. Munshi, R. Sen, S. J. Snipas, G. S. Salvesen, R. Fridman, M. S. Stack, *J. Biol. Chem.*, 2004, **279**, 8278.
90. J. Meiler, *J. Biomolec. NMR.*, 2003, **26**, 25.
91. C. A. E. M. Spronk, S. B. Nabuurs, A. M. J. J. Bonvin, E. Kieiger, G. W. Vuister, G. Vriend, *J. Biomolec. NMR.*, 2003, **25**, 225.
92. J. H. Prestegard, N. U. Jain, S. B. Levery, *Encycloped. Nuclr. Magn. Reson.*, 2002, **9**, 441.
93. M. Martin-Pastor, A. Canales-Mayordomo, J. Jimenez-Barbero, *J. Biomoleclr. NMR*, 2003, **26**, 345.
94. O. Millet, R. P. Hudson, L. E. Kay, *Proc. Natl. Acad. Sci. U. S. A.*, 2003, **100**, 12700.
95. F. Belot, A. Otter, M. Fukuda, O. Hindsgaul, *Synlett*, 2003, **9**, 1315.
96. R. Lucas, J. Angulo, P. M. Niesto, M. Martin-Lomas, *Org. Biomolec. Chem.*, 2003, **1**, 2253.
97. G. D'Auria, G. Flores, L. Falcigno, R. Oliva, M. Vacatello, M. M. Corsaro, M. Parrilli, L. Paolillo, *Biopolymers*, 2003, **70**, 260.
98. H. Nakatani, *Biochem. J.*, 2002, **365**, 701.
99. M. Takeda, H. Terasawa, M. Sakakura, Y. Yamaguchi, M. Kajiwara, H. Kawashima, M. Miyasaka, I. Shimada, *J. Biol. Chem.*, 2003, **278**, 43550.
100. J. S. Grinstead, J. T. Schuman, A. P. Campbell, *Biochem.*, 2003, **42**, 14293.
101. R. Gutierrez Gallego, G. Dudziak, U. Kragl, C. Wandrey, J. P. Kamerling, J. F. G. Vliegenthart, *Biochemie*, 2003, **85**, 275.
102. R. D. Brokx, L. Revers, Q. Zhang, S. Yang, T. K. Mal, M. Ikura, J. Gariepy, *Biochem.*, 2003, **42**, 13817.
103. M. E. Daley, B. D. Sykes, *J. Biomolec. NMR*, 2004, **29**, 139.
104. C. Robbe, C. Capon, E. Maes, M. Rousset, A. Zweibaum, J-P. Zanetta, J-C. Michalski, *J. Biol. Chem.*, 2003, **278**, 46337.
105. M. A. Ringenberg, S. M. Steenbergen, E. R. Vimr, *Molec. Microbiol.*, 2003, **50**, 961.
106. P. Cescutti, G. Impallomeni, D. Garozzo, L. Sturiale, Y. Herasimenka, C. Lagatolla, R. Rizzo, *Carbohydr. Res.*, 2003, **338**, 2687.
107. O. A. Agrellos, C. Jones, A. R. Todeschini, J. O. Previato, L. Mendonca-Previato, *Molec. Biochem. Parasitol.*, 2003, **126**, 93.
108. D. Arosio, S. Baretti, S. Cattaldo, D. Potenza, A. Benardi, *Bioorgan. Medicin. Chem. Letts.*, 2003, **13**, 3831.
109. H-C. Siebert, S. Andre, S-Y. Lu, M. Frank, H. Kaltner, J. A. Van Kuik, E. Y. Korchagina, N. Bovin, E. Tajkhorshid, R. Kaptein, J. F. G. Vliegenthart, C-W. Von der Lieth, J. Jimenez-Barbero, J. Kopitz, H-J. Gabius, *Biochem.*, 2003, **42**, 14762.
110. F. Berti, P. Constantino, M. Fragai, C. Luchinat, *Biophys. J.*, 2004, **86**, 3.
111. J-R. Brisson, H. J. Jennings, *Adv. Expermntl. Med. Biol.*, 2001, **491**, 543.
112. M-J. Clement, A. Imberty, A. Phalipon, S. Perez, C. Simenel, L. A. Mulard, M. Delepierre, *J. Biol. Chem.*, 2003, **278**, 47928.
113. J. A. F. Joosten, B. J. Lazet, J. P. Kamerling, J. F. G. Vliegenthart, *Carbohydr. Res.*, 2003, **338**, 2629.
114. K. Lycknert, G. Widmalm, *Biomacromols.*, 2004, ACS ASAP.
115. J. Shao, M. Li, Q. Jia, Y. Lu, P. G. Wang, *FEBS Letts.*, 2003, **553**, 99.
116. E. V. Vinogradov, L. Brade, H. Brade, O. Holst, *Carbohydr. Res.*, 2003, **338**, 2751.
117. A. N. Kondakova, S. N. Senchenkova, A. I. Gremyakov, A. S. Shashkov, Y. A. Knirel, R. Fudala, W. Kaca, *Carbohydr. Res.*, 2003, **338**, 2387.
118. K. Kolodziejska, A. N. Kondakova, K. Zych, S. N. Senchenkova, A. S. Shashkov, Y. A. Knirel, Z Sidorczyk, *Carbohydr. Res.*, 2003, **338**, 2105.
119. R. Fudala, A. N. Kondakova, K. Bednarska, S. N. Senchenkova, A. S. Shashkov, Y.

A. Knirel, U. Zahringer, W. Kaca, *Carbohydr. Res.*, 2003, **338**, 1835.
120. A. Rozalski, A. V. Perepelov, B. Bartodziejska, S. N. Senchenkova, D. Babicka, W. Kaca, Y. A. Knirel, *Arch. Imm. Ther. Exp.*, 2003, **51**, 69.
121. A. N. Kondakova, K. Kolodziejska, K. Zych, S. N. Senchenkova, A. S. Shashkov, Y. A. Knirel, Z. Sidorczyk, *Carbohydr. Res.*, 2003, **338**, 1999.
122. K. Feher, P. Pristovsek, L. Szilagyi, D. Ljevakovic, J. Tomasic, *Bioorgan. Medicin. Chem.*, 2003, **11**, 3133.
123. E. Katzenellenbogen, N. A. Kocharova, G. V. Zatonsky, A. Korzeniowska-Kowal, A. S. Shashkov, Y. A. Knirel, *Carbohydr. Res.*, 2003, **338**, 2153.
124. O. V. Bystrova, B. Lindner, H. Moll, N. A. Kocharova, Y. A. Knirel, *Carbohydr. Res.*, 2003, **338**, 1801.
125. E. Vinogradov, A. Korenevsky, T. J. Beveridge, *Carbohydr. Res.*, 2003, **338**, 1991.
126. A. Molinaro, C. De Castro, R. Lanzetta, M. Parrilli, A. Raio, A. Zoina, *Carbohydr. Res.*, 2003, **338**, 2721.
127. D. N. Ostrovsky, G. R. Diomina, V. I. Biniukov, A. S. Shashkov, M. Schloter, *Microbiol.*, 2003, **72**, 528.
128. S. N. Senchenkova, Y. A. Knirel, A. S. Shashkov, M. Ahmed, A. Mavridis, K. Rudolph, *Carbohydr. Res.*, 2003, **338**, 2025.
129. A. S. Shashkov, G. M. Streshinskaya, L. N. Kosmachevskaya, S. N. Senchenkova, L. I. Evtushenko, I. B. Naumova, *Carbohydr. Res.*, 2003, **338**, 2021.
130. N. V. Potekhina, A. S. Shashkov, L. I. Evtushenko, S. N. Senchenkova, I. B. Naumova, *Carbohydr. Res.*, 2003, **338**, 2745.
131. C. Villeneuve, G. Etienne, V. Abadie, H. Montrozier, C. Bordier, F. Laval, M. Daffe, I. Marionneau-Parini, C. Astaric-Dequeker, *J. Biol. Chem.*, 2003, **278**, 51291.
132. E. A. Leitao, V. C. B. Bittencourt, R. M. T. Haido, A. P. Valente, J. Peter-Katalinic, M. Letzel, L. M. de Souza, E. Barreto-Bergter, *Glycobiol.*, 2003, **13**, 681.
133. S. Kumazawa, M. Kanda, M. Utagawa, N. Chiba, H. Ohtani, T. Mikawa, *J. Antiobiot.*, 2003, **56**, 652.
134. Z. Liu, P. R. Jensen, W. Fenical, *Phytochem.*, 2003, **64**, 571.
135. S. G. Batrakov, I. V. Konova, V. I. Sheichenko, L. A. Galanina, *Chem. Phys. Lipids*, 2003, **123**, 157.
136. B. Larsen, D. M. S. A. Salem, M. A. E. Sallam, M. M. Mishrikey, A. I. Beltagy, *Carbohydr. Res.*, 2003, **338**, 2325.
137. C. S. Vairappan, *Sci. Int.* (*Lahore*), 2003, **15**, 49.
138. T. R. Storseth, K. Hansen, J. Skjermo, J. Krane, *Carbohydr. Res.*, 2004, **339**, 421.
139. H. D. Chludil, A. P. Murray, A. M. Seldes, M. S. Maier, *Studies Natr. Prods. Chem.*, 2003, **28**, 587.
140. N. M. Carballeira, H. Cruz, E. A. Orellano, F. A. Gonzalez, *Chem. Phys. Lipids*, 2003, **126**, 149.
141. R. A. Andesen, C. L. Broadhurst, M. M. Polansky, W. F. Schmidt, A. Khan, V. P. Flanagan, N. W. Schoene, D. J. Graves, *J. Agricul. Food Chem.*, 2004, **52**, 65.
142. C. C. Barnes, M. K. Smalley, K. P. Manfredi, K. Kindscher, H. Loring, D. M. Sheeley, *J. Natr. Prods.*, 2003, **66**, 1457.
143. H. Liu, Z. Xiong, F. Li, G. Qu, H. Kobayashi, X. Yao, *Chem. Pharmaceut. Bull.*, 2003, **51**, 1089.
144. A. Tolonen, M. Pakonen, A. Hohtola, J. Jalonen, *Chem. Pharmaceut. Bull.*, 2003, **51**, 467.
145. A-C. Mitaine-Offer, T. Miyamoto, V. Laurens, C. Delaude, M-A. Lacaille-Dubois, *Helvetica Chim. Acta*, 2003, **86**, 2404.
146. K. Kazuma, N. Noda, M. Suzuki, , *Phytochem.*, 2003, **64**, 1133.

147. E. Pale, M. Kouda-Bonafos, M. Nacro, M. Vanhaelen, R. Vanhaelen-Fastre, *Phytochem.*, 2003, **64**, 1395.
148. T. Fossen, R. Slimestad, O. M. Andersen, *Phytochem.*, 2003, **64**, 1367.
149. S. Bonnely, A. L. Davis, J. R. Lewis, C. Astill, *Food Chem.*, 2003, **83**, 485.
150. Y. Tachibana, H. Kikuzaki, N. H. Lajis, N. Nakatani, *J. Agricul. Food Chem.*, 2003, **51**,6461.
151. T. Peterbauer, I. Brereton, A. Richter, *Carbohydr. Res.*, 2003, **338**, 2017.
152. P. Avato, M. A. Pesante, F. P. Fanizzi, C. Aimbire de Moraes Santos, *Lipids*, 2003, **38**, 773.
153. A. Braca, A. R. Bilia, J. Mendez, C. Pizza, I. Morelli, N. De Tommasi, *Studies Natr. Prod. Chem.*, 2003, **28**, 35.
154. A. Karioti, H. Skaltsa, J. Heilmann, O. Stitcher, *Phytochem.*, 2003, **64**, 655.
155. I. O. Vvedenskaya, R. T. Rosen, J. E. Guido, D. J. Russell, K. A. Mills, N. Vorsa, *J. Agricul. Food Chem.*, 2004, **52**, 188.
156. J. S. Roach, S. McLean, W. F. Reynolds, W. F. Tinto, *J. Natr. Prods.*, 2003, **66**,1378.
157. S. Khera, G. M. Woldemichael, M. P. Singh, E. Suarez, B. N. Timmermann, *J. Natr. Prod.*, 2003, **66**, 1628.
158. Y. Su, K. Koike, T. Nikaido, J. Liu, J. Zheng, D. Guo, , *J. Natr. Prod.*, 2003, **66**, 1593.
159. N. Germonprez, L. Van Puyvelde, L. Maes, M. V. Tri, N. De Kimpe, *Tetrahedron*, 2004, **60**, 219.
160. Y. Kumarasamy, L. Nahar, P. J. Cox, M. Jaspars, S. D. Sarker, *Phytomed.*, 2003, **10**, 344.
161. D-J. Yang, T-J. Lu, L. S. Hwang, *J. Agricul. Food Chem.*, 2003, **51**, 6438.
162. K. Ori, M. Koroda, Y. Mimaki, H. Sakagami, Y. Sashida, *Phytochem.*, 2003, **64**, 1351.
163. J. H. Chen, G. Y. Cui, J. Y. Liu, R. X. Tan, *Phytochem.*, 2003, **64**, 903.
164. L. Voutquenne, P. Guinot, O. Thoison, T. Sevenet, C. Lavaud, *Phytochem.*, 2003, **64**, 781.
165. A. Kardosova, A. Ebringerova, J. Alfoldi, G. Nosal'ova, S. Franova, V. Hribalova, *Int. J. Biologcl. Macromol.*, 2003, **33**, 135.
166. M. R. Vignon, L. Heux, M-E. Malainine, M. Mahrouz, *Carbohydr. Res.*, 2004, **339**, 123.
167. M. A. Kabel, H. A. Schols, A. G. J. Voragen, *ACS Symp. Series*, 2004, **864**, 108.
168. D. J. Kiemle, A. J. Stipanovic, K. E. Mayo, *ACS Symp. Series*, 2004, **864**, 122.
169. K. M. Holtman, H-m. Chang, J. F. Kadla, *J. Agricul. Food Chem.*, 2004, **52**, 720.
170. Y. Tamaki, S. Uechi, T. Taira, M. Ishihara, S. Adaniya, K. Uesato, M. Fukuda, M. Tako, *J. Appl. Glycosci.*, 2004, **51**, 19.
171. T. Hannuksela, C. Herve du Penhoat, *Carbohydr. Res.*, 2004, **339**, 301.
172. P. Rapp, L. H. E. Gabriel-Juergens, *Microbiol.*, 2003, **149**, 2879.
173. J. T. de Souza, M. de Boer, P. de Waard, T. A. van Beek, J,M. Raaijmakers, *Appl. Environmen. Microbiol.*, 2003, **69**, 7161.
174. J-L. Bonmatin, O. Laprevote, F. Peypoux, *Combinat. Chem. High Throughput Screen.*, 2003, **6**, 541.
175. S. Moutard, B. Perly, P. Gode, G. Demailly, F. Djedaini-Pilard, *J. Inclusion. Phenom. Macrocyc. Chem.*, 2003, **44**, 317.
176. N. Funasaki, S. Ishikawa, S. Neya, *J. Phys. Chem.*, 2003, **107**, 10094.
177. E. P. O'Brien, G. Moyna, *Carbohydr. Res.*, 2004, **339**, 87.
178. S. Kwon, J. H. Park, H. Chung, I. C. Kwon, S. Y. Jeong, I-S. Kim, *Langmuir*, 2003, **19**, 10188.

179. C. W. Harrell, M. E. McCarroll, K. F. Morris, E. J. Billiot, I. M. Warner, *Langmuir*, 2003, **19**, 10684.
180. E. Micklander, L. G. Thygesen, H. T. Pedersen, F. van den Berg, R. Bro, D. N. RutledgeS. B. Engelsen, *Special Publication – Roy. Soc. Chem. Magnetic resonance in Food Science. Royal Society of Chemistry Press*, 2002, **286**, 239.
181. D. R. Martin, S. Ablett, H. T. Pedersen, M. J. D. Mallett, *Special Publication Roy. Soc. Chem. Magnetic resonance in Food Science. Royal Society of Chemistry Press*, 2002, **286**, 54.
182. B. P. Hills, L. Meriodeau, K. M. Wright, *Special Publication – Roy. Soc. Chem.*, 2002, **286**, 186.
183. G. Knothe, *Lipid Technol.*, 2003, **15**, 111.
184. M. D. Guillen, A. Ruiz, *Eur. J. Lipid Sci. Tecnol.*, 2003, **105**, 688.
185. J. J. G. van Soest, *Chem. Funct. Props. Food Sacchs.*, 2004, 371.
186. K. P. Nott, S. M. Shaarani, L. D. Hall, *Special Publication – Roy. Soc. Chem.*, 2002, **286**, 38.
187. C. D. Nandini, P. V. Salimath, *J. Sci. Food Agricul.*, 2003, **83**, 1297.
188. A. P. Deshmukh, A. J. Simpson, P. G. Hatcher, *Phytochem.*, 2003, **64**, 1163.
189. M. J. Simpson, B. Chefetz, P. G. Hatcher, *J. Environ. Qual.*, 2003, **32**, 1750.
190. S. Hiradate, N. U. Yamaguchi, *J. Inorg. Biochem.*, 2003, **97**, 26.

11
Synthetic Macromolecules

BY HIROMICHI KUROSU AND TAKESHI YAMANOBE

1 Introduction

For synthetic macromolecules, NMR has been the most powerful method to characterize and to investigate the relationship between the structure and the physical properties. In the field of synthetic macromolecules, NMR is used not only as the routine analytical method but also as the method that has the infinite possibility. In this chapter, NMR applications for synthetic polymers are reviewed.

Cheng and English edited ACS symposium series which covers the solution and solid state NMR investigations for dendrimers, cellulose, polyurethane, polyolefins biopolymers, copolymers and so on[1]. Spiess described a historical overview of role of NMR spectroscopy in polymer science[2]. Newmark summarizes the two dimensional and pulsed gradient diffusion NMR experiments and their applications to polymers[3]. Shit *et al.* reviewed the analysis of polymer molecular weight and copolymer composition by NMR[4]. Sasanuma summarized the the analysis of polyethers and polysulfides by NMR and theoretical calculations[5]. Ardelean et al described the principle and its applications of diffusion studies by NMR[6]. Roy et al summarized the structural analysis of Novolak resins by multidimensional NMR[7]. Reviews about NMR study of surfactant[8], polymer blends[9] and the structural elucidation of supramocules[10] are published.

2 Primary structure

Characterizations of primary structures such as tacticity, regioregularity, end group, sequence distribution, and so on are investigated mainly by solution NMR. Table 1 summarizes the papers in which NMR is used to investigate the primary structure of polymers.

Nuclear Magnetic Resonance, Volume 34
© The Royal Society of Chemistry, 2005

Table 1

Polymer, monomer	*Nucleus*	*Contents*	*Ref.*
binaphthyl-polythiophene	H	molecular weight	11
block copolymer, 2-(1H,1H,2H,2H-perfluorohexyl)-2- oxazoline, 2-nonyl-2-oxazoline,2-methyl-2-oxazoline	H	molecular weight, end group	12
chlorinated polyethylene-graft-poly(methyle methacrylate)	H	graft degree, reaction kinetics	13
copolyamide, terephthaloyl chloride, p-phenylenediamine, 3,4′-diaminodiphenyl ether	C	sequence distribution, regioregularity	14
copolycarbonate, 1,4:3,6-dianhydro-D-glucitol, 1,4:3,6-dianhydro-D-mannitol	C	sequence distribution	15
copolyester, p,p′-bibenzoic acid, dimer acid, alkylene glycol		sequence distribution, composition	16
copolyester, poly(ethylene terephthalate) , p-hydroxybenzoic acid, bis(2-oxazoline)	H	sequence length	17
copolyetster, isophthalic acid , terephthalic acid, 2,2-bis(4-hydroxyphenyl)propane, hydroquinone, bisphenols		sequence distribution	18
copolyimide,polysiloxane, isophorone, aromatic tetracarboxylic dianhydride	H	sequence distribution	19
epoxy resin	H	branch	20
fluoropolyester, dicyclohexylcarbodiimide, 4-(dimethylamino)pyridium 4-toluenesulfonate	C	branch	21
fluoropolymers, poly(vinylidene fluoride-co-hexafluoropropene)	H, C,		22
liquid crystal polyester,4-(5-pentenyloxy)benzoic acid 1,4-phenylene ester, 4-(5-pentenyloxy)benzoic acid 1,4-t-butyl-phenylene ester	H	end group, molecular weight	23
natural rubber	C	configuration	24
novolak resins	H, C	reaction mechanism	25
nylon	O	hydrolysis, oxidation	26
nylon 66	O	hydrolysis, oxidation	27
perfluoroalkoxy resin		end group, branch, crosslinks	28
perfluoroalkyl end-capped poly(ethylene oxide)		end group	29
Phenolic resin	C	crosslink	30
phenolic resin	C	crosslink	31
poly((2-cyclopentylidene-1,3-dioxolane-4-yl)methyl methacrylate-co-styrene),poly((2-cyclopentylidene-1,3-dioxolane-4-yl)methyl methacrylate -co- acrylonitrile)	H, C	composition	32

poly((3S)-3-[(Benzyloxycarbonyl)methyl]morpholine-2,5-dione -co- ε-caprolactone)	C	sequence distribution	33
poly(1,1-dimethyl silabutane)	H,C	regioregularity	34
poly(1,2:5,6-dianhydro-D-mannitol)	C	branch	35
poly(1,3-cyclohexadiene)	H,C	configuration	36
poly(1,4-Anhydroerythritol), poly(1,4-anhydro-L-threitol)	C	branch	37
poly(1,4-Pentadiene-3-one-1-p-hydroxyphenyl-5-p-Ph methacrylate),poly(1,4-Pentadiene-3-one-1-p-hydroxyphenyl-5-p-Ph methacrylate-co-ethyl acrylate)	H	composition	38
poly(1,5-dioxepan-2-one) ,poly(1,5-dioxepan-2-one), poly(L-lactide)	H	crosslink	39
poly(1,7-octadiyne)		branch	40
poly(1,7-octadiyne)		branch	41
poly(1,9-decadiene)		configuration	42
poly(1-alkoxy-2,4-m-phenylenevinylene)	H	configuration	43
poly(1-hexene)	C	polymerization kinetics	44
poly(1-trimethylsilyl-1-propyne)	C	configuration	45
poly(1-vinylimidazole)	H	molecular weight	46
poly(2,3-dicarboalkoxynorbornene), poly(2,3-norbornadienes)		tacticity	47
poly(2,4,6-trinitrotoluene)	C, 15N	hydrolysis	48
poly(2-(2-bromoisobutyroyloxy)ethyl methacrylate-co-2-(diethylamino)ethyl methacrylate)	H,C	branch	49
poly(2-(4-tert-butylphenoxy)-2-oxo-ethyl methacrylate-co-methyl methacrylate)	H,C	composition	50
poly(2-(dimethylamino)ethyl methacrylate), poly(2-(dimethylamino)ethyl-co-polyethylene glycol methacrylate)	H	branch	51
poly(2-(dimethylamino)ethyl methacrylate-co-methoxy hexa(ethylene glycol) methacrylate)	H	composition	52
poly(2-(dimethylamino)ethyl-2-methacrylate)-graft-poly(ethylene oxide)	C	graft length	53
poly(2-[(2-bromopropionyl)oxy]ethyl acrylate-co-me acrylate)		branch	54
poly(2-ethylhexyl acrylates)	H	branch	55
poly(2-hydroxyethyl aspartamide)-graft-dehydrocholic acid	H	composition, graft	56
poly(2-hydroxyethyl methacrylate)		composition	57
poly(2-hydroxyethyl methacrylate)-linked-polyisobutylene	H	composition	58
poly(2-methyl-1,3-pentadiene-block-styrene)		composition	59
poly(2-vinylnaphthalene)	H	end group	60
poly(3,3-bis(hydroxymethyl)oxetane)	C	branch	61

Table 1 *(cont.)*

Polymer, monomer	*Nucleus*	*Contents*	*Ref.*
poly(3.5-dihydroxybenzoic acid)	C	polycondensation kinetics, composition	62
poly(3-alkoxythiophenes)		regioregularity	63
poly(3-alkoxythiophenes)	H	regioregularity	64
poly(3-ethyl-3-(hydroxymethyl)oxetane)	C	branch	65
poly(4,4-dialkylcyclopentadithiophenes)		end group	66
poly(4-(3′,4′-Dimethoxycinnamoyl)phenyl acrylate-co-methyl methacrylate)	H	composition	67
poly(4-(Benzyloxycarbonyl)phenyl acrylate), poly(4-(Benzyloxycarbonyl)phenyl acrylate -co-glycidyl methacrylate)	H,C	composition	68
poly(4-benzyloxycarbonylphenyl acrylate-co-methyl methacrylate)	H,C	composition	69
poly(4-benzyloxycarbonylphenyl methacrylate-co-glycidyl methacrylate)	H, C	composition	70
poly(4-ethynylbenzoic acid)		configuration	71
poly(4-methyl-1-pentene)	H,C	configuration	72
poly(4-propanoylphenyl methacrylate-co-glycidyl methacrylate)	H	composition	73
poly(4-Vinyl pyridine-co-methacrylonitrile)	H,C	composition	74
poly(5,6-Benzo-2-methylene-1,3-dioxepane-co-methyl methacrylate)	H	composition	75
poly(5,6-benzo-2-methylene-1,3-dioxepane-co-styrene	H	composition	76
poly(5-(methacryloyl oxyethylene amino carboxyl)methylene bicyclo[2.2.1]hept-2-ene), poly(methylmethacrylate)	H, C	configuration	77
poly(5-(methacryloyloxyethyleneaminocarboxyl)methylene bicyclo[2.2.1]hept-2-ene)	H,C	configuration	78
poly(6-{4-[4-(2-(2-bromoisobutyryloxy)hexyloxy)phenylazo]phenoxy}hexyl methacrylate)	H	branch	79
poly(8-aminoquinoline-co-o-anisidine)	H,C	composition	80
poly(acetalethers)	H	regioregularity	81
poly(acrylamide-co-4-vinylpyridine)	H	composition	82
poly(acrylamide-co-trans-4-methacroyloxyazobenzene)	C	composition	83
poly(acrylic acid)		branch	84
poly(acrylonitrile)		tacticity	85
poly(acrylonitrile-co-maethacrylic acid), poly(acrylonitrile-co-itaconic acid)	H,C	composition, sequence distribution	86

poly(acrylonitrile-co-methyl methacrylate), poly(acrylonitrile-co-glycidyl methacrylate), poly(acrylonitrile-co-acrylic acid), poly(acrylonitrile-co-styrene),poly(acrylonitrile-co-vinylidene chloride)	H,C	composition, sequence distribution	87
poly(acrylonitrile-co-methyle methacrylate), poly(acrylonitrile-co-glycidyl methacrylate)	H, C	tacticity	88
poly(acrylonitrile-co-styrene-co-acrylic acid)	H,C	composition, assignment	89
poly(alkylene D-glucaramides),	H	end group, stereoregularity	90
poly(alkynylsilane)	H, C, Si, P	regioregularity	91
poly(allyl chloride)	H	branch	92
poly(α-(trifluoromethyl)acrylic acid-co-vinylidene fluoride)	H,	composition	93
poly(amide-imide)	H	branch	94
poly(aryl ester)	H	branch	95
poly(arylene arylene phosphine oxide)	P	branch	96
poly(arylene arylene phosphine oxide)	P	branch	97
poly(aryleneethynylene), 1,3,5-triethynylbenzene, 1-hexyloxy-2,4,6-triethynylbenzene, tris(4-ethynylphenyl)phenylsilane, tris(4-ethynylphenyl)phosphine oxide	P	branch	98
poly(aspartic acid-co-lactic acid)		branch	99
poly(behenyl acrylate-co-behenyl fumarate)	H	composition	100
poly(benzyl methacrylate-co-2-(dimethylamino)ethyl methacrylate), poly(enzyl methacrylate-co-hexa(ethylene glycol) methacrylate)	H	composition	101
poly(benzyl-malate) (PMLABe), poly(hexyl-malate) (PMLAHe), and poly(malic acid-co-benzyl-malate)	H	degradation	102
poly(beta-D,L-butyrolactone)	C	tacticity	103
poly(butadiene)	H, C	configuration	104
poly(butadiene), poly(butadiene-co-styrene), poly(butadiene-co-glycidyl methacrylate)	C	configuration	105
poly(butadiene-co-isoprene)	C	composition, tacticity, sequence distribution	106
poly(butyl vinyl ether)	C	tacticity	107
poly(butylene succinate-co-butylene fumarate)	H	composition	108
poly(butylene terephthalate)-co-poly(butylene succinate)-block-poly(ethylene glycol)	H	sequence length	109

Table 1 *(cont.)*

Polymer, monomer	*Nucleus*	*Contents*	*Ref.*
poly(butylene terephthalate)-poly(ethylene terephthalate-co-isophthalate-co-sebacate)	H	sequence length	110
poly(butylene terephthalate-co-cyclohexylenedimethylene terephthalate)	C	sequence distribution	111
Poly(carbosilane)	Si	branch	112
poly(carbosiloxane), 1,4-bis(dimethylsilyl)benzene, 1,3-bis(dimethylsilyl)benzene, 4,4′-bis(dimethylsilyl)benzene, 9,9′-bis[4-(dimethylsilyl)-phenyl]fluorene	H	sequential distribution	113
poly(catechin-aldehyde)		regioregularity	114
poly(chloromethyl styrene)	H	molecular weight	115
poly(chlorotrifluoroethylene)		branch, end group	116
poly(cyclic ketene acetals-co-styrene),2-ethylidene-4-methyl-1, 3-dioxolane, 2-ethylidene-4 ethyl-1,3-dioxolane, 2-ethylidene-1,3-dioxepane, 2-ethylidene-1,3-dioxane	H	composition	117
poly(cyclohexa-1,3-diene)	H,C	configuration	118
poly(cyclohexene carbonate).	H	sequence distribution	119
poly(cyclohexene oxide)	P,	end group	120
Poly(D,L-lactic acid)-methoxypoly(ethylene glycol)	H	composition	121
poly(D,L-lactide)	C	tacticity	122
Poly(dimethyl siloxane)-polyamide, isophthaloyl dichloride, diamino poly(di-Me siloxane) 3,4′-diaminodiphenyl ether	H	sequence distribution	123
poly(dimethylsiloxane-co-acrylate)		composition	124
poly(DL-lactide-co-ethylphosphate)	H,P	composition	125
poly(ε.-caprolactone-co-L-lactide)	H,C	sequence distribution	126
poly(ε-caprolactone)	H	end group	127
poly(ε-caprolactone-block-tetrahydrofuran-block-ε-caprolactone)	H,C	composition	128
poly(ε-caprolactone)	H	end group	129
poly(ε-caprolactone)	H	degree of polymerization	130
poly(ester amide), glutaric anhydride, α-ω-aminoalcohols	H	sequence distribution	131
poly(ester amide),chloroacetic acid, N-chloroacetyl-beta-alanine		sequence distribution	132
poly(ester urethane)	15N	degradation	133
poly(ester-amide)		branch	134

poly(ester-imide), N-[3- or 4-bis(4-acetoxyphenyl)toluoyl]-4-carboxyl-phthalimide, N-{3- or 4-[1,1-bis(4-acetoxyphenyl)]ethylphenyl}-4-carboxy phthalimides	H,C	branch	135
poly(ethene-co-1-octene)		end group	136
poly(Ethene-co-norbornene)	C	sequence distribution	137
poly(ether imide)	H	branch	138
poly(ether imide),N-[3- or 4-bis(4-hydroxyphenyl)toluoyl]-4-chlorophthalimide, N-{3- or 4-[1,1-bis(4-hydroxyphenyl)]ethylphenyl}-4-chlorophthalimides	H	branch	139
Poly(ether sulfone), polycondensation of silylated 4-tert-butylcatechol, 4,4′-difluorodiphenylsulfone	H	end group	140
poly(ethyl glyoxylate)-	H, C	tacticity	141
poly(ethyl methacrylate-co-N-phenylmaleimide-co-itaconic acid)	H	composition	142
poly(ethylene acrylate-block-ethylene oxide-block-ethylene acrylate)		composition	143
poly(ethylene glycol)	H,C	end group	144
poly(ethylene glycol) endcapped poly(ethylene terephthalate)	H	end group	145
poly(ethylene glycol) methacrylate,poly(propylene glycol) methacrylate		end group, branch	146
poly(ethylene glycol), poly(ethylene oxide)	H, C, Si	branch	147
poly(ethylene glycol-block- butylene terephthalate),poly(ethylene glycol-block-butylene succinate)		composition	148
poly(ethylene oxide)	H,P	end group	149
poly(ethylene oxide)		molecular weight	150
poly(ethylene oxide)-block-poly[(R)-3-hydroxy butyrate]-block-poly(ethylene oxide)	H	sequence distribution	151
poly(ethylene oxide-block-1,1,2,2-tetrahydroperfluorodecyl acrylate)	H	molecular weight	152
poly(ethylene terephthalate)		end group	153
poly(ethylene terephthalate)	H	degradation	154
poly(ethylene terephthalate)	H	degradation	155
poly(ethylene terephthalate-block-1,4-butylene succinate)	H, C	composition	156
poly(ethylene terephthalate-co-butylene terephthalate)	C	sequential distribution	157
poly(ethylene terephthalate-co-epsiln-caprolactone)		composition, sequence distribution	158
poly(ethylene/1,4-cyclohexanedimethylene terephthalate)	H,C	sequence distribution	159
poly(ethylene/trimethylene terephthalate/2,6-naphthalate),	H	sequence distribution	160

Table 1 *(cont.)*

Polymer, monomer	*Nucleus*	*Contents*	*Ref.*
poly(ethylene-Bu acrylate-carbon monoxide)	H, P, Si, Sn	end group, tacticity	161
poly(ethylene-co-1-butene)	H,C	tacticity, sequence distribution	162
poly(ethylene-co-1-octene)		end group	163
poly(ethylene-co-5-hexen-1-ol)	C	sequence distribution	164
poly(ethylene-co-9-(bicyclo[2.2.1.]hept-5-en-2-ylmethyl)-9h-carbazole)	H,C	configuration	165
poly(ethylene-co-α-Olefin)	C	sequence distribution	166
poly(ethylene-co-butene)	H, C	tacticity, sequence distribution	167
poly(ethylene-co-butene)	H,C	tacticity,sequence distribution	168
poly(ethylene-co-hexene), poly(ethylene-co-octene)		branch	169
poly(ethylene-co-n-butylacrylate-co-carbon monoxide)	2H, P, Si, 119Sn	end group, tacticity	170
poly(ethylene-co-propylene)		branch	171
poly(ethylene-co-propylene)	C	regioregularity	172
poly(ethylene-co-propylene-co-1-decene)	C	sequence distribution	173
poly(etramethyl-p-silphenylene-3,3,3-trifluoropropylmethyl-co-di-Me siloxane)	H,Si	composition	174
poly(γ-butyrolactone-co-ε-caprolactone)	H,C	sequence distribution	175
poly(glycidyl methacrylate-co-butyl acrylate)	H, C	composition, reactivity	176
poly(glycidyl methacrylate-co-vinylidene chloride)	H, C	composition	177
poly(hexene-1)		branch	178
poly(hydroquinone), poly(resorcinol)	C	branch	179
Poly(hydroxybutyrate-co-hydroxyvalerate)	H	composition	180
poly(hydroxyethyl methacrylate),poly(hydroxypropyl methacrylate), poly(ethylene glycol)-graft-poly(methacrylate), poly(propylene glycol) -graft-poly(methacrylate)		end group	181
poly(hydroxyethyl methacrylate-block-methylphenylsilane- block-hydroxyethyl methacrylate), poly[oligo(ethylene glycol) Me ether methacrylate-block-methylphenylsilane- block-oligo(ethylene glycol) Me ether methacrylate]	H, C	molecular weight	182

poly(isoprene-block-styrene)	H	configuration	183
poly(L,L-lactide-co-ε-caprolactone)		sequence distribution, sequence length	184
poly(L-alanine)-block-poly(2-acryloyloxyethyl-lactoside)-block-poly(L-alanine)		composition, molecular weight	185
poly(L-lactide)	H,C	tacticity	186
poly(L-lactide)	H	molecular weight	187
poly(L-lactide), poly(D,L-lactide)	H	tacticity	188
poly(L-lactide),poly(ε-caprolactone)	H	composition	189
poly(L-lactide)-block-poly(ε-caprolactone)	H	degradation	190
poly(L-lactide-block-butylene succinate-block-L-lactide)	C	sequence distribution, sequence length	191
poly(L-lactide-co-beta-malic acid)	H	composition	192
poly(L-lactide-co-RS-beta-malic acid)	H	composition	193
poly(leucine-beta-Bzl-aspartate-valine)	H	composition	194
poly(m-phenylenevinylene-co-2,5-dioctyl-oxy-p-phenylenevinylene)		configuration	195
poly(maleimide-co-styrene),4-maleimidobenzoic acid, hydroquinone, hexadecyloxybenzoic acid	H,C	sequence distribution	196
poly(Me methacrylate), polystyrene, poly(Bu acrylate), polybutadiene		composition, sequence distribution	197
poly(methacrylic acid-co-ethyl acrylate)	H,C	composition	198
poly(methacrylimide)		composition	199
poly(methacrylonitrile-co-styrene-co-methyl methacrylate)	H,C	composition	200
poly(methl methacrylate-block-butyl acrylate)	H,C	end group	201
poly(methyl 2,4-hexadienoate), poly(ethyl 2,4-hexadienoate)		tacticity	202
poly(methyl acrylate-co-styrene),poly(butyl acrylate-co-styrene)	C	sequence distribution, sequence length	203
poly(methyl α-isobutylacrylate)		configuration	204
poly(methyl methacrylate)	C	tacticity	205
poly(methyl methacrylate)	H	branch	206
poly(methyl methacrylate)	C	tacticity	207
poly(methyl methacrylate)	H,C	composition, branch	208
poly(methyl methacrylate)	H	tacticity	209

Table 1 *(cont.)*

Polymer, monomer	*Nucleus*	*Contents*	*Ref.*
poly(methyl methacrylate)	H,C	end group	210
poly(methyl methacrylate).	H	tacticity	211
poly(methyl methacrylate-co- N-(p-tolyl)itaconimide),poly(methyl methacrylate-co-N-phenylitaconimide)	H	composition	212
poly(methyl methacrylate-co-ethyl acrylate)	C	sequence distribution, configuration	213
poly(methyl methacrylate-co-methyl acrylate), poly(methyl methacrylate-co-ethyl acrylate), poly(methyl methacrylate-co-butyl acrylate)	H, C	composition, tacticity	214
poly(methyl methacrylate-co-N,N-dimethylacrylamide)		composition	215
poly(methyl methacrylate-co-styrene)	H,C	sequential distribution	216
poly(methyl vinyl ether-co-maleic anhydride)		crosslink	217
poly(methylene oxide-co-butylene oxide)	C	sequence distribution	218
poly(methylidene-co-trimethylsilylmethylidene)	H,C	sequence distribution	219
poly(N-(5-sorbyl-pentyl)-N′,N″-di(n-octyl)benzene-1,3,5-tricarboxamide)	H,C	configuration	220
poly(N-(o-/m-/p-chlorophenyl) itaconimide-co-methyl methacrylate)	H	composition	221
poly(N-2-biphenylmaleimide) , poly(N-(2-phenoxy)-phenylmaleimide)	C	tacticity	222
poly(N-acryloyl β-alanine-block-N-iso-propyl acrylamide),poly(N-acryloyl β-alanine)	H	molecular weight	223
poly(N-acryloylmorpholine)	H	molecular weight	224
poly(n-butyl acrylate-co-carbon monoxide-co-ethylene)	H,C	composition, branch	225
poly(n-butyl acrylate-co-carbon monoxide-co-ethylene)	H,C	sequence distribution	226
poly(n-decyl itaconate),poly(n-dodecyl itaconate),poly(n-decyl itaconate-co-styrene),poly(n-dodecyl itaconate-co-styrene)	H	composition	227
poly(N-hexyl isocyanate -block-isoprene-block-N-hexyl isocyanate)	H	composition	228
poly(N-hydroxysuccinimide methacrylate)	H	molecular weight	229
poly(N-isopropylacrylamide)	H	end group	230
poly(N-isopropylacrylamide), poly(acrylamide)	H	reaction kinetics	231
poly(n-octyl acrylate-co-styrene)	H	sequence distribution	232
poly(N-phenyl methacrylamide-co-methyl methacrylate)	H	composition	233

poly(N-propargylamides)	H	stereoregularity	234
poly(N-triphenylmethylmethacrylamide)	H	stereoregularity	235
poly(N-vinyl-2-pyrrolidone-co- methacrylonitrile)	H,C	composition	236
poly(norbornene)		configuration	237
poly(norbornene)		configuration	238
poly(norbornene)		end group	239
poly(norbornene),poly(norbornadiene)	H,C	tacticity	240
poly(ortho ester), poly(d,l-lactide-co-glycolide)	H	degradation	241
poly(oxypropylene) and poly(oxypropylene-co-glycerol)	H, C	sequence distribution, irregularity	242
poly(p-(iodomethyl)styrene)		branch	243
poly(p-(p-methoxyphenylethynyl)phenylacetylene),poly(p-(p-butoxyphenylethynyl)phenylacetylene)		configuration	244
poly(phenylenevinylene-block-phenyleneethynylene)	C	sequence distribution	245
poly(phenylethyl acrylate-co-methacrylate)	H	composition	246
poly(phosphate ester)	H,P	composition, molecular weight, end group	247
poly(propene-co-norbornene)	C	sequential distribution	248
poly(propylene carbonate)		sequential distribution	249
poly(propylene carbonate)	C	sequence distribution	250
poly(propylene glycol) methacrylate		molecular weight	251
poly(propylene oxide)	C	tacticity, regioregularity	252
poly(propylene)	C	tacticity	253
poly(propylene-co-1-butene)	C	sequence distribution	254
poly(propylene-co-1-butene), poly(propylene-co-1-hexene), poly(propylene-co-1-octene)	C	branch, sequence distribution	255
poly(propylene-co-ethylene-co-butene-1)	C	sequence distribution	256
poly(propylene-co-ethylene-co-butene-1)	C	composition, sequence distribution	257
poly(siloxane)	C	crosslink	258
poly(silphenylenesiloxane)	H, C, Si	sequence distribution	259
poly(silsesquioxane), poly(dimethylsiloxane)	H,Si	sequence distribution, ladder, cage	260
poly(silylenemethylene)		configuration	261
poly(stearyl methacrylate-co-styrene-co-vinyl pyrrolidinone)		molecular weight	262
poly(styrene-α-methylstyrene-co-acrylonitrile)	C	degradation	263

Table 1 *(cont.)*

Polymer, monomer	*Nucleus*	*Contents*	*Ref.*
poly(styrene-block- tert-butyl acrylate-block-methyl methacrylate)	H	composition	264
poly(styrene-co-1-(vinylbenzyl)thymine)	H	composition	265
poly(styrene-co-α-methylstyrene)	H	composition	266
poly(styrene-co-butadiene)	C	sequence distribution	267
poly(styrene-co-Et acrylate)		end group, tacticity, composition	268
poly(styrene-co-ethylene), poly(α-methylstyrene-co-ethylene)	C	degradation	269
poly(styrene-co-maleic anhydride)	C	sequence distribution	270
poly(styrene-co-maleic anhydride)	C	sequence distribution	271
poly(styryl)lithium	H,C	end group, configuration	272
poly(styryl)lithium	C	end group, configuration	273
poly(tetrafluoroethylene), poly(chlorotrifluoroethylene), poly(ethylene-chlorotrifluoroethylene), poly(tetrafluoroethylene-co-tetrafluoro-ethylene perfluoropropyl ether)		composition	274
poly(tetrafluoroethylene-co-4,5,5-trifluoro-4-ene pentyl acetate)		composition	275
poly(tetrafluoroethylene-co-hexafluoropropylene)		composition	276
poly(tetrafluoroethylene-co-hexafluoropropylene)		branch	277
poly(tetrafluoroethylene-co-perfluoropropyl vinyl ether)		branch	278
poly(thiophene-co-thiazole)	H	regioregularity	279
poly(trimethylene-co-butylene terephthalate)	C	sequence distribution, sequence length	280
poly(urea-urethane)	H,C	branch	281
poly(vinyl acetate)	H	end group	282
poly(vinyl acetate-co-dibutyl maleate)	H	composition	283
Poly(vinyl acetate-co-vinyl alcohol)	C	hydrolysis	284
poly(vinyl alcohol)		tacticity, irregularities	285
poly(vinyl alcohol)	H, C	tacticity	286
poly(vinyl chloride)	C	tacticity	287
poly(vinyl chloride),polypropylene	C	tacticity	288

poly(vinyl pyrrolidone-co-vinyl acetate),poly(acrylate-co-vinyl acetate)		composition	289
poly(vinyl pyrrolidone-co-vinyl acetate),poly(acrylate-co-vinyl acetate)		composition	290
poly(vinylbenzyl abietate), poly(vinylbenzyl abietate -co- methyl methacrylate)	H	composition	291
poly(vinylene-arsine)	H, C	sequence distribution	292
poly(vinylidene fluoride-co-hexafluoropropylene)	H,	end group	293
poly[(N-isopropylacrylamide-co-maleic anhydride)-γ-poly(ethylene oxide)],polyethylenimine	H,C	composition	294
poly[ω-(4′-cyano-4-biphenyloxy)alkyl-1-glycidylether]	H,C	regioregularity, tacticity	295
poly[pseudo(methyl methacrylate)-rotaxa-(dimethyl siloxane)]	H	composition	296
poly{2,5-bis[4′-2-(N,N-diethylamino)ethoxyphenyl]-1,4-phenylenevinylene}, poly{2,5-bis(4′-decyloxyphenyl)-1,4-phenylenevinylene-alt-2,5-bis[4′-2-(N,N-diethylamino)ethoxyphenyl]-1,4-phenylenevinylene}, poly(2,5-bis{4′-2-[2-(2- methoxyethoxy)ethoxy]ethoxyphenyl}-1,4-phenylenevinylene-alt-2,5-bis[4′-2-(N,N-diethylamino)ethoxyphenyl]-1,4-phenylenevinylene) , poly{2,5-bis(4′-decyloxyphenyl)-1,4-phenylenevinylene-alt-2,5-bis[4′-2-(N,N,N-triethylammonium)ethoxyphenyl]-1,4-phenylenevinylene} dibromide	H	configuration	297
Poly{bis(4,4′-tert-butyl-2,2′-bipyridine)-(2,2′-bipyridine-5,5′-diyl-[1,4-phenylene])-ruthenium(II)bishexafluorophosphate}, poly{bis(4,4′-tert-butyl-2,2′-bipyridine)-(2,2′-bipyridine-4,4′-diyl-[1,4-phenylene])-ruthenium(II)bishexafluorophosphate}, poly{bis(2,2′-bipyridine)-(2,2′-bipyridine-5,5′-diyl-[1,4-phenylene])-ruthenium(II)bishexafluorophosphate}	H,C	sequence distribution	298
poly{methylsulfonio-1,4-phenylenemethylsulfonio-1,4-phenyleneoxy-1,4-phenylene bis(triflate)}	H	branch	299
poly-1,2-(4-methyl-1,3-pentadiene)		tacticity	300
polyacetylene	H	configuration	301
polyalkoxysilane	Si	branch	302
polyamide-polyether-polyimide , trimellitic anhydride/4,4′-oxydianiline/m-phenylenediamine	H,C	composition	303
polyamides, polyurethane3,5-bis(4-aminophenoxy)benzoic acid	H,C	branch	304

Table 1 *(cont.)*

Polymer, monomer	*Nucleus*	*Contents*	*Ref.*
polyaniline	H,C	regioregularity	305
polyarylate, polyestercarbonate	H	sequence distribution	306
polybutadiene	H	tacticity	307
polybutadiene	C	tacticity	308
polydimethylsiloxane, polyhydrogenmethylsiloxane, polymethylphenylsiloxane	Si	sequence distribution	309
polydisilahydrocarbon, poly(tetramethyl-disilylene-ethylene)	Si	composition	310
polyepichlorohydrin	C	configuration	311
polyeste	H	end group, molecular weight	312
polyester	H	branch	313
polyester	C	branch	314
polyester, isophthalic acid, terephthalic acid,tetrachlorobisphenol A		sequence distribution	315
polyesteramide	H	degradation	316
polyether polyol	H,	end group	317
polyethercarbonate	H,C	sequence distribution	318
polyetherurethane,poly(tetramethylene oxide), poly(ethylene oxide), 4,4′-diphenylmethane diisocyanate	C	degradation	319
polyethylene	C	branch	320
polyethylene	C	branch	321
polyethylene	C	branch	322
polyethylene	C	branch	323
polyethylene	C	branch	324
polyethylene	C	branch	325
polyethylene	C	branch	326
polyethylene	C	branch	327
polyethylene		branch	328
polyethylene	C	branch	329
polyethylene	C	branch	330
polyethylene	C	branch	331
polyethylene		branch	332

polyethylene		branch	333
polyethylene	C	branch	334
polyethylene,poly(ethylene-co-1-heptene), poly(ethylene-co-1-octene),poly(ethylene-co-1-nonene)	H, C	irregularity, additives	335
polyethylene,poly(ethylene-co-1-heptene), poly(ethylene-co-1-octene),poly(ethylene-co-1-nonene)	H, C	irregularity, additives	336
polyethylene-graft-poly(ethylene oxide)		composition	337
polyethyleneimine		crosslink	338
polyglycidol	C	branch	339
polyglycidol	C	branch	340
polyglycidol	C	branch	341
polyimide	H	crosslink	342
polyimide	C	end group	343
polyimide, Cis-1,2,3,4-cyclohexanetetracarboxylic dianhydride,4,4′-oxydianiline, 4,4′-methylenedianiline, 4,4′-diamino-3,3′-dimethyldiphenylmethane, 4,4′-bis(4-aminophenoxy)benzene (TPEQ), 2,2-bis[4-(4-aminophenoxy)phenyl]propane	H	configuration, conformation	344
polyimide,di-phenyl (2,3-dihydro-2-thioxo-3-benzoxazolyl)phosphonate	H	branch	345
polyimide-poly(dimethylsiloxane)		end group	346
polyisobutylene	H	end group	347
polyisobutylene	H,C	end group	348
polyisoprene		tacticity	349
polyketone, 2-phenyl-1-methylenecyclopropane, carbon monoxide	H,C	configuration	350
polyketone, carbon monoxide, ethylene	C	sequence distribution	351
polylactide	H	end group, tacticity	352
polylactide-graft- chitosan	H	branch	353
polymethylhydrosiloxane	Si	pyrolysis	354
polynorbornadiene	H,C	configuration, branch	355
polynorbornane	H, C	tacticity	356
polynorbornene	C	reaction kinetics	357
polynorbornene	C	configuration	358
polynorbornene	C	configuration	359
polyoxyethylene		branch	360

Table 1 *(cont.)*

Polymer, monomer	*Nucleus*	*Contents*	*Ref.*
polypentadiene	C	configuration, tacticity	361
Polypropylene	C	tacticity	362
Polypropylene	C	end group	363
polypropylene	C	branch, tacticity	364
polypropylene	C	tacticity	365
polypropylene		polymerization kinetics	366
polypropylene	C	tacticity, branch	367
polypropylene	H	end group	368
polypropylene	C	tacticity, end group, regioselectivity	369
polypropylene	C	branch	370
polypropylene		end group	371
polypropylene	C	tacticity	372
polypropylene	C	tacticity	373
polypropylene	C	tacticity	374
polypropylene	C	tacticity	375
polypropylene	C	tacticity	376
polypropylene	C	tacticity	377
polypropylene	C	tacticity	378
polypropylene	C	branch	379
polypropylene	H	tacticity	380
polypropylene, poly(proprylene-co-ehtylene)	C	end group	381
polypropylene,poly(ethylene-co-propylene)	C	composition, blend	382
polysilane	H,Si	end group	383
polysilane	Si	sequence distribution	384
polysiloxane		tacticity	385
polysilsesquioxanes	Si	ladder polymer	386
polystyrene	C	tacticity	387

polystyrene	C	tacticity	388
polystyrene	C	tacticity	389
polystyrene, poly(methyl methacrylate)	H, C, P	polymerization kinetics	390
polystyrene, poly(methyl methacrylate), poly(styrene-co-methyl methacrylate)	C	end group	391
polystyrene, poly(methyl methacrylate), poly(styrene-co-methyl methacrylate)	C	end group	392
polythiophene, copolythiophene		composition	393
polytrimethylene terephthalate	H	end group, repeat unit	394
polyvinyl chloride	H	degradation	395
polyvinylbenzoate		composition, end group	396
sulfonated polystyrene		crosslink degradation	397
sulfur-cured natural rubber	C	crosslink	398
syndiotactic 1,2-polybutadiene	C	tacticity	399
tCum[poly(isobutylene-β-norbornadiene)]3, tCum[poly(norbornadiene-β-isobutylene)]3		molecular weight	400
telechelic hydroxy-terminated poly(ethylenebutylene)		end group	401
trans-1,4-polyisoprene	H	configuration	402

3 Liquid Crystalline Polymers

The self diffusion coefficient of poly(diethylsiloxane) in the temperature range from 10 to 50°C (in the solid and liquid crystalline state) is measured by steady field-gradient spin-echo ^{1}H NMR method and the diffusional behavior of poly(diethylsiloxane) in the liquid crystalline phase is elucidated[403-405]. The isotropic and anisotropic diffusion coefficients of highly oriented poly(γ-n-dodecyl L-glutamate) are measured as a function of temperature from 50-80°C by PFGSE ^{1}H NMR method and NMR imaging. The diffusion behavior in the thermo-tropic liquid crystalline state is analysed by the translational diffusion equation for rod-like polymers[406]. The orientational ordering and the electro-optical properties of nematic liquid crystal droplets confined to cross-linked polymer networks are studied as a function of the anchoring conditions at the polymer-liquid crystal interface by ^{13}C NMR[407]. Phase transition , structure and dynamics have been investigated for polyesters and polyurethanes with the same mesogen and spacer units by solid state ^{13}C NMR spectroscopy[408]. The dynamics of 5CB liquid crystalline molecules dispersed in the form of spherical microdroplets in a PDLC material is studied by ^{1}H NMR. From $T_{1\rho}$, the relaxation mechanism is discussed[409]. ^{2}H-NMR measurements were performed on dimer liquid crystals having an oxyethylene spacer. The orientational characteristics of the mesophase were studied by the ^{2}H-NMR method, leading to a conclusion that the oxyethylene-type spacer takes spatial arrangements characteristic of the nematic phase over a wide range of temperatures[410]. The director dynamics lyotropic cholesteric system PBLG/m-cresol 14% is investigated by Rheo NMR experiments where the sample is subjected to viscous, elastic and magnetic torques[411]. The rheological history dependent mechanical property of solutions of hydroxypropylcellulose in H_2O is studied by rheo-NMR method. The difference of high and low modulus state is elucidated[412]. The stereoselective separations of a cholesteric, chiral, liquid crystalline polyester PTOBEE is investigated by NMR diffusion measurements. The high degree of formation of a complex by self association of several polymer unit is presented[413]. The variable-angle ^{2}H-NMR measurements are applied to nematic liquid crystalline side-chain polymers. The existence of a biaxial nematic phase with the mesogenic group to the polymer backbone is obtained[414].

4 Imaging

The structure of the novolac-type phenolic resin/silica hybrid organic-inorganic nanocomposite is investigated by ^{29}Si NMR imaging. Obtained results revealed that tetrasubstituted and trisubstituted are the dominant microstructures[415]. The photopolymerization of acrylamide gels are studied by magnetic resonance imaging. The polymerization rate is constant until the monomer concentration is significantly depleted[416]. The penetration of water into the polyglycolid disks is monitored by MRI. Before 13 days, little change is observed, but after this time, water began to penetrate toward the center of disks. The combination of MRI

and drug release data support the hypothesis that drug releases quickly from the swollen regions behind the fronts where the polymer is open and porous, and that release finishes when the fronts meet in the center of the sample[417]. T_1, T_2 and diffusion coefficient measurements of PMMA and NIPA gel in situ and synchronized to phase transition are carried out. For the PMMA gel T_1, T_2 and diffusion coefficient decrease when gels undergo volume phase transition. At its contracted state, T_1 is reduced to a little less than one order of magnitude, T_2 over two orders of magnitude, and D over one order of magnitude, smaller from values of PMMA gel at the swollen state. At an elevated temperature, the thermosensitive NIPA gel is at a contracted state, with its D reduced to almost one order of magnitude smaller than that of the swollen NIPA at room temp[418]. The diffusion mechanism for water/ethanol in diacrylate dental resin is investigated by STRAFI method. It is obtained that the diffusion of this system is Fickian with coefficients that increases with alcohol contents[419]. MRI is used to get informations about the spatial distribution of the absorbed dose in the irradiated dosimeter[420]. Copolymers of 2-hydroxyethyl methacrylate and 1-vinyl-2-pyrrolidone in the form of cylindrical hydrogels have been prepared radiochemically and the sorption of water into these cylinders has been studied by the mass-uptake methods and by MRI. Diffusion coefficients of water are measured and the behavior of the obtained diffusion coefficients varies depending on the copolymer compositions[421]. The effect of the membrane thickness on the performance of polymer electrolyte membrane fuel cells was studied by MRI. The optimal conditions for the polymer electrolyte membrane fuel cell is discussed[422]. Penetration and spacial distribution of aborbed water are investigated for low density polyethylene-calcium lactate composite by NMR and MRI[423]. The diffusion behavior of water into poly(2-hydroxyethyl methacrylate) containing Aspirin or Vitamin B12 are studied. Depending on the containing drugs, the development of cracks is obserbed. It is concluded that the drugs work as plasticizer or antiplasticizer[424]. MRI and NMR are used to study the water absorption by nylon46, and its copolymers. The relation between water uptake, morphology and mobility is discussed[425]. The diffusion of water into cylinders of polyHEMA and copolymers of HEMA with THFMA, BMA and CHMA were studied over a range of copolymer compositions. The diffusion behaviors of water into the polymers are discussed[426]. ^{1}H-chem. shift NMR imaging patterns of a poly(methacrylic acid) gel containing water with paramagnetic praseodymium ions(Pr^{3+}) were successfully observed. By analysing these experimental results, the immersion process of Pr^{3+} ions into the network of the polymer gel was spatially clarified[427]. The potential for a polyelectrolyte gel to serve as a barrier to the migration of sodium chloride is examined[428]. A lot of papers about MRI contras agents are published[429-435].

5 Characterization of the Synthetic Macromolecules

Both the nanocomposites prepared by in-situ polymerization of 2-ethnylpyridine (2Epy) in the presence of a layered aluminosilicate such as Ca^{2+} -

montmorilonite (MMT) and enzymically synthesized conducting polyaniline (PANI) materials were investigated by solid-state ^{13}C cross-polarization/magic angle spinning (CP/MAS) NMR spectroscopy. The results of solid state NMR and X-ray diffraction (XRD) suggests that polymers are formed in the galleries of MMT of the nanocomposite. The polymers in the nanocomposite are mostly bound to the surface of the MMT either at the Broensted or Lewis acid sites. In the case of PANI, structure, dynamics of conducting polymer chains were probed by solid-state NMR spectroscopy[436]. Temperature-dependent ^{1}H NMR and dilute solution viscometry coupled with dynamic light scattering techniques were used to elucidate the aqueous phase conformation of several poly(vinyl alcohol)s (PVAs) differing in their molecular architecture (*i.e.*, degree of blockiness, molecular wt., and degree of hydrolysis). The aqueous phase conformation of semidilute poly(vinyl alcohol) solutions possessing different residual acetate sequence distributions (degree of blockiness) and molecular weights were studied as a function of polymer concentration[437]. ^{2}H NMR and small angle neutron scattering data are reported for deuterated guest chains of polydiethysiloxane (PDES) in end-linked PDES networks as a function of the molecular weight of guest chains relative to that of the network elastic chains. The ability of PDES networks to form a strain-induced mesophase is exploited to demonstrate the tendency of longer guest chains to phase separation or partition selectively to the amorphous phase and the tendency of smaller guest chains to remain distributed between the mesophase and the amorphous phase. The segmental orientation of the guest chains measured *via* ^{2}H NMR peak splitting can be interpreted in terms of an enthalpic orientational coupling of the chain segments in the amorphous state[438]. It is reported that the implementation of modern proton multiple-quantum NMR methods for the characterization of molecular order and dynamics in polymer networks and melts on cost-efficient low-resolution low-field NMR instrumentation. The method permits the extension of chain order parameter distributions, and is therefore sensitive to a heterogeneity of cross-links and other topology constraints. Experiments were carried out on polydimethylsiloxane model networks prepared by end-linking of precursor polymers with average molecular weights of 40,700 and 780 g/mol. Data from samples with bimodal network chain length distributions acquired at 20 MHz (0.47 T) are in quantitative agreement with results obtained at high field (500 MHz). It is shown for the first time that the chain order distribution is broadened upon swelling, providing evidence for the nontrivial nature of the swelling process[439]. The prediction of amorphous physical stability by differential scanning calorimetry (DSC) was compared to proton relaxation measurements using variable temperature solid state NMR for drug melts and drug/polyvinylpyrrolidone (PVP) co-melts. Such proton relaxation measurements are a valuable additional tool to thermal analytical methods for predicting the amorphous physical stability. For amorphous drug melts and drug/PVP co-melts, measurements of the spin-lattice relaxation time in the rotating frame provide an insight into amorphous stability that is different to that of DSC glass transition temperature (Tg) measurements. NMR relaxation measurements lead to an improved est. of amorphous physical stability compared to DSC Tg determination[440]. ^{13}C MAS NMR was used to

determine the conformational change of hydrophobically end-capped poly(ethylene oxide), HEUR. The hydrophobic alkyl chains on both ends changed from trans to gauche with increasing temperature, while the poly(ethylene oxide) (PEO) main chain was either crystalline or amorphous (less-ordered crystalline) depending on temperature. The increased crystallinity due to intermolecular interaction of the PEO main chains increases the affinity of end hydrocarbons and results in a phase transition from trans to gauche form. Hydrocarbons on both ends functioned as spacers, and they increase the intermolecular spacing between the PEO main chains, where deshielding of ^{13}C signal and distinct crystalline and amorphous ^{13}C NMR peaks were observed[441]. Acrylonitrile-styrene-acrylic acid (N/S/A) terpolymers were prepared and analysed by NMR spectroscopy. The compositions of terpolymers were determined by quantitative ^{13}C $\{^1H\}$ NMR spectra and compared with those calculated by Goldfinger's equation using comonomer reactivity ratios: rns = 0.04, rsn = 0.35; rna = 0.81, ran = 2.99; rsa = 0.80, ras = 0.10. Complete spectral assignments of ^{13}C and ^1H NMR spectra were done with the help of DEPT and two dimensional ^{13}C -^1H heteronuclear single quantum coherence (HSQC) and total correlated spectroscopy (TOCSY). The methine and methylene carbon resonances showed compositional sensitivity. 2D NOESY was used to ascertain the spatial proton-proton couplings[442]. The dyad and triad-level sequence analysis of polyarylate; U-Polymer, which is an aromatic copolyester of bisphenol-A and 50/50 isophthalic/terephthalic acid, and of polyestercarbonate prepared from U-Polymer and bisphenol-A polycarbonate were reported in a solvent system of o-chlorophenol/deuterated chloroform mixture (75/25 vol./vol.) at 80°C using 600 MHz proton NMR (^1H NMR). The well-resolved proton peaks were observed, which made the detailed sequence analysis possible. The methyl proton peaks of the bisphenol-A units were split into the dyad sequence in the chain. The aromatic proton peaks of the isophthalic and terephthalic units were split into the triad sequence in the chain. It was confirmed that the sequence distribution in U-Polymer and the polyestercarbonate are random and obey Bernoullian statistics, and the dyad and triad information obtained coincides with each other by a comparison of the number-average sequence lengths from the dyad and triad sequences. ^{13}C NMR peaks of the aliphatic quaternary carbons of bisphenol-A units were also split into the dyad sequence in the chain. It was confirmed that the solvent system of the 75/25 (vol./vol.) mixture of o-chlorophenol /deuterated chloroform has the potentiality for the detailed sequence analysis of polyarylate and polyestercarbonate[443]. The microphase composition. of poly(butylene terephthalate)-block-poly(tetramethylene oxide) multiblock (PBT-block-PTMO) copolymers with varying content of PTMO soft block and varying block length was studied by ^1H NMR transverse magnetization relaxation (T_2 relaxation) and ^1H 2D DQ NMR experiments under fast MAS. The 2D NMR method showed the existence of the molecular scale mixing of PBT and PTMO blocks. The ^1H and previously obtained ^{13}C NMR relaxation data provided detailed information on the microphase composition. The content of soft domains (*i.e.*, viscoelastic material which is composed of the soft block and mixed PBT) and hard domains (*i.e.*, crystal PBT and immobilized PBT chain portions

at the crystal-amorphous PBT interface) depends largely on temperature. It was shown that about 15-25% of PBT in the samples is soft due to molecular mixing with PTMO. The results suggest that at 40 °C the mixed phase is composed of approximately one PBT chain unit per eight PTMO chain units. The PBT crystallinity in the copolymers slightly increases with increasing length of the soft block, since this causes increase of the average length of PBT blocks. The content of crystalline PBT is nearly constant for samples with hard blocks containing more than five monomer units and decreases for shorter PBT block lengths[444]. By introducing dipolar recoupling methods to high-resolution MAS NMR spectroscopy, a class of experiments has been delevoped that allows the measurement of residual dipole-dipole couplings of approximately 1 Hz in weakly immobilized molecules. Using homonuclear ^{1}H -^{1}H recoupling, distances of up to approximately 8 angstrom can be selectively determined, while heteronuclear ^{1}H-^{13}C recoupling provides access to dynamic order parameters of individual molecular segments on the order of approximately 10^{-3}.[445] The ^{129}Xe-NMR method was used for evaluation of the sizes of free volume elements in amorphous glassy materials – random copolymers of tetrafluoroethylene and perfluorodioxoles of different structures. ^{129}Xe chemical shifts were measured at different pressures up to 1060 Torr. The zero pressure chemical shifts obtained by extrapolation were used for calculation of the diameters of microcavities having spherical and cylindrical shapes. The sizes of microcavities are consistent with those found by means of positron annihilation lifetimes and inverse gas chromatography methods[446]. A large number of para-substituted benzene thiols and the corresponding disulfides were synthesized and characterized by ^{1}H NMR, ^{13}C NMR, and IR spectroscopies. Geometries of all sixteen thiols and fourteen disulfide compounds were optimized at the B3LYP/6-31G(d) level, while the electronic structure and the ^{13}C isotropic shifts were calculated by ab initio Hartree-Fock method coupled with the Gauge-Independent AO (GIAO) algorithm and a 6-31+G(d,p) basis set. The calculated ^{13}C NMR isotropic shifts exhibit admirable agreement (δ rmsd 4.6 ppm) with the experimental data. The chemical shift of *para*-substituted carbon showed a linear correlation with Hammett constants (σ_p and σ_p^+). Using this methodology the σ_p^+ constants for the dendritic ligands have been estimated to be 0.25 and 0.24 for 2(n) and 2(o), respectively. In addition, the NBO charges on the sulfur atoms shows a latent response with the σ_p^+ parameter. The atomic charge on the thiophenolato sulfur is invariant with the electron withdrawing ability of the substituents, however, the charge increases with increasing electron-withdrawing power[447]. Two-dimensional Nuclear Overhauser Enhancement Spectroscopy(NOESY) NMR has been applied to study sodiumdodecylsulfate (SDS)/polyethyleneoxide (PEO)/D_2O at 10, 20, 25, and 40 °C. The results indicate that PEO interacts preferentially with the surface of the micelle aggregates at 20 and 25 °C, displacing some water molecules from the hydration sphere. At 40 °C the polymer tends to penetrate the interior of the SDS micelle, since its solubility in hydrophobic media increases with temperature[448]. The morphology of high-densty polyethylene (HDPE) extrusion coating layer on high-density paper (HDP) has been investigated. An uneven layer with a high content of crystallinity against the paper surface was

discovered. The methods applied were solid-state ^{13}C NMR Spectroscopy and Atmic Force Microscopy. The highly crystalline layer was found to be mainly monoclinic crystallinity. The formation of the monoclinic crystallites was probably initiated by orientation of the polyethylene molecules by drawing, adhesion to the fibrous paper surface, and pressure[449]. Aqueous solutions of sodium dodecyl sulfate (SDS) at various concentrations in 2 g/L polyvinylpyrrolidone (PVP) and 2 g/L polyvinyl alcohol (PVA), respectively, were studied by ^{1}H NMR. Two-dimensional NOESY experiments show that SDS starts to micellize at a concentration of 2.5 mmol/L, with PVP solubilized in the interior of the micelles. At SDS concentrations lower than 2.5 mmol/L, no sinificant interaction could be detected. Spin-spin relaxation measurements support this conclusion. The interaction between PVA and SDS was hardly detected[450]. Advanced ^{1}H solid-state NMR methods are applied for studying the hydrogen bond formation occurring in polymer hydrogels based on N-isopropylacrylamide (NIPAAm) and methacrylic acid (MAA). For P(NIPAAm-co-MAA) copolymers collapsed at low pH, two populations of water can be distinguished in ^{1}H magic-angle spinning (MAS) NMR spectra, one of which is probably situated near stable hydrogen-bonded regions, while the other behaves similarly to free water. The pH-induced polymer collapse can be followed in detail using 2D ^{1}H -^{1}H double quantum (DQ) MAS NMR experiments on dried samples. For collapsed copolymers as well as interpenetrating polymer networks, the appearance of characteristic signals shows that hydrogen bonding takes place between NIPAAm and MMA monomers. The temperature dependence of the DQ spectra indicates that acid-amide hydrogen bonds formed between both comonomers are more stable than the acid-acid hydrogen bonds formed among MAA moieties alone. Correspondingly, by analysing ^{1}H -^{1}H DQ sideband patterns, a relatively short distance of 270 pm is found for the NIPAAm-MMA hydrogen bond[451]. Complete comonomer sequence assignments were made for a series of propylene-1-olefin copolymers to establish the effect of branch length on the sequence sensitivity of the backbone carbon chemical shifts. Particular attention was paid to the effect of branch length on the monomer sequence sensitivity of the $\alpha\alpha$ carbon chemcal shifts. As opposed to the ethylene-1-olefin copolymers where the reported $\alpha\alpha$ carbon chemical shifts were exclusively tetrad sensitive regardless of the branch length, the $\alpha\alpha$ carbons in each of the three propylene-1-olefin systems examined showed apparent tetrad, triad, and dyad monomer sequence sensitivities as the center dyad changed from PP to PX to XX where X represents the individual 1-olefin[452]. Poly(buthyl acrylate-co-carbon monoxide-co-ethylene) (polyEBC) samples prepared from ^{13}C -labeled monomer,n-buthyl acrylate, were characterized using two dimensional (2D) pulsed field gradient (PFG) 750 MHz NMR spectroscopy. To elucidate the complex structure of the terpolymer, 2D-^{1}H/^{13}C-heteronuclear single quantum coherence (HSQC) and heteronuclear multiple bond correlation (HMBC) experiments were conducted by selectively exciting the enhanced resonances in the spectra of two polymer samples, one polymer resulting from synthesis with 1-^{13}C- buthyl acrylate monomer and a second polymer obtained from a synthesis with 2-^{13}C- buthyl acrylate monomer. In all experiments, the sample temperature was 120 °C, to ensure a homogeneous solution and sufficient

molecular mobility[453]. The rate of conversion of the monomers and crosslinker in the formation of a novel semi-interpenetrating poly(ethylene glycol)/ poly(2-acrylamido-2-methylpropane sulfonic acid-co-N-isopropylacrylamide) copolymer hydrogel was determined by using ^{1}H-NMR spectroscopy. It was established that poly(ethylene glycol) does not participate in the polymerization reactions and that crosslinking by methylenebisacrylamide occurs predominantly in the early stages of copolymer chain growth[454]. Poly(buthyl acrylate-co-carbon monoxide-co-ethylene) samples with varying monomer components and degrees of branching (g') were characterized using 750 MHz 2D pulsed-field gradient (PFG) NMR spectroscopy. The NMR experiments were performed in solution at 100 °C to ensure sample homogeneity and sufficient mobility of the ethylene-based terpolymer. Since the ^{1}H and ^{13}C NMR spectra of the terpolymer samples were complex, 2D-^{1}H /^{13}C -heteronuclear multiple quantum coherence (HMQC) and HMBC experiments were conducted. The distinctive resonances of the ketone and ester carbonyl groups facilitated spectral assignments, such that chain-end resonances were apparent and the effects of short-chain-branching reactions and monomer sequence distributions were readily observed[455]. The precise estimation of the degree of derivatization of functional groups in polymers is important for determining their macroscopic properties. In this work, the quantitative estimation of the extent of esterification of novolac copolymers with di-tert- buthyl dicarbonate was studied. Although the extent of esterification has been calculated previously by quantifying the signals from FT-IR and UV-Vis spectroscopy, these were restricted to monitoring the progress of the derivatization process. The ^{13}C NMR signal intensities from the inverse-gated ^{1}H -decoupled NMR spectrum have been used recently for the quantitative estimation of the degree of esterification of polymers. An alternative methodology has been suggested based on the fully relaxed ^{1}H chemical shift intensities. However, since the proton signals of novolac resins are generally broad and overlapping, the proton decoupled ^{13}C NMR spectrum was used to identify the ^{1}H NMR signals using the 2-D HSQC technique[456]. Pulse field gradient-NMR (PFG-NMR) spectroscopy is determined to be a more suitable method for the investigation of self-association processes in multi-component (co)polymer systems than light scattering methods. The co-micellization of mixtures of the diblock copolymer polystyrene-block-(hydrogenated polyisoprene) (PS-HPI) and the triblock copolymer polystyrene-block-(hydrogenated polybutadiene)-block-polystyrene (PS-HPB-PS) in decane is investigated by PFG-NMR spectroscopy and the results compared to those experimentally determined by static (SLS) and dynamic (DLS) light scattering. As expected, diffusion coefficients determined by PFG-NMR spectroscopy are systematically lower than those from DLS. The PFG-NMR measurements provided higher values of $c_{tr}^{e}(X)/c_{tot}$ than the model calculations, illustrating that the basic assumption used in the calculations, *i.e.*, that the number concentration of co-micelles in mixed solutions follows thedilution with a triblock copolymer solution, 1 – X, is not fully valid at high X (weight fraction of PS-HPB) values[457]. The measurements of molecular self-diffusion coefficients by the Pulsed Gradient Spin-Echo (PGSE) NMR have evolved to become a very important method to characterize complex aqueous mixtures.

The ability to visualize and quantify the mobility of particular component in multi-component mixtures has had a profound impact on the polymer science because the mobility of species under investigations is determined not only by its chemical structure and size, but also by the phys. environment in which it is located. This review reports the most recent results, realized from our group in Calabria, on the field of the NMR-self-diffusion in aqueous polymer mixtures. Water, polymer, surfactant and oil self-diffusion coefficients were determined in different complex polymer mixtures (*e.g.* micellar solutions, lyotropic liquid crystal phases, microemulsions) in order to define their super-molecular structure as a function of composition and temperature. PGSE-NMR permitted a non-perturbing in-situ probing of structured solutions and this is especially true for aqueous solutions of amphiphilic polymers since the their characteristic structural dimension[458]. PFG NMR results are reported on H_2O, PEG200, PEG1500, PEG8000, and PEG20000 in wet cotton fibers and H_2O in wet cotton linters. The data are analysed in terms of a two-site exchange model (water/cotton) and show that the probe molecules in fibers are trapped in cages. The cage size decreases from 10 to 2 μm as the probes' size increases from 0.23 to 9.2 nm, although the overall accessible volume only decreases from 50 to 20-30%. This behaviour may be explained by size-exclusion effects on the connectivity and accessibility. Analysis of the diffusion coefficients at short diffusion times indicates that fiber cages are water pools held between the growth rings of the fiber. In linters these cages do not occur, and a freely diffusing signal from H_2O in the amorphous region is observed with $D = (4.5\text{-}8.9) \times 10^{-11}\ m^2\ s^{-1}$, which when compared to the predicted value from the microviscosity of the amorphous regions gives a tortuosity of 2-4. Exit of all probes from linters and fibers takes 0.2 s and requires hydrogen bonds to be broken with an activation energy of 50 kJ mol^{-1}[459]. ^1H spin-diffusion experiments employing a double-quantum (DQ) dipolar filter were performed for the characterization of the microdomain structure of heterogeneous samples. For this purpose the NMR spin-diffusion process was analysed based on a model morphology of three different domains with arbitrary sizes, diffusivities, and filter efficiency. General analytical solutions for z magnetization source and sink were obtained valid for a one-dimensional lamellar morphology in the full range of spin-diffusion times. These solutions of the spin-diffusion equations were used for determining the crystal, interface, and amorphous domain sizes in polystyrene-poly(ethylene oxide) (PS-PEO) and poly(hydroxyethyl methacrylate)-poly(ethylene oxide) (PHEMA-PEO). The DQ dipolar filter has a good efficiency for PS-PEO but is only partially efficient in filtering the signal of the mobile domains in the PHEMA-PEO diblock copolymer. The domain sizes measured by the DQ filter method are compared to those obtained using the traditional dipolar filter creating z magnetization in the mobile domains[460]. Measurements of the self-diffusion coefficient of water in Nafion-117 as a function of pressure have been carried out. The natural field gradient of a 7.3 T superconducting magnet was used for the diffusion measurement. The measurements were carried out at 288 K and variable pressure up to 0.25 GPa. The high-pressure diffusion data were obtained for four different water contents between 6.6 and 22 wt %. The

calculated activation vol. decreased from 13.2 to 2.7 cm^3/mol as the water content increased from 6.6 to 22 wt %. It is suggested that segmental motions within the polymer play a significant role in the transport mechanism for low water content membranes, and that the transport mechanism for high water content membranes is similar to that in liquid bulk water[461]. Nanocomposites result from combinations of materials with vastly different properties in the nanometer scale. These materials exhibit many unique properties such as improved thermal stability, reduced flammability, and improved mech. properties. Many of the properties associated with polymer-clay nanocomposites are a function of the extent of exfoliation of the individual clay sheets or the quality of the nanodispersion. This work demonstrates that solid-state NMR can be used to characterize, quantitatively, the nanodispersion of variously modified montmorillonite (MMT) clays in polystyrene (PS) matrixes. The direct influence of the paramagnetic Fe^{3+}, embedded in the aluminosilicate layers of MMT, on polymer protons within about 1 nm from the clay surfaces creates relaxation sources, which, *via* spin diffusion, significantly shorten the overall proton longitudinal relaxation time (T_1^H). Deoxygenated samples were used to avoid the particularly strong contribution to the T_1^H of PS from paramagnetic molecular oxygen. T_1^H value was used as an indicator of the nanodispersion of the clay in PS. A quick assay of T_1^H is reported for samples equilibrated with atomspheric oxygen. Included are these samples as well as 28 PS/MMT nanocomposite samples prepared by extrusion. These measurements are related to the development of high-throughput characterization techniques. This approach gives qualitative indications about dispersion; however, the more time-consuming analysis, of a few deoxygenated samples from this latter set, offers significantly greater insight into the clay dispersion[462]. Colloidal poly(4-vinylpyridine)/silica and polystyrene/silica nanocomposites particles comprising 38% and 48% silica by mass, respectively, have been characterized by solid-state NMR spectroscopy in order to probe the nature of the molecular interactions between the polymer and silica phases. For polyvinylpyridine/silica nanocomposites particles, our results indicate hydrogen bond formation between the pyridine nitrogen and a surface hydroxyl proton. In contrast, a π-interaction between the aromatic ring and the silica surface is the most likely model for the PS/silica nanocomposites particles. Nonspecific binding interactions do not appear to play an important role in nanocomposites particle formation in either case. The high-resolution ^1H-^{13}C and ^1H-^{29}Si correlation experiments used to extend this information are a novel combination of multipulse proton decoupling and Lee-Goldberg cross-polarization[463].

6 Polymer Blend of the Synthetic Macromolecules

Copolymer ethylene-dimethyl-aminoethyl methacrylate (EDAM) with 3.9% DAM side groups and ultra-high molecular weight polyethylene (UHMWPE) were blended in decalin solvent. The hot homogenized solution was poured into an aluminum tray to form gels and the decalin was allowed to evaporate from the

resultant gels under ambient condition. Surprisingly, the resultant dry blend films could be elongated to more than 200-fold ($\lambda = 200$) even for the blend film with 90% EDAM content (9/1 composition), although the maximum draw ratio of EDAM homopolymer films was 1.6-fold ($\lambda = 1.6$). The mechanism of the great drawability was dependent upon the content of EDAM. The drawability for the 9/1 composite films was attributed to large crystal lamellae of UHMWPE ensuring crystal transition from a folded to a fibrous type. Accordingly, EDAM chains were independent of ultradrawing of UHMWPE and kept a random orientation under ultra-drawing process. The storage (Young's) modulus was 10 GPa at 20 °C. In contrast, EDAM chains within the 1/1 composite films were oriented drastically together with UHMWPE crystallites. The modulus of the 1/1 composition at 20 °C reached 68 GPa, which was higher than the value (40 GPa) of polypropylene films with $\lambda = 100$. Such considerable difference of modulus due to EDAM content was analysed in relation to the gelation/crystallization from solutions[464]. Physical blends of poly(ethylene terephthalate) (PET) and poly(ethylene isophthalate) (PEI), abbreviated PET/PEI (80/20) blends, and of PET and a random poly(ethylene terephthalate-*co*-isophthalate) copolymer containing 40% ethylene isophthalate ($PET_{60}I_{40}$), abbreviated PET/$PET_{60}I_{40}$ (50/50) blends, were melt-mixed at 270°C for different reactive blending times to give a series of copolymers containing 20 mol % of ethylene isophthalic units with different degrees of randomness. ^{13}C NMR spectroscopy precisely determined the microstructure of the blends. The thermal and mechanical properties of the blends were evaluated by DSC and tensile assays, and the obtained results were compared with those obtained for PET and a statistically random PETI copolymer with the same composition. The microstructure of the blends gradually changed from a physical blend into a block copolymer, and finally into a random copolymer with the advance of transreaction time. Isothermal crystallization studies carried out on molten samples revealed the same trend for the crystallization rate. The effect of reaction time on crystallizability was more pronounced in the case of the PET/$PET_{60}I_{40}$ (50/50) blends. The Young's modulus of the melt-mixed blends was comparable to that of PET, whereas the maximum tensile stress decreased with respect to that of PET. All blend samples showed a noticeable brittleness[465]. Binary blends formed by poly(methylmethacrylate)/poly(ethylene oxide), PMMA/PEO, were studied by different solution and solid state NMR techniques to obtain information on blends homogeneity and compatibility. The values of $T_{1\rho}^{H}$ obtained by variable contact time and delayed contact time experiments, for each composition, were distinct and this fact suggests that regions with different molecular mobilities exist, as a consequence of blending interaction[466]. The molecular mobility in PEG-PVP blends as a function of the time of system storage and the PVP molecular mass is studied by the PFG NMR method. The distribution of PEG molecules over their mobilities is found in a blend containing 36 vol.% PEG with molecular mass 400 g/mol. As the storage time of the system increases, the spectrum of diffusion coefficient values varies, thereby indicating the redistribution of PEG400 molecules in blends with PVP. A partly restricted diffusion of PEG400 molecules is discovered, reflecting the influence of PVP macromolecules on the motion of

short PEG chains. It is shown that, during the redistribution of PEG molecules in the blend, they are involved in a complex with PVP, which is characterized by its own transport properties. The data obtained by the NMR relaxation technique are in agreement with the results of NMR diffusion measurements in the studied systems[467]. Blend films of poly(ε-caprolactone) (PCL) with chitin or chitosan were prepared as completely biodegradable polyester/polysaccharide composites. Differential scanning calorimetry and FTIR spectroscopy revealed that the crystallization of PCL, which had been suppressed by blending with chitin and chitosan, progressed with the elapse of time after film preparation. The suppression of crystallization of PCL by blending with polysaccharides was also observed by solid-state ^{13}C NMR spectroscopy[468]. Natural abundance solid-state ^{15}N NMR spectroscopy was applied to investigate films of nylon 6 and their blends with poly(propylene oxide) (PPO). The ^{15}N NMR results showed that the crystalline forms presented in these blends and also confirmed the previous NMR results obtained by ^{13}C NMR study. From all NMR data the antiplasticization phenomena and plasticization effects caused by PPO content in the blends were characterized. The polyoxide action is a function of its proportion. However, because the samples were prepared by solution casting, residual solvent action cannot be ignored. The ^{15}N chemical shift changes were influenced by both PPO and residual solvent[469]. The extent of mixing in blends of poly(hydroxybutyrate-co-hydroxyvalerate) (73:27) and poly(vinyl acetate) (PVAc) has been measured using a number of different techniques, principally solid-state NMR. DSC measurements indicated effective mixing of the polymer chains on a scale of several nanometers. The results of T_1^H and $T_{1\rho}^H$ measurements confirm intimate mixing of the chains. A change on blending in the $T_{1\rho}^H$, and the ^1H NMR line width of the signal from the protons of PVAc was consistent with an increase in the amplitude and frequency of motion of this component. The PVAc chains reside within the inter-lamellar space, as confirmed by spin diffusion measurements after $T_{1\rho}^H$ preparation[470]. Melt blends of poly(butylene terephthalate) (PBT) and poly(ethylene 2,6-naphthalate) (PEN) with 30, 40, 50, 60, and 70 wt.% PEN were prepared using a single-screw extruder and injection-molding machine. ^{13}C and ^1H NMR spectra were obtained on solutions prepared by dissolving samples of the polyesters and each blend in deuterated trifluoroacetic acid + chloroform mixts. (1:1 by vol.). The absence of new signals in ^1H and ^{13}C spectra, that would be expected to result from transesterification reactions in the PBT + PEN blend system, provides convincing evidence that such reactions do not occur in these blends under the melt processing conditions that were used. In the light of published work on solid-state NMR studies of these and related blend systems, and the observations of partial miscibility with a very small domain size, together with substantial enhancement of the mechanical properties of PBT by blending with PEN, it can be concluded that any improvement in mechanical properties arises from molecular scale mixing of the polyesters and strong but non-covalent bonding interactions over the very large interfacial area between the PBT-rich and PEN-rich phases[471]. Binary blends formed by PMMA and PVP were prepared by solution casting and evaluated by solution and solid-state NMR. Variations

in the microstructure of PMMA were analysed by ^{13}C solution NMR. From the NMR solution, it was possible to evaluate the microstructure of both polymer blend components; they were atactic. From the solid state, good compatibility between both polymer components was characterized[472]. The phase structures of thermally processed wheat proteins (WP) and PVA blends were studied by solid-state high-resolution NMR spectroscopy. The intermolecular interactions among the multi-component systems and the behaviour of each component in the blends on scales of nanometers were examined. The mechanical properties of the blends were also measured and related to the phase structure studies. The results indicated that the polymer chains of WP could be homogeneously mobilized when thermally processed with glycerol and water as plasticisers, but the glycerol predominately associated with WP rather than PVA in the blends. The intermolecular hydrogen bonding interactions between WP and PVA caused some extent of miscibility in the system on scales of nanometers especially when the PVA content was low. The tensile strength and modulus of the blends were improved as compared to WP. However, the intermolecular interactions were relatively weak and could not be further enhanced by increasing PVA component in the blends. The particle miscible WP/PVA blends contained plasticised WP and PVA phases in conjunction with the miscible WP/PVA phase. Increasing the PVA content in the blends did not result in an increase of the percentage of the miscible phase and the blends tented to be immiscible while the elongation of the blends was reduced when increasing the PVA content in the blends[473]. The broad-line ^{1}H NMR study of the polymer blend composed of isotactic polypropylene and ethylene-propylene-diene monomer rubber was carried out. The NMR measurements were performed on the samples of the polymer blend and on the components of the blend in the temperature range covering the glass-transition regions of all studied polymers. Conclusions were drawn from the temperature dependencies of the second moment M_2 and of the data obtained by the decomposition of the spectra into the components related to the motionally distinct regions of the partially crystalline polymer. The mass fractions of the amorphous, intermediate, and crystalline domains and the widths of the spectra related to the particular phases were computed from the spectra. A double glass transition was revealed for the polymer blend. Different mechanisms of the motional processes related to the glass transition were deduced from the data. The gradual increase of the number of the chains and the enhancement of the chain mobility within noncrystalline regions of the polymer blend are responsible for the motion related to the lower glass transition and only transformation of the hindered motion into free motion was found in the temperature region of the upper glass transition[474]. PFG NMR measurements have been made to study the diffusion of diethyl ether in blends of PEO and PMMA. The blends have 10-30 wt % PEO, a composition range within which these materials are amorphous glasses. The diffusion of diethyl ether through the blends is quite rapid, with diffusion constants in the range of 10^{-7} to 10^{-8} cm^2/s. In PFG NMR experiments, the apparent diffusion constant depends on the timescale over which diffusion is observed. The values decrease to a plateau as the time increases, this being the signature of tortuous diffusion. In these blends,

PEO is known to undergo rapid segmental motion typical of a rubbery state well below the glass transition, whereas the segmental motion of PMMA is slower by many orders of magnitude. Mobile PEO provides a pathway for the diffusion of structurally similar diethyl ether, whereas solid-like PMMA acts as a barrier. The size of the domains can be estimated either from a lattice model or from equations for tortuous diffusion. Micrometer sizes are indicated that are unexpectedly large, given the size of the polymer chains and the size of the concentration fluctuations, both of which are thought to be in the tens of nanometers. The lattice model and the equations for tortuous diffusion assume a random dispersion of impenetrable or less penetrable objects. This may not be the appropriate morphology for the diffusion pathway. Recently, large sizes have been indicated by PFG NMR experiments, in which a penetrant is thought to diffuse in a curvilinear fashion. In these blends, the pathway for diethyl ether is along the PEO backbone. A plot of the logarithm of the mean-square displacement versus the logarithm of time has a slope of about 0.6, close to the value of 0.5 for pure curvilinear diffusion. Exponents with values in this range can also be associated with diffusion in a fractal space, which, in this situation, still consists of mobile PEO[475]. Natural abundance two-dimensional exchange ^{13}C NMR spectra revealed the very close proximity between the carboxyl carbons of poly(methacrylic acid) (PMAA) and carbonyl carbons of PVAc in miscible 3:1 PMAA/PVAc blends. The estimated distance between the CO carbons is approximately 0.37 nm. This close distance is induced by strong hydrogen bonding between the hydrogens of the carboxyl groups of PMAA and the oxygens of the carbonyl groups of PVAc. Molecular mechanics (MM) calculation reveals that the distance of the hydrogen bond between the hydrogen of the carboxyl group and the oxygen of the carbonyl group is approximately 0.2 nm by fixing the intermolecular (inter-polymer) C-C distance between the CO carbons to be 0.37 nm. This value is reasonable for very strong hydrogen bonding interaction. This interaction makes the ^{13}C chemical shift value of PVAc carbonyl carbon peak toward lower field by 4 ppm and that of PMAA carboxyl carbon peak to change toward upper field by 4 ppm [476]. Chain-level mixing in polyolefins is investigated for blends of polyisobutylene (PIB) and polyethylene-co-1-butene (PEB). Variable-temperature ^{1}H, ^{2}H, ^{13}C, and ^{129}Xe NMR experiments are used to characterize local PIB chain dynamics in blends with PEB in which the concentration of 1-butene comonomer units is 23 or 66 wt%. Results from 1D and 2D solid-state ^{13}C exchange experiments, ^{1}H relaxation measurements, and ^{2}H line shape analysis indicate that local conformational dynamics of the PIB CH_2 group in the polymer backbone increase significantly in blends with PEB copolymers containing 66 wt.% butene comonomer (PEB-66). Even though the PEB-66 is a higher Tg polymer than PIB, PIB exhibits a lower effective Tg when the blend is formed relative to its pure state. Similar perturbations are not observed in the PIB/PEB-23 blend, indicating that this blend is not miscible at the chain level. These results are directly relevant to the length scale of glass transitions in polyolefins, indicating that local interchain packing plays an important role in the conformational dynamics that occur within a chain, and are suggestive of local configurational entropy contributions to mixing. Although ^{1}H spin-diffu-

sion experiments could not reveal quantitative length scales of mixing in the these blends due to insufficient contrast between the constituents, ^{129}Xe NMR experiments showed that the PIB/PEB-66 blend was homogeneous on a 50 nm length scale. In agreement with the heterogeneous morphology indicated by the dynamic NMR experiments, ^{129}Xe NMR showed two resolved peaks for the PIB/PEB-23 blend, indicative of phase separation on a 50 nm length scale. The compilation of all the data, most of which were obtained at natural abundance, indicates that the PIB/PEB-66 blend exhibits intimate chain-level mixing on a length scale much shorter than Rg (*ca.* 8 nm). More importantly, the data show that reduced chain packing constraints occur in the miscible blend and suggest that local entropic contributions are the driving force for miscibility[477].

7 Dynamics of the Synthetic Macromolecules

A poly(ethylene acrylate) (PEA) homopolymer and an ethylene acrylate-acrylic acid copolymer Na salt ionomer containing 8.4 mol % ionic groups (PEANa-8.4) were studied by using ^{13}C CP/MAS NMR. The ^{13}C spin-lattice relaxation times in a rotating frame, $T_{1\rho}^{C}$, were measured as functions of the temperature. Using these $T_{1\rho}^{C}$ times, the chain mobility, correlation time, and activation energy for carbon of PEA and PEANa-8.4 were obtained. It was found that the molecular motion in PEA needed a higher activation energy than that in PEANa-8.4. In addition, we observed that motion of the 1-methyl carbons in PEANa-8.4 was distinctly different from that in PEA: the value of $T_{1\rho}^{C}$ for 1-methyl carbon is ascribed to stronger interactions between the polymer chains in the homopolymer[478]. The local dynamics of three poly(propylene imine) dendrimers with hydrophilic triethylenoxy methyl ether terminal groups were studied in D_2O by the measurement of the ^{1}H NMR relaxation times, which were treated with the Lipari-Szabo model-free approach. The results showed that the overall mobility increased with temperature and decreased with increasing dendrimer size. An Arrhenius trend was observed for both overall and local motions. The local mobility decreased from the outer part to the inner part of the dendrimer and with the dendrimer size. The spatial restriction of local motions decreased with increasing temperature up to 55 °C and remained constant above 55 °C. Local motions were more restricted when the dendrimer size increased. The results showed that the hydrophilic end groups of the dendrimers were located preferentially at the periphery of the molecules and were extended in the aqueous environment[479]. Direct measurement of chemical exchange events in the crystalline polycarbonate monomer 4,4'- isopropylidenediphenol (bisphenol A, BPA) *via* 2D ^{13}C solid-state NMR reveals slow, large-amplitude aromatic ring reorientations. X-ray diffraction, however, indicates a static crystal structure. Experiments with multiple exchange times show that ring flips occur in all of the three unique conformers found in the crystal unit cell of this compound, but in specific cases, two of the three unique molecules actually switch conformations. All room-temperature exchange events may be quenched at 213 K, at least on the time scale (up to several seconds) probed. Simulation of the potential-energy

surface of BPA molecules reveals that the lowest-energy pathway for ring flips (maximum energy of 1.9 kcal/mol) involves +110° flips of one ring coincident with +70° flips of the second. The mechanism of the ring dynamics in the crystalline monomer is unique relative to those previously reported for the polycarbonate in that the collective motion of both rings in a monomer unit is 180°, whereas single-ring flips of 180° occur in the polymer[480]. The relationship between the morphology and the mechanical properties of copolymer ethylene-methyl methacrylate (EMMA) films with different MMA contents was investigated as a function of temperature by using positron annihilation, X-ray diffraction, and ^{13}C solid-state NMR. To make clear the effect of MMA side groups on the morphology and molecular mobility of EMMA as a function of temperature, the characteristics of EMMA were discussed together with those of copolymer (dimethylamino)ethyl methacrylate and branched polyethylene. Three kinds of transitions were confirmed by positron annihilation: the first at temperatures around -130 °C, the second around -40 °C, and the third around 50 °C. The first and the second transitions were due to the commencement of molecular motions, which can remove trapped electrons from their shallow potentials, while the third transition around 50 °C was attributed to the partial melting of unstable small crystallites[481]. Dry and hydrated PVA gels with 55% (α-PVA) and 61% (s-PVA) syndiotacticity and related PVA/lactosyl chitosan (LC) blends were investigated with ^{129}Xe and CP/MAS ^{13}C NMR techniques. Although the dry gels exhibit two broad ^{129}Xe resonances in the slow-to-intermediate exchange limit, both hydrated gels show three resonances. The corresponding dry blends exhibit two signals, the chem. shifts and line widths of which change with respect to those of pure PVA, whereas one (α-PVA/LC) or two (s-PVA/LC) signals appear in the spectra of the hydrated blends. A comparative analysis of the data demonstrates that LC rearranges the domains of the polymeric matrix in both the dry and hydrated blends according to the syndiotacticity of the PVA chains. Information on the molecular motions of the amorphous and swollen polymeric domains in the kilohertz range has been obtained from an analysis of the spin-lattice relaxation times. These data indicate that the dynamics and arrangement of the PVA chains in the gels are strongly affected by their tacticity and the addition of the copolymer LC[482]. ^{13}C and ^{2}H NMR relaxation time measurements were performed on four linear styrene-isoprene tetrablock copolymers (SISI) of overall molecular weight about 12,000 g/mol in order to characterize the segmental dynamics of both components. The two isoprene blocks are equal in length as are the two styrene blocks. A wide range of temperatures (from 285 to 530K) and several compositions (volume fraction of styrene: 23%, 42%, 60%, and 80%) were investigated. The segmental correlation times for both components in SISI were extended by fitting the experimental data to the modified Kohlrausch-Williams-Watts orientation autocorrelation function and Vogel-Tammann-Fulcher temperature dependence. While previous measurements found that the global dynamics in this system are quite homogeneous, these NMR measurements show that the segmental relaxation times of styrene and isoprene segments differ by orders of magnitude. At high temperatures, the dynamics of styrene segments are about 10 times slower than

that of isoprene segments; this can be attributed to the difference in the intrinsic mobility of the two types of segments. The segmental dynamics of 5% polyisoprene tracers in one tetrablock matrix are very similar to that of the matrix isoprene segments[483]. T_1^C and nuclear Overhauser effect (NOE) relaxation data for hydroxyl-terminated polybutadiene (HTPB), obtained as a function of temperature (-50 to +70°C) in $CDCl_3$, suggest that a log χ^2 distribution model is the most appropriate in describing polymer chain segmental motions. The local segmental motions are the major sources of relaxations for the HTPB protonated carbons. The relaxation data show the chain segmental motions taking place in very short time intervals (on the order of tenth of a nanosecond). The activation energies of such conversions from one conformer to another are found to be on the order of kilojoules[484]. Poly(p-phenylenevinylene) (PPV) has shown a great potential for electro-optical applications due to its electroluminescent and semiconducting properties. Such properties are directly related with the polymer chain conformation and dynamics. Then, it is important to understand in detail the local chain motions. In this work, three ^{13}C solid-state MAS exchange NMR techniques were used to study conformational dynamics of phenylene rings in PPV. The standard 2D MAS exchange experiment was used to identify exchange processes between equivalent and nonequivalent sites. Centerband-only detection of exchange (CODEX) experiments were applied to determine the amplitude of the phenylene ring flips and small-angle oscillations. Additionally, a new version of the CODEX technique, which allows for the selective observation of segments executing exchange between non- equivalent sites, is demonstrated and applied to determine the flipping fractions and the activation energies of the phenylene ring rotations. It was found that, at -15 °C, (26 ± 3)% of the rings undergo 180° flips in the millisecond time scale, with average imprecision of $(30 \pm 5)°$ and activation energies of (23 ± 3) kJ/mol. Other (31 ± 10)% of the rings perform only small-angle oscillations with an average amplitude of $(9 \pm 2)°$[485]. The segmental ordering within sublayers of a lamellar polystyrene-poly(dimethylsiloxane)- polystyrene triblock (PS-PDMS-PS) was studied by NMR. The carbon and deuterium NMR line shapes of the PDMS sequence (soft block) reveal clearly a wide distribution of segmental orientational order S in the lamellae and thus a distribution of constraints probed by the chains. This distribution is mainly due to the coexistence of positive and negative S, resulting from a competitive ordering effect induced by the presence of glassy interfaces ($S < 0$ in their vicinity) and the chain-end anchoring junctions ($S > 0$)[486]. Solid-state ^{13}C NMR analyses have been carried out on the temperature dependence of the molecular mobility and phase structure of biodegradable poly[(R)-3-hydroxybutyric acid-co-(R)-3-hydroxyhexanoic acid] [P(3HB-co-3HH)] copolyesters. ^{13}C spin-lattice relaxation time (T_1^C) experiments for the main chain CH and CH_2 carbons have shown the existence of two components with different T_1^C values for each carbon. This T_1^C result is in accord with the previous T_1^C results for poly[(R)-3-hydroxybutyric acid] [P(3HB)] homopolymer and other P(3HB)-type random copolyesters. In previous papers, however, the assignment of the two components with different T_1^C values have been remained unsolved. By performing variable-temperature experiments and by comparing with the results

of other partially crystalline polymers, the assignment of the two components was investigated in detail. As the results, it has been concluded that both the two components are crystalline components. The crystalline component with longer T_1^C value is assignable to the internal region of crystalline lamellae and the shorter T_1^C component is ascribed to the interfacial crystalline region near amorphous phase. T_1^C analysis have also detected the gradual increase in molecular mobility with an increase of temperature. When compared with the previous T_1^C results for poly(butylene adipate) (PBA), poly(ethylene succinate) (PES), and poly(butylene succinate) (PBS), the tendency of the temperature change observedd for P(3HB-co-3HH) has been close to that for PES[487]. Polymer diffusion and its temperature dependence in poly(vinyl acetate-co-dibutyl maleate) [P(VAc-DBM)] latex films prepared from 4:1 wt./wt. ratio of VAc:DBM are described. Two sets of polymers were investigated: one set containing 50% gel (high-M); the other set, with Mw $\approx$ 250 000 (M250K), free of a measurable gel content. Despite their similar chemical components, as determined by ^{1}H NMR, these 2 sets of samples exhibited different glass transition temperatures (Tg). Latex particles were labeled with 9-methacryloxymethylphenanthrene as the donor dye and 2′-acryloxy-4′-methyl-4-(N,N-dimethylamino) benzophenone as the acceptor. Polymer diffusion was monitored by nonradiative energy transfer (ET), and apparent diffusion coefficients (Dapp) were calculated from the ET data using a simple diffusion model. These values increased with temperature and were characterized by an apparent activation energy (Ea) of 37 $\pm$ 2 kcal/mol for the high-M polymer and 45 $\pm$ 2 kcal/mol for the M250K sample[488]. Information about segmental mobility in thermoplastic elastomers was obtained using static ^{1}H double quantum (DQ) NMR experiments in combination with homo- and heteronuclear dipolar filters, *e.g.* ^{13}C editing of ^{1}H DQ buildup curves. Block copolymers of poly(butylene terephthalate) (PBT) as hard blocks and polytetramethylene oxide (PTMO) as soft blocks (PBT-*block*-PTMO) were investigated by varying composition and block length. By simulation of the DQ buildup curves, residual dipolar couplings and with this the average order parameter were deduced for the mobile PTMO blocks which are sensitive to the segmental mobility responsible for the viscoelastic properties of thermoplastic elastomers. A strong correlation exists between residual dipolar coupling and composition. Furthermore, the average order parameter correlates linearly with the amt. of PTMO in a PTMO-rich phase as determined in previous studies. Additionally, ^{1}H transverse magnetization relaxation measurements revealed a direct correlation between the effective T_2 relaxation time of the soft domain and the composition of the thermoplastic elastomers[489]. An approach towards the analysis of the intensity decay in proton multiple-quantum experiments on polymeric networks in terms of slow fluctuations of the residual dipole-dipole coupling tensor were reported. Solutions for individual spin pairs as well as the three-spin system of methyl groups are derived, and the influence of the cycle time of the multiple-quantum pulse sequence is evaluated. The multiple-quantum strategy discussed herein features the advantage that the magnitude of the fluctuating part of the residual dipole-dipole coupling const. and the correlation time of the slow process can be

determined independently of the integral residual coupling constant as well as its distribution. The theory is applied to experiments on end-linked poly(dimethylsiloxane) model networks with mono- and bimodal chain length distributions, where it is found that, for all samples, correlation times of the slow processes av. to about 1 ms, and that the magnitude of the fluctuating part of the dipole-dipole coupling is significantly smaller than the av. dipole-dipole coupling constant. This observation is interpreted in terms of considerably restricted reorientations of topologycal constraints[490]. Spin-lattice NMR relaxation times T_1 in the laboratory frame and $T_{1\rho}$ as well as $T_{1\rho}^{off}$ in the rotating frame off-resonance were employed to the study of molecular dynamics of both pristine poly(*p*-phenylene sulfide) (PPS) and thermally treated PPS. The temperature dependence of T_1 was exponential in the whole temperature range studied, whereas $T_{1\rho}$ only in low temperatures. In the high temperature range the distribution of relaxation times $T_{1\rho}$ and correlation times τ_c as well as activation energy E_a was observed. The distribution of activation energy determined from T_1 minima at 15 and 30 MHz and from low temperature slopes of $T_{1\rho}$ dependence as well as from spectral density functions (estimated from proton off-resonance technique) was attributed to the reorientation of phenylene groups around the sulfur-phenyl-sulfur axis in amorphous and crystalline phases of PPS. Furthermore, it is suggested that an additional relaxation mechanism related to interactions of protons with paramagnetic centers is operative in a low temperature range. After thermal treatment of PPS the low temperature minima disappeared and the relaxation times shortened in the low temperature regime. Both these facts were attributed to an increased contribution of spin diffusion in the relaxation process[491]. Two series of ethylene-dimethylaminoethyl methacrylate and ethylene-methylene acrylate copolymers with different comonomer content were studied by high-resolution solid-state ^{13}C NMR spectroscopy. Biexponential ^{13}C spin-lattice relaxation behaviours of the crystalline region were observed for all copolymer samples either melt-quenched or isothermally crystallized. The relative content of the shorter T_1^C component to that of the longer T_1^C component was found to increase with comonomer content. By employing a new pulse sequence which can be considered as a combination of Goldman-Shen's and Torchia's pulse sequences, it was demonstrated that the shorter T_1^C component is corresponding to the intermediate part of the crystalline region. The thickness of the intermediate part is estimated to be about 0.85 nm[492].

References

1. Cheng, H.N. and English, A. D., eds. '*NMR Spectroscopy of Polymers in Solution and in the Solid State* (*ACS Symposium Series* 834)', Oxford Univ. Pr., 2003
2. Spiess, H. W., *Macromolecular Chemistry and Physics*, 2003, **204**, 340-346
3. Newmark, R., *Polymer News*, 2003, **28**, 40-49
4. Shit, S. C. and Maiti, S. Editor(s): Maiti, S., *Analysis and Characterization of Polymers*, 2003, 71-84
5. Sasanuma, Y., *Annual Reports on NMR Spectroscopy*, 2003, **49**, 213-280

6. Ardelean, I. and Kimmich, R., *Annual Reports on NMR Spectroscopy*, 2003, **49**, 43-115
7. Roy, D.; Basu, P. K.; Raghunathan, P.; Eswaran, S.V., *Polymer International* 2003, **52**, 757-767
8. Mao, S.-Z.; Du, Y.-R., *Huaxue Xuebao* , 2003, **19**, 675-680
9. Whittaker, A. K., Editor(s): Simon, G. P. *Polymer Characterization Techniques and Their Application to Blends* , 2003, 461-503
10. Spiess, H. W., *Macromolecular Symposia*, 2003, **201**, 85-88
11. Li, Jun; Rajca, Andrzej; Rajca, Suchada., *Synthetic Metals* , 2003, **137**, 1507-1508
12. Komenda, Thomas; Jordan, Rainer., *Polymer Preprints (American Chemical Society, Division of Polymer Chemistry)* , 2003, **44**, 986-987
13. Zhao, Ji-Ruo; Feng, Ying; Chen, Xin-Feng., *Journal of Applied Polymer Science*, 2003, **89**, 811-816.
14. Matsuda, Hironori; Asakura, Tetsuo; Nakagawa, Yasuo, *Macromolecules*, 2003, **36**, 6160-6165.
15. Yokoe, Makito; Aoi, Keigo; Okada, Masahiko, *Journal of Polymer Science, Part A: Polymer Chemistry*, 2003, **41**, 2312-2321.
16. Tsai, Hong-Bing; Lee, Da-Kong; Tsai, Rucy-Shi., *Journal of Applied Polymer Science*, 2003, **88**, 750-758.
17. Zhou, Chongfu; Ma, Jinghong; Yang, Shenglin; Liang, Borun, *Colloid and Polymer Science*, 2003, **281**, 887-891.
18. Higashi, Fukuji; Koyanagi, Sakura, *Journal of Polymer Science, Part A: Polymer Chemistry*, 2004, **42**, 1100-1106.
19. Leu, Tsu-Shang; Wang, Chun-Shan, *Journal of Applied Polymer Science*, 2003, **88**, 1963-1970.
20. Bogdal, Dariusz; Gorczyk, Jaroslaw, *Polymer* , 2003, **44**, 7795-7800.
21. Kang, Seok Ho; Luo, Jingdong; Ma, Hong; Barto, Richard R.; Frank, Curtis W.; Dalton, Larry R.; Jen, Alex K. Y, *Macromolecules*, 2003, **36**, 4355-4359.
22. Assemat, Olivier; Rinaldi, Peter L. , *ACS Symposium Series* , 2003, 834(*NMR Spectroscopy of Polymers in Solution and in the Solid State*), 123-136.
23. Qin, Haihu; Chakulski, Brian J.; Mather, Patrick T.; Constable, Gregory S.; Coughlin, Bryan E., *Polymer Preprints (American Chemical Society, Division of Polymer Chemistry)* , 2003, **44**, 40-41.
24. Mori, Makio, *Technical Papers – American Chemical Society, Rubber Division, Spring Technical Meeting, 163rd, San Francisco, CA, United States, Apr. 28-30, 2003*, 2003, 60-84.
25. Roy, Debmalya; Basu, P. K.; Raghunathan, P.; Eswaran, S. V., *Magnetic Resonance in Chemistry* , 2003, **41**, 84-90
26. Alam, T. M.; Winters, Sean T.; Bernstein, Robert; Derzon, Dora K., *Abstracts of Papers, 225th ACS National Meeting, New Orleans, LA, United States, March 23-27, 2003*, 2003, POLY-344.
27. Alam, Todd M.; Winters, Sean; Bernstein, Robert; Derzon, Dora., *Polymer Preprints (American Chemical Society, Division of Polymer Chemistry)* , 2003, **44**, 247-248.
28. Dargaville, T. R.; George, G. A.; Hill, D. J. T.; Scheler, U.; Whittaker, A. K., *Macromolecules*, 2003, **36**, 7138-7142.
29. Calvet, Damien; Collet, Andre; Viguier, Michel; Berret, Jean-Francois; Serero, Yaelle., *Macromolecules*, 2003, **36**, 449-457.
30. Bouajila, J.; Raffin, G.; Waton, H.; Sanglar, C.; Paisse, J. O.; Grenier-Loustalot, M. F., *Polymers & Polymer Composites*, 2003, **11**, 233-262.

31. Bouajila, J.; Raffin, G.; Alamercery, S.; Waton, H.; Sanglar, C.; Grenier-Loustalot, M. F,*Polymers & Polymer Composites*, 2003, **11**, 345-357.
32. Ilter, Zuelfiye; Soykan, Cengiz; Koca, Murat., *Journal of Polymer Science, Part A: Polymer Chemistry*, 2003, **41**, 2996-3005.
33. Lee, Jin-kook; Ryou, Jin-ho; Lee, Won-ki; Park, Chan-young; Park, Sang-bo; Min, Seong-kee, *Macromolecular Research* , 2003, **11**, 476-480.
34. Kawahara, Seiichi; Nagai, Akinori; Kazama, Takeo; Takano, Atsushi; Isono, Yoshinobu, *Macromolecules*, 2004, **37**, 315-321.
35. Imai, Tomoko; Satoh, Toshifumi; Kaga, Harumi; Kaneko, Noriaki; Kakuchi, Toyoji, *Macromolecules*, 2003, **36**, 6359-6363.
36. Quirk, Roderic P.; You, Fengxiang., *Polymeric Materials Science and Engineering*, 2003, **88**, 540-541.
37. Imai, Tomoko; Satoh, Toshifumi; Kaga, Harumi; Kaneko, Noriaki; Kakuchi, Toyoji, *Macromolecules*, 2004, **37**, 3113-3119.
38. Arun, A.; Reddy, B. S. R., *Journal of Polymer Science, Part A: Polymer Chemistry* , 2003, **41**, 1632-1640.
39. Finne, Anna; Albertsson, Ann-Christine., *Journal of Polymer Science, Part A: Polymer Chemistry*, 2003, **41**, 1296-1305.
40. Zheng, Ronghua; Peng, Han; Lam, Jacky Wing Yip; Chen, Junwu; Hauss, Matthias; Tang, Ben Zhong., *Polymer Preprints (American Chemical Society, Division of Polymer Chemistry)*, 2003, **44**, 956-957.
41. Zheng, Ronghua; Peng, Han; Lam, Jacky Wing Yip; Chen, Junwu; Hausler, Matthias; Tang, Ben Zhong., *Abstracts of Papers, 225th ACS National Meeting, New Orleans, LA, United States, March* 23-27, 2003, 2003, POLY-270.
42. Dereli, Okan; Duz, Bulent; Zumreoglu-Karan, Birgul; Imamoglu, Yavuz., Applied Organometallic Chemistry, 2003, **17**, 23-27.
43. Liang, Hui; Yan, Jiaguo; Lu, Jiang, *Synthetic Metals*, 2004, **142**, 143-145.
44. Sacchi, Maria Carmela; Forlini, Fabrizio; Losio, Simona; Tritto, Incoronata; *Macromolecular Symposia*, 2003, **193**(5th Annual UNESCO School & IUPAC Conference on *Macromolecules* & Materials Science, 2002), 45-56.
45. Teplyakov, V. V.; Roizard, D.; Favre, E.; Khotimsky, V. S., *Journal of Membrane Science*, 2003, **220**, 165-175.
46. Takafuji, Makoto; Ide, Shunichi; Ihara, Hirotaka; Xu, Zhenghe, *Chemistry of Materials*, 2004, **16**, 1977-1983.
47. Delaude, L.; Demonceau, A.; Noels, A. F., *NATO Science Series, II: Mathematics, Physics and Chemistry* , 2003, **122**(Novel Metathesis Chemistry), 249-261.
48. Thorn, Kevin A.; Thorne, Philip G.; Cox, Larry G., *Environmental Science and Technology*, 2004, **38**, 2224-2231.
49. Mori, Hideharu; Walther, Andreas; Andre, Xavier; Lanzendoerfer, Michael G.; Mueller, Axel H. E., *Macromolecules*, 2004, **37**, 2054-2066.
50. Soykan, Cengiz; Erol, Ibrahim, *Journal of Polymer Research*, 2004, **11**, 53-63.
51. Rudisin, Amanda N.; Eyestone, Willard H.; Huckle, William R.; Long, Timothy E., *Polymer Preprints (American Chemical Society, Division of Polymer Chemistry)*, 2004, **45**, 129-130.
52. Georgiou, Theoni K.; Yamasaki, Edna N.; Phylactou, Leonidas A.; Vamvakaki, Maria; Patrickios, Costas S., *Abstracts of Papers, 227th ACS National Meeting, Anaheim, CA, United States, March* 28-*April* 1, 2004 , 2004, BIOT-304.
53. Stalgren, J. J. R.; Pamedytyte, V.; Makuska, R.; Claesson, P. M.; Brown, W.; Jacobsson, U., *Polymer International*, 2003, **52**, 399-405.
54. Hong, Chun-Yan; Zou, Ying-Fang; Pan, Cai-Yuan.,*Polymer International*, 2003,

52, 257-264.

55. Kilian, Lars; Perry, Matthew D.; Dick, Rebecca R.; Long, Timothy E., *Abstracts of Papers, 225th ACS National Meeting, New Orleans, LA, United States, March* 23-27, 2003, 2003, POLY-596.
56. Yang, Seung Rim; Jeong, Jae Hyun; Park, Kinam; Kim, Jong-Duk.,*Colloid and Polymer Science* , 2003, **281**, 852-861.
57. Ji, Xiang-Ling; Jiang, Shi-Chun; Qiu, Xue-Peng; Dong, De-Wen; Yu, Dong-Hong; Jiang, Bing-Zheng., *Journal of Applied Polymer Science*, 2003, **88**, 3168-3175.
58. Domjan, Attila; Erdoedi, Gabor; Wilhelm, Manfred; Neidhoefer, Michael; Landfester, Katharina; Ivan, Bela; Spiess, Hans Wolfgang, *Macromolecules*, 2003, **36**, 9107-9114.
59. Mavroudis, Anastasios; Avgeropoulos, Apostolos; Hadjichristidis, Nikos; Thomas, Edwin L.; Lohse, David J., *Chemistry of Materials*, 2003,**15**, 1976-1983.
60. Lizotte, Jeremy R.; Long, Timothy E., *Macromolecular Chemistry and Physics*, 2003, **204**, 570-576.
61. Morita, Ayako; Kudo, Hiroto; Nishikubo, Tadatomi., Polymer Journal (Tokyo, Japan), 2004, **36**, 413-421.
62. Schmaljohann, Dirk; Komber, Hartmut; Barratt, Joshua G.; Appelhans, Dietmar; Voit, Brigitte I., *Macromolecules*, 2003, **36**, 97-108.
63. Sheina, Elena E.; McCullough, Richard D., *Polymer Preprints (American Chemical Society, Division of Polymer Chemistry)*, 2003, **44**, 885.
64. Sheina, Elena E.; McCullough, Richard D. , *Abstracts of Papers, 226th ACS National Meeting, New York, NY, United States, September* 7-11, 2003, 2003, POLY-136.
65. Mai, Yiyong; Zhou, Yongfeng; Yan, Deyue; Lu, Hongwu., China. *Macromolecules*, 2003, **36**, 9667-9669.
66. Coppo, Paolo; Cupertino, Domenico C.; Yeates, Stephen G.; Turner, Michael L.,*Macromolecules*, 2003, **36**, 2705-2711.
67. Selvam, P.; Babu, K. Victor; Penlidis, A.; Nanjundan, S., *Journal of Macromolecular Science, Pure and Applied Chemistry*, 2004, **41**, 791-809.
68. Selvamalar, C. S. Jone; Vijayanand, P. S.; Penlidis, A.; Nanjundan, S., *Journal of Applied Polymer Science*, 2004, **91**, 3604-3612.
69. Vijayanand, P. S.; Penlidis, A.; Nanjundan, S., *Journal of Macromolecular Science, Pure and Applied Chemistry*, 2003, **A40**, 125-140.
70. Selvamalar, C. S. Jone; Krithiga, T.; Penlidis, A.; Nanjundan, S., *Reactive & Functional Polymers* , 2003, **56**, 89-101.
71. Njus, Jeffrey M.; Yang, Lin; Foxman, Bruce M.; Sandman, Daniel J., *Polymer Preprints (American Chemical Society, Division of Polymer Chemistry)*, 2003, **44**, 905-906.
72. Balaji, R.; Kothandaraman, H.; Rajarathnam, D., *Journal of Applied Polymer Science*, 2003, **88**, 2468-2477.
73. Godwin, Gordon G.; Jone Selvamalar, C. S.; Penlidis, A.; Nanjundan, S., *Reactive & Functional Polymers*, 2004, **59**, 197-209.
74. Hooda, Sunita; Brar, A. S., *Journal of Applied Polymer Science*, 2003, **88**, 3232-3238.
75. Wickel, Holger; Agarwal, Seema; Greiner, Andreas., *Macromolecules*, 2003, **36**, 2397-2403.
76. Wickel, Holger; Agarwal, Seema., *Macromolecules*, 2003, **36**, 6152-6159.
77. Liaw, Der-Jang; Huang, Ching-Cheng; Hong, Shou-Mau., *Abstracts of Papers, 225th ACS National Meeting, New Orleans, LA, United States, March* 23-27, 2003 , 2003, POLY-263.

78. Liaw, Der-Jang; Huang, Ching-Cheng; Hong, Shou-Mau., *Polymer Preprints (American Chemical Society, Division of Polymer Chemistry)*, 2003, **44**, 943-944.
79. Jin, Ming; Lu, Ran; Bao, Chunyan; Xu, Tinghua; Zhao, Yingying, *Polymer*, 2004, **45**, 1125-1131.
80. Li, Xin-Gui; Huang, Mei-Rong; Hua, Yi-Min; Zhu, Mei-Fang; Chen, Qun, *Polymer*, 2004, **45**, 4693-4704.
81. Maslinska-Solich, Jolanta; Kukowka, Sylwia, *Macromolecular Bioscience*, 2004, **4**, 421-430.
82. Gao, Baojiao; Lu, Yuexian; Jiu, Hongfang, *Polymer International*, 2003, **52**, 1468-1473.
83. Moniruzzaman, M.; Fernando, G. F.; Talbot, J. D. R., *Journal of Polymer Science, Part A: Polymer Chemistry*, 2004, **42**, 2886-2896.
84. Loiseau, J.; Doeerr, N.; Suau, J. M.; Egraz, J. B.; Llauro, M. F.; Ladaviere, C.; Claverie, J., *Macromolecules*, 2003, **36**, 3066-3077.
85. Sawai, Daisuke; Kanamoto, Tetsuo; Yamazaki, Hitoshi; Hisatani, Kunio, *Macromolecules*, 2004, **37**, 2839-2846.
86. Bajaj, Pushpa; Sreekumar, T. V.; Sen, Kushal; Kumar, Rajeev; Brar, Ajaib Singh., *Journal of Applied Polymer Science*, 2003, **88**, 1211-1217.
87. Brar, A. S., *International Journal of Plastics Technology*, 2003, **6**, 77-80.
88. Brar, A. S. , *ACS Symposium Series*, 2003, **834**(NMR Spectroscopy of Polymers in Solution and in the Solid State), 166-173.
89. Brar, A. S.; Pradhan, D. R., *Journal of Polymer Materials*, 2003, **20**, 31-42.
90. Styron, Susan D.; Kiely, Donald E.; Ponder, Glenn., Journal of Carbohydrate Chemistry, 2003, **22**, 123-142.
91. Wong, Wai-Yeung; Wong, Chun-Kin; Lu, Guo-Liang; Lee, Albert Wai-Ming; Cheah, Kok-Wai; Shi, Jian-Xin., *Macromolecules*, 2003, **36**, 983-990.
92. Gaur, B.; Lochab, B.; Choudhary, V.; Varma, I. K., Journal of Thermal Analysis and Calorimetry, 2003, **71**, 467-479.
93. Souzy, Renaud; Ameduri, Bruno; Boutevin, Bernard, *Macromolecular Chemistry and Physics*, 2004, **205**, 476-485.
94. Chang, Yao-Te; Shu, Ching-Fong. Department of Applied Chemistry, *Macromolecules*, 2003, **36**, 661-666.
95. Lin, Qin; Long, Timothy E., *Macromolecules*, 2003, **36**, 9809-9816.
96. Fossum, Eric; Tan, Loon-Seng., *Polymer Preprints (American Chemical Society, Division of Polymer Chemistry)*, 2003, **44**, 862-863.
97. Fossum, Eric; Tan, L-S., *Abstracts of Papers, 225th ACS National Meeting, New Orleans, LA, United States, March* 23-27, 2003, 2003, POLY-219.
98. Haeussler, Matthias; Lam, Jacky Wing Yip; Hui, Tong; Zheng, Ronghua; Tang, Ben Zhong, *Abstracts of Papers, 227th ACS National Meeting, Anaheim, CA, United States, March* 28-*April* 1, 2004, 2004, POLY-129.
99. Shinoda, Hosei; Asou, Yukiko; Suetsugu, Akio; Tanaka, Kimiko., *Macromolecular Bioscience*, 2003, **3**, 34-43.
100. Sarmah, Diganta; Baruah, Shashi D., *Journal of Applied Polymer Science*, 2003, **90**, 2721-2726.
101. Hadjiyannakou, Stella C.; Vamvakaki, Maria; Patrickios, Costas S., *Abstracts of Papers, 225th ACS National Meeting, New Orleans, LA, United States, March* 23-27, 2003, 2003, COLL-292.
102. Barbosa, Maria Elisa Martinez; Cammas, Sandrine; Appel, Martine; Ponchel, Gilles, *BioMacromolecules*, 2004, **5**, 137-143.
103. Kricheldorf, Hans R.; Eggerstedt, Sven, *Journal of Macromolecular Science, Pure*

and Applied Chemistry, 2003, **A40**, 1009-1018.
104. Deb Nath, Dilip Chandra; Shiono, Takeshi; Ikeda, Tomiki, *Applied Catalysis, A: General*, 2003, **238**, 193-199.
105. Gromada, Jerome; le Pichon, Luc; Mortreux, Andre; Leising, Frederic; Carpentier, Jean-Francois., *Journal of Organometallic Chemistry*, 2003, **683**, 44-55
106. Bertini, Fabio; Canetti, Maurizio; De Chirico, Aurelio; Ricci, Giovanni., *Journal of Applied Polymer Science*, 2003, **88**, 2737-2743
107. Nagy, Miklos; Keki, Sandor; Deak, Gyoergy; Zsuga, Miklos., *Polymers for Advanced Technologies*, 2003, **14**, 807-812
108. Nikolic, Marija S.; Poleti, Dejan; Djonlagic, Jasna, *European Polymer Journal*, 2003, **39**, 2183-2192
109. Zhang, Yong; Feng, Zeng-Guo; Zhang, Ai-Ying., *Polymer International*, 2003, **52**, 1351-1358
110. Zhao, Yun Hui; Xu, Gen Hui; Jia, Hong Tao; Sheng, Jing., *Journal of Macromolecular Science, Pure and Applied Chemistry*, 2003, **A40**, 461-473
111. Sandhya, T. E.; Ramesh, C.; Sivaram, S., *Macromolecular Symposia*, 2003, **199**(Polycondensation 2002), 467-482
112. Rim, Chinwon; Son, David Y., *Macromolecules*, 2003, **36**, 5580-5584
113. Kawakami, Yusuke., Polymers for Advanced Technologies, 2003, **14**, 314-319
114. Kim, Young-jin; Chung, Joo Eun; Kurisawa, Motoichi; Uyama, Hiroshi; Kobayashi, Shiro, *Macromolecular Chemistry and Physics*, 2003, **204**, 1863-1868
115. An, Sung Guk; Cho, Chang Gi., *Polymer Bulletin (Heidelberg, Germany)*, 2004, **51**, 255-262
116. Hill, David J. T.; Thurecht, Kristofer J.; Whittaker, Andrew K., *Radiation Physics and Chemistry*, 2003, **67**, 729-736
117. Bhatia, Dhiraj; Braun, D.; Choudhary, Veena, *Indian Journal of Chemical Technology*, 2003, **10**, 548-557
118. Quirk, Roderic P.; You, Fengxiang; Zhu, Lei; Cheng, Stephen Z. D. ,*Macromolecular Chemistry and Physics*, 2003, **204**, 755-761
119. Hsu, Tsung-Ju; Tan, Chung-Sung., *Journal of the Chinese Institute of Chemical Engineers*, 2003, **34**, 335-344.
120. Wackerly, Jay Wm., Jr.; Nalli, Thomas W., *Abstracts of Papers, 225th ACS National Meeting, New Orleans, LA, United States, March* 23-27, 2003, 2003, CHED-615.
121. Nguyen, Cung An; Allemann, Eric; Schwach, Gregoire; Doelker, Eric; Gurny, Robert., *International Journal of Pharmaceutics*, 2003, **254**, 69-72.
122. Belleney, J.; Wisniewski, M.; Le Borgne, A., *European Polymer Journal*, 2004, **40**, 523-530.
123. Kang, Eui-Chul; Kaneko, Tatsuo; Shiino, Daijiro; Akashi, Mitsuru., *Journal of Polymer Science, Part A: Polymer Chemistry*, 2003, **41**, 841-852.
124. Dai, Qiu; Zhang, Zhicheng; Wang, Feng; Liu, Jie., *Journal of Applied Polymer Science*, 2003, **88**, 2732-2736.
125. Chaubal, Mahesh V.; Wang, Bing; Su, Geraldine; Zhao, Zhong, *Journal of Applied Polymer Science*, 2003, **90**, 4021-4031.
126. Zhang, Lifang; Shen, Zhiquan; Yu, Cuiping; Fan, Ling., *Journal of Macromolecular Science, Pure and Applied Chemistry*, 2004, **41**, 927-935.
127. Zhang, Lifang; Yu, Cuiping; Shen, Zhiquan, *Polymer Bulletin (Heidelberg, Germany)*, 2003, **51**, 47-53.
128. Li, Jun; Chen, Bin; Wang, Xin; Goh, Suat Hong.,*Polymer*, 2004, **45**, 1777-1785.
129. Choi, Jeongsoo; Kwak, Seung-Yeop., *Macromolecules*, 2003, **36**, 8630-8637.
130. Cui, Yanjun; Ma, Xiaomei; Tang, Xiaozhen; Luo, Yinpei, *European Polymer Jour-*

nal, 2003, Volume Date 2004, **40**, 299-305.
131. Fey, Thomas; Keul, Helmut; Hoecker, Hartwig., *e-Polymers*, 2003.
132. Rodriguez-galan, Alfonso; Vera, Montserrat; Jimenez, Katia; Franco, Lourdes; Puiggali, Jordi, *Macromolecular Chemistry and Physics*, 2003, **204**, 2078-2089.
133. Wrobleski, Debra A.; Langlois, David A.; Orler, E. Bruce; Dattelbaum, Dana M.; Small, James H., *Abstracts of Papers, 227th ACS National Meeting, Anaheim, CA, United States, March* 28-*April* 1, 2004, 2004, POLY-651.
134. Su, Ya-li; Li, Xiu-ru; Tong, Yue-jin; Li, Yue-sheng., *Chinese Journal of Polymer Science*, 2004, **22**, 1-5.
135. Li, Xiu-Ru; Li, Yue-Sheng., *Polymer*, 2003, **44**, 3855-3863.
136. Van Axel Castelli, Valeria; Segre, Anna L.; Busico, Vincenzo; Friederichs, Nicolaas; van der Velden, Geert.,*Abstracts of Papers, 225th ACS National Meeting, New Orleans, LA, United States, March* 23-27, 2003, 2003, POLY-576
137. Wendt, Ralf Alexander; Fink, Gerhard, *Journal of Molecular Catalysis A: Chemical*, 2003, **203**, 101-111.
138. Chang, Yao-te; Shu, Ching-fong; Leu, Chyi-ming; Wei, Kung-hwa, *Journal of Polymer Science, Part A: Polymer Chemistry*, 2003, **41**, 3726-3735.
139. Li, Xiuru; Li, Yuesheng; Tong, Yuejin; Shi, Linqi; Liu, Xiaohang., *Macromolecules*, 2003, **36**, 5537-5544.
140. Kricheldorf, Hans R.; Vakhtangishvili, Lali; Schwarz, Gert; Schulz, Gunter; Kruger, Ralf-Peter, *Polymer*, 2003, **44**, 4471-4480.
141. Burel, Fabrice; Rossignol, Laetitia; Pontvianne, Pascale; Hartman, Jonas; Couesnon, Nicole; Bunel, Claude., *e-Polymers*, 2003, Paper No. 31.
142. Naguib, Hala F.; Mokhtar, Samia M.; Ali, Raouf O.; Elsabee, Maher Z., *Journal of Polymer Science, Part A: Polymer Chemistry*, 2003, **41**, 3180-3187.
143. Dai, S.; Ravi, P.; Leong, C. Y.; Tam, K. C.; Gan, L. H., Langmuir, 2004, **20**, 1597-1604.
144. Akiyama, Yoshitsugu; Nagasaki, Yukio; Kataoka, Kazunori, Bioconjugate Chemistry, 2004, **15**, 424-427.
145. Lin, Qin; Unal, Serkan; Fornof, Ann R.; Wei, Yuping; Long, Timothy E. , *Polymer Preprints (American Chemical Society, Division of Polymer Chemistry)*, 2003, **44**, 191-192.
146. Jia, Zhifeng; Yan, Deyue., *Abstracts of Papers, 225th ACS National Meeting, New Orleans, LA, United States, March* 23-27, 2003, 2003, POLY-240.
147. Powell, Kenya T.; Gudipati, Chakravarthy; Wooley, Karen L., *Abstracts of Papers, 226th ACS National Meeting, New York, NY, United States, September* 7-11, 2003, 2003, PMSE-469.
148. van Dijkhuizen-Radersma, R.; Roosma, J. R.; Kaim, P.; Metairie, S.; Peters, F. L. A. M. A.; de Wijn, J.; Zijlstra, P. G.; de Groot, K.; Bezemer, J. M., Journal of Biomedical Materials Research, Part A, 2003, **67A**, 1294-1304.
149. Lapienis, Grzegorz; Penczek, Stanislaw, *Journal of Polymer Science, Part A: Polymer Chemistry*, 2004, **42**, 1576-1598.
150. Saf, Robert; Schwarzenbacher, Gerald; Mirtl, Christian; Hayn, Gertraud; Hobisch, Josefine; Gatterer, Karl, Macromolecular Rapid Communications, 2004, **25**, 911-915.
151. Li, Jun; Li, Xu; Ni, Xiping; Leong, Kam W., *Macromolecules*, 2003, **36**, 2661-2667.
152. Ma, Zhi; Lacroix-Desmazes, Patrick, *Journal of Polymer Science, Part A: Polymer Chemistry*, 2004, **42**, 2405-2415.
153. Ma, Y.; Agarwal, U. S.; Vekemans, J. A. J. M.; Sikkema, D. J., *Polymer*, 2003, **44**, 4429-4434

154. Samperi, Filippo; Puglisi, Concetto; Alicata, Rossana; Montaudo, Giorgio., *Polymer Degradation and Stability*, 2004, **83**, 11-17.
155. Samperi, Filippo; Puglisi, Concetto; Alicata, Rossana; Montaudo, Giorgio, *Polymer Degradation and Stability*, 2004, **83**, 3-10.
156. Kint, Darwin P. R.; Alla, Abdelilah; Deloret, Elise; Campos, Josefina L.; Munoz-Guerra, Sebastian. *Polymer*, 2003, **44**, 1321-1330.
157. Kamau, Stephen D.; Hodge, Philip; Helliwell, Madeleine, *Polymers for Advanced Technologies*, 2003, **14**, 492-501.
158. Tessier, Martine; Fradet, Alain, *e-Polymers*, 2003, Paper No. 30.
159. Matsuda, Hironori; Nagasaka, Bunsow; Asakura, Tetsuo, *Polymer*, 2003, **44**, 4681-4687.
160. Matsuda, Hironori; Asakura, Tetsuo, *Macromolecules*, 2004, **37**, 2163-2170.
161. Monwar, Masud; Rinaldi, Peter L.; McCord, Elizabeth F.; Marshall, Donald R.; Buback, Michael; Latz, Henning., *Polymer Preprints (American Chemical Society, Division of Polymer Chemistry)*, 2003, **44**, 257-258.
162. Sahoo, Sangrama K.; Zhang, Tong; Reddy, D. Venkat; Rinaldi, Peter L.; McIntosh, Lester H.; Quirk, Roderick P., *Macromolecules*, 2003, **36**, 4017-4028.
163. Van Axel Castelli, Valeria; Segre, AnnaLaura; Busico, Vincenzo; Friederichs, Nicolaas; van der Velden, Geert., *Polymer Preprints (American Chemical Society, Division of Polymer Chemistry)*, 2003, **44**, 379-380.
164. Hagihara, Hideaki; Tsuchihara, Kenji; Takeuchi, Kazuhiko; Murata, Masahide; Ozaki, Hiroyuki; Shiono, Takeshi, *Journal of Polymer Science, Part A: Polymer Chemistry*, 2003, **42**, 52-58.
165. Mustonen, Ilpo; Hukka, Terttu; Pakkanen, Tuula T., *Macromolecular Chemistry and Physics*, 2003, **204**, 471-480.
166. Jongsomjit, Bunjerd; Kaewkrajang, Paninee; Wanke, Sieghard E.; Praserthdam, Piyasan, *Catalysis Letters*, 2004, **94**, 205-208.
167. Sahoo, Sangrama K.; Reddy, D. Venkat; Zhang, Tong; Rinaldi, Peter L.; McIntosh, Lester H.; Quirk, Roderick P., *Abstracts of Papers, 225th ACS National Meeting, New Orleans, LA, United States, March* 23-27, 2003, 2003, POLY-573.
168. Sahoo, Sangrama K.; Reddy, D. Venkat; Zhang, Tong; Rinaldi, Peter L.; McIntosh, Lester H.; Quirk, Roderick P., *Polymer Preprints (American Chemical Society, Division of Polymer Chemistry)*, 2003, **44**, 373-374.
169. Savitski, Edward P.; Caflisch, George B.; Killian, Christopher M.; Meadows, Michael D.; Merkley, Joseph H.; Huff, Brenda J., *Journal of Applied Polymer Science*, 2003, **90**, 722-728.
170. Rinaldi, Peter L.; Monwar, Masud; McCord, Elizabeth F.; Marshall, Donald R.; Buback, Michael; Latz, Henning., *Abstracts of Papers, 225th ACS National Meeting, New Orleans, LA, United States, March* 23-27, 2003, 2003, POLY-376.
171. Sworen, John C.; Smith, Jason A.; Wagener, Kenneth B.; Baugh, Lisa S.; Rucker, Steven P. Journal of the American Chemical Society, 2003, **125**, 2228-2240.
172. Busico, Vincenzo; Cipullo, Roberta; Polzone, Carmen; Talarico, Giovanni; Chadwick, John C., *Macromolecules*, 2003, **36**, 2616-2622.
173. Escher, Fernanda F. Nunes; Galland, Griselda Barrera; Ferreira, Marcio, *Journal of Polymer Science, Part A: Polymer Chemistry*, 2003, **41**, 2531-2541.
174. Mayer, Bernhard X.; Rauter, Walfried; Kaehlig, Hanspeter; Zoellner, Peter, *Journal of Separation Science*, 2003, **26**, 1436-1442.
175. Agarwal, Seema; Xie, Xiulan.,*Macromolecules*, 2003, **36**, 3545-3549.
176. Brar, A. S.; Yadav, A.; Kaur, Manpreet., *Abstracts of Papers, 225th ACS National Meeting, New Orleans, LA, United States, March* 23-27, 2003, 2003, POLY-580.

177. Brar, Ajaib Singh; Yadav, Anil.,*Polymer Journal (Tokyo, Japan)*, 2003, **35**, 37-43.
178. Subramanyam, U.; Rajamohanan, P. R.; Sivaram, S., *Polymer*, 2004, **45**, 4063-4076.
179. Benson, Adrienne; Graves, Erin; Omrane, Kamel; Haas, Amy Lynn; Mandalaywala, Monisha; Mueller, Anja, *Polymer Preprints (American Chemical Society, Division of Polymer Chemistry)*, 2004, **45**, 108-109.
180. Nakas, James; Keenan, T. J.; Stipanovic, A.; Tanenbaum, S. W., *Abstracts of Papers, 227th ACS National Meeting, Anaheim, CA, United States, March* 28-*April* 1, 2004, 2004, CELL-130.
181. Jia, Zhifeng; Yan, Deyue., *Polymer Preprints (American Chemical Society, Division of Polymer Chemistry)*, 2003, **44**, 901-902.
182. Holder, Simon J.; Rossi, Nicholas A. A.; Yeoh, Chert-Tsun; Durand, Geraldine G.; Boerakker, Mark J.; Sommerdijk, Nico A., *J. M., Journal of Materials Chemistry*, 2003, **13**, 2771-2778.
183. Phinyocheep, Pranee; Pasiri, Sureemas; Tavichai, Orasa., *Journal of Applied Polymer Science*, 2003, **87**, 76-82.
184. Leonora de Castro, Maria; Wang, Shu Hui, *Polymer Bulletin (Heidelberg, Germany)*, 2003, **51**, 151-158.
185. Dong, Chang-Ming; Sun, Xue-Long; Faucher, Keith M.; Apkarian, Robert P.; Chaikof, Elliot L., Bio*Macromolecules*, 2004, **5**, 224-231
186. Li, Hong; Wang, Chenhong; Bai, Feng; Yue, Jin; Woo, Hee-Gweon, Organometallics, 2004, **23**, 1411-1415
187. Zhao, Youliang; Shuai, Xintao; Chen, Chuanfu; Xi, Fu., *Chemistry of Materials*, 2003, **15**, 2836-2843
188. Gamble, Carolyn L.; Hall, Kirsten C.; Hofmeister, Gretchen E., *Abstracts of Papers, 225th ACS National Meeting, New Orleans, LA, United States, March* 23-27, 2003, 2003, CHED-1041
189. Guerpinar, Oe. Aylin; Tuzlakoglu, Kadriye; Onur, M. Ali; Tuemer, Askin; Serdar, Muhittin A.; Uenal, Nilay; Piskin, Erhan, *Journal of Biomaterials Science, Polymer Edition*, 2003, **14**, 589-600
190. Jeon, Oju; Lee, Soo-Hong; Kim, Soo Hyun; Lee, Young Moo; Kim, Young Ha., *Macromolecules*, 2003, **36**, 5585-5592
191. Ba, Chaoyi; Yang, Jing; Hao, Qinghui; Liu, Xiaoyun; Cao, Amin, *BioMacromolecules*, 2003, **4**, 1827-1834
192. He, Bin; Bei, Jianzhong; Wang, Shenguo, *Polymers for Advanced Technologies*, 2003, **14**, 645-652.
193. He, Bin; Bei, Jianzhong; Wang, Shenguo., *Polymer*, 2003, **44**, 989-994.
194. Wamsley, Andrea; Jasti, Bhaskara; Phiasivongsa, Pasit; Li, Xiaoling, *Journal of Polymer Science, Part A: Polymer Chemistry*, 2003, Volume Date 2004, **42**, 317-325.
195. Drury, Anna; Maier, Stefanie; Ruether, Manuel; Blau, Werner J., *Journal of Materials Chemistry*, 2003, **13**, 485-490.
196. Cianga, L.; Yagci, Y.; Fernandes, E. G.; Galli, G., *Designed Monomers and Polymers*, 2003, **6**, 145-158.
197. Wu, Jian; Beshah, Kebede. *ACS Symposium series*, 2003, **834**(NMR Spectroscopy of Polymers in Solution and in the Solid State), 345-357.
198. Jassal, Manjeet; Acharya, Badri Narayan; Bajaj, Pushpa, *Journal of Applied Polymer Science*, 2003, **89**, 1430-1441.
199. Ritter, Helmut; Schwarz-Barac, Sabine; Stein, Peter, *Macromolecules*, 2003, **36**, 318-322.
200. Brar, A. S.; Pradhan, D. R., *Journal of Molecular Structure*, 2003, **649**, 245-255.
201. Zhang, Huiqi; Jiang, Xulin; van der Linde, Rob., *Polymer*, 2004, **45**, 1455-1466.

202. Takasu, Akinori; Ishii, Masaya; Inai, Yoshihito; Hirabayashi, Tadamichi; Inomata, Katsuhiro., *Macromolecules*, 2003, **36**, 7055-7064.
203. Zhang, Hongwei; Mays, Jimmy W., *Abstracts of Papers, 227th ACS National Meeting, Anaheim, CA, United States, March* 28-*April* 1, 2004, 2004, POLY-484.
204. Rzayev, Javid; Dickinson, L. Charles; Penelle, Jacques, *Macromolecules*, 2003, **36**, 6273-6275.
205. Chen, Gaojian; Zhu, Xiulin; Cheng, Zhenping; Lu, Jianmei; Chen, Jianying, *Polymer International*, 2004, **53**, 357-363.
206. Isaure, Francoise; Cormack, Peter A. G.; Sherrington, David C., *Journal of Materials Chemistry*, 2003, **13**, 2701-2710.
207. He, Xiaohui; Yao, Yingzheng; Luo, Xiang; Zhang, Junkai; Liu, Yunhai; Zhang, Ling; Wu, Qing., *Organometallics*, 2003, **22**, 4952-4957.
208. Isaure, Francoise; Cormack, Peter A. G.; Sherrington, David C., *Macromolecules*, 2004, **37**, 2096-2105.
209. Melis, Karen; Verpoort, Francis., *Journal of Molecular Catalysis A: Chemical*, 2003, **201**, 33-41.
210. Hatada, Koichi; Kitayama, Tatsuki; Terawaki, Yoshio; Sato, Hisaya; Horii, Fumitaka; Araki, T.; Chujo, R.; Hashimoto, M.; Ikeyama, M.; Isokawa, A.; Kanda, M.; Kurosu, H.; Lee, K.; Matsumoto, A.; Matsumura, K.; Mizuno, A.; Mori, T.; Ninomiya, H.; Saito, H.; Sangen, S.; Shimoda, M.; Sueoka, K.; Takai, Y., *Polymer Journal (Tokyo, Japan)*, 2003, **35**, 393-398.
211. Carriere, Pascal; Feller, Jean-Francois; Dupuis, *Journal of Colloid and Interface Science*, 2004, **272**, 218-224.
212. Anand, Vishal; Choudhary, Veena.,*Journal of Applied Polymer Science*, 2003, **89**, 1195-1202.
213. Matlengiewicz, M., Advances in Plastics Technology, *International Conference, 5th, Katowice, Poland, Nov.* 4-6, 2003, 2003, P28/1-P28/6.
214. Brar, A. S., *Abstracts of Papers, 225th ACS National Meeting, New Orleans, LA, United States, March* 23-27, 2003, 2003, POLY-339.
215. Galia, Alessandro; Muratore, Antonino; Filardo, Giuseppe., Industrial & Engineering Chemistry Research, 2003, **42**, 448-455.
216. Hirai, Hidefumi., Polymers for Advanced Technologies, 2003, **14**, 266-272.
217. McCarron, Paul A.; Woolfson, A. David; Donnelly, Ryan F.; Andrews, Gavin P.; Zawislak, Agnieszka; Price, John H., *Journal of Applied Polymer Science*, 2004, **91**, 1576-1589.
218. Cui, Min-Hui; Zhang, Yuli; Werner, Mark; Yang, Nan-Loh; Fenelli, Steven P.; Grates, John A., *ACS Symposium Series*, 2003, **834**(NMR Spectroscopy of Polymers in Solution and in the Solid State), 228-241.
219. Bai, Jie; Shea, Kenneth J., *Abstracts of Papers, 227th ACS National Meeting, Anaheim, CA, United States, March* 28-*April* 1, 2004, 2004, POLY-233.
220. Masuda, Mitsutoshi; Jonkheijm, Pascal; Sijbesma, Rint P.; Meijer, E. W., *Journal of the American Chemical Society*, 2003, **125**, 15935-15940.
221. Anand, Vishal; Kumar, Rajeev; Choudhary, Veena, *Journal of Applied Polymer Science*, 2004, **91**, 2016-2027.
222. Oishi, Tsutomu; Isobe, Yukio; Onimura, Kenjiro; Tsutsumi, Hiromori., *Polymer Journal (Tokyo, Japan)*, 2003, **35**, 245-254.
223. Chung, Ildoo; Britt, Phillip; Mays, Jimmy W. Department of Chemistry, *Abstracts of Papers, 227th ACS National Meeting, Anaheim, CA, United States, March* 28-*April* 1, 2004, 2004, POLY-234.
224. Favier, Arnaud; Ladaviere, Catherine; Charreyre, Marie-Therese; Pichot, Chris-

tian, *Macromolecules*, 2004, **37**, 2026-2034.
225. Wysgoski, Faith J.; Rinaldi, Peter L.; McCord, Elizabeth F.; Stewart, Mark A.; Marshall, Donald R., *Macromolecules*, 2004, **37**, 846-855
226. Monwar, Masud; Oh, Sung Joon; Rinaldi, Peter L.; McCord, Elizabeth F.; Hutchinson, Robin A.; Buback, Michael M.; Latz, Henning, Analytical and Bioanalytical Chemistry, 2004, **378**, 1414-1427.
227. Kumar, Gulshan; Aggarwal, Saroj; Choudhary, Veena, Indian Journal of Chemistry, Section A: Inorganic, Bio-inorganic, Physical, Theoretical & Analytical Chemistry, 2004, **43A**, 278-281.
228. Ahn, Jun-Hwan; Shin, Yeong-Deuk; Kim, Sun-Young; Lee, Jae-Suk, *Polymer*, 2003, **44**, 3847-3854.
229. Monge, Sophie; Haddleton, David M.,*European Polymer Journal*, 2003, **40**, 37-45.
230. Ray, Biswajit; Isobe, Yutaka; Matsumoto, Kozo; Habaue, Shigeki; Okamoto, Yoshio; Kamigaito, Masami; Sawamoto, Mitsuo. *Macromolecules*, 2004, **37**, 1702-1710.
231. Guo, M. M. Polymer Science Institute, *Abstracts of Papers, 225th ACS National Meeting, New Orleans, LA, United States, March* 23-27, 2003, 2003, PMSE-152.
232. Bisht, Harender S.; Ray, Siddharth S.; Chatterjee, Alok K.,*European Polymer Journal*, 2003, **39**, 1413-1420.
233. Reddy, G. Jayasimha; Naidu, S. Venkata; Reddy, A. V. Rami, *Journal of Applied Polymer Science*, 2003, **90**, 2179-2186.
234. Tabei, Junichi; Nomura, Ryoji; Sanda, Fumio; Masuda, Toshio, *Macromolecules*, 2003, **36**, 8603-8608.
235. Hoshikawa, Naohiro; Hotta, Yuji; Okamoto, Yoshio, *Journal of the American Chemical Society*, 2003, **125**, 12380-12381.
236. Brar, A. S.; Kumar, Rajeev; Kaur, Manpreet., Journal of Molecular Structure, 2003, **650**, 85-92.
237. Myagmarsuren, G.; Lee, Ki-Soo; Jeong, O-Yong; Ihm, Son-Ki., Catalysis Communications, 2003, **4**, 615-619.
238. Myagmarsuren, G.; Lee, Ki-Soo; Jeong, O-Yong; Ihm, Son-Ki, *Polymer*, 2004, **45**, 3227-3232.
239. Yeh, An-chi., *Journal of the Chinese Chemical Society (Taipei, Taiwan)*, 2003, 50, 959-964.
240. Cobo, Noelia; Esteruelas, Miguel A.; Gonzalez, Fernando; Herrero, Juana; Lopez, Ana M.; Lucio, Patricia; Olivan, Montserrat, *Journal of Catalysis*, 2004, **223**, 319-327.
241. Yang, Yi-Yan; Shi, Meng; Goh, Suat-Hong; Moochhala, Shabbir M.; Ng, Steve; Heller, Jorge., *Journal of Controlled Release*, 2003, **88**, 201-213.
242. Chen, Su; Chen, Li. Chemical College, *Colloid and Polymer Science*, 2003, 281, 288-291.
243. Kowalczuk-Bleja, A.; Trzebicka, B.; Komber, H.; Voit, B.; Dworak, A., *Polymer*, 2004, **45**, 9-18.
244. Mawatari, Yasuteru; Tabata, Masayoshi; Sadahiro, Yohikazu., *Polymer Preprints (American Chemical Society, Division of Polymer Chemistry)*, 2003, **44**, 691-692.
245. Chu, Qinghui; Pang, Yi; Ding, Liming; Karasz, Frank E., *Macromolecules*, 2003, **36**, 3848-3853.
246. Senthilkumar, U.; Ganesan, Kilivelu; Reddy, B. S. R., *Journal of Polymer Research*, 2003, **10**, 21-29.
247. Narendran, N.; Kishore, K., *Journal of Applied Polymer Science*, 2003, **87**, 626-631.
248. Boggioni, Laura; Bertini, Fabio; Zannoni, Giulio; Tritto, Incoronata; Carbone,

Paola; Ragazzi, Massimo; Ferro, Dino R., Milan, Italy. *Macromolecules*, 2003, **36**, 882-890.
249. Zhu, Q.; Meng, Y. Z.; Tjong, S. C.; Zhang, Y. M.; Wan, W.,*Polymer International*, 2003, **52**, 799-804.
250. Du, L. C.; Meng, Y. Z.; Wang, S. J.; Tjong, S. C., *Journal of Applied Polymer Science*, 2004, **92**, 1840-1846.
251. Shemper, Bianca S.; Mathias, Lon J., *European Polymer Journal*, 2004, **40**, 651-665.
252. Chakraborty, Debashis; Rodriguez, Antonio; Chen, Eugene Y.-X., *Macromolecules*, 2003, **36**, 5470-5481.
253. Randall, James C.; Alamo, Rufina G.; Agarwal, Pawan K.; Ruff, Charles J., *Macromolecules*, 2003, **36**, 1572-1584.
254. Zhang, Yu-Dong, *Macromolecules*, 2004, **37**, 2471-2477.
255. Zhang, Yudong, *Polymer*, 2004, **45**, 2651-2656.
256. Zhang, Yudong; Qiao, Jinliang; Wu, Changjiang., *Polymer Preprints* (*American Chemical Society, Division of Polymer Chemistry*), 2003, 44, 375-376.
257. Zhang, Yudong; Wu, Changjiang., *Abstracts of Papers, 225th ACS National Meeting, New Orleans, LA, United States, March* 23-27, 2003, 2003, POLY-574.
258. Kowalewska, A.; Stanczyk, W. A., *Chemistry of Materials*, 2003, **15**, 2991-2997.
259. Liu, Yang; Imae, Ichiro; Makishima, Akio; Kawakami, Yusuke., Science and Technology of Advanced Materials, 2003, **4**, 27-34.
260. Suzuki, Hiroshi; Tajima, Seitarou; Sasaki, Hiroshi, *ACS Symposium Series*, 2003, **847**(Photoinitiated Polymerization), 306-316.
261. Lienhard, M.; Wiegand, C.; Apple, T.; Interrante, L. V., Journal of Organometallic Chemistry, 2003, **686**, 272-280.
262. Torres, Edgar; Dutta, Naba; Choudhury, Namita Roy; Matisons, Janis, Polymer Engineering and Science, 2004, **44**, 736-748.
263. Nogueira, Regina F.; Tavares, Maria Ines B., *Journal of Applied Polymer Science*, 2003, **88**, 1004-1009.
264. Ramakrishnan, A.; Dhamodharan, R, *Macromolecules*, 2003, **36**, 1039-1046. .
265. Dahman, Yaser; Puskas, Judit E.; Margaritis, Argyrios; Merali, Zaheer; Cunningham, Michael., *Macromolecules*, 2003, **36**, 2198-2205.
266. Taskiran, Isa; Sunal, Guerkan; Erbay, Erol; Uyanik, Nurseli, *Journal of Applied Polymer Science*, 2003, **90**, 609-614.
267. Iovu, Mihaela-Corina; Buzdugan, Emil; Ghioca, Paul; Britchi, Alina Gabriela; Mapolie, Selwyn F.; Iovu, Horia., Revue Roumaine de Chimie, 2003, **48**, 163-171.
268. Hiller, Wolf; Pasch, Harald., *ACS Symposium Series*, 2003, **834**(NMR Spectroscopy of Polymers in Solution and in the Solid State), 338-343.
269. Cardona, Francisco; Hill, David J. T.; Pomery, Peter J.; Whittaker, Andrew K., *Polymer International*, 2003, **52**, 1711-1718.
270. Liang, Guozheng; Meng, Jiru; Zhao, Lei, *Polymer International*, 2003, **52**, 966-972.
271. Wu, De-Cheng; Hong, Chun-Yan; Pan, Cai-Yuan; He, Wei-Dong.,*Polymer International*, 2003, **52**, 98-103.
272. Quirk, Roderic P.; Gomochak, Deanna L.; Wesdemiotis, Chrys; Arnould, Mark A., *Journal of Polymer Science, Part A: Polymer Chemistry*, 2003, **41**, 947-957.
273. Quirk, Roderic P.; Gomochak, Deanna L.; Bhatia, Rajeev S.; Wesdemiotis, Chrys; Arnould, Mark A.; Wollyung, Kathleen, *Macromolecular Chemistry and Physics*, 2003, **204**, 2183-2196.
274. Ellis, David A.; Martin, Jonathan W.; Muir, Derek C. G.; Mabury, Scott A., *Analyst* (*Cambridge, United Kingdom*), 2003, **128**, 756-764.
275. Kostov, George; Ameduri, Bruno; Boutevin, Bernard; Bauduin, Gerard; Stankova,

Maya, *Journal of Polymer Science, Part A: Polymer Chemistry*, 2004, **42**, 1693-1706
276. Hutchenson, Keith W., *Journal of Chemical and Engineering Data*, 2003, **48**, 1028-1036
277. Hill, D. J. T.; Mohajerani, S.; Whittaker, A. K.; Scheler, U., *Polymer International*, 2003, **52**, 1725-1733
278. Lappan, U.; Geissler, U.; Scheler, U.; Lunkwitz, K., *Radiation Physics and Chemistry*, 2003, **67**, 447-451
279. Yamamoto, Takakazu; Arai, Minoru; Kokubo, Hisashi; Sasaki, Shintaro., *Macromolecules*, 2003, **36**, 7986-7993
280. Kim, Joon Ho; Park, Jun Ho; Jang, Ho Kyu; Yoon, Ji Young; Lyoo, Won Seok, *Journal of Applied Polymer Science*, 2003, **90**, 2200-2205
281. Abdelrehim, Mona; Komber, Hartmut; Langenwalter, Joseph; Voit, Brigitte; Bruchmann, Bernd, *Journal of Polymer Science, Part A: Polymer Chemistry*, 2004, **42**, 3062-3081.
282. Iovu, Mihaela Corina; Matyjaszewski, Krzysztof, *Macromolecules*, 2003, **36**, 9346-9354.
283. Wu, Jun; Oh, Jung Kwon; Yang, Jian; Winnik, Mitchell A.; Farwaha, Rajeev; Rademacher, Jude., *Macromolecules*, 2003, **36**, 8139-8147.
284. Park, Jun Wuk; Im, Seung Soon., *Polymer*, 2003, **44**, 4341-4354.
285. Myers, Sharon A.; Tsou, Li-Chun; Heiler, David J. *Abstracts of Papers, 225th ACS National Meeting, New Orleans, LA, United States, March* 23-27, 2003, 2003, POLY-570.
286. Brar, A. S.; Kumar, R.; Yadav, A.; Kaur, M. *ACS Symposium Series*, 2003, **834**(NMR Spectroscopy of Polymers in Solution and in the Solid State), 174-178.
287. Martinez, G.; Millan, J.; Contreras, J., *Journal of Polymer Science, Part A: Polymer Chemistry*, 2003, **41**, 508-519.
288. Guarrotxena, Nekane; Schue, Francois; Collet, Andre; Millan, Jose-Luis., *Polymer International*, 2003, **52**, 420-428.
289. Wu, June Y.; Pathre, Sadanand V., *Polymer Preprints (American Chemical Society, Division of Polymer Chemistry)*, 2003, **44**, 394-395.
290. Wu, June; Pathre, Sadanand V., *Abstracts of Papers, 225th ACS National Meeting, New Orleans, LA, United States, March* 23-27, 2003, 2003, POLY-584.
291. Kim, Woo-Sik; Byun, Kyung-Rock; Lee, Dong-Ho; Min, Kyung-Eun; Park, Lee-Soon; Seo, Kwan-Ho; Kang, Inn-Kyu; Park, Soo-Young, Polymer Journal (Tokyo, Japan), 2003, **35**, 450-454.
292. Naka, Kensuke; Umeyama, Tomokazu; Nakahashi, Akiko; Chujo, Yoshiki., *Abstracts of Papers, 225th ACS National Meeting, New Orleans, LA, United States, March* 23-27, 2003, 2003.
293. Souzy, Renaud; Ameduri, Bruno; von Ahsen, Stefan; Willner, Helge; Arguello, Gustavo A, *Journal of Fluorine Chemistry*, 2003, **123**, 85-93.
294. Koseli, Volkan; Rzaev, Zakir M. O.; Piskin, Erhan., *Journal of Polymer Science, Part A: Polymer Chemistry*, 2003, **41**, 1580-1593.
295. Montornes, J. M.; Reina, J. A.; Ronda, J. C.,*Journal of Polymer Science, Part A: Polymer Chemistry*, 2004, **42**, 3002-3012.
296. White, Bryan M.; Watson, W. Philip; Beckham, Haskell W., *Polymer Preprints (American Chemical Society, Division of Polymer Chemistry)*, 2003, **44**, 839-840.
297. Fan, Qu-Li; Lu, Su; Lai, Yee-Hing; Hou, Xiao-Yuan; Huang, Wei., *Macromolecules*, 2003, **36**, 6976-6984.
298. Pautzsch, Thomas; Klemm, Elisabeth, *Journal of Polymer Science, Part A: Polymer Chemistry*, 2004, 42, 2911-2919.

299. Oyaizu, Kenichi; Yonemaru, Hiroyuki; Iwasaki, Tomokazu; Matsubara, Ryohei; Tsuchida, Eishun., *Journal of Macromolecular Science, Pure and Applied Chemistry*, 2003, **A40**, 415-423.
300. Proto, Antonio; Capacchione, Carmine; Venditto, Vincenzo; Okuda, Jun, *Macromolecules*, 2003, **36**, 9249-9251.
301. Masayoshi, Tabata; Takeyuki, Sone; Yasuteru, Mawatari; Daigo, Yonemoto; Atsushi, Miyasaka; Takashi, Fukushima; Yoshikazu, Sadahiro., *Macromolecular Symposia*, 2003, **192**(7th Pacific Polymer Conference, 2001), 75-97.
302. Jaumann, Manfred; Rebrov, Eugene A.; Kazakova, Valentina V.; Muzafarov, Aziz M.; Moller, Martin., *Macromolecular Chemistry and Physics*, 2003, **204**, 1014-1026.
303. Robertson, Gilles P.; Guiver, Michael D.; Yoshikawa, Masakazu; Brownstein, Sydney, *Polymer*, 2004, **45**, 1111-1117.
304. Nasar, A. Sultan; Jikei, Mitsutoshi; Kakimoto, Masa-aki., *European Polymer Journal*, 2003, **39**, 1201-1208.
305. Ward, Rachel E.; Meyer, Tara Y., *Macromolecules*, 2003, 36, 4368-4373.
306. Matsuda, Hironori; Nagasaka, Bunsow; Asakura, Tetsuo, Polymer Journal (Tokyo, Japan), 2003, **35**, 740-747.
307. Nath, Dilip Chandra Deb; Shiono, Takeshi; Ikeda, Tomiki, Institute of Technology, Yokohama, Japan. *Macromolecular Chemistry and Physics*, 2003, **204**, 2017-2022.
308. Bertini, Fabio; Canetti, Maurizio; Ricci, Giovanni, *Journal of Applied Polymer Science*, 2004, **92**, 1680-1687.
309. Yang, Mei-Hui; Lin, Hsin-Tso; Lin, Chih-Chun., Journal of the Chinese Chemical Society (Taipei, Taiwan), 2003, **50**, 51-57.
310. Packirisamy, S.; Ambadas, Govind; Rama Rao, M.; Ninan, K. N., *European Polymer Journal*, 2003, **39**, 1077-1080.
311. Francis, A. U.; Venkatachalam, S.; Kanakavel, M.; Ravindran, P. V.; Ninan, K. N., *European Polymer Journal*, 2003, **39**, 831-841.
312. Qin, Haihu; Chakulski, Brian J.; Mather, P. T.; Constable, Gregory S.; Coughlin, E. Bryan.,*Abstracts of Papers, 225th ACS National Meeting, New Orleans, LA, United States, March* 23-27, 2003, 2003, POLY-335.
313. Kou, Huiguang; Shi, Wenfang; Lu, Yonghua; Hai, Ming., *Polymer International*, 2003, **52**, 1088-1094.
314. De Luca, Edoardo; Richards, Randal W., *Journal of Polymer Science, Part B: Polymer Physics*, 2003, **41**, 1339-1351.
315. Higashi, Fukuji; Moriya, Miwako., *Journal of Polymer Science, Part A: Polymer Chemistry*, 2003, **41**, 821-830.
316. Qian, Zhiyong; Li, Sai; Zhang, Hailian; Liu, Xiaobo., *Colloid and Polymer Science*, 2003, **281**, 869-875.
317. Yamamoto, Kiyoshi; Kakita, Reiko; Suzuki, Chitoshi; Meno, Masanori; Nozawa, Yoko, *Applied Spectroscopy*, 2003, **57**, 353-355.
318. Tan, Chung-Sung; Juan, Chun-Chieh; Kuo, Ting-Wu., *Polymer*, 2004, **45**, 1805-1814.
319. Kim, Young Shin; Park, Jae Hyung; Bae, You Han., *Journal of Applied Polymer Science*, 2003, **89**, 2270-2276.
320. Yu, Youlu; Rohlfing, David C.; Hawley, Gil R.; DesLauriers, Paul J., *Polymer Preprints (American Chemical Society, Division of Polymer Chemistry)*, 2003, **44**, 49-50.
321. Kasi, Rajeswari M.; Coughlin, E. Bryan, *Macromolecules*, 2003, **36**, 6300-6304.
322. Conboy, Claire; Hsi, Ed; Redwine, David; Taha, Angela; Xiong, Jincheng; Zhang,

Shanmin; Gorenstein, David; Lin, Feng; Mainz, Vera, *Polymer Preprints* (*American Chemical Society, Division of Polymer Chemistry*), 2003, 44, 371-372.

323. Stibrany, Robert T.; Patil, Abhimanyu O.; Zushma, Stephen, *ACS Symposium Series*, 2003, **857**(Beyond Metallocenes), 194-209.
324. Beigzadeh, Daryoosh; Soares, Joao B. P.; Duever, Thomas A., *Journal of Polymer Science, Part A: Polymer Chemistry*, 2004, **42**, 3055-3061
325. de Vries, Tjerk J.; Kemmere, Maartje F.; Keurentjes, Jos T. F. Process Development Group and Dutch Polymer Institute, Department of Chemical Engineering and Chemistry, *Macromolecules*, 2004, **37**, 4241-4246
326. Bailly, C.; Stephenne, V.; Daoust, D.; Godard, P.; van Ruymbeke, E.; Keunings, R., *Polymer Preprints* (*American Chemical Society, Division of Polymer Chemistry*), 2003, **44**, 35-36
327. Bailly, Christian; Stephenne, Vincent; Daoust, Daniel; Godard, Pierre; Van Ruymbeke, Evelyne; Keunings, Roland., *Abstracts of Papers, 226th ACS National Meeting, New York, NY, United States, September* 7-11, 2003, 2003, POLY-216
328. Yu, Youlu; Rolfing, David C.; Hawley, Gil R.; DesLauriers, Paul J., *Abstracts of Papers, 226th ACS National Meeting, New York, NY, United States, September* 7-11, 2003, 2003, POLY-353
329. Pollard, M.; Spiess, H. W.; Sperber, M. Wilhelm O.; Piel, C.; Kaminsky, W., *Polymer Preprints* (*American Chemical Society, Division of Polymer Chemistry*), 2003, **44**, 369-370
330. Majeste, J. C.; Carrot, C.; Stanescu, P., *Polymer Preprints* (*American Chemical Society, Division of Polymer Chemistry*), 2003, **44**, 39-40
331. Pollard, M.; Klimke, K.; Graf, R.; Spiess, H. W.; Wilhelm, M.; Sperber, O.; Piel, C.; Kaminsky, W., *Macromolecules*, 2004, **37**, 813-825
332. Majeste, J. C.; Carrot, C.; Stanescu, P., *Rheologica Acta*, 2003, **42**, 432-442
333. Leatherman, Mark D.; Svejda, Steven A.; Johnson, Lynda K.; Brookhart, Maurice., Journal of the American Chemical Society, 2003, **125**, 3068-3081
334. Furlan, Luciano G.; Kunrath, Fabio A.; Mauler, Raquel S.; De Souza, Roberto F.; Casagrande, Osvaldo L., Jr., Journal of Molecular Catalysis A: Chemical, 2004, **214**, 207-211
335. Brar, A. S., *Polymer Preprints* (*American Chemical Society, Division of Polymer Chemistry*), 2003, **44**, 238-239
336. van der Velden, Geert; Linssen, H., *Abstracts of Papers, 225th ACS National Meeting, New Orleans, LA, United States, March* 23-27, 2003, 2003, POLY-341
337. Lu, Yingying; Ma, Zhi; Hu, Youliang; Xu, G. X.; Chung, T. C.,*Chinese Science Bulletin*, 2003, **48**, 523-525
338. Hanson, James E.; Li, Sue Yuan, *Abstracts of Papers, 226th ACS National Meeting, New York, NY, United States, September* 7-11, 2003, 2003, PMSE-339
339. Khan, Majad; Huck, Wilhelm T. S., *Polymer Preprints* (*American Chemical Society, Division of Polymer Chemistry*), 2003, 44, 476-477
340. Huck, Wilhelm T. S.; Khan, Majad. Melville Laboratory, *Abstracts of Papers, 225th ACS National Meeting, New Orleans, LA, United States, March* 23-27, 2003, 2003, POLY-699
341. Khan, Majad; Huck, Wilhelm T. S., *Macromolecules*, 2003, **36**, 5088-5093
342. Wind, John D.; Staudt-Bickel, Claudia; Paul, Donald R.; Koros, William J., *Macromolecules*, 2003, **36**, 1882-1888
343. Meador, Mary Ann B.; Frimer, Aryeh A., *Abstracts of Papers, 225th ACS National Meeting, New Orleans, LA, United States, March* 23-27, 2003, 2003, POLY-340
344. Fang, Xingzhong; Yang, Zhenghua; Zhang, Suobo; Gao, Lianxun; Ding,

Mengxian, *Polymer*, 2004, **45**, 2539-2549
345. Hao, Jianjun; Jikei, Mitsutoshi; Kakimoto, Masaaki., *Macromolecules*, 2003, **36**, 3519-3528
346. Kripotou, S.; Pissis, P.; Bershtein, V. A.; Sysel, P.; Hobzova, R., *Polymer*, 2003, **44**, 2781-2791
347. Kim, Il-Jin; Faust, Rudolf, *Journal of Macromolecular Science, Pure and Applied Chemistry*, 2003, **A40**, 991-1008
348. Machl, Doris; Kunz, Michael J.; Binder, Wolfgang H., *Abstracts of Papers, 226th ACS National Meeting, New York, NY, United States, September* 7-11, 2003, 2003, POLY-121
349. Bazzini, Cristina; Giarrusso, Antonino; Porri, Lido; Pirozzi, Beniamino; Napolitano, Roberto, *Polymer*, 2004, **45**, 2871-2875
350. Kim, Sunwook; Takeuchi, Daisuke; Osakada, Kohtaro.,*Macromolecular Chemistry and Physics*, 2003, **204**, 666-673
351. Vavasori, Andrea; Toniolo, Luigi; Cavinato, Gianni, *Journal of Molecular Catalysis A: Chemical*, 2004, **215**, 63-72
352. Tang, Zhaohui; Chen, Xuesi; Pang, Xuan; Yang, Yongkun; Zhang, Xuefei; Jing, Xiabin, *BioMacromolecules*, 2004, **5**, 965-970
353. Liu, Y.; Tian, F.; Hu, K. A., Carbohydrate Research, 2004, **339**, 845-851
354. Moalla, S.; Kalfat, R.; Legrand, A. P.; Zarrouk, H., *Journal of Sol-Gel Science and Technology*, 2003, **26**, 125-129
355. Peetz, Ralf M.; Moustafa, Ahmed F.; Kennedy, Joseph P., *Journal of Polymer Science, Part A: Polymer Chemistry*, 2003, **41**, 732-739
356. Delaude, Lionel; Demonceau, Albert; Noels, Alfred F., *Macromolecules*, 2003, **36**, 1446-1456
357. Patil, Abhimanyu O.; Zushma, Stephen; Stibrany, Robert T.; Rucker, Steven P.; Wheeler, Louise M., *Journal of Polymer Science, Part A: Polymer Chemistry*, 2003, **41**, 2095-2106
358. Patil, Abhimanyu O.; Zushma, Stephen; Stibrany, Robert T.; Rucker, Steven P.; Wheeler, Louise M., *ACS Symposium Series*, 2003, **857**(Beyond Metallocenes), 173-191
359. Amir-Ebrahimi, Valia; Rooney, John J., *Journal of Molecular Catalysis A: Chemical*, 2004, **208**, 103-108
360. Walach, Wojciech; Trzebicka, Barbara; Justynska, Justyna; Dworak, Andrzej, *Polymer*, 2004, **45**, 1755-1762
361. Costabile, Chiara; Guerra, Gaetano; Longo, Pasquale; Pragliola, Stefania, *Macromolecules*, 2004, **37**, 2016-2020
362. Busico, Vincenzo; Cipullo, Roberta; Cutillo, Francesco; Talarico, Giovanni; Razavi, Abbas., *Macromolecular Chemistry and Physics*, 2003, **204**, 1269-1274
363. Lahelin, Mika; Kokko, Esa; Lehmus, Petri; Pitkaenen, Paeivi; Loefgren, Barbro; Seppaelae, Jukka., *Macromolecular Chemistry and Physics*, 2003, **204**, 1323-1337
364. Ye, Zhibin; Zhu, Shiping., *Journal of Polymer Science, Part A: Polymer Chemistry*, 2003, **41**, 1152-1159
365. Arrighi, Valeria; Batt-Coutrot, Delphine; Zhang, Chuhong; Telling, Mark T. F.; Triolo, Alessandro, *Journal of Chemical Physics*, 2003, **119**, 1271-1278
366. Al-Humydi, Abdulaziz; Collins, Scott; Garrison, Jered C.; Youngs, Wiley J., *Abstracts of Papers, 226th ACS National Meeting, New York, NY, United States, September* 7-11, 2003, 2003, INOR-401
367. Galland, Griselda Barrera; Da Silva, Luciana P.; Dias, Marcos L.; Crossetti, Geraldo L.; Ziglio, Claudio M.; Filgueiras, Carlos A. L., *Journal of Polymer Science,*

Part A: Polymer Chemistry, 2004, **42**, 2171-2178
368. Long, J.; Tzoganakis, C.; Chen, P., *Polymer Engineering and Science*, 2004, **44**, 56-71
369. Mitani, Makoto; Furuyama, Rieko; Mohri, Junichi; Saito, Junji; Ishii, Seiichi; Terao, Hiroshi; Nakano, Takashi; Tanaka, Hidetsugu; Fujita, Terunori., *Journal of the American Chemical Society*, 2003, **125**, 4293-4305.
370. Weng, Weiqing; Hu, Weiguo; Dekmezian, Armenag H., *Abstracts of Papers, 226th ACS National Meeting, New York, NY, United States, September* 7-11, 2003, 2003, POLY-037
371. Kawahara, Nobuo; Kojoh, Shin-ichi; Matsuo, Shingo; Kaneko, Hideyuki; Matsugi, Tomoaki; Toda, Yoshihisa; Mizuno, Akira; Kashiwa, Norio, *Polymer*, 2004, **45**, 2883-2888
372. Nishii, Kei; Matsumae, Takashi; Dare, Enock O.; Shiono, Takeshi; Ikeda, Tomiki, *Macromolecular Chemistry and Physics*, 2004, **205**, 363-369
373. Kissin, Yury V.; Ohnishi, Rikuo; Konakazawa, Takehito, *Macromolecular Chemistry and Physics*, 2004, **205**, 284-301
374. Miller, Stephen A. Department of Chemistry, *Macromolecules*, 2004, 37, 3983-3995
375. Miller, Stephen A.; Bercaw, John E., Organometallics, 2004, 23, 1777-1789
376. Staal, Oetze K. B.; Beetstra, Dirk J.; Jekel, Andries P.; Hessen, Bart; Teuben, Jan H.; Stepnicka, Petr; Gyepes, Robert; Horacek, Michal; Pinkas, Jiri; Mach, Karel., *Collection of Czechoslovak Chemical Communications*, 2003, **68**, 1119-1130
377. Busico, Vincenzo; Castelli, Valeria Van Axel; Aprea, Paola; Cipullo, Roberta; Segre, Annalaura; Talarico, Giovanni; Vacatello, Michele., *Journal of the American Chemical Society*, 2003, **125**, 5451-5460
378. Busico, V.; Mannina, L.; Segre, A. L.; Van Axel Castelli, V., *ACS Symposium Series*, 2003, **834**(NMR Spectroscopy of Polymers in Solution and in the Solid State), 192-207
379. Weng, Weiqing; Hu, Weiguo, *Polymer Preprints* (*American Chemical Society, Division of Polymer Chemistry*), 2003, **44**, 17
380. Saule, Myriam; Navarre, Sebastien; Babot, Odile; Maslow, Wasil; Vertommen, Luc; Maillard, Bernard, *Macromolecules*, 2003, **36**, 7469-7476
381. Lamberti, Marina; Gliubizzi, Rocco; Mazzeo, Mina; Tedesco, Consiglia; Pellecchia, Claudio, *Macromolecules*, 2004, **37**, 276-282
382. Fu, Zhi-sheng; Fan, Zhi-qiang; Zhang, Yu-qing; Feng, Lin-xian. Institute of Polymer Science, *European Polymer Journal*, 2003, **39**, 795-804
383. Saxena, Anubhav; Okoshi, Kento; Fujiki, Michiya; Naito, Masanobu; Guo, Guangqing; Hagihara, Takahiro; Ishikawa, Masaaki, *Macromolecules*, 2004, **37**, 367-370
384. Uhlig, Wolfram., *Journal of Organometallic Chemistry*, 2003, **685**, 70-78
385. Kawakami, Yusuke; Imae, Ichiro, *ACS Symposium Series*, 2003, **838**(Synthesis and Properties of Silicones and Silicone-Modified Materials), 61-71
386. Chiang, Chin-Lung; Ma, Chen-Chi M., *Journal of Polymer Science, Part A: Polymer Chemistry*, 2003, **41**, 1371-1379
387. Capacchione, Carmine; D'Acunzi, Maria; Motta, Oriana; Oliva, Leone; Proto, Antonio; Okuda, Jun., *Macromolecular Chemistry and Physics*, 2004, **205**, 370-373
388. Nakaoki, Takahiko; Kobayashi, Masamichi,*Journal of Molecular Structure*, 2003, **655**, 343-349
389. Abbondanza, Luigi; Abis, Luigi; Cardi, Nicoletta; Garbassi, Fabio; Po, Riccardo, *Macromolecular Chemistry and Physics*, 2003, **204**, 1428-1438
390. Guo, M. M., *Abstracts of Papers, 226th ACS National Meeting, New York, NY, United States, September* 7-11, 2003, 2003, IEC-150
391. Wysgoski, Faith; McNamara, Kristin; Harwood, H.; Rinaldi, Peter, *Abstracts, 35th*

Central Regional Meeting of the American Chemical Society, Pittsburgh, PA, United States, October 19-22, 2003, 104

392. Wysgoski, Faith; McNamara, Kristin; Harwood, H.; Rinaldi, Peter, *Abstracts, 35th Central Regional Meeting of the American Chemical Society, Pittsburgh, PA, United States, October* 19-22, 2003, 31
393. Catellani, Marinella; Luzzati, Silvia; Lupsac, Natalia-O.; Mendichi, Raniero; Consonni, Roberto; Famulari, Antonino; Meille, Stefano Valdo; Giacalone, Francesco; Segura, Jose L.; Martin, Nazario, *Journal of Materials Chemistry*, 2004, **14**, 67-74
394. Anon, *Research Disclosure*, 2003, **472**, P940
395. Liang, Zhu-Mei; Wan, Chao-Ying; Zhang, Yong; Wei, Ping; Yin, Jie. *Journal of Applied Polymer Science*, 2004, **92**, 567-575
396. Gerber, Michael; Walker, Lynn, *Abstracts, 35th Central Regional Meeting of the American Chemical Society, Pittsburgh, PA, United States, October* 19-22, 2003, 86
397. Carvalho, Antonio J. F.; Curvelo, Antonio A. S., *Macromolecules*, 2003, **36**, 5304-5310
398. Buzare, Jean-Yves; Silly, G.; Emery, J.; Boccaccio, Guy; Rouault, Eric., *Journal of Applied Polymer Science*, 2003, **87**, 3-8
399. Chen, Ye; Yang, Decai; Hu, Yanming; Zhang, Xuequan, *Crystal Growth & Design*, 2004, **4**, 117-121
400. Peetz, Ralf M.; Moustafa, Ahmed F.; Kennedy, Joseph P., *Journal of Polymer Science, Part A: Polymer Chemistry*, 2003, **41**, 740-751
401. Keizer, Henk M.; van Kessel, Rik; Sijbesma, Rint P.; Meijer, E. W., *Polymer*, 2003, **44**, 5505-5511
402. Bonnet, Fanny; Visseaux, Marc; Pereira, Angela; Bouyer, Frederic; Barbier-Baudry, Denise, *Macromolecular Rapid Communications*, 2004, **25**, 873-877
403. Kanesaka, Sho; Kimura, Hideaki Kuroki; Shigeki; Fujishige, Shouei; Ando, Isao, *Abstracts of Papers, 225th ACS National Meeting, New Orleans, LA, United States, March* 23-27, 2003, 2003, POLY-565
404. Kanesaka, Sho; Kimura, Hideaki; Kuroki, Shigeki; Ando, Isao; Fujishige, Shouei, *Polymer Preprints (American Chemical Society, Division of Polymer Chemistry)*, 2003, **44**, 357-358
405. Kanesaka, Sho; Kimura, Hideaki; Kuroki, Shigeki; Ando, Isao; Fujishige, Shouei, *Macromolecules*, 2004, **37**, 453-458
406. Ando, Isao; Yin, Yige; Zhao, Chenhua; Kuroki, Shigeki, *Polymer Preprints (American Chemical Society, Division of Polymer Chemistry)*, 2003, 44, 323-324
407. Roussel, Frederick; Fung, Bing M, *Physical Review E: Statistical, Nonlinear, and Soft Matter Physics*, 2003, **67**, 041709/1-041709/4
408. Murakami, Miwa; Ishida, Hiroyuki; Miyazaki, Masayuki; Kaji, Hironori; Horii, Fumitaka, *Macromolecules*, 2003, **36**, 4160-4167
409. Vilfan, M.; Lahajnar, G.; Zupancic, I.; Zalar, B., *Magnetic Resonance Imaging*, 2003, **21**, 169-175
410. Hiejima, Toshihiro; Seki, Kiyoshi; Kobayashi, Yoshinori; Abe, Akihiro, *Journal of Macromolecular Science, Physics*, 2003, **B42**, 431-439
411. Orian, Laura; Feio, Gabriel; Veron, Alain; Martins, Assis Farinha; Polimeno, Antonino, *Molecular Crystals and Liquid Crystals*, 2003, **394** 63-75
412. Godinho, M. H; van der Klink, J. J; Martins, A. F, *Journal of Physics: Condensed Matter*, 2003, **15**, 5461-5468
413. Perez-Mendez, Mercedes; Berenguel, Roser Marsal; Garrido, Leoncio; Martin-Pastor, Manuel, *Macromolecules*, 2003, **36**, 8049-8055
414. Severing, Kirsten; Saalwachter, Kay, *Physical Review Letters*, 2004, **92**, 125501/1-

125501/4
415. Chiang, Chin-Lung; Ma, Chen-Chi M; Wu, Dai-Lin; Kuan, Hsu-Chiang, *Journal of Polymer Science, Part A: Polymer Chemistry*, 2003, **41**, 905-913
416. Lees, Tom J; Balcom, Bruce J; *Magnetic Resonance in Chemistry*, 2003, **41**, 229-236
417. Milroy, Georgina E; Cameron, Ruth E; Mantle, Michael D; Gladden, Lynn F; Huatan, Hiep, *Journal of Materials Science: Materials in Medicine*, 2003, **14**, 465-473
418. Yung, Kaung-T, *Magnetic Resonance Imaging*, 2003, **21**, 135-144
419. Hunter, Geoffrey; Lane, Deirdre M; Scrimgeour, Sheelagh N; McDonald, Peter J; Lloyd, Charles H, *Dental Materials*, 2003, **19**, 632-638
420. Hurley, C; De Deene, Y; Meder, R; Pope, J. M; Baldock, *Physics in Medicine & Biology*, 2003, **48**, 3043-3058
421. Malak, Mark; Hill, David J. T.; Whittaker, Andrew K., *Polymer International*, 2003, **52**, 1740-1748
422. Teranishi, Kazuhiro; Tsushima, Shoji; Hirai, Shuichiro, *Thermal Science and Engineering*, 2003, **11**, 35-38
423. Kusmia, S; Kozak, M; Szczesniak, E; Domka, L; Jurga, S., *Solid State Nuclear Magnetic Resonance*, 2004, **25**, 173-176
424. Chowdhury, Mohammad A.; Hill, David J. T.; Whittaker, Andrew K., *BioMacromolecules*, 2004, **5**, 971-976
425. Adriaensens, Peter; Pollaris, Anne; Rulkens, Rudy; Litvinov, Victor M; Gelan, Jan, *Polymer*, 2004, **45**, 2465-2473
426. Hill, David J. T.; Chowdhury, Mohammad; Ghi, Phuong Y.; Moss, Naomi G.; Whittaker, Andrew K., *Macromolecular Symposia* , 2004, **207**(Fundamentals and Applications of Polymer Gels), 111-123
427. Yokota, Satomi., Sasaki, Akitsugu., Hotta, Yoshio., Yamane, Yuji., Kimura, Hideaki., Kuroki, Shigeki., Ando, Isao, *Macromolecular Symposia*, 2004, 207(Fundamentals and Applications of Polymer Gels), 105-109
428. Darwish, M. I. M.; Rowe, R. K.; van der Maarel, J. R. C.; Pel, L.; Huinink, H.; Zitha, P. L. J., Canadian Geotechnical Journal, 2004, **41**, 106-117
429. Guo, Jian; Jiang, Xiqun; Hu, Yong; Yang, Changzheng, Journal of Materials Science: Materials in Medicine, 2003, **14**, 283-286
430. Lu, Zheng-Rong; Wang, Xinghe; Parker, Dennis L; Goodrich, K. Craig; Buswell, Henry R., Bioconjugate Chemistry, 2003, **14**, 715-719
431. Kobayashi, Hisataka; Brechbiel, Martin W., Molecular Imaging, 2003, 2, 1-10
432. Yordanov, Alexander T.; Kobayashi, Hisataka; English, Sean J.; Reijnders, Koen; Milenic, Diane; Krishna, Murali C; Mitchell, James B; Brechbiel, Martin W., Journal of Materials Chemistry, 2003, **13**, 1523-1525
433. Kalish, H.; Arbab, A. S.; Miller, B. R.; Lewis, B. K.; Zywicke, H. A.; Bulte, J. W. M.; Bryant, L. H., Jr.; Frank, J. A., Magnetic Resonance in Medicine, 2003, **50**, 275-282
434. Kim, Do Kyung; Mikhaylova, Maria; Wang, Fu Hua; Kehr, Jan; Bjelke, Boerje; Zhang, Yu; Tsakalakos, Thomas; Muhammed, Mamoun, *Chemistry of Materials*, 2003, **15**(23), 4343-4351
435. Langereis, Sander; De Lussanet, Quido G.; Van Genderen, Marcel H. P; Backes, Walter H.; Meijer, E. W., *Macromolecules*, 2004, **37**, 3084-3091
436. Cholli, A. L.; Sahoo, S. K.; Kim, Dong Wook; Samuelson, L.; Kumar, J.; Blumstein, A., *International Journal of Plastics Technology* (2003), **6**(1), 1-5.
437. Budhlall, B. M.; Landfester, K.; Sudol, E. D.; Dimonie, V. L.; Klein, A.; El-Aasser, M. S., *Macromolecules* (2003), **36**(25), 9477-9484.
438. Batra, Ashish; Hedden, Ronald C.; Schofield, Paula; Barnes, Aaron; Cohen, Claude;

Duncan, T. M., *Macromolecules* (2003), **36**(25), 9458-9466.
439. Saalwaechter, Kay., *Journal of the American Chemical Society* (2003), **125**(48), 14684-14685.
440. Forster, A.; Apperley, D.; Hempenstall, J.; Lancaster, R.; Rades, T., *Pharmazie* (2003), **58**(10), 761-762.
441. Lee, Youngil; Choi, Jinwoo; Choi, Young-Wook; Sohn, Daewon., *Journal of Physical Chemistry B* (2003), **107**(45), 12373-12377.
442. Brar, A. S.; Pradhan, D. R., *Journal of Polymer Materials* (2003), **20**(1), 31-42.
443. Matsuda, Hironori; Nagasaka, Bunsow; Asakura, Tetsuo, *Polymer Journal (Tokyo, Japan)* (2003), **35**(9), 740-747.
444. Litvinov, V. M.; Bertmer, M.; Gasper, L.; Demco, D. E.; Bluemich, B., *Macromolecules* (2003), **36**(20), 7598-7606.
445. Thieme, Karena; Schnell, Ingo, *Journal of the American Chemical Society* (2003), **125**(40), 12100-12101.
446. Golemme, G.; Nagy, J. B.; Fonseca, A.; Algieri, C.; Yampolskii, Yu, *Polymer* (2003), **44**(17), 5039-5045
447. Sengar, Raghvendra S.; Nemykin, Victor N.; Basu, Partha. Department of Chemistry and Biochemistry, Duquesne University, Pittsburgh, PA, USA. *New Journal of Chemistry* (2003), **27**(7), 1115-1123.
448. De Alvarenga, Elson S.; Lima, Claudio F.; Denadai, Angelo M. L, *Physical Sciences* (2004), **59**(4/5), 291-294.
449. Furuheim, Knut Magne; Axelson, David E.; Antonsen, Henrik W.; Helle, Torbjorn, *Journal of Applied Polymer Science* (2004), **91**(1), 218-225.
450. Feng, Yang; Fang, Xiao-wen; Mao, Shi-zhen; Zhao, Sui; Yuan, Han-zhen; Yu, Jia-yong; Du, You-ru, *Bopuxue Zazhi* (2004), **21**(1), 49-55.
451. Diez-Pena, Eva; Quijada-Garrido, Isabel; Barrales-Rienda, Jose Manuel; Schnell, Ingo; Spiess, Hans Wolfgang, *Macromolecular Chemistry and Physics* (2004), 205(4), 430-437.
452. Zhang, Yudong, *Polymer* (2004), **45**(8), 2651-2656.
453. Monwar, Masud; Oh, Sung Joon; Rinaldi, Peter L.; McCord, Elizabeth F.; Hutchinson, Robin A.; Buback, Michael M.; Latz, Henning, *Analytical and Bioanalytical Chemistry* (2004), **378**(6), 1414-1427.
454. Zhang, Chi; Easteal, Allan J, *Journal of Applied Polymer Science* (2004), **91**(6), 3635-3641.
455. Wysgoski, Faith J.; Rinaldi, Peter L.; McCord, Elizabeth F.; Stewart, Mark A.; Marshall, Donald R, *Macromolecules* (2004), **37**(3), 846-855.
456. Roy, Debmalya; Basu, P. K.; Raghunathan, P.; Eswaran, S. V, *Magnetic Resonance in Chemistry* (2004), **42**(1), 76-80.
457. Groeger, Stefan; Geschke, Dieter; Kaerger, Joerg; Stallmach, Frank; Konak, Cestmi, *Macromolecular Rapid Communications* (2004), **25**(10), 1015-1018.
458. Coppola, Luigi; Gianferri, Raffaella; Nicotera, Isabella; Oliviero, Cesare; Ranieri, Giuseppe Antonio; Terenzi, Mario, *Recent Research Developments in Applied Polymer Science* (2003), **2** , 1-12.
459. Newling, B.; Batchelor, S. N, *Journal of Physical Chemistry B* (2003), **107**(45),
460. Buda, A.; Demco, D. E.; Bertmer, M.; Blumich, B.; Reining, B.; Keul, H.; Hocker, H, *Solid State Nuclear Magnetic Resonance* (2003), **24**(1), 39-67.
461. Jayakody, J. R. P.; Stallworth, P. E.; Mananga, E. S.; Farrington-Zapata, J.; Greenbaum, S. G, Journal of Physical Chemistry B (2004), **108**(14), 4260-4262.
462. Bourbigot, Serge; Vanderhart, David L.; Gilman, Jeffrey W.; Awad, Walid H.; Davis, Rick D.; Morgan, Alexander B.; Wilkie, Charles A, *Journal of Polymer*

Science, Part B: Polymer Physics (2003), **41**(24), 3188-3213.
463. Agarwal, Gyan K.; Titman, Jeremy J.; Percy, Matthew J.; Armes, Steven P, *Journal of Physical Chemistry B* (2003), **107**(45), 12497-12502.
464. Azima, Mami; Ma, Lin; He, Chunqing; Suzuki, Takenori; Bin, Yuezhen; Kurosu Hiromichi; Matsuo, Masaru, *Polymer* (2004), **45**(2), 409-412.
465. Kint, Darwin P. R.; Martinez de Ilarduya, Antxon; Sansalvado, A.; Ferrer, Josep; Munoz-Guerra, Sebastian, *Journal of Applied Polymer Science* (2003), **90**(11), 3076-3086.
466. Diniz, Teresinha M. F. F.; Tavares, Maria I. B, *Journal of Applied Polymer Science* (2003), **90**(11), 2955-2958.
467. Vartapetyan, R. Sh.; Khozina, E. V.; Chalykh, A. E.; Skirda, V. D.; Feldstein, M. M.; Kaerger, J.; Geschke, D, *Colloid Journal (Translation of Kolloidnyi Zhurnal)* (2003), **65**(6), 684-690.
468. Honma, Tomonori; Senda, Toshihiko; Inoue, Yoshio, *Polymer International* (2003), **52**(12), 1839-1846.
469. Ines, Maria; Tavares, B.; de Souza, Claudia M. G, *Journal of Applied Polymer Science* (2003), **90**(14), 3872-3875.
470. Hill, David J. T.; Markotsis, Martin; Whittaker, Andrew K.; Wong, Kathy W, *Polymer International* (2003), **52**(11), 1780-1789.
471. Jung, Dylan Dae Bong; Easteal, Allan J.; Bhattacharyya, Debes, *Materials Research Innovations* (2003), **7**(5), 269-274.
472. Diniz, Teresinha M. F. F.; Tavares, Maria I. B, *Journal of Applied Polymer Science* (2004), **93**(1), 372-377.
473. Zhang, Xiaoqing; Burgar, Iko; Lourbakos, Eleni; Beh, Henry, *Polymer* (2004), **45**(10), 3305-3312.
474. Olcak, Dusan; Onufer, Jozef; Mucha, L'ubomir; Raab, Miroslav; Spevacek, Jiri, *Journal of Applied Polymer Science* (2004), **91**(1), 247-252.
475. Cao, Haihui; Lin, Guoxing; Jones, Alan A, *Journal of Polymer Science, Part B: Polymer Physics* (2004), **42**(6), 1053-1067.
476. Asano, Atsushi, *Polymer Journal (Tokyo, Japan)* (2004), **36**(1), 23-27.
477. Wolak, Justyna; Jia, Xin; Gracz, Hanna; Stejskal, Edward O.; White, Jeffery L.; Wachowicz, Marcin; Jurga, Stefan, *Macromolecules* (2003), **36**(13), 4844-4850.
478. Lim, Ae Ran; Kwark, Young-Je; Kim, Joon-Seop, *Journal of Applied Physics* (2003), **94**(11), 7351-7355.
479. Malveau, C.; Baille, W. E.; Zhu, X. X.; Ford, W. T, *Journal of Polymer Science, Part B: Polymer Physics* (2003), **41**(22), 2969-2975.
480. Wolak, J. E.; Knutson, J.; Martin, J. D.; Boyle, P.; Sargent, Andrew L.; White, Jeffery L, *Journal of Physical Chemistry B* (2003), **107**(48), 13293-13299.
481. Ma, Lin; He, Chunqing; Suzuki, Takenori; Azuma, Mami; Bin, Yuezhen; Kurosu, Hiromichi; Matsuo, Masaru, *Macromolecules* (2003), **36**(21), 8056-8065.
482. Lai, Simona; Locci, Emanuela; Saba, Giuseppe; Husu, Ivan; Masci, Giancarlo; Crescenzi, Vittorio; Lai, Adolfo, *Journal of Polymer Science, Part A: Polymer Chemistry* (2003), **41**(20), 3123-3131.
483. He, Yiyong; Lutz, T. R.; Ediger, M. D, *Macromolecules* (2003), **36**(21),8040-8048.
484. Kassaee, M. Z.; Heydari, H.; Hattami, M.; Nia, A. Fazli, *Macromolecules* (2003), **36**(18), 6773-6779.
485. De Azevedo, E. R.; Franco, R. W. A.; Marletta, A.; Faria, R. M.; Bonagamba, T. J, *Journal of Chemical Physics* (2003), **119**(5), 2923-2934.
486. Lorthioir, C.; Deloche, B.; Auroy, P.; Gallot, Y, *Europhysics Letters* (2003), **62**(5), 746-752.

487. Kuwabara, Kazuhiro; Gan, Zhihua; Nakamura, Takashi; Abe, Hideki; Doi, Yoshiharu, *Polymer Degradation and Stability* (2004), **84**(1), 135-141.
488. Wu, Jun; Tomba, J. Pablo; Winnik, Mitchell A.; Farwaha, Rajeev; Rademacher, Jude, *Macromolecules* (2004), **37**(6), 2299-2306.
489. Bertmer, Marko; Gasper, Lothar; Demco, Dan E.; Bluemich, Bernhard; Litvinov, Victor M, *Macromolecular Chemistry and Physics* (2004), **205**(1), 83-94.
490. Saalwachter, Kay, *Journal of Chemical Physics* (2004), **120**(1), 454-464.
491. Jurga, J.; Wozniak-Braszak, A.; Fojud, Z.; Jurga, K, *Solid State Nuclear Magnetic Resonance* (2004), **25**(1-3), 47-52.
492. Lin, Weixin; Zhang, Qiujin; Yang, Guang; Chen, Qun, *Journal of Molecular Structure* (2003), **655**(1), 37-45.

12
NMR in Living Systems

By M. J. W. PRIOR

1 General Applications and Methodologies

1.1 Spectral Analysis. – The basic principles of metabolic modelling, applied to ^{13}C-labeling experiments, have been reviewed.[1]

A fast, automated, observer-independent technique for processing ^{1}H-decoupled ^{13}C spectra has been developed. The method has been demonstrated on ^{13}C spectra from human subjects following the administration of [1-^{13}C] glucose and/or [1-^{13}C]acetate. [2] Restricted metabolite diffusion in skeletal myofibril systems has been analysed by the random walk method. Modelling allowed the calculation of apparent diffusion coefficients of particles in the axial and radial directions.[3]

1.2 New Applications. – Non-invasive methods for the study of drug distribution have been reviewed.[4]

Localised ^{13}C NMR spectra have been obtained from the rat brain, over a region of 15 to 100 ppm, with <10% chemical shift displacement. A semi-adiabatic distortionless enhancement by polarization transfer (DEPT) method was combined with ^{1}H localization, and a new gradient dephasing scheme was employed to eliminate unwanted coherences. Naturally abundant resonances from N-acetyl aspartate (NAA), myo inositol (mI) and glutamate were detected in the rat brain. After infusion of [^{13}C]glucose, many resonances were detected including Glu, Gln, Asp, glucose (Glc), NAA, γ-aminobutyric acid (GABA), lactate and alanine.[5] The chemical shifts of C-2 and C-4 of carnosine in ^{1}H spectra of frog muscle have been used to measure intracellular pH (pH$_i$). Measurements were verified by comparison with pH measurements using other ^{1}H chemical shifts and ^{31}P data. Values for pH$_i$ were obtained for glycolytic and oxidative fibres.[6]

2 Cells

2.1 Bacteria. – ^{31}P NMR has been used to investigate *Zymomonas mobilis* ZM4/Ac^{R}, an acetic acid resistant strain of *Z. mobilis* ZM4, to determine the possible mechanisms of resistance to acetic acid. The mutant strain showed

Nuclear Magnetic Resonance, Volume 34
© The Royal Society of Chemistry, 2005

resistance to ethanol or low extracellular pH (pH_e) in the presence of acetic acid compared to the parent strain. In *Z. mobilis*ZM4/Ac^R, pH_i and energy status were less affected by acetic acid.[7] The effects of substrate on xanthosine-5′-monophosphate over-production in *Corynebacterium ammoniagenes* has been studied with ^{31}P NMR. For the most efficient XMP production, a ratio of 0.31 of Glu to Glc was required. In the early phase of substrate utilization when Glu and Glc were utilised, the average ATP concentration was 0.50 ± 0.17 μM g^{-1} of dry cell weight. The ATP level decrease to an undetectable level later when the Glu had been consumed and XMP production had been replaced by production of hypoxanthine.[8]

2.2 Blood. – The pH_i and free intracellular Mg^{2+} ($[Mg^{2+}]_{free}$)in human sickle cells has been determined using the chemical shifts of ATP and 2,3-diphosphoglycerate(2,3-DPG). Theoretical equations were employed to express the observed chemical shifts as a function of pH_i, $[K^+]$ and intracellular $[Mg^{2+}]$ ($[Mg^{2+}]_i$), although this requires knowledge of the intracellular concentrations of ATP, 2,3-DPG, K^+ and haemoglobin. Measurements on oxygenated, normal whole blood showed $pH_i = 7.20 \pm 0.02$, $[Mg^{2+}]_{free} = 0.41 \pm 0.03$ mM and [2,3-DPG] = 7.69 ± 0.47 mM. Results from sickle cell blood showed $pH_i = 7.10 \pm 0.03$, $[Mg^{2+}]_{free} = 0.32 \pm 0.05$ mM and [2,3-DPG] = 10.8 ± 1.2 mM.[9]

2.3 Mammalian. – The use of NMR imaging and spectroscopy for the detection of apoptosis has been reviewed.[10]

The effects of 2,5-Anhydro-D-mannitol (2,5-DM) on intracellular Na^+ (Na^+_i) and phosphate metabolites have been investigated in superfused hepatocytes. Exposure to 2,5-DM, which is known to stimulate feeding in rats, caused an increase in Na^+_i and phosphomonoesters (PME) and a 60% decease in ATP levels. However, exposure of hepatocytes to fructose did not raise Na^+_i and caused a smaller increase in PME and a smaller decrease in ATP levels.[11] The effects of 30 mM glucose or the anti-diabetic sulfonylurea compound glyburide on energy metabolism, Na^+-flux, insulin secretion and cAMP release has been investigated in superfused β-HCp cells encapsulated in microcarrier beads. High glucose and glyburide increased oxygen consumption by 15 – 30 % and increased insulin release by 15- or 25-fold, respectively. However, 30 mM glucose caused an increased in phosphocreatine (PCr) and a decrease in Pi, whereas glyburide caused the opposite effect. ^{31}P NMR detected no change in ATP after 30 mM glucose or glyburide treatment. Exposure of cells to 5 mM glucose caused a decrease in Na^+, and 30 mM glucose caused a further decrease. In contrast, Na^+ increased when glyburide was added to media containing 5 mM glucose.[12]

Cortical astrocytes, cerebellar neurons and O-2A progenitor cells have been investigated with MASS ^1H NMR. All cells contained creatine and significant amounts of lipid resonances even when a T_2-edited CPMG pulse sequence was used to selectively attenuated resonances from macromolecules. Principle component analysis readily differentiated the spectra, however the lipid content of the cells contributed most to the separation of cell types.[13] The nature of the NMR-visible mobile lipid signal that is observed under certain conditions in

some cells has been investigated with ^{1}H NMR. Spectra were obtained from CEM-T4, THP-1 and stimulated Jurkat cells and compared to spectra from membrane fractions separated by density gradient centrifugation. Cytoplasmic lipid droplets contributed much of the NMR-visible lipid signal, but a significant proportion was also from detergent-resistant membrane domains. The latter were found to contain a greater proportion of cholesterol, ganglioside GM1 and unsaturated fatty acids compared to lipid droplets.[14]

2.4 Tumour. – The formation of NMR-visible mobile lipids has been observed to occur in two stages in human erythroleukemia cells exposed to Taxol for 3 hours. A first wave of mobile lipid generation was detected in treated cells at the onset of the effector phase, 8 – 24 h after exposure to the drug. The levels then reached a plateau at 24 – 48 h post treatment, but increased further during the degradation phase 48 to 72 h post-treatment.[15] The effects of Harringtonine on HL-60 cells has been investigated with ^{31}P and ^{1}H NMR. After cells were treated for 2 hours there was a significant decrease in ATP, PME and pH_i, whilst ^{1}H detected an increase in the methylene resonance and a slight decrease in choline-containing compounds (Cho).[16] The effects of treatment with indomethacin on malignant human mammary epithelial (MDA-MB-231) cells have been investigated with ^{31}P and diffusion-weighted ^{1}H NMR. An accumulation of glycerophosphocholine and a decrease of phosphocholine were detected within 2 h of treatment with 200 μM indomethacine. The changes were not related to changes in pH_i or extracellular pH (pH_e).[17] A murine leukaemic cell line (L1210 cells) and L1210 cells adapted to vincristine (L1210/VCR cells) have been investigated with ^{31}P NMR to examine changes due to multidrug resistance. There was a lower level of ATP and a much lower level of UDP-saccharides in L1210/VCR cells compared to L1210 cells.[18]

3 Plants

The uptake and metabolism of 3-O-methylglucose (3-OMG) into excised root tips has been investigated in *Zea mays* L. cv DEA. The effects of 3-OMG on protein content and endopeptidase activity were similar to the effects of glucose starvation or 6-deoxyglucose exposure. The time course of changes in major metabolites were monitored using ^{13}C and ^{31}P NMR in root tips. When root tips were incubated with 3-OMG, it accumulated to a level of around 120 mM. Furthermore, there was a transient increase in nucleoside triphosphates (NTP) and uridine diphosphoglucose followed by a continuous decrease to about 60% of their initial values after about 48 hours on 3-OMG treatment. During incubation with 3-OMG, there was also an increase in concentrations of phosphorylcholine, vacuolar pH (Pi_{vac}) and Asn, which are markers of intracellular autophagy. The presence of 3-O-methylglucose-6-phosphate was detected in root tips during incubation with 3-OMG.[19] An NMR flow quantification method applicable to measurement of metabolite flow in plants has been presented. Flow sensitivity was accomplished by magnetization preparation based upon stimu-

lated echo experiments prior to slice selective spectroscopy. The technique allowed the detection of low levels of metabolites and very slow velocities, down to 0.1 mm s^{-1}, despite large background water signals.[20]

4 Tissues

4.1 Brain. – The contribution of ^{13}C NMR in the study of lactate metabolism in the brain has been reviewed.[21] A review of the measurement of neuro-glial metabolism by *in vivo* NMR has been produced.[22] The use of ^{1}H-detected ^{13}C NMR for the study of brain metabolism has been reviewed.[23] A review of NAA in the vertebrate brain has been produced.[24] NMR spectroscopy and imaging methods for studies of neurodegenerative diseases in rodent models has been reviewed.[25]

^{1}H spectroscopic imaging has been used to measure metabolite levels in adult bonnet macaque (Macaca *radiata*) that had been exposed to early-life stress ten years prior to the NMR measurements. Significantly decreased ratios of NAA/total creatine (NAA/tCr) and Glu + Gln/tCr (Glx/tCr) was observed in the anterior cingulate, and a significantly increased ratio of Cho/tCr was found in the medial temporal lobe.[26] The effects of 60 s inhalation of 90% CO_2 on pH_i in the pig brain has been investigated with ^{31}P NMR. During inhalation, the pH_i paralleled the arterial pH and P_{co2}, O_2 saturation and HCO_3^- concentration. The pH_i decreased to approximately 6.7 within the 60 s inhalation period and reversed after that.[27] Magnetic resonance perfusion imaging and ^{31}P NMR have been used to investigate the effects of expression of myoglobin in the brains of transgenic mice. There were no gross morphological changes observed and no differences in the cellular energetics or perfusion of the brain.[28] The effects of perinatal iron-deficiency has been investigated with ^{1}H NMR in the rat brain hippocampus. Iron was withheld from gestational day 3 to post-natal day 7; the brain iron concentration in the iron-deficient group was 60% lower at post-natal day 7 and 19% lower at post-natal day 28. In the iron-deficient group, PCr, Glu, NAA, Asp, GABA, phosphoethanolamine and Tau concentrations were elevated.[29] Changes in the T_2 relaxation times for water and NAA at 9.4 T have been detected in the rat brain during ischaemia. There was a fall of approximately 10% in the value of T_2 during ischaemia and a reversal of this reduction following reperfusion. However, no changes were seen in the value of T_2 for tCr during these experiments.[30]

The LCmodel method has been adapted to analyse data from localised *in vivo* ^{13}C spectra obtained from the rat brain. The relative distribution of isotopomers in Glu, Gln, and Asp was in excellent agreement with that determined in extracts.[31] Microdialysis and mass-spectrometry have been used to measure the enrichment of extracellular Glu from ^{13}C-glucose in the rat brain. The fractional 13C enrichment of basal dialysate Glu C5, collected during 0.75 – 1.25 h of [2,5-^{13}C]glucose infusion, was 0.263 $\pm$ 0.01, which is close to the value obtained in parallel NMR measurements.[32] Localised water-suppressed ^{1}H-[^{13}C]-NMR has been used to follow the incorporation of [1,6-^{13}C]glucose in the rat brain.

The labelling of [^{13}C]glutamate and [^{13}C]glutamine was observed in positions 4,3 and 2 whilst label was also incorporated into, [2-^{13}C]aspartate, [3-^{13}C] aspartate, [3-^{13}C]alanine and [3-^{13}C]lactate. The TCA cycle flux was 0.52 $\pm$ 0.04 μmol min^{-1} g^{-1}, and the glutamatergic neurotransmitter flux was 0.25 $\pm$ 0.05 μmol min^{-1} g^{-1}, when calculated from the labelling patterns.[33] Regional rates of ^{13}C incorporation from glucose into glutamate have been measured in the anaesthetized rat brain. Time courses of regional [^{13}C]glutamate turnover and cerebral metabolic rate of oxygen consumption were fitted by a model to obtain regional TCA cycle flux.[34]

The effects of deep pentobarbital anaesthesia on glucose metabolism has been studied in the rat brain. Brain glucose levels were elevated two-fold compared to those during light α-chloralose anaesthesia. A mathematical model of neurotransmitter metabolism was used to estimate several metabolic reaction rates from the data obtained under pentobarbital anaesthesia. Total oxidative glucose metabolism was 0.33 μmol g^{-1} min^{-1} and the TCA cycle rate was 0.35 and 0.26 μmol g^{-1} min^{-1} in the neurons and glia, respectively. The rate of pyruvate carboxylation and the exchange rate between cytosolic Glu and mitochondrial 2-oxaglutarate was 0.33 μmol g^{-1} min^{-1}. The apparent rate of glutamatergic neurotransmission was o.44 μmol g^{-1} min^{-1}. However, the rate of cerebral oxidative glucose metabolism and glutamatergic neurotransmission did not have a 1:1 stoichiometry.[35] The effects of hyperglycaemia or hypoglycaemia on brain glycogen levels have been investigated in the rat brain. During hyperinsulinaemia with 10 mM blood glucose, brain glycogen levels increased. When rats were subjected to moderate, insulin-induced hypoglycaemia, brain glycogen levels decreased after brain glucose levels approached zero, though glycogen levels never became undetectable. Following hypoglycaemia, glucose was infused and brain glycogen levels increased to levels higher than baseline values.[36]

The utilisation of various substrates by rat brain slices in artificial cerebrospinal fluid (ACSF) has been investigated with ^{31}P NMR. When brain slices were depolarised with 60 mM K^+, the recovery of PCr levels was equally supported by glucose, lactate or pyruvate. In slices pre-treated with iodoacetate, there was no recovery of PCr levels following depolarisation in slices provided with glucose, though pyruvate and lactate did support recovery. Pre-treatment of slices with fluorocitrate, prevented lactate from supporting recovery, but did not affect recovery supported by glucose or pyruvate. However, glucose and lactate were unable to support recovery in slices pre-treated with iodoacetate and fluorocitrate, whereas the action of pyruvate was unaffected. Lactate was able to support recovery from depolarisation in the presence of iodoacetate and fluorocitrate when brain slices were obtained from rats subjected to ischaemia.[37] Non-volume selected ^{1}H spectroscopic imaging has been used to measure changes in metabolites during the acute stage of focal ischaemia in the rat brain. The results were compared to histopathological finings. In the peri-ischaemic area, NAA was maintained, but the decline of NAA in the ischaemic lesion was linear over the first 10 hours after middle cerebral artery occlusion and there was an accumulation of lactate.[38]

4.2 Heart. – A review of studies of creatine kinase flux and ATP energy transfer in the perfused heart has been produced.[39] The scaling relationships between heart design, cellular bioenergetics and mitochondria efficiencies in mammals of different body sizes has been reviewed.[40]

In an investigation of the effects of pH_i and temperature on measurements of intracellular $[Ca^{2+}]$ ($[Ca^{2+}]_i$) during ischaemic reperfusion injury, ^{31}P NMR has been used to determine intracellular pH in the perfused rabbit heart.[41] The protective properties of R 56865, a inhibitor of slowly inactivating Na^+-channels, have been investigated in the isolated guinea pig heart. During ischaemia, and increase of 2.6 and 4.4 fold in Na^+_i was detected by ^{23}Na NMR within 30 and 60 min, respectively. Treatment with R 56865 did not affect this increase, but did improve the recovery of left ventricular diastolic pressure (LVDP), ATP and PCr levels whilst reducing the development of contractor.[42] The effects of diazoxide, K_{ATP} channel opener, have been compared to ischaemic preconditioning. Diazoxide caused a potentiation of the ischaemic inhibition of the mitochondrial ATP synthase and produced cardioprotection. The administration of diazoxide did not affect cellular energy detected by ^{31}P NMR. The actions of diazoxide and ischaemic preconditioning were prevented by 5-hydroxydecanoate.[43] The effects of inhibition of Na^+/H^+ exchange on moderately hypertrophied hyperthyroid hearts, compared to euthyroid hearts, subjected to 28 min of global ischaemia and reperfusion have been investigated with ^{31}P and ^{23}Na NMR. Ischaemia caused a greater and greater Na^+_i accumulation, less acidification and faster hydrolysis of ATP compared to euthyroid hearts. Inhibition of Na^+/H^+ exchange with 1 mM amiloride in hyperthyroid hearts resulted in delayed and lower Na^+_i accumulation, faster and greater acidification and delayed ATP degradation. There was also an improved cardiac function in treated hyperthyroid hearts during reperfusion.[44] The role of Na^+-accumulation in the uptake of Ca^{2+} during ischaemia has been investigated in newborn and adult, Langendorff-perfused isolated rabbit hearts. After Na^+/K^+ ATPase inhibition, hypoxic hearts gained Na^+, whereas normoxic controls did not. In normoxic hearts acidified using a NH_4Cl pre-pulse, pH_i fell rapidly and recovered, whereas Na^+_i rose from 31 ± 18.2 to 117.7 ± 20.5 meq kg dry weight^{-1}. Hypoxia and intracellular acidification caused an accumulation of Ca^{2+}_i, though the accumulation was less in newborn, compared to adult, hearts. Increases in Na^+_i and Ca^{2+}_i were inhibited by the Na^+/H^+ exchange inhibitor methylisobutylamiloride as well as by increasing perfusate osmolarity immediately before or during hypoxia.[45] The effects of inhibition of the Na^+/H^+ exchanger on post-ischaemic recovery has been investigated with ^{23}Na and ^{31}P NMR in the Langendorff-perfused rat heart. Treatment with EIPA, cariporide or eniporide began 5 min prior to 30 min of ischaemia followed by 30 min of drug free reperfusion. Following ischaemia $[Na^+]_i$ was 293 ± 26, 212 ± 6, 157 ± 5 and 146 ± 6% above baseline for controls, EIPA, cariporide and eniporide hearts respectively. Ischaemic acidosis did not vary significantly, but pH_i recovery during reperfusion was significantly delayed in treated hearts.[46]

The mechanism of action of resveratrol has been investigated in the perfused rat heart. Treatment with a 10 min infusion of resveratrol increased adenosine

release and coronary flow in Langendorff-perfused, normoxic hearts and hearts subjected to 30 min low flow ischaemia. Furthermore, there was a decrease in PCr and the phosphorylation potential with an increase in Pi. Treatment with resveratrol plus and adenosine antagonist abolished post-ischaemic vasodilatation. Hearts from rats provided with drinking water containing 25 mg dm^{-3} resvertrol showed better functional recovery and vasodilatation from 60 min low flow ischaemia, however, there were no differences in the ATP, PCr, Pi or pH in the treated compared to the control hearts.[47] The toxicity and the effects of the antiarrythmia drug amiodarone has been investigated in the Langendorff-perfused heart, isolated cadiomycetes, hepatocytes, pancreatic cells and isolated mitochondria. Low concentrations of amiodarone protected heart and mitochondrial energy metabolism from ischaemia-reperfusion damage. The toxicity of the drug was significantly higher in hepatocytes and pancreatic cells than on cardiomycetes. In isolated mitochondria, up to 10 μM amiodaone considerably inhibited Ca^{2+}-induced permeability transition.[48] The effects of metformin on cellular energetics in the isolated rabbit heart has been investigated using ^{31}P NMR. Metformin was administered 60 min prior to the induction of global ischaemia with or without the nitric oxide synthase inhibitor L-NAME given 5 or 60 min prior to ischaemia. During ischaemia, the decrease in ATP was significantly inhibited by the presence of metformin. However, the preservation of ATP by metformin was inhibited by treatment with L-NAME.[49] The effects of pioglitazone and metformin on high energy phosphate metabolism has been studied in the perfused rabbit heart. Pioglitazone or metformin were administered 60 min prior to 45 min of global ischaemia with, or without, administration of L-NAME 60 or 5 min prior to global ischaemia. The decrease in ATP during ischaemia was significantly inhibited by pioglitazone or metformin treatment. However, this affect was abolished by treatment with L-NAME 5 min prior to ischaemia. Treatment with L-NAME 60 min prior to ischaemia, resulted in the protection of ATP levels for part of the ischaemic period.[50]

The effects of exposure to H_2O_2 in the Langendorff-perfused rat heart has been studied with ^{31}P NMR. Hearts were exposed to two, 5 min periods of ischaemic pre-conditioning, or two periods of exposure to H_2O_2, followed by 35 min of global ischaemia and 40 min reperfusion. Exposure to 2 μmol dm^{-3} H_2O_2 or ischaemic preconditioning significantly improved LVDP and the levels of PCr and ATP compared to control hearts. However, exposure to 0.5 μmol dm^{-3} or 10 μmol dm^{-3} H_2O_2 had no effect. There was a significant correlation between LVDP and ATP levels in hearts treated with 2 μmol dm^{-3} H_2O_2. However, the mean LVDP was greater in hearts following ischaemic pre-conditioning compared to that in hearts treated with H_2O_2, although the level of ATP was similar. Furthermore, hearts treated with ischaemic pre-conditioning had less intracellular acidification compared to controls or hearts treated with H_2O_2.[51] The cardioprotective effects of a free radical-scavenging agent (HO-3073) have been investigated in the Langendorff-perfused rat heart. Following 25 min of global ischaemia, hearts were reperfused with HO-3073 and/or wortmannin. Treatment with HO-3073 facilitated the recovery of ATP levels to 76 ± 5% compared to 32 ± 4% in controls, improved recovery of the rate-pressure product to 47 ± 3%

compared to 12 ± 3% in controls as well as reducing infarct size, lipid peroxidation and protein oxidation. Wortmannin administration neutralised the effects of HO-3073.[52]

The role of peroxynitrite on energy metabolism and cardiac function has been investigated in the Langendorff-perfused rat heart. Hearts were treated with either urate, a scavenger of peroxynitrite, or nitro-L-arginine, an inhibitor of peroxynitrite synthesis and were subjected to 30 min ischaemia and 60 min of reperfusion. Treatment with urate or nitro-L-arginine produced a recovery of cardiac function, creatine kinase activity and ^{31}P NMR-detected ATP levels.[53] Myocardial energy metabolism has been measured in the mouse heart *in vivo*. An i.v. infusion of 24 μg min^{-1} kg^{-1} dobutamine was used to increase the mean heart rate by 39%, from 482 ± 46 min^{-1} to 669 ± 77 min^{-1} whilst ^{31}P NMR spectra were recorded. There was no change in the PCr/ATP ratio caused by the dobutamine infusion.[54] The effects of angiotensin II stimulation on the energetics and pH_i of the intact rabbit heart have been investigated with ^{31}P NMR. Exposure to angiotensin II increased developed pressure by 14 ± 2 mmHg and increased pH_i by 0.08 ± 0.03 units, but did not cause any changes in PCr, ATP or Pi concentrations. Inhibition of Na^+/H^+ exchange with 1 μM Hoe642 abolished the increase in pH_i, but did not prevent the increase in developed pressure caused by angiotensin II. Inhibition of protein kinase C using 25 μM chelerythrine chloride prevented the positive inotropic and alkalinising effects of angiotensin II.[55] The oxidative capacity of the failing heart has been investigated in isolated hearts from pigs. Left ventricular hypertrophy was produced by ascending aortic banding in 21 swine, 9 of which developed chronic heart failure. Basal levels of PCr/ATP were 2.07 ± 0.07, 1.86 ± 0.09 and 1.68 ± 0.07 in normal, left ventricular hypertrophy and chronic heart failure, respectively. An infusion of dobutamine and dopamine caused an approximate doubling of myocardial oxygen consumption (MV_{o2}) in all groups, but only decreased PCr/ATP in the normal and left ventricular hypertrophy groups. When heart were also infused with 2,4-dinitrophenol, the was a further increase in MV_{o2} with no change in PCr/ATP in normal and left ventricular hypertrophy hearts.[56] Cardiac adaptation to exercise has been studied in the rat following a exercise regime of 30 min day^{-1} at 0.8 km h^{-1} for 5 days $week^{-1}$. Exercise endurance increased by 318% after 6 weeks and 609% after 12 weeks. ^{31}P NMR of isolated hearts from trained rats showed decreased PCr and decreased PCr/ATP ratios with increased creatine, AMP and ADP concentrations.[57]

Changes in cardiac energetics have been investigated in the transgenic mouse heart overexpressing the β-adrenergic receptor. Left ventricular performance and contractile reserve were identical for hearts of 4 month old transgenic and wild-type mice; older transgenic mice initially have increased contractility followed by left ventricular hypertrophy and heart failure. However in 4 month old transgenic mice, the ratio of PCr/ATP and the total creatine content of transgenic hearts was significantly reduced.[58] Cardiac energetics have been studied in transgenic mice bearing the missense mutation R92Q within the tropomyosin-binding domain of the thin filament protein cardiac troponin T. Simultaneous observation of contractile performance and measurements of cardiac energetics

with ^{31}P NMR revealed a decrease in free energy of ATP hydrolysis available to support contractile work and a marked inability to increase contractile performance upon acute inotropic challenge in hearts bearing the R92Q mutation.[59] The role of myoglobin in the hearts of transgenic mice over-expressing inducible nitric oxide synthase (iNOS) has been investigated with ^{31}P and 1H NMR. The formation of NO by iNOS resulted in a significant decrease of the oxymyoglobin signal and the appearance of a signal for metmyoglobin in ^{1}H NMR spectra of hearts, although contractility and energetics were unaffected. When carbon monoxide was used to inhibit myoglobin-mediated degradation of NO there was a deterioration of contractility in the transgenic hearts and a perturbation of the cardiac energy status.[60] Transgenic mouse hearts, over-expressing a dominant negative mutation of the AMP-activated protein kinase $\alpha 2$ catalytic subunit have been investigated with ^{31}P NMR. During 10 min of ischaemia, AMP-activated protein kinase activity increase 4.5-fold, whereas there was no increase in transgenic hearts. Furthermore, there was an accelerated decrease in ATP in transgenic hearts, which also developed left ventricular dysfunction.[61]

^{31}P NMR has been used to investigate the effects of perfusion with blood cardioplegic or UW solution on coronary metabolism in 14 dog hearts stored at 4° in UW solution. Hearts perfused with had significant recovery of PCr and ATP, lower levels of creatine phosphokinase activity and lower release of lactic acid. Although water content was significantly increased after perfusion with blood cardioplegic solution, there were no significant differences in found with histological examination.[62] The Val E11 signal of myoglobin at -2.76 ppm has been used to detect CO binding to myoglobin *in vivo*. When CO was infused a signal at -2.26 appeared and no effects on PCr or the oxygen consumption rate were seen when was saturated with 80% CO.[63] The labelling patterns from [2-^{13}C]acetate in the perfused rat heart under different working conditions and substrate supply have been measured with ^{13}C NMR in combination with *in vitro* methods. The hearts were perfused with: (1) 5 mM glucose + 40 μU cm^{-3} and 5 mM [2-^{13}C]acetate under high workload, (2) 2.5 mM pyruvate and 5 mM [2-^{13}C] acetate under normal workload or (3) 1 mM propionate and 5 mM [2-^{13}C] acetate under normal workload. The equilibrium of glutamate and glutamine labelling occurred after 50 min and the fractional enrichment of glutamine was 31% of the enrichment of glutamate under all conditions.[64]

4.3 Eye. – ^{1}H-detected gradient-enhanced hetronuclear multiple quantum coherence spectroscopy has been used to map the distribution of [1-^{13}C]glucose and [1-^{13}C]sorbitol in the bovine lens that have been incubated with 50mM [1-^{13}C]glucose for 1, 2 or 4 days. The majority of the [1-^{13}C]glucose and [1-^{13}C] sorbitol was found in the cortex of the lens.[65]

4.4 Liver. – ^{31}P and ^{1}H NMR have been used to examine donor livers prior to transplantation in a pilot study of the use of NMR in the assessment of donor livers. The method allowed NMR assessment of organ status without removal of the organ from the ice transportation box.[66] The synthesis of glycogen in perfused livers from fed and starved rats has been investigated with ^{1}H-decoupled ^{13}C

NMR. Livers were perfused with 99% ^{13}C glucose for 60 min followed by perfusion with natural abundance glucose. The release of ^{13}C during the latter perfusion allowed the calculation of futile glycogen cycling. The rate of glycogen synthesis was 0.31 $\pm$ 0.04 and 0.99 $\pm$ 0.04 μmol glucose g^{-1} min^{-1} and the net turnover of glycogen was less than 2 $\pm$ 0.7% and 0.6 $\pm$ 0.02% in starved and fed livers, respectively. During the chase period, however, a small broad component was observed in the glycogen signals that caused an apparent decline of glycogen by 15 $\pm$ 4 and 12 $\pm$ 2 % in starved and fed rats, respectively.[67] In an investigation of liver metabolism, ^{31}P NMR has been used to measure a decrease in high energy phosphorous metabolites when livers were perfused with lactate and pyruvate in the presence of acetylcholine.[68] The metabolism of 500 mg kg^{-1} ifosfamide has been studied using ^{31}P NMR in the guinea pig. It was found that decoupling approximately doubled the signal of detected peaks, but polarization transfer had no effect. Chemical shift imaging showed that significant proportions of the signal came from the liver and also from the gall bladder. The half life of signal in the liver was approximately 74 min, but the was no change in the signal level in the gall bladder over a 2.5 h period.[69]

4.5 Muscle. — ^{1}H and ^{31}P NMR have been used to examine knockout mice with a deficiency in guanidinoacetate methyltransferase. ^{1}H NMR revealed reduced tCr in brain and muscle with a large increase in guanidinoacetate in the muscle, but little or no increase in guanidinoacetate in the brain. ^{31}P NMR spectra of hind leg muscle and brain demonstrated reduced levels of PCr and a signal for phosphorylated guanidinoacetate, which was much higher in muscle than brain. The level of phosphorylated guanidinoacetate was reduced when muscle was made ischaemic, but increased upon reperfusion.[70] The effects of temperature and pH_e on the anaerobic metabolism of the resting frog (*Rana* esculenta) muscle has been investigated with ^{31}P and ^{1}H NMR. In the temperature range of 15 to 25°C, the temperature dependence of anaerobic glycolysis was found to be higher than that of PCr depletion. The rate of PCr hydrolysis did not appear to be affected by extracellular pH changes. However, at 25°C, lowering the pH_e from 7.9 to 7.0 caused a depression in lactate accumulation. The calculated intracellular buffering capacity was related to intra- and extracellular pH and temperature. At an extracellular pH of 7.9 and a temperature of 15°C and 25°C, the buffering capacity was calculated to be 29.5 μmol g^{-1} pH $unit^{-1}$ and 69.98 μmol g^{-1} pH $unit^{-1}$, respectively.[71] A comparison has been made of the effects of muscle contraction caused by magnetic stimulation, electric stimulation and nerve stimulation measured by ^{31}P NMR. Changes in PCr/Pi and pH_i were greater in muscles following direct electrical stimulation compared to that following magnetic stimulation or nerve stimulation.[72] The effects of the insulin sensitizer rosiglitazone on the intramyocellular lipid (IMCL) and extramyocellular lipid (EMCL) content in the tibialis anterior muscle and whole body lipid disposition in Zucker rats has been investigated with ^{1}H NMR. The ratio of IMCL/EMCL decline over the first 4 days of treatment, and was significantly lower at 7, 14, 21, 28 days following treatment with 3 mg kg^{-1} day^{-1} rosiglitazone. The absolute IMCL content was also lower at 28 days compared to

controls. At 7 days treatment, there was negative correlation between absolute IMCL content and glucose infusion rate during euglycaemic-hyperinsulinaemic clamp. treatment with rosiglitazone increased the whole body lipid content after 28 days treatment.[73]

4.6 Smooth Muscle. – A review of studies using NMR to investigate smooth muscle metabolism has been produced.[74] The effects of amiloride and KB-R7943 on Mg^{2+} levels in pig carotid artery smooth muscle have been measured with ^{31}P NMR. Both compounds caused a decrease in intracellular $[Mg^{2+}]$ ($[Mg^{2+}]_i$) in the tissue perfused with normal solution. However, both compounds caused an increase in $[Mg^{2+}]_i$ in Ca^{2+}-free conditions. In Na^+-free conditions, in the presence of Ca^{2+}, there was an increase in $[Mg^{2+}]_i$ caused by amiloride and KB-R7943.[75]

4.7 Tumour. – A review choline phospholipid metabolism in cancer cells and tumours has been produced.[76]

A new series of fluorinated porphyrin photosensitisers have been developed. The uptake of the drug into murine RIF tumours was confirmed with ^{19}F NMR.[77] Human neuroblastoma xenografts growing in nude mice have been investigated with ^1H NMR. Signals from Cho and mobile lipids (ML) dominated the spectra. Individual ratios of ML/Cho in treated and untreated tumours positively correlated with tumour volume and there was an inverse correlation between the ML/Cho ratio and the viable tumour fraction. Higher ratios of ML/Cho concomitant with pronounced histological changes were seen in tumours treated with the antiangiogenic drug TNP-470 compared to untreated tumours.[78] The role of polyunsaturated fatty acids in BTC4 gliomas during granciclovir-thymidine kinase gene therapy-induced programmed cell death has been studied with ^1H NMR. Spectra were obtained *in vivo* and analysed by pattern recognition. Spectra from ex vivo tumours showed similar macromolecular peaks to those detected in vivo and showed that the signals were largely from 18:1 and 18:2 lipids.[79] Metabolite levels in BT4C rat gliomas have been studied with ^1H NMR during granciclovir-thymidine kinase gene therapy-induced programmed cell death. The level of Gly and tCr followed changes in cell density, but the level of Cho was unaffected by up to 60% cell loss. During this period increases in saturated and unsaturated mobile lipids were observed. Metabolites observed *in vivo* were further identified using MAS NMR and high resolution NMR of cell extracts.[80] Selective multiple quantum coherence spectroscopy has been used to monitor lactate levels in RIF-1 tumours before, 24 and 72 h after 300 mg kg^{-1} cyclophosphamide treatment. There was a decline in the steady-state lactate concentration following treatment. Dynamic contrast MRI was used to show that there was an increase in Gd-DTPA up take in response to treatment. Further identification of metabolite changes were accomplished by NMR analysis of extracts.[81]

4.8 Whole Organisms. – ^{31}P NMR has been used to measure pH changes in the white muscle tissue of three eelpout populations exposed to temperature changes

of 1°C in three hours. Intracellular pH changes of 0.015 pH units $°C^{-1}$ was observed, in accordance with the α-stat hypothesis, in all populations studied. In the stenothemal Antarctic species (*Pachycara brachycephalum*), pH changes were completed earlier (with 4 hours). In *Zoarces viviparus*, from Baltic populations, pH changes occurred with 8 hours, whereas in *Z. viviparus* from North sea populations pH changes had not completed in 12 hours.[82] The effects of acute increases in temperature on blood oxygenation and muscle energy metabolism has been studies in the Atlantic cod (*Gadus morhua*). Arterial P_{O2} remained more or less constant and arterial oxygen uptake did not become limiting during warming. However, a progressive drop in venous P_{O2} was observed at greater than 10°C. ^{31}P NMR of white muscle demonstrated a decrease in pH, of 0.025 pH units $°C^{-1}$ with temperature increases between 10 and 16 °C although there was no effect on high energy phosphorous metabolites.[83] The effects of osmotic shock on the high energy metabolism and arginine kinase flux of juvenile blue crabs (*Callinectes sapidus*) has been investigated with ^{31}P NMR. Crabs were acclimated for 7 days to a salinity of 5 or 35% before examination by NMR and exposure to 35 or 5% saline, respectively. Neither acclimation salinity nor osmotic shock resulted in any change in ATP, AP on Pi. Furthermore, there was no effect on arginine kinase flux measured by ^{31}P saturation transfer. These results were in contrast to those obtained previously from isolated crab muscle.[84] The effects of acyl-L-carnitine and myo-inositol have been investigated with ^{31}P NMR in free swimming zebra fish. Those fish exposed to acyl-L-carnitine or myo-inositol had higher PCr and lower Pi levels compared to controls. No effects on PME or ATP levels were observed.[85]

5 Clinical Studies

5.1 Brain. – The use of ^{1}H NMR in diagnosis based on MRI of diseases of the central nervous system has been reviewed.[86] A review of creatine deficiency syndromes, including the use of ^{1}H and ^{31}P NMR for diagnosis, has been produced.[87] Methods and applications of ^{13}C NMR in the study of brain metabolism has been reviewed.[88] A review of ^{13}C-labeling studies of neurotransmitter flux and neuronal energetics and their relationship to fMRI has been produced.[89]

A localised proton 2D double-quantum spin-echo spectroscopy method has been used to investigate three children with intractable epilepsy. The method allowed the separation of the peak for GABA from those that would interfere with its measurement in 1D spectra. Following the onset of a ketogenic diet, one patient showed decreasing levels of GABA, whilst the other two had initial low levels that increased with time.[90] The levels of Glx and GABA have been measured in the occipital lobes of patients with idiopathic generalised epilepsy, occipital lobe epilepsy and healthy controls.[91] The level of GABA and Glx were elevated in patients with idiopathic generalised epilepsy though no correlation was found between these levels and seizure frequency, or time since last seizure. ^{1}H NMR has been used to examine patients with juvenile myoclonic epilepsy. The ratio of NAA/tCr was significantly decreased in the left and right thalami

compared to controls.[92] The concentrations of NAA, tCr and Cho have been determined in a 480 cm^3 volume of normal appearing white matter (measured by MRI) centred on the corpus collosum of relapsing-remitting multiple sclerosis patients and compared to control subjects. The choline level was the only single metric differentiating patients from controls at 100% specificity and 90% sensitivity.[93] Four patients with infantile Alexander's disease have been examined with ^{1}H NMR. A wide spread increase in myo inositol (mI) with normal or elevated Cho were observed along with a reduction of NAA in the cerebral and cerebellar white matter. There was also an accumulation of lactate in affected white matter.[94] Changes in the metabolites of affected white matter in patients with adrenoleukodystrophy have been investigated with ^{1}H NMR before and after haematopoietic stem cell transplantation. Disease progression before haematopoietic stem cell transplantation was mainly characterised by a further increase of elevated Cho levels. A positive outcome after haematopoietic stem cell transplantation was correlated with high NAA levels in affected white matter before treatment.[95] The metabolite levels in the basal ganglia and thalamus of patients with idiopathic unilateral symptomatic Parkinson's disease have been measured with ^{1}H NMR. The ratio of NAA/tCr was significantly lower in the brain contralateral to the clinically affected side.[96]

Dementia The patterns of loss of NAA in subcortical ischaemic vascular dementia (SIVD) and Alzheimer's disease has been studied using ^{1}H NMR. NAA levels in patients with SIVD were 18% lower in the frontal cortex and 27% lower in the parietal cortex compared to controls. Patients with SIVD had no NAA reduction in the white matter and medial temporal lobe. Compared to Alzheimer's disease patients, NAA levels in SIVD patients were 13% lower in the frontal cortex and 20% lower in the left parietal cortex. Cortical NAA decreased in SIVD with increasing white matter lesions and the number of lacunae. Thalamic lacunae were associated with greater NAA reduction in the frontal cortex than were lacuna outside the thalamus.[97] Patients with Alzheimer's disease, subcortical vascular dementia and subjective cognitive impairment have been investigated with ^{1}H NMR. Significantly reduced NAA levels were found in patients with Alzheimer's disease and vascular dementia compared with to those with subjective cognitive impairment. The ratio of NAA/tCr and NAA/mI were significantly lower in patients with Alzheimer's disease compared with to those with vascular dementia or subjective cognitive impairment. The ratios of NAA/tCr and NAA/mI were positively correlated with the degree of cerebral atrophy.[98] ^{1}H NMR has been used to examine the occipital cortex of 22 non-demented elderly subjects with or without the ApoE ε4 allele. There were no differences in the levels of NAA, mI and Cho, though the level of tCr was significantly lower in the ApoE ε4 allele carriers. The level of tCr only correlated with performance on the Mini-Mental state Examination in ApoE ε4 allele carriers.[99] The levels of metabolites in the dorsolateral prefrontal cortex and in the left anterior cingulum have been measured with ^{1}H NMR and the results were related to verbal intelligence. Out of a total of 52 measurements in the dorsolateral prefrontal cortex 23 were in female subjects and out of 62 measurements made in the left anterior cingulum 22 were in female subjects. The level of

NAA in the dorsolateral prefrontal cortex and in the left anterior cingulate cortex in female subjects was positively correlated to vocabulary scores.[100] The effects of hyperammonaemia on brain function has been studied using psychological tests, ^{1}H NMR and magnetization transfer MRI. Patients were given 75 g of amino acids in solution or a placebo. In those given amino acids, blood ammonia levels changed from 76 $\pm$ 7.3 to 121 $\pm$ 6.4 μM. Neuropsychological function improved in the control group, but no change was observed in the amino acid-treated group. There was a significant increase in the ratio of Glx/tCr and a significant decrease in the magnetization transfer value in the brains of the amino acid-treated group.[101] ^{1}H NMR has been used to investigate lactate levels in subjects with nocturnal apnoeic episodes and/or habitual snoring. Spectra obtained from the right centrum semiovale showed significant lactate levels in patients aged 50 years or older with an apnoea index of 26 or above.[102]

The concentrations Cho in the left and right medial thalamus of patients with obsessive-compulsive disorder have been found to be significantly increased when compared to patients with major depressive disorder or control subjects.[103] Medial thalamus Cho concentrations were not significantly different between patients with major depressive disorder and control subjects. Higher levels of Glx have been detected in the dorsolateral prefrontal cortex of patients with acute mania when compared to matched controls.[104] ^{1}H NMR spectroscopic imaging has been used to investigate brain metabolite levels in 22 autistic children, compared to age matched controls. In autistic children, it was found that the level of Cho was 27.2% lower in the left inferior anterior cingulate and 19.1% higher in the head of the right caudate nucleus, tCr was 21.1% higher in the head of the right caudate nucleus, but 17.6% lower in the body of the left caudate nucleus and 16.6% lower in the right occipital cortex.[105] ^{1}H NMR has been used to measure metabolite levels in the left striatal area of first-episode, antipsychotic-naive schizophrenic patients. The ratio of NAA/Cho was negatively correlated with performance of a procedural task.[106] The ratios of NAA, tCr and Cho have been measured in the left prefrontal cortex, hippocampus and basal ganglia of patients with schizophrenia. A significant reduction of NAA/tCr was observed in the hippocampus of anti-psychotic naive patients relative to those already treated or control subjects.[107] No differences were observed in follow-up examinations. The concentrations of NAA, tCr, Cho and mI and there ratios have been determined in the prefrontal region of 17 depressed patients.[108] The ratios of NAA/tCr, Cho/tCr and mI/tCr were significantly lower in depressed patients compared to control subjects. This was found to be due to a higher concentration of tCr in patients. The metabolite levels in the grey and white matter of the frontal lobe of patients with bipolar disorder have been detected with ^{1}H NMR. Patients had lower levels of NAA and Cho in the grey matter and higher levels of amino acids in the white matter when compared to controls.[109] ^{1}H NMR has been used to examine the metabolite levels in the dorsolateral prefrontal cortex of children (mean age 12.6 years) with bipolar disorder. Lower NAA/tCr was observed in the right dorsolateral prefrontal cortex, but not in the left, and no differences were observed in mI or Cho levels.[110] The level of NAA in the right and left dorsolateral prefrontal cortex, orbitofrontal cortex, cingulate

and thalamus has been measured by ^{1}H NMR in patients with chronic back pain and depression compared to the relationship between depression and NAA in normal subjects. A reduction of NAA was found in the right dorsolateral prefrontal cortex of chronic back pain patients, and the levels of NAA were highly correlated with depression.[111] The effects of electroconvulsive therapy (ECT) on the metabolite levels in the brains of patients with depression have been investigated using ^{1}H NMR. Measurements were made in the left amygdala region before and after unilateral ECT. A significant increase in NAA was observed in those responding to ECT. Furthermore, five patients that responded later to a combination of ECT and antidepressants also showed a significant increase in NAA. There were no changes observed in Cho, tCr and Glx in patients who responded to treatment.[112]

In a similar study, however, reduced Glx levels were observed in the anterior cingulum of depressed patients. The level of Glx was found to increase upon effective ECT.[113] The effects of selective serotonin reuptake inhibitor discontinuation syndrome have been investigated in patients with unipolar major depression who had been stabilised on paroxetine or fluoxetine. ^{1}H NMR spectroscopic imaging of the rostral anterior cingulate was carried out 3 days after substitution of medication with a selective serotonin reuptake inhibitor or a placebo. The ratio of Cho/tCr was deceased in patients who met the criteria of selective serotonin reuptake inhibitor discontinuation syndrome compared to asymptomatic subjects.[114]

Metabolite levels in the foetal brain have been measured using ^{1}H NMR STEAM and PRESS throughout the 30 to 41 week gestational period. During this period the absolute concentrations of NAA increased, the ratio of NAA/tCr and NAA/Cho increased and the ratio of Cho/tCr decreased.[115] ^{1}H NMR has been used to in the diagnosis of a creatine transport disorder. The patient had an absence of tCr in the brain, though no absence of tCr was observed in the muscle.[116]Time-resolved ^{1}H NMR has been used to measure changes in Lactate levels following a brief visual stimulation paradigm. A significant decrease in lactate concentration was observed 5 s after stimulation; after 12 s levels had returned to baseline.[117]

The unidirectional flux from Pi to ATP has been measured using progressive saturation transfer. The synthesis rate was 12.1 ± 2.8 μmol ATP g^{-1} min^{-1} in the human primary visual cortex.[118] The variation of relaxation times of metabolites in the human brain has been investigated in human subjects at 1.5 T. Saturation recovery spectra were obtained with a TE of 30 ms from the occipital grey matter, parietal white matter and frontal white matter. In all tissues, mI had the shortest T1, followed by Cho, NAA and then tCr. The value of T1 increased from that in occipital grey matter to that in parietal white matter and frontal white matter had the highest values. In test solutions, the order of shortest to longest T1 was mI, NAA, tCr and Cho.[119]The use of the ratio of Lactate/Cho as a predictive indicator of adverse outcome in acute perinatal asphyxia has been investigated. Logistic regression confirmed that the lactate/Cho ratio detected in the basal ganglia and thalamus could be used to differentiate normal, abnormal or fatal outcome.[120] ^{1}H NMR has been used to examine the occipital grey matter and

parietal white matter of patients with diabetes mellitus. Compared to control subjects, patients had a significantly elevated mI/tCr ratio in both areas, and elevated Cho/tCr in the grey matter. In patients with polyneuropathy, the level of mI was increased further.[121] Single voxel ^{1}H PRESS has been used to measure metabolite levels in the brains of patients before and after radiotherapy for lung cancer. Changes in NAA levels were seen in all patients irrespective of age or treatment, with greater effects seen in the deeper frontal lobes compared to the occipital lobes.[122]

5.2 Heart. – A review of applications of NMR to the study of the heart has been produced.[123] Clinical applications of cardiovascular NMR have been reviewed.[124]

High energy phosphate metabolism of cardiac and skeletal muscle has been measure in patients with type 2 diabetes. Although cardiac morphology, mass and function appear to be normal, patients with diabetes had significantly lower PCr/ATP ratios 1.50 ± 0.11 compared to controls (2.30 ± 0.12) and also showed a negative correlation of PCr/ATP with fasting plasma free fatty acids (FFA) concentrations. During exercise, diabetic patients also appeared to have a faster decrease of muscle PCr and pH, which recovered more slowly afterwards.[125] The level of tCr in the septum has been measured with image-guided, cardiac-gated, ^{1}H PRESS in patients with dilated cardiomyopathy or hypertrophic cardiomyopathy. Myocardial tCr was significantly lower in patients with dilated cardiomyopathy compared to controls. Furthermore, tCr was lower in patients with hypertrophic cardiomyopathy compared to controls, though it was significantly higher than in patients with dilated cardiomyopathy. Myocardial tCr was significantly correlated with left ventricular ejection fraction, but negatively correlated with plasma B-type natriuretic peptide in patients with dilated cardiomyopathy or hypertrophic cardiomyopathy.[126] ^{1}H NMR has been used to measure myocardial triglycerides in rats and humans in a study of cardiac steatosis. In ex vivo tissue from Zucker rats, ^{1}H NMR measurement of myocardial triglycerides agreed with those obtained from biochemical measurement. In human subjects, myocardial triglyceride was detected *in vivo* even in very lean subjects and was elevated in overweight and obese subjects.[127]

5.3 Liver. – The use of ^{31}P NMR for the assessment of hepatitis has been investigated in patients with mild hepatitis, moderate/severe hepatitis or cirrhosis assessed by liver biopsy. Changes in the ratio of PME/phosphodiesters (PME/PDE) were used to separate patients with mild disease from those with moderate disease, and both of these groups were separated from patients with cirrhosis.[128] The effects of amino acids on hepatic glucose metabolism has been assessed using ^{13}C NMR to measure glycogenolysis in the liver and using the incorporation of D_2O into [6,6-^{2}H]glucose to determine gluconeogenesis and endogenous glucose production. When subjects were given an infusion of amino acids or glucose in the presence of somatostatin, plasma glucose rose by about 50% due to an increase in endogenous glucose production. The infusion of amino acids produced a 53% increase in total glucose production and a 65%

increase in net glucose production. When amino acids were infused without somatostatin there was no change in plasma glucose levels despite a near doubling of production from gluconeogenesis.[129] The uptake and metabolism of the fluorinated non-steroidal anti-inflammatory drug niflumic acid has been studied with ^{19}F NMR. Spectra from the liver indicated the presence of niflumic acid and a metabolite, possibly 4′-hydroxyniflumic acid. There was a 0.7 to 0.9 ratio of the drug to metabolite detected in the liver.[130]

5.4 Muscle. – The assessment of insulin resistance by NMR has been reviewed.[131]

The effects of cigarette smoking on glycogen recovery following exercise in gastrocnemius muscle has been investigated in young, male smokers compared to control subjects. Single-leg toe raises were used to deplete glycogen to 23.5 $\pm$ 1.2 and 19.1 $\pm$ 1.3 mM in smokers and controls subjects, respectively. During the first hour of recovery, glycogen synthesis was 13.8 $\pm$ 1.1 and 15.3 $\pm$ 11.3 mM h^{-1} in smokers and controls subjects, respectively. Between hours 1 to 4, glycogen synthesis was 0.8 $\pm$ 0.2 and 4.5 $\pm$ 0.5 mM h^{-1} in smokers and controls subjects, respectively. Furthermore, the level of G6P during hours 1 to 4 was 0.105 $\pm$ 0.006 and 0.217 $\pm$ 0.019 in smokers and controls subjects, respectively.[132] The effects of dietary carbohydrate on muscle glycogen has been investigated in 12 male and 8 female healthy volunteers. One hour of treadmill or toe-raise exercises were performed before a 3-day low carbohydrate (loCHO) diet (20% carbohydrate, 60% fat and 20% protein). On day 3 the exercise was repeated before the volunteers began a four-day high carbohydrate (HiCHO) diet (90% carbohydrate, 2% fat and 8% protein). ^{31}P and ^{13}C NMR were used before and after exercise to determine glycogen, G6P and muscle pH. During the 3-day LoCHO diet, fasting levels of G6P were not different from resting levels, although resting G6P was elevated compared to that before the study during the first three days of the HiCHO diet. By the final day, muscle glycogen was 1.6-fold greater than before the protocol, while G6P had retuned to baseline.[133] The IMCL content of the predominantly non-oxidative tibialis anterior muscle and the oxidative soleus muscle has been measured with ^{1}H NMR in a study of the effects of serum adiponectin concentration on intramyocellular lipids. Changes in IMCL content of both muscle types were measured after a three day dietary lipid challenge and after i.v. lipid challenge with suppressed lipid oxidation under hyperinsulinaemia. Aponectin concentrations were negatively correlated with IMCL in the soleus muscle independent of measures of obesity, but not correlated with IMCL in the non-oxidative tibialis anterior muscle. Adiponectin concentrations were negatively correlated with the increase in IMCL after dietary lipid challenge in the tibialis but not the soleus muscle. During suppression of lipid oxidation by hyperinsulinaemia, no effects on IMCL by adiponectin were observed in either muscle type.[134] The relationship between adiponectin levels, IMCL levels and insulin resistance has been investigated in 14 obese adolescents and 8 age-matched, non-obese controls. Adiponectin levels were lower in obese adolescents and were positively related to insulin sensitivity. Strong inverse relationships were found between adiponectin levels and tri-

glyceride levels or IMCL content of muscles.[135]

The T_1 and T_2 relaxation times of phosphorous metabolites have been measured in the human calf muscle at 3T using ^{31}P-STEAM. T_1 relaxation times were 5.2 ± 1.0, 6.4 ± 0.2, 4.5 ± 0.3, 2.6 ± 0.9 and 3.5 ± 1.1 s for Pi, PCr, γ-ATP, α-ATP and β-ATP, respectively. Values for T_2 were 148 ± 17, 334 ± 30, 78 ± 13, 55 ± 7 and 55 ± 10 ms, respectively. The effects of creatine supplementation on ATP synthesis during a 10 s maximal dynamic handgrip exercise has been investigated with ^{31}P NMR. Creatine supplementation produced an 11 ± 4.6% increase in the resting muscle PCr concentration and a 65 ± 4.2% increase in the PCr degradation during exercise. Following supplementation, the ATP synthesis rate through PCr hydrolysis increased from 0.64 ± 0.08 to 0.86 ± 0.14 μmol kg-wet-weight^{-1} s^{-1} and the total anaerobic ATP synthesis rate during exercise increased from 0.97 ± 0.16 to 1.33 ± 0.27 μmol kg-wet-weight^{-1} s^{-1}. Furthermore, supplementation produced a 15.1 ± 3.8% increase in the mean power output during exercise, but there was no difference in the mean power output per unit of total anaerobic ATP synthesis. However, the ATP synthesis rate through PCr hydrolysis positively correlated with mean power output during exercise.[136]

5.5 Tumour. – Patients with oligodendrogliomas have been examined with MRI and short-echo ^{1}H spectroscopic imaging. Tumours contained lower NAA and increased Cho and Glx compared to contralateral white matter. Furthermore, the level of Glx was significantly higher in patients with low-grade oligodendrogliomas compared with patients with low-grade astrocytomas. Large resonances of lipids plus lactate were observed high-grade oligodendrogliomas compared to low-grade tumours.[137] An elevated level of glutathione has been detected by ^{1}H NMR in meningiomas compared to normal white matter and low-grade gliomas. Concentrations of Glx were also found to be elevated in meningiomas compared to astrocytomas or normal white matter.[138] The differentiation of tumour types has been investigated using ^{1}H NMR spectra from primitive neuroectodermal tumours compared to meningiomas, low-grade astrocytomas, anaplastic astrocytomas, glioblastomas and metastases. The resonances for alanine and Glx were decreased in primitive neuroectodermal tumours compared to meningiomas, choline was increased compared to low-grade and anaplastic astrocytomas, and lipids, at 1.30 ppm, decreased whilst Cho increased with respect to glioblastomas and metastases.[139] Patients with primary central nervous system lymphoma or glioma have been examined with ^{1}H NMR. All patients with primary central nervous system lymphoma had massively increased lipid resonances and markedly elevated Cho levels. Increased lipid resonances were also found in necrotic glioblastomas, but massively increased lipid levels distinguished primary central nervous system lymphoma from all solid astrocytomas.[140] ^{31}P NMR has been used to examine the Pi/NTP ratio in bone sarcoma before therapy. In this study of 20 patients, it was found that the Pi/NTP ratio of the sarcoma was higher in those patients that went on to survive.[141]

References

1. Mason, G. F. and Rothman, D. L. *Metab. Engineer.* 2004, **6(1)**, 75-84.
2. Shic, F. and Ross, B. *J. Magn. Reson.* 2003, **162(2)**, 259-268.
3. Aliev, M. K. and Tikhonov, A. N. *Mol. Cell. Biochem.* 2004, **256/257(1&2)**, 257-266.
4. Port, R. E. and Wolf, W. *Invest. New Drug* 2003, **21(2)**, 157-168.
5. Henry, P. G.; Tkac, I. and Gruetter, R. *Magn. Reson. Med.* 2003, **50(4)**, 684-692.
6. Damon, B. M.; Hsu, A. C.; Stark, H. J. and Dawson, M. *Magn. Reson. Med.* 2003, **49(2)**, 233-240.
7. Kim, I. S.; Barrow, K. D. and Rogers, P. L. *J. Microbiol. Biotechnol.* 2003, **13(1)**, 90-98.
8. Noguchi, Y.; Shimba, N.; Kawahara, Y.; Suzuki, E.- I. and Sugimoto, S. *Eur. J. Biochem.* 2003, **270(12)**, 2622-2626.
9. Willcocks, J. P.; Mulquiney, P. J.; Ellory, J. C.; Veech, R. L.; Radda, G. K. and Clarke, K. *J. Biol. Chem.* 2002, **277(51)**, 49911-49920.
10. Hakumaki, J. M. and Brindle, K. M. *Trends Pharmacol. Sci.* 2003, **24(3)** 146-149.
11. Friedman, M. I.; Graczyk-Millbrandt, G.; Ji, H.; Rawson, N. E. and Osbakken, M. D. *Biochim. Biophys. Acta* 2003, **1642(1-2)**, 53-58.
12. Doliba, N. M.; Vatamaniuk, M. Z.; Buettger, C. W.; Qin, W.; Collins, H. W.; Wehrli, S. L.; Carr, R. D. and Matschinsky, F. M. *Diabetes* 2003, **52(2)**, 394-402.
13. Griffin, J. L.; Bollard, M.; Nicholson, J. A. and Bhakoo, K. *NMR Biomed.* 2002, **15(6)**, 375-384.
14. Wright, L. C.; Djordjevic, J. T.; Schibeci, S. D.; Himmelreich, U.; Muljadi, N.; Williamson, P. and Lynch, G. W. *Eur. J. Biochem.* 2003, **270(9)**, 2091-2100.
15. Brisdelli, F.; Iorio, E.; Knijn, A.; Ferretti, A.; Marcheggiani, D.; Lenti, L.; Strom, R.; Podo, F. and Bozzi, A. *Biochem. Pharmacol.* 2003, **65(8)**, 1271-1280.
16. Wu, C.- L.; Qian, M. and Huang, Y. *Bopuxue Zazhi* 2002, **19(4)**, 353-358.
17. Glunde, K.; Ackerstaff, E.; Natarajan, K.; Artemov, D. and Bhujwalla, Z. M. *Magn. Reson. Med.* 2002, **48(5)**, 819-825.
18. Fiala, Z.; El-Saggan, A. H.; Uhrik, B.; Liptaj, T.; Dovinova, I.; Hanusovska, E.; Drobna, Z., Barancik, M. and Breier, A. *Biochim. Biophys. Acta* 2003, **1639(3)**, 213-224.
19. Cortes, S.; Gromova, M.; Evrard, A.; Roby, C.; Heyraud, A.; Rolin, D. B.; Raymond, P.; Brouquisse, R. *Plant Physiol.* 2003, **131(2)**, 824-837.
20. Szimtenings, M.; Olt, S. and Hasse, A. *J. Magn. Reson.* 2003, **161(1)**, 70-76.
21. Bouzier-Sore, A.- K.; Serres, S.; Canioni, P. and Merle, M. *Biochimie* 2003, **85(9)**, 841-848.
22. Gruetter, R. *Adv. Mol. Cell Biol.* 2004, **31(Non-neuronal cells of the nervous system:Function and Dysfunction, Part 2)**, 409-433.
23. de Graaf, R. A.; Mason, G. F.; Patel, A. B.; Behar, K. L. and Rothman, D. L. *NMR Biomed.* 2003, **16(6/7)**, 339-357.
24. Baslow, M. H. *Neurochem. Res.* 2003, **28(6)**, 941-953.
25. Choi, I.- Y.; Lee, S.- P.; Guilfoyle, D. N. and Helpern, J. A. *Neurochem. Res.* 2003, **28(7)**, 987-1001.
26. Mathew, S. J.; Shungu, D. C.; Mao, X.; Smith, E. L. P.; Perera, G. M.; Kegeles, L. S.; Perera, T.; Lisanby, S. H.; Rosenblum, L. A.; Gorman, J. M. and Coplan, J. D. *Biol. Psychiatr.* 2003, **54(7)**, 727-735.
27. Martoft, L.; Stodkilde-Jorgensen, H.; Forslid, A.; Pedersen, H. D. and Jorgensen, P. F. *Lab Animal* 2003, **37(3)**, 241-248.
28. Shonat, R. D. and Koretsky, A. P. *Adv. Exp. Med. Biol.* 2003, **530(Oxygen Trans-**

port to Tissues XXIV), 331-345.
29. Rao, R.; Tkac, I.; Townsend, E. L.; Gruetter, R. and Georgieff, M. K. *J. Nutrition* 2003, **133(10)**, 3215-3221.
30. Lei, H.; Zhang, Y.; Zhu, X.- H. and Chen, W. *Magn. Reson. Med.* 2003, **49(6)**, 979-984.
31. Henry, P.- I.; Oz, G.; Provencher, S. and Gruetter, R. *NMR Biomed.* 2003, **16(6/7)**, 400-412.
32. Kondrat, R. W.; Kanamori, K. and Ross, B. D. *J. Neurosci. Methods* 2003, **120(2)**, 179-192.
33. de Graaf, R. A.; Brown, P. B.; Mason, G. F.; Rothman, D. L. and Behar, K. L. *Magn. Reson. Med.* 2003, **49(1)**, 37-46.
34. Hyder, F.; Brown, P.; Nixon, T. W. and Behar, K. L. *Adv. Exp. Med. Biol.* 2003, **530(Oxygen transport to tissue XXIV)**, 29-39.
35. Choi, I.- Y.; Lei, H. and Gruetter, R. *J. Cereb. Blood Flow Metab.* 2002, **22(11)**, 1343-1351.
36. Choi, I.- Y.; Seaquist, E. R. and Gruetter, R. *J. Neurosci. Res.* 2003, **72(1)**, 25-32.
37. Kitano, N.; Shibata, E.; Iwasaka, H.; Noguchi, T.; Yokoi, I. *Mol. Cell. Biochem.* 2003, **244(1&2)**, 77-81.
38. Igarashi, H.; Kwee, I. L.; Okubo, S.; Nakada, T. and Katayama, Y. *Int. Congress Ser.* 2003, **1252(Molecular Mechanisms and Epochal Therapeutics of Ischemic Stroke and Dementia)**, 341-344.
39. Joubert, F.; Mateo, P.; Gillet, B.; Beloeil, J.- C.; Mazet, J-L. and Hoerter, J. A. *Mol. Cell. Biochem.* 2004, **256/257(1&2)**, 43-58.
40. Dobson, G. P. *Clin. Exp. Pharmacol. Physiol.* 2003, **30(8)**, 590-597.
41. Stamm, C.; Friehs, I.; Choi, Y.- H.; Zurakowski, D.; McGowan, F. X. and del Nido, P. J.; *Cardiovasc. Res.* 2003, **59(3)**, 695-704.
42. Hartmann, M. and Decking, U. K. M. *N-S Arch Pharmacol.* 2003, **368(3)**, 160-165.
43. Ala-Rami, A.; Ylitalo, K. and Hassinen, I. E. *Basic Res. Cardiol.* 2003, **98(4)**, 250-258.
44. Baki, M. I. and Ingwall, J. S. *Cardiovasc. Res.* 2003, **57(4)**, 1004-1014.
45. Anderson, S. E.; Liu, H.; Ho, H. S.; Lewis, E. J. and Cala, P. M. *Am. J. Physiol.* 2003, **284(5, Pt. 1)**, C1123-C1132.
46. Ten Hove, M.; Van Emous, J. G. and Van Echteld, C. J. A. *Mol. Cell. Biochem.* 2003, **250(1&2)**, 47-54.
47. Bradamante, S.; Berenghi, L.; Piccinini, F.; Bertelli, A. A. E.; De Jonge, R.; Beemster, P. and De Jong, J. W. *Eur. J. Pharmacol.* 2003, **465(1-2)**, 115-123.
48. Varbiro, G.; Toth, A.; Tapodi, A.; Veres, B.; Sumegi, B. and Gallyas, F. *Biochem. Pharmacol.* 2003, **65(7)**, 1115-1128.
49. Kawabata, K. and Ishikawa, K. *Hypertens. Res.* 2003, **26(1)**, 107-110.
50. Kawabata, H. and Ishikawa, K. *Diabetes/Metab. Res. Review.* 2003, **19(4)**, 299-305.
51. Yaguchi, Y.; Satoh, H.; Wakahara, N.; Katoh, H.; Uehara, A.; Terada, H.; Fujise, Y. and Hayashi, H. *Circ. J.* 2003, **67(3)**, 253-258.
52. Toth, A.; Kovacs, K.; Deres, P.; Halmosi, R.; Czopf, L.; Hanto, K.; Kalai, T.; Hideg, K.; Sumegi, B. and Toth, K. *Biochem. Pharmacol.* 2003, **66(11)**, 2263-2272.
53. Lee, W. H.; Gounarides, J. S.; Roos, E. S. and Wolin, M. S. *Am. J. Physiol.* 2003, **285(4, Pt. 2)**, H1385-H1395.
54. Naumova, A. V.; Weiss, R. G. and Chacko, V. P. *Am. J. Physiol.* 2003, **283(5, Pt. 2)**, H1976-H1979.
55. Mielke, M.; Paterson, D. J.; Sang, A. E.; Radda, G. K. and Clarke, K. *Int. J. Biochem. Cell Biol.* 2003, **35(6)**, 984-991.

56. Gong, G.; Liu, J.; Liang, P.; Guo, T.; Hu, Q.; Ochiai, K.; Hou, M.; Ye, Y.; Wu, X.; Mansoor, A.; From, A. H. L.; Urgurbil, K.; Bache, R. J. and Zhang, J. *Am. J. Physiol.* 2003, **285(2, Pt. 2)**, H541-H548.
57. Fenning, A.; Harrison, G.; Dwyer, D.; Rose'Meyer, R. and Brown, L. *Mol. Cell. Biochem.* 2003, **251(1&2)**, 51-59.
58. Spindler, M.; Engelhardt, S.; Niebler, R.; Wagner, Hein, L.; Lohse, M. J. and Neubauer, S. *J. Mol. Cell. Cardiol.* 2003, **35(4)**, 389-397.
59. Javadpour, M. M.; Tardiff, J. C.; Pinz, I. and Ingwall, J. S. *J. Clin. INvest.* 2003, **112(5)**, 768-775.
60. Wunderlich, C.; Floegel, U.; Goedecke, A.; Heger, J. and Schrader, J. *Circ. Res.* 2003, **92(12)**, 1352-1358.
61. Xing, Y.; Musi, N.; Fujii, N.; Zou, L.; Luptak, I.; Hirshman, M. F.; Goodyear, L. J. and Tian, R. *J. Biol. Chem.* 2003, **278(31)**, 28372-28377.
62. Suzuki, M.; Hasegawa, Y.; Ohtaki, A.; Takahashi, T. and Morishita, Y. *Kitakanto Medical Journal* 2003, **53(3)**, 243-249.
63. Jue, T. and Chung, Y. *Adv. Exp. Med. Biol.* 2003, **530(Oxygen Transport to tissue XXIV)**, 671-680.
64. Cohen, D. M.; Guthrie, P. H.; Gao, X.; Sakai, R. and Taegtmeyer, H. *Am. J. Physiol.* 2003, **285(6, Pt. 1)**, E1312-E1316.
65. Sawada, T.; Nakamura, J.; Nishida, Y.; Kani, K.; Okamoto, R.; Morikawa, S. and Inubushi, T. *MAgn. Reson. Imag.* 2003, **21(9)**, 1029-1031.
66. Changani, K. K.; So, P.- W.; Bell, J. D.; Davidson, B.; Rolles, K. and Fuller, B. J. *Cell Preserv. Tech.* 2003, **1(2)**, 105-109.
67. Bergans, N.; Dresselaers, T.; Vanhamme, L.; Van Hecke, P.; Van Huffel, S. and Vanstapel, F. *NMR Biomed.* 2003, **16(1)**, 36-46.
68. Vatamaniuk, M. Z.; Horyn, O. V.; Vatamaniuk, O. K. and Doliba, N. M. *Life Sci.* 2003, **72(16)**, 1871-1882.
69. Mancini, L.; Payne, G. S.; Dzik-Jurasz, A. S. K. and Leach, M. O. *Magn. Reson. Med.* 2003, **50(2)**, 249-255.
70. Renema, W. K. J.; Schmidt, A.; van Asten, J. J. A.; Oerlemans, F.; Ullrich, K.; Wieringa, B.; Isbrandt, D. and Heerschap, A.; *Magn. Reson. Med.* 2003, **50(5)**, 936-943.
71. Vezzoli, A.; Gussoni, M.; Greco, F.; Zetta, L. *J. Exp. Biol.* 2003, **206(17)**, 3043-3052.
72. Chiba, A. and Inase, M. *Bioelectromagn.* 2003, **24(5)**, 366-371.
73. Jucker, B. M. Schaeffer, T. R.; Haimbach, R. E.; Mayer, M. E.; Ohlstein, D. H.; Smith, S. A.; Cobitz, A. R. and Sarkar, S. K. *Metab. Clin. Exp.* 2003, **52(2)**, 218-225.
74. Nakayama, S. and Clark, J. F. *Mol. Cell. Biochem.* 2003, **244(1&2)**, 17-30.
75. Uetani, T.; Matsubara, T.; Nomura, H.; Murahara, T. and Nakayama, S. *J. Biol. Chem.* 2003, **278(48)**, 47491-47497.
76. Ackerstaff, E.; Glunde, K. and Bhujwalla, Z. *J. Cell. Biochem.* 2003, **90(3)**, 525-533.
77. Pandey, S. K.; Gryshuk, A. L.; Graham, A.; Ohkubo, K.; Fukuzumi, S.; Dobhal, M. P.; Zheng, G.; Ou, Z.; Zhan, R.; Kadish, K. M.; Oseroff, A.; Ramaprassed, S. and Pandey, R. K. *Tetrahedron* 2003, **59(50)**, 10059-10073.
78. Linskog, M.; Kogner, P.; Ponthan, F.; Schweinhardt, P.; Sandstedt, B.; Heiden, T.; Helms, G. and Spenger, C. *Brit. J. Cancer*2003, **88(3)**, 478-485.
79. Griffin, J. L.; Lehtimaeki, K. K.; Valonen, P. K.; Groehn, O. H. J.; Kettunen, M. I.; Ylae-Herttuala, S.; Pitkaenen, A.; Nicholson, J. K. and Kaupinen, R. A. *Cancer Res* 2003, **63(12)**, 3195-3201.
80. Lehtimaeki, K. K.; Valonen, P. K.; Griffin, J. L.; Vaeisaenen, T. H.; Groehn, O. H. J.; Kettunen, M. I.; Vepsaelaeinen, J.; Ylae-Herttuala, S.; Nicholson, J. and Kaup-

pinen, R. A. *J. Biol. Chem.* 2003, **278(46)**, 45915-45923.
81. Poptani, H.; Bansal, N.; Graham, R. A.; Mancuso, A.; Nelson, D. S. and Glickson, J. D. *NMR Biomed.* 2003, **16(2)**, 102-111.
82. Sartoris, F. J.; Bock, C. and Pörtner, H. O. *J. Therm. Biol.* 2003, **28**, 363-371.
83. Sartoris, F. J.; Bock, C.; Serendero, I.; Lannig, G. and Pörtner, H. O. *J. Fish Biol.* 2003, **62(6)**, 1239-1253.
84. Kinsey, S. T. and Lee, B. C. *Comp. Biochem. Phys. B* 2003, **135B(3)**, 521-531.
85. Levine, J.; Panchalingam, K.; McClure, R. J.; Gershon, S. and Pettegrew, J. W. *Neurochem. Res.* 2003, **28(5)**, 687-690.
86. Ida, M.; Nakamura, K.; Arai, T. and Tokuyama, T. *Brain and Nerve* 2002, **54(11)**, 935-941.
87. Schulze, A. *Mol. Cell. Biochem.* 2003, **244(1&2)**, 143-150.
88. Gruetter, R.; Adriany, G.; Choi, I.- Y.; Henry, P.- G.; Lei, H. and Oz, G. *NMR Biomed.* 2003, **16(6/7)**, 313-338.
89. Rothman, D. L.; Behar, K. L.; Hyder, F.; Shulman, R. G. *Ann. Rev. Physiol.* 2003, **65**, 401-427.
90. Wang, Z. J.; Bergqvist, C.; Hunter, J. V.; Jin, D.; Wang, D.- J.; Wehrli, S. and Zimmerman, R. A. *Magn. Reson. Med.* 2003, **49(4)**, 615-619.
91. Simister, R. J.; McLean, M. A.; Barker, G. J. and Duncan, J. S. *Epilepsia* 2003, **44(4)**, 550-558.
92. Mory, S. B.; Li, L. M.; Guerreiro, C. A. M. and Cendes, F. *Epilepsia* 203, **44(11)**, 1402-1405.
93. Inglese, M.; Li, B. S. Y.; Rusinek, H.; Babb, J. S.; Grossman, R. I. and Gonen, O. *Magn. Reson. Med.* 2003, **50(1)**, 190-195.
94. Brockimann, K.; Dechent, P.; Meins, M.; Haupt, M. Sperner, J.; Stephani, U.; Frahm, J. and Hanefeld, F. *J. Neurology* 2003, **250(3)**, 300-306.
95. Wilken, B.; Dechent, P.; Brackmann, K.; Finsterbusch, J.; Baumann, M.; Ebell, W.; Korenke, G. C.; Pouwels, P. J. W.; Hanefeld, F. A. and Frahm, J. *Neuopediatr.* 2003, **34(5)**, 237-246.
96. Kim, J.- K.; Kim, B.- C.; Lee, K.- R.; Song, M.- K.; Park, M.- S.; Kim, M.- K.; Cho, K.- H. and Seo, J.- J. *Taehan Sin'gyong Kwahak Hoechi* 2003, **21(6)**, 622-627.
97. Schuff, N.; Capizzano, A. A.; Du, A. T.; Amend, D. L; O'Neill, J.; Norman, D.; Jagust, W. J.; Chui, H. C.; Kramer, J. H.; Reed, B. R.; Miller, B. L.; Yaffe, K. and Weiner, M. W. *Neurology* 2003, **61(3)**, 358-364.
98. Weiss, U.; BAcher, R.; Vonbank, H.; Kemmler, G.; Lingg, A. and Marksteiner J. *J. Clin. Psychiatr.* 2003, **64(3)**, 235-242.
99. Laakso, M. P.; Hiltunen, Y.; Koenoenen, M.; Kivipelto, M.; Koivisto, A.; Hallikainen, M. and Soininen, H. *J. Neuro. Transmission* 2003, **110(3)**, 267-275.
100. Pfleiderer, B.; Ohrmann, P.; Suslow, T.; Wolgast, M.; Gerlach, A. L.; Heindel, W.; Michael, N. *Neurosci.* 2004, **123(4)**, 1053-1058.
101. Balata, S.; Olde, D.; Steven, W. M.; Ferguson, K.; MArshall, I.; Hayes, P. C.; Deutz, N. E. P.; Williams, R.; Wardlaw, J. and Jalan, R. *Hepatology* 2003, **37(4)**, 931-939.
102. Kamba, M.; Inoue, Y.; Higami, S. and Suto, Y. *Neurobiol. Aging* 2003 **24(5)**, 753-760.
103. Smith, E. A.; Russell, A.; Lorch Banerjee, S. P.; Rose, M.; Ivey, J.; Bhandari, R.; Moore, G. J. and Rosenberg, D. R. *Biol. Psych.* 2003, **54(12)**, 1399-1405.
104. Michael, N.; Erfurth, A.; Ohrmann, P.; Goessling, M.; Arolt, V.; Heindel, W. and Pfleiderer, B. *Psychopharmacol.* 2003, **168(3)**, 344-346.
105. Levitt, J. G.; O'Neill, J.; Blanton, R. E.; Smalley, S.; Fadale, D.; McCracken, J. T.; Guthrie, D.; Toga, A. W. and Alger, J. R. *Biol. Psych.* 2003, **54(12)**, 1355-1366.

106. Gimenez, M.; Junque, C.; Perez, M.; Vendrell, P.; Baeza, I.; Salamero, M.; Mercader, J. M. and Bernado, M. *Neurosci. Letts.* 2003, **347(2)**, 97-100.
107. Fannon, D.; Simmons, A.; Tenakoon, L.; O'Ceallaigh, S.; Sumich, A.; Doku, V.; Shew, C. and Sharma, T. *Biol. Psychiatr.* 2003, **54(6)**, 587-598.
108. Gruber, S.; Frey, R.; Mlynarik, V.; Stadlbauer, A.; Heiden, A.; Kasper, S.; Kemp, G. J. and Moser, E.; *Invest. Radiol.* 2003, **38(7)**, 403-408.
109. Cecil, K. M.; Del-Bello, M. P.; Morey, R. and Strakowski, S. M. *Bipolar Disord.* 2002, **4(6)**, 357-365.
110. Chang, K.; Adleman, N.; Dienes, K.; Barnea-Goraly, N.; Reiss, A. and Ketter, T. *Biol. Psychiatr.* 2003, **53(11)**, 1059-1065.
111. Grachev, I. D.; Ramachandran, T. S.; Thomas, P. S.; Szeverenyi, N. M. and Fredrickson, B. E. *J. Neuro. Transmission* 2003, **110(3)**, 287-312.
112. Michael, N.; Erfurth, A.; Ohrmann, P.; Arolt, V.; Heindel, W. and Pfleiderer, B. *Neuropsychopharmacol.* 2003, **28(4)**, 720-725.
113. Pfleiderer, B.; Michael, N.; Erfurth, A.; Ohrmann, P.; Hohmann, U.; Wolgast, M.; Fiebich, M.; Arolt, V. and Heindel, W. *Psych. Res.* 2003, **122(3)**, 185-192.
114. Kqaufman, M. J.; Henry, M. E.; Frederick, B. deB.; Hennen, J.; Villafuerte, R. A.; Stoddard, E. P.; Schmidt, M. E.; Cohen, B. M. and Renshaw, P. F. *Biol. Psychiatr.* 2003, **54(5)**, 534-539.
115. Kok, R. D.; van den Berg, P. P.; van den Berg, A. J.; Nijland, R. and Heerschap, A. *Magn. Reson. Med.* 2002, **48(4)**, 611-616.
116. De Grauw, T. J.; Cecil, K. M.; Byars, A. W.; Salomons, G. S.; Ball, W. S. and Jacobs, C. *Mol. Cell. Biochem.* 2003, **244(1&2)**, 45-48.
117. Mangia, S.; Garreffa, G.; Bianciardi, M.; Giove, F.; Di Salle, F. and Maraviglia, B. *Neurosci.* 2003, **118(1)**, 7-10.
118. Lei, H.; Ugurbil, K. and Chen, W. *Proc. Natl. Acad. Sci. U. S. A.* 2003, **10(24)**, 14409-14414.
119. Brief, E. E.; Whittall, K. P.; Li, D. K. P. and MacKay, A. *NMR Biomed.* 2003, **16(8)**, 503-509.
120. Zarifi, M. K.; Astrakas, L. G.; Poussaint, T. Y.; du Plessis, A.; Zurakowski, D. and Tzika, A. A. *Raiology* 2002, **225(3)**, 859-870.
121. Geissler, A.; Fruend, R.; Schoelmerich, J.; Feuerbach, S. and Zietz, B. *Exp. Clin. Endocrinol. Diabetes* 2003, **111(7)**, 421-427.
122. Cichon, A.; Matulewicz, L. and Sokol, M. *Mol. Phys. Rep.* 2003, **37**, 71-74.
123. Forder, J. R. and Pohost, G. M. *J. Clin. Invest.* 2003, **111(11)**, 1630-1639.
124. Forder, J. R.; Pohost, G. M. *J. Clin Invest.* 2003, **111(11)**, 1630-1639.
125. Scheuermann-Freestone, M.; Madsen, P. L.; Manners, D.; Blamire, A. M.; Buckingham, R. E.; Styles, P.; Radda, G. K.; Neubauer, S. and Clarke, K. *Circulation* 2003, **107(24)**, 3040-3046.
126. Nakae, I.; Mitsunami, K.; Omura, T.; Yae, T.; Tsunamoto, T.; Matsuo, S.; Takahashi, M.; Morikawa, S.; Inubushi, T.; Nakamura, Y.; Kinoshita, M. and Horie, M. *J. Am. Coll. Cardiol.* 2003, **42(9)**, 1587-1593.
127. Szczepaniak,L. S.; Dobbins, R. L.; Metzger, G. J.; Sartoni-D'Ambrosia, G.; Arbique, D.; Vongpatanasin, W.; Unger, R. and Victor, R. G. *Magn. Reson. Med.* 2003, **49(3)**, 417-423.
128. Lim, A. K. P.; Patel, M.; Hamilton, G.; Hajnal, J. V.; Goldin, R. D. and Taylor-Robinson, S. D. *Hepatology* 2003, **37(4)**, 788-794.
129. Krebs, M.; Brehm, A.; Krssak, M.; Anderwald, C.; Bernroider, E.; Nowotny, P.; Roth, E.; Chandramouli, V.; Landau, B. R.; Waldhaeusl, W. and Roden, M. *Diabetologia* 2003, **46(7)**, 917-925.

130. Bilecen, D.; Schulte, A.- C.; Kaspar, A.; Kuestermann, E.; Seelig, J.; Elverfeldt, D.; Scheffler, K. *NMR Biomed.* 2003, **16(3)**, 144-151.
131. Ohara, T. *Bunshi Tonyobyogaku no Shinpo* 2003, 91-96.
132. Price, T. B.; Krishnan-Sarin, S.; and Rothman, D. L. *Am. J. Physiol.* 2003, **285(1, Pt. 1)**, E116-E122.
133. Price, T. B.; Laurent, D. and Petersen, K. F. *Int. J. Sport. Med.* 2003, **24(4)**, 238-244.
134. Thamer, C.; Machann, J.; Tschritter, O.; Haap, M.; Wietek, B.; Dahl, D.; Bachmann, O.; Fritsche, A.; Jacob, S.; Stumvoll, M.; Schick, F. and Haring, H.- U. *Horm. metab. Res.* 2002, **34(11/12)**, 646-649.
135. Weiss, R.; Dufour, S.; Groszmann, A.; Petersen, K.; Dziura, J.; Taksali, S. E.; Shulman, G. and Caprio, S. *Clin. Endocrinol. Metab.* 2003, **88(5)**, 2014-2018.
136. Kurosawa, Y.; Hamaoka, T.; Katsumura, T.; Kuwamori, M.; Kimura, N.; Sako, T. and Chance, B. *Mol. Cell. Biochem.* 2003, **244(1&2)**, 105-112.
137. Rijpkema, M.; Schuuring, J.; van der Meulen, Y.; van der Graaf, M.; Bersen, H.; Boerman, R. van der Kogel, A. and Heerschap, A. *NMR Biomed.* 2003, **16(1)**, 12-18.
138. Opstad, K. S.; Provencher, S. W.; Bell, B. A.; Griffiths, J. R. and Howe, F. A. *Magn. Reson. Med.* 2003, **49(4)**, 632-637.
139. Majos, C.; Alonso, J.; Aguilera, C.; Serrallonga, M.; Acebes, J. J.; Arus, C. and Gili, J. *Radiology* 2002, **225(2)**, 556-566.
140. Harting, I.; Hartmann, M.; Jost, G.; Sommer, C.; Ahmadi, R.; Heiland, S. and Sartor, K. *Neurosci. Lett.* 2003, **342(3)**, 163-166.
141. Zakian, K. L.; Shukla-Dave, A.; Meyers, P.; Gorlick, R.; Healey, J.; Thaler, H. T.; Huvos, A. G.; Panicek, D. M. and Koutcher, J. A. *Cancer Res.* 2003, **63(24)**, 9042-9047.

13
Nuclear Magnetic Resonance Imaging

BY TOKUKO WATANABE

1 Introduction

This review is a continuation of the last eight years[1] and covers the progress in the field of NMR imaging (NMRI), NMR microimaging, NMR microscopy or MR (micro) tomography as well as MRI (Magnetic Resonance Imaging). Papers mainly recorded in CA Selects on Proton Magnetic Resonance and on Carbon & Heteroatom NMR over a period from June 2003 to May 2004 are collected. The topics are limited to mainly basic, technical, and applicable aspects in the non-clinical research field, such as physicochemical, biological, botanical, physiological, pharmaceutical, geological, environmental, food science and technology, and various industrial applications. Almost all of the clinically oriented papers on whole body MRI machines have not been picked up because they are more professional topics with clinical or medical interest. Recently, however, papers concerning more basic applications in the in vivo-biological, medical or clinical topics have been increasingly published because of utilization of horizontal MRI instruments with higher magnetic field such as 4 T to 9 Tesla. These topics are partly picked up. The term 'MRI' instead of the term 'NMR imaging' becomes much more popular, even in the non-clinical fields of research. In this review, the author has quoted the term used by the original author(s). Review articles are included separately as reviews in the first part of each section.

In some cases the technical development for imaging methods or pulse sequences proceed in the clinical MRI machine rather than in the high-resolution NMR machine or MRI machine for animal use because of the more severe, specific demands for using with patients. Such technical developments have been exploited in the high-resolution NMR machine. Journals shown below concentrate on the developments and applications within the topics: *Journal of Magnetic Resonance*, *Magnetic Resonance of Medicine*, *Journal of Magnetic Resonance Imaging*, *Magnetic Resonance Imaging*, *NMR in Biomedicine*, *Magnetic Resonance in Chemistry*, *Journal of Computer Assisted of Tomography*, as well as more clinical publications such as *Radiology*, *American Journal of Roentgenology*, *American Journal of Neuroradiology*, *Neuroimage and Investive Radiology*. Theoretical aspects of the field are often documented in *Medical Physics* and hardware developments regularly make appearance in the *Review of Scientific Instruments*. *Concepts in Magnetic Resonance* which presents fundamental aspects of

Nuclear Magnetic Resonance, Volume 34
© The Royal Society of Chemistry, 2005

the technique and *Magnetic Resonance Quarterly* which contains review articles of various topics of the field are recommended from the educational view point. The abstract from the *Annual Meeting of International Society for Magnetic Resonance in Medicine* (*ISMRM*) is strongly recommended as a means of deriving concise, up to data information on developments within the subjects.

2 Overview and Catalysed Reactions

In this period, applications to characterize the heterogeneity and the distribution of relevant properties in materials like gels, polymers, elastomers, and catalysts, were consecutively increasing, as reviewed in section 7. The number of papers concerning the analysis of engineering or industrial processes in specific conditions are increasing, reviewed in section 6. In these fields, or materials science, combination between standard NMR spectroscopic method for structural analysis and NMR imaging exploited to visualize structures in heterogeneous objects has been widely practiced.
In situ reaction processes, such as catalysed reactions, and in situ melting, freezing processes, are interesting as targets for visualization. Such applications have appeared in this term and reviewed as a new trend in section 2 and 7. The use of NMR imaging or MRI in dynamic phenomena, such as diffusion, flow velocity, and mass transportation, has successively become of interest in recent years, especially in the industrial applications, which is reviewed in sections 5, 6 and 8.

Gas-phase NMR has also great potential as a probe for a variety of interesting physical, biomedical, and industrial problems. In this period, papers have not been much published in chemical fields. In physical and medical fields more papers were presented. Although the optical pumping techniques for enhancing the polarization of the noble gases, ^{3}He and ^{129}Xe, has developed and recently we can get the gases at lower cost and more easily in the laboratory, distribution of the system is limited.

Molecular imaging, an emerging field of study that deals with imaging of disease on a cellular or genetic level, is becoming a big project in medical field. Usefulness of NMR imaging to molecular imaging is not clear at moment, if we compare SPECT, because of difficulty for preparing appropriate contrast agents. Many challenging researches has been done, which is reviewed in section 11.

2.1 Review. – Short reviews concerning a specified topic are summarized in each session below. Here, more general reviews are picked up. Although some of the reviews are concerned rather with a specific region, the content may be useful to researchers in other fields.

Non-traditional applications of NMR imaging to studies of chemical reactions including polymerization reactions and the Belousov-Zhabotinsky oscillating reaction are considered.[2] Publications concerning applications of NMR imaging to studies of the temperature and electric current density distributions in various specimens are discussed. NMR studies of hyperpolarized gases and gases

with equilibrium nuclear spin polarization and NMR imaging of solids (in particular, polymers and elastomers) are described.

Non-invasive characterization of human skeletal muscle by the methods of proton NMR imaging and spectroscopy is reported.[3] Basic knowledge about muscle structure and function is provided, followed by examples showing the appearance of musculature in contrast to surrounding tissue using established NMR imaging sequences. Special imaging techniques for musculature are presented including a spectral-spatial technique for highly selective detection of muscular lipids and magnetization transfer imaging. Methods and strategies for quantification of muscular spectra are described, focusing on the separation and assessment of intramyocellular (IMCL) and extramyocellular lipids (EMCL). Experiments used for measuring relaxation times, magnetization transfer rates, and diffusion coefficients of water and lipids and typical results are described. Studies on lipid metabolites in human skeletal musculature are presented with the main emphasis on the role of IMCL in the pathogenesis of insulin resistance and the regulation of IMCL by exogene interventions. Finally, a brief overview on muscle NMR spectroscopy at higher field strength is given, and promising applications with other nuclei such as ^{31}P and ^{13}C are discussed.

Measurement of the apparent diffusion coefficient (ADC) of tissue water *via* diffusion-weighted NMR imaging (DWI) and its relationship to cell volume change in pathological states are reviewed from the clinical point and animal experiments.[4] Although the mechanism is still not completely understood, the cellular swelling that accompanies cell membrane depolarization results in a reduction in the net displacement of diffusing water molecules and thus a concomitant reduction in the ADC of tissue water. Affect on water ADC values by the presence and orientation of barriers to translational motion (such as cell membranes and myelin fibers) and thus sensitivity of NMR measures of anisotropic diffusion to more chronic pathological states are described. Both theoretical prediction and experimental evidence suggest that the ADC of tissue water is related to the volume fraction of the interstitial space *via* the electric condition of the tissue and chemical communication between cells through the extracellular space (*i.e.*, extrasynaptic or volume transmission).

2.2 Catalysed Reaction. – In situ ^{1}H NMR imaging study of propagation of concentration waves in an autocatalytic reaction in a fixed granular bed has been demonstrated.[5,6] The interplay of mass transport and chemical reaction in porous media was studied by NMR microimaging. The NMR imaging technique was employed to visualize the propagation of autocatalytic waves for the Belousov-Zhabotinsky (BZ) reaction which is carried out in a model porous medium.[5] It is demonstrated that the wave propagation velocity decreases as the wave crosses the boundary between the bulk liquid and the flooded bead pack. The images detected during the catalytic hydrogenation of α-methylstyrene on a single catalyst pellet at elevated temperatures have revealed that the reaction and the accompanying phase transition alter the distribution of the liquid phase within the pellet. The in situ ^{1}H NMR technique was used to study the propagation of chemical waves during the liquid-phase BZ reaction in a model fixed bed of

grains consisting of chemically inert glass beads or quartz sand.[6] The propagation of autocatalytic chemical waves in this bed is determined by the size of pores between the grains. The rate of wave front propagation is independent of the size of the grains involved in this bed but is much lower than that in the bulk of the homogeneous aqueous phase.

The first application of NMR imaging to study the behavior of a gas-liquid-solid model catalytic reactor operating at elevated temperatures was reported.[7] Two techniques, namely functional MRI and NMR spectroscopic imaging, were employed to perform a dynamic in situ study of α-methylstyrene catalytic hydrogenation on a single catalyst pellet or in a granular bed. The results represent a first direct MRI visualization of the mutual effect of mass and heat transport processes and a chemical reaction in an operating reactor and demonstrate that NMR imaging and spectroscopy techniques can be used successfully to study the development of critical phenomena in operating multiphase reactors. Further development of the applications of the MRI toolkit in chemical and process engineering and catalysis hold significant promise for the development of safe and efficient technologies based on a detailed understanding of the interplay of various processes in an operating gas-liquid-solid reactor.

2.3 Xe Ice Melting Process. – The melting and dissolution processes of xenon (Xe) ice into different solvents have been visualized, using the methods of NMR spectroscopy, imaging, and time resolved spectroscopic imaging by means of hyperpolarized ^{129}Xe.[8] Starting from the initial condition of a hyperpolarized solid Xe layer frozen on top of an ethanol (ethanol/water) ice block, the Xe phase transitions were measured as a function of time and temperature. In the ethanol/water mixture (80 vol%/20%), most of the polarized Xe liquid first stays on top of the ethanol/water ice block and then starts to penetrate into the pores and cracks of the ethanol/water ice block.

3 Instruments and Materials

3.1 Reviews. – The development of both in vivo EPR spectroscopy and the mapping of free radicals in living systems required a large number of changes from classical X-band spectroscopy, such as the high water content of living tissue and the large sample volume. In order to obtain information about active oxygen free radicals in biological systems such as small animals, in vivo EPR spectroscopy is carried out with loop-gap and other low-frequency resonators operating at L-band microwave or lower (*Ca.*250 MHz) frequency.[9] L-band EPR imaging instrumentation has been developed in order to elucidate spatially defined differences in tissue metabolite and the redox status. Very recently, a new magnetic resonance imaging method was presented that can 'visualize' free radical generation in animals by means of MRI. The advantages of MRI, the combination of MRI and EPR, and PEDRI (proton electron double resonance imaging), and recent progress of these methods were summarized.

3.2 Magnets. – Precise information on gradient waveform shape and rise-

times is often most useful in experimental MRI, because magnetic field gradient is fundamental in almost all NMR imaging and localized spectroscopic methods. A very simple and robust method for measuring the time evolution of a magnetic field gradient is reported.[10] The method is based on the analysis of the NMR signal in the time domain, and requires no specialized field measurement probes for its implementation. The technique makes use of the principal that for small flip angles the excitation profile is a good approximation to the Fourier transform of the radio frequency pulse shape. Although originally designed for measurement of the rise time only, the technique hasbeen extendedto measure the exact time course of the gradient. The theory is confirmed by experimental results for gradient waveform field measurements in a high-field vertical bore system.

3.3 Surface Coil. – In NMR imaging the use of HTS coils can greatly improve the image quality when internal losses of conventional Cu coil are the dominant loss mechanism. To optimize HTS coil performances, *i.e.* quality factor, Q, and resonance frequency, f_0, the knowledge of its superconducting properties is required. The influence of static magnetic field ranging from 2 mT to 1.5 T on the performances of a small YBCO surface coil dedicated to NMR microscopy was investigated.[11]From these measurements, the field dependence of the surface resistance Rs and of the London penetration depth λab were extended. At low field, the dependence of Rs on H was found to be quadratic while it became linear >0.1 T and λab exhibited a linear dependence on H.

3.4 Optical Pumping System for Polarized Gases. – Large amounts of hyperpolarized ^{3}He gas with high nuclear polarization rates are required for use in neutron spin filters for NMR imaging of the human lung. Very high efficiency can be obtained by metastability exchange optical pumping using multimode lasers to excite the 23S-23P transition at 1083 nm. Broadband Yb-doped tunable fiber lasers were designed for that particular application.[12] A linear cavity configuration that includes a high reflectivity fiber mirror and a low reflectivity tunable fiber Bragg grating is emphasized. Multi-mode operation matching the 2 GHz Doppler-broadened He response line and tunability over >200 GHz are demonstrated. Boosting the output of this fiber laser with a Yb-doped fiber power amplifier, all-fiber devices are built to provide robust, high power turnkey sources at 1083 nm for improved production of laser polarized ^{3}He.

3.5 Rapid Sample-mixing Technique. – A novel rapid sample-mixing technique for real-time NMR spectroscopy is developed and applied to real-time protein folding.[13] The application consists of an insert inside a conventional NMR tube coupled to a rapid injection syringe outside the NMR magnet. Efficient and homogeneous mixing of solutions in the NMR tube is achieved with a dead time of tens of milliseconds, without modification of the NMR probe or additional hardware inside the magnet. The performance of the device has been tested and optimized by a variety of methods, including sensitive detection of residual pH gradients and the use of NMR imaging to monitor the extent of

mixing in real time. The potential utility of this device, in conjunction with the sensitivity and selectivity of photo-CIDNP, is demonstrated by experiments on the protein hen lysozyme.

4 Pulse Sequences and Data Processing

4.1 Force-detected NMR Imaging. – NMR imaging using magnetic resonance force microscopy (MRFM) is demonstrated in combination with optical pumping to increase the nuclear spin polarization.[14, 15] The ability of force-detected magnetic resonance to apply NMR imaging to semiconductor devices and other nanostructures is demonstrated.[14] The authors demonstrated 1-dimensional NMR imaging of the semiconductor GaAs with 170 nm slice separation and resolve two regions of reduced nuclear spin polarization density separated by only 500 nm. Optical pumping of the GaAs created spin polarization up to 12 times larger than the thermal nuclear spin polarization at 5 K and 4 T. The experiment was sensitive to sample vols. of 50 μm^3 containing approximately 4×10^{11} $^{71}Ga/\sqrt{Hz}$. A versatile method for Fourier encoding the spatial distribution of spins detected by magnetic resonance force microscopy is presented.[15] Shuttling a magnetic particle in synchrony with an radiofrequency pulse sequence causes spins in a constant-field slice near the particle to precess at a rate proportional to their x or y coordinate. A two-dimensional spin-density map is recovered by a linear Fourier transform of a set of integrated force signals. Performance of the radiofrequency sequence is demonstrated experimentally and numerical simulations show that the method can achieve nanoscale resolution. The authors' approach offers a new route to manipulating spin wave functions down to the atomic scale.

4.2 Imaging Techniques. – New imaging techniques have been developed especially for solid or semi-solid materials with dipolar broadened spectra.[16-19] High-resolution NMR imaging of objects with dipolar-broadened spectra was proposed.[16] It is shown that, in some substances with dipolar-broadened conventional NMR spectra, it is possible to use long-lived coherent response signals, excited by long and weak radiofrequency pulses, for producing NMR images with high spatial resolution. Compared to other techniques, the method does not require high field gradients or strong radiofrequency fields, and therefore, can be applied to large objects.

Imaging of the ^1H NMR 2nd moment was demonstrated by using the Jeener-Broekaert (JB) dipolar signal instead of the Zeeman FID signal commonly employed.[17] The JB dipolar signal was induced by applying a JB pulse sequence, $90°x$-τ-$45°y$-τ'-$45°y$, which was followed by the time-suspension magic echo sequence, TREV-16TS, for imaging detection. Scanning the imaging detection to cover the whole evolution of the JB dipolar signal finally results in producing spatially resolved JB dipolar signals. The local value of the quantity called the JB 2nd moment, $M_2(JB)$, is then estimated from the initial slope of each resolved JB dipolar signal. The t dependence of $M_2(JB)$ is potentially useful for characterizing

the 2nd moment distribution resulting from the crystal orientation dependence. This is illustrated by preliminary experiments performed on test samples. Multi-point k-space mapping,which is a hybrid between const.-time (single-point mapping) and spin-warp imaging, involving sampling of a k-line segment of r points per TR cycle, was implemented for NMR imaging of semi-solid materials on a 400 MHz micro-imaging system and two different k-space sampling strategies were studied to minimize the adverse effects from relaxation-induced k-space signal modulation.[18] Implementation of a T_2 selective RF excitation demonstrated the feasibility of obtaining short-T_2 contrast even in the presence of tissues with long-T_2. The method's potential is illustrated with 3-dimensional proton images of short-T_2 materials such as synthetic polymers and bone. Proton multipolar spin states associated with dipolar encoded longitudinal magnetization (DELM) and double-quantum (DQ) coherences of bound water are investigated for bovine and sheep Achilles tendon under mechanical load.[19] DELM decay curves and DQ buildup and decay curves reveal changes of the 1H residual dipolar couplings for tendon at rest and under local compression forces. Quotient images obtained from DQ-filtered images by matched and mismatched excitation/reconversion periods are encoded only by the residual dipolar couplings. Semi-quantitative parameter maps of the residual dipolar couplings of bound water were obtained from these quotient images using a reference elastomer sample. This method can be used to quantify NMR imaging of injured ordered tissues.

A novel magnetic resonance imaging (MRI) technique, chemically selective NMR imaging, which resolves the separate components of the evolving vertical concentration profiles of 3-component non-colloidal suspensions, is described.[20] This methodexploits the sensitivity of MRI to chemical differences between the three phases to directly image the fluid phase and one of the solid phases, with the third phase obtained by subtraction.

A new NMR method is presented to measure selectively the self-diffusion coefficient of molecules with ^{13}C-^{1}H bonds.[21] The method is based on the selection of spectral lines by both ^{13}C chemical-shift and ^{13}C-^{1}H J-coupling encoding, which generally is adequate to individuate a molecular species. The method may also be utilized to attain self-diffusion weighted NMR imaging (MRI) of single molecular species. Results on glucose metabolites in aqueous solutions are presented. The approach shows a chemical selectivity, which is higher than the traditional NMR stimulated echo approach.

Frequency-swept stray-field magnetic resonance imaging was used for determining the diffusion mechanism for water/ethanol mixtures in a diacrylate dental resin by direct observation of the absorbed liquid profiles.[22] The diffusion profiles were recorded periodically for diffusion times up to 10 h, to a depth of 360 μm and with readings taken at 24 mm intervals. Frequency-swept STRAFI offers a new and unique opportunity to produce spatially resolved measurements of the liquids in dental resins to high resolution. STRAFI has great potential for other applications, for example drying, liquid exchange, *etc.*

4.3 Data Processing. – Amide's a Medical Image Data Examiner (AMIDE)

has been developed as a user-friendly, open-source software tool for displaying and analysing multimodality volumetric medical images.[23] Central to the package's abilities to simultaneously display multiple data sets (*e.g.*, PET, CT, MRI) and regions of interest is the on-demand data reslicing implemented within the program. Data sets can be freely shifted, rotated, viewed, and analysed with the program automatically handling interpolation as needed from the original data. Validation has been performed by comparing the output of AMIDE with that of several existing software packages. AMIDE runs on UNIX, Macintosh OS X, and Microsoft Windows platforms, and it is freely available with source code under the terms of the GNU General Public License.

5 Hyperpolarized Noble Gases, Gas Phase Imaging and Other Nuclei

5.1 Review. – Laboratory optical pumping experiments in atomic gases are overviewed with physical explanation.[24] Optical pumping is the non-equilibrium redistribution of atoms among the energy sublevels of the ground state by resonant absorption of light and allows control of populations of the Zeeman sublevels, *i.e.* control of the electronic and nuclear angular momenta in the ground state *via* selective depopulation and repopulation processes. Based on this technique, very precise measurements of energy separations in the ground state, the operation of atomic clocks, and laser optical pumping of alkali and noble gas atoms, notably helium atoms (both ^{3}He and ^{4}He, with I = 1/2 and I = 0) were explained. Laser optical pumping has various established or emerging applications, *e.g.* polarized targets for nuclear physics, neutron spin filters, and NMR imaging of lungs.

5.2 Hyperporalized Nobel Gases. – The new bis-cryptophanes, deuterium-labeled $(Xe)_2$@bis-cryptophane complex, were prepared from cryptophanols, suggesting the synthetic possibilities offered by the latter for the design of new host systems featuring the preparation of large supramolecular receptors and new polycryptophane bio-sensors for NMR imaging.[25] The complexation of xenon by the dissymmetric bis-cryptophane was studied by ^{129}Xe NMR spectroscopy. At low temperature, a strong discrimination ($\Delta\delta$ = 1.16 ppm) of the encapsulated xenon guests inside the two cryptophane cavities was observed. The kinetic parameters for the complexation process were determined from 1D-EXSY ^{129}Xe NMR experiments.

The melting and dissolution process of Xe ice into different solvents have been visualized by means of hyperpolarized ^{129}Xe.[8] A broadband Ytterbium-doped tunable fiber laser for ^{3}He optical pumping at 1083 nm was developed and a supply of large amount of ^{3}He gas becomes available with high efficacy.[12]

5.3 Nanopore Structure Analysis. – MRI has provided direct visualization of gaseous xenon and methane in the void spaces of aerogels, offering unique information and insights into the pore structure and molecular diffusivities of occluded sorbates.[26, 27] Pore structure and sorption properties of silica aerogels

were studied by magnetic resonance imaging and pulsed-field gradient (PHG) spectroscopy.[26] PFG-NMR techniques were used to characterize exchange and diffusive motion of sorbed xenon gas at equiliblium. PFG measurements showed evidence of anisotropic diffusion; nominal self-diffusion coefficients of xenon on the order of $D = 10^{-7}$ m^2/s were determined. Based on a mathematical relationship for the restricted diffusion of gases in confined environments, an expression for estimating the mean free path was derived, from which the average pore size could be obtained from the extrapolated value of the diffusion coefficient to low xenon pressures. Nondestructive characterization of nanopore microstructure was performed by using NMR imaging of gas adsorption/desorption in nanoporous solids.[27] NMR images obtained as a function of the equilibrium pressure, at constant temperature, form a pixel-by-pixel map of adsorption isotherms. Spatial maps of the specific surface area, the net energy of adsorption, and the pore morphology were resulted by analysis of these isotherms using Brunauer-Emmett-Teller (BET) theory. Results for γ-Al_2O_3 and ZnO powders and partially sintered ceramics of these materials, as well as Vycor porous glass, compare well to results for bulk samples obtained using conventional N_2 BET adsorption. MRI studies of gas adsorption are shown to provide statistical averages of the pore microstructure parameters, resolved on a macroscopic scale.

5.4 Other Nuclei. – Functional oxygen-17 MR imaging and localized spectroscopy is defined as the ensemble of MR measurements aiming at in vivo, noninvasive characterization of oxygen transport and utilization.[28] After a brief description of the present status of in vivo ^{17}O-MR, preliminary results are reported on oxygen delivery and consumption in cell suspensions of *Saccharomyces cerevisiae.* It is shown that parallel ^{31}P-MR at high magnetic fields has an important corroborative value.

6 Dynamics: Diffusion, Flow and Velocity Imaging

6.1 Diffusion. – The self-diffusion coefficient of molecules with ^{13}C-^{1}H bonds was selectively measured and utilized to attain self-diffusion weighted NMR imaging of single molecular species (see section 4.2).[21]

The diffusive properties of anaerobic methanogenic and sulfidogenic aggregates in wastewater treatment bioreactors were studied using diffusion analysis by relaxation time-separated pulsed-field gradient NMR spectroscopy and NMR imaging.[29] NMR spectroscopy measurements were performed at 22°C with 10 mL of granular sludge at a magnetic field strength of 0.5 T (20 MHz). Self-diffusion coefficients D of water in the studied series of mesophilic aggregates were 51-78% lower than D of free water and interestingly, were independent of the aggregate size. Analysis of NMR images of a single aggregate shows that methanogenic aggregates possess a spin-spin relaxation time and self-diffusion coefficient distribution, which are due to both physical (porosity) and chemical (metal sulfide precipitations) factors.

Direct observation of the absorbed liquid profiles by using frequency-swept

stray-field magnetic resonance imaging (STRAFI) was reported.[22] For all water/ethanol mixtures in a diacrylate dental resin, diffusion was found to be Fickian with coefficients, that increased progressively and smoothly with alcohol content in the diffusing mixture, from 2.4×10^{-13} to 150×10^{-13} m^2s^{-1}. A rule of mixtures approach, as suggested by Kwei and Zupko, gave a satisfactory description of the ethanol fraction dependence of the diffusivity.

6.2 Flow in Emulsion, Suspensions and Colloids. – The flow of homogeneous, concentrated, oil-in-water emulsions, subjected to a shear flow between rotating horizontal concentric cylinders, were investigated.[30,31] NMR imaging was used to measure velocity profiles within a flowing, concentrated emulsion.[30] It was observed that below a critical velocity, in a portion of the gap, the fluid moves in a direction opposite to the outer, rotating cylinder. Above this critical velocity, the emulsion corotates with the outer cylinder. Theoretical analysis suggests that the transitions are driven by buoyancy effects. The corotating and counter-rotating flow states at different rotation speeds can be characterized by a single dimensionless parameter Γ, which relates buoyancy and viscous effects.Time-of-flight and chemical shift imaging methods were used to measure velocity profiles and concentration maps in an emulsion that was mixed after being allowed to cream for several hours.[31]Detailed information about mixing in concentrated emulsions was revealed. A simple model is introduced that gives a plausible explanation of the experimental observations. The results indicate that the mixing mechanism in concentrated emulsions is significantly different from that in single-phase liquids. A three-dimensional granular system fluidized by vertical container vibrations was studied using pulsed field gradient (PFG) NMR coupled with 1-dimensional magnetic resonance imaging (MRI).[32] The system consisted of mustard seeds vibrated vertically at 50 Hz, and the number of layers $N_l \leqslant 4$ was sufficiently low to achieve a nearly time-independent granular fluid. Using NMR, the vertical profiles of density and granular temperature were directly measured, along with the distributions of vertical and horizontal grain velocities. The velocity distributions showed modest deviations from Maxwell-Boltzmann statistics, except for the vertical velocity distribution near the sample bottom which was highly skewed and non-Gaussian. Data taken for three values of N_l and two dimensionless accelerations $\Gamma = 15, 18$ were fit to a hydrodynamic theory, which successfully models the density and temperature profiles including a temperature inversion near the free upper surface.

6.3 Flow in Tubes. – The spatially resolved determination of velocities in two-phase systems consisting of water and oil by means of NMR imaging techniques is described and applied to steady tube flows with regard to the total flow rate.[33] The insight into the inner micro flow processes and microstructure allows characterization of fluid mixtures or emulsions. Flow rate and preparation/mixing method were varied in order to realize changes of the flow pattern and the structure of the mixture during flow. Physical models of the flow behavior and physics stability of these complex systems can be based upon this information.

6.4 Gas Flow. - A growing demand for efficient air quality management quickens the progress for the development of technologies capable of meeting the stringent requirements now being applied in areas of chemistry, biology and medical activities. Currently, filtration is the most effective process available for removal of fine particles from carrier gases. Purification of gaseous pollutants is associated with adsorption, absorption and incineration. The paper which discusses a new technique for highly efficient simultaneous purification of gaseous and particulate pollutants from carrier gases was presented.[34] This technique involves the passage of contaminated carrier gases through a porous medium submerged into a liquid, leading to the formation of narrow and tortuous pathways through the medium. The wet walls of these pathways result in outstanding purification of gaseous, liquid and solid alien additives. NMR imaging was successfully used to map the gas pathways inside the porous medium submerged into the liquid layer.

NMR imaging of gas adsorption/desorption in nanoporous solids, such as γ-Al_2O_3 and ZnO powders and partially sintered ceramics of these materials, as well as Vycor porous glass was analysed using Brunauer-Emmett-Teller (BET) theory.[27] Visualization of gaseous xenon and methane in the void spaces of aerogels offered unique information and insights into the pore structure and molecular diffusivities of occluded sorbates.[26]

6.5 Steady State Flow in Porous Media. – Hydrodynamic dispersion at the microscopic scale during steady-state flow through water-saturated glass beads was analysed by using NMR imaging.[35] The flow rate through the porous medium was chosen high enough in order to neglect the influence of molecular diffusion on dispersion. Velocity statistics were measured, by NMRI, within slices of increasing thickness perpendicular to the direction of flow. It was found that the point-like preferential influx and efflux boundary condition increased velocity variances and thus enhanced longitudinal hydrodynamic dispersion. Using the transverse correlation length of longitudinal velocity variance, a mean transverse dispersivity was derived, which agreed well with Saffman's (1959) model. So, authors gave for the first time a direct observation verification of a part of Saffman's conjectures. By NMRI this value is proved to be independent of the observation scale of the slice thickness.

7 Polymer

7.1 Reviews. – A review describes NMR methodologies for characterizing nano-scale structure and dynamics of soft polymers such as polymer gels and polymer liquid crystals, and hard polymers such as solid organic and inorganic polymers by using field-gradient NMR, three-dimensional NMR imaging and solid state NMR.[36]

7.2 Characterization. – A study of the behavior of polymers in supercritical CO_2 by NMR spectroscopy and imaging was presented.[37] The effect of the

presence of SC-CO_2 on the volume of common materials such as crosslinked PDMS, EPR and LDPE was studied. Of these three polymers only PDMS is known to swell to any appreciable extent in SC-CO2. The fully-amorphous EPR was found to swell by *ca.* 15 % on exposure to liquid CO_2 at a pressure of 50 Bar at 45 °C. The diffusion of styrene monomer and the morphology of subsequently-polymerized blend were examined by MRI and solid-state NMR. Solid-state ^{13}C NMR spin diffusion measurements were used to detect the extent of mixing of the usually-incompatible components of the blend after polymerization.

Noninvasive magnetic resonance imaging, biochemical analyses, and mechanical testing of engineered neocartilage grown in a hollow-fiber bioreactor (HFBR) was employed to establish tissue properties, and the hypothesis that MRI can be used to monitor biochemical and biomechanical properties of neocartilage was tested.[38] Chondrocytes from day 16 embryonic chick sterna were inoculated into an HFBR and maintained for up to 4 wk with and without exposure to chondroitinase ABC. The fixed-charge density (FCD) of the cartilage was determined using the MRI gadolinium exclusion method. A HFBR-derived neocartilage showed regional variation in sulfated glycosaminoglycan (S-GAG) content under control conditions, and in the decrease of S-GAG in response to enzyme treatment. In addition, the results support the hypothesis that tissue parameters derived from MRI can be used to noninvasively monitor focal neocartilage formation and biochemical and biomechanical properties.

7.3 Diffusion Process Analysis. – The diffusion of water into cylinders of poly-HEMA and copolymers of HEMA with THFMA, BMA and CHMA were studied.[39] The diffusion of water into the polymers was found to follow a Fickian, or case I mechanism. The diffusion coefficients of water were determined from mass measurements and NMR imaging studies. They were found to vary from $1.7 \pm 0.2 \times 10^{-11}$ m^2 s^{-1} for polyHEMA at 37 °C to lower values for the copolymers. The mass of water absorbed at equilibrium relative to the mass of dry polymer varied from 52-58 wt% for polyHEMA to lower values for the copolymers.

The ingress of water into poly(2-hydroxyethyl methacrylate), PHEMA, loaded with either one of two model drugs, vitamin B12 or aspirin, was studied at 37° using three-dimensional NMR imaging.[40] PHEMA was loaded with 5 and 10 wt. % of the drugs. From the imaging profiles, it was observed that crack formation on sorption of water was enhanced in PHEMA-vitamin B12 systems, but inhibited in the PHEMA-aspirin systems. The reason is accounted for by the anti-plasticization of PHEMA by vitamin B12 and the plasticizing effect of the aspirin on the PHEMA matrix. All of the polymers were found to absorb water according to an underlying Fickian diffusion mechanism.

Magnetic resonance imaging, NMR relaxometry, thermal analysis and gravimetric experiments are performed to study the water absorption by neat PA46 and copolymers of PA46 and PA4n (PA46-co-PA4n) with 4 mol% n = 8, 12 and 16.[41] The observed reduction in water uptake, ingress rate and water molecule mobility with increasing value of n was explained by a combination of several physico-chemical molecular properties. It is shown that the increased

chain mobility of the PA46 segments in the copolymers allows an improved coupling of the amide groups in the amorphous phase, explaining the observed decrease in water uptake. The important role of the morphology of the amorphous phase for water uptake is further demonstrated by annealing results and NMR relaxation experiments as a function of temperature.

Diffusion of rodlike polypeptides, poly(γ-n-dodecyl L-glutamate) film in the thermotropic and lyotropic liquid crystalline phases was studied by high field gradient ^{1}H NMR spectroscopy at 50-80°C.[42] The main-chain length dependence of diffusion behavior as elucidated. The diffusion behavior in the thermotropic liquid crystal state is analysed by the translational diffusion equation based on the Kirkwood theory of diffusion for rod-like polymers derived by M. Doi and S. F. Edwards (1986). Further, the diffusional behavior of a-helical poly(γ-n-octadecyl L-glutamate) was elucidated in chloroform as solvent in the isotropic, biphasic and liquid crystal phases by using high field-PFGSE ^{1}H NMR and diffusion ^{1}H NMR imaging.

Copolymers of 2-hydroxyethyl methacrylate (HEMA) and 1-vinyl-2-pyrrolidone (VP) in the form of cylindrical hydrogels (≈ 8 mm $\times$ 20 mm) have been prepared radiochemically and the sorption of water into these cylinders has been studied by the mass-uptake methods and by magnetic-resonance imaging at 310 K.[43] The equilibrium water contents for the cylinders were found to vary systematically with the copolymer composition. NMR-imaging studies showed that, while the profiles of the water diffusion fronts for cylinders with high HEMA contents were Fickian, those for the 1:1 copolymer was not and indicated that the mechanism was Case III. The polymers which were rich in VP were characterized by a water-sorption process which follows Case-III behavior.

7.4 Polymer Gel and Sol-Gel Transition. – Alginate microcapsules (between 400 mm and 600 mm in diameter) that advanced ^{1}H NMR imaging, along with paramagnetic Cu^{2+} as contrast agent, can be used to validate the crosslinking process.[44] Two- and three-dimensional images and maps of the spin-lattice relaxation time T_1 of Ba^{2+} cross-linked microcapsules exposed to external Cu^{2+} yielded qualitative as well as quantitative information about the accumulation of Cu^{2+} within and removal from microcapsules upon washing with Cu^{2+} free saline solution. The use of Cu^{2+} (having a slightly higher affinity constant to alginate than Ba^{2+}) for gelling gave a complementary insight into the spatial homogeneity of the crosslinking process together with information about the mechanical stability of the microcapsules. The potential of this technique was demonstrated for alginates extended from two different algal sources and cross-linked either externally by the conventional air-jet dropping method or internally by the 'crystal gun' method.

^{1}H-chemical shift NMR imaging patterns of a poly(methacrylic acid) gel containing water with paramagnetic praseodymium ions (Pr^{3+}) were successfully observed, in order to elucidate spatial distribution of Pr^{3+} ions in the gel.[45] The chemical shift of water associated with Pr^{3+} ions in the gel moves largely downfield. By analysing these experimental results, the immersion process of Pr^{3+} ions into the network of the polymer gel was spatially clarified.

Poly(γ-benzyl L-glutamate) (PBLG) gels with highly oriented α-helix chains were prepared by the crosslinking of PBLG chains through changes in the concentration of ethylenediamine crosslinker, in 1,4-dioxane in the presence of the strong magnetic field of an NMR magnet (10.5 T).[46] In one of these gels, long channels with an average diameter of about 100 μm were formed by phase separation between crosslinked PBLG and the solvent. Also, 3-dimensional ^{1}H-NMR imaging patterns showed that the long channels were aligned in the direction parallel to the α-helix axis. The PBLG gel was swollen in the direction perpendicular to the α-helix axis, but it was not swollen in the direction parallel to the α-helix axis.

7.5 Rubbers, Elastmers, and Elastgraphy. – NMR imaging by radio-frequency field gradients (B_1 gradients) is especially convenient for heterogeneous samples and/or in the case of relatively short transverse relaxation times. The method has been combined with the application of two spin-lock periods of different duration so as to produce rotating-frame spin-lattice relaxation time ($T_1\rho$) images.[47] The strained crosslinked natural rubber was visualized by the $T_1\rho$ images, which was not only characteristic of the crosslink density but also revealed the way in which the material has been stressed. The strained parts can be visualized either directly or through histograms showing the $T_1\rho$ distribution over the whole sample.

The dynamics of the sol/gel phase transition in agarose was analysed with magnetic resonance elastography (MRE) and diffusion-weighted imaging, providing complementary information on a microstructural as well as on a macroscopic spatial scale.[48] In thermal equilibrium, the diffusion coefficient of agarose is linearly correlated with temperature, independent of the sol/gel phase transition. The experiments supported the approach to derive temperature maps from the apparent diffusion coefficient maps by a linear relationship. The elastisities were determined from the spatially resolved dynamics of the temperature maps. Finally, experimental MRE data were simulated using a model of coupled harmonic oscillators. The calculated images agreed well with the experimentally observed MRE wave patterns.

Gravimetric Flory-Rehner experiments were combined with MRI experiments to study the spatially dependent degree of crosslinking in unfilled, 1,6-hexamethylenediamine-cured poly(isobutylene-p-methylstyrene-p-bromomethylstyrene) terpolymers.[49] MRI relaxometry revealed two proton T_2 relaxation decay times in CCl_4 swollen specimens: a fast decaying component reflecting the constrained chain segments near crosslinks and entanglements and a slow decaying component originating from less constrained, remote chains. The local crosslink density in inhomogeneously cross-linked specimens was determined by the spatially dependent T_2 decay times. MRI solvent diffusion experiments reveal that the ingress kinetics of cyclohexane in PIB terpolymers is Fickian. The diffusion coefficient varies linearly with the cure state and the volume-averaged T_2 decay times.

7.6 Swelling, Drug Release. – Gelation of alginate by external Ba^{2+} (or other

divalent cations) produces non-homogeneous crosslinking of the polymeric mannuronic (M) and guluronic (G) acid chains. The stability of such microcapsules is rather limited. Homogeneous crosslinking has been achieved by injecting $BaCl_2$ crystals into alginate droplets before they come into contact with external $BaCl_2$.[50] The high effectiveness of this crystal gun method was demonstrated by confocal laser scanning microscopy and by advanced NMR imaging. Both techniques gave clear-cut evidence that homogeneous cross-linkage throughout the microcapsule is only obtained with simultaneous internal and external gelation. Cross-linked alginate microcapsules of sufficient mechanical strength can immunoisolate cells for the long-term treatment of hormone and other deficiency diseases in human beings. In vitro experiments showed greatly suppressed swelling for crystal gun microcapsules.

Carbohydrate polymers are widely used for pharmaceutical applications such as the controlled release of drugs. The swelling and water mobility in high-amylose starch tablets are important parameters to be determined for these applications. These tablets have a hydrophilic matrix, which swells anisotropically and forms a hydrogel in water. NMR imaging shows clearly the anisotropy of the water penetration and the swelling along the radial and axial dimensions of the tablets.[51] Empirical relationships are established to describe the kinetics of water penetration and swelling of the tablets. Gravimetric measurements of water uptake were also performed in comparison with the NMR imaging results.

7.7 Silica Network. – The silica network was characterized by NMR imaging and ^{29}Si NMR for novolac-type phenolic/SiO2 hybrid organic-inorganic nanocomposite materials prepared by sol-gel method.[52] The coupling agent was used to improve the interface between the organic and inorganic phases. Results revealed that Q4 (tetrasubstituted) and T3 (trisubstituted) are the dominant microstructures. The size of the silica in the phenolic resin was characterized with a scanning electron microscope. Properties and limiting oxygen index of the nanocomposite were evaluated.

8 Chemical Engineering and Industrial Application

8.1 Reviews. – Drying is an important process technology for both the food and pharmaceutical industries. However, despite their common interest in processing and their usage of biological and organic materials there has been little overlap or exchange of ideas and methods. The paper is probing the significance and requirements of drying in each industry and identifies divergent and convergent interests.[53] Areas of relative strengths and weaknesses in the applied science of each industry is presented, together with some issues of current or future synergy and mutual benefit. Reviews on industrial application of NMR techniques to steelmaking process and related advanced materials. Analysis of materials and processes by solid-state NMR is discussed with reference to the manufacture of cast iron and steel and catalysts relating to energy and environmental issues.[54, 55] NMR imaging is described in relation to the analysis of

changes in the materials during heating and voids in porous materials.

8.2 Process Analysis. – Dynamics of size segregation and mixing of granular materials in a 3D-blender was investigated by NMR imaging. Magnetic Resonance Imaging was used to characterize the kinematics of mixing and size segregation of dry binary mixtures (diameters, d_{min} and d_{max}) in a Turbula shaker-mixer.[56] It is demonstrated that this blender is very efficient for dry materials within the three following conditions: (i) the rotation speed is fast enough, (ii) one tries to mix a little amount of small particles in a sea of large ones, and (iii) the concentration of the smaller particles does not exceeds 10%. A segregation index S, based on density fluctuation, has been defined. Segregation in Turbula results from both surface and bulk segregation mechanisms. The surface effect is related to shear percolation during flow close to the free surface and it is observed whatever the rotation speed is. At last, it is proved that a low concentration system can be understood *via* a self-consistent approach with a single small particle in a 'sea' of large ones.

Possible optimization of pastes and the according apparatus in process engineering by MRI flow experiments were described.[57] The spatially resolved determination of velocities in suspensions by means of NMR imaging techniques was applied to steady tube flows (with regard to the total flow rate) in different geometries. Three types of suspensions with different solid volumetric concentrations were examined in order to demonstrate the effect of the material-specific flow-behavior and of the geometry of the experimental set-up on the observed flow pattern. The local probability distribution of single velocity components is determined and then both the local mean value and the standard deviation can be derived from the probability distribution. The standard deviation can be interpreted as the local dispersion coefficient of the velocity component.

Various latex dispersions based on poly(vinyl acetate) stabilized by different surfactants and polyelectrolytes were investigated by NMR methods to elucidate the macroscopic and molecular film-formation process of these latex dispersions.[58] Macroscopically the inhomogeneous drying in the film-formation process was investigated by NMR-imaging techniques. The influence of different amounts of surfactant on the homogeneity of the drying process was monitored. The molecular film-formation process was investigated by ^{1}H, ^{2}H, and ^{13}C solid-state NMR spectroscopy. For these bulk measurements, films of latex dispersions were homogeneously dried to different defined solid contents. Spectroscopic analysis allows the investigation of the drying process of the water at different solid contents with a pronounced influence on the polymer water interface and the latex particle core. The film-formation process is correlated to the drying mechanism of different types of water within the film. External water, water at ionic and non-ionic groups at surfactants in the polymer/water interface, and water in the swollen and mobilized polymer, could be distinguished during the drying process.

8.3 Filtration Process for Air Quality Management. – Purification of gaseous pollutants is associated with adsorption, absorption and incineration. A new

technique was proposed for highly efficient simultaneous purification of gaseous and particulate pollutants from carrier gases, and was investigated by NMR imaging.[34]

8.4 Oil Distribution. – Answering general questions such as 'Where is the oil?' 'How much oil is there?,' and 'Can we expect it?' is a challenging task for a large fractured field in southern Italy. Various studies were conducted to gain more insight into the way. NMR imaging was conducted on several whole core samples and the different porosity contributions (microporosity, vugs, and fissures) defined on a 3D basis.[59] An analytical approach based on the percolation theory was used to separate the permeability contributions and define the conditions under which vugs and fissures may form a conducting system. Wettability was a key parameter for productional estimations. All the data contributed to our current understanding of the reservoir.

9 Plants, Trees and Woods

9.1 Reviews. – Imaging of water transport, including transfer and flow speed, in plant cells by diffusion coefficient analysis using NMR microscopy was reviewed, with discussing methodology and its merits.[60]

9.2 Trees. – Lipids play a crucial role in the maintenance of the structural and functional integrity of the water-conducting elements and cells of the resurrection plant Myrothamnus flabellifolia during complete dehydration. Lipid composition, mobility and distribution within the internodal and nodal xylem regions (including short shoots and leaves) were investigated in the presence and absence of water by using various NMR spectroscopy and imaging techniques differing greatly in the level of spatial resolution and acquisition of lipid parameters.[61] Significant findings elucidated part of the strategy used by the resurrection plant to cope with extreme drought and to minimize transpirational water loss upon hydration.

10 Food

10.1 Review. – Drying is an important process technology for both the food and pharmaceutical industries. Status and needs in drying technology for the food and pharmaceutical industry are summarized.[53] An overview of the current state of knowledge in foods is presented, together with suggestions for borrowing or co-developing materials science and measurement techniques from each of the industries.

10.2 Freezing Process. – MRI gives a unique opportunity to better-understand the dynamic phenomena that occur during processing and storage of food. By measuring apparent diffusion coefficient, both axially and radially in meat, the

influence of intracellular diffusional barriers or post-mortem structural changes was probed.[62] The effects of different freezing methods on trout muscle were investigated using MRI. The structural changes of tissue produced by the freezing process were characterized by variations of T_2 and the radial diffusion coefficient.

The formation of ice during freezing of pasta filata and non-pasta filata Mozzarella cheeses, and the spatial redistribution of water T_2 relaxation time and the changes of water self-diffusion coeff. (D) within the unfrozen and frozen-stored cheese samples were observed by NMR imaging.[63] There was a significant change in T_2 and D values of water following freezing-thawing, which can be used to characterize the effect of freezing on cheeses. The difference of D values and T_2 distribution between the frozen-stored pasta filata Mozzarella cheese samples and the non-pasta filata Mozzarella cheese samples may be attributed to the microstructure differences between the two cheeses.

10.3 Moisture Migration. – NMR proton density imaging was used to study water transfer analysis, *i.e.*, isothermal and unidirectional drying of pork semi membranous muscle samples at temperatures of 12, 16 and 20 °C.[64] An independent calibration of the transversal relaxation time T_2 as a function of the moisture content was carried out to convert the signal amplitude into moisture content. Due to spatial heterogeneity in drying, 2D images were needed to assess the evolution of 1D moisture profiles. The relationship between the effective water diffusivity (D) was calculated in function of water content (X) using the Boltzman transformation which needs no a priori on the relationship $D = f(X)$.

The water characteristics in cooked pressure-heat treated (45°C for 45 min prior to pressurisation at 150 MPa for 30 min) and non-pressurised, cooked (control) samples of beef Longissimus aged for 1, 3, 8 or 16 days were studied by NMR microscopy.[65] A multi-echo sequence was used to obtain T_2 images. The effect of ageing duration and cooking condition to the T_2 values were discussed and revealed that the mechanisms changing the water properties in beef during ageing are different from those occurring during pressure-heat treatment of meat.

The structure, moisture distribution, and oil distribution in the coating of tempura, the 3-layered fine structure of the coating of the Japanese oil-fried battered food,was observed by NMR micro imaging.[66]The porosity of the intermediate layer was correlated to the moisture content of the batter. Chemical shift imaging, which gave moisture distribution and oil distribution images, revealed the changes in the coating after cooking.

The ^{1}H-magnetic resonance imaging technique was applied for monitoring the extent of the heat coagulation in the shell egg.[67] It is demonstrated that spin-spin relaxation time (T_2) is an effective marker to observe the extent of coagulation in egg white and yolk and that the T_2 value image is quite useful to recognize non-destructively the extent and status of coagulation of the heated eggs. This technique can also be applied to the material science as well as food science for observation of the inner status of the objects.

10.4 Fat Contents, Distribution and Migration. – A novel methodology to non-

invasively and objectively predict sensory traits and intramuscular fat content of dry-cured Iberian loins was studied.[68] Texture analysis of MRI was performed on 47 dry-cured Iberian loins. Appearance and texture traits were assessed by a 18-member trained panel, and intramuscular fat content was chemically extracted and quantified for the same samples. Three classes of dry-cured loin according to each sensory and chemical trait were established (low, medium and high). The application of this methodology, allowing in situ, automatic, objective and non-destructive classification of loins will be useful.

10.5 Fruits and Vegetables. – Low-field NMR relaxation and T1 weighted NMR-imaging were used as tools in differentiation between potato sample and determination of dry matter content in potatoes.[69] The low-field NMR relaxation parameters T_1 ($r = -0.85$) and full CPMG relaxation curves ($r = 0.95$) were correlated with the dry matter content of the potatoes. T_{21} and T_{22} obtained upon bi-exponential analysis of CPMG relaxation curves, were also highly correlated with the dry matter content ($r = -0.66$ and 0.78, respectively). On the other side, the applied image analysed features based on the histogram analysis were not correlated with dry matter content in whole potatoes in the present study. Thus, MR-imaging did not complement the correlations between NMR data and dry matter content, meaning that the way the spatial distribution of water in the material was determined did not cover the full information about dry matter content.

NMR-imaging was performed on five potato varieties stored at 4°C and 95% relative humidity for two and eight months, respectively.[70] An image analysis and subsequent sensory analysis of the cooked potatoes displayed the high potential of employing advanced image analysis on MR-imaging data from raw potatoes to predict sensory attributes related to the texture of cooked potatoes. Authors suggest that information about water distribution and anatomic structures within raw potatoes obtained by NMR imaging are importance for the perceived textural properties of the cooked potatoes.

11 In Vivo Application

11.1 Reviews. – A review describes the state-of-the-art of imaging and spectroscopy, particularly NMR spectroscopy and chemical shift imaging.[71] Current application of these imaging techniques are in peripheral angiography, myocardial-viability assessment, and in myocardial contractile function. Future imaging techniques application include radiofrequency tagging, phase tracking, coronary angiography, plaque imaging and characterization, image-guided catheter placement and myocardial-perfusion imaging. Future spectroscopic applications include ^{31}P stress test, ^{23}Na measurement of sarcolemmal integrity and myocardial intracellular lipid content.

Imaging of brain function and neurotransmission is an important bridge between basic and clinical research. Regional cerebral energy metabolite and blood flow are normally coupled to regional cerebral function. Positron

tomography (PET) studies of cerebral glucose metabolite and blood flow, single photon tomography (SPECT) and MRI studies of cerebral perfusion, have been used to image cerebral development and aging in man. The sensitivity, temporal resolution, spatial resolution and lack of radiation have led to the widespread utilization of blood oxygen level dependent (BOLD) and MRI perfusion techniques. The strengths, limitations, and application of these modalities are reviewed.[72] The application of these methods to cerebral development and aging are briefly discussed. A review described a brain imaging technique that pinpoints regions of neural activity by detecting changes in tissue oxygenation and blood volume.[73] It was demonstrated that local tissue oxygenation is reduced following neural activity, and that neurons do in fact increase their oxygen consumption following activation.

Glioblastoma multiforme are infiltrative lesions that have a high degree of heterogeneity, both within and between different patients. Imaging is critical for all phases in the evaluation and treatment of these lesions, but has been limited in providing information that is reliable enough to stratify patients into groups with uniform behavior and to predict outcome. A review of recent advances in magnetic resonance, which have made possible the routine acquisition of physiological data such as perfusion-and diffusion-weighted images and of metabolic data such as water suppressed proton spectroscopic images, was described.[74] Quantitative measurements are more closely related to the biological properties of the tumor and reflect changes in tumor vascularity, cellularity and proliferation that are associated with tumor progression. These new magnetic resonance techniques are able to contribute to diagnosis, characterization of malignant potential, treatment planning and assessment of response to therapy.

The use of anatomical imaging in clinical oncology practice traditionally relies on comparison of patient scans acquired before and following completion of therapeutic intervention. Therapeutic success is typically determined from inspection of gross anatomical images to assess changes in tumor size. The use of imaging could assist in delineating therapeutic-induced spatial heterogeneity within a tumor mass by providing information related to specific regions that are resistant or responsive to treatment. Largely untapped potential resides in exploratory methods such as diffusion MRI. Alterations in water mobility reflect changes in tissue structure at the cellular level. While the clinical utility of diffusion MRI for oncologic practice is still under active investigation, the overview on the use of diffusion MRI for the evaluation of brain tumors was introduced how this approach may be applied in the future for the management of patients with solid tumors.[75]

A review gives an overview of analysis of metabolites in neural systems by MRS technologies, especially brain, and the application of the NMR imaging to diagnosis.[76] The NMR measurement of the substances that could be used as metabolic markers such as phosphates and choline was also described. Proton NMR, ^{31}P-NMR and ^{13}C-NMR spectrometry and the data processing procedures in these analyses were discussed.

A review was described a new generation of contrast agents, which could be developed by making greater use of soft modeling techniques such as

QSAR/QSPR after a suitable description of their molecular structure, especially in the design of gadolinium (III) chelates in the field of modern medical diagnostics.[77] Some of the general potential directions of macromolecular MRI contrast agents were reviewed, using the recently reported families of dendrimer-based agents as examples.[78] Changes in molecular size altered the route of excretion. Smaller-sized contrast agents less than 60 kDa molecular weight were excreted through the kidney resulting in these agents being potentially suitable as functional renal contrast agents. Hydrophilic and larger-sized contrast agents were found better suited for use as blood pool contrast agents. Hydrophobic variants formed with polypropylenimine diaminobutane dendrimer cores created liver contrast agents. Larger hydrophilic agents are useful for lymphatic imaging. Finally, contrast agents conjugated with either monoclonal antibodies or with avidin are able to function as tumor-specific contrast agents, which also might be employed as therapeutic drugs for either gadolinium neutron capture therapy or in conjunction with radio-immunotherapy.

11.2 Cell and Molecular Imaging. – It was demonstrates that a commercially available contrast agent can be used as a marker for the long-term noninvasive MR tracking of implanted cells.[79] Bone marrow stromal cells (MSCs) are pluripotent progenitor cells that have the capacity to migrate toward lesions and induce or facilitate site-dependent differentiation in response to environmental signals. In animals with a cortical photochemical lesion, the fate of rat MSCs colabeled with superparamagnetic iron-oxide nanoparticles (Endorem) and bromodeoxyuridine (BrdU) was studied. In vivo MRI was used to track their fate. During the first week post transplantation, the transplanted cells migrated to the lesion site and populated the border zone of the damaged cortical tissue. The implanted cells were visible on MR images as a hypo-intense area at the injection site and in the lesion. Three to four weeks after injection, <3% of MSCs around the lesion expressed the neuronal marker NeuN.

The HER-2/neu receptor is a member of the epidermal growth factor family and is amplified in multiple cancers. It is under intense investigation both as a prognostic marker and for therapy, using monoclonal antibodies targeted against the receptor. A novel two-component gadolinium-based MR contrast agent to image the HER-2/neu receptor was developed.[80] Positive T_1 contrast in MR images was generated by the specific binding of avidin-gadolinium complexes to tumor cells prelabeled with a biotinylated anti-HER-2/neu antibody. Significant intensity enhancement was observed in HER-2/neu-expressing cell lines and in vivo in a breast cancer model.

pH-sensitive MRI contrast was produced by exploiting the exchange between the hydrogen atoms of water and the amide hydrogen atoms of endogenous mobile cellular proteins and peptides.[81] The pH dependence of the amide proton signal was calibrated in situ, using phosphorus spectroscopy to determine pH, and proton exchange spectroscopy to measure the amide proton transfer rate. To show the potential of amide proton transfer (APT) contrast for detecting acute stroke, pH effects were noninvasively imaged in ischemic rat brain. This observation opens the possibility of using intrinsic pH contrast, as well as

protein- and/or peptide-content contrast, as diagnostic tools in clinical imaging.

11.3 Functional MRI. – In order to study the behavior of cerebral physiological parameters and to further the understanding of the fMRI blood-oxygen-level-dependent (BOLD) effect, simultaneously multi-source frequency-domain near-IR and BOLD fMRI signals were recorded during motor functional activation in humans.[82] In order to relate the observations to changes in cerebral blood flow the 'balloon' model of cerebral perfusion was employed. The data showed that the deoxyHb concentration is the major factor determiningthe time course of the BOLD signal. Functional MRI was used to determine the acute blood oxygen level dependent effect (BOLD) of neuroleptic drugs in healthy male subjects.[83] Using a robust simultaneous visuo-acoustic stimulation paradigm fMRI measurements were obtained prior to as well as 1 h and 24 h after i.v. infusion of 5 mg haloperidol to six healthy young men. It was emphasize the necessity to control for interactions through acute medication and confirm fMRI as a non-invasive method for studying cerebral psychopharmacological effects.

11.4 Contrast Agents. – Paramagnetic manganese ions (Mn^{2+}) are taken up into cardiomyocytes where they are retained for hours. Mn content and relaxation parameters, T_1 and T_2, were measured in right plus left ventricular myocardium excised from isolated perfused rat hearts.[84]Variations in perfusate calcium (Ca^{2+}) during wash-in of $MnCl_2$ and experiments including nifedipine showed that myocardial slow Ca^{2+} channels are the main pathway for Mn^{2+} uptake and that Mn^{2+} acts as a pure Ca^{2+} competitor and a preferred substrate for slow Ca^{2+} channel entry. Inversion recovery analysis at 20 MHz revealed 2 components for T_1 relaxation. Applying 2-site exchange analyses on the obtained T_1 data yielded results in parallel to, but also differing from, results reported with an ec contrast agent. The longitudinal relaxivity of Mn ions in ic water [60 (s mM)-1] was about one order of magnitude higher than that of $MnCl_2$ in water in vitro [6.9 (s mM)-1], indicating that ic Mn-protein binding is an important potentiating factor in relaxation enhancement.

MRI would be ideally suited to monitor cell trafficking in vivo because of its noninvasive and three-dimensional visualization of whole organisms over time. However, systemically injected cells had been difficult to visualize by MRI because of relatively inefficient labeling methods. A novel, biocompatible, and physiologically inert nanoparticle (highly derivatized cross-linked iron oxide nanoparticle; CLIO-HD) was developed, which is available for highly efficient intracellular labeling of a variety of cell types.[85] CLIO-HD allows in vivo MRI tracking of systemically injected cells at near single-cell resolution. The authors have revealed the extensive three-dimensional spatial heterogeneity of T-cell recruitment to target tumors and demonstrated a temporal regulation of T-cell recruitment within the tumor. These results demonstrate that CLIO-HD is uniquely suited for quantitatively repetitive MRI of adoptively transferred cells and that this approach may be particularly useful for evaluating novel cell-based therapies in vivo.

The ability to visualize cell infiltration in experimental auto-immune encepha-

lomyelitis (EAE), a well-known animal model for multiple sclerosis in humans, was investigated using a clinical 1.5-T MRI scanner, a custom-built, high-strength gradient coil insert, a 3-D fast imaging employing steady-state acquisition (FIESTA) imaging sequence and a superparamagnetic iron oxide (SPIO) contrast agent.[86] An 'active labeling' approach was used with SPIO administered intravenously during inflammation in EAE. This work provides early evidence that cellular abnormalities that are the basis of diseases can be probed using cellular MRI and supports authors' earlier work which indicates that tracking of iron-labeled cells will be possible using clinical MR scanners.

Gadolinium-chelating cationic lipids have been synthesized to obtain lipoplexes with MRI contrast properties.[87] These compounds were designed to follow the biodistribution of synthetic DNA for gene delivery by NMR imaging. The lipid MCO-I-68 and chelate complexes with gadolinium were formed and characterized in terms of physicochemical and DNA binding properties. The transfection activity of MCO-I-68-Gd/DNA complexes was assayed in vitro on NIH 3T3. Different formulations of the product were tested. When up to 5% of the gadolinium lipid complexes were co-formulated with the cationic lipid RPR120535 used as a reference, the transfection levels were maintained as compared to RPR120535 alone. To date, only a liposomal formulation of a gadolinium-cationic lipid chelate without DNA had been observed using MRI. In vivo intratumoral administration of MCO-I-68-Gd/DNA lipoplexes to tumor model led to an important increase of the NMR signal. It was demonstrated that the new complexes also acted as transfection carriers when they were formulated from liposomes.

A novel polyacrylamide superparamagnetic iron oxide nanoparticle platform is described which has been synthetically prepared such that multiple crystals of iron oxide are encapsulated within a single polyacrylamide matrix (PolyAcrylamide Magnetic [PAM] nanoparticles).[88] This formulation provides for an extremely large T_2 and T_2* relaxivity of between 620 and 1140 sec^{-1} mM^{-1}. Addition of polyethylene glycol of varying sizes (0.6, 2, and 10 kDa) to the surface of the PAM nanoparticles resulted in an increase in plasma half-life and affected tumor uptake and retention of the nanoparticles as quantified by changes in tissue contrast using MRI. The flexible formulation of these nanoparticles suggests that future modifications could be accomplished allowing for their use as a targeted molecular imaging contrast agent and/or therapeutic platform for multiple indications.

11.5 Animal Model. – Loss of proteoglycans (PGs) from the extracellular matrix of cartilage is an early event of osteoarthritis. The capability of $Gd(DTPA)^{2-}$enhanced MRI to quantitatively assess PG content was explored in a goat model of cartilage degeneration.[89]A close correlation was found between the extent of the PG loss and the $Gd(DTPA)^{2-}$-induced T_1 decrease. As long as a preinjection T_1 map was obtained, the $Gd(DTPA)^{2-}$-enhanced MRI technique provided good sensitivity in detecting partial loss of PG in articular cartilage. This was true only when the animal was maintained in a resting state during diffusion of the $Gd(DTPA)^{2-}$. This approach is of particular interest for long-

term evaluations of cartilage degeneration and regeneration.

Using single-shot ultrafast spin-echo (SSFSE) NMR imaging of hearts of Wistar-Kyoto rats and spontaneously hypertensive rats at 4 T, high-quality NMR images of the rat heart was performed.[90] The images can be generated very reliably with sufficient contrast and temporal and spatial resolution, and allow precise, non-invasive and fast characterization of left ventricular hypertrophy in a hypertensive rat model.

In orthotopically transplanted murine models of brain tumors, cross-section micro-MRI at 11.7 T allows for visualization and measurement of the physically inaccessible tumors.[91] To allow for long resident times of a contrast agent in the tumor, intraperitoneal administration was used as a route of injection for contrast-enhanced micro-MRI, and a simple method for relative tumor volume measurements was examined. A strategy for visualizing the variability of the delayed tumor enhancement was developed. These strategies were applied to monitor the growth of brain tumors xenotransplanted into nude mice and either treated with the antiangiogenic peptide EMD 121974 or an inactive control peptide.

Neurocysticercosis (NCC) is the most frequent parasitic disease of central nervous system. Creatine [(creatine + phosphocreatine); (tCr)] was observed on ex vivo proton MR spectroscopy (1H MRS) in some of the cysticercus cyst fluid samples obtained from swine's brain parenchyma. In the current study, swine brains of freshly slaughtered animals naturally infected with NCC were subjected to ex vivo magnetic resonance (MR) imaging on a 1.5 T MR system.[92] Cysticercus cysts (n = 12) were removed from these brains and were labeled depending upon presence or absence of edema around cysts as observed on imaging. Cysticercus cyst fluid (100 μL) was subjected to different ^{1}H MRS experiments and results were compared with histopathological examinations to look for any relationship between tCr and parameters like quantification of musculature, and cellular infiltration in wall of the parasite. Histopathology of cyst wall was categorized into two groups based on cellular characteristics and the amount of musculature. Grade I cysts (n = 5) with no or minimal inflammation and large amount of musculature showed tCr on ^{1}H MRS. However, grade II cysts (n = 7) with profuse inflammation and less amount of musculature in the cyst wall lacked tCr. Higher amount of musculature in grade I cysts was associated with higher concentration of tCr in the cyst fluid ($r2 = 0.93$, $P = 0.007$). Creatine appears to be a marker of innocuous and viable NCC.

A recently developed pinhole high-resolution SPECT system and a 1.5 T clinical MRI scanner with a specially developed surface coil were used for rats (n = 9) after injection of the dopamine transporter ligand ^{123}I-FP-CIT.[93] The SPECT images showed clear striatal uptake. On the MR images, cerebral and extra-cerebral structures could be easily delineated.

MPTP (1-methyl-4-phenyl-1,2,3,6-tetrahydropyridine) was administrated to adult, male cats to model Parkinson's disease (PD), and MRI and spectroscopy (MRS) at 1.5 T was utilized to identify metabolic degenerative changes in the striatum in vivo.[94]Neurological status and somatosensory-evoked potentials in vivo, as well as postmortem striatal histopathol. and immunohistochem. par-

ameters, were examined.

Clenbuterol and beta-adrenergic receptor agonist drugs are illegally used as growth promoters in animal production. Pharmacologically active residues in edible tissues led to intoxication outbreaks in several countries. Two new compounds named 'A' and 'G4', was found in feeding stuffs.[95] Their chemical structure was studied through NMR-imaging and IR spectroscopy, and β1- and β2-adrenergic activity was evaluated on isolated guinea-pig atrium and trachea in comparison with clenbuterol. It was resulted that the pharmacodynamic properties and stronger lipophilic properties shown by the two compounds may result in increased cardiovascular risk for consumers of illicitly treated animals.

References

1. Watanabe, T., *Nuclear Magnetic Resonance*, 1997, **26**, 447-; ibid., 1998, **27**, 431-; ibid., 1999, **28**, 468-484; ibid, 2000, **29**, 509-533; ibid., 2001, **30**, 453-476; ibid., 2002, **31**, 428-463; ibid., 2003, **32**, 433-472, ibid., **33**, 465-496.
2. Koptyug, I. V.; Sagdeev, R. Z., *Russ. Chem. Rev.*, 2003, **72**, 165-191.
3. Machann, J., Steidle, G., Thamer, C., Mader, I., Schick, F. *Ann. Rep. NMR Spectrosc.* 2003, **50**, 1-74.
4. Sotak, C.H., *Neurochem. Int.*, 2004, **45**(4), 569-582.
5. Koptyug, I.V., Lysova, A.A., Matveev, A.V., Ilyina, L.Yu., Sagdeev, R.Z., and Parmon, V.N., *Magn. Reson. Imaging*, 2003, **21**, 337-343.
6. Koptyug, I.V., Lysova, A.A., Parmon, V.N., and Sagdeev, R.Z., *Kinet. Catal.* (Translation of Kinetika i Kataliz), 2003, **44**, 401-407.
7. Koptyug, I.V., Lysova, A.A., Kulikov, A.V., Kirillov, V.A., Parmon, V.N., and Sagdeev, R.Z., *Appl. Catal.*, A: General, 2004, **267**, 143-148.
8. Han, S., Kuehn, H., Haesing, F.W., Muennemann, K., Bluemich, B., and Appelt, S., *J. Magn. Reson.*, 2004, **167**, 298-305.
9. Fujii, H., and Berliner, L.J., *Biomed. Res. Trace Elements*, 2003, **14**, 6-10.
10. Jellus, V., Sharp, J. C., Tomanek, B., and Latta, P., *J. Magn. Reson.*, 2003, **162**, 189-197.
11. Ginefri, J.-C., Crozat, P., and Darrasse, L., *Adv. Sci. Tech.* (*Faenza, Italy*), 2003, **38**(Sci. Eng. HTC Supercon. IV), 449-456.
12. Tastevin, G., Grot, S., Courtade, E., Bordais, S., and Nacher, P.-J., *Appl. Phys. B Laser and Optics*, 2004, **78**, 145-156.
13. Mok, K.H., Nagashima, T., Day, I.J., Jones, J.A., Jones, C.J.V., Dobson, C.M., and Hore, P.J., *J. Am. Chem. Soc.*, 2003, **125**, 12484-12492.
14. Thurber, K.R., Harrell, L.E., Smith, and D.D., J. Magn. Reson. 2003, **162**, 336-340.
15. Kempf, J.G. and Marohn, J.A., *Phys. Rev. Lett.*, 2003, **90**, 087601/1-087601/4.
16. Antochshuk, V., Kim, M.-J., and Khitrin, A.K., *J. Magn. Reson.*, 2004, **167**, 133-137.
17. Matsui, S., Saito, S., Hashimoto, T., and Inouye, T., *J. Magn. Reson.*, 2003, **160**, 13-19.
18. Fernandez-Seara, M.A., Wehrli, S.L., and Wehrli, F.W., *J. Magn. Reson.*, 2003, **160**,144-150.
19. Fechete, R., Demco, D.E., and Blumich, B., *J. Magn. Reson.*, 2003, **165**, 9-17.
20. Beyea, S.D., Altobelli, S.A., and Mondy, L.A., *J. Magn. Reson.*, 2003, **161**, 198-203.
21. Casieri, C., Testa, C., Paci, M., and De Luca, F., *Chem. Phys. Lett.*, 2004, **387**, 295-300.

22. Hunter, G., Lane, D.M., Scrimgeour, S.N., McDonald, P.J., and Lloyd, C.H., *Dental Mater.*, 2003, **19**, 632-638.
23. Loening, A.M., and Gambhir, S.S., *Mol Imaging*, 2003, **2**,131-137.
24. Nacher, P.-J., *Astr. Soc. Pacific Conf. Series*, 2003, **307**, 151-163.
25. Darzac, M., Brotin, T., Rousset-Arzel, L., Bouchu, D., Dutasta, J.-P., *New J. Chem.*, 2004, **28**, 502-512.
26. Gregory, D.M., and Botto, R.E., *Appl. Spectr.* 2003, **57**, 245-250.
27. Beyea, S.D., Caprihan, A., Glass, S.J., and DiGiovanni, A., *J. Appl. Phys.*, 2003, 94(2), 935-941.
28. Mateescu, G.D., *Adv. Exp. Med. Biol.*, 2003, **510**(Oxygen Transport to Tissue XXIII), 213-218.
29. Lens, P.N. L., Gastesi, R., Vergeldt, F., van Aelst, A.C., Pisabarro, A.G., and Van As, H., *Appl. Environ. Microbiol.*, 2003, **69**, 6644-6649.
30. Shapley, N.C., d'Avila, M.A., Walton, J.H., Powell, R.L., Dungan, S.R., and Phillips, R.J., *Phys. Fluids*, 2003, **15**, 881-891.
31. d'Avila, M.A., Shapley, N.C., Walton, J,H., Phillips, R.J., Dungan, S.R., and Powell, R.L. *Phys. Fluids*, 2003, **15**, 2499-2511.
32. Huan, C., Yang, X., Candela, D., Mair, R.W., and Walsworth, R.L., *Los Alamos Nat. Lab., Preprint Arch., Condensed Matter*, 2003, 1-14.
33. Gotz, J., and Zick, K., *Chem. Eng. Tech.*, 2003, **26**, 59-68.
34. Agranovski, *I.E.*, Braddock, R.D., Crozier, S., Whittaker, A., Minty, S., and Myojo, T., *Separn Purifn Tech.*, 2003, **30**, 129-137.
35. Deurer, M., Vogeler, I., Clothier, B.E., and Scotter, D.R., *Transport Porous Media*, 2004, **54**, 145-166.
36. Ando, I., Yamane, Y., Koizumi, S., Matsui, M., Kuroki, S., *J. Ion Exchange*, 2003, **14**, 87-95.
37. Hill, D.J.T., Thurecht, K., and Whittaker, A.K., *Polym. Preprints* (*Am. Chem. Soc., Polym. Chem.*), 2003, **44**, 265-266.
38. Chen, C.-T., Fishbein, K.W., Torzilli, P.A., Hilger, A., Spencer, R.G.S., and Horton, W.E., Jr., *Arthritis & Rheumatism*, 2003, **48**, 1047-1056.
39. Hill, D.J.T., Chowdhury, M., Ghi, P.Y., Moss, N.G., and Whittaker, A.K., *Macromol. Symp.*, 2004, **207**(Fund. Appl. Polym. Gels), 111-123.
40. Chowdhury, Mohammad A.; Hill, D.J.T., and Whittaker, A.K., *Biomacromol.*, 2004, **5**, 971-976.
41. Adriaensens, P., Pollaris, A., Rulkens, R., Litvinov, V.M., and Gelan, *J.*, *Polymer*, 2004, **45**, 2465-2473.
42. Ando, I., Yin, Y., Zhao, C., Kuroki, S.,. *Polym. Preprints* (*Am. Chem. Soc., Div.Polym. Chem.*), 2003, **44**, 323-324.
43. Malak, M., Hill, D.J.T., Whittaker, A.K., *Polym. Int.*, 2003, **52**, 1740-1748.
44. Manz, B., Hillgaertner, M., Zimmermann, H., Zimmermann, D., Volke, F., and Zimmermann, U., *Eur. Biophys. J.*, 2004, **33**, 50-58.
45. Yokota, S., Sasaki, A., Hotta, Y., Yamane, Y., Kimura, H., Kuroki, S., and Ando, I., *Macromol. Symp.*, 2004, **207**, 105-109.
46. Yamane, Y., Kanekiyo, M., Koizumi, S., Zhao, C., Kuroki, S., and Ando, I., *J. Appl. Polym. Sci.*, 2004, **92**, 1053-1060.
47. Chaumette, H., Grandclaude, D., and Canet, D., *J. Magn. Reson.*, 2003, **163**, 369-373.
48. Sack, I., Gedat, E., Bernarding, J., Buntkowsky, G., and Braun, J., *J. Magn. Reson.*, 2004, **166**, 252-261.
49. Adriaensens, P., Pollaris, A., Kelchtermans, M., and Gelan, J., *Macromol.*, 2003, **36**,

706-711.
50. Zimmermann, H., Hillgartner, M., Manz, B., Feilen, P., Brunnenmeier, F., Leinfelder, U., Weber, M., Cramer, H., Schneider, S., Hendrich, C., Volke, F., and Zimmermann, U., *Biomaterials*, 2003, **24**, 2083-2096.
51. Malveau, C., Baille, W.E., Zhu, X.-X., and Marchessault, R.H., *Biomacromol.*, **3**, 1249-1254.
52. Chiang, C.-L., Ma, C.-M., Wu, D.-Lin., and Kuan, H.-C., *J. Polym. Sci.*, A, 2003, **41**, 905-913.
53. Lillford, P. J., *Food Sci. Tech. Int.* 2003, **9** , 145-149.
54. Saito, K., Interijento Zairyo, *Gijutsu no Saishin Kaihatsu Doko*, 2003, 214-219.
55. Saito, K., *Foramu*, 2003, **8**, 747-753.
56. Porion, P., Sommier, N., Faugere, A.-M., and Evesque, P., *Powder Tech.*, 2004, **141**, 55-68.
57. Gotz, J., Zick, K., and Kreibich, W., *Chem. Engin. Process.*, 2003, **42**, 517-534.
58. Rottstegge, J., Traub, B., Wilhelm, M., Landfester, K., Heldmann, C., and Spiess, H.W., Macromol. *Chem. Phys.*, 2003, **204**, 787-802.
59. Bona, N., Radaelli, F., Ortenzi, A., De Poli, A., Peduzzi, C., and Giorgioni, M., SPE *Reserv. Eval. Eng.* 2003, **6**, 226-233.
60. Ishida, N., *Kagaku to Seibutsu*, 2003, **41**, 147-149.
61. Schneider, H., Manz, B., Westhoff, M., Mimietz, S., Szimtenings, M., Neuberger, T., Faber, C., Krohne, G., Haase, A., Volke, F., and Zimmermann, U., *New Phytologis*, **159**, 487-505.
62. Renou, J. P., Foucat, L., and Bonny, J.M., *Food Chem.*, 2003, **82**, 35-39.
63. Kuo, M.-I., Anderson, M.E., and Gunasekaran, S., *J. Dairy Sci.*, 2003, **86**, 2525-2536.
64. Ruiz-Cabrera, M. A., Gou, P., Foucat, L., Renou, J.P., and Daudin, J.D., *Meat Science*, 2004, **67**, 169-178.
65. Bertram, H.C., Whittaker, A.K., Shorthose, W.R., Andersen, H.J., and Karlsson, A.H., *Meat Science*, **66** , 301-306.
66. Horigane, A.K., Motoi, H., Irie, K., and Yoshida, M., *J. Food Sci.*, 2003, **68**, 2034-2039.
67. Tashiro, M., Ishida, N., Shimotakahara, S., Tanabe, S., and Okubo, A.,. *Anal. Sci.*, 2003, **19**, 933-936.
68. Antequera, T., Muriel, E., Rodriguez, P.G.., Cernadas, E., Ruiz, J., *J.,Sci. Food Agri.* 2003, **83**, 268-274.
69. Thybo, A.K., Andersen, H.J., Karlsson, A.H., Donstrup, S., and Stodkilde-Jorgensen, H., *Lebensm.-Wiss. Tech.*, 2003, **36**, 315-322.
70. Thybo, A.K., Szczypinski, P.M., Karlsson, A.H.; Donstrup, S., Stodkilde-Jorgensen, H.S., and Andersen, H.J. *J. Food Eng.*, **61** , 91-100.
71. Forder, J.R., and Pohost, G,M., *J. Clin. Invest.*, 2003, **111**, 1630-1639.
72. Kessler, R.M., *Neurobiol. Aging*, 2003, **24**, S21-S35.
73. Mayhew, J.E., *Science*, 2003, **299**, 1023-1024.
74. Nelson, S.J., Cha, S., *Cancer J.*, 2003, **9**, 134-145.
75. Umeda, M., and Tanaka, T., *Ann. Rev. Shinkei*, 2003, 32-45.
76. Chenevert, T.L., Meyer, C.R., Moffat, B.A., Rehemtulla, A., Mukherji, S.K., Gebarski, S.S., Quint, D.J., Robertson, P.L., Lawrence, T.S., Junck, L., Taylor, J.M., Johnson, T.D., Dong, Q., Muraszko, K.M., Brunberg, J.A., and Ross, B.D., *Mol Imaging*, 2002, **1**, 336-43.
77. Maiocchi, A., *Mini-Rev. Med. Chem.*, 2003, **3**, 845-859.
78. Kobayashi H., and Brechbiel M.W., *Mol. Imaging*, 2003, **2**, 1-10.

79. Glogarova, K., Andersson, B., Hajek, M., Sykova, E., *Magn. Reson. Med.*, 2003, **50**, 767-776.
80. Artemov, D., Mori, N., Ravi, R., Bhujwalla, Z.M., *Cancer Res.*, 2003, **63**, 2723-2727.
81. Zhou, J., Payen, J.-F., Wilson, D.A., 80. Traystman, R.J., and van Zijl, P.C.M., *Nature Medicine*, 2003, **9**, 1085-1090.
82. Toronov, V., Webb, A., Walker, S., Gupta, R., Choi, J.H., Gratton, E., and Hueber, D.M., *Proc. SPIE-Int. Soc. Opt. Eng.*, 2003, **5068**, 222-226.
83. Brassen, S., Tost, H., Hoehn, F., Weber-Fahr, W., Klein, S., and Braus, D.F., *Neurosci. Lett.*, 2003, **340**, 193-196.
84. Nordhoy, W., Anthonsen, H.W., Bruvold, M., Jynge, P., Krane, J., and Brurok, H., *NMR Biomed.*, 2003, **16**, 82-95.
85. Kircher, M.F., Allport, J.R., Graves, E.E., Love, V., Josephson, L., Lichtman, A.H., and Weissleder, R., *Cancer Research*, 2003, **63**, 6838-6846.
86. Oweida, A.J., Dunn, E.A., and Foster, P.J., *Mol Imaging*, 2004, **3**, 85-95.
87. Leclercq, F., Cohen-Ohana, M., Mignet, N., Sbarbati, A., Herscovici, J., Scherman, D., and Byk, G., *Bioconjugate Chem.*, 2003, **14**, 112-119.
86. Moffat, B.A., Reddy, G.R., McConville, P., Hall, D.E., Chenevert, T.L, Kopelman, R.R, Philbert M, Weissleder R, Rehemtulla A, and Ross B.D., *Mol. Imaging*, 2003, **2**, 324-332.
87. Laurent, D., Wasvary, J., Rudin, M., O'Byrne, E., and Pellas, T., *Magn. Reson. Med.*, 2003, **49**, 1037-1046.
88. Parzy, E., Fromes, Y., Wary, C,. Vignaux, O., Giacomini, E., Leroy-Willig, A., and Carlier, P.G., *J. Hypertension*, 2003, **21**, 429-436.
89. Moats, R.A, Velan-Mullan, S., Jacobs, R., Gonzalez-Gomez, I., Dubowitz, D.J., Taga, T., Khankaldyyan, V., Schultz, L., Fraser, S., Nelson, M.D., and Laug, W.E., *Mol Imaging*, 2003, **2**, 150-158.
90. Chawla, S., Gupta, R.K., Husain, N., Garg, M., Kumar, R., and Kumar, S., *Life Sci.*, 2004, **74**, 1081-1092.
91. Booij, J., de Bruin, K., de Win, M.M.L., Lavini, C., den Heeten, G.J., and Habraken, J.B.A., *Nucl. Med. Biol.*, 2003, **30**, 643-649.
92. Podell, M., Hadjiconstantinou, M., Smith, M.A., and Neff, N.H., *Exp. Neur.*, 2003, **179**, 159-166.
93. Mazzanti, G., Daniele, C., Boatto, G., Manca, G., Brambilla, G., and Loizzo, A., *Toxicology*, 2003, **187**, 91-99.

14
NMR of Liquid Crystals and Micellar Solutions

BY MAURA MONDUZZI

1 Introduction

This chapter presents recent papers (June 2003-May 2004) focussing on the use of N.M.R. techniques to elucidate the microstructure and dynamics of self-assembled systems. As reported in the analogous chapter of last year [1], here the relevant concepts and acronym related to liquid crystals and micellar solutions will be briefly revised.

Self-assembly of amphiphilic molecules and of molecules with a fairly rigid elongated shape is mainly determined by molecular shape and intermolecular interactions. The latter molecules can form in determined range of temperatures thermotropic liquid crystals (L.C.) which generally self-assemble according to nematic, smectic A, B and C or cholesteric – when chiral atoms occur – long-range order. Amphiphilic molecules form micelles, and lyotropic L.C. having a variety of supramolecular structures when polar or apolar solvents are used. In the presence of both polar and apolar solvent besides L.C. phases mciroemulsions, or emulsions, stabilized by an amphiphilic interface, may also form. The structured polar-apolar interfaces are addressed by molecular shape and composition. The shape of the amphiphilic molecules is typically described by the packing parameter v/al (where v is the volume of the hydrophobic chain, a is the area of the polar head and l is the length of the hydrophobic chain). The interfacial curvature of the amphiphilic interface, responsible of the self-assembly type, is taken as positive (normal, H>0, and $v/al<1$) for oil-in-water (o/w) L_1 phases (normal micellar solutions), I_1 (discrete cubic L.C.) and H_1 (normal hexagonal L.C.). For water-in-oil (w/o) L_2 phases (reverse micellar solutions), I_2 (reverse discrete cubic L.C.) and H_2 (reverse hexagonal L.C.) phases negative curvatures (H<0, and $v/al>0$) are assumed. The lamellar L_α L.C. phases, and, similarly, also bicontinuous cubic (V_1 and V_2) phases show an average $H \approx 0$, due to $v/al \approx 1$. In the bicontinuous cubic phases amphiphilic domains are usually constituted by bilayers with the bilayers mid-plane surface described by an Infinite Periodical Minimal Surface (IPMS).

2 General Articles: Reviews, Methods, Models

Interesting review articles have appeared. Some of interest for this chapter are

Nuclear Magnetic Resonance, Volume 34
© The Royal Society of Chemistry, 2005

comprised in 'Encyclopedia of Nuclear Magnetic Resonance', and are related to local field experiments in liquid crystals,[2] and to the use of liquid crystals in macromolecular structure determinations.[3] Many general reviews have been reported. They are listed as follows: NMR methods used to investigate amphiphile self-assembly in aqueous solution, included two-dimensional (2D) NMR techniques,[4] and to elucidate micellization of fluorinated amphiphiles.[5] Studies based on NMR cross-polarization used to characterize ordering in nematic liquid crystals.[6, 7] A methodological review on the use of ^{31}P NMR to characterize phospholipids (PL) composition in tissues and body fluids.[8] Method for the qualitative and quantitative characterization of PLs in a monophasic solvent *via* ^{31}P NMR.[9] NMR methods along with a variety of techniques used to investigate amphiphile-polymer interactions.[10] A review on the role of different magnetic susceptibility between various compartments in heterogeneous samples, used to interpret NMR spectra.[11] Another on the distributions of the static and dynamic director fluctuations in thin nematic L.C. formed by a 5Cyano-Biphenyl (5CB) derivative deuterated in the α-position of the pentyl chain, through the use of ^{2}H NMR.[12] A method based on separated local field spectroscopy suggested to investigate columnar and nematic L.C. phases,[13] where, particularly, the proton-detected local field sequence was shown to provide in most cases the best dipolar resolution. A series of NMR experiments proposed to investigate structure and dynamics of a uniformly ^{15}N labelled membrane protein in micellar environment.[14] Seven interesting articles on NMR self-diffusion techniques related to restricted diffusion measurements, which are of great interest for investigating emulsion systems, were reported. 2D PGSE (Pulsed Gradient Spin Echo sequence) methods,[15] based on the use of the gradient domain, in which molecular displacements are measured, or of the time domain, in which relaxation is measured, were proposed. With this method the case of water diffusion in a lamellar L.C. was examined. Alternative methods to measure self-diffusion were shown to offer promising applications. One concerned with a modification of the Carr-Purcell-Meiboom-Gill (CPMG) pulse sequence,[16] for rapid characterization of diffusion. Another was based on the use of successive stimulated echoes from a single excitation pulse called Difftrain,[17] much less time consuming than typical PGSE NMR experiments. A third article discussed a novel procedure that couples diffusion measurements (PGSE) with transverse relaxation rate measurements (CPMG) to overcome many problems related to the assumptions which are typically introduced to extract size distribution functions in emulsion droplets.[18] Another paper was reported on the use of PGSE NMR to analyse large colloidal materials, particularly vesicles and nanoparticles.[19] A novel method, so called 'regularization methods', to extract size distribution functions from PGSE NMR data in emulsion droplets, was proposed;[20] the method does not require an 'a priori' choice of the distribution function form (typically various data analysis methods assume a lognormal distribution function). Predictions of pulsed field gradient NMR echo-decays for molecules diffusing in various restricted geometries were reported in another article of very general interest.[21] Finally a general article on the use of micellar catalysis as a tool to improve performance and environmental impact of indus-

trial productions was reported.[22]

3 Liquid Crystals

In this paragraph NMR studies on thermotropic and lyotropic L.C. phases and their use as solubilizing media are reported. The use of the typical NMR parameters of the ^2H quadrupolar nucleus ($I = 1$), such as $\Delta\nu_q$ quadrupolar splittings and lineshape analysis in anisotropic environments is extensively adopted to investigate self-assembly features. Deuterium oxide (^2H_2O), used as solvent in the particular case of lamellar and hexagonal lyotropic L.C. phases or, alternatively, perdeuterated and selectively deuterated mesogens and amphiphiles are the main sources of this type of quadrupolar nuclei. Other important topics are related to structural investigations of molecules such as drugs, proteins, peptides solubilized into an anisotropic L.C. phase that aligns in the magnetic field. Indeed the microstructural features of a solubilizate can be obtained from parameters related to the degree of long-range order and also to steric and anisotropic molecular interactions. Besides NMR methods, a variety of techniques were used, among which X-ray diffraction (Small and Wide Angle, SAXS and WAXRD), Small Angle Neutron Scattering (SANS), cryo-Transmission Electron Microscopy (cryo-TEM), polarizing optical microscopy (POM), Fourier Transform Infrared spectroscopy (FT-IR) and differential scanning calorimetry (DSC) are the most used to obtain complementary information.

3.1 Thermotropic Liquid Crystals. – Organic molecules, having aromatic rings or unsaturations thus producing elongated shapes, and also polymeric molecules often show thermotropic phase behavior. Mesomorphism comprises typically nematic, smectic A and B, and cholesteric thermotropic phases, but in several cases columnar, discotic and rod-disk self-assembly shapes of thermosensitive mesogens have been observed.

3.1.1 Phase Behavior. Many articles related to synthesis of new mesogens and to the characterization of the thermotropic phase behavior have appeared. In many cases these new mesogens are polymeric materials. New azobenzene-based mesogens were synthesized, particularly a series of side-chain L.C. homopolymers of poly[6-(4-methoxy-4′-oxy-azobenzene) hexyl methacrylate] with different degree of polymerization;[23] these homopolymers showed smectic and nematic phases. A series of novel L.C. coil tri-block copolymers with narrow polidispersity was obtained, and through ^1H NMR, FTIR and gel permeation chromatography the phase behavior was investigated. The smectic-nematic, and nematic-isotropic phase transition temperatures were found to increase with increasing the molecular weight (MW) of the new L.C. block. The use of ^1H NMR, FTIR, DSC and WAXRD allowed to characterize the phase behavior of an ethyl cellulose derivative containing azobenzene-based mesogens;[24] L.C. phase behavior was ascertained in the temperature range 125-172 °C. The presence of L.C.

phases in zwitterionic mesogens was suggested to be potentially useful for optoelectronic switching.[25] Several L.C. compounds were derived from 2-aminonaphtalene and showed nematic phase behavior as demonstrated by NMR and FTIR.[26] The structure and properties of fully aromatic L.C. copolyesters containing m-hydroxybenzoic acid units were investigated through ^{1}H NMR and other techniques;[27] nematic L.C. phases were identified when the content of linear units was over 67 mol%. The linear polymer obtained from novel L.C. monomers having acrylate and allyl functional groups, showed nematic phase behavior as demonstrated by NMR and polarizing optical microscopy textures.[28] Nematic L.C. phases were found for 5-butoxy-2-[(4-butylphenyl) azo] phenol mesogen where the L.C. structure was determined by the formation of intramolecular H-bond as demonstrated *via* ^{13}C NMR spectroscopy from the ^{2}H-^{13}C dipolar coupling constants measured for the specifically deuterated mesogen.[29] Chemically-induced discotic L.C. phases were ascertained through NMR methods in two systems;[30] in one case the inductor was a nitrate fluorenone and in the second case a substituted o-xylene. Semi-flexible star-shaped oligoester mesogens with a benzoyloxy scaffold form were found to form columnar L.C. characterized by 2D X-ray and solid-state NMR.[31] Nematic columnar mesophases of polyethers obtained by chemical modification of poly(epichlorohydrin) with potassium 3,4,5-tris (dodecyloxy) benzoate were characterized through NMR;[32] the stability range depended on the modification degree. Rod-like poly(diethylsiloxane) L.C. polymers were identified and characterized at 30 °C through ^{1}H PGSE NMR measurements.[33, 34] The transitions of L.C. phases formed by polyesters containing variable spacer length in the side chain and in the main chain were shown to depend on the spacer through 2D ^{13}C NMR spectroscopy.[35] A series of new side-chain cholesteric L.C. elastomers derived from mesogenic cross-linking agent revealed that in the case of a carboxylate derivative the cholesteric phase is retained, whereas for the benzenediol bisate smectic and nematic phases formed as identified by NMR and other techniques.[36, 37] A smectic L.C. phase was observed during the preparation of an epoxy resin as suggested by ^{1}H and ^{13}C NMR.[38] Other smectic L.C. polymers containing five-membered heterocyclic groups were investigated by ^{1}H NMR;[39] the most peculiar feature of these mesogens was that they showed photoluminescent properties. Smectic phases were ascertained by NMR methods and other techniques also for poly(phenylacetylene) containing stigmasterols pendants,[40] and for polystirene-poly (dimethylsiloxane)-polystirene tri-block polymer;[41] in the latter case ^{13}C and ^{2}H NMR revealed a wide distribution of segmental orientational order due to the presence of glassy interfaces and chain-end anchoring junctions. The number of alkoxy chains present around the dendritic core of a series of poly (amidoamine) determined lamellar-columnar phase transitions as proven by NMR and X-ray methods.[42] Cholesteric L.C. elastomers containing cross-linking agent pentaerythriol tetra-p-allyloxybenzoate and mesogenic monomer 4-cholesteryl-4'-undecenyloyloxybenzoate were investigated by ^{1}H NMR and characterized for the different elasticity properties as a function of the degree of cross-linking.[43]

3.1.2 Dynamics and Solubilization. NMR relaxation and self-diffusion are the most useful methods to investigate dynamics of soft matter at a molecular level. The technique PGSE NMR combined with a quadrupole-coil rotation was applied to the study of anisotropic self-diffusion in smectic A L.C.;[44] the diffusion across the layer was faster for cyano compounds, whereas the diffusion within the layer was faster for the trifluoromethoxy derivatives. Studies of the field-induced alignment of a Smectic A L.C. phase, formed by 8CB-d_2 using ^{2}H NMR revealed a complex dynamics behavior depending on the electric field angle;[45] computer simulations were then used to razionalize the dynamics of the alignment.[46] ^{2}H NMR along with spectral simulations, performed on nematic L.C. phases of a 5CB derivative confined in a slab between two electrodes, revealed that the relaxation of the field-induced director occurs on a timescale comparable to that of the experiment, which is the effective spin-spin relaxation time.[47] Rheo-NMR experiments were performed on nematic L.C. confined in cylindrical Couette geometry and the competing forces influencing the director were analysed through a numerical study that revealed a distribution of orientations.[48] A variety of chiral L.C. phases including blue, cholesteric, TGBA (twisted grain boundary of a smectic A L.C. block), Smectic A, Smectic C, and Smectic I, formed by ^{2}H- labelled biphenyl-benzoate derivatives, were investigated for orientational order parameters, and diffusion coefficients of the various overall and internal motions through ^{2}H NMR spectra and relaxation measurements.[49] The measurements of ^{2}H NMR spin-lattice relaxation, at various frequencies, for 4,4'-diheptylazoxybenzene in the isotropic, nematic, and smectic A phases, gave, using suitable theoretical models, the principal components of the diffusional tensor as well as the diffusion coefficient.[50] ^{2}H NMR spin-spin relaxation measurements, using CPMG sequences, were used to determine the anisotropic elastic constants of a polymer L.C. in the nematic phase.[51, 52] Ultrasound-order director fluctuations interaction in nematic 5CB based L.C. were investigated through field-cycling NMR relaxometry;[53] sonication was shown to shorten the spin-lattice relaxation time on a broad frequency range. Using ^{1}H NMR relaxometry in the kilohertz frequency range the dynamics of 5CB L.C. phases dispersed in the form of spherical microdroplets in a polymeric material was investigated above the nematic-isotropic transition temperature;[54] due to the slowing down of translational diffusion of the molecules in contact with the polymeric surface, an average dwell-time of 10^{-5} s was estimated for the molecules residing in the superficial layer. The analysis of NMR lineshape of a CB nematic L.C. derivative in the presence of a variable external magnetic field (fast field-cycling NMR technique) revealed the occurrence of a high frequency regime where magnetic torque governs the dynamics of reorientation, and of a low frequency domain where thermal fluctuations are responsible for the dynamics.[55] In the case of 5CB and 8CB in nematic and smectic A phases the ^{1}H NMR relaxation was analysed as a function of a multipulse sequence where both pulse width and pulse delay time were changed;[56] the results allowed to relate anomalies observed in the low-field spin-lattice relaxation rates with the dipolar effects. The temperature dependence of the spin-lattice relaxation rate was investigated for an antiferroelectric L.C. in the chiral smectic phase of S-4-(1-

methylheptyloxy-carbonyl) phenyl 4′-octyloxybiphenyl-4-carboxylate, using solid-state ^{13}C NMR;[57] in the chiral smectic C phase the activation energy was larger than in the smectic A, thus suggesting that the molecular rotation is hindered in the former L.C. phase. NMR diffusion and cross saturation transferred NMR experiments were used to investigate the structural features and the local dynamics stability in a chiral cholesteric L.C. polyester prepared from a racemic mixture of monomers as a result of different amounts of the two enantiomers.[58] Finally, two papers deal with solubilization in thermotropic L.C. phases. In the first case a multiscale statistical analysis was used to interpret the mobility of H_2O diffusing within nematic aqueous dispersion of charged anisotropic synthetic Laponite clays;[59] ^{1}H PGSE NMR along with ^{7}Li and ^{23}Na NMR quadrupolar splittings were used for the experiments, whereas semi-empirical quantum calculations (MINDO coupled to perturbation theory for dispersion forces), Monte Carlo (MC), and Molecular Dynamics (MD) calculations were used for the analysis. The second investigation was related to modelling the macromolecular alignment in nematic virus suspensions for which the residual dipolar couplings between ^{15}N and ^{1}H were determined and predicted.[60]

3.2 Lyotropic Liquid Crystals. – As mentioned above $^{2}H_2O$ is often used to investigate lyotropic L.C. phase behavior. ^{2}H NMR quadrupolar splittings $\Delta\nu_q$ appear in the case of anisotropic lamellar and hexagonal L.C. phases while isotropic ^{2}H NMR signals appear in isotropic L.C. phases such as cubic arrangements. Moreover, this method allows ascertaining the occurrence of multiphase systems, *i.e.* the coexistence of different L.C. phase types in the characterization of phase diagrams. Fully or specifically deuterated molecules, particularly in the case of lipids and PLs, can be used. For structural investigations of PLs ^{31}P NMR is widely used also. Generally, the phase behavior of amphiphile molecules in binary or multi-component systems is fully characterized not only by NMR techniques, but also by SAXS, SANS, POM, DSC, and TEM measurements. As to NMR methods, it should be emphasized that self-diffusion measurements can give important information on the dimensions of the organized micro-domains, on the obstruction effects (due to concentration, shape and soft boundaries), and on the spatial connectivity of the micro-domains, *i.e.* the topology of the long-range ordered structure. The huge number of investigations that make use of PGSE NMR methods to prove structural features trustworthily testifies this. In addition, the growing number of articles dealing with improved methods to acquire and to model the NMR self-diffusion experiments, is also significant. Recently great attention has been also given to study the molecular conformational properties and the interactions with additives leading to the formation of defective L.C. phases. Here the lyotropic L.C. phase behavior is presented according to the chemical nature of the amphiphiles, *e.g.* ionic, nonionic, polymeric, lipidic and phospholipidic types and their use as solubilizing matrices. Vesicles, bicelles, liposomes and other dispersed L.C. phases are presented separately for their importance in the characterization of solubilized protein and peptides, besides their use as drug delivery systems.

3.2.1 Ionic Amphiphiles. A variety of ionic amphiphiles, mostly cationic, were

investigated for their phase behavior in water (W). Some articles dealing with alkylammonium chlorides and bromides have been reported. In an article the hexagonal-to-lamellar phase transition was investigated for a nanostructured silica/amphiphile composite where eicosyltrimethyl ammonium bromide is the cationic amphiphile;[61] the use of several techniques along with ^{1}H, ^{13}C and ^{29}Si NMR allowed to estimate energetics of the L.C. phase transition. ^{1}H NMR self-diffusion measurements were used to characterize the microstructure of a discrete cubic L.C. phase (Pm3n space group as determined by SAXS), in comparison with the L_1 micellar phase, formed by cetyltrimethyl ammonium with mixed acetate and polyacrylate counterions;[62] electrostatic attractions and obstruction effects were demonstrated to account for the measured self-diffusion coefficients. ^{2}H and ^{14}N NMR spectra of lyotropic L.C. phases formed by cetylpyridinium bromide (CPyBr) with pentanol and NaBr brine as compared to those obtained for thermotropic L.C. phases of pure CPyBr indicated similar behavior of the amphiphile polar head.[63] PGSE NMR diffusion and relaxation measurements were used to investigate how the Na^+ ionophore monensin affects the dynamics of sodium ions in a Myverol 18-99/saline bicontinuous Ia3d cubic L.C. phase;[64] the monensin-Na^+ binding number was estimated from ^{23}Na NMR line width to be between 3 and 6. Moreover, the dependence of the apparent Na^+ diffusion coefficient on the concentration of monensin revealed monensin-induced Na^+ transport. The orientation of simple amides, such as FM, NMF, DMF, was investigated through NMR in the L.C. phases formed by Cs pentadecafluorooctanoate/water.[65]

3.2.2 Nonionic Amphiphiles. A linear alkyl chain bound to a number of ethylenoxide groups with the general formula CH_3-$(CH_2)_{n-1}$-$(O$-CH_2-$CH_2)_mOH$, for short C_nEO_m, typically forms the most popular nonionic amphiphiles. Only one paper reports on these typical nonionic amphiphiles. The poly-domain L_α L.C. phases formed by $C_{12}EO_5$/decane/water were investigated through ^{1}H PGSE self-diffusion and ^{2}H NMR line shape analysis for samples prepared with $^{2}H_2O$;[66] three types of bilayer were found. At low amphiphile and oil concentrations, the L_α phase consists of a stack of flat parallel bilayers, whereas at intermediate concentration water-filled bilayers exist as demonstrated by three-dimensional water diffusion. At high concentrations, the defective lamellar phase is oriented in the magnetic field thus giving a mono-domain structure. In the context of nonionic amphiphiles sugar-esters have also become very popular, although they are expensive, due to highly specific performances in many biocompatible applications. A detailed characterization of the phase diagram of n-octyl-α-D-glucoside in water was performed through DSC, SAXS, and NMR;[67] lamellar, cubic, and hexagonal L.C. phases were identified and van der Waals differential equation was used to predict the slopes of the phase boundaries. An investigation by SAXS, WAXRD, and ^{1}H NMR on an organogel system prepared from methyl 4,6-O-benzylidene-α-D-mannopyranoside and p-xylene suggested that the solvent molecules are incorporated into the hexagonal packing of fibres thus obtaining a 'wet gel';[68] indeed the gelator molecules were shown to retain thermal motion also in the gel state. The dihydrochloride of

bis-(N,N-diethylaminoethyl) perylene-3,4,9,10-tetracarboxylic diimide showed a peculiar phase behavior in aqueous solution as demonstrated by ^{2}H NMR along with POM;[69] an isotropic-nematic phase transition across a biphasic region was investigated as a function of concentration and temperature. An order parameter of 0.97 was obtained for the tetradeuterated derivative in the nematic phase at high amphiphile concentration. A complex polymorphism and thermotropic mesomorphism also was ascertained by IR and NMR spectra for three gemini amphiphiles in which n-dodecylammonium bromide and n-tetradecylammonium bromide were connected at the polar head-groups by a flexible -$(CH_2)_s$- spacer;[70] surprisingly, with the spacer having s = 6 the gemini amphiphile forms interdigitated bilayers-based L.C. phases, whereas with s = 2, or 10, only monolayers based L.C. phases were identified.

3.2.3 Polymer Amphiphiles. Polymer amphiphiles are typically based on blocks of groups having different hydrophilicity, *e.g.*, the hydrophilic ethylenoxide EO and the more hydrophobic propylenoxide PO units, often referred as A and B blocks respectively. Two tri-block copolymers $(EO)_4(PO)_{59}(EO)_4$ and $(EO)_{17}(PO)_{59}(EO)_{17}$ were investigated for the phase behavior at 25 °C;[71] the phase boundaries were identified using ^{2}H NMR, and a variety of L.C. phases having positive and negative H curvature were characterized, whereas the highly hydrophobic core of the copolymers containing four EO units was shown to favour reverse curvature L.C. microstructures. Micelle-L.C. phase transitions were shown to depend on both temperature and composition for other ABA tri-block copolymers from ^{1}H NMR relaxation measurements.[72] The dynamic-structural changes and polymer-solvent interactions during the thermotropic phase transitions in poly(vinyl-methylether)/^2H_2O system, in a wide range of composition, were studied using ^{1}H NMR spectra and relaxation measurements;[73] compact globular-like microstructures were identified. Lamellar and hexagonal packing was ascertained for functional polymer colloids built from octadecyldimethyl(3-trimethoxysilylpropyl)-ammonium chloride condensed with the trisodium salt of triacetic acid N-(trimethoxysilylpropyl) ethylenediamine using NMR and other techniques.[74] The influence of netropsin, a minor groove binder, on the organization of calf thymus polymeric poly-electrolyte DNA in the aqueous cholesteric phase was investigated by POM and ^{2}H, ^{23}Na, and ^{31}P NMR spectroscopy;[75] a significant increase of the cholesteric pitch upon complex formation was ascertained.

3.2.4 Lipids. Natural lipids, particularly mono-acyl glycerides, steroids and PLs, show a very rich polymorphism that is always a topic of great interest. Many investigations have been reported on the structural characterization and/or the phase transitions observed for either single lipids or mixtures of them in water and in the presence of other additives (salts, drugs, peptides, etc). The rich phase behavior of the hydrated palmitic acid/palmitin system was investigated at different pH values by ^{2}H NMR;[76] the orientation of the lamellar bilayers and of the cylinders in the hexagonal phases was analysed in NMR spectra obtained using perdeuterated lipids. A number of investigations focussing on the 1-

monoglycerol-oleate, also referred as monoolein (MO), has been reported. The existence of two types of bicontinuous cubic phases, namely the gyroid Q^G (Ia3d space group) and the diamond Q^D(Pn3m space group), is well known and demonstrated for the MO/W system. The MO/poly ethylene glycol (PEG)/W sponge L_3 phase was investigated using PGSE NMR self-diffusion;[77] the data allowed the L_3 phase to be modelled as a bicontinuous system with respect to the lipid and water domains. The addition of n-octyl-β-D-glucopyranoside (OG) to MO/^2H_2O system produced significant effects as determined by SAXS and ^2H NMR;[78] a hexagonal phase occurs at high OG content, while the addition of 1.5 wt% of OG converts the cubic phases, which occur in the binary MO/^2H_2O system, to a lamellar phase. On the contrary the cubic phase of the OG/^2H_2O system can incorporate up to 15-wt% of MO. The action of Humicola lanuginosa lipase on the cubic L.C. phase formed by MO/sodium oleate/W system was investigated using ^1H, ^{13}C NMR spectra and ^1H PGSE NMR diffusion measurements;[79] a sequence of different L.C. phases, namely bicontinuous cubic, hexagonal and discrete cubic L.C. phases, was ascertained as a result of lipase action. ^2H NMR was used to monitor changes of the L.C. phases during the extraction of supercritical carbon dioxide;[80] due to the presence of the supercritical fluid, a sample containing 18 wt% of water showed a L_2 phase at all the investigated temperatures, while a sample containing 9 wt% of water showed a L_α-L_2 phase transition with increasing temperature.

3.2.5 Phospholipids and Solubilization in PL Bilayers. Many scientific NMR investigations comprise PL based systems among which PL bilayers used as membrane models, PL dispersions and unilamellar (so called bicelles) and multilamellar vesicles are particularly considered. Important studies based on PLs mixtures and PLs/lipids of different nature, particularly cholesterol (CHOL) and polyunsaturated fatty acid (FA) species mixtures, and also PLs/additives of biological interest have been reported. In consideration of the huge number of articles dealing with PLs (here only those dealing with L.C. phases characterization are mentioned) it seems interesting to show in Fig. 1 the most common polar heads occurring in PLs and in Fig. 2 some other lipids of great interest in biological systems such as CHOL and the simplest bile salts' components, *e.g.* cholic and deoxycholic acids. The phosphatidylcholine (PC) and phosphatidylethanolamine (PE) polar heads are the most abundant PL moieties in the naturally available sources, *e.g.* lecithin (LCT) from soybean seeds and egg yolk. Among sphingophospholipids (SPLs) sphingomyelin (SM) is the most abundant in animal fluids and membranes. Other PLs, *e.g.* phosphatidylglycerol (PG), phosphatidylserine(PS), phosphatidylinositol (PI), and phosphatidic acid (PA) occur in nature at a much lesser extent. ^{31}P nuclei, from the lipid polar head, and ^2H nuclei, from ^2H_2O used as solvent, and perdeuterated or selectively deuterated carbons of the alkyl chains, are the usually investigated NMR nuclei. Moreover many studies dealing with peptide interactions and orientation in PL bilayers have been reported. The phase diagram of the ternary systems LCT/W/isooctane (ISO) and LCT/W/decane (DEC) was investigated by SAXS and NMR techniques to elucidate the complex phase behavior and the variety of

L.C. phases which form along water dilution lines.[81] The simulation of ^{31}P NMR line shapes of unoriented PL bilayers in the L_α phase and of oriented bilayers in both L_α and $L_{\beta'}$ phases was performed through van Faassen's method;[82] it was demonstrated that this method, used for dimyristoylPC (DMPC) and dipalmitoylPC (DPPC) PLs bilayers, involving only numerical integration, is less computationally consuming than other approaches.

Three pairs of PC-based lipids were designed to cross-link at the termini of

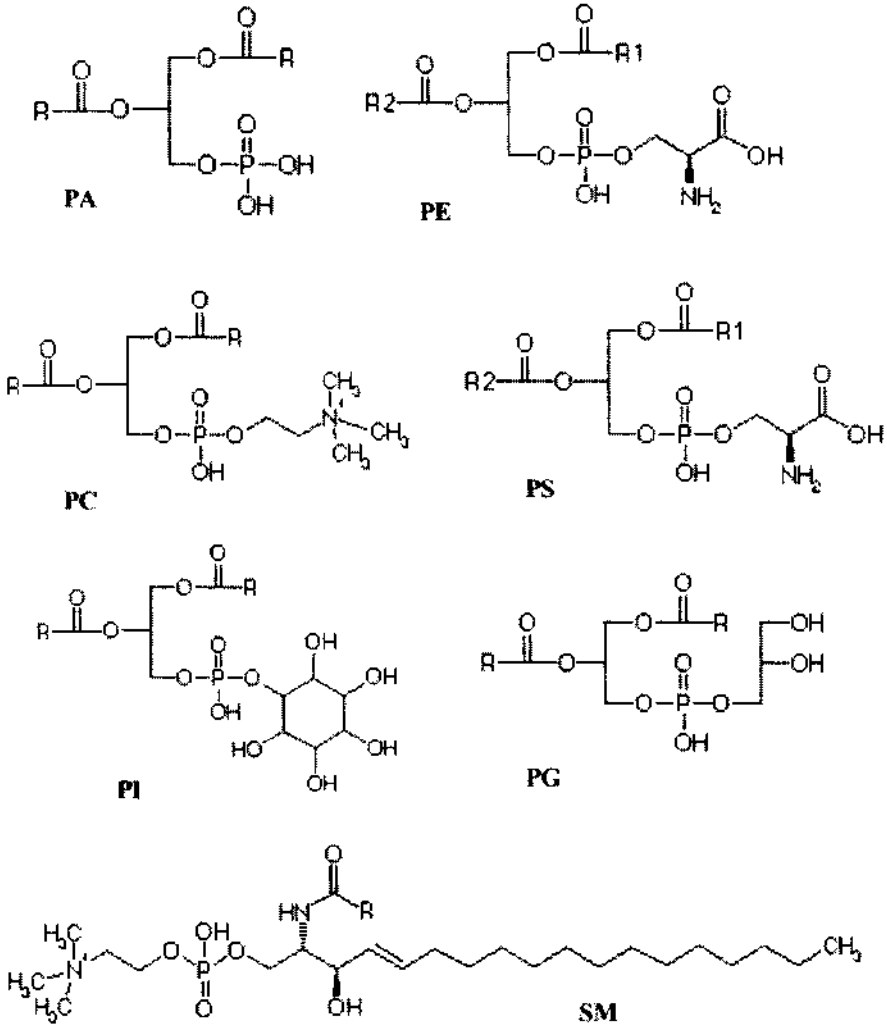

Figure 1 *Schematic formulas of the most common Phospholipid polar heads. Phosphatidic Acid (PA), Phosphatidylethanolamine (PE), Phosphatidylcholine (PC), Phosphatidylserine (PS), Phosphatidylinositol (PI), Phosphatidylglycerol (PG), sphingomyelin (SM).*

their 2-position acyl chain upon the formation of bilayers;[83] the microstructure was investigated by ^{1}H NMR, whereas the ability to enhance the bilayer stability was tested incorporating these new PLs into DMPC. Different mixtures of egg yolk PC, diolein (DO) in Tris-buffered saline were investigated by SAXS and ^{31}P NMR;[84] with increasing DO content phase transitions from lamellar L_α to reverse hexagonal H_2 through two different bicontinuous cubic L.C. phases, namely a primitive C_P (Im3m space group), and a diamond C_D (Pn3m space group), were demonstrated. The effect of DO in promoting a reverse curvature of the polar-apolar interface was clearly remarked, although ^{31}P NMR spectra showed that the H_2 L.C. phase always coexists with cubic L.C. phases.

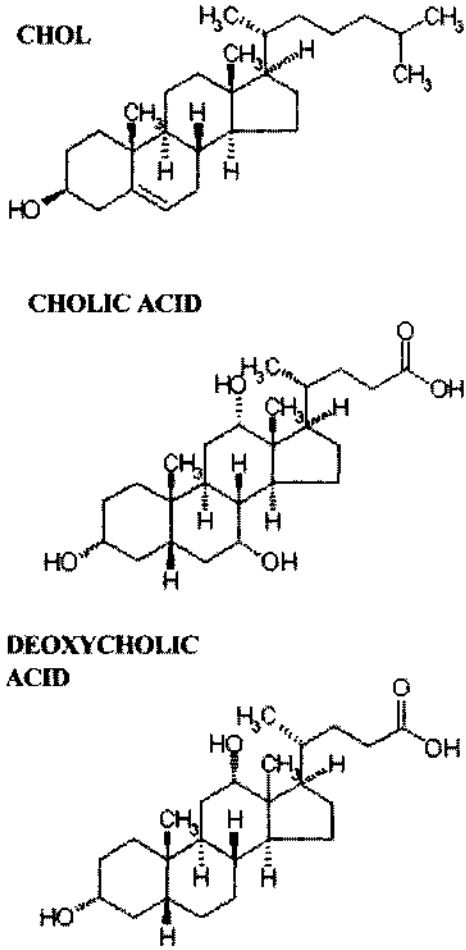

Figure 2 *Schematic formulas of cholesterol (CHOL), cholic and deoxycholic acids.*

Several articles deal with the effect of addition of CHOL, protein and peptides to PL bilayers. The interest is justified by the fact the CHOL and some proteins or peptides are natural constituents of biological membranes. Particularly, it

should be noticed that the fairly rigid structure of CHOL molecule, shown in Fig. 2, confers the necessary stiffness to the PLs bilayer when it is incorporated onto a biological membrane. Different mixtures of DMPC, dioleylPC (DOPC), palmitoyloleylPC (POPC), SM, CHOL and water were investigated through PGSE NMR to obtain the lateral diffusion of the various lipids in the range of temperature 293-333 K;[85, 86] strong evidence was found that fluid domains with high molecular order form within a single bilayer. These domains may play a role for protein-membrane interactions. Moreover, a so-called CORE method was used to separate the diffusion coefficients into a fast and a slow spectral component. Other lipid mixtures, based on CHOL, DOPC, SM, and DPPC were investigated by ^{2}H NMR;[87] from the order of the various acyl chain (^{2}H-labelled) a preferential interaction of CHOL for sphingoPLs over glyceroPLs was suggested. The presence of a protein, NAP-22, present in high abundance in the synaptic cell membrane and synaptic vesicles, was shown to promote the formation of CHOL-rich domains in mixtures of PC-based PL but not of PE-based PL bilayers as demonstrated *via* NMR experiments.[88] Novel properties of CHOL/DOPC mixtures and other PLs were investigated by ^{31}P NMR.[89] ^{13}C MAS NMR was used to investigate the role of CHOL in bilayers of SM or dihydroSM at concentrations found in ocular lens membranes.[90] Miscibility and phase behavior of binary mixtures of N-palmitoyl-ethanolamine, an endogenous ligand for the peripheral cannabinoid receptor, and DPPC were characterized by ^{31}P NMR and SAXS;[91] the influence of N-acylethanolamines, whose content is known to increase significantly in cell membranes when injury or stress occurs, was also investigated. The effects of unsaturated FA and their tri-glycerides (TG) on PE-based membrane were investigated by ^{31}P NMR and SAXS;[92] as expected these unsaturated lipids promote L_α-H_2 phase transitions, and, depending on type of FA or TG, different temperatures of the transitions were found. Among the polyunsaturated FA (PUFA) docosahexaenoic FA (DHA, C22:6 Ω-3) has been recognized to play an important role in cerebral membranes, whereas its conformations seem to be involved in peculiar diseases such as bipolar depression, attention deficit hyperactivity disorder (ADHD) and also autism. Recent results of solid-state NMR investigations on the high flexibility of DHA in PL membranes were reported.[93] The interaction of CHOL with DHA-containing PE-PLs was analysed by ^{2}H NMR and SAXS;[94] depending on compositions, a variety of phase transitions, L_α, H_2, gel L.C., was ascertained. The incorporation of various membrane proteins or peptides in PL bilayers generally alters the original protein secondary structures. To investigate these modifications through NMR techniques specifically labelled proteins and peptides, or alternatively, specifically deuterated lipids can be used. Charge effects of protein interaction at lipid-water interface were investigated by ^{2}H NMR using DMPC-d_4 pure or mixed with DMPG;[95] in the mixed PL bilayers a strong interaction between the charged lysine residues of myosin and the negative charged DMPG was ascertained. 2D solid-state NMR (^{2}H, ^{15}N, ^{31}P) was used to investigate the structure, topology and dynamics interaction of a myristoylated, and specifically labelled, recoverin, a protein involved as calcium sensor in retinal rod cells, with PL bilayers;[96] particularly, it was shown that Ca^{2+}-bound protein is located on

the membrane surface with its long molecular axis oriented at 45° with respect to the membrane normal. The structure of Gramicidin A in a PL bilayer was determined using MD simulations coupled to solid-state NMR data.[97] In another article, using ^{2}H NMR, the hydrophilic glycoprotein SP-A, the main pulmonary amphiphile protein, was shown to interact with DPPC bilayers reducing DPPC chain orientational order significantly.[98] The lateral diffusion of a trans-membrane peptide in PL bilayers was studied by PFG NMR in combination with MAS NMR using a two-dimensional diffusion model.[99] In a multi-technique study on the interaction of the peptidic conantokins with synaptic membranes in conjunction with a high affinity binding to the N-methyl-D-aspartate receptor, it was found that the conantokins preserve a high degree of helical conformation when bound to PL vesicles and bilayers in the presence of Ca^{2+}.[100] The initial structure and dynamic characterization of M2 protein from influenza A virus was investigated in hydrated DMPC/DMPG PL bilayers above the gel-L.C. phase transition by solid-state NMR;[101] the presence of aqueous pores was suggested. The mechanism of PE-based PL bilayers disruption by the human anti-microbial peptide LL-37 was elucidated by ^{31}P NMR.[102] The reversible association of α-lactalbumin with PS and mixed PS/PC based PL bilayers was investigated as a function of pH by ^{2}H NMR.[103] The alanine residues of proteins and peptides in PL bilayers were found to be affected by paramagnetic relaxation induced by doxyl ESR spin label covalently attached to the 5th, 10th, and 16th carbons of the stearic chain of 1-palmitoyl-2-stearoylPC.[104] ^{13}C solid-state NMR was used to provide information on the depth of insertion of an anti-microbial peptide, protegrin 1, in dilaurylPC bilayers using paramagnetic Mn^{2+}.[105] The interaction between two cardio-toxins from cobra snake and membrane PL bilayers was reported in two articles.[106, 107] The interaction of anti-microbial peptides from Australian amphibians with DMPC/dihexanoylPC (DHPC) bicelles and aligned DMPC bilayers was elucidated by ^{2}H and ^{15}N NMR.[108] The effect of fructans, fructose based oligo- and poly-saccharides which protect membranes during dehydration, was investigated in POPC and DMPC bilayers using ^{2}H and ^{31}P NMR;[109] data suggested that fructans insert among the head-groups of PLs, thus spacing the acyl chains. The effect of tricyclic antidepressants on the conformation of PL head-groups was studied by ^{2}H and ^{14}N solid-state NMR;[110] particularly, incorporation of imipramine was shown to change both PL head-group conformation and dynamics. Finally, synthesis and characterization of novel lipid and CHOL-coated gold nanoparticles and their interaction with DMPC membranes was reported.[111]

3.2.6 Vesicles, Bicelles and L.C. Dispersions. Vesicles, liposomes, bicelles form as a result of an effective packing parameter $v/al \approx 1$ of the amphiphilic constituents accompanied by an interplay of different favourable factors. Often, to reach these favourable conditions a mixture of different molecules are needed to combine different conformations of the polar head, different hydration shells, different lengths and conformations (presence of insaturations with different location) of the chain. The result is an arrangement of the bilayer with opposite

interfacial curvature in the inner and in the outer layers. Shape fluctuations in DMPC based vesicles with controlled size were analysed through transverse nuclear spin relaxation measurements using the CPMG sequence.[112] Lateral diffusion measurements and multi-dimensional PFG MAS NMR experiments on POPC liposomes embedded with the hydrophobic drug ibuprofen were used to provide insight into the location and dynamics of lipids, drug, and water.[113, 114] Phase transitions of 100 nm large unilamellar PL vesicles of DPPC were investigated using ^{1}H NMR in $^{2}H_2O$.[115] Using NOE measurements the intermolecular interactions between dimethylsulfoxide and lipid vesicles were investigated.[116] Mixed lipid vesicles containing gangliosides were shown to impose different ^{2}H NMR dynamical parameters on water environment depending on the lipid composition.[117] Multilamellar liposomes formed by phosphatidyl nucleosides were investigated to elucidate intermolecular interactions through NOESY cross-peaks experiments.[118] The location of isoniazid and rifampicin, two tuberculostatics, in DMPC and DMPG bilayers was investigated by ^{1}H NMR;[119] rifampicin in DMPC liposomes was located along the acyl chains of the bilayer. Organic/inorganic hybrid vesicles based on block copolymer were characterized by TEM, SEM, and NMR techniques.[120] Spontaneous formation of silver nanoparticles was observed in multilamellar vesicles favoured by a higher onion internal pH as probed by ^{31}P NMR.[121] ^{1}H NMR and other techniques were used to monitor the formation of vesicular aggregates with spherical and tubular shapes from porphyrin-centered amphiphilic star block copolymer in DMF/water mixed solvent.[122] A ^{1}H NMR conformational study on the complex DNA-based non-viral vector liposomes, stabilised by novel carbohydrate-based agents was reported.[123] The macrolide antibiotic azithromycin was found to reduce the mobility of PL head-groups, as proven by ^{31}P NMR, in Langmuir-Blodgett monolayers and liposomes.[124]

Unilamellar bilayered micelles (vesicles) constituted by a mixture of long and short chain PLs are generally referred as bicelles and are used as membrane model systems. Depending on PL types, concentration and temperature these nanoparticles may form an isotropic phase or an aligned phase in the magnetic field. The effects of bilayer surface charge on the conformation of PC group were studied using torsional angle analysis of ^{2}H quadrupolar and ^{13}C dipolar splittings of POPC labelled with either deuterons or carbon in the PC group, and incorporated into magnetically aligned bicelles based on the cationic DM-trimethylammoniumpropane or the anionic DMPG;[125] the torsional angle constraints and order parameters were obtained. Location of the myristoylated alanine-rich C-kinase substrate, which is a highly basic, unstructured protein segment, was investigated by NMR for its capacity to sequester phosphoinosities within the plane of a bilayer when bound to PL bicelles;[126] the phenylalanine residues of this protein were found to be located within the membrane hydrophobic domain a few Å from the polar-apolar interface. A ^{2}H NMR and Molecular Mechanics study was reported on the structure and dynamics of PL bicelles incorporating selectively deuterated and perdeuterated DMPC.[127] Bicelles formed from DMPC/DHPC were examined by ^{31}P NMR under variable-angle sample-spinning thus inducing different orientations of the L.C. director;[128] the

method was used to investigate the interaction of the bicelle with the opioid pentapeptide leucine-enkephalin.[129] A ^{31}P NMR enzymic assay system was used to examine the kinetic behavior of cobra venom phospholipase A_2 toward a variety of bicellar substrates;[130] no significant preference for long or short PLs was found. The stability of bicelles towards disruption induced by the membrane-lytic peptide melittin was increased significantly by adding CHOL as demonstrated by ^{31}P NMR.[131] PGSE-NMR in the presence of paramagnetic probes was used to investigate motilin-bicelles interactions and relative locations;[132] the N-terminus of motilin is inserted into the bicelle, whereas the helix is likely to reside at the head-group layer.

4 Micellar Solutions

Micelles are the simplest organised form of the self-assembly produced by amphiphilic molecules due to the so-called 'hydrophobic effect', firstly recognized by Tanford.NMR parameters experience dramatic effects as a result of the strong intermolecular interactions among the amphiphiles. In the case of isotropic liquid systems, NMR experiments can be easily performed and modelled, since many advances have been produced in the last two decades.Hence, information on critical micelle concentration (c.m.c.), molecular conformations and interactions, counterion binding, hydration can be obtained from chemical shifts, relaxation, and self-diffusion NMR measurements, also in mixed systems.

4.1 Micelles in Amphiphile-Solvent Systems. – In this paragraph studies on micellar solutions formed by single and mixed amphiphiles are reported according to the amphiphile type, *e.g.* ionic, nonionic, polymer, and mixed amphiphiles (mixtures of different types).

4.1.1 Ionic Amphiphiles. Among ionic amphiphiles that have been used for many years in technological applications only few are still extensively adopted and investigated. Some cationic amphiphiles are of interest because of their antibacteric, immunosuppressive or other specific properties. Indeed ionic amphiphiles tend to be aggressive towards biological membranes. Few ionic amphiphiles possess biocompatibility. Examples are peptide-based amphiphiles. Also cholate derivatives should be mentioned since they are based on bile salt components such as cholic or deoxycholic acids, shown in Fig. 2. A 2D NMR study using NOESY and ROESY spectra was performed to obtain information on the structures of micelles of sodium taurocholate (NaTC).[133] In another article collective and self-diffusion coefficients of sodium taurodeoxycholate (NaTDC) and NaTC in ^2H_2O micellar solutions were measured as a function of ionic strength (NaCl) and bile salt concentration;[134] the cylindrical micelles were shown to be affected by NaCl concentration, particularly NaTDC diffusivity and size were significantly modified. The influence of monovalent Li, Na, K, Rb, and Cs counterions on micellar properties and chiral recognition of poly-N-undecenoyl-L-leucinate was investigated through PFG-NMR and other tech-

niques;[135] significant differences in the chiral selectivity and resolution as well as retention factors were found for Rb and Cs counterions. With these counterions a dramatic increase of c.m.c. was also found. A progressive structural change of the self-assembly from spherical micelles at 0.5 wt% to small disk-like and then to cylindrical micelles at 10 wt% was identified for a hybrid anionic fluorocarbon/hydrocarbon amphiphile, sodium 1-oxo-1[4-(tridecafluorohexyl)phenyl]-2-hexanesulfate using cryo-TEM, rheological and NMR self-diffusion measurements.[136] Some articles deal with sulfonate amphiphiles, that have been very much used in the past for detergency. Differences in micellar properties of Na-dodecylsulfonate and Na-4-decyl naphtalene sulfonate in ^2H_2O were identified by ^1H NMR relaxation and 2D NOESY spectra;[137, 138] the presence of the naphtyl ring was shown to produce a more tightly packed micellar core than that of Na-dodecyl sulfonate.[139] Sodium octane-1-sulfonate was chosen as reference to investigate the effect of replacing sodium with alkylpyridinium counterions having different number of carbons, n_c, in the alkyl chain, namely from $n_c = 1$ to $n_c = 8$;[140] all amphiphiles, as demonstrated by ^1H, and ^2H NMR, PGSE NMR and other techniques, formed L_1 micellar and H_1 L.C. phases. The use of ^1H, and ^2H NMR relaxation and self-diffusion to investigate the micellar solution formed by K-nonanoate allowed to identify slow and fast components of the diffusion process, due to the micelle and the amphiphile monomer, respectively.[141] Two articles dealing with cationic amphiphiles based on ammonium chloride derivatives have been reported. ^1H and ^{13}C NMR spectra and relaxation, used to study a series of benzyl(2-acylaminoethyl) dimethylammonium chlorides in ^2H_2O, allowed to determine c.m.c. and thermodynamic parameters;[142] acyl chains with $n_c = 10$-16 were examined, and, in another investigation, aggregation numbers were estimated also in different solvents such as $CDCl_3$ and $CD_3OD/^2H_2O$.[143] The mixtures of sodium and ammonium salts of three homologous perfluoropolyether carboxylic acids having Cl- terminated perfluoroalkyl group and differing in the average molecular weight were examined using ^{19}F NMR;[144] the analysis of chemical shift variations allowed to evaluate the partition of the various amphiphiles in the mixed aggregates thus proving that ideal mixing, particularly at high amphiphile concentration, occurs.

4.1.2 Nonionic Amphiphiles. Nonionic amphiphiles generally display a lower biological aggressiveness than ionic species. In the last decade typical nonionic EO-based amphiphiles have been widely produced and investigated although they do not undergo easy biodegradation. More recently different classes of sugar-esters have become important types of nonionic amphiphiles. The most interesting features of these amphiphiles consist in the full biocompatibility and on the possibility of modulating their hydrophilic-lipophilic balance (HLB) by changing the hydrophobic moiety, particularly the chain length, and the nature of the polar sugar head, from a monosaccharide to polysaccharides. This confers all the characteristics observed for typical C_nEO_m-type amphiphiles. An investigation on three sugar-esters, having different sugar polar heads, using NMR and other techniques, revealed the influence of the flexibility of the polar heads;[145] different c.m.c. values and aggregation numbers were identified as well as import-

ant deviations from spherical shape of micelles were suggested on the basis of NMR self-diffusion data. An interesting article was reported on the amphiphile diffusion through bicontinuous micellar network formed by n-decyl-β-D-glucopyranoside and n-nonyl-β-D-glucopyranoside mixtures;[146] NMR self-diffusion data allowed to justify the phase behavior and phase separations observed in the ternary phase diagram. Self-diffusion coefficients of Triton X-100 micelles in dextran gel were found of the same order of the dextran chain diffusion,[147] thus emphasizing the potential role of the polysaccharide gels as bacterial bio-films. Structural and transport properties were determined for bola C-16 micelles, based on [α,ω-(4,7,10,13-pentaoxa-16-azacyclooctadecane)hexadecane] amphiphile, in water and aqueous electrolyte solutions using SANS, NMR self-diffusion and other techniques;[148] the addition of LiCl, NaCl and HCl induced different effects from simple screening of electrostatic repulsion between micelles in the case of LiCl, to a significant reduction of micellar size in the presence of HCl. The self-micellization of Gemfibrozil 1-O-b acylglucuronide, a model drug-glucuronide conjugate, was investigated in aqueous solution by micro-calorimetry and ^{1}H NMR;[149] micellization was detected in acetate buffer. The self-association of hydrophobically modified glycol chitosans by 5β-cholanic acid was investigated by ^{1}H NMR and other techniques;[150] depending on the degree of substitution the critical aggregation concentrations decreased with increasing MW.

4.1.3 Polymer Amphiphiles. Modification of polymer-based amphiphiles may introduce specific functional groups that confer a variety of selective applications. Amino acid residues and sugar groups have been often used to modify particularly the HLB properties.

A new biodegradable amphiphilic tri-block copolymers, based on hydrophilic poly-EO (PEO) groups and on hydrophobic poly[(R)-3-hydroxybutyrate] (PHB)groups, was synthesized and characterized for micellar properties by ^{1}H NMR;[151] very low c.m.c. values were measured whereas micellization was found to be temperature insensitive. A novel series of water-soluble polyethylenglycol (PEG) – maleic anhydride – polydimethylsiloxane polyester amphiphiles were characterized for surface properties.[152] Polymerizable cationic amphiphiles, constituted by methacryloyl and acryloyl derivatives, were used as mixed micelles to obtain polymers which can form lamellar phases;[153] NMR and SAXS were used to characterize phase behavior. A pH-dependent micellization was characterized by ^{1}H NMR relaxation and other techniques for the di-block copolymer poly(sodium 2-(acrylamido)-2-methylpropanesulfonate-block-sodium 6-acrylamidohexanoate).[154] A pH-induced reversible micellization was found also for poly(methacrylic acid-block-(2-diethylamino)ethyl methacrylate) and the mechanism was elucidated *via* ^{1}H NMR.[155] The effects of acyl chain length on the micelle properties of the diblock copolymer PEO-block-poly(N-hexyl-L-aspartamide)-acyl conjugates was investigated by ^{1}H NMR, TEM and DLS;[156] c.m.c. values decreased with increasing the acyl chain length.

4.1.4 Mixed Amphiphiles Systems. Mixed micellar systems are very important

either for industrial applications or scientific investigations. Several mixed systems containing sodium dodecyl sulfate (SDS) have been reported. The interactions between the nonionic polymer PEO (MW 20000) and amphiphiles of various type, such as SDS, dodecyl trimethylammonium bromide, octyl β-D-glucoside, and potassium laurate were investigated by ^{1}H PGSE NMR;[157] a detailed picture of binding and aggregation processes was obtained. SANS, electrophoretic NMR and other techniques were used to study the mixed micelles formed by SDS and $C_{12}EO_4$;[158] particularly, NMR studies provided interesting estimation of the ionic character of the micelle: with increasing nonionic amphiphile content, aggregation numbers were shown to increase whereas micelles became more elliptical and the head-group region less hydrated. The interaction between a polybetaine and anionic, cationic, zwitterionic and neutral amphiphiles were investigated by several techniques;[159] the polybetaine, being a phosphorylcholine-based polymer, showed strong association with anionic amphiphiles such as SDS *via* a cooperative mechanism driven by electrostatic interactions. ^{1}H and ^{19}F NMR measurements on micellar solutions of mixed sodium perfluorooctanoate and sodium dodecanoate were reported;[160] NMR data indicated that below the c.m.c. each monomer is not affected by the presence of the other, while above the c.m.c. fluorinated chains aggregate forming islands among hydrocarbon chain domains. Hybrid threadlike micelles, formed by cetyltrimethylammonium bromide (CTAB), sodium p-toluensulfonate (NaTS) and sodium poly(p-vinylbenzoate) varying pH and compositions, were investigated using NMR and viscoelastic measurements;[161] when NaTS concentration is higher than 60% of CTAB concentration, hybrid threadlike micelles, that are long enough to become entangled, form. Mixed micelles of cationic-nonionic amphiphiles, based on CTAB and Triton X-100, were studied using ^{1}H PGSE NMR self-diffusion.[162] ^{1}H and ^{13}C NMR parameters were used to elucidate the structure and to evaluate the interactions in several binary mixtures of the following amphiphiles: benzyldimethylhexadecylammonium chloride mixed with hexadecyltrimethylammonium bromide (HTABr), hexadecylpyridinium bromide (HPyBr) and chloride (HPyCl) where the strong binding ability of bromide counterion induced compactness in the mixed micelles;[163] HTABr mixed with hexadecyltriphenylphosphonium bromide (HTPBr), hexadecyltributylphosphonium bromide (HTBBr), and HPyBr mixed with HTPBr and HTBBr;[164] sodium deoxycholate mixed with HTABr, HPyBr, and HPyCl;[165] cationic amphiphile mixtures and anionic poly-electrolytes where the mixtures were constituted by benzylhexadecyl-dimethylammonium chloride (BHDACl) and HPyBr or HPyCl in the presence of dextran sulfate and polyacrylic acid sodium salts;[166] and also mixed BHDACl/HTABr in the presence of cellulose sodium salt.[167] In these investigations the role of the head-groups was evaluated to elucidate the mixed micelles formation mechanism and to ascertain their stability in relation to the electrolyte-modified bulky properties. Interfacial, thermodynamics, and self-association properties were determined using ^{1}H NMR for binary mixtures of $C_{14}H_{29}CH(SO_3Na)COOCH_3$ and $C_{12}EO_6$ amphiphiles;[168] very low c.m.c. were determined for the mixed micelles along with synergic effects as determined using Rubingh and Maeda theory. The mixed

system Lysozime (Ly)-octyl sulfate (OS) was reported to form in the presence of an excess of OS micelles which, at high protein and OS concentration coexist with gel aggregates;[169] OS micelles containing a single Ly molecule were suggested to form when the molar ration OS/Ly exceeds 30, as demonstrated by NMR diffusometry and UV spectroscopy. The Ly protein was investigated also in the presence of lithium perfluorononanoate using ^{19}F NMR; [170] micelles and interconnected necklace structures were suggested. The mixed micellar aggregates based on CCK peptides and Gd complexes, designed as tumor-specific contrast agents in MRI were investigated through PGSE NMR and other techniques;[171] spherical micelles with an external shell of ≈ 21 Å and an inner core of ≈ 20 Å were proposed.

4.2 Solubilization, Microemulsions and Emulsions. – Micellar solutions with both normal (L_1) and reverse (L_2) curvature, *e.g.* o/w and w/o type systems, can be swollen by oil and water to obtain water/oil/amphiphile ternary or pseudo-ternary systems. These systems have been widely used as solubilizing media for structural investigations of the immobilized solubilizate (a protein for instance), for drug delivery systems, and also for reaction media. (micellar catalysis). Ternary systems based on water, oil, and amphiphile mixtures can form a variety of L_1 and L_2 monophasic regions. When these systems form isotropic solutions spontaneously, they are termed microemulsions. The formation of a microemulsion is related mainly to a substantial decrease of the interfacial tension ($\gamma_{o/w}$) at the oil-water interface, due to the amphiphilic molecules located at the polar-apolar interface. This occurs in agreement with the typical equation:

$$\Delta G = \Delta A\, \gamma_{o/w} - T\Delta S \qquad (1)$$

where ΔG is the Gibbs free energy, ΔA is the interfacial area variation, and ΔS is the configurational entropy associated to the dispersion process, at the defined temperature T. If the amphiphile decreases the interfacial tension $\gamma_{o/w}$ sufficiently to allow spontaneous emulsification, thermodynamically stable microemulsions form. They are characterized by small aggregates and low polydispersity. When emulsification needs additional work the kinetically stable systems that form are defined emulsions. Crucial factors to determine the spontaneous curvature, H_o, of the amphiphilic interface for both microemulsions and emulsions are the hydration of the polar head group and the oil penetration which, in turn, determines the elasticity of the interfacial film and thus the stability towards the rupture. Several additional parameters among which the relative densities and viscosities of the dispersed phase and of the dispersing media influence particularly the emulsion stability with respect to the typical destabilizing processes, *e.g.* creaming, sedimentation, flocculation, coalescence and Ostwald ripening.

4.2.1 Solubilization Media. Many investigations have been reported on the interaction between a solubilizate and a micellar system. Several solubilization media can constitute interesting drug delivery systems. In other cases, solubilization in micelles represents a simplified model for mimicking interactions with biological membranes as an alternative to bicelles, liposomes and PL bilayers.

The polymeric micelles formed by poly(2-ethyl-2-oxazoline)-block-poly(ε-caprolactone) was used as carrier for paclitaxel, a drug used to inhibit the growth of some carcinoma cells;[172] ^{1}H NMR was used to characterize the micelles with and without the entrapped drug. A complex solubilization of non-steroidal anti-inflammatory drugs ibuprofen and diflunisal in cyclodextrin was investigated by NMR and UV spectroscopy as a function of pH.[173] Micelles based on copolymeric blends of polycaprolactone-PEG were designed and characterized by NMR and IR for delivery of nimesulide.[174] Physiological mixtures of bile salts forming mixed micellar aggregates were investigated by NMR self-diffusion as delivery systems for several types of drugs.[175] Diffusion-ordered (DOSY) NMR measurements were performed to clarify the solubilization process of artemisinin, a natural drug, in octanoyl-6-O-ascorbic acid micelles used to improve drug availability in hydrophilic media.[176] A polymeric micellar carrier based on poly(D,L-lactide) was used as carrier for the solubilization of biphenyl dimethyl dicarboxylate and investigated for its performance as a function of the preparation methods using NMR and other techniques.[177] ^{1}H NMR was used to prove the solubilization of 1,6-diphenyl-1,3,5-hexatriene in the hydrophobic core of the micelles formed by the tri-block copolymer poly(p-dioxanone-co-1-lactide)-block-PEG.[178] Several articles dealing with solubilization in SDS micelles, and based on the use of NMR techniques, have been reported. This is the case of an amyloid polypeptide hormone which orients at the micellar polar-apolar interface,[179] of different types of Penetratin, peptides which have the ability to penetrate biological membranes,[180, 181] of poly(vinylpyrrolidone) for which a micelle-like cluster bound onto the polymer was suggested to form,[182] of Spinigerin, an antibacterial peptide derived from termite which forms an α-helic also in the presence of other types of micelles such as DPC,[183] and of Orexin-B, a neuropeptide implicated in sleep-wakefulness and feeding regulation, where the helix II was suggested to be involved in membrane recognition.[184] Other investigations have focussed on the solubilization and/or interaction between SDS and macromolecules of biological interest. This is the case of the modification of the secondary structure of a β-casein supramolecular micellar aggregate due to the solubilization of small amounts of SDS, whose micelles can form only after saturation of the casein hydrophobic binding sites,[185] and of the variation of rheological properties of maize starch granules due to the formation of rigid complexes with the exterior chains of amylopectin.[186] In addition, it was shown that humic substances enhance SDS aggregation prior to micellization, whereas form ion pairs with the positive charged CTAB.[187] Micelles of DHPC or dodecylPC (DPC) seem to be drug delivery systems or membrane-like models more promising than SDS. Indeed several articles dealing with solubilization in DHPC and DPC micelles have appeared. DHPC micelles were used to elucidate and to refine the structure of the Escherichia coli outer membrane protein OmpX through different ^{15}N and ^{13}C NMR experiments.[188, 189] The structure and topological orientation of recombinant, biological active, monomeric Phospholamban, an integral membrane protein regulating contractility of cardiac muscle, in lipid-mimicking DPC micelles were determined by multidimensional NMR experiments;[190] the topological arrangement makes the two phosphoryla-

tion sites (Ser-16 and Thr-17) more accessible to kinase. DPC micelles were used generally to identify the most probable binding site of proteins, peptides, as in the case of the prion protein where also the binding to Cu^{2+} ions was found to play a physiological role,[191] the polypeptide hormone glucagon,[192] the Pediocin-like anti-microbial peptide Sakacin P and a variant of it stabilized by an inserted C-terminal disulfide bridge.[193] Different binding sites were observed by 2D NMR experiments for ($Ala^{8,13,18}$)magainin peptides in DPC or SDS micelles;[194] the peptide adopts an α-helical secondary structure involving residues 2-16 in the case of DPC micelles and residues 7-17 in the presence of SDS micelles. PGSE NMR was used to investigate the binding of cationic neuropeptides having different charges (+1 to +3) to zwitterionic DPC and anionic SDS micelles;[195] peptides with a larger net charge were found to bind at a greater extent than those with a lesser net charge, *i.e.* in the order bradykinin > substance P > neurokinin A >Met-enkephalin, whereas almost the opposite order was found in the presence of DPC micelles. 2D NMR experiments were used to evaluate the conformations adopted by glycosyl enkephalin analogues in the presence of DPC or SDS micelles;[196] glycosylation did not produce significant modifications of the peptides, while deep conformational changes were observed in the presence of the micellar aggregates.

4.2.2 Microemulsions. As in the case of simple micellar solutions, the development and the use of NMR techniques in the characterization of microstructural features and transitions in microemulsion systems has produced a wide and unique insight of knowledge. In L_1 and L_2 microemulsion phases a variety of microstructures from discrete to bicontinuous aggregate, exactly as in the L.C. state, occur. Not only o/w or w/o droplets exist. The shape of the amphiphile and the delicate interplay of intermolecular forces (van der Waals, electrostatic, hydration, polarizability, specific ion effects, etc) that balance the location of the amphiphile between the apolar and the polar domains are crucial factors. They can be simply embodied in an effective packing parameter '*v/al*'. However, it is not easy to evaluate the contributions of the various intermolecular forces. For instance, the transition of the dispersed phase from a disconnected to an interconnected domain has been generally referred as percolative threshold. It has been shown that these transitions can be clearly identified. In addition, a percolative behavior is typically expected upon increasing the amphiphile/oil ratio. All these are phenomenological observations that have been also modelled trustworthily. However a deeper insight into the role of the various intermolecular forces which address the delicate balance among different nanostructures within the same monophasic and macroscopically isotropic region, is necessary. Indeed recent trends of the investigations on microemulsions point towards a more detailed analysis of experiments, performed at a molecular level, to improve predictive theories. Another recent trend of the reported investigations is the highlight on biocompatible systems. Some articles dealing with Lecithin (LCT) based microemulsions have been reported. A time-resolved ^2H NMR study performed in the isotropic and concentrated region of the ternary system LCT/^2H_2O/cyclohexane allowed to investigate the relaxation of a shear-induced

nematic back to the isotropic liquid w/o microemulsion, after cessation of shear;[197] the process was clarified by monitoring the decrease of the ^2H quadrupolar splittings induced by the nematic phase. LCT microemulsions in dimethylether and propane were investigated by NMR to generate pharmaceutical aerosols containing polar solutes;[198] sphere-to string micellar shape changes as the solvent mixture was varied were observed. Peculiar o/w microemulsions were identified from PGSE NMR measurements for the ternary system $C_{18:1}EO_{10}$/oil/W systems where oils were medium chain TG or retinyl palmitate mixtures.[199] Temperature-insensitive microemulsions spanning the whole water-oil composition range, and formulated using W/n-octane/n-octyl-β-D-glucopyranoside/1-octanol were investigated by SANS and NMR diffusometry;[200] clear evidence of transition from o/w to w/o microstructures *via* bicontinuous networks in a wide range of compositions around phase inversion was obtained. ^1H NMR self diffusion measurements were used to study bicontinuous microemulsions formed by water, SDS, and polymers of methyl methacrylate and 2-hydroxyethyl methacrylate, cross-linked with ethylene glycol dimethacrylate;[201] evidence for bicontinuity of the microporosity of these polymeric materials was given. Some articles still dealing with another well known w/o microemulsion forming amphiphile such as sodium bis-ethylhexyl sulfosuccinate, commonly referred as Aerosol-OT (AOT), have been reported. The effect of α-lactalabumin on the microstructure of the microemulsions formed by AOT/W/isooctane was investigated by NMR and other techniques for different protein/AOT ratios.[202] Light sensitive w/o microemulsions were obtained adding a photo-destructible amphiphile, Na 4-hexylphenylazosulfonate to AOT/W/n-heptane microemulsion systems;[203, 204] ^1H NMR measurements indicated that the added amphiphile undergoes UV-induced decomposition to yield a mixture of 4-hexylphenol and hexylbenzene which altered the AOT microemulsion phase behavior. The microstructure of the w/o microemulsion which forms close to the oil corner of the four-component sulfobetaine/pentanol/toluene/W system was found to be altered by adding suitable amounts of the polyelectrolyte Na polyacrylate;[205] indeed ^1H NMR self-diffusion measurements demonstrated a L_2-L_α L.C. phase transition which implies a significant modification of the curvature of the polar-apolar interface. The microemulsion formed by the fluorinated amphiphile tetraethylammonium perfluorooctyl sulfonate, water, and the fluorinated oil 1H-perfluorohexane was investigated by ^1H and ^{19}F NMR self-diffusion method;[206] along oil dilution lines a microstructural transition from threadlike to spherical reverse micelles was ascertained.

4.2.3 Emulsions. Emulsions are widely used, and thus of great interest for technological formulations in agrochemical, cosmetic, pesticide, lubricant, detergent, food, pharmaceutical and crude oil industry. Not less important is the use of emulsion systems as polymerization reactors. Emulsions are systems characterized by minimal thermodynamic stability when they form, and tend to phase separate. The technological interest on emulsions is clearly demonstrated by the growing number of investigations and by the development of several NMR-based experiments aimed to gain information on the formation, microstructural

features and stability of these systems. NMR self-diffusion measurements appear to be of paramount importance to investigate polydispersity and thus the potential stability towards coalescence and phase separation. This is further demonstrated by the development also of acquisition techniques in NMR measurements – modified spin-echo sequences, combined CPMG/PGSE sequences, 2D PGSE experiments, modelling approaches – as reported in paragraph 2. Some articles dealing with emulsions as polimerization reactors have been reported.[207, 208] The influence of crude oil fractions on the stability of crude oil emulsions was investigated using ^{1}H and ^{13}C NMR;[209] it was ascertained that the presence of aliphatic acids with different structures in crude oil decreases the stability of the thin liquid films formed by interfacial active components, thus influencing the emulsion stability. Two cosmetic emulsions containing the stearyl phosphate emulsifier were examined using ^{1}H and ^{31}P NMR techniques;[210] solid-state cross polarization MAS and water self-diffusion experiments proved the existence of the emulsifier either as solid phase or gel network phase. MRI technique was used to investigate the mixing process of concentrated oil-in-water emulsions in a horizontal, concentric-cylinder geometry;[211] a simple modelling of the experimental data to elucidate the mixing mechanism was proposed. The self-diffusion of different species in highly concentrated w/o emulsions, where n-heptane was the continuous oil phase, was studied by NMR diffusometry approach;[212] the transport of various substances, such as water, tetramethylammonium ions, glucose, and mixtures of acetic acid/acetate ions was investigated. Results showed that water and acetic acid/acetate ions diffuse between emulsion droplets whereas tetramethylammonium ions, and glucose do not on the relevant time scale of the experiments. The last article to be mentioned in this paragraph deserves some additional remarks since unusual, although transient, microstructures of the investigated emulsions were identified through the cooperative used of PGSE NMR, rheology, conductivity and freeze-fracture TEM.[213] Emulsions prepared in different composition range of the ternary Triton X-100/toluene/W system were o/w type emulsions at all Triton X-100 wt%. At high concentration of the amphiphile a stable closed-cell foam emulsion appeared. Around 6 wt% of amphiphile a bicontinuous emulsion can be stabilized for several hours provided that a minimal input energy was given in the preparation. This unusual microstructure was shown to be extremely sensitive to external stimuli, and, again unusually, to coexist with a more regular o/w emulsion. To comment on these finding it can be emphasized that for the first time a bicontinuous microstructure has been trustworthily identified in an emulsion system.

References

1. M. Monduzzi, in 'Nuclear Magnetic Resonance', ed. G.A. Webb, Royal Society of Chemistry, Cambridge, 2004, **33**, 531
2. S. Caldarelli, in 'Encyclopedia of Nuclear Magnetic Resonance', ed. D.M. David R.K. Harris, John Wiley & Sons, Chichester, 2002, **9**, 291

3. A. Bax, J. J. Chou, and B. E. Ramirez, in 'Encyclopedia of Nuclear Magnetic Resonance', ed. D.M. David, R.K. Harris, John Wiley & Sons, Chichester, 2002, **9**, 401
4. S. Z. Mao and Y. R. Du, *Wuli Huaxue Xuebao*, 2003, **19**, 675.
5. K. Matsuoka and Y. Moroi, *Curr. Opin. Colloid Interface Sci.*, 2003, **8**, 227.
6. K. V. Ramanathan and N. Sinha, *Monatshefte fuer Chemie*, 2002, **133**, 1535.
7. K. V. Ramanathan and N. Sinha, *Pramana*, 2003, **61**, 249.
8. J. Schiller and K. Arnold, *Med. Sci. Monitor*, 2002, **8**, MT205.
9. S. Murgia, S. Mele, and M. Monduzzi, *Lipids*, 2003, **38**, 585.
10. B. Sesta and C. LaMesa, *Curr. Topics Colloid & Interface Sci.*, 2002, **5**, 261.
11. P. W. Kuchel, B. E. Chapman, W. A. Bubb, P. E. Hansen, C. J. Durrant, and M. P. Hertzberg, *Concepts Magn. Reson. Part A*, 2003, **18A**, 56.
12. A. Sugimura and G. R. Luckhurst, in 'Nanotechnology and Nano-Interface Controlled Electronic Devices', ed. M. Iwamoto, K. Kaneto, S. Mashiko, Elsevier Sci., Amsterdam, 2003, 313
13. S. V. Dvinskikh, H. Zimmermann, A. Maliniak, and D. Sandstrom, *J. Magn. Reson.*, 2003, **163**, 46.
14. S. Lee, M. F. Mesleh, and S. J. Opella, *J. Biomol. NMR*, 2003, **26**, 327.
15. P. T. Callaghan, S. Godefroy, and B. N. Ryland, *Magn. Reson. Imaging*, 2003, **21**, 243.
16. Y. Q. Song, M. D. Hurlimann, and C. Flaum, *J. Magn. Reson.*, 2003, **161**, 222.
17. C. Buckley, K. G. Hollingsworth, A. J. Sederman, D. J. Holland, M. L. Johns, and L. F. Gladden, *J. Magn. Reson.*, 2003, **161**, 112.
18. A. A. Pena and G. J. Hirasaki, *Adv. Colloid Interface Sci.*, 2003, **105**, 103.
19. M. Valentini, A. Vaccaro, A. Rehor, A. Napoli, J. A. Hubbell, and N. Tirelli, *J. Am. Chem. Soc.*, 2004, **126**, 2142.
20. K. G. Hollingsworth and M. L. Johns, *J. Colloid Interface Sci.*, 2003, **258**, 383.
21. H. Hagslatt, B. Jonsson, M. Nyden, and O. Soderman, *J. Magn. Reson.*, 2003, **161**, 138.
22. V. C. Reinsborough, in 'Interfacial Catalysis', ed. A.G. Volkov, M. Dekker, New York, 2003, 377
23. X. He, H. Zhang, D. Yan, and X. Wang, *J. Polym. Sci., Part A: Polym. Chem.*, 2003, **41**, 2854.
24. C. Wu, Q. Gu, Y. Huang, and S. Chen, *Liq. Crys.*, 2003, **30**, 733.
25. A. E. Riley, G. W. Mitchell, P. A. Koutentis, M. Bendikov, P. Kaszynki, F. Wudl, and S. H. Tolbert, *Adv. Functional Mater.*, 2003, **13**, 531.
26. N. D. Jadav, B. A. Prajapati, and A. K. Prajapati, *Mol. Cryst. Liq. Cryst.*, 2003, **399**, 53.
27. Z. Yerlikaya, S. Aksoy, and E. Bayramli, *J. Appl. Polym. Sci.*, 2003, **90**, 3260.
28. J. S. Hu, Y. Wang, B. Y. Zhang, and Y. H. Li, *Polym. J. (Japan)*, 2003, **35**, 728.
29. C. Tan and B. M. Fung, *J. Phys. Chem. B*, 2003, **107**, 5787.
30. J. R. Hughes, G. R. Luckhurst, K. Praefcke, D. Singer, and W. M. Tearle, *Mol. Cryst. Liq. Cryst.*, 2003, **396**, 187.
31. M. Lehmann, R. I. Gearba, M. H. J. Kock, and D. A. Ivanov, *Chem. Mater.*, 2004, **16**, 374.
32. J. C. Ronda, J. A. Reina, V. Cadiz, M. Gamberini, and L. Nicolais, *J. Polym. Sci., Part A: Polym. Chem.*, 2003, **41**, 2918.
33. S. Kanesaka, H. Kimura, S. Kuroki, I. Ando, and S. Fujishige, *Polym. Preprint A.C.S.*, 2003, **44**, 357.
34. S. Kanesaka, H. Kimura, S. Kuroki, I. Ando, and S. Fujishige, *Macromolecules*,

2004, **37**, 453.
35. G. Hempel, A. Dimitrova, J. Lindau, D. Reichert, and H. Schneider, *Macromol. Chem. Phys.*, 2003, **204**, 674.
36. J. S. Hu, B. J. Zhang, K. Sun, and Q. Y. Li, *Liq. Crys.*, 2003, **30**, 1267.
37. J. S. Hu, B. Y. Zhang, Y. G. Jia, and S. Chen, *Macromolecules*, 2003, **36**, 9060.
38. K. Sadagopan, D. Ratna, and A. B. Samui, *J. Polym. Sci., Part A: Polym. Chem.*, 2003, **41**, 3375.
39. M. Sato and Y. Kitani, *Liq. Crys.*, 2003, **30**, 1109.
40. L. M. Lai, J. W. Y. Lam, K. K. L. Cheuk, and B. Z. Tang, *Polym. Preprint A.C.S.*, 2003, **44**, 954.
41. C. Lorthioir, B. Deloche, P. Auroy, and Y. Gallot, *Europhys. Lett.*, 2003, **62**, 746.
42. J. M. Rueff, J. Barbera, B. Donnio, D. Guillon, M. Marcos, and J. L. Serrano, *Macromolecules*, 2003, **36**, 8368.
43. B. Y. Zhang, J. S. Hu, Y. Wang, and J. H. Qian, *Polym. J. (Japan)*, 2003, **35**, 476.
44. O. Oishi and S. Miyajima, *J. Magn. Reson.*, 2003, **160**, 74.
45. G. R. Luckhurst, B. A. Timimi, T. Miyamoto, and A. Sugimura, *Mol. Cryst. Liq. Cryst.*, 2003, **402**, 339.
46. G. R. Luckhurst and K. Satoh, *Mol. Cryst. Liq. Cryst.*, 2003, **394**, 153.
47. A. M. Kantola, G. R. Luckhurst, B. A. Timimi, and A. Sugimura, *Mol. Cryst. Liq. Cryst.*, 2003, **402**, 353.
48. L. Orian, G. Feio, A. Veron, A. F. Martins, and A. Polimeno, *Mol. Cryst. Liq. Cryst.*, 2003, **394**, 63.
49. D. Catalano, L. Chiezzi, V. Domenici, M. Geppi, and C. A. Veracini, *J. Phys. Chem. B*, 2003, **107**, 10104.
50. V. Domenici, J. Czub, M. Geppi, B. Gestblom, S. Urban, and C. A. Veracini, *Liq. Crys.*, 2004, **31**, 91.
51. D. Frezzato, G. Kothe, D.Frezzato, and G. J. Moro, *Mol. Cryst. Liq. Cryst.*, 2003, **394**, 107.
52. D. Frezzato, G. J. Moro, M. Tittelbach, and G. Kothe, *J. Chem. Phys.*, 2003, **119**, 4060.
53. F. Bonetto, E. Anoardo, and R. Kimmich, *J. Chem. Phys.*, 2003, **118**, 9037.
54. M. Vilfan, G. Lahajnar, I. Zupancic, and B. Zalar, *Magn. Reson. Imaging*, 2003, **21**, 169.
55. R. H. Acosta and D. J. Pusiol, *J. Chem. Phys.*, 2003, **119**, 3461.
56. R. H. Acosta, R. C. Zamar, and G. A. Monti, *Phys. Rev. E: Stat., Nonlinear, Soft Matter Phys.*, 2003, **68**, 41705/1.
57. T. Seki, K. Miyayama, H. Satoh, M. Kanekiyo, K. Hiraoka, and Y. Uematsu, *Jap. J. Applied Phys. Part* 1, 2003, **42**, 3535.
58. M. Perez-Mendez, R. M. Berenguel, L. Garrido, and M. Martin-Pastor, *Macromolecules*, 2003, **36**, 8049.
59. P. Porion, M. Al Mukhtar, A. M. Faugere, R. J. M. Pellenq, S. Meyer, and A. Delville, *J. Phys. Chem. B*, 2003, **107**, 4012.
60. A. Ferrarini, *J. Phys. Chem. B*, 2003, **107**, 7923.
61. A. F. Gross, S. Yang, A. Navrotsky, and S. H. Tolbert, *J. Phys. Chem. B*, 2003, **107**, 2709.
62. A. Svensson, D. Topgaard, L. Piculell, and O. Soderman, *J. Phys. Chem. B*, 2003, **107**, 13241.
63. F. Asaro, G. Pellizer, and B. Pergolese, *Mol. Cryst. Liq. Cryst.*, 2003, **394**, 127.
64. K. I. Momot, P. W. Kuchel, and D. Whittaker, *Langmuir*, 2004, **20**, 2660.
65. C. F. Weise and J. C. Weisshaar, *J. Phys. Chem. B*, 2003, **107**, 6552.

66. L. Coppola, R. Gianferri, I. Nicotera, and C. Oliviero, *Mol. Cryst. Liq. Cryst.*, 2003, **398**, 157.
67. V. Kocherbitov and O. Soderman, *Phys. Chem. Chem. Phys.*, 2003, **5**, 5262.
68. K. Sakurai, Y. Jeong, K. Koumoto, A. Friggeri, O. Gronwald, S. Sakurai, S. Okamoto, K. Inoue, and S. Shinkai, *Langmuir*, 2003, **19**, 8211.
69. S. W. Tam-Chang, I. K. Iverson, and J. Helbley, *Langmuir*, 2004, **20**, 342.
70. M. Sikiric, I. Smit, L. Tusek-Bozic, V. Tomasic, I. Pucic, I. Primozic, and N. Filipovic-Vincekovic, *Langmuir*, 2003, **19**, 10044.
71. P. Kipkemboi, A. Khan, B. Lindman, and V. Alfredsson, *Can. J. Chem.*, 2003, **81**, 897.
72. A. Lovino, C. La Mesa, D. Capitani, and A. L. Segre, *Colloid & Polymer Sci.*, 2003, **281**, 1136.
73. J. Spevacek and L. Hanykova, *Macromol. Symposia*, 2003, **203**, 229.
74. L. M. Bronstein, C. Linton, R. Karlinsey, B. Stein, G. I. Timofeeva, D. I. Svergun, P. I. Konarev, M. Kozin, J. Tomaszewski, U. Werner-Zwanziger, and J. W. Zwanziger, *Langmuir*, 2004, **20**, 1100.
75. F. Cesare-Marincola, G. Saba, and A. Lai, *Phys. Chem. Chem. Phys.*, 2003, **5**, 1678.
76. J. P. Douliez, *Langmuir*, 2004, **20**, 1543.
77. H. Evertsson, P. Stilbs, G. Lindblom, and S. Engstrom, *Colloids Surf., B: Biointerfaces*, 2002, **26**, 21.
78. G. Persson, H. Edlund, H. Amenitsch, P. Laggner, and G. Lindblom, *Langmuir*, 2003, **19**, 5813.
79. F. Caboi, J. Borne, T. Nylander, A. Khan, A. Svendsen, and S. Patkar, *Colloids Surf., B: Biointerfaces*, 2002, **26**, 159.
80. J. da Cruz-Francisco, C. Turner, D. Topgaard, B. Sivik, and B. Bergenståhl, *Colloids Surf., A: Phys. Eng. Aspects*, 2003, **213**, 69.
81. R. Angelico, A. Ceglie, G. Colafemmina, F. Delfine, U. Olsson, and G. Palazzo, *Langmuir*, 2004, **20**, 619.
82. I. C. Malcolm, Y. Z. Wu, and J. Higinbotham, *Solid State Nucl. Magn. Reson.*, 2003, **24**, 1.
83. M. Halter, Y. Nogata, O. Dannenberger, T. Sasaki, and V. Vogel, *Langmuir*, 2004, **20**, 2416.
84. T. Kamo, M. Nakano, W. Leesajakul, A. Sugita, H. Matsuoka, and T. Handa, *Langmuir*, 2003, **19**, 9191.
85. A. Filippov, G. Oradd, and G. Lindblom, *Biophys. J.*, 2003, **84**, 3079.
86. A. Filippov, G. Oradd, and G. Lindblom, *Biophys. J.*, 2004, **86**, 891.
87. B. Y. van Duyl, D. Ganchev, V. Chupin, B. de Kruijff, and J. A. Killian, *FEBS Lett.*, 2003, **547**, 101.
88. R. M. Epand, R. F. Epand, and S. Maekawa, *Chem. Phys. Lipids*, 2003, **122**, 33.
89. R. M. Epand, D. W. Hughes, B. G. Sayer, N. Borochov, D. Bach, and E. Wachtel, *Biochim. Biophys. Acta*, 2003, **1616**, 196.
90. R. M. Epand, *Biophys. J.*, 2003, **84**, 3102.
91. M. J. Swamy, M. Ramakrishnan, D. Marsh, and U. Wurz, *Biochim. Biophys. Acta*, 2003, **1616**, 174.
92. J. Prades, S. S. Funari, P. V. Escriba, and F. Barcelo, *J. Lipid Research*, 2003, **44**, 1720.
93. K. Gawrisch, N. V. Eldho, and L. L. Holte, *Lipids*, 2003, **38**, 445.
94. S. R. Shaikh, V. Cherezov, M. Caffrey, W. Stillwell, and S. R. Wassall, *Biochemistry*, 2003, **42**, 12028.
95. J. A. G. Areas and A. Watts, *Magnetic Resonance in Food Science Spec. Publ. R.S.C.*,

2002, **286**, 70.
96. K. G. Valentine, M. F. Mesleh, S. J. Opella, M. Ikura, and J. B. Ames, *Biochemistry*, 2003, **42**, 6333.
97. T. W. Allen, O. S. Andersen, and B. Roux, *J. Am. Chem. Soc.*, 2003, **125**, 9868.
98. M. R. Morrow, N. Abu-Libdeh, J. Stewart, and K. M. W. Keough, *Biophys. J.*, 2003, **85**, 2397.
99. A. Pampel, J. Karger, and D. Michel, *Chem. Phys. Lett.*, 2003, **379**, 555.
100. Q. Dai, J. Zajicek, F. J. Castellino, and M. Porok, *Biochemstry*, 2003, **42**, 12511.
101. C. Tian, P. F. Gao, L. H. Pinto, R. A. Lamb, and T. A. Cross, *Protein Science*, 2003, **12**, 2597.
102. K. A. Henzler-Wildman, D. K. Lee, and A. Ramamoorthy, *Biochemistry*, 2003, **42**, 6545.
103. A. V. Agasoster, O. Halskau, E. Fuglebakk, N. A. Froystein, A. Muga, H. Holmsen, and A. Martinez, *J. Biol. Chem.*, 2003, **278**, 21790.
104. A. Vogel, H. A. Scheidt, and D. Huster, *Biophys. J.*, 2003, **85**, 1691.
105. J. J. Buffy, T. Hong, S. Yamaguchi, A. J. Waring, R. I. Lehrer, and M. Hong, *Biophys. J.*, 2003, **85**, 2363.
106. P. V. Dubovskii, D. M. Lesovoy, M. A. Dubinnyi, Y. N. Utkin, and A. S. Arseniev, *Eur. J. Biochem.*, 2003, **270**, 2038.
107. F. Forouhar, W. N. Huang, J. H. Liu, K. Y. Chien, W. G. Wu, and C. D. Hsiao, *J. Biol. Chem.*, 2003, **278**, 21980.
108. I. Marcotte, K. L. Wegener, Y. H. Lam, B. C. S. Chia, M. R. R. DePlanque, J. H. Bowie, M. Auger, and F. Separovic, *Chem. Phys. Lipids*, 2003, **122**, 107.
109. I. J. Vereyken, V. Chupin, F. A. Hoekstra, S. C. M. Smeekens, and B. deKruijff, *Biophys. J.*, 2003, **84**, 3759.
110. J. S. Santos, D. K. Lee, and A. Ramamoorthy, *Magn. Reson. Chem.*, 2004, **42**, 105.
111. S. Bhattacharya and A. Srivastava, *Langmuir*, 2003, **19**, 4439.
112. G. Althoff, D. Frezzato, G. Kothe, D. Frezzato, G. J. Moro, M. Vilfan, I. Vilfan, O. Stauch, and R. Schubert, *Mol. Cryst. Liq. Cryst.*, 2003, **394**, 93.
113. H. C. Gaede and K. Gawrisch, *Biophys. J.*, 2003, **85**, 1734.
114. H. C. Gaede and K. Gawrisch, *Magn. Reson. Chem.*, 2004, **42**, 115.
115. A. Kennedy, P. J. Hmel, J. Seelbaugh, J. G. Quiles, R. Hicks, and T. J. Reid, *J. Liposome Research*, 2002, **12**, 221.
116. A. Kennedy, C. J. Long, P. J. Hmel, and T. J. Reid, *J. Liposome Research*, 2003, **13**, 259.
117. C. Arnulphi, C. A. Martin, and G. D. Fidelio, *Molecular Membrane Biology*, 2003, **20**, 319.
118. O. Cruciani, L. Mannina, A. P. Sobolev, A. Segre, and P. Luisi, *Langmuir*, 2004, **20**, 1144.
119. C. Rodrigues, P. Gameiro, M. Prieto, and B. de Castro, *Biochim. Biophys. Acta*, 2003, **1620**, 151.
120. J. Du, Y. Chen, Y. Zhang, C. C. Han, K. Fischer, and M. Schmidt, *J. Am. Chem. Soc.*, 2003, **125**, 14710.
121. C. Faure, A. Derre, and W. Neri, *J. Phys. Chem. B*, 2003, **107**, 4738.
122. R. H. Jin, *Macromol. Chem. Phys.*, 2003, **204**, 403.
123. E. Perouzel, M. R. Jorgensen, M. Keller, and A. D. Miller, *Bioconjugate Chem.*, 2003, **14**, 884.
124. D. Tyteca, A. Schanck, Y. F. Dufrene, M. Deleu, P. J. Courtoy, P. M. Tulkens, and M. P. Mingeot-Leclercq, *J. Membr. Biol.*, 2003, **192**, 203.
125. D. J. Semchyschyn and P. M. Macdonald, *Magn. Reson. Chem.*, 2004, **42**, 89.

126. J. F. Ellena, M. C. Burnitz, and D. S. Cafiso, *Biophys. J.*, 2003, **85**, 2442.
127. F. Aussenac, M. Laguerre, J. M. Schmitter, and E. J. Dufourc, *Langmuir*, 2003, **19**, 10468.
128. G. Zandomeneghi, M. Tomaselli, P. T. F. Williamson, and B. H. Meier, *J. Biomol. NMR*, 2003, **25**, 113.
129. G. Zandomeneghi, P. T. F. Williamson, A. Hunkeler, and B. H. Meier, *J. Biomol. NMR*, 2003, **25**, 125.
130. J. A. Whiles, R. Deems, R. R. Vold, and E. A. Dennis, *Bioorganic Chem.*, 2002, **30**, 431.
131. H. Sasaki, S. Fukuzawa, J. Kikuchi, S. Yokoyama, H. Hirota, and K. Tachibana, *Langmuir*, 2003, **19**, 9841.
132. A. Andersson and L. Maleer, *FEBS Lett.*, 2003, **545**, 139.
133. N. Funasaki, M. Fukuba, T. Kitagawa, M. Nomura, S. Ishikawa, S. Hirota, and S. Neya, *J. Phys. Chem. B*, 2004, **108**, 438.
134. L. Galantini and N. V. Pavel, *J. Chem. Phys.*, 2003, **118**, 2865.
135. J. Tarus, S. A. Shamsi, K. Morris, R. A. Agbaria, and I. M. Warner, *Langmuir*, 2003, **19**, 7173.
136. D. Danino, D. Weihs, R. Zana, G. Oradd, G. Lindblom, M. Abe, and Y. Talmon, *J. Colloid Interface Sci.*, 2003, **259**, 382.
137. X.-Y. Yang, X.-L. Tan, H.-Z. Yuan, S.-Z. Mao, S. Zhao, L. Zhang, J.-Y. An, J.-Y. Yu, and Y.-R. Du, *Bopuxue Zazhi*, 2003, **20**, 329.
138. H. Z. Yuan, X. L. Tan, G. Z. Cheng, S. Zhao, L. Zhang, S. Z. Mao, J. Y. An, J. Y. Yu, and Y. R. Du, *J. Phys. Chem. B*, 2003, **107**, 3644.
139. X. Y. Yang, H. C. Gao, H. L. Tan, H. Z. Yuan, G. Z. Cheng, S. Z. Mao, S. Zhao, L. Zhang, J. Y. An, J. Y. Yu, and Y. R. Du, *Colloid & Polymer Sci.*, 2004, **282**, 280.
140. G. Persson, H. Edlund, E. Hedenstrom, and G. Lindblom, *Langmuir*, 2004, **20**, 1168.
141. M. V. Popova, Y. S. Tchernyshev, and D. Michel, *Langmuir*, 2004, **20**, 632.
142. S. Shimizu, P. A. R. Pires, H. Fish, T. K. Halstead, and O. A. El Seoud, *Phys. Chem. Chem. Phys.*, 2003, **5**, 3489.
143. S. Shimizu, P. A. R. Pires, and O. A. El Seoud, *Langmuir*, 2003, **19**, 9645.
144. S. Mele, S. Murgia, and M. Monduzzi, *J. Fluorine Chem.*, 2004, **125**, 261.
145. U. R. M. Kjellin, J. Reimer, and P. Hansson, *J. Colloid Interface Sci.*, 2003, **262**, 506.
146. C. Whiddon, J. Reimer, and O. Soderman, *Langmuir*, 2004, **20**, 2172.
147. S. J. Kwak and M. Lafleur, *Macromolecules*, 2003, **36**, 3189.
148. E. Caponetti, D. Chillura-Martino, C. La Mesa, R. Muzzalupo, and L. Pedone, *J. Phys. Chem. B*, 2004, **108**, 1214.
149. D. M. Shackleford, R. J. Prankerd, M. J. Scanlon, and W. N. Charman, *Pharm. Res.*, 2003, **20**, 465.
150. S. Kwon, J. H. Park, H. Chung, I. C. Kwon, S. Y. Jeong, and I. S. Kim, *Langmuir*, 2003, **19**, 10188.
151. J. Li, X. Ni, X. Li, Z. Zhou, and K. W. Leong, *Polym. Preprint A.C.S.*, 2003, **44**, 707.
152. H. J. Liu, L. H. Lin, and K. M. Chen, *Colloids Surf., A: Phys. Eng. Aspects*, 2003, **215**, 213.
153. M. Summers, J. Eastoe, and R. M. Richardson, *Langmuir*, 2003, **19**, 6357.
154. S. Yusa, Y. Shimada, Y. Mitsukani, T. Yamamoto, and Y. Morishima, *Macromolecules*, 2003, **36**, 4208.
155. S. Dai, P. Ravi, K. C. Tam, B. W. Mao, and L. H. Gan, *Langmuir*, 2003, **19**, 5175.
156. M. L. Adams and G. S. Kwon, *J. Biomaterial Sci., Polym. Ed.*, 2002, **13**, 991.
157. E. Pettersson, D. Topgaard, P. Stilbs, and O. Soderman, *Langmuir*, 2004, **20**, 1138.

158. P. C. Griffiths, A. Y. F. Cheung, C. Farley, A. Paul, R. K. Heenan, S. M. King, E. Pettersson, P. Stilbs, and R. Ranganathan, *J. Phys. Chem. B*, 2004, **108**, 1351.
159. K. Miyazawa and F. M. Winnik, *Progr. Colloid & Polym. Sci.*, 2003, **122**, 149.
160. M. E. Amato, E. Caponetti, D. Chillura-Martino, and L. Pedone, *J. Phys. Chem. B*, 2003, **107**, 10048.
161. K. Nakamura, K. Yamanaka, and T. Shikata, *Langmuir*, 2003, **19**, 8654.
162. X. W. Fang, S. Zhao, S. Z. Mao, J. Y. Yu, and Y. R. Du, *Colloid & Polymer Sci.*, 2003, **281**, 455.
163. M. S. Bakshi, I. Kaur, R. Sood, and K. Singh, *Colloid & Polymer Sci.*, 2003, **281**, 771.
164. M. S. Bakshi and I. Kaur, *Colloid & Polymer Sci.*, 2003, **281**, 935.
165. M. S. Bakshi, I. Kaur, and R. Sood, *Colloid & Polymer Sci.*, 2003, **281**, 928.
166. M. S. Bakshi and I. Kaur, *Colloids Surf., A: Phys. Eng. Aspects*, 2003, **224**, 185.
167. M. S. Bakshi and I. Kaur, *Progr. Colloid & Polym. Sci.*, 2003, **122**, 37.
168. S. R. Patil, T. Mukaiyama, and A. K. Rakshit, *J. Surf. Deterg.*, 2004, **7**, 87.
169. A. Stenstam, D. Topgaard, and H. Wennerstrom, *J. Phys. Chem. B*, 2003, **107**, 7987.
170. B. Sesta, G. Gente, A. Iovino, F. Laureti, P. Michiotti, O. Paiusco, A. C. Palacios, L. Persi, A. Princi, S. Sallustio, C. Sarnthein-Graf, A. Capalbi, and C. LaMesa, *J. Phys. Chem. B*, 2004, **108**, 3036.
171. A. Accardo, D. Tesauro, P. Roscigno, E. Gianolio, L. Paduano, G. D'Errico, C. Pedone, and G. Morelli, *J. Am. Chem. Soc.*, 2004, **126**, 3097.
172. S. C. Lee, C. Kim, I. C. Kwon, H. Chung, and S. Y. Jeong, *J. Controlled Release*, 2003, **89**, 437.
173. A. Magnusdottir, M. Masson, and T. Loftsson, *J. Inclus. Phenom.& Macrocyclic Chem.*, 2003, **44**, 213.
174. S. Bhadra, D. Bhadra, and G. P. Agrawal, *Indian J. Pharm. Sci.*, 2003, **65**, 139.
175. T. S. Wiedmann, W. Liang, and L. Kamel, *Pharm. Res.*, 2002, **19**, 1203.
176. A. R. Bilia, M. C. Bergonzi, F. F. Vincieri, P. Lo Nostro, and G. A. Morris, *J. Pharm. Sci.*, 2002, **91**, 2265.
177. S. C. Chi, D. I. Yeom, S. C. Kim, and E. S. Park, *Archives Pharm. Research*, 2003, **26**, 173.
178. N. Bhattarai, S. R. Bhattarai, M. S. Khil, D. R. Lee, and H. Y. Kim, *European Polym. J.*, 2003, **39**, 1603.
179. A. Mascioni, F. Porcelli, U. Ilangovan, A. Ramamoorthy, and G. Veglia, *Biopolymers*, 2003, **69**, 29.
180. A. Andersson, J. Almqvist, F. Hagn, and L. Maler, *Biochim. Biophys. Acta*, 2004, **1661**, 18.
181. M. Lindberg, H. Biverstahl, A. Graeslund, and L. Maeler, *European J. Biochem.*, 2003, **270**, 3055.
182. P. Roscigno, F. Asaro, G. Pellizer, O. Ortona, and L. Paduano, *Langmuir*, 2003, **19**, 9638.
183. K. H. Lee, S. Y. Shin, J. E. Hong, S. T. Yang, J. I. Kim, K. S. Hahm, and Y. Kim, *Biochem. Biophys. Res. Commun.*, 2003, **309**, 591.
184. M. Miskolzie, S. Lucyk, and G. Kotovych, *J. Biomol. Struc. & Dynamics*, 2003, **21**, 341.
185. Y. Zuev, D. Faizullin, B. Idiyatullin, F. Mukhitova, J. M. Chobert, V. Fedotov, and T. Haertle, *Colloid & Polymer Sci.*, 2004, **282**, 264.
186. M. Kurakake, H. Hagiwara, and T. Komaki, *Cereal Chemistry*, 2004, **81**, 108.
187. W. H. Otto, D. J. Britten, and C. K. Larive, *J. Colloid Interface Sci.*, 2003, **261**, 508.
188. C. Fernandez and K. Wuthrich, *FEBS Lett.*, 2003, **555**, 144.
189. C. Hilty, G. Wider, C. Fernandez, and K. Wuthrich, *J. Biomol. NMR*, 2003, **27**, 377.

190. J. Zamoon, A. Mascioni, D. D. Thomas, and G. Veglia, *Biophys. J.*, 2003, **85**, 2589.
191. C. Renner, S. Fiori, F. Fiorino, D. Landgraf, D. Deluca, M. Mentler, K. Grantner, F. G. Parak, H. Kretzschmar, and L. Moroder, *Biopolymers*, 2004, **73**, 421.
192. G. Wider, *Magn. Reson. Chem.*, 2003, **41**, S56.
193. M. Uteng, H. H. Hauge, P. R. L. Markwick, G. Fimland, D. Mantzilas, J. Nissen-Meyer, and C. Muhle-Goll, *Biochemistry*, 2003, **42**, 11417.
194. R. P. Hicks, E. Mones, H. Kim, B. W. Koser, D. A. Nichols, and A. K. Bhattacharjee, *Biopolymers*, 2003, **68**, 459.
195. T. L. Whitehead, L. M. Jones, and R. P. Hicks, *J. Biomol. Struc. & Dynamics*, 2003, **21**, 567.
196. M. M. Palian, V. I. Boguslavsky, D. F. O'Brien, and R. Polt, *J. Am. Chem. Soc.*, 2003, **125**, 5823.
197. R. Angelico, D. Burgemeister, A. Ceglie, U. Olsson, G. Palazzo, and C. Schmidt, *J. Phys. Chem. B*, 2003, **107**, 10325.
198. M. L. Sommerville, C. S. Johnson Jr., J. B. Cain, F. Rypacek, and A. J. Hickey, *Pharm. Dev. Technol.*, 2002, **7**, 273.
199. C. J. Ko, Y. J. Ko, D. M. Kim, and H. J. Park, *Colloids Surf., A: Phys. Eng. Aspects*, 2003, **216**, 55.
200. J. Reimer, O. Soderman, T. Sottmann, K. Kluge, and R. Strey, *Langmuir*, 2003, **19**, 10692.
201. V. Challa, K. Kuta, S. Lopina, H. M. Cheung, and E. von Meerwall, *Langmuir*, 2003, **19**, 4154.
202. C. M. Rohloff, J. W. Shimek, and S. R. Dungan, *J. Colloid Interface Sci.*, 2003, **261**, 514.
203. J. Eastoe, M. Sanchez-Dominguez, H. Cumber, G. Burnett, P. Wyatt, and R. K. Heenan, *Langmuir*, 2003, **19**, 6579.
204. J. Eastoe, M. S. Dominguez, H. Cumber, P. Wyatt, and R. K. Heenan, *Langmuir*, 2004, **20**, 1120.
205. J. Koetz, C. Gunther, S. Kosmella, E. Kleinpeter, and G. Wolf, *Prog. Colloid Polym. Sci.*, 2003, **122**, 27.
206. E. Johannessen, H. Walderhaug, and B. Balinov, *Langmuir*, 2004, **20**, 336.
207. S. Bhawal, D. Dhoble, and S. Devi, *J. Appl. Polym. Sci.*, 2003, **90**, 2593.
208. C. C. Blackwell, S. N. Shah, S. Mendon, K. Diamond, O. W. Smith, and S. F. Thames, *Polym. Preprint A.C.S.*, 2003, **44**, 880.
209. Z. Xu, J. An, L. Zhang, S. Zhao, and J. Yu, *J. Dispersion Sci. Technol.*, 2003, **24**, 803.
210. J. Plass and D. Emeis, *NATO Sciences Series, Series, II: Mathematics, Physics and Chemistry*, 2002, **76**, 375.
211. M. A. d'Avila, N. C. Shapley, J. H. Walton, R. J. Phillips, S. R. Dungan, and R. L. Powell, *Phys. Fluids*, 2003, **15**, 2499.
212. C. Malmborg, D. Topgaard, and O. Soderman, *J. Colloid Interface Sci.*, 2003, **263**, 270.
213. E. H. Liu, P. T. Callaghan, and K. M. McGarth, *Langmuir*, 2003, **19**, 7249.

15
Paramagnetic NMR

BY R. R. SHARP

1 Introduction

NMR of paramagnetic systems continues to be a highly active field, indicative of the richness of the physics of coupled electron-nuclear spin systems and the importance of paramagnetic metal ions in chemistry and biochemistry. Intensive work continues on the optimization of paramagnetic complexes for use as clinical MRI contrast agents. Because of the high level of current interest in contrast agent development, this area will be reviewed first. Important advances have occured in a number of other areas, among which the development of new methodologies for determining solution structures of paramagnetic proteins has been particularly active. Determination of the protein structure near a paramagnetic center has historically been difficult because the standard techniques of spectral assignment and NOE-based distance constrants used for diamagnetic proteins are not readily applied to paramagnetically perturbed resonances. However, new kinds of paramagnetism-based distance constraints have been devised, and suitable approaches now appear to be available for all but the most difficult cases.

The review covers the primary refereed literature and scholarly review articles between June, 2002, and May, 2004. Patent applications, meeting abstracts and dissertations are not included.

2 MRI Contrast Agents

2.1 Optimization of Gd Complexes. – Paramagnetic metal complexes that are strong NMR relaxers of solvent protons are widely used clinically as MRI contrast agents, and a great deal of recent work has been directed toward optimizing Gd complexes for this purpose. Current commercial contrast agents are based on Gd(III), which, because of its half-filled f-shell, has a large magnetic moment and exceptionally long electron spin relaxation times, typically 3-4 orders of magnitude longer than for other lanthanides (except Eu(II), which is a very strong reducing agent). Two contrast agents used clinically are Gd-DOTA

Nuclear Magnetic Resonance, Volume 34
© The Royal Society of Chemistry, 2005

(I) and Gd-DTPA (VII), both of which are octadentate and bear one exchangeable water molecule. Synthetic work directed toward improving the MRI properties of Gd complexes continues. In clinical applications, small dosage, reasonable aqueous solubility, good metal retention, and high proton relaxivity are obviously desirable. In addition, proton relaxivity depends on several physical parameters, including the number of exchangeable water molecules, the chemical exchange residence time of bound water, the electron-nuclear interspin distance, the reorientational correlation time, and the electron spin relaxation time. Various aspects of contrast agent research have recently been reviewed.[1,2,3,4,5]

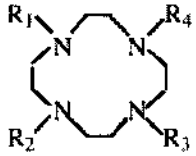

(I) DOTA, all R_i = $-CH_2COOH$
(II) DO3A: like DOTA but R_1=H
(III) DO2A: like DOTA but R_1, R_2=H
(IV) DOTAM, all R_i = $-CH_2CONH_2$
(V) HPDO3A: like DOTA but R_1= $-CH_2CHOHCH_3$
(VI) DOTP: all R_i = $-CH_2PO(OH)_2$

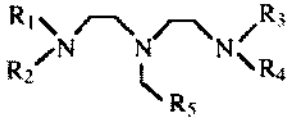

(VII) DTPA, all R_i = $-CH_2COOH$
(VIII) DTPA-BMA: like DTPA but R_1, R_3 = $-CH_2CONHCH_3$

2.1.1 Interspin Distance. The interspin distance between the electron spin (which is assumed to be located at the metal nucleus) and the protons of metal-bound waters have in most studies been inferred from crystal structure data. However, proton positions are usually not determined directly by x-ray diffraction, and distances may differ in crystal and solution phases. Noting that complexes that have similar correlation times and the same number of bound waters often exhibit proton relaxivities that differ by factors of as much as three, Atashkin *et al.*[6] and Caravan *et al.*[7] have explored the possibility that these differences reflect variability in the interspin distance (which enters as r^{-6}). They used pulsed ENDOR to measure the Gd-water proton distance in glasses of Gd^{3+}(aq) and five Gd contrast agents. They find a single distance, r(Gd-H) = 0.31 ± 0.01 nm, for all of these species.

2.1.2 Electron Spin Relaxation. Proton relaxivity also depends on electron spin relaxation, which is in general a multi-exponential, magnetic field-dependent phenomenon. Electron spin relaxation in Gd chelates, which are $S = 7/2$ species, is a complex phenomenon that depends on stochastic zero field splitting (zfs) interactions, which may arise from both (1) collisional distortion of the zfs tensor and (2) Brownian reorientation of the zfs principal axes. The importance of both mechanistic contributions has been emphasized in recent study of electron spin relaxation in $Gd(DOTA)^{2-}$ and $Gd(DPTA)^{-}$ by Borel *et al.*,[8] which reanalyses

multifrequency ESR linewidth data and longitudinally detected ESR T_{1e} data using recent theory.

2.1.3 Isomers and Conformations. Lanthanide chelates of DOTA-like macrocycles exhibit interesting conformational equilibria involving twists of both the tetraazamacrocycle moiety and the side-arm conformations that induce chirality in the chelate. Ln(DOTA) complexes exist in solution as a mixture of two enantiomeric pairs of diastereoisomers differing in the ligand conformation termed square antiprismatic (SA) and twisted square antiprismatic (TSA) geometries. In addition, there is an equilibrium between 9- and 8-coordinate species. Benetollo *et al.*[9] have obtained crystal structures of six Ln(DOTA) complexes representative of all four coordination geometry typologies. Woods *et al.*[10] have shown that different coordination isomers (SA and TSA) of Eu(III) and Gd(III) DOTA complexes may be isolated by choosing substituents on the ring and arms. Substituents with identical chirality produced the twisted square antiprism, while opposite chirality produced the square antiprism. Water exchange rates of the two coordination isomers were found to differ by an order of magnitude. In further work, Woods *et al.*[11] have found that functionalization of the DOTA macrocycle with a *p*-NO_2-benzyl substituent increases the population of the square antiprism and locks the ring into the (δδδδ) configuration.

Terreno *et al.*[12] have investigated the coordination equilibria of three Gd- and Yb-tetraazamacrocyclic chelates by proton NMR. Burai *et al.*[13] have separated the diastereomers of two Ln(III)-EPTPA (EPTPA = ethyleneprophylene triamine pentaacetate) derivatives by HPLC and measured the water exchange rate of the diastereomers by ^{17}O NMR. The EPTPA ligand has been shown to provide rapid water exchange and hence potentially high proton relaxivity.
Internal molecular motions and conformational equilibria of lanthanide chelates often have a marked influence on proton relaxivity. These internal motions have been studied by Yerly *et al.*,[14,15] who used MD simulation to assist the interpretation of proton NMR relaxivity data for several Gd(III) complexes currently used as contrast agents. Yerly *et al.*[16] have also used MD in conjunction with ^{1}H and ^{17}O NMR to study conformational equilibria of binuclear polyaminocarboxylate lanthanide

2.1.4 Integrated Data Analysis. X-ray crystal structures and *ab initio* calculations of conformational barriers likewise provide related information which strengthens the analysis. In addition, variable pressure NMR relaxation measurements provide insight into the chemical exchange reaction mechanism, demonstrating whether a dissociative or associative mechanism is involved (*i.e.*, whether the solvent coordination number increases or decreases in the activated complex). Increasingly, the interpretation of NMR relaxation data is approached as a comprehensive study involving the simultaneous analysis of NMR (^{1}H, ^{17}O, and occasionally ^{13}C) and ESR data sets, any of which can be measured as a function of magnetic field strength, temperature, and (for NMR data) pressure. A comprehensive mechanistic analysis of this sort of course imposes much tighter constraints on the analysis than do NMRD data alone.

Dunand *et al.*[17] describe a global analysis of EPR, ^{17}O NMR relaxation and chemical shift and proton NMRD profiles for aqueous $[Gd(DOTA)(H_2O)]^-$ and $[Gd(DTPA)(H_2O)]^{2-}$ The analysis is more detailed than in previous studies in that it incorporates theoretical advances in EPR relaxation theory (primarily involving the reorientation of the static zfs tensor) as well as the results of MD simulations describing the internal motions of bound water. The authors conclude that complexes in which Gd is in a symmetric chemical environment should have relatively long electron spin relaxation times, thus enhancing proton relaxivity. They also conclude that, because of permanent zfs interactions, very low frequency NMRD-data and slowly tumbling complexes cannot be analysed by their methods.

2.1.5 Water Chemical Exchange Rate. Fast chemical exchange of coordinated water usually correlates with high proton relaxivity (although in CEST-MRI, the reverse is true – slow chemical exchange is desirable). The chemical exchange rate in various Gd-chelates can vary from the low nsec to low microsecond timescale, depending of the chemical environment of the metal ion. In large aggregates with long reorientational correlation times, the relaxivity of Gd complexes is generally limited by the chemical exchange rate. Solvent exchange on metal ions has been reviewed by Dunand *et al.*[18], and the use of variable pressure measurements in mechanistic studies have been reviewed by Helm and Merbach[19]. Thompson *et al.*[20] have studied an 8-coordinate Gd complex, the metal coordination sphere of which contains six coordinating oxo groups plus two exchangeable waters. The water exchange rate, determined from ^{17}O T_2 measurements, is high, as is the thermodynamic stability.[21] The combination of rapid chemical exchange, good thermodynamic stability, and two, rather than one, exchangeable water ligands makes this complex interesting from the standpoint of next generation contrast agents.

Laus *et al.*[22] and Ruloff *et al.*[23] have pursued a strategy for increasing the water chemical exchange rate by modifications in the ligand that result in steric crowding of the water. Increased crowding also causes the chemical exchange mechanism to change from dissociative to associative. The authors show that two new ligands prepared by modification of the parent ligands (DTPA, DOTA, or TRITA) exhibit the predicted enhancement of water exchange rate and the predicted change of mechanism. Aime *et al.*[24] have studied the factors that control the rate of exchange of the axial water of a series of lanthanide complexes with ligands based on the DOTAM tetraazamacrocycle (IV). They conclude that the exchange rate is controlled by the extent of second sphere hydration, which is determined by hydrophobicity of the complex and by the counter-ion. Kruk and Danuta[25] have formulated a theoretical model of outer sphere paramagnetic relaxation enhancement for Gd(III) complexes.

The ligands DO3A (II) and DO2A (III) are related to DOTA by the removal of 1 (or 2) of the carboxymethyl sidechains. The lower denticity of these ligands results in higher hydration numbers. Terreno *et al.*[26] find that the rate of exchange of the two waters coordinated to the Gd(III) center in neutral complexes with heptadentate DO3A derivatives depends on the basicity of the macrocyclic

nitrogen bearing the pendant group: a lower basicity results in a slower water-exchange rate.

Laurent *et al.*[27] and Botteman *et al.*[28] have explored a synthetic strategy to enhance the water exchange rate of the clinical contrast agent, Gd-DTPA, by derivatizing the methylene carbon of the ligand. ^{17}O T_2 measurements confirmed that the rate of water exchange is enhanced in two bisamide esters of DTPA (VIII), which were functionalized at the C_4 methylenic carbon. In complexes with slow water exchange rates, such as *bis*-amide derivatives of DTPA, prototropic chemical exchange, which is a pH-dependent process, can contribute significantly to τ_M. Aime *et al.*[29] have measured the prototropic exchange rate in Gd chelates to assess whether this mechanism can be controlled by chemical modification.

2.1.6 New GD Ligands. New ligands with improved properties have been reported[30,31,32,33,34]. Feng *et al.*[35] have characterized two polyoxometalates of Gd(III), $Gd_2P_2W_{18}O_{62}$ and $K_{15}[(GdO)_3(PW_9O_{34})_2]$, both of which have higher molar relaxivities than the clinical contrast agent, Gd-DTPA. Ruloff *et al.*[36] have synthesized a novel trinuclear metal complex containing one Fe(III) and two Gd(III) ions. Mayoral *et al.*[37] describe a series of new Gd mixed ligands with N-donor atoms which display enhanced proton relaxivity, apparently due to increased solvent exchange rate and slowed reorientation. Monzani *et al.*[38] describe a new Gd ligand with N5O3 donor atoms and high proton relaxivity.

2.2 Macromolecular Agents. – Efforts to increase the relaxivity of Gd complexes have focused on slowing molecular reorientation (see review by Aime *et al.*[39]). Vander Elst *et al.*[40] have prepared a hydrophilic derivative of Gd-DOTA with a molecular weight of 5.6 kD, which they have characterized by proton relaxometry, by ^{17}O relaxometry (to measure water chemical exchange rates, by pulsed magnetic field gradient spin echo measurements. The reorientational correlation time (9.2 ns) was determined from ^2H T_2's of the labeled La^{3+} analog. Aime *et al.*[41] have prepared and characterized adducts of Gd complexes to cyclodextrin.

2.2.1 Micellar Contrast Agents. One strategy for increasing reorientational correlation time is to incorporate the Gd complex into a micelle. Kimpe *et al.*[42] have prepared Gd-DTPA-BMA (VIII) derivatives which are linked to alkyl chains containing 14, 16 and 18 carbons. These complexes, which were incorporated into mixed micelles and studied by NMRD, display higher relaxivity values than Gd-DTPA. In other studies, Hovland *et al.*[43] have prepared an amphipathic Gd complex which forms micelles in aqueous solution with low critical micelle concentration and high proton relaxivity. Nicolle *et al.*[44] have studied the factors which control proton relaxivity in a series of micelle-forming Gd-DOTA derivatives which bear alkyl chains, C_{10}-C_{18} in length. Nicolle *et al.*[45] have studied electron spin relaxation of binuclear $Gd(III)_2$ chelates incorporated into micelles. They found that electron-electron dipole-dipole interactions shorten electron spin relaxation times slightly, broadening the ESR linewidths and decreasing proton relaxivity.

2.2.2 Metallofullerenes. Kato *et al.*[46] have synthesized and characterized new water-soluble multi-hydroxyl lanthanoid (La, Ce, Gd, Dy, and Er) endohedral metallofullerenes ($M@C_{82}(OH)_n$) as potential contrast agents. The water proton R_1 relaxivity of the Gd metallofullerene ($R_1 \approx 80$ sec^{-1} mM^{-1}),is significantly higher than that of Gd-DTPA. These complexes are viewed as ideal models for future high relaxivity contrast agents. Bolskar *et al.*47 *and Masafumi et al.*48 have prepared and characterized new water-solubilized paramagnetic endohedral metallofullerenes based on $Gd@C_{60}$, the proton relaxivies of which are comparable to that of clinically used agents.

2.2.3 Nanoparticles. Gossuin *et al.*[49] have studied the physical mechanism of solvent ^1H relaxation due to superparamagnetic particles of apoferritin, a 24-subunit protein aggregate (13 nm diameter) which contains a ferrihydrite ($5Fe_2O_3 - 9H_2O$) mineral core that is 8 nm in diameter. The authors evaluated inner and outer sphere (*i.e.*, chemical exchange-mediated vs diffusive) contributions to the relaxation mechanism through studies in mixed methanol-water solvents. Methanol was assumed to be non-coordinating, so that differences in molar relaxivity of water and methanol protons were attributed to the inner sphere relaxation mechanism of water. Aime *et al.*[50] have prepared a novel contrast agent in which the apoferritin shell is loaded with several molecules of a Gd-chelate (Gd-HPDO3A, V). Water molecules exchange freely between the internal and external spaces, but the chelate does not. The proton relaxivity of the sequestered Gd-chelate is about 20 times greater than that of the unsequestered chelate.

Morales *et al.*[51] report the synthesis and proton relaxivity of colloidal dextran-coated Fe-O nanoparticles approximately 50 nm in diameter with a unimodal size distribution. Kim *et al.*[52]report the synthesis and relaxation properties of starch-coated Fe-O nanoparticles 6 nm in diameter.

2.2.4 Dendrimeric Contrast Agents. A review has been prepared by Kobayashi and Brechbiel[53]. In recent work, Wang *et al.*[54] report the T_1 field dispersion profiles of a new Gd(III) contrast agent prepared from polypropyleneimine dendrimers, generation 2. Yordanov *et al.*[55] have used Gd(III) dendrimers as biometric nanoprobes to detect vascular permeability. Francese *et al.*[56] have characterized proton relaxivity of PAMAM dendrimers functionalized by nitronyl nitroxide radicals.

Maliakal *et al.*[57] have studied the proton relaxivity produced by dinitroxide spin labels attached to poly(propylene imine) dendrimers as potential MRI contrast agents. They find that proton relaxivity, which is substantially higher than for mononitroxide spin labels, is not seriously affected by electron self-exchange.

2.3 Intelligent Contrast Agents. – Intellligent contrast agents are those for which the relaxivity reflects local conditions, such as pH, pO_2, temperature, or concentration of a particular metabolite. As an agent which reflects changes in temperature, Muller *et al.*[58] have studied Fe(II)-containing polymers which exhibit a critical spin transition temperature, above which Fe(II) is paramagnetic

(S = 2), below which, it is diamagnetic (S = 0). In the paramagnetic state, the particles enhance R_2* providing contrast. This phenomenon was confirmed in phantoms prepared from cyclohexane solutions.

Li *et al.*[59] have devised an interesting contrast agent that is responsive to Ca^{2+} concentrations. The agent (DOPTA-Gd), contains a pair of chelated Gd(III) which, in the absence of Ca^{2+}, are sequestered from inner sphere water so that the paramagnetic relaxation enhancement results from outer sphere interactions. Ca^{2+} binding induces a conformation change which dramatically increases the accessibility of chelated Gd to the solvent, increasing relaxivity.

Glogard *et al.*[60] have devised a novel contrast agent which is responsive to the concentration of free radicals. They used a Gd-chelate conjugated to a liposome by a disulfide linkage. Radical-induced cleavage of the disulfide bond frees the Gd-chelate from the liposome, reducing its relaxivity (due to faster reorientation). They report *in vitro* tests in which gamma radiation and dithiothreitol were both used to cleave the disulfide bond.

New pH-sensitive contrast agents are reported by Raghunand *et al.*[61], who propose a dual-contrast agent strategy for mapping pH *in vivo*. One agent, Gd-DOTA-4AmP^{5-}, is pH-sensitive, the other, Gd-DOTP^{5-} (VI), is pH-insensitive, the latter providing a baseline response. Woods *et al.*[62] have prepared a new DOTA-based Gd complex that exhibits pH-dependent proton relaxivity. The physical origin of the R_1 enhancement is attributed to a pH-dependent increase of solution structure in the second hydration sphere. Lockling *et al.*[63] describe the optimization of paramagnetic pH-responsive liposomes for use as MRI contrast agent.

2.4 Targeted Contrast Agents. – Woods *et al.*[64] have prepared a review. Corneillie *et al.*[65] have prepared an antibody which selectively binds metallo-DOTA complexes and have determined crystal structures[66] for the Y-DOTA and Gd-DOTA adducts, which are potential docking stations for targeted MRI probes. Pirko *et al.*[67] have used superparamagnetic antibodies specific for cell surface markers to image immune cell location in the central nervous system. They report that superparamagnetic antibodies have excellent T_1, T_2, and T_2* relaxivity, making them ideal for targeted contrast applications. Morawski *et al.*[68]have characterized a highly paramagnetic liquid perfluorocarbon nanoparticle agent 250 nm in diameter that contains >90000 Gd^{3+} per particle. Using this highly potent contrast agent, they were able to quantify molecular epitopes in picomolar concentrations.

Accardo *et al.*[69] report a novel targeting strategy based on the use of mixed micellar aggregates. The micelles were formed from two monomers, both containing C_{18} hydrophobic chains but with different polar head groups. One monomer possessed a DTPA-Gd head group, thus providing MRI contrast, while the other possessed the CCK8 peptide. This peptide displays high affinity for cholecystokinin cell surface receptors, which are over-expressed in a number of tumors. Lattuada and Lux[70] have synthesized a lipophilic Gd-cholesterol complex for use in mixed micelles.

Laurent *et al.*[71] have designed a new contrast agent to target inflammation.

Feng *et al.*[72] have evaluated neutral bis-amide derivates of Gd-DTPA as potential liver-targeting agents. Caravan *et al.*[73] describe a highly relaxive Gd agent that targets DNA. The Gd ligand is a peptide with a helix-turn-helix motif. The relaxivity of the Gd-peptide complex increases 100% upon binding to DNA.

2.4.1 Intracellular Contrast Agent. Allen and Meade[74] describe a Gd(III)-based MR contrast agent conjungated to polyarginine that is able to permeate cell membranes.

2.5 Differentiating Intra- and Extracellular $^{23}Na^+$ and $^{35}Cl^-$. – Chemical shift imaging employing lanthanide shift reagents has also been used to differentiate intracellular and extracellular pools of $^{23}Na^+$ and $^{35}Cl^-$ resonances *in vivo*. Weidensteiner[75] have used the highly negatively charged LSR, $Tm(DOTP)^{5-}$ (VI), to distinguish extracellular from intracellular Na^+. The high charge of this LSR ensures that it is membrane-impermeant, and the negative charge ensures an ion-pair interaction with Na^+. Avicella *et al.*[76] have determined the x-ray crystal structure of the Na^+-$Gd(DOTP)^{5-}$ adduct. Delort *et al.*[77] have compared three different Na^+ lanthanide shift reagents, $(Dy(PPPi)_2^7$, $Tm(DOTP)^{5-}$, and $Dy(TTHA)^{3-}$), in measurements of intracellular Na^+ concentrations in resting cells of Fibrobacter succinogenes S85. Among these reagents, $Tm(DOTP)^{5-}$ gave the most satisfactory results.

Chemical shift reagents which bear a high negative charge are unsuitable for monitoring $^{35}Cl^-$. For this purpose, Diven *et al.*[78] have evaluated the mono-anionic complex, tris-glycinatocobaltate(II), and find that, although the ^{35}Cl chemical shifts are small (smaller than for Co(II)(aq)) this complex offers advantages with respect to chemical stability and also gives narrow ^{35}Cl linewidths.

2.6 Chemical Exchange Saturation Transfer (CEST). – CEST (also referred to as Magnetization Transfer, MT) is a relatively recent T_2 imaging modality, which relies on chemical exchange of solvent protons into a chemically shifted site on the contrast agent (see review by Zhang *et al.*[79]). In the regime of slow chemical exchange ($(\Delta\omega_M)\tau_M > 1$), the solvent and ligand resonances are resolved, and saturation of ligand site can strongly suppress the NMR signal of the solvent. A large chemical shift and a relatively slow chemical exchange rate (which is opposite the requirement for high relaxivity, is required. Seeking to optimize the CEST experiment, Zhang *et al.*[80] have used ^1H and ^{17}O NMR to measure water chemical exchange rates in DOTAM (IV) chelates of a series of lanthanide ions. They found that the water exchange time, τ_M, is longest for Eu(III) and exhibits a sharp break between Eu(III) and Gd(III). Zhang *et al.*[81] have prepared several DOTA-tetra(amide) ligands and have evaluated their Eu(III) chelates as CEST agents.

2.6.1 Intelligent CEST Agents. Aime *et al.*[82] have designed a new Yb(III) CEST agent (MBDO3AM) which responds to lactate concentration. This agent is heptadentate with six exchangeable amide protons, which have been described[83] as providing efficient 'antennae' for the transfer of saturated proton magnetiz-

ation to water. Lactate ion forms a ternary adduct with Yb(III)-MBDO3AM, blocking a coordination site of water. Botta *et al.*[84] have evaluated two heptadentate triamide Gd chelates with respect to ternary complex formation with simple anions and the resulting modulation of proton relaxivity and water exchange rate. Dickens *et al.*[85] have used ^{1}H and ^{17}O NMR in conjunction with X-ray structure analysis and CD to examine the nature of aqueous ternary complexes formed on reversible binding of acetate, lactate, citrate, amino acids and peptides to chiral diaqua europium, gadolinium, or ytterbium chelates.

Zhang *et al.*[86] have developed a CEST agent that responds to glucose concentration. The agent is 9-coordinate with a single bound water molecule, the proton resonance of which is 50 ppm upfield of TMS. The pendant sidearms of the complex contain boronic acids, which bind selectively and reversibly to structures containing cis-diols. The presence of glucose slowed the chemical exchange rate of bound water molecule, and the resulting change in CEST ratio was readily observed in phantom studies. Aime *et al.*[87] descibe a pH-responsive CEST agent. Aime *et al.*[88] describe a CEST agent based on supramolecular reversible adducts between poly-L-arginine and $[Tm(III)(HDOTP)]^{4-}$.

2.7 Non Gd-Based Contrast Agents. – *2.7.1 Eu(II) Complexes.* Most MR contrast agent work has centered on complexes of Gd(III). Eu(II) is isoelectronic with Gd(III) and likewise has very long electron spin relaxation times, hence the potential for producing high water proton relaxivity. Because of the lower ionic charge and long Eu-O distance, chemical exchange rates of Eu(II)-bound water are rapid, further enhancing proton relaxivity. However, Eu(II) is a highly reducing species. Burai *et al.*[89] have prepared an interesting cryptate of Eu(II) which is relatively stable against oxidation, has two inner sphere waters, and rates of water chemical exchange and electron spin relaxation that are nearly optimal with respect to proton relaxivity. This agent is also pO_2-responsive. In another study, Burai *et al.*[90] have characterized the redox stability and water exchange rates of Eu(II)-DOTA and Eu(II)-TETA. The former has extremely high water exchange rates, while the latter has no inner sphere bound water.

Moreau *et al.*[91,92] have studied the solution structures of Eu(II) chelates and solvates by XAFS. The Eu(II)$DOTA^{4-}$, $DTPA^{5-}$ and $ODDA^{2-}$ chelates were found to adopt the twisted-square antiprism conformation because of the large radius of the metal ion.

2.7.2 Mn(II) Complexes. Mn(II) is a divalent cation which, like Eu(II), exhibits much faster water chemical exchange rates than does Gd(III). Aime *et al.*[93] show that the rapid solvent chemical exchange of Mn(II) can be exploited in slowly rotating macromolecular adducts to produce intrinsic proton relaxivities comparable to those of commercial Gd-based contrast agents. Kruk and Kowalewski[94] have reinterpreted these data using new theoretical models of the motion of the zero field splitting tensor. Other non-Gd based contrast agents have been reviewed[95]. Unchelated Mn(II) forms well-known binary complexes to serum albumin, binding at 1 tight and several loose sites. Aime *et al.*[96] have characterized these by ^{1}H NMRD and by variable temperature ^{17}O R_2 measure-

ments. They report that 3-4 exchangeable waters with rapid chemical exchange kinetics ($\tau_M \approx 22$ nsec) contribute to the proton relaxivity.

Dy(III) acts as a negative (T_2) imaging agent due to its large hyperfine chemical shifts. Vander Elst *et al.*[97] point out that in the regime of fast chemical exchange ($\tau_M < T_{2M}$), the R_2 relaxivity of these agents increases as the square of Zeeman field strength and as the first power of chemical exchange residence time (τ_M). Hence high field strengths and slow chemical exchange are generally desirable as long as $\tau_M < T_{2M}$. They compare five complexes which illustrate both fast and slow exchange behavior.

2.8 Free Radical Imaging (PEDRI). – Endogenous free radicals can in principle be imaged directly by ESR, although clinical applications have not yet emerged because of experimental difficulties, notably the inability of microwaves to penetrate bulky aqueous samples[98]. Nevertheless, direct CW imaging of free radicals can be done at very low field strengths (≈ 20 mT) where the electron spin resonance frequency is <1 GHz. An indirect method relies on PEDRI[99] (Proton Electron Double Resonance Imaging, also called Overhauser MRI), in which the electron spin is saturated during the collection of an MR image, with NOE of the water proton resonance providing contrast enhancement. This experiment can be done with conventional MRI equipment and software, but the problem of irradiating the electron spin at NMR field strengths remains. Lurie *et al.*[100] have modified a 0.38 T whole body imager for operation at 20.1 mT as a small animal PEDRI-imager. Liebgott *et al.*[101],[102] describe a 20.1 mT PEDRI imager, which they have used to image nitroxide free radicals in isolated beating rat hearts and triarylmethyl free radicals in living rat. Guanglong *et al.*[103] describe experimental modifications of a whole-body imager for combined ^{1}H MRI imaging at 16 MHz and free radical ESR imaging at 750 MHz.

2.8.1 ^{19}F PEDRI. Murugesan *et al.*[104] have generated ^{19}F PEDRI images at 15 mT. In these experiments, the enhancement in ^{19}F NMR images depended on the concentration of free radical contrast agent, the pO_2, and the ESR irradiation power. The authors conclude that the sensitivity is sufficient for monitoring ^{19}F tracers. Khramtsov *et al.*[105] have assessed stable nitroxides of imidazoline and imidazolidine types as potential probes of pH and of sulfhydryl groups.

2.8.2 Field-cycling PEDRI. In this technique, the electron spin is initially saturated in a low polarizing field, which is then stepped to a higher value for the MRI scan. Youngdee *et al.*[106], describe a new pulse sequence for rapid imaging of free radicals in field-cycled PEDRI. The sequence optimizes the number of EPR irradiation periods for acceptable S/N and spatial resolution of the final image while reducing the RF power deposition and increasing the temporal resolution.

3 Lanthanide-Induced Shifts (LIS)

3.1 Analysis of LIS data. – Most lanthanide ions possess larger magnetic

moments than d-block ions, and they induce large paramagnetic shifts and relaxation enhancements in nuclear resonances. The LIS depends on the orientation of the interspin vector with respect to the molecular axes, as well as to the interspin distance, and thus the LIS provides a potentially rich source of molecular structure data (both angle and distance) in solution. Although their magnetic properties are complex (L-S coupling does not hold), the chemistry of lanthanides is simplified by the fact that 4f orbitals have relatively small radii and are thought to participate relatively little in chemical bonding. For this reason, the crystal field parameters and hyperfine coupling constants in a series of isostructural lanthanide complexes can be treated approximately as varying linearly across the Lanthanide Series. In addition, it is often assumed that magnetic and electronic parameters of a given lanthanide ion can be transferred from the aquo ion to the complex of interest. The use of paramagnetic NMR lanthanide induced shifts for extracting solution structures has been reviewed[107].

Ren *et al.*[108] have discussed the analysis of LIS data. In complexes with a 3-fold or higher rotational symmetry, the LIS, $\Delta_{a,i}$, can be expressed as a sum of contact and pseudocontact terms:

$$\Delta_{a,i} = F_a \langle S_z \rangle_i + D_i (A_2^\circ \langle r2 \rangle)_i G_a \qquad \text{Eq. (1)}$$

where the subscripts, a and i, label the nuclear spin and the lanthanide ion. The two terms on the r.h.s. describe, respectively, the contact and pseudocontact chemical shifts. F_a is a hyperfine coupling constant, D_i is proportional to the magnetic susceptibility anisotropy of the lanthanide ion, A_2° is the quadratic cylindrical crystal field parameter, and G_a is a molecular structure factor which describes on the orientation of the interspin (electron-nucleus) vector with respect to the molecular z-axis. The molecular structure factor, G_a, is usually of greatest chemical interest. Using NMR data from LIS measurements on a single nuclear resonance, Eq. (1) can be analysed graphically, although the results are not entirely satisfactory, presumably due to breakdown of the assumption that magnetic and crystal field parameters are transferable between lanthanide ions or the assumption that homologous lanthanide complexes are isostructural.

To remove questionable assumptions from the analysis, these authors propose a method that provides ratios of structural factors rather than absolute values. Building on this work, Geraldes *et al.*[109] have developed methods involving chemical shift data for two and three nuclear spins and have applyied these methods to complexes with a 4-fold symmetry axis. In further work[110], the same group has used a combination of 1-, 2- and 3-nucleus methods in the analysis of LIS data for complexes with a C_3 rotation axis.

Oali *et al.*[111] have developed new multi-center methods for analysing LIS data that are appropriate when the paramagnetic complex contains more the one lanthanide ion. Their specific chemical focus involves the solution structures of triple-stranded homotrimetallic lanthanide helicates, $[Ln_3(lig)_3]$, (Ln = Ce-Yb, except Pm, Gd). The multi-center approach incorporates different crystal field parameters for the center and terminal lanthanide ions. In the same study, the authors developed and applied a novel 3-nucleus crystal field-independent method of analysis, which they used to demonstrate that all members of the

homologous series of helicates adopt a single solution structure with D_3 symmetry.

Oali *et al.*[112]have also developed a 3-nucleus crystal-field independent method for the purpose of demonstrating isostructurality in homologous lanthanide complexes in which the paramagnetic ions are in sites of strong orthorhombic symmetry. The method is applied to homologous heterotrimetallic sandwich complexes containing a single lanthanide ion in a site of C_{2v} symmetry plus two diamagnetic Lu^{3+} ions. The treatment is then extended to complexes with two and three paramagnetic centers. Oali *et al.*[113] have also used these techniques to investigate isostructurality of triple-helix lanthanide complexes with 2,6-dipicolinic acid. They find an abrupt variation of crystal field parameter, thus reversing an earlier conclusion that the homologous complexes are isostructural. In both studies, the authors note that variation of the second-rank crystal-field parametersalong the Lanthanide Series prevents reliable structural analyses with the classical one-nucleus equation.

DiBari *et al.*[114] describe a new program, PERSEUS, for solution structures derived from LIS and lanthanide-induced NMR relaxation data.

Ishikawa[115] has a proposed a new method for determining the crystal field parameters, A_2^0, of an isostructural series of lanthanide complexes which utilizes both ^1H paramagnetic chemical shifts and static magnetic susceptibility data. The method has been demonstrated[116] using hetero-dinuclear phthalocyanine complexes which contain a diamagnetic Y(III) and a paramagnetic lanthanide. Ishikawa *et al.*[117] have carried out a detailed experimental and theoretical (DFT) study of ^1H pseudocontact chemical shifts in dinuclear lanthanide complexes with phthalocyanin ligands. In this study, the two lanthanide ions of the dinuclear complex were found to contribute additively to the pseudocontact chemical shift. In another study of homo-dinuclear lanthanide phthalocyanine complexes, Ishikawa *et al.*[118] report the detection of magnetic interactions between lanthanide ions.

3.2 Solution structures deduced from LIS data. – Andre *et al.*[119] have prepared new ditopic trihelicate lanthanide (La-La′-L_3) complexes, which they consider of potential utility as biomedical probes. The solution structures of these species were determined by analyses of lanthanide-induced chemical shifts and proton spin relaxation data of mixed complexes containing one diamagnetic Lu^{3+} ion and one paramagnetic lanthanide ion.

Valencia *et al.*[120] have used proton pseudocontact chemical shift data in conjuction with x-ray crystal structures to determine the solution geometries of the lanthanide complexes with the ligand $Py_2N_6Ac_4$, which contains four acetate pendant arms. The aqueous solution structures of diamagnetic$La^{3+}$and Lu^{3+} complexes were characterized by their COSY NMR spectra. The structures of the paramagnetic complexes were determined by fits of ^1H pseudocontact chemical shift data and spin relaxation data to a model that assumed rhombic magnetic susceptibility tensors.

Lisowsky *et al.*[121] have studied proton pseudocontact chemical shifts in a series of chiral macrocyclic Yb(III) complexes which differ in the axial ligands. They

calculated magnetic susceptibility tensors for each complex. Hussain *et al.*[122] have used ^{1}H pseudocontact shifts to characterize the solution structures of Ln(III) chelates with 2,2′-bipyridine and with 1,10-phenanthroline[123]. Dickens *et al.*[124] have used ^{1}H pseudocontact shifts to characterize the solution structures in ternary adducts composed of a chiral, diaqua-Yb(III) chelate plus one of the 20 common α-amino acids. Babailov and Mainichev[125] have studied the molecular structure, dynamics and paramagnetic properties of lanthanide chelates with crown ethers. Babailov *et al.*[126] have used ^{1}H and ^{13}C NMR to study intramolecular dynamics in tetraoxadiaza macrocycle complexes.

D'Amelio *et al.*[127] have determined the solution structure of the Ca^{2+}-angiotensin complex, using Ce(III) as a paramagnetic surrogate for Ca^{2+}. Distance and angle constraints used in a simulated annealing MD analysis of the complex were provided by ROESY cross-peaks and ^{3}J(HN-H$_\alpha$) coupling constants. Pseudocontact chemical shift measurements were used to determine the dissociation constant and the stoichiometry of the complex.

3.2.1 Determination of Absolute Configuration and Solution Conformation. Abraham *et al.*[128] have employed ^{1}H and ^{13}C lanthanide induced shifts produced by Yb(fod)$_3$ as an experimental probe of the solution conformations of cyclopentanol and *cis*- and *trans*-cyclopentane-1,2-diol. Analysis of the LIS was undertaken in conjunction with molecular mechanics and *ab initio* calculations of structure.

DiBari *et al.*[129] discuss the use of Yb(fod)$_3$ for determining absolute configurations of chiral diols. Analysis of the pseudocontact shifts of protons of the diol provided structural information about the diol-Yb(fod)$_3$ solution complex, from which the absolute configuration of the diol is inferred.

Schenato *et al.*[130] describe the use of Eu(fod)$_3$ in the analysis of the ^{1}H and ^{13}C NMR spectra of *cis* and *trans*-fused β-hydroxydecalones. In this study, the PMLIS algorithm was used to determine the Eu ion position in the complex, from which the relative configurations of the substituents were determined.

4 Characterization of Solution Species

Crans *et al.*[131] propose that paramagnetic ^{1}H NMR provides a simple yet powerful approach to monitoring transition-metal complex stoichiometry and speciation in solution. Their experimental work involves Cr^{3+}, Fe^{3+}, Fe^{2+}, Co^{2+}, and Ni^{2+} complexes of 2,6-pyridinedicarboxylic acid. Panyushkin *et al.*[132] have used ^{1}H NMR to study compexation in solutions containing carboxylic acids and two cations, Mg^{2+} and Tm^{3+}. Kiremire *et al.*[133] describe qualitative trends of paramagnetic chemical shifts in a series of 3-imidazolidine nitroxyl free radical transition metal complexes.

Ebihara *et al.*[134] have used ^{1}H contact chemical shifts to estimate electron spin density on the ligands of a benzylidyne-capped tricobalt cluster.

Yoder *et al.*[135] have used ^{1}H NMR to measure the rates of electron and H-atom self exchange reactions of iron and cobalt coordination complexes.

5 Analytical Applications

5.1 Chemical Shift Reagents. – Chemical shift reagents (CSR) were first proposed about 35 years ago as a means of separating overlapping ^{1}H spectra of solution components. Although these applications have largely been superceeded by developments in 2D NMR and by the availability of higher field spectrometers, CSR applications are still useful in certain problems, particularly those involving chiral resolution. Aspinal[136] has prepared a review of chiral lanthanide complexes and their uses as chemical shift reagents.

Besli *et al.*[137] describe a problem involving the use of CSR to determine meso and racemic forms of diastereoisomers in which the stereogenic centers of the molecules are separated by achiral spacers. In these cases, the NMR signals of both meso and racemic forms of diastereoisomers may exhibit doubling on addition of the CSR. Unequivocal assignments can be made only by characterizing the effects for separate meso and racemic forms.

Smith *et al.*[138] have prepared 11 chiral calix[4]arenes, calix[4]resorcarenes, and anionic cyclodextrin derivatives and investigated the properties of their lanthanide (Yb^{3+}, Dy^{3+}) complexes as chiral lanthanide shift reagents (LSR). Baldovini *et al.*[139] report an application of a camphor-derived chiral complex, $Yb(hfc)_3$ (hfc = tris[3-(heptafluoropropylhydroxymethylene)-(+)-camphorate]) to differentiate the ^{13}C NMR spectra of enantiomers of bornyl acetate.

5.2 T_1 Relaxation Agents. – Fischer *et al.*[140] have studied the use of immobilized free radicals and Gd complexes as relaxation agents to shorten T_1's of analytes in quantitative continuous-flow ^{13}C NMR. Tamburini *et al.*[141] have prepared a schiff base Gd(III) chelate which they propose as a T_1 relaxation agent in standard ^{2}H NMR analyses which identify the natural origin of ethanol from different sources. The ^{2}H NMR technique is well established, but the protocol has the disadvantage of long data collection times (8 hr) due to the long T_1's of ^{2}H.

Fasano *et al.*[142] propose using water proton T_1 measurements in physiological media as a quantitative assay of ferric-heme serum albumin, which has a high intrinsic proton relaxivity.

6 Metallo-porphyrins

Work related to heme proteins is described under Biological NMR. Most of the studies reported in this section relate to Fe(III) porphyrins and are organized according to spin state.

6.1 Low spin Fe(III). – Low spin Fe(III) porphyrinates can have either a $(d_{xy})^2(d_{xz}, d_{yz})^3$ or $(d_{xz}, d_{yz})^4(d_{xy})^1$ electron configuration, the latter being uncommon although stabilized by ruffling of the porphyrin ring. Yatsunyk and Walker[143] have investigated the ground state electron configuration of three sterically crowded low spin Fe(III) porphyrins, one with a ruffled configuration, the other

two saddled. On the basis of ^{1}H NMR and ESR data, they report the first $(d_{xz}, d_{ys})^4(d_{xy})^1$ configuration for a purely saddled geometry and conclude that although a ruffled geometry stabilizes this configuration, it is not required. Using the same decasubstituted porphyrins with axial *bis*(4-cyanopyridine) ligands, the same authors[144] measured the kinetics of ring inversion of the ligand by NOESY spectroscopy.

In low-spin Fe(III)-porphyrins with two cyano axial ligands, the electron configuration often depends on the solvent polarity, changing from $(d_{xy})^2(d_{xz},d_{ys})^3$ in low-polarity aprotic solvents to $(d_{xz},d_{ys})^4(d_{xy})^1$ in protic solvents, evidently due to hydrogen bonding between the solvent and the ligand. Weak hydrogen bonding between a coordinated cyanide and solvent molecules decreases the s-donating and increases the π-accepting ability of the cyanide ligand, thus decreasing the energy difference between the (d_{xz}, d_{ys}) and d_{xy} orbitals. Ikezaki and Nakamura[145] have studied the influence of solvent-cyano hydrogen bonds on the electronic state of low spin Fe(III) porphyrinates with *bis*-cyano ligation. The electron configurations were distinguished primarily on the basis of ^{13}C contact shifts of the *meso* carbons. They conclude that the $(d_{xy})^2(d_{xz}, d_{ys})^3$ configuration is stabilized in non-polar solvents (benzene), the $(d_{xz}, d_{ys})^4(d_{xy})^1$ configuration in dipolar aprotic solvents (DMSO). The same authors[146] have used proton NMR to study related phenomena in Mn(III) porphyrins with mono- and bis-cyano ligation.

Rivera *et al.*[147] have used variable temperature ^{13}C NMR hyperfine chemical shifts to probe the electron spin density in a low-spin Fe(III) porphyrinate that models the hydroperoxide intermediate (FeIII-OOH) of heme oxygenase. Variable temperature NMR measurements, in conjunction with ENDOR, indicated that the ruffled $(d_{xy})^1$ and planar $(d_{xy})^2$ spin states are in thermal equilibrium. The authors suggest that this kind of spin-state equilibrium may be important for enzymatic function. The same group[148] used ^{13}C NMR and pulsed ENDOR to characterize the electronic and spin states of ^{13}C-labeled porphyrin models of the low-spin Fe(III) hydroperoxide intermediate of heme oxygenase. The ferric hydroperoxide intermediate in heme catabolism has also been studied by Caignan *et al.*[149] using ^{13}C NMR.

6.1.1 Quantum Calculations. – Mao *et al.*[150] have carried out density functional calculations of spin density and hyperfine chemical shifts for ^{1}H, ^{13}C, ^{15}N, and ^{19}F in a series of $S = 1/2$, 2, and 5/2 metalloporphyrins as models of heme proteins. Using spin-unrestricted methods together with large, locally dense basis sets, they obtained very good correlations between experimental and theoretical results. The authors conclude that accurate quantum mechanical calculations of chemical shifts are now feasible without the use empirical methods or molecular orbital analyses. Cheng *et al.*[151] report the results of DFT calculations of high-spin ($S = 5/2$) 5- and 6-coordinate ferric porphryins. They relate calculated spin densities and orbital populations to measured NMR chemical shifts and an analysis of chemical bonding.

Johannson *et al.*[152] have carried out Density Functional Theory (DFT) calculations of spin density on low-spin ($S = 1/2$) ferric porphyrins, posing the question

of whether the unpaired electron is localized on the iron atom, as indicated by ESR g-values, or, alternatively, whether the electron is delocalized in porphyrin-centered MO's as indicated by NMR and ENDOR. The calculations show that the integrated spin density at the iron atom is nearly one, in agreement with the ESR, but that significant areas with opposite (β) spin are found along the Fe-N bond axes, thus evoking a need for additional α-spin density to be present in the porphyrin ring, ring substituents, and axial ligands to keep the net amount of unpaired spin exactly one.

6.2 High Spin Fe(III). – Hada[153] has reported the results of quantum chemical calculations of the ^{13}C chemical shift of iron-bound cyano ligands in high-spin Fe(III) porphyrins. The chemical shift, which is extraordinarily large, 2500-4000 ppm, results primarily from the Fermi contact term and reflects unpaired spin density on carbon. Hada explores the origin of the shift in ground and low-lying excited states containing ferric $(d_{xy})^2(d_{xz,ys})^3$ and $(d_{xy})^1(d_{xz,ys})^4$ configurations.

Gandini *et al.*[154] have used proton NMR in conjunction with optical and ESR spectroscopies to determine the solution forms of the water-soluble high-spin ferric porphyrin, *meso*-tetrakis(4-N-methylpyridiniumyl)porphyrin. A number of species were found, both 5- and 6-coordinate, including monomers in several states of protonation and a μ-oxo dimer. Song[155] has used proton NMR to demonstrate the formation of a novel hydride-bonded porphyrin complex in which BH_4 coordinates to the Fe(III) of Fe(III)-tetraphenylporphyrin. Wasser *et al.*[156] report the synthesis and complete proton NMR assignment of μ-oxo (O_2-)-bridged heme/non-heme diiron complexes, which they study as models for the active site of nitric oxide reductase.

6.3 Intermediate S = 3/2 Spin State of Fe(III) and Mixed Spin States. – The intermediate S = 3/2 spin state of Fe(III) porphyrinates usually occurs as a quantum mechanical admixture with the high spin S = 5/2 state. The degree of admixture depends on the peripheral substituents, which, when bulky, induce distortions, usually either ruffling or saddling (S_4), in the porphyrin moiety. Sakai *et al.*[157] have used ^{13}C chemical shifts to probe the electron configuration in distorted Fe(III) porphyrins with the intermediate S = 3/2 spin state. They point out that there are two different electron configurations which can contribute to the intermediate spin state, namely $(d_{xz}, d_{ys})^3(d_{xy})^1(d_z2)^1$ and $(d_{xy})^2(d_{xz},d_{ys})^2(d_z2)^1$. These two configurations are stabilized by peripheriphal substituents which induce, respectively, ruffled and saddled conformations of the porphyrin ring. They probe these configurations in two sterically crowded porphyrins using ^{13}C chemical shifts of the *meso*-CH carbons, which, as pointed out by Nakamura *et al.*[158], are highly sensitive to spin density in the d_{xy} orbital. Other highly ruffled 5- and 6-coordinate Fe(III) porphyrins were studied by the same group[159], again using ^{13}C chemical shifts of the *meso*-carbon in conjunction with ^1H NMR, ESR, and Moessbauer spectroscopies to characterize spin states.

Ikeue *et al.*[160] have characterized temperature-dependent spin crossover processes in a series of saddle-shaped (S_4) ferric porphyrins, using for this purpose proton chemical shifts of the axial ligand resonances. Curie plots showed dra-

matic spin cross-over phenomena between the $(d_{xz},d_{yz})^4(d_{xy})^1$ and $(d_{xy})^2(d_{xz},d_{yz})^3$ electron configurations, which the authors attribute to thermal motions and the influence of rigidity of porphyrin cores in determining the spin crossover pathways.

Garate-Morales *et al.*[161] and Sanchez-Sandoval *et al.*[162] report the preparation and spectroscopic properties of new pinch porphyrins, which have as axial ligands a pair of pyridines joined by a flexible covalent linkage (hence the 'pinch'). The authors used chemical shifts of *meso*-C-H and methyl proton resonances to characterize the mixed spin states (S = 3/2, 5/2) of these compounds.

Ikezaki and Nakamura[163] have prepared a number of mono(imidazole)-ligated complexes of perchloro(*meso*-tetramesitylporphyrinato)iron(III), which they view as models for cytochromes *c'*, a class of heme proteins found in photosynthetic, denitrifying, and nitrogen fixing bacteria, in which the heme iron is pentacoordinated with a solvent-exposed histidine residue as the fifth ligand. The spin states were all quantum mechanical admixtures of (S = 5/2, 3/2) as determined by ^{1}H and ^{13}C NMR, ESR, and solution magnetic moments.

6.3.1 ^{19}F NMR. – Yatsunyk and Walker[164] have explored the utility of ^{19}F chemical shifts for probing spin states of ferric porphyrins. They studied two pentafluorophenyl-substituted Fe(III) porphyrinates, one of which was high-spin (S = 5/2), the other, an admixture of (S = 3/2, 5/2). The chemical shifts were unexpectedly difficult to interpret by straightforward pictures of spin density in specific porphyrin MO's. The relatively large isotropic shifts of the *ortho*-fluorines appear to have a large contribution from either a ligand-centered dipolar shift or a through-space contact shift that results from direct electron cloud overlap of the ortho-fluorines with the pi-system of the porphyrin ring. Song and Yu[165] also investigated ^{19}F chemical shifts of pentafluorophenyl-substituted Fe(III) porphyrins and likewise found that the *o*-phenyl ^{19}F resonances have a substantial contact contribution. They conclude that the large phenyl ^{19}F chemical shifts are sensitive to oxidation and spin states and thus are useful for identifying the electronic structures of Fe(III) and Fe(II) porphyrins.

6.4 Fe(II) porphyrins. –

6.5 Oxaporphyrins, Corroles, and Carbaporphyrins. – *6.5.1 Oxaporphyrins.* Pawlicki, *et al.*[166] have studied oxaporphyrins, in which one of the pyrrole nitrogen atoms of porphyrin is replaced by oxygen. They report the proton NMR properties, including temperature dependence and Curie plots, of high-spin Fe(II) and Fe(III) oxaporphyrins, as well as of a low-spin dicyano Fe(III) oxaporphyrin, using chemical shift data to analyse the electron configurations and spin states of these species. Of particular interest is a tetraaryl Fe(I) porphyrin species which exhibits an unprecedented pattern of ^{1}H pyrrole and furan chemical shifts, Wojaczynski *et al.*[167] report and analyse proton chemical shifts of hydroxy- and oxo-substituted porphyrins.

6.5.2 Corroles. Corroles are related to porphyrins but have a direct link between

two pyrroles. Zakharieva *et al.*[168] have used DFT calculations in conjuction with ^{1}H NMR, magnetic susceptibility and Moessbauer data to probe spin delocalization of Fe(III) corrolates. Steene *et al.*[169] and Cai *et al.*[170] have analysed this question (*i.e.*, the degree to which the corrole ring has π-cation radical character) by DFT calculations and by ^{1}H and ^{19}F NMR chemical shift measurements on fluorine-substituted Cu(II) and Fe(III) corroles. Walker[171] points out that DFT calculations provide spin densities at positions that can be probed by ^{1}H NMR, and that good agreement between calculated spin densities and measured hyperfine shifts leads to increased confidence in the calculated spin densities at positions that cannot be directly probed by ^{1}H NMR. ^{13}C NMR data are needed to probe experimentally the nonprotonated C spin densities.

6.5.3. Carbaporphyrins. Rachlewicz *et al.*[172,173] have prepared new high-spin iron(II) 2-aza-21-carbaporphyrins, in which one of the pyrrole nitrogens is replaced by a methine carbon. This proton lies in an interor site, and its chemical shift is extremely large (812 ppm), indicating an Fe(II) C(21)-H agostic interaction.

7 Biological Applications

The electron spin relaxation times of type II Cu proteins are particularly long, and resonances near the metal center are often may be broadened beyond the limits of detection.

7.1 New Spectral Assignment Techniques for Paramagnetic Proteins. – Resonances near paramagnetic centers of proteins present special challenges requiring new strategies for detection and assignment. Severe line broadening of peaks near the metal center can interfere with detection and frequently suppresses NOE's and coherence transfer.

One important source of distance constraints for paramagnetic proteins are cross correlations between Curie spin relaxation and ^{1}H-X dipolar relaxation (X = ^{1}H, ^{13}C, or ^{15}N). These cross correlations can in principle be detected by the same pulse sequences as are commonly used in diamagnetic systems to detect cross correlation between chemical shift anisotropy and ^{1}H-^{15}N dipolar relaxation. However, in paramagnetic systems, rapid transverse self-relaxation tends to quench the build-up of relaxation allowed coherence transfer. To overcome this problem, Kateb and Piccioli[174] have proposed a modified HSQC experiment to observe and quantify relaxation-allowed coherence transfer before it is quenched by a short T_2.

Since paramagnetic broadening varies as the square of the nuclear gyromagnetic ratio, work has focused experiments involving low-γ nuclei, particularly, ^{13}C and ^{15}N. Bermel *et al.*[175] describe the use of direct detection ^{13}C in 2D NMR experiments (^{13}C-^{13}C COSY, ^{13}C-^{13}C COCAMQ, ^{13}C-^{13}C NOESY) to detect paramagnetically broadened lines in NMR spectra of paramagnetic metalloproteins. Through the use of direct detection probeheads, cryogenic technology,

and ^{13}C band-selective homodecoupling, broadened signals from nuclei as close as 4 Å to the Cu(II) center were detected. Babini *et al.*[176] likewise used direct ^{13}C detection to reduce paramagnetic line broadening. Data are reported for a calcium binding protein (human oncomodulin, substituted by Tb^{3+} at one Ca^{2+} site), for which ^{13}C resonances as close as 5.5 Å to the Tb were detected and used as structural constraints. Pintacuda *et al.*[177] describe a fast structure-based assignment of ^{15}N HSQC spectra of selectively ^{15}N-labeled paramagnetic proteins.

Machonkin *et al.*[178] emphasize the utility of $^{13}C\{^{13}C\}$ 2D NMR for observing the paramagnetically broadened resonances near the metal centers of ferre0doxins. They demonstrate the utility of $^{13}C\{^{13}C\}$ CT-COSY in identifying connectivity information from fast relaxing carbon nuclei on ligands of the metal center. In further work, Machonkin *et al.*[179] describe a six-step strategy based largely on direct-detection of ^{13}C for assigning and detecting paramagnetically broadened resonances in [2Fe-2S] and [4Fe-4S] ferredoxins. Kostic *et al.*[180] propose the use of $^{13}C_{\alpha}\{^{13}C'\}$ and $^{13}C'\{^{15}N\}$ HMQC and MQC experiments for assigning backbone resonances in the neighborhood of a paramagnetic center.

In a review, Nocek *et al.*[181] discuss the use of proton pseudocontact chemical shift data to analyse structural perturbations in proteins that are too large for solution structure determination. The discussion focuses on oxygenated and deoxygenated states of hemoglobin.

7.1.1 Determination of electron spin relaxation times. Electron spin relaxation times of paramagnetic metal centers in proteins can, at least in principle, be determined from NMR relaxation rates. Jensen and Led[182] have discussed four different approaches to this problem based on from NMR T_1 measurements of ^{1}H and ^{15}N backbone nuclei. They conclude that only two of these methods are reliable when reorientation is slow.

7.2 Paramagnetic Constraints for Structure Analysis. – Paramagnetism-based constraints for protein structure determination have been based on hyperfine chemical shifts, paramagnetic relaxation enhancements, residual dipolar couplings due to paramagnetically-induced self-orientation (usually by a lanthanide ion), and by cross correlations between Curie relaxation and dipolar relaxation.[183] Work from the laboratories of Bertini and Luchinat[184,185,186] uses the PARAMAGNETIC-DYANA program to incorporate paramagnetic constraints in the structure determination. Modules containing paramagnetic constraints are also available for the program XPlor-NIH. Comparisons of these two programs give comparable results[187].

Torano *et al.*[188] describe the use of paramagnetism-based constraints for the solution structure of high-spin Fe(III) met-myoglobin. This system is challenging due to the high magnetic anisotropy and relatively long electron relaxation times. The constraints included cross correlation between the internuclear dipole-dipole interaction and the dipole-dipole interaction between nuclear spins and the Curie spin magnetic moment. Pintacuda *et al.*[189] have measured the dipole-dipole-Curie-spin cross-correlated relaxation rates in ^{15}N-HSQC spectra

of low-spin cyano-met-myoglobin and high-spin fluoro-met-myoglobin. These cross-correlation rates are shown to contain long-range angular information about the orientation of the ^1H-^{15}N bond with respect to the iron-^1H vector, and angular information was measurable up to 25 Å.

Barbieri *et al.*[190] describe how a medium-resolution solution structure of a protein (Tb^{3+} substituted calbindin D_{9k}) can be obtained with the sole assignment of the protein backbone and backbone-related constriants if a derivative with a firmly bound paramagnetic metal is available. The following paramagnetism-based constraints were used: 1) pseudocontact shifts, acquired by substituting one (or more) lanthanide(s) in the C-terminal calcium binding site; 2) N-HN residual dipolar couplings due to self-orientation induced by the paramagnetic lanthanide(s); 3) cross-correlations between the Curie and internuclear dipole-dipole interactions; and 4) paramagnetism-induced relaxation rate enhancements. The method is suitable for high molecular weight proteins.

The conformational space sampled by the two-domain protein calmodulin has been explored by an approach based on four sets of NMR observables obtained on Tb^{3+} and Tm^{3+}-substituted proteins. The observables are the pseudocontact shifts and residual dipolar couplings of the C-terminal domain when lanthanide substitution is at the N-terminal domain. Each set of observables provides independent information on the conformations experienced by the molecule. It was found that not all sterically allowed conformations are equally populated. For example, taking the N-terminal domain as the reference, the C-terminal domain preferentially resides in a region of space inscribed in a wide elliptical cone.

Determinations based on this approach include human α-parvalbumin by substitution of Dy^{3+} in a Ca^{2+} binding site[191]; the Rhodopseudomonas palustris cytochrome c_{556}; oxidized cytochrome b_5 and $Met_{80}Ala$ cyano-cytochrome c.[192] Banci *et al.*[193] have determined the solution structure of oxidized cytochrome c_{553} from Bacillus pasteurii.

Assfalg *et al.*[194] have determined the solution structure of ^{15}N enriched yeast iso-1-ferricytochrome c which contained three mutations designed to produce a single conformer. The global structure of the protein was determined using NOE's, backbone angle constraints, and pseudocontact shifts as constraints. Yao *et al.*[195] have determined the solution structure of cyanoferricytochrome c.

Assfalg *et al.*[196] have determined the solution structure of fully oxidized mutant form of cytochrome c_7, which is paramagnetic with three paramagnetic centers. The assignment strategy and the algorithm of an automated program used in the analysis of ^1H NMR spectra are described.

Bertini *et al.*[197] have studied the question of whether reliable models for a protein of unknown structure can be constructed from that of a protein of known structure if the sequence homology is greater than 30%. They modeled the structure of cytochrome c556 on that of cyt c and validated the model using paramagnetic structure constraints (pseudocontact shifts and self-orientation residual dipolar couplings) without determining the full solution structure.

7.2.1 Residual Dipolar Couplings. There is currently a great deal of interest in

macroscopic orientation of samples as a source of residual dipolar couplings as supplemental information in protein structure determinations. Paramagnetic metal ions, particularly (1) Co(II) among the d-block ions and (2) lanthanide ions other than Gd(III), possess highly anisotropic magnetic susceptibility tensors. At high field strengths, these ions have been shown to orient membranes or proteins to which they are attached.

Barbieri *et al.*[198] discuss the problem of determining alignment tensors and propose that since any specific lanthanide ion orients according to its specific magnetic susceptibility tensor, data sets obtained using several lanthanide ions should be analysed using pseudocontact chemical shift data to provide independent knowledge of the magnetic susceptibility anisotropy tensor of each metal. A module of the PARAMAGNETIC-DYANA program is described that incorporates the derived orientations as constraints in the solution structure calculation. The method is applied using calbindin D9k, to which Ce^{3+}, Tb^{3+}, Dy^{3+}, Ho^{3+}, Er^{3+}, Tm^{3+}, and Yb^{3+} are bound in the C-terminal site. Jimenez *et al.*[199] describe the use of this program in analysing early steps of unfolding of the 8.5 kD di-Ca^{2+} binding protein calbindin D9k. Non-conventional distance constraints were obtained from pseudocontact chemical shifts measurements on a modified (1 Ca^{2+}, 1 Ce^{3+}) protein. Allegrozzi *et al.*[200] have also used lanthanide-substituted protein to induce pseudocontact shifts in calbindin D9k. Longinetti *et al.*[201] discuss the uniqueness problem in the localization of some rigid structural elements using constraints available for proteins containing paramagnetic ions. They find that a unique analysis is provided by multiple magnetic tensors and propose a numerical strategy for dealing with multiple datasets.

7.2.2 Paramagnetic Labels. – Paramagnetic probe complexes (such as Me-ETDA) covalently attached to a diamagnetic protein can provide additional constraints for protein structure analysis. Both lanthanide ions and Co(II), have been used as paramagnetic labels. Gochin *et al.*[202] describe a synthetic peptide designed to present an all-leucine core on folding. The folded form, stabilized by Co(II) or Ni(II), exists in solution as a 3-stranded α-helical coiled coil. The solution structure was probed by pseudocontact chemical shifts in the Co(II) complex and by NOE measurements in the Ni(II) complex.

Gaponenko *et al.*[203] describe the labeling of a 123 residue protein with Co(II) *via* a thiol-reactive EDTA. Pseudocontact chemical shifts of methyl and amide protons were used to provide long-range distance constraints, which improved the accuracy of the structure determination. They propose that multiple labeling sites can be serially engineered to obtain data from alternative orientations of the paramagnetic anisotropic susceptibility tensor. The improved accuracy is cross validated by Q-factors determined from residual dipolar couplings measured as a result of magnetic susceptibility alignment.

Lanthanide-labeled proteins present a similar situation, where pseudocontact shifts are large and contact shifts are often small. In addition, the paramagnetic susceptibility tensor of lanthanide ions is expected to be only mildly dependent on chemical environment. Prudencio *et al.*[204] used a caged lanthanide complex, derivatived by two reactive thiol groups, as the paramagnetic probe. Attachment

to the protein occured in a bidentate manner at two cysteines, thus restricting the motion of the probe so that the hyperfine tensor was fixed relative to the protein. The lanthanide probe induced usable residual dipolar couplings at high fields; it also induced pseudocontact shifts in proton resonances as far as 40 Å from the probe.

Gaponenko *et al.*[205] have also demonstrated the use of a paramagnetic label, added sub-stoichiometrically, to disrupt the symmetry in the NMR spectra of homodimers. This approach, of course, requires that the probe reside on only one monomer within the dimer. The pseudocontact shifts induced by the label provide an experimental basis for determining the monomer orientation within the dimer. Goodfellow *et al.*[206] have applied a similar approach to the resolution of the NMR spectra of the homodimer Desulfovibrio gigas desulforedoxin. They studied proteins in which the endogenous [Fe-4S] centers were partially substituted with Zn.

Pintcuda *et al.*[207] have labelled the N-terminal domain of the E. coli arginine repressor with a paramagnetic ion (Co(II), Cu(II), or Mn(II)) by derivatizing a free Cys sidechain with S-cysteaminyl-EDTA. The paramagnetic perturbations were monitored with ^{15}N-HSQC spectra. Co(II) produced significant pseudocontact shifts but also in peak doubling, which was attributed to different stereoisomers. Cu^{2+} and Mn^{2+}, which have slowly relaxing electron spins, did not produce chemical shifts but yielded self-consistent sets of paramagnetic relaxation enhancements of the amide protons, providing accurate distance constraints from 9-25 Å. They comment that these long-range constraints are useful for structures inaccessible to NOEs. These methods were used to refine the structure of a solvent-exposed loop in the N-terminal domain of the E. coli arginine repressor.

Takahisa *et al.*[208] describe an enantiomerically pure EDTA-derived label that aligns more strongly due to a short linker and does not suffer from stereochemical diversity upon lanthanide complexation. They observed residual ^{15}N-^{1}H dipolar couplings as large as 8 Hz at 800 MHz. Woehnert *et al.*[209] have used a protein fusion construct of human ubiquitin with an N-terminal lanthanide binding tag to generate residual dipolar couplings of the protein. The ions Tb^{3+}, Dy^{3+}, and Tm^{3+} induced different alignment tensors, which were found to be in excellent agreement with predictions based on the x-ray structure of the protein.

Jensen *et al.*[210] have used Ni(II)-induced paramagnetic relaxation enhancements as a source of long-range distance constraints. The binding moiety was a his-his-pro (HHP) peptide fused to the N-terminus of the protein (thioredoxin). Ni(II) cross-links two HHP units, forming a dimer.

Ulmer *et al.*[211] have studied the effect of dissolved oxygen on T_1 and T_2 of the amide protons of a module peptide of fibronectin. Relaxation enhancements were observed in T_1, but not T_2, and were analysed mechanistically.

7.3 Spin Labels. – Spin labels have traditionally been a tool of ESR spectroscopy, where the ESR resonance of the free radical label (usually a nitroxide-containing species, such as TEMPO) is observed directly. However, spin labels have increasingly become a tool of NMR as T_1 relaxation enhancing agents.

Because of the very strong dependence (r^{-6}) on interspin distance and the large magnetic moment of the electron spin, this technique provides useful distance information out to quite large interspin separations (several nm). Recent work involves site-directed spin labels, in which the label has been inserted into proteins that are covalently modified at a specific amino acid residue (usually cystein). Battiste *et al.*[212] have reviewed the use of site-directed spin labels for determining global folds of large proteins. Dvoretsky *et al.*[213] describe a simple protocol for attaching a thiol-reactive EDTA to a cystein residue. McNulty *et al.*[214] have prepared a new nitroxide spin label (Dap-SL), which can be attached *via* an amide linkage to specific sites on the protein backbone.

Aime *et al.*[215] have used the coordinatively-unsaturated Gd chelate, Gd-DO3A, as a relaxation label which binds semi-selectively to solvent-exposed carboxylates on the surface of a protein. In this complex, Gd(III) is 7-coordinate, leaving two sites available for oxygen donors from the protein. In experimental studies, paramagnetic T_1 relaxation enhancements were measured for the amide protons by inversion-recovery ^{15}N-^{1}H HSQC and used to provide distance constraints for a structural analysis of Gd binding sites.

Metal ions that are bound to proteins as paramagnetic labels are often conjugated by flexible linkages, in which case the location of the metal ion with respect to the protein is not well defined. To handle this problem, Iwahara *et al.*[216] have developed a computational strategy which more accurately back-calculates the paramagnetic relaxation enhancement based on a multiple-structure representation of the paramagnetic label in simulated annealing calculations.

7.3.1 Drug-protein binding assays. Janke[217] has reviewed the use of spin labels to characterize protein-ligand interactions by NMR, with particular reference to drug screening. Bertini *et al.*[218] propose that binding assays of metalloenzymes should utilize enzymes which are substituted by a paramagnetic label in a functional metal binding site. As an example, they describe a ligand binding assay for the hydrolytic zinc enzyme, matrix metalloproteinase, which uses enzyme that has been partially substituted by Co(II) in the endogenous Zn(II) binding sites.

7.3.2 Protein-lipid interaction. Ellena *et al.*[219] have studied the localization of perfluorocarbons in lipid membranes, using for this purpose Gd^{3+} and O_2 as relaxation-enhancing agents of the ^{19}F resonance.

Hilty *et al.*[220] have used spin labels to study protein-lipid interactions in mixed micelles containing dihexanoylphosphatidylcholine and the E. coli outer-membrane protein X (OmpX). As paramagnetic relaxation probes, they used several different nitroxide spin labels attached to the lipid as well as Gd-DOTA, which remains in the aqueous phase. Spectral perturbations were monitored in ^{15}N,^{1}H TROSY and 1D ^{1}H NMR spectra.

7.3.3 Nitroxide spin labels. Lietzow *et al.*[221] have used nitroxide spin labels attached at specific mutant cysteine residues of apomyoglobin to monitor the early events of protein folding. Interestingly, they found interactions between the

C and N termini at a stage when the central region of the protein behaved as a random coil polymer.

Lindorff-Larsen *et al.*[222] have used site-directed spin labels to study partially denatured structures of bovine acyl coenzyme A binding protein. Nitroxide spin labels were covalently attached to five site-directed cystein mutants of the protein. The resulting paramagnetic relaxation enhancements were applied as constraints in Monte Carlo simulations of the partially unfolded protein structure.

Neri *et al.*[223] describe the used of the water-soluble nitroxide spin label, TEMPOL, to map the solvent-exposed surface of hen egg-white lysozyme. Pintacuda and Otting[224] have used the Gd chelate, Gd(DTPA-MBA), for the same purpose in studies of ubiquitin. The latter group reports that the correlation of maps generated using TEMPOL and the Gd agent were poor. They recommend the use of the latter, which is more strongly relaxing and less hydrophobic, hence less likely to bind to specific hydrophobic patches of the protein surface.

Lewin *et al.*[225] describe a method for site-specific labeling of proteins with cyclen-bound transition metal ions (particularly, Co(II)). The Co(II)–cyclen label is linked to a cysteine residue of the protein by a thioethyl group.

Nomura *et al.*[226] propose the use of the Cu^{2+} chelate of iminodiacetic acid, which binds to exposed hystidyl residues on proteins. They report that paramagnetic R_2 enhancements of NMR resonances within ≈ 20 Å of the metal center provide useful distance constraints in solution structure analyses. They tested the method in NMR studies of ubiquitin, where the measured R_2 enhancements agreed well with calculations based on the crystal structure.

7.3.4 Paramagnetic Labels of DNA. Complexes containing paramagnetic metal ions can bind to DNA in a sequence-selective manner. Bhattacharya *et al.*[227] have monitored proton line broadening induced by the binding of Ni(II) complexes to oligonucleotides in order to clarify the structural basis of sequence-selective binding. Watson *et al.*[228] have investigated whether ^{1}H NMR provides a useful probe of paramagnetic Cr(III) adducts of guanine in oxidatively damaged DNA (their conclusions are pessimistic).

Iwahara *et al.*[229] have shown that Mn(II)-EDTA-derivatized deoxythymidine, incorporated into DNA, can provide a site of paramagnetic labeling that can be used to ascertain the polarity of protein binding to DNA. The label also provides long range distance constraints for the refinement of nucleotide/protein solution structures. The authors point out that by using different metal ions, the method can be optimized for intermolecular distance ranges between 9 and 35 Å.

7.3.5 Metal Binding Sites in Alginate Gels . – Emmerichs *et al.*[230] have used ^{13}C NMR to monitor the binding of Mn^{2+} to algal and bacterial alginates. Manz *et al.*[231] have studied the cross-linking of alginates (which are used commercially to immobilize drugs, enzymes, *etc.*) by MRI using Cu^{2+} as a contrast agent. Gabriella *et al.*[232] have investigated the coordination of Cu(II) to an hyaluronate tetrasaccharide by ^{1}H and ^{13}C NMR.

7.4 Heme proteins. – Rivera and Caignan[233] have reviewed recent research involving ^{13}C NMR of paramagnetic hemes and heme proteins.

7.4.1 Paramagnetic Susceptibility Tensors of Heme Proteins. The NMR resonances of amino acid residues of heme proteins exhibit hyperfine shifts which are largely dipolar in origin (in contrast to the hyperfine shifts of resonances on the heme moiety itself or on the axial ligands, which usually result from both dipolar and scalar hyperfine couplings). Thus the position of these nuclei can be determined relative to the heme coordinate frame using hyperfine chemical shift measurements once the magnitude and orientation of the paramagnetic susceptibility tensor are known. A large amount of prior experimental work has been directed toward determining these quantities with a view to finding the orientation of the heme within the heme pocket of proteins.
Bertini *et al.*[234] report a detailed study of the magnetic properties of myglobin, in which they determined the axial and orthorhombic terms of the paramagnetic susceptibility tensor using a combination of hyperfine chemical shift measurements and static suscetibility measurements (Evans Method). The determination of the magnetic anisotropy provided a measurement of the residual dipolar couplings and also permitted a separation of the contact and pseudocontact chemical shift contributions of ^{1}H resonances of the Fe(III) ligands.

In recent work, de Ropp *et al.*[235] have determined the orientation and magnitude of the paramagnetic susceiptibility tensor of the cyanide-inhibited horseradish peroxidas, containing a single (his42 to ala) mutation. Proton hyperfine chemical shift measurements wer used to probe molecular and electronic structural changes of the axial heme ligands relative to the wild-type protein.

Du *et al.*[236] have determined the magnitude and orientation of the paramagnetic susceptibility tensor of the cyanomet complex of an O_2-avid hemoglobin from the trematode Paramphistomum epiclitum. They used proton hyperfine chemical shifts and paramagnetic relaxation enhancements to probe the chemical bonding at the metal center.

Ma *et al.*[237] have analysed the pseudocontact chemical shifts of high-spin, ferrous heme in deoxy myoglobin from Aplysia limacinato determine the orientation and magnetic anisotropy of the heme prosthetic group within the heme pocket. This knowledge allowed a separation of contact and pseudocontact contributions to the chemical shifts of the heme resonances, and, from these, a mapping of spin density on the heme.

Vu *et al.*[238] have carried out a detailed analysis of ^{1}H, ^{13}C, and ^{15}N hyperfine chemical shifts in two cyanobacterial hemoglobins. This study focuses on the the properties of an unusual cross-link between one of the heme vinyl groups and a histidine located in the C-terminal helix.

7.4.2 Other Studies of Heme Proteins. Monzani *et al.*[239] have used ^{1}H relaxometry to study Mn(III)-substituted heme complexes with cyanogen bromide fragments of human serum albumin.

Shokireva *et al.*[240] have assigned the ^{1}H NMR resonances of the heme substituents of the low-spin Fe(III) form of nitrophorin 2 using ^{1}H homonuclear 2D and

^{1}H-^{13}C HMQC spectroscopy.

Using triple resonance and total correlation spectroscopy, Liu *et al.*[241] have assigned the ^{1}H spectra of mutants of horse heart cytochrome c in both the diamagnetic and paramagnetic ($S = 1/2$) forms of the protein. Chemical shifts of the wild type and mutant proteins were used as a basis for refining the g-tensors.

Yamamoto *et al.*[242] have used ^{1}H and ^{19}F NMR to determine the electronic structures of deoxymyoglobins reconstituted with a fluorinated heme. They found that ^{19}F signal provides a sensitive probe of the mechanism of spin delocalization onto the heme.

Zhang *et al.*[243] have studied the heme environment and ligand binding properties of two large membrane proteins (quinol oxidases) containing multiple paramagnetic metal centers. Perturbations of hyperfine-shifted proton resonances were used to probe the chemical changes induced by oxidation-reduction reactions and cyanide addition.

Louro *et al.*[244] have used ^{13}C NMR to characterize a tetrahaem ferricytochrome from Shewanella frigidimarina. The heme electronic structure was determined from an analysis of hyperfine ^{13}C chemical shifts of the nuclei bound to the porphyrin of the four heme groups. This analysis provided g-tensors for each heme. This information was used to establish the orientation of the heme magnetic axes.

Du *et al.*[245] have studied equilibrium orientational disorder of the heme group of mouse neuroglobin using 1D proton NMR by monitoring chemical shift changes in the hyperfine-shifted resonances of the heme group and its axial ligands following cyanide addition.

Zhang *et al.*[246] have determined the solution structions of the native and a mutant form of bovine microsomal cytochrome b_5. They used 1D and 2D NMR measurements of ^{1}H pseudocontact chemical shifts to study differences the heme environments of the native and mutant forms.

Schock *et al.*[247] have engineered a water-soluble plant cyt P_{450} for improved properties with respect to purification and solubility. Proton NMR relaxation was used to characterize the orientation of the substrate (cinnamic acid) with respect to the heme to better understand the reason for selective hydroxylation of the substrate.

7.5 Copper Proteins. – Type I Cu(II) proteins possess relatively short electron spin relaxation times and their structures can be determined by standard NMR techniques tailored for fast-relaxing nuclei. Type II Cu(II) proteins are much more difficult to study because of their characteristically long electron spin relaxation times, which tend to produce strong paramagnetic broadening of nuclear resonances of the Cu(II) ligands.[248] Direct detection of ^{13}C can, to a large degree, circumvent these problems.[249]

Arnesano *et al.*[250] describe a strategy for NMR analysis of type II Cu proteins, which they applied to the study of the copper trafficking protein CopC from Pseudomonas Syringae. The electron relaxation time of the Cu(II) center was estimated from NMRD measurements and used to optimize heteronuclear experiments. In this way, they assigned 37 ^{13}C and 11 ^{15}N signals that were

undetectable using conventional approaches. Ionnis *et al.*[251] have developed a protocol for type II Cu proteins that utilizes tailored versions of 2D HSQC and 3D CBCA(CO)NH and CBCANH sequences that are widely used in studies of diamagnetic proteins. The new protocol is intended to facilitate structural studies of paramagnetic proteins by workers without special expertise in paramagnetic proteins.

Sato and Dennison[252] have assigned hyperfine shifted proton resonances of the type I Cu(II) protein, pseudoazurin, by means of saturation transfer experiments on a 1:1 mixture of diamagnetic (Cu(I)) and paramagnetic (Cu(II)) forms of the enzyme. The same authors[253] have also assigned the ^{1}H NMR spectrum of Co(II)-substituted spinach plastocyanin.

7.5.1 Electron Delocalization in Cu-Proteins. Fernandez and Vila have prepared a review.[254] Hansen and Led[255] have used proton R_1's to map electron spin delocalization in a type I Cu protein (oxidized plastocyanin from Anabaena variabilis). Their method relies on the dependence of R_1 on the spatial distribution of the unpaired electron spin.

Donaire *et al.*[256] have used proton hyperfine chemical shift data to probe the immediate liganding environment of Cu(II) in pseudoazurin and rusticyanin. Ligand resonances in the immediate vicinity of Cu(II) were observed with the use of exchange spectroscopy and, for severely broadened resonances, by indirect detection. The NMR data provided a probe of subtle changes in electron density and liganding environment that were not observable in optical and EPR experiments. Monleon *et al.*[257] have used proton NMR contact shifts in conjunction with homology modeling to characterize the coordination site of Cu(II)-halocyanin, with the objective of explaining the low observed redox potential of this protein.

7.5.2 Co(II) and Ni(II)-substituted Copper Proteins. Carrell *et al.*[258] have determined the crystallographic and NMR structures of the Co(II)-substituted form of amicyanin, a type I Cu protein. The use of Co(II) facilitated the observation of resonances of the metal ligands, which are severely broadened in the native protein. Fernandez *et al.*[259] have assigned the ^{1}H spectrum of a Co(II)-substituted pseudoazurin, a type II Cu protein. The line broadening of the Co(II) protein is much less than that of the native Cu(II) protein, and the authors conclude that assignments can be extrapolated between these forms. Dennison and Sato[260] have assigned the ^{1}H NMR spectrum of Ni(II)-substituted pseudoazurin, including resonances of the ligands of Ni(II). Dennison and Harrison[261] have studied the active site structure of the native and a Ni(II)-substituted form of the type I Cu protein, umecyanin (which is like stellacyanin but with an axial Gln ligand). Harris *et al.*[262] have used Co(II) as a surrogate for Zn(II) in the dizinc enzyme, aminopeptidase, to probe the binding site of the inhibitor, inorganic phosphate.

7.6 Ferredoxins. – Kostic and Popchapsky[263] have reviewed the approaches used in their laboratory for studying Cys4Fe2S2 ferredoxins and Ni(II)-containing acireductone dioxygenase. They emphasize the utility of ^{13}C-detected 2D

NMR for observing resonances close to the metal center.

Calzolai *et al.*[264] have used ^{1}H and ^{15}N NMR to study the paramagnetic cluster environment of ferredoxin from the hyperthermophilic archaeon, Pyrococcus furiosus. They identified dipolar connectivities involving the strongly relaxed residues near the metal centers by a combination of T_1 data, rapid pulsing and/or short delay/mixing time ^{1}H WEFT spectra, NOESY, TOCSY, and [^{1}H-^{15}N]-HSQC maps.

Sham *et al.*[265] have used paramagnetically-induced ^{1}H relaxation enhancements as distance constraints for a solution molecular model of the ferredoxin of P. furiosus. Kostic *et al.*[266] have used ^{1}H Overhauser enhancements to compare the functional C-terminal domains of three vertebrate-type ferredoxins.

Trivelli *et al.*[267] and Ubbink[268] have reviewed NMR studies of the interactions among proteins of the photosynthetic electron transfer chain. Mueller *et al.*[269] report the NMR structure of the [2Fe-2S] ferredoxin domain from soluble methane monooxygenase reductase.

7.7 Electron Self-Exchange Reactions. – Flemming and Led[270] have studied electron self-exchange in the blue copper protein plastocyanin from Anabaena variabilis. They investigated the accuracy of analyses based on approximate solutions of the Block-McConnell equations. Jensen *et al.*[271] have developed an NMR method for determining rate constants of electron self-exchange in blue copper proteins from proton T_1's that is valid outside the slow exchange limit.

Sato *et al.*[272] have used paramagnetic proton NMR to measure electron self-exchange rates in five different plastocyanins. This work attempts to understand the relationship between the self-exchange rate and the structures of acidic and hydrophobic residues on the electron transfer pathway.

Hansen *et al.*[273] describe a proton NMR method for detecting transient interactions between protein molecules in solution. The method relies on the intermolecular paramagnetic contribution to the NMR relaxation of protons at or close to the interaction surface. The method was applied to the soluble electron transfer protein, plastocyanin, and used to locate surface patches that may be involved in electron transfer.

8 Advances in Theory

This section describes theoretical work of a fundamental nature that does not clearly belong in one of the sections above. Work focused on a particular chemical system – for example, DFT calculations of hyperfine chemical shifts in porphyrins are described in the Porphyrins section.

8.1 NMR relaxation of S>1/2 Paramagnetic Ions. - Paramagnetic ions with S>1/2 experience a complex physical situation, since the electron spin hamiltonian is a sum of non-commuting terms due respectively to the Zeeman and zfs interactions. In solution phases, the zfs portion of the spin hamiltonian is an explicit function of time due to Brownian reorientation and collisional distortion

of the zfs tensor. An overview of the physical problems that are currently being addressed in this field was given in a previous contribution to this series.[274]

To describe the relaxation phenomenon theoretically, Kowalewski and his coworkers have developed a formalism based on the Stochastic Liouville Equation (SLE). In recent work, Kowalewski *et al*[275] have compared theoretical simulations of R_1 field dispersion profiles computed using the SLE formalism with the results of more restricted theory developed in Florence that neglects reorientational motion of the zfs tensor. Kruk and Kowalewski[276] describe a theoretical model that incorporates fast reorientational motion of the zfs tensor. These workers[277] also present theoretical calculations describing the situation where collisional distortions of the zfs tensor are much larger than the time-averaged zfs tensor.

Miller *et al*[278] have employed Spin Dynamics techniques to calculate NMR relaxation enhancements produced by $Cr(III)(acac)_3$, an $S = 3/2$ spin system for which sufficient physical information is available that an accurate first principles calculation should be possible (*i.e.*, a calculation without variation of undetermined physical paramaters).

8.2 Hyperfine Chemical Shifts. – Rinkevicius *et al.*[279] have investigated first principles methods for calculating the nuclear shielding tensor in open-shell, paramagnetic molecules with small spin-orbit coupling (*i.e.*, to small organic compounds). The formalism is consistent up to second order in the fine structure constant and includes orbital, fully anisotropic dipolar, and isotropic contact contributions to the tensor. The proposed method is implemented within the *ab initio* single- and multiconfiguration SCF as well as within the DFT framework. Applications include small main-group and nitroxide radicals. Telyatnyk *et al.*[280] have applied this methodology in calculations of nitronylnitroxide radicals that form core units in molecular magnets. Their work focuses on the influence of hydrogen bonding on the calculated nuclear shielding parameters.

9 Chemically Induced Dynamic Nuclear Polarization (CIDNP)

9.1 Mechanistic Studies. – Chemically Induced Dynamic Nuclear Polarization (CIDNP) is the phenomenon by which large non-equilibrium nuclear spin populations arise as a consequence of short-lived free-radical intermediates in chemical reactions. Homolysis or photolysis of a chemical bond produces a pair of free radicals (*i.e.*, spin doublets). When the radicals separate from each other chemically, the electron spins precess independently, in general at somewhat different frequencies. But in liquid phases, the diffusing radicals often re-encounter each other. When this occurs, the Heisenberg exchange coupling suddenly becomes large, and the combined spin state evolves as a singlet or triplet with a probability that depends on the relative quantum mechanical phases of the spins in the recombined pair. The triplet radical pair tends to be relatively long-lived and produces large non-equilibrium nuclear spin populations through nuclear-electron hyperfine interactions. Sagdeev *et al.*[281] describe a novel 2-dimensional

NMR method of analysing the spin polarization of a non-equilibrium system of coupled nuclei in CIDNP experiments. Using Fourier analysis of the variation of NMR line intensities as a function of the radio frequency excitation pulse length, they have established a relationship between the spectral components of various harmonic order and the alignment in the spin multiplet.

9.1.1 RYDMR. Radical recombination reactions are sensitive to applied static and/or oscillating magnetic fields. This is the basis of the RYDMR (reaction yield detected magnetic resonance technique, in which an electromagnetic field in resonance with the electron Zeeman splitting is used to perturb the singlet-triplet interconversion of the radical pair and so affect the yield of geminate recombination. Woodward *et al.*[282] describe experiments in which weak 1-80 MHz radio frequency fields are applied to radical ion pairs derived from pyrene and 1,3-dicyanobenzene in the presence of a weak static magnetic field in order to test the viability of RYDMR in low fields.

CIDNP experiments can provide various kinds of information concerning the reaction mechanism.

9.1.2 Factors Affecting Radical Pair Reencounter Probability. Popov *et al.*[283] have developed theory to describe CIDNP produced during recombination of successive radical pairs. Assuming that the spin hamiltonian changes instantly upon reaction, they express general relations for CIDNP using the quadratures of Green functions, which characterize the molecular motions.

Goez and Sartorius[284] have studied the effects of solvent permittivity on the radical pair reencounter probability, as reflected in CIDNP polarization patterns of reactions involving radical ion pairs. For this purpose, they used a sensitizer radical pair anion, which converts the initially formed radical ion pair into a neutral radical pair.

9.1.3 Third Spin Effects. Magin *et al.*[285] studied the effect of a 'third spin', on photo-CIDNP formation. They monitored the effects of the stable free radicals TEMPO and dodecanetiol-1, acting as radical traps, on the time-resolved proton photo-CIDNP generated upon photocleavage of diisopropylketone. It was found that TEMPO affects the formation of the primary radical pair not only as a radical acceptor but also through spin exchange. Polyakov *et al.*[286] have studied the effects of electron donors (triphenylphospine, triphenylamine) on electron transfer reactions produced during the photolysis of acetonitrile.

9.1.4 Localization of Radical Pairs in Micelles. CIDNP can often be enhanced by the use of micelles to enhance the recombination probability of photochemically produced radical pairs. Bagranskaya *et al.*[287] have reviewed this techique. Goez and Heun[288] have used Monte Carlo simulations of diffusional trajectories to calculate reencounter probabilitiies of micellized radical pairs. By varying the initial locations, they found that unless at least one of the radicals starts its diffusional trajectory extremely near the micelle boundary, the reencounter probability is essentially the same as in the case of free diffusion. It was concluded

that the reencounter function is influenced mainly by the short-time diffusional motion.

Lebedeva *et al.*[289] report theoretical and experimental studies of CIDNP generated in consecutive micellised radical pairs. They measured the radical pair escape rate in the photolysis reactions of three substrates (*e.g.*, dibenzyl ketone), and compared physico-chemical aspects of the process to that occurring in biradicals, where the escape of radical pairs is inhibited by the covalent linkage.

9.1.5 Chemical Reaction Mechanism. Fairly detailed conclusions can often be made concerning the chemical and spin properties of the radical pair intermediates, properties which can be difficult to obtain by other methods. Lehnig *et al.*[290] report ^{15}N CIDNP studies of the reaction of nitrous acid with hydrogen peroxide to form nitric acid. The complex mechanism involves a number of intermediates including both radicals ($OH^{\cdot}$, $OOH^{\cdot}$, $O_2NOOH^{\cdot-}$) and non-radical (ONOOH, $ONOOCO_2^-$)species.

Polyakov *et al.*[291] have investigated the effect of the electron donor triphenylamine on the photoisomerization reactions of α,β-unsaturated diketones. CIDNP has also been applied in mechanistic studies of free radical polymerization reactions[292,293].

9.2 Switched-Magnetic Field CIDNP. – The information available concerning spin dynamics and spin interactions in the radical pair and in short-lived radical intermediates can be augmented by switching the polarizing magnetic field to a lower value during the spin evolution period, thereby affecting quantum mechanical spin coherence in the spin-correlated radical pairs. Spin coherence in the doublet quantum states is influenced by time evolution of the spin wave functions and is progressively destroyed through a number of processes that affect the observed CIDNP enhancements. Hiyashi[294] has prepared a review. Khudyakov *et al.*[295] have reviewed the technique of using a moderate magnetic field to increase the efficiency of triplet photoinitiators of polymerization.

Fedin *et al.*[296] have used switched external magnetic field CIDNP to study the kinetics of appearance and disappearance of short-lived neutral radicals in solution. Benzyl, tert-butyl, and 2-hydroxy-2-propyl radical intermediates were monitored with microsecond time resolution, and their spin relaxation times spin relaxation times were determined in low magnetic fields. New theory was developed to simulate the experimental results. Ivanov *et al.*[297]have used switched magnetic fields across a range 0-7 T to study the photoreaction of excited 2,2′-dipyridyl with tyrosine. They simulated the CIDNP polarization patterns using the Green function theory of geminate reactions and found good agreement between theory and experiment for both net and multiplet polarization.

9.3 Time-Resolved CIDNP. – Petrova *et al.*[298], have used time-resolved photo-CIDNP in the dibenzyl-ketone-b-cyclodextrin inclusion complex. The photodecay of the inclusion complex generates a benzyl radical that is held in the cyclodextrin cavity for a time exceeding the nuclear spin relaxation time, from

which the rate constant for the dissociation reaction was measured. Pozdnyakov *et al.*[299] have used time-resolved CIDNP in conjunction with nanosecond laser flash photolysis and optical spectroscopy to determine photophysical and photochemical processes for 5-sulfosalicylic acid dianion in aqueous solutions and frozen matrices. Yurkovskaya *et al.*[300] have used time-resolved photo-CIDNP to study the kinetics and mechanism of the photoreaction between triplet 2,2′-dipyridyl and guanosine-50-monophosphate.

Goez and Frisch[301] have used photo-CIDNP to measure the activation energy of a biradical rearrangement reaction. Roth[302] has studied the electron transfer back reactions of photoexcited *cis*- and *trans*-1,2-diphenylcyclopropane in the presence of singlet acceptors. He finds that the pair energy relative to the reactant ground states and an accessible triplet state, respectively, determines whether the back reaction is competitive.

9.4 CIDNP Studies of Proteins. – Photochemically-induced CIDNP (photo-CIDNP) has emerged in recent years as powerful tool for the investigation of residue accessibility and structural changes of proteins, particularly as a probe of protein folding. The irradiation of aqueous protein solutions in the presence of a water-soluble dye produces triplet states of tryptophan, tyrosine, and histidine sidechains due to triplet dye quenching, resulting in CIDNP enhancement of the NMR resonances of specific sidechain[303]. Since the aqueous dye reacts only with solvent-exposed residues, the method demonstrates solvent accessibility of the sidechain or changes in accessibility due to dynamic processes such as aggregation, substrate binding, denaturation, folding, *etc.* These methods have been employed[304,305] to study oxidative folding intermediates of the Amaranthus α-amylase inhibitor, a 32-residue cystine-knot protein with three disulfide bridges, in terms of the disulfide content of the intermediate species.

9.4.1 New Techniques. Mok *et al.*[306] describe a new rapid sample-mixing technique designed for photo-CIDNP investigations of protein folding. Efficient, homogeneous mixing of solutions in the NMR tube was achieved within tens of milliseconds without modification of the NMR probe. The device was tested in studies on the partially unfolded state of hen lysozyme. Lyon *et al.*[307] have likewise employed rapid sample mixing in order to exploit the magnetic field dependence of CIDNP with the objective of more fully characterizing the radical intermediates. They illuminated solutions of an amino acid or a protein at a position in the bore of the NMR magnet where the field is between 0.1 T and 7.0 T. The polarized sample was then transferred by rapid injection into an NMR tube at the center of the magnet (at 9.4 T), where the spectrum is recorded. The field dependence of histidine, tryptophan and methionine CIDNP allowed them to determine the g values of the transient radicals. Experiments in which CIDNP polarization was generated at 0.7 T indicated that methionine could be used as a probe of surface accessibility.

Lyon *et al.*[308] have developed a technique that probes the structures of disordered, partially folded states of proteins. CIDNP is first generated photochemically in exposed aromatic side-chains of the denatured state and and the

nuclear polarizations are then transferred to the high-resolution NMR spectrum of the native state by stimulating rapid refolding of the protein. The photochemical and detection steps are carried out at field strengths of 4 T and 9.4 T to provide sensitivity enhancement. Their studies of the low pH molten-globule state of R-lactalbumin revealed that the environments of aromatic residues in the primary hydrophobic core of the protein are similar to those in the fully native protein.

9.4.2 ^{19}F Photo-CIDNP. – Kuprov and Hore[309] have used photo-CIDNP to hyperpolarize the ^{19}F nuclear magnetisation in 3-fluorotyrosine, and then monitored the effects of the ^{19}F hyperpolarization on the ^{19}F-^{1}H cross-relaxation and cross-correlation peaks. The ^{19}F polarization increased by more than an order of magnitude, producing large enhancements of the cross peaks. They discuss the potential for enhancing the sensitivity of heteronuclear NOEs in ^{19}F-labelled proteins.

9.4.3 Model Studies with Peptide and Amino Acids. In model studies, Morozova *et al.*[310,311] have used time-resolved photo-CIDNP to study the kinetics and mechanism of the photoreaction between the sensitizer, 2,2′-dipyridyl, and the dipeptide L-tryptophan-L-tyrosine. Through the use of nanosecond laser flash photolysis and microsecond time resolution, they were able to determine the full reaction scheme with all relevant transient intermediates. Tsentalovich *et al.*[312] have characterized the chemical reactions between the photoexcited triplet state of flavin mononucleotide and the aromatic amino acids, N-acetyl tryptophan, N-acetyl tyrosine, and N-acetyl histidine.

9.4.4 ^{13}C CIDNP of Photosynthetic Reaction Centers. In an exciting biophysical advance of the last few years, the primary photochemical products of the initial charge transfer step of photosynthesis have been detected *in situ* through photo-CIDNP experiments on the natural abundance ^{13}C resonances of preparations of photosynthetic reaction centers from photosynthetic bacteria[313,314]. Experiments required *in situ* illumination during magic-angle spinning in an ss-NMR spectrometer. CIDNP enhancements are thought to reflect the distribution of electron spin density across the two chlorophyll partners which constitute the Special Pair of the reaction center. The origin of the photo-CIDNP observed in these solid samples is presumably different from the radical pair recombination mechanism that occurs in solution. Jeschke and Matysik[315] have considered the mechanism and conclude that a combination of three spin mixing and differential spin relaxation may be involved.

References

1. E. Toth, L. Helm, A. E. Merbach, in 'Comp. Coord. Chem. II', Ed. J.A. McCleverty and T.J. Meyer, Elsevier, Oxford, UK, 2004, vol. 9, p. 841-881.
2. S. Aime, W. Dastru, S.G. Crich, E. Gianolio, and V. Mainero, *Biopolym.*, 2003, **66**,

419.
3. L. Helm, E. Toth, and A.E. Merbach, *Met. Ions Biol. Syst.*, 2003, **40**, 589.
4. M.P. Lowe, *Aust. J. Chem.*, 2002, **55**, 551.
5. A. Maiocchi, *Mini-Rev. Med. Chem.*, 2003, **3**, 845.
6. A.V. Astashkin, A.M. Raitsimring, and Peter Caravan, *J. Phys. Chem. A* 2004, **108**, 1990.
7. P. Caravan, A.V. Astashkin, and A.M. Raitsimring, *Inorg. Chem.*, 2003, **42**, 3972.
8. A. Borel, L. Helm, A. E. Merbach, V. A. Atsarkin, V. V. Demidov, B. M. Odintsov, R. L. Belford, and R. B. Clarkson, *J. Phys. Chem. A*, 2002, **106**, 6229.
9. F. Benetollo, G. Bombieri, L. Calabi, S. Aime, and M. Botta, *Inorg. Chem.*, 2003, **42**, 148.
10. M. Woods, Z. Kovacs, S. Zhang, and A.D. Sherry, *Angew. Chem., Int. Ed.*, 2003, **42**, 5889.
11. M. Woods, Z. Kovacs, R. Kiraly, E. Brucher, S. Zhang, and A.D. Sherry, *Inorg. Chem.* 2004, **43**, 2845.
12. E. Terreno, M. Botta, F. Fedeli, B. Mondino, L. Milone, and Silvio Aime, *Inorg Chem.*, 2003, **42**, 4891.
13. L. Burai, E. Toth, and A. E. Merbach, *Chem. Commun.*, 2003, (**21**), 2680.
14. F. Yerly, K. I. Hardcastle, L. Helm, S. Aime, M. Botta, and A.E. Merbach, *Chem. Eur. J.*, 2003, **8**, 1031.
15. F. Yerly, A. Borel, L. Helm, and A.E. Merbach, *Chem. Eur. J.*, 2003, **9**, 5468.
16. G.M. Nicolle, F. Yerly, D. Imbert, U. Boettger, J.-C. Buenzli, and A.E. Merbach, *Chem. Eur. J.*, 2003, **9**, 5453.
17. F.A. Dunand, A. Borel, and L. Helm, *Inorg. Chem. Commun.*, 2002, **5**, 811.
18. F.A. Dunand, L. Helm, and A.E. Merbach, *Adv. Inorg. Chem.*, 2003, **54**, 1-.
19. L. Helm and A.E. Merbach, 'Water exchange on metal ions: The effect of pressure' in High Pressure Chemistry, Eds. R. Van Eldik and F.G. Klaerne, Wiley-VCH Publisher, 2002, p. 131-160.
20. M. K. Thompson, M. Botta, G. Nicolle, L. Helm, S.Aime, A.E. Merbach, and K. N. Raymond, *J. Am. Chem. Soc.*,2003, **125**, 14274.
21. D.M.J. Doble, M. Melchior, B. O'Sullivan, C. Siering, J. Xu, V.C. Pierre, and K.N. Raymond, *Inorg. Chem.*, 2003, **42**, 4930.
22. S. Laus, R. Ruloff, E. Toth, and A.E. Merbach, *Chem. Eur. J.*, 2003, **9**, 3555.
23. R. Ruloff, E. Toth, R. Scopelliti, R. Tripier, H. Handel, and A.E. Merbach, Andre E., *Chem. Commun.*, 2002, (**22**), 2630.
24. S. Aime, A. Barge, A.S. Batsanov, M. Botta, D. Delli Castelli, F. Fedeli, A. Mortillaro, D. Parker, and H.Puschmann, *Chem. Commun.*, 2002, (**10**), 1120.
25. D Kruk and J. Kowalewski, *J. Chem. Phys.*, 2002, **117**, 1194.
26. E. Terreno, P. Boniforte, M. Botta, F. Fedeli, L. Milone, A. Mortillaro, and S. Aime, *Eur. J. Inorg. Chem.*, 2003, (**19**), 3530.
27. S. Laurent, F. Botteman, L. Vander Elst, and R.N. Muller, *Eur. J. Inorg. Chem.*, 2004, (**3**), 463.
28. F. Botteman, G.M. Nicolle, L. Vander Elst, S. Laurent, A.E. Merbach, and R.N. Muller, *Eur. J. Inorg. Chem.*, 2002, **10**, 2686.
29. S. Aime, E. Gianolio, A. Barge, D.Kostakis, I.C. Plakatouras, and Nick Hadjiliadis, *Eur. J. Inorg. Chem.*, 2003, (**11**), 045.
30. T. Yamamoto, K. Ikuta, K, Oi, K. Abe, T. Uwatoku, M. Murata, N. Shigetani, K. Yoshimitsu, H. Shimokawa, and Y. Katayama,, *Anal. Sci.*, 2004, **20**, 5.
31. R. Hovland, A.J. Aasen, and J. Klaveness, *Org. Biomolec. Chem.*, 2003, **1**, 1707.
32. S. Aime, E. Gianolio, D. Corpillo, C. Cavallotti, G. Palmisano, M. Sisti, G.B.

Giovenzana, and R. Pagliarin, *Helv. Chim. Acta*, 2003, **86**, 615.
33. B. O'Sullivan, D.M.J. Doble, M.K. Thompson, C. Siering, J. Xu, M. Botta, S. Aime, and K.N. Raymond, Inorg. Chem., 2003, **42**, 2577.
34. R.S. Ranganathan, N. Raju, H. Fan, X. Zhang, M.F. Tweedle, J.F. Desreux, and V. Jacques, *Inorg. Chem.*, 2002, **41**, 6856.
35. J. Feng, G. Sun, F. Pei, and M. Liu, *J. Inorg. Biochem.*, 2002, **92**, 193.
36. R. Ruloff, G. van Koten, and A.E. Merbach, *Chem. Commun.*, 2004, (**7**), 842.
37. E.P. Mayoral, M. Garcia-Amo, P. Lopez, E. Soriano, S. Cerdan, and P. Ballesteros, *Bioorg. Med. Chem.*, 2003, **11**, 5555.
38. E. Monzani, M. Curto, M. Galliano, L. Minchiotti, S. Aime, S. Baroni, M. Fasano, A. Amoresano, A.M. Salzano, P. Pucci, and L. Casella, *Biophys. J.*, 2002, **83**, 2248.
39. S. Aime, A. Barge, M. Botta, and E. Terreno, in 'Metal Ions in Biological Systems', 2003, vol. 40(Lanthanides and Their Interrelations with Biosystems), p. 643-682.
40. L. Vander Elst, M. Port, I. Raynal, C. Simonot, and R.N. Muller, *Eur. J. Inorg. Chem.*, 2003, (**13**), 2495.
41. S. Aime, E. Gianolio, E. Terreno, I. Menegotto, C. Bracco, L. Milone, and G. Cravotto, *Magn. Reson. Chem.*, 2003, **41**, 800.
42. K. Kimpe, T.N. Parac-Vogt, S. Laurent, C. Pierart, L. Vander Elst, R. N. Muller, and K. Binnemans, *Eur. J. Inorg. Chem.*, 2003, **16**, 3021.
43. R. Hovland, C. Glogard, A.J. Aasen, and J. Klaveness, *Org. Biomolec. Chem.*, 2003, **1**, 644.
44. G.M. Nicolle, E. Toth, K.-P., Eisenwiener, H.R. Macke, and A.E. Merbach, *J. Biol. Inorg. Chem.*, 2002, **7**, 757.
45. G.M. Nicolle, L. Helm, and A.E. Merbach, *Magn. Reson. Chem.*, 2003, **41**, 794.
46. H. Kato, Y. Kanazawa, M. Okumura, A. Taninaka, T. Yokawa, and H. Shinohara, *J. Am. Chem. Soc.*, 2003, **125**, 4391.
47. R.D. Bolskar, J.M. Alford, A.F. Benedetto, L.O.. Huesbo, and L.J. Wilson, in 'Fullerenes: The Exciting World of Nanocages and Nanotubes', *Proc. Electrochem. Soc.*, 2002, vol. 12, p. 398-406.
48. O. Masafumi, M. Masahito, Y. Takashi, K. Yoko, K. Haruhito, and S. Hisanori, *Acad. Radiol.*, 2002, **9**, S495.
49. Y. Gossuin, A. Roch, R.N. Muller, and P. Gillis, *J. Magn. Reson.*, 2002, **158**, 36.
50. S. Aime, L. Frullano, and S. Geninatti Crich, *Angew. Chem., Int. Ed.*, 2002, **41**, 1017.
51. M.P. Morales, O. Bomati-Miguel, R. Perez de Alejo, J. Ruiz-Cabello, S. Veintemillas-Verdaguer, K. O'Grady, *J. Magnetism Magn. Mat.*, 2003, **266**, 102.
52. D.K. Kim, M. Mikhaylova, F.H. Wang, J. Kehr, B. Bjelke, Y. Zhang, T. Tsakalakos, and M. Muhammed, *Chem. Mater.*, 2003, **15**, 4343.
53. H. Kobayashi and M.W. Brechbiel, *Molec. Imag.*, 2003, **2**, 1.
54. S. J. Wang, M. Brechbiel, and E. C. Wiener, *Invest. Radiol.*, 2003, **38**, 662.
55. A.T. Yordanov, H. Kobayashi, S.J. English, K. Reijnders, D. Milenic, M.C. Krishna, J.B. Mitchell, and M.W. Brechbiel, *J. Mater. Chem.*, 2003, **13**, 1523.
56. G. Francese, F.A. Dunand, C. Loosli, A.E. Merbach, and S. Decurtins, *Magn. Reson. Chem.*, 2003, **41**, 81.
57. A.J. Maliakal, N.F. Turro, A.W. Bosman, J. Cornel, and E.W. Meijer, *J. Phys. Chem. A*, 2003, **107**, 8467.
58. R.N. Muller, L. Vander Elst, and S. Laurent, *J. Am. Chem. Soc.*, 2003, **125**, 8405.
59. W.-H. Li, G. Parigi, M. Fragai, C. Luchinat, and T.J. Meade, *Inorg. Chem.*, 2002, **41**, 4018.
60. C. Glog, G. Stensrud, and S. Aime, *Magn. Reson. Chem.*, 2003, **41**, 585.
61. N. Raghunand, C. Howison, A.D. Sherry, S. Zhang, and R.J. Gillies, *Magn. Reson.*

Med., 2003, **49**, 249.
62. M. Woods, S. Zhang, E. Von Howard, and A.D. Sherry, *Chem. Eur. J.*, 2003, **9**, 4634.
63. K.E. Lokling, R. Skurtveit, K. Dyrstad, J. Klaveness, and S.L. Fossheim, *Internat. J. Pharmaceut.*, 2004, **274**, 75.
64. M. Woods, Z. Kovacs, A.D. Sherry, *J. Supramol. Chem.*, 2003, **2**, 1.
65. T.M. Corneillie, P.A. Whetstone, A.J. Fisher, and C.F. Meares, *J. Am. Chem. Soc.*, 2003, **125**, 3436.
66. T.M. Corneillie, P.A. Whetstone, and C.F. Meares, *J. Am. Chem. Soc.*, 2003, **125**, 15039.
67. I. Pirko, A. Johnson, B. Ciric, J. Gamez, S.I. Macura, L.R. Pease, and M. Rodriguez, *FASEB J.*, 2004, **18**, 179.
68. A.M. Morawski, P.M. Winter, K.C. Crowde, S.D. Caruthers, R.W. Fuhrhop, M.J. Scott, J.D. Robertson, D.R. Abendschein, G.M. Lanza, and S.A. Wickline, *Magn. Reson. Med.*, 2004, **51**, 480.
69. A. Accardo, D. Tesauro, P. Roscigno, E. Gianolio, L. Paduano, G. D'Errico, C Pedone, and G. Morelli, *J. Am. Chem. Soc.*, 2004, **126**, 3097.
70. L. Lattuada and G. Lux, *Tetr. Lett.*, 2003, **44**, 3893.
71. S. Laurent, L. Vander Elst, Y. Fu, and R.N. Muller, *Bioconj. Chem.*, 2004, **15**, 99.
72. J. Feng, G. Sun, F. Pei, and M. Liu, *Bioorg. Med. Chem.*, 2003, **11**, 3359.
73. P. Caravan , J.M. Greenwood , J.T. Welch. and S.J. Franklin, *Chem. Commun.*, 2003, **(20)**, 2574.
74. M.J. Allen and T.J. Meade, *J. Biol. Inorg. Chem.*, 2003, **8**, 746.
75. C. Weidensteiner, M. Horn, E. Fekete, S. Neubauer, and M. von Kienlin, *Magn. Reson. Med.*, 2002, **48**, 89.
76. F. Avecilla, J.A. Peters, and C.F.G.C. Geraldes, *Eur. J. Inorg. Chem.*, 2003, **23**, 4179.
77. A.-M. Delort, G. Gaudet, and E. Forano, *Anal. Biochem.*, 2002, **306**, 171.
78. C. F. Diven, F. Wang, A. M. Abukhdeir, W. Salah, B. T. Layden, C. F. G. C. Geraldes, and D. M. de Freitas, *Inorg. Chem.*, 2003, **42**, 2774.
79. S. Zhang, M. Merritt, D.E. Woessner, R.E. Lenkinski, A.D. Sherry, *Acc. Chem. Res.*, 2003, **36**, 783.
80. S. Zhang, K. Wu, and A.D. Sherry, *J. Am. Chem. Soc.*, 2002, **124**, 4226.
81. S. Zhang and A.D. Sherry, A. Dean, *J. Sol. State Chem.*, 2003, **171**, 38.
82. S. Aime, D. Delli Castelli, F. Fedeli, and E. Terreno, *J. Am. Chem. Soc.*, 2002, **124**, 9364.
83. S. Zhang, L. Michaudet, S. Burgess, A.D. Sherry, *Angew. Chem., Int. Ed.*, 2002, **41**, 1919.
84. M. Botta, S. Aime, A. Barge, G. Bobba, R.S. Dickins, D. Parker, and E. Terreno, *Chem. Eur. J.*, 2003, **9**, 2102.
85. R.S. Dickins, S. Aime, A.S. Batsanov, A. Beeby, M. Botta, J.I. Bruce, J.A.K. Howard, C.S. Love, D. Parker, R.D. Peacock, and H. Puschmann, *J. Am. Chem. Soc.*, 2002, **124**, 12697.
86. S. Zhang, R Trokowsk, and A.D. Sherry, *J. Am. Chem. Soc.*, 2003, **125**, 15288.
87. S. Aime, D.Delli Castelli, and E. Terreno, *Angew. Chem., Int. Ed.*, 2002, **41**, 4334.
88. S. Aime, D. Delli Castelli, and E. Terreno, *Angew. Chem., Int. Ed.*, 2003, **42**, 4527.
89. L. Burai, R. Scopelliti, and E. Toth, *Chem. Commun.*, 2002, **(20)**, 2366.
90. L. Burai, E. Toth, G. Moreau, A. Sour, R. Scopelliti, and A.E. Merbach, *Chem. Eur. J.*, 2003, **9**, 1394.
91. G. Moreau, L. Burai, L. Helm, J. Purans, and A.E. Merbach, *J. Phys. Chem. A*, 2003, **107**, 758.
92. G. Moreau, R. Scopelliti, L. Helm, J. Purans, and A.E. Merbach, *J. Phys. Chem. A*,

2002, **106**, 9612.
93. S. Aime, P.L. Anelli, M. Botta, M. Brocchetta, S. Canton, F. Fedeli, E. Gianolio, E. Terreno, *J. Biol. Inorg. Chem.*, 2002, **7**, S58.
94. D. Kruk and J. Kowalewski, *J. Biol. Inorg. Chem.*, 2003, **8**, 512.
95. D.D. Schwert, J.A. Davies, and N. Richardson, *Top. Curr. Chem.*, 2002, **221**(Contrast Agents I), 165.
96. S. Aime, S. Canton, S. Crich, G. Simonetta, and E. Terreno, *Magn. Reson. Chem.*, 2002, **40**, 41.
97. L. Vander Elst, S. Zhang, A.D. Sherry, S. Laurent, F. Botteman, and R.N. Muller, *Acad. Radiol.*, 2002, **9 Suppl 2**, S297.
98. H. Fujii and L.J. Berliner, Biomed. *Res. Trace Elem.*, 2003, **14**, 6.
99. D.J. Lurie, *Biol. Magn. Reson.*, 2003, **18**, 547.
100. D.J. Lurie, H. Li, S. and Petryakov, J.L. Zweier, *Magn, Reson. Med.*, 2002, **47**, 181.
101. T. Liebgott, H. Li, Y. Deng, and J.L. Zweier, *Magn. Reson. Med.*, 2003, **50**, 391.
102. H. Li, Y. Deng, G. He, P. Kuppusamy, D.L. Lurie, and J.L. Zweier Jay L, *Magn. Reson. Med.*, 2002, **48**, 530.
103. H. Guanglong, D. Yuanmu, L. Haihong, K. Periannan, and J.L. Zweier, *Magn. Reson. Med.*, 2002, **47**, 571.
104. R. Murugesan, S. English, K. Reijnders, K. Yamada, J.A. Cook, J.B. Mitchell, S. Subramanian, and M.C. Krishna, *Magn. Reson. Med.*, 2002, **48**, 523.
105. V.V. Khramtsov, I.A. Grigor'ev, D.J. Lurie, M.A. Foster, J.L. Zweier, and D.M. Kuppusamy, *Spectroscopy.*, 2004, **18**, 213.
106. W. Youngdee, D. Lurie, and M.A. Foster, *Phys. Med. Biol.*, 2002, **47**, 1091.
107. C. Piguet and C.F.G.C. Geraldes, *Handbook Phys. Chem. Rare Earths.*, 2003, **33**, 353.
108. J. Ren, S. Zhang, A.D. Sherry, A. Dean, and C.F.G.C. Geraldes, *Inorg. Chim. Acta*, 2002, **339**, 273.
109. C.F.G.C. Geraldes, S. Zhang, and A.D. Sherry, *Bioinorg. Chem. Appl.*, 2003, **1**, 1.
110. C.F.G.C. Geraldes, S. Zhang, and A.D. Sherry, *Inorg. Chim. Acta*, 2004, **357**, 281.
111. N. Ouali, J.-P. Rivera, P.Y. Morgantini, J. Weber, and C. Piguet, *Dalton Trans.*, 2003, (**7**), 1251.
112. N. Ouali, J.P. Rivera, D. Chapon, P. Delangle, and Claude Piguet, *Inorg Chem.*, 2004, **43**, 1517.
113. N. Ouali, B. Bocquet, S. Rigault, P.-Y. Morgantini, J. Weber, amd C. Piguet, *Inorg. Chem.* 2002, **41**, 1436.
114. L. Di Bari, G. Pintacuda, S. Ripoli, and P. Salvadori, *Magn. Reson. Chem.*, 2002, **40**, 396.
115. N. Ishikawa, *J. Phys. Chem.* A, 2003, **107**, 5831.
116. N. Ishikawa, T. Iino, and Y. Kaizu, *J. Phys. Chem. A*, 2002, **106**, 9543.
117. N. Ishikawa, T. Iino, and Y. Kaizu, *J. Phys. Chem. A*, 2003, **107**, 7879.
118. N. Ishikawa, T. Iino, and Y. Kaizu, *J. Am. Chem. Soc.*, 2002, **124**, 11440.
119. N. Andre, T.B. Jensen, R. Scopelliti, D. Imbert, M. Elhabiri,G. Hopfgartner,C.Piguet,and J.-C.G. Bu1nzli, *Inorg. Chem.* 2004, **43**, 515.
120. L. Valencia, J. Martinez, A. Macias, R. Bastida, R.A. Carvalho, and C.F.G.C. Geraldes, *Inorg. Chem.*, 2002, **41**, 5300.
121. J. Lisowski, S. Ripoli, and L. Di Bari, Inorg. Chem., 2004, **43**, 1388.
122. H.A. Hussain, A.A. Ansari, and K. Iftikhar, *Spectrochim. Acta, Part A: Molec. Biomolec. Spectr.*, 2004, **60A**, 873.

123. H.A. Hussain, and K. Iftikhar, *Spectrochim. Acta, Part A: Mol. Biomol. Spectr.*, 2003, **59A**, 1061.
124. R.S. Dickins, A.S. Batsanov, J.A.K. Howard, D. Parker, H. Puschmann, and S. Salamano, *Dalton Trans.*, 2004, (**1**), 70.
125. S.P. Babailov and D.A. Mainichev, *J. Inclusion Phenom. Macrocycl. Chem.*, 2002, **43**, 187.
126. S.P. Babailov, L.D. Nikulina, and J.H. Krieger, *J. Inclusion Phenom. Macrocyc. Chem.*, 2002, **43**, 25.
127. N. D'Amelio, E. Gaggelli, N. Gaggelli, F. Mancini, E. Molteni, D. Valensin, and G. Valensin, *J. Inorg. Biochem.*, 2003, **95**, 225.
128. R. J. Abraham , R. Koniotou and F. Sancassan, *J. Chem. Soc., Perkin Trans.* 2, 2002, (12), 2025.
129. L. Di Bari, M. Lelli, and G. Pintacuda, and S. Piero, *Chirality*, 2002, **14**, 265.
130. R.A. Schenato, E.M. Dos Santos, P.F.B. Goncalves, B.S.M. Tenius, E.R. De Oliveira, EI. Caracelli, and J. Zukerman-Schpector, *Magn. Reson. Chem.*, 2003, **41**, 53.
131. D.C. Crans, L. Yang, E. Gaidamauskas, R. Khan, W. Jin, and U. Simonis, *ACS Symp. Ser.*, 2003, **858**(Paramagn. Reson. Metallobiomol.), 304.
132. V.T. Panyushkin, I.V. Sukhno, and N.F. Vodopetova, *Russ. J. Gen. Chem.* (*Transl. Zhur. Obsh. Khim.*), 2003, **73**, 507.
133. E.M.R. Kiremire, G. Kumar, K. Chibale, J.C.A. Boeyens, J. Makhubela, and E. Matabane, *Orient. J. Chem.*, 2003, **19**, 309.
134. M. Ebihara, M. Iiba, M. Kato, H. Minami, and T. Kawamura, *Inorg. Chim. Acta*, 2004, **357**, 533.
135. J.C. Yoder, J.P. Roth, E.M. Gussenhoven, A.S. Larsen, and J.M. Mayer, *J. Am. Chem. Soc.*, 2003, **125**, 2629.
136. H. C. Aspinall, *Chem. Rev.*, 2002, **102**, 1807.
137. S. Besli, S.J. Coles, D.B. Davies, R.J. Eaton, M.B. Hursthouse, A. Kilic, R.A. Shaw, G.Y. Ciftci, and S. Yesilot, *J. Am. Chem. Soc.*, 2003, **125**, 4943.
138. K. J. Smith, J. D. Wilcox, G. E. Mirick, L. S. Wacker, N. S. Ryan, D. A. Vensel, R. Readling, H. L. Domush, E. P. Amonoo, S. S. Shariff, and T. J. Wenzel, *Chirality*, 2003, **15**, S150.
139. N. Baldovini, F. Tomi, and J. Casanova, *Phytochem. Anal.*, 2003, **14**, 241.
140. H.H. Fischer, M. Seiler, T.S. Ertl, U. Eberhardinger, H. Bertagnolli, H. Schmitt-Willich, and K. Albert, *J. Phys. Chem. B.* 2003, **107**, 4879.
141. S. Tamburini, P. Tomasin, P.A. Vigato, S. Aime, M. Botta, and M.A. Cremonini, *Inorg. Chim. Acta*, 2004, **357**, 1374.
142. M. Fasano, S. Baroni, S. Aime, M. Mattu, and P. Ascenzi, *J. Inorg. Biochem.*, 2003, **95**, 64.
143. L. A. Yatsunyk and F. A. Walker, *Inorg. Chem.*,, 2004, **43**, 4341.
144. L. A. Yatsunyk and F. A. Walker, *Inorg. Chem.*,, 2004, **43**, 757.
145. A. Ikezaki, M. Nakamura, *Inorg. Chem.*, 2002, **41**, 2761.
146. A. Ikezakiand M. Nakamura, *Inorg. Chem.*, 2003, **42**, 2301.
147. M. Rivera, G. A. Caignan, A. V. Astashkin, A. M. Raitsimring, T. Kh. Shokhireva, and F. A. Walker, *J. Am. Chem. Soc.*, 2002, 124, 6077.
148. M. Rivera, G.A. Caignan, A.V. Astashkin, A.M. Raitsimring, T.Kh. Shokhireva, and F.A. Walker, *J. Am. Chem. Soc.*, 2002, **124**, 6077.
149. G.A. Caignan, R. Deshmukh, Y. Zeng, A. Wilks, R.A. Bunce, and M. Rivera, *J. Am. Chem. Soc.*, 2003, **125**, 11842.
150. J. Mao, Y. Zhang, and E. Oldfield, *J. Am. Chem. Soc.*, 2002, **124**, 13911.
151. R.-J. Cheng, P.-Y. Chen, T. Lovell, T. Liu, L. Noodleman, and D. A. Case, *J. Am.*

Chem. Soc., 2003, **125**, 6774.
152. M. P. Johansson, D. Sundholm, G. Gerfen, and M. Wikstrom, *J. Am. Chem. Soc.*, 2002, **124**, 11771.
153. H. Hada, *J. Am. Chem. Soc.*, 2004, **126**, 486.
154. S. C. M. Gandini, E. A. Vidoto, O. R. Nascimento, and M. Tabak, *J. Inorg. Biochem.*, 2003, **94**, 127-137.
155. B. Song, *Bull. Kor. Chem. Soc.*, 2003, **24**, 1035.
156. I. M. Wasser, C. F. Martens, C. N. Verani, E. Rentschler, H.-W. Huang, P. Moeenne-Loccoz, L. N. Zakharov, A. L. Rheingold, and K. D. Karlin, *Inorg. Chem.*, 2004, **43**, 651.
157. T. Sakai, Y. Ohgo, T. Ikeue, M. Takahashi, M. Takeda, and M. Nakamura, *J. Am. Chem. Soc.*, 2003, **125**, 13028.
158. M. Nakamura, A. Hoshino, A. Ikezaki, and T. Ikeue, *Chem. Commun.*, 2003 (15), 1862.
159. T. Sakai, O. Yoshiki Ohgo, A. Hoshino, T. Ikeue, T. Saitoh, M. Takahashi, and M. Nakamura, *Inorg. Chem.*, 2004, **43**, 5034.
160. T. Ikeue, Y. Ohgo, O. Ongayi, M. G. H. Vicente, and M. Nakamura, *Inorg. Chem.* 2003, **42**, 5560.
161. J. L. Garate-Morales, Y. Reyes-Ortega, C. Alvarez-Toledano, R. Gutierrez-Perez, D. Ramirez-Rosales, R. Zamorano-Ulloa, E. Basurto-Uribe, J. Hernandez-Diaz, and R. Contreras, *Trans. Met. Chem.*, 2002, **27**, 906.
162. A. Sanchez-Sandoval, D. Ramirez-Rosales, R. Zamorano-Ulloa, C. Alvarez-Toledano , M. Moya-Cabrera , and Y. Reyes-Ortega, *Biophys. Chem.*, **106**, 2003, 253.
163. A. Ikezaki and M. Nakamura, *Inorg. Chem.*, 2002, **41**, 6225.
164. L. Yatsunyk and F. A. Walker, *Inorg. Chim. Acta*, 2002, **337**, 266.
165. B. Song, B.-S. Yu, *Bull. Kor. Chem. Soc.*, 2003, 24, 981.
166. M. Pawlicki, L. Latos-Grazynski, *Inorg. Chem.* 2002, **41**, 5866.
167. J. Wojaczynski, M. Stepien, and L. Latos-Grazynski, *Eur. J. Inorg. Chem.* **2002**, 1806.
168. O. Zakharieva, V. Schunemann, M. Gerdan, S. Licoccia, S. Cai, F. A. Walker, and A. X. Trautwein, *J. Am. Chem. Soc.*, 2002, **124**, 6636.
169. E. Steene, A. Dey, and A. Ghosh, *J. Am. Chem. Soc.*, 2003, **125**, 16300.
170. S. Cai, S. Licoccia, C. D'Ottavi, R. Paolesse, S. Nardis, V. Bulach, B. Zimmer, T.Kh. Shokhireva, and A.F. Ann Walker, *Inorg. Chim. Acta*, 2002, **339**, 171.
171. F. A. Walker, *Inorg. Chem.*, 2003, **42**, 4526.
172. K. Rachlewicz, S.-L. Wang, C.-H. Peng, C.-H. Hung, and L. Latos-Grazynski, *Inorg. Chem.* 2003, **42**, 7348.
173. K. Rachlewicz, S.-L. Wang, J.-H. Ko, C.H. Hung, and L. Latos-Grazynski, *J. Am. Chem. Soc.*, 2004, **126**, 4420.
174. F. Kateb and M. Piccioli, *J. Am. Chem. Soc.*, 2003, **125**, 14978.
175. W. Bermel, I. Bertini, I.C. Felli, R. Kuemmerle, and R. Pierattelli, *J. Am. Chem. Soc.*, 2003, **125**, 16423.
176. E. Babini I. Bertini, F. Capozzi, I.C. Felli, M. Lelli, and C. Luchinat, *J.Am. Chem. Soc.*, 2004, **126**, 10496.
177. G. Pintacuda, M.A. Keniry, T. Huber, A.Y. Park, N.E. Dixon, and G. Otting, *J. Am. Chem. Soc.*, 2004, **126**, 2963.
178. T.E. Machonkin, W.M. Westler, and J.L. Markley, *J. Am. Chem. Soc.*, 2002, **124**, 3204.
179. T.E. Machonkin, W.M. Westler, and J.L. Markley, *J. Am. Chem. Soc.*, 2004, **126**, 5413.

180. M. Kostic, S. Sondej-Pochapsky, and T.C. Pochapsky, *J. Am. Chem. Soc.*, 2002, **124**, 9054.
181. J.M. Nocek, K. Huang, and B.M. Hoffman, *ACS Symp. Ser.*, 2003, **858**(Paramag. Reson. Metallobiomol.), 227.
182. M.R. Jensen and J.J. Led, *J. Magn. Reson.*, 2004, **167**, 169.
183. I. Bertini, M. Longinetti, C. Luchinat, G. Parigi, and L. Sgheri, *J. Biomol. NMR*, 2002, **22**, 123.
184. I. Bertini, G. Cavallaro, M. Cosenza, R. Kuemmerle, C. Luchinat, M. Piccioli, and L. Poggi, *J. Biomol. NMR*, 2002, **23**, 115
185. I. Bertini, C. Luchinat, and G. Parigi, *Concepts Magn. Reson.*, 2002, **14**, 259.
186. I. Bertini, C. Luchinat, and G. Parigi, *Progr. Nucl. Magn. Reson. Spectr.*, 2002, **40**, 249.
187. L. Banci, I. Bertini, G. Cavallaro, A. Giachetti, C. Luchinat, and G. Parigi, *J. Biomol. NMR*, 2004, **28**, 249.
188. P. Turano, G. Battaini, and L. Casella, *Chem. Phys. Lett.*, 2003, **373**, 460.
189. G. Pintacuda, K. Hohenthanner, G. Otting, and N. Mueller, *J. Biomol. NMR*, 2003, **27**, 115.
190. R. Barbieri, C. Luchinat, and G. Parigi, *Chem. Phys. Phys. Chem.*, 2004, **5**, 797.
191. I. Baig, I. Bertini, C. Del Bianco, Y. K. Gupta, Y.-M. Lee, C. Luchinat, and A. Quattrone, *Biochem.*, 2004, **43**, 5562.
192. L. Banci, I. Bertini, G. Cavallaro, and C. Luchinat, *J. Biol. Inorg. Chem.*, 2002, **7**, 416.
193. L. Banci, I. Bertini, S. Ciurli , A. Dikiy, J. Dittmer, A. Rosato, G. Sciara, and A.R. Thompsett, *Chembiochem*, 2002, **3**, 299.
194. M. Assfalg, I. Bertini, A. Dolfi, P. Turano, A.G. Mauk, F.I. Rosell, and H.B. Gray, *J. Am. Chem. Soc.*, 2003, **125**, 2913.
195. Y. Yao, C. Qian, K. Ye, J. Wang, Z. Bai, and W. Tang, *J. Biol. Inorg. Chem.*, 2002, **7**, 539.
196. M. Assfalg, I. Bertini, P. Turano, M. Bruschi, M.-C. Durand, M.-T. Giudici-Orticoni, and A. Dolla, *J. Biomol. NMR*, 2002, **22**, 107.
197. I. Bertini, J. Faraone-Mennella H.B. Gray, C. Luchinat, G. Parigi, and J.R. Winkler, *J. Biol. Inorg. Chem.*, 2004, **9**, 224.
198. R. Barbieri, I. Bertini, G. Cavallaro, Y.M. Lee, C. Luchinat, A. Rosato, *J. Am. Chem. Soc.*, 2002, **124**, 5581.
199. B. Jimenez, L. Poggi, and Mario Piccioli, *Biochem.*, 2003, **42**, 13066.
200. M. Allegrozzi, I. Bertini, S.N. Choi, Y.-M. Lee, and C. Luchinat, *Eur. J. Inorg. Chem.*, 2002,(**8**), 2121.
201. M. Longinetti, G. Parigi, and L. Sgheri, *J. Phys. A: Math. Gen.*, 2002, 35, 8153.
202. M. Gochin, V. Khorosheva, and M.A. Case, *J. Am. Chem. Soc.*, 2002, **124**, 11018.
203. V. Gaponenko, S.P. Sarma, A.S. Altieri, D.A. Horita, J. Li, Jess, and A.R. Byrd, *J. Biomol. NMR*, 2004, **28**, 205.
204. M. Prudencio, J. Rohovec, J.A. Peters, E. Tocheva, M.J. Boulanger, M.E.P. Murphy, H.-J. Hupkes, W. Kosters, A. Impagliazzo, and M. Ubbink, *Chem. Eur. J.*, 2004, **10**, 3252.
205. V. Gaponenko, A.S. Altieri, J. Li, and R.A. Byrd, *J. Biomol. NMR*, 2002, **24**, 143.
206. B.J. Goodfellow, S.G. Nunes, F. Rusnak, I. Moura, C. Ascenso, J.J.G. Moura, B.F. Volkman , and J.L. Markley, *Prot. Sci.*, 2002, **11**, 2464.
207. G. Pintacuda, A. Moshref, A. Leonchiks, A. Sharipo, and G. Otting, *J. Biomol. NMR*, 2004, **29**, 351.
208. I. Takahisa, V. Laurent, S. Peyman, S. Grimm, B. Pescatore, K. Saxena, K.M.

Fiebig, and C. Griesinger, *J. Biomol. NMR*, 2004, **29**, 339.
209. J. Woehnert, K.J. Franz, M. Nitz, B. Imperiali, and H. Schwalbe, *J. Am. Chem. Soc.*, 2003, **125**, 13338.
210. M.R. Jensena, C. Lauritzenb, S.W. Dahlb, J. Pedersenb, and J.J. Leda, *J. Biomol. NMR*, 2004, **29**, 175.
211. T.S. Ulmer, I.D. Campbell, and J. Boyd, *J. Magn. Reson.*, 2002, **157**, 181.
212. J.L. Battiste, J.D. Gross, and G. Wagner, *Biol. Magn. Reson.*, 2003, **20**, 79.
213. A. Dvoretsky, V. Gaponenko, and P.R. Rosevear, *FEBS Lett.*, 2002, **528**, 189.
214. J.C. McNulty, D.A. Thompson, M.R. Carrasco, and G.L. Millhauser, *FEBS Lett.*, 2002, **529**, 243.
215. S. Aime, N. D'Amelio, M. Fragai, Y.-M. Lee, C. Luchinat, E. Terreno, and G. Valensin, *J. Biol. Inorg. Chem.*, 2002, 7, 617.
216. J. Iwahara, C.D. Schwieters, and G.M. Clore, *J. Am. Chem. Soc.*, 2004, **126**, 5879.
217. W. Jahnke, *ChemBioChem*, 2002, **3**, 167.
218. I. Bertini, M. Fragai, Y.-M. Lee, C. Luchinat, and B. Terni, *Angew. Chem., Int. Ed.*, 2004, **43**, 2254.
219. J.F. Ellena, V.V. Obraztsov, V.L. Cumbea, C.M. Woods, D.S. Cafiso, *J. Med. Chem.*, 2002, **45**, 5534.
220. C. Hilty, G. Wider, C. Fernandez, and K. Wuethrich, *ChemBioChem*, 2004, **5**, 467.
221. M.A. Lietzow, M. Jamin, D.H. Jane, and P.E. Wright, *J. Mol. Biol.*, 2002, **322**, 655.
222. K. Lindorff-Larsen, S. Kristjansdottir, K. Teilum, Kaare, W. Wolfgang, C.H. Dobson, F.M. Poulsen, and M. Vendruscolo, *J. Am. Chem. Soc.*, 2004, **126**, 3291.
223. N. Neri, O. Spiga, A. Bernini, M. Scarselli, A. Ciutti, I. Fiaschi, S. Chiellini, H. Molinari, and P.A, Temussi, *J. Mol. Biol.*, 2003, **332**, 437.
224. G. Pintacuda and G. Otting, *J. Am. Chem. Soc.*, 2002, **24**, 372.
225. A. Lewin, J.P. Hill, R. Boetzel, T. Georgiou, R. James, C. Kleanthous, and G.R. Moore, *Inorg. Chim. Acta*, 2002, **331**, 123.
226. M. Nomura, T. Kobayashi, T. Kohno, K. Fujiwara, T. Tenno, M. Shirakawa, I. Ishizaki, K. Yamamoto, T. Matsuyama, M. Mishima, and C. Kojima, *FEBS Lett.*, 2004, **566**, 157.
227. P.K. Bhattacharya, H.J. Lawson, and J.K. Barton, *Inorg. Chem.*, 2003, **42**, 8811.
228. H. Watson, J. Hatfield, and J.B. Vincent, *Inorg. Chim. Acta*, 2003, **344**, 265.
229. J. Iwahara, E.D. Anderson, E.C. Murphy, and M.G. Clore, *J. Am. Chem. Soc.*, 2003, 125, 6634.
230. N. Emmerichs, J. Wingender, H.-C. Flemming, and C. Mayer, *Int. J. Biol. Macromol.*, 2004, **34**, 73.
231. B. Manz, M. Hillgaertner, H. Zimmermann, D. Zimmermann, F. Volke, and U. Zimmermann, *Eur. Biophys. J.*, 2004, **33**, 50
232. G. D'Auria, G. Flores, L. Falcigno, R. Oliva, M. Vacatello, M.M. Corsaro, M. Parrilli, and L. Paolillo, *Biopolym.*, 2003, **70**, 260.
233. M. Rivera and G.A. Caignan, *Anal. Bioanal. Chem.*, 2004, **378**, 1464.
234. I. Bertini, C. Luchinat, P. Turano, G. Battaini, and L. Casella, *Chem.-Eur. J.*, 2003, **9**, 2316.
235. J.S. de Ropp, S. Sham, A. Asokan, S. Newmyer, P.R. Ortiz de Montellano, and G.N. La Mar, *J. Am. Chem. Soc.*, 2002, **124**, 11029.
236. W. Du, Z. Xia, S. Dewilde, L. Moens, and G.N. La Mar, *Eur. J. Biochem./ FEBS*, 2003, **270**, 2707.
237. D. Ma, R. Musto, K.M. Smith, and G.N. La Mar, *J. Am. Chem. Soc.*, 2003, **125**, 8494
238. B.C. Christie, D.A. Vuletich, S.A. Kuriakose, C.J. Falzone, J.T.J. Lecomte, *J. Biol. Inorg. Chem.*, 2004, **9**, 183.

239. E. Monzani, M. Curto, M. Galliano, L. Minchiotti, S. Aime, S. Baroni, M. Fasano, A. Amoresano, A.M. Salzano, P. Pucci, and L. Casella, *Biophys. J.*, 2002, **83**, 2248.
240. T.Kh. Shokhireva, N.V. Shokhirev, and F.A. Walker, *Biochem.*, 2003, **42**, 679.
241. W. Liu, J. Rumbley, S.W. Englander, A.J. Wand, *Prot. Sci.*, 2003, **12**, 2104.
242. Y. Yamamoto, S. Nagao, Y. Hirai, T. Inose, N. Terui, H. Mita, and A. Suzuki, *J. Biol. Inorg. Chem.*, 2004, **9**, 152.
243. J. Zhang J.P. Osborne. R.B. Gennis, and X. Wang, *Arch. Biochem. Biophys.*, 2004, **421**, 186.
244. R.O. Louro, M. Pessanha, G.A. Reid, S.K. Chapman, D.L. Turner, and C.A. Salgueiro, *FEBS Lett.*, 2002, **531**, 520.
245. W. Du, R. Syvitski, S. Dewilde, L. Moens, and Gerd N. La Mar, *J. Am. Chem. Soc.*, 2003, **125**, 8080.
246. Q. Zhang, C. Cao, Z.Q. Wang, Y.-H.Wang, H. Wu, and Z.-X. Huang, *Prot. Sci.*, 2004, **13**, 2161.
247. G.A. Schoch, R. Attias, M. Belghazi, P.M. Dansette, and D. Werck-reichhart, *Plant Phys.*, 2003, **133**, 1198.
248. L. Banci, R. Pierattelli, A.J. Vila, *Adv. Prot. Chem.*, 2002, **60**(Copper-Containing Proteins), 397.
249. I. Bertini, and R. Pierattelli, *Pure Appl. Chem.*, 2004, **76**, 321.
250. F. Arnesano, L. Banci, I. Bertini, I.C. Felli, C. Luchinat, and A.R. Thompsett, *J. Am. Chem. Soc.*, 2003, **125**, 7200.
251. I. Gelis, N. Katsaros Nikolaos, C. Luchinat, M. Piccioli , and L. Poggi, *Eur. J. Biochem./FEBS.*, 2003, **270**, 600.
252. K. Sato, and C. Dennison, *Biochem.*, 2002, **41**, 120.
253. C. Dennison and K. Sato, *Inorg. Chem.*, 2004, **43**, 1502.
254. C.O. Fernandez and A.J. Vila, *ACS Symp. Ser.*, 2003, **858**(Paramag. Reson. Metallobiomol.), 287
255. D.F. Hansen, and J.J. Led, *J. Am. Chem. Soc.*, 2004, **126**, 1247.
2256. A. Donaire, B. Jimenez, C.O. Fernandez, R. Pierattelli, T. Niizeki, J.-M. Moratal, J.F. Hall, T. Kohzuma, S.S. Hasnain, and A.J. Vila, *J. Am. Chem. Soc.*, 2002, **124**, 13698.
257. D. Monlcon, F. Ribes, H.R. Jimenez, J.M. Moratal, and B. Celda, *Inorg. Chim. Acta*, 2004, **357**, 1111.
258. C.J. Carrell, X. Wang , L. Jones, W.L. Jarrett, V.L. Davidson, and F.S. Mathews, *Biochem.*, 2004, **43**, 9381.
259. C.O. Fernandez, T. Niizeki, T. Kohzuma, and A.J. Vila, *J. Biol. Inorg. Chem.*, 2003, **8**, 75..
260. C. Dennison and K. Sato, *Inorg. Chem.*, 2002, **41**, 6662.
261. C. Dennison and M.D. Harrison, *J. Am. Chem. Soc.*, 2004, **126**, 2481.
262. M.N. Harris, C.M. Bertolucci, and L.-J. Ming, *Inorg. Chem.*, 2002, **41**, 5582.
263. M. Kostic and T.C. Pochapsky, *ACS Symp. Ser.*, 2003, **858**(Paramagn. Reson. Metallobiomol.), 214.
264. L Calzolai, H. Haarklau, P.S. Brereton, M.W.W. Adams, and G.N. La Mar, *ACS Symp. Ser.*, 2003, **858**(Paramagn. Reson. Metallobiomol.), 258
265. S. Sham, Simon, L. Calzolai, P.-L. Wang, K. Bren, H. Haarklau, P. Brereton, M.W.W. Adams, and G.N. La Mar, *Biochem.*, 2002, **41**, 12498.
266. M. Kostic, S.S. Pochapsky, J. Obenauer, H. Mo, G.M. Pagani, R. Pejchal, and T.C. Pochapsky, *Biochem.*, 2002, **41**, 5978.
267. X. Trivelli, S. Bouillac, P. Tsan, I. Krimm, and J.-M. Lancelin, *Photosynth. Res.*, 2004, **79**, 357.

268. M. Ubbink, *Photosynth. Res.*, 2004, **81**, 277.
269. J. Mueller, A.A. Lugovskoy, G. Wagner, and S.J. Lippard, *Biochem.*, 2002, **41**, 42.
270. H.D. Flemming and J.J. Led, *J. Magn. Reson.*, 2003, **163**, 215.
271. M.R. Jensen, D.F. Hansen, and J.J. Led, *J. Am. Chem. Soc.*, 2002, **124**, 4093.
272. K. Sato, T. Kohzuma, and C. Dennison, *J. Am Chem. Soc.*, 2003, **125**, 2101.
273. D.F. Hansen, M.A.S. Hass, H.M. Christensen, J. Ulstrup, and J.J. Led, *J. Am. Chem. Soc.*, 2003, **125**, 6858.
274. R.R. Sharp, in 'Paramagnetic NMR', ed. G.A. Webb, Specialist Periodical Reports, The Royal Society of Chemistry, Cambridge, UK, 2003, vo. 32, p. 473-520.
275. J. Kowalewski, C. Luchinat, T. Nilsson, and G. Parigi, *J. Phys. Chem. A*, 2002, **106**, 7376.
276. D. Kruk and J. Kowalewski, *J. Magn. Reson.*, 2003, **162**, 229.
277. D. Kruk and J. Kowalewski, *Molec. Phys.*, 2003, **101**, 2861.
278. J. Miller, N. Schaefle, and R. Sharp, *Magn. Reson. Chem.*, 2003, **41**, 806.
279. Z. Rinkevicius, J. Vaara, L. Telyatnyk, and O. Vahtras, *J. Chem. Phys.*, 2003, **118**, 2550.
280. L. Telyatnyk, J. Vaara, Z. Rinkevicius, and O. Vahtras, *J. Phys. Chem. B*, 2004, **108**, 1197.
281. K. L. Ivanov, K. Miesel, H.-M. Vieth, A. V. Yurkovskaya, and R. Z. Sagdeev, *Z. Phys. Chem.*, 2003, **217**, 1641.
282. J. R. Woodward, C. R. Timmel, P. J. Hore, and K. A. McLauchlan, *Mol. Phys.*, 2002, **100**, 1181.
283. A. V. Popov, P. A. Purtov, and A. B. Doktorov, *Appl. Magn. Reson.*, 2002, **23**, 149.
284. M. Goez and I. Sartorius, *J. Phys. Chem. A*, 2003, **107**, 8539.
285. I. M. Magin, V. S. Shevel'kov, A. A. Obynochny, A. I. Kruppa, and T.V. Leshina, *Chem. Phys. Lett.*, 2002, **357**, 351.
286. N. E. Polyakov, A. I. Kruppa, V. S. Bashurova, T. V. Leshina, and L. D. Kispert, *J. Photochem. PhotoBiol.* A, 2002, **153**, 113.
287. E. G. Bagraynskaya, N. V. Lebedeva, M. V. Fedin, R. Z. Sagdeev, *NATO Sci. Ser., II: Math., Phys. Chem.* 2002, **76**(Magn. Reson. Coll. Interf. Sci.), 173
288. M. Goez and R. Heun, *Phys. Chem. Chem. Phys.*, 2002, **4**, 5531.
289. N. V. Lebedeva, M. V. Fedin, E. G. Bagryanskaya, and R. D. Sagdeev, *Phys. Chem. Chem. Phys.*, 2003, **5**, 2595.
290. M. Lehnig, M. Kirsch,and H.-G. Korth, *Inorg. Chem.*, 2003, **42**, 4275.
291. N. E. Polyakov, V. S. Bashurova, T. V. Leshina, O. A. Luzina, and N. F. Salakhutdinov, *J. Photochem. PhotoBiol.* A, 2002, **153**, 77.
292. A. J. Maliakal, N. J. Turro, *Polym. Mat. Sci. Eng.* 2002, **87**, 166.
293. G. Gescheidt, D. Neshchadin, G. Rist, A. Borer, K. Dietliker, and K. Misteli, *Phys. Chem. Chem. Phys.*, 2003, **5**, 1071.
294. H. Hiyashi, *J. Chin. Chem. Soc.*, 2002, **49**, 137.
295. I. V. Khudyakov,A. N. Arsu, S. Jockusch, N. Turro, *Designed Monomers and Polymers*, 2003, **6**, 91.
296. M. V. Fedin, E. G. Bagryanskaya, P. A. Purtov, T. N. Makarov, and H. Paul, *J. Chem. Phys.*, 2002, **117**, 6148.
297. K. L. Ivanov, H.-M. Vieth, K. Miesel, A. V. Yurkovskaya, R. Z. Sagdeev, *Phys. Chem. Chem. Phys.*, 2003, **5**, 3407.
298. S. S. Petrova, A. I. Kruppa, T. V. Leshina, *Chem. Phys. Lett.*, 2004, **385**, 40.
299. I. P. Pozdnyakov, V. F. Plyusnin, V. P. Grivin, D. Yu. Vorobyev, A. I. Kruppa, H. Lemmetyinen, *J. Photochem. Photobiol. A: Chem.*, 2004, **162**, 153.
300. A. V. Yurkovskaya, O. A. Snytnikova, O. B. Morozova, Y. P. Tsentalovich, and R.

Z. Sagdeev, *Phys. Chem. Chem Phys.*, 2003, **5**, 3653.
301. M. Goez and I. Frisch, *J. Phys. Chem.* A, 2002, **106**, 8079.
302. H. D. Roth, *J. Phys. Chem. A* 2003, **107**, 3432.
303. D. Canet, C. E. Lyon, R. M. Scheek, G. T. Robillard, C. M. Dobson, P. J. Hore, and N. A. J. van Nuland, *J. Mol. Biol.*, 2003, **330**, 397.
304. M. Cemazar, S. Zahariev, S. Pongor, and P. J. Hore, *J. Biol. Chem.*, 2004, **279**, 16697.
305. M. Cemazar, S. Zahariev, J. J. Lopez, O. Carugo, J. A. Jones, P. J. Hore, and S. Pongor, *Proc. Nat. Acad. Sci. (U. S. A)*, 2003, **100**, 5754.
306. K. H. Mok, T. Nagashima, I. J. Day, J. A. Jones, C. J. V. Jones, C. M. Dobson, and P. J. Hore, *J. Am. Chem. Soc.*, 2003, **125**, 12484.
307. C. E. Lyon, J. J. Lopez, B.-M. Cho, and P. J. Hore, P. J., *Mol. Phys.*, 2002, **100**, 1261.
308. C. E. Lyon, E.-S. Suh, C. M. Dobson, and P. J. Hore, *J. Am. Chem. Soc.*, 2002, **124**, 13018.
309. I. Kuprov and P.J. Hore, *J. Magn. Reson.* 2004, **168**, 1.
310. O. B. Morozova, A. V. Yurkovskaya, Y. P. Tsentalovich, M. D. E. Forbes, and R. Z. Sagdeev, *J. Phys. Chem. B*, 2002, **106**, 1455.
311. O. B. Morozova, A. V. Yurkovskaya, H.-M. Vieth, and R. Z. Sagdeev, *J. Phys. Chem. B*, 2003, **107**, 1088.
312. Yu. P. Tsentalovich, J. J. Lopez, P. J. Hore, and R. Z. Sagdeev, *Spectr. Acta, Part A: Mol. Biomol. Spec.*, 2002, **58A**, 2043.
313. E. A. M. Schulten, J. Matysik, Alia, S. Kiihne, J. Raap, J. Lugtenburg, Peter Gast, A. J. Hoff, and H. J. M. de Groot, *Biochemistry*, 2002, **41**, 8708.
314. S. Prakash, Alia; P. Gast, G. Jeschke, H. J. M. de Groot, J. Matysik, *J. Mol. Struct.*, 2003, 661, 625.
315. G. Jeschke and J. Matysik, *Chem. Phys.*, 2003, **294**, 239.

As a spectroscopic method, nuclear magnetic resonance (NMR) has seen spectacular growth over the past two decades, both as a technique and in its applications. Today the applications of NMR span a wide range of scientific disciplines, from physics to biology to medicine.

Each volume of **Nuclear Magnetic Resonance** comprises a combination of annual and biennial reports which together provide comprehensive coverage of the literature on this topic. This Specialist Periodical Report reflects the growing volume of published work involving NMR techniques and applications, in particular NMR of natural macromolecules which is covered in two reports: "NMR of Proteins and Nucleic Acids" and "NMR of Carbohydrates, Lipids and Membranes".

For those wanting to become rapidly acquainted with specific areas of NMR, this title provides unrivalled scope of coverage. Seasoned practitioners of NMR will find this an invaluable source of current methods and applications.

ISBN 0-85404-352-7

9 780854 043521

SPECIALIST PERIODICAL REPORTS

Specialist Periodical Reports provide systematic and detailed review coverage in major areas of chemical research. Compiled by teams of leading authorities in the relevant subject areas, the series creates a unique service for the active research chemist, with regular, in-depth accounts of progress in particular fields of chemistry. Subject coverage within different volumes of a given title is similar and publication is on an annual or biennial basis.

Current subject areas covered are *Amino Acids, Peptides and Proteins, Carbohydrate Chemistry, Catalysis, Chemical Modelling: Applications and Theory, Electron Paramagnetic Resonance, Nuclear Magnetic Resonance, Organometallic Chemistry, Organophosphorus Chemistry, Photochemistry* and *Spectroscopic Properties of Inorganic and Organometallic Compounds.*
From time to time, the series has altered according to the fluctuating degrees of activity in the various fields, but these volumes remain a superb reference point for researchers.